HANDBOOK OF NON-FERROUS METAL POWDERS

TECHNOLOGIES AND APPLICATIONS

Edited by:
OLEG D. NEIKOV • STANISLAV S. NABOYCHENKO •
GORON DOWSON

Elsevier
The Boulevard, Langford Lane, Kidlington, Oxford OX5 1GB, UK
Radarweg 29, PO Box 211, 1000 AE Amsterdam, The Netherlands

First edition 2009

British Library Cataloguing in Publication Data
A catalogue record for this book is available from the British Library

Library of Congress Cataloging-in-Publication Data
A catalog record for this book is availabe from the Library of Congress

ISBN: 978-1-85617-422-0

For information on all Elsevier publications visit our web site at www.books.elsevier.com

Typeset by Charon Tec Ltd., A Macmillan Company. (www.macmillansolutions.com)

Printed and bound in Great Britain

09 10 10 9 8 7 6 5 4 3 2 1

Foreword

This new handbook is a comprehensive manual of the manufacture, properties and applications of non-ferrous metal powders. It was previously published in Russian in 1997, but now is completely updated and reflects the continuing improvements in traditional metal powder production technologies, as well as significant new coverage of emerging manufacturing methods; including the advanced technologies of the Post-USSR Countries, which were not published earlier in English. The fundamentals of the main methods of non-ferrous metal powder production, including mechanical methods, chemical and electrolytic methods, and physical-chemical methods are described and discussed.

In addition to in-depth articles on powder production, testing and characterization, the book expands coverage on the secondary operations, the safety engineering in the production of powders, and advanced areas of engineering research such as nanopowder processes.

Contributors and Reviewers

Oleg D. Neikov
Frantsevich Institute for Problems of Material Science (IPMS), Kiev, Ukraine

Stanislav S. Naboychenko
Ural State Technical University (UPI), Yekaterinburg, Russia

Irina V. Murashova
Ural State Technical University (UPI), Yekaterinburg, Russia

Victor G. Gopienko
Russian National Aluminium-Magnesium Institute, Saint Petersburg, Russia

Irina V. Frishberg
Fine Metal Powders R & D Company, Yekaterinburg, Russia

Dina V. Lotsko
Frantsevich Institute for Problems of Materials Science (IPMS), Kiev, Ukraine

Gordon Dowson
Technical Copyeditor, UK

Bernard Williams
European Powder Metallurgy Association, UK

Valerij G. Tokhtuyev
Frantsevich Institute for Problems of Materials Science (IPMS), Kiev, Ukraine

Ivan O. Neikov
Frantsevich Institute for Problems of Materials Science (IPMS), Kiev, Ukraine

Larissa A. Latysheva
Fine Metal Powders R & D Company, Yekaterinburg, Russia

Galina I. Vasilieva
Frantsevich Institute for Problems of Materials Science (IPMS), Kiev, Ukraine

Introduction

Oleg D. Neikov, Frantsevich Institute for Problems of Materials Science (IPMS), Kiev, Ukraine

The methods of non-ferrous powder production are multifarious and numerous. These techniques permit the manufacture of a wide spectrum of metal powders aimed to meet the requirements of a variety of applications. Various powder production processes allow precise control of the chemical composition and the physical characteristics of powders with prescribed attributes for their applications.

The relationship between shipments (tonnage) of non-ferrous and ferrous powders is about one to four but, in terms of market value, aluminum, silver and zinc are all close to the value of iron powders [1, 2]. This is illustrated by the recent data about metal powder world yield manufactured by atomization processes [2]. Figure I.1 shows the price in $/kg of powder, its volume in t/yr, and its total market value in $millions (log scale).

Basic Methods of Powder Production

Non-ferrous powders are produced by mechanical, chemical and electrochemical methods. Mechanical methods comprise the groups of disintegration of solids and atomization of melts. The disintegration of solid metals and alloys is carried out by machining, milling in impact mills, ball, vibration and edge-runner mills, medium agitating mills (attrition mills), jet mills etc. General chemical methods comprise the reduction methods, precipitation from solution, hydrometallurgical processing in leach autoclaves, carbonyl process and hydride/dehydride process. The electrolytic methods include electrolysis of aqueous solutions, cementation process and melt electrolysis (Table I.1). The evaporation–condensation method is a physical–chemical process and is one of the basic methods for the production of ultrafine (sub-micron) and nano-sized powders used in advanced miniaturization and nanotechnologies in powder metallurgy (PM), powder injection molding and creation of PM functional materials.

The shape and size of particles depend on the method of powder production and may vary within wide limits. In Figure I.2, the shapes of common particles produced by different methods are shown as depicted in ISO 3252.

Atomization is the most common method that allows the production of powders over a wide range of compositions and in a wide variety of powder particle sizes, from 1 μm to a few millimeters. While ferrous powders are currently produced by water atomization of liquid steel, the methods of non-ferrous powder production are multifarious.

Chemical and electrolytic methods are widely used for producing high-purity non-ferrous powders.

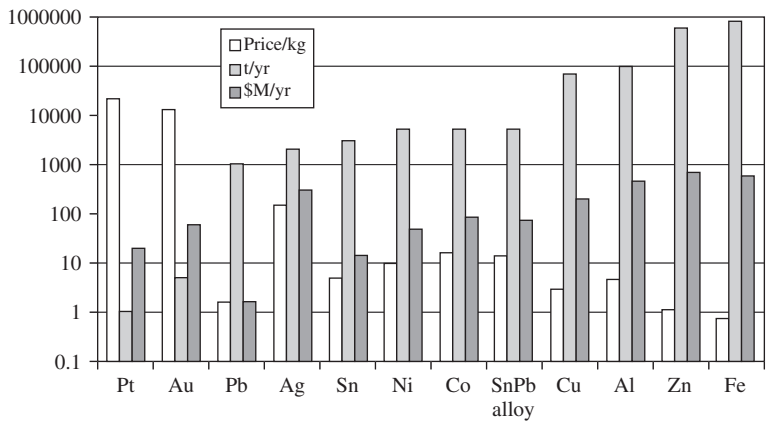

Figure I.1 Volume and value of metal powders.

Table I.1 Basic methods of non-ferrous metal powder production

Method of production	Processing character	Material	Characteristic of powder particles	
			Median mass diameter (d_m) (μm)	Shape
Mechanical methods				
Comminution of solids	Machining	Brass, bronze, Mg, Al, Cu	$3 \cdot 10^3$–10^3	Chips
	Hammer mills	Sinter cakes	$5 \cdot 10^3$–50	Angular, irregular
	Ball and rod mills, self-grinding	Bronze, Al, Ag, Ti, Ni, Cr	$5 \cdot 10^3$–10	Scaly, flake
	Mill rolls and bowl mills	The same	10^4–20	Irregular, scaly
	Vibratory mills	Metals, alloys	10–0.2	Scaly
	Medium agitating mills (attritors)	Metals, alloys	15–0.1 40–1.0	Scaly Irregular
	Jet mills	Mo, Be, tungsten alloys	<40	Flaked
Atomization of melts	Water granulation	Metals, alloys	$5 \cdot 10^3$–10^3	Spherical, irregular
	Water atomization	Metals, alloys	$2 \cdot 10^3$–1.0	Irregular
	Gas atomization	Metals, alloys	500–10	Spherical, irregular
	Centrifugal atomization	Al alloys, Be alloys, Mg, Mo, Ni alloys	150–50	Spherical, irregular
	Rotating electrode process	Ti alloys, Ni alloys	300–150	Spheroidal Irregular, angular
Chemical and electrolytic methods				
Reduction metal oxides	Oxide reduction by reducing atmospheres	Ni, Co, Cu, W, Mo	300–20	Spongy, granular, (conglomerates)
	Precipitation from solution	Ti, W, Precious metals	100 nano-size	Spongy, irregular, angular
	Hydrogenation, dehydrogenation	Ti, Zr, Hf	200–20	Irregular, angular
	Hydrometallurgical processing in leach autoclaves	Ni, Co, Cu, Precious metals	70–10	Spongy, granular, briquettes
	Metallothermy	Tantalum, niobium, magnesium, titanium, thorium, zirconium, vanadium	300–20	The same
	Carbothermy	Aluminum, magnesium, niobium, tungsten	400–20	Spongy
	Carbonyl process	Ni, Co, W, Mo	300–0.1	Spongy, acicular
Electrolysis	Electrolysis of aqueous solutions	Copper, tin, lead, zinc, nickel	400–ultrafine	Dendritic
	Electrolysis from melts	Aluminum, magnesium, titanium, tantalum, niobium, vanadium, zirconium	400–10	Dendritic
Physical-chemical methods				
Gas phase precipitation	Evaporation and condensation	Zn, Mg, Ti, Ag, Cd, Bi	Ultrafine, Nano-size	Conglomerate of particles, clusters
Other methods				
Mechanical alloying	Ball milling	Metals, alloys	Ultrafine, Nano-size	Agglomerate of particles, clusters
Spray granulation	Fluidized bed spray granulator	Al, Co, pyrophoric rare earths	$5 \cdot 10^3$–10^3	Spherical

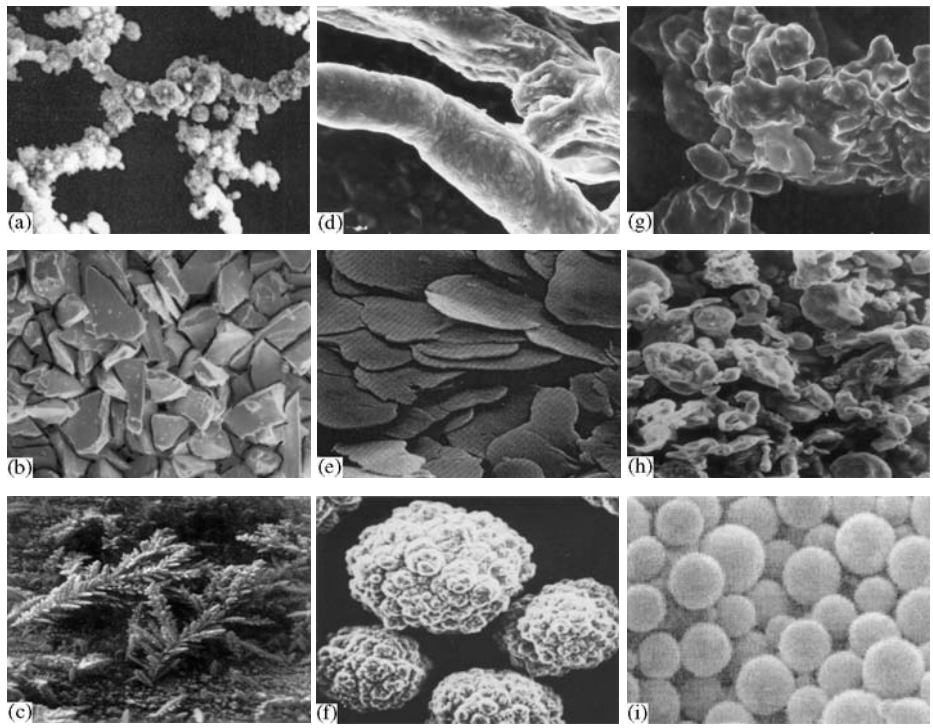

Figure I.2 Characteristic particle shapes: (a) acicular powder particles; (b) angular powder particles; (c) dendritic powder particles; (d) fibrous powder particles; (e) flake powder particles; (f) granular powder particles; (g) Irregular powder particles; (h) nodular powder particles; (i) spheroidal powder particles.

The comminution of solid metals has significant limitation due to the ductility of most of them. Nevertheless, milling in a high-energy apparatus such as an attritor finds wide application for the mechanical alloying of powders. Some basic physical and chemical methods of nanopowders and ultrafine powder production are discussed in Chapter 4, 'Nanopowders' and Chapter 6, 'Gas-phase method of metal powder production'.

Mechanical alloying is a simple and efficacious technique to synthesize both equilibrium and non-equilibrium phases of commercially and scientifically advanced materials obtained from initial elemental powders. The exclusive advantage of mechanical alloying consists of the possibility of the synthesis of unique alloys that are not accessible by any other technique, because mechanical alloying is a completely solid-state process and, therefore, limitations specified by the state diagrams do not apply here. Mechanical alloying is realized commonly by means of the high-energy ball milling technique.

Spray granulation, is when granules are formed by atomizing a binder solution into a fluidized powder bed [3]. Bulk fine powders typically have a low apparent density, do not flow, are dusty, have a low thermal conductivity and are explosive in the case of reactive metals such as aluminum, zirconium, etc. When duly granulated, the same powders in granule form are poured easily, apparent density is higher, dust emission is decreased, explosion-proofness is provided and they transfer thermal energy more efficiently.

Powder particle size is a dominant characteristic of a metal powder designated for subsequent use in PM. The area of application of powders dictates the size range required. In Figure I.3, the length of the segment lines shows approximately these application regions in terms of powder size. As is obvious, a rising number of PM applications require submicron powders that are produced by chemical or physical methods. The powder applications area embraces the range of particle sizes from a few nanometers to granules of some millimeters.

The main problems in production and processing of metallic nanopowders are caused by their high reactivity, explosibility owing to very high specific area, and agglomeration of particles. In Chapter 4, 'Nanopowders', a novel method for manufacturing semi-products directly from metal vapor, omitting

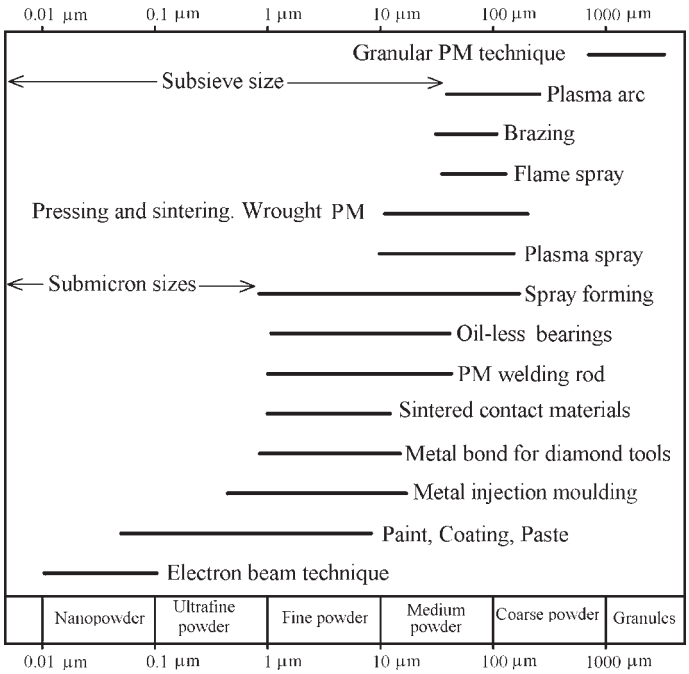

Figure I.3 Ranges of particle size suitable for different applications of non-ferrous powders.

the operation of producing nanopowder in powdered form, is discussed.

The powder characterization and testing described in Chapter 1, providing the key to the evaluation of the powder production, precede the description and discussion of the powder manufacturing methods. The main test methods and specific testing procedures that characterize the physical properties of powders, such as particle size distribution, particle shape and surface area are shown. Each of these parameters may have an important effect on the physical and mechanical behavior of powders produced for the manufacturing of PM products. Bulk properties of powders are also examined in this chapter. Finally, test methods for the determination of the compressibility, a key factor in reaching high PM production density, are given.

The fundamentals of the main methods of non-ferrous metal powder production, including mechanical methods, chemical and electrolytic methods and physical–chemical methods, are described and discussed in Section 2.

In Section 3, the techniques used for secondary operations such as dehydration, thermal drying, powder passivation, powder classification according to size, mixing, dosage and packing are described.

Production methods and techniques of copper and copper-base powders, aluminum and aluminum alloy powders, advanced aluminum alloy powders, magnesium and magnesium-base powders, titanium powders, nickel powders, zinc powders, refractory metal powders, rare metal powders, noble metal powders, and many other non-ferrous metal powders are described and discussed in Section 4.

Section 5 contains the description and discussion of safety engineering techniques and environmental protection in the production of powders.

References

1. Williams, B., Powder metallurgy – a global market review. In *International Powder Metallurgy Directory & Yearbook*, 13th edn 1, 2008/2009, pp. 5–14.
2. Dunkley, J.J., Atomisation of metals – craft or science?. In *Proceedings of 2nd International Conference on Spray Deposition and Melt Forming*, Vol. 1, edited by, K. Bauckhage, U. Fritsching, V. Uhlenwinkel, A. Leatham, Universitat Bremen, Bremen, 2003, pp. 1-3–1-11.
3. Tsukada, M., Goto, K., Yamamoto, R.H., Horio, M., Metal powder granulation in a plasma-spouted/fluidized bed. *Powder Technol.*, 1995, 82(3):347–353.

SECTION 1 Powder Characterization and Testing

Contents

Chapter 1 Powder Characterization and Testing

For a more detailed Section Contents list, please see the book Contents pages that start on page v

Chapter 1

Powder Characterization and Testing

Oleg D. Neikov, Dina V. Lotsko, Frantsevich Institute for Problems of Materials Science (IPMS), Kiev, Ukraine
Victor G. Gopienko, Russian National Aluminium-Magnesium Institute (VAMI), St. Petersburg, Russia

Apparent density, tap density, angle of repose, flow rate, compressibility and green strength are referred to as the physical–technological properties of powders. These properties, for a certain powder composition, may depend on its granulometric composition, particle shape, particle morphology, specific surface, moisture content, etc. Knowledge of technological parameters coupled with the physical properties enables evaluation of the behavior of powder during processing that is accomplished by their consolidation. The procedures described in standards are used to determine the technological properties of powders in delivery condition.

To evaluate powder properties the standard monitoring methods are used. The standard demands of the ISO are the base for the development of regional, national and branch standards. Usually, in contrast to ISO, a feature of these standards is the fact that they contain additional or refined specifications. Appendix 1 at the end of the book contains the list of the standard methods of powder characterization and testing.

Obtaining reliable powder samples is of vital importance for getting genuine data of chemical composition and the physical and technological properties of a given powder. To obtain a representative powder sample for analysis, it is necessary to follow the principles of sampling described below.

Sampling of Powders

Sampling arrangement and the subsequent partition of the selected samples that are needed for tests are laid down in ISO 3954. An analogous standard functions in North America (ASTM Standard B215) and in the USA (MPIF Standard 01).

Generally, two methods are used for obtaining samples of metal powders for subsequent testing. The first method is provided for sample take-off while the powder is in motion. A general rule in this method is that the whole of the stream of powder should be taken for many short increments of time, in preference to a single part of the stream being taken. This may be done when blenders or storage tanks are being emptied by screw or belt conveyors.

In the standard, the following sample types, represented in the sampling scheme in Figure 1.1, are distinguished. In the standard, the following terms are defined:

- lot – a definite quantity of powder processed or produced under uniform conditions
- increment – a quantity of powder obtained by a sampling device at one time from a single lot
- gross sample – a quantity of powder, adequate for the tests to be performed, consisting of all of the increments taken from a single lot
- composite sample – the blended entire gross sample
- test sample – a quantity of powder taken from the composite sample for determination of a single property or for preparing test pieces. It should normally be taken by splitting the composite sample
- test portion – a defined quantity of powder drawn from the test sample, on which the test is performed or from which test pieces are produced.

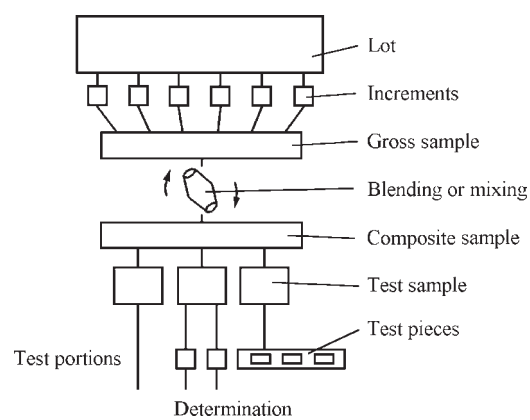

Figure 1.1 Sampling scheme.

Table 1.1 Recommended number of containers to be selected from a packaged lot

Number of containers in lot	Number of containers to be selected
1–5	All
6–11	5
12–20	6
21–35	7
36–60	8
61–99	9
100–149	10
150–199	11
200–299	12
300–399	13
More than 400	13 + 1 per 100 additional containers

At least three increments shall be taken for each lot of powder. The actual number depends on the size of the lot and the powder involved and shall be agreed upon by the parties involved.

The second method is used for sampling stored non-flowing materials: powders already packaged in containers. They may be stored in small containers such as drums or bags, or in large containers such as trucks or railway wagons. Several of these containers should be selected systematically or, preferably, using a table of random numbers. The standard recommends the number of samples depending on the total number of containers (Table 1.1). Sampling accuracy is provided by means of a sampling spear. The MPIF Standard 01 recommends the use of the keystone sampler, consisting of two coaxial tubes, outer and inner, closed from the bottom and with windows in the sides. The bottom part of the sampler is provided with a screw and from above is supplied by a handle. In the closed position, the sampler is inserted into the powder at a point 70% of the distance from the center of the cross-section to the periphery and straight down to the bottom of the container. The sampler is twisted to the open position, allowing powder to flow into the sampler tube. After filling, the sampler tube is closed and the sampler is removed from the container.

In sampling from trucks and wagons, it is recommended that eight samples be extracted [1]. No increment should be taken less than 300 mm below the surface in order to avoid sampling from the surface layer in which segregation can occur due to vibration (Figure 1.2).

The gross sample is often too large to be handled easily and may have to be reduced to a more opportune weight. Several methods are used for sample reduction.

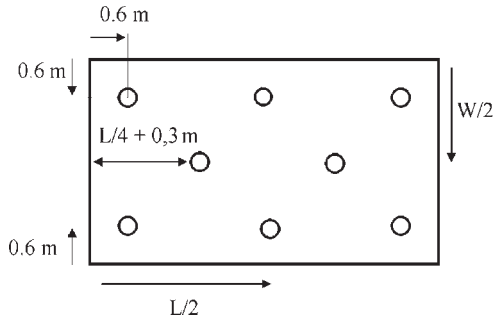

Figure 1.2 Sampling points for a truck or a wagon.

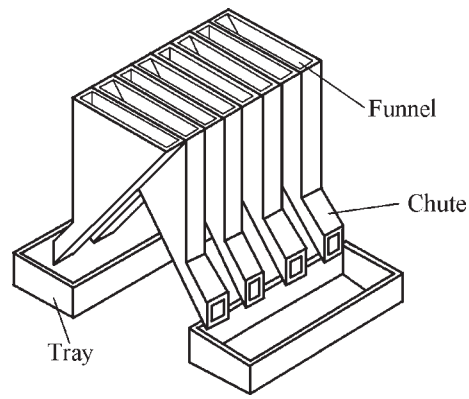

Figure 1.3 Sample splitter.

- *Scoop sampling* consists of plunging a scoop into the powder and selecting a sample. Such samples may not be representative of the bulk because the sample is taken from the surface and the sampling device does not pass through the whole heap.
- *Conical pouring and quartering* consists of pouring the powder into a heap on a flat horizontal surface and dividing by a cross-shaped cutter. The powder from two opposite portions is integrated in the common sample that in turn is divided into four parts for subsequent testing.
- *Chute splitting* is adopted for sample division. The chute splitter consists of funnels located along the bottom and forming two lines of chutes that separately feed two trays placed on either side of the chute (Figure 1.3).

All above methods are simple and therefore popular owing to the fact that samplers contain no moving parts and are inexpensive.

- A *rotary sample divider* for free-flowing powders is shown in Figure 1.4. Several versions of this device were designed for dusty powders, and some for cohesive powders.

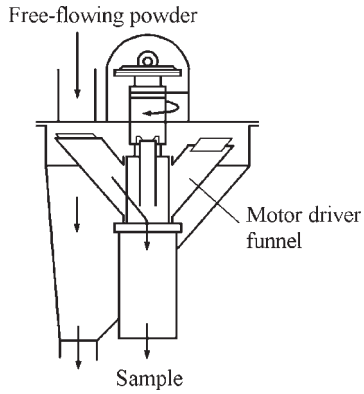

Figure 1.4 Rotary sample divider.

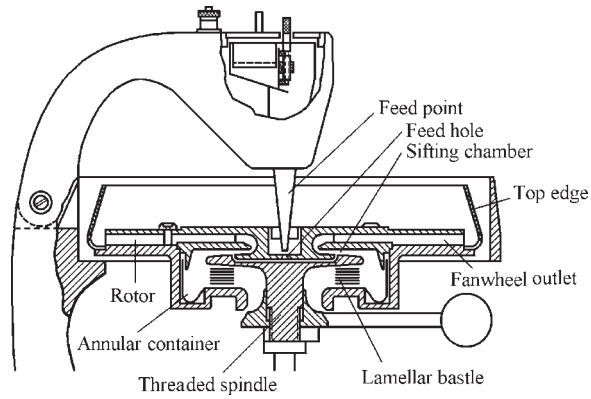

Figure 1.5 Simplified schematic draft of the Bahco classifier.

The reliability of selected methods was examined using binary mixtures of coarse and fine sand (60:40 ratio). It was deduced that the standard deviations amounted to 6.81 and 5.14%, respectively, for quartering and scoop sampling methods. Consequently, little confidence can take place in the first two techniques. For the chute splitting method and rotary sample divider, the standard deviations amount to 1.01 and 0.146%, respectively. Hence, the rotary sample divider is better than all the other methods.

Weight of Sample

The limiting (minimum) weight of the gross sample may be calculated using the following simple formula:

$$M_s = \frac{1}{2}\left(\frac{\rho}{\sigma_i^2}\right)\left(\frac{1}{w_1} - 2\right)d_1^3 \times 10^3 \qquad (1)$$

where M_s is the limiting weight in grams, ρ is the powder density in g/m^3, σ_i^2 is the variance of the tolerated sample error, w_1 is the fractional mass of the coarsest size class being sampled and d_1^3 is the arithmetic mean of the cubes of the extreme diameter in the size class in cubic centimeters. This equation is applicable when the coarsest class covers a size range of not more than 1.41:1 and w_1 is less than 50% of the total sample.

ISO 3081 recommends a minimum incremental mass depending on the maximum particle size in millimeters. According to this standard, the minimum mass of increment with maximum particle size of 10–0 mm amounts to 0.3 kg.

Particle Size Distribution Analysis

The classification process is used to determine particle size distribution or to separate certain particle sizes from a distribution. Generally, powder classification is based on the movement of the suspended particles in a fluid, under the action of a force field which is created by gravity, centrifugal or coriolis, and inertia forces. The fluid is usually air or water. The classifiers may be distinguished depending on the stream direction: counterflow equilibrium and cross-flow separation. The classifiers such as elutriators, zigzag classifiers, and Bahco centrifugal classifier, are related to the counterflow equilibrium devices [2]. The Bahco classifier (Figure 1.5) can be graded in the size range from 5 to 100 μm. For the samples, 5–10 g of powder are required.

Sieve Analysis

Sieve analysis is the method most widely used in the PM industry for determination of particle size distribution of metal powders larger 5 μm. Wire cloth sieves woven in a square mesh pattern of phosphor bronze or stainless steel are mounted in 75 or 200 mm stainless steel or brass rings. A series of sieves is selected that covers the full range of particle sizes present in a given powder. The sieving unit with sieve series, where sieves are stacked in order, with the largest mesh size at the top and a pan at the bottom, on a shaker with rotary and tapping action, is shown in Figure 1.6.

Test sieves according to the international and national standards are represented in Table 1.2. The standard sieve series are specified in ISO standards 565 and 3310/1, ASTM standard E 11 and CIS standard GOST 3584.

ISO sieve series is based on the principle of a fixed ratio between the sieve openings with selection of the row of preferable numbers: with the denominator of $\sqrt[20]{10} \approx 1.12$ (R 20) for supplementary sizes and selection of each third number from row numbers for principal sizes (R 20/3 ≈ 1.4).

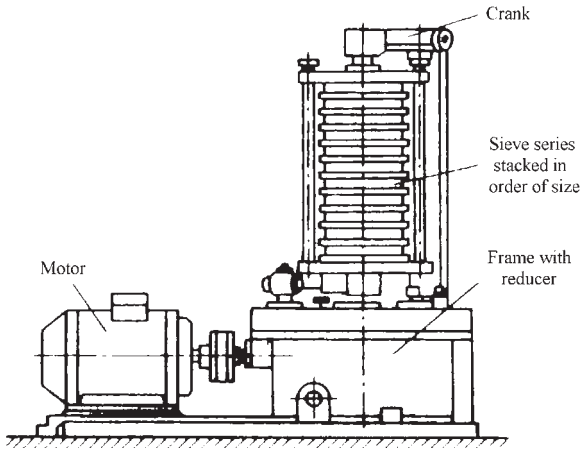

Figure 1.6 Sieving classifier.

The process for carrying out the sieve analysis of metal powders is laid down in ISO 4497. Analogous standards are used in North America (ASTM Standard B 214), in CIS (GOST 18318–94) and in the USA (MPIF Standard 05).

The main sieving problems are as follows. In the case of an overloaded sieve, the weight of the oversized powder tends to wedge the near-mesh particles into the openings or near-mesh oversized particles become entrapped in the openings. If brushing fails to remove the particles, an ultrasonic wash with a wetting agent must be used to eliminate them. Typically, the irregularly shaped particles are able to pass through sieve openings in a certain orientation only. Usually vibrating and shaking are sufficient to change the orientation of particles.

Damaged sieves may have stretched and distorted the mesh openings or may be torn. A microscope should be used to examine sieves regularly. Epoxy has been used to repair small damages.

Electrostatic charges may cause fine particles adhere to each other, forming an agglomerate of particles. Fine particles also can adhere to larger particles. The use of sieving aids, such as commercial antistatic agents, may lessen the agglomeration.

Micromesh sieves have the advantage in comparison with wire cloth sieves but they are more expensive. The micromesh sieves are manufactured by photo-etching and electrodeposition techniques. This method makes it possible to produce flat sheets of electrodeposited nickel with precise square openings. This thin gauze is supported by a coarser square-etched grid of nickel-plated cupronickel. ASTM E 11-87 specification claims a maximum deviation of only $\pm 2.0\,\mu m$ for sieves ranging from 125 to 5 μm.

Irrespective of sieve types, for sieves finer than 45 μm (325 mesh) most dry sieving techniques are deficient. For these finer size sieves, a jet type siever can

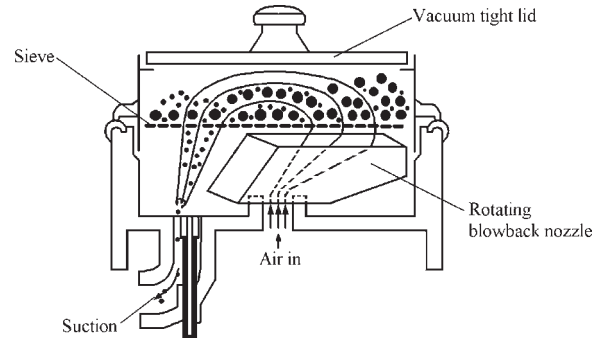

Figure 1.7 Micromesh jet sieve.

be used, such as the Alpine production (Figure 1.7). This device uses an exhaust coupled with a rotating blowback nozzle. Fine particles are suctioned through the mesh, while the blowback nozzle redistributes the powder sample on the sieve, thus disintegrating agglomerates and purging the mesh openings. The sieving operation is rapid and permits sieving down to 10 μm.

Sieves are installed consistently; sieves with the larger apertures are placed above. A set of sieves is placed on a vibrating table. The top sieve is filled with a powder shot of 100–300 g. Sieving is carried out for 15–20 min, then the residue on each sieve is weighed and the percentage of this fraction is determined. More information on analysis procedures can be found in the ASTM edition [3].

In Table 1.8 a list of the devices for determination of the granulometric structure of metal powders is given.

Sedimentation Methods

Sedimentation methods are based on the classifying of metal powders depending on the settling rate under gravity of particles situated in a fluid. This determination is based on Stokes's law of fluid dynamics by laminar current. That states that the frictional force, F_r on a spherical particle moving through a fluid at constant velocity is proportional to the product of constant velocity, the fluid velocity, ν, the fluid viscosity η and the radius of the sphere, *r*:

$$F_r = -6\pi\eta r\nu \tag{2}$$

Measuring this velocity, ν_{st}, it is possible, with the help of Stokes' equation, to determine the radius, *r*, of settling particles:

$$r = \sqrt{\frac{9\eta\nu_{st}}{2g(\rho_s - \rho_f)}} \tag{3}$$

Table 1.2 Standard sieve series

ISO 565 and 3310/1		DIN 4178	ASTM E 11	CIS GOST 3584	British Standard	
Principal sizes (R 20/3)	Supplementary sizes (R 20)				Sieve designation	
μm	μm	μm	μm	mm	μm	mesh
1000[a]	1000[a]	1000[a]	1000[a]	1.00	1000	16
	900	900				
	800	800	850	0.80	850	18
710	710	710	710		710	22
	630	630		0.63		
	560	560	600		600	25
500	500	500	500	0.50	500	30
	450	450				
	400	400	425	0.40	425	36
355	355	355	355		355	44
	315	315		0.315		
	280	280	300		300	52
250	250	250	250	0.250	250	60
	224	224				
	200	200	212	0.200	212	70
180	180	180	180		180	85
	160	160		0.160		
	140	140	150		150	100
125	125	125	125	0.125	125	120
	112	112				
	100	100	106	0.100		
90	90	90	90	0.090	90	170
	80	80		0.080		
	71	71	75	0.071	75	200
63	63	63	63	0.063	63	240
	56			0.056		
	50	50	53	0.050	53	300
45	45	45	45	0.045	45	350
	40	40		0.040		
	36	36	38		38	400
	32	32	32			
	28	28				
	25	25	25			
	22	22				
	20	20				

[a]The beginning of sieve series is 125 mm. The range up to 1000 μm is not presented here.

where ρ_s is solid density, ρ_f is fluid density and g is gravitational acceleration.

To ensure accurate results, convection currents must be eliminated in the suspending fluid and the relative rate of motion between the fluid and powder particles must be slow enough to guarantee laminar flow. Usually this technique is used for the subsieve size range. These methods are applicable for sedimentation in air with limitation to particles larger 5 μm and, in liquids, particle sizes down to 0.1 μm can be determined. As particles size decreases, this method becomes unreliable because of the Brownian motion of the particles. The upper limit is 100 μm. Particles of more than 100 μm cause the display of medium inertia forces, which are not taken into account by Stokes' equation. The method is not suitable if particle shape strongly differs from spherical, for powders which cannot be dispersed or for agglomerated powders.

The suspension must be dilute enough to ensure independent motion to the maximum particle concentration even to 1 vol% of particles in the suspension. Compositions of dispersion liquids used for sedimentation analysis are given in Table 1.3.

Table 1.3 Liquids for preparation of suspensions

Powder	Liquid for suspension	Dispersion stabilizer
Aluminum	Water with pH value amount 3–4; Cy, Cye, Isopropanole, and Vegetable oil	ST of 0.1 wt%; Sfa OII-7 of 0.075 g/L
Boron carbide	WD; Butanol/ethanol	SP of 0.5 g/L
Bronze	Cy, Cye	SP of 0.5 g/L
Chromium	WD, Butanol, Kerosene	SPP of 0.001–0.002 mole/L
Cobalt	EA, n-Butanol, Isobutane	SP of 0.5 g/L
Copper	WD, Ethanol, Acetone, Cyl, n-Butanol, Isoamyl, EA, Water/glycerin in ratio 1:1	SP of 0.5 g/L
Lead	Cy, Cye, Acetone, n-Butanol	SP of 0.5 g/L
Magnesium	EA, n-Butanol	SP of 0.5 g/L
Manganese	Cye, Isobutanole	SP of 0.5 g/L
Molybdenum	EA, Acetone, WD, Water/glycerin, Water/glycol	Sodium hexametaphosphate of 0.1 g/L
Nickel	Water/glycerin, EA, n-Butanol/acetone, Cye	Alkyl polysulphonate of 0.1 g/L
Silver	Water/glycerin, EA	. . .
Tantalum	Cy, Cye	. . .
Tin	WD, n Butanol, Isobutanole	Alkyl sulphonate of 0.1 g/L
Titanium	WD, Cye	SSP of 0.5 g/L
Tungsten	WD, Water/glycerin, Ethanol, n-Butanol	Alkyl polysulphonate of 0.1 g/L Sodium hexamethophosphate of 0.1 g/L
Tungsten carbide	Water/glycerin WD	Sodium polyphosphate Alkyl polysulphonate
Zinc	Kerosene, EA, Cy, Butanol	. . .
Zirconium	Isobutanole, Methanol	Hydrochloric acid 0.01 g/L

Abbreviations: WD: water distillate; Cy: cyclohexanol; Cye: cyclohexanone; EA: ethyl alcohol; NS: naphtha soap; SC: sodium carbonate; Sfa: surfactant; SPP: sodium pyrophosfate ($Na_4P_2O_7$•$10H_2O$); SP: sodium phosphate (Na_3PO_4); ST: sodium tartrate

Among the number of sedimentation methods available, only a few are usually used for metal powders. Devices based on the method of accumulation of the deposition from the suspension that were popular in former times find an application at present too. Turbidimetry methods are widely used to determine the particle size distribution of refractory metal powders, such as tungsten and molybdenum. The micromerographs find a use to determine the particle size of subsieve metal powders.

Accumulation of the Sediment

The method of accumulating the deposit from a suspension consists of calculating the cumulative weight of powder settled from the fixed high suspension column h as a function of time. Construction of a curve of distribution function is shown in Figure 1.8. In the initial period, the increment sediment mass m is a linear function of the time τ.

$$m = k\tau$$

where k is the proportion coefficient or corner line coefficient (tangent of corner α_1, see Figure 1.8).

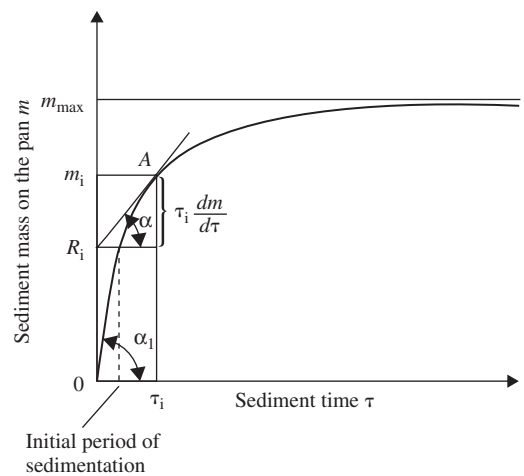

Figure 1.8 Construction of a curve of distribution function.

On completion of the initial period, the increment sediment mass on the pan starts to diminish, since all particles of the largest size have by then settled from the suspension. The increment sediment mass on the pan will continue to slow down as the sedimentation

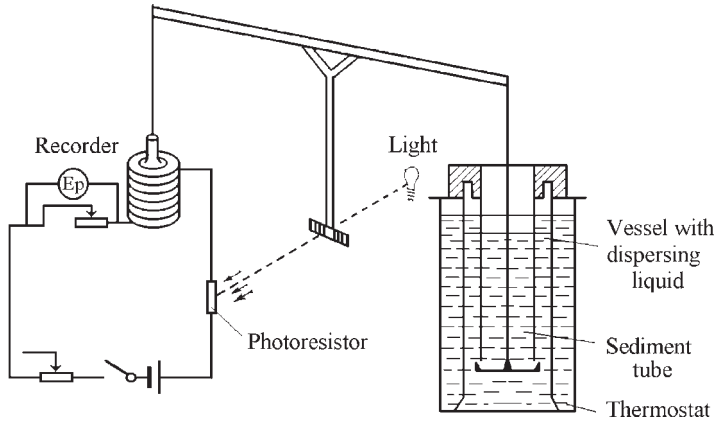

Figure 1.9 Liquid sedimentograph.

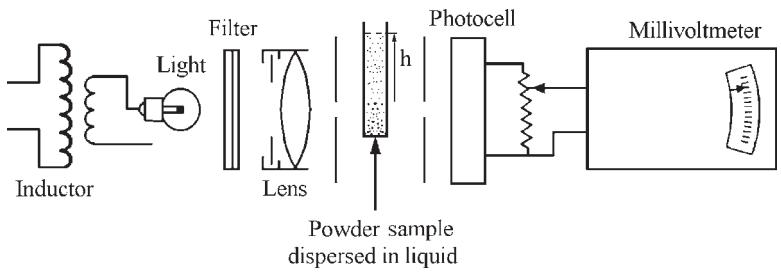

Figure 1.10 Schematic diagram of light turbidimeter.

of the particles of fixed sizes is completed. The function of sediment accumulation $m = f(\tau)$ in this period is graphically described by a smooth curve asymptotically approaching the straight line; m_{max} represents the maximum of mass sediment that can accumulate on the pan. The increment rate of the sediment $dm/d\tau$ constitutes the angle of slope of the tangent to the curve of sediment accumulation at the point corresponding to the time τ.

Since the sediment mass on the pan at the time τ_i (see Figure 1.8) is depicted by the segment projection on the ordinate line $A\tau_i$ (of the length $0m_i$) the tangent traced to this point of the curve divides this projection into two parts: a segment m_iR_i equal to τ_i $(dm/d\tau)$ that represents the mass of particles for which the settling rate is not higher than h/τ_i, and a segment $0R_i$, that constitutes the mass of particles for which the settling rate is not lower than h/τ_i, and therefore completely settled from the suspension in the column h at time τ_i. Accordingly, the ratio of $0R_i$ to $0m_{max}$ represents the fraction of particles, which have completely settled from the suspension.

Figure 1.9 shows a schematic diagram of a typical device based on the method of accumulation of the sediment from a suspension.

One serious disadvantage of the gravitational sedimentation techniques is the excessively long precipitation time for particles smaller than 5 µm. The centrifuging process can greatly accelerate the rate of settling [1].

Micromerographs

The micromerograph method consists of the accumulation of the sediment from the air of a suspended powder. A typical micromerograph includes a sediment chamber in the form of a vertical aluminum tube with an inside diameter of 10 cm and a height of 2.5 m. The pan, located at the bottom of the chamber, receives the sediment weight. Particle size distribution, being the first derivative of the function of sediment accumulation, is calculated on the basis of the obtained function $m = f(\tau)$ (see Figure 1.8) and Eqn 3. This device allows the determination of particle size distribution over the range 2 to 100 µm.

Turbidimetry

The turbidimeter is standardized in ASTM B 430. Figure 1.10 shows a schematic diagram of a typical

light turbidimeter. A sample of powder dispersed in a liquid is filled into a glass cell. A collimated beam of light passes through the cell at a level of a certain height of the vertical suspension column, h. The intensity of the light beam is determined by the current generated in a photocell and is measured by a recording millivoltmeter. The determination of the particle size distribution is based on the effect of attenuation of the light beam intensity proportionally to the projected area of the suspended particles, and consequently proportional to the square of particle diameter. As the suspension settles, the projected area of the particles in the suspension decreases, and the intensity of the light beam increases.

The information obtained consists of the residual weight of suspended powder and, accordingly, the sediment accumulation after a given time, τ_x, allows us to calculate the particle size distribution on the base of the function $m = f(\tau)$ (see Figure 1.8) and Eqn 3. The particle sizes are presented here by their projected diameters (diameter of a circle equivalent to a particle projected area).

When X-rays are used to determine particle size distribution of a particle suspension, the attenuation of the X-ray beam intensity is proportional to the mass of the powder particles in contrast to their projected area in white light.

Method of weight samples

This method of particle size measurement, known as the pipette method, is based on Stokes's law. The pipette method consists of taking consecutive suspension samples of a certain volume from a given depth, h, at time, τ_i. The powder weight in suspension samples is determined after evaporation. Thus, in the pipette method, as in turbidimetry, the residual weight of the suspended powder at the fixed time is defined and, on the base of the function $R = f(\tau)$ and Eqn 3, the particle size distribution is calculated. However, in the pipette method, the residual weight of the suspended powder is defined directly in contrast to turbidimetry where an indirect method for its measurement is used. Figure 1.11 shows a schematic diagram of typical pipette devices. In practice, for the determination of particle size distribution, the Andreasen's pipette is still used.

Light Scattering

Light scattering measurements are based on the Mie theory [1]. Figure 1.12 represents schematically the principle of light laser scattering. Light scattering intensity obtained from Mie theory is described by the following equation:

$$K(\theta, m, D) = \frac{\lambda^2}{8\pi^2 R^2}[i(\theta, m) + i(\theta, m, D)] \quad (4)$$

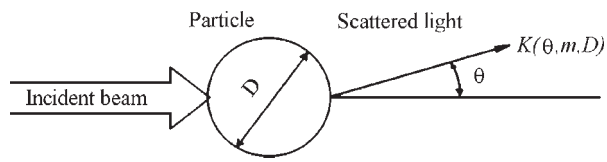

Figure 1.12 Laser scattering principle.

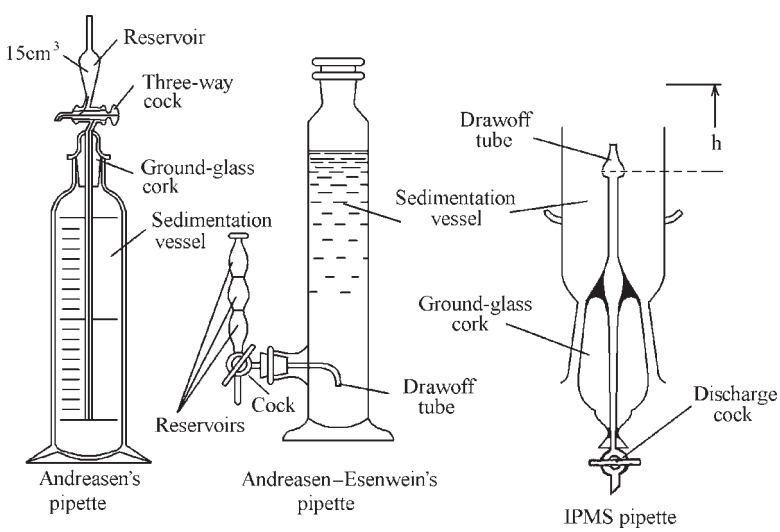

Figure 1.11 Pipette devices.

where $\pi D/\lambda$ is the size parameter, D is the particle diameter, λ is the incident light wavelength, R is the radial distance, $m = \mu_1/\mu_2$, μ_1 is the refractive index of the particle, μ_2 is the refractive index of the dispersing medium. The parameters λ and R are defined by the design of the instrument and are constant. Refractive indices (μ_1 and μ_2) in many cases are found in standard reference literature. In rare cases of newly developed materials or mixed dispersed systems, these values can be determined experimentally.

The complexity of exact solving of the Mie problem on the diffraction of electro-magnetic waves on a sphere or an ellipse generated numerous methods to simplify its solving, but the accuracy of particle size measurements is lowered. Modern computers make it possible to solve the complex Mie equation (4).

The light scattering method is capable of providing particle size analysis in a broad range of particle sizes. This technique ensures a rapid determination of the sought parameters, and is easy.

A typical recent device for laser light scattering measurement consists of a light source, particle dispersion and delivery systems, a detector to measure the light scattering by the specimen and a computer to control the system and to define the particle size distribution. Previous versions of laser particle analyzers were only capable of measuring the scattering pattern at small angles, lower than 20°, and were limited to measuring particles coarser than 1.0 μm. Modern instruments collect scattering data at larger angles. This allows accurate measuring of particles of 1.0 μm down to 0.1 μm in size. Particles in a parallel laser beam deflect the light at a fixed angle that depends on the particle diameter. A lens focuses the scattered light in a ring on the sensor that is mounted in the focal plane of the lens, whereas undiffracted light converges at the focal point on the optical axis. A certain scattering angle is allocated to each individual particle size. The energy distribution measured in the sensor elements that are arranged radially and symmetrically is evaluated, and the particle size distribution is calculated.

The major difficulty in accurate, reproducible particle size measuring is the dispersion. In previous instruments, the analyzer usually did not envisage this need. It was accepted that the dispersion would be performed external to the instrument particle analyzers. This, however, did not provide the stable dispersion and was not handy.

The recent instruments, such as for example, laser particle sizer 'Analysette 22' (produced by Fritsch company), are supplied with liquid and dry dispersing units. These two analyses give comparable results. For the liquid process, a mixture of liquids for suspension preparation is selected as for sedimentation analyses depending on the powder material composition (see Table 1.3). Usually, an integrated ultrasonic bath is used for the dispersion. The amount of sample required is approximately 0.2–1.0 g. The dispersing unit for dry samples processes the agglomerates by means of mechanical forces. A vibratory feeder meters the amount of sample supplied. Dispersion occurs in a two-phase annular gap nozzle due to cooling fins causing waves at the nozzle outlet with a high flow rate.

The popular tendency has been to incorporate a centrifugal pumping system. This type of pump provides sufficient power to pump particles of down to 2.0 mm in size around the system in a uniform condition. In this system, the ultrasonic probe is placed directly into the stream of the flowing liquid. The rapid flow rate and its position immediately in front of the cell where the laser beam is focused makes it possible to analyze even strongly agglomerating samples. These accessories have extended the range of samples that these instruments can analyze. Similar systems are incorporated into all newer devices.

There is also another tendency consisting of total removal of the pumping module from the system. This option is viable only for smaller particles; larger particles tend to become sediment below the laser beam. This approach is useful for analyzing particles in obnoxious fluids. It minimizes the use of the solvent and simplifies moving the sample.

The popularity in the last 10–15 years of laser light scattering as a method of particle size analysis has led to the development of new capabilities. The analysis has been automated and the reproducibility and the repeatability have been improved.

Surface and Bulk Characterization of Powders

Particle Image Analysis

Particle image analysis includes measurement of particle size, particle shape characterization, morphological analysis and surface chemistry analysis. Light microscopy is a very precise method of particle image analysis and allows us to observe and to measure individual particles. But some of the analyzing techniques used are more art than measurements. At the same time, the basic principles of sampling, preparation and measurement permit a precise count to be made with the thorough conception of the essence of the observable particles. Details of using optical microscopy for particle sizing are included

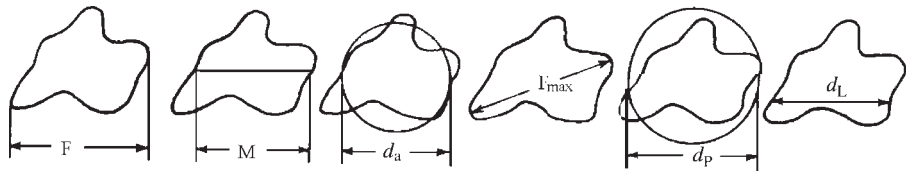

Figure 1.13 Measuring of irregular particles.

in ASTM standard E 20 and the Commonwealth of Independent States (CIS) standard GOST 25846 (see Appendix 1).

Size Measurements

These measurements consist of the determination of particle sizes, which are used to classify the two-dimensional particle images in terms of an equivalent spherical particle. Accepted particle measurements shown in Figure 1.13 include:

- d_F, the maximum length of the particle measured in a fixed position (called also Feret's diameter, *F*)
- d_M, the length of the line that bisects the area of the particle image, all particles being measured in the same direction (called Martin's diameter, *M*)
- d_a (project area diameter), the diameter of a circle with the same area as the two-dimensional image of the particle
- $d_{F\,max}$ (the longest diameter), maximum diameter of each particle, no set direction
- d_p (perimeter diameter), the diameter of a circle having the same circumference as the perimeter of the particle
- d_L (maximum horizontal intercept), the length of the longest line that can be drawn through the particle in a fixed direction.

The easiest for manual measuring is the diameter d_F. The average Feret's diameter, F_{av} is related to the perimeter of the convex hull of the particle P_{CH} and calculated by:

$$F_{av} = \frac{P_{CH}}{\pi}$$

Martin's diameter is related to the specific surface S_p of the particle by:

$$M = \frac{4}{S_p}$$

The first three diameters are related to one another by the expression $d_M < d_a < d_F$. The ratio d_F/d_M is used as a shape function, which is equal to 1.0 for spherical particles and increases in magnitude as particle shape becomes more irregular. The projected area diameter, d_a, gives the best evaluation of the accurate cross-sectional area of the particle.

The sampling techniques are described at the beginning of this chapter.

Particle Shape

Photomicrographs of several types of loose powders described in the International Standards Organization standard ISO 3252 (see Appendix 1) are shown in Figure I.2 in the Introduction to this book.

The British Standards Institute has prepared a standard glossary of terms for use in the description of the appearance of powder grains (British Standards 2955 Glossary of Terms Relating to Powders):

- *Acicular*: needle-shaped
- *Angular*: sharp-edged or roughly polyhedral shaped. (Polyhedral derives from poly, meaning many: therefore, polyhedral is understood to be a geometric shape having many faces, each of which can act as a base.)
- *Crystalline*: a geometric shape freely developed in liquid
- *Dendritic*: a branched crystalline shape
- *Fibrous*: regularly or irregularly threadlike
- *Flaky*: no normal definition in the British Standards. (It is assumed that a flaky fine particle is recognizable.)
- *Lamellar*: plate-like
- *Granular*: approximately equidimensional but irregularly shaped
- *Irregular*: lacking any symmetry
- *Modular*: rounded, irregularly shaped
- *Spherical*: globular shaped

Various shape terms have been proposed quantitatively to represent particle shape. Early systems tended to measure one specific feature of a particle.

There are known conventional shape factors [1], including the three ratios: elongation factor (x), bulkiness factor (y) and surface factor (z).

A rectangle of minimum area is drawn around the cross-section of a particle (particle projection). The ratio of the rectangle side length permits calculation of a particle's elongation factor:

$$x = \frac{a}{b}$$

where a and b are side lengths of rectangle.

The ratio of the area (A) of the projected particle to the area of the enveloping rectangle of minimum area ($a \times b$) indicates the bulkiness factor of the particle:

$$y = \frac{A}{a \times b}$$

Thus, the cross-sectional area of the particle is correlated with some of its linear dimensions.

To characterize the surface configuration by surface factor, which is an essential factor of shape, the surface of the respective particle should be compared with the surface of a sphere of equivalent volume or a cross-section should be compared with that of the particle:

$$z = \frac{c^2}{12.6A}$$

where c is the perimeter of the projection profile of the particles. For a spherical particle, $z = 1$, and for particles of other shape, $z > 1$.

Although the three ratios (x, y and z) do not permit exact characterization of particle shape, they are nevertheless descriptive.

Optical Microscopy

Optical microscopy allows the counting and sizing of particles from 100 to 0.5 μm in size. The depth of field of an optical microscope is about 10 μm at 100 and 0.5 μm at 1000 magnification. This requires the specimen powders to be placed in one plane and eliminates the wide particle size range by using automatic counting devices. Another limitation is that owing to the small number of particles usually counted, only the field of view can be characterized, not the representative lot from which the specimen was obtained.

Preparation techniques of slides for optical microscopy depend on the type of powder, particle size, particle size range and particle composition.

When a permanent slide is not required, and the powder develops good flow characteristics, slides can be prepared by applying dry powder onto the slide with a brush.

In conditions that require action to disperse the powder, a dispersing fluid can be used. The simplest technique involves placing a drop of the dispersing fluid on a glass slide and placing a small amount of powder onto the drop. This sample is then fixed by cover slip.

Obtaining permanent slides consists of preparation of thin films that can be produced by dissolving parlodion in amyl acetate, Canada balsam in xylene and polystyrene in xylene. Films are formed from a 0.5% solution directly on the glass slide. After the films dry, the powder is applied by spraying on the surface. The particles sink into the medium, forming a permanent slide.

A filar micrometer eyepiece is used for direct measuring of particle diameters in an optical microscope. This eyepiece contains a dial and a movable cross hair that is operated by a calibrated knob. During measuring, a particle is moved so that one side touches one of the fixed mesh markings, while the cross hair is moved to touch the other side of the particle. The difference between the two readings is the particle diameter, d_F, i.e. the maximum length of the particle measured in a fixed position, known also as the Feret's diameter [1]. This is a time-consuming technique. Eyepiece graticules are usually used to shorten the time required for particle size measurement.

A typical example of eyepiece graticules is given in British Standard 3406 (Figure 1.14) showing seven circles in a root-2 progression of sizes and five different geometric areas. A similar eyepiece graticule is used in the Commonwealth of Independent States. The last presents a disk comparator with ten circles and Vigdorchik's denumerably-measuring scale with twenty geometric areas [4].

These stencils are etched on glass disks that are positioned in the back focal plane of the microscope ocular and are thus in the same focal plane as the particle images. Feret's diameter, project area diameter (d_a), or perimeter diameter (d_p) (see Figure 1.13) are measured expediently with graticules.

Data Presentation

The percentage of fractions obtained as a result of analyzing the granulometric composition is conveniently presented in the form of a step-like graph (histogram). Particle sizes are plotted (at a uniform

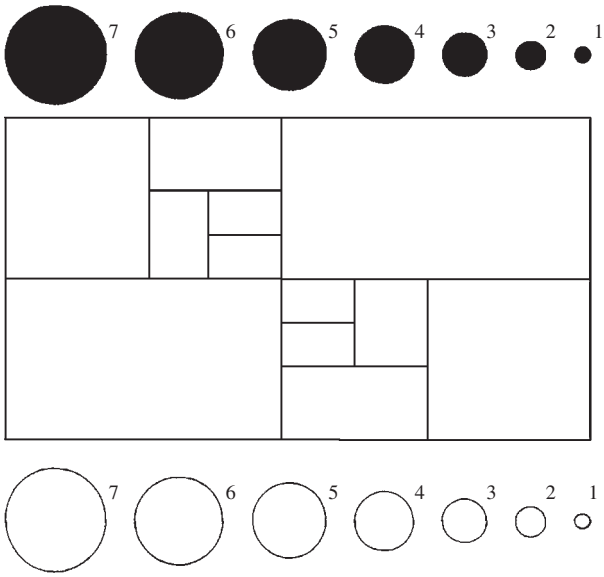

Figure 1.14 The British Standard eyepiece graticule for particle diameters measuring in optical microscope.

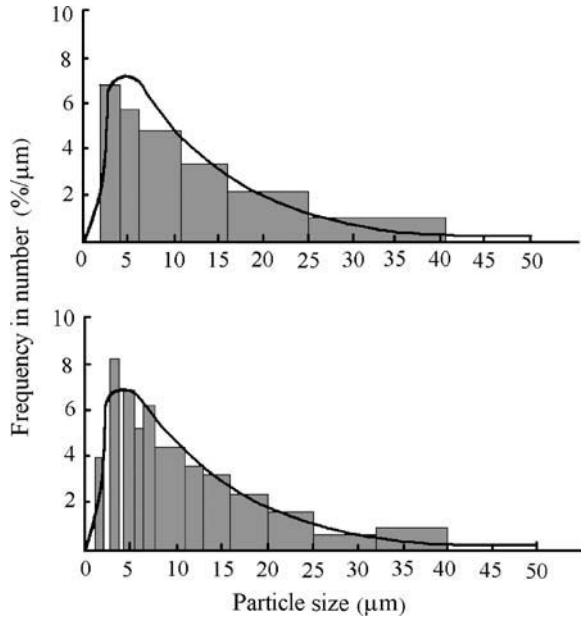

Figure 1.15 Histograms and size frequency curves of the two identical powder specimens by different particle size fraction ranges.

or non-uniform scale) as abscissas and relative fraction contents, i.e. percentages of each fraction, as ordinates.

In constructing the diagrams, it should be borne in mind that the ranges of separate fractions are usually taken to be non-equal. It is caused by technical conditions of analyzing as well as by the fact that, for a complete powder characteristic, the range of fractions should be increased with particle size increase. Indeed, the surface area of a particle of 1 μm in diameter is 4 times lower than the surface area of a particle of 2 μm in diameter, whereas for particles of 10 and 11 μm in diameter the difference in their surface areas is only 20%, and for particles of 100 and 101 μm in diameter it is as small as 2%. As powder properties significantly depend on their surface area, in the ranges coarser than 10 μm, a difference of 1–2 μm has a very small effect on particle properties and the separation into such small ranges is in this case non-expedient. Therefore, an increase of fraction ranges in geometric series with the growth of particle size seems to be justified.

In practice, the ranges of separate fractions are usually taken to be non-equal without a strict adherence to this condition. As a consequence, while constructing the histograms of weight distribution throughout particle sizes, the relative contents of fractions plotted on the ordinate are counted by dividing the weight percentage of each fraction by its range (difference in the limiting sizes in the fraction). The histogram gives a vivid presentation of powder disperse composition and the correctness of the presentation increases with narrowing the range limits. In Figure 1.15, the influence of the sizes of fraction range on the form of histograms is seen.

Metallographic Microscope

The requirement for the metallographic optical microscopes used for analyzing powders is that they form the image by a transmission principle. The powder sample is placed on a glass plate, each particle lying separately. Modern microscopes are equipped with digital photo-cameras and computers with a special program for powder analysis.

Techniques of Chemical Analysis for Powders

Chemical analysis of powders is carried out for quantitative and qualitative information. This is a complicated process with difficulties that can arise in the selection of the appropriate instrument and the correct interpretation of the results. The chart in Figure 1.16 can be used for the selection of the appropriate analytical technique.

Atomic absorption spectroscopy (AAS), atomic emission spectrometry (AES) and inductively coupled

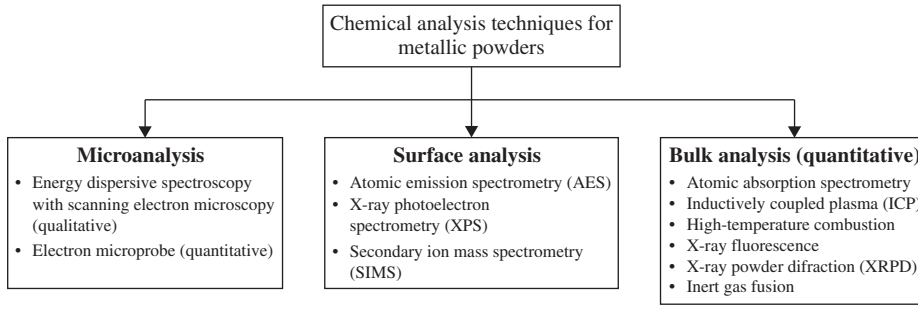

Figure 1.16 Chemical analysis techniques for metallic powders.

plasma optical emission spectroscopy (ICP-OES) are widely employed for chemical analysis of metal powders. AAS can detect the element content in parts per billion (ppb), but analyzes one element at a time. ICP-OES has a lower resolution, typically of 0.2–0.5 wt% for dissolved elements; however, the analysis ensures quantitative data for twenty or more elements simultaneously.

X-ray fluorescence allows the same broad element determination as ICP-OES; however, the material can be analyzed in the bulk solid condition. For trace analyses, this method has a lower resolution limit of approximately 100 ppm. The scanning electron microscopy (SEM) equipped with an energy dispersive spectroscopy (EDS) system can ensure a qualitative analysis of a metal particle. The microprobe analysis is regarded as microchemical analysis because of the small sample volume used to obtain the data.

Auger electron spectroscopy (AES), ion-scattering spectroscopy and X-ray photoelectron spectroscopy (XPS) can be used. The last is also known as electron spectroscopy for chemical analysis. Higher sensitivities are achievable by the use of the secondary ion mass spectrometry (SIMS). Microanalysis is also done with some SIMS techniques that can be used to measure composition and trace impurity levels as a function of depth, ensuring a detection limit in the ppb to ppm range for many elements.

X-ray diffraction analysis is one of the few methods that are available for a quantitative determination of the amount of phases existing in a powder sample. It should be remembered that the sensitivity of the X-ray diffraction technique in revealing the phase strongly depends on phase chemical composition and lattice type and is, in general, of about 3–5 vol%. X-ray diffractometers are widely used for this purpose, though the photographic technique can have a better sensitivity. The sensitivity can be strongly increased by using synchrotron radiation.

To obtain specific information for a particular phase in the powder (size and shape of phase particles, crystallographic orientation etc.) as well as to detect phases existing in a small amount, the transmission electron microscopy should be employed. Thin foils of about 0.2 μm in thickness are obtained from individual particles by microtome technique, most often with a fine diamond cutter [5]. In general, some defects are introduced into the foil in the cutting process, but for phase analysis it is quite suitable.

Scanning Electron Microscopy (SEM)

As a device for examining particle surfaces, the scanning electron microscope provides the following general possibilities: imaging of surface features is from 10 to 100 000×; resolution of features is from 3 to 100 nm depending on the sample; when equipped with a backscattered detector, this microscope allows us to observe grain boundaries on unetched surfaces; evaluation of the crystallographic orientations of grains down to 2–10 μm in size; and imaging of second phases on unetched surfaces when the second phase has a different average atomic number. This allows us to evaluate individual grains, precipitated phases and dendrites; to identify the chemistry of features down to micron sizes on the particle surface; to evaluate chemical composition gradients on the surface over distances approaching 1 μm.

Electron probe X-ray microanalysis provides qualitative and quantitative analysis of elements with atomic number of 11 (sodium) and greater with detection limits of approximately 1 μm, qualitative elemental analysis for light elements with atomic number from 5 (boron) to 10 (neon), and elemental compositional mapping of areas with dimensions as large as millimeters with spatial resolution to 1 μm. These capabilities are used for compositional analysis of individual phases at microstructural level in multiphase samples, analysis of compositional gradients close to boundaries, and compositional mapping of

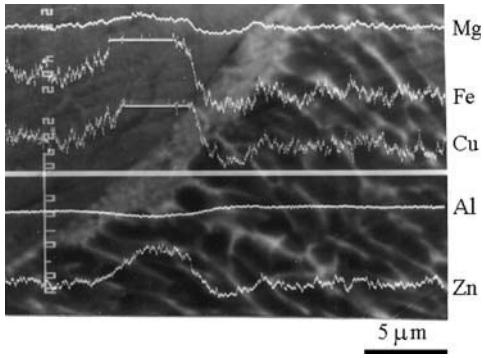

Figure 1.17 Scanning electron micrograph of the polished sample of Al-9.0Zn-3.0Mg-1.2Cu-1.0Fe alloy with elemental distribution along the secant line.

specimens to produce maps of element location and concentration.

Figure 1.17 illustrates an example of electron probe X-ray microanalysis for the analysis of element gradients at grain boundaries, in particle section along the secant line.

Auger Electron Spectroscopy

In Auger electron spectroscopy (AES), Auger electrons are produced whenever incident radiation (electrons, ions, photons or neutral atoms) interacts with an atom with an energy exceeding that necessary to remove an inner-shell electron (K, L, M,) from the atom. This scattering process leaves the atom in an excited state with a core hole, that is, a missing inner-shell electron.

In AES, the powder sample to be analyzed is bombarded with electrons. When an incident electron strikes a K-shell (core-level) electron with sufficient energy to free it, the atom is left in a singly ionized state with a core-level electron vacancy. If the atom is near the surface, both the incident electron and the core-level electron are emitted from the sample as backscattered electrons, with energies below approximately 25 eV.

These knockout results occur within to 3 nm depth under the surface that permits compositional analysis of the surface for all elements except hydrogen and helium. Auger analysis has some advantages for the analysis of light elements because the probability for Auger emission exceeds that for X-ray emission as atomic number decreases.

AES instrumentation typically includes an electron gun for primary electron excitation of the sample, an electron spectrometer for energy analysis of secondary electrons, a secondary electron detector for secondary electron imaging, a stage for sample manipulation and an ion gun for sputter removal of atoms from the sample surface. Depth-profiling analysis versus sputter is simultaneous or sequential.

Detection sensitivity for most elements (except hydrogen and helium) is from 0.1 to 1.0 at%. The accuracy of quantitative analysis is limited to ±30% of the element present when calculated using published elemental sensitivity factors. Better quantification (±10%) is possible by using standards that closely resemble the sample. Samples can be solid materials with relatively low vapor pressures at room temperature ($<10^{-8}$ torr). Higher vapor pressure materials can be handled by sample cooling or by applying a thin film onto a conductive substrate. Sample size can be individual powder particles as small as 1 μm in diameter. The maximum sample size depends on the specific device.

Secondary Ion Mass Spectrometry (SIMS) Analysis

The principle of SIMS consists of ion bombardment directed at the sample surface in a high or ultrahigh vacuum environment. The transfer of momentum from the impinging primary ions to the sample surface effects the sputtering of surface atoms and molecules. Some of the sputtering corpuscles are ejected with positive or negative charges that are termed secondary ions. These are then mass-analyzed using a double-focusing mass spectrometer or an energy filtered quadrupole mass spectrometer.

The method allows us to get a variety of information about the surface, subsurface or bulk composition of the sample. If the rate of sputtering is high, the intensity of peaks in the mass spectrum can be continuously recorded to provide an in-depth concentration profile of the near-surface region. At very high sputtering rates, trace element or impurity analysis in the bulk is possible.

Figure 1.18 illustrates an example of SIMS together with X-ray photoelectron spectroscopy (XPS) analysis of element depth distribution on particle surfaces. An O_2^+ primary beam was used to record positive secondary ions, while both O_2^+ and C^+ primary beams were used for analysis of negative secondary ions. The powder surface was scanned ranging from $35 \times 35\,\mu m^2$ to $50 \times 50\,\mu m^2$ with focused oxygen or cesium ion beams over an area. The spot size of the primary ion beam was approximately 3 μm. A mass resolution of $m/\Delta m = 300$ was used for all measurements.

Typical profiles of some elements are shown in Figure 1.18. Only Mg exhibits a pronounced enrichment of subsurface layers. Both Zn and Cu are distributed more or less homogeneously with some deviations from an ideal plane profile. Main metallic

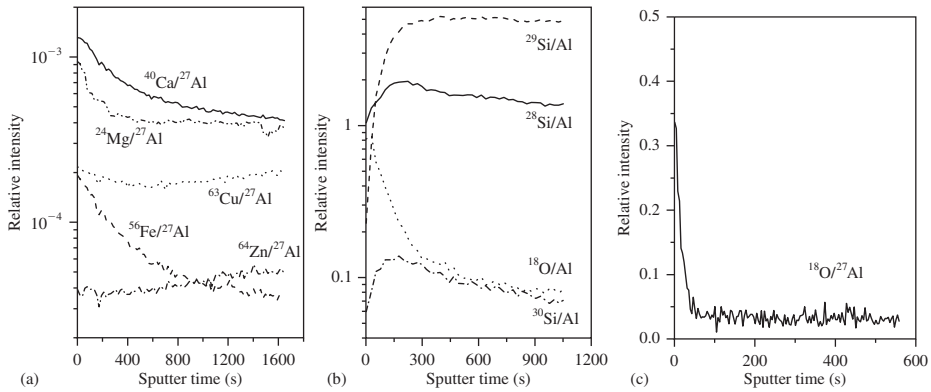

Figure 1.18 Typical depth profiles for: (a) Mg, Ca, Cu, Zn and Fe ions normalizsed to Al (primary O_2^+ and secondary positive ions); (b) Si and ^{18}O ions normalized to Al (primary Cs^+ and secondary negative ions); (c) $^{18}O/^{27}Al$ (primary O_2^+ and secondary negative ions).

impurities, Fe and Ca, are typically enriched in the subsurface as is seen from Figure 1.18a. The average thickness of the surface oxide film as well as the widths of the observed Mg, Fe and Ca segregation zones are estimated on the basis of the available depth profiles and respective ion sputter rate data. These thicknesses are taken to be proportional to the sputtering times required for a 50% drop in the element profiles [6, 7]. The average thickness of the surface oxide usually varies from 4 to 10 nm.The widths of Mg, Ca and Fe enrichment layers range between 30 and 70 nm.

Although a useful method of operation, it is not yet a routine analytical technique. More information on AES and SIMS methods can be found in http://www.cea.com/tutorial.htm.

Bulk Analysis

Many methods are available to determine the chemical composition of powders. A brief description of methods used in powder analysis is summarized below.

X-Ray Powder Diffraction (XRPD)

This technique allows us to make various investigations, including qualitative and quantitative phase identification and analysis, determination of crystallinity, lattice-parameters determinations, high-temperature studies, thin film characterization and analysis of crystal structure.

On the whole, an XRPD characterization of a substance consists of placing a powder sample in a collimated monochromatic X-ray beam. In XRPD analysis, samples are usually a fine powder fraction (ordinarily less than 50 μm in size). The particles in the sample comprise one or more independently diffracting regions that coherently diffract the X-ray beam. These small crystalline regions are termed crystallites. Although larger grain sizes can sometimes be used in XRPD, the size limitation is important because most applications of powder diffraction rely on X-ray signals from a statistical sample of crystallites. The angular position, θ, of the diffracted X-ray beam depends on the spacing, d, between planes of atoms in a crystalline phase and on the X-ray wavelength, λ, in accordance with the Wulf–Bragg equation:

$$2d \sin \theta = n\lambda$$

The intensity of the diffracted beam depends on the arrangement of the atoms on these planes. For the determination of the phase amount in the sample in the case of known phases, graphs constructed on the basis of X-ray patterns of standard mixtures can be used. A diffraction pattern can be recorded using film, analog or digital methods. Many modern automated powder diffractometers can provide further data reduction, including peak finding, a tabular listing of peak intensity versus interplanar spacing, and various computer utilities.

Phase identification using XRPD is based on the unique pattern produced by every crystalline phase. Qualitative identification of phases can be accomplished by pattern-recognition methods that include established manual techniques and the newer methods that use computers. All of these methods make use of the database maintained by the JCPDS International Centre for Diffraction Data (Joint Committee on Powder Diffraction Methods, International Centre for Diffraction Data, Swathmore, PA).

Inert Gas Fusion

This method is used to determine the quantitative content of oxygen, nitrogen and hydrogen in materials. Gases introduced into the material are quantitatively determined using inert gas fusion. Inert gas fusion reverses the physical and chemical bonding between the gases and metals to dissociate the gases and sweep them from the fusion area with an inert carrier gas. Because the gas/metal bonds are formed over a wide temperature range, bonds can be broken only by heating the sample above the highest temperature at which the gas/metal bonding occurred. Required powder sample mass is usually 2 g or less, depending on material type and the expected amount of gases present. Special precautions are required for metals with low boiling points. Materials with stabile nitrides or oxides require addition of fluxes. The method is destructive of the material.

Inductively Coupled Plasma Atomic Emission Spectroscopy (ICP-AES)

The ICP-AES is an analytical technique, based on the principles of atomic spectroscopy, for the determination of over 70 elements with detection limits in the parts per billion (ng/ml) to parts per million (μg/ml) range. In theory, the technique allows us to analyze all elements except argon. The samples can be introduced as liquids, solids or gases. In practice, favorable analytical results are obtained for approximately 70 elements, with detection limits usually reaching the ppb level, and most samples are introduced in liquid form as aqueous solutions. The inductive coupled plasma is the excitation source for atomic emission spectroscopy. Argon plasma operates at atmospheric pressure and is kept by inductive coupling to a radio frequency so that the standard frequency of operation is of 27.17 MHz or, less commonly, of 40.68 MHz (the frequencies permitted by the Federal Communication Commission for scientific and medical instrumentation [8]). The resulting plasma is a highly ionized gas with temperatures about 10 000 K. The ICP provides the capability of simultaneous multi-element analysis for as many as 60 elements in 1–2 min. The precision and accuracy are of the order of 1%.

Atomic Adsorption Spectrometry (AAS)

AAS is commonly used for the analysis of relatively low concentrations of approximately 70 metallic elements in solution samples [9].

There exist three types of AAS (Figure 1.19). Several features are common to all three techniques:

- flame atomic emission spectrometry (AES) (Figure 1.19a), where hot flame gases, to produce the desired signal, must thermally excite a significant fraction of the free atoms produced by dissociation in the atomizer from the ground-state level to one or more electronically excited states. AES usually necessitates scanning the monochromator completely over the analytical spectral line to obtain the background signal values necessary for the calculation of a correct response
- flame atomic absorption spectrometry (Figure 1.19b), where the radiation from a lamp emitting a discrete wavelength of light that has an energy corresponding to the difference in energies between the ground state and an excited state of the analyzed element is passed through the atomizer. Free analyzed atoms within the atomizer absorb source-lamp light at wavelengths within their absorption profiles. In contrast to AES, the ground-state (not excited state) atomic population is observed. The source light not absorbed in the atomizer passes through the monochromator to the light detector and the data reduction/display system of the spectrometer outputs an absorbance response directly proportional to the concentration of the analyzed atoms in the sample solution
- flame atomic fluorescence spectrometry (AFS) (Figure 1.19c) is an emission method based on an external light beam to excite analyte atoms radiatively. The absorption of light from the light source composes a higher count of excited-state atoms in the atomizer than that predicted by the Boltzmann equation at that temperature. Therefore, the absolute sizes of the atomic emission signals detected are larger than those seen in AES analysis performed with the same concentration of analyzed atoms within the atomizer. AFS has two major sources of error. The first is chemical scavenging of the non-equilibrium excited-state of the analyzed atom population before a useful light signal can be emitted. The second source of error is a scatter of the exacting radiation by particulate matter within the atomizer. For example, some refractory metals, such as zirconium and uranium, if present in high concentration in the sample, have a tendency to be incompletely dissociated or gasified in conventional atomizers.

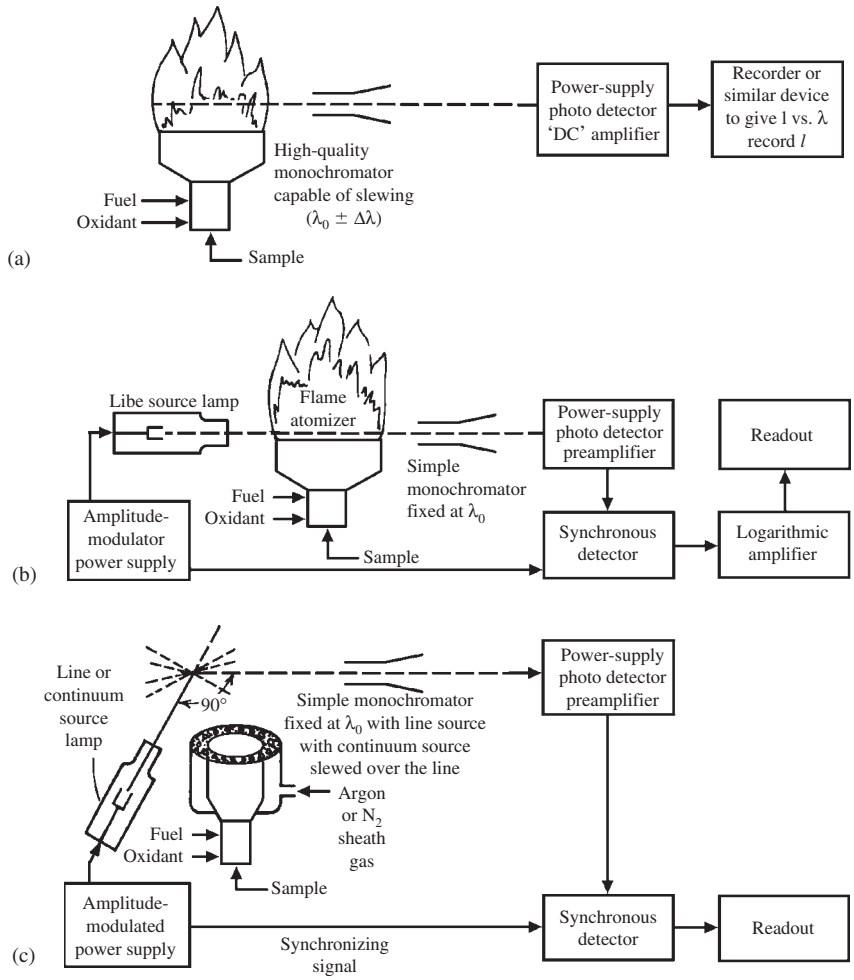

Figure 1.19 Comparison of (a) flame atomic emission spectrometry, (b) flame atomic absorption spectrometry, (c) flame atomic fluorescence spectrometry. (Source: Ref [9]®)

The sensitivity of atomic absorption spectroscopy is characterized by the magnitude of the atomic absorbance signal expected when a 1 ppm solution of the element is continuously aspirated into a flame atomizer or introduced as a discrete 25 µl aliquot into a graphite furnace.

On the whole, the AAS method has been one of the most widely used techniques of trace element analysis.

The capabilities of the contiguous techniques can be summarized as follows:

- Optical microscopy: provides superior image quality on relatively flat samples at less than 300 to 400×.
- X-ray diffraction: provides bulk crystallographic information.
- Scanning electron microscopy: minimum area for surface pictures of 4–5 nm (conventional scanning microscope), and for microchemical analysis of 1–3 µm (energy-dispersive spectrometry and/or wavelength-dispersive spectrometry).
- Scanning transmission electron microscopy: minimum area for surface pictures of 2–3 nm (SEM mode, in-lens), and for microchemical analysis of 5–30 nm (energy-dispersive spectrometry).
- Auger electron microscopy: minimum area for surface pictures of ≈100 nm (Auger), and of 10 nm (SEM mode), and for microchemical analysis of ≈100 nm (Auger), of 1–3 µm (energy-dispersive spectrometry).
- Transmission electron microscopy: provides information from within the volume of material, such as dislocation images, small angle boundary distribution, and vacancy clusters. The conventional resolution is of about 1–2 nm. A superior resolution requires very thin samples.

Determination of Oxygen Content by Reduction Methods

The methods for the determination of oxygen content by reduction in hydrogen are laid down in ISO 4491 Standard. They include: determination of loss of mass on hydrogen reduction (ISO 4491–2:1997), determination of reducible oxygen (ISO 4491–3:1997) and determination of total oxygen by reduction–extraction (ISO 4491–4:19889). Analogous standards function in the Commonwealth of Independent States (CIS): GOST 29006–91, GOST 27417–87 and GOST 18897–73 (see Appendix 1).

Standard ISO 4491–3:1997 establishes the technique for the determination of the oxygen content reduced by hydrogen in metallic powders that contain from 0.05 to 3 wt% of oxygen. This technique is applicable to powders of elemental metals and alloys. It cannot be used for powders containing a binder but can be extended over powders containing carbon by using a special catalytic device.

The principle of the process is in reducing a powder sample in the stream of pure dry hydrogen at a given temperature. The water formed by reduction is absorbed by methanol and titrated by Karl Fisher's reagent. In the case of analyzing powders containing carbon, a conversion of carbon monoxide and dioxide in methane with nickel catalyst is carried out.

The reduction is performed in an apparatus equipped with a reducing tube with closed end, or in an apparatus with a running reducing tube with open end (Figure 1.20). A weighed powder sample is from 1 to 5 g, depending on the oxygen content. The temperature and the optimum duration of the reduction are determined for each type of powder. Thus, the temperature for reducing oxides in nickel and cobalt powders is 900 ± 20°C with a duration of 20 min, and for molybdenum and tungsten oxides it is 1100 ± 20°C.

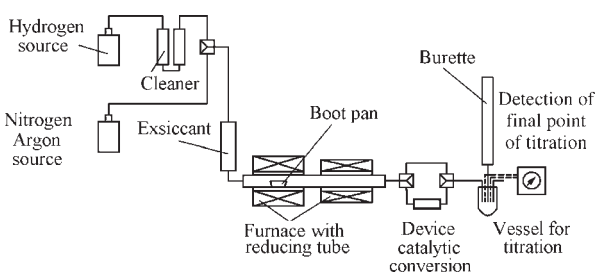

Figure 1.20 Flowchart of apparatus for oxygen content determination.

Surface Area and Porosity of Powders

The surface area in a quadratic degree, strongly depends on the powder particle size and not so strongly on their morphology and open porosity. At the same time, all these characteristics are significant factors for understanding and controlling product properties and processing behavior.

Various techniques can be used to determine these characteristics. However, the results of various test methods can differ owing to their inherent features. Mainly, the following methods to determine powder surface area, porosity and density are used: gas adsorption method, permeametry, pycnometry and mercury porosimetry.

Gas Adsorption

The gas adsorption technique is based on the Brunauer–Emmet–Teller (BET) model included in the determination of the amount of the gas that is adsorbed on the surface of the sample at low temperatures [10]. The specific surface area (m^2/g) defined by this method comprises the outward as well as the internal (open pores) surface area. However, the surface area of closed pores cannot be determined because of its inaccessibility for adsorbing gas molecules.

Brunauer, Emmett and Teller extended Langmuir's kinetic monolayer physical adsorption theory (1916) to a multilayer adsorption theory (1938). For convenience of a chart creation, the BET relationship is entered in the following form:

$$\frac{P}{V(P_0 - P)} = \frac{1}{V_m C} + \frac{C-1}{V_m C}\frac{P}{P_0} \tag{5}$$

The BET relationship is significantly complicated in the case when the number of adsorbed layers is limited:

$$\frac{V}{V_m} = \frac{C(P/P_0)}{1 - P/P_0}\,\frac{1-(n+1)(P/P_0)^n + n(P/P_0)^{n+1}}{1+(C-1)(P/P_0) - C(P/P_0)^{n+1}} \tag{6}$$

where V_m is the monolayer capacity; in the actual experiment, the adsorbed amount of gas, V, is measured as a function of gas pressure, P; P_0 is the saturation pressure of the liquefied gas at the corresponding temperature of the adsorption measurement; P/P_0 is often referred to as the relative pressure; the

parameters C and n are parts of the BET conception. The parameter C is:

$$C \approx \exp\left\{\frac{q_1 - q_c}{RT}\right\} \tag{7}$$

where the parameters q, R and T are the heat of adsorption, gas constant and temperature, respectively.

Due to the complexity of Eqn (6), it is seldom used in practice. Calculations are simplified by graphical construction. A diagram of $P/[V(P_0 - P)]$ dependence on P/P_0 in accordance with Eqn (5) generally gives a straight line in the range of $P/P_0 = 0.06$ to 0.3. The amount of gas adsorbed in a monomolecular layer, V_m, is determined from the slope of this line and its intercept with the ordinate axis. The total surface of the sample can then be calculated based on the specific size of the adsorbing molecule. It should also be taken into account that the value of C is rather sensitive to errors in the measurement and it can vary by 50% or more depending on how accurately the data points are taken and which data points are omitted in the calculation.

An isotherm of nitrogen adsorption on metallic powder surface of a typical gibbous shape of its initial part is illustrated in Figure 1.21. The initial supposition is that the process of the formation of the first adsorption layer on the surface of the powder sample is finished at point B of the beginning of the rectilinear section of the BC isotherm. A comparison of the values of monomolecular coatings by low temperature nitrogen adsorption (78 K) for different particulate materials calculated by the BET (V_m) technique and with the help of point B (V_b) in most cases show a satisfactory coincidence: the average value of the ratio V_b/V_m equals 0.97 and varies between 0.65 and 1.3 [11]. The results of investigations by the technique of low temperature (78 K) nitrogen adsorption of other authors for different metallic powders have shown the V_b/V_m ratio to lie between 0.9 and 1.04 [12].

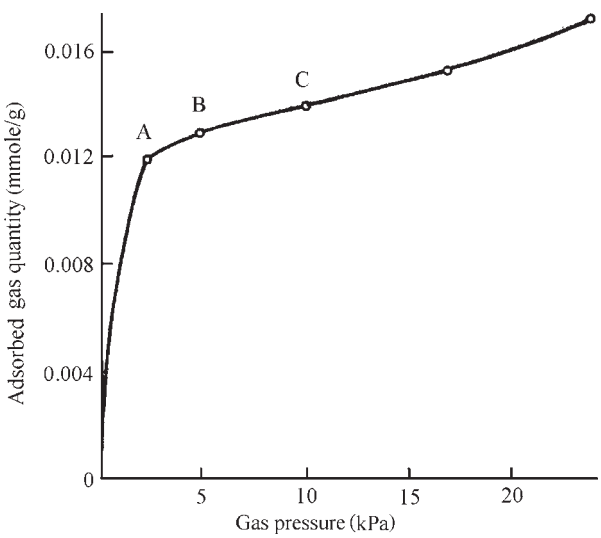

Figure 1.21 Adsorption nitrogen isotherm on metallic powder surface at 78 K.

In CIS countries, there is a standardized technique for the determination of the specific surface of metallic powders from 0.1 to 500 m^2/g by the thermal desorption of argon (Appendix 1, GOST 23401–90). The essence of the adsorption/desorption technique is in the determination of the amount of argon adsorbed on the surface of the adsorbent from the argon–helium mixture of a predetermined concentration at liquid nitrogen temperature and its subsequent desorption into the same mixture on increasing the temperature to 293 K. A maximum diversity between two parallel determinations does not exceed 20% for adsorbents with the specific surface from 0.1 to 10 m^2/g and 10% for adsorbents with the specific surface of 10 m^2/g and higher.

Gas adsorption/desorption methods can also be used to study the pore size distribution in the sample. Pores of up to 100 or 200 nm in size can be determined. The method is based on the capillary condensation, which means that a gas will condense into a liquid phase below its saturation point when it is confined in small pores. The fundamental relation between relative pressure and pore size is described by the Kelvin equation:

$$\ln\left(\frac{P}{P_0}\right) = -\left(\frac{2\gamma_{1v}V_1}{RTr}\right) \tag{8}$$

where γ_{1v} is the interfacial tension of the liquid–gas interface, V_1 is the molar volume of the liquid gas phase, and other symbols are gas constant, R, temperature, T, and radius of curvature of the liquid–gas interface, r. The adsorption/desorption isotherm shows a hysteresis and the relative pressure range where the hysteresis appears provides the information about the pore size. The explanation and the analysis of the hysteresis effect in more detail, including the information about network and connectivity effects of the pore system in a sample, are described in several manuals [13,14].

For the determination of the specific surface area various gases can be used. Usually, nitrogen or argon is used. The use of krypton or argon as the adsorbent improves the accuracy of measuring low specific surface areas.

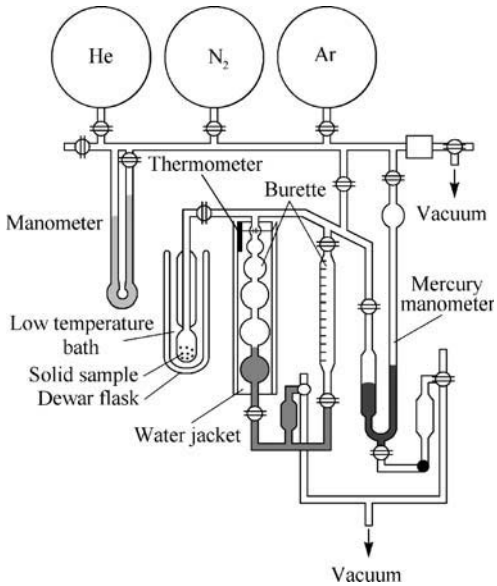

Figure 1.22 BET apparatus for specific surface area determination.

The apparatus for the determination of the specific surface area originally developed by Emmett is shown in Figure 1.22. Commercial instruments are now completely automated. In these devices, instead of the burette-type mechanism to measure the adsorbed gas volume, very precise pressure transducers are used to calculate the adsorbed amount from the known volume of a calibration chamber and the pressure drop that happens when the valve between sample and calibration chamber is opened. Further details are described in all manual books [13–15].

Permeametry

Among the indirect methods for the determination of powder specific surface, the methods based on measuring the gas permeability of the powder have gained ground. The quickness of the analysis and simplicity of the apparatus design have led to a wide usage of this method in industry.

Noteworthy is that, in all cases, the measured quantity is the resistance to fluid flow through a compact powder layer. In this way, the outer particle surface, as though 'smoothed out', without regard to their roughness and blind pores is determined, therefore the value of the permeability specific surface area (S_h) is even less than one determined by BET (S_{BET}).

The Kozeny–Carman equation is the widely used basis for all permeametry modifications. It expresses a connection between the pressure drop across the powder layer (ΔP), the velocity of fluid flow (ν) and parameters characterizing the powder layer including the permeable porosity (ε_v), the viscosity of fluid (η), the layer thickness (l), the average length of the path through the powder layer (l_0) and the density of powder material (ρ_p), and has the following form:

$$S_h^2 = \frac{l^2}{2\eta\nu l_0^2}\frac{\Delta p}{l}\frac{\varepsilon_v^2}{(1-\varepsilon_v)^3} \tag{9}$$

The method for the determination of specific surface of metallic powders by means of measuring the powder layer air-penetrability is laid down in ISO 10070. An analogous standard functions in the Commonwealth of Independent States (GOST 23401–90).

The value of the specific surface of powder, of which the permeable porosity is known, is determined by measuring volumetric flow (q) and the pressure drop of a dry gas (air as a rule) passing through the powder layer in laminar mode, and is calculated by equation:

$$S_h = \sqrt{\frac{\varepsilon_p^3 A\,\Delta p}{5.0(1-\varepsilon_p)^2 q\eta l\rho_p}} \tag{10}$$

where A is section area (m^2), ΔP(Pa), q(m^3/s), η(kg/(m · s)), l(m), ρ_p(kg/m^3) are as defined above.

The equivalent diameter of a spheroidal particle may be calculated as a diameter of the non-porous spheroidal particle having the same specific surface area as the particles of the investigated powder (measured by same method).

Commercial permeametry is applicable for powders with specific surface area and particle size in a range of 70–20,000 cm^2/g and of 0.5–50 μm, respectively [16, 17].

Several designs of permeametry apparatus are used. These instruments can be classified in two groups depending on whether the mass flow of the gas across the powder layer is constant or changing. The apparatus developed by Lea and Nurse [18] and Tovarov [4] (Figure 1.23) refer to the first group.

The Lea and Nurse apparatus was modified by Gooden and Smith by means of an addition of a self-calculating diagram that allows the direct readout of the specific surface. The commercial version of their modification is known as the Fisher subsieve sizer (Figure 1.24) [17].

The instruments of the second group are simplified in comparison with the first. The Blaine permeameter [15], IICX and ADII designs (Figure 1.25) [4] represent this type of apparatus. A variable pressure technique is used. Like this, a hand-operated pump in the form of a rubber pear is used in ADII apparatus.

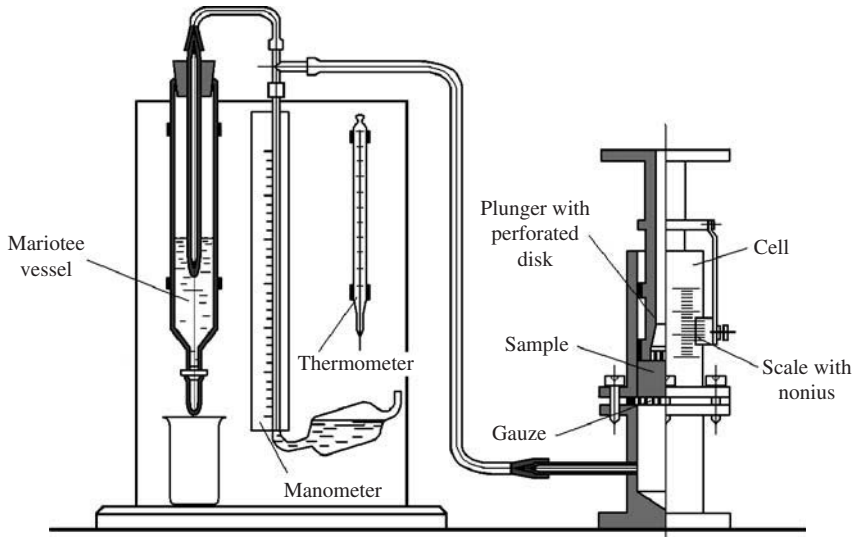

Figure 1.23 Tovarov's apparatus.

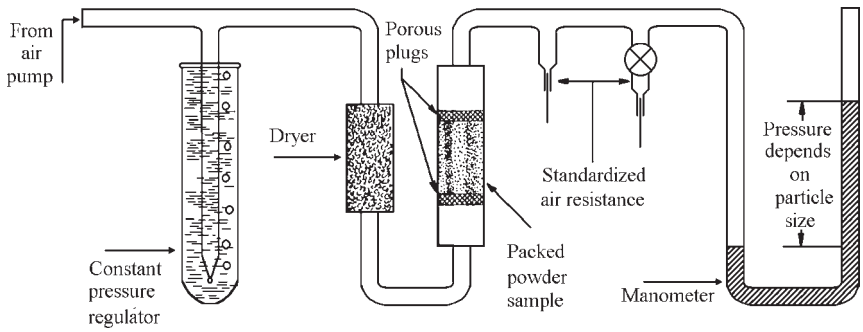

Figure 1.24 Fisher subsieve sizer.

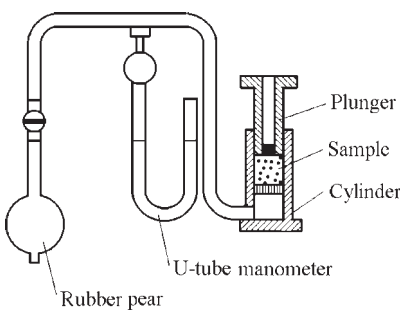

Figure 1.25 ADII apparatus for specific surface area determination.

A typical sample occupies a volume of about 5 cm^3 and, depending on its apparent density, is from 5 to 20 g in weight.

ADII apparatus consists of a cylinder (pan) with a perforated bottom, under which there is a connecting pipe for connecting the cylinder to the manometer. A hollow plunger is inserted into the cylinder, a circle of filter paper is put into the cylinder and a powder sample weighed to within ±0.01 g is put in. The sample is coated with a circle of filter paper and is densified by a plunger. The height of the sample layer is measured by means of the points indicated on the plunger, then the plunger is removed and, by means of a rubber pear, the underpressure under the false bottom measured by the manometer is created. Underpressure gradually decreases due to air penetration through a layer. A stopwatch fixes the duration.

Using the empirical formula, powder specific surface (S, cm^2/g) is calculated:

$$s = k\frac{M\sqrt{t}}{P}$$

where K is the device constant (determined by a reference specimen); M is the coefficient found from the table for measured layer height and air temperature; t is the time of a manometric liquid lowering between two readings, s; P is the sample weight, g.

Specific surface determined by such a method characterizes the external surface of a powder without taking into account a relief of particle surface, their porosity, etc.

In the advanced design of the device, the evacuation with vibration at a frequency of 50 Hz is applied that prevents aggregation of particles and provides the stacking of particles with the porosity within the limits of 0.4–0.8. It increases the accuracy and reproducibility of the measurement.

Picnometry

Picnometry is used for the determination of the true density of PM materials. Density is one of the most important properties of metallic powders.

In addition to its use in measuring the true density of a powder, picnometry can also be used to discriminate among different crystalline phases or grades of materials, different alloys, compositions or prior treatments. Picnometry allows information to be obtained on the porosity of a material if the sample volume is known as well. Then the pore volume can be calculated as the difference between the bulk volume and specific volume.

Archimedes' law is the basis for defining the true density by means of the displacement principle. These can be measured using either liquid or gas picnometry. In liquid picnometry, the volume displacement is measured directly, as liquids are incompressible. The inability of the liquid to permeate pores, chemical reaction or adsorption onto the particle surface, wetting or interfacial tension problems lead to errors in density measurement. In these cases, the gas picnometry has an advantage over the liquid one.

Powder density defined by the liquid picnometry is calculated by the following expression:

$$\rho_p = \frac{m_2 - m}{V_p - V_L} \tag{11}$$

where m_2 is the weight of picnometer bottle with the powder and the liquid (g), m is the weight of the bottle with the liquid (g), V_L is the liquid volume in the picnometer (ml), V_p is the volume of the liquid with submerged powder in the bottle (ml).

In gas picnometry, the volume displacement is measured indirectly from the pressure/volume relationship of the gas under controlled conditions. Gas picnometry requires the use of high-purity, dry, inert, non-adsorbed gases such as argon, neon, dry nitrogen, dry air or helium. Of these, helium is recommended because it can penetrate into pores as small as 0.1 nm and behaves like an ideal gas.

In commercial picnometers, the powder sample is first conditioned to remove contaminants that fill or occlude pores and influence in such a way the surface characteristics. This is achieved by the exhaustion of the system and heating it to elevated temperatures followed by a purging with an inert gas. A typical commercial gas picnometer is a helium-filled sample system consisting of the sample cell, the calibrated reference cell, the vessel with a gas such as helium, the pressure transducer and the connecting pipes with flow control valves. This system is in 'zero' condition if it achieves the environmental pressure and temperature. At this point, the sample cell and the reference cell are isolated from each other and from the system by closed valves [19]. In the process of measuring, the gas is fed by opening the valves first into the reference cell, then it enters the sample cell where a given pressure value is established. Before the measurement in the sample cell starts, there is established a pressure P_2 that exceeds the ambient pressure by 100 kPa, then the pressure is elevated to the P_3 value.

The state of the system can be characterizsed by the equations:

$$PV = nRT \tag{12}$$

for the sample cell and

$$PV_R = n_R RT \tag{13}$$

for the calibrated reference cell and, when a solid sample of the volume V_S is placed in the sample cell

$$P(V - V_S) = n_1 RT \tag{14}$$

where P is the ambient pressure, Pa; V is the volume of the sealed empty sample cell, cm^3; V_R is the volume of the calibrated reference cell, cm^3; n is the amount of the gas (moles) in the sample cell volume at a pressure P; n_R is the amount of the gas (moles) in the reference cell volume at a pressure P; n_1 is the amount of the gas (moles) occupying the remaining volume in the sample cell at a pressure P; R is the universal gas constant; T is the ambient temperature, K.

Omitting the intermediate computations that characterize the changes of the gas state in the sample cell at a pressure of P_2 and the following pressure elevation, we deduce the expression for the gas volume V_S that penetrated into the pores at a pressure of P_3 (working equation):

$$V_s = V + V_R/[1 - (P_2/P_3)] \tag{15}$$

In recent years, the gas picnometer has been further improved by means of a more accurate pressure transducer, a better temperature control and automation. Modern picnometers can now reach an accuracy of 0.01% [19].

Porosimetry

Mercury and gas porosimetry are mutually complementing techniques with the former covering a much wider pore size range, from 0.3 mm to 3.5 nm, and the latter applicable to pores of 0.2 μm and smaller in size [20]. Mercury porosimetry consists of the step-by-step intrusion of mercury into an evacuated porous medium at increasing pressures followed by extrusion as the pressure is lowered.

Mercury porosimetry is based on the capillary rise phenomenon in which a surplus pressure is required to cause a non-wetting liquid to enter a narrow capillary. The pressure difference across the interface is described by the equation of Laplace (1806) and Young (1855), and its peculiarity is such that the pressure is lower if the contact angle θ (Figure 1.26) is greater than 90° or higher if θ is smaller than 90°. In the case of a capillary circular in cross-section and not too large in radius, the mercury meniscus will be approximately hemispherical. The curvature of the meniscus can be functionally related to the radius of the capillary that is given by Young–Laplace–Washburn equation (1921):

$$\Delta P = \frac{2\eta_{1v}}{r_p}\cos\theta \qquad (16)$$

where η_{1v} is the surface tension of the liquid (of 0.485 N/m for mercury), r_p is the capillary radius. The angle θ is the angle of contact between the liquid and the capillary walls.

Every mercury porosimeter contains a penetrometer unit into which the sample is placed. It is then evacuated to a given vacuum level before the sample cell is filled with mercury. The increasing pressure forces the mercury to penetrate into the largest pores in the sample. The amount of mercury penetrating into the sample is recorded at each pressure point respective to the pore size. The first reading is usually carried out at a pressure of 3 kPa, though a reading at a pressure of 0.07 kPa is possible [20]. The pressure is increased up to a final pressure of 400 MPa. Commercial units work either in a consecutive discrete or in a continuous mode. In the former, the pressure is increased in steps and the system is allowed to stabilize at each pressure point before the next step. In case of the continuous mode, the pressure is increased continuously at a given rate.

As is obvious (Eqn 16), two parameters play the most important role in the determination of pore size from the accurately measured applied pressure: the contact angle, θ, and the surface tension, $\eta_{1v.}$

The pressure is usually measured with an electronic pressure transducer or with a Heise–Bourden manometer used in older manual units.

Various methods are available to determine the contact angle.

Usually the sessile drop mode is used. A drop of mercury is placed on the flat surface of the sample and the resulting contact angle is observed visually and usually measured in its shadowgraph on a screen [21]. The same technique can be used to measure the contact angle in transparent capillaries. In the case of non-transparent capillaries, to obtain a shadowgraph such techniques as X-ray and ultrasonic flow-detection can be employed. It is necessary to take into account the difference between microscopic and macroscopic measurement of the contact angle under conditions of wetting and non-wetting [22].

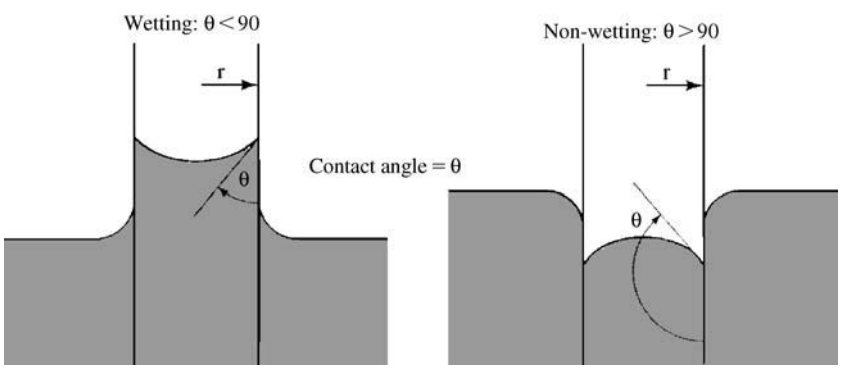

Figure 1.26 Contact angle (*θ*) of a liquid in capillary.

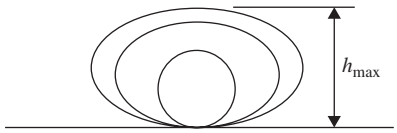

Figure 1.27 Change of mercury-drop shape with size.

Table 1.4 Contact angle between mercury and select PM non-ferrous materials

Powder	Angle (degrees)
Aluminum	140
Copper	116
Zinc	133
Tungsten carbide	121
Tungsten	135

The contact angle depends on the drop size (Figure 1.27). A simplified formula can be used when the maximum height of the drop, h_{max}, is determined:

$$\cos\theta = 1 - \frac{\rho g h_{max}^2}{2\eta_{lv}} \qquad (17)$$

where g is the acceleration of gravity and ρ is the density of the liquid.

The Willhelmy plate method [23] based on the effect of contact angle hysteresis for emersion and immersion is also known. Surface roughness or a change in surface composition during the contact with mercury can explain the presence of this difference. No surface roughness effects manifest themselves below pore size of about 100 nm.

Another technique consists in pressing a powder compact onto a disk with a well-defined hole. Mercury is now placed on the face plane of this disk and the contact angle can be calculated from the required pressure to force the mercury through this cylindrical pore with the size measured directly.

The contact angle, θ, is frequently supposed to be equal to 130° or 140°. This assumption is perhaps the largest source of error. The contact angles of mercury with various materials may significantly differ. Contact angle values between mercury and select PM non-ferrous metals [24] are shown in Table 1.4.

Samples of such metals as zinc, silver and lead can react with mercury. This can strongly change the non-wetting behavior of mercury with the sample. In this case, using a protective film, for example, of satiric acid formed on the pore surface can prevent this reaction. Moreover, for some reactive metals, such as aluminum, their natural oxide layer on the surface ensures sufficient protection.

Surface Tension of Mercury

The purity of mercury strongly influences the surface tension. Mercury is very sensitive to contamination and, probably for this reason, the evaluations of its surface tension values in earlier publications showed a lack of reproducibility. Later works [13], however, showed very consistent data. The effect of temperature is minimal, because the temperature coefficient of the surface tension of mercury is only of 2.1×10^{-4} N/(m°C).

Another error is caused by very small radii of pore surface curvature. The following correction has been suggested by Kloubek [25]:

$$\eta_{corr} = \eta - 2.66 \times 10^{-4}\ \Delta P$$

For $\Delta P = 200$ MPa, the correction term gives an error of 12%.

Restrictions and Limitations

The principal limitations of the results obtainable by mercury porosimetry are the following:

- The extent of the pore volume filled with mercury is limited by a maximum pressure. In such conditions mercury cannot penetrate into very small pores.
- Contrary to the former, the penetration into very large pores is limited by the height of the sample, which determines a minimum pressure. Consequently, very large pores may remain unfilled.
- In the process of porosity measurement, mercury not only penetrates into pores, but it also fills the space between particles that distorts the results obtained for the true volume of coarse pores.

Detailed discussion about restrictions and limitations of mercury porosimetry can be found in a series of works [26, 27].

Surface Area Determination

The surface area of a sample is calculated from mercury porosimetry measurements under a supposition of specific pore geometry. Many publications show a relatively good correlation between surface area values derived from mercury porosimetry measurements and corresponding nitrogen adsorption BET values (Table 1.5) [13, 24].

The value of the specific surface area is often used to calculate the contact angle of mercury on the

Table 1.5 Comparison of surface area measurements with nitrogen adsorption and mercury porosimetry

Sample	Surface area (m^2/g)	
	N_2-adsorption	Hg-porosimetry
Aluminum dust	1.14	1.35
Anatase powder	10.3	15.1
Boron nitride	20.0	19.6
Copper powder	0.49	0.34
Silver iodide	0.53	0.48
Tungsten powder	0.10	0.11
Zinc dust	0.32	0.34

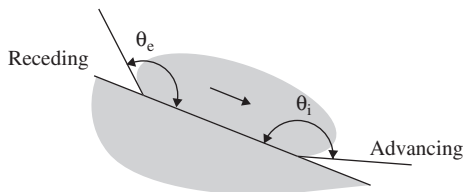

Figure 1.28 Contact advancing (θ_i) and receding (θ_e) angles.

sample material by varying the contact angle till the specific surface area computed from mercury porosimetry measurements correlates with the values determined from nitrogen adsorption data. This method might be a well-grounded alternative to determine the contact angle for materials that are able to withstand a strong effect of compressibility and have no pores smaller than about 10 nm.

Hysteresis and Detained Mercury

The interpretation of the penetration data from mercury porosimetry measurements has been mostly neglected because the interpretation was vague. Generally, three theories are used to explain the hysteresis between the intrusion and extrusion curves in mercury porosimetry measurements: contact angle hysteresis, ink-bottle theory, and connectivity model [27].

Numerous data of contact angle hysteresis indicate different values for advancing and receding contact angles (Figure 1.28). This model does not offer any explanation for the penetrated mercury that can remain in the sample pores after complete depressurization.

The ink-bottle model describes the condition in which mercury enters and leaves pores. It shows how some mercury remains trapped in the sample pores. However, for most samples, the ink-bottle theory prognosticates a much larger amount of mercury remaining in samples than one obtained in actual measurements.

The connectivity model represents a network of pores. In the regular network model, a porous medium is presented in the form of a regular two-dimensional or three-dimensional grid, the sites of which are connected by pores of a constant section. The main characteristics of the grid are obtained experimentally. The peculiarities of a real porous solid in its grid model are taken into account by the selection of the place of the principal pores volume concentration (in connections or in sites of the grid), the amount and the succession of the connections, the size of elements and their combination. This model probably describes the real condition better. However, in spite of a relatively large number of works in the field of mercury penetrability in porous media, the hysteresis problem remains unsolved to the present day.

Standardization

ASTM standards D 4284 [28] and C 493 [29] contain the recommendations for procedures accomplishing the mercury intrusion porometry.

Bubble Test of Pore Size

The essence of this method consists of measuring the pressure necessary for the appearance of the first air bubble on the surface of the sample completely saturated by a liquid to determine the maximum pore size, and in measuring a pressure that corresponds to the beginning of air bubbles discharge on the total sample surface to determine the average pore size. Ethyl alcohol is used as a liquid for sample saturation.

ISO 4003 standard establishes the recommendations for the procedures accomplishing the method of bubble test of pore size. An analogous standard is CIS (GOST 26849–86) (see Appendix 1).

Bulk Properties of Powders

Apparent density, tap density, angle of repose and flow rate are the main attributes that characterize bulk properties of powders. For accurate determination of these properties, a knowledge of the problems of powder movement plays an important part. Thus, the flow of metal powders in bins, hoppers, feeders, conveyors, as well as filling a die cavity is not always reliable or uniform. This often results in the press having to operate at pressing cycle times and wasted product due to composition or apparent density variations. A powder

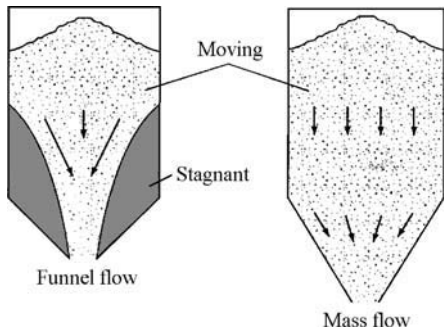

Figure 1.29 Two movement types of powder that can develop in the bin: funnel flow and mass flow.

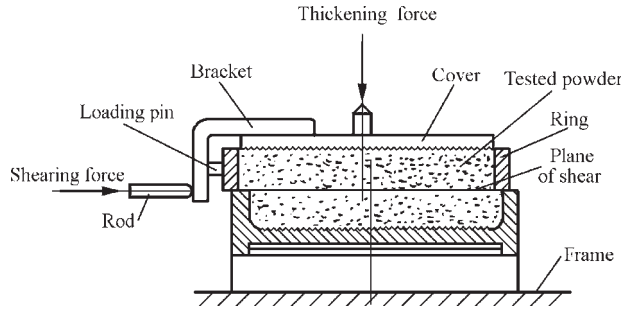

Figure 1.30 Jenike shear cell in initial offset shearing position.

may form a stable arch or a hollow; particle segregation may happen, that results in unacceptable variations in bulk density of the powder delivered to the feed shoe, or the powder may flood uncontrollably.

Bulk Flow Parameters

There are two virtual movement types that can develop in a bin: funnel flow and mass flow that are shown in Figure 1.29.

In funnel flow, an active flow channel is formed above the outlet with non-flowing powder at the periphery. As the level of powder in the bin decreases, layers of non-flowing powder may not slide into the flowing channel, which can result in the formation of stable hollows. Along with this, funnel flow can cause powder caking, form a first-in non-flowing powder, and increase the extent of sifting segregation.

In mass flow, all of the powder is in motion. Powder from the center as well as the periphery moves toward the outlet. Mass flow hoppers provide the flow sequence, eliminate stagnation of powder, reduce sifting segregation, and provide a steady discharge with a consistent bulk density and a flow that is continuous and well controlled. Conditions for the attainment of mass flow are accomplished by means of making the hopper walls smooth and steep as well as the outlet sufficiently large to prevent arching.

Having the information about bulk properties of powders, engineers can optimize the selection of storage and handling equipment. These same properties can be used to modify prevalent processes to correct flow problems. The following bulk solids handling properties are relevant to constitutive flow behavior: cohesive strength and frictional.

Cohesive Strength

When the powders are placed in bins, hoppers or containers, the consolidation pressures range from zero at the surface to relatively large values at increasing depth within the vessels. If a powder acquires a cohesive strength because of the pressures applied to it, an arch or hollow can form. An arch is a stable obstruction that forms over the point of narrowed cross-section of the vessel. The arch supports the rest of the contents vessel, hindering discharge. A hollow (called also a rathole) is a stable pipe or vertical cavity that connects with the outlet. Powder is left in stagnant zones that remain in their place until an external force is applied to destroy them.

The cohesive strength can be measured as a function of the applied consolidation pressure on a Jenike apparatus [30], shown in Figure 1.30 and accepted in ASTM D 6128 Standard [31]. The bottom of the cover and the inside of the base are roughened to increase friction with the powder under test. The base and the ring are filled with the powder being tested, and a vertical load is applied to the cover. A horizontal shearing force that acts on the section of contact between the ring and the base is transferred from the bracket to the ring through a loading pin. The standard shear cell is 95 mm in inside diameter. The present shear tester is equipped with a shear cell, a gravity vertical loading system and an electronic shearing force applicator with shearing rate of 2.54 mm/min. This arrangement produces a permanent record of the stress–strain relationship.

Shear testing is a two-step process that consists of consolidation (also called preshear) and shear. The consolidation is realized by accomplishment of specimen to flow under given stresses until a steady state is reached or closely approached. Measurement of the shear stress σ_{40} consists of obtaining its dependence on the pressure normal stress σ_p in yield locus. The determination of one yield locus requires the measurement of three to five points of the locus. For each point, the specimen is first consolidated and then sheared. The value of shear normal stress typically ranges between 25 and 80% of the preshear normal stress σ_p.

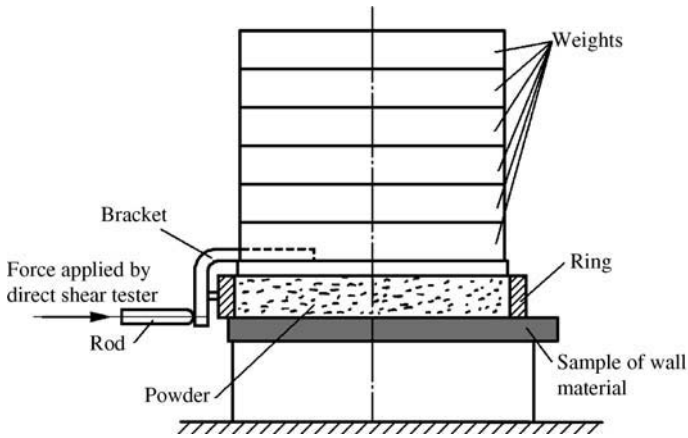

Figure 1.31 Shear cell used in measuring wall friction properties.

The flow condition of a powder is used for a variety of engineering decisions, for example, to design an optimal outlet assembly to prevent the formation of cohesive arches and ratholes. Details can be found in Jenike [30].

Moisture, particle size and shape, long-term storage at rest in vessels and some chemical additives influence the cohesiveness of the bulk powder.

Typically, cohesiveness rises as moisture content increases, but not in direct proportion. Hygroscopic materials can suffer significant increases during exposure to humid air.

As a rule, as a powder becomes finer, it also becomes more cohesive and difficult to handle. Dendritic, flaky or fiber particles are more cohesive than those that are spheroidal.

When a powder is kept in a bin or hopper for a period without moving, it can become more cohesive and difficult to handle. Such cohesion may result from settling and compaction, crystallization, adhesive bonding and agglomeration.

In some cases, adding a small amount of a chemical additive such as calcium, lithium or zinc stearate can make a cohesive powder flow more easily.

Frictional Properties

Both internal and external friction values can be determined by measuring cohesive strength with a shear tester (Figure 1.31) like the Jenike shear cell. Internal friction is conditioned by solid particles moving against each other and is characterized by the angle of internal friction and the effective angle of internal friction. External friction is characterized by the wall friction angle or coefficient of sliding friction. The higher the coefficient of sliding friction, the steeper the hopper walls that are necessary for mass powder flow.

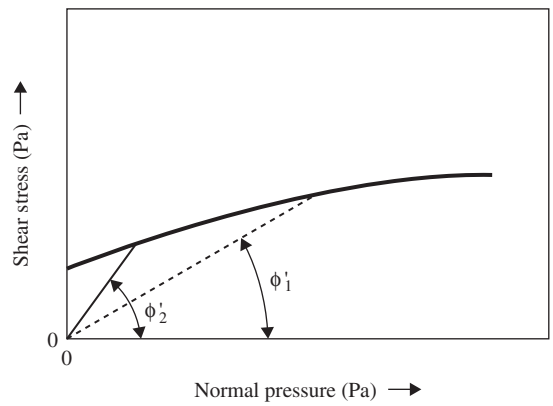

Figure 1.32 Typical results of the wall friction properties measured by means of shear cell test setup shown in Figure 1.31 to determine wall friction angle.

In the shear cell (Figure 1.31), a sample of wall material is placed on a disk so that the top surface of the wall material is the horizontal section of the force measuring stem. The ring is placed over the wall material sample and filled with the powder. After scraping off the excess powder, a cover is placed over the powder. A vertical force is applied to the cover by means of weight disks. This force creates a vertical pressure σ_w in the powder. Several (usually upto six) 0.5 or 1 kg weights are placed directly on the top of the cover of the shear cell to give the largest required normal pressure σ_w. The stem is moved. When the shear stress τ_w is leveled off with recording its value, one weight is removed. Thus, sequentially removing away the weights, the τ_w is determined for every magnitude of σ_w.

Characteristic results of the test for wall friction angle determination in the shear tester are shown in Figure 1.32. Typically, as vertical pressure increases, the wall friction angle decreases.

Table 1.6 Influence of particle size and particle shape on apparent density for several non-ferrous metal powders

Material	Manufacture method	Particle diameter (μm)	Specific surface Fisher (m^2/g)	Particle shape	Apparent density (g/cm^3)	Source
Aluminum	Granulation	500–2500	...	Needle	1.4	ECKA
Aluminum	Grinding	1000–2000	...	Irregular to semi-spheroidal	1.3	– " –
		500 max	...	– " –	0.8–1.2	– " –
		150 max	...	– " –	0.8–1.2	– " –
Aluminum	Air atomization	160 max	...	Irregular	1.0	– " –
		18 (a)	...	– " –	1.09	[32]
		15.5 (a)	...	– " –	0.98	– " –
		6.0 (b)	0.6	– " –	0.60	ECKA
Copper	Air atomization	500 max	...	Irregular	5.2	ECKA
		315 max	...	– " –	5.1	– " –
	Water atomization	315 max	...	Irregular	4.2	– " –
	Air atomization	160 max	...	Irregular	5.0	– " –
	Water atomization	100 max	...	Irregular	4.2	– " –
	Air atomization	63 max	...	Irregular	4.7	– " –
		45 max	...	– " –	4.4	– " –
	Grinding	...	0.3	Flake	1.1	– " –
		...	0.4	– " –	1.1	– " –
		...	1.0	– " –	0.8	– " –
	Electrodeposition	63 max	0.23	Dendritic	0.7	– " –
Zinc	Air atomization	315 max	...	Irregular	3.0	ECKA
		45 max	...	– " –		
Tin	Gas atomization	200 max	...	Teardrop-shaped	4.0	ESKA
		63 max	...	– " –	3.7	– " –
		40 max	...	– " –	3.5	– " –
		32 max	...	– " –	2.2	– " –
		8 (b)	0.25	– " –	2.0	– " –
Nickel	Carbonyl	3.2 (a)	...	Acicular	0.61	[32]
		3.8 (a)	...	– " –	1.87	– " –
		4.1 (a)	...	– " –	2.10	– " –
Nickel	Precipitation	3.5 (a)	...	Roundish	1.81	[32]
		4.4 (a)	...	– " –	2.09	– " –
		8.0 (a)	...	– " –	2.60	– " –

(a): Average particle diameter; (b): Median mass diameter; ESKA: ESKART- GRANULES Company

The pressure, moisture, particle size and shape, long-term of storage at rest in vessels, and wall surface condition influence both the internal and external friction values of metal powders.

Typically, as the consolidating pressure increases, the effective angle of friction decreases. Similarly, the coefficient of sliding friction often decreases as the pressure acting normal to the plate increases. When a powder is kept in a bin or a hopper for a period without moving, many powders experience an increase in friction between the particles and the wall surface.

Fine powders and those with a wide range of particle sizes are usually more frictional than coarse powders or those with a narrow particle size distribution. Dendritic, flaky or fiber particles are more frictional than roundish ones. An increase of moisture content in many powders leads to an increase in their friction.

The wall surface condition can appreciably manifest itself in sliding powders along it. Thus, smooth surfaces are typically less frictional.

Values of both internal friction angle and wall friction angle are required to design chutes, mass flow hoppers and other vessels.

Bulk Density

The term powder bulk density includes its apparent density and top density that differ from one another in their effect on compressibility of powder samples. This is one of the fundamental properties of a powder.

Apparent Density

Apparent density of metal powder is the weight of a unit volume of loose powder expressed in grams per cubic centimeter. This characteristic determines the actual volume allocated by a mass of loose powder that directly defines the processing parameters such as the design of consolidation tooling and the range of the press motions required to pack and to compact the loose powder.

Apparent density of a metal powder strongly depends on the particle size. Usually, it decreases with decreasing particle size. Table 1.6 shows the influence of particle size on the apparent density for several non-ferrous powders.

Apparent density decreases as the particle shape becomes more irregular, decreases with increasing surface roughness, and depends on particle size distribution. In the case of powders with a wide range of particle sizes, the apparent density increases because the space between coarse particles is filled with smaller particles.

Funnel Method

The most prevalent method for the determination of apparent density of metal powders uses the Hall funnel illustrated in Figure 1.33. ISO 3923/1 standard establishes recommendations for using this method with the application of the Hall funnel (Figure 1.33). An analogous standard functions in CIS (GOST 19440-94-86) (see Appendix 1). Both ASTM B 212 and MPIF Standard 04 describe this method of using the Hall funnel. Both ASTM B 417 and MPIF Standard 28 provide for the Carney funnel. This funnel differs in the design of the discharge opening (Figure 1.33). The orifice diameters amount to 2.5 and 5 mm, respectively.

The equipment assembly for the determination of the apparent density is shown in Figure 1.34.

Apparent density measurements are carried out by pouring powder into the funnel from which it flows into the 25 cm^3 density cup. After filling the cup, the funnel is moved away and the excess powder is leveled off using a spatula. The apparent density in grams per cubic centimeter is then defined by weighing the powder in the cup in grams and dividing by 25 cm^3.

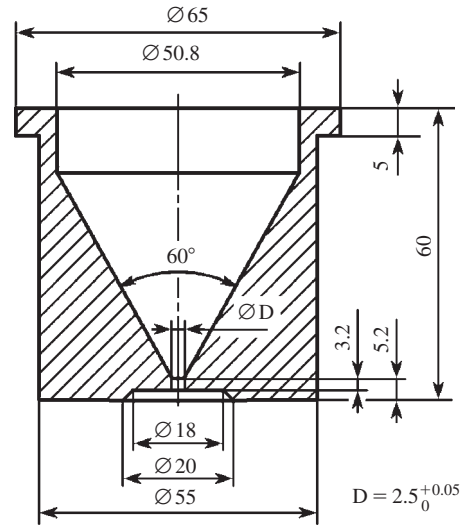

Figure 1.33 Hall funnel.

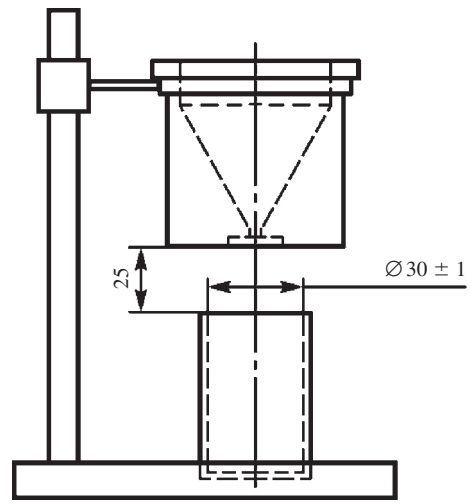

Figure 1.34 Equipment assembly for apparent density determination.

For powders that do not flow freely, the Carney funnel is used. The larger opening allows a greater variety of powders to flow. If the powder does not flow readily, its flow can be stimulated by poking a wire up and down in the orifice without entering the density cup.

Scott Volumeter

This method is used for powders that do not flow freely through a Carney funnel. In the Scott volumeter, the bulk condition of the powder is obtained

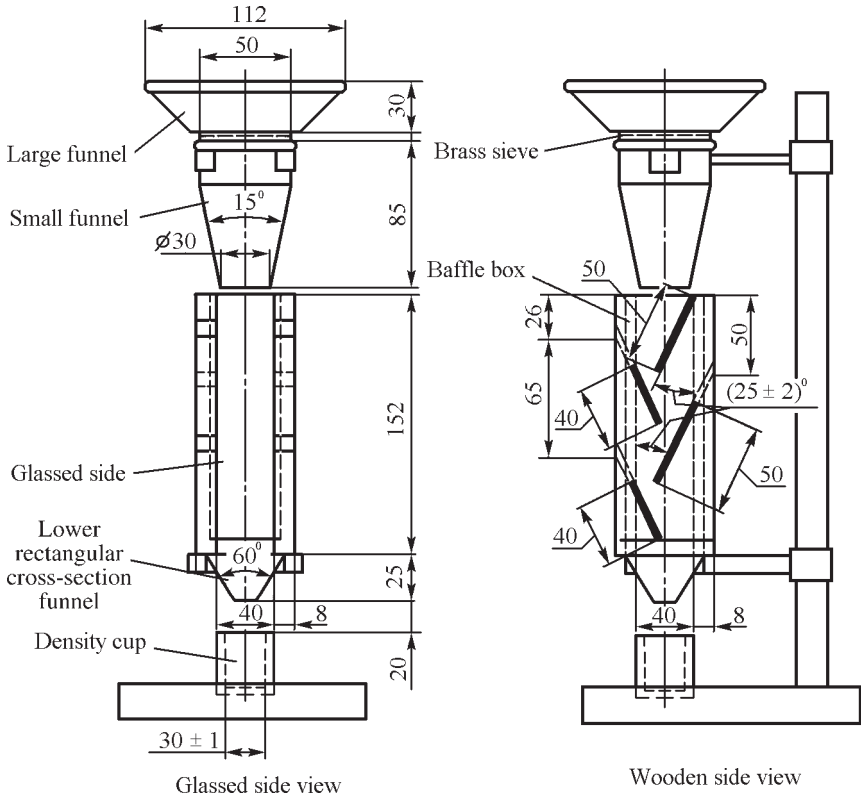

Figure 1.35 Scott volumeter.

by filling the density cup as a result of passing the gravitational powder jet through a system of inclined plates of the volumeter. As shown in Figure 1.35, the apparatus consists of a large funnel with a metallic screen and a smaller funnel that has a straight stem directing the powder into the baffle box. The latter with glass sides and two wooden sides contains a series of glass baffle plates and a funnel at the bottom to direct the powder into the density cup.

Pouring the test specimen carefully into the funnel begins the operating procedure. Ultrafine powders may require a light brushing with a synthetic brush to stimulate the powder to flow through the screen into the funnel. The powder is permitted to stream into the density cup until it completely fills and overflows the circumference of the cup. The excess powder should be removed from the cup by passing a spatula blade in flat contact with the top of the cup. The powder weight is determined accurate to 0.05 g. The density of the powder is given in grams per cubic centimeter if a metric cup is used, or grams per cubic inch if a non-metric cup is used.

Tap Density

The method for the determination of tap density, which is defined as the density of a powder when the volume container is tapped or vibrated under specified conditions, is established by ISO 3953. This method in accordance with ISO 3953 is accepted in ASTM B 527, MPIF 46, GOST 25279–93 and MIL-STD-1233 standards (see Appendix 1).

Tap density is a function of particle size distribution, particle shape and surface roughness. It is always higher than the free-flow apparent density.

A graduated glass cylinder with a volume of 100 ml and a multiplying factor of 0.2 ml (or a smaller graduated cylinder may be used for high-density powders) is used for tap density measurement. The amount of the powder for tap density testing is shown in Table 1.7. If mechanical tapping is used, the filled cylinder is placed in the mechanical apparatus, which operates till no further decrease in volume of the powder is observed (Figure 1.36). The amplitude of tapping or vibrating must be of 3 mm and frequency shall be from 100 to 300 impulses per minute. In both the latter or hand tapping, care must be taken to exclude loosening the surface layers of the sample during the procedure. The tap density in grams per cubic centimeter is then defined by weighing the powder in the cylinder in grams and dividing by the volume of the tapped powder in cubic centimeters. The results should be obtained with accuracy not worse than $\pm 0.1\ g/cm^3$.

Table 1.7 Typical tap density in comparison with apparent density of non-ferrous powders

Powder	Particle size (μm)	Apparent density (g/cm^3)	Particle size (μm)	Tap density (g/cm^3)	Increase (%)
Aluminum [32]	6.00 (a)	0.60 (b)	5.05 (a)	1.30	117
Cobalt [33]	99.6 wt% $< 40\,\mu m$	1.8	99.6 wt% $< 40\,\mu m$	3.0	67
Copper [34] (c): Spherical	...	4.5	...	5.3	18
Irregular	...	0.4	...	0.7	35
Flake	...	0.4	...	0.7	75
Nickel [35, 32]	3.0 (a)	1.0	3.0 (a)	1.9	90
Tin [32] (b):	8.0 (d)	2.0	2.45 (a)	3.15	57
Tungsten fine [36, 32]	3.27 (a)	2.16	1.15 (a)	4.45	106

(a): Fisher subsieve size; (b): ESKA Metal Powders; (c): Particle size distribution is the same for apparent and tap density; (d): Mass median particle size measured by means of laser granulometer

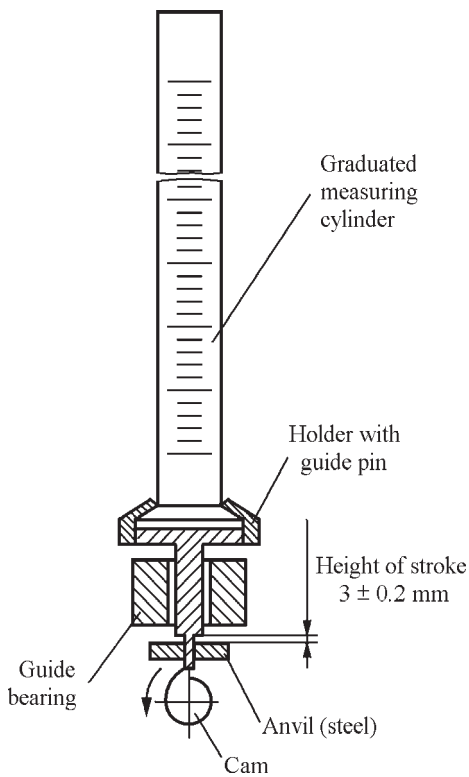

Figure 1.36 Diagram of tapping apparatus.

The amount of increase from apparent to tap density depends to a great extent on particle shape and particle size. Usually, the lower the apparent density, the higher the percentage increase in density on tapping.

Flow Rate

Flow rate is the time required for a powder sample of a standard weight (50 g) to flow gravitationally under atmospheric conditions through the Hall funnel into the cup. A determination of the flow rate of the powder is important in high-volume manufacturing, which depends on rapid, uniform, consistent filling of the die. Poor flow characteristics cause slow and non-uniform press feeding and even difficulty in filling of the die cavity. In modern automatic presses, the die cavity shall be filled with a certain constant amount of the powder in about 1 s.

ISO 4490 establishes the method of flow rate determination of metallic powders by means of the Hall funnel. The description of this method is contained also in ASTM B 213, MPIF 03 and GOST 20899-75 standards (see Appendix 1). Japanese standard JIS 7-2502-1966 and German standard 82–96 are standards equivalent to ISO 4490. The funnel with a calibrated orifice of 2.5 mm in diameter is made of aluminum alloy 6061–T6 with a smooth finish to minimize wall friction.

The test procedure consists of the following. A dry sample of 50 g in weight is poured into the funnel, the orifice of which is covered by the operator's finger. The stopwatch is started when the fingertip is removed and is stopped when the last powder leaves the funnel. The flow rate (s/50 g) of the sample is expressed as the time in seconds necessary for 50 g in weight of the powder to flow through the orifice. A powder that does not flow through the 2.5 mm orifice of a Hall funnel is classed as non-free-flowing powder.

The Hall funnel is calibrated using a standard powder (150-mesh Turkish corundum) that has a flow

rate of 40.0 s/50 g in the standard funnel. Real funnels can give somewhat different values of the flow rate of this powder due to peculiarities of their manufacture and this value is usually stamped on the funnel. The correction coefficient of the funnel equals 40.0 divided by this value. Calibration with Ballotini solid glass spheres with particle size ranges of 0.090 to 0.102 mm and 0.065 to 0.090 mm in diameters, has flow rates of 35.6 and 33.4 s/50 g, respectively.

Sliding at Impact Point

The chute angle and the roughness of the chute surface at the point of impact are the key factors in chute design. Optimum is the chute angle that does not facilitate an accelerated movement of powder in the chute with the transformation of constrained moving to free one, which is accompanied by a transition into suspension state of dust powder fractions (mainly of particles smaller than 50 μm in size) and by enhancing particle segregation in the reservoir filled with the powder. All of the factors affecting frictional properties can influence the optimum chute angle.

Segregation of Particles

A uniformity of the mixture is very important in achieving high-quality PM manufacture. In the case where a particulate material is represented by both a polydisperse powder and a mixture of powders differing in their physical–chemical properties, segregation results in the heterogeneity of the particle size distribution as well as of physical–chemical properties. This requires not only a proper mixing, but also suitable storing, feeding and transporting of powders.

Three phenomena have been identified as the primary cause of most segregation problems in metallic powders. They are the simple segregation mechanisms under gravity considered below.

Trajectory Effect

While pouring the powder by the chute onto the pile, particles are separated in size. The frictional drag on particles moving on a pile surface is higher for finer particles than for coarser particles. This results in a concentration of finer particles nearer to the end of the chute, while coarser particles come to rest at a much greater distance, to the base of the pile (Figure 1.37).

Screening Model (also called Sifting Phenomenon)

This effect occurs when finer particles move through a matrix of coarser particles. The screening effect occurs in typical PM processes connected with filling of different volumes. In these processes, there is revealed also an impingement effect when, under the impact of falling coarser particles, the pile of finer particles becomes more dense and that causes the slope angle of the upper part of the pile to become higher that the angle of repose (see Figure 1.37).

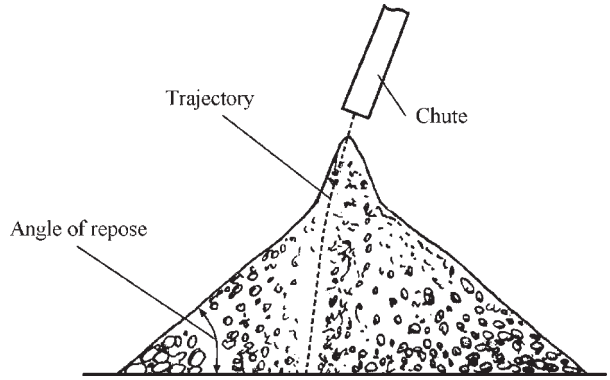

Figure 1.37 Trajectory effect segregation of particles.

Fluidization

Fine particles retain the ability to remain in suspension for a long time, whereas coarser particles settle first (according to their sedimentation rate). This results in a vertical segregation of particles within the powder layer. If the powder is segregated by air entrainment, fine particles will be located close to the top of the bottom-poured container. Air currents can carry the airborne fine and light particles away from a fill point to certain parts of a bin, such as toward vents and dust collectors.

Using the following data can help to influence the powder segregation during the production of PM parts:

- The more cohesive a powder, the less probable its segregation. Therefore, for some materials, the opportunity for segregation can be reduced by adding binders. This causes fine particles to stick to coarse ones and makes the powder less free-flowing. However, an additive must be optimized to avoid the possibility of reducing to zero the powder flow in the chute.
- The type of the displacement device can appreciably influence the segregation tendency of powders. It is significant that funnel flow patterns strengthen segregation, while a mass flow pattern tends to minimize such problems.

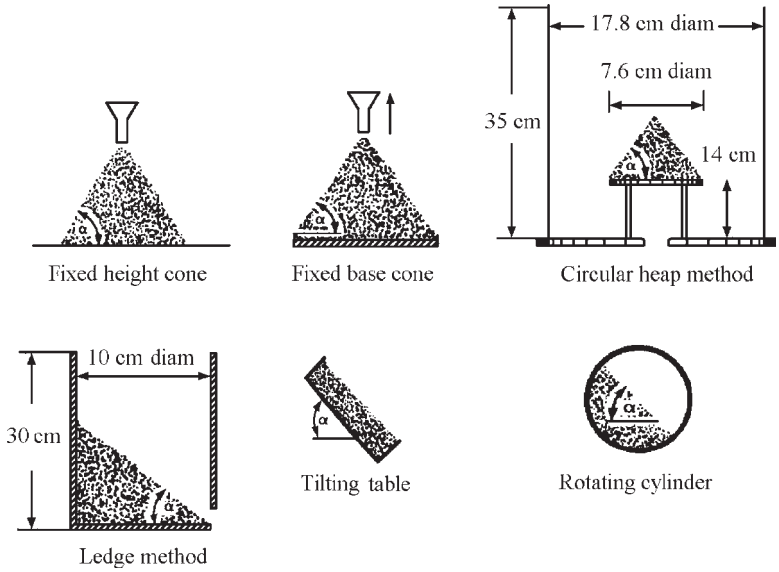

Figure 1.38 Six methods used to measure the angle of repose.

- Trajectory effect segregation is most likely to occur when the powder has a wide particle size distribution and when there is interparticle motion during operation. Usually, particles greater than about 100 μm in diameter are most subject to trajectory effect segregation. If most of the particles are smaller than 100 μm, the segregation by fluidization and particle entrainment is more probable.

Angle of Repose

The angle of repose is related to interparticle friction and the flowability of powders. It is not standardized. Several methods are used to measure this parameter. However, it is necessary to have in mind that the reliability of measuring the ultimate angle of repose depends on the measuring method used. Therefore, the measuring method should be carefully selected so that it best represents the property to be quantified.

A popular method for the determination of the angle of repose consists of the calculation of the tangent of the angle as the ratio of the height to the mean base radius of the powder heap. This powder cone is formed by means of carefully pouring the powder through a funnel. It can be formed as a fixed height cone, as a fixed base cone, or by means of using a circular method (Figure 1.38) measuring the angle.

The following methods have also found a use for measuring the angle of repose [37]:

- *Titling table*, where a rectangular box filled with powder is tilted until the contents begin to slide.

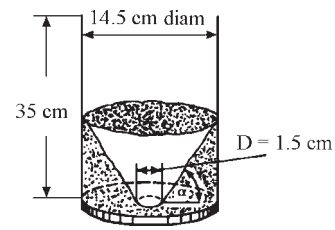

Figure 1.39 Crater method used to measure the angle of repose.

- *Rotating cylinder*, where a sealed hollow cylinder half full of powder is rotated until the powder surface shows its maximum angle with the horizontal. This angle is the angle of repose.
- *Ledge method*, where the powder is initially charged into a rectangular box (see Figure 1.38). A slot at the base of one vertical wall is closed by a board. The closure board is then removed to allow the material to flow slowly through the narrow slot. The angle with the horizontal plane of the surface of the powder equilibrium when the flow stops is calculated as the angle of repose.
- *Crater method* (called also *Discharge method* [38]), where a circular tube is placed vertically on a plate with an orifice in the center (Figure 1.39). The height of the remaining powder against the wall of the tube is measured at eight equidistant points around the circumference to determine the angle of repose [39].

- *Dynamic angle of repose* is determined in the apparatus consisting of a drum with a roughened internal surface that is half filled with powder and slowly rotated around its horizontal axis. Within a certain range of rotation speeds (usually from 2.5 to 6 rpm), the surface of the powder in the drum comes to a sufficiently steady condition. The maximum angle of bed inclination just before slump occurs is designated as the dynamic angle of repose [32].

Factors Influencing the Angle of Repose

There are internal and external factors affecting the angle of repose. Internal factors include particle size, particle shape and cohesiveness. Generally, coarser particles have higher angles of repose. However, very fine particles may reveal cohesiveness owing to the electrostatic effect, which increases the angle of repose. Typically, spherical particles have smaller angles of repose than irregularly shaped ones, owing to spherical particles having a greater tendency to roll.

External factors include the method of measurement and presence of other components including moisture. The effect of measuring method is discussed in detail above. It is significant that the ledge and crater methods give a higher angle of repose than that obtained from the heap formation methods. The angle of repose of loose dry powder increases by compacting, as well as by introducing moisture.

Compactibility of Metal Powders

Compressibility and compactibility define the ability to form unsintered ('green') compacts by die pressing of powders. Generally, the compressibility is quantified as the value of the compacting pressure required to ensure a specified green density of the sample. Therefore, the compressibility of the powder is an important factor in the design of pressing equipment. It is usually expressed in terms of green density. The compressibility is also measured by the compression ratio, which is the ratio of the green density to the apparent density of the powder.

The compactibility is evaluated by the green strength of a powder compact and relates to the sample complexity, fragility and the ability of the compact to be ejected from the die. The relation between the compressibility and the compactibility is complex, because some factors can improve one of them to the detriment of the other. Thus, particles of a spherical shape generally have a higher compressibility. In contrast, an increase of particle surface area, which can be achieved by increasing the particle surface irregularity, usually increases the green strength. At the same time, such factors as increasing the compaction pressure and the temperature have competing effects on the compressibility and the green strength. These factors promote intense particle movement and deformation, which are the bases to improve mechanical interlocking.

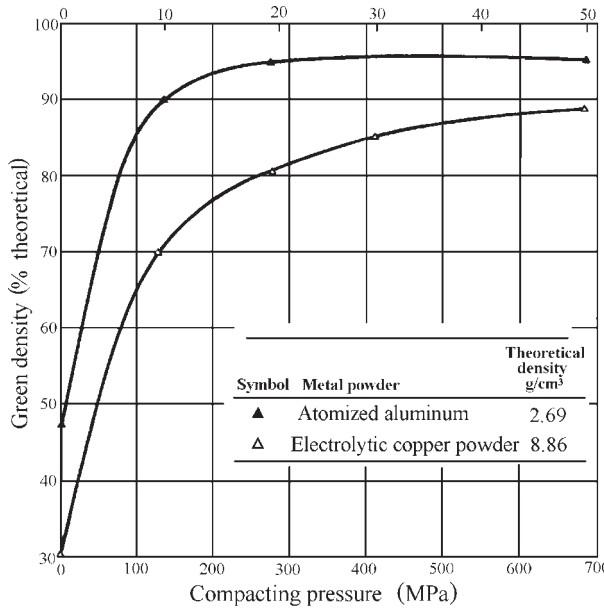

Figure 1.40 Compressibility curves for gas atomized aluminum powder and electrolytic copper powder.

Compressibility

Characteristic compressibility data for gas atomized aluminum powder and electrolytic copper powder are shown in Figure 1.40 as a functional dependence of the percentage of the theoretical density on the compacting pressure [40].

Lubricants are used to promote the ejection of the compacted samples from the die. At higher compacting pressures, lubricants reduce the green density owing to the fact that they are taken up by the available pores. There are two lubrication techniques. One method consists of mixing a dry lubricant such as zinc stearate, amide wax and stearic acid, with the metallic powder. By the other method, the die walls and punches are greased by the lubricants. In the case of the powder lubrication method, the lubricant addition may range from 0.5 to 1.5 wt%. With the wall lubrication, a solid lubricant is mixed with a volatile organic liquid, for example 100 g zinc

stearate with 1 l methylchloroform. This mix is either painted or sprayed on the tooling. The organic liquid evaporates, leaving a thin film of dry lubricant on the working surface of the die cavity and punches.

ISO 3927, 'Metallic Powders Excluding Powders for Hardmetals – Determination of Compactibility (Compressibility) in Uniaxial Compression', establishes the method for the compressibility. The description of this method is contained also in ASTM B331, MPIF 45 and GOST 25290-90 standards (see Appendix 1).

For pressing, dies of tool steel hard metal are used, one of them for cylindrical and the other for rectangular compacts. The cylindrical die shall ensure the manufacture of compacts of 20–26 mm in diameter and with the height-to-diameter ratio of 0.8–1.0, and the rectangular die shall ensure the manufacture of compacts in the form of plates of $30 \times 12\,\text{mm}^2$ in size and of 5–7 mm in thickness. The shaping is carried out in a press with the loading to 500 kN, which is controlled for a uniform growth with a rate not higher than of 50 kN/s. To construct the curve of powder compressibility at repeated pressing, loadings of 200, 400, 500, 600 and 800 MPa are used. If the compressibility at a single pressing is needed, it is measured at one of the above pressure values.

After pressing, the green samples are weighed to ± 1 mg and their sizes are measured by a micrometer to ± 1 μm. The compressibility (ρ_p) that is determined by the density of the pressed sample is calculated by the formula:

$$\rho_p = \frac{m}{V}$$

where ρ_p is the compressibility, g/cm^3; m is the weight of the green compact, g; V is the volume of the green compact, cm^3.

Green Strength

Necessary and sufficient mechanical strength of a cold pressed green specimen allows the ejection of the green specimen from the die and its transfer to the sintering furnace or die head without breakage. This is particularly important for thin-walled specimens, thin sections of large parts and finned specimens. The strength of green compacts depends mainly on mechanical interpenetration of superficial irregularities of particles, which is favored by plastic deformation during pressing. Therefore, spherical particles show the lowest degree of mechanical strength because of low initial surface contact between neighboring particles. Green strength is also decreased when oxidation and contamination of particle surfaces and the amount of adsorbed gases increase.

Standard test methods to determine green strength of an unsintered compact are specified in ISO 3995, 'Metallic Powders – Determination of Green Strength by Transverse Rupture of Rectangular Compacts'; the description of this method is contained also in ASTM B312, MPIF 15 and GOST 25282-93 standards (see Appendix 1).

The main point of the method consists of the determination of the bending stress of green samples of a rectangular section by means of the action on the sample of a uniformly growing load up to fracture. The strength is determined as the stress calculated by the bending equation that is necessary to crack the rectangular billet installed on the two supports along the edges and subjected to the load imposed in the centre. An example of the device for testing the sample strength is shown in Figure 1.41.

For the test, samples of not less that 30 mm in length, 10–13 mm in width and 5.5–6.5 mm in thickness are used. The load is increased with a constant rate till the sample fails (not quicker than 10 s). The strength of the non-sintered material is calculated by the formula:

$$S = \frac{3PL}{2t^2W}$$

where S is the green strength, MPa; P is the force at the instant of the failure, N; L is the distance between the supports, mm; t is the thickness of the specimen, mm; W is the width of the specimen cross section, mm.

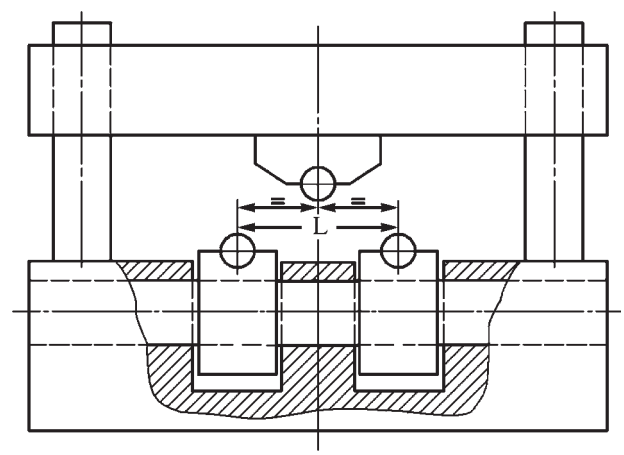

Figure 1.41 Device for testing of green strength of an unsintered compact.

Table 1.8 Apparatus for powder analysis

Apparatus	Principle of operation	Measurement range (μm)	Measuring time	Source
Particle size analysis techniques				
SediGraph III 5120 particle size analyzer	It determines particle size by using the sedimentation technique which measures, with the help of narrow X-ray beam, the settling rates of different size particles in a liquid with known properties	Particles ranging from 300 to 0.10 μm equivalent spherical diameter	Runs up to 18 samples unattended operation in 15 minutes max	MIC
Saturn DigiSizer	The digital presentation of the pattern is obtained as a result of laser light scattering from a sample. The resulting information is then processed using data reduction based on Mie theory	Particles ranging from 1000 to 0.10 μm equivalent spherical diameter. Accuracy in particle range: from 0.10 to 1.0 μm relative error amounts 10%; from 1.0 to 1000 μm one 3%	Approx. 10 s	MIC
Laser-Particle-Sizer 'analysette 22' (comfort)	Method utilizes a principle of the scattering of electromagnetic waves to determine particle size distribution	• Liquid dispersing unit: from 0.1 to 1250 μm • Dry dispersing unit: from 0.8 to 1250 μm • Free-flowing samples: from 0.8 to 1250 μm	Approx. 10 s	Fr
Surface area, porosity and density measurements				
TriStar 3000	Surface area determination and porosimetry are based on the technique of gas adsorption	Measures surface are as low as 0.01 m^2/g	Performs three BET surface area measurements in approx. 20 minutes	MIC
ASAP 2020	Surface area and porosimetry analyzer uses the gas sorption technique to determine the percent metal dispersion, active metal surface area, size of particles, and surface acidity of catalyst materials	Pressure range: 0 to 950 mmHg	Accuracy: • 1000 mmHg range: within 0.15% of reading (high vacuum systems); • 1 mmHg range: within 0.12% of reading (micropore)	MIC
FlowSorb III	It measures surface area using the flowing gas method, which involves the continuous flow of the adsorptive and inert gas mixture over the sample at atmospheric pressure	Samples with surface areas from 0.01 m^2/g to 1000 m^2/g	Reproducibility is better than 0.5%	MIC
AutoPore IV 9500	Porosity of material is characterized by applying various levels of pressure to a sample immersed in mercury	Ability to measure pore diameters from 0.003 to 360 μm	Better than 0.1 μl for mercury intrusion and extrusion volumes	MIC
MultiVolume Pycnometer 1305	Method utilizes a principle of gas picnometry, where volume displacement is determined from the pressure/volume relationship of a gas, preferably helium, under controlled conditions	Range of sample volumes: from 0.5 to 150 cm^3	Accuracy: of ±0.1 to 0.2%	MIC

MIC: Micromeritics Instrument Corporation. More information on these apparatuses can be found in http: www.micromeritics.com; Fr: Fritsch GmbH (Germany)

For most applications, green strength values of 5.0–6.0 MPa or higher allow safe handling of green specimens. Lower green strength may cause horizontal lamination in the specimen. Specimens with sharp contours or thin sections, or specimens made from a blend of several powders in which some of the components detract from the overall strength of the specimen, require higher green strength characteristics.

Apparatus for Powder Analysis

Several advanced designs of apparatus for powder analysis have been developed in recent years. These include the particle size techniques as well as surface area, porosity and density measurements. Table 1.8 contains the list of some of these devices.

Laser particle sizer 'analysette 22' Comfort from Fritsch GmbH (Germany) is a versatile instrument for determination of the size distribution of suspensions, emulsions and powders. The usable inverse Fourier optics provides measurement of particle size distribution with a very high resolution. With the computer-controlled location of the measuring cell (max. 310 positions) in the convergent beam between laser and sensor, it is possible to utilize up to 310 measurement signals for the calculation. The new generation SediGraph III 5120 Particle Size Analyz with advanced instrumentation from Micromeritics Instrument Corporation (United States/Germany/Italy) provides accurate and reproducible results. Particles with diameters in the range of 300 to 0.1 μm can be measured. Scanning the sedimentation cell from bottom to top permits accurate inventory of particles while minimizing the time required to resolve the separation of fine particles. Vibratory sieve 'analysette 3 M' from Fritsch GmbH provides microprecision sieving with automatic weighing of sieve sets, while particle size distribution is determined by sieving. The TriStar 3000 gas adsorption analyzer from Micromeritics Instrument Corporation is a fully automated surface area and porosimetry analyzer, providing three BET surface area measurements simultaneously in approximately 20 minutes. The AutoPore IV 9500 Series from Micromeritics Instrument Corporation characterizes a material's porosity by applying various levels of pressure to a sample immersed in mercury. Mercury porosimetry is applied over a capillary diameter range from 0.003 to 360 μm. The operating details and special features of these devices can be found in the respective brochures available from the manufacturers.

References

1. Allen, T., *Particle Size Measurements*, 4th edn. Chapman & Hall Publishers, 1990.
2. Allen, T., Sampling and classification of powders. In *ASM Handbook*, Vol. 7. ASM International Publishers, 1998, pp. 205–221.
3. Pope, L.R., Ward, Ch.W., *Manual on Test Sieving Methods*, 4th edn. ASTM Publisher, Mayfield, PA, 1998.
4. Kouzov, P.A., *Fundamentals of Particle-Size Analysis of Industrial Dusts and Particulate Materials*. Himiy Publishers, Leningrad, 1987 (in Russian).
5. Shimizu, K., Brown, G.M., Kobayashi, K., Skeldon, P., Thompson, G.E., Wood, G.C., Ultramicrotomy – a route towards the enhanced understanding of the corrosion and filming behaviour of aluminium and its alloys. *Corrosion Science*, 1988, 40(7):1049–1072.
6. Krajnikov, A., Gastel, M., Orter, H.M., Likutin, V.V., Surface chemistry of water atomised aluminium alloy powders. *Applied Surface Science*, 2002, 191: 26–43.
7. Neikov, O.D. et al., Advanced PM Aluminium Alloys Produced by New Rapid Solidification Technology. In *Proceedings of 2004 Powder Metallurgy World Congress*, Vol. 1. European Powder Metallurgy Association, 2004, pp. 230–235.
8. Faires, L.M., Inductively coupled plasma emission spectroscopy. In *ASM Handbook*, Vol. 10. ASM International Publishers, 1996, pp. 31–42.
9. Iacocca, R., Bulk and surface characterization of powders. In *ASM Handbook*, Vol. 7. ASM International Publishers, 1998, pp. 223–233.
10. Brunauer, S., Emmett, P.H., Teller, J., *Am. Chem. Soc.*, 1938, 60:309.
11. Young, D.M., Crowell, A.D., *Physical adsorption of cases*. Butterworth Publishers, London, 1962.
12. Panichkina, V.V., Uvarova, I.V., *Testing Methods of Dispersity and Specific Surface Area of Metallic Powders*. Naukova Dumka Publishers, Kiev, 1973 (in Russian).
13. Gregg, S.J., Sing, K.S.W., *Adsorption, Surface Area and Porosity*. Academic Press Publishers, 1982.
14. Lowell, S., Shields, J.E., *Powder Surface Area and Porosity*. Chapman & Hall Publishers, 1991.
15. Allen, T., *Particle Size Measurement, Vol. 2, Surface Size and Pore Size Determination*. Chapman & Hall Publishers, 1997.
16. Callis, C.F., Irani, R.R., *Miscellaneous Techniques, Particle Size: Measurements, Interpretation, and Application*. John Wiley & Sons Publishers, 1963.

17. *Method for Determination of Average Particle Size of Metal Powders Using the Fisher Subsieve Sizer, MPIF Standard 32*. MPIF Publishers, Princeton, 2003, pp 45–47.
18. Heinzer, P.J., Permeametry. In *ASM Handbook*, Vol. 7. ASM International Publishers, 1998, pp. 277–278.
19. Heinzer, P.J., Pycnometry. In *ASM Handbook*, Vol. 7. ASM International Publishers, 1998, pp. 278–280.
20. AutoPore 1V Operator's Manual, Micrometrics, 2004.
21. Naidich, Yu.V., Perevertailo, V.M., Lavrinenko, I. A., Kolesnichenko, G.A., Zhuravlev, V.S., *Surface Properties of Melts and Solids and their Usage in Material Science*. Naukova Dumka Publisher, Kiev, 1991 (in Russian).
22. Good, R.J., Mikhail, R.Sh., *Powder Technol.*, 1981 29(53).
23. Hiemenz, P.C., Rajagopalan, R., *Principles of Colloid and Surface Chemistry.* Marcel Dekker Puplisher, 1997.
24. Rootare, H.M., A Review of Mercury Porosimetry. In *Advanced Techniques in Powder Metallurgy, Vol. 5. Perspectives in Powder Metallurgy.* Plenum Press Publisher, 1970.
25. Kloubek, J., *Powder Technology*, Vol. 7. 1981, pp. 63–162.
26. Plachenov, T.G., Kolesencev, S.D., *Porosimetry*. Himiy Publishers, Leningrad, 1988 (in Russian).
27. Giesche, H., Mercury Porosimetry. In *ASM Handbook*, Vol. 7. ASM International Publishers, 1998, pp. 280–286.
28. ASTM standard D 4284, Pore Volume Distribution of Catalysts by Mercury Intrusion Porosimetry. In *Annual Book of ASTM Standards*, Vol. 5.03, ASTM International Publishers, 2003.
29. ASTM standard C 493, Bulk Density and Porosity of Granular Refractory Materials by Mercury Intrusion Porosimetry. In *Annual Book of ASTM Standards*, Vol. 15.01, ASTM International Publishers, 2003.
30. Jenike, A.W., Storage and Flow of Solids, *Bulletin of the University of Utah*, Vol. 53, No. 26. University of Utah Publisher, Salt Lake City, 1964.
31. ASTM standard D 6128, *Standard Shear Testing Method for Bulk Solids Using the Jenike Shear Cell*. ASTM Publishers, 1977.
32. Carson, J.W., Bulk properties of powders. In *ASM Handbook*, Vol. 7. ASM International Publishers, 1998, pp. 287–301.
33. Freeman, G., Production of Cobalt-Base Powders. In *ASM Handbook*, Vol. 7. ASM International Publishers, 1998, pp. 179–181.
34. Poster, A.R. (ed.), *Handbook of Metal Powders*. Reinhold Publisher, 1966.
35. Tundermann, J.H., Production of Nickel-Base Powders. In *ASM Handbook*, Vol. 7. ASM International Publishers, 1998, pp. 167–171.
36. Lux, B., Zeiler, B., Production of Tungsten and Tungsten Carbide Powders. In *ASM Handbook*, Vol. 7. ASM International Publishers, 1998, pp. 189–201.
37. Brown, R.L., Richards, J.C., *Principles of Powder Mechanics*. Pergamon Press Publisher, 1977.
38. Yokoyama, T., Fluidity of Powder. In *Powder Technology Handbook*. Marcel Dekker, Inc, 1997, pp. 413–425.
39. Henein, H., Brimacombe, J.K., Watkinson, A. P., The Modeling of Transverse Solids Motion in Rotary Kilns. *Metall. Trans. B*, 1983, 14:191–205.
40. Lumpman, S., Compressibility and Compactibility of Metal Powders, In *ASM Handbook*. ASM International Publishers, Vol. 7, 1998, pp. 302–309.

SECTION 2 Powder Production Methods

Contents

For a more detailed Section Contents list, please see the book Contents pages that start on page v

Chapter 2

Mechanical Crushing and Grinding

Oleg D. Neikov, Frantsevich Institute for Problems of Materials Science (IPMS), Kiev, Ukraine

Comminution is the oldest mechanical operation for size reduction of solid materials and an important step in many processes where raw materials are converted into intermediate or final products. It is the most widely used method of powder production for hard metals and oxide powders. Secondary grinding of spongy cakes of reduced oxide, electrolytic or atomized powders is the most common milling process; hammer crushers and rod mills are used for this purpose. Depending on the degree to which the material is sintered, every primary particle size distribution is re-established during grinding or larger agglomerates are produced.

Demand for fine or ultrafine particles is increasing in many kinds of industries, particularly in solid-state alloying or high-energy milling, but grinding of proper metal powders has received minimal attention to date. The energy efficiency of comminution is very low and the energy required for comminution increases with a decrease in produced particle size.

The main purposes of grinding include:

- Particle size reduction
- Particle size growth
- Particle shape change (to flake shape)
- Agglomeration
- Mechanical alloying (solid-state alloying)
- Blending of two or more materials or mixed phases
- Modifying or changing of properties of a material (density, flowability or work hardening)
- Non-equilibrium processing of metastable phases such as amorphous alloys, extended solid solutions and nanocrystalline structures.

The grinding process disintegrates, deforms or cold welds the impacted particles. Grinding also may produce polymorphic transformation [1]. The specific effect that grinding has on a powder depends on its physical and chemical properties, the vacuum, gaseous or liquid environment in which the operation is performed and grinding conditions.

Four types of forces act on particulate material during grinding: impact, attrition, shear and compression. Impact is the instantaneous striking of one object by another; both objects may be moving or one may be stationary. Attrition is the producing of particles by the rubbing action between two bodies or wear debris. Shear consists of cutting or cleaving of particles and usually is combined with other types of force. Shear contributes to breaking particles into separate pieces with a minimum fine yield. Compression is the slow application of compressive forces to a solid. This type of grinding action is realized in jaw crushers, predominantly when the material is hard and non-ductile.

Design and process advances have been based principally on empirical and semi-empirical data. Fundamental research of grinding ductile metals is missing, although much is known phenomenologically about the process.

Breaking occurs in hard, brittle materials, with minimal particle deformation and agglomeration due to welding. Deformation, cold welding and breaking happen in varying degree with both hard and soft, ductile materials.

Principles of Grinding

Existent theoretical views on the crushing and grinding patterns of relationships are based on the mechanics of continua positions. The disruption process of a solid passes through several phases:

- Accumulation of defects leading to local concentration of strains

- Formation of the embryonic microcracks, i.e. rupture of continuity crystal lattice in several cells
- Development and joining of embryonic microcracks down to formation of main disruption crack
- Disruption of solid into several parts.

Let us discuss these disruption process stages in more detail.

The dislocations, arising from unequal atom numbers in neighboring lattice planes, are a main type of crystal lattice defect which defines the strengthening properties of a solid. Odd atoms in a structure remain without a chemical bond. In that case, a defect of structure, i.e. a dislocation, occurs (Figure 2.1).

The action of an external load can displace this defect from one part of a crystal to the other and, finally, if on the path of motion the obstacles do not meet, the dislocation appears on the surface where a step in one atom is formed. To such unimpeded displacement of dislocations (in extremely schematic form), a ductile deformation mechanism is represented.

By application of deformative load to a solid in which there are braking cen-ters of dislocations, the accumulation of dislocations is observed by obstacles interfering with their motion. In these locations, high local stresses appear which can turn out to be sufficient for integration of some of the dislocations together and the formation of an embryonic microcrack (Figure 2.2). At that stage, the stresses in material directly adjoining the microcrack boundaries decrease and elastic energy is released. The value of the latter is approximately proportional to the square of the crack length or its depth penetration in the crystal. Energy, which is needed for forming two new surfaces, is proportional to crack length in the first power. Thus, a small crack, for its growth, consumes more surface energy due to relaxation of the stresses that designate its stability.

However, if a crack affected by applied stress begins to develop, the character of the process is changed. With growth of crack size, the released energy is increased in proportion to the second power of the crack length. At a definite crack length, the crack begins to release more energy than it consumes. Then, an abrupt change occurs and the crack can propagate in the body of the metal at high speed and is ramified, forming a break surface.

The conception about the breaking as a process and its subsequent growth arose because the usually observed ultimate strength values, from 10 to 1000 MPa, differ markedly from theoretical data calculated at the strength of interatomic bonding, amounts to 10 to 100 GPa.

Application of compressive forces to solids can significantly increase the durability of solids by prevention of the development of the microcracks. Therefore, the slow application of compressive forces to solids accounts for the high power-consumption and low efficiency of this technique. The microcracks can readily develop under the influence of tensile and shear stresses.

In the development phase of microcracks, the adsorption of surfactants has great importance. Their penetration into the microcrack mouth weakens interatomic bonding and facilitates crack propagation, while adsorption on newly formed surfaces prevents its closing (Rebinder's effect). Thus, the breaking process acquires a mechanochemical character.

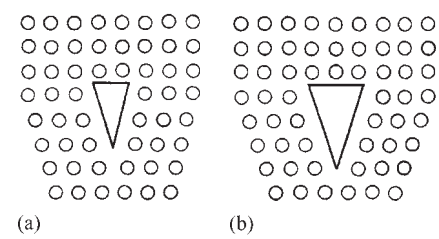

Figure 2.2 Confluence of dislocations with formation of the embryonic microcrack at (a) two and (b) three dislocations.

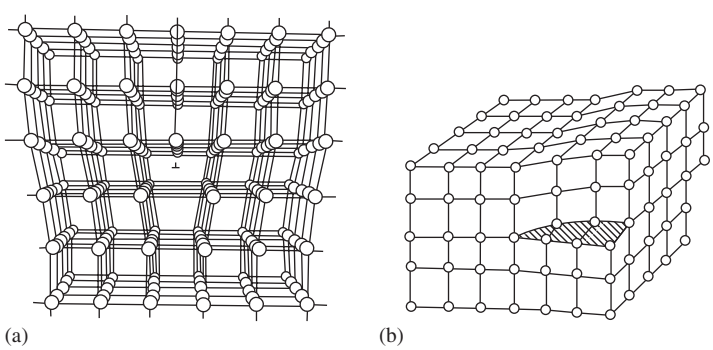

Figure 2.1 Scheme of (a) linear and (b) helical dislocations in crystal lattice.

However, observance of a number of conditions is necessary for the development of Rebinder's effect. Above all, action of surfactant becomes apparent when a solid is in the strained state. Environmental high pressure promotes penetration of surfactant into embryonic microcracks. Optimum temperature in the range 100–150°C is also a requisite condition, while the intensive thermal fluctuations which occur above a certain limit may result in dissipation of dislocation clusters and stabilization of microcracks.

It is possible to represent the impact process in the following way. A process model at the moment of collision, at which particles are trapped between two colliding balls, is shown in Figure 2.3.

This effect is typical in dry and wet grinding operations that use colliding devices such as tumbling, vibratory and attrition ball mills. The number of particles within the incremental volume subjected to impact compression stress may range from a single to a multitude, depending on the average particle size and the radius of the ball or curved surfaces contacting the trapped incremental volume.

The number of particles trapped between two balls on impact in a loose powder mass increases as the ratio of the ball diameter D to the particle diameter d increases. At the high ratios of D/d characteristic in milling of fine particles (less 150 μm), the trapped volume consists of particles within the mini-volume BB′DD′ (see Figure 2.3). Outside this incremental volume, the seeming (apparent) density of the powder sharply decreases to the density of the agitated loose particulate material or suspension in the case of wet milling.

The amount of powder trapped and the size of the trapped volume depends on many factors, along with ratios of D/d, including particle size, apparent density of the particle cloud, the presence of slurry and its concentration and viscosity, air or gas pressure within the mill, surface roughness of the balls, velocity of the balls and kinetic energy of the balls at the instant of collision.

In the gaseous atmosphere prior to impact, the majority of particles, of lesser size for the most part, is ejected as the balls approach each other, while the remaining fraction becomes trapped and compacted between the decelerating balls at the moment of collision. If the impacting force is sufficient, the trapped incremental volume of powder is compacted to an agglomerate particle (Figure 2.4), which is released when elastic energy impels the balls apart.

If bonding by welding or adhesion occurs between contacting surfaces and bonding forces are sufficient, the agglomerate does not break apart. Similarly, particles may bond to the surfaces of the balls, which may become coated with the powder. If the compressive impact forces exerted by the balls and particles are sufficient, particles fracture (see Figure 2.4d) or compact (see Figure 2.4c) within a critical zone of diameter X_c and thickness t, within the boundaries of BB′ and DD′ (see Figure 2.3). The initial zone of compaction theoretically does not exceed AA′EE′. Density of the trapped bed of particles varies from

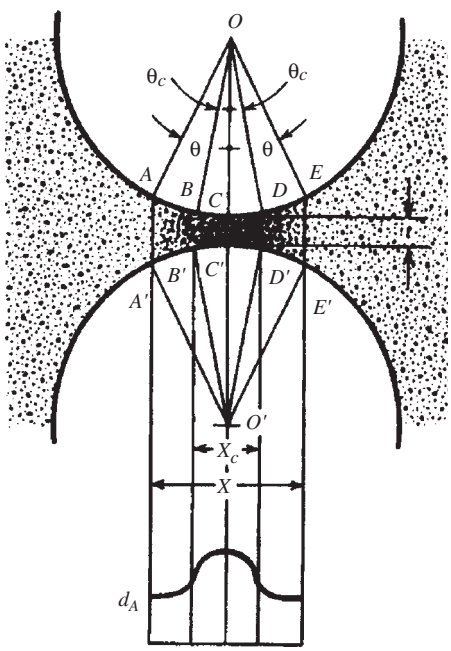

Figure 2.3 Model of impact act at a moment of maximum impacting force illustrating the formation of a microcompact. (Source: Ref 2®)

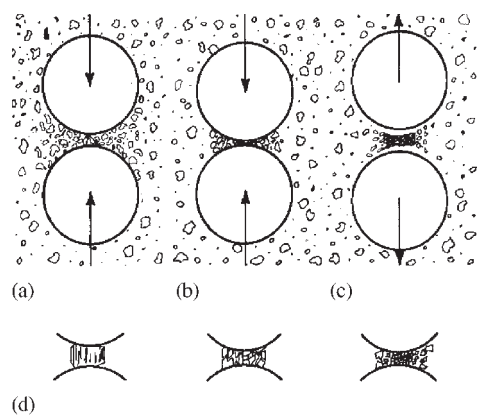

Figure 2.4 Model of process trapping an incremental volume of ductile powder between two balls including (a) series of balls coming together, (b) impact event, (c) release of agglomerate by elastic energy and (d) brittle single particle.

the maximum at the point CC′ to the density of the freely agitated powder outside the two *A*–*A*′ and *E*–*E*′ boundaries.

Fragmentation is similar to impact compacting of a radially micropowder compact. Compaction begins with a powder mass that is characterized by relatively large spaces between particles compared to the particle size.

The first stage of compaction represents rearrangement of the particles. Particles slide past one another with a minimum of deformation and fracture, producing some fines, especially from brittle particles. During this stage, flowability is reduced and void spaces are partially filled with fine particles. During this stage, particle shape plays a vital part. Spherical particles, having the least friction, are almost totally ejected from between colliding balls; flake or irregular particles, having the greatest frictional resistance to flow, tend to be retained between the nearing balls.

During the second stage, plastic deformation and cold welding have major effects on comminution for ductile materials. For hard and brittle metallic materials, plastic deformation and welding have little effect on comminution. Most metals become harder during the second stage, which increases deformation resistance.

The closing, third stage of compaction, involving particle fracture, results in further deformation and/or fragmentation of the particles. The microcompacts range from very small for slightly ductile materials to relatively large for highly ductile metal powders, depending on the strength of the bonds between particles which, in turn, depends on factors such as conformance of the impact force, bonding surfaces, oxide films, surface cleanliness and temperature.

A. Griffith's theory supposes that a brittle material has instant cracks fragmented within it and that fracture arises from these cracks [2,3]. The stress σ_c at which a crack spreads depends on the size of the crack. The general form of the fracture equation is:

$$\sigma_c = A\left[\frac{\gamma E}{c\left(1-\mu^2\right)}\right]^{0.5}$$

where A is a numerical constant that depends on crack geometry and its location, mode of loading and particle sizes (for example, A is $\sqrt{2/\pi}$ for the slit crack in an infinite sheet), c is the size of the crack, E is modulus of elasticity, μ is Poisson's ratio and γ is the surface energy of ground material. Thus, according to the above equation, measured strength depends on the size of the crack, elastic properties and surface energy. For brittle materials, γ ranges from 10^3 to 10^4 erg/cm^2. The Griffith's equation leads to gross errors.

The stress σ for fracture of a particle is represented by [3]:

$$\sigma = \sqrt{\frac{2Er}{L}}$$

where L is the length of the crack and r is the radius of the crack tip. When stress at the crack tip equals the strength of the cohesion between atoms, all new surface energy is supplied by the stress itself from elastic strain energy and corresponds approximately to the Griffith's model.

Three types of flaw have been identified by Gilvarry [4], with respect to location on the surface or interior of single particles: facial, volume or edge. According to Gilvarry, flaws exhibit a Poisson-type distribution and the three types of flaw are distributed interdepedently of each other, as a consequence of the randomness of fracture surface orientation and the fracturing stress.

During grinding, a major part of the energy input is expended on various internal processes that do not contribute to particle fragmentation. As grinding proceeds into the ultrafine region, fracturing mode varies and conditions that were insignificant when particles were relatively large become controlling factors.

If the particle deforms plastically, fracture is difficult to induce and the probability that stress will occur is reduced further. As fragments decrease in size, the tendency to aggregate increases and fracture resistance increases. Particle fineness approaches a limit as grinding continues and maximum energy is expended. Generally, as batch comminution proceeds over an extended time, the mean applied stress needed for particle failure increases, while the magnitude of local stresses available to initiate fracture decreases.

Typical changes in ductile powder particle morphology are shown in Figure 2.5. These occur during wet milling of gas atomized cobalt-base alloy powders due to the following processes: microforging, fracture, agglomeration and deagglomeration.

Microforging is the predominant process during initial grinding as a result of compression shape forming of ductile metal particles by impact from the milling medium (see Figure 2.5b).

After a certain period of grinding, particles deform to the state that cracks initiate, propagate and ultimately fracture the particles. Particles formed from irregular or spongy particles contain fissures and cracks that facilitate compression, fatigue failure and

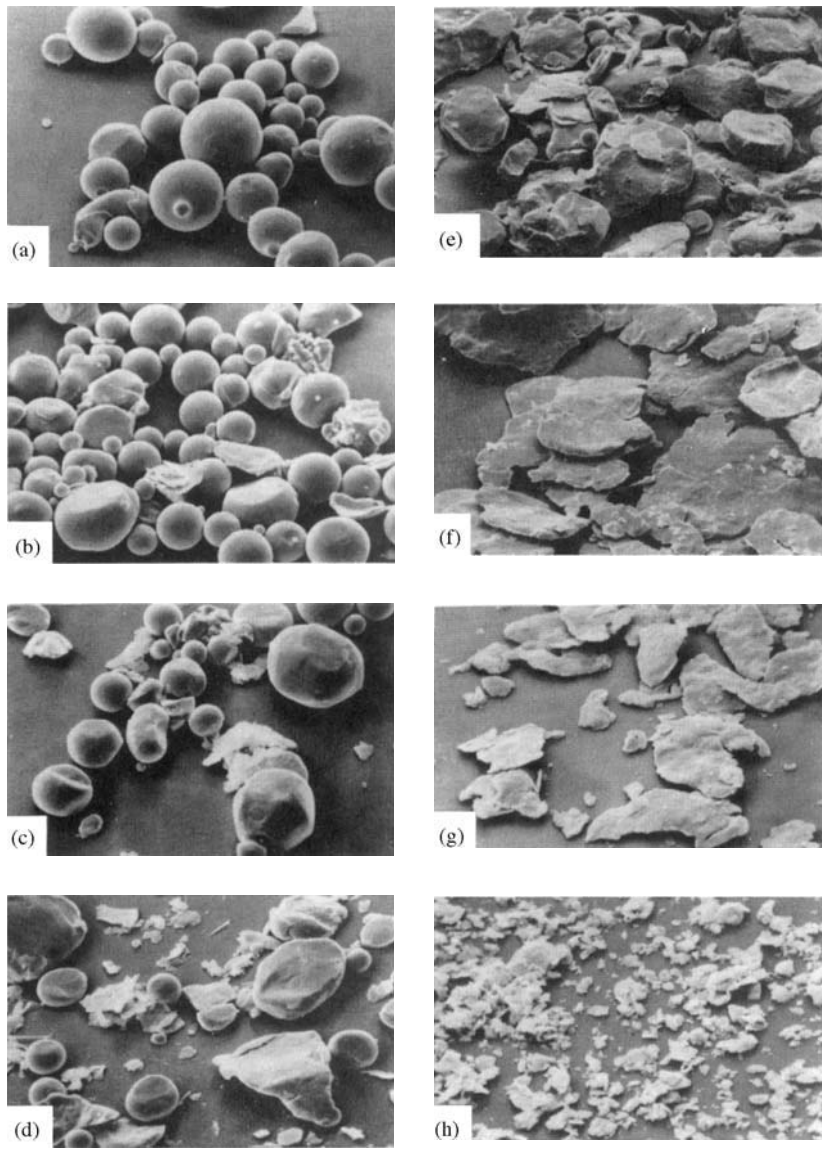

Figure 2.5 Scanning electron micrographs of stellite 21 cobalt base alloy powder, wet milled in ethyl alcohol with aluminum nitrate grinding aid. (a) As produced gas atomized powder; (b) after 1 h grinding; (c) after 2 h; (d) after 4 h. (e) after 8 h; (f) after 16 h; (g) after 32 h; (h) after 64 h. (Source: Ref 2®)

fragmentation, compared to the smooth, relatively non-porous spheroidal particles formed by atomization. Some friable metals (such as antimony, bismuth, silicon, manganese and chromium) and brittle intermetallic alloys (for example, copper–aluminum, aluminum–magnesium, copper–tin, nickel–iron, nickel–zirconium and phosphorus–copper) can be milled easily.

Agglomeration of particles may appear by welding, locking of spongy or rough surfaces, or autoadhesion. Autoadhesion is the molecular interaction themselves, characterized by van der Waals forces.

Deagglomeration is a process that breaks up agglomerates formed by autoadhesion.

Grindability

When a metal is plastically deformed by cold working, most of the mechanical energy of the deformation process is converted in the heat. However, a

small amount (approximately 5%) is conserved in the metal, thereby raising its internal energy. The energy connected with permanent lattice strain or cold work is minimal for hard, brittle particles, but can be large for ductile materials. The energy expended to overcome the friction between particles is translated to heat and fulfils no useful work in grinding.

If the temperature of the powder rises above a certain level, the cold processed metal particles may undergo recovery and recrystallization. Heat is generated by particle deformation and by elastic deformation of the metal grinding balls and grinding chamber. Generally, the temperature rises during severe cold working, abruptly falls just before cold work attains saturation levels and then slowly decreases after extended milling time. Water-jacketed milling chambers usually are required for large, high-energy vibratory and attrition mills that reach temperatures above 200°C.

Grindability characterizes the comminution efficiency of a grinding technique and is determined by a strictly defined mode. Usually one of the two following methods is used.

Hardgrove Grindability Index (ASTM D409 Standard)

The device to measure the grindability consists of a top rotating ring with eight balls of 1 inch (25.4 mm) diameter. A load of 64 ± 0.5 lb (29.5 ± 0.23 kg) is applied on the top rotating ring.

The hardgrove grindability index is defined as:

$$\text{HGI} = 13 + 6.93w$$

where w (g) is the mass of ground product finer than 74 μm.

Bong's Work Index (JIS M4002 Standard)

Bong's Work Index is used in Bong's law of comminution energy. It states that the total work useful in breakage is inversely proportional to the length of the square root of the size of the product particles, directly proportional to the length of the formed crack tips and directly proportional to the square root of the formed surface:

$$W = W_i\left(\frac{10}{\sqrt{d_p}} - \frac{10}{\sqrt{d_f}}\right) = C'_B\left(S_p^{0.5} - S_f^{0.5}\right)$$

where W is specific energy expenditure in kilowatt-hours per tonne and d_p and d_f are the particle size in microns at which 80% of the corresponding product and feed passes through the sieve; C'_B is a constant depending on the characteristics of materials; S_p and S_f are the specific surface areas of product and initial feed, respectively. W_i is called Bond's Work Index in kilowatt-hours per tonne. It is given by the empirical equation:

Table 2.1 Set of steel balls for test by Bond's Work Index

Diameter (mm)	Number of balls
36.5	43
30.2	67
25.4	10
19.1	71
15.9	94
Total	285

$$W_i = \frac{1.1 \times 44.5}{P_1^{0.23} G_{b.p}^{0.82}\left(\frac{10}{\sqrt{d_p}} - \frac{10}{\sqrt{d_f}}\right)}$$

where P_1 is the sieve opening in microns for the grindability test, $G_{b.p.}$ (g/rev) is the ball mill grindability, d_p is the product particle size in microns (80% of product finer than size P_1 passes) and d_f is the initial feed size in microns (80% of feed passes). A standard ball mill is 305 mm in internal diameter and 305 mm in internal length charged with 285 balls as tabulated in Table 2.1. The lowest limit of the total mass of balls is 19.5 kg. The mill is rotated at 70 rev/min. The process is continued until the net mass of undersize produced by revolution becomes a constant $G_{b.p}$ in the above equation.

In fine grinding, when P is smaller than 70 μm, the Work Index W_i is multiplied by a factor f to account for the increased work input. The factor f is found from the following empirical equation:

$$f = \frac{P + 10.3}{1.145P}$$

The Work Index is an important factor in designing comminution processes and has been widely used.

Crushing and Grinding Equipment

A major objective of comminution is to liberate minerals for concentration processes. Another objective

is to manufacture powder with particles of required sizes. Comminution processes generally consist of several stages in series. Various types of crushing and grinding equipment have been used industrially for these objectives.

Crushers

Crushers are widely used as a primary stage to produce the particulate product finer than about 50–100 mm in size. They are classified as jaw, gyratory and cone crushers based on compression, cutter mill based on shear and hammer crusher based on impact.

A *jaw crusher* consists essentially of two crushing plates, inclined to each other forming a horizontal opening by their lower borders. Material is crushed between a fixed and a movable plate by reciprocating pressure until the crushed product becomes small enough to pass through the gap between the crushing plates. Jaw crushers find a wide application for brittle materials. For example, they are used for comminution of porous copper cake.

A *gyratory crusher* includes a solid cone set on a revolving shaft and placed within a hollow body, which has conical or vertical sloping sides. Material is crushed when the crushing surfaces approach each other and the crushed products fall through the discharging opening.

Hammer crushers are used either as a one-step primary crusher or as a secondary crusher for products from a primary crusher. They are widely used for crushing of hard metal scrap for different hard metal recycling processes.

Pivoted hammers are pendulous, mounted on the horizontal axes symmetrically located along the perimeter of a rotor and crushing takes place by the impact of material pieces with the high speed moving hammers and by contact with breaker plates. A cylindrical grating or screen is placed beneath the rotor. Materials are reduced to a size small enough pass through the openings of the grating or screen. The size of product can be regulated by changing the spacing of the grate bars or the opening of the screen.

The feature of the hammer crushers is the appearance of elevated pressure of air in the discharging unit of the crusher and underpressure in the zone around of the shaft close to the inside surface of the body side walls. Thus, the hammer crushers also act as high-pressure forced-draught fans. This may lead to environmental pollution and product losses in fine powder fractions.

A design for a hammer crusher (Figure 2.6) allows essentially a decrease of the elevated pressure of air in the crusher discharging unit [5]. The A-zone beneath the screen is communicated through the hollow ribs and openings in the body side walls with the B-zone around the shaft close to the inside surface of body side walls. As a result, circulation of suspended matter in the gas between A- and B-zones is established and high pressure of air in the discharging unit of crusher is reduced.

Grinding Techniques

Ball-medium Types

In ball-medium types, the grinding energy is transferred to materials through such media as balls, rods and pebbles by moving the mill body. Based on the mode of motion of the mill body, ball-medium mills are classified as tumbling ball mills, vibration mills and planetary mills.

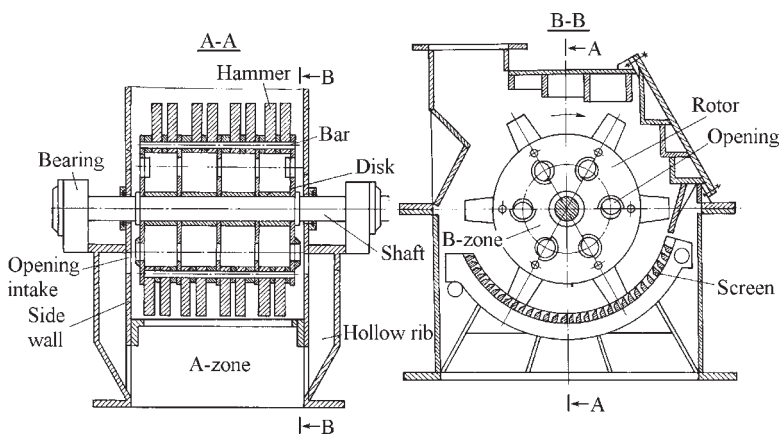

Figure 2.6 Hammer crusher.

Tumbling Ball Mills

Tumbling ball mills or ball mills are most widely used in both wet and dry systems, in batch and continuous operations, and on a small and large scale.

Grinding elements in ball mills travel at different velocities. Therefore, collision force, direction and kinetic energy between two or more elements vary greatly within the ball charge. Frictional wear or rubbing forces act on the particles, as well as collision energy. These forces are derived from the rotational motion of the balls and movement of particles within the mill and contact zones of colliding balls.

By rotation of the mill body, due to friction between mill wall and balls, the latter rise in the direction of rotation till a helix angle does not exceed the angle of repose, whereupon, the balls roll down. Increasing of rotation rate leads to growth of the centrifugal force and the helix angle increases, correspondingly, till the component of weight strength of balls become larger than the centrifugal force. From this moment the balls are beginning to fall down, describing during falling certain parabolic curves (Figure 2.7). With the further increase of rotation rate, the centrifugal force may become so large that balls will turn together with the mill body without falling down. The critical speed n (rpm) when the balls are attached to the wall due to centrifugation:

$$n = \frac{42.3}{\sqrt{D_m}}$$

where D_m is the mill diameter in meters. The optimum rotational speed is usually set at 65–80% of the critical speed. These data are approximate and may not be valid for metal particles that tend to agglomerate by welding.

The minimal magnitude of ball size is calculated in millimeters from the equation:

$$d_{b.min} = 10 d_{b.max} \sqrt[3]{\frac{\sigma^2}{0.128 E \rho_b D}}$$

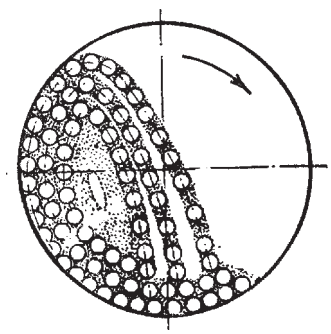

Figure 2.7 Displacement of balls in mill.

where $d_{b.max}$ is the maximum size of feed (mm); σ is compression strength (MPa); E is modulus of elasticity (MPa); ρ_b is density of material of balls (kg/m^3); D is inner diameter of the mill body (m).

Generally, a maximum allowed ball size is situated in the range from $D/18$ to $D/24$.

The degree of filling the mill with balls also influences productivity of the mill and milling efficiency. With excessive filling, the rising balls collide with falling ones. Generally, filling the mill by balls must not exceed 30–35% of its volume.

Productivity of ball mills depends on drum diameter and the relation of drum diameter and length. Optimum ratio between length L and diameter D, L:D is, usually, accepted in the range 1.56–1.64.

The mill productivity also depends on many other factors: physical–chemical properties of feed material, filling of the mill by balls and their sizes, armor surface shape, speed of rotation, milling fineness and timely moving off of ground product.

It is possible to make an approximate calculation of the capacity of a ball mill by means of the equation:

$$N = (0.104 D^3 L \rho_{b.ap} \phi^{0.88} + 0.1 L n) \frac{1}{\eta_1 \eta_2}$$

where $\rho_{b.ap}$ is the apparent density of the balls; ϕ is the degree of filling of the mill by balls; n is revolutions per minute; η_1, and η_2 are coefficients of efficiency of electric engine and drive, respectively.

A feature of ball mills is their high specific energy consumption; a mill filled with balls, working idle, consumes approximately as much energy as at full-scale capacity, i.e. during grinding of material. Therefore, it is most disadvantageous to use a ball mill at less than full capacity.

Ball mills have the following advantages:

- universality and high capacity
- permanence of a prescribed milling fineness by certain capacity over long periods of time (with periodical addition of balls for compensation of their wear)
- reliability and safety, simplicity of servicing.

Shortcomings of ball mills:

- unhandiness and large weight
- grinding high specific energy consumption; energy is mainly consumed on wear of balls and wall armor, friction, heating of material, etc.
- noise during working.

Depending on the form of the body, ball mills are differentiated as cylindrical, tube and conical.

Depending on the discharging method, they are differentiated:

- mills with free discharge of ground product through a hollow trunnion
- mills with discharge along all length of the drum through a cylindrical sieve
- mills with an external separation system, in which a prepared product is separated from the under milled powder in separators outside of the mill drum.

Cylindrical Ball Mills

The steel drum of a ball mill (Figure 2.8) is lined inside by armor slabs. They have different sizes and form a rough inside surface. Due to such juts, the impact force of falling balls is strengthened. Initial material is fed into the mill by a screw feeder located in a hollow trunnion; ground product is discharged through the opposite hollow trunnion.

Cylindrical screen ball mills have a drum with spiral curved plates with longitudinal slits between them. Ground product passes into these slits and then through a cylindrical sieve and is discharged via the unloading funnel of the mill body.

Conical Ball Mills

A conical mill body consists of two cones and short cylindrical part located between them (Figure 2.9). Such a ball mill body is expedient, since efficiency is appreciably increased. Peripheral velocity along the conical drum scales down in the direction from the cylindrical part to the discharge outlet; the helix angle of balls is decreased and, consequently, their kinetic energy. The size of disintegrated particles also decreases as the discharge outlet is approached and the energy used decreases.

In a conical mill, most big balls take up position in the deeper, cylindrical part of body, thus the size of balls scales down in the direction of the discharge outlet.

For emptying, the conical mill is installed with a slope from bearing to one. In wet grinding, emptying is realized by the decantation principle, i.e. by means of unloading through one of two trunnions.

With dry grinding, these mills often work in a closed cycle. A scheme of the conical ball mill supplied with air separator is shown in Figure 2.10.

Air is fed to the mill by means of a fan. Carried off by air current, the product arrives at the air separator, from which the coarse particles are returned by

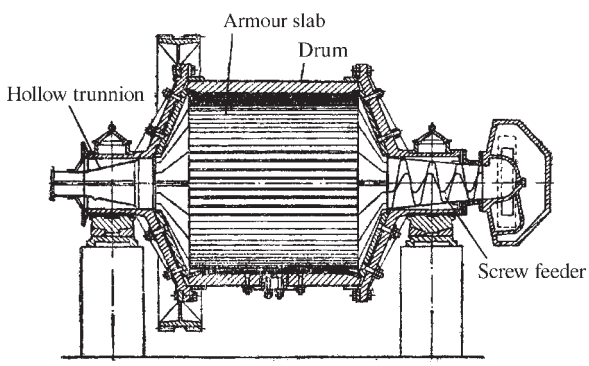

Figure 2.8 Cylindrical ball mill.

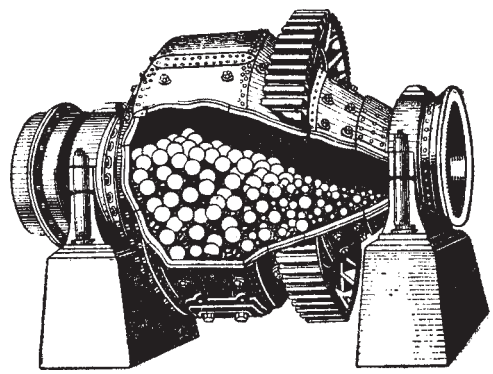

Figure 2.9 Conical ball mill.

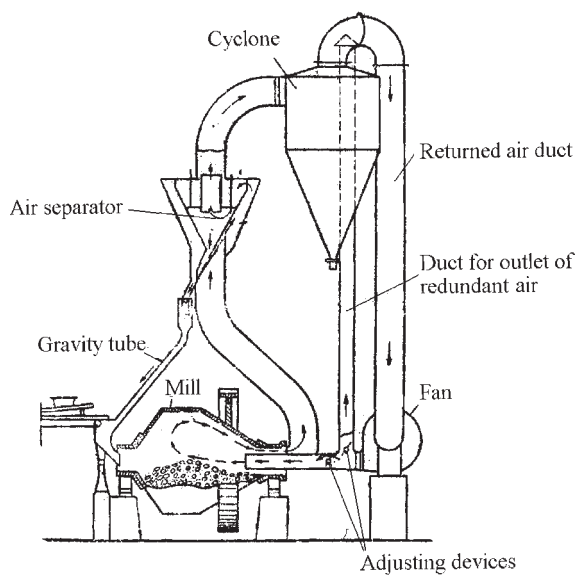

Figure 2.10 Conical ball mill supplied by air separator, working in closed cycle.

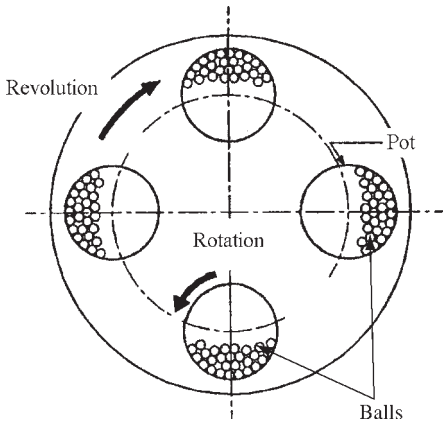

Figure 2.11 Schematic drawing of a planetary ball mill.

gravity via a tube into the mill. The finished product is entrapped in a cyclone, while the air is returned in the fan.

Rod Mills

For fine grinding, rod mills are also used, in which the rods are 40–80 mm in diameter and play a part in the grinding media. In such mills, the contacts between grinding rods and material occur along a line, not at separate points as in ball grinding.

Furthermore, coarse particles prevent the fine ones from welding together; consequently a more homogeneous product is produced.

Planetary Mills

A planetary mill consists of a revolving base disk and rotating mill pots as shown in Figure 2.11. Materials are ground by the large centrifugal force generated during revolution and rotation. The intensity of acceleration can be increased up to 150 g on the scale of the gravitational acceleration. Thus, the pot containing the grinding media rotates about two separate parallel axes. A planetary arm of radius, R_p, is centered at a point about which it rotates at angular velocity, ω_{pl}. The pot with radius r_p, rotates (usually in the direction opposite to the planetary arm) with angular velocity, ω_p.

Planetary ball mills have often been used for research studies. Typically, the commercially available Fritsch Pulverisette P-5 four-station planetary ball mill has been used (Figure 2.12). Grinding pots and balls are available in several different materials: agate, silicon nitride, sintered corundum, zirconia, chrome steel, chrome–nickel steel, tungsten carbide and plastic polyamide.

Figure 2.12 Fritsch planetary ball mill Pulverisette 5 with 4 bowl fasteners.

Vibratory Ball Mills

In the vibratory tube mill, oscillatory motion of the balls is used. The trajectories of the balls and particles are determined by many factors, including vibrational speed, amplitude and curvature of the mill chamber side walls. The balls gyrate around the chamber wall, sometimes traveling horizontally in a spiral trajectory. Balls also revolve at different rates and directions, causing substantial shearing action, which is desirable in blending operations.

Impact forces acting on powders in a vibratory mill are a function of the rate of milling, amplitude of vibration and mass of the milling medium. High-energy milling forces can be obtained by using high vibrational frequencies and small amplitudes of vibration.

Large production mills operate at relatively low vibrational frequencies and high amplitude, for example, 1000–1500 rpm and up to 12 mm.

The vibratory ball mill is also an excellent means of producing solid-state alloyed and dispersion strengthened metals.

Figure 2.13 shows the pilot- and production-size cascade two-stage vibratory mills. The material passes sequentially through two steps of the grinding. In large tube mills, vibratory motion of the medium decreases from the chamber walls to the center of the mill tube; consequently, the grinding effect is less at the center of the mill than adjacent to the chamber

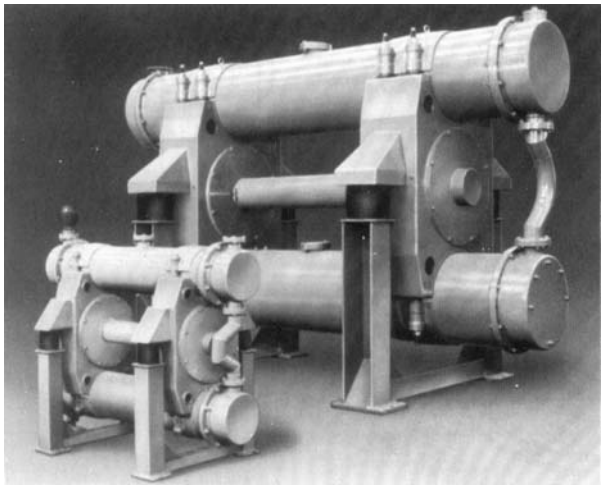

Figure 2.13 The pilot- and production-size cascade two-stage vibratory mills.

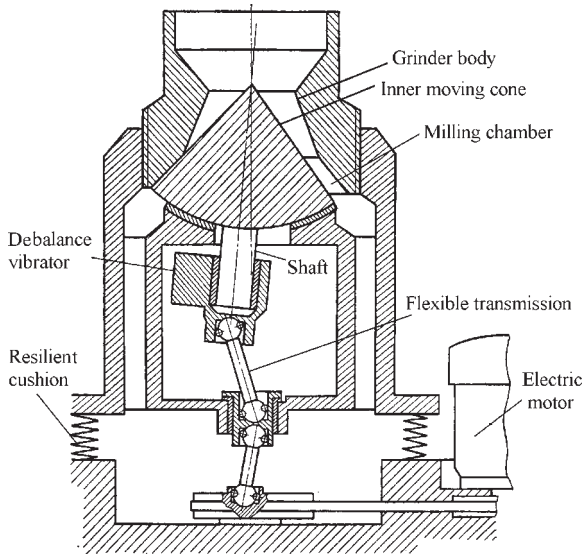

Figure 2.14 Principal constructional diagram of cone inertia crusher KID. (Source: Ref 6)

walls. Efficient operation is obtained at a ball fill of 60–80% of the volume of the mill chamber for tubes about 500 mm in diameter, with 100% fill of the volume between the balls.

In vibratory mills, the grinding medium receives rapid impulses at a rate proportional to the vibrational frequency of the mill. Impact forces acting on the powder exceed shearing and friction forces. Vibratory mills utilize smaller grinding media because of higher impact forces, frequencies and acceleration.

The rate of processing in a vibratory mill is proportional to the diameter of the balls and their density, proportional to the cube of the frequency of vibration, while not significantly affected by chamber diameter. The rate of processing increases as the amount of powder in the mill decreases and is greater with balls than other shapes, but rods provide the more homogeneous product.

Vibrating Grinders

Vibrating grinders are also called cone inertia crushers (KID) [6]. The principal constructional diagram of a KID is shown in Figure 2.14.

The grinder consists of a body with a conical inner surface in which is arranged an internal moving milling cone. The two cones form the milling chamber. On the axle of the internal moving milling cone a debalancing vibrator is fitted, which is driven through a flexible transmission. During vibrator rotation, the centrifugal force is generated, leading the internal cone to roll along the inner cone surface of the grinder body without clearance, if material is absent in the milling chamber or across a material layer. Such inner cone movement difference is possible owing to the absence in these machines of kinematic limitation of inner cone amplitude. Thus, KID does not have a discharging gap as for eccentric crushers, therefore, the diametric annular between cones is received by coincidence of their axes.

The idea of using the vibrator drive of the cone crusher appeared as long ago as 1925 (US Patent 1 553 333) and then its later versions (German Patent 679 800, 1952; Austrian Patent 200 598, 1957; and Japanese Patent 1256, 1972) were published. In the Soviet Union, the first experimental KID specimens had been created by the early 1950s. Now, in the various branches of industry in the Commonwealth of Independent States, KIDs with capacity from 1 to 300 t/h are produced.

The basic KID feature – absence of rigid kinematic bondings between the cones – allows the inner moving cone to change its amplitude depending on the variation of grindable material resistance or to stop if a large non-grindable body is encountered; but this is not detrimental and does not lead to plugging. Another KID feature is the nature of the crushing force. In KID, the crushing force is the sum of the centrifugal force of debalance of the inner cone by its gyrating movement. Such force is determined by mechanics and does not depend on the properties of the processed material. The crushing force acts as well on idle running as the result of gapless running in of cones. Therefore, the stability of the inner cone on its spherical support during idle running is ensured.

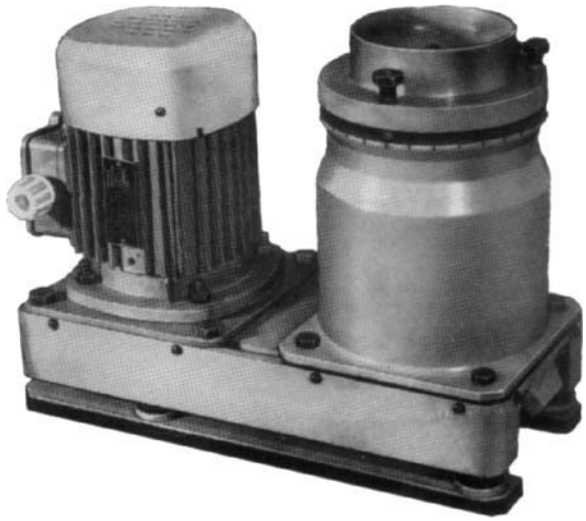

Figure 2.15 Vibrating grinder KID-60.

Table 2.2 Attributes of vibrating grinder KID-60

Characteristic	Unit	Magnitude
Piece size of a feedstock	mm	max 6
Productivity depending on particle sizes of obtained product:		
up to 71 μm	kg/h	3
up to 100 μm	kg/h	5
up to 0.5 mm	kg/h	10
up to 1.0 mm	kg/h	20
Capacity of motor	kW	0.55
Vibrational frequency	rpm	2800, 2300 and 1900
Overall dimension	mm	370 × 160 × 300
Weight	kg	25

This characteristic in combination with resilient isolation of KID from foundation allows a twofold increase in the inner cone vibration frequency.

The vibrating grinder KID-60 is shown in Figure 2.15. It can be adjusted to yield powder finer than 71 μm or coarser powder with almost complete absence of minus 71 μm powder (Table 2.2).

Technical characteristics of the main KID dimension-types are given in Table 2.3.

Medium Agitating Mills

In this technique, a large number of small grinding media are agitated by impellers, screws or disks in a chamber. Breakage occurs mainly by collision of the media. There are designs of the mill with a vertical or horizontal rotating shaft with wet or dry systems (Figure 2.16).

The medium agitating mill is regarded as one of the most efficient devices for micronizing materials and has been in regular use for the production of fine particles and mechanical alloying processes.

A typical stirred mill with a vertical rotating shaft and horizontal arms is shown in Figure 2.17. This stirring action causes a differential movement between balls and the material being milled, thus, ensuring that there is a substantially higher degree of surface contact than is achieved in tumbling or vibratory mills.

Milling takes place by impact and shear forces. The rotating charge of balls and milling product form a whirl, where the milling product is impacted by ball movement in various trajectories that collide within the dilated charge of grinding medium and powder.

The attrition mill agitator rotates at speeds ranging from 60 rpm for production units to 300 rpm for laboratory units and uses media that range from 3 to

Table 2.3 Technical characteristics of main cone inertia crushers (KID) dimension-types

Parameter		KID dimension-types							
	Unit	KID-100	KID-200	KID-300	KID-450	KID-600	KID-900	KID-1200	KID-2200
Productivity on minerals	t/h	0.03	0.16	2	7	25	45	80	300
Piece size of a feedstock, max	mm	10	35	20	30	50	70	80	110
Particle size in product, max	mm	0.3	1	2	3	5	6	8	12
Installed capacity	kW	1	5.5	11	30	75	160	250	600
Overall dimensions:									
depth	mm	400	920	1300	1400	2170	3115	3800	6600
width	mm	210	365	800	1000	1280	1970	2500	4000
height	mm	350	755	1450	1650	2170	2290	3000	6000
Weight	t	0.06	0.32	2	4	7.5	17	30	140

Source: Ref [6]

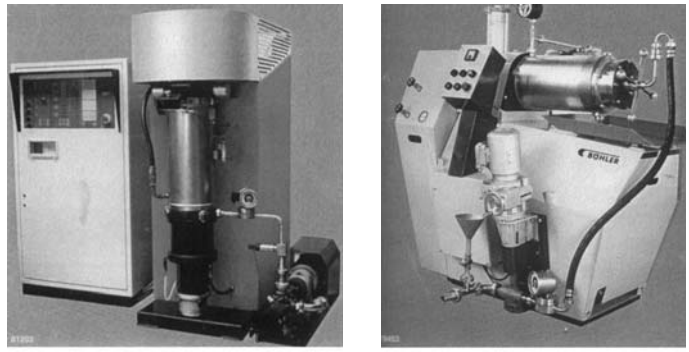

Figure 2.16 Attrition mill designs with (a) vertical or (b) horizontal rotating shaft.

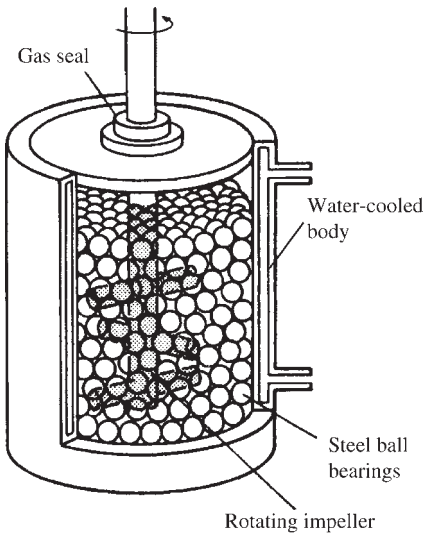

Figure 2.17 Schematic drawing of an attrition ball mill.

6 mm, while ball mills use large grinding media, usually 12 mm or larger, and run at low rotational speeds of 10–50 rpm. Power input to attrition mills is used to agitate the medium, not to rotate or vibrate heavy drums. Therefore, specific energy consumption of attrition mills is significantly less than with ball mills.

In the attrition grinding process, grinding time is related to medium diameter and agitator speeds [2], within given limits, as:

$$t = \frac{kd}{\sqrt{n}}$$

where t is grinding time required to reach a certain medium particle size; k is a constant that varies with the suspension being processed and the type of medium and mill being used; d is the diameter of the grinding medium; and n is shaft movement, in rpm.

Attrittion mills are classified as batch-, continuous- or circulation-type mills. In the batch mill, material is loaded into the chamber and ground until the desired dispersion and particle size are achieved. Chamber walls are jacketed so that either hot or cold water can be circulated to control and maintain the temperature of the charge. The batch attrition mills can process high-density material, such as tungsten carbide, as well as viscous materials, and are suitable for dry grinding and for producing dispersion-strengthened metals by means of mechanical alloying.

Continuous attrition mills, more appropriate for large production output, consist of a tall, jacketed chamber through which previously prepared slurry is pumped in at the bottom and discharged at the top. Grids located at the bottom and top retain the grinding medium as shown in Figure 2.18.

The circulation grinding system comprises an attrition mill and a large holding tank, generally ten times the volume of the grinding unit. The attrition mill contains grids that restrain the medium while the slurry passes through. Usually, the contents of the holding tank are passed through the system at a rate ten times per hour. The slurry can be monitored continuously and processing is stopped when the desired particle size dispersion is achieved.

Attrition mills find application for hard materials such as carbides and hard metals, where conventional tumbling and vibratory ball mills are less efficient. The principal advantages of attrition mills for mixing and blending tungsten carbide with cobalt as binder metal cutting tool powders include short milling time, production of fine particle size (submicron sizes) and enhanced coating of cobalt onto the surface of tungsten carbide particles [7]. Attrition mills effectively grind metals in inert atmospheres, such as in solid-state or mechanical alloying, but are not cost-effective.

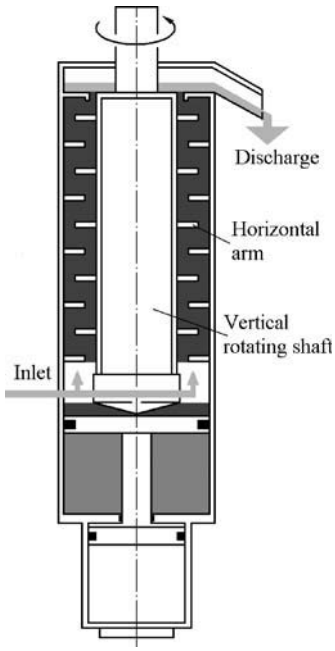

Figure 2.18 Schematic drawing of continuous attrition mill.

Jet Mills

The jet mill, also called the fluid-energy mill, is based on a coldstream impact process in which the materials are disintegrated by collision of a particle with a particle, a stationary target or a wall of the containing chamber. The collision energy is generated by a high-speed jet flow.

Fluid energy mills may be classified in terms of the mill action. In a fluidized bed jet mill, schematically illustrated in Figure 2.19, the grinding energy is created by gas streams from horizontal grinding air nozzles. Particles in the fluidized bed created by the gas streams are accelerated towards the center mill chamber colliding with slower moving particles. The particle-laden air transports the particles to the classifier. Coarse particles are rejected by the classifier and returned into mill. The particle-to-particle milling system prevents wear of the internal mill components. The supersonic nozzles are made of cemented tungsten carbide, but other wear-resistant materials or products being comminuted can be used to make these parts. Commercial jet mills are available from NETZSCH-Feinmahltechnik Company. The CGS 50 fluidized bed jet mill is shown in Figure 2.20. These jet mills allow finenesses ranging from $d_{97} = 2\,\mu m$ to $d_{97} = 70\,\mu m$. The adjustment of the desired finenesses is carried out by a dynamic air classifier integrated into the housing.

In another type of mill, two streams convey particles at high velocity into a chamber where they impact on each other.

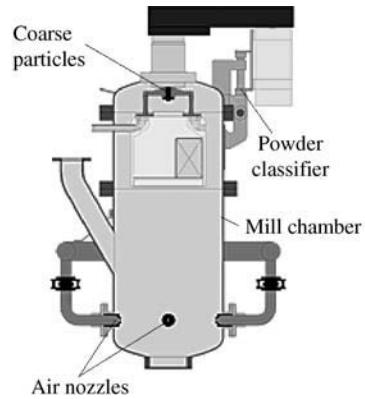

Figure 2.19 Schematic drawing of fluidized bed jet mill.

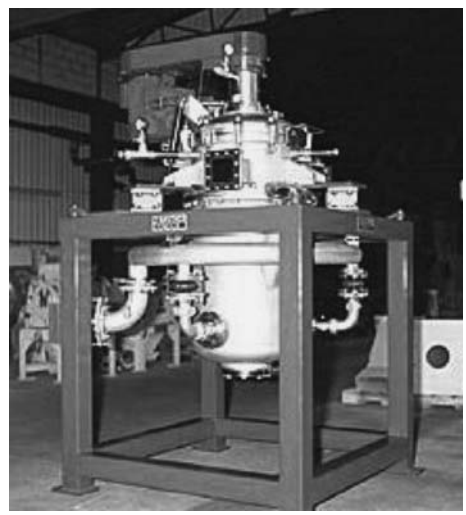

Figure 2.20 CGS 50 fluidized bed jet mill commercialy available from NETZSCH-Feinmahltechnik.

Rapidly expanding gases emerging from the nozzle create a cooling effect by adiabatic expansion. This effect is greater than the heat generated in the process. Thus, the process operates at well below room temperature. For example [2], a compressor operating at $56\,m^3$/min and 6.9 MPa is used.

The coldstream impact process is used to disintegrate hard, abrasive, relatively expensive materials such as tungsten carbide, tungsten alloys, molybdenum, beryllium and other alloys. The process rapidly reduces an initial particulate material of particles 3 mm or smaller to micron size. Process advantages include simplicity, low operating temperature, which prevents oxidation, and the ability to retain high purity and particle size control over the material being ground. The coldstream process generally produces a relatively oxide free powder. Most atomized powders have a slight oxide film on the surface of the particles. The coldstream process leads to the removal

Table 2.4 Technical characteristics of Fritsch Pulverisette planetary mills

Parameter	Unit	Planetary mill types			
		Pulverisette 4	Pulverisette 5	Pulverisette 6	Pulverisette 7
Grinding process	...	dry/wet	dry/wet	dry/wet	dry/wet
Speed of main disk	rpm	0 to 400	50 to 400	100 to 650	100 to 800
Input powder	W	9000	1500/1300	880	880
Max. feed size, depending on the material	mm	10	10	10	5
Max. sample quantity	ml	400	900	225	40
Final fineness	µm	<1µm	<1µm	<1µm	<1µm
Bowl number	n-d*	2	4	1	2
Overall dimensions:					
width	mm	600	580	370	370
depth	mm	800	670	530	530
height	mm	1100	570	500	500
Weight	kg	320	120	63	35
Physical properties of the sample materials**		H, Md-H, S, Br, T, M	H, Md-H, S, Br, M	H, Md-H, S, Br, M	H, Md-H, Br, M

*n-d, non-dimensional quantity

**H, hard; Md-H, medium-hard; S, soft; Br, brittle; T, tough; M, moist

of this oxide film and thus improves the properties of the powder. During processing, this brittle oxide film is stripped from the metal and broken up into fine dust. Lower density and smaller particle size of the latter facilitate its separation from the metal particles by air classification.

Other High-energy Milling Methods

Vibratory, attrition and large-diameter tumbling mills may be classified as high-energy ball mills and, as such, may be used effectively in solid state or mechanical alloying processes. Fluid energy mills are also related to high-energy mills.

Many commercially available high-energy laboratory-scale mills have been developed and used for research as a result of the sharp rise in interest in the last 20 years in the use of mechanical milling/alloying for the production of metastable materials such as amorphous alloys, quasicrystalline materials, metastable crystalline phases and nanostructured materials. These mills pro-cess small quantities of powder and, in some cases, they are more energy-efficient than larger industrial mills. Planetary ball mills have often been used for research studies. Frequently, the commercially available various types of Fritch Pulverisette planetary mills are used (Table 2.4). A Vario-planetary mill pulverisette 4 with wide variable grinding conditions is a perfect mill for mechanical activation and mechanical alloying for different materials.

A mill often used in research, especially in the USA, is the Model 8000 shaker mill of Spex. This high-energy ball mill agitates the charge of powder and grinding medium in three mutually perpendicular directions at approximately 1200 rpm. Ball velocities in such shaker mills are high, about 5 m/s. Glenmills Ultra centrifugal mill as well as Laboratory jet mill, Covington Engineering bead mills, Hwa Maw Machine bead mills, and Fritsch Vibratory micro mill Pulverisette 0 are also used in research investigations.

There are several other examples of specially designed mills for experimental investigations. These include the experimental ball mill designed by Calka and co-workers [2], which can change the milling action from predominantly impact to mainly shearing by changing the placement of strong permanent magnets, which are external to the vial. A disintegrator installation for fine grinding of metals and alloys, which are liable to form explosive airborne dust has also been designed [7]. The couple counter-rotation reinforced by hard alloy rotors are located in a chamber with controlled inert gas atmosphere. The stepless regulation of rotor speed in a wide range up to 15 000 rpm allows investigation of the grinding process and mechanical activation condition. The explosion-proof disintegrator technique is described in more detail in Section 5 'Safety engineering in the production of powders'.

Netzsch–Feinmahltechnik attritors are both horizontal and vertical; they include industrial as well as laboratory mills. The Netzsch LMZ horizontal type

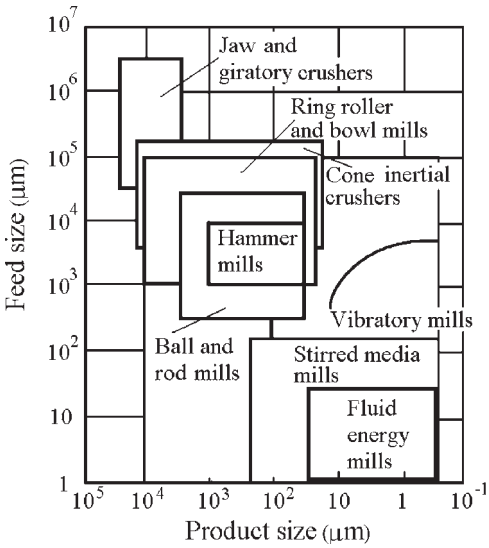

Figure 2.21 Possibilities of typical size reduction equipment for grinding a material of a given feed size to a desired product size.

attritor permits the production of ultrafine and nanopowders. The Zoz Simoloyer horizontal attritor mills are produced for both laboratory and pilot plant powder quantities [8,9].

High-energy ball milling has been employed to synthesize metastable structures analogous to other non-equilibrium processing methods such as rapid solidification and physical vapor deposition. However, the initial phase in the case of mechanical alloying is generally a crystalline solid or solids rather than liquid or vapor. The thermodynamics and kinetic factors that govern metastable phase formation can be very different. The more in detail mechanical alloying technique is described in Chapter 3.

Figure 2.21 shows the possibilities of typical size reduction equipment for grinding a material of a given feed size to a desired product size, when the purpose is comminution of a hard and/or brittle metal or ceramic material.

References

1. Senna, M., Kuno, H., Polymorphic transformation of PbO by isothermal wet ball-milling. *J. Am. Ceram. Soc.*, 1971, 54(5).
2. Koch, C.C., Milling of brittle and ductile materials. In *ASM Handbook*, Vol. 7. ASM International Publishers, 1998, pp. 53–66.
3. Griffith, A.A., *Trans. Roy. Soc. Lond.*, 1921, A221:163.
4. Gilvarry, J.J., Borgstrom, B.M., Fracture and comminution of brittle solids. *AIME Trans.*, 1961, 220. AIME.
5. Soviet Union Patent 1,242,233, Dec 1984.
6. Revnivcev, V.I., Denisov, H.A., Zarogatsky, L.P., Turkin, V.J., *Vibrating Disintegration of Solid Materials*. Nedra Publishers, Moscow, 1992.
7. Soviet Union Patent 1,044,328, June 1981.
8. Zoz, H. et al., Mechanical alloying of Ti-24Al-11Nb (at %) using the Simoloyer. *Metall.*, 1996, 59(9):575–579.
9. Zoz, H., Reichardt, R., Ernst, D., Simoloyer CM100s, semi-continuously mechanical alloying in a production scale using cycle operation – Part II. *Metall*, 1998, 51(9):521–527.

Chapter 3

Mechanical Alloying

Oleg D. Neikov, Frantsevich Institute for Problems of Materials Science (IPMS), Kiev, Ukraine

Mechanical alloying (MA) is a completely solid-state processing technique and phase diagram constraints do not impose here. This process permits the synthesis of novel alloys that are not possible by any other technique. Mechanical alloying is usually a dry, high-energy milling process and has been employed to manufacture a variety of commercially advanced materials. This technique was developed during the late 1960s by John Benjamin and his colleagues at the International Nickel Company (INCO) mainly to combine the advantages of precipitation strengthening and oxide-dispersion hardening in some nickel- and iron-base superalloys [1, 2].

The process consists of repeated welding–fracturing–welding of a mixture of powder particles in a high-energy ball mill. The powder particles are trapped between the colliding balls during the milling and undergo deformation, welding or fracture, depending on the mechanical behavior of the powder components. The process is used to produce a variety of materials and alloys: supersaturated solid solutions, amorphous materials, intermetallic compounds and metal–matrix composites.

The mechanical alloying stages with two ductile metal powders can be schematized in the following way. First, the particles undergo deformation and their morphology changes from the initial to a flattened one. In the following stage, the welding mechanism predominates, causing equiaxed particle formation. At this stage, oriented welding lines are observed. Then, welding and fracture mechanisms reach equilibrium and the formation of particles with randomly oriented welding lines predominates. The final stage is characterized by the steady state process, in which the microstructural refinement can continue, but the particle size and size distribution remain approximately stable.

The main attributes of mechanical alloying can be summarized:

- Production of a fine dispersion of second phase particles
- Extension of solid solubility limits
- Refinement of grain sizes down to nanometer range
- Synthesis of novel crystalline and quasi-crystalline phases
- Development of amorphous phases
- Disordering of ordered intermetallics
- Possibility of alloying difficult to alloy elements
- Inducement of chemical reactions at low temperatures
- Scaleable process.

The different aspects of MA have been widely discussed and reviewed in periodicals, in the proceedings of the International Symposia on Metastable and Mechanically Alloyed and Nanocrystalline Materials, and proceedings of international conferences on powder metallurgy. An annotated bibliography of the available literature has also been published [3].

Several terms in the literature are used to designate the processing of powders in high-energy mills. Mechanical alloying is the process when mixtures of powders, of different metals or alloys/compounds, are milled together. In this process, material transformation is accomplished to obtain a homogeneous alloy. While milling of homogeneous composition of powders, such as pure metal, intermetallic or prealloyed powders, has been usually named mechanical milling (MM), the term mechanical grinding (MG) is also used as a synonym of MM. However, in this article the term MA as fixed notion term is used to include both MA and MM.

Mechanical Alloying Process

The MA process starts with mixing of powders in the given proportion and charging the powder into the mill along with the grinding medium. This mixture is then milled for the required time till the final state is reached. This state occurs when the composition of every powder particle is the same as the proportion of the elements in the starting powder mixture. Sometimes the powder is milled either to form

metastable phases or to achieve certain desired properties. The obtained powder is further consolidated into the bulk shape and heat processed to achieve the specified microstructure and properties.

The raw materials used for MA are widely available as commercially pure powders with particle sizes usually up to 200 μm. At the same time, the powder particle size is not especially crucial. If it should be smaller than the grinding ball size, the powder particle size decreases exponentially with time and reaches a small value after a few minutes of milling. These powders include many kinds of pure metals, master alloys, prealloyed powders and refractory compounds. The oxygen content of commercially pure metal powders generally ranges from 0.05 to 0.2 wt%. Therefore, if it is relevant to phase formation, it becomes important to choose the appropriate purity of the powder. It is significant because, as a rule, the nature and amount of impurities in the system determine the character of the final phase formed and the chemical constitution of the alloy. Dispersion strengthened materials usually contain additions of oxides, carbides or nitrides. Oxides are the most common and such alloys are known as oxide-strengthened (ODS) materials.

MA allows the production of novel alloys by milling of ductile–ductile, ductile–brittle and fully brittle powder mixtures.

For MA process control, a process control agent (PCA) is introduced into the powder mixture, especially when the latter involves a substantial fraction of a ductile component. The PCAs are ordinary organic compounds which act as surfactant agents. They are adsorbed onto the surface of the powder particles and minimize contact between particles and thereby inhibit agglomeration.

In the development phase of microcracks in solids, the adsorption of surfactants has great importance. Their penetration into the microcrack mouth weakens the interatomic bonding, which facilitates the dissemination of cracks, while adsorption on a newly formed surface prevents its closing (Rebinder's effect). Thus, the breaking process acquires a mechanochemical character. This effect was discovered by P. Rebinder in 1928. The molecular nature of Rebinder's effect consists in facilitation of rupture and reconstruction of the intermolecular (interatomic) bonding in solids over active adsorption and, moreover, enough movable extrinsic molecules (atoms and ions) [4].

A wide range of PCAs has been used in practice. There are mostly organic compounds in the range from 0.3 to 4 wt% of the total powder charge and include stearic acid ($CH_3(CH_2)_{16}COOH$), hexane (C_6H_{14}), oxalic acid ($(COOH)_2 \cdot H_2O$), methanol, ethanol, acetone, isopropyl alcohol, heptane, Norcowax-22DSP, octane, toluene, trichlorotrifluoroethane, organosilicon compounds, etc. Alumina, aluminum nitrate, graphite and sodium chloride have also been used as PCAs [5, 6]. Most of these compounds decompose during milling and interact with the powder and form compounds, which are incorporated in the form of dispersions into the powder particles during milling.

Reactive metals such as aluminum, titanium and zirconium, when milled in the presence of air, can gather substantial amounts of oxygen and nitrogen and effect phase changes, including formation of new phases [7]. Completely non-oxidized finely milled powders may self-ignite when contacting the air [8]. Some metals, such as aluminum, nickel and copper, react with certain alcohols during milling to form complex metallo-organic compounds. Thus, aluminum reacts with isopropyl alcohol. Other metals such as titanium and zirconium can react explosively with chlorinated fluids such as carbon tetrachloride. Therefore, chlorinated fluids should never be used with reactive metals. Reactive milling (milling of metal powders in the presence of reactive solids/liquids/gases causing a chemical reaction to occur) has also been used to synthesize metal oxides, carbides and nitrides [9, 10]. Thus, milling of titanium in a nitrogen atmosphere has produced titanium nitride; several other nitrides have also been produced in a similar way. Milling of aluminum with carbon, or by use of PCA containing carbon, produced aluminum carbide ($A1_4C_3$), which appears dispersed inside the aluminum matrix and improves the properties of the alloy. The carbide in this case is only partially formed during milling; further heat treatment is required to accomplish the reaction of carbon with aluminum. Milling of tungsten with carbon (graphite) has produced tungsten carbide.

Use of a PCA ordinarily introduces some impurities into the powder. Therefore, to produce a high-purity alloy, use of a PCA should be eschewed. Generally, the choice of a PCA for milling depends on the nature of the powder being milled and the final product specification.

Milling Equipment

Tumbling ball mills, planetary mills, attritors and vibratory (shaker) mills are widely used for laboratory investigations of mechanical alloying processes. Attritors and ball mills are commercially available for MA and are much larger in size than such types of mills in laboratory use. The former are different in capacity, efficiency of milling and have additional arrangements for cooling, heating, etc.

Figure 3.1 Vario-planetary mill Pulverisette 4.

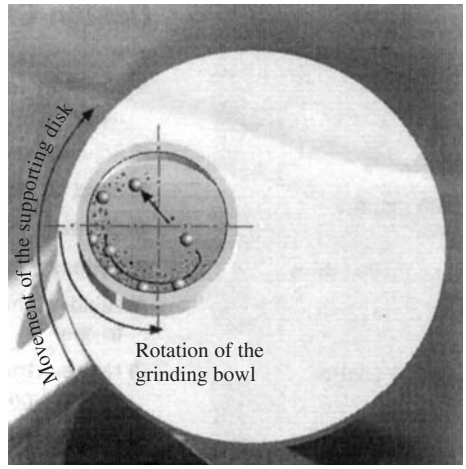

Figure 3.2 Schematic depiction of the ball motion inside the bowl of a planetary mill.

Planetary Ball Mills

Planetary ball mills have often been used for research studies, in particular by European investigators. These planetary mills are manufactured by Fritsch GmbH in Germany and marketed by Gilson Co., Inc. in the USA and Canada. Vario-planetary mill Pulverisette 4 with infinitely variable grinding conditions is the perfect mill for mechanical alloying and activation. It is equipped with two bowls (Figure 3.1). The bowls are arranged on a rotating support disk and a special drive mechanism causes them to rotate around their own axes. The centrifugal force produced by the bowls rotating around their axes and by the rotating support disc acts on the bowl contents, consisting of material to be milled and grinding balls. Because the bowls and the supporting disk rotate in opposite directions (Figure 3.2), the centrifugal forces alternately act in like and opposite directions. This results in the grinding balls running down the inside wall of the bowl stimulating the friction effect followed by the impact effect when the material being ground and the grinding balls lift off and travel freely through the inner area of the bowl and collide against the opposing inside wall.

In the vario-planetary Pulverisette 4 mill, the rotational speeds of grinding bowls and supporting disk can be adjusted completely independently of each other in contrast to standard planetary mills. By changing the transmission ratio, it is possible to accomplish mechanical alloying as well as mechanical activation. The performance features of Pulverisette 4 are:

- free selectable controlled rotation speed for grinding bowls and supporting disk
- programming of the grinding parameters by PC software
- reversing option to improve the milling results
- real-time display of the speeds to monitor the milling process.

Grinding bowls and balls are available in several different materials: agate, hard metal tungsten carbide, stainless steel, silicon oxide, zirconium oxide and sintered corundum. The mills are provided by grinding balls with diameter sizes: 5, 10, 15, 20 and 30 mm. Additional technical attributes of planetary mills are given in Chapter 2.

Shaker Mills

SPEX mill (SPEX CertPref, Inc., Metuchen, NJ), a shaker type mill, is another popular mill, which is often used in research, especially in the USA. It mills about 10 g of the powder at a time and is most commonly used for laboratory investigations and for powder sieving. The common kind of the mill has one bowl containing the sample and grinding balls, attached in the clamp and swung energetically several thousand times a minute. The shaking motion is combined with lateral movements of the ends of the bowl so that it appears to be tracing a figure of 8. Thus, the charge of powder and balls is agitated in three mutually perpendicular directions at approximately 1200 rpm. With each swing of the bowl, the balls impact against the sample and the end of the bowl, both milling and mixing the sample. Due to $\approx$5 cm amplitude and the high agitating rate of the bowl and grinding balls, the ball velocities are high and, consequently, the force of the ball impact is very large.

A variety of bowl materials is available for the SPEX mills and these include alumina, agate, hardened steel, silicon nitride, stainless steel, tungsten carbide, zirconia, plastic and methacrylate.

Attritors

Attritors of different sizes and capacities are available (from a few to 50 kg). A vertical attritor is shown in diagram form in Figure 3.3. The powder to be milled is placed in a stationary chamber (tank) with the grinding medium. This mixture is then agitated by a vertical shaft with horizontal arms, rotating at a high speed of about 250 rpm. Commercial attritors are available from NETZSCH-Feinmahltechnik, Union Process, Akron, OH, and Modis Company. Commercial batch NETZSCH attritors (Figure 3.4) used industrially today are available in sizes from 115 to 720 L (Table 3.1). The grinding tanks of attritors produced by Union Process, Akron, OH are available in stainless steel or stainless steel coated inside with alumina, silicon carbide, zirconia, rubber or polyurethane. A variety of grinding media also is available, including alumina, zirconium, zirconium silicate, stainless steel, chrome steel, tungsten carbide, silicon carbide, silicon nitride, sialon, mullite, steatite ceramic, glass and flint-stones. NETZSCH laboratory attritors (Figure 3.5) are available in batch sizes from 0.15 to 2 L (see Table 3.1).

High-energy attritors with horizontal performance have been developed by Zoz Maschinenbau GmbH for laboratory application as well as for commercial use. These attritors are called 'simoloyers'. A laboratory simoloyer CM01-051 is shown in Figure 3.6; the impeller arms have a typical shape (Figure 3.7) [11]. The process parameters depend on the alloy composition that is created during mechanical alloying. Thus, mechanical alloying of $Ti_{65}Al_{24}Nb_{11}$ alloy is accomplished by the following milling conditions: powder components with milling balls of diameter 5.1 mm are processed in an argon atmosphere in a water cooled tank with a rotation speed of the impeller

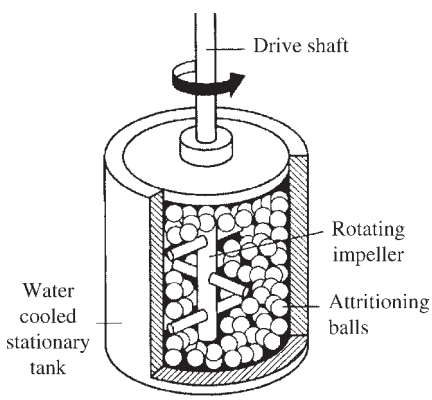

Figure 3.3 The diagram of a custom vertical attritor with rotating impeller.

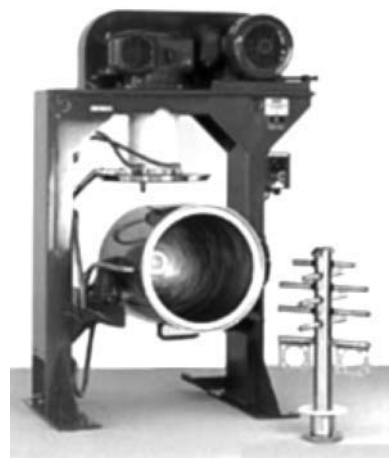

Figure 3.4 Commercial batch NETZSCH attritor PRK 52 S. Courtesy of NETZSCH Incorporated.

Table 3.1 Technical characteristic of main Netzch attritors dimension-types

Technical data	Unit	Attritor dimension-types			
Laboratory batch mills					
Machine type		PE 075	PE 5	PR 01	PR 1
Drive	kW	0.25	2.5	0.25	2
Speed	rpm	233–2100	400–1500	71–530	80–400
Batch size	L	0.15–0.3	2–2.5	0.15–0.3	2
Commercial batch mills					
Machine type		PRK 17 S	PRK 32 S	PRK 102 S	PRK 201 S
Tank volume	L	115	250	490	720
Drive	kW	14/15	22/24	55/58	75/84

Figure 3.5 Laboratory batch NETZSCH attritor PE 5. Courtesy of NETZSCH Incorporated.

Figure 3.6 Laboratory Simoloyer CM01-051 attritor in horizontal performance. (Source: Ref 11)

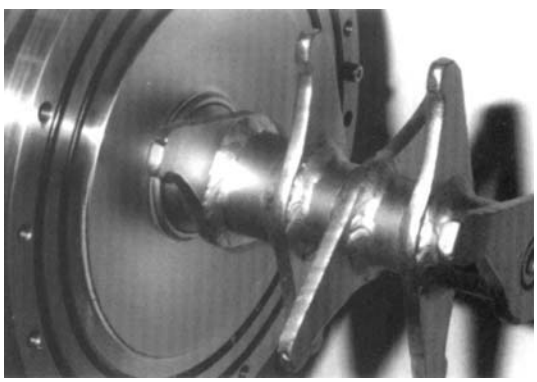

Figure 3.7 Impeller of laboratory Simoloyer CM01-051 attritor. (Source: Ref 11)

up to 1300 rpm and weight of powder charge 130 g and powder to ball weight ratio of 1 to 10.

The Simoloyer CM100s with 100 L capacity has the 30 kW drive at a maximum rotation speed of 430 rpm (Figure 3.8) [12]. This leads to the maximum relative velocity of grinding media in the tank of approximately 10 m/s. For continuous operation fulfillment, the compression method, where a pressured carrier gas is needed, or the depression method based on the suction principle is used.

Commercial Tumbling Ball Mills

Commercial tumbling ball mills for mechanical alloying are much larger in size than the mills described above and can process from several hundred kilograms to up to 1 tonne at a time. The milling time increases with a decrease in the specific energy of the mill. Thus, a process that takes only a few minutes in a planetary mill can take hours in attritors and several days in commercial tumbling ball mills.

Safety Engineering

Because of the very small particle sizes and large surface area of mechanical alloyed powders, they are highly reactive and can be pyrophoric and can cause health problems when inhaled. Therefore, mechanical alloyed powders should be handled with caution and care. Precautions should be taken not to open the powder container immediately after milling as this can lead to abrupt oxidation of the powders and, in some conditions, can cause ignition and explosion. Further, such reactive powder processing must be fulfilled in a protective atmosphere. In cases when reactive powders are processed in air, they must be previously covered by an oxidation-resistant film. Safety engineering technique is described in more detail in Section 5 'Safety engineering in the Production of Powders'.

Mechanical Alloying Fundamentals

For realization of chemical reaction between solids, which are able from thermodynamic considerations to interact, it is necessary to satisfy at least two conditions – bring them together at acting distance of interatomic forces and impart to the atoms sufficient excess energy for redistribution of electron density, by which a chemical conversion is accomplished. Realization of the first condition is not so complicated as the latter. The average energy density transmitted to matter, as a rule, is much less than the energy of

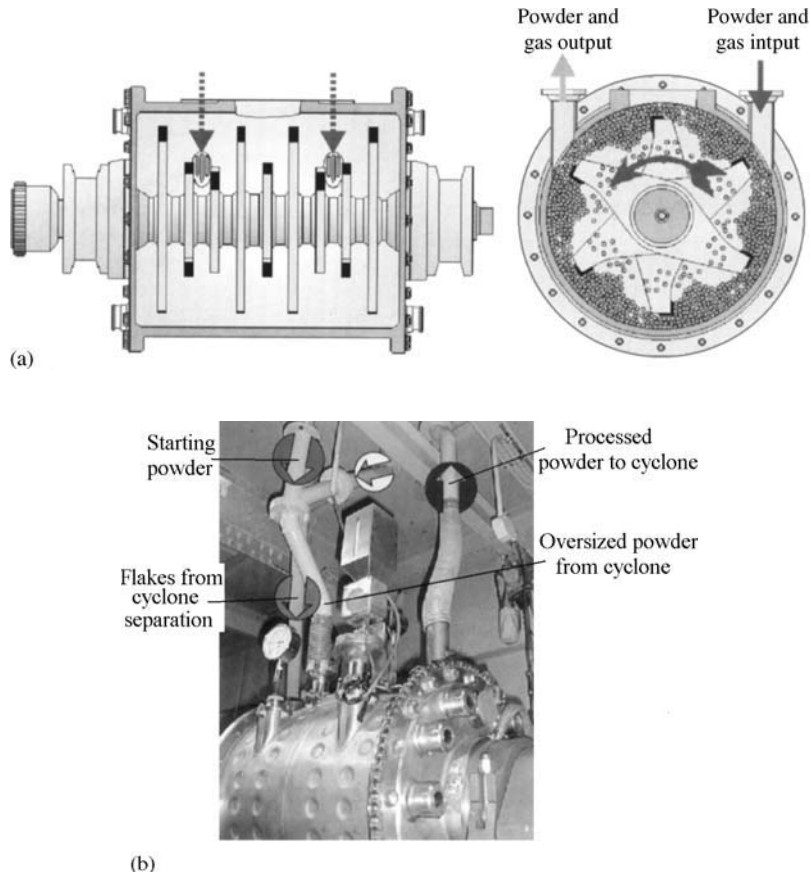

Figure 3.8 Simoloyer CM100 s attritor with 100 L capacity: (a) longitudinal section; (b) piping configuration. (Source: Ref 12)

the interatomic bonds. Therefore, the concentration factor of the former in local points amounts to a quantity sufficient for the fulfillment of the second condition to become of primary importance.

There are several approaches to an explanation of the mechanism of mechanical alloying [9, 13]. One theory, which is called 'Thermal', reckons that the activation of chemical processes is provided by heat caused by friction and collision of particles with the grinding medium and with each other [14]. In the second approach – 'Dislocation' – it is reckoned that the activation occurs at the expense of energy of exit dislocations on particle surfaces by plastic deformation of particles which are being ground [15, 16]. In the third approach, the activation of chemical processes is connected with the 'trip-out' of a resilient energy at distraction of solid and with formation of short-lived active centers [17–21]. The presence of numerous effects, such as luminescence, emission of electrons and other charged particles, the appearance of electric charges on the surface and 'evaporation' of crystal lattice components, leads to the creation of the 'deformation' model. The above models, without exception, complement each other.

The evolutional course of the MA process, following modification of shape and powder particle structures, occurs in the following way. During high-energy milling, the powder particles are repeatedly flattened, fractured and rewelded. Whenever two steel balls collide, some powder is trapped between them. This plastically deforms the powder particles, creates new surfaces and enables the particles to weld together, which leads to an increase in particle size. In the early stages of milling, the particles are soft (in conditions when either ductile–ductile or ductile–brittle material combination are used) and their tendency to weld together and form large particles is high. The composite particles at this stage have a typical layered structure consisting of various combinations of the initial components. With continued deformation, the particles become work-hardened and fracture by a fatigue failure mechanism and/or by

the fragmentation of fragile flakes. At this stage, the inclination to fracture predominates over cold welding. Due to the continued impact of grinding balls, the structure of particles is steadily refined, while the particle size continues to be the same. As a result, the interlayer space decreases while the number of layers in a particle increases. The rate of the internal structure refinement of the particles is roughly logarithmic with processing time, while the initial size of the particles is relatively unimportant [3, 5].

Milling for a certain length of time leads to a steady-state equilibrium when a balance is reached between the rate of welding, which tends to increase the average particle size, and the rate of fracturing, which tends to decrease the average composite particle size. At this stage, generally, each particle contains substantially all of the initial ingredients in the proportion in which they were mixed together, and the particles attain saturation hardness. The particle size distribution at this stage is narrow, because particles larger than average are reduced in size at the same rate as fragments smaller than average grow through agglomeration of smaller particles. The average particle size obtained at this stage depends on the relative ease with which agglomerates can be formed by cold welding, fatigue and fracture strength of composite particles and the resistance of particles to deformation.

As previously mentioned, during MA, heavy deformation of the particles occurs. This is manifested by the presence of a variety of crystal defects and an increased number of grain boundaries. The presence of these structural defects increases the diffusivity of solute elements into the matrix. Additionally, the small rise in temperature during milling further aids the diffusion behavior.

As widespread application of mechanically alloyed powders requires production of the powders in tonnage quantities, efficient methods of consolidating the powders into bulk shape are also necessary. All the consolidation methods generally used in powder metallurgy processes can also be used for mechanically alloyed powders. At the same time, mechanically alloyed condition features, where the powder particles are smaller in size than those used in conventional powder metallurgy operations, some special precautions are needed. Conventional consolidation of powder to full density through processes such as hot extrusion and hot isostatic pressing normally requires use of high pressures and high temperatures for extended periods of time. However, this results in loss of the benefits achieved by the nanostructures obtained by MA. Because mechanical alloyed powders have a high hardness, cold compaction is not a viable process. Along with this, oxide dispersion strengthened alloys (ODS) have been found not to densify during simple sintering.

The most common method of MA powder consolidation is hot compaction followed by hot extrusion, or by direct hot extrusion at temperatures greater than half the melting point, consequently at temperatures considerably lower than those used for coventional powders, in order to minimize MA powder activity. For example, while conventional γ-TiAl powders are hot isostatically pressed at about 1100°C, mechanical alloyed γ-TiAl powders can be consolidated to full density by hot isostatically pressing them at about 750°C [5].

The consolidation methods used for mechanically alloyed powders, both on laboratory and industrial scales, include plasma activated sintering, electrodischarge compaction, Ceracon processing and explosive forming. These processes could be used if their application does not lead to the loss of metastable effects, such as the crystallization of the amorphous phase in the powder.

Oxide Dispersion Strengthened (ODS) Alloys

The main use of MA of non-ferrous metals has been in the present-day developments of commercial ODS nickel-, copper-, and aluminum-base alloys. The feature of these materials is elevated temperature strength, which is derived from several mechanisms. First, their structure is characterized by uniform dispersion, with a spacing of about 100 nm, of very fine (from 5 to 50 nm), oxide particles of stable oxides such as alumina (Al_2O_3), titania (TiO_2), thoria (ThO_2), yttria (Y_2O_3), lanthana (La_2O_3) and beryllia (BeO). This dispersion inhibits dislocation motion in the metal matrix and increases the resistance of the alloy to creep deformation. Another function of the dispersoid particles is to inhibit the recovery and recrystallization processes. Secondly, the homogeneous distribution of alloying elements due to MA gives both the solid solution strengthened and precipitation hardened alloys more stability at elevated temperatures and improvement in properties. Mechanically alloyed materials have also high oxidation and hot corrosion resistance.

The production of ODS alloys on a commercial scale uses as raw materials elemental powders, crushed master alloy (intermetallic) powders, and prealloyed powders. Yttria powder, as well as other oxide particle powders, with narrow ranges of crystallite size (preferably when the crystallite size is below 30 nm) and metal powders are mixed together to form a bulk feedstock. These mixtures are charged into large tumbling

ball mills with steel balls. During milling, an equilibrium powder particle size distribution is established till each individual particle achieves the alloying constituents in the given proportions. The mechanically alloyed powder from the mill is then filled into stainless steel containers. Then the powder is consolidated at elevated temperatures usually by either extrusion or hot isostatic pressing (HIP). In most cases, extrusion is preferred because it is less expensive then HIP. The former is accomplished in the following way. The powder is loaded into mild steel extrusion cans with characteristic sizes up to 300 mm in diameter and 900 mm in length and containing up to 280 kg. The batch is held for several hours in a furnace at the extrusion temperature, during which time homogenization of the powder and complete alloying occur, if it has not already been accomplished during milling. Extrusion is done in commercial presses at temperatures, ratios and speeds that are independent variables depending on the properties of the material.

The consolidated mechanically alloyed billets are worked to final shape, such as sheet, plate, rod, bar, tube, etc., using typical hot working techniques such as extrusion and hot rolling.

Contact Displacement Reactions

Contact displacement reactions (cementation) in solutions are well known. The electrolytic nature of these are described in 'Contact displacement method (Cementation)' in Chapter 9. Electrolytically precipitated powder is produced by the displacement of one metal from the solution due to conjugated dissolution of the other metal.

Mechanical activation of solids to cause chemical reactions has been used for over 40 years [13]. A revival in this activity arose later when, in 1989, it was discovered that MA can be used as a refining process [5] by showing that pure metallic copper can be synthesized as a result of ball milling copper oxide and calcium together at room temperature. Numerous metals, including Zn, Ti, Zr, Ta, Gd, Er, Sm, V, W and some intermetallics, e.g., $SmCo_5$, can be now synthesized directly from oxides or chlorides.

The general equations for the displacement reactions of the metal oxides as well as chlorides may be represented as:

$$MO + R \rightarrow M + RO$$

$$MCl + R \rightarrow M + RCl$$

where a metal oxide (MO) or metal chloride (MCl) is reduced by a reductant (R) to the metal (M).

The displacement reactions realized by MA are characterized by a large negative free energy conversion at room temperature and are therefore thermodynamically practicable at room temperature. At the same time, commercial operations by pyrometallurgical techniques are conducted at elevated temperatures to overcome the kinetic barriers and achieve sufficiently high reaction rates.

Mechanical alloying can provide the means to increase the reaction kinetics of the displacement reactions because the repetitive fracturing and welding of powder particles increases the area of contact between the particles and allows newly formed surfaces to come into contact many times. Due to this, the reaction proceeds without diffusion through the product layer. Parallel with this, the high surface defects caused during MA accelerate the diffusion process. As a result these reactions will now occur at room temperature. In the case when reaction cannot occur at room temperature, the particle surface refinement and consequent reduction in diffusion distance can considerably reduce the reaction temperature.

Two different reaction kinetics (depending on milling conditions) have been distinguished. The reaction can extend to a very small volume during each collision between the grinding media leading to a gradual conversion. Alternatively, when the reaction enthalpy is high enough, a self-propagating combustion reaction can be initiated. Such reactions require a critical milling time for the combustion reaction to be ignited. If the temperature of the powder is recorded during MA, a sudden increase in temperature at a critical time indicates combustion. Measurements of the ignition time and temperature provide a means of characterizing the structural and chemical evolution during MA as well as preventing the risk of explosion.

The displacement reaction products normally consist of two phases – the metal or a compound and the oxide or chloride connected with a reductant. The by-product phase can be easily removed if the metal particles are embedded in a continuous matrix. Removal of the by-product is achieved by leaching the product mixture in a dilute acid or hot water, or by vacuum distillation. The use of carbon or hydrogen as the reductant leads to the formation of gaseous carbon dioxide or water vapor as the by-product and avoids the need for leaching and distillation.

Process parameters, including ball-to powder weight ratio, ball diameter, milling temperature, use of a process control agent, and relative proportion of the reactant phases, play an important role in the nature and amount of product phases obtained by the displacement reactions and these need to be optimized for the best yields.

The mechanically driven displacement reaction shows a number of advantages over conventional metal processing techniques:

- Mechanically driven displacement reaction allows the direct formation of powder product without first having to manufacture the bulk alloy and then convert it to powder
- It enables the reduction of a number of oxides and halides to pure metals at room temperature, which ensures energy savings
- If a number of components are reduced simultaneously, it is possible to produce an alloy without first having to convert the oxides to pure metals and then to the desired alloy.

Thus, a number of high-temperature conventional technical processes can be combined into one single-room temperature process with the potential for considerable cost savings.

Powder Contamination

A most important problem in the MA process is the impurities that get into the powder particles during milling and contaminate them. Because of the small size of the particles, their surface area is large which promotes contamination of the powders. The magnitude of contamination depends on the milling medium, time of milling, the intensity of milling, the atmosphere in which the powder is milled, and the difference in strength to hardness of the powder. As is well known, from 1 to 4 wt% of iron has been found as normally present in most of the powders milled with the steel grinding medium, amounts as large as 7 wt% (20 at.%) iron in a tungsten-carbon mixture milled for 310 h and 13 wt% (33 at.%) iron in pure tungsten milled for 50 h in a SPEX mill [5].

The origins of contamination of metal powders can be chemical purity of the initial powders, milling equipment, milling atmosphere and the process control agents (PCA) added to the powders. Contamination from milling equipment is mainly substitutional and that from the milling atmosphere is in essence interstitial in nature, while contamination from chemical purity can be either substitutional or interstitial in nature. The PCA additions lead to interstitial contamination. The interstitial impurities oxygen and nitrogen are deleterious to reactive metals such as titanium and zirconium and the presence of these impurities leads to a change in the constitution of the alloys [22, 23].

The level of contamination can be different under different processing conditions and is dependent on the type of mill, intensity of milling, nature of powder, nature of the grinding medium and tank, ambient atmosphere, etc.

Several attempts have been made to minimize powder contamination during mechanical alloying. The following ways to minimizing powder contamination are known:

- Using the same material for the mill body (tank) and grinding medium as the powder being milled
- Grinding medium and tank should be harder and stronger than the powder being milled
- Preventing the outside atmosphere leaking into the mill by using a controlled milling atmosphere
- Proper cleaning of the tank that was previously used for another powder
- Optimization of the milling process.

The first way is of restricted use because it is difficult in many cases due to the non-availability of the special grinding media and tanks. The problem is becoming more and more complicated because the MA technique is being applied to a variety of materials, including metals, alloys, ceramics, polymers and composites, and it is impossible to get tanks and grinding media of all these types of materials. But it is possible to find another solution, using a thin adherent coating on the internal surface of the tank of the material to be milled.

Independently of the above, a simple rule that must be followed to minimize contamination is that the tank and grinding medium should be harder/stronger than the powder being milled.

The problem of the milling atmosphere is also important. It has been observed [5] that when the tank is not properly sealed, the atmosphere surrounding the tank, usually air, leaks into the tank and contaminates the powder. So, when reactive metal such as titanium and zirconium are milled in incompletely sealed containers, the powders are contaminated with nitrogen and oxygen. Flushing with argon does not remove oxygen and nitrogen absorbed on the internal surfaces.

Attempts have been made to improve the tank-sealing integrity to prevent the surrounding atmosphere leaking in. It has been reported [23] that the use of a high-purity argon (99.998%) milling atmosphere and improvements of the sealing quality resulted in the processing of high-quality titanium alloy powder with less than 100 ppm oxygen and 15 ppm nitrogen. However, this technique may not be economically viable and therefore may not be acceptable on a commercial scale.

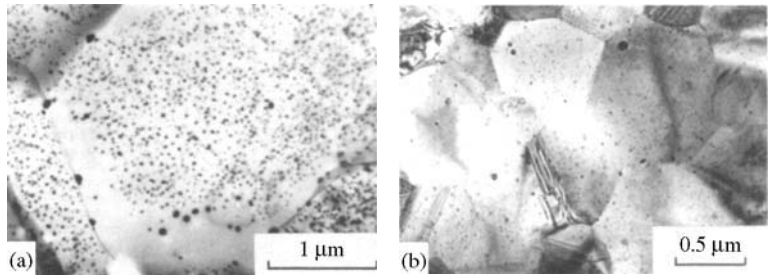

Figure 3.9 Transmission electron micrographs of two polished metallographic sections showing the difference in the matrix grain size and size and distribution of dispersoids. (a) Rapidly solidified and hot isostatically pressed at 850°C. (b) Mechanically alloyed and hot isostatically pressed at 1000°C. (Source: Ref 5®)

Attempts to minimize the powder contamination by means of milling process optimization are known. Such a method for minimizing the powders contamination during ball milling was recently described [24]. Because the optimum milling conditions ensuring a minimum of contamination are different from the conditions for maximum productivity for a specified quality of the powder being milled, the authors propose a solution for achieving a compromise between the targets mentioned above.

Summing the foregoing about the state of the problem of the powder contamination during milling, it is noted that claims have been made in the literature for the superiority of certain mills and practices over others, but systematic investigations on milling the same powder under identical conditions in different mills and evaluating the contamination levels have not been undertaken.

Applications

The main industrial applications of mechanical alloyed materials have been used in thermal processing, power engineering, glass processing, aerospace and other industries. These applications are based on the ability of MA to synthesize materials with metastable phases, such as supersaturated solid solutions, non-equilibrium crystalline or quasicrystalline intermediate phases, and amorphous alloys [3, 21, 25].

Comparison of the ability to produce metastable phases by MA with the results of rapid solidification, shows differences in the nature of the mechanisms by which metastable phases form as well in processing techniques. For example, solid solutions have been obtained in the full composition range in the Cu–Co, Cu–Fe and AlSb–InSb systems by MA, but not by rapid solidification.

The formation of metastable intermediate phases and amorphous alloys also differs in various systems using the two techniques. For example, the formation of an amorphous phase in the titanium–aluminum system by MA is realizable, while it is not possible by rapid solidification [5]. An important difference between these methods is that whereas amorphous phases form in the vicinity of eutectic compositions by rapid solidification, they form near the equiatomic composition by MA. Another considerable difference between mechanically alloyed and rapidly solidified alloys containing dispersoids becomes apparent in the size and distribution of the dispersoids. Typical transmission electron micrographs showing the difference for mechanically alloyed material and rapidly solidified alloy in the matrix grain size, and size and distribution of dispersoids, are shown in Figure 3.9 [5]. The rapidly solidified alloy is Ti_3Al to which 2 wt% Er was added and then hot isostatically pressed at 850°C. The mechanically alloyed material is $Ti_{61}Al_{25}Nb_{10}V_3Mo_1$ to which 2 wt% Er was added and the alloy powder was hot isostatically pressed at 1000°C. As is obvious, even after HIP at the higher temperature, in comparison with the rapidly solidified alloy, the mechanically alloyed material showed a finer matrix grain size, more uniform distribution, absence of large dispersoids at grain boundaries and absence of dispersoid-free zones near the grain boundaries.

The major use of MA has been in the applications of commercial oxide dispersion strengthened nickel-, aluminum-, and copper-base alloys.

Nickel-base Alloys

Compositions of several typical grades of the commercially available mechanically alloyed nickel-base superalloys are given in Table 3.2. The term 'superalloy' is employed to characterize the materials with high strength at high temperatures that are used principally in turbine engines for aircraft and power generation.

Table 3.2 Nominal compositions (wt%) of mechanically alloyed nickel-base superalloys

Elements	Trade grade. Source					
	MA 754 [27, 28]	MA 757 [28]	MA 758 [29]	MA 760 [27, 28]	MA 6000 [30, 31]	TMO-2 [27, 28]
Aluminum	0.3	4.0	0.3	6.0	4.5	4.2
Boron	...	...	...	...	0.01	...
Carbon	0.05	...	0.05	...	0.05	...
Cobalt	...	...	...	...	...	9.7
Chromium	20	16	30	20	15	6.0
Iron	1.0	...	...	...	...	...
Molybdenum	...	...	...	2.0	2.0	2.0
Tungsten	...	...	...	3.5	4.0	12.4
Tantalum	...	...	...	...	2.0	4.7
Titanium	0.5	0.5	0.5	...	2.5	0.8
Yttrium oxide	0.6	0.6	0.6	0.95	1.1	1.1
Zirconium	...	...	...	...	0.15	...
Nickel	bal	bal	bal	bal	bal	bal

The oxide dispersion strengthened alloys continue to find applications in a wide variety of industries. It was observed [5] that the two production facilities of INCO Alloys International have a combined annual powder capacity approaching 300 tonnes. The MA nickel-base superalloys are used mainly for gas turbine engine components and sheet for use in oxidizing/corrosive atmospheres. Thus, the largest use of MA 754 is as vanes and bands for aircraft gas turbine engines. It is also used for brazed nozzle guide vane and band assemblies in aero engines. The principal advantages of the alloy for these applications are thermal fatigue resistance, high melting point and long-term creep strength. Alloy MA 758 is used in a number of industrial applications where its high chromium content makes it resistant to extremes of temperature and environment. This alloy is used in the glass industry for high-temperature components requiring both elevated temperature strength and resistance to extremely corrosive molten glass. New product forms of the commercial alloys continue to be developed. Large diameter, thin wall tubing of alloy MA 754 has been produced and evaluated for radiant tube applications and alloy MA 758 has been used as tubing in heat exchangers and process equipment operating at very high temperatures.

The alloy MA 6000, because of its complex composition, has excellent resistance to oxidation and sulfidation. It is used for first- and second-stage advanced gas turbine vanes and blades machined from solid bar.

Data about room temperature and elevated temperature mechanical properties of commercial oxide dispersion strengthened nickel-base superalloys are given in 'Production of Nickel and Nickel-alloy powders' (Chapter 17).

Aluminum-base Alloys

Through the presence of durable surface oxide film, the initial aluminum powder during processing in high-energy mill is easy granulated. Thus, it has been reported [21] that at the end of 5 minutes milling in a vibratory ball mill, the powder becomes a lamellar state. An increase in the specific surface of particles as a result of shape change leads to disruption of the oxide layer continuity and the appearance of fresh surfaces. During this stage, cold welding dominates over fracture. Then, during processing in the range from 5 to 20 minutes, fracture prevails, leading to an appreciable decrease in lamellar particle sizes. They range from 100 to 200 μm in two directions with thickness at most 4–5 μm. Further processing has no perceptible influence on the particle thickness, but decreases particle sizes in two other directions resulting in a steep decrease of apparent density from the initial 1.1–1.3 g/cm^3 to 0.4–0.6 g/cm^3 at the end of 20 minutes milling. Along with the comminution process, a reverse process takes place including agglomeration and cold welding of metallic aluminum on the one hand and oxide splinters and products of interaction between oxides and adsorbed gases on the other (Figure 3.10). This process prevails over breakdown after 30 minutes which leads to an increase of granules and apparent density. The latter reaches a maximum of 1.3–1.4 g/cm^3 after processing for 2 h, and does not change significantly on further processing.

Increase of milling time above 30 minutes changes the shape of particles. It is altered from lamellar to fission-fragment shape. Adhesion processes lead to agglomeration of particles as well as attachment of

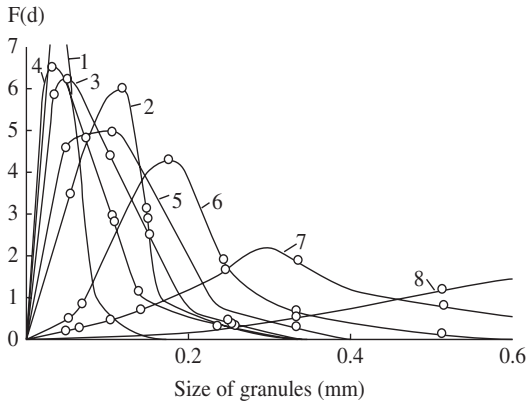

Figure 3.10 Change of aluminum granule sizes distribution during mechanical alloying processing at the end of: (1) 0 minutes, (2) 5 minutes, (3) 10 minutes, (4) 20 minutes, (5) 30 minutes, (6) 40 minutes, (7) 60 minutes and (8) 90 minutes. (Source: Ref 21)

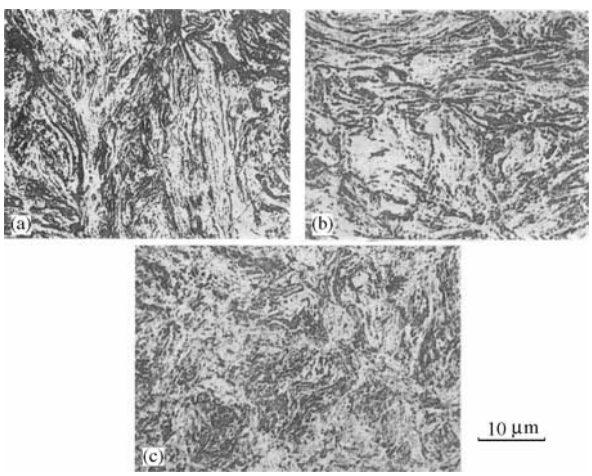

Figure 3.11 Microstructure of granules obtained by processing of aluminum powder in vibratory ball mill at the end of: (a) 1 h, (b) 4 h and (c) 8 h. (Source: Ref 21)

fragments to the grinding balls. From now on the balls are not only a milling medium but also their surface becomes the site of granule formation. By ball collisions, the particles are welded layerwise on the particle incrustations due to action of normal strength component, while the tangential strength component causes the break up of the incrustations. After one hour, a dynamic balance is established, at which approximately 10 wt% of the charge is found on the balls.

Under multiple plastic deformation action, the granules assume a shape near to spheroidal. Simultaneously, the structure of composition is also transformed (Figure 3.11). At the first granulation stage, the structure of granules is characterized by pronounced lamination. During further processing, the thickness of layers is continuously decreased and gradual homogenization of composition occurs. However, in granulated aluminum and in aluminum-base compositions obtained without surfactant, typical lamination is observed after long-continued processing. Increasing the processing time up to 6–8 h leads to continuous growth of the average size of the granules. By that time, the average granule size reaches 2 mm and a dynamic balance between welding and destruction of granules is established.

Mechanical alloying of aluminum alloys of various compositions generally brings an increase of granule hardness. Table 3.3 contains the data about microhardness of granulated compositions obtained by mechanical alloying of aluminum with various elements and their oxides.

Here it is shown that strengthening does not depend on the initial hardness of the alloying component but, rather, on the kinetics of mechanochemical reactions defining the formation of the strengthening phases. Thus, a correlation is observed between Gibbs function oxidation–reduction reaction values and hardness of the compositions. The latter increases with decreasing ΔG value.

It is typical that aluminum milling with aqua addition, as well as its processing in carbon dioxide or sodium superoxide, leads to significantly greater strengthening in comparison with mechanical alloying with oxides, Cr_2O_3, TiO_2 and ZrO_2, which have high hardness and low value of Gibbs function of oxidation–reduction reaction. Mechanical alloying with oxides, such as CuO, Co_3O_4, MoO_3 and V_2O_5, is more advantageous.

The characteristics of room- and elevated-temperature mechanical properties for mechanical alloyed aluminum of various compositions are summarized in Table 3.4.

IncoMAP alloy AL-9052 has a density 5% less than that of conventional age-hardenable aluminum alloy of comparable strengths such as 2024 and so its combination of light weight, high strength and corrosion resistance is useful for aerospace applications. The addition of lithium to mechanically alloyed aluminum alloys produces an ultra-lightweight alloy, IncoMAP AL-905XL. Its density is lower and its stiffness 10% greater than the age-hardenable alloy 7075-T73 of comparable strength. The excellent combination of the properties makes this alloy useful for airframe applications.

Increasing the alloying component content leads generally to an appreciable increase of the durability of the semi-finished products. However, their plasticity ductility is decreased down to the lower

Table 3.3 Microhardness of granulated compositions obtained by mechanical alloying of aluminum with various elements and their oxides

Alloyed component		Gibbs function of oxide formation $-\Delta G_T$ (kJ/mole at)	Gibbs function of electronation reaction $-\Delta G_T$ (kJ/mole at)	Microhardness of granulated composition (MPa)	
Substance	Content (wt%)			Without surfactant	With 0.5 wt% surfactant
Without alloying component		...	...	720	850
Al_2O_3	14.83	527	0	950	1150
B	4.0	...	...	1150	1600
B_2O_3	4.42	395	132	950	1500
CO_2	4.19	197	330	1400	1550
Co	5.0	...	...	1000	1100
Co_3O_4	11.47	189	338	1300	1550
Cr	5.0	...	...	1150	1250
Cr_2O_3	9.6	350	177	1100	1350
Cu	5.0	...	...	1200	1300
CuO	6.26	128	399	1350	1500
Fe	5.0	...	...	1000	1150
Fe_2O_3	5.0	247	280	1150	1350
La	5.0	...	...	1100	1250
Li	5.0	...	...	1300	1550
Mn	5.0	...	...	1050	1200
MnO_2	8.28	233	294	1200	1450
MoO_3	9.14	226	301	1250	1550
Ni	5.0	...	...	1050	1150
NiO	10.50	215	312	1300	1400
NO_2	4.38	103	630	1450	1600
Pb	10.0	...	...	650	750
SiO_2	10.25	413	114	1050	1350
Ti	5.0	...	...	950	1100
TiO_2	7.62	445	82	950	1250
ZnO	15.5	317	210	1050	1300
Zr	5.0	...	...	1150	1300
ZrO_2	14.83	514	13	950	1200

(Source: Ref 21).

limit admissible for construction materials. Thus, the introduction of 9.14 wt% molybdenum trioxide together with 5 wt% magnesium in an aluminum-base MA composition resulted in increasing the ultimate tensile strength of the rod to 660 MPa with 2% elongation in comparison with alloy without molybdenum trioxide addition –580 MPa and 5%, respectively (see Table 3.4). Highly alloyed compositions retain sufficient high mechanical properties up to 300°C.

The largest tensile strength values are achieved by alloying with organic compounds: 700–770 MPa. Organic compounds contoured by different groups were used: oxalic acid (COOH·COOH), carbamide ($HN_2 \cdot CO \cdot NH_2$), dinitrotoluene ($CH_2 \cdot C_6H_3(NO_2)_2$), diphenyline carbazide ($C_{13}H_{14}N_4O$), and others. Thus, organic compounds successfully serve as donors of the elements for hardening phases such as Al_4C_3, AlN, Al_2O_3, etc.

The Al_3Nb intermetallic compounds due to their high elasticity coefficient and oxidation resistance are suitable for high-temperature structural materials such as in aerospace, gas turbines, etc. The Al_3Nb alloy has a comparatively low density (4.54 g/cm^3) which is lower than that of comparable advanced Ni_3Al- based compound (7.6 g/cm^3), but it is difficult to fabricate the alloy by conventional methods due to the large difference in melting point between Al and Nb. Furthermore, due to intrinsic brittleness, Al_3Nb ingots crack during solidification. It is reported [34] that some of these problems can be overcome by MA. The relationships between MA processing parameters

Table 3.4 Mechanical properties of mechanical alloyed aluminum alloys

Alloyed component			Temperature (°C)	Mechanical properties			Reference
Substance	Content (wt%)	Mg content (wt%)		Hardness (MPa)	UTS (MPa) (a)	Elongation (%)	
Al-Mg-Li- O-C (b)			20	...	510	10	Ref 32
SiC (c)	8.2	...	20	...	480	3.78	Ref 5
4.0Mg-0.75O-1.0C Al balance(d)			20	...	450	13	Ref 32
4.0Mg-1.3 Li-0.6O-1.1C Al balance(e)			20	...	520	9	Ref 33
Without alloyed composition		5.0	20	1550	580	5	Ref 21
			200	700	290	23	
			350	250	100	10	
			400	150	70	9	
NO_2	4.4	5.0	20	1650	650	2	Ref 21
			200	1100	370	16	
			350	650	200	21	
			400	550	160	19	
			500	...	100	12	
CO_2	4.2	5.0	20	1650	670	2	Ref 21
			200	1100	360	15	
			350	600	190	19	
			400	550	150	16	
			500	...	100	8	
MoO_3	9.14	5.0	20	1700	680	2	Ref 21
			200	1150	380	12	
			350	900	210	16	
			500	...	120	10	
V_2O_5	6.93	5.0	20	1650	580	3	Ref 21
			200	1150	350	15	
			350	800	180	17	
			400	650	140	14	
			500	...	90	11	
B_2O_3	4.42	5.0	20	1650	630	2	Ref 21
			200	1200	340	17	
			350	800	170	19	
			400	600	120	14	
			500	...	70	10	
SiO_2	5.78	5.0	20	1400	500	3	Ref 21
			200	1000	300	19	
			350	700	160	14	
			400	500	120	12	
			500	...	60	8	
ZrO_2	12.5	5.0	20	1650	660	2	Ref 21
			200	1200	370	16	
			350	900	200	18	
			400	700	160	15	
			500	..	110	9	
Al_2O_3	6.5	5.0	20	1500	520	4	Ref 21
			200	1050	310	22	
			350	600	130	23	
			400	450	100	17	
			500	...	60	10	

(*Continued*)

Table 3.4 (Continued)

Alloyed component			Temperature (°C)	Mechanical properties			Reference
Substance	Content (wt%)	Mg content (wt%)		Hardness (MPa)	UTS (MPa) (a)	Elongation (%)	
$CH_4\,ON_2$	2.5	2.0	20	...	720	2	Ref 21
			200	...	420	8	
			300	...	310	15	
			400	...	240	12	
$C_7H_6\,(NO_2)_2$	2.5	2.0	20	...	770	2	Ref 21
			200	...	480	8	
			300	...	360	14	
			400	...	260	10	
			500	...	190	8	
$C_{13}H_{14}\,N_4O$	2.5	2.0	20	...	760	2	Ref 21
			200	...	480	7	
			300	...	370	15	
			400	...	270	11	
			500	...	190	9	
$C_{10}H_{10}\,ON_2$	2.5	2.0	20	...	750	2	Ref 21
			200	...	470	8	
			300	...	360	14	
			400	...	250	11	

(a) Ultimate tensile strength; Commercial production grade: (b) MAP Al-Mg-Li- O-C; (c) MAP AA8090; (d) MAP alloy 9052Al; (e) IncoMAPalloy AL-905XL

and structural characteristics of Al_3Nb nanocrystalline powders are described. The homogeneous Al_3Nb powder particles were obtained by means of ball milling using of 3 wt% stearic acid as PSA.

Recently, high-strength aluminum–titanium alloys have been developed using MA by dispersing nanometer or submicron-sized Al_3Ti intermetallic particles (in addition to the Al_2O_3 and Al_4C_3 dispersoids by the addition of PCAs) in an aluminum matrix. Similar approaches could be used to develop high- strength alloys in other systems. High mechanical properties where achieved in Al–10Ti alloy obtained by MA [35]. A mixture of aluminum and 10 wt% titanium powders were attrition-milled in the presence of 1.5 wt% wax. After 10 h milling time aluminum had dissolved about 9 wt% Ti. The powder prepared in this way showed a Vickers microhardness of 192 HV.

Copper-base Alloys

The fundamentals of the formation of phase composition, structure and properties of mechanical alloyed aluminum alloys are typical also for MA copper alloys. One of the features of copper composition formation distinguishing them from aluminum is their high tendency to granulation. This is caused by the absence of durable oxide film on the powder particle surfaces. It is reported [21] that MA processing in a vibratory mill can be done using the following conditions: acceleration of milling bodies in the range from 100 to 150 m/s^2, 70–80% of the mill volume occupied by the balls, the ratio of the balls to charge volumes must be 7–10, and temperature must not exceed 80°C, and processing duration ranges from 6 to 10 h. The properties of main granulated compositions are given in Table 3.5.

The apparent density ranges from 4.5 to 5.5 g/cm^3 at the end of 20–30 minutes processing. The structure of the majority of the granulated copper compositions is homogeneous. Grain size does not exceed tenth quantums of micron (Figure 3.12). Depending on the nature of the main phase transformations during MA processing of the alloys, it is possible to recognize three groups. The main phase change in the first group of alloys is the formation of solid solutions; in the second, formation of compounds. The third group includes systems which do not have a fundamental phase change.

Electrical applications are the main areas served by MA copper alloys. Notable are the electrodes for welding and electro-erosion processes, where costs can be reduced and productivity increased by the longer life-time of the electrodes [35].

Table 3.5 Properties of granulated copper-base compositions obtained by processing in vibratory ball mill and MA copper-base alloys

Alloyed components and their contents (wt%)	Duration of mechanical alloying (h)	Properties of granulated compositions			Properties of MA alloys			
		Granule shape	Average size of granules (mm)	Micro-hardness (MPa)	Hardness (MPa)	Ultimate tensile strength (MPa)	Elongation (%)	Electrical resistivity ($10^{-8}\Omega$·m)
Al (1.00)	6	Lamellar	0.6	2700	2250	850	6	4.453
Al (5.00)	6	Angular	0.6	3100	2750	1060	3	4.976
Be (0.50)	6	Lamellar	1.1	2300	2200	810	6	4.338
Be (1.50)	...	...	...	...	2900	1120	3	6.043
Be (2.00)	6	Angular	0.4	3100	...	...	...	...
Mo (5.00)	6	Spheroidal	0.4	2300	...	...	...	...
Nb (5.00)	6	Lamellar	1.1	3200	2650	990	3	2.386
Al(0.80), CuO (3.56)	8	Angular	0.3	2600	2600	1040	3	2.350
Al (0.80), CH_4ON_2 (0.44)	8	Angular	0.3	2900	2650	1130	2	2.383
Be(0.40), CuO (3.56)	8	Angular	0.3	2600	2400	980	3	2.413
Al (0.80), C (0.30)	8	Lamellar	1.1	2400	2300	830	6	4.338
Zr (2.00), C (0.30)	8	Lamellar	1.0	2700	2450	970	4	2.452
Nb (5.00)	6	Lamellar	1.1	3200	2650	990	3	2.386
Al_2O_3 (1.88)	...	...	...		2300	760	2	2.452

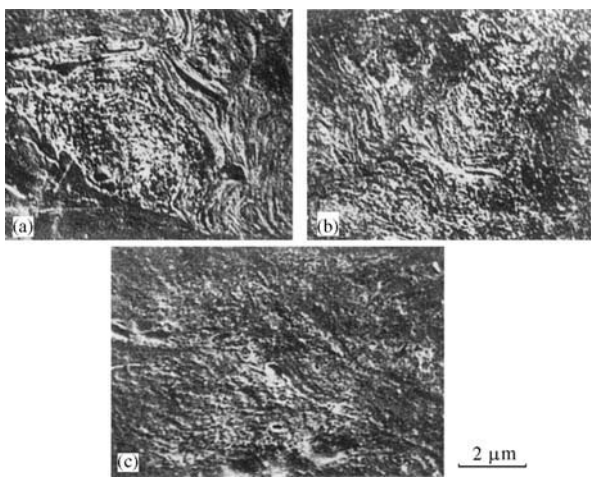

Figure 3.12 Microstructure of granules obtained by processing of copper alloy powders in vibratory ball mill at the end of 8 h milling time: (a) Cu-0.4Be-3.56CuO; (b) Cu-0.5Al; (c) Cu-20Zn.

References

1. Benjamin, J.T., Mechanical alloying. *Sci. Amer.*, 1976, 234(5):40–48.
2. FRG Patent 1,909,781, 1968.
3. Suryanarayana, C., *Bibliography on Mechanical Alloying and Milling*. Cambridge International Science Publishing, 1995.
4. Rebinder, P.A., Shchukin, E.D., Surface phenomena in solids during deformation and destruction processes. *Uspehy physicheskih nauk*, 1972, 108(1):3–8 (in Russian).
5. Suryanarayana, C., Mechanical alloying. In *ASM Handbook*, Vol. 7. ASM International Publishers, 1998, pp. 80–90.
6. Soviet Union Patent 1,436,341, July 1988.
7. Masters, K., *Spray Drying*, 4th edn. John Wiley & Sons, 1985.
8. Alekseev, A.G., Neikov, O.D., The explosion risk of metal powders. *Staub Reinhaltung der Luft*, 1990, 50:245–250.
9. Avvakumov, E.G., *Mechanical Methods of Activation of Chemical Processes*. Nauka Publishers, Novosibirsk, 1986 (in Russian).
10. Jang, G., In *New Materials by Mechanical Alloying Techniques*. Deutsche Gesellschaft für Metallkunde, Oberursel, Germany, 1989, pp. 39–52.
11. Zoz, H. et al., Mechanical alloying of Ti-24Al-11Nb (at%) using the Simoloyer. *Metall*, 1996, 50(9):575–579.
12. Zoz, H., Reichardt, R., Ernst, D., Simoloyer CM100s, semi-continuous mechanical alloying in

a production scale using cycle operation – Part II. *Metall*, 1998, 51(9):521–527.
13. Heinicke, G., *Tribochemistry*. Academie-Verlag, Berlin, 1984.
14. Bowden, F.P., Tabor, D., *The Friction and Lubrication of Solids*. The Clarendon Press, Oxford, 1964.
15. Kraculin, Y.A., Dislocation as active centres in topo-chemical reactions. *Theoretical and Experimental Chemistry*, 1967, 3(1) (in Russian).
16. Schradar, R., Stadter, W., Octtel, H., Untersuchungen an mechanisch aktivirten. XIII Festkorperstruktur und Katalishe Verhalten von Nickel-pulver. *Z. Phys. Chem.*, 1972, 249:87–100.
17. Streletskiy, A.N. et al., Regularities of mechano-chemical synthesis of the complicated oxides in Pb–Fe_2O_3–Nb_2O_5 system. In *Proceedings 'Mechanical synthesis in inorganic chemistry'*. Novosibirsk, 1991, pp. 66–83 (in Russian).
18. Butjagin, P., Yur, P., Initial active centres in mechanochemical reactions. *VChO imeni D.I.Mendeleeva*, 1973, 18:90–95 (in Russian).
19. Butjagin, P. Yur., Bystrikov, A.V., About initiation chemical reactions by destruction of solids. In *Proc. of V All-Union Symp. for mechano-emission and mechanochemistry of solids*, Tallin, 1977, Part 1, pp. 63–78 (in Russian).
20. Clemens, B.M., Solid-state reaction and structure in compositionally modulated zirconium-nickel and titanium-nickel films. *Physical Review B.*, 1986, 33(11):7615–7626.
21. Vitjaz, P.A., Lovshenko, F.G., Lovshenko, G.F., *Mechanical Alloyed Alloys Based on Aluminium and Copper*. Belaruskaja Nauka Publishers, Minsk, 1998.
22. Chen, G.-H., Suryanarayana, C., Froes, F.H., Structure of mechanically alloyed Ti-Al-Nb powders. *Metallurgical Mater. Trans.* A, 1995, 26(6):1379–1387.
23. Goodwin, P.S., Ward-Close, C.M., Contamination control in the mechanical alloying of nanocrystalline intermetallic compound based alloys. *Materials Science Forum*, 1995, 179/181: 411–418.
24. Spârchez, Z., Chicinaş, I., Method for minimising the powders contamination during the ball milling process. In *Proceedings of 2005 Powder Metallurgy European Conference*, compiled by European Powder Metallurgy Association, UK, 2005, Vol. 1, pp. 107–112.
25. Koch, C.C., Mechanical milling and alloying. In *Proceedings: Materials Science and Technology – A Comprehensive Treatment*. VCH, 1991, pp. 193–245.
26. deBarbadillo, J., Fischer, J., Dispersion-strengthened nickel-base and iron-base alloys. In *ASM Handbook*, Vol. 2. ASM International Publisher, 1990, p. 722.
27. Gilman, P., Benjamin, J.S., Nickel- and iron-based dispersion strengthened alloys. In *ASM Handbook*, Vol. 7. ASM International Publishers, 1985, p. 722.
28. Inconel Alloy MA 754, Alloy Dig., 1990, ASM International, Rev. March 1990.
29. Inconel Alloy MA 758, Alloy Dig., 1990, ASM International, Rev. May 1996.
30. Pettit, F.S., Meier, G.H., Oxidation and hot corrosion of superalloys. In *Proceedings of Fifth International Symposium on Superalloys*. The Metallurgical Society, 1984, pp. 651–687.
31. Inconel Alloy MA 6000, Alloy Dig., 1980, ASM International, Rev. July 1983.
32. Murakami, Y., Aluminum-based alloys. *Materials Science and Technology*, 1996, 8:213–276.
33. Buhl, H. (ed.), *Advanced Aerospace Materials*. Springer-Verlag Publishers, 1992.
34. Gallardo, J.M., Rodrigues, J.A., Herrera, E.J., Structure and properties of attrition-milled aluminium-10% titanium powder. In *Proceedings of 1998 Powder Metallurgy World Congress*, compiled by European Powder Metallurgy Association, UK, 1998, Vol. 1, pp. 378–383.
35. Hofmockel, M., Neubing, H-Cl., ECKA Discup – new high performance PM-copper materials process, properties and applications. In *Proceedings of 2004 Powder Metallurgy World Congress*, compiled by European Powder Metallurgy Association, UK, 2004, Vol. 1, pp. 231–236.

Chapter 4

Nanopowders

Oleg D. Neikov, Frantsevich Institute for Problems of Materials Science (IPMS), Kiev, Ukraine

Currently, it is the convention to consider several kinds of nanomaterials. Under conditions, they can be denoted as consolidated objects, nanosemiconductors, nanoporous structures, numerous nanotubular objects, nanopolymers, catalysts and supramolecular structures [1]. Here, however, we are concerned with their use as powders. The general rule is that the size of the basic structural components (crystallites, phases, pores, particles and molecular ensembles) does not exceed 100 nm.

Such traditional materials as dispersion-strengthened alloys, the structure of which includes ultrafine- and nanoparticles, occupying usually only some 5–10 vol%, as well as wrought metals and alloys, in which assemblies and local non-oriented areas are small but the original coarse grain size remains, do not come into the category of nanomaterials.

It is necessary to note several terminological peculiarities. The terms with 'nano-' prefix such as nanotechnology, nanochemistry, nanoscience, etc. have a wide dissemination. In American literature [2], the nanotechnology concept is accepted as the ability to create and use the materials, devices and systems in which structural elements have sizes ranging from 1 to 100 nm. The nanoscience is science about low-sized matters – that is an aggregate of knowledge about properties of substances and effects on the nanometer scale.

Nanoparticles are low-sized hard substances, the geometrical size of which ranges from tenths to 100 nm. The nanopowders and nanoparticles concepts are in many respects overlapping. But, certainly, it is necessary to bear in mind the possible separate nature of the former and the necessarily aggregated state of the latter (the powder – that is an aggregate of the separate hard small particles ranging from 0.001 to1000 μm).

The fundamental importance of the low-sized objects was underscored in 1959 by Nobel Prize Winner Richard Feynman in a lecture (Feynman, R.P. 'There is plenty of room at the bottom'. In *Miniaturization*. New York: Reinhold, 1961), which later became famous. Feynman told the audience about fantastic perspectives which the creation of the materials on atomic or molecular level promises. He also showed that the necessity will arise to create an absolutely new class of operative and measuring apparatus for handling such small, nanosize objects.

The apparatus predicted by Feynman appeared only in 1980 (scanning tunnel and atomic power microscopes and other devices). At the same time, considerable progress in computer techniques had been made, which allowed us to model the material characteristics on the nanoscale. In this connection a new paradigm, based on submicron assembling, arose. In the traditional technological approach, which is termed 'top-down', the fine and ultrafine objects are created (miniaturization) from large ones (for example, by means of comminution). The second approach termed 'bottom-out', which is popularized in organic chemistry and chemistry of high-molecular compositions, is based on submicron erection of the material with given composition and structure followed by an increase in its size.

Starting with the pioneer work of H. Gleiter and his colleagues [3–5], the interest in nanomaterials is growing steadily. The nanomaterials, because of their unique properties, occupy key positions in state-of-the-art materials science. The nanotechnologies and nanomaterials information grows greatly – articles in journals (*Nanotechnology*, UK; *Journal of Cluster Science including Nanostructured Materials*, The Netherlands, USA; *Journal of Metastable and Nanocrystalline Materials*, Switzerland, Germany; *Journal of Computational and Theoretical Nanoscience*, USA; *Journal of Nanoparticle Research*, The Netherlands, USA; *Journal of Nanoscience and Nanotechnology*, USA; *Materials Science of Nanostructures*, Ukraine; *Physics of Low-Dimensional Structures*, Switzerland; *International Journal of Nanoscience*, Singapore; and *Journal of Aerosol Science*, USA), the proceedings of the numerous conferences and annual symposia, patents and monographs.

In this chapter, the main attention focuses on the production of ultrafine and nanopowders and their application in the particulate condition and consolidated state.

Production Methods

Several methods are available for the production of ultrafine powders used for manufacturing nanomaterials. Conventionally, they can be subdivided into chemical and physical. Such subdivision is yet greatly tentative. Thus, chemical reactions take a large part, for example by evaporation in reacting gas media, while many chemical methods are based on the physical phenomena (such as low-temperature plasma, laser emission and others). The most typical methods of obtaining ultrafine powders are the following:

- evaporation and condensation in a vacuum or inert gas
- gas-phase method of reacting in a gaseous medium
- high-energy disintegration (high-energy comminution, detonation gun spray process and electro-bursting)
- plasma spray process
- mechano-chemical method
- electrochemical precipitation
- chemical precipitation from solution
- self-propagating high-temperature process
- thermal decomposition.

One of the basic processes is inert gas condensation (IGC). With IGC, high-quality powders with low chemical impurities from precursor materials and low amounts of oxides or nitrides from the production process can be produced. Other processes, like flame reduction or plasma reduction, use the decomposition and reduction of metal in a gas flame or plasma. The chemical vapor reaction (CVR) process uses the reaction of metal chlorides and hydrogen in a hot wall reactor. A wet-chemical approach in which the nanoparticles are produced by gelation, precipitation and hydrothermal treatment is used in the so-called sol–gel processes. Let us consider some of these methods of producing ultrafine powder in more detail.

Condensation Technique

The process of powder formation comprises three stages:

1. vaporization, either by evaporating the metal or by its chemical interaction with the components of a gas phase
2. feeding the vapor into the zone of condensation (decomposition)
3. formation of solid particles by condensing or decomposing the gaseous chemical compounds (nucleation and growth of a new condensed phase).

In the case of physical condensation, the temperature of the vapor source is higher than that of the powder formation zone; in most cases of chemical precipitation it is vice versa.

The following conditions are necessary for the condensation of metallic vapor and the formation of a particulate phase: high supersaturation of the vapor sufficient to trigger simultaneous and multiple formation of nucleation centers, and the presence of a neutral gas acting as a medium preventing the coagulation and growth of particles due to diffusion, or evaporation in a vacuum and following physical vapor deposition.

The presence of foreign inclusions, ions and chemically active compounds in the neutral gas promotes the nucleation. Forced or natural circulation of the gas ensures the transfer of the condensation heat and of the particulate matter and contributes to a variety of modes of their growth.

Temperature (T) and pressure (p) are the principal thermodynamic characteristics of the process. The evaporation and precipitation take place at T_1 and p_1 (zone evaporation), at T_2 and p_2 (zone precipitation), respectively.

Under the equilibrium conditions, the phase rule is observed in each zone:

$$G = N - \varphi + 2$$

where G, φ and N stand for the number of components, phases and degrees of freedom, respectively.

Homogeneous and heterogeneous nucleations are distinguished. The former represents the volumetrical condensation. Realizing the evaporation in an inert gas over a deposition surface, it is possible to provoke heterogeneous nucleation, for which the nucleation energy barrier is much lower in comparison with the volumetrical condensation.

By changing the system of supersaturation (by increasing or lowering of vapor pressure, varying, for example, the process temperature), it is possible to adjust the critical nucleus size and obtain the required powder particle size.

Detailed information on the theoretical basis of the gas-phase method and mechanism of powder formation during vapor condensation can be found in Chapter 6.

The inert gas condensation (IGC) is realized by evaporating and condensing a suitable material in a vacuum chamber filled with low pressure inert

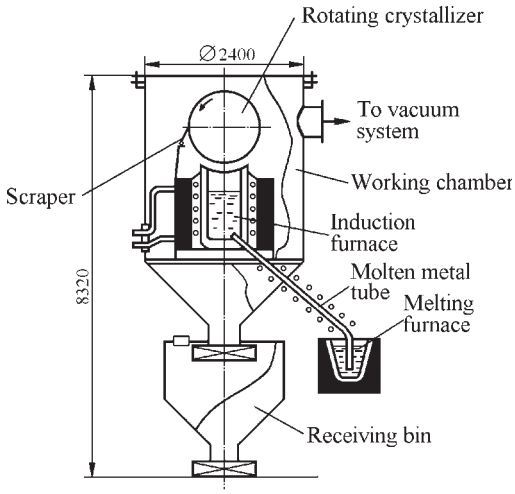

Figure 4.1 Scheme of equipment to produce metallic nanopowders by the inert gas condensation process.

gas (e.g. 100 Pa helium) [6]. The evaporation of the material is performed by electron beam, magnetron sputtering laser, either in a resistance or induction furnace. The vapor forms particles homogeneously due to collisions with the cold inert gas. The particle fog condenses on cooled substrates (crystallizers) that are inserted into the vacuum chamber.

Figure 4.1 shows the scheme of well-known installation utilizing an induction furnace for the metal evaporation. A nitrogen stream directs the zinc vapor to the rotating crystallizer. The particles form a flaky powder layer on the cooling crystallizer surface that is removed continuously by a scraper. The operating conditions for producing zinc nanopowders are as follows: the melt temperature in the induction furnace ranges from 650 to 800°C, the pressure of nitrogen from 3 to 20 kPa and the powder yield in the range from 10 to 15 kg/h.

Figure 4.2 shows the scheme of equipment used on the lab scale by Fraunhofer for the production of precious metal nanopowders with a rate of about 1 to 2 kg per day [7]. The particles are transported to and deposited on cooled surfaces due to free thermal convention (Figure 4.2(a)); by this scheme it is difficult to achieve real control of the powder deposition process resulting, e.g. in a rather low output of usable powder material. A closed-loop gas flow design, as outlined in Figure 4.2(b) has improved on the above concept and may operate at a higher level of gas pressure (ranging from 2 to 5 kPa). The condensed silver particles coagulate within the gas flow forming highly porous (spongy) aggregates that deposit as a fluffy layer on a filter substrate. By using backflow pressure pulses, the powder is easily removed.

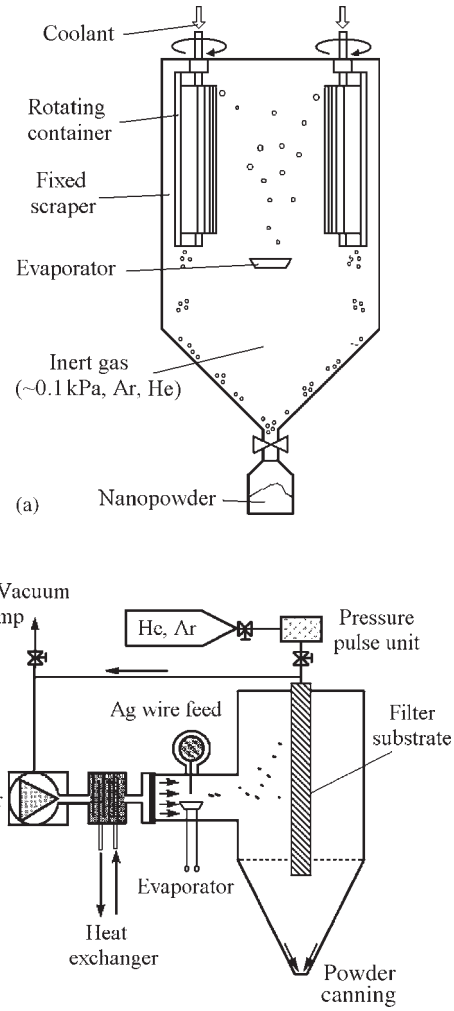

Figure 4.2 Draft of two different variants of the inert gas condensation process: (a) purely convective powder transport and thermophoretic deposition on cooled surfaces followed by mechanical stripping-out of the powder deposits; (b) nanoparticles are transported to the filter substrate by enforced gas flow. Powder removal is realized by means of pressurized backflow pulses.

The excess inert gas volume thereby introduced into the system is pumped off within a few seconds. Thus the process basically runs at a constant background pressure.

The main problem in the production and processing of metallic nanopowders is their high reactivity, explosibility because of very high specific area, and agglomeration of particles.

In the Gleiter's installation, the ultrafine powder obtained in the atmosphere of the evacuated inert gas is combined with vacuum compacting [3]. Condensed on the cooled rotating cylinder, surface

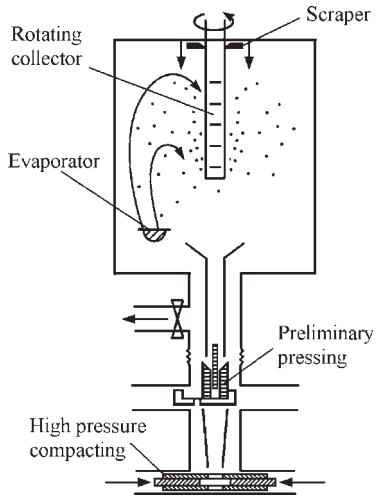

Figure 4.3 Scheme of Gleiter's installation. (Source: Ref 3)

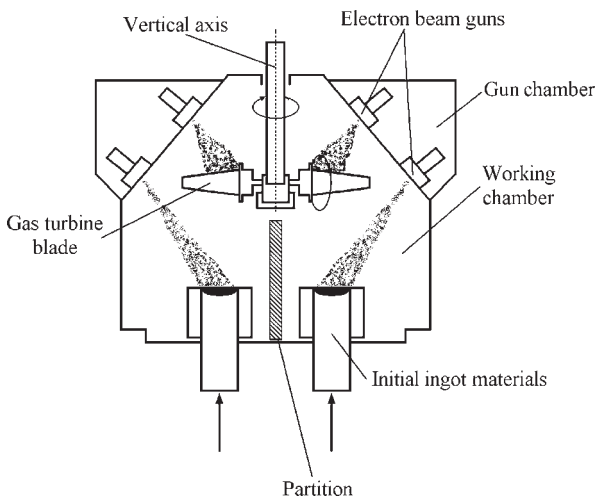

Figure 4.4 Scheme of microlayered material deposition on gas turbine blades. (Source: Ref 8)

powder particles are taken away by a scraper and collected in a press mold of the preliminary pressing, under pressure up to 1 GPa (Figure 4.3), then the green compact is re-pressed at higher pressures (3–5 GPa).

A novel technology for manufacture of semi-products directly from metal vapor, omitting the operation of producing nanopowder, is promising (Figure 4.4) [8]. The simultaneous evaporation of several materials, mixing their vapor flows, followed by condensation on a substrate and subsequent thermomechanical treatment allows the construction of materials with unique properties.

In high vacuum, molecular evaporation from an open surface takes place at a rate that is determined by the Langmuir formula [9]:

$$V = 4.4 \times 10^{-4} \times P_0 \left(\frac{M}{T}\right)^{1/2}$$

where V is the material mass (g), evaporating from 1 cm^2 in 1 s; P_0 is the equilibrium pressure of material vapor at a given temperature, Pa; M is the material molecular mass; T is the evaporation temperature, K. Experimental values of vapor pressures and evaporation rates of the elements and inorganic compounds are given in publications [10,11].

At the beginning of the 1960s, the EO Paton Electric Welding Institute started systematic research and equipment development of electron beam evaporation followed by physical vapor deposition in a vacuum (EBPVD) to produce thick films (1–2 mm) and bulk condensates of inorganic materials with preset structure and properties [12].

The electron beam evaporation of materials in a vacuum differs from other methods in such conditions, namely thermal and ion plasma, primarily by its versatility, technological flexibility and cost effectiveness. During collision of flying electrons with the solid surface, their kinetic energy is consumed in heating, secondary emission and in excitation of X-ray radiation. The main part of the kinetic energy of the electrons on their collision with a solid surface is transformed into thermal energy in a thin subsurface layer of 1–2 μm thickness. At a voltage of 20–25 kV and beam current several amperes, energy losses for X-ray radiation excitation are about 0.1% of the total power of the electron beam. X-ray radiation arising in the above voltage range, has a low penetrability and is completely absorbed by the chamber's metal walls, which are several millimeters thick. Energy losses for excitation of secondary emission (really true secondary emission and reflected electrons) are about 15%. Here, in heating by an electron beam, the heat source is located in the working chamber (see Figure 4.4), and provides the maximum complete transformation of the electric energy into thermal energy.

Modern electron guns of 50–100 kW power enable evaporation of metallic materials at high enough rates, approximately to 10^{-2} g/cm^2s. The evaporators usually used contain a water cooled copper crucible, which collects the evaporated material in the form of an ingot (cast or compacted) with diameter ranging from 25 to 70 mm. The level of the liquid pool surface from which evaporation proceeds is kept constant in most cases, using the mechanism of

vertical displacement of the ingot. For evaporation in a vacuum of 10^{-4}–10^{-6} torr, the spatial density of the vapor flow above the evaporator follows the cosinusoidal law of distribution, according to which the maximum density is observed in the direction normal to the evaporation surface (angle $\alpha = 0$) [10]. At a vacuum down to 10^{-2} torr, the vapor flow is dissipated to produce a more uniform density distribution.

For evaporation of a 70 mm diameter ingot, the rate of vapor flow condensation on a flat stationary substrate located above the liquid pool surface at 300 mm distance, can be up to 30–50 μm per minute for metals and alloys and 15–20 μm per minute for ceramics (i.e. oxides, carbides and borides).

Similar to alloys, pure metals are evaporated as individual atoms. For most alloys, however, the composition of the vapor phase above the liquid alloy is not equivalent to the average ingot alloy composition. Alloy fractionation occurs, namely condensate layers beside the condensation surface, and contains maximum amounts of volatile components. Condensates of multicomponent metallic materials of a composition homogeneous across their thickness are produced, using various evaporation techniques, including evaporation of individual alloy components from independent sources.

Evaporation of compounds (e.g. oxides, carbides and borides, etc.) is, as a rule, accompanied by change of the initial molecules. Many refractory compounds are characterized by dissociation of initial molecules with the formation of gaseous products, for instance: O, Al, AlO_3 and Al_2O form during Al_2O_3 evaporation. Results of analysis of thermal dissociation of compounds are generalized [10,13]. Producing condensates by direct evaporation from one source without any change of the initial composition of the compounds is possible only under the condition that dissociation products have practically the same volatility, i.e. a harmonized 'congruent' evaporation of the compounds is required. Refractory oxides (i.e. Al_2O_3, Y_2O_3, ZrO_2 and MgO), carbides (i.e. TiC, ZrC and NbC) and borides (i.e. TiB_2 and ZrB_2) can be evaporated from water cooled copper crucibles using electron beam heating with practically no change in the composition.

A number of compounds, for instance, WC, SiC, TiN, AlN and ZrN cannot be deposited by direct evaporation because they decompose on heating, forming products with markedly different volatilities. Such compounds can be produced in the form of condensates by component evaporation from two independent sources (i.e. WC and SiC) or using the so-called reactive evaporation, bleeding the appropriate gas into the working chamber and vapor flow ionization [10].

Figure 4.5(a) and (b) shows the schematics of electron beam evaporation of material A from one and A and B from two sources, and subsequent vapor flow condensation on flat surfaces. The condensation surfaces can also be cylindrical or have a more complex shape and can be stationary (Figure 4.5(a)) or make certain movements in space, using an appropriate feed mechanism for motion transfer (Figure 4.5(b)). The schematic (Figure 4.5(b)) corresponds to the technological process of deposition of a two component material AB, for instance WC or SiC, on a flat surface in the form of a circle rotating about a vertical axis. Substrate rotation is required to produce a uniform composition across the condensate thickness.

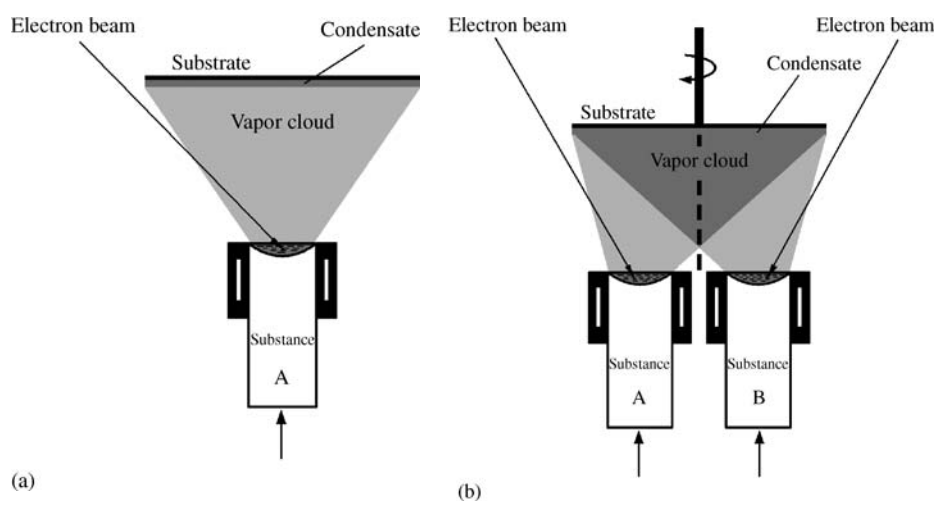

Figure 4.5 Material evaporation process following by condensation: (a) from one source; (b) from two sources. (Source: Ref 12)

It should be noted that such a technological process could be easily transformed during production of multilayer condensates of A/B type by placing a partition between the sources (marked by a dotted line in Figure 4.4). At a constant rate of evaporation of substances A and B, the substrate rotation rate will be a simple and reliable process parameter for adjustment of the thicknesses of alternate layers. Laboratory and production units, developed by the EO Paton Institute have three or four independent evaporators (water cooled crucibles) and corresponding electron beam guns for evaporation of three to four materials by a preset program [12].

However, with regard to simplicity and cost effectiveness of the deposition process, the technology variants of evaporation from one source of mixtures of dissimilar materials, prepared in the form of special tablets or composite ingots, are particularly interesting.

Chemical Precipitation from Solution

Ultrafine copper powders find wide application for microelectronic components, multilayer ceramic capacitors (MLCCs) and μ-metal injection molding (μ-MIM).

μ-MIM is an advanced method of metal injection molding, using sub-μm-sized metal powders and very fine molds to produce extremely small three-dimensional structures with very high resolution, sharp edges and outstanding aspect ratios, while the cheap and well established method of injection molding is applied.

Based on microelectronic components design criteria, the sub-μm particle size of metal powders used is one key component, as e.g. the internal electrodes in MLCCs are only about 1–2 μm in thickness. Theses layers are manufactured by screen printing of metal paste, a technique widely used in electronic components manufacture [14].

Therefore, products like ceramic capacitors and also μ-MIM parts need to use sub-μm-sized metal powders to assure the requirements defined by their dimensional design. It is consequently essential to characterize the particle size not only by means of distribution in general, but also to find a method to characterize the biggest particles present in such powders: for example ceramic capacitor manufacturing normally defines values of $d_{100} < 1.5\,\mu m$ or even $d_{100} < 1.0\,\mu m$.

Industrial consumption of sub-μm powders in quantities of tonnes/month, as well as the cost aspect, emphasizes that the wet chemical process of powder production by precipitation from solution is able to fulfill these requirements in a competitive and economical way.

This process is in principle shown in Figure 4.6. By precise selection of process parameters, including concentrations, temperatures, negative logarithm of hydrogen-ion activity (pH) value, and time, it is possible to control and adjust properties such as particle size, apparent density, specific surface, and overall morphology to customers' requirements.

Nano-sized copper powder produced by the wet chemical precipitation process on a lab-scale is shown in Figure 4.7.

The wet chemical precipitation process can be controlled in such a way as to adjust properties like particle size and it is also able to produce agglomerated as well as non-agglomerated powders (Figure 4.8).

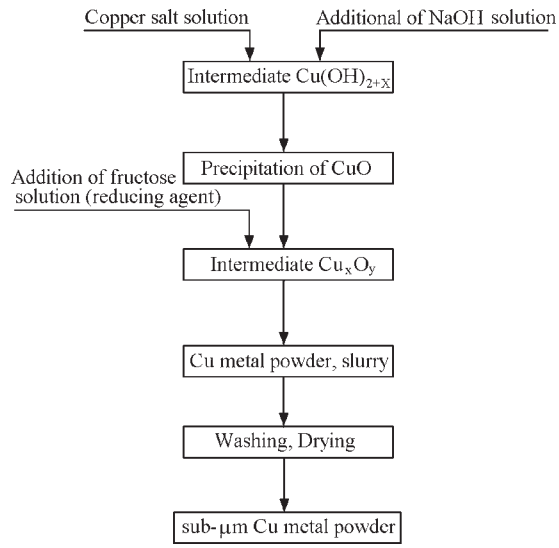

Figure 4.6 Process flow sheet for the wet chemical production of copper powder.

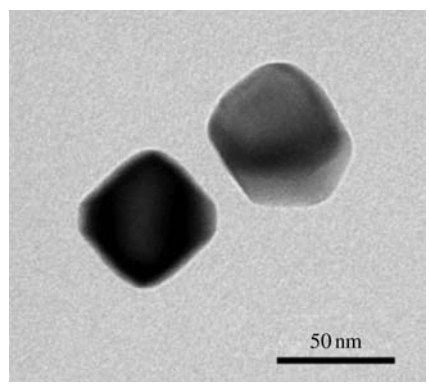

Figure 4.7 Transmission electron micrograph of nanosized copper powder, produced by wet chemical precipitation process in lab-scale. (Source: Ref 14)

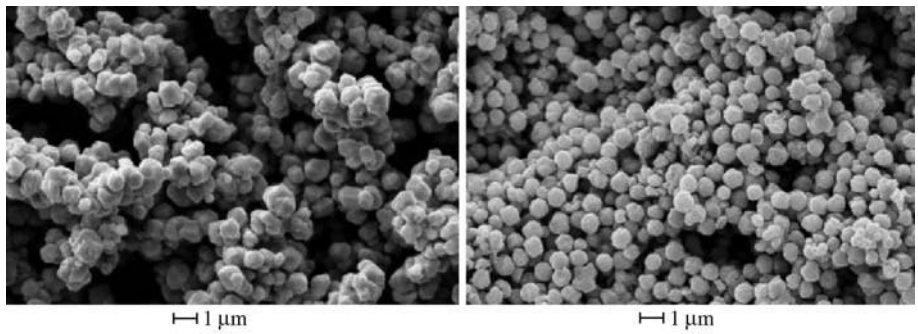

Figure 4.8 Copper powders of different particle size and morphology produced by wet chemical precipitation from copper salt solution: (a) agglomerated powder grade, (b) non-agglomerated powder grade. (Source: Ref 14)

The latter are best suited for metal pastes used for screen printing deposition of thin layers.

It is well known that, for a given cobalt content, the hardness of WC–Co cemented carbides can be increased by decreasing the WC mean particle size. The classical ways of production of WC, described in Chapter 21, allow the production a WC particle size ranging from 0.5 to 20 μm. During the production of ultrafine powders – 0.3–1 μm – starting for instance with WO_3, the formation of $W_{18}O_{49}$, should be skipped over, and the two main reduction steps $WO_3 \rightarrow WO_2$, and $WO_2 \rightarrow W$ should take place in the lowest possible humidity environment [15]. The formation of ultrafine powders is favored by:

- decreasing the amount of tungsten oxide in the boats
- increasing the hydrogen flow rate
- decreasing the passing through rate of the boats
- decreasing the reduction temperature – below 1400°C
- having a smooth temperature gradient in the furnace
- using hydrogen with the lowest dew point
- using a two-step reduction process.

In the production of ultrafine and nanometric powders, the carburization temperature must be kept in the range of 750–1000°C. For such powder production, special ultrafine cobalt powders are needed, since the conventional ones, ranging from 1 to 3 μm, are too coarse.

A new process has been developed for the production of cobalt powder based on the reduction at 210°C of cobaltous hydroxide by a mixture of ethylene- and de-ethylene-glycol [16]. This powder named 'polyol cobalt' is characterized by spherical shape, narrow particle size distribution and non-agglomerated particles (Figures 4.9 and 4.10).

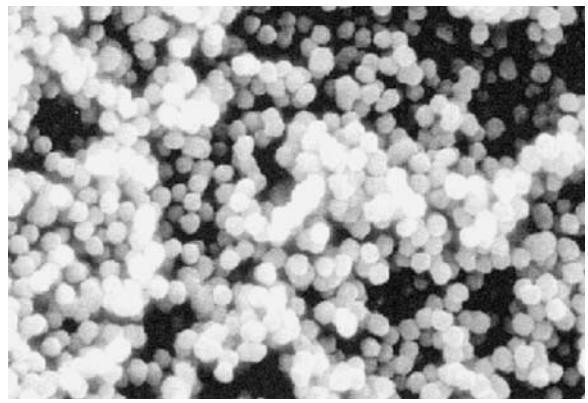

Figure 4.9 SEM micrograph of polyol cobalt powder. (Source: Ref 15)

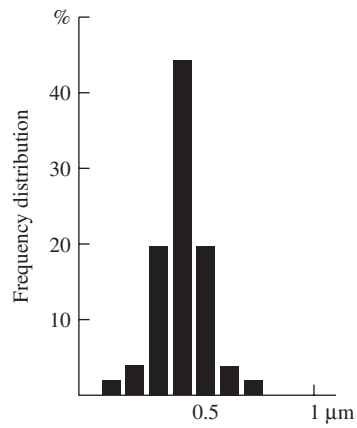

Figure 4.10 Polyol powder particle sizes distribution. (Source: Ref 15)

Replacement of the conventional 'hydrogen reduced cobalt' by 'polyol cobalt' greatly improves the microstructure of the sintered product and allows a decrease of the milling (mixing) time by

half, a decrease in the sintering temperature from 50 to 75°C, and even the avoidance of HIP of low cobalt content grades.

The nanostructured WC-Co cermets starting from water soluble precursor compounds have the advantage that the cobalt can be mixed homogeneously with tungsten at the molecular level, Co to W can be varied over a large range, and additional constituents (Ti, Ta) or grain growth inhibitors (Cr, V) can be introduced homogeneously at the same time.

It is a three step process:

1. preparation and mixing of the starting reactants
   - cobalt tris-ethylenediamine tungstate, obtained by reaction between an aqueous solution of $CoCl_2$ and a solution of H_2WO_4 in ethylene diamine [17,18]
   - ammonium metatungstate or ammonium paratungstate (APT) + cobalt salt + ammonia (aqueous solution, pH = 7) precipitating: $(NH_4)_8(H_2Co_2W_{11}O_{40}) \cdot H_2O$ [19–21],
   - APT + cobalt salt + Cr(Cl O_4) and VCl_3 (grain growth inhibitors) [22]
2. fixed bed- or spray-drying (600–700°C) of the resulting precursor to a chemically homogeneous mixture of oxides
3. classical or fluid-bed thermochemical conversion (700–1000°C, H_2, CH_4, $CO + CO_2$) of the dried mixture into the desired nanoscale (20–50 nm WC powder) composite WC–Co powder.

Nano-sized platinum particles are very active and commercially important as catalysts. One method of production of platinum powder with a size of about 30 nm is the reduction of chloroplatinic acid with sodium borohydride. The reduction process can be written:

$$H_2PtCl_6 + NaBH_4 + 3H_2O \rightarrow Pt_{(s)} + H_3BO_3 + 5HCl + NaCl + 2H_{2(g)}$$

An organic protective agent such as poly (vinylpyrrolidone) is commonly added to prevent coagulation of these ultrafine platinum particles.

Spray Conversion Method

With the advent of closed-cycle systems, production of cemented carbides by spray drying increased considerably in the 1980s. Spray conversion processing

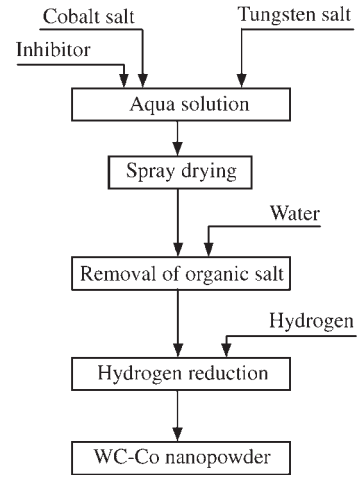

Figure 4.11 Spray conversion process for production of tungsten carbide-cobalt nanopowders.

is a versatile technology which can be applied to a variety of metal–metal systems (e.g. W–Cu) [15,16].

The nitrogen drying gas that is used in spray drying is heated to 75–100°C, depending on the milling liquid used. The solids content of the slurry varies from 75 to 80%. Pressures for single-fluid nozzle atomization range from 590 to 1500 kPa.

Nanotech (Korea) manufactures WC–Co nanopowders by a novel process named the spray conversion method [23]. This process consists of synthesizing a liquid solution, spray drying, hydrogen reduction and carburization for the purpose of the refinement and homogeneous distribution of WC particles and cobalt binder (Figure 4.11).

The commercially produced WC-10 wt% Co nanopowder manufactured by Nanotech using a patented liquid spray conversion process followed by hydrogen reduction and carburization [24] is shown in Figure 4.12.

In order to produce ultrafine and nanometric powders, the carburization temperature must be kept in the range of 750–1000°C.

Plasmachemical Synthesis

Synthesis realized at temperatures of 6000–8000 K allows high supersaturation level, high reaction and condensation process rates. The arc plasmatrons, as well as high- and plasma-microwave generators, are used. The former is more efficient, however, the latter ensures the production of fine and pure powders. The diagram of such an installation is shown in Figure 4.13 [25].

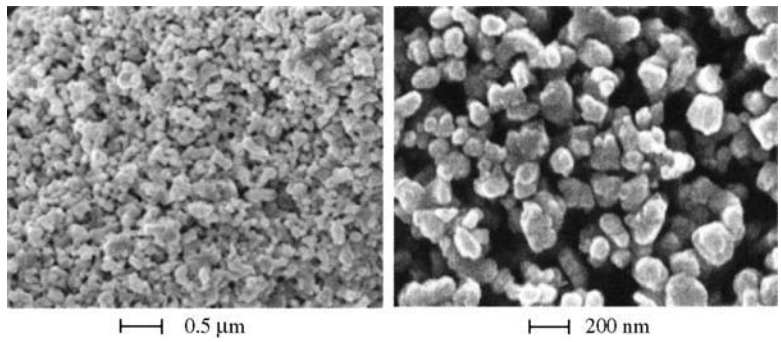

Figure 4.12 SEM micrograph (at different magnifications) of Nanotech (Korea) commercially manufactured WC-10 wt%Co nanopowder produced by spray draying of liquid sources, subsequent hydrogen reduction and carburization.

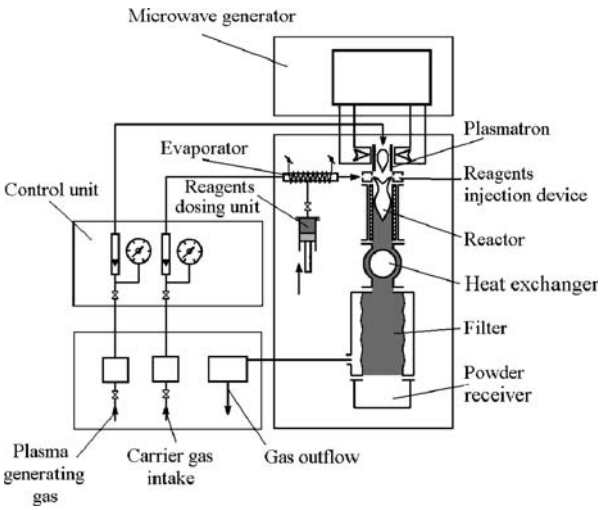

Figure 4.13 Flowchart of plasmachemical synthesis installation.

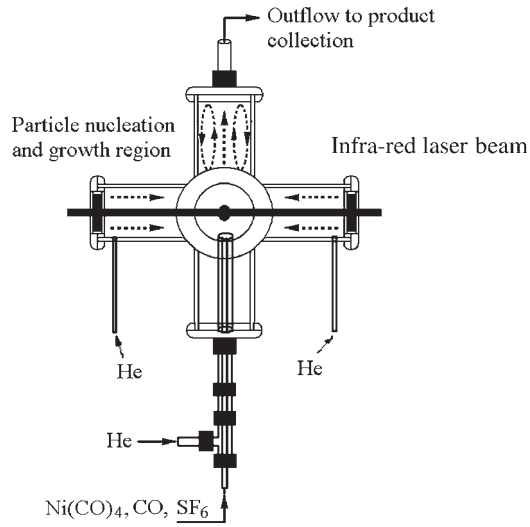

Figure 4.14 Schematic drawing of the lab laser pyrolysis reactor for nickel nanopowders production.

As the initial product, metal chlorides, metal powders and silicon- and metallo-organic compounds are used. Plasma microwave generators and plasmachemical powders of nitrides, metal oxides and other compounds are manufactured.

The plasmachemical technique provides for a production of refractory metal ultrafine powders (W, Mo, Ni), compounds (TiN, AlN, Al_2O_3, SiC, Si_2N_4, Ti(C, N) and others), and composite material types such as Si_3N_4 + SiC and TiB_2 + TiN and others. Due to the features of plasmachemical synthesis (non-isothermal process, coagulation of particles, and others), the particle size distribution range is, in most cases, rather wide.

Laser pyrolysis has been developed for the production of nickel nanopowders [26, 27]. A schematic drawing of the lab laser pyrolysis reactor is shown in Figure 4.14.

This process makes possible the production of nickel particles by laser-driven decomposition of a nickel precursor, such as nickel carbonyl (NiCO). Here, an infrared laser rapidly heats a dilute mixture of nickel carbonyl and a photo-sensitizer in a carrier gas, to decompose the precursor and initiate particle nucleation. The photosensitizer is selected from the group consisting of sulfur hexafluoride, ethylene, silicon tetrafluoride, and ammonia. Nickel carbonyl was generated in situ from activated nickel powder and carbon monoxide at room temperature. During the synthesis process, laser heating allows for rapid cooling of the freshly nucleated particles by mixing with unheated gas. By varying the precursor flow rate, laser energy and unheated gas flow rate to change the residence time, precursor concentration and reaction temperature, the average particle size can

be controlled over a range of primary diameters from 5 to 50 μm. Figure 4.15 illustrates the nickel nanoparticle average sizes versus the carbon monoxide flow rate. Figure 4.16 shows the TEM image and selected area electron diffraction pattern of nickel particles produced with ethylene as photosensitizer. With ethylene, in comparison with the other above photosensitizers, a much larger amount is needed, but there is no risk of nickel fluoride formation and there may be some beneficial effect on the particle morphology as well.

Such powders are of growing interest in the development of nanostructured magnetic materials, motivated by the potential of these materials in a broad range of applications including data storage, biomedicine and telecommunications.

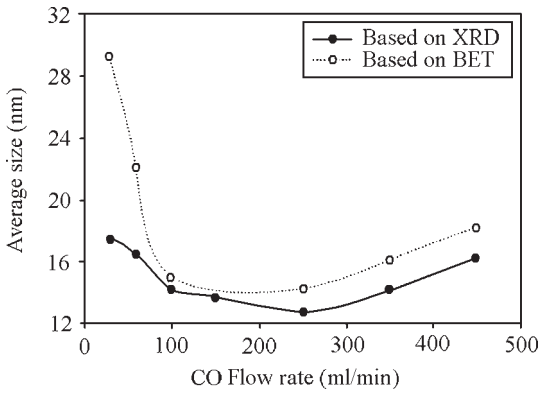

Figure 4.15 Nickel nanoparticle average sizes versus carbon monoxide flow rate.

The plasma arc discharge process is used for synthesis of ultrafine zirconium based alloy powder [28]. Such powders are of particular interest in hydrogen storage and gas absorption application.

Figure 4.17 shows the flowchart of the plasma arc process. This installation mainly consists of

Figure 4.16 TEM image and selected area electron diffraction pattern of nickel particles produced with ethylene as photosensitizer. (Source: Ref 26)

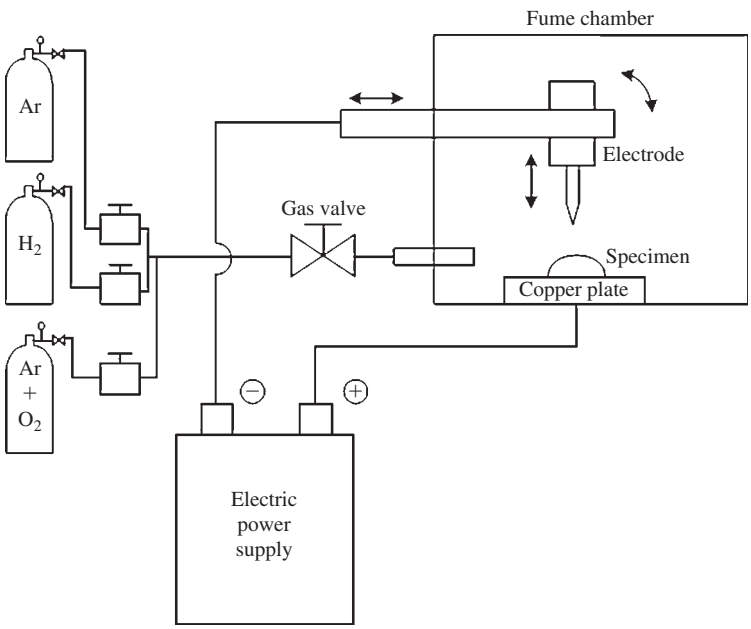

Figure 4.17 Flowchart of plasma arc process for synthesis of ultrafine zirconium-based alloy powder. (Source: Ref 28)

the vacuum chamber, tungsten cathode, copper anode, gas flow system and electric power supply.

$Zr_{57}V_{36}Fe_7$ bulk alloy was used as a raw material. The vacuum chamber was evacuated down to 10^{-5} torr and then backfilled with the hydrogen/argon mixture gas to 300–550 torr. The arc plasma was then initiated between the tungsten cathode and the bulk alloy on the copper anode using an arc current 140 A and an arc voltage of 21–25 V. The mixture ratio of the hydrogen to argon was changed from 4 to 6 to equal volumes.

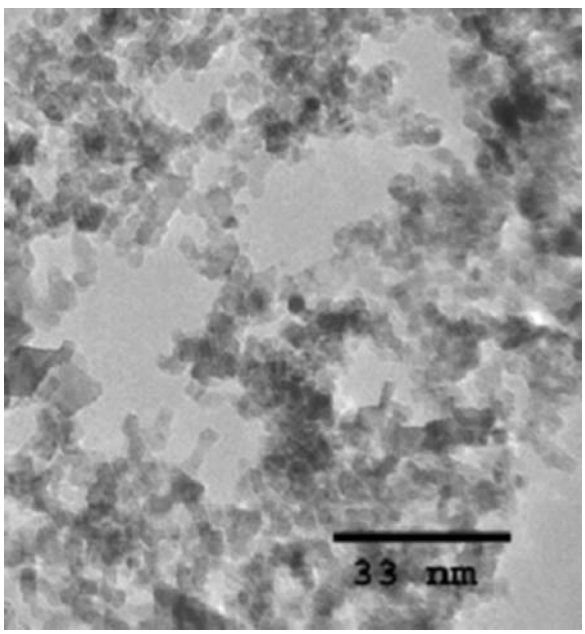

Figure 4.18 Transition electron microscopy image of cerium oxide powder particles. (Source: Ref 29)

The chemical composition of the synthesized powder strongly depends on the volume content of hydrogen in the synthesis atmosphere. The chemical composition of the synthesized powder approaches that of the raw material with increasing hydrogen – up to 50% hydrogen atmosphere. The synthesized powder has an average particle size of 50 nm.

By means of the plasma technique, nanoscale metal oxide powders are produced on a commercial scale [29]. A high resolution TEM image of cerium oxide is shown in Figure 4.18. Particle size distribution of this powder is illustrated in Figure 4.19.

High-energy Comminution

The lower limit of particle size of powders produced by high pressure gas or water atomization is between 1 and 5 μm. Examples are trademark product FLQT5 of aluminum atomized powder with medium diameter 2 ± 1 μm or trademark of silver atomized powder with average diameter 1.2 μm [30].

Vibratory, attrition, jet, planetary and large-diameter tumbler mills may be classified as high-energy mills.

The agglomerated particles of nano-sized WO_2 and W to WC powder, generated by direct carburization, were crushed by a jet mill [31]. This ensured disintegration of the agglomerated particles and led to a decrease of the average particle size of powders, separated in a bag filter, from 72 to 61 nm and increased specific surface area from 5.28 to 6.28 m^2/g.

Commercial jet mills are available from NETZSCH-Feinmahltechnik Company. A fluidized bed jet mill CGS 16, which is able to realize the finest jet milling in the existing CGS series, is shown in Figure 4.20.

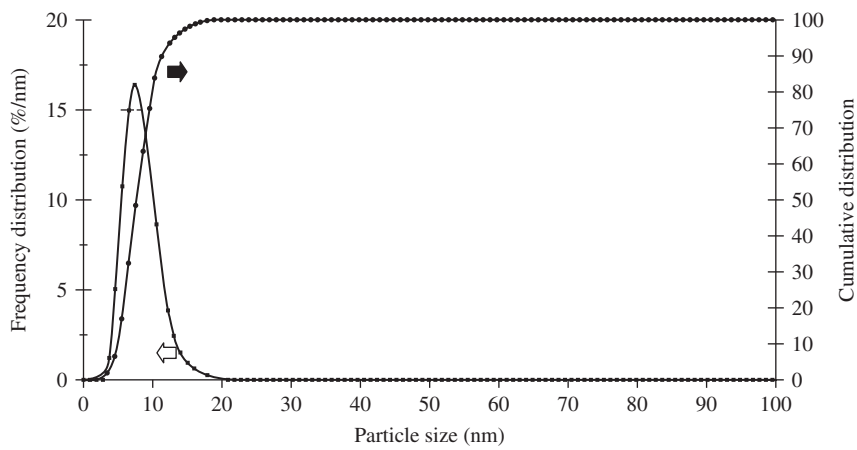

Figure 4.19 Cerium oxide nanopowder particle size distribution. (Source: Ref 29)

The product to be milled is fed through a double flap valve and inlet into the milling chamber above the milling nozzles (Figure 4.21). The material is formed in the bottom of the milling chamber on a fluidized bed by the gas stream from the milling nozzles. Particles from the fluidized bed are drawn into the gas stream and accelerated with increasing velocity towards the center of the chamber. The milling gas, laden with ground particles, rises centrally to the classifier wheel, which is driven by a controlled variable speed motor. Coarse particles are rejected by the classifier wheel and return directly to the fluidized bed. Fine particles together with worked-out gas leave by the fines outlet and are separated sequentially in a cyclone and filter. The CGS 16 mills hard materials down to median particle size $d_{50} = 0.8\,\mu m$ with powder yield of 4.5 kg/h.

For nanotechnologies, NETZSCH-Feinmahltechnik offers a commercial attritor LMZ Type (Figure 4.22) [32]. The circulation mill LMZ 60 is used for pigment production, including titanium dioxide, the most effective white pigment. Its particle sizes are below 1 μm with a throughput above 5000 kg/h.

To produce composition materials of the TiN–AlN system, the initial raw materials consist of titanium hydride and aluminum powder with specific surface 1.5 and 2.1 m^2/g, respectively and are treated in a planetary mill where mechanical activation accelerates the nitriding process which takes place in liquid

Figure 4.20 Model CGS 16 fluidized bed jet mill. Courtesy of NETZSCH-Feinmahltechnik Company.

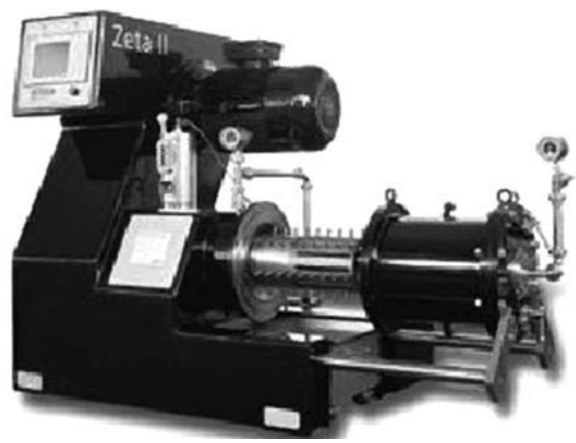

Figure 4.22 Type LMZ wet attritor. Courtesy of NETZSCH-Feinmahltechnik Company.

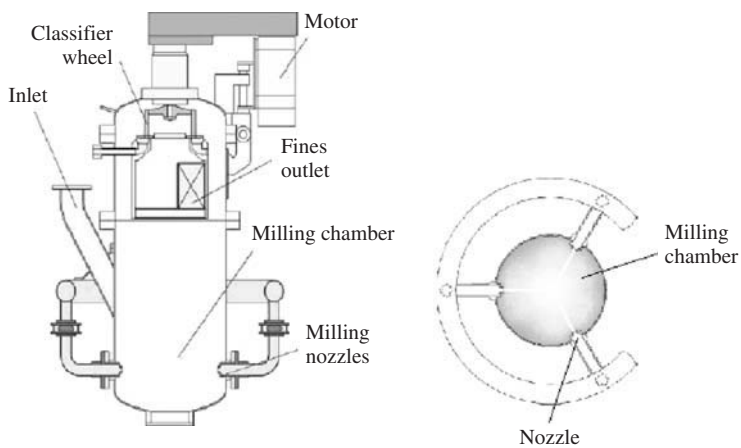

Figure 4.21 Draft of a fluidized bed jet mill.

nitrogen [33]. The processing was fulfilled with 1440 promptness per minute in liquid nitrogen. The proportions of the ingredients corresponds to the equilibrium for the reaction:

$$3TiH_2 + Al + 2N_2 = 3TiN + AlN + 3H_2$$

The specific surface of the product amounts to 2.8, 4.39, 6.16 and 9.49 m^2/g as a result of milling for 10, 30, 40 and 60 minutes, respectively. The average particle size was 160 nm. The mechanical activation accelerates the nitriding process.

Some bulk alloys are easily crushed to fine powder in a hydrogen atmosphere. The Nb–Ti alloys are examples of this kind [34]. These alloys were hydrogenated by a gas–solid thermal reaction system: they were placed in a furnace containing high-purity hydrogen gas and annealed at 1200°C for 3 hours, followed by furnace cooling to room temperature. The hydrogenated Nb–Ti alloys are brittle and friable in comparison with the original alloys. The hydrogenated $Nb_{94}Ti_6$ powders milled in a planetary ball mill with tungsten-carbide balls in air for 60 minutes at room temperature have an average particle size of 2.3 μm, while by milling at a temperature lower than 203 K, the average particle size is less than 1 μm with better uniformity.

Porous compact structures of pure niobium and niobium alloys such as Nb–Ti and Nb–N are widely used as a metal substrate for electrolytic capacitors, which realize a large electrical capacity in a surface layer of niobium pentoxide. Here, the porous compacts are generally produced from powders and one of the ways to improve the performance is to employ powders having finer particle size under 1 μm and higher impurity so as to increase the relative surface area of porous compacts with solid niobium pentoxide layers.

Ultrasonic milling was used for obtaining of tungsten heavy alloy [35]. This process uses ultrasonic cavitation, which leads to the violent collapse of macroscopic bubbles, producing extremely high energy densities [36]. This energy source can be used to produce nanopowders free of impurities. The design of the interface structure of tungsten heavy alloys such as 93W–4.9Ni–2.1Fe is essential for property improvement. In particular, it is necessary to reduce particle sizes, to homogenize the powder mixture, and to maintain purity, in order to reinforce interface strength. Previously, mechanical alloying in an attritor was used, but this resulted in deterioration of the properties of the powder as a result of the pick-up of impurities.

In an ultrasonic milling process [35] with WO_3, NiO and Fe_2O_3 as source materials, powders were mixed together to give a 93W–4.9Ni–2.1Fe composition using a turbular mixer. The mixture was milled in an ultrasonic bath for 50 and 100 h. After drying at 80°C, the powder was sieved. Mean particle size of samples after 50 and 100 h was measured as 500 and 400 nm, respectively. Particle size distribution of the 100 h sample is narrower and the mean size of agglomerates is smaller. The mixture was then reduced at 800°C in hydrogen atmosphere for 1 h.

Explosive evaporation of metal followed by condensation of the vapor is another technique for producing fine particles. It is possible to obtain, in one installation, between 50 and 200 kg/h powders with particle size ranging from 50 to 100 nm using power inputs 25–50 kWh/kg [37]. The explosive metal evaporation occurs by passing through a relatively thin wire of current impulses of 10^4–10^6 A/mm^2. Depending on the atmosphere, the particles may be metallic (in neutral atmospheres) or oxide or nitride. Required particle sizes and powder yield are controlled by the discharge circuit parameters and wire diameter. The particle shape is mainly spheroidal.

Powder Processing Methods

The powder processing methods such as classification, blending, thermal treatment and compaction are complicated with nanodispersed metallic systems due to their high surface activities and, in many cases, new approaches are required. While the influence of the free surface and interfacial energies in the micrometer scale is limited to the well known powder metallurgy phenomena of driving forces for sintering, wetting behavior, and grain growth – on moving to the nanometer scale, even characteristics that generally are considered to be constant will change. So the melting temperature may be lowered by hundreds of degrees, the lattice parameter decreases while the vapor pressure over the solid surface strongly increases if the particle size is as small as 10 nm [38]. With the decreasing particle size, the proportion of atoms located in surfaces or interfaces increases and the surface and grain boundary diffusion with coefficients 10^3 to 10^4 times higher than those of volume diffusion [39] become dominant in thermally activated processes. Important factors for the properties of nanostructured materials are the interactions between lattice defects and interfaces or surfaces as well as dimensional electric and magnetic effects. Fundamentals on this matter are given in [40, 41].

Without arrangements specified during powder production, strong agglomeration of powder particles can take place owing to surface diffusion.

Table 4.1 The relative density data of Ni and Si_3N_4 from various particle size powders pressed at 1 GPa

Particle sizes (μm)	Conventional pressing		Hydrostatic pressing	
	Ni	Si_3N_4	Ni	Si_3N_4
50	0.82	...	0.86	...
5	0.73	...	0.77	...
1.1	...	0.64	...	0.69
0.05	0.58	0.54	0.68	0.60
0.015–0.017	0.49	0.47	0.61	0.50

The powder keeps a high specific surface area, but particles cannot be separated. To prevent agglomeration, particles may be introduced into a liquid before they come into contact. The interactions between powder particles and the environment can also be minimized by coating procedures included in the powder production process [42].

Densification by compaction is difficult as for ductile metals when the particles become very small and their hardness increases. At particles sizes of 50–100 nm, dislocation mechanisms are still active to enable plastic deformation. Smaller particles are dislocation free and the image forces counteract dislocations to penetrate into particles [42]. Higher densities are achieved at elevated temperatures during compaction [43]. The relative density data of Ni and Si_2N_4 powders of various particle size pressed at 1 GPa are given in Table 4.1 [44]. They illustrate the aforesaid: the ductile nickel powders and brittle silicon nitride powders in the ultrafine state are pressed equally.

Higher densities are achieved at elevated temperature during compaction [40]. The biggest problem, however, is connected with grain growth if dense and nanostructured materials have to be obtained by free sintering. Grain growth in the nanostructure can be reduced at least to a certain extent by multiphase alloy design and pressure sintering at lower temperatures. For example, sintering of titanium nitride powders with initial average particle size 60 nm at temperature ranges from 500 to 800°C and pressing pressure 7.7 GPa gives compacts with low porosity (below 3–5%), while by conventional sintering without high pressure, the porosity ranges from 10 to 12% [45].

Applications

At present, there are a number of application fields of nanopowders and numerous potential applications in advanced engineering and technology. Some of these are: nanocomposites, coatings, catalysts, magnetic recording materials, electrically conductive inks and pastes, power engineering, chemical industry, biotechnologies and environmental control [1,2].

Vapor Deposition in a Vacuum

Today, the prevailing methods to produce nanopowders in a controlled way are gas-phase processes and sol–gel techniques.

Due to the high reactivity of nanopowders, the main problem of pickup of oxides or nitrides during processing or storage needs to be prevented. As nanopowders are used or processed in suspension, agglomeration is also a quality issue because of the need of deagglomeration of the powders. Both parameters, the pickup of gaseous impurities and agglomeration, increase with decreasing particle size. Therefore, for nanopowders, the development of technologies that combine production and processing is essential. Just such a principle was used in Gleiter's lab installation [3] and is used in recent commercial units [24,29,46–49]. While the IGC process equipment was in the beginning used only in fundamental studies [3,7], tonnage quantities of nanopowders are now being produced [47–50].

The general view of the UE-204 installation of the EO Paton Electric Welding Institute International center for electron beam technologies is presented in Figure 4.23. Its work chamber amounts to one cubic meter in size and is provided with four independent evaporators and six beam guns, each 60 kW in capacity. The vapor yield in such installation amounts to 10 kg/h.

Figure 4.4 shows the scheme of the installation in the process of microlaminate coating forming on the rotating blade of a gas turbine. Electron beam guns located in the gun chambers isolated from the working chamber perform the evaporation of the initial ingot materials. The two upper guns heat the substrate to the required temperature. The partition prevents

mixing of the vapor flows formed in the left and right parts of the working chamber and the substrate rotation provides the formation of a microlaminate condensate [51].

Typical distribution of the main elements in the coating cross-section, produced by successive evaporation of CrAlY alloy ingot and of the above composite ingot is shown in Figure 4.24 [52]. In the evaporation of the NiCrAl alloy, chromium is the first to evaporate and it forms a chromium rich layer (55 wt% Cr) 4–5 μm thick on the bed coat surface. Then, as the insert evaporates, NiAl intermetallic with 5%Cr forms approximately 10 μm thick. The second bond coat consists of two layers: first, a chromium rich layer and then an NiAl intermetallic layer.

Figure 4.25 gives typical data of ultimate strength (a) and microhardness (b) of two phase Fe–Cu, C–Cu and Mo–Cu condensates, produced by deposition from two independent sources at substrate temperatures of 600, 850 and 950°C.

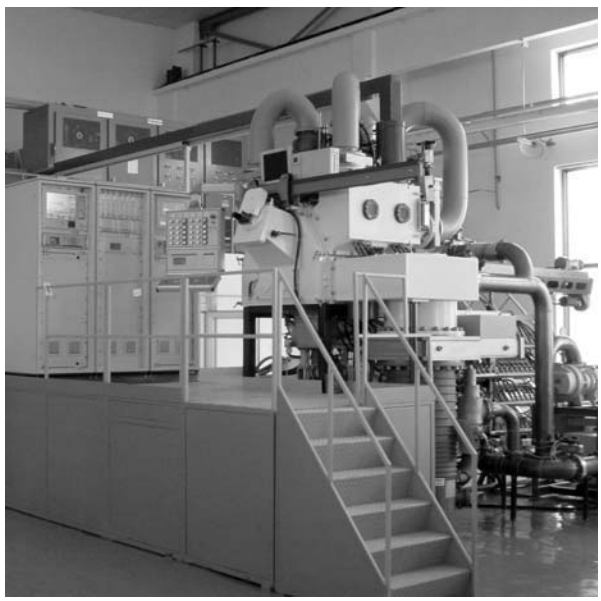

Figure 4.23 Installation UE-204 of the EO Paton Electric Welding Institute International center for electron beam technologies used for electron beam evaporation and following physical vapor deposition in a vacuum and the manufacture of various materials and components. Courtesy of Professor BA Movchan.

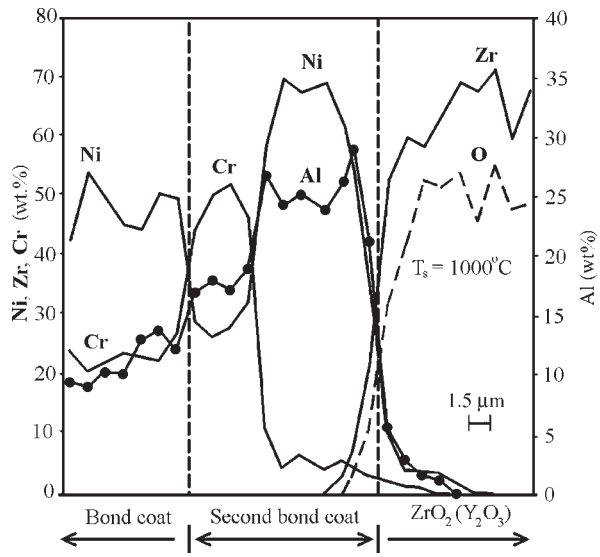

Figure 4.24 Element distributions across the coating thickness produced by evaporation of CrAlY alloy. (Source: Ref 52)

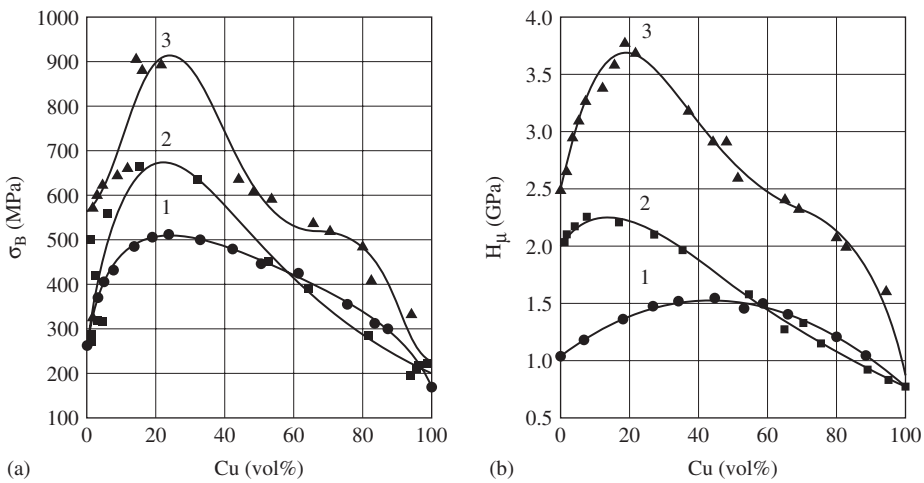

Figure 4.25 Ultimate strength and microhardness of two phase (1) Fe–Cu, (2) Cr–Cu and (3) Mo–Cu condensates depending on copper volume concentration. (Source: Ref 12)

Because the structural coatings have a greater thickness as compared with normal protective coatings, they can perform the function of the bearing members. The bimetal structures in which the second layer is produced by the EBPVD method is the simplest example of structural coatings. Some experience is available on the application of structural coatings for producing channeled components. First, precise casting or machining is used to make semiproducts with open channels. Then the channels are filled with a salt mask and structural coatings are deposited on the surface of the masked channels. Next the aforenamed component is heated to a temperature above the condensation one. Salt filler evaporates to empty the channels. Figure 4.26 shows the blade and vane blanks with channels, produced by precise casting, before (on the left) and after (on the right) deposition of the about 0.7 mm structural coating.

Figure 4.27 shows examples of a disk and billets produced by EBPVD process [12].

At present, the following examples of existing and currently developed practical applications of vapor phase technologies are given [12]:

- protective and structural coatings on gas turbine blades for various purposes
- solid oxide fuel cells
- superhard coatings on tools for material processing
- catalysts in the form of graded coatings on an appropriate surface (e.g. wire and strip, etc)
- materials and coatings with special physical properties (e.g. optical, electric, magnetic, etc)
- biomaterials and biocoatings.

Because of their high reactivity, ultrafine powders are provided with a passivating surface layer to aid handling and incorporation into the final product [49]. The commercial ultrafine aluminum powder is passivated with an oxide layer less than 5 nm thick. The powder particles have a spherical shape, controlled size distribution in the range 100 nm ± 50 nm, and high surface area to volume ratio ranging from 25 to 30 m^2/g. The residual metal content is 65%. QinetiQ Nanomaterials Ltd [49] is developing the process to cover a range of metals including copper, nickel, tungsten and silver.

An assessment of the worldwide value of physical vapor deposition (PVD) industry development (published in July 2005) [53] showed that the value of worldwide shipments of PVD equipment was estimated to be $5.2 billion by 2005 and was forecast to rise at an average annual growth rate (AAGR) of

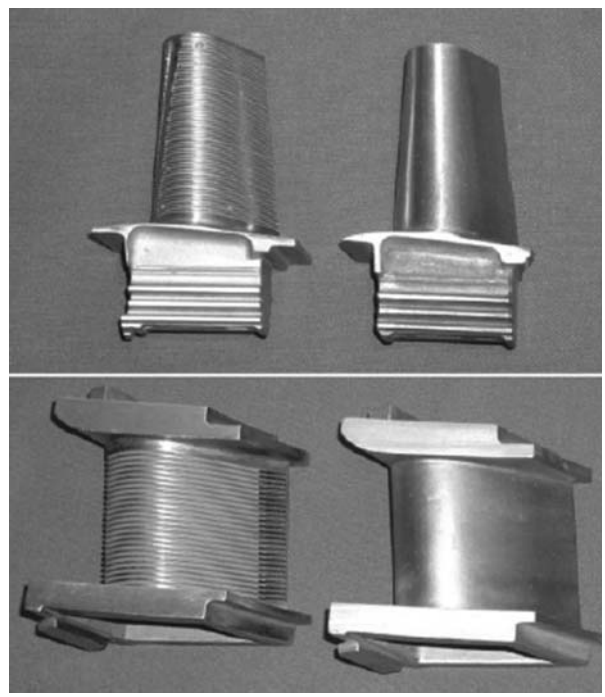

Figure 4.26 Channel blade and vane with channels, produced by precision casting, before (left) and after (right) deposition of the about 0.7 mm structural coating.

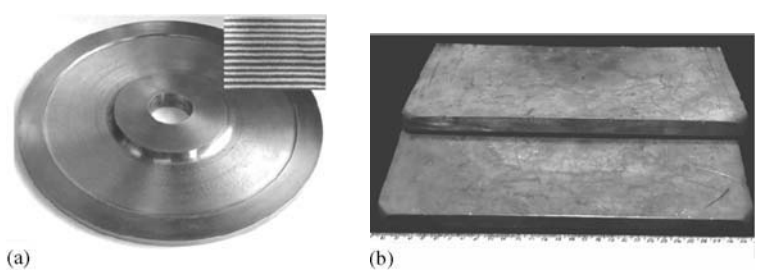

Figure 4.27 (a) 220 mm diameter and 15 mm thickness disk, composed of 10 000 alternating TiAl/Ti microlayers; (b) 300 × 80 × 16 mm strips of Cu–Cr–Nb alloy.

10.1%, and reach $8.4 billion by 2010. The value of materials deposited was estimated to be $1.1 billion by 2005 and was expected to rise at an AAGR of 11.1% to $1.8 billion by 2010. According to this forecast, the microelectronics industry, encompassing semiconductors, components and flat panel displays, remains the largest market segment with data storage representing the fastest growing sector.

Non-consolidated nanopowders find wide application due to their special catalytic, optical, biological, electrical and magnetic properties. A broad spectrum of metal oxide nanopowders is produced for various purposes [48], including antimicrobial (wood preservation, marine antifouling, textile fibers, thermoplastics and permanent coatings), catalysts (environmental catalysts and fuel cells), performance coatings (abrasion-resistant coatings), personal care, polishing (glass polishing and semiconductor polishing).

Cemented Carbides

The discovery that a reduction of the carbide particle size results in considerable improvement in hardness and wear, as well as strength, makes further grain refinement down to real nanostructures interesting [15,54,55]. Along with this, the preparation of a homogeneous microstructure and the reduction of size of crack initiating defects in parallel with the carbide grain size are important [53]. Commercial cemented carbide powders with particle sizes below 200 nm are available (Table 4.2).

The greatest challenge is grain coarsening during sintering. The reduction of the sintering temperature appears to be the important factor. Two ways appear to be possible to reduce grain coarsening:

- adjustment of a favorable initial state for sintering with a homogeneous distribution of the cobalt phase and homogeneous packing of the carbide particles in order to avoid local densification during sintering connected with the formation of large pores [53]; extensive densification during solid state sintering
- densification at low temperatures using pressure assisted sintering (hot pressing, HIP or SPS).

Several processes are under development for the production of nanostructured cemented carbides, like the Nanodyne Process [55–58], mechanochemical

Table 4.2 Commercial cemented carbide and cobalt powders

Property	Unit	Trade grade					
		NC6	NC8	NC9	NC10	NC12	NACO-UF
Nominal composition:							
Cobalt	wt%	6	8	9	10	12	99.85 min
Tungsten carbide + dopant	wt%	85–94	85–94	85–94	85–94	85–94	...
Total carbon	wt%	5.85–5.95	5.75–5.85	5.72–5.82	5.65–5.75	5.55–5.65	0.05 max
Impurities max:							
Aluminum	ppm	20	20	20	20	20	...
Calcium	ppm	10	10	10	10	10	40
Copper	ppm	40	40	40	40	40	...
Iron	ppm	5	5	5	5	5	50
Magnesium	ppm	4	4	4	4	4	20
Manganese	ppm	4	4	4	4	4	50
Molybdenum	ppm	10	10	10	10	10	...
Nickel	ppm	80	80	80	80	80	80
Lead	ppm	2	2	2	2	2	20
Potassium	ppm	1	1	1	1	1	...
Silicon	ppm	...	...	...	...	...	50
Sodium	ppm	7	7	7	7	7	...
Sulfur	ppm	40	40	40	40	40	50
Oxygen	wt%	...	...	...	...	...	0.5
Zinc	ppm	...	...	...	...	...	5
Particle sizes	μm	<0.2	<0.2	<0.2	<0.2	<0.2	2–4[a]
Apparent density	g/cm^3	≤1.95	≤1.80	≤1.70	≤1.65	≤1.50	0.5–0.9

[a]Median diameter of lognormal distribution of particle sizes. Source: Ref 24

synthesis [59], gas phase carburization [54], or high energy milling.

Thus, mechano-chemical synthesis is accomplished in the following way [60]. Mixtures of elemental powders (tungsten, graphite and cobalt with particle size smaller than 75 μm) are milled under argon in a planetary ball mill. The particle size decreases to 16 nm after 20 h and to 11 nm after 100 h of milling. The integrated mechanical and thermal activation process [61] consist of high energy milling of a mixture WO_3 + CaO + graphite. The milled powder is subsequently subjected to reduction and carburization at 1000°C in argon.

High-purity nanosized WC–Co powders with a mean WC particle size of 60 nm and a cobalt content of 11 wt% can be prepared from $CoWO_4$ by a two-step process: hydrogen-plasma reduction giving W–Co powders around 40 nm in a very short time (10^{-3} s); carburization at low temperature (550–950°C) in CO + H_2 atmosphere [62].

The problem of grain growth preventing sintering of ultrafine and nanometric WC–Co powders has often been solved in recent decades by adding grain growth inhibitors (mainly VC, Cr_3C_2 and TaC).

A new class of solid solution grain growth inhibitor alloys, which are solid solutions of VC and Cr_3C_2 in a Co-rich matrix, has been developed [63]. These alloys form multicomponent liquids at temperatures as low as 1200°C, so that the inhibitor carbide phase can be dispersed in the Co-rich liquid phase at a lower temperature than is common. Thus ultrafine and nanometric grades can be sintered to full density at 1250°C, resulting in a finer microstructure with high magnetic coercivity; this leads to higher hardness and toughness.

The ultrafine- and nanometric-grained tungsten carbide-cobalt cemented carbides exceed the classical fine-grained WC–Co in hardness at identical toughness, by displaying a 2 to 6 times higher wear resistance. They are finding increasing application, about 35% of the total cemented carbide production, in wear parts, round tools, end mills, drills (Figure 4.28), helical cutters, chipless forming tools, circular shearing and cutting blades for paper and plastics, dental tools and microdrills for the electronic industry. For instance, in this last application, a WC (0.4 μm)−6 wt% Co grade, with a hardness of HV_{30} = 2050 (94 HRA) is used to produce drills with a particularly sharp cutting edge, working at a rotating speed of 40 000 revolutions/min.

Figure 4.28 Selection of nanometric WC-Co solid carbide end mills, drills and rods. (Source: Ref 24)

Fiber-reinforced Material

Tungsten carbide nanorods, with diameters between 2 and 40 nm and a length to diameter ratio of 10 to 1000, can be produced by a chemical vapor transport process carried out in a continuous flow reactor, using a support metal catalyst – a carrier tungsten carbide coated with a metal catalyst (Co/P) – a volatile species source (tungsten oxide), and a carbon source (carbon black). Iodine acts as the transport reagent. The powder thus obtained (WC nanorods + Co) is mixed with paraffin wax or stearate-based lubricants, formed by extrusion (which facilitates the directional arrangement of the tungsten carbide nanorods), and hot pressed in a hydrogen + ammonia atmosphere. As a result of the nanorods' parallel orientation, the contact area between the rods is considerably decreased while, in the radial direction, the characteristics of this fiber-reinforced material is strengthened [64].

Gradient Materials

Since the late 1960s, hundreds of patents and papers have been published on PVD and CVD coating of the surface of cutting inserts by a variety of functionally different materials [15]. This shows the considerable success of the coated cutting tools. But, nearly simultaneously, many attempts have been made to create and develop cemented carbides with a combination of different layers which complement the properties of each other, for instance by reciprocal co-sintering, common gradual pressing, sputtering or electrophoretic deposition of different compositions [65].

Nanopowder-polymer Composites

Metallic filling powders in polymers play an important role in the realization of electrical conductive adhesives, radio frequency shielding polymers, or magnetic polymeric layers. In most cases, the use of high-aspect ratio fibers and flake is advantageous.

The PVD process may be used for nanopowder polymer composites [12]. Coming back to the process sequence in Figure 4.5, it should be noted that if one of the evaporated metals A or B is to be replaced by a polymer, a variant of the nanopowder polymer will be obtained.

A reduction of the relative amount of metal powder in an electrical conductive adhesive or polymer is possible by using porous nanoscale powders. With this reduction of filler volume, adhesives with a better thermo-cycling behavior can be produced for applications in microelectronics [66].

Thin Film Technique

The manufacture of films of a variety of makeup in a non-porous state is possible in a wide range of particle sizes, beginning at 1–2 nm and higher. Physical vapor deposition (PVD) methods, as well as chemical vapor deposition (CVD), and also electrodeposition, ion deposition, and others are used. Excitation of the voltaic arc in a nitrogen or carbon-bearing atmosphere is one of the most widespread ion deposition technology variants; metallic cathodes are used as metal ion sources. The electric arc evaporation is a highly productive process but is companioned by formation of a dripping metal phase. The magnetron variant of ion-plasma deposition, in which a target (cathode) is atomized by means of gas discharge ion-plasma bombardment, is free from the above imperfection. The transversal magnetostatic field localizes the plasma at the atomized target surface and increases the atomization efficiency. By magnetron deposition, the substrate temperatures are moderate (below 100–200°C), that widens the opportunities of nanograin and amorphous thin films. But spraying yields are some times less than by the electric arc evaporation.

Nanograin films represent a diamagnetic (as copper) or paramagnetic (as rhenium) matrix with nanoparticle inclusions of ferromagnetic metal (cobalt, iron and nickel) [45,67]. The devices for information recording (recording heads, magnetic carriers, disks, etc) are an important field of application of the magnetic nanomaterials. Lightness reproducibility, stability in storage, high recording density and low cost are only some of the demands of these systems. The giant magnetic resistance (GMR) manifestations in multilayer magnetic/non-magnetic films like Fe/Cr, Co/Cu, etc, have proved to be very useful for efficient recording of information [68]. Various makeups of nanostructure Co–Cu films obtained by electrolytic precipitation were studied [69–71].

Multilayer films of Nb/Fe and Nb/Gd systems consisting of ferromagnetic and superconducting layers are also considered as a promising area for electronics and measurement technology.

Semiconductors

In the case of semiconductors, the conversion to nanostructures is accompanied by shift of luminescence spectra in the short-wave area, increase of energy gap width, and other phenomena, and finds interesting and important applications [2]. Monocrystalline CdSe particles in polymeric matrices are considered as light diodes and optical switches for the laser systems, as well as sensors in biological applications.

The semiconductor nanoparticles are synthesized by colloidal methods, hydrolysis treatment, gas phase technique (included phase evaporation), etc.

Application of heterogeneous structures with multilayers as AlGaAs/GaAs in semiconductor lasers has allowed a considerable decrease in the threshold currents, uses more short radiation waves, and improved other field-performance factors in fast optical fiber information transfer systems. The conversion to nanostructures with quantum wires and dots leads to still more considerable effects (further decrease of the threshold current, increase temperature stability and others) important for lasers, optical modulators, detectors and emitters, working in the far-infrared region. The semiconductor nanostructures are very promising for solar energy conversion systems. Thus the advance in the creation of heterogeneous structures with quantum wires and dots will make possible improvements to the performance of present day and future techniques.

Miniaturized Systems

Miniaturization of advanced techniques defines the specifications of components used to design and produce, for example, highly integrated printed circuit boards (PCB) for PCs and cell phones. All these advanced PCBs each use hundreds of capacitors – so-called MLCCs (multilayer ceramic capacitor) contain components with ultrafine metal powders. A modern cell phone for example, contains about 300–500 MLCCs and perfected electronics used in modern cars consume about 5000 MLCCs per car. To keep the units small in size, these capacitors are all typically not more

than 1.2 mm in thickness, although they have a quite complicated internal laminate structure consisting of several hundreds of layers; most advanced MLCCs already have even more than 1000 layers.

Though the internal structure of these components is really complicated and miniaturized, MLCCs have become a cheap mass product: e.g. in 2000 about 581 billion MLCCs were consumed at an average price level of only US$ 0.0107 per capacitor [72].

Another application requiring the use of ultrafine metal powders is μ-MIM, an advanced kind of metal injection molding (MIM) able to produce μm-sized three-dimensional structures with high resolution as a low cost mass product.

A lot of work is going on in the field of microelectromechanical and nano-electromechanical (less than 100 nm) systems that find application in superminiature sensors, electric motors, transformers, valves, shutters, etc. Currently, there are already pilot models of microelectric motors with rotor size about 1 mm and rotor speed up to 40 000 revolutions per minute.

References

1. Andrievski, R.A., Nanomaterials: conceptions and up-to-date problems. *Russian Chemical Journal*, 2002, XLVI(5):50–56.
2. Nanotechnology research directions: IWGN Workshop report. Vision for Nanotechnology R&D in the next decade. On behalf of NSTS/CT/IWGN, eds. M.C., Roco, R.S., Williams, P. Alivisatos. Kluwer Academic Publishers, Dorbrecht, 1999.
3. Gleiter, H., Nanocrystalline materials. *Prog. Mater. Sci.*, 1989, 33:223–315.
4. Birringer, R., Gleiter, H., Klein, H.-P., Marquard, P., Nanocrystalline materials: an approach to the novel solid structure with gas-like disorder? *Phys. Lett.*, 1984, 102:365–369.
5. Birringer, R., Herr, U., Gleiter, H., Nanocrystalline materials – a first report. *Trans. Jap. Inst. Met. Suppl.*, 1986, 27:43–52.
6. Eifert, H., Metallic Nanopowders. In *ASM Handbook*, Vol. 7. ASM International Publishers, 1998, pp. 77–79.
7. Günther, B., Schäfer. In *Proceedings of 1998 Powder Metallurgy World Congress, Granada*, European Powder Metallurgy Association Publishers, Shrewsbury, UK. 1998, Vol. 1, pp. 567–572.
8. Movchan, B.A., EB-PVD Technology in the gas turbine industry: present and future. *J. Metals. Miner. Mater. Soc.*, 1996, 48:40–45.
9. Langmuir, I., *Physic Rev.*, 1913, 2(5):329–342.
10. Maissel, L., Gland, R. (eds). *Handbook of Thin Film Technology*, Vol. 1. McGraw Hill Company Publishers, New York, 1970.
11. Nesmiyanov, A.N., *Vapour Pressure of Chemical Elements*. AN USSR Publishing House, Moscow, 1961.
12. Movchan, B.A., Inorganic materials and coatings produced by EBPED. *Surface Engineering*, 2006, 22(1):35–46.
13. Kulikov, I.S., *Thermal Dissociation of Compounds*. Metallurgia Publishing House, Moscow, 1969 (in Russian).
14. Huenert, R., Ultrafine copper powder. In *Proceedings of 2002 Powder Metallurgy World Congress, Princeton*, MPIF Publishers, New Jersey, 2002, Vol. 10, pp. 1–11.
15. Pastor, H., Developments in tungsten carbide-cobalt cemented carbides. In *International Powder Metallurgy Directory & Yearbook*, 12th edn, 2006/2007, pp 99–108.
16. Pastor, H. et al., New spherical mono-dispersed and non-agglomerated cobalt powder. In *Proceedings of Int. Conf. on Advanced in Hard Materials Production*. EPMA, Shrewsbury, 1992, pp. 6-1–6-11.
17. US Patent 5,338,330 (Aug. 16, 1994), July 24, 1991.
18. US Patent 5,352,269 (Oct. 4, 1994) July 9, 1991.
19. Intern. Pat. WO 96 / 03239 (Feb. 8, 1996), Swed. Appl. July 21, 1994.
20. Intern. Pat. WO 96 / 14952 (May 23, 1996), Swed. Appl. Nov. 16, 1994.
21. Wahlberg, S., Nano-structured hard material composites by molecular engineering. 1. Synthesis from soluble tungsten salts. *Nanostruct. Mater.*, 1997, 9:105–108.
22. Intern. Pat. WO 96 14962 (Feb. 8, 1996), Swed. Appl. July 22, 1994.
23. Spray drying and granulation. In Powder metal technologies and applications, *ASM Handbook*, Vol. 7. ASM International Publishers, 1998, pp. 91–96.
24. Nanotech (Korea). www.nanopowder.co.kr
25. Troizkiy, V.N., Production of ultrafine powders in plasma microwave discharge. In Proceedings 'Plasma microwave generators: physics, technique, and application'. *Energoatomizdat*, Moscow, 1988, pp. 175–221.
26. US Patent Application 20060225534, Oct. 12, 2006.
27. Ténégal, F. et al., Large scale production of nanoparticles by laser pyrolysis. In *Proceedings of 2006 Powder Metallurgy World Congress*, Korean Powder Metallurgy Institute, Busan, Korea, 2006, pp. 235–236.
28. Lee, Gil-Geun, Park, Je-Shin, Kim, Won-Baek, Synthesis of Ultrafine Zr based alloy powder by plasma arc discharge process. In *Proceedings of 2006 Powder Metallurgy World Congress*, Korean

Powder Metallurgy Institute, Busan, Korea, 2006, pp. 505–506.
29. NanoProducts Corporation, Colorado, USA, www.nanoproducts.com
30. Nippon Metal Powder Corporation, Japan, www.Syhitech.en.alibaba.com
31. Yamonato, Y., Mizukami, M., Development of nano-sized WC powder for hardmetal In *Proceedings of 2006 Powder Metallurgy World Congress*, Korean Powder Metallurgy Institute, Busan, Korea, 2006, pp. 427–428.
32. NETZSCH-Feinmahltechnik: Technologie – Nano, www.netzsch-feinmahltechnik.de
33. Krushinskaya, L.A. et al., Production of ultrafine Ti–AlN powders. *Material Science of Nanostructures*, 2006, (1):3–8.
34. Semboshi, S., Masahashi, N., Kono, T.J., Hanada, S., Powder fabrication of Nb–Ti alloys using hydrogenation process. In *Proceedings of 2006 Powder Metallurgy World Congress*, Korean Powder Metallurgy Institute, Busan, Korea, 2006, pp. 250–251.
35. Lee, Ch-W., Lee, S-Ch., Lee, J-S, Synthesis of nanocomposite powder for tungsten heavy alloy by hydrogen reduction of ultrasonic-milled oxide nanopowders. In *Proceedings of 2006 Powder Metallurgy World Congress*, Korean Powder Metallurgy Institute, Busan, Korea, 2006, pp. 507–506.
36. Suslick, K.S., Price, G.J., Applications of ultrasound to materials chemistry. *Annual Review Materials Science*, 1999, 24:295–326.
37. Kotov, Yu.A., Nanopowders derivable with using of target heating by impulse technique. *Advance materials*, 2003, 4:79–81 (in Russian).
38. Geguzin, J.E., *Physik des Sinterns*. Deutscher Verlag für Grundstoffindustrie Publishers, Leipzig, 1973.
39. Kolobov, Yu.P., *Grain Boundary Diffusion and Properties of Nanostructured Materials*. Nauka Publishers, Novosibirsk, 2001.
40. Morris, D.G., *Mechanical Behaviour of Nanostructured Materials.* Trans Tech Publications, Zurich, 1998.
41. Ajayan, P.M. et al., *Nanocomposite Science and Technology*. Willey-VCH Publishers, Weinheim, 2003.
42. Siegel, R.W., Hu, E., Rocco, M.C., *Nanostructure Science and Technology – a Worldwide Study*. WTEC, Loyola College Publishers, Maryland, 1999.
43. Sanders, P.G. et al., The strength of nanocrystalline metals with and without flaws. *Mater. Sci. Eng.*, A, 1999, 234:77–82.
44. Andrievski, R.A., *Powder Material Science*. Metallurgia Publishers, Moscow, 1991 (in Russian).
45. Andrievski, R.A., Ragulya, A.V., *Nanostructure Materials*. Academa Publishers, Moscow, 2005 (in Russian).
46. Biogate, www.bio-gate.de/index2.html
47. TECHNANOGY, www.technanogy.net
48. Nanophase Technologies, www.nanophase.com
49. QinetiQ Nanomaterials Ltd (UK), www.nano.qinetiq.com
50. www.k-set.com/ebpvd.htm
51. Movchan, B.A., EB-PVD Technology in the gas turbine industry: present and future. *J. Metals. Miner. Mater. Soc.*, 1996, 48:40–45.
52. Movchan, B.A., Functionally graded EB PVD coatings. *Surface and Coatings Technology*, 2002, 149:252–262.
53. Moran, R., Physical vapor deposition (PVD), Report ID: MFG015B. BCC Research Publishers, 2005.
54. Gille, G. et al., Submicron and ultrafine grained hard metals for microdrills and metal cutting inserts. In *Proceedings of 15th Int. Plansee Seminar. Plansee Holding AG,* Vol. 2, 2001, pp. 782–816.
55. Fridrichs, K., Moertl, K., Development of new types of carbides with ultrafine and even finer tungsten carbide powders. In *Proceedings of 2002 Powder Metallurgy World Congress, Princeton*, MPIF Publishers, New Jersey, 2002, Vol. 6, pp. 1–11.
56. McCandish, L.E., Seegopaul, P., Development and application of nanostructured tungsten carbide/cobalt powders. In *Proceedings of Europ. Conf. Advances in hard material production*, Stockholm, EPMA, 1995, pp. 93–100.
57. Yao, Z. et al., Nanosized WC-Co holds promise for the future. *Metal Powder Report*, 1998, 53(3):26–33.
58. Seegopaul, P. et al., Production capability and powder processing methods for nanostructured WC-Co powders. *Int. J. Refractory & Hard Materials*, 1997, 15:133–138.
59. Cha, S.I. et al., Mechanical properties of WC-10Co cemented carbides sintered from nanocrystalline spray conversion processed powders. *Int. J. Refract. Met. & Hard Materials*, 2001, 19:397–403.
60. Xueming, M.A., Gang, J.I., Nanostructured WC–Co alloy prepared by mechanical alloying. *J. Alloy & Compounds*, 1996, 245:L30–L32.
61. Ban, Z.G., Shaw, L.L., On the reaction sequence of WC–Co formation using an integrated mechanical and thermal activation process. *Acta Materiala*, 2001, 49(15):2933–2939.
62. Fu, L., Cao, L.H., Fan, Y.S., Two-step synthesis of nanostructured WC–Co powders. *Scripta Materiala*, 2001, 44(7):1061–1068.

63. Sadangi, R.K. et al., Liquid phase sintering aids for nanograin and micrograin WC–Co. In *Proceedings: Advances in Powder Metallurgy & Particulate Materials. Cemented Carbides*, MPIF, Princeton, USA, 1999, pp. 10/15–10/22.
64. Zhang et al., WC nanorod reinforced cemented carbide material and technology design for PCB micro drill. *Powder Metallurgy Sci. & Technol. Briefs*, 2001, 3(4):8–11.
65. Spasil, J., Functionally gradient materials in the cemented carbide field creation and application. In *Proceedings of 14th Int. Plansee Seminar. Plansee Holding AG*, Vol. 2, 1997, pp. 338–351.
66. Outthous, S. et al., Study of isotropically conductive bondings filled with aggregates of nanosized Ag particles. *IEEE Transactions on Components, Packaging and Manufacturing Technology*, Part A, 1997, 20(1):15–20.
67. Fedosyuk, V.M., Nanogranular electrodeposit magnet: cobalt alloys. In *Encyclopedia of Nanoscience and Nanotechnology*, Vol. 2. American Scientific Publishers, 2004, pp. 895–918.
68. Mizuseci, H., Kikuchi, K., Tanaka, K., Modeling of magnetic multivalued recording in granular materials. *Japan. J. Appl. Phys. B.*, 1996, 37(4):2155–2158.
69. Fedosyuk, V.M., Kasyutich, O.I., Blythe, H.J., Composition and annealing influence on the superparamagnetizm of granular Cu–Co films. *J. Magm. Magn. Matter*, 1996, 156:77–78.
70. Fedosyuk, V.M., Blythe, H.J., Magnetic of electrodeposited inhomogenious alloyed CuCo films. *Phys. Status. Solidi* (a), 1994, 146(2):k13–k17.
71. Fedosyuk, V.M., Magnetic and magnetoresistive properties of granulated films in the Co–Cu system. *Material Science of Nanostructures*, 2005(2–6):3–11.
72. Multilayered ceramic chip capacitors, World Market, Technology and Opportunities: 2001–2005. Paumanok Publications, Inc., Cary, North Carolina 27511.

Chapter 5

Atomization and Granulation

Oleg D. Neikov, Frantsevich Institute for Problems of Materials Science (IPMS), Kiev, Ukraine

Because of the ease with which a liquid can be broken up into fine droplets, atomization has become the prevailing mode of powder production of non-ferrous metals and their alloys. Currently, the world-wide atomization capacity of non-ferrous metals amounts to 10 million metric tonnes per year [1]. Atomization allows the manufacture of rapidly solidified metal alloys. The use of rapid solidification of melts to produce new structural and other materials with complex properties unachievable by traditional metallurgy is not only a very popular subject of investigation but also finds a wide industrial application nowadays.

The basic types of atomization processes include (Figure 5.1):

- Jet atomization of the melt, where a liquid metal is dispersed into droplets by the impingement of high-pressure jets of gas, water or oil (Figure 5.1(a) and (b))
- Centrifugal atomization, where a liquid stream is dispersed into droplets, flakes, or ribbons by the centrifugal force effect of a rotating disk, spinning cup, spinning roller or consumable electrode (Figure 5.1(c))
- Disintegration of liquid metal (Figure 5.1(d))
- Impact atomization a liquid stream (Figure 5.1(e))
- Ultrasonic atomization, where a liquid metal film is subjected to ultrasonic vibration (Figure 5.1(f))
- Impulse atomization, where impulses are mechanically applied to the melt (Figure 5.1(g))
- Vacuum atomization, where heavily saturated molten metal with a gas is atomized in the vacuum (Figure 5.1(h)).

Particle size distribution is one of the most important parameters of powders. The particle size distribution of atomized powders generally follows the log normal law. This signifies that the particle size distributions form straight or nearly straight lines on the log-probability paper (Figure 5.2).

Granulation of a melt is realized by means of free fall into cold liquid, usually water. During the free fall and by impact with the water surface, the melt stream is broken up into droplets which then solidify. The melt is caused to flow through a nozzle plate (see Figure 5.1(g)) in order to obtain granules of pellet shape. Particulate materials coarser than 1 mm in diameter are conventionally referred to as granules (see Introduction). Thus, several types of conventional atomization processes are useful for granule production.

Water Atomization

Water atomization (WA) is used for commercial production of copper, copper alloys, nickel-base alloys and zinc powders. Water atomized precious metals are used in dental techniques, sintered electrical contacts and brazing pastes. WA is less expensive than other methods of atomization. It allows the production of powders within wide yield limits from 1 to 500 kg/min for a single nozzle. The main limitation of WA is powder purity, especially for metals and alloys inclined to oxidation. However, owing to the higher cooling rate of the melt by WA, the average thickness of surface oxides is similar to that in gas atomized powders. This is realized, in particular, in water atomized aluminum alloys [4] (discussed in Chapter 13).

Technique

The major components of a conventional water atomization system are a melting unit, a tundish, an atomizing chamber, a water pumping/recycling system, and the dewatering and drying units. A flow diagram of the typical water atomization process for copper and copper alloy powders production is shown in Chapter 16.

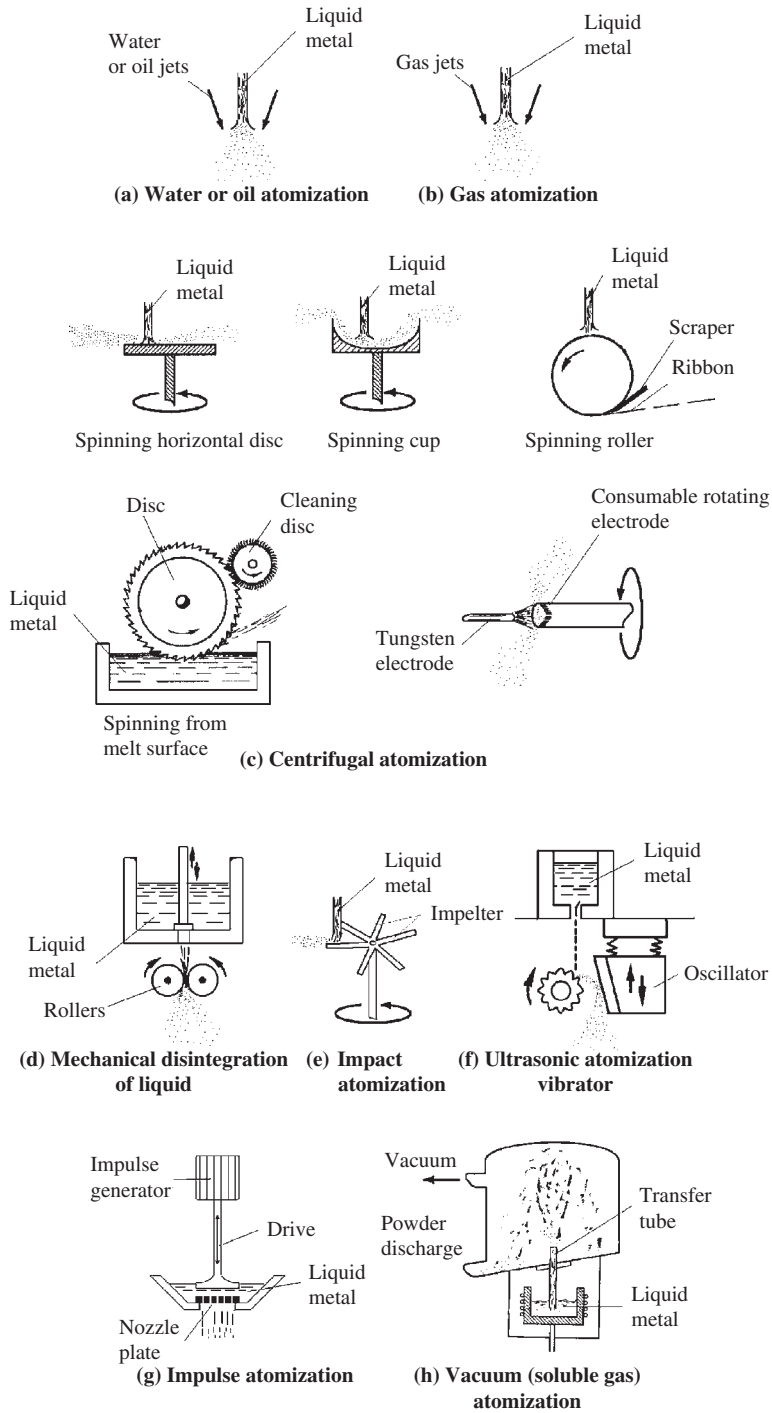

Figure 5.1 Schematic drawing of atomization processes.

Conventional installations usually operate with water pressure in the region of 5–20 MPa, producing the powders with mass median particle sizes of 30–50 μm. Significantly higher water pressures of 50–150 MPa are used to manufacture finer powders with mass median particles sizes of 1–20 μm. These powders are used for injection molding processes, binders in diamond tools, sintered bearings, paints, coatings and pastes.

Generally, the water atomizer designs are based on 'V' configurations with some nozzles (at the minimum two) located symmetrically about the axis of the liquid metal stream (Figure 5.3).

A representation of the overall processing stages in water atomization is shown in Figure 5.3. The associated melting process variables include the charge ingredients, atmosphere and superheat of the melt; the associated atomization stage variables are nozzle

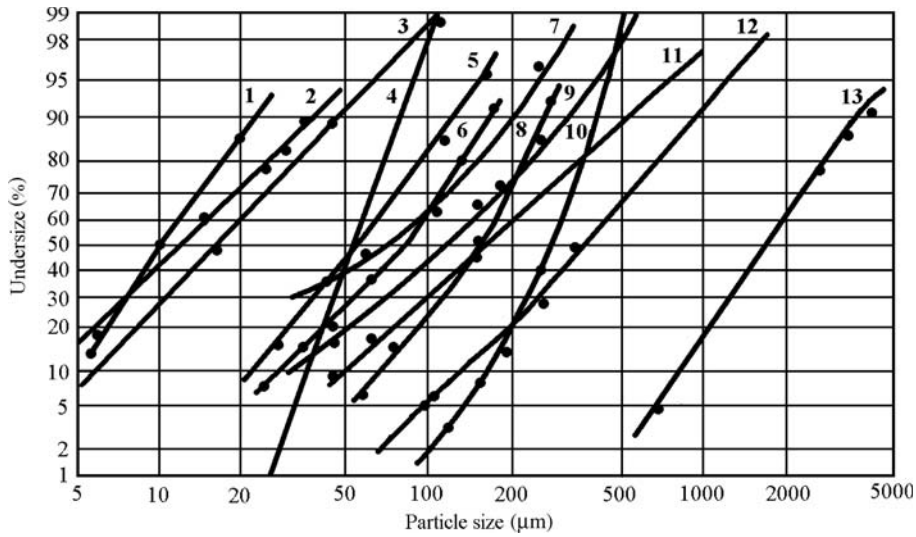

Figure 5.2 Typical particle size distribution of atomized powders.

Curve No	Powder	Median mass diameter (d_m), μm	Geometric standard deviation (σ_g)	Ref
1	Copper, hot-gas atomized at 4.5 MPa in nitrogen at 500°C	10	2.0	(Ref 2)
2	Copper, water atomized at 54 MPa	12.5	2.4	(Ref 3)
3	Zinc, gas atomized at 2 MPa	16	2.1	(Ref 3)
4	67Pb-33Sn ultrasonically atomized	64	1.31	(Ref 3)
5	44.85Al-13.7Fe-28.55Cu-12.9Cr, water atomized at 10 MPa	55	1.83	A*
6	43Al-40Cu17Fe, argon atomized at 0.6 MPa	87	2.48	–
7	60Pb-40Sn solder, gas atomized at 0.8 MPa	70	2.5	(Ref 3)
8	Aluminum, water atomized at 4.8 MPa	150	2.0	A*
9	Bronze, air atomized at 0.5 MPa	120	2.33	(Ref 3)
10	Zinc, centrifugally atomized	270	1.4	(Ref 3)
11	Zinc, water atomized at 5.5 MPa	170	2.58	(Ref 3)
12	Copper shot, water atomized at 2 MPa	280	2.1	(Ref3)
13	Phosphor shot, water atomized at 0.05 MPa	1950	1.9	(Ref 3)

A*, author's data have first been published

diameter, metal stream length, density of metal, surface tension of the melt, viscosity of the melt, water pressure, jet geometry and apex angle; key variables in the particle solidification stage are melting point, droplet size, heat transfer, quenching medium, temperature of suspended solid in atomization chamber and flight path. Basic water-jet configurations are shown in Figure 5.4.

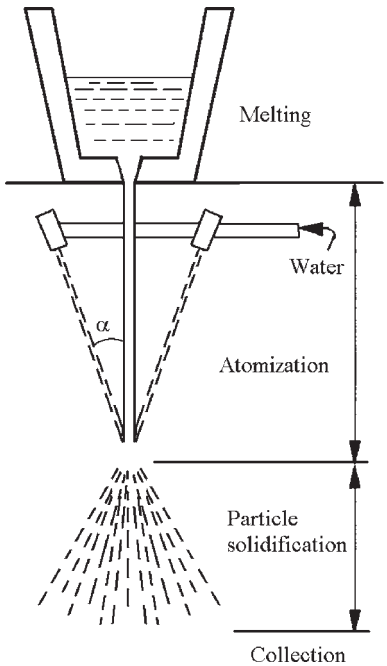

Figure 5.3 Stages in water atomization.

Typical range of operating conditions in water atomization are as follows [3]:

- Metal flow rate (single nozzle), 1–90 kg/min
- Water flow rate, 20–380 L/min
- Water velocity (at nozzle exit), 10–500 m/s
- Water pressure (at exit or in manifold), 5–150 MPa
- Metal superheat, 75–170 (above melting point).

Commercial water atomization plants typically operate with water flow to metal flow ratios between 2/1 and 15/1. Table 5.1 comprises the operating conditions for specific powders and their properties.

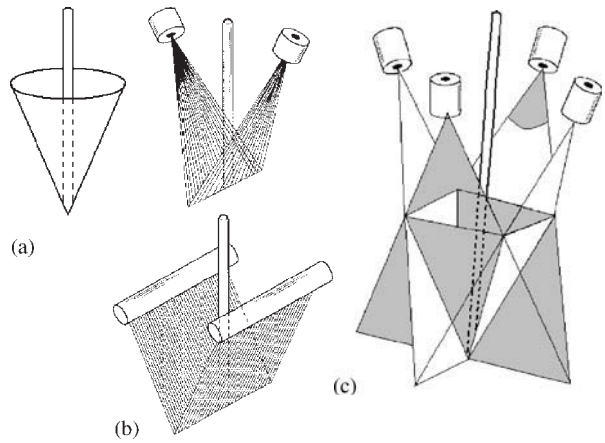

Figure 5.4 Water jet configurations: (a) annular jet; (b) open V-jets; (c) closed V-jets.

Table 5.1 Properties of several water-atomized powders

Alloy	Operating parameters				Powder properties		
	Metal flow (M) (kg/min)	Water flow (W) (L/min)	W/M ratio	Water pressure (MPa)	Median diameter r (μm)	Apparent density (g/mL)	Oxygen (ppm)
Ag (a)	18	100	5.5	50	21	3.4 (c)	...
Al-5Zn-3Mg-0.49Fe (b)	6.5	90	13.8	10	60	0.9 (d)	...
Al-1.3F-1.5Cr (b)	7.0	90	12.8	15	45	0.98 (d)	600
Cu-5Cr (a)	27	180	6.7	20	24	3.18 (c)	...
Co (a)	27	180	6.7	20	29	3.28 (c)	...
Au-2Cu (a)	7	40	5.7	13.7	88	...	...
Ag-22Cu-3Zn (a)	9	42	4.7	17.2	72	3.95 (c)	110
Ni-B-Si (a)	24	160	6.7	17.2	51	4.26 (c)	...

[a]All data from V-jet atomizer with 40–50 degrees apex angle, nitrogen purged;
[b]IPMS atomizer equipped with eight discrete nozzles;
[c]apparent density for fractions under size 250 μm;
[d]apparent density for fractions under size 63 μm;
(a) and (c) Source: Ref 3; (b) and (d) Source: IPMS

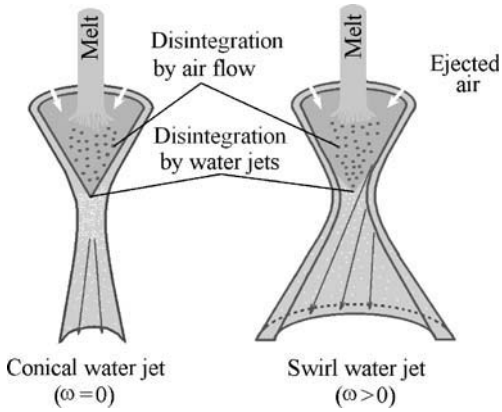

Figure 5.5 High-pressure water atomization using conical swirl water jet.

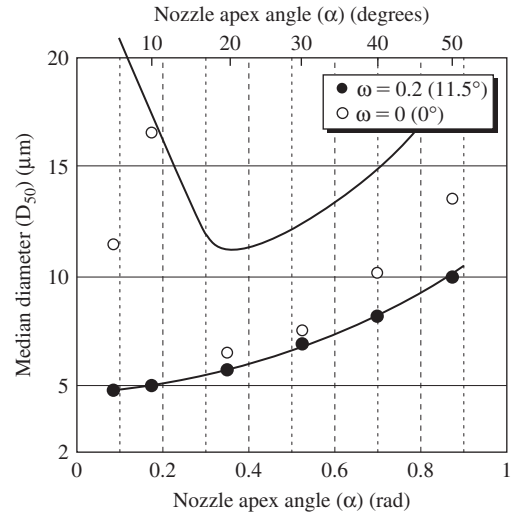

Figure 5.6 Dependence of powder median diameter on jet apex angle of conical swirl water jet atomizer.

Atomizer

The atomizers play the main role in ensuring the efficiency of the disintegration of a liquid metal stream. In the literature on atomization, the terms nozzles and jets are often used interchangeably. The jet is the stream of liquid or gas that flows out from the nozzle, whereas a nozzle is one part of the atomizer. As far as possible, the use of these terms throughout the book is consistent with these definitions.

Though numerous patents of atomizer design have been filed, only a few types of atomizer are used in most commercial water atomization units. Atomizer design in most commercial water atomization units are variants of either V-jet nozzles (see Figure 5.4) or annular cone-jet nozzles that are concentric with the metal stream. Annular ring nozzles are utilized in some large-capacity plants, but are rarely used elsewhere because they are less flexible and harder to make than designs based on V-nozzle configurations with two or more discrete openings located symmetrically about the axis defined by the metal stream.

The liquid metal stream typically falls a certain distance (usually about 15–25 cm) before meeting the water jets. A partial vacuum is often created above the impingement point with the water and the gas/air sucked by the water streams can disrupt the liquid metal before it actually meets the water jets [5].

A swirl water atomizer for fine powder production has been developed [6]. Figure 5.5 shows a schematic of high-pressure water atomization by 'free fall' design and swirl water jet. This unit allows the production of bronze (Cu–10 mass% Sn) powder with median particle size 7.5 μm and apparent density 2.8 g/cm^3 with water pressure of 83.3 MPa.

Figure 5.6 shows the effect of the jet configuration apex angle (θ) on the median diameter of swirl water atomized copper powder (δ_{50}) [7]. The water jets are generated at water pressure 90 MPa with flow rate 5 l/s on the jet swirl angle, ω = 0.2 rad (≈11.5 degrees) and ω = 0.0 rad (0.0 degrees), i.e. usual conical jet configuration. For ω = 0.0 rad, δ_{50} of common conical jet configuration atomized powders decreases with decreasing θ down to 0.35 rad, but as θ becomes less than 0.35 rad, δ_{50} increases abruptly with decreasing θ, while, by swirl jet configuration for ω = 0.2 rad, δ_{50} keeps decreasing with θ decreasing. As can be seen from dependences of δ_{50} on θ in the range θ = 0.35 to θ = 0.87 rad, δ_{50} for swirl jet configuration is less than one order of magnitude in comparison with common conical jet configuration. Via the latter, there are many coarse particles with wide size distribution (Figure 5.7). The particles are spherical or drip shaped, but with increasing θ up to 0.87 (≈50 degrees) the powders become irregular in shape. In the former, there are few irregular aggregates. Almost all particles were spherical and particle sizes decreased with decreasing θ.

Applications for such ultrafine powders include metal injection molding (MIM), sintered filters, conductive pastes and corrosion-resistant paints.

In atomization installations using an atomizer with a binary water cone configuration (Figure 5.8) [8], a second convergent water cone performing angular motion relative to the melt stream axis affects the atomized melt droplets. The lower annular nozzle is provided with tangential channels at 27–29 degrees that create swirl jet configuration. The apex angle of the upper nozzle ranges from 54 to 58 degrees and

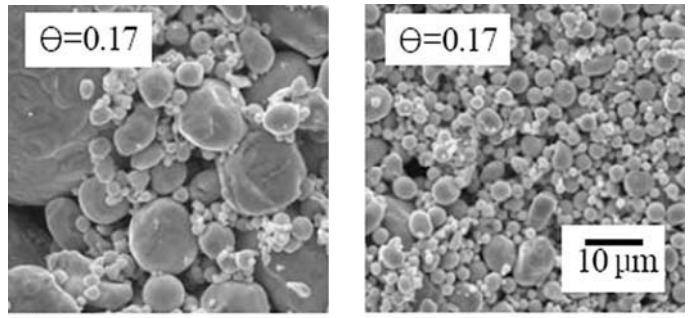

Figure 5.7 SEM micrographs of copper powders produced by the high-pressure water atomization using conical swirl water jet with apex angle 0.17 rad (≈9.7 degrees) and jet swirl angle, ω = 0 (a) i.e. common cone water jet configuration, and ω≈50 degrees (b), accordingly.

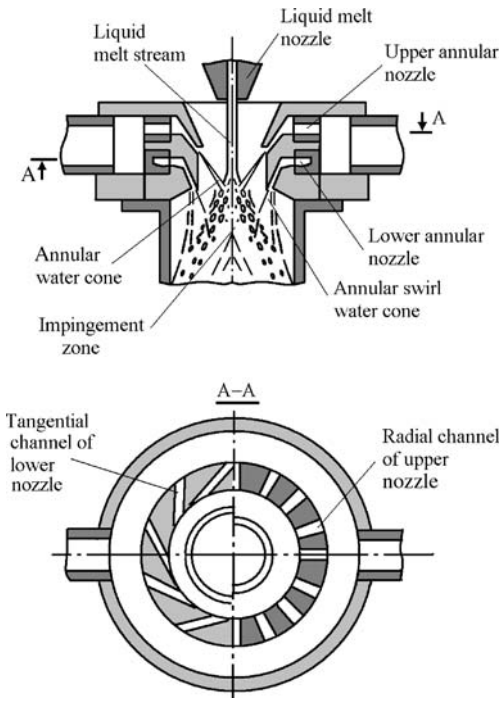

Figure 5.8 Atomizer with binary water cone configuration.

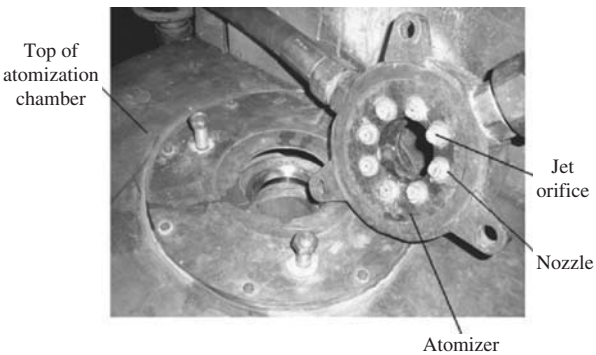

Figure 5.9 IPMS atomizer equipped with eight discrete nozzles. Courtesy of IPMS.

the lower one ranges from 36 to 40 degrees. The liquid melt outflow orifice is 9 mm.

The IPMS atomizer is equipped with eight discrete nozzles located symmetrically about the axis defined by the metal stream (Figure 5.9), four nozzles create closed V-jet configuration and disintegrate the metal stream on meeting the atomizing fluid. A second closed V-jet configuration is created by means of four nozzles that impinge on the melt stream at a more acute apex angle than the former. Thus, they meet the melt droplets after the impingement point.

Atomization Mechanism

The water-atomization process is distinguished by high density of the energy carrier, high cooling rate and steam formation in the contact zone between water and melt. High water density $\rho_{H_2O} \approx 10^3 \rho_{air}$ leads to an essential increase of impulse linear momentum $(p = mv)$ and kinetic energy $(E_k = mv^2/2)$ of the energy carrier.

Steam film originating around a drop decreases the heat transfer from drop to surroundings; if the film is disrupted and the contact of melt with water is provided, the cooling rate is appreciably accelerated. The high density of the energy carrier preserves the high velocity of water jets over a long distance that allows a wide range of positional relationships of melt streams and water jets and simplifies the design of hydraulic atomizers.

Liquid metal drops are disintegrated by a superheated compressed steam, which is formed on melt contact surface with water. The breakdown force of the steam film on the melt drop depends on the

physical conditions in the contact zone: temperature and density of steam as well as water pressure and volume.

The mechanism of liquid melt drop formation under the impact from the exploding water–steam packet rather than shear was first proposed by Grandzol and Tallmadge for water atomization [9]. This model reflects the dispersed nature of the water and an inverse proportionality between particle size and the normal velocity component of the water, with respect to the metal stream axis. Grandzol and Tallmadge represent the dependence of mass median particle size (δ_m) on the water drop velocity (v_w) such that:

$$\delta_m = \frac{A}{v_w} = \frac{14,900}{v_w}\left(\frac{1}{n}\right)^{1/3} \quad (1)$$

where A is a constant, δ_m is in μm, v_w is in m/s, and n is the number of metal droplets formed from the disintegration of one water droplet. In this equation, water flow rate, water pressure, momentum and energy, jet length and metal flow are not primary parameters influencing δ_m; they do, however, affect particle size by influencing water-jet velocities and the number of water droplets. Impingements during atomization can also influence particle size, particle size distribution and particle shape [10].

From subsequent experimental observations on the influence of the angle between the metal stream axis and the water jet axis on δ_m, it was concluded that the velocity component of the water normal to the liquid metal stream, rather than the velocity component parallel to the liquid metal stream, is the dominant parameter in controlling δ_m [11]. Thus, the refined model [12] gives a relation between δ_m and v_w of:

$$\delta_m = \frac{B}{v_w}\sin\alpha \quad (2)$$

where δ_m is in μm, v_w is in m/s, α is the angle (in degrees) between the axis of the metal stream and the water jets, and B is a constant. The value of B in conditions of the refined model [12] is 2750.

The relation between δ_m and water pressure (p_w) for various metal powders [13] is shown in Figure 5.10.

Based on the straight log–log plots in Figure 5.10, the relationship between δ_w and p_w can be expressed:

$$\delta_m = Kp_w^{-m} \quad (3)$$

where K and m are constants for a given material and atomization unit. For atomizer modification with two nozzles, when δ_m is in μm, the parameter m is typically in the range 0.6 to 0.8 for water pressure from 0.1 to 50 MPa [14].

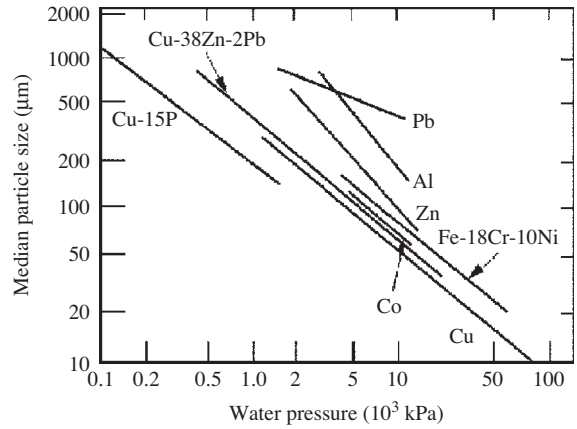

Figure 5.10 Particle size of water atomized metals as function of water atomized pressure.

Values of K are almost one order of magnitude higher for aluminum and zinc than for copper. In practice, this means that for two alloys water atomized under identical operating conditions, δ_m can vary by a factor of about 6. The K value evidently depends strongly on the physical and chemical properties of the molten alloy, in particular, viscosity and surface tension. Modification of the surface tension by the atmosphere (steam) to allow the formation of oxides is also expected to be important in terms of disintegration of the molten metal stream.

Increasing the melt superheat reduces δ_m in water atomization, primarily through the effect of temperature on viscosity and surface tension. For example, for zinc, an increase in superheat from 100 to 300°C reduces δ_m from 150 to 100 μm [13]. Similarly, in a cobalt-base alloy, increasing the superheat by about 150°C leads to decrease in δ_m of about 13.5% [15]. In addition to its effect on particle size, superheat is used as an operating variable to prevent freezing of the alloy in the exit nozzle of the tundish; simultaneously, the superheating leads to increase of melt flow rate through the tundish orifice, due to a decrease in melt viscosity.

The apex angle also influences particle size. With the apex angle increasing, the velocity component normal to the metal stream increases. It is shown [12,16] that δ_m decreases with increasing angle between the axis of the water jet nozzle and the liquid stream. Grandzol and Tallmadge represent this dependence in the form:

$$\delta_m = \frac{1}{v_w \sin\alpha} \quad (4)$$

However, there is a practical limit to the magnitude of the apex angle. Above about 50 degrees, flow

of the molten metal from the orifice of the tundish is impeded by the upward thrust of water, and the incidence of metal freeze-up at higher axis angles, especially at higher pressures (Figure 5.11). To decrease attenuation in water pressure, a short water-jet length is preferred, but again there are practical limits. It is normally found that using the apex angle to control fineness leads to dangerously unstable conditions. It is better to select a good stable setup with essentially zero rejection of melt and spray toward the jets and tundish and then provide the necessary pressure to achieve the desired particle size.

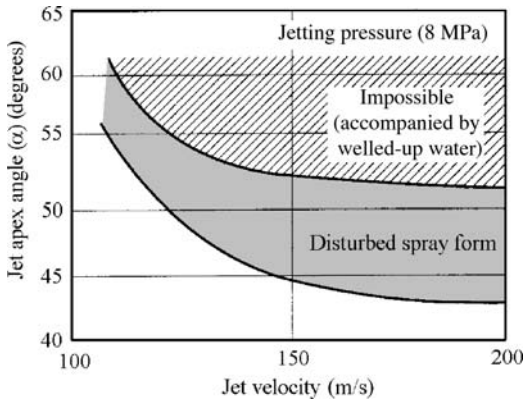

Figure 5.11 Effect of jet apex angle on stability of water atomization at various water velocities. (Source: Ref 16)

Powder Characteristics

Particles of water-atomized powder have generally an irregular shape with a pronounced uneven surface compared to gas atomized powders. For high-yield, low-cost production, and safe engineering, water atomization is usually preferred over gas atomization, providing powder characteristics are compatible with the application.

Particle Size Distribution

Generally, water-atomized powders exhibit log normal size distribution. Typical data for a range of metals and alloys and for differing operating conditions in water atomization are shown in Figure 5.12. Deviations from linearity using log normal-probability coordinates usually indicate operational instability, sampling errors or loss of fines. Minimum values of standard deviations (σ) are normally in the range 1.8 to 2.3, with some alloys on the low end of this range, e.g. Ni–B–Si and Fe–Si, while, for aluminum alloys

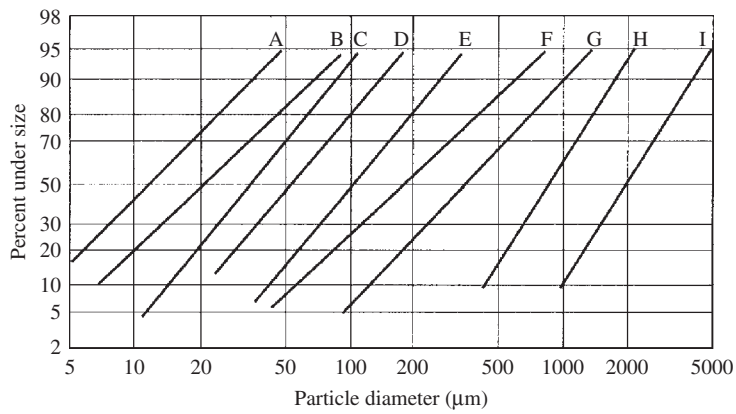

Figure 5.12 Typical water atomized particle mass size distribution. (Source: Ref 12)

	Alloy and water pressure	δ_{50}	σ
A	Copper atomized at 54 MPa	12	2.40
B	18Cr-10Ni-2.5Mo stainless steel atomized at 5 MPa	20	2.40
C	Fe-15Si atomized at 20 MPa	40	1.70
D	M2 high-speed steel atomized at 140 MPa	55	2.11
E	Fe-45Si for welding electrodes atomized at 4 MPa	100	1.70
F	Zinc for alkaline manganese batteries atomized at 5.5 MPa	180	2.34
G	Copper shot atomized at 2.0 MPa	400	2.30
H	15% phosphor copper shoot atomized at 0.15	800	1.76
I	15% phosphor copper shoot atomized at 0.05	2000	1.75

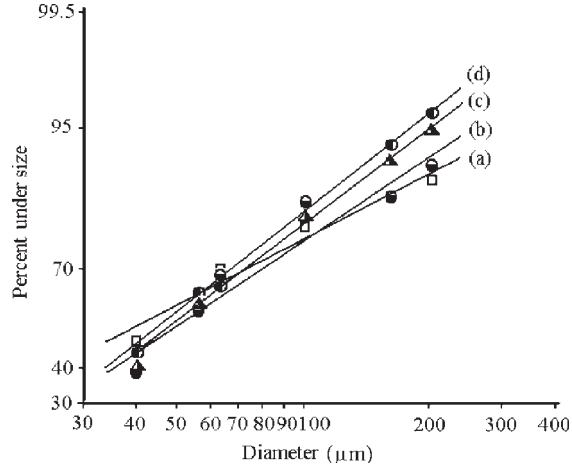

Figure 5.13 Typical particle mass size distribution of water atomized aluminum alloys:

Alloy and water pressure		δ_{50}	σ
(a)	$Al_{94}Fe_{2.0}Cr_{2.0}Ti_{2.0}$ alloy atomized at 15 MPa	40.5	2.96
(b)	$Al_{94}Fe_{2.5}Cr_{2.5}Ti_{0.7}Zr_{0.3}$ alloy atomized at 15 MPa	46	2.83
(c)	$Al_{94}Fe_{4.1}Cr_{1.3}Zr_{0.6}$ alloy atomized at 15 MPa	43	2.51
(d)	$Al_{94}Fe_{4.1}Cr_{1.3}\,Ti_{0.47}Zr_{0.13}$ alloy atomized at 15 MPa	42	2.5

(Figure 5.13) and the alloys which contain aluminum and chromium which form refractory oxides, values of σ are typically higher, namely 2.0 to 3.0. The standard deviation is calculated by:

$$\sigma = \frac{\delta_{84.1}}{\delta_{50}} = \frac{\delta_{50}}{\delta_{15.9}} \qquad (5)$$

where δ_{50}, $\delta_{84.1}$, and $\delta_{15.9}$, correspond to the particle sizes at the 50%, 84.1%, 15.9% cumulative weight percent levels, respectively.

Thus, the main influence on standard deviation, once a good and stable atomizing jet set-up is ensured, appears to be melt chemistry.

As a general characteristic of water atomization, δ_m and σ are not particularly sensitive to metal flow rate or the ratio of water flow to metal flow rate.

Figures 5.14 and 5.15 [17] illustrate the effects of melt nozzle diameter and pouring temperature for water-atomized copper powders on standard deviation and mass median diameter. The large effect of the atmosphere is observed (Figure 5.14). In fact, it is confirmed [3] that if copper is atomized with a large dissolved oxygen content, the powder is much finer. Thus, the large difference between nitrogen and air atmosphere may be due to this effect. Similarly, the chemistry may be directly influencing the standard deviation. The generally lower values of standard deviation at lower metal flow rates reflect

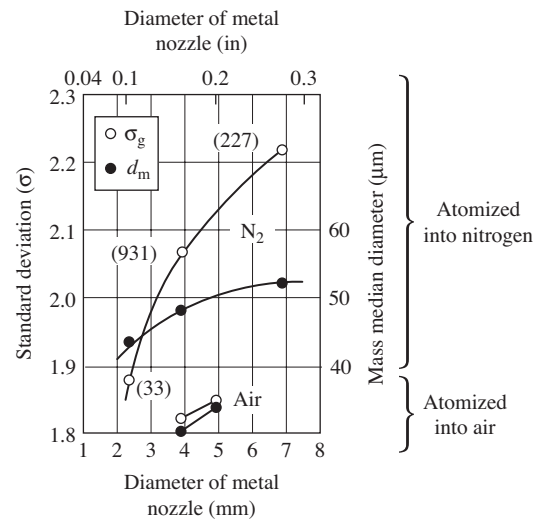

Figure 5.14 Effect of metal stream diameter on standard deviation of particle mass size distribution of water atomized copper powder. Pouring temperature 1200°C; figures in parenthesis show average metal flow in g/s. (Source: Ref 18)

the importance of collisions in broadening the size distributions.

It is appropriate to mention here that each commercial water atomization unit has its own feature operating characteristics. However, well-established proprietary empirical relations give a high degree

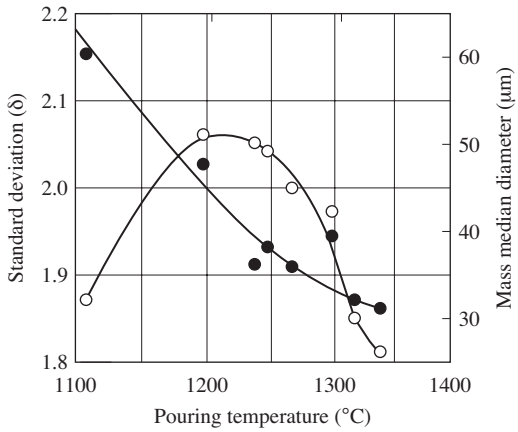

Figure 5.15 Effect of pouring temperature on distribution of water atomized copper powder. Metal stream diameter 4 mm; water flow 320 l/minute; water pressure 13.2 MPa; atmosphere nitrogen. (Source: 13)

of predictability in terms of operating conditions and powder properties, in particular, particle size. In addition to the aforesaid empirical formulas, there are others in the published literature that have been annotated by Beddov [19].

Particle Shape

The shape of water-atomized powder particles can vary appreciably. Most water-atomized powders are somewhat irregular in shape. Certain alloys can be produced with spherical or near-spherical shape, exhibiting apparent densities about 50% of theoretical, while others can be sponge like and extremely irregular in shape, in which case apparent densities are as low as 10–15% of theoretical.

During melt atomization, the irregular liquid metal drops under action of the surface tension forces tend to a spherical shape, the surface of which is minimal for a certain volume that corresponds to minimum free energy. At that, a particle shape is defined by relation of drop residence time in liquid state to spheroidizing time. Calculated values of the time necessary for solidification and spheroidizing of copper melt drops of different sizes [19] are shown in Figure 5.16. The heat-transfer coefficient dependence on water pressure, melt temperature and droplet size was taken into account. If the droplets' solidification time to spheroidizing time ratio value is equal to one or less, the solidified droplets will have an irregular shape.

In water atomization, the estimated spheroidization time for a 100 μm diameter droplet is in the range from 0.1 to 10 μs, depending on the magnitude of surface tension forces [12]. Freezing (solidification)

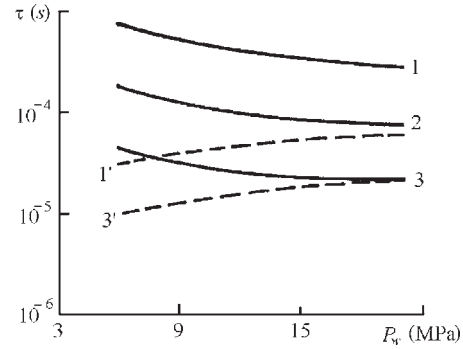

Figure 5.16 Solidification and spheroidizing times of copper melt droplets by pouring temperature 1140°C: 1–3 are cooling time curves; 1′and 3′ are spheroidizing time curves; droplet sizes in 640 μm diameter (1 and 1′), in 255 μm (2) and 102°μm (3 and 3′), accordingly. (Source: Ref 20)

times are of the order of 50–750 μs for elevated temperature aluminum alloys by pouring melt temperature 1250–1300°C (details of the analysis of droplet cooling rate are given in Chapter 13). Thus, solidification times are near to or shorter than spheroidization times, which are two or three orders of magnitude shorter than freezing times, and water-atomized particles are therefore predicted to be predominantly spheroidal in shape.

The formation of an oxide film on the surface of the droplet before it is in free fall and able to spheroidize can drastically affect particle shape. Elements that form refractory oxides prevent spheroidization by producing an oxide film with sufficient strength to oppose the forces of surface tension.

Thus, in terms of particle shape, droplets with very short freezing times tend to be more irregular and, in turn, are associated with low apparent densities. Accordingly, the longer freezing times characteristic of high melting point elements or alloys result in a more spherical particle shape.

Surface Morphology and Internal Structure

Water-atomized powders, along with their irregular shape, typically show a rough surface morphology and honeycomb. This characteristic is illustrated in water-atomized Al-6.0Zn-0.3 Mg-0.3Zr-0.5 Mn high-strength alloy (Figure 5.17) and Al-5.0Fe-5.0Cr-2.0Ti-1.0Zr elevated temperature alloy (Figure 5.18). The combination of irregular shape, surface roughness and porosity is an important feature of water-atomized powders, since green strength is enhanced by the mechanical interpenetration of irregular powders during die pressing.

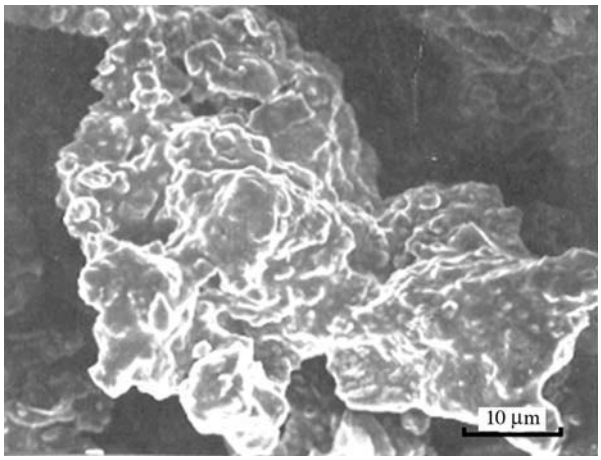

Figure 5.17 SEM micrograph of water-atomized powder of Al-6.0Zn-0.3Mg-0.3Zr-0.5Mn high strength alloy.

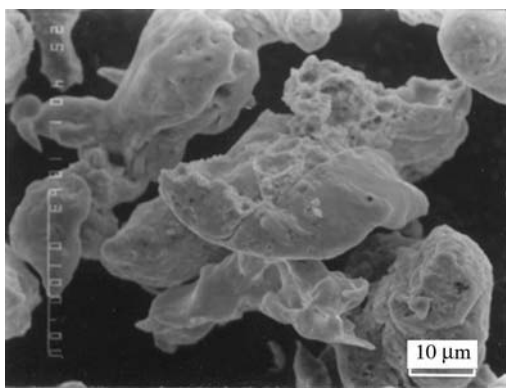

Figure 5.18 SEM micrograph of water-atomized powder of Al-5.0Fe-5.0Cr-2.0Ti-1.0Zr elevated temperature alloy. Superheat 200°C; diameter of gravity melt stream 7.0 mm.

Individual particles, or even different grains within a powder particle, differ in microstructure (Figure 5.19(a)). This is caused by differences in solidification behaviors of the solidifying fronts growing into the melt and of primary intermetallic phases distributed in the melt. Most of the particles exhibit a cellular or non-dendritic-like structure with an arm spacing of a few hundred nanometers in colonies a few microns in diameter (Figure 5.19(b)). Some other grains show a coarser background network structure where coarse primary intermetallics act as separate growth centers.

In addition to a non-dendritic structure, some other areas of individual particles show a subdendritic and cellular structure. Such observations can be explained by a significant intensification of the nucleation during crystallization by deep super cooling of the melt. The non-dendritic and subdendritic cell sizes are different for different particles. For example, the calculated cell size values shown in Figure 5.19(b) range from 1.2 to 0.94 µm that, in accordance with Eqn (1) in Chapter 13, correspond to cooling rates from 0.83 to 1.7°C/µs.

Powder Purity

Deoxidation of the melt plays an important role in the atomization process. The oxygen content of water-atomized powder is a function of the free energy of the reaction of the metal with water vapor and also of the reaction kinetics. For many water-atomized powders, oxygen levels are in the range 1000–4000 ppm by weight. The importance of the kinetic effect is exemplified by the appropriate oxygen levels in aluminum or high silicon alloys. In these alloys, a protective oxide film arises on the particle surface which prevents or retards further oxidation.

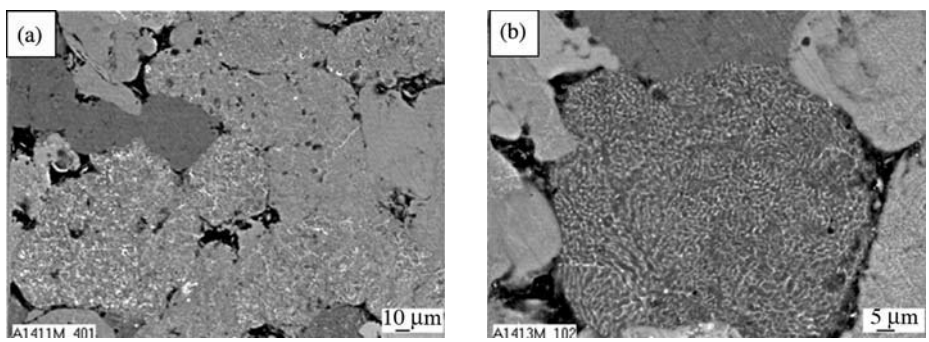

Figure 5.19 Microstructures of two typical metallographic sections of water-atomized powder particles of Al-Fe-Ce alloy in backscattering electrons with lower (a) and higher (b) magnifications.

Table 5.2 Characteristic properties of water-atomized powders

Metal alloys	Mass median particle size (δ_m) (μm)	Standard deviation σ_g	Apparent density (g/mL)	Oxygen content (ppm)
Ag	37	2.16	3.76	...
Ag-28Cu	32	2.3	3.37	285
Ag-25Sn-5Cu-1Zn	35	2.40	5.11	260
Al-3.92Fe-3.65Cr-3.3 Ti*	40.5	2.96	1.07	1200
Au	130	2.69	7.82	...
Au-20Ni	62	2.9	...	57
Bi	79	3.33	3.58	...
Cd	185	2.00	1.29	...
Cu	46	2.30	3.48	350
Cu	90	2.40	5.07	397
Cu-0.3Mg	31	2.51	2.01	1105
Ni	100	2.10	4.50	645
Ni-5Al	34	2.29	2.85	710
Ni-Cr-B-Si	51	1.69	4.26	...
Pt-10Rb	250	2.80	12.3	...
Sn	160	2.19	1.48	314
Sn	90	2.19	1.23	620
Zn	58	2.05	1.82	...

Source: Ref 12 and *IPMS data

The surface oxide of water-atomized powders is non-uniform in thickness. So, with water-atomized powders, three-dimensional film islets with a typical thickness of 30–40 monolayers usually cover 30–70% of the particle surface. The rest is covered by a thin oxide film about 3 to maximum 8 monolayers [21]. Table 5.2 gives the characteristic properties of water-atomized powders, including oxygen content.

The increase of oxygen content can be accommodated by modifying the atomization conditions. For example, the use of inhibitors in combination with the control of hydrogen ion level, and suspension temperature, during the atomization process can lead to a decrease in the oxygen content to the level of gas-atomized powders [22]. The Au-Ni brazing alloys normally have an oxygen contain about 200 ppm. By using inert purging gases in the melting process, the oxygen level is reduced to 150 ppm. Further reductions in oxygen level to 100 ppm and 40–50 ppm can be achieved by deionized water or by the addition of alcohol to the water. The use of anti-foaming agents in the atomizing water can further reduce oxidation and increase the cooling rate [15].

Oil Atomization

The oil-atomization process should avoid the problem of powder oxidation. In the early 1980s, Simetomo Metals developed the oil atomization process for the commercial production of relatively high carbon (0.4 wt%) steel [15]. Oil-atomized powders resembled water-atomized powder in particle size. Their densities are intermediate between water- and gas-atomized powders as the cooling rate is slower and oxidation much less. However, carbon pickup occurs to an extent depending on metal temperature and carbide-forming tendency of the melt [23].

Gas Atomization

Gas atomization (GA) is the process in which the liquid metal is dispersed by a high-velocity jet of air, nitrogen, argon or helium. Gas atomization is used for the commercial production of powders of copper, copper alloys, aluminum and its alloys, magnesium, zinc, titanium, titanium alloys, nickel-base alloys, cobalt-base alloys, lead, tin, solder, precious metals, refractory metals, beryllium, etc.

Air atomization of aluminum, copper, brass and zinc powder accounts for about 250 000 tonnes. Inert gases are used when the oxygen content must be kept low, or when atomizing reactive metals such as the superalloys and titanium. The worldwide annual tonnage of inert gas atomized metal powders is much less than for water-atomized powders. The relationship between the shipments of ferrous and non-ferrous

powders is about 4 to 1. But, in market value terms, aluminum, silver and zinc are all close to the value of iron powders [1, 24]. The price in $/kg of metal powders produced, their volume in t/year, and their total market values in $billions are shown in the Introduction in this book.

Gas atomization differs from water atomization in many aspects. Rather than being dominated by the pressure of the medium like water atomization, it is found that the gas-to-metal ratio is the dominant factor in controlling particle size. A feature of GA is the fact that an increase of pressure above 0.1 MPa, at which the sonic velocity is reached, gives only small increments in gas velocity. In contrast, to reach sonic velocity (in air or nitrogen) with a water jet, a pressure of nearly 40 MPa is needed and the velocity increases according to the square root of the pressure. Moreover, gas atomization takes place by the action of a continuum on another, while in water atomization a stream of droplets in an entrained gas flow acts on a continuum. The density of the water medium is about a thousand times higher than the gases used, giving much greater impact.

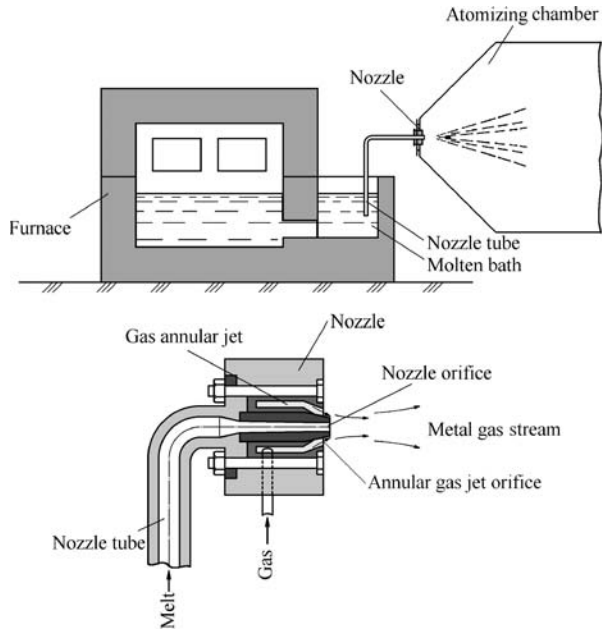

Figure 5.20 VAMI aspirating nozzle design with horizontally molten metal stream.

Gas Atomizing Units

Gas atomizing units also come in a much wider range of designs than water atomizers. The earliest gas atomization was with steam, patented in 1872 by Marriott of Huddersfield. The very simplest design of atomizer is to let a metal stream to fall onto a horizontal gas jet and this has been used for zinc powder production. The earliest scientific worker in this field seems to have been Professor Hall, founder of the Metals Disintegrating Co. His patent in the late 1920s [25] represents a kind of close-coupled atomizer for aluminum atom-ization. The basic design shown in this patent is still in use and has yet to be improved in any radical manner. A similar unit developed by VAMI is shown in Figure 5.20. The atomizing gas is delivered through an annular orifice around the nozzle at the converging angle. The gas flow creates the suction (aspiration) effect at the tip of the nozzle that draws the molten metal into the nozzle. The amount of gas delivered by the nozzle is controlled by the size of the air gap and pressure and temperature of the gas. Rate of metal flow and resultant powder particle size are influenced by the aspirating force, the nozzle metal orifice diameter and the vertical distance between the nozzle and molten metal level.

This atomizer design aims to contact the liquid metal stream with the gas at or close to the gas jet exit plane where the highest jet velocities exist. It leads to efficient break-up of the liquid, resulting in finer powders and is the preferred method for aluminum and other low-melting-point metals. It can be operated vertically upwards or down wards or in the horizontal position. Careful design of the atomizer is required, however, to avoid freezing of the metal by the gas jet, which can lead to solidification at the nozzle tip.

Many gas atomizer designs are known. They are classified as 'free fall', 'confined' or closed nozzles (Figure 5.21(a)) and 'internal mixing'. The closed nozzle designs are also as known as close-coupled nozzle designs.

For free gas atomization (Figure 5.21a), the key process variables are similar to those of water atomization (see Figure 5.3). In this atomizer, the liquid metal issues in the form of a stream from a tundish and falls 100–200 mm by gravity. Then it is atomized either by means of discrete or an annular directed at the point of meeting with the metal stream. This method is easy to operate but inefficient and is not suitable for making fine powders.

In the 'internal mixing prefilming' atomizer type, the gas and liquid metal are mixed together before expanding into the atomizing chamber [26].

Confined Nozzle Designs

This nozzle design (see Figure 5.21(b)) makes it possible to increase the yield of median particle size powder

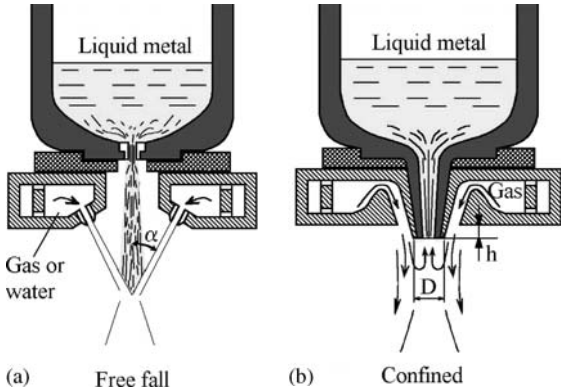

Figure 5.21 Atomizer designs of two types: (a), free fall design (gas or water) and (b) confined nozzle design (only gas). Design characteristics: α, angle formed by free-falling molten metal and atomizing medium jet; D, diameter of confined molten metal nozzle end; h, protrusion length of melt nozzle.

(40–60 μm) by maximizing the gas velocity and density at the meeting with the metal stream [16]. However, the use of these units can cause the freezing of the molten metal at the end of the tundish nozzle, which immediately stops the atomizing. Along with this, the interaction of the gas stream with the nozzle tip can form either under pressure or positive pressure, varying from an underpressure that can significantly increase melt flow rate to an inverse pressure sufficient to stop it and blow gas into the tundish. Thus, great care is needed in setting up closed nozzles and control during atomization.

The WIDEFLOW gas atomizer based on the confined nozzle principle is illustrated in linear modification (Figure 5.22) [27]. This atomizer involves two chambers, a high-pressure chamber (autoclave), containing melting and pouring units, and a low pressure atomization chamber divided by a linear Laval gas nozzle. The pressure difference between the two chambers forces the gas accelerated flow through the converging linear Laval nozzle to sonic velocity, when the pressure ratio exceeds the critical value. Kinetic energy of ultrahigh velocity gas flow is transferred efficiently to the atomization of thin melt film. Using nitrogen or argon, mean particle diameters about 10 μm can be achieved with pressures of 2.0–2.5 MPa [28].

Ultrasonic Gas Atomization

Confined atomizers are of two types: conventional (see Figure 5.21(b)) and ultrasonic (Figure 5.23). The ultrasonic designs use the Hartman tube principle to apply high-frequency pulsation to the gas stream, with gas exit velocities reported to be Mach

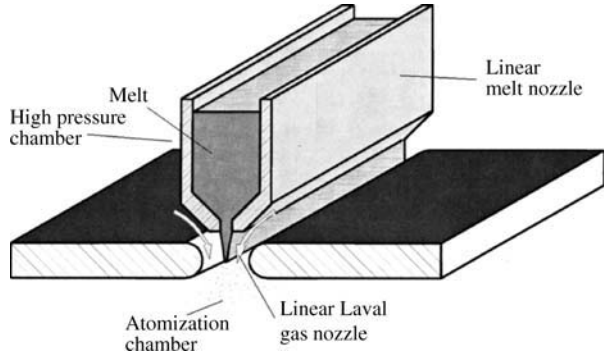

Figure 5.22 Simplified drawing of the WIDEFL0W confined linear nozzle design.

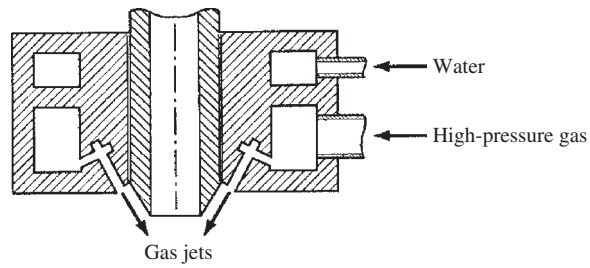

Figure 5.23 Ultrasonic gas atomizer. (Source: US Patent 2,997,245, Aug 1961)

2 to 2.5 and the major pulsation frequency at about 100 000 Hz. HEVs ultrasonic atomization unit includes an induction melting unit, atomizer, transducer, transfer tube and tubular resonator [29]. Classification of the pneumo-acoustic atomizers, development of new devices and procedures for ultrasonic gas atomization are given in [30].

Prefilming Nozzle Design

In several confined designs, the circulation created by the gas flowing up the side of the tundish nozzle causes, due to aspiration force action, the molten metal to spread across the face of the ceramic nozzle to its edge, where it is sheared by the flowing gas [31]. These nozzle designs are referred to as 'prefilming' (Figure 5.24(a)) and are quite widely used.

The regime when a thin film is formed on the melt nozzle top is the preferred operating regime for producing fine powders. When the metal flow rate is too high, the filming effect is partially lost and some of the metal is entrained into the low-velocity wake and does not film effectively [32]. Such a regime leads to coarser powders and to the formation of undesirable flakes in the powder.

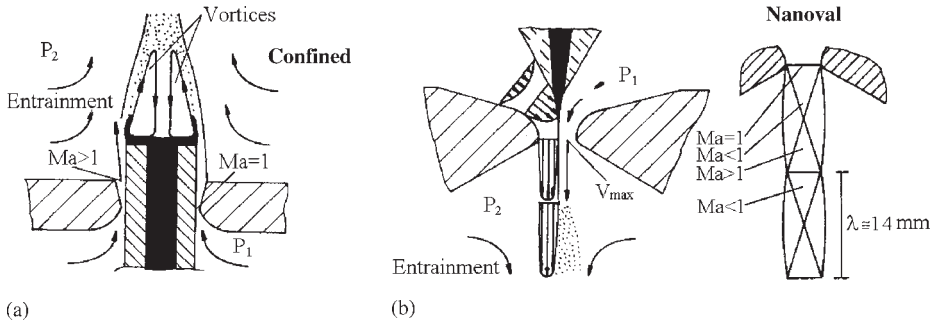

Figure 5.24 Schematic of prefilming nozzle design (a) and Nanoval design (b).

The low pressure (suction, aspiration) created at the nozzle tip is a useful feature of the prefilming nozzle design. It is employed to draw the liquid metal into the melt nozzle from the crucible in up-draught operation, as mentioned above. Additionally, the presence of suction at a point of contact between the gas and liquid avoids the potentially hazardous blowback effects observed in free fall nozzle designs for certain jet geometries.

At the same time, by the air atomization a sudden stoppage or decrease of its flow rate can lead to ignition or explosion of the suspended solid powder in case of active metals or alloys.

The level of suction created by a nozzle is found to be extremely sensitive to nozzle geometry, atomizing gas nature and operating gas pressure [32].

Nanoval Nozzle Design

In the Nanoval nozzle design [33], a metal melt stream is broken up by the action of friction forces between the atomization gas and the liquid (Figure 5.24(b)). Because the metal stream is always kept very thin and it is delivered directly to the throat of the nozzle, this design is capable of producing very fine powders. The comparison of mean particle sizes by Nanoval and conventional confined nozzle design is represented in the form of mass median diameter dependence on specific gas momentum, shown in Figure 5.25.

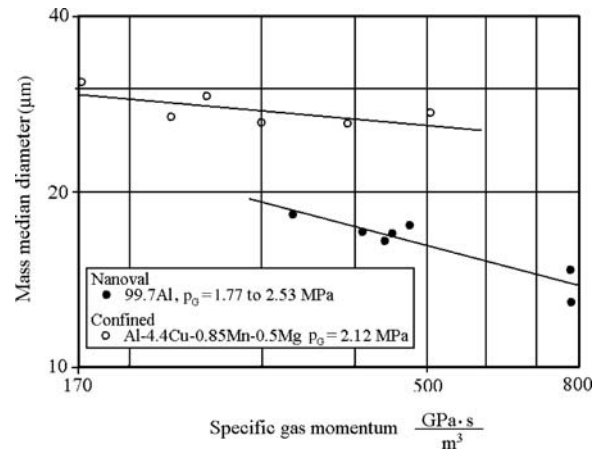

Figure 5.25 Comparison of mean particle sizes by Nanoval and conventional confined atomizing nozzle designs.

Pressure-swirl Hybrid Prefilming Atomizer

This atomizer combines pressure-swirl atomization and ring-gas atomization. In the first stage, a film is generated followed by gas jet atomization in the second step [34]. The pressure-swirl-metal chamber, atomization chamber and gas-recirculation system are the main components of the powder atomization unit. Figure 5.26 [35] shows schematically a pressure-swirl atomizer. Due to overpressure, the molten metal flows tangentially into the swirl chamber, leaves it through a small cylindrical hole (D_L) and forms a

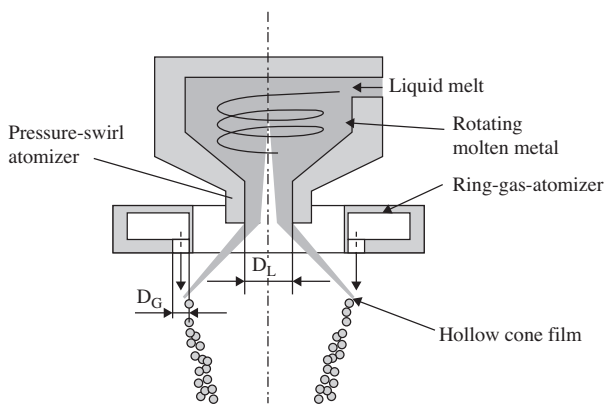

Figure 5.26 Pressure-swirl hybrid prefilming atomizer.

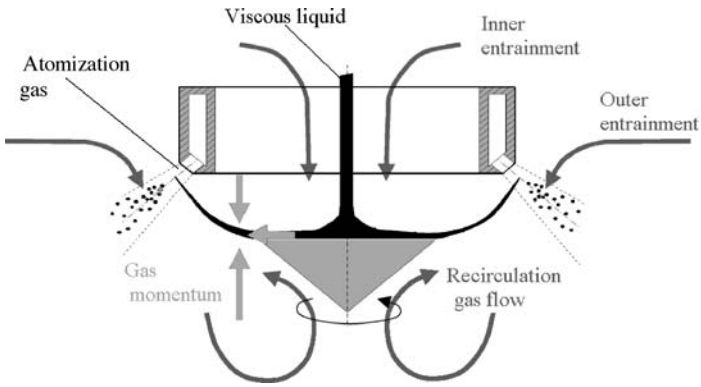

Figure 5.27 Prefilming hybrid atomizer for viscous melt atomization. (Source: Ref 36)

swivelling hollow cone film of molten metal. The film is subsequently atomized by the gas jets through the orifices (D_G).

Spherical tin powders with median diameter 10–20 μm and standard deviation below 2 were obtained by superheat 100°C, gas (nitrogen) pressure 1.0 MPa, gas to metal ratio 1.3, and with a melt flow rate between 160 and 190 kg/h.

Prefilming Hybrid Atomizer

This has been developed for viscous melt atomization [36]. Viscous melts, such as oxidized metals or slags, have a comparably high viscosity. The prefilming hybrid atomizer is shown in Figure 5.27. Their local flow regimes are distinguished by the difference from where the ambient gas interacts with the atomization gas. The inner entrainment reaches the atomization area through the atomizer liquid stream passage. The outer entrainment reaches the atomization area directly and the recirculation gas flow reaches the atomization area from below the rotary disk. The aim of the prefilming hybrid design is to generate a maximum recirculation momentum so that the film is transported closer to the external mixing atomizer gas outlet.

Process Parameters

In conventional gas-atomization processes, the atomization pressures are typically in the range 0.5 to 4 MPa and gas velocities in the nozzles range from Mach 1 to 3. However, in free-fall atomizers, gas velocities in the impingement zone usually have fallen to 50–150 m/s (for air or nitrogen). Typically, gas-atomized powders are usually spherical with log normal size distribution. Average particle sizes are usually in the range 10 to 300 μm with a standard deviation of about 2; oxygen content is the range of 100 to 1000 ppm. Prealloyed alloys are made commonly by inert gas atomization. Worldwide annual tonnage of inert gas-atomized powder is much less than that of water-atomized powders, probably amounting to more than 50 000 tonnes per year. Metal feed rates are lower than in water atomization and melt batch is smaller. However, total tonnage of air-atomized powders, especially zinc and aluminum, as well as copper, tin, lead and copper alloys, probably exceeds 400 000 tonnes per year [1]. Air atomizers operate continuously for many hours or round-the-clock. Multinozzle units are often used to boost yield on aluminum and zinc.

In conventional inert gas or air atomization, typical metal flow rates through single-orifice nozzles are in the range 1–90 kg/min. Capability of plants varies from very little laboratory units to immense plant such as ANVAL Atomizer 1 (Figure 5.28), which is the biggest inert-gas atomizer and is designed for producing large tonnages of superalloy and other alloy powders. Melting takes place in two 5.5-tonne induction furnaces. A plasma-heated tundish is used. Due to the height of the tower, powder with up to 1 mm particle size can de produced. Very fine powder can also be produced for applications such as MIM.

In conventional atomizers, typical gas flow rate ranges from 1 to 50 m^3/min at a pressure range of 350 kPa to 4 MPa. The superheat of molten metal (the temperature differential between the melting point and the temperature at which the molten metal is atomized) is generally about 75–150°C. In gas atomization with inert gas, the cost of gas consumption is significant, and a means of circulation to promote gas reuse is desirable, especially in large-scale facilities.

In practice, for a given gas nozzle design and size, mean particle size is controlled by the pressure of the atomizing medium and the melt flow rate, which is regulated by nozzle diameter and nozzle suction. For all nozzles, the velocity of the gas usually 'chokes' at sonic velocity (about 300 m/s for nitrogen and argon) in the narrowest region of the nozzle.

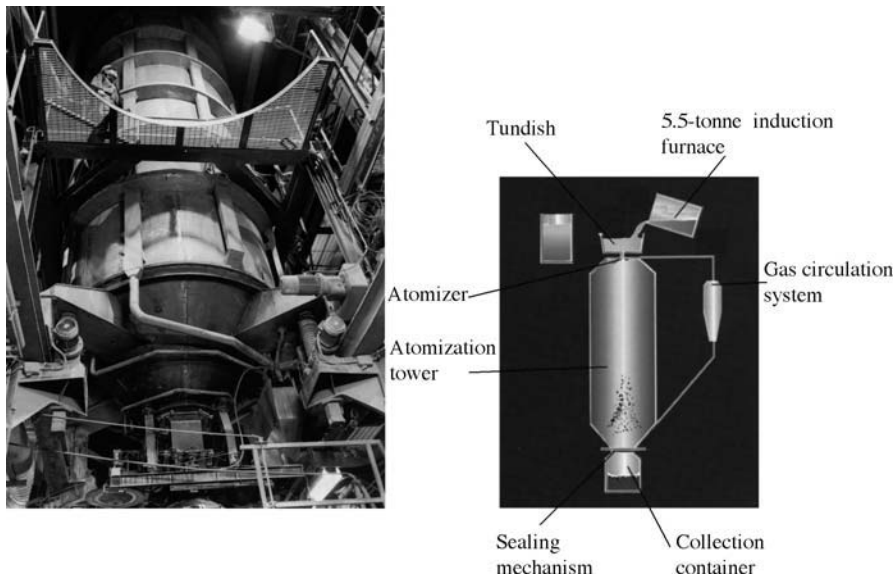

Figure 5.28 ANVAL Atomizer 1. Courtesy of ANVAL.

Therefore, the amount of gas flow (Q) depends on gas pressure, temperature and nozzle area. For ideal conditions and zero velocity on the entrance side of the nozzle, gas flow can be expressed [3]:

$$Q = \omega\left(\frac{2}{k+1}\right)^{\frac{k+1}{2(k-1)}} g\frac{p\sqrt{2g}}{\sqrt{RT}} \tag{6}$$

where ω is the cross-section of gas nozzle at exit; k equals C_p/C_v, the ratio of specific heat at constant pressure and volume, correspondingly; p is the gas pressure in reservoir; T is the temperature in gas reservoir; R is the gas constant; and g is the acceleration due to gravity. For nitrogen $k = 1.4$.

As a compressible fluid passes through a nozzle, a drop in pressure and a simultaneous increase in velocity result. If the pressure drops sufficiently, a point is reached where, in order to accommodate the increased volume due to expansion, the nozzle design must diverge. Thus, nozzles for supersonic velocities must converge to a minimum section and diverge again.

A comparison on the basis of how much powder surface is generated per unit of atomization gas spent can be used for evaluation the gas efficiency. This criterion accounts for higher gas consumption requirements when higher gas pressures are applied to produce finer powders. Confined nozzle designs in comparison with consumption ones give higher efficiencies at a comparable gas to metal ratio [37].

A simple equation of median particle size dependence on gas/metal ratios can be used:

$$\delta_m = \frac{k}{\sqrt{G/M}} \tag{7}$$

where k is a constant for the process and G/M is the gas/metal ratio, which is variously measured in kg/kg or cubic meters of gas per metal mass (m^3/kg). Source [16] involves typical values of k for confined nozzle designs.

Models of Gas Atomization

Superheated metal melts may be considered as Newtonian liquids; in this connection their interaction with the gas jet is expressed by criterial dependences. The most empirical formulations for definition of an average particle size in real atomization systems use the aerodynamic Weber number:

$$We_g = \frac{\rho_g v_g^2 d_0}{\sigma_m} \tag{8}$$

This criterion represents the balance of the break-up force, related to gas kinetic energy through the gas density, ρ_g, and v_g^2, that is resisted by melt surface tension, σ_m, acting over a specific melt stream diameter, d_0.

Generally, in each model of droplet formation, a stability criterion involves the Weber number of the liquid metal. The first attempt to develop a model

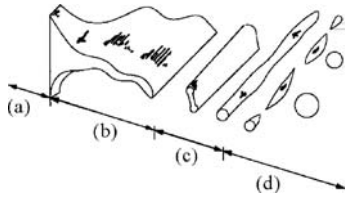

Figure 5.29 Model for the disintegration of a liquid sheet by a high velocity jet of gas: (a) stable sheet; (b) growth of waves in sheet; (c) ligament formation; (d) ligament breakdown.

of the three steps droplet formation process seems to have been made by Dombrovski and Johns [38]. Proposed mechanisms of droplet formation involve:

- the initiation of a sinuous wave which rapidly increases in amplitude
- detachment of the wave from the layer of the liquid to became a ligament whose dimensions depend on the wave length λ at disintegration on wave number k_w (i.e. $2\pi/k_w$)
- breakdown of ligaments into droplets (Figure 5.29).

In Bradley's mathematical model, known as the capillary wave model [39,40], the liquid is considered to be a horizontal infinitely deep phase, initially not moving, being swept by a compressible gas phase with a uniform velocity parallel to the liquid surface. Rayleigh instability was invoked for the break-up of the ligament into spherical drops. In the first stage of the atomization process, the critical wave number k_{max} with the fastest growing amplitude is determined from quadratic equation in k and includes a dependence on the kinematic viscosity of the liquid, the densities of the gas and liquid phases, the liquid/gas interfacial energy that opposes the growth of the wave, and the Mach number M of the atomizing gas.

In the second stage of atomization, Bradley suggested that the ligament diameter D is related to the wavelength λ_{max}, i.e. $2\pi/k_{max}$ by linear dependence:

$$D = \varepsilon\lambda_{max} = \frac{2\pi\varepsilon}{k_{max}} \tag{9}$$

where the parameter ε (of the order of 0.25) was defined in earlier studies on the air atomization of water.

The resultant droplet diameter δ is expressed:

$$\delta = \frac{2.95\sigma_m}{L\rho_g v_g^2} \tag{10}$$

where σ_m is the liquid surface tension (N/m), ρ_g is the density of the gas (kg/m^3), v_g is the sonic gas velocity (m/s), L is a dimensionless parameter, the function of the Mach number M and knowing the value of M during gas atomization; L can be defined by [41].

A comparison of the experimental data of See and Johnston to Bradley's predictions for the nitrogen atomization of lead sees that the model gives agreement approximately within a factor of two [42]. At its present design, Bradley's model does not give any indication of the origin of the spread in powder production by gas atomization.

The other often-cited models are the capillary and acceleration wave models of Ingebo [43]. Here, the Reynolds number is an important part of the Ingebo expressions for both capillary and acceleration wave break-up. The Reynolds number

$$Re_L = \frac{\rho_L (v_g - v_L)^2 d_0}{\mu_L} \tag{11}$$

contains the dimensionless balance of gas kinetic energy through $(v_g - v_L)^2$, as related to the dynamic viscosity, μ_L, in the melt with a density, ρ_L, in the melt stream diameter, d_0.

The resulting Ingebo equation is:

$$\frac{d_0}{\delta_m} = c_0 (We\ Re_L)^m \tag{12}$$

where c_0 and m are adjustable constants; for area $WeRe_L > 10^6$ $c_0 = 0.027$ and $m = 0.4$, then

$$\delta_m = 37 d_0 [We\ Re_L]^{-0.4}$$

A modified capillary wave model in melt atomization was applied in several works [44,45]. Ternovoy and colleagues [45] considered the atomization of free melt stream by annular gas jet with hollow cone of metal formation. The instability wavelength λ_f with the fastest-growing amplitude in the metal film was defined in accordance with [46]:

$$\lambda_f = \frac{1.5\gamma}{\rho_g v_g^2} \tag{13}$$

where γ is the specific surface energy of a melt, ρ_g is the gas density, v_g is the gas velocity at the exit of the melt nozzle.

The droplet formation is considered as break-up of the melt micro-jets by instability wavelength $\lambda_{\mu j}$ with the fastest growing amplitude in metal micro-jets and is described in accordance with [46] by the expression:

$$\lambda_{\mu j} \approx 4\pi \left(\frac{v_m^2 \rho_m \delta_{\mu j}^3}{8\gamma} \right)^{1/4} \tag{14}$$

where v_m is the kinematic viscosity of a melt, ρ_m is the melt density and $\delta_{\mu j}$ is the diameter of the micro-jet.

The resulting semi-empirical formula for the droplet diameter definition is:

$$\delta_m = \frac{1.88 v_m^{0.4} \rho_m^{0.2} d_m^{1.26}}{\gamma^{0.026} \rho_g^{0.17} R_{tr}^{0.63} v_g^{0.34}} \left(\frac{gh\rho_m + \Delta p}{gh\rho_m - 2\Delta p} \right) \left(\frac{G_m}{G_g} \right)^{0.3} \quad (15)$$

where d_m is the melt jet diameter at the exit of the melt nozzle, R_{tr} is the film opening radius in position of toroidal thickening on its periphery, g is the acceleration due to gravity, h is the melt height in the tundish, Δp is the pressure differential between furnace chamber and the exit of the melt nozzle, G_m melt mass flow, and G_g gas mass flow.

More recently, improved flow visualization techniques used to study melt atomization dynamics do not confirm the formation of film hollow cone in conditions of atomization of free melt stream by annular gas jet [47]. Through that, the authors [45] obtained the tolerable convergence of median particle size values calculated on the suggested formula with measures for argon or argon/helium mixture atomization on a confined nickel alloy jet.

The pressure-swirl atomization principle allows formation of the film metal hollow cone as is shown in Figure 5.26. Here, a conical film of melt created by a pressure swirl nozzle and shaped by centrifugal forces is atomized by high- velocity gas jets. The physical model of such combined atomization process was represented in work [48]. There are considered to be the following stages of the atomization process (Figure 5.30):

1. transmission of instability wave in a film across and along the velocity vector owing to oscillation processes caused by external and internal factors. The instability wavelength κ_f with the fastest-growing amplitude in a metal film was introduced in accordance with [46]. Depending on the physical properties of the liquid and gas, two schemes are suggested: with a thickening of a film in toroidal form in accordance with wavelength (Figure 5.30 (side a)) and when a film is just bending (Figure 5.30(side b))
2. formation of a liquid torus on peripherals of a film as a result of transmission of a longitudinal wave with the fastest growing amplitude

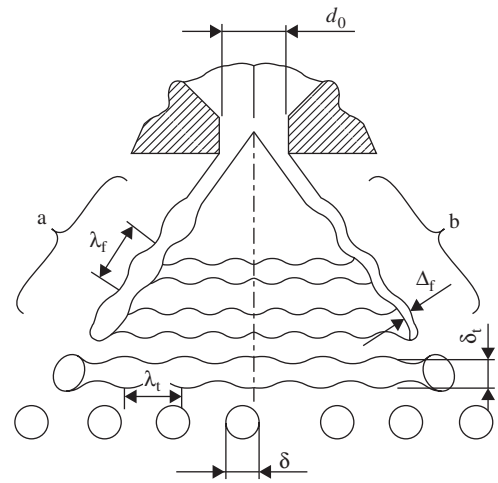

Figure 5.30 Model of the pressure-swirl atomization process: d_0 is the melt metal nozzle orifice diameter, Δ_f is film thickness in zone of impingement with secondary atomization gas jet, δ_t is the diameter of max torus cross-section in zone of impingement with secondary atomization gas jet, λ_f is the wavelength of film instability, λ_t is the wavelength of liquid torus and δ is the atomized particle diameter. (Source: Ref 48)

3. transmission of instability of toroidal peripheral area
4. all previous stages coincide with the above described model [45], while the final stage differs because it consists of secondary atomization of previously broken up film ligaments (torus or drops in dependence on atom-ization conditions) under the action of a high gas pressure jet.

The thin film represents a surface for efficient disintegration in order to achieve fine particle sizes and narrow size distribution using low specific gas consumption.

On the basis of this model, a formula for definition of particle diameter was suggested:

$$\delta = k\varphi^{0.46} \frac{v_m^{0.17} \rho_m^{0.08} \sigma^{0.38} d^{0.92}}{R_f^{0.46} \rho_g^{0.46} v_g^{0.92}} \quad (16)$$

where k is the coefficient of the nozzle geometry; φ is the unfilled coefficient for the melt nozzle orifice of d diameter; v_m is the kinematic viscosity of a melt; ρ_m is the density of a melt; σ is the surface tension of the melt; R_f is the radius of the film at the point of break-up; ρ_g and v_g are the density and velocity of a gas stimulating the film disturbance.

Table 5.3 Tin powder properties produced by means of the pressure-swirl atomization process

Oxygen contentin the atomization chamber (ppm)	Melt temperature (°C)	Melt pressure (MPa)	Melt flow rate (kg/h)	Gas pressure (MPa)	Gas flow rate (m^3/h)	Mass median diameter (μm)	Standard deviation (δ_{84}/δ_{50})
<100	290	0.7	180	0.7	109	33.5	1.85
100	290	0.7	180	0.7	109	22.8	1.6
300	290	0.7	180	0.7	109	22.1	1.6
500	290	0.7	180	0.7	109	24.6	1.6

The estimation of the mass median diameter offered by Eqn (16) shows sufficient comparability between calculated and experimental values for tin, tin–lead solder (61Sn–39Pb) and copper alloy (Cu–15Sn–5Pb–4Ni) in experiments by gas/metal ratio values in the range from 0.15 to 0.35 m^3/kg [48]. An effect of oxygen content on powder properties was revealed (Table 5.3).

Traditionally, gas atomization by means of close-coupled nozzles is believed to involve the formation of a melt film at the nozzle edge [49], as shown in Figure 5.31. Fine particles are thought to form as a result of the primary breakup of the melt film upon its interaction with supersonic gas flow at the nozzle edge. Further, even if low melt flow conditions that favor filming are used, it has been suggested that secondary breakup still plays an important role in determining particle size [50].

More recently, a microsecond-exposure spark schlieren technique allow us to visualize the melt atomization process along with the atomizing gas flow features, providing a look at the fluid dynamic interactions during atomization [47]. These experiments indicated more complex atomization behavior, including a primary breakup stage close to the nozzle tip, followed by a finer secondary breakup stage where the coarse droplets are disintegrated under high shear into fine powder. Therefore, several authors [50,51] have discussed the apparent dominance of secondary atomization and break-up mechanisms in most studies of close-coupled gas atomization. However, this model version does not exclude the importance of primary atomization to minimize the spread of $\Delta v \mid v_g - v_m \mid$ values.

The increased understanding of the atomization process discovers new ways to approach the problem of particle size control and atomization efficiency. In this connection, in close-coupled gas atomization, there is a considered description of the two gas flow situations that are termed open wake condition

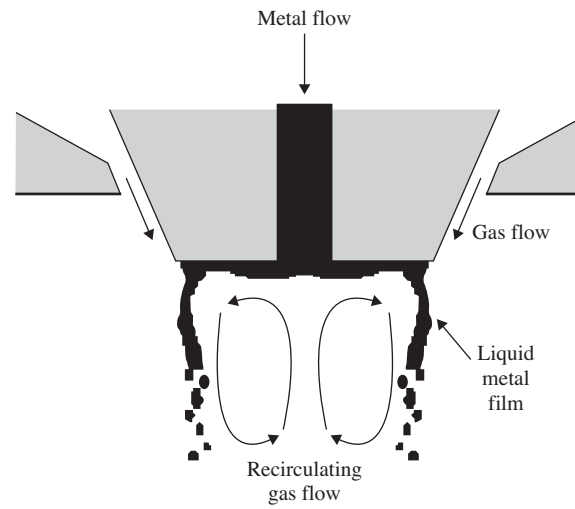

Figure 5.31 Metal filming view in gas atomization. (Source: Ref 49)

[51,52], as shown in Figure 5.32(a) and closed wake conditions in Figure 5.32(b), where the sketches are of a central cross-section and may apply to either a discrete jet nozzle ensemble or an annular slit nozzle with the same melt tube arrangement.

A more complicated gas flow situation has often been developed purposefully for the production of high yields of fine droplets where the shear wall gas flow is interrupted by a Mach shock disk. The Mach shock disk can appear during high pressure operation of either an annular slit [52] or discrete jet [53]. The wake closure effect and its associated Mach shock can present an additional kind of atomization energy coupling.

The pressure value on the liquid metal nozzle tip is an important parameter in close-coupled gas atomization. The pressure formation on the melt nozzle tip in dependence on gas pressure is shown in Figure 5.33.

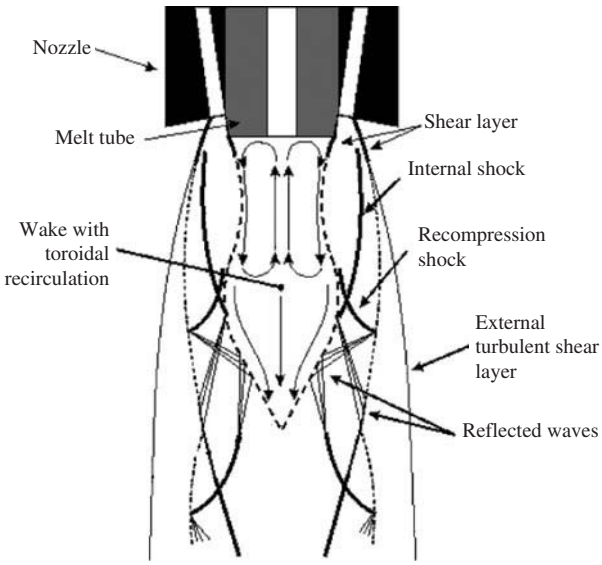

Figure 5.32 Schematic of (a) open wake and (b) closed wake gas flow patterns in close coupled gas atomization. (Source: Ref 53)

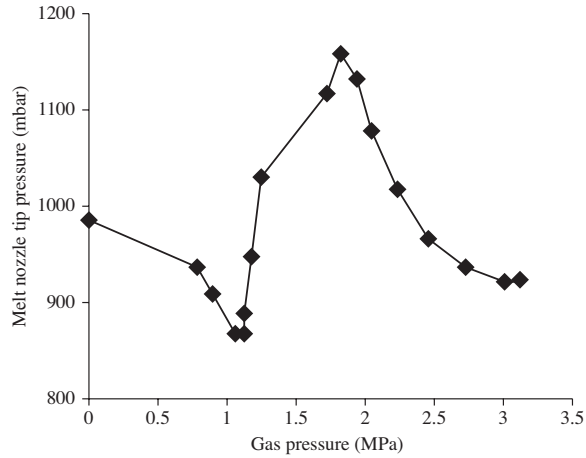

Figure 5.33 The pressure formation on the melt nozzle tip in dependence on gas pressure in close-coupled slotted nozzle design (by the constant protrusion length 10 mm).

Gas Atomized Powders

Particle Size, Size Distribution, Shape and Surface Morphology

There is a comprehensive literature base on gas atomization in terms of the effect of operating conditions on powder properties [14,15,56].

One of the most important single parameters controlling particle size in gas atomization is specific gas consumption. It can be expressed as a mass ratio of gas to metal flow or as the ratio of gas volume to metal mass. Data for several metals and alloys conform to an equation of the form:

$$\delta_m = KF^{-1/2} \tag{17}$$

where K is a constant and F is the specific gas consumption in m^3/kg. The value of K is a function of nozzle design and alloy properties [15].

Specific gas consumption is also an important process parameter in controlling δ_m in ultrasonic gas atomization [42,57]. For an aluminum alloy at a fixed atomizing gas pressure, median diameter value can be varied from $\approx 250\,\mu m$ to below $50\,\mu m$ when the mass flow ratio of gas to metal increases from 0.3 to 2.0. A decrease in δ_m is also predicted with increasing gas pressure.

Gas-atomized powders generally have a log normal size distribution, with standard deviation normally around 2.0 ± 0.3. The values of π generally decrease as δ_m decreases and most data show an in empirical relation of the form [56,58]:

$$\sigma = a\delta_m^b \tag{18}$$

where a and b are constants.

Lubanska [58], by comparing the literature on gas-atomized metal powders and by using a relationship

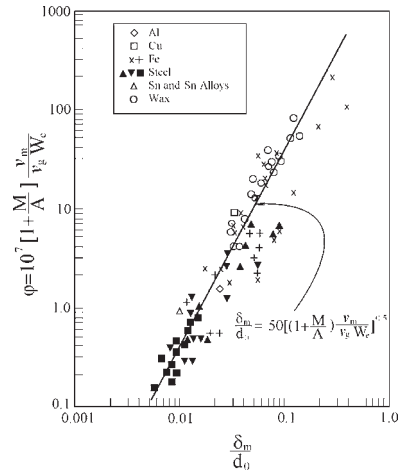

Figure 5.34 Lubanska correlation (Eqn 19) for air atomization.

developed by Wigg [59], derived an empirical equation for the average particle size (δ_m). In dimensionless form, Lubanska's formula is:

$$\frac{\delta_m}{d_0} = K\left[\frac{v_m}{v_g}\frac{1}{We}\left(1+\frac{M}{A}\right)\right]^{1/2} \tag{19}$$

where *We* is the Weber number, δ_m is the mass median particle diameter, d_0 is the diameter of the metal stream, v_m is the kinematic viscosity of liquid metal, v_g is the kinematic viscosity of the atomizing medium, M/A is the mass flow rate to gas, K is a constant.

Data from source [58] for various metals are depicted graphically on log/log scale in Figure 5.34 and show consistent agreement with experimental data.

Various other empirical equations have been published.

Miller and Giles [12] have analyzed the atomization of a variety of metals and conclude that acceleration wave break-up predominates at high gas velocity. They define a modified Weber number and correlate it to material properties and the ratio of gas-to-metal mass flow rates. The functional (dimensionless) form of the relationship was obtained from experiments.

Some empirical relationships can be transformed in terms of physical models for droplet formation. That referred to as maximum stability criterion, for instance, gives maximum drop size as a function of surface tension of the liquid metal (σ), gas density (ρ_g) and velocity (v) of the atomizing medium as:

$$\delta_{crit} = \frac{\sigma}{\rho_g v^2} \tag{20}$$

This equation applies to the breakup of ligaments [42]. Secondary disintegration into particles smaller than δ_{crit} occurs only if the dynamic pressure due to the gas stream velocity exceeds the restarting force of surface tension. Owing primarily to the higher surface tension of liquid metals, energy requirements and, therefore, gas pressures used for atomizing metals is typically between 0.35 and 2.75 MPa.

Similar to water atomization, commercial gas-atomization units exhibit non-uniformly operating characteristics. Proprietary empirical relations have been established between operating conditions, material properties and powder characteristics, in particular, median particle size and standard deviation. Beddov [19] has annotated several of these empirical relations for gas atomization.

The majority of gas-atomized powders are spherical or near-spherical in shape. Small satellite particles attached to the larger particle give rise to a variable shape factor in gas atomization. The satellites are caused by collision between particles in flight and the incidence of this effect increases as overall powder size decreases due to the fine particles drown up into the atomizing zone [60].

In the absence of impurity effects and surface oxide films, particle shape is controlled by the relative magnitudes of the times for solidification and spheroidization, provided the residence time of the particle in suspended solid state in the gas is greater than either of these times. Models of both phenomena are given in [61].

In the model for solidification time in gas atomization, it was assumed that the molten droplets did not undercool, that the relative velocity between the gas phase and the particle is constant and that convective heat transfer is dominant [42]. Then, the total solidification time t_{sol} (in seconds) [42, 61] is expressed by:

$$t_{sol} = \frac{\delta_m \rho_m}{6h_g}\left[(c_p)_m \ln\left(\frac{t_{in}-t_g}{t_m-t_g}\right)+\left(\frac{\Delta H_m}{t_m-t_g}\right)\right] \tag{21}$$

where δ_m is the mass median particle diameter (m), h_g is the convective heat transfer coefficient of the gas (W/(m^2°C)), ρ_m is the density of the liquid metal (kg/m^3), $(c_p)_m$ is the heat capacity of the liquid metal (J/(kg°C)), t_{in} is the initial temperature of the particle (°C), t_g is the gas temperature (°C), t_m is the melting

point of the metal/liquidus temperature for alloys (°C), ΔH_m is the latent heat of fusion of the metal (J/kg).

The value of h_g is given by:

$$h_g = \frac{k_g}{\delta_m}(2.0 + 0.6Re^{0.5}Pr^{0.33}) \quad (22)$$

where k_g is the thermal conductivity of the gas (W/(m°C)), *Re* is the Reynolds number relative to the particle, *Pr* is the Prandtl number for the gas.

Under the influence of surface tension forces alone, the time for spheroidization t_{sph} is expressed by:

$$t_{sph} = \frac{3}{4}\frac{\pi^2\mu_m}{V\sigma_m}(r^4 - r_{tr}^4) \quad (23)$$

where μ_m is the dynamic viscosity of the liquid metal (Pa·s), V is the particle volume (m^3), σ_m is the surface tension of the liquid metal (N/m), r is the radius of spheroidized droplet (m), r_{tr} is the metal liquid trickle radius before transformation to spherical droplets (m).

A more detailed and general model to estimate the time for spheroidization of a droplet has been given by Rao and Tallmadge [62]. Lawley [15] notes that their predicted spheroidization times are not significantly different from those given by Eqn (23).

Based on these models, See and Johnston [42] have calculated the times for spheroidization and solidification of a range of droplet sizes (149–420 μm) for tin. Spheroidization times ($<2 \times 10^{-5}$ s) lower than the times required for solidification, so that only spherical particles should be produced in gas atomization, if there are no factors which hinder this transformation. The presence of ligament-shaped particles of Sn, particularly at small particle size fractions, is attributed to the presence of an oxide layer (SnO_2) which opposes the action of the surface tension.

The surface of gas atomized powders is generally smooth. The particle surfaces frequently exhibit a cellular or dendritic morphology, subject to cooling rate during solidification of the droplets. When reactive elements are prealloyed with the base elements, some surface oxidation can occur during gas atomization.

The spherical shape and smooth surface inhibit the development of green strength in cold compaction. In addition, prealloying before atomization increases particle hardness and strength which reduces compressibility. These inherent limitations of gas-atomized powders have stimulated development of elevated temperature consolidation processes to achieve high density: examples include hot extrusion and hot pressing. It is possible, by increasing the cooling rate via decrease in particle size, to change particle shape towards non-sphericity. It is also possible to add elements that alter the surface tension values (Li, Mg, Si, Ca, Mn, etc.).

The relatively high cooling rates intrinsic to gas atomization result in fine-scale microstructures. In NiAl and Ni_3Al powders, sonic gas atomized using nitrogen produced either dendritic or equiaxed structures depending on the particle size and consequently on the cooling rate [63]. The $Al_{82}Ni_{10}Y_8$ alloy powder produced in a close-coupled nozzle atomizer unit at 3.03 MPa argon jet pressure has perfectly spherical and smooth particles (Figure 5.35). In particles of several micrometers the dendritic and cellular microstructures were not detected and they tend to be amorphous (Figure 5.36).

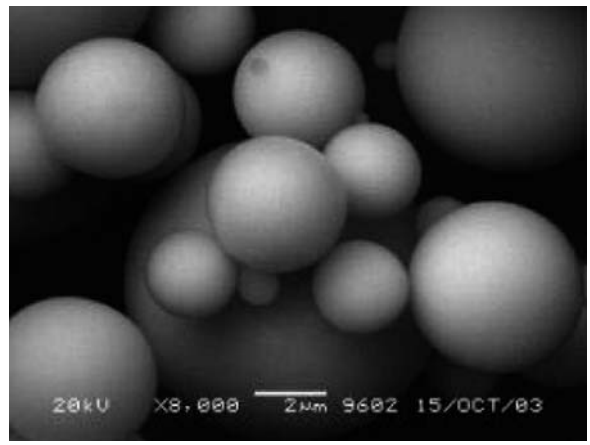

Figure 5.35 Surface morphology of $Al_{82}Ni_{10}Y_8$ alloy powder with particle diameter below 15 μm. (Source: Ref 64®)

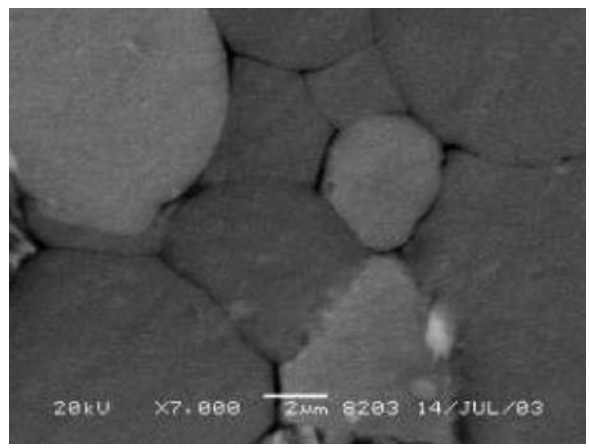

Figure 5.36 SEM microstructure of $Al_{82}Ni_{10}Y_8$ alloy powder with particle diameter below 15 μm. (Source: Ref 64®)

Internal pores can be present in gas atomized powder and may be detrimental in several respects. The effect of closed porosity leads to reduced apparent density, causes gas bubbling in thermal spray deposits and gives rise to uncontrolled dimensional change during sintering. Internal pores are of most concern in superalloy powders atomized with argon. The argon in the pores is insoluble in the alloy and this gives rise to the phenomenon of thermally induced porosity following densification by hot isostatic pressing with attendant decrease in the mechanical properties. From the study [65], it is concluded that internal closed porosity is a common phenomenon in gas atomization and that its extent increases with increasing particle size. A major source of internal porosity is gas entrapment, especially when the gas is insoluble in the solid powder particles.

Powder Cleanliness

Impurity control is of paramount importance for high-performance applications. Powder cleanliness is a major concern with atomized specialty alloys. These alloys are used frequently in applications with exacting combinations of strength, ductility, toughness and fatigue resistance. In these conditions, there are non-metallic inclusions in the powder that limit performance when the powder is consolidated. Inclusions may be introduced during melting and inert gas atomization; their source is the refractory tundish or pouring nozzle used in conventional gas atomization. The inclusions act as sites of stress concentration and can result in the initiation of fatigue cracks. This effect is of prime concern in components for aircraft engine applications.

Using practicable induction melting technique, it is possible to replicate closely the composition of the melt stock in the resulting gas-atomized powder. Thus, specialty alloys based on aluminum, copper, nickel, cobalt and titanium can be gas-atomized to exacting compositional specifications. Partial loss of elements with a high vapor pressure or reactive elements can be quantitatively compensated for during melting prior to atomization. Primary sources of intermediate impurities are initial charge impurities, the melting atmosphere, the atomizing gas and refractory ceramics (crucible, tundish and tundish nozzle). In the case of the most critical superalloys, a bottom pouring electroslag remelting furnace that discharges using a ceramic-free pouring nozzle to minimize all possibility of inclusion pickup [66] has been developed. In the EIGA (Electrode Induction Melting Gas Atomization) process [67], prealloyed rods as an electrode are inductively melted without a crucible. The metal liquid droplets from the electrode fall into the atomization nozzle design and are atomized with an inert gas jet. The EIGA process is used for titanium and niobium alloy powder production [68] and can also be applied to other alloys. Process developments in EIGA technique [69] allow this process to be conducted crucible- and ceramic-free, with larger electrode diameters up to 61 mm and increased melt flow rates of 26.4 kg/h. The optimized technique was applied for the atomization of pure Ti, Ti–6Al–7Nb and gamma-TiAl-based Ti–46Al–9Nb alloy powders. The oxygen level of the Ti–6Al–7Nb rod was about 1800 ppm; for the argon atomized powder, fraction $<20\,\mu m$, the oxygen content increases to 2300 ppm. The TiAl rod had an oxygen level of 560 ppm; for powder fraction 63–90 μm this level was maintained.

The control of the level of interstitial is very important, particularly in titanium alloys, titanium aluminides and beryllium. The control of interstitial levels in titanium alloys and aluminides is particularly important because ductility is very sensitive to carbon, oxygen, nitrogen and hydrogen impurities. Typical interstitial impurity contents of gas-atomized gamma titanium aluminide, alpha two titanium aluminide and alpha titanium alloy powders are given in Table 5.4. There is, in the main, no increase in carbon, nitrogen and hydrogen over the starting material during atomization. The increase in oxygen content from the starting material to the $<500\,\mu m$ powder is typically 200 ppm [42,70]. Nitrogen content appears

Table 5.4 Typical interstitial impurity contents of gas-atomized gamma titanium aluminide, alpha two titanium aluminide and alpha titanium alloy powders

Alloy	Impurity elements, ppm (weight)			
	Carbon	Oxygen	Nitrogen	Hydrogen
Gamma titanium aluminide	200	800	50	20
Alpha two titanium aluminide	200	800	50	50
Alpha titanium alloys	200	800	50	75

(Source: Ref 12 and Ref 70)

to be independent of particle size but the oxygen content shows an increase from 800 ppm in $<500\,\mu m$ powder to 1020 ppm in $<45\,\mu m$ powder due to the large increase in surface area.

In helium-atomized beryllium powder, it is possible to keep the oxide content to a relatively low level [12, 71].

Other Gas Atomization Methods

Internal Mixing Nozzles

In an internal mixing atomizer, gas and liquid metal are mixed under pressure and expansion and atomization occur at the nozzle exit into the chamber [72]. As is shown (Figure 5.37), the gas enters with high velocity through tangential inlets into a nozzle to which the liquid metal flows axially and is carried by the rotational gas flow in film form on the inner surface of the nozzle walls to the outlet in the bottom. The narrowing of the lower nozzle part forces the gas to accelerate so that the liquid film becomes thinner. At the outlet, the film breaks into small droplets. Concerning its working principle this nozzle design is termed a prefilming spin nozzle (PFSN). The lab melt feeding unit allowed the control of melt flow rates between 0.4 and 5 ml/min for temperatures up to 200°C. The atomization conditions were as follows: atomizing gas was argon, gas pressure max 0.6 MPa and initial metal was 62Bi–38Sn (weight). Its physical data were as follows: melting point 144°C, viscosity 2.2 mPa s at 200°C, surface tension 0.41 N/m at 150°C, density 8.7 g/m^3. The average particle diameters range from 14 to 25 μm.

The pressure swirl hybrid prefilming atomizer described above (see Figure 5.26), contains an internal mixing nozzle in combination with ring gas atomizer.

The fundamental disadvantage of the internal mixing technique is the engineering difficulty of arranging to pressurize the melt to the same pressure as the gas. There are also problems with erosion of the ceramic nozzles employed because of the metal velocity, normally only 1–3 m/s in a pouring nozzle could be expected to rise to the same order of magnitude as the gas velocities, i.e. possibly about 100 m/s. Thus, applications are so far very limited.

Soluble-Gas-Atomization Process

The soluble-gas-atomization process is also known as vacuum atomization (see Figure 5.1(h)). This process [73] is based on the rapid expansion of gas-saturated molten metal, resulting in a fine atomization of molten droplets that form as the dissolved gas, usually hydrogen or an argon hydrogen mixture, is suddenly released in an evacuated powder collection tank (Figure 5.38). The droplets solidify at a rate of about 1000°C/s. The powder collection tank is cooled under vacuum, powder is sealed and then backfilled with an inert gas. This technique is capable of atomizating up to 1000 kg of superalloy in one fusion and produces spherical powder. This process has been employed in commercial scale for LC Astroloy, MERL 76 and IN-100 production.

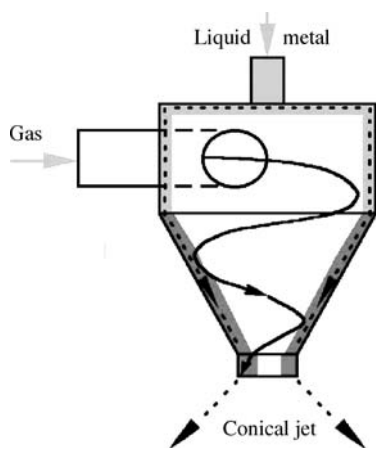

Figure 5.37 Principle of the internal mixing nozzle.

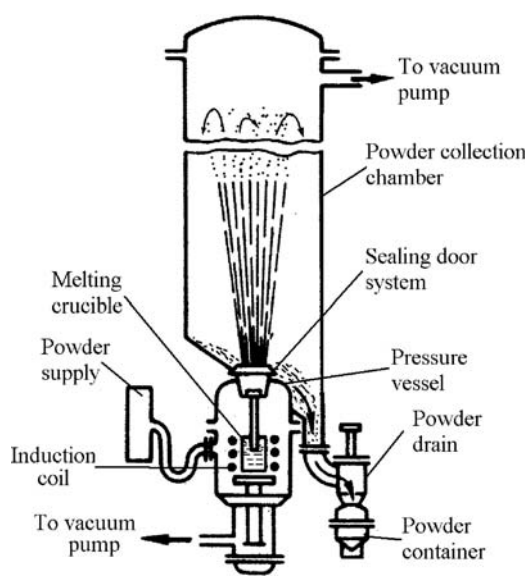

Figure 5.38 Soluble gas atomization system.

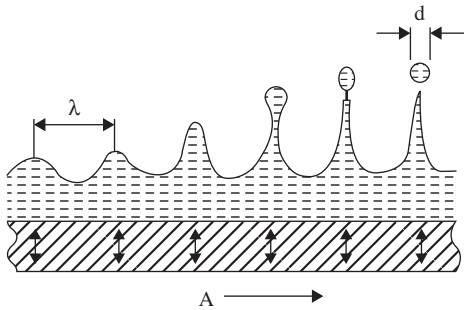

Figure 5.39 Capillary wave atomization model.

Ultrasonic Gas Atomization

Lierke and Griesshammer seem to have been first to report the experimental production of metal powders by ultrasonic atomization in 1967 [74]. Later, they achieved atomization of silver [75]. Many experimental studies have been carried out to evaluate particle size distributions. There are differences between low-frequency (20–100 kHz) and high-frequency (up to 3 MHz) atomizers. Analytical studies work on two assumptions: either the breakup mechanism results from growing instabilities in a capillary wave pattern created at the surface of the liquid film, or it derives from cavitational phenomena [76].

According to the capillary-wave hypothesis (Figure 5.39), a thin layer of a liquid wetting the surface of a solid resonator that vibrates vertically to its surface plan, forms a chessboard-like pattern of stationary capillary waves. This occurs when the vibration amplitude exceeds a threshold value. On further increase of the amplitude, ligament breakup of the liquid follows and droplets are hurled from the crests of the capillary waves. The parameter of interest is λ, the capillary wavelength.

Rayleigh [77] stated that

$$\lambda = \left(\frac{2\pi\sigma}{\rho v^2} \right)^{1/3} \tag{24}$$

where σ is the liquid surface tension, ρ is the liquid density, and v is the oscillation frequency, if the oscillation frequency in the liquid is half that in the solid resonator then

$$\lambda = \left(\frac{8\pi\sigma}{\rho f^2} \right)^{1/3} \tag{25}$$

where f is the ultrasonic frequency.

Later Ruthardt and Lierke [75] measured the particle diameter amounting to 0.25 λ for silver.

Theoretical predictions based on the capillary-wave hypothesis are numerous and essentially apply to low-frequency, low-flow-rate atomizers, whereas cavitation is supposed to occur at higher regimes [76,78]. Yule [79,80] has shown that capillary-wave atomization is not as orderly as foreseen theoretically. As an alternative, Dumouchel and Boyaval [81] used the maximum entropy formalism (MEF) to model size distribution. A detailed description of the MEF can be found in Kapur's paper [82]. In general, the MEF is a mathematical tool for the elaboration of probability distributions.

On HEV's (University of Applied Sciences of Western Switzerland) ultrasonic atomizer [29], magnesium alloy, AZ63 and pure silver were atomized at 20 kHz. Atomizer, induction melting unit, transfer tube, transducer and tubular resonator are the principal parts of HEV's ultrasonic atomizer. Experimental results show a spheroidal particle shape (Figure 5.40); the powder fraction $<50\,\mu m$ yields are about 65 and 71 vol% for magnesium alloy and silver powders, accordingly.

No commercial operator is known to use this method and the largest melter used has been in the 10–50 kg size range.

Hot Gas Atomization

In practice, the hot gas process has been partly motivated by an appreciation of the fact that it allowed the production of finer powders, and partly by the fact that it reduced or avoided the problems of nozzle freezing when processing lower melting point alloys (e.g. Li, Sn, Bi, Cd, Pb, Zn and Al). This allows the use of smaller nozzles and pouring rates which, in turn, allows convenient continuous production as well as the production of finer powders than is possible at higher melt flow rates.

The effect of gas temperature on particle size is shown in Figure 5.41. These data are the result of computation [83] based on dependence of the decrease in the median size of the powder on the square root of gas absolute temperature. In this case, a gas temperature of 200°C reduces the size by 11% and 400°C by 19%. The effect of gas temperature on gas consumption for a constant particle size is shown in Figure 5.42.

A calculation of the economic effect in the case of steel powder production [83] shows that going from 20°C to 200°C reduces costs by 16% and 400°C by 34% (this calculation assumes a gas cost of 0.14 €/m^3 for nitrogen and electricity cost for heating of 0.14 €/kWh). Heating gas to 200°C or even 400°C is not very demanding technically, while to reach 1000°C is far more difficult. Besides that,

savings from going from 499°C to 1000°C are only a further 18%.

Hot gas atomization was applied for the production of inexpensive copper powder for metal injection molding (MIM) where powder costs currently form a high component part [2]. The powder with median diameter about 10 μm was produced by the following process parameters: pouring temperature 1400°C (melting point 1083°C) and atomization gas temperature 500°C.

However, hot gas atomization leads to an increase in the time needed for solidification rather than to a decrease in median diameter and that necessitates an increase in the size of the atomizer chamber. The cooling rate decrease adversely affects the possibility of creating advanced nanostructure alloys.

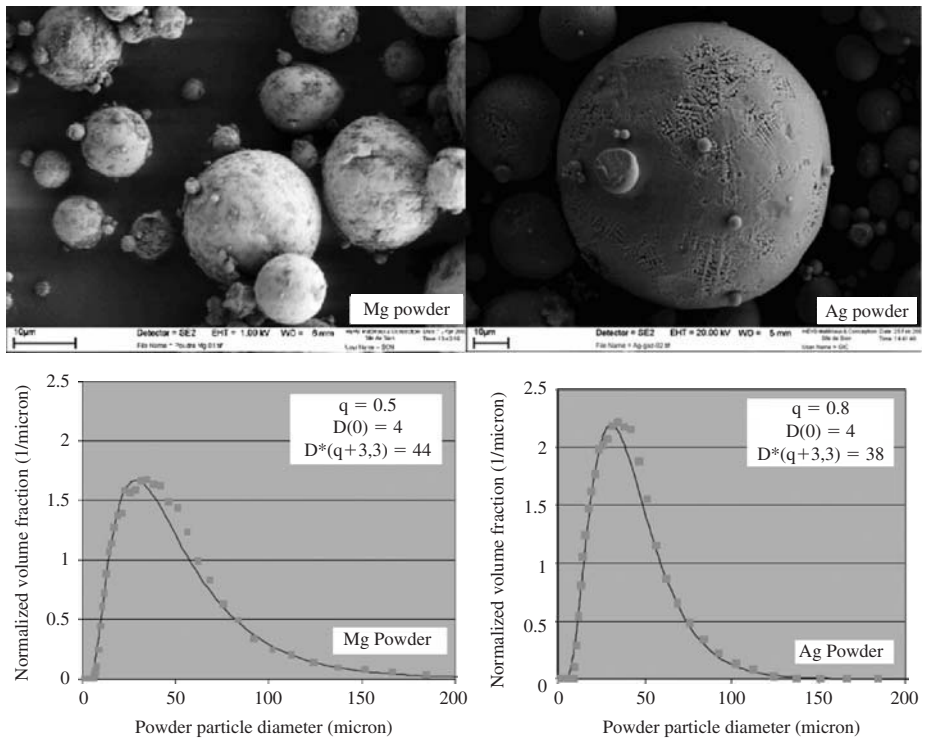

Figure 5.40 Scanning electron micrographs of the ultrasonic atomized magnesium alloy and silver powders and their size distribution. (Source: Ref 29)

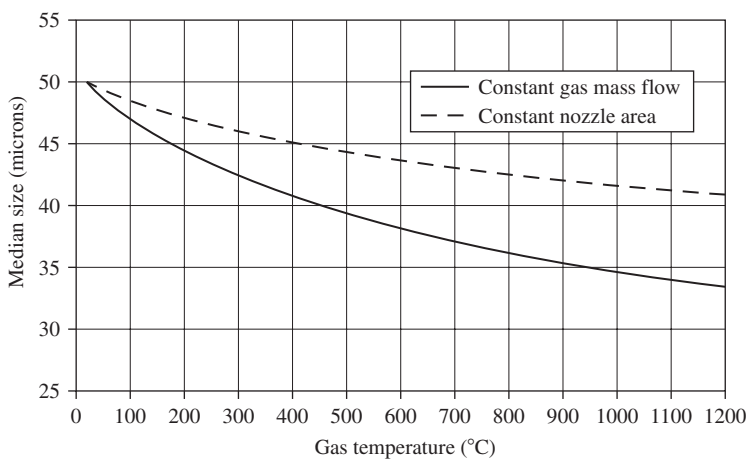

Figure 5.41 Effect of gas temperature on particle size. (Source: Ref 83)

Liquefied Gas Atomization

The atomization of melts with liquefied, cryogenic gases seems to have been developed in 1988 [84]. The so-termed liquefied gas-atomization (LGA) is, in principle, similar to the well-established water-atomization technique (WA) and results in comparable or even higher cooling rates than WA. During LGA no oxidation occurs between the atomizing fluid and melt. Materials exhibiting high sensitivity to oxidation have been atomized via LGA, such as the rare earth NdFeB [85] and NiLa or special solder alloys. Starting with atomizing arrangements similar to WA (free-fall design), the technique has been further developed for the use of confined nozzles, similar or identical to the one used for gas atomization (GA).

Two identical inert gas atomization units at ATZ-EVUS, a laboratory unit up to 30 kg and a pilot unit 100 kg per batch have been used for GA and LGA powder production [86]. Melting is done by inductive heating. The melt orifice diameters range from 1.7 up to 4 mm, the melt superheat temperatures are typically 100–200°C, the atomizing pressures range from 1.0 to 25 MPa. Liquefied gas after cooling to cryogenic temperatures flows to the atomizer when the flow of the superheated melt begins. The mass median diameters range from 30 to 80 μm for NdFeB alloy, copper and Sn–37Pb alloy. The cooling rate achieved is $>10^6$ °C/s in the above laboratory size unit by melt flow rates up to 20 kg/minute [85].

No commercial operator is known to use this method. More detailed data, including powder characteristics, economic effect, and safety engineering aspects, are necessary to evaluate liquefied-gas-atomization process.

Centrifugal Atomization

Models of Centrifugal Atomization

According to the studies of Hinze [87], Tanasawa [88], Champagne and Angers [89, 90] and Halada [91], in centrifugal atomization, there are three basic droplet formation modes. These models conform to the rotating electrode process and are shown in Figure 5.43. Their analysis is applicable to centrifugal atomization in general.

The direct drop formation (DDF) mode occurs at relatively small rotating speeds and small rates of liquid supply. In this mode, a lot of protuberances grow

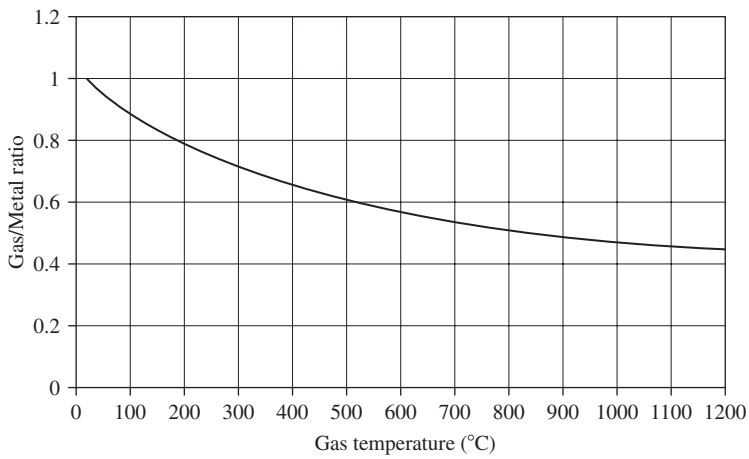

Figure 5.42 Effect of gas temperature on gas consumption for constant particle size. (Source: Ref 83)

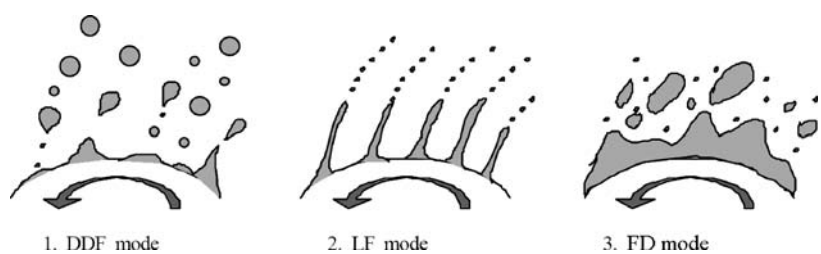

Figure 5.43 Three disintegration modes in centrifugal atomization.

under the balance between centrifugal force and surface tension. When surface tension is lower than the centrifugal force, droplets are separated and ejected from the protuberances. The major part of every protuberance form the main drops in large sizes. Its tail usually becomes satellites. Therefore, the typical powder size distribution in this mode has two peaks with equal numbers of large and small droplets.

The ligament formation mode (LF) occurs when the rate of supply of molten metal at the periphery of the electrode increases. Here the protuberances develop larger amplitude than in the DDP mode before Rayleigh instability breaks up the elongated ligaments. Droplet size increases and, though still bimodal, the weight fractions of the small and large droplets become similar as the liquid supply rate increases.

When the liquid flow rates are very high, ligaments become unstable and the disintegration mode changes gradually to formation disintegration (FD). The transition conditions among these modes had been studied experimentally in a broad range: $10^3 < We < 10^7$ and $10^2 < Re < 10^6$ by Masumoto [92]. The condition range for metal centrifugal atomization is Weber number: 10^4–10^5 and Reynolds number: 10^5–10^6.

Champagne and Angers [89,90] observe that for various metals (e.g. Al, Cu and Zn), the final droplet shape seen in the DDF mode is spherical. In the LF mode a more ellipsoidal shape is formed.

Champagne and Angers [89,90] discovered that the ratio of two parameters determines the transitions from the DDF to the LF and LF to the FD modes:

$$X = \frac{\left(\dfrac{Q\omega^{0.60}}{D^{0.68}}\right)}{\left(\dfrac{\sigma^{0.88}}{\eta_L^{0.17}\rho_L^{0.71}}\right)} \tag{26}$$

where Q is the liquid supply rate (m^3/s), ω is the angular velocity of the anode (rad/s), D is the anode diameter (m), σ is the surface tension (N/m}, η_L is the dynamic liquid metal viscosity (Pa s), and ρ_L is the density of the liquid (kg/m^3).

The numerator includes only process variables while the denominator includes only the material variables. Using the above units for the process and material variables, the DDF to LF mode change occurs when $X = 0.07$. The second mode change to FD mode occurs when $X = 1.33$. These relations are plotted in Figure 5.44. Thus, an increase in melting rate and angular velocity and decrease in rotating anode diameter favor a transition from the DDF to the LF mode and finally to the FD mode. Close agreement exists between model predictions of the transitions in atomization modes for various metals (Figure 5.44).

Centrifugal atomization generally leads to a narrower spread in particle size than does gas atomization. The analysis of centrifugal atomization developed by Champagne and Angers allows for a quantitative prediction of mean particle diameter in the direct droplet formation mode. In its present form, the model gives no indication of the extent of droplet sizes.

The median particle size d_{50} for the rotating electrode process is approximately defined [93] by

$$d_{50} = \frac{K}{\omega\sqrt{D}} \tag{27}$$

where K is a constant for a given alloy for a limited range of arc power.

In a simple model [94], which considers force balance between centrifugal force and surface tension forces, the particle size is expressed as:

$$d = \sqrt{\frac{A\sigma}{\rho_m\omega^2 R}} \tag{28}$$

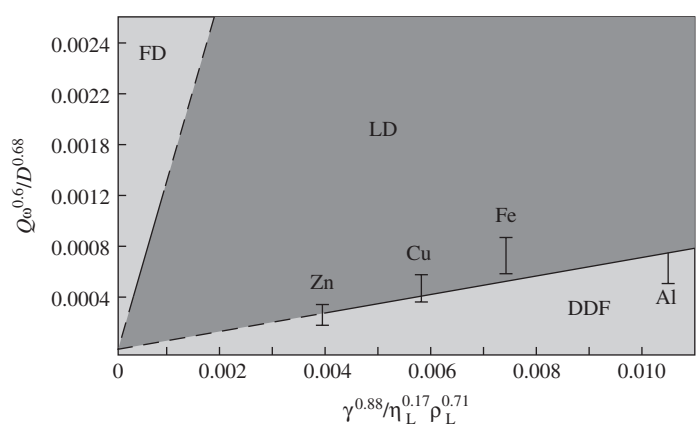

Figure 5.44 Atomization mechanism domains in centrifugal atomization. (Source: 12)

where ω is the angular velocity (rad/s) of the rotating disc (or the electrode), R is the radius of the atomizer (or electrode) (m), ρ_m is the liquid density (kg/m^3) and σ is the surface tension (N/m). A is a constant with value 6 [95] in the elementary case (spheroidal particle shape).

Actual powder sizes are coarser then those predicted [76], which may be explained by the influence of viscosity, particularly at higher speeds. In effect, the molten film is 'slipping' on the disc surface, making its speed less than the peripheral speed of the disc. If a term that is counteracting the centrifugal acceleration, and that includes both the viscosity and the speed at the rim of the disk, is added to the basic model (Eqn 28), the following relationship is suggested by Tornberg [37]:

$$d = \sqrt{\frac{A\sigma}{\rho_m \omega^2 R(1 - (\omega R)^n \eta)}} \qquad (29)$$

where the constant $A = 4.8$ and the exponent $n = 0.93$.

Centrifugal Atomization Methods

There are several different types of centrifugal atomization process (see Figure 5.1) which are discussed. In general, centrifugal atomization methods are far more energy-efficient than gas and water atomization, where only about 1% of the jet energy is used in the disintegration of the metal stream [12]. In contrast, the energy used in centrifugal methods is low as it all goes into acceleration of the metal droplets instead of into atomizing fluid, as in the case of two-fluid techniques. Centrifugal atomization also generally leads to a narrower spread in particle size than does gas atomization (see Figure 5.2), with σ_g as low as about 1.2 in some cases.

As the process depends on the solution to the problem of finding a compatible material for the spinning disk or cup, the applications that have been, and are currently, used on a significant industrial scale are quite distinct.

Spinning Disc Atomization

Solder powder for electronic applications has a very demanding specification: it must be perfectly spherical and satellite-free, it must be very low in oxygen content (≈100 ppm), and it must have a very narrow size distribution. In 1997, more than half of the demand was for size grade that is nominally −45 + 25 μm. Attempts to make this product with inert gas atomization have practically ceased as yields are as little as 5% and the avoidance of satellites is very difficult.

In the USA, Europe and Japan, there are many producers using spinning disc methods to make this product. This is possible because a steel disk is well wetted by ordinary Sn63Pb37 solder and is not very quickly eroded. A disk with diameter of 40–100 mm running at speeds of 30 000–60 000 rpm can produce this material with good yields of 30–70% and at rates of 50–100 kg/h. Annual production is probably several thousand tonnes per year.

When used with higher melting point metals, it is difficult to run at the level of speeds that are used on solder, because of the need to increase the plant diameter. However, there are markets for coarser powders of zinc (alkaline batteries), aluminum (chemical) and magnesium (flares) that are made by this process. In all cases, the cup is 100–200 mm diameter, running at moderately high speeds, from 3000 to 10 000 rpm. The chamber size needed is very large, up to 12 m in diameter, but productivity can be very high. Battery applications commonly require −600 + 100 μm zinc powder. Using a 5 kW spinning cup, 98% can be achieved, at outputs of several tonnes per hour, and with compressed air costs.

Course aluminum powder is also produced in this way but, because the large size of plant needed freezes large droplets, it is done in the open air, which produces a needle-shaped powder. In this case, a perforated steel or cast iron cup is used to make a series of streams of metal, which break up into needles due to the oxide film on them. Production is probably thousands of tonnes per year.

The spinning cup water granulation process [96] allows an increase in the cooling rate and notable decrease of the size of plant owing to cooling the molten droplets in water. Thus, the chiller chamber size is only 1.2–1.5 m in diameter in comparison with 12 m in diameter in open air granulation. Chapter 13 includes more detailed information about this technique.

Rapid Solidification Rate (RSR) Process

RSR process is another design of centrifugal disk or cup atomization, which was developed for superalloy powder production. To overcome the problems of the material in handling high melting and aggressive alloys, the process [97] employs a high-speed water-cooled rotating disk (20 000–50 000 rpm), which breaks up the molten metal stream. To enhance solidification rates, the resulting droplets are then struck by high-pressure helium gas as they leave the periphery of the rotating disk. Powders produced by the RSR

process are spherical, satellite-free and have smooth surfaces. Particle sizes are usually below about 200 μm with a mass median particle diameter <90 μm and a low standard deviation in the range 1.4–1.6.

RSR facilities currently in use incorporate closed-loop helium recirculation. Based on Ni-base alloys, the largest unit has a melt capacity of about 900 kg with an atomization chamber close to 5 m in diameter. In the intermediate size unit, melt sizes are 135 kg with an atomization chamber of about 2.3 m in diameter. Production rates can be varied between 0.05 and 0.3 kg/s, for Ni-base alloys. Typically, RSR droplets smaller than 100 μm in diameter cool at rates of about 10^5°C/s. Apart from these operating variables, the superheat of the melt has a strong influence on particle size and hence particle cooling rate.

More detailed data can be found in Chapters 13 and 14.

Melt Spinning Roller Technique

At present, maximum melt cooling rate has been achieved under heat abstraction from a melt by means of a contact with metallic substrate. The main conditions for advance of high melt cooling rate due to heat conductivity are the following:

- minimal loss of heat during carrying from furnace to cooling point
- minimal melt thickness in the line of heat sink
- high heat conductivity of freezing metallic material (substrate)
- sufficiently high melting point of the substrate
- good heat contact (first of all cleanness of the substrate surface) of the freezing and cooling materials.

As freezing material, pure copper or its alloys (e.g. beryllium bronze) mostly serve. For good heat contact, the substrate surface is thoroughly polished. The most advanced method of obtaining particles (ribbons, flakes) by means of their freezing on a substrate is the spinning roller technique [96]. A liquid metal stream (Figure 5.45) collides with surface of a rapidly rotating roller and wets it. At the contact point a liquid metal bath is formed. The moving roller surface expands the bath into a ribbon, which begins to move with the same velocity as that of the roller surface. The solidified ribbon is then released from the roller under the action of centrifugal force.

The cooling rate of liquid metals achieves 10^5 – 10^7°C/s depending on ribbon thickness, which is changed from 20 to 80 μm; the roller circumferential speed is ≈30 m/s [94], output of the Al alloy is 4–6 kg/minute.

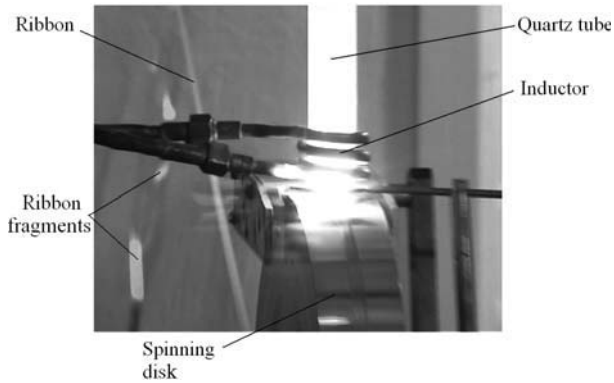

Figure 5.45 Aluminum alloy ribbon obtaining on melt spinning roller. Courtesy of IPMS.

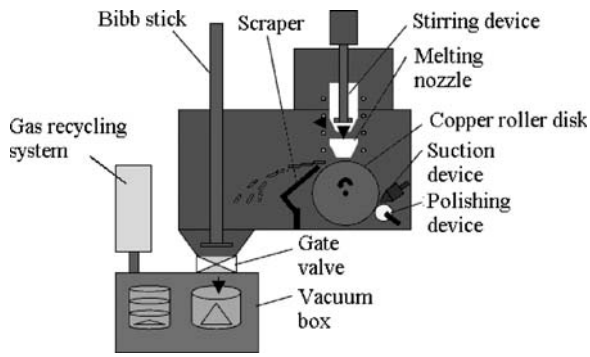

Figure 5.46 The diagram of flaky powder production by melt spinning roller technique.

The phenomenon of heightened solubility becomes possible by such cooling rates. Thus, for example, in aluminum alloy ribbons an increase of the non-equilibrium solubility of scandium up to 2 wt% was achieved [98]. Alloying of aluminum with scandium leads to hardnesses of 950, 1200 and 1800 MPa for scandium concentrations of 0.6, 1.0, and 2.0 wt%, respectively (significantly higher than the maximum hardness achieved for aluminum alloys by traditional technology, i.e. 800 MPa).

At the plant shown in Figure 5.46, a flaky magnesium powder is manufactured [99]. $Mg_{97}Zn_1Y_2$ alloy was melted by high-frequency induction heating in an argon atmosphere and flaky powder was produced by spinning roller atomization. In the experiments, the distance between the melt nozzle end and copper roller surface was 0.3, 15, and 30 mm, while the roller circumferential speed was 30, 40, and 50 m/s. As a result, the flaky powders are produced in the range from 20 to 65 μm and Vickers hardness from 104 to 134 depending on experimental conditions.

The melt spinning roller technique is widely used in laboratory investigations, but no commercial operator is known to use this method.

Rotating Electrode Atomization

In the rotating electrode process (REP), one end of a metal bar is melted while it is rotated around its longitudinal axis (see Figure 5.1). The molten metal is ejected by centrifugal force in the form of droplets from the periphery of the bar. The REP process was developed by Nuclear Metals, Inc. and patented [100,101].

In the original process, the consumable rotating bar is the anode of a direct current power circuit and the permanent (non-melted) stationary cathode is either a cooled tungsten tipped device or a transferred arc plasma torch. When the later mode is used to melt the end of the rotating anode, the atomization process is termed the plasma rotating electrode process (PREP). A chamber of 2440 mm in diameter is used with the circular section oriented. Anode rotational speeds are normally 1570 rad/s. Melting of the anode is conducted in an inert atmosphere. Helium gas enhances both arc stability and the convective cooling efficiency of the atomized droplets.

Powder particles produced by REP and PREP are spherical with smooth high quality surfaces. The particle size range is typically from 50 to 400 μm with a mass median particle size around 200 μm [12]. Particle cooling rates are lower than in water or gas atomization. From secondary dendrite arm spacing measurements, the cooling rate is $\leq 10^2$°C/s, depending on the gas in the chamber and the particle size.

However, a major drawback is the mechanical limitations on rotational speed, which limit the minimum median particle size to about 50–150 μm [3]. Also, the cost of making a high-quality bar of metal is very significant and productivity is low and energy consumption high compared with other techniques.

Other Methods

Impact Atomization

Impact atomization was developed [102] for producing rapidly solidified particulates. In this method, a molten alloy and volatile liquid coolant are fed simultaneously to a rapidly rotating impeller. As the molten alloy is atomized, the coolant vaporizes; the necessary heat of vaporization of the coolant is taken from the droplets as they solidify. Patents covering this process were issued to the Dow Corning Corporation [103,104]. Powders have been prepared from a variety of stainless steels, nickel, copper and a glass forming alloy [102]. Coolants used included water, liquid ammonia, methanol and hexane at flow rates from 60 to 200 L/minute, depending on the heat of solidification of the alloy, the heat of evaporation of the coolant, the degree of superheat and molten metal feed rate.

This process has been used in Argentina where, since 1997, two commercial plants have been operating using induction melting furnaces with 80 and 500 kg capacity, respectively [105]. Both plants include: furnace, tundish, rotating impeller, atomization tank with water, reservoir of circulating water and a pump feeding circulating water to the impeller. The speeds of impeller rotation are from 2000 to 3500 rpm depending on alloy type, required particle size distribution and powder apparent density values. The commercial bronze (Cu–5Sn–5Zn–5Pb) powder contains size fraction ≤44 μm up to 26 wt% and size fraction ≥47 μm max 20 wt%. For 2.2–2.5 t/h atomized powder yield a 10 kW belted drive is used.

Besides the industrial types of atomization processes, there are also many atomization methods with scientific potential that have been described in the literature. There are the following methods.

Vibrating Electrode Atomization

Powder is atomized at the molten end of a vibrating consumable electrode in rod form that is continuously fed between rollers into an atomization chamber. A water-cooled rotating electrode of copper or graphite is located opposite the end of the consumable electrode. The rollers are attached to an electrodynamic oscillator which transfers vibration to the rod electrode. Thus, the electrode forms a resonant rod with one free and one fixed end. Atomization takes place in an inert atmosphere when the arc is struck between the rotating electrode and the vibrating end of the rod electrode.

In the facility described in the literature [106], currents between 600 and 1200 A were generated at a potential between 30 and 60 V. Electrode vibration frequencies up to 500 Hz were evaluated. Powder particles are spherical with mass median sizes typically in the range 300–500 μm. Vibrating rod diameter range is 1–4 mm and feed rate 1.7–4.3 m/minute. Disadvantages of the vibrating electrode atomization are that particles are coarse, productivity is low and cost high.

Melt Drop Orifice Technique

There are several types of such technique, which include impulse atomization (IA), melt drop vibrating orifice method and pulsated orifice ejection method.

Impulse Atomization Method

A schematic of the process is shown in Figure 5.1(g). This unit includes the impulse generator, the mechanical drive, a tundish and a nozzle plate complete with orifices [107]. There are two modes of impulse atomization operation: the first (gravity impulse mode) is the generation of monosized granules larger than 1 mm in diameter and the second (impulse mode) is the atomization of droplets with a narrow size distribution less than 1 mm up to 150–180 μm. In the impulse mode of operation, by varying the plunger acceleration, orifice size, orifice shape, melt superheat temperature and type of gas atmosphere, the powder particle sizes and distribution, shape and microstructure can be controlled to the required specifications. In gravity impulse mode, the melt stream free falls out through the orifice and impulses are applied to generate millimeter-sized droplets. The powders have been produced in an experimental tower 0.5 m in diameter and 4 m in height. In the atomization chamber, the quiescent gas atmosphere into which the melt has been atomized includes helium, nitrogen, argon and air. The nozzle plate contained over 500 orifices. Standard refractory materials are used for the tundish, plunger and orifice plate. There are no temperature limitations to the use of impulse atomization provided an appropriate refractory material is available for use. For example, a nickel–aluminum alloy was atomized at 1600°C.

Table 5.5 includes a summary of the materials and range of particle sizes reported in [107]. The powders have a narrow particle size distribution; the standard deviation (δ_{84}/δ_{50}) range is $1.1 \leq \pi \leq 1.6$, typically 1.4, for the impulse mode.

In the impulse mode of operation, mass flow rates of 225 kg/h have been attained in pilot scale tests with, to date, 2.5 h of continuous operation with zinc. This corresponds to a mass throughput of 7300 kg/(m^2 s) based on the area of orifices in the nozzle plate; while the mass throughput for aluminum range in these experiments from 2000 to 3000 kg/($m^2 \cdot$ s). The mass flow rate attained with the gravity impulse mode was 15 kg/h for 2 mm magnesium granules. Alcoa has developed a forecast model for the conversion cost of a commercial gravity impulse unit [107].

Table 5.5 Powders and granules produced using impulse atomization method

Metal or alloy	Atomization mode	Average particle sizes	
		Unit	Volume
Aluminum	Impulse mode	μm	310
Aluminum	Gravity impulse mode	mm	2–10
Al–(5–24 wt%)Cu alloys	Impulse mode	μm	250–710
Al 6061 and Al 6111 alloys	Impulse mode	μm	250–850
Al 357 alloy	Impulse mode	μm	560–700
Al–(0.1–8.0 wt%)Fe alloys	Impulse mode	μm	400
Al–(10 & 24 wt%)Sr alloys	Impulse mode	μm	1000
Al–Al_2O_3 composite powders (5 to 20 vol% of 35 μm reinforcement)	Impulse mode	μm	1000
Copper	Impulse mode	μm	200–1400
Bronze 90/10 and bronze 94/6	Impulse mode	μm	180–720
Pb–(10 &12 wt%)Sn alloys	Impulse mode	μm	200–1000
Magnesium	Impulse mode	μm	850–1000
Magnesium	Gravity impulse mode	mm	2 and 4
Mg–9Al–1Zr alloy	Impulse mode	μm	850–1000
AZ91D alloy	Impulse mode	μm	850
Knife alloy	Impulse mode	μm	1000
90Ni–10Al alloy	Impulse mode	μm	350
34Ti–45Cu–1Zr–8Ni alloy	Impulse mode	μm	350
Zinc	Impulse mode	μm	150
Zn–500 ppmPb	Impulse mode	μm	250

Melt Drop Vibrating Orifice Method

In this method, molten metal contained within a closed, pressurized crucible is subjected to vibratory oscillations. Forcing the metal through a nozzle at the bottom of the crucible and into a vacuum or inert gas chamber causes it to form a jet and break up into uniform droplets. The technique has been demonstrated with aluminum, beryllium, copper, lead and some superalloys [108] and has been proposed for solder [109]. The technique was in limited industrial use in the 1990s, making precision solder balls for electronics with sizes in the range 500 to 1000 μm. It is limited as production is related to the square of particle size and nozzle blockage is a problem for orifices in the 200–20 μm range.

Pulsated Orifice Ejection Method

This method is intended for the production of monosized spherical particles [110]. Figure 5.47 shows a schematic diagram of a pulsated orifice ejection method. A piezoelectric actuator was used as a driving device of a metal diaphragm, in which the maximum displacement is 14.7 μm and the frequency is 69 kHz. Rectangular waves were generated by a function generator for controlling the output waveform of a power amplifier. A hole about 0.2 mm in diameter, as an orifice, was machined at the center of the bottom of the tundish. Each pressure pulse produced one melt droplet. The apparatus allows the preparation of particles having very narrow particle size distribution with size deviation less than 2% of mean particle size. It has been found that the pulsated orifice ejection method is applicable for preparing monosized particles of various metals and alloys. For example, the monosized Sn–3.5 wt% Ag powder with mean particle size of 187 μm with 0.8% deviation was demonstrated.

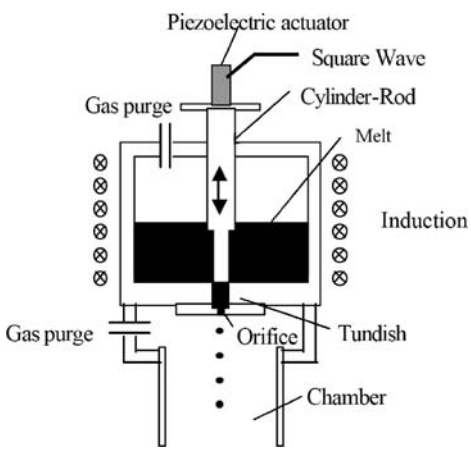

Figure 5.47 Schematic illustration of pulsated orifice ejection apparatus.

Roller Atomization

In roller atomization, a molten metal stream is fed between rapidly rotating twin rollers (see Figure 5.1(d)). Its feature is that little conductive heat transfer between the liquid metal and the rollers takes place [111]. This distinguishes roller atomization from spinning roller in which rapidly solidified ribbon or flaky particles are produced. Epoxy and phenolic resin coatings on the rollers were found to satisfy the heat transfer requirements for temperatures below 300°C, because of poor thermal stability. Epoxy/alumina roller coatings have been used for the atomization of higher melting point metals and alloys. The original atomization facility consisted of a pair of 150 mm diameter rollers contra-rotated at speeds up to 1250 rad/s with a roller gap in the range 50 to 100 μm. The process has been used to atomize a range of metals including lead, tin, aluminum and copper at metal flow rates up to 6 kg/minute. The particle shapes can be irregular, acicular, spheroidal, or flaky, depending on the operating conditions and the metal properties. The spheroidal particles are relatively coarse; mass median particle diameters for Sn powder are in the range 250 to 680 μm. Primary operating variables are roller speed, roller gap, metal flow rate, metal stream velocity and metal superheat.

Plasma Atomization Process

This process was developed to produce fine spherical titanium powder using titanium wire as the starting material [112]. The wire is fed into the apex of three plasma torches, where it is melted and atomized in an argon atmosphere. Droplets are then cooled during flight in the argon atmosphere with a cooling rate in the range 10^2–10^3 K/s and solidify, forming spherical powder particles. Spherical titanium and Ti-6Al-4V alloy powders with diameters from 5 to 150–250 μm have been produced commercially in four grades differing as to particle sizes. The oxygen content depends on particle size and is in the range 0.1–0.3 wt %. The flow rate varies depending on particle size. PyroGenesis Inc. proposes the use of plasma-atomized titanium powders for producing porous filters, applications in injection molding and thermal spray processes and biomedical applications.

Vacuum-dynamic Atomization

This method is based on the use of energy of two contrary rotating gas flows (Figure 5.48) with initiation of tornado result (USSR Patent 1,082,566, Jan., 1984). However, there are no known evaluations of vacuum level and the rapid expansion of gas-saturated molten metal.

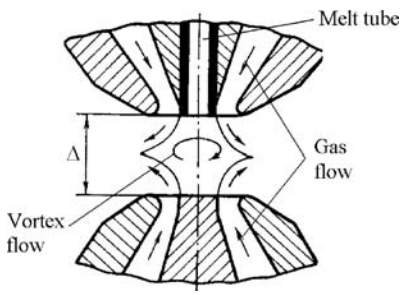

Figure 5.48 Schematic representation of vacuum-dynamic atomization.

Granulation

Granulation is a term that is used to define two dissimilar processes. In one definition, granulation is defined as the production of a metal product by atomization of molten metal. These processes have been discussed above. In the other definition, the most commonly used techniques are spray drying and spray granulation. Granulation is the purposeful agglomeration of fine particles into larger clusters to improve certain powder properties. For example, bulk powders characteristically have low density, do not readily flow, are dusty and have low thermal conductivity. When properly granulated, the same powder pours easily, exhibits a high and uniform bulk density, does not 'dust' and transfers thermal energy more efficiently.

Spray Granulation

The basic method for making granules in a fluidized bed can be by the combination of the hot gaseous fluidized bed and a two-fluid spray nozzle. A binding liquid or solution is spread onto a bed surface of fluidized particles or is sprayed directly into the bed (Figure 5.49). It tends to show that compared to seed particles, larger spray droplets generally result in the formation of agglomerates, which is influenced by variation of operating conditions. In relation to granule growth of simultaneous coating and agglomeration in a hot fluidized bed, the size distribution and growth rate of granules under continuous operation can be derived from the material balance of the bed particles. Granule size increases as the fraction of the bed exposed to the binding liquid is reduced and the spray nozzles are adjusted to give coarser droplets. Increasing the intensity of agi-tation of the bed (with of higher velocity) decreases the size of granules. There is an upper limit on granule size because of the tendency of the powder bed to defluidize. However, spray granulation can form larger granules than are usually possible by spray drying because of longer residence time.

Both spray granulation and spray drying are scaleable technologies and provide the means for producing bulk quantities of nanophase composite powders at low manufacturing cost.

A direct current plasma fluidized bed was applied to the granulation of spheroidal alloy grains from

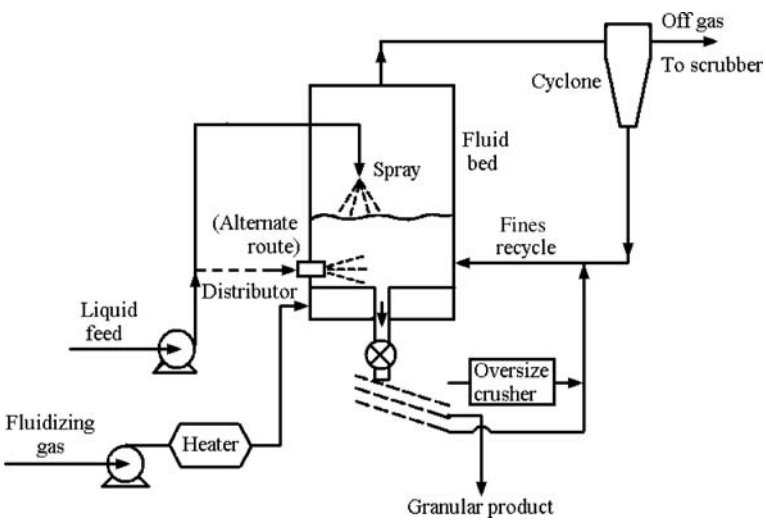

Figure 5.49 Fluidized bed spray granulator. (Source: Ref 113®)

metal powder mixtures [114]. From a mixture of aluminum powder (74–88 μm and 125–149 μm) and iron powder (149–210 μm), alloy grains from 1 to 5 mm in diameter were produced. The grains exhibited a dense homogeneous core and a porous non-homogenous shell structure.

A fluidized bed process facilitates the production of contamination free pyrophoric rare earths and abrasive ceramic powders [115]. The production of exactly limited particle fractions is an important process for rare earths (Sm–Co, Nd–Fe–B) and ceramic oxide (oxides, carbides, nitrides, and borides) products.

Spray Drying

Spray drying is a powder production process in which a slurry or a solution is atomized into droplets in a chamber through which heated gases, usually air, are passed. A typical spray dryer utilizes a disc atomized with co-current air flow. This process is described in Chapter 11.

Spray drying offers several advantages over other powder-processing techniques, particularly in applications requiring agglomerates for subsequent pressing and sintering operations. Spray drying also is one of the most economical ways of drying slurries.

Control of Powder Properties

Most of the applications of spray drying in the metal industry require the formation of free-flowing agglomerates, including the powder injection molding process. Many of these powders are used for producing pressed parts. Therefore, the agglomerate size distribution and bulk density are the two most important properties of spray-dried powders. Agglomeration is achieved by using a binder.

Agglomerate size distribution is a function of atomization conditions and properties of slurry. Commonly, a lower solids content yields a finer average agglomerate size. The maximum attainable solids content varies with material, but usually can be increased by using deflocculating or suspending agents.

Bulk density is a function of the solids content of the slurry additives. Lower bulk densities are generally achieved from slurries with low solids contents. Also, excessive inlet temperatures can cause lower bulk densities. Rapid evaporation of the liquids causes the partially dried droplets to expand rapidly, thus decreasing density. Introduction of frothing agents may draw air into the slurry, which also leads to lower bulk densities. Typically, frothing agents are not added in metallurgical applications.

Moisture content of a powder can be controlled by the inlet and outlet temperature of the spray dryer in conjunction with the slurry feed rate. Moisture levels below 0.1% are possible. For a given airflow and inlet temperature, outlet temperature is controlled by the rate of slurry feed and the solids content. With higher percentages of solids, less water will be evaporated, which leads to higher throughput of dry product.

Binders for agglomeration. Suitable binder materials must be homogeneously dispersable (preferably soluble) in the liquid introduced to form the slurry. When dry, binders must form a coating and/or adhere to the material being agglomerated. They must impart the required strength and crush resistance to the granule for subsequent handling. In addition to the liquid, solids and binders used to formulate a slurry, various other additives may be necessary. Table 5.6 includes typical components of spray-dried slurries.

Plasticizers may be used with binding materials that are hard and that tend to crack during drying. Suspending agents may be needed to prevent solids

Table 5.6 Binders for agglomeration of spray drying slurries

Binder classification	Binder
Organic binders	Polyvinyl alcohol, gum arabic, other natural gums, carboxy-methyl cellulose salts, polyvinyl acetate, methyl cellulose, ethyl cellulose, polyvinyl butyral dispersions, protein colloids, acrylic resin emulsion, ethylene oxide polymers, water-soluble phenolics, lignin sulfonates, propylene glycol alginates, flour, starches
Inorganic binders	Sodium silicate, boric acid, borax, carbonates, nitrates, oxylates, oxychlorides
Plasticizers	Glycerine, ethylene glycol, triathylene glycol, dibutyl phthalate, ethanolamines, propylene glycol, glycenol monochlorhydrin, polyoxyethylene arylether
Deflocculating agents	Sodium hexametaphosphate, sodium molybdenate, tetrasodium pyrophosphate, ammonium citrate, ammonium oxalate, ammonium tartrate, ammonium chloride, monoethylamine
Wetting agents	Synthetic detergents, alkylaryl sulfonates, alkylaryl sulfates, soaps

from settling within the slurry. Deflocculating agents aid the formation of slurries by preventing the agglomeration of fine particles. Wetting agents also may be used to maintain solids in suspension. Some slurries have a tendency to foam during mixing. Antifoaming agents or defoamers may be used to control this action. Chemical activators also may be used as additives to aid in subsequent sintering or processing of powders.

Water Granulation

Water granulation is a process for producing metal granules by pouring molten metals through a screen into water or by agitating molten metals into droplets with subsequent water quenching. Granulation of liquid metal offers a simple technique for solidification of metals, but pouring of liquid metal into water has always been regarded as hazardous. In order to prevent the steam explosion and ignition and explosion of reactive metals like aluminum, a large water tank must be used.

Atomization Techniques

The following conventional atomization processes are used to atomize slurries for spray drying:

- Melt drop orifice atomization
- Centrifugal (rotating disk) atomization
- Two fluid jets atomization.

Table 5.7 includes data about the range sizes of powders produced by the above atomization processes

Table 5.7 The range sizes of powders produced by several atomization processes

Atomization method	Average agglomerate size (μm)
Centrifugal atomization (rotating disk)	
High speed	25–100
Medium speed	50–200
Low speed	100–300
Melt drop orifice atomization	
High pressure	25–100
Medium pressure	50–200
Low pressure	100–300
Very low pressure	200–600
Two fluid jets atomization	
High pressure	10–50
Medium pressure	25–100
Low pressure	50–200

[116]. As shown, the largest agglomerate sizes (600 μm) are achieved by the melt drop orifice atomization. However, recently, this agglomerate size level has been raised up to 2 and 4 mm by using the impulse atomization method [107]. The subsection Melt Drop Orifice Technique in this chapter (p. 213) contains a description of this method, and other paragraphs include the description of centrifugal (rotating disk) atomization and two fluid jets atomization.

Applications

Spray drying applications include production of cemented carbides, mineral processing, production of oxide-dispersion-strengthened alloys and production of powders for thermal spraying applications.

Closed-cycle spray drying is required for most cemented carbide powders because the binders that are used are soluble only in volatile organic fluids. The nitrogen drying gas that is used in the spray drying of cemented carbides is heated to 75–100°C. Viscosity of milled slurries is sometimes modified with stabilizers such as stearic acid (0.3–0.5 wt%). Pressures for melt drop orifice atomization ranges from 590 to 1470 kPa. More detailed description of this is given in Chapter 21.

Multicomponent oxide powders for plasma spraying is an other area of spray drying. The concept of multicomponent powders consists of two steps. The first step is the agglomeration of the starting powder by the drying process. The second step involves plasma densification [117,118]. The plasma densified powder obtained has a spheroidal, smooth surface, a high density and a porosity approaching zero. Experience in this technique concerning the plasma densification of metals, metallic hard materials and ceramics shows that the multicomponent powder concept is practicable for nearly all materials. It has been shown that coatings of plasma densified powders reveal better resistance to wear than coatings of agglomerated powders.

References

1. Dunkley, J.J., Atomization of metals – craft or science? In *Proceedings of 2nd International Conference on Spray Deposition and Melt Atomization*. Bremen Universität, 2003, pp. 3–11.
2. Hopkins, W.G., Hot gas atomization. *European Congress and Exhibition on Powder Metallurgy*, Vol. 4. European Powder Metallurgy Association, 2001, pp. 194–200.
3. Dunkley, J.J., Atomization. In *ASM Handbook*, Vol 7, *Powder Metal Technologies and Applications*. ASM International Publishers, 1998, pp. 35–52.

4. Neikov, O.D., Vasilieva, G.I., Sameljuk, A.V., Krajnikov, A.V., Water atomized aluminium alloy powders. *Materials Science and Engineering* A, 2004, 383:7–13.
5. Seki, Y., Takigava, H., Kawai, N., Effect of atomization variables on powder characteristics. *Met. Powder Rep*., January 1990:38–40.
6. Kikukawa, M., Matsunaga, S., Inaba, T., Iwatsu, O., Takeda, T., Development of spherical fine powders by high-pressure water atomization using swirl water jet. In *Proceedings of 2000 Powder Metallurgy World Congress*. Japan Society of Powder and Powder Metallurgy, Kyoto, 2000, pp. 363–366.
7. Terai, S., Kikukava, M., Inaba, T., Koyata, T., Development of spherical fine powders by high-pressure water atomization using swirl water jet. In *Proceedings of 2006 Powder Metallurgy World Congress*. Korean Powder Metallurgy Institute, 2006, pp. 18–19.
8. Russian Federation Patent 1,812,731, May 1990.
9. Grandzol, R.J., Tallmadge, J.A., Water jet atomization of molten steel. *Am. Inst. Chem. Engineers* J., 1973, 19(6):1149–1158.
10. Klar, E., Fesko, J., On the particle shape of atomized metal powders. *Prog. Powder Metall.*, 1981, 37:47–66.
11. Grandzol, R.J., Tallmadge, J.A., Effect of jet angle of water atomization. *Int. J. Powder Metall. Powder Technol.*, 1975, 11(2):103–116.
12. Lawley, A., *Atomization*. Metal Powder Industries Federation Publishers, Princeton, 2003.
13. Dunkley, J.J., The production of metal powders by water atomization. *Powder Metall. Int.*, 1978, 10(1):38–41.
14. Seki, Y., Okamoto, H., Takigava, H., Kavai, N., Effect of atomization variables on powder characteristics in the high-pressure water atomization process. *Met. Powder Rep.*, 1990, 45(1):38–45.
15. Small, S., Bruce, T.J., The comparison of characteristics of water and inert gas atomized powders. *Int. J. Powder Metall.*, 1968, 4(3):7.
16. Dunkley, J.J., *Atomization of Metal Powders in Powder Metallurgy.* Institute of Metals Publishers, 1991.
17. Levis, G.C. et al., Atomization of liquids in high velocity gas streams. *Ind. Eng. Chem.*, 1948, 40(1):67–74.
18. Yule, A.J., Dunkley, J.J., *Atomization of Melts*. Oxford University Press, 1994.
19. Beddov, J.K., *The Production of Metal Powders by Atomization*. Heyden Press Publishers, Philadelphia, 1978.
20. Sanin, A.F., Nichiporenko, O.S., Influence of water pressure on the powder particle shape during atomization. *Powder Metallurgy and Metal Ceramics,* 1988, 10:1–8.
21. Neikov, O.D., Krajnikov, A.V., Milman, Yu.V. et al., Advanced PM aluminium alloys produced by new rapid solidification technology. In *Proc. PM 2004 World Congress*, European Powder Metallurgy Association, Shrewsbury, UK, 2004, Vol. 1, pp. 237–242.
22. Neikov, O.D., Milman, Yu.V., Sirko, A.I., Sameljuk, A.V., Krajnikov, A.V., Elevated temperature aluminium alloys produced by water atomization. *Materials Science and Engineering* A, 2008, 477:80–85.
23. Dunkley, J.J., An assessment of atomization with hydrocarbon. *Met. Powder Rep.*, February 1992, 22–23.
24. Williams, B., Powder metallurgy – a global market review, 13th edn. 1. Article in *International Powder Metallurgy Directory & Yearbook*, 2008/2009, pp 5–14.
25. US Patent 1,659,291, 1917, February 1928.
26. Wiggers, H., Koster, S.,Walzel, P., Experiments to liquid metal atomization with a new prefilming nozzle. In *Proceedings of International Conference on Spray Deposition and Melt Forming*. Bremen Universität, 2000, pp. 569–578.
27. US Patent 6,481, 638, November 2002.
28. Schulz, G., Concepts for a continuous operation of a WIDEFLOW gas atomizer. In *Proceedings of 2nd International Conference on Spray Deposition and Melt Atomization*. Bremen Universität, 2003, 2, pp. 59–66.
29. Caccioppoli, G., Clausen, B., Bonjour, Ch., Hofman, H., Ultrasonic atomization of metallic melts: modelling and case studies. In *Proc. PM 2004 World Congress, European Powder Metallurgy Association*, Shrewsbury, UK, 2004, Vol. 1, pp. 59–64.
30. Sparchez, Z., Development of new procedures and devices for ultrasonic gas atomization of metallic melts using specific methods of engineering creativity. In *Proc. PM 2004 World Congress, European Powder Metallurgy Association*, UK, 2004, Vol. 1, pp. 25–32.
31. Ünal, A., Flow separation and liquid rundown in a gas atomization process. *Metall. Trans.* B., 1989, 20B(10):613–621.
32. Ünal, A., Influence of nozzle geometry in gas atomization of rapidly solidified aluminium alloy. *Mater. Sci. Technol.*, 1988, 4:909–915.
33. Stobik, M., Nanoval atomizing – superior flow design for finer powder. In *Proceedings of International Conference on Spray Deposition and Melt Atomization.* Bremen Universität, 2000, pp. 511–520.
34. Germany Patent DE 102 37 213.6, August 2002.
35. Achelis, L., Uhlenwinkel, V., Characterization of metal powders generated by pressure-gas-atomizer. *Materials Science and Engineering* A, 2008, 477:60–65.

36. Crisch, C., Fritsching, U., Nozzle design for viscous melt atomization. *Materials Science and Engineering* A, 2008, 477:70–75.
37. Tornberg, C. Gas efficiency in different atomization system. In *Proceedings 'Powder production and spray forming'*, Vol. 1, Metal Powder Industries Federation, 1992, pp. 127–135
38. Dombrovski, N., Johns, W.R., The aerodynamic instability and disintegration of viscous liquid sheets. *Chem Eng. Sci.*, 1963, 18:203–214.
39. Bradley, D., On the atomization of a liquid by high velocity gases: I. *J. Phys. D: Appl. Phys.*, 1973, 6:1724–1736.
40. Bradley, D., On the atomization of a liquid by high velocity gases: II. *J. Phys. D: Appl. Phys.*, 1973, 6:2267–2272.
41. Allen, T., *Particle Size Measurement*, 3rd edn, Chapman and Hall Publishers, 1981.
42. See, J.B., Johnston, G.H., Interactions between nitrogen jets and liquid lead and tin streams. *Powder Tech.*, 1978, 21:119–125.
43. Ingebo, R.D., Capillary and acceleration wave breakup of liquid lets in axial-flow airstreams. NASA Technical Paper 1791, National Aeronautics and Space Administration, Scientific Technical Information Branch, 1981.
44. Sheichaliev, Sh.M., Sharonov, I.V., Karpov, M. P., Centrifugal-hydraulic method of powder production. *Sov. Powder Metall. Met. Ceram.*, 1989, 6:16–21.
45. Ternovoy, Yu.F., Pashetneva, N.N., Manegin, Yu.V., Physicomathematical model of the process of gas spraying of the melt jet. *Sov. Powder Metall. Met. Ceram.*, 1992, (3):11–15.
46. Levich, V.G., *Physicochemical Hydrodynamics.* Phizmatgiz Publishers, Moscow, 1958 (in Russian).
47. Mates, S.P., Biancaniello, F.S., Ridder, S.D., An alternative view of close-coupled gas atomization of liquid metals. In *Proc. 2002 World Congress of PM & Particulate Mater. Metal Powder Ind. Fed.*, Princeton, NJ, 2002, 3, pp. 178–187.
48. Lagutkin, S., Uhlenwinkel, V., Achelis, L., Pulbere, S., Sheikhaliev, Sh., Centrifugal – gas atomization: preliminary investigation of the method. In *Proceedings of PM 2004 World Congress*, European Powder Metallurgy Association, 2004, Vol. 1, pp. 71–76.
49. Klar, E., Fesko, J.W., Atomization. In *Metals Handbook*, Vol. 7, 9th edn., American Society for Metals Publishers, Metals Park, OH, 1984 pp. 25–51.
50. Ünal, A., Effect of processing variables on particle size in gas atomization of rapidly solidified aluminium powders. *Materials Science and Technology*, 1987, 3:1029–1039.
51. Mates, S.P., Ridder, S.D., Biancaniello, F.S., Comparison of the supersonic length and dynamic pressure characteristics of discrete-jet and annular close-coupled nozzles used to produce fine metal powders. In *Proc. Liquid Metal Atomization: Fundamentals and Practice*, The Minerals, Metals, and Materials Society, Warrendale, PA, 2000, pp. 71–81.
52. Ting, J., Peretti, M.W., Eisen, W.B., Control of fine powder production and melt flow rate using gas dynamics. In *Proc. Advances in Powder Metallurgy and Particulate Materials 2000*, Metal Powder Ind. Fed., Princeton, NJ, 2000, 2, pp. 27–40.
53. Anderson, I.E., Terpsta, R.I., Figliola, R., Gas recirculation flow in the melt feeding zone of a close-coupled gas atomization nozzle: modelling and measurement. In *Proceedings of 2nd International Conference on Spray Deposition and Melt Atomization.* Bremen Universität, 2003, 2, pp. 19–30.
54. Anderson, I.E., Figliola, R., Terpsta, R.I., Rau, S., Rauscher, B., Progress in experimental analysis of gas atomization process physics. In *Proc. 2002 World Congress of PM & Particulate Mater.* Metal Powder Ind. Fed., Princeton, NJ, 2002, 3, pp. 150–162.
55. Ünal, R., Effect of the pressure formation at the tip of the melt delivery tube in close-coupled nozzles in gas atomization process. In *Proceedings of 2006 Powder Metallurgy World Congress*, Korean Powder Metallurgy Institute, Busan, Korea, 2006, pp. 562–563.
56. Klar, E., Shafer, W.M., High-pressure gas atomization of metals. *Powder Metallurgy for High-Performance Applications*. Syracuse University Press, Syracuse, NY, 1972.
57. Rai, G., Lavernia, E., Grant, N.J., Powder size distribution in ultrasonic gas atomization. *J. Met.*, 1985, 37(8):22–29.
58. Lubanska, H., Correlation of spray ring data for gas atomization of liquid metals. *J. Met.*, 1970, 22(2):45–49.
59. Wigg, L.D., Drop-size prediction for twin-fluid atomizers. *J. Inst. Fuel*, 1964, (November), 500–505.
60. Dunkley, J.J., Telford, B., Control of 'satellite' particles in gas atomization. In *Proc. 2002 World Congress of PM & Particulate Mater*. Metal Powder Ind. Fed., Princeton, NJ, 2002, 3, pp. 103–110.
61. Nichiporenko, O.S., On the effect of blast energy on the formation process of melt drops during atomization. *Soviet Powder Metall. Ceramics*, 1974, 6:1–7.
62. Rao, P., Tallmadge, J.A., Change of shape of metal droplets in quench atomization. In *Proc. of 1971 Powder Metallurgy Conference*, Metal Powder Industries Federation, 1972, NY, pp. 251–258.

63. Zambon, A., Badan, B., Ramous, E., Gas atomization of nickel aluminide powders. In *Proc. PM 1998 World Congress.* European Powder Metallurgy Association, UK, 1998, Vol. 1, pp. 173–178.
64. Liu, Y., Guo, Sh., Huang, B., Liu, Z., Du, Y., Densification behaviour of Al-Ni-Y powder containing amorphous and nanocrystalline phases. In *Proc. PM 2004 World Congress*, European Powder Metallurgy Association, UK, 2004, Vol. 1, pp. 425–430.
65. L'Estrada, L., Halén, H., Ljunggren, R., Internal porosity of gas atomized powders. In *Proc. Modern Developments in Powder Metallurgy.* Metal Powder Industries Federation, Princeton, NJ, 1988, Vol. 20, pp.187–195.
66. US Patent 5,310,165, May, 1994.
67. German Patent DE 4,102,101 Al, 1991.
68. Pleier, S., Hohmann, M., Goy, W., Schaub, B., Actual improvements of ceramic-free metal powder production. In *Proc. PM 2004 World Congress*. European Powder Metallurgy Association, UK, 2004, Vol. 1, pp. 89–90.
69. Gerling, R., Schimansky, F.P., Crucible- and ceramic-free melting and atomization of Ti-based alloys. In *Proc. PM 2004 World Congress*, European Powder Metallurgy Association, UK, 2004, Vol. 1, pp. 77–82.
70. Yolton, C.F., Gas atomized titanium and titanium aluminide alloys. In *P/M in Aerospace and Defence Technologies*. Metal Powder Industries Federation, Princeton, NJ, 1989. pp. 128–136
71. Babun, A.V., Neklyudov, I.M., Azhazha, V.M., Kovtun, K.V., Vasiliev, A.A., Bobylev, G.G., Beryllium powder metallurgy: developments of the National Scientific Centre 'Kharkov Physicotechnical Institute'. *Powder Metallurgy and Metal Ceramics*, 2006, 3/4:118–125.
72. Wiggers, H., Köster, S., Walzel, P., Experiments to liquid metal atomization with a new prefilming nozzle. In *Proceedings of SDMA 2000 International Conference on Spray Deposition and Melt Atomization*. Bremen Universität, 2000, 2, pp. 569–578.
73. Reichman, S., Chang, D.S., *Superalloys II.* John Wiley & Sons Publishers, 1987.
74. Lierke, E.G., Griesshammer, G., The formation of metal powders by ultrasonic atomization of molten metal. *Ultrasonic*, 1967, 5:224–228.
75. Ruthardt, R., Lierke, E.G., A new ultrasonic atomization technique for the production of metal powder. In *Proc. Modern Developments in Powder Metallurgy*, Metal Powder Industries Federation, Princeton, NJ, 12, 1980, pp. 105–111.
76. Rajan, R., Pandit, A.B., Correlation to predict droplet size in ultrasonic atomization. *Ultrasonics*, 2001, 39:235–255.
77. Lord Rayleigh, *The Theory of Sound*, Vol. II. Dover, NY, 1945.
78. Barreras, F., Amaveda, H., Lozano, A., Transient high-frequency ultrasonic water atomization. *Experiments in Fluids*, 2002, 33:405–413.
79. Yule, A.J., Al-Suleimani, Y., On droplet formation form capillary waves on a vibrating surface. *Proceedings of the Royal Society London, A,* 2000, 456:1069–1085.
80. Al-Suleimani, Y., Yule, A.J. A CFD Prediction of wave development and droplet production on surface under ultrasonic excitation. In *Proc. ILASS-Europe 2002*, 2002, pp. 9–11.
81. Dumouchel, C., Boyaval, S., Use of the maximum entropy formalism to determine drop size distribution characteristics. *Particle and Particle Systems Characterization*, 1999, 16:177–184.
82. Kapur, J.N., Twenty-five years of maximum entropy principle. *Journal Mathematical and Physical Sciences*, 1983, 17:103–156.
83. Dunkley, J.J., Hot gas atomization – economic and engineering aspects. In *Proc. PM 2004 World Congress*, European Powder Metallurgy Association, UK, 2004, Vol. 1, pp. 13–18.
84. Bergmann, H.W., Vetter, J., Cai, Q., Die Erzeugung von Metallpulvern durch Verdüung ihrer Schmelzen mit flüssigen Gasen. *Steels & Met. Mag.*, 1988, 26(10):985–1003.
85. Wolf, G., Nöth, M., Schubert, Martin, V.E., Bergmann, H.W., Production and characterization of liquid gas atomized hard magnetic NdFeB alloy powders for bonded isotropic magnets. *Proc. of the Powd. Met. World Congr.*, 1994, Vol. 3:1745–1753.
86. Wolf, G., Lang, A., Bergmann, H.W., Investigations on melt atomization with gas and liquefied cryogenic gas. In *Proceedings of International Conference on Spray Deposition and Melt Forming*. Bremen Universität, 2000, pp. 535–547.
87. Hinze, H., Milborn, H., Atomization of liquids by means of rotating cup. *J. Appl. Mech.*, 1950, 17(2):145–153.
88. Tanasawa, Y., Miyasaka, Y., Umehara, M., On the filamentation of liquid by means of rotating discs. *J. Japan Mech.* Soc., 1959, 25(156):879–897.
89. Champagne, B., Angers, R., Fabrication of powder by rotating electrode process. *Int. J. Powder Metall. Powder Tech.*, 1980, 16(4):359–364.
90. Champagne, B., Angers, R., REP atomization mechanism. *Powder Metall. Int.*, 1984, 16(3): 125–128.
91. Halada, K., Suga, H., Theoretical investigation on parameters of centrifugal atomization of metal powder. *Powder and Powder Metallurgy*, 1990, 37(4):492–499 (in Japanese).

92. Matsumoto, S., Saito, K., Takashima, Y., Disintegration modes of centrifugal atomization. *J. Eng. Japan,* 1974, 7(1):13–15.
93. Angers, R. et al., Inverted disc centrifugal atomization of 2024. *Int. J. Powder Metall.*, 1994, 30(4):429–434.
94. Dunkley, J.J., Aderhold, D., Centrifugal atomization for powder production. In *Proceedings of International Conference on Spray Deposition and Melt Forming*. Bremen Universität, 2006, pp. 1–6.
95. Superplastic PM superalloys by centrifugal atomization. *Met. Powder Rep.*, 1988, 43(10):688.
96. Bondarev, B.I., Shmakov, Yu.V., *Technology of Rapidly Solidified Al Alloy Production*. All-Russian Institute of Light Alloys Publishers, Moscow, 1997 (in Russian).
97. U.S. Patent 4,343,750, August 10, 1982.
98. Pan, S.V., Slypenyuk, O.M., Kuprin, V.V., Milman, Yu.V., Troy Tacke, V., Influence of scandium concentration on structure peculiarities and hardness of the rapidly-quenched Al–Sc alloys. *Met. Phys. Adv. Tech*., 1999, 18:452–455.
99. Hitoshi, O., Takashi, O., Nobuyki, I., Motonori, N., Development of safe production system for Mg-Zn-Re rapidly solidified powders. In *Proc. PM 2004 World Congress*, European Powder Metallurgy Association, UK, 2004, Vol. 1, pp. 111–115.
100. U.S. Patent 3,099,041, July, 1963.
101. U.S. Patent 3,802,816, April, 1974.
102. Liles, D.T., Deleeuw, D. C., Rapid solidification via centrifugal atomization with a volatile liquid coolant. In *Proc. Rapidly Solidified Crystalline Alloys*. The Metallurgical Society, Warrendale, PA, 1985, p. 285.
103. U.S. Patent 4,347,199, August, 1985.
104. U.S. Patent 4,419,060, December, 1983.
105. Naida, Yu.I., Stepanchuk, A.N., Naida, A.Yu., Industrial production of copper alloys powders using impact atomization method. *Powder Metallurgy and Metal Ceramics*, 2006, 1/2: 112–117.
106. Matei, G., Bicsak, E., Huppmann, W.J., Claussen, N., Atomization of metal powders using the vibrating electrode method. In *Proc. Modern Development in Powder Metallurgy*. Metal Powder Industries Federation, Vol. 9, 1977, pp. 153–160.
107. Henein, H., Impulse atomization: as innovative approach for the generation of powders and spray deposits. In *Proceedings of 2nd International Conference on Spray Deposition and Melt Atomization*. Bremen Universität, 2003, Vol. 1, pp. 31–39.
108. Aldinger, F., Linck, L., Claussen, N., A melt drop technique for the production of high-purity metal powder. *Mod. Dev. P/M,* 1977, 9:141–151.
109. Yim, P. et al., Production and characterisation of mono-sized Sn38Pb alloy balls. *Int. Metall. Powder Technol*, 1996, 32(2):155–164.
110. Kawasaki, A., Watanebe, R., Preparation of monosized spherical particles of metals and alloys by POEM process. In *Proc. 2002 World Congress of PM & Particulate Mater.* Metal Powder Ind. Fed., Princeton, NJ, 2002, 3, pp. 96–102.
111. Singer, A.R.E., Roche, A.D., Roller atomization of molten metals for the production of powder. *Proc. Modern Developments in Powder Metallurgy.* Metal Powder Industries Federation, Princeton, NJ, 1977, 9, p.127.
112. Smagorinski, M.E., Tsantrizos, P.G., Production of spherical titanium powder by plasma atomization. In *Proc. 2002 World Congress of PM & Particulate Mater.* Metal Powder Ind. Fed., Princeton, NJ, 2002, 3, pp. 248–260.
113. Capes, C.E., Particle size enlargement. *Handbook of Powder Technology*. Elsevier Scientific Publishers, 1980.
114. Tsukada, M., Goto, K., Yamamoto, R.H., Horio, M., Metal powder granulation in a plasma-spouted/fluidized bed. *Powder Technol*., 1995, 82(3):347–353.
115. Prem, H., Eddington, D.J., Contamination-free processing of pyrophoric rare earths and abrasive ceramic powders. *Powder Handl. Process.*, 1989, 1(1):101–107.
116. Masters, K., *Spray Drying*, 4th edn. John Wiley & Sons Publishers, 1985.
117. Luo, P., Strutt, P.R., Xiao, T.D., Synthesis of chromium silicide-silicon carbide composite powders. Mater. Sci. Eng. B, 1993, 17(1–3):126–130.
118. Lugscheider, E., Loch, M., Suk, H.G., Powder technology – state of the art. In *Proc. Thermal Spray: Int. Advances in Coatings Technology*. ASM International, 1992, pp. 552–559.

Selected References

Lawley, A., *Atomization*. Metal Powder Industries Federation Publishers, Princeton, 2003.
Dunkley, J.J., Atomization, In *ASM Handbook*, Volume 7, *Powder Metal Technologies and Applications*. ASM International, 1998. pp. 35–52.
Spray drying and granulation. In *ASM Handbook*, Volume 7, *Powder Metal Technologies and Applications*. ASM International, 1998, pp. 91–96.

Chapter 6

Gas-phase Method of Metal Powder Production

Irina V. Frishberg, Fine Metal Powders R&D Company, Yekaterinburg, Russia

Theory and technique of obtaining particulate precipitates from the vapors of metals or their compounds are the essence of the gas-phase method [1,2]. Two types of gas-phase precipitation, physical vapor deposition (PVD) and chemical vapor deposition (CVD) are known. In the former, the powder is formed as a result of evaporation of a metal followed by condensation of its vapor; the second one involves chemical interactions (see Chapter 19). These techniques are usually called inert gas condensation (IGC) and chemical vapor reaction (CVR) respectively. The gas-phase methods are universal and sufficiently economical. They are versatile and allow manufacturing of powders with targeted properties. The technique is applicable for producing powders from volatile metals such as zinc, cadmium, lead, magnesium, aluminum, tin, copper and their alloys, as well as from a variety of metals capable of forming volatile halides, carbonyls and metal organic compounds. Inert gas condensation methods are available for the production of nanopowders.

The process of powder formation comprises three stages:

1. vaporization, either by evaporating the metal or by its chemical interaction with the components of the gas phase,
2. feeding the vapor into the zone of condensation (decomposition)
3. formation of solid particles by condensing or decomposing the gaseous chemical compounds (nucleation and growth of a new condensed phase).

In the case of physical condensation, the temperature of the vapor source is higher than that of powder formation zone; in most cases of chemical precipitation it is vice versa.

Theoretical Basis of the Gas-phase Method

Temperature (T) and pressure (p) are the principal thermodynamic characteristics of the process. The evaporation and precipitation take place at T_1 and p_1 (zone 1), at T_2 and p_2 (zone 2), respectively.

Under the equilibrium conditions, the phase rule is observed in each zone:

$$G = N - \varphi + 2 \tag{1}$$

where G, φ and N stand for the number of components, phases, and degrees of freedom, respectively.

In the first zone, the vapor of a pure metal consists of a single component and the system possesses two degrees of freedom (the system is bivariant): T and p change independently and no formation of a new phase takes place. In the second zone, a new liquid or solid phase is precipitated from the vapor. As a result, the number of degrees of freedom decreases to one, the system becomes monovariant, and changing T automatically leads to changes in p according to the dependence of equilibrium vapor pressure (p_e) on T known for each substance. Changing T to the value at which the liquid phase begins to solidify or the solid phase begins to melt makes the system invariant: it exists only at one temperature and one pressure – the so-called 'triple point'. Adding a new component brings in a new independent variable, namely the composition, and the system now acquires one more degree of freedom. The phase rule is observed when there is dissociation of a compound or interaction between several solids during evaporation. In this case the 'reaction pressure' characterizes the system. In the case of the condensed phases, the system is also monovariant.

The formation of a new condensed phase is zone 2 is a consequence of a certain degree of vapor supersaturation (S) occurring either due to decreasing the vapor temperature or to its decomposition:

$$S = \frac{p_1(T_1)}{p_2(T_2)} \tag{2}$$

where T and p are brought into correlation by the Clausius–Clapeyron equation $p_e(T) = p_0 \exp(-E/T)$ with $E = Q/R$; Q stands for the molar heat of evaporation; R is the universal gas constant. The value

of S depends on the degree of the vapor saturation; $S = 1.0$ for saturated vapors, $S > 1.0$ for supersaturated vapors and $S < 1.0$ for non-saturated vapors.

The relation (3) gives the probability of the development of a new phase nucleus in a unit volume of the supersaturated vapor:

$$J = K\mathrm{e}^{-\Delta G/kT} \tag{3}$$

where K is a coefficient; k is the Boltzmann constant; $\Delta G = 16\pi M^2\sigma^3/3\rho^2 \times k^2T^2\ln^2 S$ displays the work of the formation of a condensed phase uncleus (M standing for the molecular mass of the vapor; σ is the surface tension of the nucleus drop; ρ is the vapour density).

The physical state of the new phase can be controlled via the degree of vapor supersaturation; $S = p_1(T_1)/P_2(T_2)$, to yield either a monolith or a disperse phase. With $S > 1$, the vapor is supersaturated and is ready for condensation, a quite definite critical value of the degree of supersaturation existing for each substance. The critical supersaturation S_{cr} generated in zone 2 (for metals $S_{cr} > 10^{20}$) is instantaneously realized in building up complexes of vapor molecules – clusters that grow to the critical nuclei of the new condensed phase having their own structure.

In the case of chemical precipitation from the gas phase, there exists an analogous parameter, S_{cr} that connects the vapor pressure of the substance in the gas phase with the equilibrium vapor pressure of the metal.

The Hertz–Knudsen equation (4) describes the rate of substance evaporation and vapor condensation:

$$J = \frac{\alpha(p - p_e)}{(2\pi MRT)^{1/2}} \tag{4}$$

where α stands either for the coefficient of evaporation depending on the nature of the substance and on the properties of the surface or, in the case of precipitation from vapor, for the coefficient of condensation (the portion in the total flux of the vapor molecules condensing under given conditions) [3].

The value of the coefficient of evaporation is close to unity in the case of a clear surface of evaporation, while the condensation coefficient varies from 10^{-6} to 1.0. In the case when the evaporation–condensation process strongly depends on the total pressure, Eqn (4) assumes the form of a simple Langmuir diffusion equation:

$$J = \frac{\alpha D(p - p_e)}{L\,\Delta\,T} \tag{5}$$

or of the Hirsh–Pound equation:

$$J = \frac{\alpha(p - p_e)/(2\pi MRT)^{1/2}}{1 + \alpha(RT/2\pi M)^{1/2}(L - \Delta)/D} \tag{6}$$

where D is the diffusion coefficient; Δ is the mean free path of the vapor molecules; L is the thickness of the diffusion layer adjacent to the surface of evaporation or condensation. Eqn (5) describes the rate of transfer of vapor molecules when that rate is determined by molecular diffusion [4].

Mechanisms of Powder Formation During Vapor Condensation

The following conditions are necessary for the condensation of metallic vapor and the formation of a particulate phase:

1. high supersaturation of the vapor sufficient to trigger simultaneous and multiple formation of nucleation centers
2. the presence of a neutral gas acting as a medium preventing the coagulation and growth of particles due to diffusion. The presence of foreign inclusions, ions and chemically active compounds in the neutral gas promotes the nucleation. Forced or natural circulation of the gas ensures the transfer of the condensation heat and of the particulate matter and contributes to a variety of modes of their growth.

The formation of powders calls for a molecular-viscous or a viscous flow state of the gas medium (Knudsen number $Kn < 0.01$ and the pressure between 0.01 Pa and 100 kPa). Decreasing the temperature of powder particles, their removal from the zone of condensation, passivation of the surface and dilution of the vapor add to the stability of the disperse system and enable control of particle growth.

The condensation of the metallic vapor and the formation of powder can take place on a cooled surface (a heterophase process), in the bulk gas volume (a homophase process) and as a mixed homo-heterophase process as well. The interval of the vapor supersaturation of 10^4–10^8 is assumed as a boundary between the first and the second processes. At supersaturation values below 10^4, the formation of the powder occurs on the surface; at values above 10^8, it occurs in the volume; within this interval, a mixed process often takes place.

The formation and properties of the particulate system depend on the heat and mass transfer in the condensation zone. The driving force of the process, i.e. the temperature difference between the initial and the final state of the vapor, results from the joint effect of the boundary conditions and the heat evolution during condensation.

Powder formation on a cooled surface (a heterophase process) takes place as a mass growth of crystalline particles nucleated on macroscopic defects of

the surface. First, there is formed a multiplicity of little 'islands' growing parallel to the substrate along the *C*-axis of the crystals. The 'islands' are shaped as prisms and pyramids of up to 10–20 μm. Then the formation of a second front of crystals occurs with crystals having the *C*-axis perpendicular to the substrate and dominant particles growing through one another appear. The following generation consists of smaller particles. The density and the thickness of the precipitate depend on the growth conditions. The precipitate stays dispersed until its relative density value falls below 30% of that of the metal. The particle size distribution varies from fractions of micron to several millimeters, the particles being shaped like dendrites or platelets, sometimes with a monocrystalline structure.

In the case of rarefied and dilute gas mixtures, the rate of precipitate formation can be influenced by the geometry of the volume and of the substrate surface.

The heterophase process is characterized by a high rate of heat and mass transfer interactions, specific thermo-hydrodynamic phenomena occurring on the boundary of the gaseous and particulate phases and the formation of intermediate particulate structures.

Different conditions can lead to the formation of powder in the volume (a homophase process), among them adiabatic expansion of the gas medium in the condensation chamber; supercooling of the gas layer adjacent to the intensely cooled surface; feeding cold neutral gas into the vapors; the presence of chemically active substances able to interact with the gas.

In real processes, almost all the above conditions are present. The particles grow mainly by coagulation, coalescing in the gas flow and precipitating onto cooled surfaces under the influence of thermo- and diffusion-phoretic force [5, 6].

The shape, structure and size of powder particles depend on the dynamics of gas and of heat and mass transfer in the gas phase. At gas temperatures exceeding 0.7 of the metal melting temperature, particles mostly take a spherical shape and their formation occurs according to the 'solid–liquid–solid' mode. At temperatures below that value, faceted crystalline shapes develop (prisms, pyramids and more complex shapes) according to the 'vapor–crystal' mode, the particles sometimes having a monocrystalline structure. The lower the pressure and the vapor concentration, the smaller the size of the particles formed. Varying the methods and conditions of condensation allows production of powders with particle sizes ranging from 0.01 to 50 μm.

Three major types of volume condensation of metallic vapor that are of practical interest can be singled out:

1. Diffusion condensation when zones 1 and 2 are combined and evaporation occurs over the open surface of the melted metal
2. Condensation in flame when zone 1 and zone 2 are separated and the vapor enters zone 2 through an orifice, condensing by the action of convection currents
3. Condensation in a vapor jet.

The condensation type is specified by the values of the parameters involved in the equation

$$j = A/p_{vg} \tag{7}$$

that describes the relation between the rate of evaporation (condensation), j, and the total pressure of the vapor–gas medium, p_{vg} (Table 6.1). In the last two cases, the values of current temperature along the jet (flame) axis are inversely proportional to the apparatus length.

The jet (flame) exhibits three zones: metallic vapor zone (near the jet inlet), vapor condensation zone and aerosol zone. The jet parameters and the linear dimensions of the apparatus determine the ratio between zones.

The particle size distribution of powder at volume condensation is determined by the rate and mechanism of the growth of condensation nuclei. Particle size distributions in diffusion, flame and jet modes do not differ substantially, as is shown in Figure 6.1.

Table 6.1 The condensation parameters

The condensation type	Partial pressure of the metal vapor (p_i)	The degree indicator (n)	The evaporation/ condensation rate J (kg/m^{2}s)	The gas feeding rate, v (m/s)	The value of the Reynolds criterion (Re)	The value of the Richardson number criterion for the stability of the flow (Ri)
Diffusion	$\ll p_{vg}$	1	$\leqslant$0.001	–	–	–
In-flame	$\leqslant p_{vg}$	2–4	0.001–0.1	1–5	$<$30	$>$1
In-jet	$\geqslant p_{vg}$	4–15	0.1–1.0	5–15	500–1000	$<$1

p_{vg} is the total vapor-gas pressure.

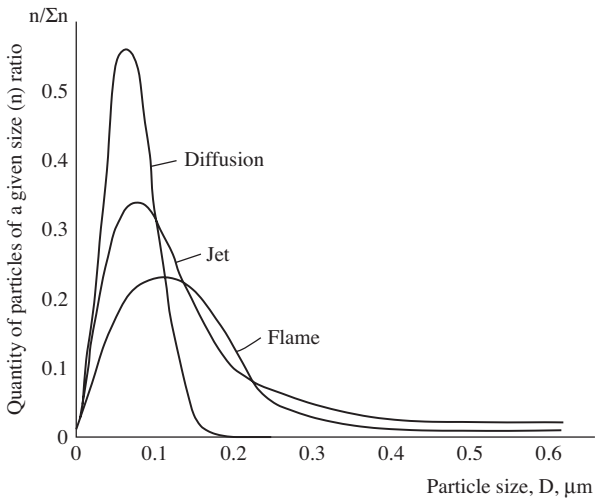

Figure 6.1 Particle size distribution of copper powder in diffusion, jet and flame condensation regimes.

A dominant feature in the diffusion regime is that powder particles increase in size owing to the vapor condensing on them. Particle size distribution is close to normal. In the flame, the distribution is log-normal; particle growth is controlled by Brownian coagulation on the free-molecular model. Powder formation in the jet occupies an intermediate position.

The crystal morphology of particles depends on the growth conditions, the properties of the metal and on the rate of heat and mass transfer processes in the gas medium. Spherical particles form, for the most part, by the 'vapor–liquid–solid' mode and are typical of low-melting metals (tin, zinc, cadmium and lead). Faceted crystalline forms are produced by the 'vapor–solid' mode (manganese) [5].

At certain combinations of the process parameters (surface temperature, volume geometry and dimensions, amounts of vapor and gas, etc.), the formation of powder in the bulk may be accompanied by the growth of particles on the cooled surface. Powders obtained by a mixed process are 'bimodal' and contain particles of mixed shapes and structures, faceted, spherical, poly- and monocrystalline. Their dimensions range from tens of nanometers to several millimeters. Ultrafine particles are formed in the bulk, while large ones are formed on the surface. Like the heterophase process, the process conditions control the fraction content of the powder and the maximum particle size.

The rate of the metal powder formation obeys the equation:

$$W = KF\rho X^{n+1}$$

where F stands for the geometric factor specifying the mass flow to a unit of the volume section; n is the order of the reaction; $X = p_v/p$; p_v standing for the partial pressure of the vapor in the mixture with a total pressure of p; steam density, ρ is defined as

$$\rho = \frac{X}{X + (1 - X)M_g/M_v}$$

M_g and M_v standing for molecular weights of the gas and the vapor, respectively; K being the process rate constant.

Typical constant values are $K < 0.3$ and $n = 1/2$ for volume condensation; $K > 0.6$ and $n > 1$ for surface condensation; $0.3 < K < 0.6$ and $n = 1/2$ for the mixed process. The later value of the parameter n is specific to chemical chain reactions with a quadratic breakage of chains. Parallel to these reactions, the neutral gas initiates the process at $p < 1$ kPa and inhibits it at higher pressures.

During volume condensation, the empirical activation energy values turn out to be lower than the corresponding calculated theoretical values, whereas at surface condensation, on the contrary they are higher than the theoretical values and, in the case of a mixed process, of the values almost coincide.

In the process of condensation of metal vapors, the 'vapor–solid' phase transition is accompanied by a rise in temperature due to the release of the internal heat of crystallization ΔH_c, the value of which for metals is significantly high (ccal/kg): Zn – 450; Mn – 1103; Mg – 1350; Al – 2200. Empirical equations exist, displaying the interrelations of the basic dimensionless criteria of heat transfer (Nusselt), mass flow (Reynolds), peculiarities of the gaseous medium (Prandtl, Schimdt and Lewis criteria) and of the 'vapor–solid' phase transition process (Kutateladze criterion) [8].

Intensive heat and mass transfer interactions occurring at the gas–solid boundary, at the front of growth of the particulate phase, lead to superheating of the adjacent gas layer that, in its turn, results in a considerable difference between theoretical and empirical values of the coefficients of heat and mass transfer.

The mechanism of heat and mass transfer processes, e.g. for the heterophase process of powder formation, can be assumed to be as follows. In the gas phase, convective streams and turbulent flows occurring at the growth front of the disperse precipitate enable the heat transfer so that the average temperature of the gas near the boundary becomes higher than the temperature of the metal powder particles.

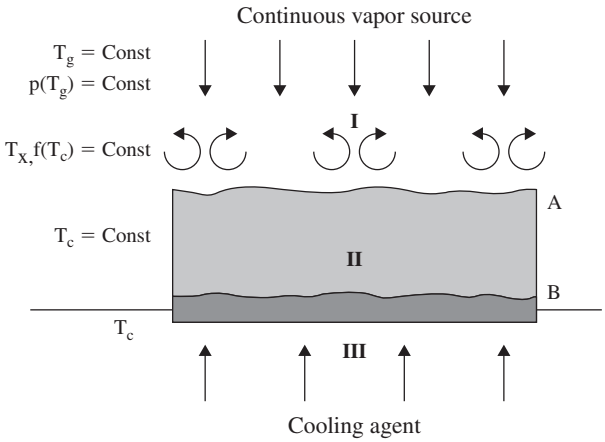

Figure 6.2 Scheme of heat and mass transfer during crystallization: I is the gas solution region; II is crystal deposit; III is cooling agent. Designation of the parameters: T_g is the gas temperature; p is the gas pressure. At the boundary A between II and I: T_x is the gas temperature; T_c is the crystal temperature; the vapor pressure $p = f(T_c)$. The temperature of the condensation surface B equals T_c.

In the boundary region, a temperature gradient arises growing as the dilution of the medium and the rate of condensation increase (Figure 6.2).

If T_g is the temperature of the gas off the phase boundary; $p_v(T_g)$ is the equilibrium vapor pressure in the mixture; T_c, p_v, (T_c) are the temperature and the equilibrium vapor pressure at the front of crystal growth, respectively, then the driving force of the mass transfer depends on $\Delta T_1 = (T_g - T_c)$ and $\Delta p = p_v(T_g) - p_v(T_c)$. In this case, the gas temperature in the layer adjacent to the front of crystal growth $T_x > T_c$ and the driving force for the heat-transfer is $\Delta T_2 = (T_g - T_x)$. The total heat flow through the phase boundary from the first region into the second one is given by

$$\alpha \Delta T_1 = \Delta H W + W C p_g \left(\frac{1}{X \mu p_v} - 1 \right) \Delta T_2 \qquad (9)$$

The first member of the Eqn (9) represents the heat of the phase transition; the second one is the physical heat of the gas at the total coefficient of heat exchange α, where the equation for the mixture flow is replaced by the relations

$$\frac{WM}{XM_v} \quad \text{and} \quad \mu p_v = \frac{M_v}{M_v X + M_g (1 - X)}$$

An analogous Eqn (10) for heat and mass transfer at vapor condensation follows from the assumed transfer model:

$$\alpha = \beta K C_p L e^{2/3} \sigma \qquad (10)$$

or

$$\alpha = W C_p K u \qquad (11)$$

where β stands for the mass transfer coefficient; K stands for the Ackerman's process rate correction [9]; C_p stands for the specific heat capacity of the vapor–gas mixture; Le is the Lewis criterion for the vapor–gas mixture; $Ku = \Delta H / C_p T_m$, stands for the Kutateladze phase transition criterion, where T_m is the average temperature value; σ is a dimensionless parameter displaying the effect of the thermo-hydro-dynamic interactions at the phase boundary:

$$\sigma = \frac{\Delta P_{\Delta T_1}}{\Delta P_{\Delta T_2}}$$

where $\Delta P_{\Delta T_1}$ is difference of partial pressures at T_g and T_c temperatures; $\Delta P_{\Delta T_2}$ is difference of partial pressures at T_g and T_x temperatures.

Increasing T_x leads to an exponential growth of σ.

General criterion Eqns (12) and (13) displaying the interrelations of the basic criteria were obtained by processing the empirical data for condensation of metal vapors in various conditions (Figure 6.3):

$$Nu = AKu(Re \cdot Pr/F)^B \qquad (12)$$

where F stands for the geometrical criterion, reflecting the effect of the geometry of the condensation volume; A and B are empirical constants, calculated as 0.6 and 0.5 for homophase processes, and as 1.1 and 2.0 for heterophase processes, respectively.

In the case of forced convection at a flow rate of 0.001–0.1 m/s, the above equation assumes the form of

$$Nu = AM_v/M_g(Re \cdot Pr/F)^B \qquad (13)$$

A dimensionless relative thermodynamic criterion has been suggested for evaluation of the hydro-thermodynamic effects at the phase boundary:

$$S = \frac{c_{PG}(1 - X\mu_{pr})\,\Delta T_2}{\Delta H X \mu_{pr} + c_{PG}\,\Delta T_2} \times \frac{\Delta T_2 T_{st}}{\Delta T_1 T_x} \qquad (14)$$

where $S \leqslant 1$.

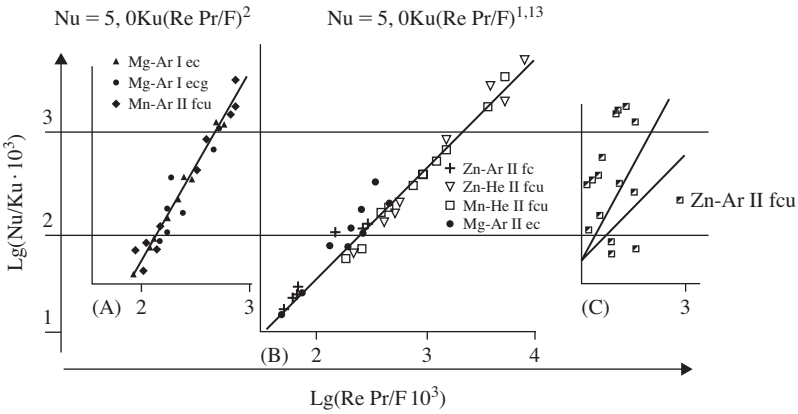

Figure 6.3 The general criteria interrelations for (A) heterophase, (B) homophase, and (C) hetero-homo-phase processes: I and II are the first and the second series of experiments; *ec* is eliminated thermo convection; *ecg* is eliminated thermo convection and varying geometry of the condensation volume; *fc* is free convection; *fcu* is free convection in an unlimited volume; Mg–Ar is condensation of magnesium vapor in argon; Zn–He is condensation of zinc vapor in helium.

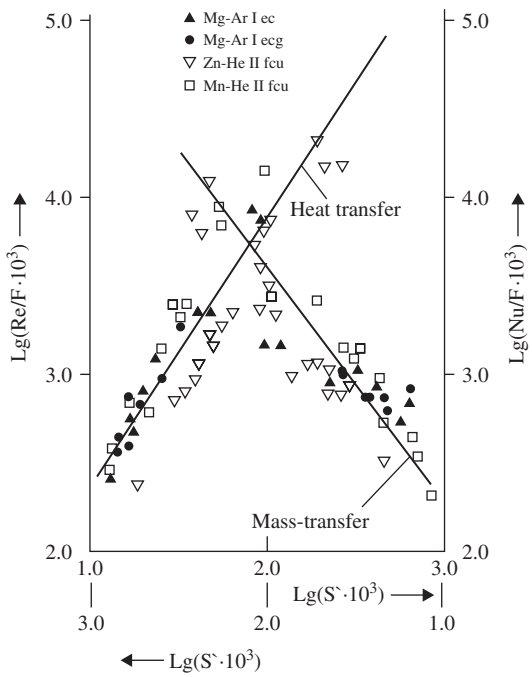

Figure 6.4 The nomogram for estimation of the rate of the mass-transfer (I) and the heat transfer (II) through the thermodynamic criterion S (designations of the nomogram parameters see Figure 6.3).

The *Re* and *Nu* criteria as well as the rates of crystallization and of the mass transfer can be evaluated using the semi-empirical nomogram in Figure 6.4.

Peculiarities of the Formation of Alloy Powders

If the vapor–gas mixture contains several metals at a given stoichiometric ratio, a powder of the corresponding alloy is produced. This can normally be achieved either by evaporating an alloy of required composition, or by evaporation of the components of the alloy separately from independent sources, or by co-precipitation of powders produced by decomposition of a mixture of metal-containing gaseous compounds.

The composition and properties of the final powder depend mostly on the type of the corresponding phase diagram. The formation of a mixture of particles of individual components is a feature of eutectic alloys with the mixing energy $U > 0$ (Pb–Sb). For the alloys featuring the 'cigar'-shaped phase diagram with $U = 0$ (Bi–Sb, Mg–Cd), a joint condensation of metals takes place on common nuclei and the resulting powder consists of particles of the alloy. In the case of metals forming congruently and incongruently melting compounds with $U < 0$ (Cd–Sb, Pb–Bi), the powder often comprises particles of intermetallic compounds.

The formation of alloy powders displays peculiarities associated with their phase diagram. The latter determines the composition and structure of the surface layer of the evaporating melt and, therefore, the properties of powders and coatings. In cases when the alloy constituents form no chemical compounds, the knowledge of the phase diagram suffices to predict those properties. For alloys displaying strong particle interaction, whose components form

a number of intermetallic compounds, vapor and melt composition dependent on the temperature and pressure values obey the Vrevsky laws. It has been found that for such alloys S_{cr} approaches unity due to the presence of ready cluster groups (condensation nuclei) in the vapor.

The rate j of evaporation (condensation) of an n-component alloy obeys the equation:

$$j = \sum_{1}^{n} j_i (a_i b_i) \qquad (15)$$

where a stands for the activity of the alloy component and b stands for the mole fraction of clusters in the vapor. The latter can be evaluated correctly enough from the model of ideal associated solutions.

Figure 6.5 shows the phase equilibrium diagram in the condensation process of a copper–tin alloy. Evidently, using the temperature as a control parameter enables production of either spherical ('supercooled phase'; Figure 6.6(a)), or faceted crystalline particles (region 'crystalline solid phase', Figure 6.6(b)) or amorphous powder (Figure 6.6(c)) [7].

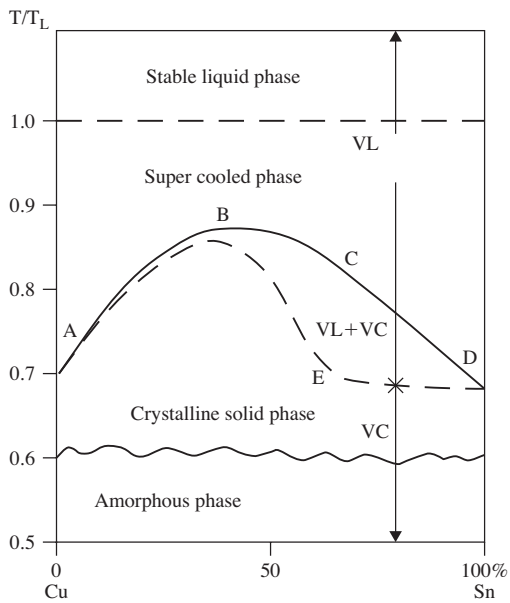

Figure 6.5 Phase equilibrium diagram of the copper–tin alloy: VL is 'vapor–liquid'; VC is 'crystal–crystal'; ABCDE is transitory (intermediate) region: T_L is the temperature of the liquidus (the boundary between the vapor and liquid phases).

Principles of the Controlled Condensation Process and the Technique of Powder Production

The theoretical concepts given above made a foundation for the development of the basic IGC technology for production of metal powders. The condensation process is carried out by one of three modes depending on the targeted powder properties:

1. in the bulk of the condensation zone at the starting supersaturation degree of the vapor $S_{cr} > 10^6$
2. on a cooled surface placed in the condensation zone at $S_{cr} < 10^6$
3. in a mixed process, simultaneously in the volume and on the cooled surface. In the absence of thermoconvection, the temperature gradients can be evaluated using the equation

$$T = T_2 - (T_2 - T_1)\frac{e^B - 1}{e^b - 1} \qquad (16)$$

with

$$b = \frac{Q_v C_v (r_2 - r_1)}{\lambda 2\pi r_1 r_2 (1 - \cos\alpha)} \quad \text{and} \quad B = \frac{b(r_2 - r_1)r_1}{(r_2 - r_1)r}$$

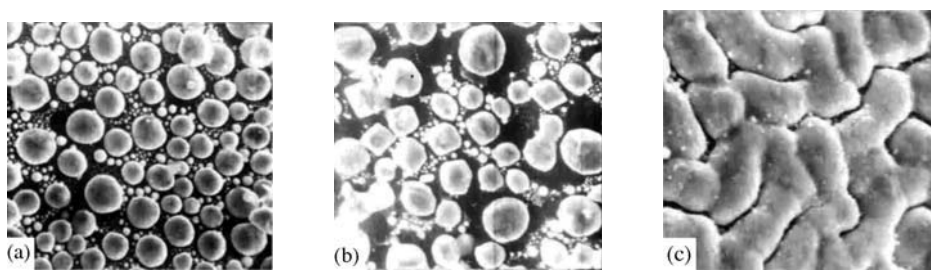

Figure 6.6 Micrographs of the cooper–tin alloy powders obtained in condensation process in several regions phase equilibrium diagram: (a) VL, 'vapor–liquid' × 1200; (b) VC, 'crystal–crystal' × 2500; (c), ABCDE × 500.

where b and B are distances between the vapor source and the powder receiver; Q_v, C_v are the flow and the specific heat capacity of the vapor; r_1, r_2 are the radii of a cell at the source and the receiver levels; r is the radius of the cell when the latter has the shape of a sphere; λ is heat conductivity coefficient.

The concentration and vapor supersaturation gradients are determined by differential equations displaying the interrelations of the parameters of the vapor–gas medium (density, viscosity, partial pressure etc.) and the geometrical characteristics of the condensation volume (shape, linear dimensions, distance from the vapor source to the crystallization surface etc.).

The control of the powder dispersivity is realized through the residence time of the powder in the condensation zone and by selecting appropriate values of the condensation parameters. Quick cooling of the vapor and short residence time in the condensation zone result in the formation of fine and ultrafine powders, while full or partial condensation on the cooled surface give more coarse powders with the particle size in the range from several microns to several millimeters.

In the case of bulk condensation, the control of the shape and the structure of particles are realized through selecting such boundary conditions and rate of the heat transfer, which can provide the condensation process going in either 'vapor–solid' or 'vapor–liquid–solid' mode. In the first case, faceted monocrystalline particles and in the other one, particles of spherical shape and semi-crystalline structure are formed.

In the case of condensation on the surface, particles of faceted shapes and of mono or polycrystalline structure prevail.

Steady boundary conditions and permanent geometrical parameters of the condensation zone provide stable quality characteristics of the powder.

The criterion Eqns (12), (13) and the nomogram (see Figure 6.4) are helpful for designing the equipment and selecting the process parameters.

The process includes melting the metal; producing a vapor; feeding the vapor into the zone of condensation; condensing the vapor into powder either in the free space or on a cooled surface (in a static or moving gas medium); accumulating the powder in the cold part of the volume. The process is carried out in the presence of a neutral gas, sometimes with addition of an oxidant or, on the contrary, of a passivating agent. Sealed furnaces of various types (resistance furnace, inducting etc.) are the conventional equipment for the process.

Manufacture of powders of relatively volatile and low-melting metals is conventionally performed in retorts (see Chapter 19), the powder being deposited either in their top sections, or in 'wells'.

Zinc powder of high purity is manufactured in plate-type rectifying columns. Zinc vapor is fed via vapor pipes into one or several large tanks with water-cooled walls that act as condensers. A neutral gas is fed into the column. The lower part of the column is equipped with a bunker for accumulation of the powder and with an appliance for its discharge. The discharged powder is subjected to classification. Typically, the output of columns and condensers is within the range of 200–400 kg/h; the rejected fractions are normally recycled. The temperature of the column controls the powder quality.

There are different types of equipment of laboratory and pilot plant scale intended for production of powders by the evaporation–condensation method. As a rule, an apparatus is fitted with induction or resistance heated evaporator and moving cooled surfaces (drum, belt or disk) for the vapor to condense on. Sometimes a common volume is used both for the evaporation and condensation. Such a feature facilitates the control of powder properties, but limits the output of the unit due to less intensive heat transfer. The nature of the metal governs the process. Manufacturing of volatile metal powders (zinc, magnesium, cadmium, lead) calls for atmospheric pressure, while aluminum and copper powders are produced at a considerably reduced pressure of a neutral gas. The lower the pressure, the lower the evaporator temperature.

One of the installations for manufacturing zinc powder is shown in Figure 6.7. A vertical apparatus of over 10 m^3 in volume equipped with a sealed water-cooled body consists of several sections each of up to 1 m high, made so as to permit dismantling to enable the regulation of the volume of the condensation zone.

One of the sections houses a 100 kW inductor and a graphite crucible with a capacity up to 300 kg of molten zinc. The design of the crucible facilitates feeding nitrogen into the condensation zone. The zinc vapors are directed by the nitrogen flow towards a rotating water-cooled drum condenser. The powder deposited on the surface of the drum is cut away with a special blade and dropped into a bunker. The unit operates at the evaporator temperature of 650–800°C in a rarefied atmosphere at 3–20 kPa. The operation control system includes the automatic control of evaporator temperature, nitrogen pressure and flow rate, rotation and cooling rates of the drum and

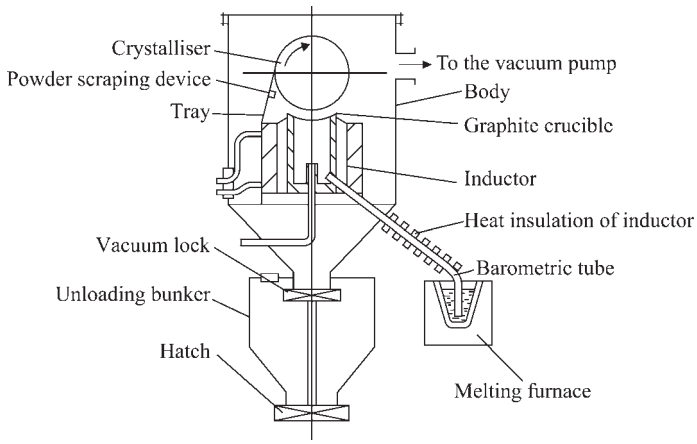

Figure 6.7 An apparatus for the production of ultrafine powders.

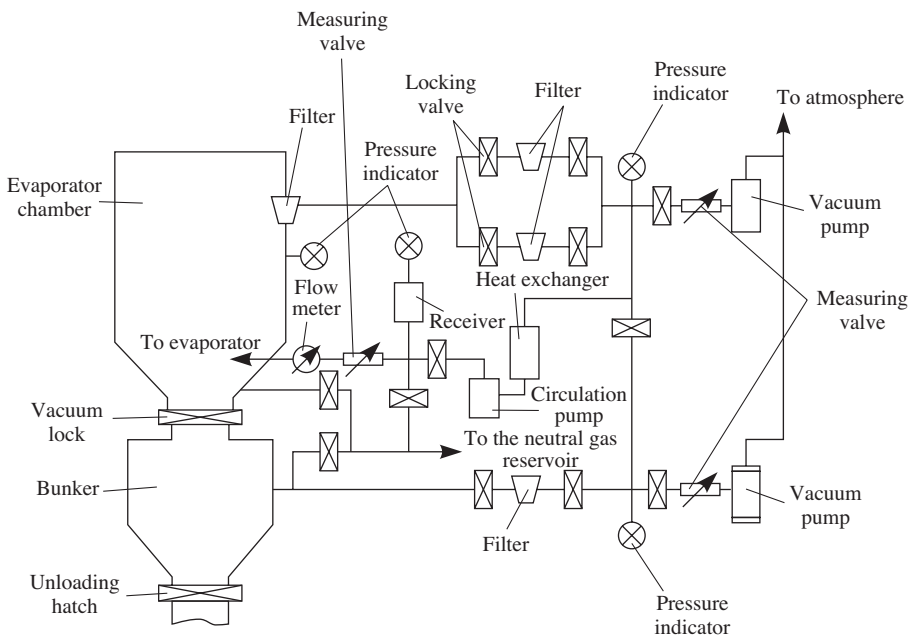

Figure 6.8 The flow sheet of the vacuum system of the apparatus in Figure 6.7.

discharging the powder (Figure 6.8). The unit yields 10–15 kg/h of ultrafine zinc.

A modular type apparatus named 'Tuman' ('Fog') was developed at the Institute of Metallurgy, Ural Branch of the Russian Academy of Science. It can feature either combined or separate zones of evaporation and condensation and is less sophisticated in design and easier in operation in comparison with the above installation.

The 'Tuman' unit (Figure 6.9) of 2.5 m^3 volume, 2 t weight and up to 50 m^2 floor area has an annual output of 120 of zinc powder. Electric power consumption is up to 40 kW; the operational cycle of 25 days is followed by a one-day stop for maintenance. The machine is easy to operate and to convert from the production of one powder type to another.

The controllable process ensures production of metal powders with a targeted particle size in micron, sub-micron and nanometer ranges with high product yields. The operational costs at a continuous production cycle do not exceed 60% of the cost of the source material.

Commercial scale 'Tuman' units are in use at Vysokodispersnye Metallicheskiye Poroshki (Fine Metal

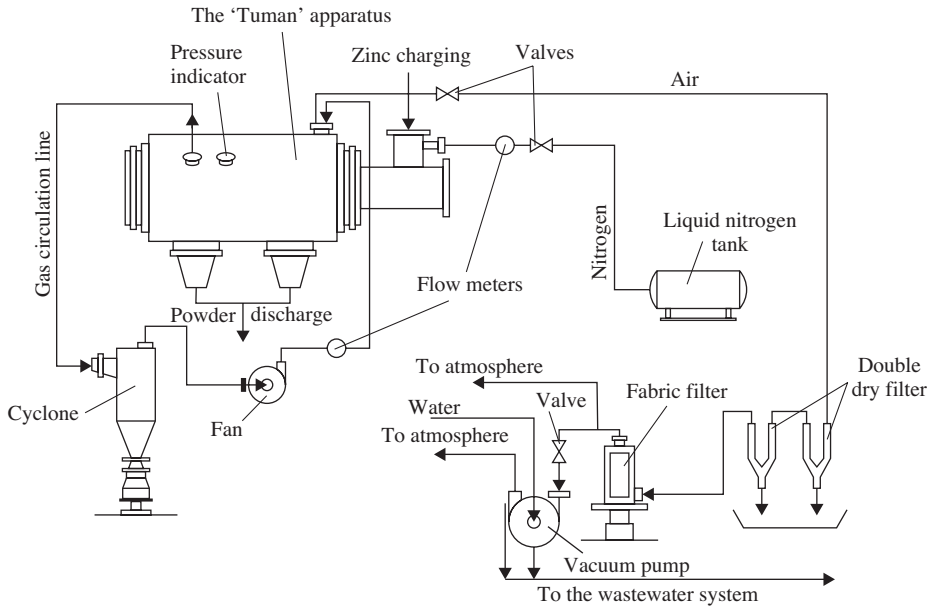

Figure 6.9 The schematic drawing of the 'Tuman' ('Fog') unit.

Table 6.2 Specification of metal powders produced by the IGC technique (manufacturer – Fine Metal Powders Company)

The powder mark (as given by the manufacturer)	Active metal content (% (min))	Bulk density (g/cm^3)	Specific surface area (m^2/g)	Average particle size (μm)
Zinc powder PZHD	96.0	1.4–2.0	0.1–0.6	4–12
Copper powder PCND	99.98	0.4–1.3	8.0–12.0	0.1–0.3
Bronze powder PBND	Cu 89.0–98.0 Sn 1.0–10.0 (typical)	0.3–1.2	3.0–8.0	0.1–0.2
Lead powder PLHD	94.0–95.0	1.8–3.6		0.5–3.0

Powders) R&D Company's plant in Yekaterinburg, Russia, for manufacturing fine and ultrafine powders of non-ferrous metals and alloys (Table 6.2) (see also Chapters 16 and 19).

The safety system for the plants operating the evaporation–condensation-based processes must include, apart from the conventional topics relating to the high-temperature and vacuum processes, the issues meeting safety requirements for flammable and explosive materials. In terms of environmental protection and health, special measures are required such as neutralization of gas and water effluents, cleaning the working areas, providing the workers with the necessary individual protection gear, etc. More specific requirements are described in the chapters dealing with the production of powders of individual metals.

Properties of Powders and Areas of their Usage

Powders produced by the evaporation–condensation process may be divided into two categories according to their particles size: ultrafine (micron and submicron) and nano-sized powders, the categories differing radically in their chemical and physical properties. The nanopowders display higher activity due to their high specific surface area and a peculiar 'non-equilibrium' structure of particles (see Figure 6.10 and Table 6.1). This makes them fit for such specific fields as production of rocket fuel, catalysts, heat absorbents and micro-electronics. The properties of ultrafine powders are more ordinary and the range of their application is much wider, from pigments for paints and varnishes to items of powder metallurgy.

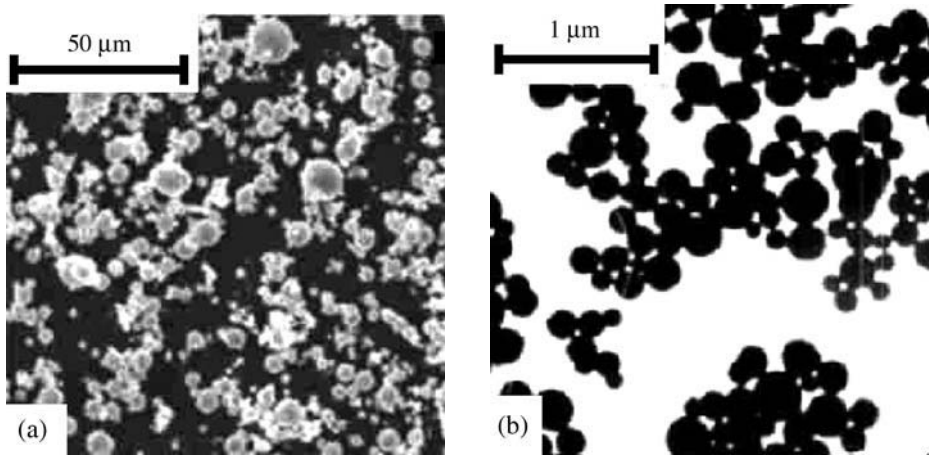

Figure 6.10 Micrographs of fine (a) and ultrafine (b) powders produced by the IGC technique.

Nanopowders of copper and of its alloys have an average particle size of 100–200 nm. Areas of application of these powders are considered in more detail in Chapter 16.

References

1. Frishberg, I.V., Kvater, L.I., Kuz'min, B.P., Gribovskii, S.V., *The Gas-phase Method of Preparing Powders*. Nauka Publishers, Moscow, 1978 (in Russian).
2. *Handbook Non-ferrous Metal Powdered Naboychenko, S.S.* Metallurgya Publishers, Moscow, 1997, pp. 67–95 (in Russian).
3. Brock, J.R., The dynamics of ultrafine particles: a survey. *J. Aerosol Sci.*, 1979, 10(2): 192–193, 195.
4. Hirsh, D., Pound, G., *Evaporation and Condensation*. Metallurgya Publishers, Moscow, 1966 (in Russian).
5. Subbotina, O.Yu., Kishkoparov, N.V., Frishberg, I.V., Genesis of ultra-fine metal powders built on their particle size distribution. In *Proceedings of the 5th All-Russian Conf. On Physical Chemistry of Ultra Disperse Systems*, Part 1. The Ural Branch of the Russian Academy of Sciences, Ekaterinburg, 2001, pp. 53–57 (in Russian).
6. Subbotina, O.Yu., Kishkoparov, N.V., Frishberg, I.V., Mechanism and kinetics of coagulation of ultrafine metal particles formed at an IGC process. In *Proceedings of the 5th All-Russian Conf. On Physical Chemistry of Ultra Disperse Systems*, Part 1. The Ural Branch of the Russian Academy of Sciences, Ekaterinburg, 2001, pp. 58–63 (in Russian).
7. Frishberg, I.V., Gas-phase Metallurgy: from an idea to the commercial manufacturing of fine metal powders and products based thereon. In *Proceedings of the Euro PM 1997 International Conference*, Munich. EPMA, 1998, pp. 252–254.
8. Kutateladzhe, S.S., *The Heat Transfer at Condensation and Boiling*. Mashgiz, Moscow, Leningrad, 1952 (in Russian).
9. Ackerman, G., Wärmeübergang und molekuläre Stoffübertragung im gleichen Feld bei grossen Temperatur- und Partialdruck-differenzen. *VDJ-Forschungshefte*, 1937, 382: 1–16.

Chapter 7

Carbonyl Method of Metal Powder Production

Irina V. Frishberg, Fine Metal Powders R&D Company, Yekaterinburg, Russia

Chemical Precipitation

Physical and chemical techniques of gas-phase manufacturing of metal powders have a common theoretical basis, so that in a number of processes they can hardly be separated. A chemical reaction may answer for the formation of the metal vapor; its precipitation may proceed as a result of simple condensation. At the same time, the evaporation–condensation processes also involve chemical interactions.

The process of chemical vapor deposition (CVD) mainly of high purity refractory metals requires reagents able to vaporize without decomposition, creating a sufficient concentration of the vapor of the metal-containing compound and giving, upon decomposition of the latter and deposition of the metal, only gaseous and chemically inert substances.

The decomposition of metal-containing compounds takes place as a result of a heat impact (plasma discharge, laser radiation). For chemical deposition, reducing agents are used, e.g. hydrogen for deposition of tungsten from halides (see Chapter 21) and zinc or magnesium vapors for a quick deposition of titanium, zirconium and beryllium from their halides. Using hydrogen lowers the process temperature.

When a metal is used as a reducing agent, its quantity must strictly correspond to the stoichiometry of the reaction to prevent its co-precipitation and appearance in the powder. A lowered pressure serves the same purpose.

The method of chemical deposition from the gas phase is universal; it enables the manufacture of powders of the highest purity of the majority of refractory metals with targeted chemical composition, particle size and shape, and the introduction of necessary additives as well.

Preparation of Metal Carbonyls

The carbonyl method is one of the most widely used methods of chemical deposition [1–4]. Its basis consists of the treatment of metal-containing materials with carbon monoxide at elevated pressures and temperatures followed by thermal decomposition of the metal carbonyls with deposition of the metal as powder, and recycling of the carbon monoxide according to the scheme:

$$M_xB_z + yCO \rightarrow [zB] + M_x(CO)_y \rightarrow xM + yCO$$

Synthesis of carbonyl — Thermal decomposition of carbonyl

where B stands for the 'ballast' matters (oxygen, salt residue, impurities, etc.); x, y and z stand for the coefficients, the values of which depend on the nature of the metal; $M_x(CO)_y$ is the carbonyl of the metal M.

The flow sheet of the synthesis and decomposition of carbonyls is shown in Figure 7.1.

The carbonyl process is used for manufacturing powders of non-ferrous metals of VI, VII and VIII groups of the Periodic Table (nickel, partly tungsten, molybdenum, cobalt and some platinum group metals). Characteristic features of this process are low raw material and energy consumption, versatility of raw materials, high yield and purity of powders produced, possibility of completely automated operation. The technique affords control of particle size, shape and structure. It makes possible the production of metallic films, coatings, filamentary crystals, as well as of composite materials.

Applicability only to a limited range of metals is one of the shortcomings of the method. The others are the toxicity of the materials and high pressures involved in the process, necessity of environmental control and of health and safety measures.

Theoretical Basis of the Synthesis

Metal carbonyls are volatile and low-melting compounds of the $M_x(CO)_y$ type that decompose on heating into carbon monoxide and metal, their properties

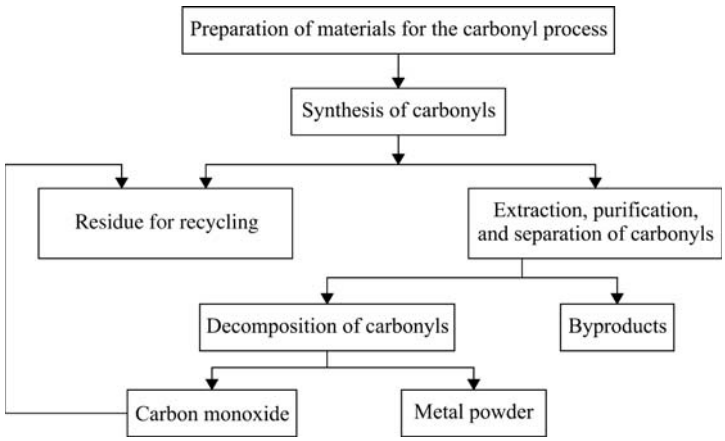

Figure 7.1 Flow sheet of the carbonyl process.

being conditioned by the structure of the carbonyl molecules and the type of chemical bonds in them. In the molecules of metal carbonyls, CO-groups are bound to the atom of the metal via carbon atoms: the electron pair of the carbon atom is transferred to the metal atom with formation a σ-bond, and α-electrons of the metal are transferred to vacant anti-bonding π*-orbitals of CO (π-bond). The metal coordinates such a number of CO-groups as to fill its electron orbitals to the electron structure of the following inert gas. It is assumed that CO donates two electrons and the metal is in the zero oxidation state (in the neutral metal carbonyls).

There are metal carbonyls of mononuclear and polynuclear structure. In the polynuclear carbonyls, the metal atoms are bound to each other directly and, in many cases, also via bridging CO-groups. The formula of carbonyls is determined according to the equations:

$$G - \frac{(xm + 2y)}{x} = x - 1 \qquad (1)$$

and

$$Y = (x/2) \cdot (G - m - x + 1) \qquad (2)$$

where m stands for the metal atomic number and G stands for the atomic number of the nearest inert gas following the metal in the Periodic Table.

Some properties of metal carbonyls are given in Table 7.1.

Metal carbonyls arise upon reaction of the metal, in its active state, with carbon monoxide according to the reversible reaction:

$$x\mathrm{M} + y\mathrm{CO} \leftrightarrow \mathrm{M}_x(\mathrm{CO})_y \qquad (3)$$

The reaction is exothermic, it is accompanied by a decrease in the number of moles of the products formed compared to the starting materials. Therefore, the process requires high pressures and moderate temperatures (Figure 7.2).

The synthesis of carbonyls takes place at the gas–solid boundary and goes through the following stages: carbon monoxide diffusion from the gas phase towards the solid surface that has cracks and pores; formation of an absorbed layer of CO on the surface; chemical reaction of CO with the metal in this layer, with the initial formation of sub-carbonyls, followed by the formation of the $M_x(CO)_y$ molecule; diffusion of metal carbonyl molecules from the solid surface into the gas phase. The reaction rate is, as a rule, limited by the diffusion of the gaseous compounds. Activation of the solid surface accelerates the synthesis reaction.

Metal carbonyls are obtained by a direct reaction of carbon monoxide with free metals according to the reaction (Eqn (1)) or by the reaction of carbon monoxide with metal compounds in the presence of reducing agents such as H_2, Zn, Mg, Na, aluminum-organic compounds, complex metal hydrides etc, for example:

$$\mathrm{Ni_3S_2} + 4\mathrm{Cu} + 12\mathrm{CO} \rightarrow 3\mathrm{Ni(CO)_4} + 2\mathrm{Cu_2S} \qquad (4)$$

The latter method is widely employed in practice due to its higher tolerance to the purity grade of the raw materials.

Another known technique is carbonyl formation carried out in aqueous media or organic solvents:

$$2\mathrm{MoCl_5} + 5\mathrm{Zn} + 12\mathrm{CO} \xrightarrow{ether,\ dichloroethane} 2\mathrm{Mo(CO)_6} + 5\mathrm{ZnCl_2} \qquad (5)$$

$$\mathrm{WCl_6} + 3\mathrm{Zn} + 6\mathrm{CO} \xrightarrow{ether} \mathrm{W(CO)_6} + 3\mathrm{ZnCl_2} \qquad (6)$$

Table 7.1 Properties of metal carbonyls

Carbonyl	Physical state	Color	Temperature (°C)				Density at 20°C (kg/m^3)	Reaction with air	Solvents of carbonyls
			Evaporation (sublimation)	Boiling	Melting	Decomposition			
Group V of Periodic table									
$V(CO)_6$	Solid	Blue-green	40	...	...	70	...	Yes	Ethers, pyridine, toluene, benzene
Group VI									
$Cr(CO)_6$	Solid	Colorless	30	153	147	90–230	1.77	No	Chloroform, ethers, benzene, alcohols
$Mo(CO)_6$	Solid	Colorless	40	155	148	130–400	1.96	No	Ethers, benzene
$W(CO)_6$	Solid	Colorless	50	175	169	140–500	2.65	No	Chloroform, ethers, alcohols
Group VII									
$Mn_2(CO)_{10}$	Solid	Golden-yellow	50	P	154	110–300	1.81	Weak	Ethers, organic solvents
$Tc_2(CO)_{10}$	Solid	Colorless	50	...	159	60–70	-	No	Ether, acetone
Group VIII									
$Fe(CO)_6$	Liquid	Light-yellow	100	103	−20 (freezing)	60–250	1.47	No	Petrol, benzene, ethers
$Os(CO)_5$	Liquid	Colorless	...	...	−15 (freezing)	...	...	-	Benzene (weakly)
$Os_3(CO)_{12}$	Solid	Light-yellow	130	...	224	...	...	No	Benzene (weakly)
$Co_2(CO)_8$	Solid	Orange	45	P	51	25–52	1.82	Yes	Petrol, benzene, alcohols
$Co_4(CO)_{12}$	Solid	Dark green	...	P	...	60	...	Yes	Pentene, benzene
$Rh_2(CO)_8$	Solid	Orange-yellow	-	P	76	...	...	Yes	Organic solvents
$[Rh(CO)_3]_x$	Solid	Brown -red	...	...	...	200	...	No	Benzene (weakly)
$Rh_6(CO)_{15}$	Solid	Black	...	...	...	220	...	Yes	Organic solvents (weakly)
$Ir_2(CO)_8$	Solid	Greenish-yellow	160	...	...	100–160	...	Yes	Ethers, CCl_4
$Ni(CO)_4$	Liquid	Colorless	30	43	−25 (freezing)	60–200	1.31	No	Ethers, benzene, alcohols, acetone
$[Pt(CO)_2]_x$	Solid	Dark red	...	P	...	210	3.55	Yes	Ketones, aniline, pyridine, alcohols

P-decomposes below boiling point.

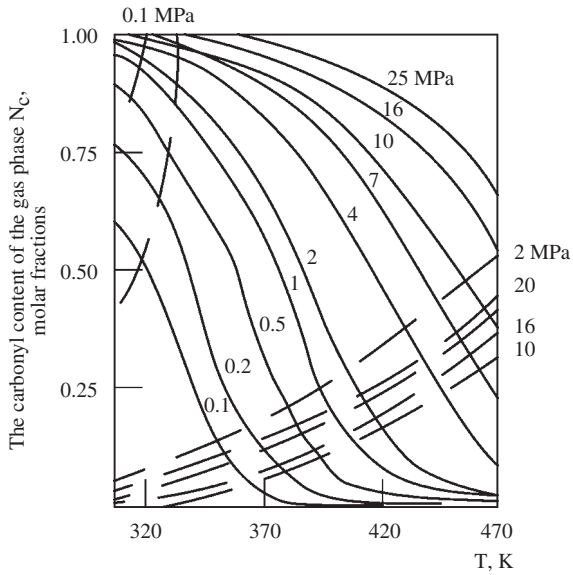

Figure 7.2 The equilibrium content of nickel carbonyl in the gas phase as a function of the synthesis temperature under reaction 3. Dashed lines divide the regions of condensed and gaseous state of the carbonyl.

In the process of synthesis of carbonyls of metals belonging to groups VI–VIII, a selective extraction of the metal from starting raw materials takes place due to the fact that all the elements of the groups I–V except vanadium do not form carbonyls.

Preparation of the Starting Materials for Carbonyl Production

Carbonyls of cobalt and nickel are obtained either by direct reaction with pure metal or with metal-containing compounds. Thus, various oxidized and sulfide materials such as scrap metal, alloys based on Ni–Fe–Cu, Ni–Fe–Cu–S, Ni–Cu–S systems etc. are in use as starting materials for commercial production of nickel carbonyl. To produce tungsten and molybdenum carbonyls, chlorides of these metals obtained from the ore concentrates are used.

The reactivity of the starting materials depends on their structure, degree of defects and chemical composition and increases with the growth of surface area accessible for the chemical interaction. Therefore, a disintegration of the starting materials to the optimal particle size in the range from 10 to 25 mm is preferable. Technological operations of crushing, granulating, or briquetting the starting materials including simultaneous addition of sulfur and oxidation, quenching, treatment with abrasives etc. are used for this purpose.

Impurities can act either as inhibitors or as catalysts of the synthesis. Thus, copper, mercury, iron, sulfur, selenium, phosphorus and some other elements increase the rate of carbonyl formation of nickel-containing materials, while carbon, silicon and chromium act conversely. The catalytic effect of impurities depends on their content and usually has a maximum, e.g. for copper and for sulfur it equals ≈3% and 3–8%, respectively.

In order to increase the metal content in the starting material and to intensify the reaction, raw materials are subjected to a pretreatment using the techniques of pyro- and hydrometallurgy described in the chapters relating to the individual metals.

Synthesis of Carbonyls

The synthesis of most carbonyls is carried out at carbon monoxide pressures in the range of 0.1–20 MPa and at temperatures of 47–277°C.

The main parameters of the process are pressure, temperature, flow rate of the gas stream and the processing time. An increase of the carbon monoxide pressure results in a higher stability of the carbonyls that, in its turn, allows the reaction temperature to increase accordingly the process rate and the yield of the carbonyls (see Figure 7.2). However, the use of expensive high-pressure equipment involves an increase in both capital outlay and operational costs due to more sophisticated organization of the continuous manufacturing process. The higher the reactivity of the starting material, the lower the optimal value of the synthesis pressure.

The yield of carbonyl depends on the temperature, growing with the rise in temperature up to the point where thermal decomposition of the carbonyl begins. A further rise of the temperature results in lowering the yield of the product. The intensity of heat and mass transfer in the reactor depends on the flow rate of the gas stream. Increasing the flow rate allows the use of a lower operating pressure of CO or, at a given pressure, boosts the output. The processing time determines the average rate of the process and influences the extraction ratio of the metal.

Synthesis of carbonyls is performed in a hermetic vertical or horizontal reactor with cold walls cooled naturally or by external cooling means. A counterflow of metal and gas, rotation of the reactor

body and special mechanical devices ensure close contact and interaction of the compounds. The reactors are usually provided with charging and unloading devices, with those preventing dust release. There are reactors of continuous or batch action. The use of reactors with fluidized beds is quite promising.

Carbonyl production in aqueous media is carried out in autoclaves equipped with stirring devices or in column reactors of a scrubber type. Pumps are used for the transportation of the reagents. The favorable features of these techniques are continuity of the process and ease of control.

Extraction, Purification and Separation of Carbonyls

Normally, the mixture of metal carbonyl vapor and carbon monoxide arising in the synthesis contains many admixtures including: carbonyls of elements belonging to groups close to the base metal; water (up to 0.5%) that comes from the gas-holder; oil from compressors and pumps; chlorine- and sulfur-containing compounds introduced at the pretreatment of the raw materials. To eliminate the admixtures from the vapor–gas mixture, carbonyls are liquefied by condensation at a pressure of 2–7 MPa. The purification of liquid carbonyls to a significant degree of purity is carried out in rectification columns by a conventional technology at atmospheric pressure. This technique is applicable to purification of nickel carbonyl containing 2–3% max of iron carbonyl. Tungsten and molybdenum carbonyls are purified by steam distillation followed by alkaline washing to remove traces of chlorides.

If two or more carbonyls are formed in the process of synthesis in comparable quantities, their purification and especially separation become more difficult. Thus, despite different volatilities of nickel, iron and cobalt carbonyls, there are no means to prevent their decomposition when they are separated at atmospheric pressure. The problem calls for more sophisticated and expensive methods of separation such as rectification under pressure, fractional condensation, or some other special method. Therefore, in the commercial production of nickel, either starting materials with low iron content are used or mixed iron–nickel powders are produced.

In processing tungsten–molybdenum raw materials where full separation of W $(CO)_6$ and Mo $(CO)_6$ is practically impossible, a preliminary separation of the metal chlorides is performed.

Manufacture of Powders by Thermal Decomposition of Metal Carbonyls

Physico-chemical Basis of the Process

Thermal decomposition of metal carbonyls is an endothermic process and, according to the reaction (Eqn 7), it proceeds with the increase of the amount of the formed substances, therefore it is expedient to use low pressures and high temperatures. According to the thermodynamic calculations (Figure 7.3), trinuclear carbonyls are most prone and mononuclear ones are least prone to thermal decomposition.

The nucleation and growth of the new phase can proceed either heterogeneously on a prepared surface or in the gas volume. In the first case, a metal coating and, in the second case, a metal powder arises.

The decomposition of the metal carbonyls proceeds stepwise, starting with the formation of unstable primary sub-carbonyls and followed by splitting the carbon monoxide molecules off until only the metal atoms are left. The latter combine to form nuclei of powder particles. The particles, the dimensions of which reach 4–20 nm, continue to grow due to thermal decomposition of the remaining carbonyl vapor on their surface.

At high concentrations of carbonyl in the gas phase, the fragments of the carbonyl can aggregate

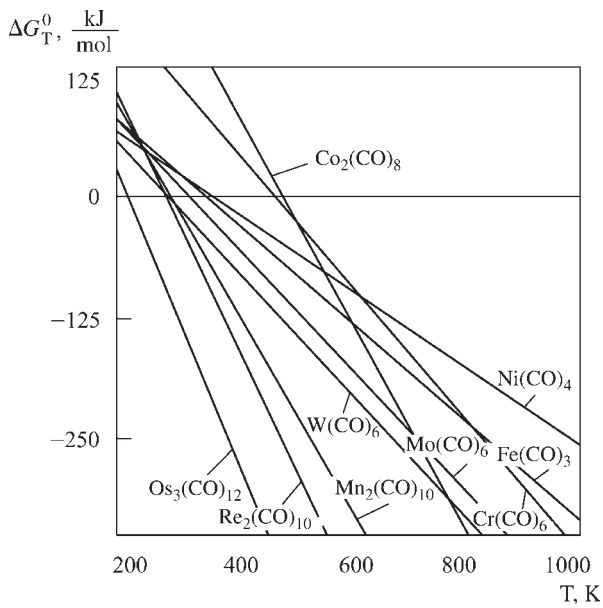

Figure 7.3 Dependence ΔG^0_T temperature for the reaction of thermal decomposition of metal carbonyls.

and this process is accompanied by a partial loss of CO-group according to the scheme:

$$M_a(CO)_i + M_b(CO)_j \rightarrow M_{a+b}(CO)_{i+j-k} + kCO \quad (7)$$

These aggregates act as nuclei of the new phase. The process of nucleation depends on the kinetics of the reaction Eqn (7), in the course of which the aggregates transform into metal particles with CO molecules sorbed on their surface. Sintering and coagulation of the particles also contribute to their growth.

Side reactions of decomposition of the carbonyls lead to the formation of carbon, metal oxides and carbides:

$$\left.\begin{aligned} CO &\leftrightarrow 0.5CO_2 + 0.5C \\ 2M + CO &\leftrightarrow MO + MC \\ M + CO &\leftrightarrow MO + C \\ M + 2CO &\leftrightarrow MC + CO_2 \end{aligned}\right\} \quad (8)$$

These reactions are typical for all the metals except rhenium and the metals of the platinum group.

The impurities influence the shape and structure of powder particles. The decomposition of CO, according to Eqn (8), results in a laminated 'onion'-type structure of particles of carbonyl powders.

The carbon and oxygen content of the powders depends on the nature of the metal and on the parameters of the process. Side reactions exert practically no influence on the properties of the metal powder. However, an exception must be made for metals which either do not form stable carbides and are not prone to oxidation or can act as weak catalysts of the reaction of CO disproportionation (e.g. nickel). The influence of the side reactions is considerably higher for W and Mo. Oxidation of the metal by carbon dioxide can take place when the latter is present in a considerable amount. The presence of the iron carbonyl $Fe(CO)_5$ in the amount of 1–2% also promotes the decomposition of the carbon monoxide.

The higher the process temperature, the lower the thermodynamic probability of the formation of carbides, oxides and other undesirable compounds. Therefore, the decomposition process should be carried out at a maximal allowable temperature to ensure the purity of the metals produced.

The Technique of Powder Manufacture

The decomposition of carbonyls is performed at carbon monoxide pressures close to atmospheric and at temperatures depending on the metal: 197–397°C for nickel, 347–1197°C for tungsten and molybdenum, 147–247°C for cobalt. The reaction is carried out in a vertical column with external heating and filled with carbon monoxide. Carbonyl vapors from the evaporator are fed into the column. The greater part of the carbonyl decomposes in the upper section of the column; the growth and the sintering of the particles formed take place in the middle and lower sections. The particles are present initially suspended in the volume of the gas and then they precipitate and fall into a receptacle. In some cases, forced circulation of CO is applied.

The main process parameters are the temperature in the sections of the apparatus, the concentration of the carbonyl vapor at the entrance and its feed rate, the volume flow rate of the gases and the presence of seeds. The temperature is the most important parameter controlling the powder particle shape and size. The higher the temperature in the top section of the apparatus, the more centers of nucleation of the metal arise and the finer the size of powder particles.

Raising the temperature from the top to the lower part of the apparatus intensifies the circulation of the reaction gas leading to a many-fold increase of the particle residence time within the apparatus. The result is an increase of particle size.

Diluting the carbonyl vapor with an inert gas or carbon monoxide leads to the formation of finer powders; increasing the vapor concentration leads to an increase of the particle size. The higher the gas volume flow rate, the shorter the period the particles stay in the apparatus and, accordingly, the finer powder is produced, and vice versa.

There are two basic modes of powder production in commercial usage:

1. a moderate rate of carbonyl feed at a comparatively low temperature in order to stimulate the formation of a relatively small number of coarse primary particles and to obtain 'heavy' powders (with high bulk density); or
2. a high feed rate at a high temperature leading to the formation of a large number of small primary particles prone to coagulation into aggregates that results in the formation of 'light' powders (with low bulk density).

In order to obtain fine and almost monodisperse powder, carbonyl vapors undergo decomposition by instantaneous mixing with a large volume of hot inert gas followed by quenching the aerosol formed by diluting and cooling.

Introduction of nucleation seeds (metallic aerosol, solid particles) or appropriate chemical agents (oxygen, halogens, ammonia, HCl or HNO_3 vapors, chlorides or bromides of arsenic, boron, silicon, titanium, etc.) adds to the productivity of carbonyl decomposition. The presence of these agents stimulates transformation of carbonyls into oxides or other metal compounds serving as crystallization nuclei.

The parameters of heat and mass transfer and, accordingly, the design of the apparatus can influence the powder properties and process productivity. Heating or cooling of the apparatus sections as well as heating the introduced inert gas are used. To prevent metal deposition on the walls of the apparatus as well as to increase the process productivity, the gas flow is rendered turbulent either with a stirrer or with a tangentially placed feeding inlet for the gas. Adding to the height of the apparatus while lessening its diameter results in producing coarser powder. Placing a broad tube along the axis of the reactor decreases the free section and ensures the uniformity of powder particle size, etc. Feeding the carbonyl into the apparatus through spraying devices makes it more widely dispersed, the reaction volume is used more evenly and the powder is more uniform. The influence of temperature in this case is a little lowered.

The details of the carbonyl process for such metals as Ni, Co, W and Mo are given in the corresponding chapters.

A number of special methods for the decomposition of carbonyls are known. Ultraviolet and pulsed laser radiation, acoustic vibrations and magnetic field can be used for the manufacture of finely dispersed uniform powders. In this process, a magnetic field below the Curie point results in a domain structure of the ferromagnetic particles formed.

In the plasma process, the reaction is carried out in highly ionized argon at a temperature of 4800–5300 K. Under those conditions, the number of nucleation centers increases sharply and dilution of the carbonyl vapors by the inert gas prevents coagulation of the particles. The result is the formation of sub-micron powders.

Manufacture of Composite Powders

The methods of producing composite powders by the carbonyl process are based either on the mutual solubility of metal carbonyls or on their ability to dissolve compounds prone to dissociation. Iron–nickel (permalloy) powders containing 5 to 50% of nickel can be manufactured by simultaneous decomposition of a mixture of liquid iron and nickel carbonyls; addition of cobalt and molybdenum is also possible.

Another method is based on the decomposition of a metal carbonyl on the surface of 'seeds' (dispersed particles of metals, non-metals, or oxides, carbides, sulfides, silicates of metals, and their mixtures) introduced into the reaction volume. In this case, a layer of metal encapsulates both single particles and agglomerates of particles having different properties. The process is carried out in a fluidized bed. The intense stirring of the particles results in uniform thickness of the metal coatings obtained.

The deposition of a metal coating onto the particles imparts corrosion protection, electrical conductivity, increases heat conductivity etc.

Properties and Applications of the Metal Carbonyl Powders

The size of carbonyl powder particles varies in a broad range from 0.5 to 20 μm. The features of these powders are high specific surface and considerable defects of crystalline structure; they are more active as compared to the powders manufactured by other techniques. However, these powders are not inflammable due to absorbed carbon monoxide that passivates the particle surface. The particle shape is close to spherical. Sometimes particles have a laminated 'onion' structure, imparting specific electromagnetic properties to the material.

Carbonyl powders can contain 1–3% of carbon and oxygen (that is equivalent to about 30% of metallic compounds) while the amount of other impurities does not exceed 1×10^{-3}%.

The powders can be subjected to additional treatments with the purpose of bringing them into accordance with the requirements relating to the purity and the particle size. Mechanical methods (crushing, mixing, sieving, separating and trapping) and thermal treatment are in use. The latter may cause changes in the crystalline structure of particles, thus enabling production of powders with targeted properties, e.g. light powders with coarse and porous particles, as well as to increase the metal content of the powder up to 99.96% as a result of the elimination of carbon and oxygen.

Carbonyl powders of metals, alloys and composites are used for manufacturing pure malleable metals, precision alloys, various solid and porous items (parts, strips, rods, filters, etc.), in electric and radio engineering, mechanical engineering, automation and other areas.

Detailed characteristics of powders are given for each metal in the corresponding chapters of Section 4.

Health and Environmental Protection Measures in the Carbonyl Industry

The carbonyl process involves considerable danger issues such as increased flammability and explosiveness of the materials used, their high toxicity and the high pressures employed in the process.

Toxic carbon monoxide can be responsible for acute and chronic poisoning in the manufacturing process. Under 'Health and Safety' legislation in the European PM industry, the long- and short-term occupational exposure limits (OELs) for carbon monoxide in the workplace atmosphere are 50 vpm (60 mg/m^3) and 300 vpm (360 mg/m^3), respectively [5]. The long-term OELs for carbon monoxide in the workplace atmosphere is 20 mg/m^3 (≈17 vpm) according to 'Health and Safety' legislation in the Commonwealth of Independents States (CIS) [6].

Metal carbonyls are also toxic; volatile ones such as nickel carbonyl being particularly dangerous. The toxicity of some carbonyls has not yet been sufficiently studied. The OELs of the carbonyls in the workplace atmosphere under the legislation in CIS are (in mg/m^3): Ni $(CO)_4$, 0.0005; CO_2 $(CO)_8$, 0.01; Mo $(CO)_6$, 1.0; and W $(CO)_6$, 2.0. The powders are also toxic, especially nickel powder which affects the breathing organs and is also carcinogenic. The long-term OELs of the powders in the air (mg/m^3) are for: Ni, 0.05; Co, 0.5; Mo metal, 0.5; and W, 6.0.

The industrial equipment for the carbonyl process must pass strict control for gas tightness. All equipment and pipe work must be purged with an inert gas prior to feeding in the toxic and explosive compounds with the object of checking their gas-tightness and to eliminate oxygen. When feeding in the carbon monoxide at operating pressures, control of its content in the air is a must. The production premises must be equipped with automatic analyzing and alarm appliances for control of the presence of carbonyl vapors and carbon monoxide in the air. In all dangerous areas, personnel must wear protective breathing masks.

The methods of determining small concentrations of carbonyls in the air are based on absorption, decomposition or chemosorption of carbonyls by using various chemical reagents, combined with instrumental methods of analysis (colorimetric, gas chromatography, spectral analysis, etc.). The method for determining the carbonyl content in water is based on volatility of carbonyls and consists of purging them from the aqueous solution using nitrogen, followed by chemosorption from the gas phase using porous active materials and chemical reagents.

Liquid carbonyls must be poured only into special tanks under a water layer. Special gas-tight vessels must be used for the transportation of carbonyls and carbonyl-contaminated wastes to the place of disposal according to local regulations. Solid wastes of carbonization fit for recycling and further processing undergo a pretreatment with oxidizing agents.

Rubber-impregnated suits, rubber boots, gloves and gas masks are a must for the personnel involved in handling liquid carbonyls.

The major environmental protection requirements as to the carbonyl technology are purification of the atmospheric ventilation discharges from toxic compounds and preventing the release of liquid wastes. The carbonyls can be present in considerable amounts in the liquid wastes due to their solubility in the water employed in the production process. Contaminated effluents, especially from the rectification unit, may have a dangerous impact on the human body mainly via inhalation. The limits of concentration of carbonyls in aqueous media must be evaluated in accordance with the local environment regulations.

Purification of ventilation effluents from carbonyls is complicated by their small concentration. The traditional way of air decontamination consists of thermal treatment or oxidation by using various agents (oxygen, chlorine, gaseous hydrogen chloride, phosphorus, etc.) on active porous materials (activated carbon, silicate absorbents, dry aluminium oxide, etc.). In a high-frequency electric discharge, the molecules of carbonyls are destroyed and oxidized by ozone. The degree of air decontamination reaches 97–99%.

The method of decontamination of carbonyl-containing water to a concentration below that of the admissible concentration limit [7] consists of purging of the carbonyls by nitrogen followed by the passing water through the columns filled with activated carbon. After purging, the gas is directed into the ventilation system and subjected to decontamination together with other gaseous effluents.

References

1. *Handbook of Non-ferrous Metal Powders*. Naboychenko, S.S. (Ed.) Metullurgiya, Moscow, 1997 (in Russian).
2. Mnukhin, A.S., Shvartsman, R.A., Zaitsev, A.Yu., Synthesis of nickel tetra carbonyl at average pressure.

Tsvetnaya Metallurgiya Publ., 1998, 64–66 (in Russian).
3. Syrkin, V.G., *CVD-process*. Nauka Publ., Moscow, 2001 (in Russian).
4. Biketova, L.V., Kozyrev, V.F., Mnukhin, A.S., Carbonyl nickel powders for manufacturing of batteries. *Tsvetnaya Metallurgiya Publ.*, 2001, 73–75 (in Russian).
5. *Guide to EU Legislation and 'Health and Safety' in the European PM Industry*. EPMA, Bellstone, 1997.
6. Commonwealth of Independents States Standard GOST 12.1.005−88 (in Russian).
7. Sanitary Regulations and Standards of surface waters from pollution. *SanPiN* 4630-88 (in Russian).

Chapter 8

Reduction Methods of Powder Production

Stanislav S. Naboychenko, Ural State Technical University (UPI), Yekaterinburg, Russia

Solid-phase Reduction of Metal Oxides and Salts

In the solid-phase reduction process, metal oxides or metal salts (carbonates, halides, oxalates and formates) are treated by a reducing agent at temperatures below their melting point.

Oxide-reduced powders characteristically exhibit the presence of pores within powder particles and thus are called sponge powders. This sponginess is controlled by the number and size of the pores and accounts for the high green strength, good compactibility and sinterability of such powders. Typically, high reduction temperatures ($>0.6\ T_m$) facilitate the formation of large intraparticle pores and powders of a small specific surface area that are required for a high compressibility. Parallel with these, elevated temperatures may cause excessive sintering and agglomeration, which cause difficulties with the disintegration of the sintered cake. Low reduction temperatures lead to the production of powders with fine pores, large specific surface area and high green strength. But extremely low reduction temperatures ($<0.3\ T_m$) can readily produce pyrophoric powders.

For the metals with very high melting points, such as tungsten and molybdenum, oxide reduction benefits partly for economic reasons. Thus, for molybdenum trioxide, because of its high vapor pressure, the reduction is accomplished in two stages to control particle size. The first step, the reduction of molybdenum trioxide to molybdenum dioxide, is carried out at a temperature between 873 and 973°C. The second step, the reduction of molybdenum dioxide to molybdenum monoxide, is carried out at around 1173–1373°C.

In contrast to atomized powders, where oxides usually are concentrated on the surface of the particles, oxide reduced powders, at least when freshly reduced or stabilized against tarnishing, contain most of their residual oxide within the particles.

Process Theory [1, 2]

Thermodynamics of metal oxide reduction by hydrogen or carbon monoxide is determined based on the analysis of the generalized reaction:

$$\frac{1}{y}M_xO_y + H_2(CO) \leftrightarrow \frac{x}{y}M + H_2O(CO_2)$$

The latter is analyzed as a set of oxide dissociation reaction

$$M_xO_y \leftrightarrow xM + \frac{y}{2}O_2$$

and gaseous reducer combustion:

$$xB + \frac{y}{2}O_2 \leftrightarrow B_xO_y$$

Further, the corresponding equations for the dependence of equilibrium constant on temperature for the reactions of hydrogen combustion ($2H_2 + O_2 \rightarrow 2H_2O$) are given:

$$\lg K_{eq} = \frac{12\,543}{T} - 0.473 \lg T - 3.6 \times 10^{-4} T + 8.1 \times 10^{-6} T^2 - 0.865$$

and carbon monoxide combustion ($CO + 0.5O_2 \leftrightarrow CO_2$):

$$\lg K_{eq} = \frac{14\,250}{T} - 2.65 \lg T - 0.08 \times 10^{-3} T + 100 T^{-0.5} - 15.4$$

This process is possible only if the partial pressure of the reducing gas is higher than its equilibrium value typical for the reduction of the oxide of the given metal.

An opposite development of the reaction is possible in the cases of low concentration of the reducing gas or high concentration of its oxidation products.

The reduction system is a three-component and three-phased one (oxide, metal, gas), therefore there

are two degrees of freedom. The equilibrium constant (K) of the reduction reaction is determined by the ratio of partial pressure of the reducing gas and the product of its oxidation; the equilibrium gas composition is determined by its pressure and temperature.

Only temperature influences the equilibrium constant (K) at low pressures of the gas since the reaction proceeds without changing the number of gas moles.

If the reaction constant $K \leqslant 1.0$, the oxides are difficult to reduce and vice versa. The stronger the metal bond with oxygen, the higher is the oxide formation heat and the more positive the thermal effect of its reduction reaction.

The utilization factor of the gaseous reducer ($\eta\%$) is determined by the equilibrium constant of the reaction

$$\eta = \frac{K}{1+K} \cdot 100$$

and can never achieve 100%. The lower the value of equilibrium constant, the higher is the hydrogen consumption; the utilization factor of hydrogen increases with its dehumidification.

The partial pressure of the metal in the gas phase appears in the equation for the reaction equilibrium constant in the case of the reduction of metal compounds with high vapor pressure. Decrease of the total pressure and increase of temperature and reducing gas concentration facilitate the development of similar processes. If the equilibrium metal pressure is higher than its saturated vapor pressures, production of metal by condensation is possible.

If the reduction reaction is endothermic, the opposite reaction (i.e. oxidation by carbon dioxide or water vapor) is possible during the cooling of the gaseous mixture together with the condensation of metal vapors. The formation of oxides on metal particle surfaces is possible in the presence of oxidizers in the gaseous phase. This makes the coalescence of metal particles difficult.

Kinetics and Mechanism of the Process

Reduction processes are developed in accordance with Baykov principle on the sequence of transformations of all chemical compounds formed in the given system.

The reactions of indirect reduction are special cases of topochemical reactions; they proceed on the interphase boundary [3].

The kinetics of solid phase reduction depends on the process parameters (temperature, pressure, reducer type and mass transfer conditions) as well as on the physical and chemical properties of the initial raw material (structure defects, dispersivity and surface).

According to adsorption-autocatalytic theory, the main stages of the process are:

1. supply of a gaseous reducer to the surface of the processed material
2. adsorption of a reducing gas molecule on active centers of solid surface
3. splitting up and recombination of the reducing gas molecule under the influence of crystal lattice forces that is accomplished by the formation of an activated form at atomic level
4. diffusion of reducing gas atoms through pores and cracks along the defects of the crystals lattice; and filling of electron vacancies
5. chemical interaction (electron interchange, nucleation and growth of metallic phase crystals); the latter accelerates adsorption and dissociation of molecules and provides the autocatalytic nature of further reduction due to high surface activity
6. desorption of gaseous products of reducer oxidation through the layer of the metallic phase
7. diffusion of ions of metal and oxygen; electron transfer inside the crystalline phase.

Supply of the reducing gas (an act of external diffusion) in conditions of its excess consumption, purity and optimal rate of feed does not retard the process.

The process rate limited by the adsorption stage depends on the pressure of the reducing gas (p_g) and is described by one of the following equations:

$$v = k\frac{bp_g}{1+bp_g}$$

$$v = k \cdot p_g^n$$

where k is the rate constant; b and n are experimental coefficients, which usually are not higher than 1.0.

For reversible reactions:

$$v = k\frac{p_g - p_g^l}{p_{pr}}$$

where p_g, p_{pr} are partial pressures of the reducing gas and reaction product; p_g^l is the equilibrium pressure of the reducing gas.

Reducing gas comes to the reaction zone in accordance with laws of internal diffusion and its supply is

increased with the growth of the gas pressure and lowering the temperature.

Adsorption of the reducing gas molecule is accompanied by transmission of electrons in the oxide lattice. Adsorption mechanisms are different for oxides of hole (p-type) semiconductors with cation vacancies (Cu_2O, NiO) and electronic (n-type) semiconductors (ZnO, CdO and Ti_2O) with cations in interstitial spaces or with vacancies in the oxygen lattice.

In consequence of its insignificant affinity to electrons, hydrogen is a donor in the case of adsorption of its molecule on the oxide surface; in this case a positive charge containing H^+ ions arises.

As the process develops, a metallic phase layer is formed that makes diffusion conditions complicated and decelerates the reduction rate. The negative influence of the metallic film is weaker when hydrogen is used, because the molecule size is smaller than that of carbon monoxide while the diffusion coefficient is larger ($D_{H_2} = 3.74\, D_{CO}$). Elevated activity of hydrogen especially appears in the region of lower temperature. Diffusion of metal ions and electrons to the boundary layer accomplishes the metallic phase nuclei and its further growth:

$$n\mathrm{M}^{2+} + 2n\bar{\mathrm{e}} \leftrightarrow n\mathrm{M} \rightarrow (\mathrm{M})_n$$

A chemical reaction includes three sequential stages: chemisorption of reducing gas molecule on the reaction surface; separation of an oxygen ion from the oxide lattice and its interaction with activated atoms (molecules) of the reducer that is completed by metallic phase formation; adsorption of gaseous products of the reduction.

In the first stage, the reduction develops slowly due to different rates of reducing gas chemisorption at centers of the oxide surface that differ by their activity.

In the first stage with p-type semiconductors, all holes are involved and adsorbed H^+ ions are formed:

$$\mathrm{H}_{2(\mathrm{g})} \leftrightarrow 2\mathrm{H}^+_{\mathrm{adi}}(\mathrm{M}^{2-}_{\beta})$$

The free electrons are formed in the boundary layer:

$$0,5\mathrm{H}_2(\mathrm{g}) \leftrightarrow \mathrm{H}^+_{\mathrm{adi}} + \mathrm{e}$$

Reduction develops with filling of cation vacancies M^{2-}_{β}

$$2\mathrm{H}^+_{\mathrm{adi}} + \mathrm{MO} + \mathrm{M}^{2-}_{\beta} \leftrightarrow \mathrm{H}_2\mathrm{O}_{\mathrm{g}} + \mathrm{M}$$

and further with electron usage:

$$2\mathrm{H}^+_{\mathrm{adi}} + \mathrm{MO} + 2\mathrm{e} \leftrightarrow \mathrm{H}_2\mathrm{O}_{\mathrm{g}} + \mathrm{M}$$

For *n*-type semiconductors, the reduction process includes the following stages:

- chemisorption of hydrogen and ionization of atoms:

$$\mathrm{H}_{2(\mathrm{g})} \leftrightarrow \mathrm{H}_{2\mathrm{adi}} \leftrightarrow 2\mathrm{H}_{\mathrm{adi}} \leftrightarrow 2\mathrm{H}^+_{\mathrm{adi}} + 2\mathrm{e}$$

- connection of free electrons by metal oxide ions
- elimination of oxygen with formation of vacancies on the surface

$$\mathrm{H}_{2(\mathrm{g})} \leftrightarrow \mathrm{H}_2\mathrm{O}_{\mathrm{g}} + \mathrm{O}^{2+}_{\beta} + 2\mathrm{e}$$

and collection of holes on metal oxide surface

- metal ion formation in interstitial spaces of (x) lattice

$$\mathrm{H}_{2(\mathrm{g})} + \mathrm{MO} \leftrightarrow \mathrm{H}_2\mathrm{O} + \mathrm{M}^{2+}(\mathrm{x}) + 2\mathrm{e}$$

In the case of a multistage mechanism of the reduction process, which includes a series-parallel formation of the lowest oxides, the reaction rate is determined by the lowest rate among these stages. A process zonality of an autocatalytic type is observed, specified by different catalytic activity of the formed phases.

Transformation of the lattice of the highest metal oxide into the lattice of the lowest oxide or metal lattice occurs in accordance with the principle of phase structure succession. With decreasing temperature, the induction period is extended and the speed of interphase boundary movement decreases. Metal ions as well as oxygen atoms can take part in diffusion stages; the limiting stage is determined by the ratio of their diffusion rates. The diffusion is performed through crystal lattice volume and along the grain boundaries.

In real conditions, due to the use of elevated temperatures, the rate of crystal chemical transformations is much higher than the rate of reducer supply or elimination of gaseous reaction products, i.e. the reduction process flows in the diffusion area.

S.T. Rostovtsev suggested a kinetic equation describing the diffusion-kinetics range of the reduction process:

$$\tau = \frac{q}{\Delta N}\left[\frac{1}{k}\ln\frac{\mathrm{e}^{S}(S-1)+\mathrm{e}^{-S}(S+1)}{\mathrm{e}^{S\cdot\xi}(S\cdot\xi-1)+\mathrm{e}^{-S\cdot\xi}(S\cdot\xi+1)} + \frac{R^2}{D_{2\mathrm{e}}}\left(\frac{1-\xi^2}{2}-\frac{1-\xi^3}{3}\right)+\frac{4R^2(1-\xi^3)}{3D_{1\mathrm{e}}(\sqrt{Re}+4)}\right]$$

where τ is reduction duration, s; q is gas mass necessary for full reduction of $1\,cm^3$ of raw material, mole/cm^3; R is radius of a spherical piece, cm; ΔN is reducer excess over its equilibrium concentration; k is constant of crystal transformation rate; $S = R\sqrt{k / D_{1e}}$ is dimensionless similarity parameter; D_{1e}, D_{2e} are coefficients of internal diffusion in volumes of an initial material particle and a particle after reduction, mole/(cm·s); ξ is dimensionless parameter; $\xi = (1 - \omega)^{1/3}$, where ω is reduction degree, in fraction unity; *Re* is Reynolds's criterion.

As the criterion S decreases, the process shifts to the kinetics area; in the transition area S ranges from 10 to 50; diffusion limits become defining at high values of this criterion.

The following features are useful for metal powder production practice:

1. Some impurities contained in the gaseous reducer can be adsorbed on active surface centers more rapidly and preferably reducing the front of productive reaction. Therefore, it is necessary to use pure gases with prior drying.
2. Increasing of particle surface and dispersivity, decreasing of the thickness of the material layer, enhancing of mass transfer conditions (increasing of active concentration and reducing gas speed and layer stirring) are required for process acceleration by its course in the diffusion area.
3. Temperature monitoring excluding subsmelting of particles of newly reduced metal and retaining the gas-permeability of the treated layer.
4. Oxides reduction rate increases in the presence of a number of impurities in the basic material. The degree of oxide structure disorder increases by partial replacing of matrix phase cations, for example, by selenium and tellurium cations: a number of vacancies and holes in p-type oxide-semiconductors increase that simplifies ion diffusion, accelerates chemisorption of the reducing gas, makes easier crystal transformations.
5. Oxides of alkali metals interact with microimpurities (sulfur, phosphorus and arsenic) with their transfer into water-soluble compounds, which are eliminated in the process of cake washing that increases the powder purity.
6. Size of powder particles significantly depends on the initial product dispersivity and the temperature; the finest powders are produced by reduction of chemically precipitated salts at a moderate temperature (300–500°C), high reducer consumption and limited duration.
7. To increase the layer gas-permeability, to exclude powder sintering and grain coarsening, it is useful to granulate the charge by injection of 1–3% binders (alcohols, organic acids or chlorides of alkali-earth metals), which then are sublimated at reduction temperatures.
8. Powder purity greatly depends on the composition of the basic raw material, as only impurities forming volatile compounds (C, As, S, O and Cl^-) can be eliminated in the reduction process.

Feed Stock and Reagent-reducers

Reducers are gaseous (hydrogen, carbon monoxide, converted natural gas and dissociated ammonia), solid (graphite, charcoal and other carbon-bearing reagents with limited content of sulfur, phosphorus and arsenic) or combined reducers (for example, carbon monoxide and charcoal). The gases are produced in dedicated plants and oxygen and water vapor are removed.

Hydrogen is the most effective reducer. Four industrial methods of hydrogen production (conversion of natural gas and electrolysis of aqueous solutions) are well known and readily available commercially. They are: A, by electrolysis of aqueous solutions; B, by iron-steam method and by interaction of ferroslag with alkaline solution; C, by chloride electrolysis; D, by steam conversion of hydrocarbon gases (Table 8.1).

Hydrogen is freed from oxygen in vertical furnaces filled with a catalyst (copper sponge, chromium–nickel powder or iron–nickel–copper mixture at 400–450°C; temperatures ranging from 250 to 300°C are required when using the palladinized asbestos). The dehydration is carried out in columns filled by silica gel and cement; residual moisture content is not higher than $20\,mg/m^3$, which corresponds to a dew point about −45°C. Silica gel is periodically regenerated at 177°C. Even better dehydration of hydrogen, giving a residual content 2–4 mg/m^3 and removal of carbon dioxide is achieved by passing the gas through columns with granulated potassium hydroxide. To exclude the formation of explosive mixtures, the gas is supplied with a surplus to the stoichiometry (the efficiency is below 15–20%), therefore the discharge gases are burned or directed to regeneration. The latter provides cleaning from dust, moisture and oxygen. Methods of diffusion separation on palladium-containing membranes and of short-cycled adsorption under a pressure with blowing off adsorbent regeneration are used in case of need to free hydrogen from

Table 8.1 Physical and chemical properties of technical hydrogen

Properties	Brand					
	A	B	C		D	
			1	2	1	2
Chemical composition:						
Hydrogen content, vol% , min	99.8	98	98.5	97.5	97.5	95
Impurties: vol%, max						
Oxygen	0.2	0.3	0.3	0.5	0.2	0.2
Carbon monoxide	–	0.3	0.2	0.3	0.5	1.2
Carbon dioxide	–	0.5	9.2	0.3	0.5	1.0
Water steam content (25°C, 0.1 MPa) (g/m^3)	25	25	25	25	25	25
max: transportation via gas conduits and storage in rubber-textile gasholders						
storage and transportation in metallic vessels	0.5	1.0	1.0	1.0	1.0	1.0

CH_4, CO, H_2S and N_2 and producing particularly pure hydrogen. The former is implemented for devices with low capacity; the latter for devices with hydrogen consumption amounts 1000 m^3/h and higher, but purification efficiency in this case is smaller. Losses of the reaction gas through leakages of charging and discharging assemblies are inevitable.

Hydrogen is an explosive gas which requires special permissions according to safety measures. When choosing structural steels to manufacture devices that operate in hydrogen atmospheres, it is necessary take into account that the formation of volatile hydrides with impurities contained in the steel (sulfur, phosphorus and carbon) is possible at high temperatures. Recrystallization of the metal structure and a decrease of strength properties are possible during long-term operation.

Endothermic gas is produced by incomplete combustion ($\alpha = 0.25$–0.3) of the natural gas at 1030°C. It has the following composition: 38–40 vol% H_2, 18–20 vol% CO, 1–2 vol% CO_2, balance N_2; the dew point is in the range from −5 to 0°C.

Exothermic gas is produced by means of combustion of the natural gas with somewhat higher air consumption.

Dissociated ammonia is produced from liquid ammonia by means of its vaporization, heating and dissociation, cooling and drying. The gas has the following composition: 75 vol% H_2 and 25 vol% N_2; dew point is in the range −60 to −43°C without afterburning; and with afterburning: 4–20 vol% H_2 and nitrogen balance.

Converted natural gas is produced by processing of natural gas by steam at 897–1097°C in the presence of a catalyst. A volume of 4 m^3 of reaction gas is produced from 1 m^3 of natural gas. Conversion furnaces with a capacity 1000 m^3/h are used for the process. The gas has the following composition: 75–76 vol% H_2, 22–23 vol% CO, 1–2 vol% CO_2, 1–1.5 vol% H_2O, 0.5 vol% N_2, max, and 0.4 vol% CH_4; the dew point is 20°C.

The furnace is purged with nitrogen before the introduction of the explosive and combustible gases into the furnace, in the case of the formation of a neutral atmosphere or as a reagent for nitration of refractory metals and alloys. Nitrogen is produced by cryogenic separation of air, its properties are given in Table 8.2. Nitrogen costs about three times less than hydrogen. Argon is used as a neutral atmosphere in the production of extreme purity metals.

In industrial practice, coke, anthracite culm, charcoal, carbon black are among the solid reducers. Coke is produced by means of heat treatment of special coals or petroleum. It is an effective reducer containing 93–98 vol% carbon and up to 5 vol% hydrogen in the form of hydrocarbons. However, depending on the composition of the initial raw material, coke includes up to 2–4% sulfur and 0.5–1.0% ash, i.e. impurities, which lower the quality of the metal powder produced.

Anthracite culm is produced by means of anthracite heat treatment. It contains up to 75% active carbon, but also a considerable amount of ash (10–20%) and sulfur (3–3.5%).

Charcoal is the solid reducing agent with the lowest sulfur content, but it has a high ash content (2–2.5%) and is also high in volatile matter (17–20%).

Carbon black is an ultrafine product of hydrocarbon heat treatment: its chemical activity is determined by its large specific surface (up to 15–18 m^2/g). Lampblack is produced by combustion of liquid petroleum products in wick burners with air deficiency at 1197°C. It contains 0.1% ash and 0.5% moisture maximum. Gas black is produced by combustion of natural gas with air deficit. It contains 0.06% ash and 2.5% moisture maximum.

Table 8.2 Commercially available nitrogen

Properties	Technical gaseous nitrogen	Gaseous and liquid nitrogen			
		Grades			
		Extra pure	I grade	II grade	III grade
Chemical composition:					
Nitrogen content (vol%, min)	99.994	99.996	99.6	99	97
Impurities content (vol% max):					
Oxygen	0.005	0.001	0.4	1.0	3.0
Water (20°C, 0.1 MPa)	0.005	0.005	0.07	...	...
Hydrogen	...	0.001	...	...	...
CO, CO_2, C_nH_m, total	–	0.001	...	...	...
Dew point (0.1 MPa), °C	−63	−63	−43	...	...

When coal-based solid reducers are used it is necessary take the following into account:

- process parameters depend significantly on purity, porosity, dispersity and surplus concentration
- in the case of an excess of the reducer and high temperature (especially up to 1197°C), there is a high probability of carbon monoxide formation by oxidation of carbon by the carbon dioxide generated
- kinetics of carbon monoxide formation is the critical item for the rate of the total reduction process
- carbon monoxide yield increases with lower pressure (the reaction proceeds with the increase of molar volumes)
- decomposition of carbon monoxide with solid phase formation (soot carbon) is possible in the presence of catalysts (for example, just formed powders of the iron sub-group)
- formation of carbides of series metals and powder contamination with carbon are possible at temperatures above 497–597°C.

Gaseous reducers are preferable to solid phase ones as they are more active and contaminate the powder to a lesser degree. Hydrogen has the greatest commercial importance for metal powder production; carbon monoxide is a product of natural gas conversion or oxidation of solid carbonaceous reagents.

Powder Production

The flow sheet of powder production by solid-phase reduction of metal compounds includes three main stages: preparation of raw material (blending, milling, drying and degreasing), reduction and powder processing (milling, classification and mixing).

Preparation of the raw material may also include an oxidation process of the metallic part, as in the copper oxide process for the manufacture of a typical starting material for both the red cuprous oxide, Cu_2O, and the black cupric oxide, CuO, for producing pure copper powder. The oxidation of air-atomized, water-atomized, or shotted copper leads to a radical change in powder particle shape and thus enhances the control of various engineering properties of powders. More detailed information is found in Section 4, which is devoted to the methods of individual powder production.

For producing PM alloys and composites, initial components are thoroughly mixed in the required proportion and finely milled if necessary; more homogeneous mixtures are produced by chemical precipitation.

Solid-phase reduction is carried out in electrical muffle furnaces of discontinuous or continuous operation. Furnaces of continuous operation (drum, push type, conveyor and walking beam) are the most popular. These are productive, mechanized devices with moderate energy consumption, but they are more complicated in design and in operation compared to furnaces of discontinuous operation.

Push Type Furnaces

The furnaces (Figure 8.1) have metallic, water-cooled housing lined internally with layers of fire brick. The metal oxide powder is filled into flat metal boats, which are loaded and unloaded automatically. This results in a static powder layer throughout the whole reduction process. Through individual heating zones, temperature profiles may be applied. Typical reduction temperatures range from 600 to 1100°C.

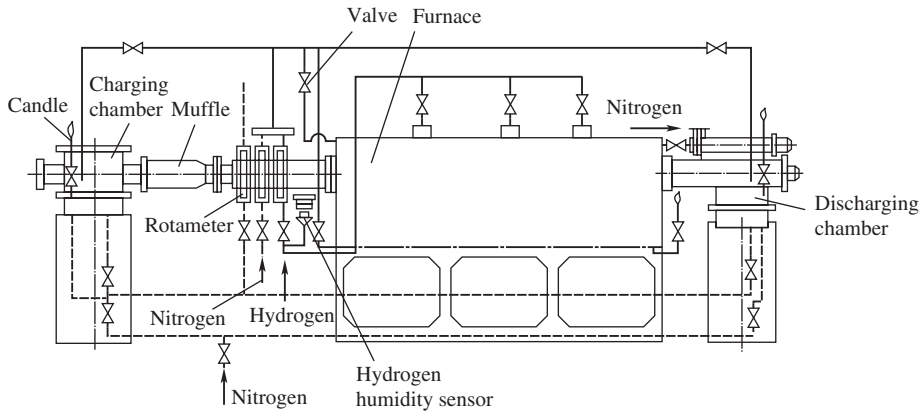

Figure 8.1 Tying scheme for push-type furnace working on hydrogen.

Removal of the water vapor formed during reduction occurs from the powder layer surface and is carried away by the reducer gas flow. Several thermal zones are provided along the furnace length. The flow of reaction gas is usually in the countercurrent direction. By variation of reduction parameters like temperature and powder layer thickness, the particle size can be controlled over a wide interval. For instance, in the case of tungsten powder, the particle sizes can be controlled in the range between 0.1 and 100 μm. The operation of the furnace is complicated by fast wear of the guides used for boat movement and by danger of their jamming.

Drum Furnaces

This type of furnace, called also a rotary furnace, is convenient for use in automatic lines. The metal oxide is directly introduced into the rotating furnace tube. As a consequence, there is no static but a dynamic powder layer. Depth of the layer is influenced by the feed rate, rotational speed, incline and lifters inside the tube. The temperature range is comparable to that of push type furnaces and the hydrogen flow direction is also, in most cases, countercurrent. As regards changes of particle size of the metal powder produced, the rotary furnace is not as flexible as the push-type furnace. They have high heat efficiency, easy pressurization; provide heat uniformity and good contact of the material with the reaction gas. But there is a danger of material nodulizing and adhering to the internal wall of the muffle (in cases of wet material processing and local submelting). In addition with these, there is appreciable erosive wear, additional energy consumption (for rotator drive), more complicated pressurization of powder charging and discharging units and increased dust production.

Conveyor Furnaces

These continuous furnaces are used for chemical–thermal treatment and sintering of powders at temperatures not higher than 1150°C. The furnace operation also alters some properties, particularly particle size and shape, apparent density and green strength of the powder production.

For example, roasting of air-atomized, water-atomized, or shotted copper is accomplished in belt conveyor furnaces. In commercial practice, oxidation or roasting copper powder is normally done in air at temperatures above 650°C. Reduction of the copper oxide thus produced is generally accomplished in a continuous belt furnace.

In a typical operation, the powder is transferred into the charge bin of a stainless steel mesh belt electric furnace. To prevent the powder from falling through the belt, a continuous sheet of high wet-strength paper covers the belt and then the powder is loaded onto the paper. A roller compresses the powder to improve heat transfer. As it enters the furnace, water is driven off and the paper burns, but not before the powder has sintered sufficiently to prevent it from falling through the belt. The gas enters the furnace from the discharge end and, because it is refrigerated, aids cooling the powder cake. By varying the furnace temperature between 480 and 760°C and altering the time of exposure, considerable variation can be made in the content of fines, apparent density and shape. To exclude powder oxidation, it is cooled down to 27–57°C in a reducing gas atmosphere and on completion of the furnace operation, the cake is broken and is ready for grinding.

The reliability of furnace operation is determined by the lifetime of the conveyor belt, which is operated in conditions of elevated temperatures, mechanical loads and a corrosive environment.

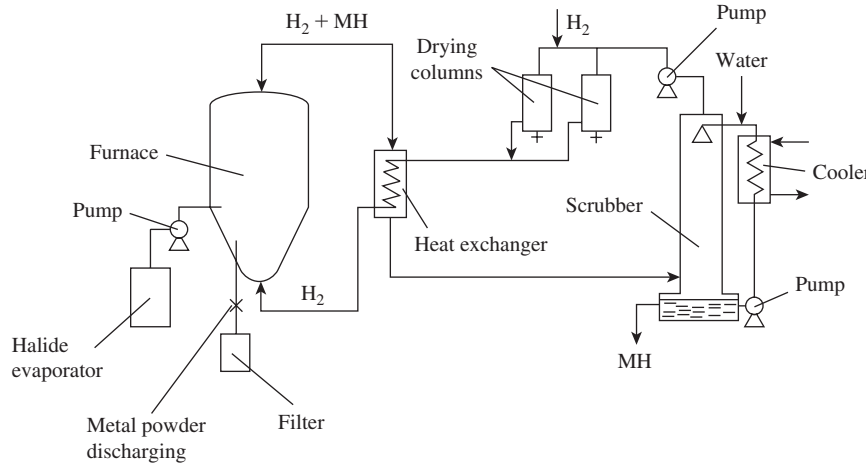

Figure 8.2 Scheme of device circuit for halide metal (MH) reduction by hydrogen in fluid-bed furnace.

The reduction process is accelerated 3 to 4 times when using fluidized bed furnaces due to increasing the contact area between powder and gas-reducer. However, the reduction operations are more difficult to control than reduction in a conveyor furnace. Along with this, dust entrainment, reducing gas consumption and, as a consequence, cost of purification and regeneration of the forming gas phase increase.

When using calcium carbide or hydride as solid reducer, the initial material is thoroughly dried and ball milled together with the reducer to $-100\,\mu m$ particle size, thoroughly blended and processed in the furnace at a required temperature that provides the reduction of the metal or metal compound oxides. A dispersing agent (calcium oxide or sodium chloride) is injected to decrease agglomeration of metallic particle components. Discharge of the resulting cake is performed by water jet (with simultaneous cooling and removal of excess calcium compounds); the pulp is processed in hydrocyclones for lime separation, acidulated by hydrochloric acid, and then washed free from the calcium chloride formed; the powder is dewatered in a centrifuge and dried in a non-oxidizing atmosphere.

The extra pure metal powders are produced by reacting low-boiling metal halides (MH) (chlorides and fluorides of molybdenum, rhenium, tungsten, tantalum and niobium) by hydrogen. A mixture of hydrogen and inert gas, usually argon (in ratio H_2 to Ar – 1.5 to 2.0), is supplied in the amount that provides a stable fluidized bed in the reactor (Figure 8.2). Hydrogen consumption exceeds the theoretically required H_2 to MH ratio several times, therefore exhausted gases are regenerated in order to utilize both the hydrogen and hydrogen chloride (hydrogen fluoride) which are returned to the technological process. The total degree of reduction achieves 98–99%; the precipitation takes place on seed particles 10–50 μm in size, which are produced by fine powder milling. The precipitation degree on the powder achieves 96–97%. Particle sizes of the powder produced range from 200 to 500 μm; particles are spherical and grain texture is dense.

Reduction processes are significantly accelerated and the produced powder is distinguished by ultrafine dispersivity (0.03–0.07 μm) by using low-temperature plasma. Hydrogen or convertible natural gas is used as a reducer.

Safety Engineering

The main hazards in metal powder production by reduction processes are dust formation, thermal and electrical action and explosion risk.

The building is constructed in conformity with the standards of technical design (discussed in Section 5). The standards cover adequate ventilation, explosion-proof lighting, lightning protection and additional safety exits.

Governing conditions for safe operation are:

- good working order of the equipment (explosion-proof and fire-proof design, gas tightness, earthing, protective cover of rotating units and performance of local ventilation according to standard requirements)
- safe methods of process conducted by experienced personnel (mechanization, remote tests and control, correct application of personnel protection and fire-fighting means, dust handling, sanitation precautions and so on)

Table 8.3 Combustion data of burning gases mixed with air

Gas	Combustion limits, vol%		T_B, °C
	Lower	Upper	
Ammonia	14.0	33.0	780
Butane	1.5	8.5	475–550
Carbon oxide	12.5	74.2	640–658
Hydrogen	4.0	74.2	580–590
Methane	5.0	15.0	650–705
Propane	2.4	9.5	518
Exogas*	17.5	87.5	...
Endogas*	8.5	80	...

*Ignition temperature depends on gas composition.

- maintenance of design specifications concerning thermal and water supply, arrangement of freight flow and usage of leak tight package for powders, audible and light alarm, warning labels.

Explosibility data of burning gases mixed with air are shown in Table 8.3 [4,5]. Design, installation and gas tubing operation have to meet 'Regulations for installation and safe operation for combustible, toxic and condensed gases' [6]. The European Development Centre, in Sheffield, UK, has Material Safety Data Sheets (MSDS) for industrial gases and gas mixtures available in published form [5].

Reaction gas is supplied either directly to the cold furnace, or after purging with inert gas. Gas pressure ranges from 0.1 to 0.2 MPa, a klaxon is activated if it fails.

The furnaces are equipped with special chambers with double doors from the charging and discharging sides to prevent the ingress of atmospheric air. Automatic temperature control is provided. The temperature shall not exceed 45°C on the external surface of the thermal insulation of furnace screens.

Before the arrangement of dump flame, the absence of flap while inflame (test-tube trial) and flame combustion stability are controlled. In the case of a sudden failure of gas supply and flame disappearance, it is necessary immediately to close the output gas fitting and stop the furnace charging and discharging processes. The line of gas supply to the furnace is blocked quickly in the case of gas inflammation.

The speed of gas movement through the suction tubes is chosen to prevent dust precipitation in them. The gases are freed from dust in devices equipped with explosive valves. During furnace repair, access inside is permitted only after cutting off all services, cooling below 40°C with constant rate, blowing by steam or inert gas that contains 4 vol% O_2 maximum, and water washing of precipitated powder if necessary.

Metallothermy

This process is the reduction of oxides and salts of metal by another metal that has a greater affinity for the metalloid included into the composition of the initial compound. Calcium, magnesium, aluminum and sodium are mostly used for the reduction. The reducer is chosen according to its activity, availability and volatility, ability to form compounds and to alloy with the produced metallic powder, and the ease with which it can be removed from the final product.

Calcium hydrides or carbides are kinds of reducers.

Metallothermy excludes metal powder contamination by carbon. It is very important for the production of precise materials and units made of them. However, the more complicated the reduction reaction, the more probable is the contamination of the powder by the metal-reducer.

Metallothermy reaction equilibrium is determined by the equality, for example, of oxygen pressures by dissociation of the initial metal oxide and the produced oxide of the metal-reducer. The metallothermy process proceeds in autogenous mode if the heat of reaction is not less than 2300 kJ per 1 kg of the reaction mixture.

In metallothermic reduction a cake is usually produced; its finishing to commercial powder requires the usage of milling, screening, and uniform mixing.

Chemical Reduction

Chemical Precipitation from Solutions

Chemical precipitation of metal as a powder is an oxidation–reduction reaction which can proceed in aqueous as well in non-aqueous medium. [7]

Table 8.4 Standard oxidation–reduction potentials of some metals in aqueous solutions at 25°C

Electrode reaction	Potential E (V(nhe))
$Ni^{2+} + 2e = Ni$	−0.23
$[Ni(NH_3)_6]^{2+} + 2e = Ni + 6NH_3$	−0.476
$Co^{2+} + 2e = Co$	−0.277
$Cu^{2+} + 2e = Cu$	+0.337
$[CuCOOH]^{+} + 2e = Cu + HCOO^{-}$	+0.285
$[CuCH_3COO] + 2e = Cu + CH_3COO^{-}$	+0.276
$[Cu(NH_3)_4]^{2+} + 2e = Cu + 4NH_3$	−0.05
$[Cu(NH_3)_2]^{+} + e = Cu + 2NH_3$	−0.11
$Ag^{+} + e = Ag$	+0.799
$[Ag(NH_3)]^{+} + e = Ag + NH_3$	+0.603
$[AgCH_3COO]^{+} + e = Ag + CH_3COO^{-}$	+0.643
$[AgCHOO]^{+} + e = Ag + HCOO^{-}$	+0.502
$[Ag(NH_3)_2]^{+} + e = Ag + 2NH_3$	+0.373
$AgCN + e = Ag + CN^{-}$	−0.04
$[Ag(CN)_3]^{2-} + e = Ag + 3CN^{-}$	−0.51
$Au^{+} + e = Au$	+1.692
$[AuCl_2]^{-} + e = Au + 2Cl^{-}$	+1.154
$[AuCl_4]^{-} + 3e = Au + 4Cl^{-}$	+1.002

Chemical precipitation from an aqueous medium permits production of all metals capable of coexistence with water: cadmium, thallium, cobalt, nickel, tin, lead, bismuth, rhenium, indium, copper and noble metals. However, thermodynamically possible reactions are often impracticable due to their extremely low rate affected by great kinetic difficulties of the reaction.

Thermodynamic Peculiarities of Metal Chemical Reduction

Electromotive force of the oxidation–reduction reaction is determined by the difference of oxidizer (Table 8.4) and reducer (Table 8.5) potentials. The potentials V (nhe) are measured relative to normal hydrogen electrode. Values of oxidation–reduction potentials in real systems as a rule differ from standard values given in tables according to component activities in the solution and pH of the medium.

To form a fine, highly dispersed product of reduction, it is necessary to provide a maximum difference of oxidation-reduction potentials of the reduced metal and the reducer. The ligands forming complexes with reduced metal ions are injected into the solution to prevent metal hydroxides forming in the alkaline medium.

Metal reduction is possible thermodynamically if oxidation–reduction potentials of the metal and the reducer are within the zone of their stability (shaded area I, II in Figure 8.3, with the example of chemical precipitation of nickel). Soluble complexes of nickel are formed in the presence of ligands (citrate-ions) at pH = 7, so the zone of nickel chemical precipitation is significantly expanded (I) so that nickel precipitation by means of formaldehyde becomes possible (Figure 8.3, zone II).

Thermodynamic data allow determination of a principal possibility of oxidation–reduction reaction performance, but do not provide any information concerning the rate of the process.

Kinetics of Solid Phase Formation in Solution [7]

The rate of metal chemical reduction from solutions is determined by kinetic factors: constant of process rate, and duration of induction period. The reaction in the first stage depends on the formation of stable particles of solid phase, which show an autocatalytic effect in the following stages. During the first stage, the reaction proceeds by successive coarsening of non-stable fine particles of the solid product. For example, the crystallization of silver nuclei is performed step by step through the formation of successively coarsening clusters:

$$\begin{aligned} &Ag^{+} + Red \leftrightarrow Ag_1 + Red^{+}.\\ &Ag_1 + Ag^{+} \leftrightarrow Ag_2^{+},\\ &\underline{Ag_2^{+} + Red \leftrightarrow Ag_2 + Red^{+}}\\ &Ag_m + Ag_n = Ag_{m+n} \end{aligned}$$

where Red is nucleus of reductant.

Table 8.5 Oxidation–reduction potentials of reducers in aqueous solutions [7]

Electrode reaction	Potential E, V(nhe)
$H_2PO_2^- + 3OH^- = HPO_3^{2-} + 2H_2O + 2e$	−0.31–0.09pH
$HPO_3^{2-} + 3OH^- = PO_4^{3-} + 2H_2O + 2e$	+0.14–0.09pH
$H_3PO_2 + H_2O = H_3PO_3 + 2H^+ + 2e$	−0.499–0.06pH
$H_3PO_2 + H_2O = H_2PO_3^- + 3H^+ + 2e$	−0.446–0.09pH
$H_2PO_2^- + H_2O = HPO_3^{2-} + 3H^+ + 2e$	−0.323–0.09pH
$H_2PO_2^- + 2H^+ + e = 2H_2O + P$ (red form)	−0.248–0.12pH
$HCHO + 3OH^- = HCOO^- + 2H_2O + 2e$	+0.19–0.09pH
$HCHO + H_2O = HCOOH + 2H^+ + 2e$	+0.056–0.06pH
$2HCHO + 4OH^- = 2HCOO^- + 2H_2O + 2e$	+0.32–0.12pH
$BH_4^- + 8OH^- = BO_2^- + 6H_2O + 8e$	−0.45–0.06pH
$N_2H_4 + 4OH^- = N_2 + 4H_2O + 4e$	−0.31–0.06pH
$N_2H_4 + 2OH^- = 2NH_2OH + 2e$	+1.57–0.06pH
$N_2H_5^+ = N_2 + 5H^+ + 4e$	−0.23–0.075pH
$NH_2OH + 7OH^- = NO_3^- + 5H_2O + 6e$	+ 0.683–0.07pH
$2NH_2OH + 4OH^- = N_2O + 5H_2O + 4e$	−0.21–0.06pH
$S_2O_4^{2-} + 4OH^- = 2SO_3^{2-} + 2H_2O + 2e$	+0.56–0.12pH
$SO_3^{2-} + 2OH^- = SO_4^{2-} + H_2O + 2e$	−0.09–0.06pH
$S_2O_3^{2-} + 6OH^- = 2SO_3^{2-} + 3H_2O + 4e$	+0.69–0.09pH
$HSnO_2^- + H_2O + 3OH^- = Sn(OH)_6^{2-} + 2e$	+0.33–0.09pH
$Ti^{3+} = Ti^{4+} + e$	−0.04
$Sn^{2+} = Sn^{4+} + 2e$	+0.151
$Cr^{2+} = Cr^{3+} + e$	+0.41
$Fe^{2+} = Fe^{3+} + e$	+0.771
$V^{2+} = V^{3+} + e$	−0.25
$R_2NHBH_3 + 3H_2O = R_2H_2N^+ + H_3BO_3 + 5H^+ + 6e$	E* −0.05 pH

*E is dependent on nature of R

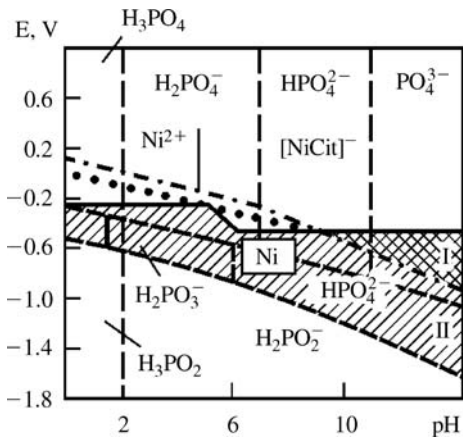

Figure 8.3 Dependence of potential on pH: upper dashed line is balance of HPO_3^{2-}/PO_4^{3-} point line is $2H^+/H_2$; solid line corresponds to Ni^{2+}/Ni (left part) and $[NiCit]^-/Ni$; (right part); upper dotted line corresponds to $H_2PO_2^-/HPO_3^{2-}$; lower dotted line corresponds to $H_3PO_2/H_2PO_3^-$ (left part) and $H_2PO_2^-/H_2PO_3^-$ (right part).

Clusters containing a small number of atoms are thermodynamically non-stable (oxidation–reduction potential of atomic silver is 1.8 V (nhe) instead 0.799 V for the metallic silver phase). Metal particles become stable in the reaction medium after achieving 1–5 nm particle size. Assuming the number of growing metal particles to be unchanged after the induction period and particles to have a spherical shape, the rate of their growth is constant and proportional to the surface S:

$$\frac{d\alpha}{dt} = k_1 S = k_2 \alpha^{2/3}$$

where α is the reduced metal yield in the fractional part of unity; k_1 and k_2 are constants of reaction rate.

The integral form of the equation is:

$$\alpha = kt^3$$

where k is integration constant and describes initial sections of reaction kinetic curves (Figure 8.4).

In the case of diffusion control of metal reduction, the rate of particle growth is proportional to its radius and is described by the equation

$$\alpha = kt^{3/2}$$

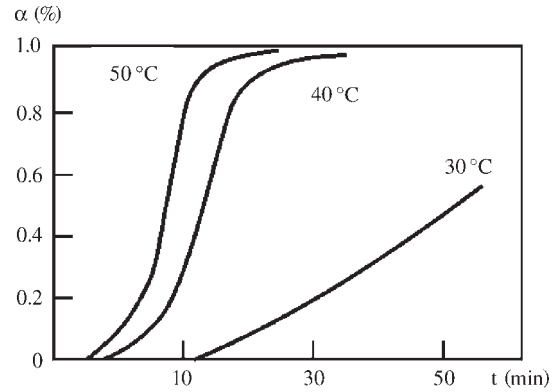

Figure 8.4 Kinetic curves of Cu (II) reduction by formaldehyde.

where k is rate constant (its value for temperature ranges from 40 to 50°C amounts to 1.66–1.67).

In the general case of stage formation of crystallization centers, the equation of kinetics of the metal crystallization process from liquid melt is developed:

$$\alpha = 1 - \exp(-kt^{n})$$

which, after expansion, becomes $\alpha = kt^{n}$ and describes the reduction of metal ions (copper and silver) from aqueous solutions by various reducers, and n can vary from 1.5 to 10.

The initial stages of reduction reaction are followed by the period when the process rate depends not only on the value of particle surface, but on the concentration of ions of the metal $(C_{M^{n+}})$ and reducer (C_{Red}).

$$\frac{d\alpha}{dt} = kC^{a}_{M^{n+}}C^{b}_{Red}S$$

where α is the reduced metal yield as the fraction of unity, a and b are constants.

In the case of reducer excess in the solution, the proportion (*) describes the kinetic reduction curves for some metals rather well; copper (II) is reduced by formaldehyde; tellurium (IV) is reduced by hydrazine; silver (I) is reduced by ascorbic acid and hydroquinone etc.

$$kt_1 = 0.5 \ln\left(\frac{1+\alpha^{1/3}+\alpha^{2/3}}{\left(1-\alpha^{1/3}\right)^2}\right) + \sqrt{3}\,\mathrm{arctg}\left(\frac{2\alpha^{1/3}+1}{\sqrt{3}}\right)$$

By chemical reduction, metals can be produced as sols or powders depending on the chosen method. Particle shape and size are controlled by the nucleation rate. In the case of sol formation, the reduction is controlled by the formation of new metal nuclei; the rate of the development of these nuclei is small. In the case of powder production, the conditions for nucleation are less favorable, but the rate of particle growth is appreciable, and also aggregation of fine particles into larger agglomerates takes place.

A momentary formation of finely divided reduction product is realized at large values of the difference of chemical reagents oxidation–reduction potentials and in the absence of autocatalytic effect of newly formed surface of metallic particles. Metallic colloids are usually formed at maximum allowable concentration of the reducer and rather low concentration of metal ions. Ligands and protective colloids are injected into the solution for stabilization of metals sols. Sols of various metals in borohydride solution are produced at elevated temperature and in the presence of a protective colloid (for example, gelatin). In such a way, sols of Ag, Au, Pd, Os, Rh, Pt, Cu, Sn, Tl, Te, Co(B) and Ni(B) can be synthesized. In the case of non-complex metal ions, sols are homogeneous and finely dispersed. In the case of the reduction of complexes, the degree of sol homogeneity decreases with the growth of their strength.

Growth rate and size of powder particles are controlled by changing the nature and concentration of the reducer, the concentration of precipitated metal ions, the solution temperature and the concentration of complexing agents or surfactant. Monodisperse powders are formed during cooling by thorough and intensive stirring of the reaction medium. To reduce particle size, the solution temperature is decreased and complexing agents and surfactants are introduced.

Application of Chemically Reduced Powders and Sols

Metal powders and sols are used as catalysts in many organic reactions. The catalyst's activity increases by dispersing it on a carrier.

Monodispersed powders with uniform distribution of the catalyst over the surface are produced by applying chemically reduced metal sols to the surface carrier particles. There are several methods of applying sol:

- Metal colloid is precipitated by a chemical method and a metallized dispersed carrier is produced in a brief contact of the metal colloid with the carrier particles as a result of colloid adsorption. This method is possible if the rate of colloid adsorption is higher than its aggregation rate.

- Colloid production directly in the presence of the carrier is preferable.
- Carrier particles covered by a salt of reducible metal are put into the reducer solution and colloid metal particles are formed on the carrier surface. $Al(OH)_3$, TiO_2, Si, MgO, $CaCO_3$, ZrO and carbon fiber material are used as carriers.
- Selective precipitation of chemically reduced metal on the carrier is performed by preliminary activation of the carrier surface by microcrystals of silver or palladium. Depending on the conditions of preliminary activation and precipitation, it is possible to produce particle islets with controlled dispersivity.

Autoclave Precipitation of Metal Powders

This method includes processing of a metal salt solution (solutions of metal hydroxide or carbonate pulp are rather rare) by a reagent-reducer at elevated temperatures and pressures [1,2]. The autoclave scheme for hydrogen reduction is shown in Figure 8.5. Some companies use the autoclave method to produce nickel, cobalt and copper powders. The processing of laterite deposits of nickel and cobalt ore high in iron is accomplished through pressure leaching with sulfuric acid in Moa, Cuba. The nickel and cobalt sulfide concentrates so produced are the principal feed to the Sherritt International refinery in Fort-Saskatchewan, Alberta, Canada. The Sherritt refining process includes the leaching at elevated temperature and pressure in the leach autoclaves. The Sherritt process is adaptable to handle a wide variety of different feedstocks. It has been adopted by Western Mining Corporation in a refinery at Kwinana, Western Australia. The Sherritt nickel and cobalt refining processes are further discussed in Chapters 17 and 18, respectively.

Organic reagents (glucose, formaldehyde, hydrazine etc.) are used as reducers, but they contaminate the final solution and powder by their dissociation products. Gaseous precipitators, i.e. sulfur oxide, carbon monoxide, hydrogen are more effective.

Hydrogen is the most widely used gaseous reducer; it is an effective, readily available reagent, which does not contaminate the solution.

According to the experience of autoclave plants, hydrogen is produced by natural gas conversion. Possible impurities (CO_2, CO, H_2O and H_2S) lead to decreasing hydrogen activity, increasing the total pressure in the autoclave, contaminate the metal powder, and lead to the formation of carbonate ions in ammonia media. This fact increases ammonia consumption and changes the molar ratio NH_3 (free) and $(NH_4)_2CO_3$, which is a kinetically important parameter.

Sulfur dioxide is a well-known reagent, but it is toxic, has limited critical parameters, leads to accumulation of sulfuric acid in the solution and powder contamination. This reagent, like carbon monoxide, is rather useful for precipitation of metal powders from alkaline and ammonium media. But carbon monoxide possesses some shortcomings: it is toxic, explosive, difficult to synthesize, expensive and it changes the acid–base balance.

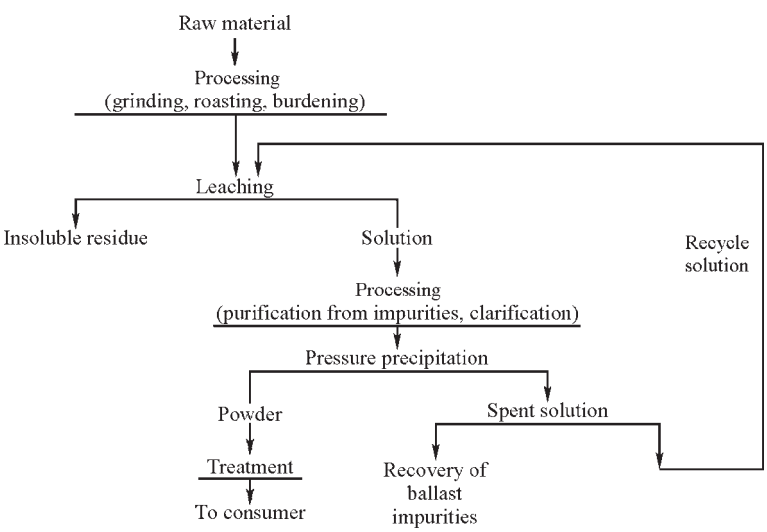

Figure 8.5 Flowsheet for metal powder production by autoclave method.

Theory of Autoclave Metal Ions Reduction

The reaction of metal ions reduction by hydrogen

$$M^{n+} + \frac{n}{2}H_2 \rightarrow M + nH^+$$

will proceed to the right until the hydrogen potential (E_{H_2}) is more electronegative than the potential of metal ion (E_M^{n+1}). The limiting degree of metal ion reduction is achieved at the moment when $E_{H_2} = E_{M^{n+}}$.

Moving strength of the summary reaction is defined by the difference of potential boundary phases $M^{n+}|M$ and $H^+|H_2$. These potentials are determinated in accordance with the Nernst equation [8]:

$$E_{M^{n+}|M} = E^0_{M^{n+}|M} + \frac{RT}{nF}\ln(a_{M^{n+}}) \qquad (1)$$

Here $E^0_{M^{n+}|M}$ is the standard potential of this boundary phases (standard conditions: $T = 298$ K, activity metal ions in solution $a_{M^{n+}} = 1$ g-ion/L), n is metal ion charge. The remaining parameters (R, T, F) are common. $a_{M^{n+}} = f_{M^{n+}} \cdot C_{M^{n+}}$; $f_{M^{n+}}$ – activity factor for M^{n+}.

For hydrogen, as its standard potential is zero by definition, boundary potential is connected with a_{H^+} – hydrogen-ion activity in the following manner:

$$E_{H^+|H} = 0 + \frac{RT}{2F}\ln\left(\frac{(a_{H^+})^2}{p_{H_2}}\right) = \frac{RT}{F}\ln(a_{H^+}) - \frac{RT}{2F}\ln(p_{H_2})$$
$$= \frac{2.303 \cdot RT}{F}\lg(a_{H^+}) - \frac{2.303 \cdot RT}{2F}\lg(p_{H_2})$$

Substitution of negative logarithm of hydrogen-ion activity $-\lg(a_{H+})$ by conventional symbol pH gives:

$$E_{H^+|H} = 0 + \frac{RT}{2F}\ln\left(\frac{(a_{H^+})^2}{p_{H_2}}\right) = \frac{RT}{F}\ln(a_{H^+}) - \frac{RT}{2F}\ln(p_{H_2})$$
$$= -\frac{2.303 \cdot RT}{F}\left(pH + \frac{1}{2}\lg(p_H)\right) \qquad (2)$$

The equilibrium activity $a_{M^{n+}}$ and concentration of metal ions $C_{M^{n+}}$ in the solution are calculated by means of joint decision of Eqns (1) and (2). The intermediate transformations lead to the equation:

$$\lg(a_{M^{n+}}) = -n \cdot pH - \frac{n}{2}\lg(p_{H_2}) - \frac{nF \cdot E^T_{M^{n+}}}{2.303 \cdot RT}$$

where $E^T_{M^{n+}}$ is standard potential for metal with correction with respect to temperature T.

This equation is acceptable for conditions in dilute solutions (with ion concentration below 0.1 mole/L), in which activity factor for M^{n+} is near to 1.

In concentrated solutions, it is necessary to take into account the bond of activity factor for M^n with ionic force of solution and after that calculate the equilibrium concentration of metal ions $C_{M^{n+}}$.

$$\lg(C_{M^{n+}}) = -n \cdot pH - \frac{n}{2}\lg(p_{H_2}) - \frac{nF \cdot E^T_{M^{n+}}}{2.303 \cdot RT}$$
$$- \lg(f_{M^{n+}})$$

Values of activity factors are given in reference literature; for sulfate media the following equation is valid:

$$f_{M^{n+}} = 0.056(\lg\mu)^2 + 0.016$$

where μ is the ionic force of solution equal to $\frac{1}{2}\sum n_i^2 \cdot c_i$; c_i is concentration of i-th ions, g-mole/L.

To denote X, the share of reduced metal ions (M^{n+1}), the degree of its reduction is calculated according to the equation:

$$E^0_{M^{n+}/M} - \frac{0.0592}{n}\lg(1 - X) = 0.05921\lg n \cdot X$$

As the influence of pH is most significant, for precipitation of electronegative metals the alkali solutions are preferable. In the presence of ammonia and other complex ligands, metal ions and complex ions with different number of addenda are in the solution. For this case, the potential of metal ion (E_{M_K}) is calculated as follows:

$$E_{M_K} = E_{M^{n+}/M} - \frac{RT}{nF}\ln\sum_0^m \beta_i \cdot a^i_{i_{free}}$$

where $E_{M^{n+}}$ is the potential of metal ion in the solution with the same concentration without complex ligands; i is the number of addenda in the complex; β_i is the stability constant of the complex that contains i complexing groups; a^i_{ifree} is the efficiency of excess complexing ligands; m is coordination number.

The pH value of ammonia solution containing free ammonia and ammonium salt is calculated as:

$$pH = pK^2\beta + \lg a_{NH_{3free}} + \lg\frac{a_{NH_4^+} \cdot a_{OH^-}}{a_{NH_4OH}} - \lg a_{NH_4^+}$$

The concentration of free ammonia in the solution is determined by pH-potentiometric titration or from Byerumm formation curves.

Thermodynamically, the reduction of many metal ions by hydrogen is possible already at 25°C and $p_{H_2} = 0.1$ MPa. But the implementation is determined first of all by kinetic factors.

The rate of autoclave precipitation of metals is defined by hydrodynamics, pressure of gas-reducer, temperature and solution (pulp) composition.

Hydrodynamics

Effective saturation of the liquid phase by the reaction gas and uniform density of the formed pulp with minimal energy consumption are achieved by sufficiently intensive stirring. Mechanical mixers that provide mass exchange on the account of configuration aerated units or rotation intensity are used; the latter is limited by increasing energy consumption of mixer drives, complexity of tightening units for their inlet into the reactor, and intensive foaming. Aerated units are more effective, but they lose the effect of the presence of powder surface deposits.

Reaction Gas Pressure

When the gas pressure is increased, the concentration of dissolved gas diluted in the pulp proportionally increases, and that accelerates the process, especially in the case of imperfect aeration. Critical pressures are limited by design reasons, extra cost for gas compression, complexity and danger of plant servicing. Partial pressures of reducing gas are varied between 0.05 and 3.0 MPa.

Temperature

The use of higher temperature is partcularly justified by effective aeration, but it involves a greater consumption of energy, more risk of corrosion and greater pressure in the autoclave, especially if volatile reagents such as ammonia are used. Also, the composition of the solution may change because of hydrolysis, sintering of powder particles and decreasing solubility of the salts. Moreover, the operation of equipment is more difficult. Usually the precipitation is performed in the temperature range from 127 to 227°C.

Solution Composition

Ammonia, sulfuric acid, hydrochloric acid and organic media are used; increasing attention is paid to the processing of metal hydroxides pulps. Process rate and powder yield per unit volume increase with the growth of precipitable metal content on condition that a reducing gas deficit is avoided. The upper limit is determined by solution stability (restricted solubility and metal salt hydrolysis); flow characteristics of pulps and effectiveness of total mass exchange become limiting factors in pulp processing. The lower limit is determined by economic indexes of the process.

Free acid in the solution complicates the corrosion condition and decelerates the rate of reducing gas molecule activation. A minimal acidity sufficient for hydrolysis prevention at elevated temperatures and introducing buffering salts (ammonia salts and alkali metal salts are preferable) are recommended.

When using ammonia media, the concentration of free ammonia is chosen taking into account the provision of the stability of diammine complexes of $(M(NH_3)_m)^{n+}$ type, where $m = 2.2$ to 2.5. In the case of ammonia excess, the total pressure in the autoclave and loss of gas vapor mixture are increased.

Depending on the initial raw composition, the solutions used for autoclave precipitation contain various impurities, especially when using acid technologies closed with respect to the solution. With organic ammonia-based solvents, which provide highly selective leaching, the problem of coprecipitation of metallic impurities arises – for example, in nickel powder production cobalt and copper may be precipitated. Therefore, a prior solution purification is required.

Accumulated impurities cause increased reducing gas consumption, change of solution properties (kinematic viscosity, solubility and pH) and lead to powder contamination. To exclude the ingress of suspended solids, the initial solution must be thoroughly filtered.

During metal precipitation, the process of ion reduction is developed by homogeneous mechanism of reaction, gas activation and ions with alternating valence play a significant part. They can accelerate the process or oxidize the intermediate ions formed with lower valence of the precipitated metal and cause the increase of reaction gas consumption and lengthen the precipitation process.

Some impurity anions form insoluble compounds with metal ions which are reduced to intermediate valences. For example, the formed copper halides are insoluble and will contaminate copper powder and decrease its yield.

Seed

Introduced dispersed solid substances (such as powder, graphite, carbides, borides, etc.) influence the metal precipitation process, which meets regularities of heterogeneous catalysis per reducing gas molecules activation (for example, under hydrogen precipitation of nickel and cobalt). Introduction of

a seed not only accelerates the process, but helps to control particle size and to cover seed particles with a precipitated metal layer to obtain composite powders.

Autoclave cladding technique provides for the treatment of materials with different particle size, layer thickness control, high rate and absence of toxic emissions.

Surfactants

Insignificant additions of organic substances (polyacrylic salts, anthraquinone and its derivatives) eliminate powder deposits on the autoclave inside surface, influence powder dispersal, shape and texture of powder particles, provide uniform covering of the precipitated metal on the surface of inert seeds and accelerate the process. But then, the surfactants introduced and products of their decomposition contaminate the powder with carbon.

In general, the method of autoclave precipitation of metal powder includes the following stages:

- Gas dissolution and saturation of the aqueous phase by it
- Adsorption of the gas on the seed surface and its activation with the formation of intermediate metal hydride (heterolytic mechanism):

$$MX_n^{m-n} + H_2 \leftrightarrow MX_{n-1}H^{m-n} + H^+ + X^-$$

- gas activation by metal ions with alternating valence (homolytical mechanism):

$$2MX_n^{m-n} + H_2 \leftrightarrow 2MH^{m^+} + 2nX^-$$

- Electrochemical reaction of metal ion reduction
- Reaction products transfer to solution volume.

Autoclave Processing of Hydroxide and Metal Carbonate Pulps

Hydroxides or carbonates of metals are semiproducts of their extraction from low-grade raw materials or are produced during neutralization of technological overflow solutions. Direct autoclave processing of pulps provides high volume of powder and it is useful for the production of powders with special properties (catalytically active powders, powders with narrow size distribution, powders with roundish shape particles and ultrafine powders). Solid-phase composition and morphology, temperature, hydrogen pressure, catalyst consumption and metal content in the aqueous phase are the main factors influencing on choice of pulp processing parameters.

As in hydrothermal conditions, base metal carbonate undergoes destruction and is transformed into metal hydroxide, the theoretical positions will be considered using hydroxide as example.

Summary reaction $M(OH)_2 + H_2 \rightarrow M + 2H_2O$ consists of two sub-reactions:

$$M^{2+} + 2e \rightarrow M^0,\ E_1^0 \quad \text{and} \quad 2H^+ + 2e \rightarrow H_2,\ E_2^0$$

the difference in potential for them is the following:

$$\Delta E = E_1^0 - E_2^0 - 2.303\frac{RT}{2F}(2\lg K_W - \lg Lp_{M(OH)_2} - \lg[H_2])$$

where

$K_W = [H^+][OH^-]$; $Lp_{M(OH)_2} = [M^{2+}][OH^-]^2$ and $Lp_{M(OH)_2}$ is the solubility product of $M(OH)_2$.

Temperature, dissolved hydrogen concentration and metal hydroxide solubility are characteristic parameters of this system.

The process is carried out at a temperature range from 197 to 247°C, $p_{H_2} = 2–3$ MPa over 1 to 1.5 h using pulps which contain 25–40% of solid phase. Powder properties depend on pulp composition, shape and size of solid phase particles and process parameters. Contents of carbon dioxide and ammonia influence the value of apparent density; powder particle size depends on metal concentration, temperature and hydrogen pressure.

If semiproducts are used, then, for pure powder production, it is recommended to dissolve them, to purify the solution and to produce secondary carbonate after solution re-distillation.

Autoclave Precipitation of Metal Powders from Organic Phases

This method of powder production allows us to produce ultrafine powders with developed surface and also to widen the choice of raw material allowing low-grade raw material to be used, which can be processed by a leaching–extraction process. This method has been developed for the production of nickel, cobalt, copper and noble metal powders.

Organic phase should be thermally stable with low solubility in water and be quantitatively regenerated during autoclave processing. Carboxylic acids and derivatives on their base and chelate compounds relate to similar reagents. Tertiary carboxylic acid $(CH_3)_3$ CCOOH is most thermally stable, up to temperatures 247–297°C. It is used in a mixture with diluent in the ratio of 1 to 2.

The advantages of autoclave metal precipitation from organometallic phases are their non-corrosiveness to stainless steels; significant decreasing of total pressure in the unit (lower than vapor pressure, below 0.5 MPa at 297°C); prevention of particles flocculation; property features of powder (roundish shape of particles, and fine particle sizes within several micrometers); organic phase regeneration and more compact flow diagram of powder production in an extraction–precipitation cycle.

But commercial application is restricted by limited choice of available reagents stable at 75–210°C, their unavoidable partial decomposition and contamination of the powder by carbon, sulfur and phosphorus, fire-risk, difficulties in separation of produced powder pulp and high power-consumption of the process (owing to lean solutions and elevated temperatures).

Equipment

For hydrogen precipitation of metals, the vertical and horizontal autoclaves with mechanical stirring are used; the latter type is predominantly used for large-capacity production. The autoclave body is made of carbon steel clad inside with a corrosion-proof material: stainless steels (for processing of ammonia, organic media and pulp of metal hydroxides) or high-alloyed steels and titanium (for processing of sulfurous and chloride media).

The autoclaves are equipped with a hatch for inside inspection and maintenance, fittings for installation of gauges for process characteristics control (thermocouples and pressure gauges), safety fittings (explosive valve, check valve), tubings for supply of solution, gas feeding and discharge of the products produced.

Gases and initial solution are supplied from the top into the autoclave; powder pulp is discharged through a dipping tube. The diagrammatic pattern for a horizontal autoclave is given in Figure 8.6.

Autoclaves for powder precipitation work parallel in periodic mode. Continuous mode is also possible, but it is complicated because of the possibility of autoclave 'obliteration', risk of hydrogen leakages and complexity of operation of units for solution supply and especially for powder pulp discharge. Also there is difficulty with control of particle size and powder particle density. The load to stirrers drives is controlled, especially at the end of the process when pulp density increases and it is quickly demixed. Overheating and shut down of the stirrer is an emergency situation. Stirrer drives are equipped by guard relay actuators for thermal protection.

Autoclaves are shut down annually for inspection and maintenance with particular attention to the condition of the protective cladding and of the welds.

Self-evaporators are capacitive devices with a conical bottom, which are equipped with a fitting for transfer of the solution and release of the gas-vapor phase. They are made of a corrosion-proof material (like autoclave) and operate at atmospheric pressure. One self-evaporator is connected with 2 or 3 autoclaves as the duration of powder pulp processing and discharge is much smaller than the duration of the powder producing cycle in the autoclave.

A double-pipe heat exchanger is the most popular type; it is manufactured from high-alloyed steel or titanium. Heat transfer efficiency deteriorates in the long run due to the precipitation of basic salts of metals and calcium sulfate. The rate of deposit formation depends on solution composition and temperature. Alkaline salts and sulfate deposits are dissolved by the spent solution and by nitric acid, respectively.

Centrifugal pumps are used and their supply into vessels operating under pressure is carried out by pumps of a plunger type. The amount of the solution supplied is controlled by the duration of pump operation, taking into account a prior measurement of the rate of solution supply.

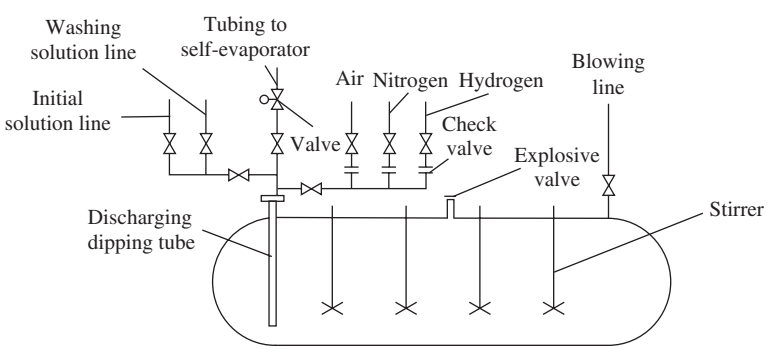

Figure 8.6 Diagrammatic scheme for hydrogen reduction in an autoclave.

Discharging units of the autoclaves, the self-evaporator and line for powder pulp transportation are subject to serious erosion, so they should be changed periodically. Discharging lines are designed with the minimum number of elbows. Relief valves are changed from time to time.

The equipment used for powder treatment (drying, screening, mixing and stirring, milling and packing) typical for powder metallurgy is described in Section 3.

Safety Engineering

Autoclaves for reduction are located in a separate building with easy dropping-cover and big window openings. The hydrogen content in the atmosphere in the building is controlled continuously [5,6,9].

The process gases are supplied into the autoclave via the separate gas tubings; the line for each gas has two faucets and a check valve allowing unused lines to be sealed.

The whole system, including autoclaves, is purged with nitrogen ($p = 0.11$ MPa) before hydrogen or air is let in. Gas-vapor mixture is continuously vented from self-evaporators to eliminate hydrogen accumulation to critical concentration.

Oxygen content in the gaseous phase after venting of equipment shall not exceed 2%.

Hydrogen-containing gases from the autoclave and the self-evaporator are passed through a drip pan and released via a chimney out of the building area.

Welding works have to be performed only after equipment shutdown, its purging and ventilation of building with continuous monitoring of the hydrogen content in the air.

Autoclave operation must be largely automated and be carried out by remote control. Control valves, electric drives of autoclaves stirrers, ventilation systems, and pumps must have explosion-proof performance.

Intermittent inspection, monitoring, high maintenance culture and personnel experience are required.

References

1. Kiparisov, S.S., Padalko, O.V., *Equipment in Powder Metallurgical Enterprises*. Metallurgy, Moscow, 1988 (in Russian).
2. Kakovsky, I.A., Naboychenko, S.S., *Thermodynamics and Kinetics of Hydrometallurgical Processes*. Nauka, Alma-Ata, 1986 (in Russian).
3. Chopra, K.L., *Thin Film Solar Cells*. Plenum Press, New York, London, 1983.
4. Fire- and explosion-proof of matters and materials and means for their quenching. *Handbook*, ed. Baratov, A.N., Korolychenko, A.J., Chimia, Moscow, 1990 (in Russian).
5. Guide to EU Legislation and 'Health and Safety' in the European PM Industry. EPMA Publisher, Shrewsbury, 1997.
6. Regulations for installation and safe operation for combustible, toxic and condensed gases. BOC Gases, European Development Centre, UK.
7. Sviridov, V.V., Vorob'eva, T.N., Gaevskaja, T.V., Stepanova, L.I., *Chemical Deposition of Metals from Aqueous Solutions*. Minsk University Publishing, Minsk, 1987.
8. Uhlig, H.H., Winston, R.R., Viley, A., Corrosion and Corrosion Control. *An Introduction to Corrosion Science and Engineering Interscience*, 3rd edn. John Wiley & Sons, New York, 1985.
9. All-Union norms of technological designing. Determination of explosion-proof and fire-safe categories of rooms and buildings. ONTP 24-86.

Chapter 9

Electrochemical Methods of Metal Powder Production

Irina B. Murashova, Ural State Technical University (UPI), Yekaterinburg, Russia

Nomenclature and Symbols

A	cross section of N nucleii formed on the boundary « solution-mercury, m^2
C_0	bulk concentration of discharging metal ions in the solution, mol/m^3
C_{SAA}	bulk surfactant concentration
C_2; $C_{2,0}$	instant and initial concentrations of discharging ions in the solution, mol/m^3
C	the instant ion concentration of dissolving metal, mol/m^3
Ce_k	cathode current efficiency
Ce_a	anode current efficiency
Ce_{ins}	current efficiency in the cells with insoluble anodes
D	diffusion coefficient, m^2/s
DLA	mechanism of diffusion-limited aggregation of metal particles
E	electrode potential, V
E_{eq}	the equilibrium potential on the interfacial boundary $Me\,|\,Me^{z+}$, V
$E^0_{M_1}, E^0_{M_2}$	standard potentials, a_{st} is standard activity equal to 1000 mol/m^3
E^0_{loc},	local standard potential (depends on curvature radii of the surface)
F	Faraday constant, A·s/mol, A·h/mol
I	current load on the electrolyser, A
I_{ins}	current load on the electrolyser with insoluble anodes, A
$I(t)$	current changing in galvanodynamic electrolysis by linear mode, A
I_{M_2}	current of metal M_2 reduction per unit area of the growth front, A/m^2
I_{TAH}	reduction current of metal M_2 on tangential spreading film per unit area of initial electrode surface, A/m^2
I_{M_1}	dissolution current of M_1 in areas free from the precipitated metal per unit area of initial electrode surface, A/m^2
K	rate constant for the contact displacement reaction of the first order, s^{-1}, Eq (33)
K	empirical rate constant for elongation of silver dendrites electrodeposited from the melts $m/(sV^n)$, Table 9
K'	empirical united rate constant for accumulation of ions-cementator $M_1^{z_1^+}$ in solution, s^{-1}, Eq (34)
$K_{dep} = i/i_{lim}$	depletion factor
$K_{dep\cdot eff}$	effective depletion factor – quotient of current density on the surface of the growth front to i_{lim}
N	dendrite distribution density on area unit of dendrite deposit growth front N, m^{-2}
N_0	number of columns per unit electrode surface formed as a result of electrolytic precipitator contact with the solution m^{-2}, the compact growth block of a radius r and a height h is spread over the surface
R	universal constant, J/(mol·K)
S	electrode surface, m^2
S_μ	thermodynamic criterion for stability of the flat growth front stability, Ohm·m
S_E	field criterion for stability of the flat growth front stability, V/m
S_w	specific volume surface of dendrite deposit, m^2/m^3
T	temperature, K
V	molar volume of the metal, m^3/mol
V_Σ	electrolyte volume in n electrolysers, m^3
ΔC	tolerable oscillation of electrolyte concentration in bath, mol/m^3, kg/dm^3
ΔE_{all}	the effect of depolarization, shift of the equilibrium potential of the j-th metal component to more positive values, V
$a_M{}^{z+}$	activity of metal ions in the solution, mol/dm^3
$a_{M(Hg)}$	metal activity in amalgam, mol/dm^3
dQ_j	quantity of electricity consumed to reduce the metal on the deposit growth front within the time interval dt_j
$dt_{r_{tip_j}}$	time period corresponding to one of m intervals when r_{tip} changes on dr_{tip}, s
d_0	initial diameter of cylindric cathode, m

h	height of growth block, m
i	current density or current per unit area of initial electrode surface, A/m^2
i_k	kinetic current density controlled by slow charge transfer through interfacial boundary, A/m^2, at settled potential i_k may be calculated as $i_k = i_0 \exp\left(-\frac{\alpha z F}{RT}(\eta)\right)$, where $\eta = E - E_{eq}$
i_0	exchange current density on equilibrium interfacial boundary $Me \mid Me^{z+}$, A/m^2
i_0^{st}	standard exchange current density, A · m/mol
i_{0,M_1}	exchange current density for metal M_1, A/m^2
i_{0,M_2}	exchange current density for metal M_2, A/m^2
i_{lim}	limit current density, A/m^2, Eq (1)
i_{limsph}	limit current density of the spherical diffusion Eq (5) when dendrite height exceeds the diffusion layer thickness, A/m^2
$i_{H,1}$	current density of hydrogen emission on M_1 surface which is free from M_2 deposit, A/m^2
$i_{H,2}$	current density of hydrogen discharge on M_2 surface formed as a result of contact displacement, A/m^2
i_{0,H_1}	exchange current density of hydrogen emission on M_1 surface, A/m^2
i_{0,H_2}	exchange current density for hydrogen emission on M_2 surface, A/m^2
i_{0,M_1}	exchange current density for metal-precipitator M_1, A/m^2
i_{0,M_2}	exchange current density for crystallising metal M_2, A/m^2
i_{tip}	current density on tips of growing dendrites, A/m^2, calculated accordingly to Eq (4)
m	number of equal intervals dr_{tip_j}, in which the interval of the tip radius change for the period of dendrite growth, t, is divided
m	constant for the given metal (Table 10) for calculation the particle size distribution in accordance with Gauss law
n	quantity of electrolysers with soluble anodes
n_{ins}	the quantity of electrolysers with insoluble anodes, which are necessary to keep material balance in batch
q	electrochemical equivalent, A·s/mol; A·h/mol
r	radius of compact film spreading over the surface during contact displacement, m
r_{tip}	radius of dendrite tip,.m
t	time, s, h
t_k	a number of cations transfer (the share of ion conductivity among a summary solution conductivity)
t_{cor}	period between corrections of electrolyte concentration, h
y	dendrite length; the height of dendrite layer on electrode, m
z, z_j	metal ion charge
1000	standard concentration, mol/m^3
α, α_j	transfer factor for reaction on interfacial boundary
α_2 and $(1 - \alpha_1)$	apparent transfer factors for cathode and anode reactions
αr_{tip_j}	share of the dendrite deposit with the tip radius $r_{tip,j}$ at any moment of electrolysis
β	rate of current rise in galvanodynamic electrolysis, A/h
δ	thickness of the diffusion layer, m
γ	specific surface energy of interface boundary, J/m^2
η	overvoltage, $\eta = E - E_{eq}$, V
ν	rate of dendrite elongation at overvoltage η, cm/s (Table 2.9)
ρ_s	solution resistivity, Ohm·m
ρ_{dep}	deposit resistivity, Ohm·m
τ	transient time interval, *s*

Electrochemical methods can be used to produce a variety of metal powders (Figure 9.1). They provide production of powders with particle size ranging from a few nanometers (by the method of zone electrochemistry) to several millimeters (electrolysis of melts) [1].

The main properties of such powders are purity, dendritic shape of particles (Figure 9.2) and good compressibility.

Electrochemical methods make it possible to control crystallization (definite shape and size of powder particles) by selecting the process parameters: concentration of the metal and hydrogen ion exponent pH of the electrolyte, cathode potential, current density, temperature and rate of circulation of the electrolyte, type and size of anode and cathode and their distance from each other, type and quantity of addition agents and conditions of removing deposits at the electrodes. The use of some techniques (permanent anodes, electrochemical reduction from solid phase, electrodes with highly developed surface) makes it possible to utilize production waste and to achieve

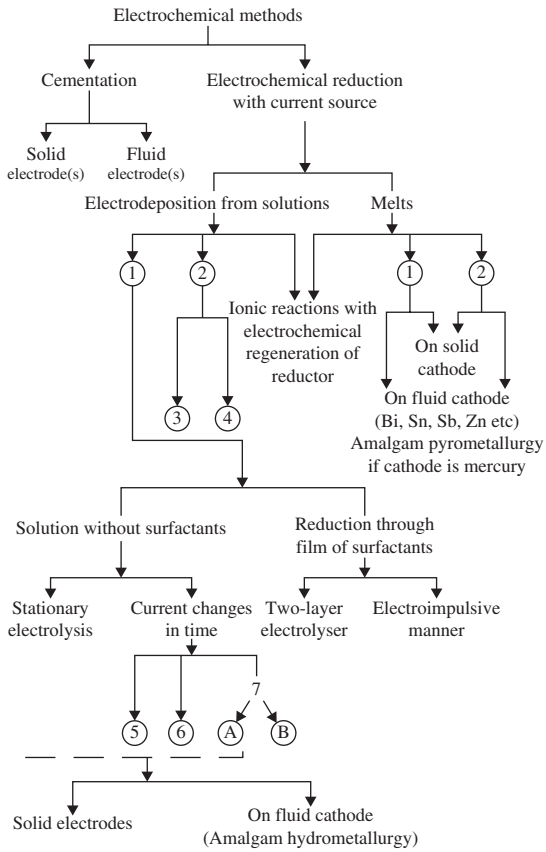

Figure 9.1 Methods of producing metal powders by electrolysis of metals: 1, with non-permanent anodes; 2, with permanent anodes; 3, on smooth electrodes; 4, on electrodes with developed surface and heightened transient factor; 5, galvodynamic electrolysis; 6, controlled potential electrolysis; 7, impulse electrolysis: (a) current impulses; (b) current impulses alternated with ultrasonic impulses (zone electro-chemistry).

complete recovery of the metal as powder. Electrolytic powder alloys do not require chemical homogenization; moreover, some alloys are produced only by the electrochemical method. Nanoparticles display a unique catalytic activity.

Powders of the majority of metals such as copper, nickel, cobalt, cadmium, zinc, silver, may be manufactured by electrodeposition of metals from aqueous solutions. This method is differentiated by the properties of the electrodepositions: the first method, namely 'direct deposition' of a friable or spongy deposit that can easily be disintegrated mechanically into fine particles, and the second method named 'brittle process' deposition of a dense, smooth, brittle layer that can be ground into powder [2]. Both deposition types are achieved by controlling the suitable composition and operating conditions. Such metals as nickel and cobalt are characterized by a high electrolytic polarization and form deposits that can form brittle layers.

Unique possibilities to produce a wide list of metals in powder form are provided by amalgam metallurgy.

Physical and Chemical Principles of Electrolytic Crystallization of Dendrite Deposits

In the course of electrolysis, the metal is crystallized in dendrites due to the destroyed stability of the flat front of growth of particles of the newly formed metallic phase that occurs at positive values of the thermodynamic criterion S_μ or the field criterion S_E (Table 9.1) [3]. The trend of the transition to dendritic

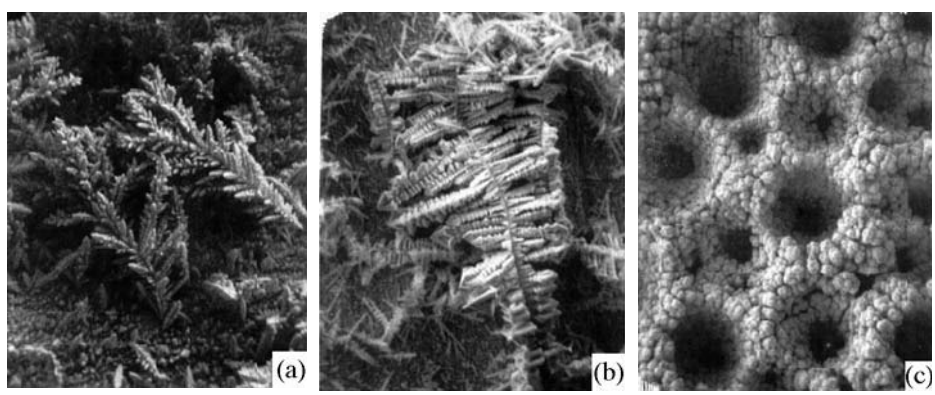

Figure 9.2 Scanning electron micrographs of electrolytic dendrite deposits on the cathode in the water solution: (a) copper, (b) lead, (c) nickel.

Table 9.1 Criteria of the stability of growth flat front*

Electrochemical precipitation	Equation for S_μ, S_E	Condition at failure of growth flat front $S_\mu > 0$; $S_E > 0$
Thermodynamic criterion		
From specific melt	$zF \cdot i \cdot (\rho_s - \rho_{dep})$	$\rho_s > \rho_{dep}$
From melted down solution or melt	$zF \cdot \left[\frac{RT}{zFDC_0 \cdot (1 - i/i_{lim})}\right] + \rho_s - \rho_{dep}$	$\rho_s + \frac{RT}{(zF)^2 DC_0 (1 - i/i_{lim})} > \rho_{dep}$
From complex electrolyte	$\frac{RT}{zF} \cdot \left[\frac{1}{D_{MX} \cdot C_{MX}} + \frac{m^2}{D_X \cdot C_X}\right] + zFi(\rho_s - \rho_{dep})$	$\frac{RT}{(zF)^2} \cdot \left[\frac{1}{D_{MX} \cdot C_{MX}} + \frac{m^2}{D_X \cdot C_X}\right] + \rho_s > \rho_{dep}$
Diffusion saturation	$RT\left[\left(\frac{d\ln(C)}{dx}\right)_s - \left(\frac{d\ln(C_c)}{dx}\right)_{dep}\right] + zFi(\rho_s - \rho_{dep})$	$D_C C_C > D_P C_P$
*Field stability criterion of growth flat front** S_E		
From specific melt	$(\rho_s - \rho_{dep}) \cdot i - \frac{d\beta}{dx} i + \frac{dE_1^0}{dx}$	$\frac{d\eta_a}{dx} < \rho_s i \quad \text{at } \frac{d\eta}{dx} = 0$
From melted down solution or melt	$-\frac{d}{dx}(\eta_a - E_1^0) + \left[\frac{RT}{(zF)^2 DC_0 (1 - i/i_{lim})} - \rho_{dep}\right] \cdot i$	$S_E > 0$

*Designation: i, A/m^2 current density; ρ_s, Ohm m resistivity of solution; ρ_{dep}, Ohm m resistivity of deposit; i_{lim}, A/m^2 limit current density; m number of ligands in the complex ion MX_m; C_X, mol/m^3 concentration of ligands; C_C, mol/m^3 concentration of precipitated metal in the alloy; η, V activated component of overvoltage; β, Ohm m^2 ($\beta = d\eta/di$) polarity of the process; E_1^0, V local value of standard potential.

deposit may be evaluated with the help of comparative computing of the values of the criterion when new electrolysis conditions are used.

In many cases, metal deposition is controlled by material transfer towards the phase boundary. The maximum rate of such electrochemical reaction is characterized by limit current density (i_{lim}, A/m^2):

$$i_{lim} = \frac{zFDC_0}{(1 - t_k)\delta} \quad (1)$$

where z is the number of electrons in the cathode process; F is the Faraday constant (96 500 Kl/mol or 26.8 A.h/mol); D is the diffusion coefficient, m^2/s ($\approx 10^{-9}$); C_0 is the concentration of discharging metal ions in the solution, mol/m^3; t_k is the number of cations transfer (0.4–0.6); δ is the thickness of the diffusion layer, m ($\approx 10^{-4}$).

As a rule, the resistivity of the solution ρ_s is considerably higher than the resistivity of the deposit ρ_{dep}, therefore, during the electric precipitation, the metal surface is gradually covered by growths in the form of dendrites. The more the stability of the flat growth front is destroyed, the higher is crystal branching, the thinner are the dendrites and the smaller is the curvature radius of their tips r_{tip}. Dendrite growth is favored by low concentration of ions in the solution, diffusion limitations, low polarizability (crystallization from non-complex solutions free from surfactants).

The structure of particles of the dendritic deposit depends on of the metal, the nucleation mechanism and the dynamics of the dendrite growth (Table 9.2). The deposit type does not always directly determine the morphological characteristics of the particles. Both sponges and electrolytic powders can include two- or three-dimensional fern-like dendrites. Different nucleation and growth mechanisms define different particle size (less than 10 μm in sponge). Strands obtained after deep passivation of the cathode surface with surfactants differ in dimension and properties anisotropy. The particle structure is influenced by the degree and the character of the cathode over-voltage. If the diffusion over-voltage prevails, ribbed sharply cut dendrites of various degrees of twinning are formed. An increase in the transition over-voltage share (for copper up to 70%) results in the crystallization of smooth spheroidal granules.

Subsieve dendritic particles (up to 1–10 μm) are obtained by the electrolysis in a two-layered cell and by the chemical reduction from solutions. Big well-cut dendrites of 50–100 mm are crystallized from the melts. Particles of 5–200 μm are produced by electrolysis of aqueous solutions.

Diffusion limitations are provided by high depletion factor $K_{dep} = i/i_{lim}$, named so by A.Pomosov ($K_{dep} = 5$, 10 and higher) [4]. In the course of dendrite deposit growing, the electrochemical reaction is forced out to the dendrite tips, while the electrical crystallization occurs only in the thin upper layer which is the growth front. The process rate slows down rapidly towards to the inner part of a three-dimensional electrode. The extension of the cathode size (together with the dendrite deposit layer) is followed by decrease in the effective depletion factor $K_{dep\text{-}eff}$ (the ratio of the dimension current density to the limit current density) in the galvanostatic electrolysis.

An anisotropic shape of dendritic particles is connected with the difference between electrolytic crystallization rate at the tips (i_{tip}) and on the rest of the deposit surface and is determined by the dynamics of their elongation [5] because

$$i_{tip} = \frac{dy}{dt} \cdot \frac{zF}{V} \quad (2)$$

Table 9.2 Types of dendrite deposits, peculiarities of their nucleation and morphology

Deposit	Nucleation mechanism	Surface morphology
Sponge	Slow nucleation at limited mass transfer. Passivation of cathode-base, decreasing of number of growth active places	Fibers, fern dendrites
Threads	Competitive layer growth of tips and passivation of side surface due to the absorption of SAA or different crystallography of cutting	Needles, fibers, whiskers
Branched dendrites	Crystallization in the condition of spherical diffusion ions transfer to the tips: (1) accelerated crystallization of faces with the highest indexes; (2) twinning; (3) dislocation pyramids; (4) three-dimensional nucleation at limited mass transfer	Needles, two- and three-dimensional dendrites; globular outgrowth

where y is dendrite length, m at a time t, s; V is molar volume of the metal, m^3/mol.

Dendrite growth dynamics in its turn completely depends upon the conditions of the electrolysis, potentiostatic and galvanostatic as well.

Under the potentiostatic conditions [5], dendrite length increases linearly during the period of their visible growth ($r_{tip}/y < 10^{-3}$).

$$y = \frac{zF}{V} i_{tip}(t - t_i) \tag{3}$$

where t_i is the period of dendrite nucleation; i_{tip} is determined by the ratio of mixed electrochemical kinetics (Eqn 4), r_{tip} is the dendrite tip radius,

$$i_{tip} = \frac{i_{lim\,sph} \cdot i_k}{i_{lim\,sph} + i_k} \tag{4}$$

where i_k is the current kinetic density determined in accordance with electrochemical laws [6] by the exchange current density i_0 and the set over-voltage η or the potential ($\eta = E - E_{eq}$).

If dendrite height exceeds the diffusion layer thickness δ, then the maximum current of the spherical diffusion is calculated as following:

$$i_{lim\cdot sph} = \frac{zFDC_0}{r_{tip}} \tag{5}$$

The tip shape that is closest to parabolic can be approximated by a semi-sphere with the radius r_{tip}. The value of r_{tip} depends on the set over-voltage and is connected with the exchange current density for the given metal which, in its turn, varies with the concentration of discharging metal ions C_0 according to the law

$$i_0 = i_0^{st} \cdot C_0^{1-\alpha} \cdot 1000^{\alpha} \tag{6}$$

where i_0^{st} is the standard exchange current density, A·m/mol; C_0 and α are determined above in the list of designations.

Thus, the dendrite growth rate is defined by the over-voltage value η, the nature (i_0^{st}, α), and concentration C_0 of discharging ions. In practice, the linear dendrite growth is preceded by the period of roughening and developing the primary surface unevenness (t_i) that increases with the electrolyte dilution and the decrease of the applied over-voltage.

Under potentiostatic conditions, uniform dendrite growth is determined by the establishment of a constant curvature radius of the dendrite tips that is correlated with the applied over-voltage. The spherical diffusion rate determined by the surface curvature radius (Eqn 6) is low on flatter tips, while very sharp tips remain unstable. Their equilibrium potential $E_{eq,tip}$ is shifted to the area of negative values by the amount of $2\gamma V/(zFr_{tip})$, so that the effective over-voltage at the tip ($E - E_{eq,tip}$) turns out to be too low to provide quick growth. Here γ is the surface energy of the 'metal-solution' boundary ($\approx$0.15 J/mol).

Such electrolysis conditions provide for the crystallization of the dendrite deposit uniform in structure during a long-term electrolysis. At that, the size and the morphological characteristics of dendrites are determined and regulated by the value of the applied over-voltage. This prospective way to obtain dendritic deposits of uniform and regulated structure is not implemented currently due to a lack of industrial potentiostats.

Since in galvanostatic electrolysis the set current is many times higher than the limit current, hydrogen is formed at the cathode together with the metals that do not possess high exchange current (in precipitation from aqueous solution). If hydrogen is not co-reduced together with the metal, then the change of the dendrite length within an interval t on a cylindrical electrode with a diameter d_0 is described in the following way, neglecting the height of the initial surface unevenness [7]:

$$y^2 + d_0 y = \frac{V}{zF} \frac{d_0 K_{dep} i_{lim}}{2\pi N r_{tip}^2} t \tag{7}$$

where N is the density of dendrite tips distribution on the front of dendrite deposit growth (10^8–10^{11} m^{-2}). The dendrite growth rate under these electrolysis conditions decreases in the course of time in accordance with Eqn (7). At high values of t, the growth rate decreases in proportion to the ratio $1/\sqrt{t}$:

$$\frac{dy}{dt} \approx \frac{1}{2} \sqrt{\frac{V d_0 K_{dep} i_{lim}}{zF 2\pi r_{tip}^2 N}} \frac{1}{\sqrt{t}} \tag{8}$$

Due to a decrease of i_{tip}, metal precipitation rates become closer in all directions, the dendrite tip curvature radius increases, the particle shape is gradually roughened and crystal-spherulites are formed. Together with the process of the dendrite deposit growth, the effective depletion factor decreases to unity; diffusion limits of the growth front are cancelled; the potential is shifted to the area of more positive values; uniform spherulite growth begins (Figure 9.3) and, finally, a continuous metal layer cover is formed. The duration of diffusion limits application, for the deposit growth front grows together with the increase of the set depletion factor and is

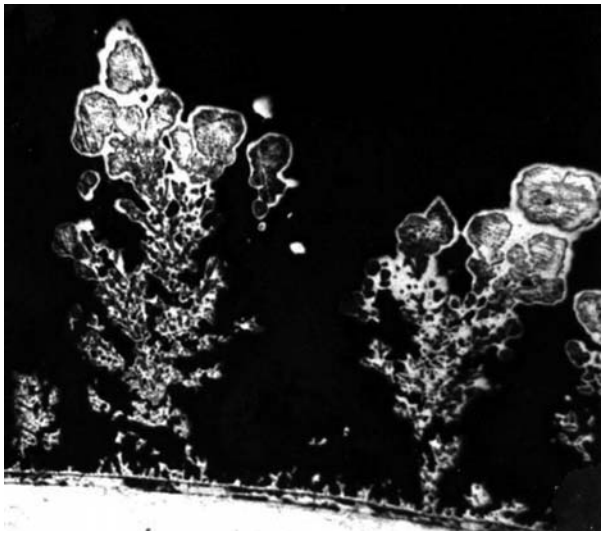

Figure 9.3 Cross-section of the loose copper deposit on the cathode with diameter of 1.5 mm.

determined by the electrode dimensions. For example, on a cylindrical electrode this period grows together with the rod diameter enlargement.

Uniform dendritic deposits can be obtained in galvanotatic electrolysis too, when the deposit growth front area is constant. For instance, in the aqueous solution together with the dendrite layer growth, the current load must be increased. Then, the initial current value and its rates of increase will determine structural and technological parameters of the powder [1]. In melts, lifting of the cathode covered with deposit from the cell should be done simultaneously with switching on the current. Solidifying melt preserves a bundle of dendritic strands. If the cathode lifting rate and the dendrite elongation rate are matched, the process in the electrolyte continues on the constant deposit growth front area [8]. The value of the set current and the cathode lifting rate determine the properties of the strands in the dendritic bundle [9].

Simulation of the electrolytic dendrite deposit growth is meant for the description of a relation between powder technological properties and electrolyte composition and electrolysis condition. In the course of processing, after the electrolysis the powder properties (particle size distribution, apparent density and specific surface) are significantly changed depending on drying, milling and screening conditions. However, the basis of particle structure is formed in the electrolysis stage. While simulating the process, we assumed the key structural parameters to be the dendrite tip curvature radius r_{tip} and the dendrite distribution density on a unit area of the dendrite deposit growth front N, m^{-2} [1].

The distribution of the obtained dendritic deposit over the dendrite tip radii is a prototype of electrolysis product distribution by particle size. The average density of tip distribution on the growth front characterizes a dendritic form of the loose deposit and is proportional to the reciprocal apparent density of the powder. The share of the dendrite deposit with the tip radius r_{tip_j} at any moment of electrolysis is $\alpha_{r_{\text{tip}_j}}$:

$$\alpha_{r_{\text{tip}_j}} = \frac{\Delta Q_j}{\sum_n \Delta Q_j} \tag{9}$$

where n is the number of equal intervals, dr_{tip_j} in which the interval of the tip radius change for the period of dendrite growth, t, is divided; ΔQ_j is the quantity of electricity consumed to reduce the metal on the deposit growth front within the time interval Δt_j. The calculated result of such distribution is determined by dendrite growth dynamics, to be more correct, by two dependences: changes with the time of the dendrite tip radius $r_{\text{tip}}(t)$ and the metal reduction current on the tips $I_{\text{tip}}(t)$ necessary to calculate every corresponding charge dQ_j. Preliminary calculation of dendrite growth dynamics is performed for galvanostatic conditions [1]. Such calculation is necessary to evaluate powder structural characteristics a priori. The process is described by a system of differential equations based on the following main principles: the laws of electrochemical kinetics (for metal reduction and for accompanying production of hydrogen) as well as the principle of charge balance on the electrode equipotential surface. The set current is distributed between metal ion discharge on the dendrite tips that create the deposit growth front, and hydrogen that reduces around the entire metal surface. The suggested equation system is solved by Runge–Kutt method that enables the relationships $r_{\text{tip}}(t)$ and $I_{\text{tip}}(t)$, required to calculate the distribution that correlates with the results of the particle size distribution analysis [10], to be obtained. Trends of maximum shifting along the curves of tip radius distribution by size show (Figure 9.4) that the average powder particle size increases with the decrease of the set current, the growth of metal ion concentration in the solution, as well as the decrease of the exchange current of the reduced metal and the increase of the hydrogen exchange current.

The use of activation control or ohmic control instead of transfer control can result in a radical change of the type of the dendrite deposit that is weakly connected with the degree of diffusion limitations.

Another kind of control (for example activation or ohmic control) instead of a transport one can

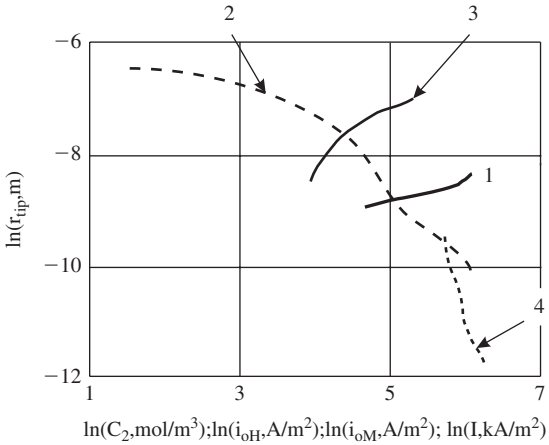

Figure 9.4 Trend of variation of predominant radii for dendrite tips of dendrite deposit depending on the parameters of galvanostatic electrolysis (model calculation): (1) C_2, mol/m^3; (2) i_{oH}, A/m^2; (3) i_{oM}, A/m^2; (4) I, A.

result in radical change of the mode of the dendrite deposit.

In such cases, the deposit structure is controlled by other technological parameters, for example, a change of discharge activation parameters (introduction of surfactants, complexing ligands) or an increase of electrolyte conductivity.

Electrolytic dendrite deposits produced under the diffusion control conditions possess fractal properties, so that the structural characteristic of such deposits is the value of the fractal dimension *D*. The process can be described by stochastic models based on the diffusion-limited aggregation (DLA) [11]. The deposit fractal properties are lost at the cancellation of transfer control of the process. This phenomenon is observed in process of the development of dendrite deposit growth front ($K_{dep} \rightarrow 1$).

Nanopowders are produced under the condition of the enforced removal of metal nuclei that develop within the period of short-term current impulses from the cathode surface [12]. In this case, the shape of the particles formed is close to spherical and the average particle size is of the order of 5–15 nm [13]. In the process of prolonged electrolysis under such conditions, one can get dendrite clusters, the mechanism of their formation is explained by the diffusion-limited aggregation.

Electrolysis of Aqueous Solutions

Electrical precipitation of metal as a loose dendritic deposit is performed from diluted solutions under a high current density. The possibility of powder precipitation on the cathode from aqueous solution is provided by the ratio of electrochemical parameters of metal and hydrogen. Intensive evolution of hydrogen is registered for the majority of metals (except mercury) ranging of the potentials from −1 to −1.2 V. This limit determines the area within which metals can be precipitated from aqueous solution on the cathode with appropriate current efficiency. Taking into account the polarizability, the most electrically negative metal that is precipitated from aqueous solution as a dendritic deposit is zinc. The use of a mercury electrode allows us to extend the range of metals precipitated from aqueous solution. The electrolysis on a solid cathode is accomplished usually at low temperature (17–57°C) with a relatively low specific power consumption (1.6–10 kW·h/kg). The crystallized deposit either falls off due to shaking or is brushed off from the cathode, it depends on the precipitated metal. The anode current density across the soluble anodes is usually lower than the cathode one to avoid passivation. The powder deposit is removed from the electrolyzer and dehydrated; it is then washed, stabilized with surfactants to protect it from oxidation, milled, screened, blended, mixed and packed. An alternative technological treatment of powder includes washing, drying, sintering in a reducing atmosphere, milling and screening. In this case, the powder is characterized by higher apparent density and flowability, but has a lower corrosion resistance owing to the destruction of stabilizing layers while sintering.

All the factors that contribute to the destabilization of the flat growth front result in comminution of powder particles. The stability is disturbed ($S_\mu > 0$; $S_E > 0$, Table 9.1) in the case of deep diffusion limitations ($i >> i_{lim}$). In conditions of diffusion control, the depletion factor K_{dep} is the key parameter that determines particle dispersity in fixed intervals of their precipitation on the cathode. If K_{dep} becomes higher, the average particle size and apparent powder density decrease, but particle branching is enhanced. Elevation of K_{dep} is achieved either by a higher current density or a decrease of the limit current density i_{lim} (by lowering the concentration C_0, decreasing the diffusion factor *D* due to lowering the temperature, addition of other electrolytes to the solution that results in lowering t_k). A decrease of current density and an increase of i_{lim} (growth of C_0, higher temperature, accelerated circulation) cause the coarsening of powder particles. Transition of metal from one phase to another in the aqueous solution can be rather difficult, and powder particle properties are significantly influenced by kinetic parameters of the electrochemical reaction: exchange current, transfer factor (see Figure 9.4). These parameters are adjusted by introduction

of complexing ligand and surfactant additives. Decrease of exchange current after introduction of complexing ligands or surfactants into the solution increases the polarization η and, consequently, the stability of flat front growth, i.e. it leads to the formation of coarser particles with simpler shape and the production of powder with higher apparent density and flowability. The passivation of the electrode surface is possible due to the formation of basic salts and hydroxides that are not readily soluble, and an intensive evolution of hydrogen.

Hydrogen evolved, together with the metal, stirs the space close to the cathode, making the diffusion layer rather thinner, and contributes to dendrite coarsening (lower K_{dep} due to i_{lim} elevation). The hydrogen ion exponent pH of the near-cathode layer is increased by hydrogen discharge and it can cause the passivation that enhances the three-dimensional nucleation and the formation of more forked dendrites. At the same time, the increased polarization due to the discharge on the passive surface facilitates its equalization and initiates the growth of spherulitic crystals.

After the current is switched on, conditions of accelerated growth of dendrites are created within the transient time interval τ and, at the end of this interval, metal ion concentration C at the cathode surface decreases from the original value C_0 to zero:

$$\tau = \pi D\left(\frac{zFC_0}{2i}\right)^2 \tag{10}$$

where i is the switched current density for geometrical electrode surface.

Then dendrites can crystallize in two ways depending on the ratio of equili-brium potentials and the exchange currents of the metal and hydrogen: either by means only of cathode process (discharge of metal ions) or together with the process of the co-reduction of metal and hydrogen ions. The first approach is applied in the case of precious metals with the equilibrium potentials much more positive than the equilibrium potentials of hydrogen as well as of metals with high over-voltage of hydrogen release on them (lead, cadmium, tin from simple electrolytes). The dynamics of dendrite growth in the first group is described by Eqns (2), (6) and (7). An intensive dendrite growth quickly removes diffusion difficulties on the growth front; the starting crystallization of huge aciculates and clusters requires a decrease in the time interval of deposit growth, to shake it off often or to brush it off from the cathode automatically.

The second group comprises the rest of the metals as well as metals of the first group precipitated from solutions of complex compounds or in the presence of surfactants. In these cases, dendrite deposit growth is accompanied by hydrogen release, dendrites grow more slowly, the cathode potential is determined by the current density of hydrogen reduction until the condition of dendrite growth $K_{dep.eff} > 1$ is reached. The removal of diffusion limitations from the growth front is accompanied by a considerable shift of potential to the more positive area. Powder properties may be regulated thus by means of the selection of the successful electrolysis conditions.

Trends of different distribution of the dendrite deposit in dendrite radii of dendrite tips under new electrolysis conditions are equal for electrolytic crystallization of all metals (see Figure 9.4). A coarsening of electrolytic powder particles is expected to follow the increase in metal ion concentration in the solution when the set current and the metal exchange current are decreased and hydrogen is released more easily. However, a combination of electrochemical parameters of metal and hydrogen provides a wide range of such changes.

Electrical crystallization of the structurally uniform deposit that grows with a constant rate is enabled along with potentiostatic electrolysis by a technically simpler galvanodynamic mode with linear change of current in time:

$$I(t) = I_{init} + \beta t \tag{11}$$

Here, I_{init} is the initial current, A; β is the rate of current change, A/h. By selection of the values of I_{init} and β, a prolonged crystallization of dendrites with required properties is achieved. Here the value of the cathode over-voltage is a reference parameter of the stability of electrical crystallization conditions. The process may be enhanced by stirring the near-anode space with fine air bubbles (without agitating the near-cathode space). An increased share of transient over-voltage causes a simplification of particle shape and an increase of powder apparent density.

The impulse mode of electrolysis is elaborated to affect the particle structure directly and enables a change of particle size distribution and powder particle shape depending on porosity, amplitude and duration of the impulse.

Constant electrolyte composition is one of the main conditions of process stability and of permanent powder quality. The requirements for the electrolyte are the following: absence of impurities able to co-reduce together with the metal; high conductivity to reduce the specific power consumption; minimum rate of hydrogen release that decreases cathode current efficiency; the lowest possibility of chemical dissolving of the precipitated metal.

Soluble anodes are manufactured from refined metal and the solution is prepared from pure reagents. Potentiostatic conditions allow selective recovery of powders of different metals from multicomponent electrolytes. The necessary conductivity of the electrolyte is provided by salts, alkali or acid. The concentration of the latter is selected according to the current efficiency since it decreases at high acidity. Approximately neutral electrolytes should be prepared with a sufficient buffer capacity to avoid quick increasing of the pH of the near-cathode space and cathode contamination due to hydrate formation.

The current efficiency of the dendrite deposit is always less than 100% for the following reasons:

- accompanying release of hydrogen
- interaction of cathode product and anode product if permanent (insoluble) anodes are used
- reduction of metal ion only to intermediate valency
- chemical dissolving, especially when powder falls down from the cathode.

The following measures contribute to the increase of the current efficiency:

- maintenance of optimal parameters of electrolysis (metal ion concentration, background, current density, stirring mode)
- installation of a diaphragm if permanent anodes are used
- extension of the interval of cathode deposit growth
- rapid powder removal out of the electrolyte and its washing to reduce secondary dissolution.

Measures to increase the current efficiency should be balanced with their effect on powder dispersivity and particle shape. As current density increases, the current efficiency passes through a maximum. At first, the proportion of current for dendrite deposit precipitation increases due to a decrease of the quantity of the compact precipitate and joints produced if current densities are comparable with the limit density. An accelerated hydrogen release leads to stirring the near-electrode space due to lowering of the current efficiency, C_{ef}. This allows C_{ef} to decelerate its drop close to the maximum. A further growth of the current density is accompanied by hydrogen effervescence and an abrupt decrease of current efficiency. When temperature and metal ion concentration in the solution increase, the current efficiency grows and powder particles coarsen.

The anode current efficiency in the case of soluble anodes is, as a rule, higher than the cathode yield and can exceed 100% taking into account chemical dissolution of the metal. In a number of electrochemical systems, anode passivation and decreasing of anode current efficiency are possible. To align current efficiencies, depassivators (for example hydrochloric acid in nickel powder production) are introduced.

The inequality of cathode and anode current efficiencies changes the electrolyte composition. Metal ions gradually accumulate; a saturation by gas of the solution close to cathode and a growth of the concentration of metal ions in the near-anode space lead to electrolyte separation into layers. The denser solution from the near-anode space drops to the bottom of the electrolyzer and, in its upper part, the solution with a lowered concentration accumulates. This effect is overcome by a periodic withdrawal of a part of the electrolyte together with the introduction of a fresh correction solution or the introduction of insoluble anodes.

Denoting the electrolyte volume in n-cells as V_Σ, m^3, the current load as I, A, the electrochemical equivalent of precipitated metal as q, kg/A·h, the permissible fluctuation of metal ion concentration as ΔC, kg/m^3, it is possible to calculate the duration of the period between corrections t_{cor}, h (without consideration of electrolyte leakage and water evaporation):

$$t_{cor} = \frac{V_\Sigma \Delta C}{nIq(Ce_a - Ce_c)} \tag{12}$$

where Ce_a and Ce_c represent anode and cathode current efficiencies, respectively.

The required quantity of cells with insoluble anodes (n_{ins}) with I_{ins}, A, being the current load on them and the current efficiency being Ce_{ins}. For the circuit consisting of n electrolyzing cells with soluble anodes, n_{ins} is calculated in the following way:

$$n_{ins} = n\frac{I}{I_{ins}}\frac{Ce_a - Ce_c}{Ce_{ins}} \tag{13}$$

If such a cell is one in the series, then its current load will be:

$$I_{ins} = nI\frac{Ce_a - Ce_c}{Ce_{ins}} \tag{14}$$

Electrolyte circulation (approximately 0.4 dcm^3/(A·h) with 12% difference in anode Ce_a and cathode Ce_c current efficiencies) is necessary to prevent electrolyte layering.

Electrolytic cells of box type with plain (disk) or cylindrical cathodes (bars or in the form of a drum) are used for water solution treatment. In electrolytic cells, devices of electrolyte input and output are

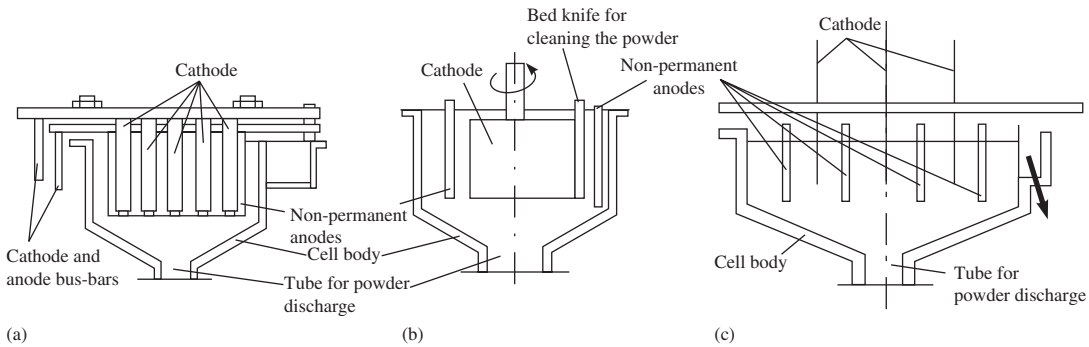

Figure 9.5 Basic types of electrolyzers with (a) rod, (b) cylinder and (c) disk cathodes.

provided. Powder is removed in the form of sludge through the bottom union. The electrolyte temperature is maintained using heat exchangers installed in the circulation scheme.

The type of the device depends upon the duration of precipitate accumulation and the strength of its binding with the cathode. Shaking off the loose precipitate (Figure 9.5(a)) or cutting it off (Figure 9.5 (b), (c)) is applied. Several types of shaking off devices for powder removal from bar cathodes are known. Using the electro-impulse method, high-voltage current is for a short time passed through dischargers installed inside the cylindrical cathode bars. When using the pneumatic shaking device, the cathode rods are preliminarily lifted up over the busbar. Then fluctuations are transferred by a pneumovibrator through a support frame to the group of cathodes supported by it at one shoulder. After shaking off powder from the bars the frame is lowered and cathode shoulder again nests on the busbar.

In the cells with disk cathodes, a quick shifting of cathode sections in the air, automatic powder cleansing from the cathode and powder washout into the collector are provided. Cathodes are placed between anodes and are manufactured in the form of sections; they are fixed on the shaft and are able to rotate around its axis. When a cathode goes from solution, each section of it is separated from others and, using a mechanism, is quickly transferred to a chamber where the powder is cut from the cathode with a knife and flushed with water into the collector.

The bath for collection of the powder from the cylindrical cathodes is installed on a platform moved in the vertical plane by a screw using a drive (Figure 9.6). The cathode is drive-rotated through an adapter and cathode arm. The scrubber approaches the cathode and cleanses the precipitate formed, which falls down into the collector. Then a software device switches on current on the electrolyzer and in the electromagnet circuit.

If a duct cathode is used, the electrolyte is supplied into it under a pressure through a fitting. The electrolyte is released through holes and falls onto plates. It is reflected from them and removed along the cathode surface. In this process, ultrasonic fluctuations with a frequency of 100 kHz arise in the solution. Metal powder precipitates on the cathode, then it is taken off the cathode by solution jets and ultrasonic fluctuations and removed into the collector in the form of a sludge.

To intensify the process of electrolysis and to simplify powder discharge, the electrolyte is fed by impulses of 5–300 s with a periodicity of 1–100 h from below the device under an angle of 5–75° to the horizontal with speeds in the range under 20 cm/s (the range under 10 cm/s is preferable) depending on the quantity and the grain-size composition of the precipitated particles.

If a vibrating ribbed cathode is used, the process of powder precipitation is accelerated 50–100 times (the amplitude is 0.8 mm and the frequency is 100 Hz). Cavitation arises close to the ribbed surface of the cathode and this intensifies electrolyte stirring and facilitates powder crumbling from the cathode.

Impulse gas feeding through holes of a hollow cathode (Figure 9.7) significantly accelerates powder precipitation. The holes are placed between ring angular flanges. As the powder accumulates, the gas is supplied into the hollow cathode through a special device. The bubbles formed accelerate the separation of the precipitate that falls into the basket.

Reduction from Solution Through Film of Surfactants

Metal particles with grain size of 0.1–10 μm are produced by electric precipitation in a bath with a two-layer electrolyte. The cathode is a rotating metal drum or disk. The bottom electrolyte layer is an aqueous

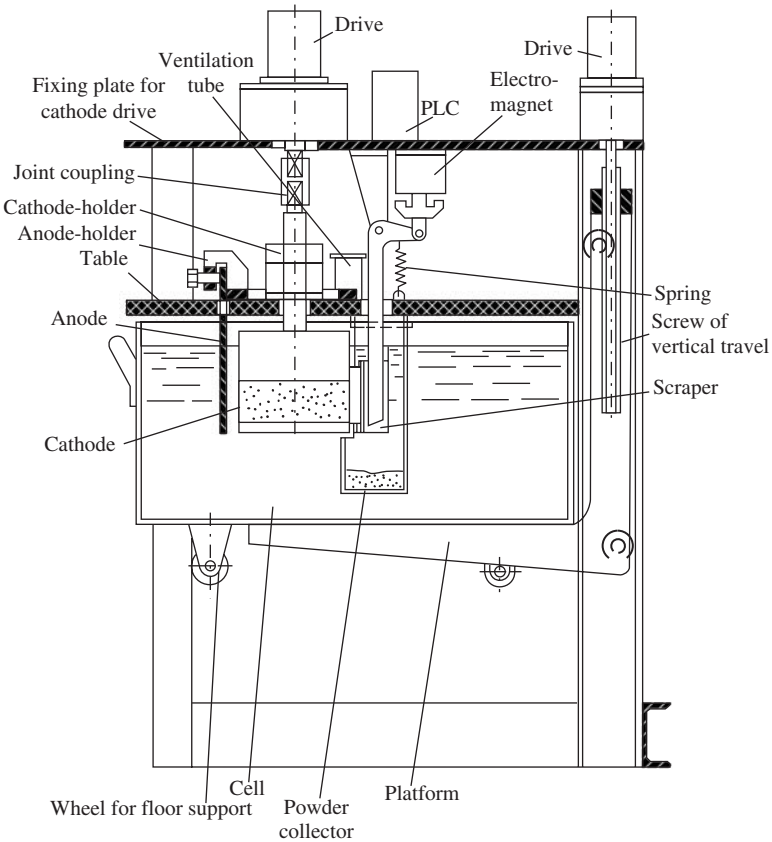

Figure 9.6 Cell with cylindrical cathode and automatic powder take-off from the cathode.

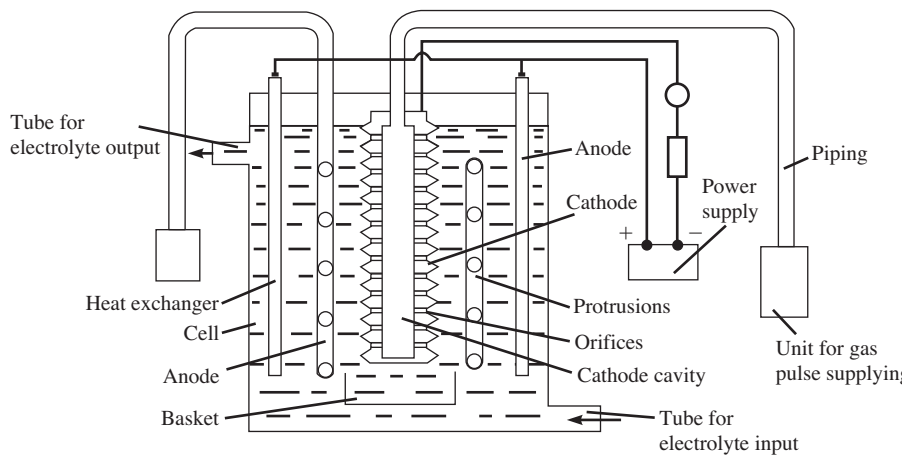

Figure 9.7 Electrolyzer with gas pulse supply to the cathode to take-off powder.

solution of a salt of the precipitated metal; the upper layer is an organic liquid (toluene, as a rule) that contains surfactants (oleic, palmitic, myristic and other acids) in the amount of 0.5–12%. Electric crystallization of fine whiskers, strands and elongated dendrites arises when the electrode passes through the water solution. The particles formed during cathode rotation pass into the layer of the organic

liquid and from here they are extracted by organic sol filtration or by centrifuge. The powder is rinsed by hot water, then it is washed free from residual organic substances by a mixture of water with spirit or acetone and dried under vacuum at room temperature. The obtained powders do not need surfactant stabilization against oxidization.

In process of crystallization of ultrafine elongated whiskers and strands precipitated from the two-layer bath several stages are distinguished:

- formation of a strong passive layer on the electrode surface
- metal ions discharge through the absorbing film by overcoming a high potential barrier
- development of three-dimensional nuclei on the electrode surface
- development of crystals inside the thin passive layer of the organic liquid
- growth of dendrites outside the film in the aqueous phase.

Under conditions of increased concentration of metal ions in the water phase, the discharge through the film of organic liquid occurs with overcoming of a high energy barrier and is controlled by the parameters of the barrier reaction. When diluted solutions of the water phase are used, diffusion factors control dendrite growth rate and qualitative links between particle structure and mass transfer parameters remain the same: particle size decreases when water solution is diluted, current density is increased and temperature is reduced. Surfactants influence the electrocrystallization process: whiskers, needles of constant section are formed due to the localization of electroprecipitation on their end surface, as crystal side faces are blocked by the layer of absorbed particles of the surfactant; the process is controlled by surfactant diffusion because of continuous nucleation and movement of growth steps with competing surfactant absorption.

In the case of precipitation from solutions saturated by surfactants, the value of the current density on the strand end is practically close to constant. According to Krichmar [1], if it is a small value and linear approximation of the absorption isotherm curve $X = G \cdot C_{SAA}$ (X is the surfactant concentration, G is the coefficient of proportionality for the linear part of the isotherm curve of Lengmoure) is taken, the rate of the process speed on the strand end is proportional to the surfactant concentration in the solution independently of its radius:

$$i \approx A\sqrt{C_{SAA}} \tag{15}$$

Introducing into the water layer a surfactant other than oleic acid that is usually present in the organic phase in the amount of 2–5 kg/m^3 is inadvisable as it can reduce dendrite wettability by the organic liquid and make difficult their transfer to the upper bath layer. As a result of the double effect (change of the proportion of organic phase components and variation of electrolysis parameter), the composition of the absorbed surfactant layer is controlled and particles not only of a certain structure, but also modified by oleic acid and oligomer, are produced. Epoxy silicon organic compounds are used as oligomers. Thermal treatment in hydrogen of the so produced powders improves their properties and increases powder resistance to oxidization.

Current efficiency of ultrafine disperse precipitation goes through a maximum with growing current density decreasing at too high current densities due to intense hydrogen emission. An excess quantity of the acid added to water phase to increase its electric conductivity leads to prevailing hydrogen discharge and reduces the current efficiency.

In alkaline media, an excessive increase of pH causes the formation of hydrates and a passivation of the electrode surface. A growth of metal ion concentration in the water layer leads to an increase of the current efficiency of the disperse precipitate. In electrolyzers, to produce metal organic sol, devices for continuous removal of disperse phase are provided (Figure 9.8). Through holes in the inner pipe the organic sol gradually goes outside through the hollow shaft. The boundary between water and nonwater layers shall be on the level of the upper line of the shaft. To reduce particle size of the organic sol, water-cooled hollow disks connected into a whole unit by the pipe are used (Figure 9.8). Particulate anodes in the form of containers made of mesh material are filled with metal chips. Laminar movement of the electrolyte around the cathode necessary for process intensification is provided by oscillatory motion of the cathode shaft.

A promising method for production of ultrafine metal powders is based on the use of emulsion devices with fixed electrodes. The method of a running magnetic field is proposed for production of ultrafine powders with the participation of non-equiaxed ferromagnetic particles (Figure 9.9). Coaxially located electrodes are placed inside an inductor that creates the mobile magnetic field. Ferromagnetic particles in the mobile magnetic field come into intense motion and stir up the electrolyte with the organic liquid. In the formed 'oil–water' emulsion, metal particles and the inner surface of the device are wetted with the organic liquid containing the surfactant. Ferromagnetic bodies are covered by a casing (for example, fluoroplast,

Figure 9.9) insoluble in the aqueous medium and organic liquid. Thus, ferromagnetic bodies that intensify the stirring efficiency of the near-electrode space do not participate in the electrode process themselves. Metal ions contained in the solution are reduced on the cathode.

The electroemulsion method involves pressing of the emulsion through the electrolyzer with fixed electrodes (Figure 9.10). The emulsion from the collecting tank is pumped through the electrolyzer by a centrifugal pump. The powder is separated by centrifuge or by magnetic separation. The velocity of emulsion motion in the electrolyzer of 0.01–10 cm/s makes it possible to intensify the process and to reduce the time of dendrite growth. Powders with particle size of 0.1 μm and specific surface of up to 30–60 m^2/g are produced [14].

Special Methods of Production of Metal Powders Recovered from Spent Solutions

High-efficiency methods of metal recovery from dilute solutions are based on the application of electrodes with developed surface together with an increase of the mass transfer coefficient that is achieved under respective hydrodynamic conditions in the electrolyzer. Metal electroprecipitation under such conditions occurs together with the formation of powder.

In the *Eco-cell* process (Ecological Engineering Ltd company design), a cathode in the form of a horizontally rotating cylinder (Figure 9.11) is used. The cathode is fixed on the shaft and surrounded by the coaxially located anode. An ion-change membrane is located between cathode and anode sections at a distance of approximately 10 mm from the cathode.

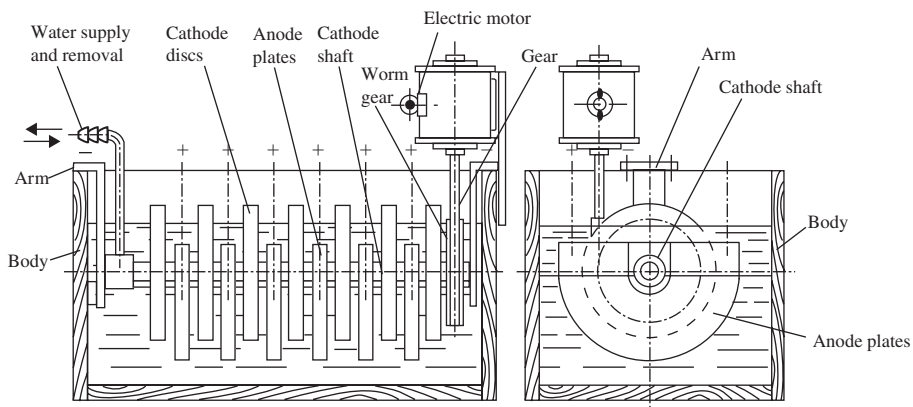

Figure 9.8 Electrolyzer with cooled cathodes and fluctuating motion of the cathode shaft.

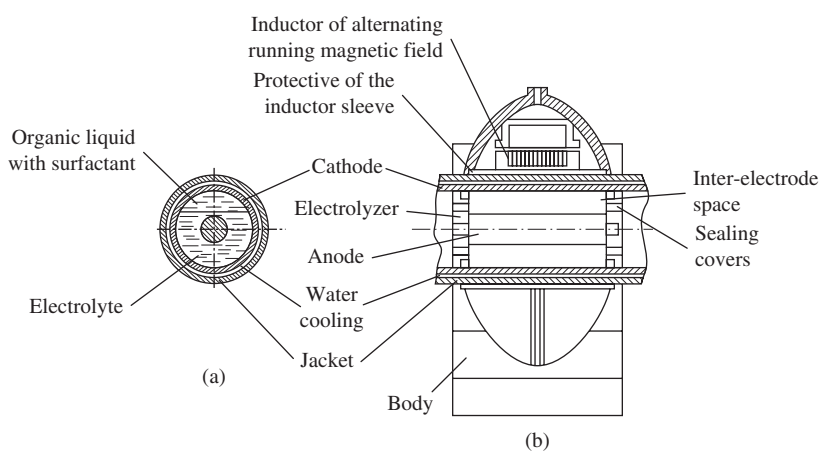

Figure 9.9 Unit for electrolytic production of ferromagnetic metals and alloys: (a) cross-section of electrode cell with cooling jacket; (b) longitudinal section of electrolyzer with cooling jacket in the inductor of alternating running magnetic field.

The powder is scrubbed from the cathode and removed by solution flow. Current connection is carried out by a sliding contact. The intensification is reached by the turbulence of liquid flow conditions even at low speeds of cathode rotation and this allows a significant increase of the current density. Thus, for metal recovery from solutions with concentrations of less than $1\,kg/m^3$, the cathode current density of $2–4\,kA/m^2$ can be used. The electrolyte is pumped through the cell at a predetermined speed. The metal is precipitated in the form of powder together with hydrogen emission. Gas is separated from the three-phase mixture in the gas-separator; the powder is extracted using a hydrocyclone or other type of thickener. Using the Eco-cell plant, it is possible to produce from solutions zinc, silver, manganese, cobalt, rhenium, rhodium, cadmium, palladium, indium, nickel, tin, iridium, platinum, gold, lead and rare-earth metals in the form of powder.

Series installation of several chambers with each of them working at a certain cathode potential allows a selective recovery of different metals from solutions (Table 9.3).

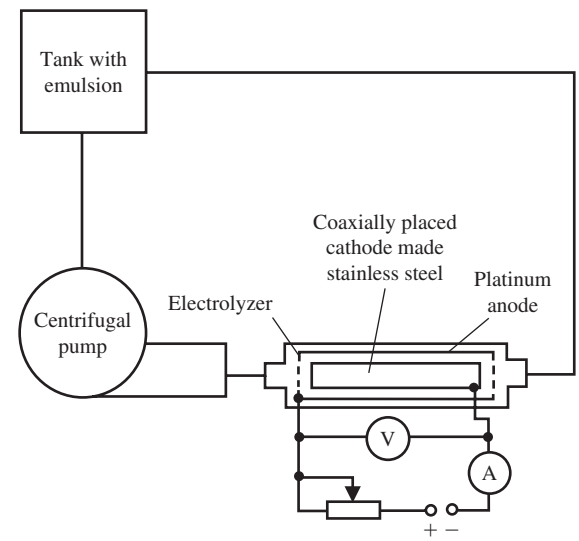

Figure 9.10 Flow-sheet for producing ultrafine powders by electro-emulsion mode.

Pump-cell

The process is activated on account of the high mass transfer coefficient in the inter-electrode space of two electrodes, the anode being rotated at a high speed and the cathode being fixed (Figure 9.12). In another variant, a bipolar electrode mounted on the ceramic axis is used. Dendrite particles up to 100 μm in size are removed from the interdisk space by electrolyte flow. The precipitation is carried out from solutions that contain up to $1\,kg/m^3$ of metal with a current density of $10\,kA/m^2$.

The electrolyzer with a rotating cylindrical layer of particles consists of two concentric perforated non-conducting cylinders (Figure 9.13(a)) and between them, conducting particles, cathodes are located. Two concentric metal mesh cylinders form anodes. The cathode cylinders are continuously rotated, so that conducting balls or particles interspaced inside them are interspersed. The electrolyte circulates through the electrolyzer. The metal is precipitated in the form of dendrites on the conducting particles inside the cathode cylinders and continuously crumbles into the bottom part of the electrolyzer, from where it is periodically removed into the collector. The thickness of the compact layer on conducting cathode particles is less than 0.01 mm.

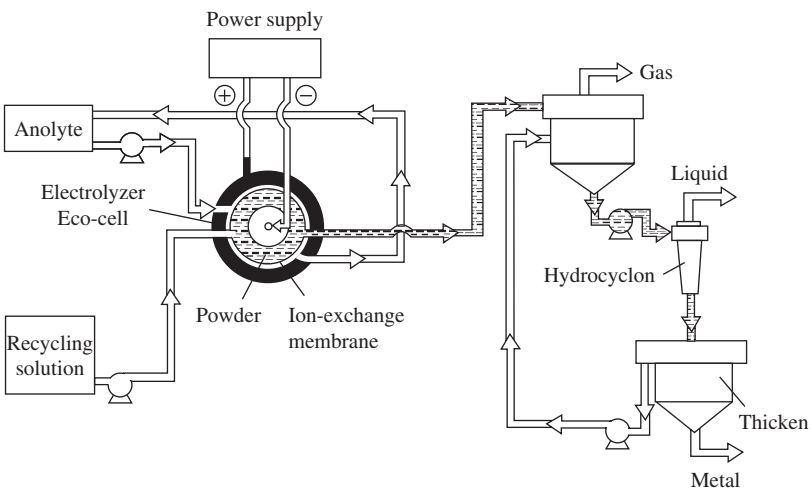

Figure 9.11 Plant Eco-cell.

Table 9.3 Parameters of selective metal extraction (Eco-cell process)

Extracted metal	Composition of origin solution (kg/m^3)	Final residual concentration of metal 10^3 (kg/m^3)
Silver	1.5 Ag; 0.9 Cu; 9.5 HNO_3	20 Ag
Copper	Cu/Zn (1:1); 147 H_2SO_4	10 Cu
Copper	Cu/Ni (1:1); 147 H_2SO_4	20 Cu
Silver, copper	Cyanide electrolyte pH 4; 0.02 Ag; 0.02 Cu	1.4 Ag; 3.0 Cu

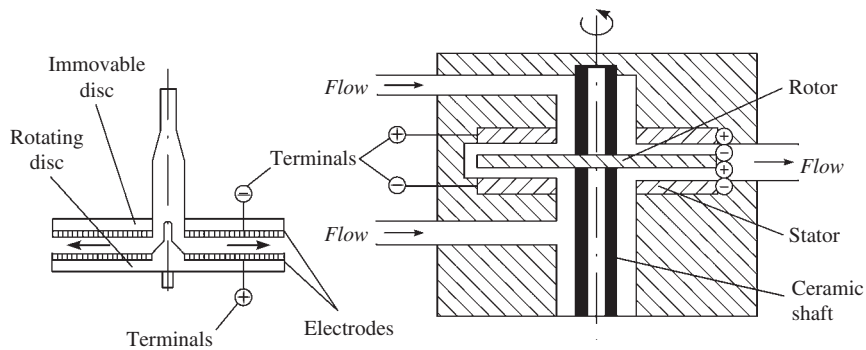

Figure 9.12 Scheme of the electrolyzer pump-cell.

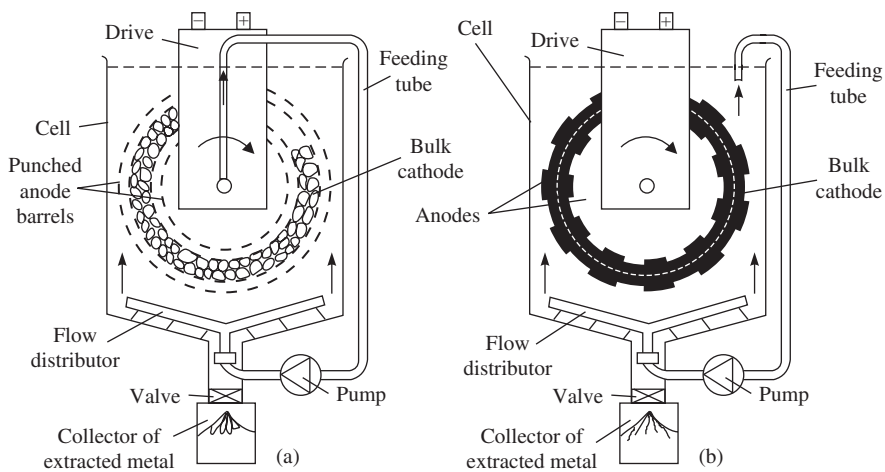

Figure 9.13 Electrolyzers: (a) with rotating cylindrical layer, (b) with striking rod.

In the electrolyzer with hammering rods (Figure 9.13(b)), the cathode consists of separate metallic rods with the ends sliding freely along ring-shaped metallic guides. The anode is in the form of two mesh cylinders located concentrically with the cathode-cylinder. The electrolyte is continuously pumped. The powder crumbles and is removed into the collector through the lock valve.

Both electrolyzers with a moving particle layer are designed for cadmium recovery from solutions containing cyanide. Metal precipitates on the cathode in the form of powder and cyanide ions oxidize on the anode to carbon dioxide. The cathode current efficiency starts to decrease significantly when the metal concentration reaches $10^{-3}\,kg/m^3$. Using the above-mentioned method, gold is recovered from

solutions with a concentration of 0.2 kg/m^3 (the final concentration is of 10^{-4} kg/m^3), silver is recovered from cyanide complex with a concentration of 5 kg/m^3 (down to 2×10^{-3} kg/m^3). This method is also applied to recover metals of the platinum group, copper, nickel and zinc.

A moving layer of steel balls 4.5 mm in diameter covered by an18 μm copper layer is used for copper recovery from the sulfate solutions. The balls fill up to 35% of the drum volume. Current is supplied to them using a free hanging lead ball 11 mm in diameter; the anode is a lead wire 3.1 mm in diameter placed along the horizontal drum axis.

Production of Metal Multicomponent Alloy Powders

The condition for the precipitation of metal alloy powders is the equality of discharge potentials of metal ions on dendrite tips. The electrocrystallization of the dendrite deposit proceeds under diffusion control and is located at the tips of growing dendrites. The conditions of mixed electrochemical kinetics with semi-spherical character of diffusion are realized:

$$E_j = E_{eq,j} - \frac{RT}{\alpha_j z_j F} \ln \frac{i_{tip,j}}{i_{0,j}} + \frac{RT}{\alpha_j z_j F} \ln \left(1 - \frac{i_{tip,j}}{i_{lim \cdot sp \cdot j}}\right) - \frac{2\gamma V}{z_j F r_{tip}} \quad (16)$$

where j is the number of alloy components.

The content of the component in the alloy is proportional to the current density of its reduction at the growing front $i_{tip,j}\ 2\pi\ r_{tip}^2\ N$, where N and r_{tip} are the density of location and the radius of alloy dendrite tips, respectively. For a two-component alloy:

$$\left(\frac{C_1}{C_2}\right)_{Alloy} = \frac{i_{tip,1}}{i_{tip,2}} \quad (17)$$

So far, diffusion limitations are not released from the growing front, the current densities $i_{tip,j}$ are comparable with limit currents of spherical diffusion $i_{tip,j} \approx i_{lim,sph,j}$ with the values proportional to the concentration of the components in the solution $C_{sol,j}$, mol/m^3,

$$i_{lim,sph,j} = \frac{z_j F D_j C_{sol,j} y}{\delta r_{tip}} \quad (18)$$

The combination of Eqns (17) and (18) gives the following:

$$\left(\frac{C_1}{C_2}\right)_{alloy} = \frac{z_1}{z_2}\frac{D_1}{D_2}\left(\frac{C_1}{C_2}\right)_{sol} \quad (19)$$

In aqueous solutions, the effective diffusion factors for different ions are close to each other, so that for $z_1 = z_2$, the proportionality coefficient $z_1 D_1 / z_2 D_2$ is close to one.

During electrolysis, the depth of diffusion limitations on the growth front of the dendrite deposit is gradually decreased and the potential shifts to the field of more positive values. In this case, the alloy component with a more electronegative potential may prove to be under conditions of activation discharge control; then the linear connection between $(C_1/C_2)_{alloy}$ and $(C_{0,1}/C_{0,2})_{sol}$ is violated and alloy composition depends upon the time of discontinuous precipitate accumulation on the cathode.

To provide diffusion control, alloys are precipitated from dilute solutions (the total concentration of metal salts is not higher then 0.2 mol/L) of simple electrolytes. The proportion of metal ions in the solution corresponds to their proportion in the alloy and a constant value of $(C_{0.1}/C_{0.2})_{sol}$ provides the stability of the alloy composition. If the difference between the equilibrium potentials of alloy components is too high (of the order of 1 V) then the electrochemical characteristics of metals (E_{eq}, i_0, α) may be juxtaposed by using their complex compounds. Meanwhile, it is important to support pH values for stabilization of ion composition of complex compounds as well as to avoid decrease of alloy current efficiency.

The methods of supporting constant solution composition depend on the nature of the anode reaction. When using insoluble anodes, it is necessary to make up the loss of reducing components in the electrolyte; an accumulation of ballast salts in the electrolyte is possible. If the soluble anodes are used, a periodical correction of electrolyte composition is required because of the difference of cathode and anode current efficiencies and uncontrolled current distribution between soluble anodes.

The most reliable method is the application of combined anodes (Figure 9.14) with independent adjustment of current in the circuit of each anode. The proportion between currents of soluble anodes shall correspond to the proportion of cathode currents of the reduction of alloy components and the part of the current passing though the insoluble anode shall be equal to 1.0 Ce_{all}, where Ce_{all} is the current efficiency.

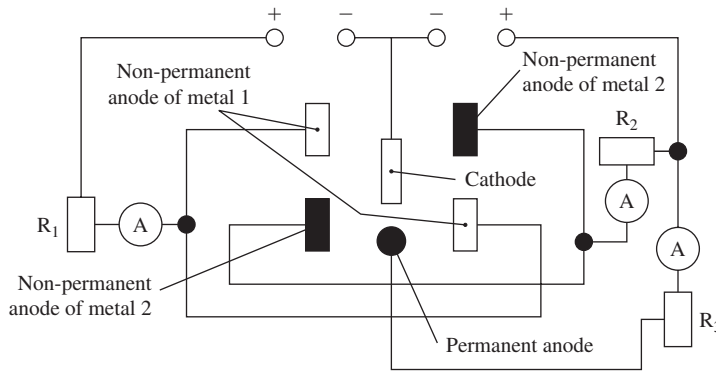

Figure 9.14 Electrical circuit to connect electrolyzer with combined anodes (R, rectifiers, A, ammeters; K, rheostats).

Alloy components can interact with each other with the formation of chemical compounds. Change of the partial mole Gibbs energy at the entrance of the *j*-metal into the alloy ΔG is expressed in the effect of depolarization, i.e. a shift of the equilibrium potential of the *j*-th metal component to more positive values:

$$\Delta E_{\text{all}} = \frac{\Delta G}{zF} \tag{20}$$

Usually the discharge of the component with more electronegative potential is obviously relieved in alloy formation. The kinetics of electrochemical reduction of metal ions depends on the nature and the character of the cathode surface that changes for each metal during alloy formation in comparison with individual discharge. If diffusion limitations on the growth front are released for any component, these effects are manifested in the change of alloy composition in comparison with one calculated according to Eqn (20).

Dispersivity, grain-size distribution and apparent density of alloy powder depend on the total concentration of metal ions and on the parameters of electrolysis (current density, temperature, pH, stirring mode). As in the case of precipitation of single component powder, the dispersivity of powders from multicomponent alloys increases, their apparent density lowers and flowability deteriorates with growing exhaust coefficient and vice versa.

The devices for producing powders of pure metals and multicomponent alloys are the same.

Powder Production Using the Method of Zone Electrochemistry

The method is based on a combination of zone chemistry and electrochemistry, and this allows the manufacture of nanopowders because of the following effects:

- substance transportation to the reaction zone is uninterrupted
- electrode surface is cleaned and degassed
- the rate of the electrochemical process is increased.

The idea of the method is that after each electrochemical impulse of constant current, during which metal nuclei form on the electrode surface, an ultrasonic (zone) impulse follows, the energy of which is the located in the reaction zone. It separates nuclei from the cathode surface and throws them into the solution.

In this method, the characteristics of impulse and zone electrolysis (interval between ultrasonic impulses, parameters of cathode-sample electrode, capacity of ultrasonic impulse) are added to the traditional factors that determine particle size and shape (solution composition, current density, electrolysis duration).

As under other electrolysis modes, the dominating particle size decreases with the growth of current impulse amplitude, with the dilution of the solution, when the time period between ultrasonic impulses is reduced and noticeably depends on their wattage. If the energy of ultrasonic impulses is low, then metal clusters formed on the cathode-sample electrode are not able to overcome the adhesion forces and to strip the deposit from the electrode into the solution. The clusters remaining on the surface affect every subsequent current impulse so that the nanoparticle yield is lowered. If the impulse energy is excessive, the temperature goes up immediately in the reaction zone, and it encourages disappearance of the transport control and leads to undesirable particle aggregation.

By means of zone electrochemistry, dendrite clusters consisting of branches like pearl necklaces can also be produced. Such formations are obtained if zone electrolysis is lengthy. One of the mechanisms of the formation of such structures is similar to the model of diffusion-limited aggregation. According to another model, particles suspended in the solution after contact with the cathode get a negative charge and act as a part of the cathode. The dependence of particle quality on a large number of parameters leads to especially high requirements to determine the range of their optimum values to provide high yield of particles of prescribed shape and size.

Contact Displacement Method (Cementation)

Electrolytically precipitated powder may be produced by the displacement of one metal M_2 from the solution due to conjugated dissolution of other metal M_1.

$$z_1 M_2^{Z_2^+} + z_2 M_1 \xrightarrow{z_1 z_2 e} z_1 M_2 + z_2 M_1^{z_1^+} \qquad (21)$$

To provide a high rate of this heterogeneous reaction, a large area of the cementing metal is provided by using it in the form of powder, chips, lumps and the intensity of the limited flow is increased. Due to excess of the precipitator, precipitated metal is deposited completely. After electrolytic precipitation, the solution is washed from the product and the precipitator surplus is eliminated (by acid solution treatment, by magnetic separation etc.).

The possibility of spontaneous proceeding of the process is estimated by the decrease of Gibbs free energy $\Delta G = zF(E^+ - E^-)$, where E^+ and E^- are respective equilibrium potentials. The reaction equilibrium is shifted to the contact deposition of M_2 metal if the initial potential of precipitated metal is more positive than the initial potential of M_1. Completeness of the precipitation is defined by equilibrium according to Nernst's equation:

$$E_{M_1} = E_{M_2} = E^0_{M_1} + \frac{RT}{z_1 F} \ln\left(\frac{a^{z_1^+}_{M_1}}{a_{st}}\right) = E^0_{M_2} + \frac{RT}{z_2 F} \ln\left(\frac{a^{z_2^+}_{M_2}}{a_{st}}\right) \qquad (22)$$

where $E^0_{M_1}$ and $E^0_{M_2}$ are standard potentials, a_{st} is standard activity equal to $1000\,mol/m^3$. The equilibrium ratio $a^{z_2^+}_{M_2} \Big/ a^{z_1^+}_{M_1}$ is calculated from the given expression. The thermodynamic completeness of the precipitation is shown in Table 9.4. Actually, the process is complicated by difficulties in kinetics of the reactions of both cathode reduction and anode dissolution.

The basis of electrolytic precipitation is corrosion (Figure 9.15). Electrolytic precipitation potential E is set where the cathode current I_c and the anode current I_a are equal. During electrolytic precipitation, the solution concentration and the state of precipitator surface are modified which leads to a change of polarization curve behavior as well as of potential

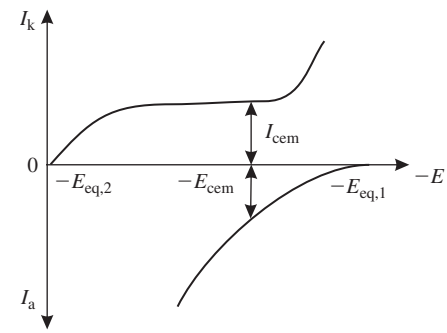

Figure 9.15 Polarization chart of contact displacement process.

Table 9.4 Parity for equilibrium activities for precipitated metal (M_2) and precipitator (M_1)

Precipitator M_1	Precipitated metal M_2	Standard potential of metal ($V_{(NHE)}$)		Equilibrium ratio $a^{z_2^+}_{M_2} \Big/ a^{z_1^+}_{M_1}$
		Precipitator	Precipitated	
Zinc	Copper	−0.763	0.34	1.0×10^{-38}
Zinc	Nickel	−0.763	−0.23	6.0×10^{-19}
Iron	Copper	−0.44	0.34	1.3×10^{-27}
Copper	Copper	−0.22	0.34	2.0×10^{-20}

and electrolytic precipitation rate. As simple solutions at high initial potential difference E_2 and E_1 are used, the metal M_2 is reduced by diffusion control with dendrite formation and accompanied by hydrogen evolution.

Metal is reduced on the tips of growing dendrites with tip location density at the growth front N (m^{-2}) and tip radius r_{tip}, and this process proceeds at current density i_{tip} (A/m^2) with current I_{M_2} per unit of area:

$$I_{M_2} = i_{tip} \cdot 2\pi N r_{tip}^2 \tag{23}$$

Around N_0 columns formed as a result of electrolytic precipitator contact with the solution the compact growth block of a radius r and a height h is spread over the surface:

$$I_{TAN} = i_{TAN}\, 2\pi N_0 rh \tag{24}$$

The precipitator M_1 is dissolved in areas free from the precipitated metal ($1 - N_0\pi r^2$):

$$I_{M_1} = i_1(1 - N_0\,\pi r^2) \tag{25}$$

The formed dendrite deposit has a volumetric specific surface S_w. Hydrogen is reduced both in precipitator M_1 areas free from dendrites with the rate $i_{H,1}$ and on developed surfaces of the precipitated metal with the rate $i_{H,2}$.

$$I_H = i_{H,2} \cdot S_w \cdot y + i_{H,1} \cdot (1 - N_0\pi r^2) \tag{26}$$

Dendrite growth rate and expansion rate of areas covered by the precipitated metal are described by Faraday's law in differential form:

$$\frac{dy}{dt} = \frac{V}{z_2 F} i_{tip} \qquad \frac{dr}{dt} = \frac{V}{z_2 F} i_{TAN} \tag{27}$$

where V m^3/mol, is mole volume of the precipitated metal. The precipitation rate of the metal on the growth front is determined by mixed kinetics at spherical character of diffusion [4]:

$$i_{tip} = i_{0,M_2}\left(1 - \frac{i_{tip}}{i_{sph}}\right) \cdot \exp\left[-\frac{\alpha_2 z_2 F}{RT}(E - E_{eq,2})\right] \tag{28}$$

On the area of the tangentially spread film, the metal is precipitated during diffusion control, as the effective value of the diffusion layer for the film is increased up to the value $\delta + y$ in advance of the dendrite deposit over a distance y:

$$i_{TAN} = \frac{z_2 FDC_2}{\delta + y} \frac{i_{lim}\delta}{\delta + y} \tag{29}$$

The precipitator dissolves according to the mechanism of delayed ionization:

$$i_1 = i_{0,M_1} \cdot \exp\left[\frac{(1 - \alpha_1) z_1 F}{RT}(E - E_{eq,1})\right] \tag{30}$$

Hydrogen emission rate is determined by its exchange current on the metal that is connected with the parameters of the kinetic equation as well as by its equilibrium potential $E_{eq,H}$:

$$\begin{aligned} i_{H,1} &= i_{0,H_1} \cdot \exp\left[-\frac{\alpha_{H1} F}{RT}(E - E_{eq,H})\right]; \\ i_{H2} &= i_{0,H_2} \cdot \exp\left[-\frac{\alpha_{H2} F}{RT}(E - E_{eq,H})\right] \end{aligned} \tag{31}$$

where $i_{H,1}, i_{H,2}$ are current densities of hydrogen discharge on the metals M_1 and M_2, respectively; i_{0,H_1}, i_{0,H_2} are exchange current densities for hydrogen on these metals; α_{H_1}, α_{H_2} are proper transfer factors for hydrogen on these metals.

The charge balance in this process is retained:

$$\begin{aligned} i_{tip}\, 2\pi N r_{tip}^2 + i_{TAN}\, 2\pi N r h + i_{H_2} S_w y + i_{H_1}(1 - N\pi r^2) \\ = i_1(1 - N\pi r^2) \end{aligned} \tag{32}$$

The dynamics of the electrocrystallization of the dendrite deposit is calculated by the solution of the system of differential equations that describe the behavior in time of its structural characteristics (y, r, r_{tip}) and of the potential. These equations are derived according to Faraday's law (Eqn 27), relations of electrochemical kinetics (Eqns 28–31), charge balance on the unit area of the electrode (Eqn 32), and conditions of its equipotential surface. It is solved numerically by the Runge–Kutt's method. In the case where an electrochemical system that excludes joint hydrogen reduction is used, this process is ignored [7].

As precipitator area is covered by the tangential film of the precipitate, the anode current density increases and the electrode potential becomes more positive. When $N_0\pi r^2$ reaches unity, the anode current density tends to infinity, the anode current decreases down to zero and the electrode potential

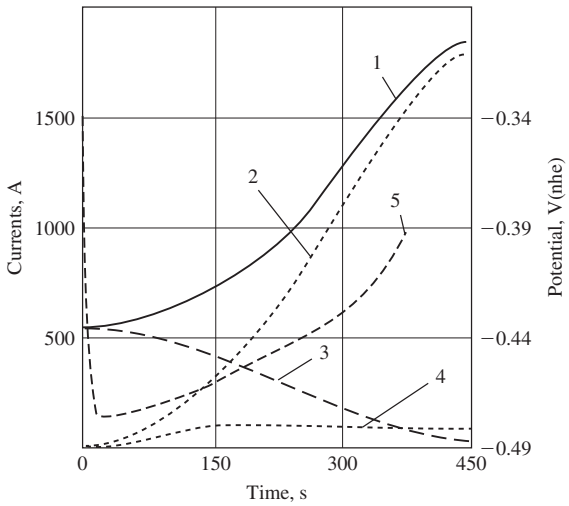

Figure 9.16 Current distribution per time and variation of precipitation potential (model calculation): 1, summary cementation current; 2, metal reduction current on the .deposit growth front; 3, current of hydrogen reduction on the metal-precipitator; 4, current of the distribution of tangential film; 5, potential alteration.

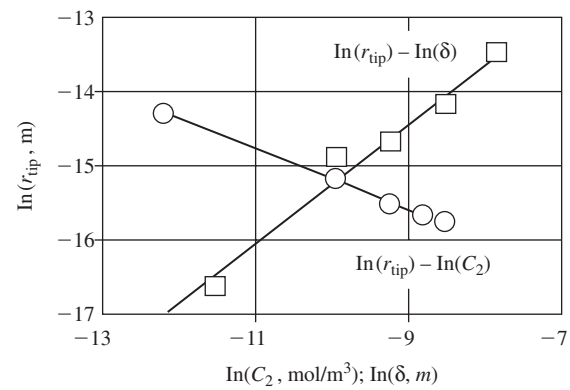

Figure 9.17 Trend of variation of predominate radii $(r_{tip_{max}})$ for dendrite tips of dendrite deposit depending on the parameters of cementation process: C_2, metal ions concentration, mol/cm^3; δ, thickness of diffusion layer, *m*.

sharply shifts to more positive values (Figures 9.15, 9.16). Later, the electrolytic precipitation process continues with negligibly small rate only through pores of the precipitated metal layer.

The solution of this task makes it possible to observe the behavior in the time domain of the dendrite tip radius and the current of metal M_2 reduction on tips of the growth front. This makes it possible to evaluate the distribution of the dendrite deposit over tip radii at various conditions of electrolytic precipitation (Eqn 5). As seen from these calculations, the higher the concentration of reducing metal ions in the solution, the larger the average dendrite tip radius (Figure 9.17). It increases also with the decrease of exchange currents of the metal M_2 and the precipitator. The average size of cement precipitator particles is changed in this direction too.

Besides, the longer the process, the larger are the particles.

The diffusion control of the process absolute at the moment of metal M_1 contact with the solution of the more electropositive component is reduced during electrolytic precipitation and can be changed for activation control. This causes difficulties in direct analytic description of the electrolytic precipitation. Besides, anode and cathode surfaces continuously change in the process of contact displacement. Numerical simulation seems to be the only possible method of adequate description.

All factors contributing to the instability of the flat growth front (see Table 9.1) lead to acceleration of dendrite growth, refining of produced particles and increase of powder specific surface. This is observed in the cases of dilute solutions, decrease of complexing ligand concentration, reduction of electrolyte conductivity and lowering of the cathode reaction polarizability. On the contrary, the extent of difficulties at the stage of the discharge and the acceleration of ion diffusion to the phase boundary lead to particle coarsening, increase of their apparent density and decrease of powder specific surface. Passivation of cathode areas by surfactants and hydroxides prevents the metal reduction and decreases the rate of electrolytic precipitation (Tables 9.5–9.8). Halogen anions, chloride ions, in particular, enhance powder dispersivity and formation of dendrite particles.

If both processes take place on the unchangeable equal surface of the cathodes S_k and the anodes S_a ($S_k = S_a = S$) and the displaced metal is reduced at the limit current, the solution depletion by ions of the discharging metal M_2 is described by first-order equation of reaction rate with rate constant K:

$$\ln \frac{C_2^0}{C_2} = Kt \tag{33}$$

where C_2^0 is the initial concentration of the solution.

The cases of delayed discharge of cathode and anode reaction are described most completely by Rotinyan–Heifez equation [1]

$$-\frac{dC_1}{dt} = K' C_2 \frac{x(1-\alpha_1)}{\alpha_2 - (1-\alpha_1)} \tag{34}$$

Table 9.5 Drum rotating velocity effect on intensity of copper precipitation with iron and powder properties

Process parameters	Drum rotation velocity (rpm)					
	0	10	20	30	40	50
Average rate of precipitation(kg/(m^2h))	0.21	0.29	0.37	0.40	0.43	0.18
Average particle size (μm)	100	115	131	139	148	165
Apparent density (kg/m_3)	1540	1800	2150	2660	2900	3140
Specific surface (m^2/kg)	60.0	57.1	53.2	40.0	38.0	33.0

Table 9.6 Precipitation parameters depending on duration between shaking of iron plates in the solution $CuSO_4$

Process parameters	Duration of deposit growth (min)				
	5	15	60	90	120
Average rate of precipitation (kg/(m^2h))	0.47	0.39	0.31	0.28	0.21
Average particle size (μm)	65	81	89	94	100
Apparent density (kg/m^3)	2910	2450	2000	1810	1540
Specific surface (m^2/kg)	60.0	52.0	58.0	49.5	48.1

where x is reaction order by ions of the reducing metal; α_2 and $(1 - \alpha_1)$ are apparent transfer factors of cathode and anode reactions; K' is combined rate constant that takes into account complexing ligand concentration in the solution, reaction order by them, relations of the surfaces of anode and cathode reactions, and electrolyte volume.

A chemical treatment of the product is most effective for cleaning the produced powder from precipitator residues. Sometimes such treatment is conducted in an inert atmosphere to prevent the produced powder from oxidation, or magnetic separation is applied.

Production of Powders by Electrolysis from Melts

Electrolysis from melts is used for producing electronegative metal powders. Their precipitation from water solutions is non-effective because of intensive hydrogen emission. High values of rate constants of electrochemical processes at high temperatures cause an insignificant polarizability and, as a result, the flat growth front becomes unstable long before the achievement of the limit current density.

As a rule, metals from melts are crystallized in dendritic form. To prevent the electrolyte from absorption of moisture and metal oxidation at high gas temperatures, the dendrite deposit is discharged from the electrolyzer in the form of solid dispersed bulk metal together with electrolyte salts. Further treatment of the powder consists of separation of powder and electrolyte either by mechanical milling, air separation, salt leaching or vacuum distillation of the electrolyte.

High electric conductivity of salt electrolytes allows use of high current densities that provide high efficiency of the process of metal takeoff and high current efficiency because of the absence of cathode hydrogen emission.

All the factors that lead to positive values of S_μ and S_E criteria (see Table 9.1) lead to the formation of small dendrites, and vice versa, the higher the metal salt concentration and temperature, the larger the electrolysis duration, and the lower the current density, the coarser are the powder particles formed. A passivation of growing faces by impurities, especially by non-metallic inclusions, by oxygen in particular, plays a significant role in dendrite structure. The passivation facilitates the increase of the nucleation rate of new crystallization centers and dendrite refining. At the same time, the increase of charge polarization on the passivated surface tends to make it smooth, so that crystals lose a strict faceting and look like spherolytes. The rate of dendrite elongation in melts is high due to high current density at the tip that achieves hundreds of amperes per square centimeter.

Table 9.7 Temperature influence on copper cementation rate with iron and on powder properties

Process parameters	Variation of process parameters for different solutions and temperatures (K)										
	0.4 mol/L $CuSO_4$				1.0 mol/L $CuSO_4$			0.4 mol/L $CuSO_4$ + 1.0 mol/L $CuSO_4$			
	298	318	338	358	318	338	358	298	318	338	358
Average rate of precipitation (kg/(m^2h))	0.21	0.76	1.04	1.26	1.91	2.34	3.62	0.30	0.38	0.68	0.65
Average particle size (μm)	100	79	68	62	187	91	81	135	165	183	200
Apparent density (kg/m^3)	1540	1280	810	560	1890	1760	1600	2030	2580	3000	3710
Specific surface (m^2/kg)	60.0	78.1	93.1	140.0	38.0	61.0	99.8	60.0	54.3	48.6	42.0

Table 9.8 Influence of solution composition on the copper precipitation rate and on powder properties

Process parameters	Variation of process parameters for different solutions and concentrations (mol/L)											
	$CuSO_4$					H_2SO_4 + 0.4$CuSO_4$			Na_2SO_4 + 0.4 M $CuSO_4$			
Average rate of precipitation (kg/(m^2h))	0.09	0.21	1.10	0.68	0.225	0.250	0.280	0.30	0.18	0.17	0.15	0.12
Average particle size (μm)	51	100	131	149	104	110	119	135	90	82	79	75
Apparent density (kg/m^3)	1600	1540	1710	2400	1560	1680	1880	2030	1470	1340	1250	1000
Specific surface (m^2/kg)	60.0	51.0	43.5	38.7	57.4	52.8	48.0	40.3	64.5	75.0	90.0	111.1

Table 9.9 Equation parameters for the growth of silver dendrites

Silver concentration (mass%)	Temperature (°C)	Direction of growth	$K \times 10^5$ cm/(s · mV)	n
Nitrate melt				
1	225	<112>	0.59	1.34
1	300	<112>	0.62	1.41
10	225	<110>	0.33	1.46
10	300	<112>	0.98	1.38
100	225	<110>	1.2	1.50
100	300	<112>	7.6	1.45
Chloride melt				
2	400	<112>	1.4	1.47
10	355	<112>	2.6	1.50
10	400	<112>	4.3	1.48
10	355	<112>	5.4	1.47

At controlled potential conditions, the experimental dependence for silver dendrite elongation v in over-voltage interval of 5–60 mV is the following:

$$v = K\eta^n \tag{35}$$

where K and n are growth parameters (Table 9.9).

At high cathode current densities, fine crystals of secondary powders are formed due to metal reduction by subions of eluted basic metals. When selecting the solvent salt, it is necessary to take into account a possibility to achieve lower electrolysis temperature and higher thermodynamic stability than the reduced metal compound. As a rule, equimolecular mixtures of metal chlorides (NaCl + KCl, KCl + LiCl, NaCl + KCl + $MgCl_2$, chloride and fluoride salts of metals) are used. The decomposition voltage of each of electrolyte components is defined by the equation:

$$E = -\frac{\Delta G}{zF}$$

where ΔG is a modification of Gibbs free energy at the formation of a given compound.

It is necessary to supply periodically or continuously the salt of the precipitated metal to the electrolyte and to add solvent salts carried away by the discharged cathode deposit. Metals and conductive metal-like compounds (carbides, nitrides, oxycarbides, carbonitrides) are used as soluble anodes.

The following factors can cause a decrease of powder yield in relation to current:

- chemical dissolution of eluted metal interaction with the solvent
- disproportionation reaction accompanied by the formation of low-valency ions
- reaction of reversed oxidation of metal in the anode area as a result of its convection or diffusion transfer
- recombination of the products of cathode and anode processes
- reduction of metals with more negative potential.

The following measures promote the increase of powder yield with respect to current:

- addition to the electrolyte of salts with cations having more negative potential and decreasing metal solubility in the electrolyte
- separation of anode and cathode areas by a diaphragm
- maintenance of temperature and current density at the optimum level.

As the temperature rises, current efficiency passes through a maximum. An excessive temperature increase intensifies chemical dissolution and facilitates diffusion and convection transfer of active substances to the anode area. At low temperature, the maximum process rate defined by the limit current density is decreased. Besides, the lower the temperature, the lower the melt electroconductivity and the larger is the specific power consumption.

The current efficiency increases when current density increases up to i_{lim}; then a growth of the part of commoving metal impurities with more negative potentials takes place. Anode passivation starts. All these processes decrease the powder yield relative current (powder current efficiency). At high anode

Table 9.10 Parameters to calculate distribution under powder particle size

Metal	*a*	*b*	α_0	*m*
Copper	1030	0.18	0.37 ± 0.015	6.8 ± 0.10
Iron	200	0.10	0.39 ± 0.01	6.7 ± 0.65
Manganese	205	0.10	0.36 ± 0.01	6.5 ± 0.60
Titanium	172	0.10	0.39 ± 0.02	7.3 ± 0.03
Tungsten	81	0.34	0.32 ± 0.01	6.7 ± 0.03

current density cation oxidation reactions are possible, for example:

$$Ti - 2e = Ti^{2\pm}; \quad Ti^{2+} - e = Ti^{3+}$$

At a 'critical' current density there is the possibility of an 'anode effect' (abundant gassing on the anode that leads to reducing the contact of the electrolyte with the anode, spark formation, and increase of the resistance, especially when the electrode is wetted poorly by electrolyte), which is undesirable. To increase the 'critical' current density, the surfactants improving anode wettability, chlorides of basic metal and oxides of the reduced metal (if oxygen is permissible in the melt) are injected into the electrolyte. If the metal oxide is considered to be an electro-active substance, the anode effect is permitted to appear with a certain regularity as the index of the oxide concentration factor in the melt.

The parameters of producing disperse precipitates of various metals are generally the same, normally sodium chloride or its eutectics with potassium chloride are used. The melt contains 10–20% of metal chlorides (usually between 3 and 7% calculated for the metal). The electrolysis temperature is between 970 and 1140 K; high cathode current density of 5–15 kA/m^2 is maintained; anode current density does not exceed 4 kA/m^2.

High densities of metal exchange current in molten media cause a rapid increase of the area of the precipitate growth front and cancel the diffusion control. This causes a corresponding coarsening of dendrite crystals during electrolysis and the deposition of the product in the form of large powder particles.

Statistical models that relate the average particle size (r_{av}) with current density and metal concentration (C, mass%) are true under the following conditions: current density of i = 5–34 kA/m^2, temperature of 1000–1020 K, metal concentration of 2–8% (in mass), the background is the equimolar mixture KCl–NaCl; precipitation time is 2 hours. According to the experimental data, the average size of powder particles obtained by electrolysis was calculated:

$$r_{av} = \Sigma \alpha_j \cdot r_j \tag{36}$$

where $r_j = 0.5 \cdot (r_{j-1} + r_{j+1})$, α_j is the total mass share of powder particles of j-th fraction in the total powder mass.

The following statistical ratio between the average particle size and electrolysis conditions is valid for metals indicated in Table 9.10:

$$r_{av} = a\left(\frac{C}{i}\right)^b \tag{37}$$

The values of constants a and b are presented for various metals in Table 9.10.

The ratio (Eqn 38) can be used to estimate the average size of powder particles in new conditions referred to the interval mentioned above. Particles are distributed around the average size under Gauss law. The fraction of particles of the size r_j with the accuracy of ±20% can be calculated by the equation:

$$\alpha_j = \alpha_0 \cdot \exp(-m^2 \Delta r_j^2) \tag{38}$$

where α_0 and m are constants for the given metal (see Table 9.10). By calculat–ing the values of α_j for a number of values Δr_j (deviations from the average value r_{av}) the curve of powder particle size distribution is obtained. The values exp $(-m^2 \Delta r_j^2)$ are obtained when using the function $\varphi(m, x) = 2/\sqrt{\pi} \cdot e^{-m^2 x^2}$ which is tabulated.

In this case it is simpler to calculate the α_j value by the formula:

$$\alpha_j = 0.885 \alpha_0 \, \varphi(m, \Delta r) \tag{39}$$

Calculations of ratios, Eqns 38–40 are based on the following dimensionalities: [i] A/cm^2; [c] mass%; [r_{av}] μm.

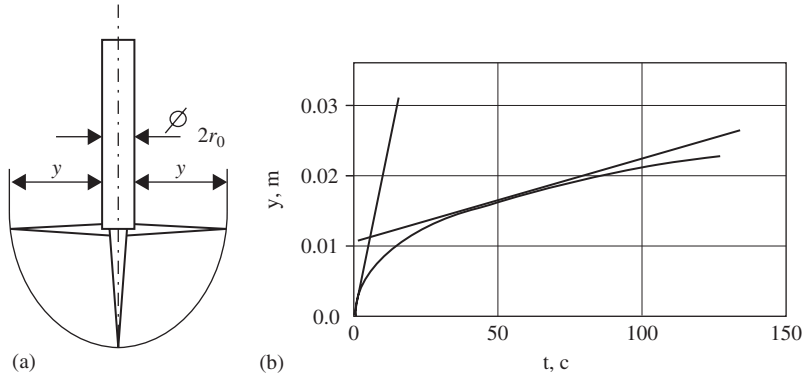

Figure 9.18 Formation of the hemispherical front by dendrites at the end of cylindrical electrode (a) and dynamic of its elongation (b) $r_0 = 2$ mm, I = 2A; $r_{tip} = 2 \times 10^{-6}$ m; $N = 3 \times 10^7$ m^{-2}; $V = 9.55 \times 10^{-6}$ m^3/mol.

When simulating the dendrite crystallization from the melt, the growth front on the cylinder end can be presented in the form of a hemisphere with radius $r_0 + y$ that increases in the course of time (Figure 9.18(a)). For the set current (I) at a dendrite arrangement density on the growth front N the differential equation for dendrite elongation (Eqn (40)) can be obtained and, after separation of variables and integration, Eqn (41) for the dependence of the dendrite length y on the time t (Figure 9.18) is obtained:

$$\frac{dy}{dt} = \frac{V}{zF} \cdot \frac{I}{4\pi^2 (r_0 + y)^2 r_{tip}^2 N} \tag{40}$$

$$r_0^2 y + r_0 \cdot y^2 + \frac{1}{3} \cdot y^3 = \frac{V}{zF} \cdot \frac{1}{4\pi^2 r_{tip}^2 \cdot N} t \tag{41}$$

The dendrite growth rate decreases in the course of time and leads to a non-homogeneous structure of the product. But, at any moment, dendrites can be lengthened linearly (see Figure 9.18(b)) by the selection of the cathode lifting speed equal to the dendrite growth rate. In this case, constant precipitation conditions are maintained on the growth front and, consequently, a homogeneous dendrite precipitate will be obtained. Structural characteristics of the dendrite precipitate are defined by the set current value and the speed of cathode lifting [1,7].

The electrolyzer with soluble anodes and immovable cathodes is a vessel with anodes and cathode cores and an inlet for inert gas injection. The graphite sleeve in the electrolyzer fulfills simultaneously the function of anode current supply in the cell with the diaphragm. A design of electrolyzer with the transfer of the cathode precipitate to a water-cooled chamber is known (Figure 9.19). The electrolyzer with the precipitate cut under electrolyte layer allows discharge without lifting the cathode. The precipitate, cut by a knife, falls into a basket that moves under each cathode in turn. Then the precipitate goes to the chamber for collection and cooling. The slime together with the electrolyte is squeezed through metal–ceramic filters.

Amalgam Metallurgy Method

Dendrites are crystallized in a mercury electrode as a result of the formation of oversaturated amalgams after achieving the limit of metal solubility in mercury (Table 9.11). The stability of mercury and amalgam depends upon the nature of anions in the solution (Table 9.12).

The metal is precipitated either by electrolysis on the liquid mercury cathode or by electrolytic precipitation by amalgam of a more negative metal (Figure 9.20).

When the metal is precipitated in the form of amalgam, continual use as the anode means that more positive impurities are left in the amalgam-anode and more negative impurities remain in the solution. The Volta series for amalgams differs from that for pure metals and depends upon the amalgam phase composition. The following Nernst equation is presented for a single-phase amalgam:

$$E = E^0_{M(Hg)} + \frac{RT}{zF} \ln \frac{a_{M^{z+}}}{a_{M(Hg)}} \tag{42}$$

where $E^0_{M(Hg)}$ is amalgam standard potential that differs from the standard potential of pure metal; $a_{M(Hg)}$ is metal activity in amalgam; $a_M{}^{z+}$ is the activity of metal ions in the solution. The standard potential of

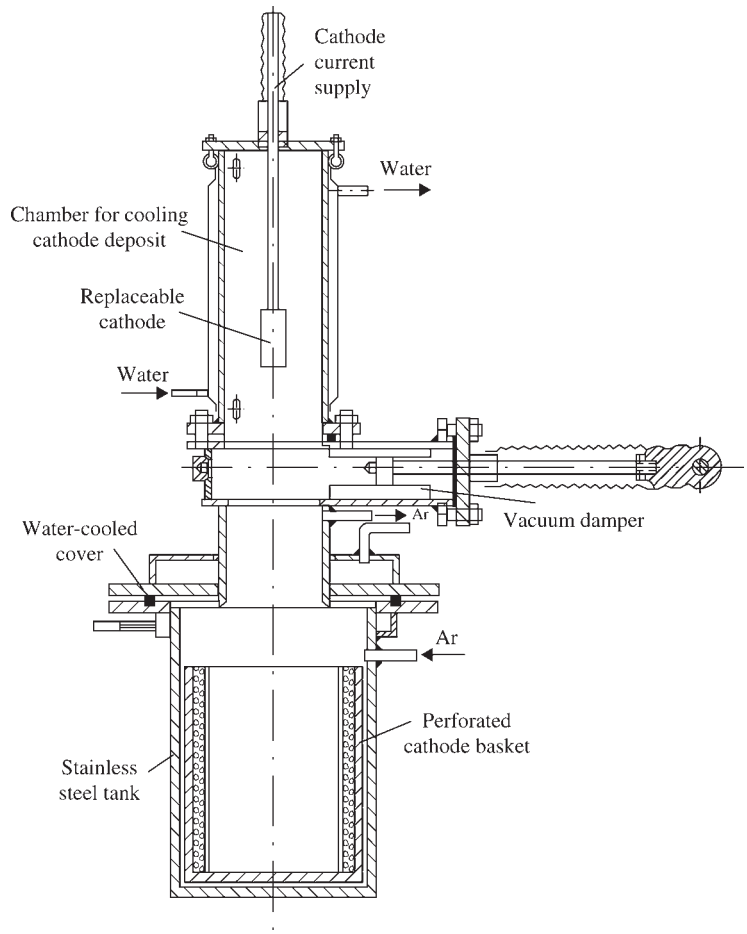

Figure 9.19 Scheme of electrolyzer for electrolytic refining of tungsten.

the amalgam is connected with the standard potential of pure metal (see Table 9.12) by the following relation:

$$E^0_{M(Hg)} = E^0_M + \frac{RT}{zF}\ln(a^{sat}_{M(Hg)}) - E_s \qquad (43)$$

where $a^{sat}_{M(Hg)}$ is metal activity in its saturated amalgam,

$$E_s = -\frac{\Delta G^0}{zF} + \frac{RT}{zF}\ln(a^{sat}_{Hg})^y \qquad (44)$$

ΔG^0 is the change of Gibbs free energy for the process of the formation solid phase that is in equilibrium with the amalgam liquid phase, a^{sat}_{Hg} is mercury activity in the saturated amalgam, y is the number of mercury moles for one metal mole in the amalgam solid phase.

In surface layers of the mercury, a supersaturated solution of metal being reduced is formed and conditions for homogeneous crystallization of metal nuclei of a size defined by the degree of amalgam oversaturation are created. Nuclei crystallization leads to amalgam depletion by metal atoms near the newly formed surface; reduced particles flow through the 'solution-mercury' phase boundary. This flow is determined by the set current density. Dendrites are crystallized under conditions of substance diffusion delivery through the amalgam layer to the surface of growing crystals.

The rate of dendrite lengthening is defined by current density on the boundary 'solution-mercury', by the number of nuclei N, m^{-2}, formed and their cross-section A, m^2, (for Co about 5 nm^2):

$$\frac{dy}{dt} = \frac{V}{zF}\frac{I}{N \cdot A} \qquad (45)$$

where V is the value of metal mole volume.

Table 9.11 Metal solubility in mercury (%(at))

Metal	Temperature (°C)			
	25	100	200	350
Indium	70.3	83.7	N/s	N/s
Thallium	43.7	56.1	76.9	N/s
Cadmium	10.1	31.9	66.7	N/s
Zinc	6.4	22.0	44.1	81.87
Lead	1.9	17.9	63.1	N/s
Bismuth	1.6	25.0	68.9	N/s
Tin	1.2	29.8	83.8	N/s
Gallium	3.6	6.8	43.5	N/s
Magnesium	3.0	9.07	22.31	28.1
Ruthenium	0.694			
Gold	0.13	0.60	2.47	26.18
Silver	0.078	0.41	1.75	10.86
Rhodium	0.012			
Aluminum	0.015	0.089	0,5	3.0
Palladium	0.012			
Uranium	0.0031	0.025	0.18	1.11
Neodymium	0.0099	0.045	0.21	0.22
Gadolinium	0.00487	5.53×10^{-2}	0.22	2.87
Samarium	0.00644	5.53×10^{-3}	0.21	0.82
Magnesium	0.00371	4.62×10^{-2}	0.32	2.24
Niobium	0.002	N/a	N/a	N/a
Iridium	0.001	The same	The same	The same
Thorium	0.00136	4.5×10^{-3}	0.011	0.052
Silicon	0.007	3.71×10^{-2}		
Copper	0.00742	3.71×10^{-3}	0.18	0.94
Vanadium	0.00022	N/a	N/a	N/a
Nickel	1.52×10^{-5}	1.7×10^{-4}	N/a	0.0123
Molybdenum	4×10^{-5}	N/a	The same	N/a
Tungsten	1×10^{-5}	N/a	N/a	N/a
Titanium	2.05×10^{-3}	9.2×10^{-5}	6.15×10^{-4}	7.12×10^{-3}
Zirconium	2.25×10^{-6}	1.86×10^{-5}	1.85×10^{-4}	9.21×10^{-4}
Chromium	6.19×10^{-7}	4.58×10^{-6}	2.27×10^{-6}	9.1×10^{-5}

N/s – non-soluble; N/a – non-available.

Table 9.12 Values of standard potentials of mercury in various media (V (nve))

Reaction	Potential
$H_2 + 2OH^- = H_2O + H_2O + 2e$	0.926
$2Hg + SO_4^{2-} = Hg_2SO_4 + 2e$	0.615
$2Hg + CrO_4^- = Hg_2CrO_4 + 2e$	0.41
$2Hg + 2IO_2^- = Hg_2(IO_3)_2 + 2e$	0.394
$2Hg + 2Cl^- = Hg_2Cl_2 + 2e$	0.268
$Hg + 4Cl^- = HgCl_4^{2-} + 2e$	0.48
$2Hg + 2Br^- = Hg_2Br_2 + 2e$	0.139
$Hg + 4Br^- = HgBr_4^{2-} + 2e$	0.21
$2Hg + 2CNS^- = Hg_2(CNS)_2 + 2e$	0.22
$2Hg + 2OH^- = Hg_2O + H_2O + 2e$	0.123
$2Hg + 2I^- = Hg_2I_2 + 2e$	0.041
$Hg + 4I^- = HgI_4^{2-} + 2e$	0.04
$Hg + 4(CN)^- = Hg(CN)_4^{2-} + 2e$	−0.37
$Hg + S^{2-} = HgS + 2e$	−0.70

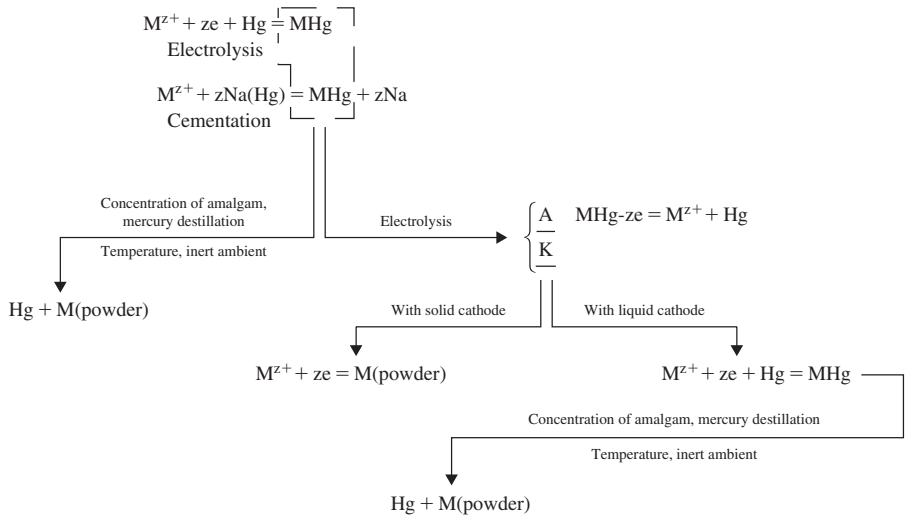

Figure 9.20 Modes of producing metal powders in amalgam metallurgy.

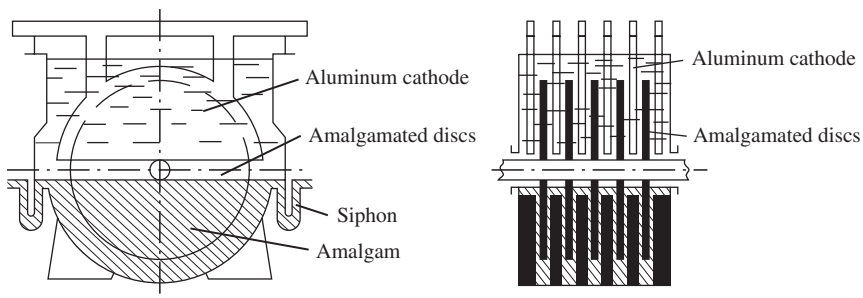

Figure 9.21 Gonsberg cell with rotating disk anodes: 1, aluminum cathode; 2, amalgamated discs; 3, siphon; 4, amalgam.

Factors increasing particle flow (increase of the current density, growth of temperature, mixing of mercury and solution) cause dendrite coarsening. Amalgams are formed by electrolysis and metals are precipitated on solid cathodes in Gonsberg's cells (Figure 9.21).

Steel amalgamated plates fitted on a slowly rotating shaft serve as anodes and feed new portions of the amalgam to the upper space containing the electrolyte.

Electrolyzers with amalgam bipolar electrodes are used to produce high-purity powders (Figure 9.22). The electrolyzer consists of series of concatenated isolated cells separated by a vertical partition that does not touch the bottom. To exclude electrolyte ingress into the next cell, a plate from an easily amalgamated metal hardly soluble in mercury is inserted in the slot in the bottom part of the partition.

For metal electrolytic precipitation by amalgams, there are in use units in which amalgams and solution are strongly mixed with an agitator. Drum precipitating devices are used to recover metals from flowing solutions. These units operate in the conditions of countercurrent flow of amalgam by means of centrifugal or magnetic pumps.

Fine powders of copper, gold, silver, cobalt, niobium, molybdenum, chromium, vanadium, tantalum, zirconium, hafnium and other metals hardly soluble in mercury are produced by precipitation from aqueous organic medium on a rotating cathode (Figure 9.23).

An oily solvent film with mercury dispersed in it is applied to the cathode surface with a roller. The electrolysis takes place in an inert atmosphere; the gas is supplied separately to anode and cathode areas separated by a diaphragm. The cathode deposit is removed from the cathode by a scraper after oil is applied to the cathode surface with a grease gun.

Amalgam is filtered in a nutsch-filter or filter press and treated in a distillation furnace. Amalgam is fed in by a screw conveyer. Inert gas or hydrogen is supplied by countercurrent flow and carries mercury fumes to a cooler. In the predistillation zone, a

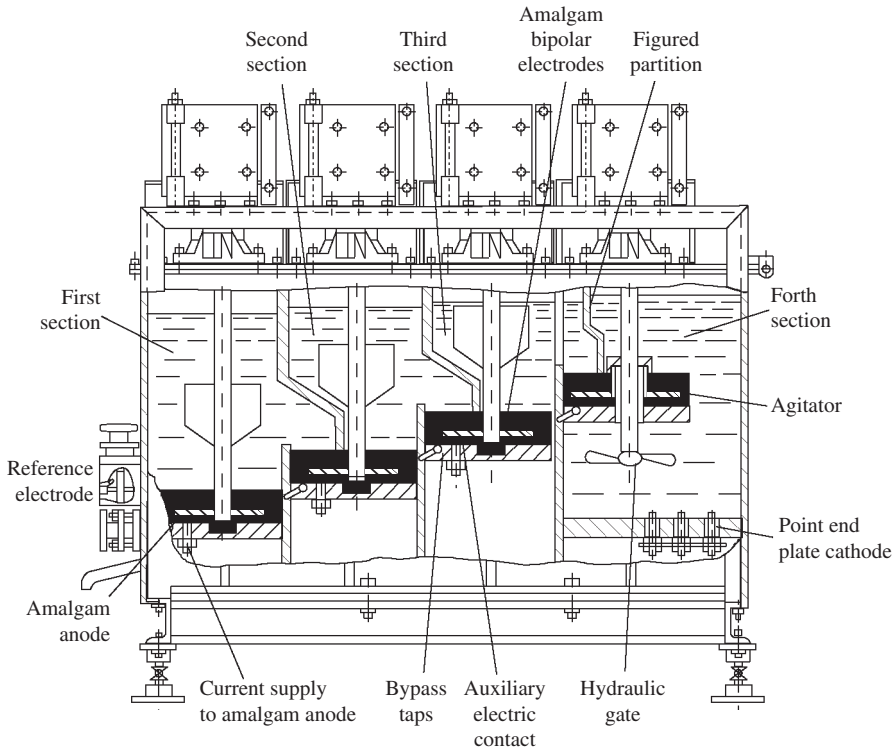

Figure 9.22 Industrial electrolyzer with cascade bipolar amalgam electrodes.

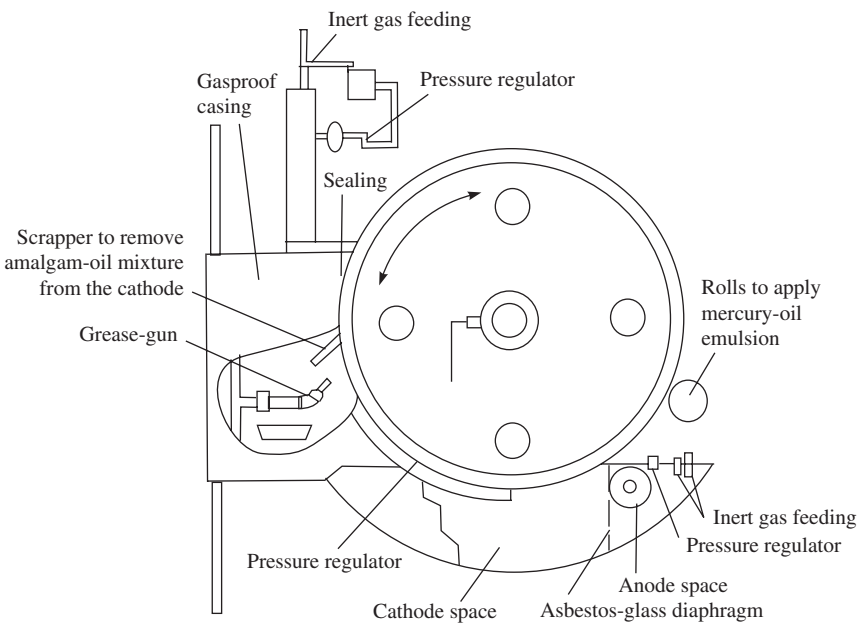

Figure 9.23 Electrolyzer for producing fine metal powders.

temperature of 670–770K is maintained, while 870K is the baking temperature. Dendrites are separated from mercury by heating under vacuum or in an inert gas atmosphere. When using amalgam as the anode together with solid (liquid) cathode, a supersaturated solution is formed and fine dendrites are then separated from mercury by a subsequent process.

References

1. Naboychenko, S.S. (Ed.) *Handbook of Non-ferrous Metal Powders*. Metullurgiya, Moscow, 1997 (in Russian).
2. Taubenblat, P.W., Chemical and electrolytic methods of powder production. In *ASM Handbook*, Vol. 7, *Powder Metal Technologies and Applications*. ASM International Publishers, 1998, pp. 67–71.
3. Baraboshkin, A.N., *Electrolytic Crystallisation of Metals from Melt Salts.* Nauka, Moscow, 1976 (in Russian).
4. Nichiporenko, O.X., Pomosov, A.V., Naboychenho, S.S., *The Powders of Copper and of its Alloys*. Metullurgiya, Moscow, 1988 (in Russian).
5. Despic, A.R., Popov, K.I., *The Modern Aspects of Electrochemistry*, Vol. 7. Plenum Press, New York, 1972, pp. 199–313.
6. Newman, J.S., *Electrochemical Systems*. Prentice-Hall Inc., Englewood Cliff, 1973.
7. I.B. Murashova, Pomosov, A.V. *Crystallisation of Metals as Dendrites*, edited by VINITI Itogi nauki, Vol. 31, Moscow, 1989, pp. 55–110 (in Russian).
8. Ivanovsky, L.E., Rozanov, I.G., Zotin, I.V., Khramov, A.P., Metal dendrite deposits production by electrolysis of ion melts and their application. *Melts*, 1997, 2:51–69 (in Russian).
9. Murashova, I.B., Khramov, A.P., Zotin, I.V., Zaikov, Yu.P., Zyryanov, V.G., Electrocrystallization of fibrous silver deposits from nitrate melts. Experience and modelling. *J. Min. Metal*, 2003, 39(1–2): 137–147.
10. Murashova, I.B., Ostarkova, G.V., Burchanova, N.G., Modelling structural changes in the deposit during galvanostatic electrolysis and contact deposition of metals. *Electrochemistry*, 2002, 38(3):284–289 (in Russian).
11. Mason, T.J., *Practical Sonoelectrochemistry*. Ellis Horwood, Chichester, 1991.
12. Mandelbrot, B.B., *Fractal Geometry of Nature*. Freeman, San Francisco, 1983.
13. Qiu, Xiao-Feng, Xu, Jin-Zhog, Zhu, Jian-Ming, Zhu, Jin-Jie, Xu, Shu, Chen, Heng-Yan, Controllable synthesis of palladium nanoparticles via a simple sonoelectrochemical method. *J. Mater. Res.*, 2003, 18(6):1399–1404.
14. Khimchenko, Yu.I., Fil, T.I., Katsyuk, O.A., New electrolytic methods for the production of very fine metal powders. *Powder Metallurgy and Ceramics*, 1983, November: 424–427.

Chapter 10

Powders for Porous Powder Metallurgy Technology

Oleg D. Neikov, Frantsevich Institute for Problems of Materials Science (IPMS), Kiev, Ukraine

Porous powder metallurgy (PM) materials find a wide variety of applications. Using similar technique and manufacturing equipment as structural PM components, porous PM materials are commonly sintered to densities between 25 and 85% of theoretical mean density (TMD), while structural PM parts are typically 85–99.9% of TMD. These designed materials provide specialized productions for applications such as filters, self-lubricating bearings, battery electrodes, flow-control devices and flow restrictors, shock-absorbers, floating structures and boundary layer control.

Cellular materials as metal foams are a species of porous PM materials. Even pure metals and metallic alloys can be produced as cellular solids or metal foams. Cellular materials find wide use in techniques for constructing, cushioning, damping, insulating and filtering and in many other applications. Highly porous materials have a high stiffness combined with a very low specific weight due to very high porosities that can achieved – above 80–85%. Because of this, cellular materials are frequently used as construction materials.

Porous Powder Metallurgy Technology

The powder metallurgy processing method is decisive for determining the final mechanical properties and porous characteristics of the porous product. Selection of the production method is based on the powder characteristics and the type of porosity required by the application. The preparation of the powders, the use of additives, the compaction methods and the sintering conditions must be closely controlled to produce uniform and repeatable porous characteristics.

Material Selection

A wide variety of PM materials can be selected depending on the application requirements and economics. The porosity is determined by the particle size distribution, particle shape, powder surface morphology and other powder characteristics that are dependent on the production technique. Because the powder characteristics are one of the major factors in determining the porous properties of the finished product, reproducible powder characteristics and manufacturing methods are critical to the production of a consistent product.

Bronze, nickel and nickel-base alloys are the most common porous PM materials, but other non-ferrous metals such as aluminum, copper, gold, niobium, silver, tantalum, titanium and zirconium are fabricated into porous materials from powder [1].

The size distribution of particles can be as a direct result of the powder production process or can be altered by classification techniques.

Bronze powders containing 89–90% Cu, 10–11% Sn and 0.1–0.5% P are the most common material for porous bronze PM parts such as filters and self-lubricating bearings. Small additions of phosphorus improve mechanical strength [2,3]. More information on bronze PM products can be found in Chapter 16.

Bearings can be manufactured from premixed elemental powders or prealloyed powders. Air or inert gas atomization of prealloyed 89/11 or 90/10 bronze yields spherical particles that can be processed to low densities by gravity sintering, as illustrated in Figure 10.1 [4]. Bronze particles were also made by coating atomized copper powder with tin with a size range of 10–850 μm depending on the powder type. Rounded particles are made by cutting tin-coated copper wire with a composition of 93–97% Cu and 3–7% Sn [5].

The filamentary-type nickel powders produced by carbonyl decomposition with fine particle size and narrow size distribution are possible using the porous PM process. This process can result in uniform pore material after working, as shown in Figure 10.2. Components with higher porosity and finer pore sizes are produced by applying very low compaction pressures less than 7 MPa [6].

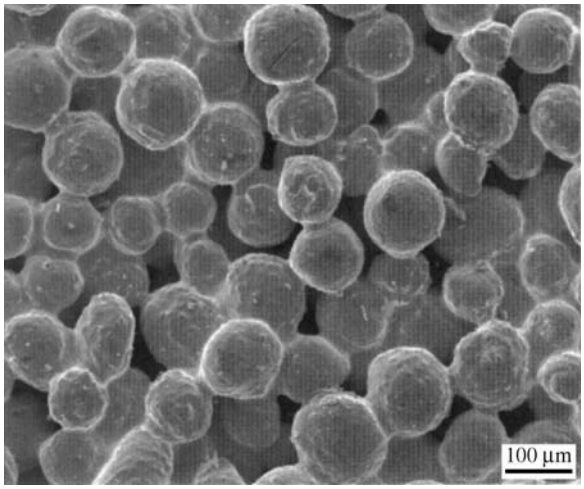

Figure 10.1 Bronze particles gravity sintered to 64% density. (Source: Ref 4®)

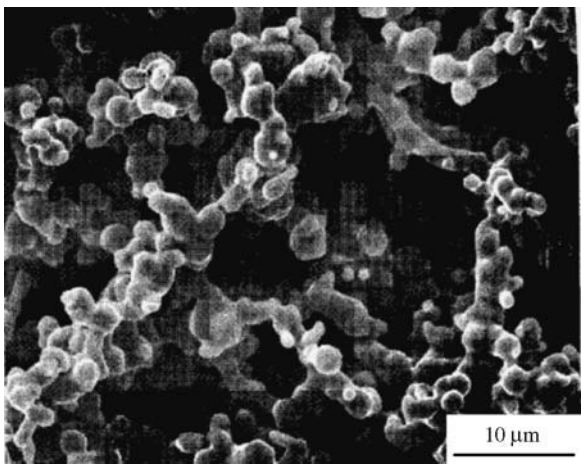

Figure 10.2 Carbonyl nickel powder particles with a size range of 2–4 μm compacted and sintered to 35% density. (Source: Ref 4®)

Powder Preparation

After the material is selected, powder preparation begins with the separation of the desired size distribution. Depending on the kind of secondary processing, commercial powders are available with either wide or narrow particle size distributions. The porous product manufacturers produce powders with narrow size distribution by removing oversize and undersize particles from the as-produced powders by screening. Vibratory or ultrasonic sieve screening methods are used for particles greater than 20 μm and other methods such as air classification or centrifugal separation are used for particles less than 20 μm.

The porous PM products manufactured from narrow particle size distribution powders have better reproducibility and uniformity of the final porosity.

When the desired particle size distribution is obtained, the powder must be thoroughly blended prior to use in order to avoid segregation and to maximize homogeneity. However, excessive blending can modify the powder characteristics as a result of the formation of additional fine powder particles or by changing the particle surface. The apparent and tap densities of the narrow powder cuts are measured and controlled by tight specifications because these characteristics control further processing steps such as powder flow and die filling. Additives such as pore formers, lubricants or binders are precisely mixed with powder when it is required during the processing [7].

The considerable amounts of powder with controlled particle size distributions are used as loose pack beds for applications such as polymer filtration, but most applications require further processing to design a more rigid porous structure.

The powder cleanliness requirements must be carefully controlled to avoid contamination with extraneous materials during powder preparation and further processing. Contamination by elements such as iron, carbon, sulfur and others can lead to a significant reduction in the mechanical properties and corrosion resistance of porous materials when used in an aggressive environment. Other trace impurities such as oxygen, alumina, silica and nitrogen can also influence the final mechanical properties.

Compaction Methods

Compaction and further sintering are usually required to produce porous materials from prepared powders in order to achieve the best combination of mechanical strength and porosity. Lower density and higher permeability parts from metals such as nickel and nickel-based alloy materials can be made by a gravity sintering process without compaction of the powders when the application does not require high strength levels.

Die compaction, isostatic pressing and roll compaction techniques are commonly used for the production of porous materials. These processes increase the green strength of the parts by cold welding of the particles with each other at contact areas because of plastic deformation.

Die compaction and sintering are the most common methods of improving mechanical properties while

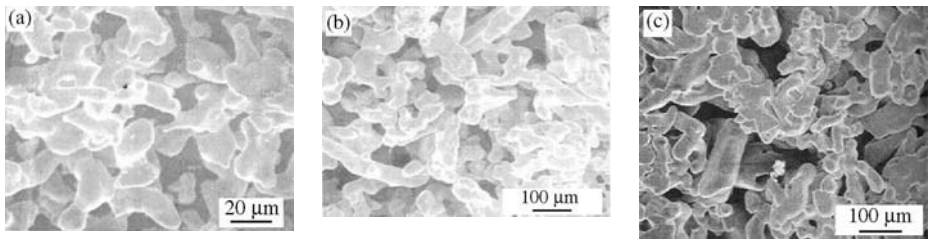

Figure 10.3 Scanning electron micrograph of (a) titanium powder produced by calcium reduction method, (b) and (c) the microstructure of the rolled plates with 30 and 50% theoretical density, correspondingly.

achieving the lowest density in order to maximize porosity and permeability. Minimum green strength can be obtained by using lower compaction forces in the range of 70–210 MPa. By comparison, higher-density structural PM components require compaction pressures of 420–840 MPa [8]. Porous components with 20–50% green densities usually have minimal green strength and require careful handling. Waxes and stearates are commonly added to the powder to reduce die-wall friction and tool wear.

Isostatic compaction is a common method of compaction for manufacturing semi-products such as tubes that have a length to diameter ratio greater than 3 to 1. Isostatic technique can produce porous components with more uniform density than can die compaction [9,10]. The wet bag cold isostatic pressing (CIP) process uses pressure ranging from 3.5 to 550 MPa applied to tooling. Other near-net shapes such as cones, funnels and tubes with splines can be manufactured by CIP [11].

Hot isostatic pressing (HIP) combines the CIP and sintering in one step and is used in applications where complex shapes are needed or when a material has low green strength for handling.

Roll compaction of porous nickel sheet materials has been commonly used in the production of battery materials [12,13]. Nickel and other powders are rolled to a thickness ranging from 0.13 to 3.8 mm and in widths up to 1 m, depending on the green strength and requirements of the application.

Titanium porous plates and foils were manufactured by rolling a billet compacted from powders produced by the calcium reduction method [14]. Detailed information on the calcium reduction method can be found in Chapter 14. Scanning electron micrographs of titanium powder produced by the calcium reduction method are shown in Figure 10.3(a). Figures 10.3(b) and (c) illustrate the microstructures of the rolled plates with 30 and 50% theoretical density respectively. Powder particles are welded to each other with honeycomb-like structure and connected pore formation.

The rolled sheet can be directly fed on a sintering furnace to minimize handling operations in certain high-volume applications. Shapes or patterns can often be designed into the rolls, or components can be stamped from the finished porous sheet. Roll compaction is used to produce an economical, uniform density material with tight dimensional tolerances.

Other forming methods used to produce porous metal components include metal injection moulding [15], centrifugal slurry casting [16], extrusion, gravity filling of shaped molds, direct typing method [17] and wet powder spraying [18]. Complicated shapes and lower-density components are formed using pore formers such as water and/or thermoplastic binders that allow adequate handling strength. Removal of the additives prior to sintering is ordinarily realized in the preheat zone of the furnace or a separately controlled baking process. Metal spraying can create a controlled porous structure with or without additives by spraying molten metal onto a base material to combine the compaction and sintering processes [19].

Sintering

Sintering of porous metal is a crucial balance between maximizing material properties and maximizing the open porosity and permeability. However, permeability and material properties such as strength and ductility are usually inversely related and the area in which the optimum compromise is obtained is quite small. Sintering temperature is selected depending on material type, the powder particle size distribution and the powder particle shape. Sintering is ordinarily done at 70–90% of the material melting temperature. Finer powder particles require a lower sintering temperature because the surface energy driving force to initiate bond growth is much higher than for a coarser particle. Sintering at too high a temperature also leads to the formation of large pores.

Table 10.1 Typical mechanical properties of bronze 90%Cu/10%Sn

Material	Filter grade (a) (μm)	Density (%)	Minimum UTS (b) (MPa)	Elongation, %	Shear strength (c) (MPa)
Bronze	10	75	48	8	130
	20	68	41	6	110
	40	62	35	4	100
	90	57	28	3	75
	150	54	21	2	40
	250	52	14	2	30

(a) Filter grades in micrometers as estimated by bubble-point test method [20,21], (b) ultimate tensile strength, (c) shear strength is the punching force divided by the sheared edge area per DIN standard V 30910 [22]

Mechanical Properties

The mechanical properties of porous materials are highly dependent on the porosity and the processing method. Table 10.1 contains typical values for tensile strength, elongation and shear strength of 90/10 tin bronze disks as a function of density and filter grade. Mechanical properties increase significantly as the pore size and the percentage of porosity decrease.

Cellular Materials

Cellular materials or metallic foams are distinguished by high porosity and high stiffness combined with a very low specific weight. Because of these features, cellular materials are frequently used as construction materials.

Cellular materials find wide use for damping, cushioning, insulating, filtering and construction purposes and in many other applications.

Production Methods

In the past, metal foams were obtained by adding a foaming agent to a molten metal when the viscosity of the melt is appropriately established [23]. The foaming agent is usually a powder of metal hydride such as TiH_2, which decomposed forming hydrogen when heated to a temperature above 400°C. As the foaming agent comes into contact with the molten metal, the latter instantly decomposes so that there is insufficient time to accomplish a homogeneous distribution of the gas-forming particles. Therefore this process is difficult to control.

The advanced PM process for production of nonferrous foams uses conventional foaming agents and metal powders [24,25]. Commercially available powders (such as aluminum, zinc, tin, or lead) are mixed with the foaming agent by conventional means, such as a drum-type mixer. Subsequent to mixing, the powder blend is compacted to give a dense, virtually non-porous body near to TMD. Several compaction methods can be employed such as uniaxial pressing, powder extrusion and even roll compaction. When this compact is heated to a temperature around the melting point, it expands into a highly porous cellular body with a closed-pore structure. This implies that each particle of the foaming agents is embedded in a gas-tight metallic matrix so that the formed gas cannot escape via interconnected pores. By heating this material to the melting point, the foaming process is initiated so that it is also possible to obtain complex-shaped foamed articles. Sandwich-type structures also can be produced by several techniques. The simplest one is to glue sheets of conventional materials to a sheet of foamed metal. However, due to the low thermal stability of resins, a metallic bonding of the sheets might be preferred. For example, a roll-cladding process can be used.

Various foaming agents have been shown to yield good results for this purpose. Among the foaming agents used are metal hydrides such as titanium, zirconium and magnesium hydrides, which have decomposition temperatures between 280 and 600°C.

Several compaction methods can be employed that range from uniaxial compaction to isostatic pressing [26,27] even to injection molding and extrusion [28,29].

Metallic hollow sphere structures (MHS) are a new kind of cellular metal. This technique ensures the controlled manufacture of single cells to single MHS and reproducible structure of the tailored components. Electrodeposition of various metals such as nickel, cobalt and copper on spherical substrates has been realized [30]. An impediment with this method is that there is a limited number of metals that can

be deposited on carrier surfaces by electrolysis, which limits the use of this technology.

A powder metallurgical process clears the way for these advantages [31]. An organic sphere substrate, mostly foamed polystyrene, has been used as a cell-forming undercoat. Fluidized deposition is provided with these foamed substrates and, by means of a nozzle system, a metal powder-binder suspension is atomized onto the outside of the styrofoam spheres [32]. Binder and styrofoam cores are removed by a subsequent heat treatment. Using the developed PM process for MHS, a wide range of powder material can be used for their production. There are several options to consolidate single hollow spheres to an MHS component, including sintering, brazing and adhesive bonding [33]. Figure 10.4 shows an overview of the spray coating process.

Properties of Metal Foams

In contrast to any other porous metal materials, metal foams are characterized by a very low specific weight. Using the PM technology, density values between 0.5 and 1 g/cm^3 are usually obtained. These values can be widened down to 0.2 g/cm^3 and up to 2.0 g/cm^3. In the case of closed porosity aluminum foam, it floats on water.

Mechanical properties of foam materials are usually determined by compression testing. The excellent strength of metal foams is illustrated by comparison

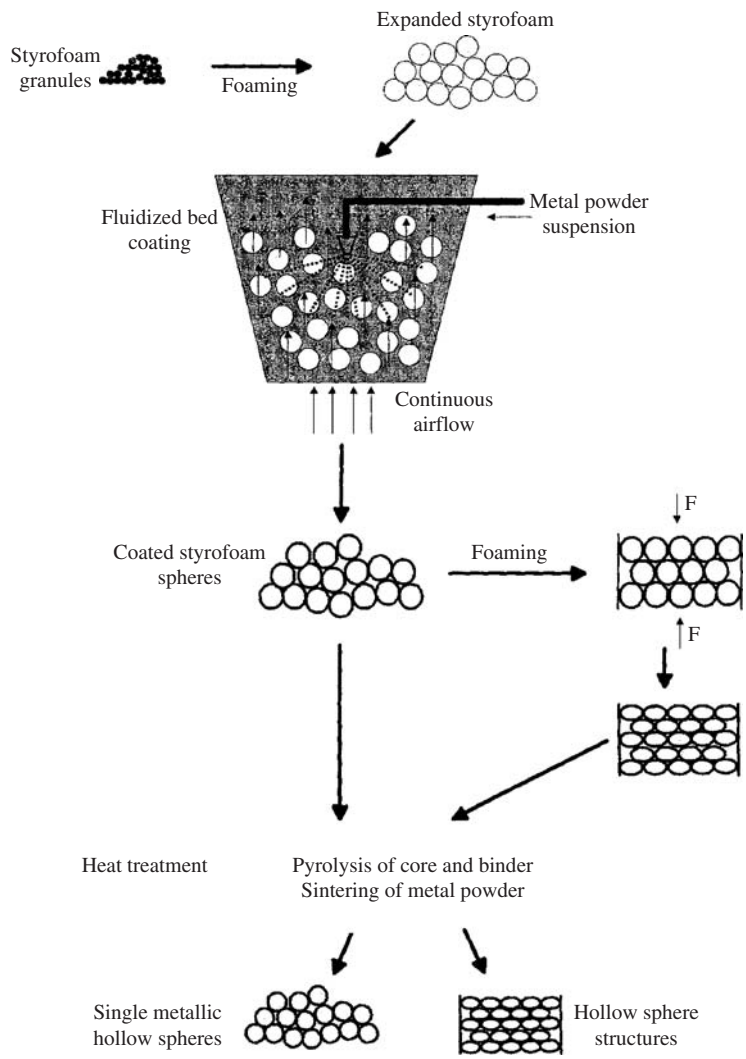

Figure 10.4 Processing of metallic hollow spheres and hollow sphere structures.

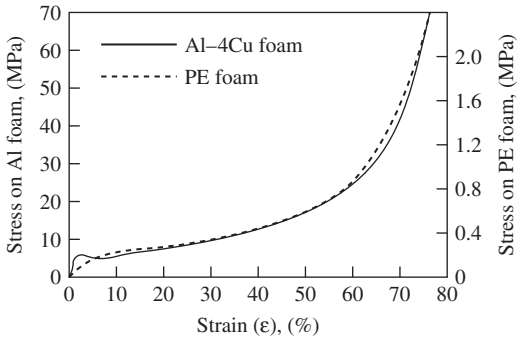

Figure 10.5 Stress–strain curve of an Al–4Cu foam (solid line, left scale) and of a polyethylene (PE) foam (broken line). (Source: Ref 34®)

of a polyethylene foam (density, 0.12 g/cm^3) with aluminum alloy foam (Al–4Cu: density, 0.45 g/cm^3) [34]. In both materials, the initial porosity is about 83–87%. The compressive strength dependence on stress shows (Figure 10.5) that, in the range from 10 to 50%, the strength values of metal foam and polyethylene foam are increased from 5.0 to 18 MPa and from 0.3 to 0.5 MPa, respectively; in strain ranges from 50 to 75%, the strength values of metal foam and polyethylene foam are increased from 18 to 60 MPa and from 0.5 to 2.0 MPa, respectively. Due to this particular form of the compressive stress–strain dependence, foamed materials have a high capacity to absorb large amounts of energy at a relatively low strength level.

The energy absorption behavior of foamed materials is determined as efficiency η. For the given strain, this parameter is defined as a ratio of the actual absorbed energy to the energy that would be absorbed by an ideal absorber.

The determination of the elastic modulus of foamed metals should not be done in the conventional way, that is, by evaluation of the slope of the elastic part of the stress–strain curve. Typical elastic modulus dependence on apparent density is available for foamed Al–12Si [34]. It was investigated using a vibrational bending test. A straight line would be expected in a double-log plot of the foam modulus versus density. Increasing the density from 0.7 to 2.5 g/cm^3 leads to growth of elastic modulus from 7 to 55 GPa.

Damping is strongest in the foams with the lowest densities. It is known that any kind of porosity enhances damping due to the stress concentration which is called mode conversion around pores. Another mechanism is of macroscopic source. The cell walls of metallic foams sometimes contain cracks and holes that may either originate from the gas released during the foaming process or from the contraction of the foamed body on cooling after foaming. These defects may give rise to an extra frictional contribution caused by the relative movement of the crack or hole walls with respect to each other. Integrally, it is also well established that PM materials have higher damping capacities than cast ones.

Applications

Filtration, battery electrodes, self-lubricated bearings and flow control are the largest commercial applications of the porous PM materials. One of the main applications of metal foams is for energy absorption. Aluminum foams can also be used for lightweight structures.

Filtration and separation technology applications [1,4,5,35,36] are the largest market for porous PM materials. Many industrial applications require fine filtration capability, excellent mechanical properties and corrosion resistance, especially at elevated temperature and high pressures. Various porous materials and design for the filters are used for gas cleaning by filtration.

Advanced porous sintered metal has been developed for diesel soot filtration [37]. The demand for a flexible porous sheet material with excellent properties needs the combination of metal powder and fully dense metal. Porous parts that are only based on powder with high porosity could not achieve good vibration resistance. Besides, weldability of highly porous materials does not meet the demands for lifetime of welded connections. Therefore latticed metal is selected for the matrix material. Water-atomized powder is preferable to reach best filtration efficiencies. Figure 10.6 shows the main process steps from the metallic powder to the manufactured article. By varying powder particle size, binder and additive contents one can adjust some properties of the filter material adapted to the demands of customers. The scanning micrographs (Figure 10.7) give a view of porous material: the surface of the porous material (a) and the interconnection between metal powder and the metallic lattice (b). In the latter one can obviously see the lattice fragments. Sintered metal filters are characterized by the following: thickness is 0.38 mm, porosity 45%, area weight is 1700 g/m^2, mean pore size is 10 μm, air permeability amounts to 100 m^3/(m^{2}h) at hydraulic pressure 200 Pa. The view of Jetfilter for passenger cars, based on the above filter material, is shown in Figure 10.8(a) and its entrance in Figure 10.8(b). The 60 filter pockets are placed symmetrically for a filter in a cylindrical casing with 150 mm diameter.

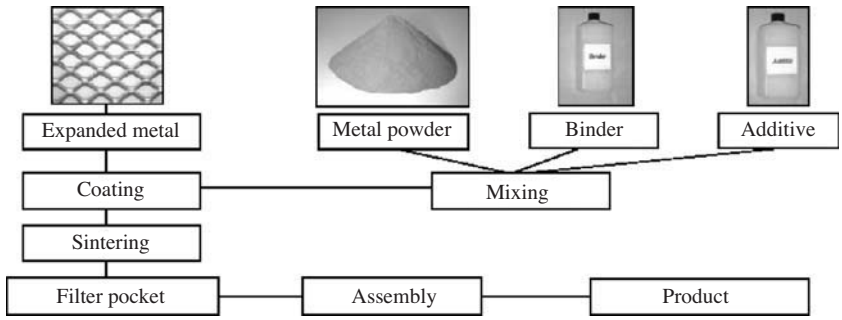

Figure 10.6 Main process steps from the metallic powder to the manufactured filter.

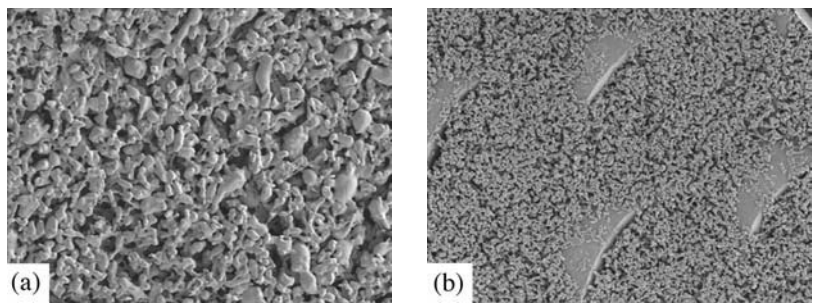

Figure 10.7 Scanning micrographs of porous material: (a) the surface of the porous material and (b) the interconnection between metal powder and the metallic lattice. (Source: Ref 37)

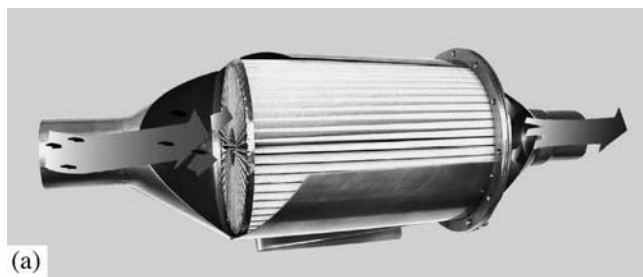

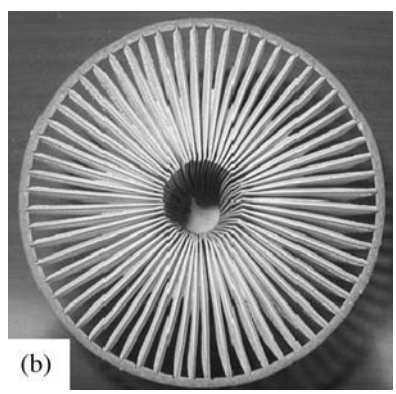

Figure 10.8 Jetfilter for passenger cars: (a) general view of jetfilter; (b) jetfilter entrance. Courtesy of HJS Fahrzeugtechnik, Germany

By selecting 250 mm for the length of the filter, a surface of 1.8 m^2 is obtained. This size is enough for diesel engines up to 2-litre cylinder and ensures gas cleaning from soot without replacement during 100 000–120 000 km running. At present, filter sizes between 1 and 10 m^2 are produced for end users.

Two-layer porous powder material has been developed for highly effective separation of mechanical impurities and water from petroleum products [38]. The substrate is made from sintered bronze or titanium powder with thickness 3–4 mm. The second layer, with average pore sizes 20–22 μm is made from fluoroplastic powder. The degree of cleaning from oil, water drops and moisture in the first layer and second layer is not less 97 and 99.3%, respectively.

Over the last decades, both intermetallic compounds such as NiAl as well as Ni-based alloys, e.g. Inconel, have been developed to serve under extreme conditions demanding excellent high-temperature stability and oxidation/corrosion resistance. For many applications such as high-temperature filtration porous structures, diesel soot traps and catalyst carriers, these materials are required but are not yet commonly available.

A technique has been developed which is suitable to produce large amounts of NiAl- and Inconel-alloy-based foams with different porosities. This process starts from pure nickel foam which is homogeneously coated and subsequently transformed into the desired material by a heat treatment [39]. The first step of the manufacturing process involves coating of the nickel foam with a binder solution. The foam is then coated with the desired powder (50 wt% for manufacturing NiAl-foam). During the subsequent sintering step, the final composition of the foam and its specific surface area and porosity can be tailored as desired. The process also allows coating of the base substrate with multiphase composite powders and is consequently also suitable for manufacturing complex alloy compositions. Figure 10.9 illustrates comparison of the individual states of the coating from the base foam to the reacted NiAl final product.

Capillary-attraction devices and reservoirs are other major application areas [1,33–35,40]. Self-lubricating bearings that store lubricants in the pores and protect the surface from wear are one of the oldest commercial applications of porous PM materials. More information on self-lubricating bearings can be found in Chapter 16. Heat removal devices for microelectronics packaging and for cooling devices used in satellites are some of the newest application areas.

Among cellular materials, hollow sphere structures manufactured by PM appear as a very attractive process due to its flexibility and easy process control. The process of coating of polymer templates with powder-binder suspension and subsequent debinding and sintering is applicable to virtually all PM materials. By forming the cells separately and joining them into a whole body, one can virtually design cellular structures by variation of structural parameters. The transfer of manufacturing technique for cellular solids to high temperature/high performance materials opens a variety of novel solutions. Such typical structures are molybdenum hollow sphere structures, which are prepared by the PM method of coating polymer templates [41]. The relative density obtained was 3% corresponding to a density of 0.3 g/cm^3. Sphere sizes were 3 mm, with shell wall thickness up to 35 μm. Thermal conductivity of hollow spheres is in the range of 1.5 $W/(m \cdot K)$, consequently, approximately 1% of solid molybdenum conductivity (there is a moderate increase of conductivity due to radiation above 800°C). Therefore molybdenum hollow sphere structures are suitable for insulating components in furnace construction.

Sound, pressure and vibration dampening components find wide industrial application [1,33–35,40,41]. Porosity acts as acoustical impedance and dampens certain sound frequencies while others pass through. A pressure pulsation in a fluid delivery system is also dampened by reducing the fluid rate when it passes through the small interconnected channels. The pressure gauges are equipped with porous metal

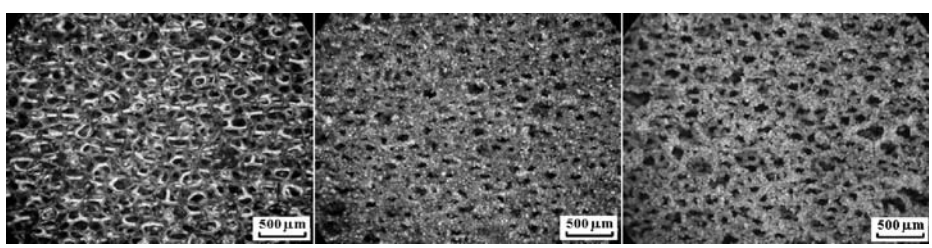

Figure 10.9 Comparison of states of the coating (from left to right: Ni base foam, coated foam, reactive sintered NiAl foam). (Source: Ref 39)

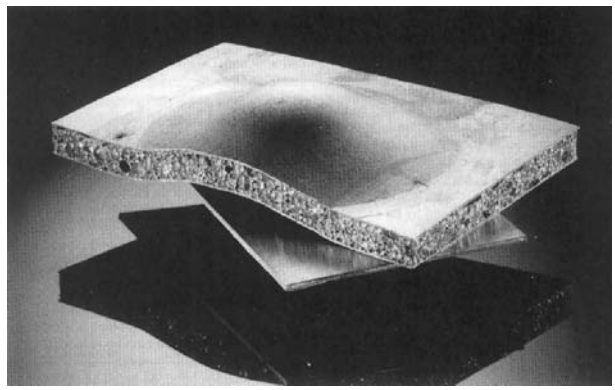

Figure 10.10 Sandwich component with a porous aluminum foam core and steel face sheets (Article of Studiengeselshaft Stahlanwendungen, Germany).

anti-vibrators to dampen the vibration or pressure fluctuation.

Energy absorption is one of the most promising application areas of metal foams. For instance, the German automotive supplier Karmann suggests sandwiches containing an aluminum foam core and aluminum face sheets for use in the bulkhead and the rear seat wall of convertible cars [34]. The components are up to ten times stiffer compared to the conventional steel parts used in the past and weigh 30–50% less. Steel is also used for sandwich face sheets. Subsequent deep drawing allows a three-dimensional structure to be produced (Figure 10.10).

As the elastic modulus can be varied within a wide range due to the choice of the foam density, it is possible to match the resonance frequency of foamed components. Thus, detrimental vibrations can be prevented. Complex-shaped parts of foamed metal can also be used to encapsulate the noise source components for their soundproofing.

Closed-cell foams are especially well suited to use as floating structures because of their high damage admissibility. These structures retain their buoyancy even when locally damaged. In particular, metal foams are able to resist higher pressure and higher temperatures than plastic foams.

Laminar flow control devices using porous PM flow throttles [1,4,35,40] are more accurate and reliable than other volumetric-flow-restricting devices such as orifices and micrometering valves that operate at higher fluid velocities. Porous PM materials are less susceptible to contamination and blockage because there are hundreds of fine jets instead of a single orifice.

Several application fields of porous PM materials demand the extremely high internal surface area and porosity available [4,13,14,42]. For example, the conductivity of the electrodes for alkaline batteries and for fuel cells can be significantly increased by large contact area with the reaction fluid. Biomedical implants use the large surface area to allow tissue growth into the porous structure to ensure good joint attachment.

In gas–liquid contacting processes, forcing gas through a fine-grade, porous PM material with high surface area produces tiny bubbles that result in high efficiency transfer contact of the gas with the liquid [43]. Conventional drilled pipe spargers produce larger bubbles that do not dissolve and react as well as the finer bubbles generated by porous metals. Simultaneously, finer pore materials prevent the liquid from penetrating back into the pores at lower internal pressures.

Boundary layer control devices such as flotation bars and vacuum hold-down plates are highly specialized applications [1,35,40,43]. A boundary layer of air in order to eliminate contact turning of thin films, tapes, or webs can be formed on the outside surface of a fine-porosity tube when the inside cavity is pressurized.

Major application areas of porous PM materials are summarized in Table 10.2. As is shown, many specialized applications have been developed to take advantage of the unique characteristics of porous materials.

Thus, the application of porous powder metallurgy technology is rapidly developing as a cost-effective, commercially viable technique that offers diverse solutions to technical challenges. The powder characteristics are key factors in determining the porous material properties of the finished product. Therefore, the powder selection and manufacturing methods are critical to the production of a consistent product.

Table 10.2 Main application areas of porous metallic powder metallurgy materials

Filtration/separation technology

Analysis instruments	Food and beverage	Polymer processing
Gas/liquid chromatography	Cooking oil, corn syrup	Caustic/sizing recovery
Gas sampling	Juice/sugar clarification	Gel dehydration
Sensor protection	Removal of yeast from beer	Polymer fibers
Chemical processing	Mineral processing/concentration	Power generation
Catalyst recovery	Catalyst manufacturing	Condensate aqua
Gases and liquids processing	Coal, silica, silicon, and metal oxides	Fossil fuel waste and flue gases
Fluid-bed reactor product and electrolytes	Metal sulfides	Radioactive material refining
Chemicals	Petrochemical industry	Semiconductor
Acids, solvents, and inks	Flue gases	Bulk gas delivery systems
Adhesives and greases	Fluid cracking catalysts	Particle removal process gas
Precipitates, solutions, and salts	Slurry oils	Purifier media retainers
Fluid power	Pharmaceutical	Other filter areas
Pneumatic equipment	Autoclave vent filters	Aircraft and marine fuel
Protect hydraulic valves	Oxygen filters	Automotive diesel soot filters and oil burners
Water separation in air lines	Process steams	Paper, pulp, and incinerators

Reservoirs and capillary attraction

Applicators	Heat sinks	Microelectronics packaging
Atomisers	Insulating components in furnace constructions	Printer ink reservoirs
Die-wall lubrication	Liquid wicks, evaporation	Self-lubricating bearings
Heat exchangers	Microelectronics satellites forcooling devices	Transpiration cooling

Dampening

Exhaust silencers/mufflers	Microphone frequency	Sound attenuation
Flame arresters/quenching	Pressure equalization	Telephone transmitters
Hearing aids	Pressure snubbers	Vibration reduction

Flow control devices

Calibrated leaks	Flow rate timing devices	Vacuum delay valves
Gas and liquid metering	Flow restrictors	Vents and breathers

Surface area devices

Batteries	Cathode dispensers	Fuel cells
Biomedical implant/prosthesis	Electrodes	Ionizers

Gas–liquid contacting

Aerators	Bubblers	Spargers
Agitation of liquids	Carbonators	Chlorine and oxygen bleaching
Bioremediation	Enhances chemical reactions	Hydrogen ion exponent control
Oxygenation, fish farming	Fermentation	Oxygen and volatile stripping
Steam injectors/heat transfer	Hydrogenation	Water/oil separation

Boundary layer control

Air bearings	Friction reduction	Polymer fiber cooling
Flotation devices	Material handling/transport	Turning bars for film/webs
Fluidizer plates for fluid bed	Mold release	Vacuum plates

Metallic foams

Buoys, life buoys	Energy absorption car components	Elevated temperature structures
Encapsulating of noise sources	Floating structures	Structure car components

References

1. Porous metal products for OEM applications, *Mott Technical Handbook*. Mott Handbook Corporation, 1996.
2. Peissker, E., *Metal powders, Norddeutsche Affinerie*. Brillant-Offset, Hamburg, 1986.
3. Neubing, H., Properties and sintering behaviour of spherical tin bronze powders for the manufacture of filters. *Int. J. Powder Metall.*, 1986, 18(4):4–10.
4. Eisenmann, M., Porous powder metallurgy technology. In *ASM Handbook*, Vol. 7. ASM International Publishers, 1998, pp. 1031–1042.
5. *Bronze Filter Powders, A Cu Powder International Brochure*. Acu Powder International Publishers, 1997.
6. Bagshaw, N., Barnes, M., Evans, J., The properties of porous nickel produced by pressing and sintering. *Powder Metall.*, 1967, 10(4):13–31.
7. Porous Metal Council, *Porous Metal Design Guidebook*. Metal Powder Industries Federation Publishers, 1980.
8. German, R., *Particle Packing Characteristics*. Metal Powder Industries Federation Publishers, 1989.
9. Albano-Muller, L., Filter elements of highly porous sintered metals. *Powder Metall. Int.*, 1982, 14:73–79.
10. Savich, V.V., Pilinevich, L.P., Tumilovich, M.V., Comparison of porous materials properties made from sponge titanium powders produced by different methods. In *Proceedings of 2004 Powder Metallurgy World Congress*, compiled by European Powder Metallurgy Association, Bellstone Shrewsbury, UK, 2004, Vol. 4, pp. 157–162.
11. Lenel, F., *Powder Metallurgy – Principles and Applications*. Metal Powder Industries Federation Publishers, 1980.
12. Tracey, V., The roll-compaction of metal powders. *Powder Metall.*, 1969, 12(24):598–612.
13. Williams, N., Tracey, V., Porous nickel for alkaline battery and fuel cell electrodes: production by roll-compaction. *Int. J. Powder Metall.*, 1968, 4(2): 47–62.
14. Moxson, V., Senkov, O.N., Froes, F.H., Production and applications of low cost titanium powders. In *Proceedings of 1998 Powder Metallurgy World Congress*, compiled by European Powder Metallurgy Association, Bellstone Shrewsbury, UK, 1998, Vol. 1, pp. 274–279.
15. Neumann, P., Amhold, V., Heiburg, K., Rohlig, R, Porous metal products with special properties. In *Proceedings of Powder Metal Materials Colloquium. Soc. Franc. De Metal. Et de Mater. Public.*, 1992, pp. 4-1-4-6.
16. Koehler, P., Seamless porous metal article and method of making, U.S. Patent No 4,828,930, 1989.
17. Andersen, O., Studnitzky, T., Bauer, J., Direct typing – a new method for the production of cellular PM parts. In *Proceedings of 2004 Powder Metallurgy World Congress*, compiled by European Powder Metallurgy Association, Bellstone Shrewsbury, UK, 2004, Vol. 4, pp. 189–194.
18. Bram, M., Buchkremer, H.P., Stöver, D., Development of porous composite membranes for microfiltration devices. In *Proceedings of 2004 Powder Metallurgy World Congress*, compiled by European Powder Metallurgy Association, Bellstone Shrewsbury, UK, 2004, Vol. 4, pp. 183–188.
19. Porous Metal Council, *From Powder to Porous Metal Parts, Design Engineering*. Metal Powder Industries Federation Publishers, 1981.
20. ISO Standard 4022, Permeable sintered metal materials – determination of fluid permeability, 1987.
21. ASTM, E 128, Standard test methods for maximum pore diameter of bubble test pore size, 1994.
22. Sinter metal materials, Part 2, Materials for filters, Standard V 30910, Normenausschuss Pulvermetallurgie, Deutsches Institut für Normung e. V., 1986.
23. Akiyama, S. et al., Foamed metal and method for producing the same. European Patent Application EP 0 210 803 Al, 1986.
24. Baumeister, J., Method for porous metal bodies. German Patent DE 40 18 360, 1990.
25. Baumeister, J., Schrader, H., Methods for manufacturing formable metal bodies. German Patent DE 41 01 630, 1991.
26. Banhart, J., Manufacture, characterisation and application of cellular metals and metal foams. *Progress in Material Science*, 2001, 46:559–632.
27. Wadley, H.N.G., Cellular metals manufacturing. *Advanced Engineering Material*, 2002, 4(10):726–733.
28. Simancik, F., Florek, R., Tobolka, P., Reinforced aluminium foam profiles. In *Proceedings of 2004 Powder Metallurgy World Congress*, compiled by European Powder Metallurgy Association, Bellstone Shrewsbury, UK, 2004, Vol. 4, pp. 113–118.
29. Matsuzaki, S., Ishida, M., Tanaka, S., Nishiyabu, K., Production of porous metal materials by injection and extrusion moulding. In *Proceedings of 2004 Powder Metallurgy World Congress*, compiled by European Powder Metallurgy Association, Bellstone Shrewsbury, UK, 2004, Vol. 4, pp. 175–181.
30. German Patent DE 37 24 156, 1986.
31. Jaeckel, M. European Patent EP 0 300 543.

32. Waag, U., Schneider, L., Löthman, P., Stephani, G., Kieback, B., Metallic hollow spheres – a new product. *Proceedings of 2000 Powder Metallurgy World Congress*. Japan Society of Powder and Powder Metallurgy, 2000, pp. 510–514.
33. Waag, U., Stephani, G., Färber, J., Venghaus, H., Bingel, G., Cellular structures based on metallic hollow spheres – mechanical and acoustical properties. In *Proceedings of 2004 Powder Metallurgy World Congress*, compiled by European Powder Metallurgy Association, Bellstone Shrewsbury, UK, 2004, Vol. 4, pp. 143–148.
34. Banhart, J., Baumeister, J., Weber, M., Metallic foam. In *ASM Handbook*, Vol. 7. ASM International Publishers, 1998, pp. 1043–1047.
35. Tracey, V., Porous materials: current and future trends. *Int. J. Powder Metall. Powder Technol.*, 1976, 12(1):25–35.
36. Ilyuschenko, A.Ph., Pilinevich, L.P., Tumilovich, M.V., Porous powder material for effective cleaning gases and liquids. In *Proceedings of 2001 European Congress and Exhibition on Powder Metallurgy*, compiled by European Powder Metallurgy Association, Bellstone Shrewsbury, UK, 2001, Vol. 1, pp. 354–358.
37. Steigert, S., Porous sintered metal for soot filtration. In *Proceedings of 2004 Powder Metallurgy World Congress*, compiled by European Powder Metallurgy Association, Bellstone Shrewsbury, UK, 2004, Vol. 4, pp. 195–200.
38. Savich, V.V., Pilinevich, L.P., Tumilovich, M.V., Petracov, A.V., Effectiveness of application of porous powder materials for separation of water from petroleum products. In *Proceedings of 2004 Powder Metallurgy World Congress*, compiled by European Powder Metallurgy Association, Bellstone Shrewsbury, UK, 2004, Vol. 4, pp. 163–167.
39. Böhm, A., Walther, G., Naumann, D., Croset, M., Bartout, J-D., Bienvenu, Y., Preparation and properties of high temperature stable NiAl and Inconel-based foams. In *Proceedings of 2004 Powder Metallurgy World Congress*, compiled by European Powder Metallurgy Association, Bellstone Shrewsbury, UK, 2004, Vol. 4, pp. 101–105.
40. Snyder, J., PM porous parts. In *ASM Handbook*, Vol. 7. ASM International Publishers, 1984, pp. 696–700.
41. Färber, J., Bojack, A., Stoiber, M., Plankensteiner, A., Goehler, H., Schneidereit, H., Molybdenum hollow sphere structures for high temperature applications. In *Proceedings of 2004 Powder Metallurgy World Congress*, compiled by European Powder Metallurgy Association, Bellstone Shrewsbury, UK, 2004, Vol. 4, pp. 131–135.
42. Savich, V.V., Pilinevich, L.P., Tumilovich, M.V., Comparison of porous materials properties made from sponge titanium powders produced by different methods. In *Proceedings of 2004 Powder Metallurgy World Congress*, compiled by European Powder Metallurgy Association, Bellstone Shrewsbury, UK, 2004, Vol. 4, pp. 157–162.
43. *Porous Metal Products for OEM Applications – A Guide to Advanced Gas Sparging and Gas-Liquid Contacting*, Mott Technical Handbook. Mott Corporation, 1996, Section 11000.

SECTION 3 Processing of Powders and Processing Equipment

Contents

For a more detailed Section Contents list, please see the book Contents pages that start on page v

Chapter 11

Processing of Powders and Processing Equipment

Oleg D. Neikov, Frantsevich Institute for Problems of Materials Science (IPMS), Kiev, Ukraine

Dehydration

In the production of non-ferrous metal and alloy powders, the technological processes and procedures effected in aqueous environment, either aqueous acidic or alkaline solutions (atomization and granulation of melts, methods of obtaining powders from solutions and electrochemical methods) are popularized. Residual moisture content in the powders is usually at the most 0.1 wt%.

The humidity w is the ratio of water mass in a product to the total mass of the wet product:

$$w = \frac{m_1 - m_2}{m_1} 100\% \tag{1}$$

where m_2 is the mass of dry product.

We can distinguish the overall humidity w_o, humidity of air-dry material w_a and surface humidity w_s, determined by difference:

$$w_s = w_o - w_a \tag{2}$$

and, consequently,

$$w_o = w_a + w_s. \tag{3}$$

Depending on physical-chemical mechanisms of material bonds with water, the free, capillary, adsorption and chemical moisture bonds are distinguished.

The free (gravitational) moisture fills the spaces between the particles and can move relative to the solid particles under the action of gravity.

The capillary moisture is in particle pores, cracks and spaces between fine particles kept by capillary forces arising on boundaries of solid, liquid and gaseous phases. The capillary moisture volume depends on the porosity of the material.

The adsorption moisture, in the form of a hydrated film, is kept on the surface of particles by adsorption forces. The adsorption moisture in turn is subdivided into hygroscopic and adhesion moisture. The hygroscopic moisture is condensed on the solid surface in the form of a film represented by water molecules layers retained by adsorption forces. The adsorption moisture is represented by water molecules layers, located above the hygroscopic moisture and bound less fast to the surface of solid particles because this bond is determined by second orientation of the water molecules and hydration by adsorbed ions.

Chemical bonded moisture is differentiated on constitutional (OH^-, H^+, H_2O^+) and crystallization (contained in crystallohydrate) forms.

Depending on the amount and form of the moisture, there are various dehydration methods. According to the water content, the powders are classified as water-bearing, wet, moist, air-dry and dry.

The water-bearing powders are a mechanical mixture of solid with water and possessing liquid mobility (as pulps and suspensions). The water atomized melts, products of electrolysis, chemical precipitation, discharges by wet milling, overflows, spills and the like are in this category. Moisture of these products is characterized by the ratio of solid to liquid (S:L) in mass units.

The quantities which characterize the pulp or suspension are connected by the following correlations.

The volumes of solid V_1 and liquid V_2 phases in 1 kg of pulp:

$$V_1 = S/\rho_1; \quad V_2 = 1 - S/\rho_1$$

where ρ_1 is density of solid, kg/m^3; S is a mass content of the solid in pulp per 1 m^3.

The solid volume-part concentration:

$$c_{1v} = \frac{1}{1+n} \tag{4}$$

where n is the volume ratio, L to S.

Then the solid mass concentration in the pulp or suspension is

$$c_{1m} = c_{1v}\rho_1$$

where ρ_1 is the mass density of solid, kg/m^3.

Such water-bearing powders are usually dehydrated in thickeners, settling-basins and sumps; previously they were thickened in hydrocyclones.

Wet powders include gravitational moisture partially, capillary, adsorption and do not possess liquid mobility.

Moist powders do not contain gravitational moisture, but include adsorption moisture and some capillary moisture.

The air-dry products are the dusts entrapped in dry cyclones and filters from dust-laden aspiration gases. They contain only hydroscopic moisture.

Dry powders are obtained by means of moisture evaporation from wet powders during thermal drying.

The basic dehydration methods of powders are listed in Table 11.1. Commonly, the powders are dehydrated in three stages with first their thickening followed by moisture receding from the thickened product by mechanical methods and drying. The dehydration of sludge (waste of technological processes) is done in two or three stages. Ordinarily, the thickened product from the settling-tank is dehydrated on a filter-press. The overflow is subjected sequentially to purification in cartridge and sand filters.

Thickening in Cyclones

The hydrocyclones of cast and welded design lined by cast ceramic or rubber for wear prevention of the walls are shown in Figures 11.1 and 11.2.

The necessary pulp pressure on entry into the hydrocyclone ranges from 0.03 to 0.25 MPa and is applied by a sand pump. If the desired capacity is not accomplished by one hydrocyclone, battery cyclones are used in which hydrocyclones are turned in parallel operation.

A calculation of hydrocyclones includes definition of the diameter D_c and throughput Q_c on pulp at given maximal size of solid particles δ_{max} in overflow, and pressure at entry into the cyclone:

$$D_c = 0.121 \times 10^{-2} \left(\frac{D_f}{D_{ov}} \right)^2 \delta_{max}^2 (\rho_1 - \rho_2) \sqrt{p_{en}}, \text{ m} \quad (5)$$

$$Q_c = 0.94 D_f D_{ov} \sqrt{H}, \text{ m}^3/\text{s} \quad (6)$$

where D_f (see Figures 11.1 and 11.2) is the diameter of feed branch pipe, m; D_{ov} is the diameter of the

Table 11.1 Dehydration methods

Method name	Apparatus	Initial product	*L*:*S*, volume ratio	
		Method essence	Initial	Final
Inertial precipitation	Hydrocyclones	Pulp Inertia precipitation	10–12	2–4
Gravity sedimentation	Cylindrical and other thickeners	Pulp Gravity sedimentation	10–12	2–4
Centrifugation	Filtrate centrifuges	Pulp; thickened product Separation under action of centrifugal forces	0.5–12	6–15%[a]
	Precipitated centrifuges	Pulp Separation under action of centrifugal forces	5–15	5–10%[a]
Filtration of slurries	Plate filters, cartridge filters	Pulp Filtration through porous partitions under pressure	5–15	20–30%[a]
Filtration of thickened products	Vacuum filters, cartridge filters	Thickened product Filtration through porous partitions under vacuum	2–4	8–15%[a]
Thermal drying[b]	Drum dryers, pneumatic conveying dryers, vibrating dryers, vacuum dryers, fluidized bed dryers	Moist product	8–15%	up to 0.1%[a]

[a]Aqua content in mas.%;
[b]heat-mass exchange by thermal drying: convection and conduction (drum dryers); convection (pneumatic conveying dryers and fluidized bed dryers); convention, conduction, and radiation (vibrating dryers); conduction (vacuum dryers).

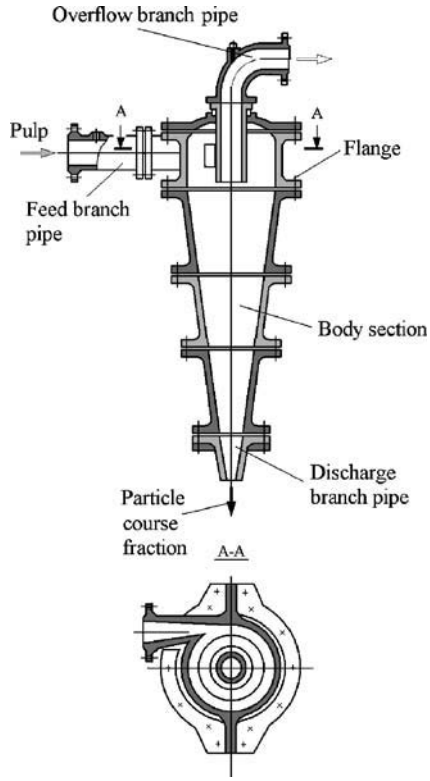

Figure 11.1 Hydrocyclone of cast design lined with cast ceramic or rubber.

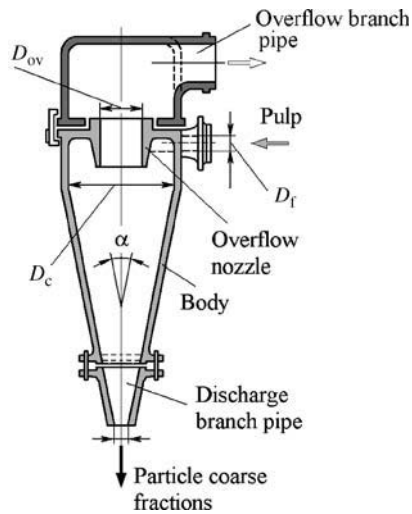

Figure 11.2 Hydrocyclone of welded design.

overflow branch pipe, m; p_{en} is pressure at entry to the cyclone, Pa; D_{dis} is the diameter of the discharge hole, m; δ_{max} is the maximum size of solid particles in overflow, mm; ρ_1, ρ_2 are mass densities of solid and liquid, respectively, kg/m^3; H is the water pressure at the entry to the cyclone, mm.

Sequence calculation:

- the diameter of the hydrocyclone D_c is defined according to Eqn (5) by ratio D_{dis}/D_{ev} values in ranges from 0.3 to 0.6 and is chosen to the nearest lesser diameter of a standard hydrocyclone (Table 11.2)
- the throughput of the hydrocyclone is defined according to Eqn (6)
- the check on unit load at the discharge opening, accepted in ranges from 0.5 to 2.0 t/h per 1 cm^2 of discharge opening cross-sectional area
- required number of hydrocyclones on given pulp yield subjected to thickening is defined.

Detailed calculation of hydrocyclones (determination of their sizes, throughput, particle sizes in overflow and their contents, in the initial slurry and overflow) can be found in Ref [1]. Table 11.2 includes the main parameters of the standard series of hydrocyclones up to 360 mm in diameter.

Conical and Cylindrical Thickeners

A typical scheme of thickener is shown in Figure 11.3. In such an apparatus, an initial pulp is fed via the vertical pipe into the thickener. The solid phase is deposited in the conical section, the clarified water rises up and is discharged into the annular chute. The thickened product is discharged continuously through orifices or by means of periodical action valves.

Capacity G(t/h) of conical thickeners is calculated from the following equation:

$$G = \frac{1.76wD_{con}^2}{[n_{st} - vn_f + (1-v)\rho_1^{-1}]} \tag{7}$$

where w is the sedimentation rate of boundary size particles, mm/s; D_{con} is cone diameter, m; n_{st} and n_f are the dilution (L:S) in initial and thickened material; v is solid in thickened material yield, part of one; ρ_1 is mass density of solid, t/m^3.

By calculation of cylindrical thickeners, the sedimentation surface is defined starting from initial pulp yield (G, t/h), (L:S) rates in initial pulp (n_{st}) and thickened product (n_f), subject to gravity sedimentation of boundary size particles w, v/h. Then the thickener specific surface is equal to

$$\overline{f} = \frac{n_{st} - n_f}{kw\rho_{ov}} \tag{8}$$

Table 11.2 Hydrocyclone characteristics

Parameter	Unit	Standard (in Russian classification)					
		HC-25	HC-50	HC-75	HC-150	HC-250	HC-360
Diameter D_c	mm	25	50	75	150	250	360
Cone angle α_{con}	degrees	10	10	10	10	10	10
Equivalent diameter of feed aperture D_f(a)	mm	6	12	17; 32	40	65	90
Diameter of overflow branch pipe D_{ov}	mm	7	13	22	40; 50	80	115
Diameter of the discharge opening D_{dis}	mm	4; 6; 8	6; 8; 12	8; 12; 17	12; 17; 24; 34	24; 34; 48; 75	35; 48; 75; 96
Pressure at entry in cyclone p_{en}	MPa	0.01–0.2	0.01–0.2	0.01–0.2	0.03–0.25	0.03–0.25	0.03–0.25
Throughput per feed with solid content up to 40% by pressure 0.1 MPa Q_c(b)	m^3/h	0.7	2.5	5	15; 20	50	95
Maximal size of solid particles in overflow δ_{max}	μm	10	10	10–60	28–95	37–135	44–180
Overall dimensions, max:							
length	mm	120	230	300	500	600	700
breadth	mm	70	100	350	450	650	750
height	mm	200	400	600	1100	1400	1900
mass	kg	2	6	20	100	220	400

(a): $D_f = \sqrt{\frac{4bh}{\pi}}$, where b and h are sizes of feed aperture (mm);

(b): if pressure p_{en} differs from 0.1 MPa, the throughput is corrected by multiplication on $\sqrt{10p_{en}}$

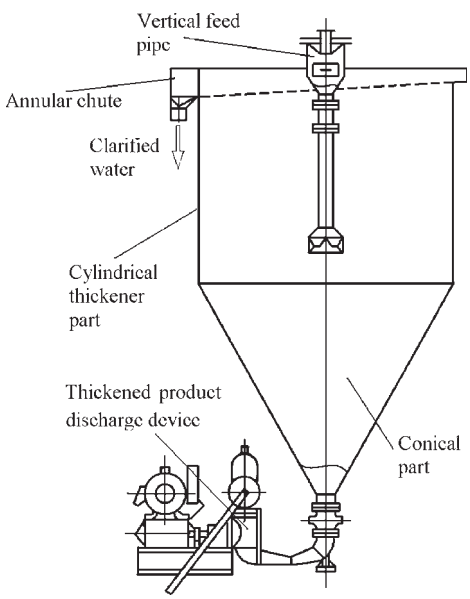

Figure 11.3 Cylindrical thickener.

where k is thickener surface use coefficient, usually $k = 0.75$; ρ_{ov} is overflow mass density, t/m^3.

The total sedimentation surface

$$F_s = \bar{f}G \tag{9}$$

then thickener diameter

$$D_{cyl} = \sqrt{1.27\bar{f}G + D_{feed}^2} \tag{10}$$

where D_{feed} is diameter of feeding conduit, m.

Filtration

Filtration is a process for separation of solids from the slurry by means of a porous medium which retains the solids and allows the liquid to pass. The operations are divided into two broad categories: 'cake' and 'depth' filtration. From the viewpoint of a driving force, cake filtration is moreover divided into pressure, vacuum, gravity and centrifugal operations. In cake filtration, particles contained in the slurry are retained in an incipient layer on the porous medium surface while the fluid passes through it. In depth filtration, particles are captured within complex pore structures of the filter medium and the cake is not formed on the medium surface. The first particles can enter the medium and, with very dilute slurries, there can be a time lag before a cake begins to form. Smaller particles enter the medium, whereas larger particles bridge the openings and start the buildup of a surface layer. Depth filtration is generally used to remove small quantities of fine particles. In practice, cake filtration is mainly employed in industry.

The equation of flow through porous media is based on Darcy's law that can be expressed in the form

$$\frac{dp_L}{dx} = \frac{\mu}{K_p} u \tag{11}$$

where dp_L/dx is the hydraulic pressure gradient, μ is the viscosity of the liquid, K_p is the permeability, and u is the apparent liquid velocity relative to the solids. This velocity is expressed as the volumetric flow rate per unit area, which is defined by

$$u = q - \frac{\theta}{1-\theta} r = q - er$$

where q is the apparent flow rate of liquid, θ is the local porosity, r is the apparent migration rate of solid particles and e is the local void ratio. In filtration, it is usual to use the volume v of dry solids per unit area instead of the distance x from medium surface. Hence, the incremental volume dv is given as

$$dv = (1-\theta)\, dx \tag{12}$$

Substituting Eqn (12) into Eqn (11) gives

$$\frac{dp_L}{dv} = \frac{\mu u}{K_p(1-\theta)} \tag{13}$$

While suspended solids are deposited during cake filtration, liquid flows through the interstices of the cake in the direction of decreasing hydraulic pressure (Figure 11.4). The solids forming the cake are compact and relatively dry at the filter medium,

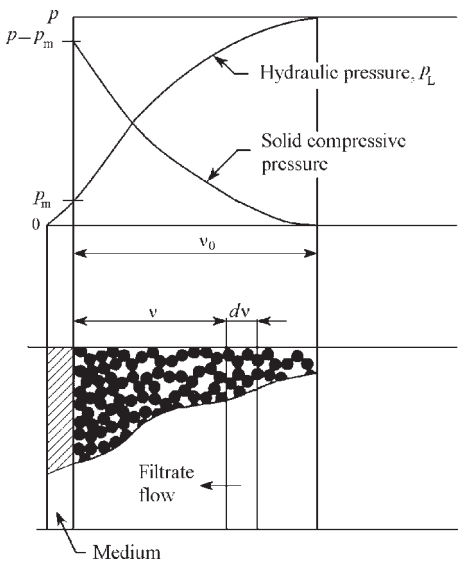

Figure 11.4 Schematic diagram of compressible filter cake. (Source: Ref 2)

whereas the surface layer is in a slurry and wet condition. So the porosity is minimum at the point of contact between the cake and the filter medium when $v = 0$ and maximum at the cake surface ($v = v_0$) where the liquid enters.

On the assumption that the inertial forces are negligible, the force balance can be written

$$p_L + p_s = 0 \tag{14}$$

where p_s is the local cake compressive pressure. Eqn (14) and Figure 11.4 show that the cake compressive pressure increases as the hydraulic pressure decreases.

It is basically assumed in compressible cake filtration theory that the local porosity and flow resistance are unique functions of the cake compressive pressure. The flow resistance α is related to the porosity ε as in Eqn (15):

$$\alpha = \frac{kS_0^2(1-\varepsilon)}{p_s \varepsilon^3} \tag{15}$$

where k is Kozeny's constant and S_0 is the effective specific surface of the solids.

Cake filtration processes are classified according to the variations of both the pressure and flow rate with time into the following kinds: (a) constant pressure filtration (by means of compressed gas maintained at a constant pressure, or a vacuum pump), (b) constant rate filtration (positive displacement pumps are employed), and (c) variable pressure, variable rate filtration (the use of a centrifugal pump results in the rate varying with the back pressure on the pump).

In practice, the original parameters for selection of the apparatus performance include specific loading per dry sediment, q_f, t/(m^2· h), filtration rate, u_f, m/h and drag during filtration, Δp, kPa.

The drag during slurry (pulp) filtering, Δp comprises the drag of the filter cake and of the filtering medium

$$\Delta p = p_\delta h + p_{fm}, \text{kPa} \tag{16}$$

where p_δ is the average specific drag of the unit thickness of the filter cake layer, kPa/m; h is the thickness of the filter cake layer, m; p_{fm} is the drag of the material of filtering medium, kPa.

The values of p_δ and p_{fm} are estimated experimentally on laboratory filtering apparatus at the adjusted values of filtration rate, u_f remaining unchanged and can also be determined by testing.

The specific loadings, q_f, t/(m^2·h) of atomized powders of copper, lead and zinc (and their alloys) are adopted as 0.1–0.2, 0.1–0.2 and 0.2–0.4, respectively.

A wide variety of filtration equipment is commercially available. The operating principles and

important features of typical filtration equipment in non-ferrous powder production conditions are described here.

Centrifugation

To dehydrate products in the metallic powder production industry, filtering centrifuges find a use.

The centrifugal settling is accomplished in centrifuges that include bowls of cylindrical or conical form with screen walls which rotate at high speed around their own axes. The product to be dehydrated (pulp) is fed into the bowl which involves the pulp rotational movement. The water present in the pulp is filtered under the action of centrifugal forces through the compressible filter cake settled upon the inner surface of the bowl wall and on the porous screen itself. The liquid phase passing through the screen is normally called the filtrate. Centrifuges with screen bowl walls are called filtering in contrast to settling centrifuges that have a solid wall.

Calculation of the centrifugal effect is restricted to the measurement of the rate of centrifugal filtering. At $Re < 1$, the rate of filtration, u_f is determined by Darcy's law:

$$u_f = k\rho_2\omega^2(R - 0.5h) \qquad (17)$$

where k is the coefficient of filtration determined either experimentally or using the Cozeny's formula:

$$k = \frac{0.2\theta^2}{S_0^2(1-\theta)\mu},\ \mathrm{m^2/(Pa\cdot s)} \qquad (18)$$

θ is the average porosity of the filter cake; S_0 is the volumetric specific surface of the solids, m^{-1}, μ is the viscosity of liquid, Pa·s (at 20°C the viscosity of water $\mu = 1.002$ mPa·s); ρ_2 is the density of liquid, kg/m^3; ω is the angular speed of rotation, c^{-1}; R is the radius of rotation circle, m; h is the thickness of filter cake layer in m; (Re is Reynolds number, determined from the formula

$$Re = \frac{\rho_2 u_f d_p}{\mu}$$

d_p is diameter of pore in the filter cake.

Calculated value, u_f and area of filtration, F_f (of screened surface of centrifuge walls) are determined starting from the required yield of dehydrated product. The F_f, R, and u_f parameters are used for selecting the desired centrifuge type.

Powders of copper and its alloys are produced using filtering centrifuges with the following performance: rotary drum internal diameter 1200 mm; the greatest number of rpm is 980; the greatest separation factor 640; shaft rotational speed 333–1000 rpm. As filtering material, a volumetric 300 mesh wire grid made from stainless steel as per CIS Standard GOST 3187-76 is used. Operating conditions are periodic, with a stopping interval for wet material feeding and manual removal of the filter cake from the walls. With the initial value of L: $S = 10$, residual humidity after dehydration ranges between 4 and 8%.

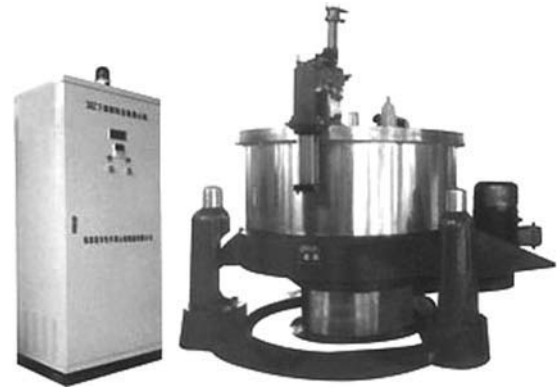

Figure 11.5 LD/SD series settling hanging-bag centrifuge. Source: Info of Jiangsu Peony Centrifuge Manufacturing Co. in China (www.Mudancentrifuge.cn).

In an improved machine, removable filtering bags are used followed by unloading normally. In another model, the centrifugal machine includes a bottom-unloading scraper. The material enters the rotary drum from the top. Under centrifugal force, the liquid passes through the filtering medium and is discharged out of the machine and the solid is left in the rotary drum. When the rotary speed falls, the scraper scrapes the solid material which is discharged from the bottom of the machine (Figure 11.5).

A more upgraded filtering as well as settling centrifuge is automatic and continuous operation, equipped by scraper scroll-type for continuous removal of the precipitated cake (Figure 11.6). Such centrifuges have maximum rotational speed of 6000 rpm, separation factor up to 4000 and ratio of basket operating length to internal diameter max 3.1.

Cartridge Vacuum Filter

Vacuum filters of batch type designed by the Design Bureau of IPMS (Figure 11.7) have filtering elements of cylindrical form made of sintered porous materials. The general filtering area of each filter element is 0.6 m^2. The filter elements are arranged horizontally

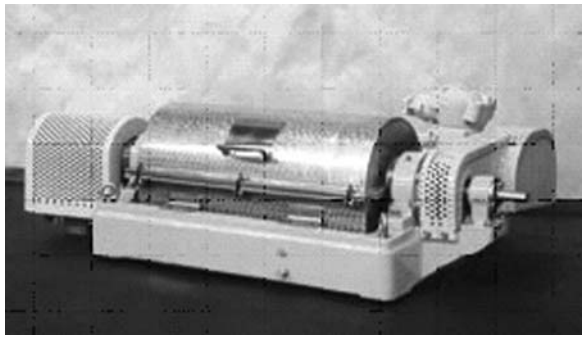

Figure 11.6 OGSh series automatic and continuously operated, horizontal performance, and equipped by scraper scroll-type for continuous removal of the precipitate cake settling centrifuge. (Source: Info of JSC Sumy Frunze NPO Company in Ukraine) (www.frunze.com.ua)

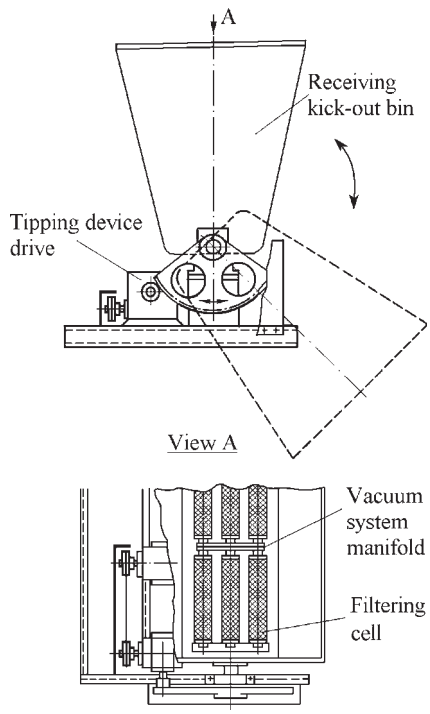

Figure 11.7 Cartridge vacuum filter.

in the lower portion of the receiving bin with a 30 mm gap relative to the bottom. One end of the cylindrical filter element is blanked-off and the second end is connected to the manifold of the vacuum system via a branch pipe. The slurry or thickened product is charged into a receiving bin and the vacuum pump is switched on. With the removal of the moisture from the material, the powder layer is densified and itself retains the fine particles, decreasing the breakthrough of particles into the filtrate and

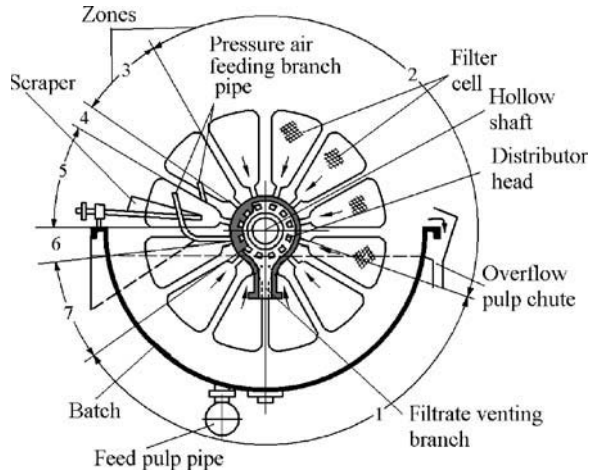

Figure 11.8 Rotary disk filter.

protecting the filter elements against blinding. The sucked-off condensed moisture (filtrate) is collected and trickles down into a container and then returned to the recycled water supply. The dehydration procedure takes from 10 to 20 minutes depending on the powder properties and water content. With the initial ratio L to S in ranges from 2 to 4 in the thickened pulp supplied to the receiving bin, the residual content of moisture will be 8–15 wt%.

When the residual moisture content reaches the required level, the vacuum pump is stopped; the receiving bin is tilted by a rotary device and the damp material discharged.

Rotary Disk Filter

Disk vacuum filters (also termed 'rotary drum filters') are designed for filtering suspensions containing particles that settle mainly at a rate of less than 18 mm/s. The process of filtering is continuous. The operation of this filter is schematically shown in Figure 11.8. The slurry is supplied via a pipeline to a bath containing sunken disks in the form of hollow chambers (filter cells) with perforated surfaces wrapped with a filter material. The slurry excess is poured down into a chute to receive overflowed slurry. The filter cake is removed from the filter cell surface by scrapers. A distributor head is intended for leading away the filtrate and exhaust air and feeding air to blow the filter cake layer off. The filter is equipped with a variable speed gear that allows variation of the number of revolutions of the shaft between 10 and 80 revolutions per hour. When rotating, the disk passes the following zones per each rotation:

1. formation of the filter cake and exhaust of the filtrate

2. drying the filter cake
3. 'dead' zone
4. blowing the filter cake away
5. removing the filter cake
6. blowing through and cleaning the filter
7. 'dead' zone.

Filter Press

The dehydration of dense suspensions, which may include fine slurries from sedimentation tanks, is performed using apparatus operating under pressure – filter presses. There are various designs of filter press: chambers, plate-and-frame, sheets and disks.

For dehydration of slurries accumulated in the settling tanks, a simple design plate-and-frame type filter press can be used having manual or electromechanical drive of the clutch (Figure 11.9). The filter is composed of vertically arranged alternating plates and frames, which are connected together and tightened by screw or hydraulic ram, formatting the chambers and making a gasket of the filter cloth.

The slurry feed is introduced into the chambers under pressure of 0.5–1.0 MPa. The liquid passes through the filter medium which, in turn, retains the solids. The filtrate is removed at a discharge outlet. Completion of the cake formation is controlled by the filtering time, decrease in the rate of the feed, on a rise in back pressure. Once the frames are full of cake, filtration is stopped and a wash liquid is applied if the solids are to be recovered. The yield per dehydration of slurries ranges from 7.5 to 15 kg/(m^2·h); residual moisture in the filter cake amounts to 19–25 wt%.

The filter press is composed of a series of horizontal filter plates that are lifted and sealed by the clutch and the filter cloth in the form of a continuous tape extending zigzag between the filter plates can eliminate the step of preliminary thickening of the pulp and automate the dehydration procedure. When discharging the filter cake, the filter cloth is relocated by the drive of tape feed. The filter cake is discharged from two sides of the tape simultaneously. The cloth is washed in the regeneration chamber. The pressure when feeding the pulp is maximum 1.2 MPa. The suspension contains from 10 to 500 kg/m^3 of solid phase. Filtering conditions for pressure filters are determined by experiment for each type of suspension.

The use of pressure filters for suspensions containing coarse particles is not recommended because of silting up of the inlet collecting manifold and the channels that feed the suspension.

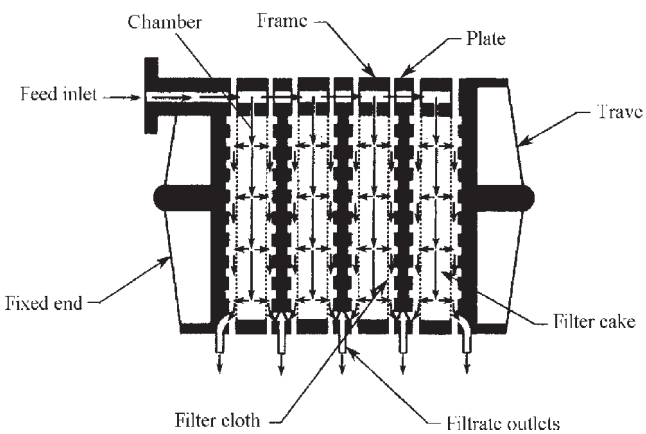

Figure 11.9 Plate-and-frame type filter press.

Thermal Drying

Introductory Conceptions and Objectives

Water Content

Thermal drying is a process for the dehydration of moist products based on moisture evaporation by heating. The heat for evaporation is transferred to the material, which is dried, either by heated hot gas or smoke fumes – fuel combustion products (convective heat transfer), or from hot surface by the material's contact with it. The heat may also be applied by radiation and high-frequency currents.

In drying techniques, the following forms of moisture in the material being dried are differentiated: free, absorbed, excess and moisture equilibrium.

The free moisture is the difference between total moisture and maximum adsorbed moisture. The absorbed moisture (w_a) is the moisture adsorbed on the powder surface, which is dependent on the hygroscopic property of the material and moisture content of the environment.

The excess moisture is the free and partly adsorbed moisture, which can be removed from material by means of evaporation in dry conditions. The moisture equilibrium (w_{eq}) is the difference between the total and excess moisture.

Heated air, smoke fumes or their mixture, with a volume of aqueous vapor may serve as a medium-term drying agent producing an evaporable moisture from the material which is being dried.

In air drying, it is necessary to avoid heating the powder to a temperature that will cause it to oxidize. The amount of water that the drying agent will absorb depends on the content of water already

present and also on the gas temperature and pressure. The moist gas pressure may be represented as

$$p_h = p_{p-d} + p_{aq-v}$$

where p_{p-d} and p_{aq-v} are partial pressure of dry gas (air) and water vapor, respectively.

A saturated gas is one that contains the maximum amount of water vapor that it can hold at the given temperature and pressure.

There are used two types of (mean) water content: dry-basis water content (w) (kg water per kg dry material) and wet-basis water content (w^*) (kg water per kg wet material). The former is much more handy for calculation than the latter:

$$w = \frac{w^*}{1 - w^*} \tag{19}$$

$$w^* = \frac{w}{1 + w} \tag{20}$$

Drying Characteristic Curve

In the conditions when a wet non-hydroscopic particulate material is being held in a hot airstream of constant temperature, humidity and velocity, the water content w and the material temperature t^m change with time during drying, as shown in Figure 11.10. The drying process after preheating consists of the following two periods: (I) constant drying rate period and (II) decreasing drying rate period.

During the preheating period, heat is transferred to the material on heating from an initial temperature t_1^m to wet-bulb temperature t_w with the humidity evaporation. This drying period is usually small in comparison with other drying periods. After preheating, there is a constant drying rate period (BC) when free water exists on the surface of the material and material temperature t^m remains constant and is equal to the wet-bulb temperature of the hot air, t_w. This period continues until the water content becomes the critical value w_{cr}, which decreases with reduction of the material size.

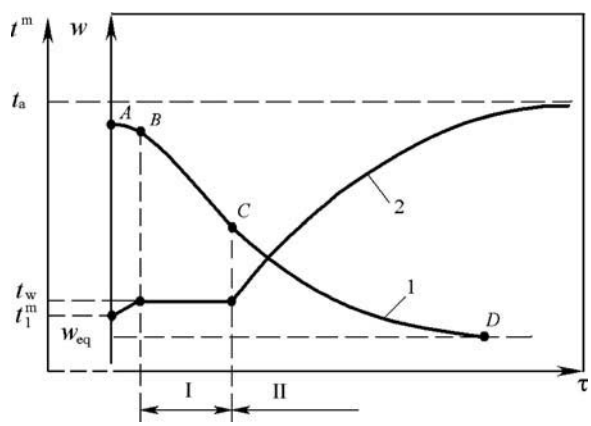

Figure 11.10 Drying characteristic curve (1) and heating curve (2) of materials for two periods: (I), constant drying rate period and (II), decreasing drying rate period.

During period II, there is no free water on the surface. As evaporation takes place from the surface and proceeds throughout the bulk by diffusion of vapor in the material, the drying rate decreases with time until, finally, drying ends at the equilibrium water content w_{eq}. Hot-air heat is consumed for heating up the material as well as for water evaporation and the temperature rises from t_w until it finally reaches hot air temperature t_a.

The shapes of drying characteristic curves are individual for each solid material, but commonly changing of average humidity content with time has the form represented in Figure 11.10.

Drying Rate

During the constant drying rate period, the drying rate R_c is apparently equal to the evaporation rate from the free water surface:

$$R_c = \frac{G}{S}\frac{dw}{d\tau} = k(H_m - H) \tag{21}$$

where G is the mass of dry material, kg; S is the drying area of material, m^2; w is the dry-basis water content (kg water/kg dry material); k is the film mass transfer coefficient, kg/(m^2·h·ΔH); H is the humidity (kg water/kg dry air); H_m is the saturated humidity at t_m (kg water/kg dry air); τ is drying time, h.

When the heat is supplied from hot air only, the material temperature t^m is equal to the wet-bulb temperature of the air t_w. Then,

$$R_c = \frac{h(t_a - t_w)}{r_w} \tag{22}$$

where r_w is the heat of water evaporation at t_w (kJ/kg).

The decreasing drying rate R_d is strongly affected by the material properties and drying method. This drying rate can be estimated [3] by

$$R_d = \rho_s \delta_s r_w \frac{dw}{d\tau}\left[1 + \left(\frac{c}{r_w}\right)\frac{dt_s}{d\tau}\right] \tag{23}$$

where ρ_s is the density of solid (kg/m^3), δ_s is the modified radius of particles (m), c is the specific heat of

the material (kJ/(kg·°C)), and t_s is the temperature of particles.

Eqn (23) is a fundamental equation of drying kinetics but, to use it, it is necessary to know the water content dependence on drying time. It is possible to obtain this dependence by solution of differential equations of system of heat and mass transfers which is a very difficult task. Approximate answers to the equation simplify a problem. Thus, Lykov [4] proposes a different method, replacing the decreasing drying rate curve by a straight line. Then the decreasing drying rate period can be described as

$$-\frac{dw}{d\tau} = K(w - w_{eq}) \tag{24}$$

where K is the proportionality coefficient, called the drying coefficient.

If the condition-dependent part is only extracted, the drying coefficient may be represented by:

$$K = \kappa R_c \tag{25}$$

where κ is the relative drying coefficient.

As it should be from Eqn (24), K is the slope ratio of the straight line and is determined in the following way:

$$K = \frac{R_c}{(w_{eq} - w)} = \kappa R_c$$

Integration of Eqn (24) gives

$$\frac{(w - w_{eq})}{(w_c - w_{eq})} = \exp(-\kappa R_c \tau) \tag{26}$$

Taking the logarithm of the last expression gives the approximate equation of the drying rate curve

$$\lg(w - w_{eq}) = \lg(w - w_c) - \frac{1}{2.3\kappa R_c \tau} \tag{27}$$

Knowing the drying coefficient, it is possible to define the decreasing drying time, and so, for the relative drying coefficient determination in practical terms, simple dependence is used

$$\kappa = \frac{1.8}{w} \tag{28}$$

Dryer Selection and Design

Many types of dryers have been developed and operated. First, dryers should be selected based on size and shape of the powder particles, water content, the production rate and the mode of drying operation. Then, the properties of the material (e.g. chemical activity, behavior at elevated temperatures, and stickiness) are taken into consideration, when the selection of dryer type is made. Finally, the volume of the dryer selected should be estimated.

For dryers receiving convective heat from hot air, the rate of heat transfer q is given approximately in batch operation by:

$$q = h_v V(t - t_m) \tag{29}$$

in continuous operation by

$$q = h_v V(t - t_m)_{lm} \tag{30}$$

For those of conductive heating type,

$$q = U_k A_k V(t_k - t_m) \tag{31}$$

where h_v is the volumetric heat transfer coefficient, kJ/(m^3 · h · ^{0}C); V is the volume of dryer, m^3; t is the hot air temperature, °C; t_m is the material temperature, °C; $(t - t_m)_{lm}$ is the logarithmic mean of the temperature differences between the hot air and the material at the material inlet and outlet; U_k is the overall heat transfer coefficient, kJ/(h · °C m^2); A_k is the heating area of material by conduction, m^2; t_k is the temperature of heat source, °C.

Pneumatic Convective Dryer

In the pneumatic convective dryers, the drying is accomplished during transport, by heat-carrying gases as a consequence of convective heat transfer. The apparatus consists of an upright directed tube where drying takes place in upward suspended solid current (Figure 11.11). Such dryers are named 'tube-dryers'. Powder time in the drying zone amounts to several seconds. The upward suspended solid current velocity must be larger than the maximum size of particle in the powder fractions subject to drying (usually in the range from 15 to 40 m/s).

A drying active regime is provided under the conditions of non-stationary interaction of phases along all drying conduits. Thus, there are rational reasons to design the tube-dryers with variable diameter (with widening), while the permanent diameter rectilinear divisions must not be taken as acceleration divisions. Calculation methods of pneumatic convective dryers are described in Refs [5, 6]. A simple and sufficiently reliable calculation method is given below.

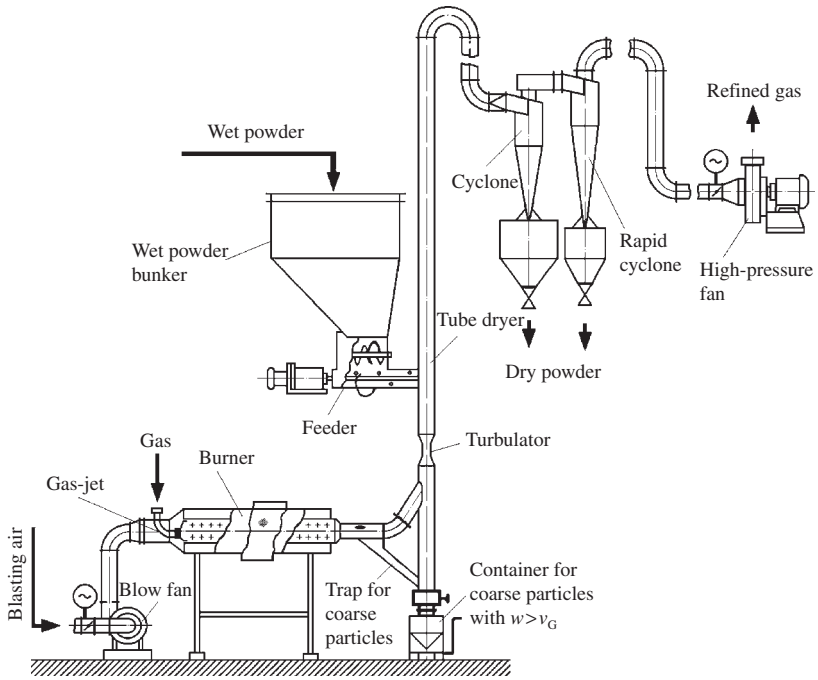

Figure 11.11 Pneumatic conveying dryer.

1. For calculation of thermal conductivity α between gas and particles before the ratio is defined according to [7]:

$$\mathrm{Nu} = 0.4\mathrm{Fe}^{0.9} \tag{32}$$

where *Fe* is Fedorov's criterion (it is also named Kirpichev's criterion):

$$\mathrm{Fe} = \bar{d}_{\mathrm{f}}\sqrt{\frac{4g(\rho_1 - \rho_2)}{3v^2\rho_2}} \tag{33}$$

where $\bar{d}_{\mathrm{f}}$ is average surface diameter, m; g is acceleration of gravity, m/s^2; ρ_1 and ρ_2 are mass density of solid particles and gas, respectively, kg/m^3; v is kinematic viscosity (at average temperature), m^2/s.
So, the average diameter of particles in order of particle number and particle mass are respectively

$$\bar{d}_{\mathrm{eq\cdot n}} = \sqrt{\frac{\sum n_{\mathrm{i}} d_{\mathrm{eq\cdot i}}^2}{\sum n_{\mathrm{i}}}}, \text{ and } \bar{d}_{\mathrm{eq\cdot m}} = \sqrt{\frac{\sum \dfrac{m_{\mathrm{i}}}{d_{\mathrm{eq\cdot m,i}}}}{\sum \dfrac{m_{\mathrm{i}}}{d_{\mathrm{eq\cdot m,i}}^3}}} \tag{34}$$

where $d_{\mathrm{eq,1}}$, $d_{\mathrm{eq,2}}$, … $d_{\mathrm{eq,n}}$, are irregular shape particle diameters modified to spherical shape; n_1, n_2, …. n_{n}, and m_1, m_2…. m_{n} are their share to total particle number and mass of particles, respectively.

2. Thermal conductivity

$$\alpha = \mathrm{Nu}\lambda/d_{\mathrm{eq}} \tag{35}$$

where λ is heat conduction coefficient of W/(m·^{0}C).

3. Summarized surface of particles, passing through the dryer during one hour

$$\sum F_{\mathrm{p}} = 6G_1/d_{\mathrm{eq}}\rho_1 \tag{36}$$

where G_1 is the material flow rate, kg/h.

4. Drying duration in seconds

$$\tau = 3600Q/\alpha\sum F_{\mathrm{p}}\Delta t_{\mathrm{av}} \tag{37}$$

where Q is heat consumption on particle heating and moisture evaporation; Δt_{av} is the average difference of temperatures between the gas and powder particles, °C.

5. The hover rate defined by a graphic approach [8] finds wide application. The $\psi\mathrm{Re}_{\mathrm{w}}^2$ complex value is defined by Eqn (38):

$$\psi\mathrm{Re}_{\mathrm{w}}^2 = \frac{4}{3}\mathrm{Ar} \tag{38}$$

where Re_w is the Reynolds number to $Re_w = wl/\nu$ at hover rate w; Ar is the Archimedes number to $Ar = g(\rho_1-\rho_2)\beta/(\rho_2\,\nu)$; l is the characteristic particle size, in this case to $l = 1.5\Omega_p/F_p$; Ω_p is the particle volume; F_p is the particle surface; ψ is the aerodynamic resistance coefficient; $\psi = 2g(\rho_1-\rho_2)\Omega_p/(w^2\rho_2 F_p)$ or in criterial form, $\psi = 4Ar/3Re_w^2$.

According to the calculation of Re_w^2 value by Eqn (38), the Re_w magnitude is found from nomographic (Figure 11.12) followed by definition of maximum particle size hover rate.

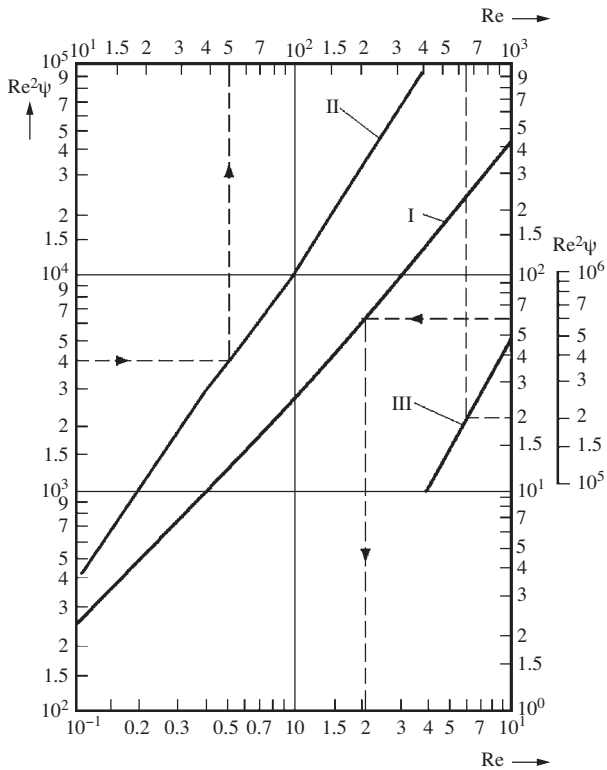

Figure 11.12 Nomographic for Re_w definition using calculated ψRe_w^2 values (use sequence of nomographic is shown by arrows; the curve I corresponds to right and lower scales in ranges ψRe_w^2 values from 3 to 400, the curve II corresponds to left and upper scales in ranges ψRe_w^2 values from 400 to 100 000 and curve III corresponds to additional scale in area ⩾100 000.

6. The influence of particle shapes is taken into account by means of a dynamic shape coefficient χ_D determined by the ratio of particle resistance force R_p to volume equivalent sphere one R_{sp} at relative velocity:

$$\chi_D = \frac{R_p}{R_p} = \frac{4\psi_p s_p}{\psi_{sp}\pi d_{sp}^2} \tag{39}$$

where ψ_p and ψ_{sp} are the aerodynamic resistance coefficients of the real particle and volume equivalent sphere; s_p is the particle midlength section. A method of the coefficient χ definition and its values are given in source [8]. Table 11.3 includes the magnitudes of χ_W, χ_D, and w for typical geometrical shape particles. Here $\chi_W = w/w_{eq}$, i.e. ratio of real shape particle sedimentation rate to volume equivalent sphere one.

7. The gas velocity in a tube-dryer is 1.3 to 1.5 times more than the hover rate of the largest size particle.

The vertical tube part length of tube-dryer amounts to $l_{t-d} = \tau(v_G - w)$.

The diameter of the vertical tube

$$D_{tub} = \sqrt{\frac{L_G}{0.785 v_G}} \tag{40}$$

where L_G is gas consumption moving in vertical tube, m^3/s; v_G is gas velocity, m/s.

Spray Drying

Spray drying is a process in which a slurry or a solution is atomized into droplets in a chamber through which heated gases, usually air, are passed. A typical spray dryer using a disc atomizer with cocurrent air flow is represented in Figure 11.13.

Spray drying is a continuous rather than a batch process that allows close control of particle size, apparent density and moisture content. Particles have very short exposure time. Residence time within

Table 11.3 Magnitudes of χ_W, χ_D, and ψ for typical geometrical shape particles

Particle shape	χ_W	χ_D	ψ
Spherical	1.0	1.0	0.5
Roundish	0.74	1.83	0.915
Angular	0.635	2.48	1.24
Oblong	0.56	3.18	1.59
Lamellar	0.392	6.50	3.25

the dryer chamber usually ranges from 2 to 20 s, depending on dryer size and mixing scheme (cocurrent, countercurrent, or mixed flow). Therefore, heat-sensitive materials can be spray dried. Lubricating additives can be added for subsequent processing.

Spray drying also has several advantages over other powder processing techniques, particularly in applications requiring agglomerates for subsequent pressing and sintering operations.

The atomized droplets dry rapidly due to their high surface-to-volume ratio. Coarse dried solids fall to the chamber bottom and are continuously collected (see Figure 11.13). The finer particles are separated by cyclone and ultrafine particles are collected by bag filter. Droplet-air mixing in spray dryers is determined by the location of the disperser and the atomizer, resulting in the given relative directions of the cooler air current and atomized droplets stream formation.

Cocurrent conditions exist when the atomizing device is located near the hot air disperser at the top of the dryer (see Figure 11.13).

In cocurrent drying, the maximum temperature to which larger dried particles are exposed is approximately 10°C less than the outlet temperature of the dryer. This is explained by the evaporative cooling effect that occurs when the liquid leaves the droplet while passing through the heated zone. Finer particles, which dry more quickly, reach temperatures approaching those of the inlet gas. In cocurrent conditions, the settling rate of particles is determined by their hover rate and drying agent velocity.

The spray dryers work also in countercurrent or mixed-flow conditions. However, cocurrent drying is mostly used, since it allows drying at high temperatures without overheating of materials.

In countercurrent conditions the settling rate is less. When the atomizing device is placed at the top of the chamber and the air disperser is located at the bottom, immediately after formation, the droplets contact cool humid air, while, as their moisture content decreases, they are exposed to increasingly hotter air. When the slurry is introduced from the bottom and gas from the top of the dryer, droplets dry both in their upward and downward movement. Therefore, narrower, shorter dryer chambers can be used. However, if partially dried products cannot be exposed to overheating, both modes of countercurrent spray drying may not be applicable.

Mixed-flow conditions are a combination of cocurrent and countercurrent air flow. This type is commonly used in fountain-type dryers, where a nozzle atomizer is located at the base of the drying chamber and the air disperser is placed at the top of the chamber (Figure 11.14).

For fine particles, precipitation and decrease of carryover of the air rate in the chamber (per its total cross-section) commonly does not exceed 0.3–0.5 m/s. But, even by such rates, the carryover is considerable and it is necessary to provide for collection of fine airborne particles.

Convective Dryer with Fluidized Bed

Convective dryers with fluidized bed have been widely used because of their high drying efficiency, resulting from intensive heat-mass exchange in the fluidized bed. The volume heat exchange coefficient related to a fluidized bed amounts to approximately 5–10 kW/(m^3·°C), while for drum dryers per total

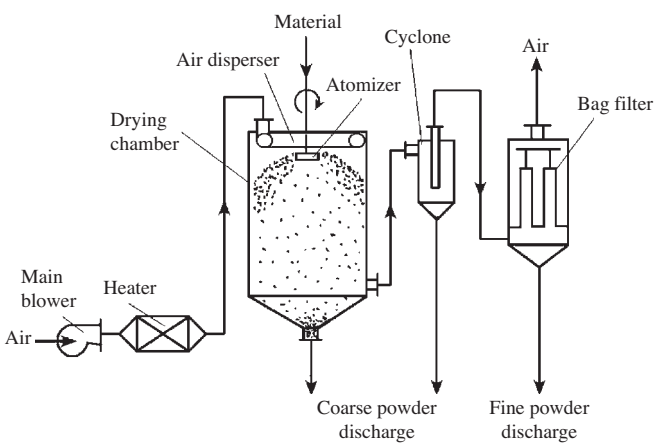

Figure 11.13 Spray dryer with cocurrent air flow.

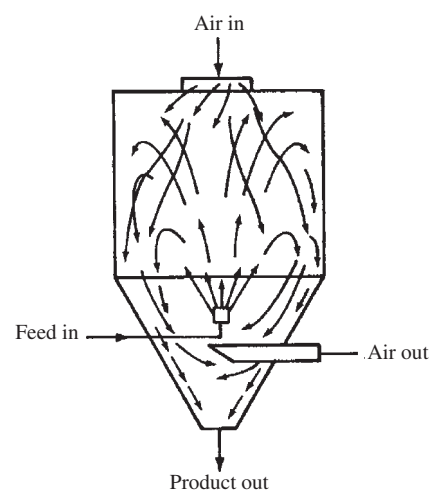

Figure 11.14 Mixed-flow type of spray dryer.

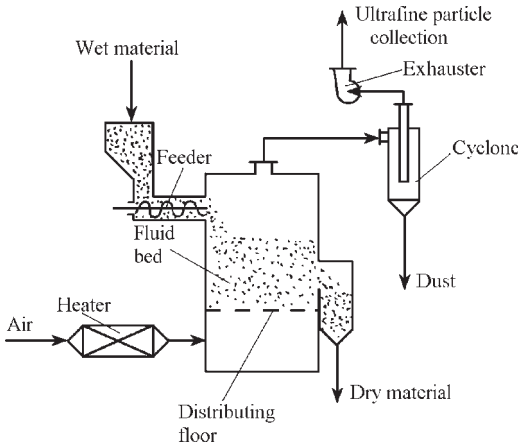

Figure 11.15 Single-stage continuously working dryer with fluidized bed.

volume attains not more than 0.5 kW/(m^3·°C). In fluidized bed installations, it is possible simultaneously to carry out several processes: drying and burning, drying and particle size classification, drying and granulation, etc. However, these dryers have disadvantages too: high energy consumption, low process rate under fine powder drying conditions, abrasion of the powder particles and dust fraction formation results, and carryover of ultrafine particle fractions.

The dryers with fluidized bed designs are multifarious. Single-stage continuously working dryers are most widespread (Figure 11.15). In dryers with a cylindrical chamber, a drying irregularity is observed, resulting from variation of dwelling time of particles in the fluidized bed chamber. In order to increase the drying uniformity, the dryers with a dilative upward section are used. Due to decreased air rate, the carryover of fine particles is decreased and the drying uniformity is increased.

Shaker Dryer

In a vertical shaker dryer, the powder is moved on a vibro-fluidized bed and is heated via convective and conductive heat [9]. A continuous operation dryer, SVT–0.5 (Figure 11.16) consists of an upright tube with a lift helical chute wound around one heat insulated casing, vibroexciters, and an elastic suspension. The chute with a vertical tube forms a freely oscillating above resonance vibration system. The casing has doors, opening externally. The inner surfaces of the doors have attached electrical heaters. The unit is supplied by loading and unloading branches attached inside the casing, and also by a branch to carry away the

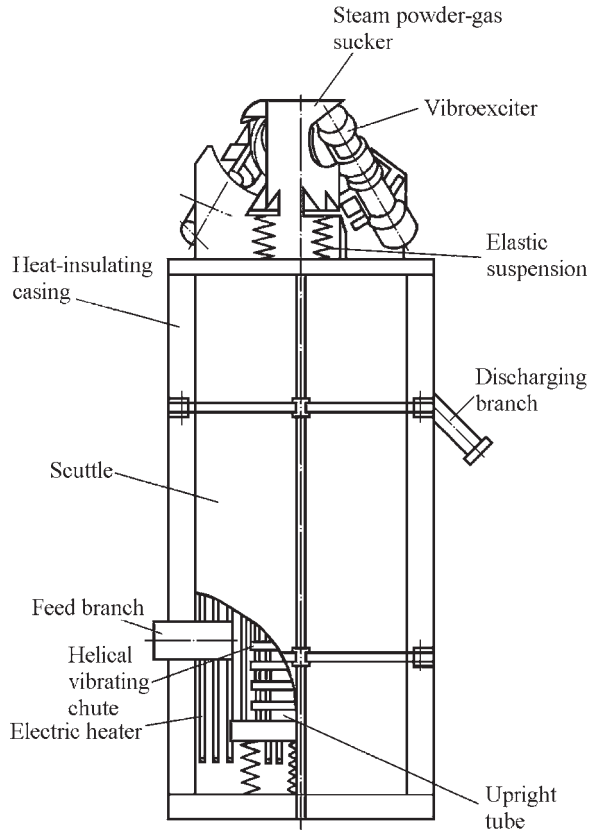

Figure 11.16 Continuous operation vertical shaker dryer, SVT–0.5.

vapour–dust–gas mixture. The air is sucked in through openings in the casing, passes via built-in channels in the casing, goes up, flows around the spiral chute with the material, which is dried and is sucked away together with the evaporated moisture through the branch. The material lifting combined with drying favors a space-saving arrangement of the dryer and adjacent units of the processing system.

The dryer throughput in terms of evaporating moisture amounts to 80 kg/h; duration of the material held in the dryer can be varied from 3 to 8 minutes by means of the oscillation amplitude from 2 to 5.2 mm at a frequency of 16.6 Hz; the volume of vapour–gas mixture to be exhausted from the dryer should not be above 1500 m^3/h. The height of lifting of the material from the loading level to the unloading level is 2.0 m. The working components adjacent to the material being dried are made from corrosion-resistant steel; the installed power of the tubular electric heaters is 120 kW. The heating power is regulated by switching on a certain number of heater segments.

For atomized bronze powder, Cu–5Sn–5Zn–5Pb with particle fraction finer than 150 μm, inclusive after centrifugation to a water content up to 7–8%, and initial temperature of 20°C, the following drying conditions in a shaker dryer are: holding period of the powder in the dryer amounts to 6 minutes, temperature of the dry powder as unloaded from the dryer is 105°C, throughput of dried powder is 400 kg/h, and the power of operating segments of heaters is 60 kW.

The drying process can be performed by preliminary warmed gas (air) in the heater with a supply to a shaker dryer. This scheme excludes zone localized overheating of the powder in the dryer.

Shaker Infrared Dryer

Such dryers operate in continuous regime, in which large quantities can be dried (Figure 11.17) [9]. During moving, a wet particulate material (powder) in a horizontal vibrating vibro-fluidized bed is formed, which is heated via infrared radiation. Typical specifications of commercially available shaker infrared dryers are given in Table 11.4.

The application of shaker dryers is limited by high content of ultrafine particles carried over by the aspirated air.

A main advantage of infrared drying in comparison with convection and contact is a possibility of obtaining large thermal currents. For instance, at radiation temperature 600°C, the thermal current amounts to 22.5 kW/m^2, while at gas temperature 600°C and flow rate about 2 m/s the heat current density does not exceed 8.0 kW/m^2. However, the large thermal current causes initiation of big temperature gradients that is not always acceptable.

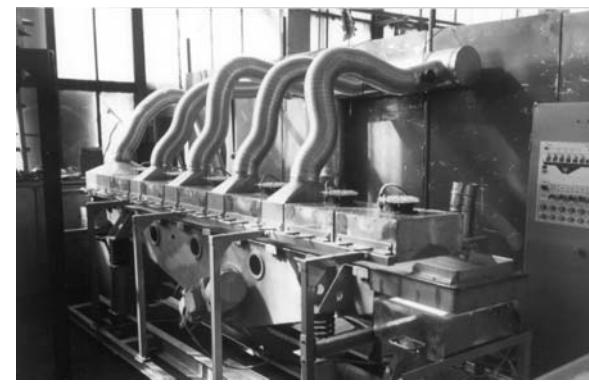

Figure 11.17 Infrared shaker dryer SVIK. Courtesy of Consit Production Company, Moscow.

Table 11.4 Typical specifications of commercial available shaker infrared dryers, SVIK

Parameter	Unit	Trademark[a]	
		SVIK-100	SVIK-350
Throughput:			
In terms of initial product	kg/h	100	350
In terms of evaporating moisture	kg/h	10–12	30–35
Number of infrared cassette	item	5	7
Parameter of cassettes number of lamps	idem	4	7
Capacity	kW	4	7
Installed power of infrareds	kW	20	49
Driving actuators	kW	0.37 × 2	0.75 × 2
Ventilators	kW	0.68	0.99
Heating temperature of material	°C	max200	max220
Drying time	minutes	max1.5	max1.5
Airflow:			
for cooling of lamps	m^3/h	800	900
for cooling of a product	m^3/h	600	1200
Extraction of water vapour	m^3/h	800	900
Overall dimensions[b]:			
length	mm	3440	4368
width	mm	930	1160
height	mm	1170	1340
mass	kg	600	900

[a]Consit shaker infrared dryers;
[b]Overall dimensions and mass are given without taking into account air conduits.

Drum Contact Dryer

There are convection as well as contact drum dryers in use. Here, combustion products of natural gas are used as drying agent. A drum dryer consists of a welded cylinder with two bands supported by radial-bearing rollers. Drum axial rotation is performed through a toothed hoop attached on the drum and made into toothing with the drive gear. One side of the drum adjoins a firebox with a mixing chamber and a loading device, the other has an unloading chamber for dried material.

The combustion gas, because of decreased content of oxygen, also plays the role of protective atmosphere and prevents oxidation of powder during drying.

Heat rate on drying under the contact heat mass exchange is higher than that of a convection one. Conduction units are justified when drying ultrafine powders for the avoidance of their carryover with combustion gas.

The design and calculation of a convective drum dryer are given in [1,3].

Among the known designs of contact drum dryers, the unit [10] exhibits essential advantages. Because of the connection of the vapor outlet tube (Figure 11.18) to the drum with the material, the counterflow of the air-vapor mixture current and material occurs along the longitudinal axis of the drum. As a result, the maximum flow rate of the air–vapor mixture occurs in the feeding part of the drum, where the material is still wet and its particles are in a bound state and dynamic interaction with the flow of air–vapor current does not lead to carryover of powder. In the discharging part of the drum, the air-current is completely absent and powder carryover does not occur, despite the fact that the material is dry in the discharging part. The material takes up the heat not only from the warmed inner drum surface, but also from the air–vapor current thus accelerating the drying process.

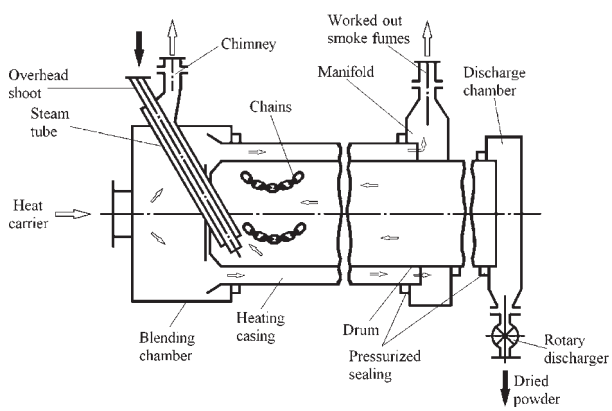

Figure 11.18 Drum conducted dryer.

Vacuum Dryers

A shelf vacuum batch dryer is a simple type of the contact batch operation dryers. Such dryers are manufactured with shelves of areas: 4.5; 16; and 33 m^2 by Berdichev plant Progress (www.progress.ua). It is a horizontal cylindrical apparatus with two pivoting butt lids. The apparatus has inside mounted shelves made in the form of heated plates. Dryers having areas of 4.5 and 16 m^2 are heated by steam. The residual pressure inside the dryer is 2.63 kPa; the maximum temperature of the plate wall is 150°C; the pressure of heat carrier in plates is 0.4 MPa.

Shelf vacuum dryers are contact apparatus of batch operation; they are used for drying heat-sensitive materials (for instance, magnesium and titanium powders). However, they are inefficient and ineffective, inasmuch as drying takes place in a motionless layer, in the presence of bad conductive heat gaps between particles and between the layer and give out warmth plates. They are used in small-capacity manufacture with a wide assortment of products.

The drying rate increases in hoe-type vacuum dryers as a result of mixing by slowly revolving horizontal stirring rod with paddles (Figure 11.19). Parallel with this they do not need the manual charging and unloading of material like shelf vacuum batch dryers.

The hoe-type vacuum dryer with batch operation has a cylindrical body with a steam jacket. The reversing motor means automatic changes every 5–6 minutes. Thus, during drying a material moves from the middle to the ends of the dryer body and back. The freely rolling rods between the paddles assist the destruction of lumps and additional mixing of materials. The dryer is connected to a steam condenser and vacuum pump.

Powder Classification by Size

Particle size and size distribution have a significant effect on the behavior during processing, thus to a considerable extent, they govern the properties of the final products made from powders.

In the technological processes commonly used, powders have a wide range of size and need to be adjusted before use. Usually the powders are classified by size, dosed in a given ratio, and blended. Classification by size can be achieved either by screen on a subdividing partition or by fluid forces. The fluid is usually water or air, and the field force may involve gravity or centrifugal or Coriolis forces. Hydroclassification in moving or motionless liquid media and dry classification in gas flows are used.

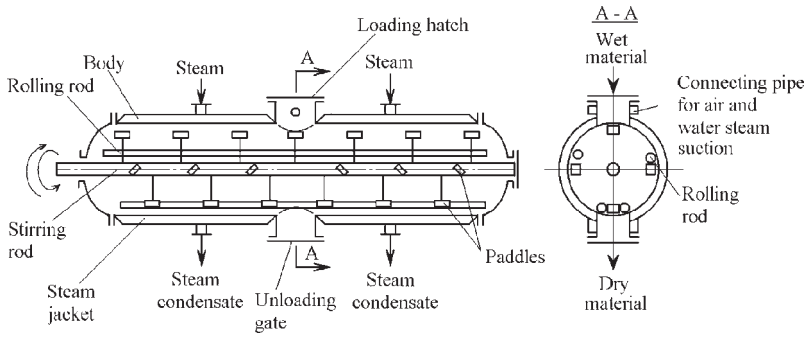

Figure 11.19 Hoe-type vacuum dryer.

The main technological characteristics of the classification process are efficiency of division size fractions and effectiveness of a size separation (ε). In evaluation of the separation process, the following parameters are participated: the weights of the feed (M), coarse stream (M_R), and fine stream (M_U); the cumulative fraction undersize of feed, $F(x)$, coarse stream, $F_R(x)$, and fine stream, $F_U(x)$; and x is particle size. Then:

$$M = M_R + M_U \tag{41}$$

The total fine efficiency

$$E_U = \frac{M_U}{M} \tag{42}$$

and the total coarse efficiency

$$E_R = \frac{M_R}{M} \tag{43}$$

so that $E_R + E_U = 1$. However, total efficiency does not enable us to determine the effectiveness of a classification process, because it only defines how much of the feed ends up in one or other of two outlet streams, not how much of the desired material arrives at the correct outlet stream. To discover this, it is necessary to determine the grade efficiency.

Thus, the grade efficiency at size x is a ratio of desired material in product of size x to the amount of desired material of size x in the feed. Therefore, coarse grade efficiency at size x may be defined as:

$$M_R(x) = \frac{M_R}{M}\frac{dF_R(x)}{dF(x)} \tag{44}$$

and taking into consideration Eqn (43)

$$M_R(x) = E_R\frac{dF_R(x)}{dF(x)} \tag{45}$$

Similarly, the fine grade efficiency is defined as:

$$M_U(x) = E_U\frac{dF_U(x)}{dF(x)} \tag{46}$$

Consequently, from Eqns (41), (42) and (46)

$$M_U(x) = 1 - M_R(x) \tag{47}$$

However, generally these ratios do not define the sharpness of the cut and it is important to know the amount of fines in the coarse and the amount of coarse in the fines.

For these cases, the evaluation of the effectiveness of a separation process for the fine yield is defined by the ratio of the weight of the fine fraction in the fine stream to the one in the feed stream. Some of the fine fraction remains in the coarse stream. The amount of fine particle content in the coarse stream c_R depends on the efficiency of the separation process and content of fine fraction in the feed stream c:

$$c_R = \frac{100(c - E_R)}{(100 - E_R)} \tag{48}$$

Sieving Methods

Sieving consists of placing a powder on a sieve containing openings of a fixed size and agitating the sieve. A variety of sieve apertures are commercially available, ranging in size from about 20 μm to millimeters for woven wire sieves, down to 5 μm or less for electroformed sieves, and greater than 1 mm for punched plate sieves. In powder manufacture, sieves with apertures smaller 40 μm generally are not used because of their very low capacity. The sieves in spread-spectrum aperture sizes are commonly used for particle-size distribution analysis.

Sieves are often referred to by their mesh size, which is the number of wires per linear inch. The American Society for Testing Materials Standards range from 635 mesh (20 μm) to 5 mesh (125 mm).

Table 11.5 Aperture sieve sizes in accordance with International and National Standards

INTERNATIONAL ISO 566 (TBL. 2):1983		AMERICAN ASTM E 11-87		TYLER STD SCRN 1910		BRITISH BS 410 1986	CIS GOST 3584	GERMAN DIN 4188: 1977		
Nominal opening mm/μm		Alt. US Std. inch/sieve		Equivalent inch/mesh		Aperture BS mesh	mm	mm/μm		DIN No 2E
26.50	mm	1.06	inch	1.05	Inch			4.00	mm	
25.00	...	1.00	...		...			2.00	...	3E
22.40	...	7/8	...	0,883	...			1.50	...	4
19.00	...	3/4	...	0.742	...			1.20	...	5
16.00	...	5/8	...	0.624	...			1.00	...	6
13.20	...	0.530	...	0.525	...			750	μm	8
12.50	...	1/2	...		...			600	...	10
11.20	...	7/16	...	0.441	...			500	...	12
9.50	...	3/8	...	0.371				430	...	14
8.00	...	5/16	...	2.5	mesh			400	...	16
6.70	...	0.265	...	3	...			340	...	18E
	...				...			300	...	20
5.60	...	3.5	sieve	3.5	...	3		250	...	24
4.75	...	4	...	4	...	3.5		200	...	30
4.00	...	5	...	5	...	4		170	...	35E
3.35	...	6	...	6	...	5		150	...	40
2.80	...	7	...	7	...	6		120	...	50
2.36	...	8	...	8	...			100	...	60
	...		...		...	...		90	...	70
2.00	...	10	...	9	...	8	2.00	75	...	80
1.70	...	12	...	10	...	10		67	...	90E
1.40	...	14	...	12	...	12		60	...	100
1.18	...	16	...	14	...	14		56	...	110
1.00	...	18	...	16	...	16	1.00	50	...	120
			...		...			36	...	130
					...			25	...	200
850	μm	20	...	20	...	18				
710	...	25	...	24	...	22	0.710	French		
600	...	30	...	28	...	25		AFNOR NFX11-50: 1970		
500	...	35	...	32	...	30	0.500	mm/μm	TAMIS	
425	...	40	...	35	...	36		5.00	mm	38
355	...	45	...	42	...	44	0.355	4.00		37
								3.15		36
300		50		48	...	52		2.50		35
250	...	60	...	60	...	60	0.250	2.00		34
212	...	70	...	65	...	72		1.60		33
180	...	80	...	80	...	85	0.180	1.25		32
	...							1.00		31
150		100	...	100	...	100		800	μm	30
125	...	120	...	115	...	120	0.125	630		29
106	...	140	...	150	...	150		500		28
90	...	170	...	170	...	170	0.090	400		27
75	...	200	...	200	...	200		315		26
63	...	230	...	250	...	240	0.063	250		25
53	...	270	...	270	...	300		200		24
45	...	325	...	325	...	350	0.045	160		23
								125		22
38		400	...	400		400		100		21
32	...	450	...			440		80		20
25	...	500	...					63		19
20	...	635	...					50		18
								40		17

The apertures for the 400 mesh are 37.5 μm; hence, the wire thickness is 26 μm and the percentage open area is 35. Table 11.5 includes the data about sieve aperture sizes in accordance with International and National Standards.

Fractionation by sieving is a function of two dimensions of particles only, maximum breadth and maximum thickness because, unless the particles are excessively elongated, the length does not affect the passage of particles through the sieve apertures. The particles much smaller in size than the sieve aperture pass through more rapidly, and larger particles pass through more slowly. The final particle that can pass through will pass through the largest opening when its two smaller dimensions are in the preferred direction. Thus, the sieving process can be divided into two regions with a transition region in between: an initial region that relates to the passage of particles much finer than the mesh apertures, and a second region that relates to the passage of near-mesh size particles (Figure. 11.20). Here the time–weight curve is plotted on log-probability paper. Near-mesh particles are defined as particles that will pass through the apertures in only a limited way, and the ultimate particle is the one that will pass only through the largest aperture in only one orientation. In practice, there is no end point to a sieving operation, since this is defined in an accidental method.

The continuous rate method is fundamentally more accurate than the time method and is used in powder manufacture processing. For that, ensuring a uniform rate of powder feeding to the screening surface is the main requirement.

Sieving Apparatus

Selection of a proper sieve surface is very important. Fine sieves are usually woven with phosphor bronze wire, medium sieves with brass and coarse sieves with stainless steel. Heavy-duty sieves are often made of perforated plate, giving size to circular apertures.

Sieving apparatus can be classified into five main categories: grizzly screens, revolving screens, vibrating screens, sifters, and air-assisted screening machines. Grizzly screens are used generally for separating material of 50 mm and coarser size, while revolving screens or trommel screens are primarily used for separations of particulate material greater than 1 mm in size. The screening machine consists usually of a cylindrical frame equipped with wire cloth or perforated plate. The material to be screened is delivered at the upper end and the oversize is discharged from the lower end. The screens rotate at a relatively low speed of 15–20 rpm. Such screens have been replaced largely by vibrating screens.

Vibrating sieves, whose sieving surface vibrates perpendicularly to its surface with a frequency greater than 600 rpm, are useful for fine powders as well as coarse powders. There is a large variety of commercially available vibrating sieves, but they can be divided basically into two main types: mechanically vibrated sieves and electrically vibrated sieves.

The most important factors for the selection of vibrating sieves are amplitude and frequency. The centrifugal effect k is characterized by the formula

$$k = \frac{r\omega^2}{2g} \tag{49}$$

where r is amplitude (in m), $\omega = 2\pi n$, n is frequency (in rpm)/60, and g is the acceleration of gravity.

If the centrifugal effect is too small, the near aperture size particles will stick in the sieve apertures. The appropriate vibrating action not only keeps the feed materials moving on the sieve but it also, more importantly, serves to reduce blinding.

Figure 11.21 shows schematically typical sieving surfaces of sifters. Sifters are characterized by

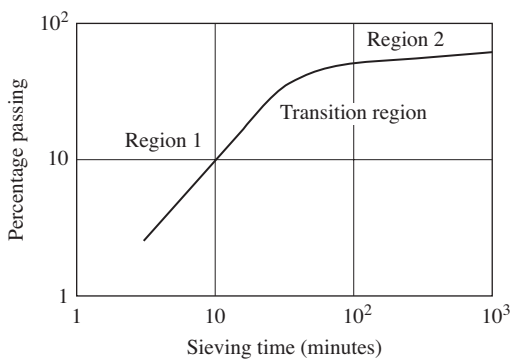

Figure 11.20 The rate of sieving process.

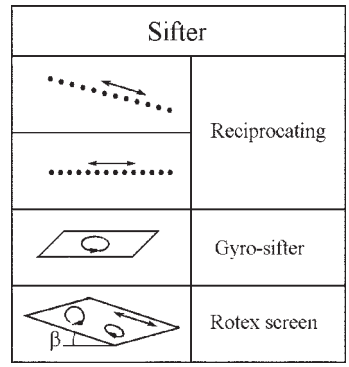

Figure 11.21 Motion of sieve surface of sifters.

low-speed (300–400 rpm), large-amplitude (up to 50 mm) vibration in a plane essentially parallel to the sieving surface. Sifters are usually used for material of 30–400 μm or more in particles sizes. Most gyratory sifters have an additional auxiliary vibration.

The relationship between 50% separation volume and sieving length may be obtained using Gaudin's theory. According to this probability theory, the passage probability P of particles of size δ_p through an aperture of size a in the sieve surface is given by

$$P = \frac{(a - \delta_p)^2}{a^2} = \left(1 - \frac{\delta_p}{a}\right)^2 \tag{50}$$

Introducing the concept of the number of passage trials i, the oversize fraction of particles after i trails, η_i, which is the partial separation efficiency, is expressed by

$$\eta_i = (1 - \delta_p)^i = \left[1 - \left(\frac{a - \delta_p}{a}\right)^2\right]^i \tag{51}$$

If i is sufficiently large, Eqn (51) is written approximately as

$$\ln \eta_i = -i\left(\frac{a - \delta_p}{a}\right)^2 \tag{52}$$

Hence, the particle size at 50% separation efficiency, δ_{p50} is derived, substituting $\delta_p = 0.5$ into Eqn (52):

$$\delta_{p50} = a - \frac{0.832a}{\sqrt{i}} \tag{53}$$

Round Vibrating Sifters

A two-decks vibrating sifter is shown in Figure 11.22. The sifter consists of a set of cylindrical sidewalls with sieving surfaces that are assembled using bow connections. The lower sidewall has a conical form bottom and is assembled on a frame by means of flexible ties. Rotation from the motor to the vibroexcitor shaft is transmitted via a V-belt drive. The loading and unloading branches are equipped

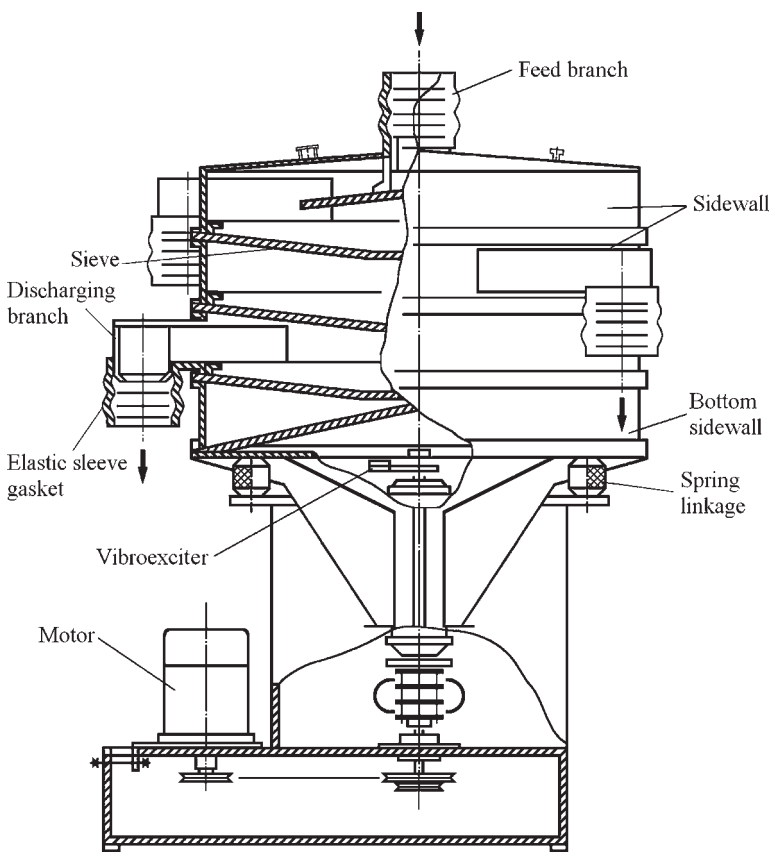

Figure 11.22 Consit two-decks vibrating sifter SV2-0.9.

with rubber sleeve gaskets to seal joints to branches of an initial material feeding device and classified product chutes. Provision is made to operate at rotational speed of 23.7 and 29.5 Hz. Adjustment is also provided for oscillation amplitude by varying the angle between the axes of debalances. The vibrosieve is equipped with points for sampling from the powder flow in the unloading branches for periodic control of sieving efficiency. The vibrosieve is soundless; the impermeability of joints is provided by air or an inert gas pressurization up to 2 kPa within the working area of the sifter.

Figure 11.23 Tetradecks Russel Finex sifter. Courtesy of RusselFinex Inc.

The area of each of two sieving sidewalls is 0.56 m^2 with an outer diameter of sidewalls 900 mm. The sifter can yield three fractions. The vibrosieve is equipped with screening meshes with openings 1.0; 0.315; 0.16; 0.1; and 0.05 mm. The throughput when sifting, for instance, an atomized bronze powder in terms of passing for the –0.16 class is 3.2 t/h. The efficiency of sizing $E = 90–95\%$. Table 11.6 contains approximate values of the throughput of Consit sifters.

The throughput, factors E and c_R are determined experimentally on a material subjected to sizing.

A tetra-deck Russell Finex sifter is shown in Figure 11.23. There are commercially available sifters (Russell Finex VDS System) that can be used in potentially explosive gaseous or dusty environments. There is also a vibrosonic system which eliminates the blinding and blocking of the apertures, allowing accurate separation down to 20 μm.

Preliminary separation of coarse fractions, for example of the water-atomized powder, can be carried out on a hydraulic sizing screen. Such flat screen [1] is equipped with a shaker. Usable area of one sieve is 0.75 m^2, tilt angle 40–50°, slot size 0.09–1.0 mm, throughput of one segment (depending on the slot size) per solid is 10–30 t/h and per pulp flow 20–40 m^3/h.

Air-assisted Sieving Machine

An air-assisted sieving machine is schematically shown in Figure 11.24. It has been predominantly used for fine powders. The stream of air accelerates the passage of fine particles through the sieve and removes the blinding particles in the apertures of the sieve.

Table 11.6 Throughput of Consit two-decks vibrating gyro sifters

Sieve aperture sizes (mm)		Throughput (m^3/h)	
Upper deck	Under deck	SV2-0.6[a]	SV2-0.9[b]
2	0.63	0.3	0.7
2	0.315	0.3	0.7
1	0.315	0.2	0.5
1	0.16	0.2	0.3
0.63	0.16	0.1	0.3
0.63	0.1	0.1	0.1
0.315	0.1	0.04	0.1
0.315	0.063	0.04	0.02
0.16	0.045	0.01	0.02
0.1	0.045	0.01	

[a]Deck 600 mm in diameter;
[b]Deck 900 mm in diameter.

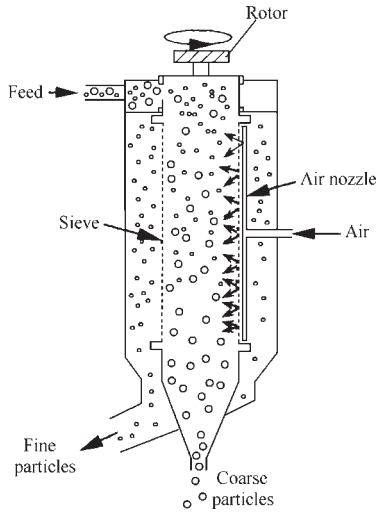

Figure 11.24 Schematic drawing of air-assisted sieving machine.

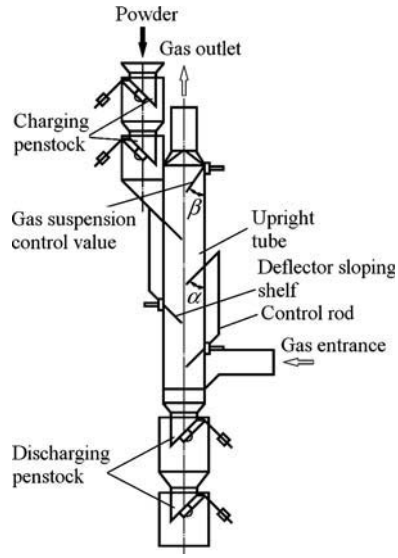

Figure 11.25 Air gravitational classifier with powder deflector sloping shelves.

Air Separation

In general, air classification is used for small particles where effective sieving is not applicable. The particle size range for air classification is mostly between a few and 150 μm but, recently, classification of submicrometer particles has been possible.

In air classification, particles are separated by their difference in settling velocity or displaced distance, which depends on the size, shape and density of particles and the types of forces applied to the particles. Such forces may be drag force, gravitational force, centrifugal force, Coriolis force, inertial force, electrostatic force, magnetic force, impaction force, adhesion force, etc.

In air classifiers, a material is usually separated into two classes: coarser and finer. If more classes are needed, classification is performed in sequence using several apparatus.

Air classifiers are divided into three groups depending on particle separation mechanism:

- the relationship between the settling velocity of particles due to the gravitational or centrifugal force and the velocity of airflow
- the displacement of particles traversing the airflow
- others.

The gravitational mechanism is used in a classifier with powder deflector sloping shelves (Figure 11.25), the powder passes through a bin with gates and is blown by the countercurrent air flow. Coarse particles discharge through the discharging penstock, while the suspension of finer particles is aspirated to the cyclone. The powder classification is adjusted by varying the air flow rate and also by positioning the deflector sloping shelves, the inclination angle of which is varied using special rods.

As air classification is accomplished by the difference in particle trajectories, the mechanism of any air classification can be investigated by solving the equation of particle motion numerically with the initial conditions of the particle and fluid flow in the classification zone.

Centrifugal classification is the most commonly used in air classification. The centrifugal force easily attains a force a few hundred times greater than gravitational force and the force strength can be controlled by the rotational speed. The centrifugal air classification is applicable to particles ranging in size from submicron to several tens of micrometers. There exists an equilibrium point: the position at which the radial velocity of a certain size of particle equals the inward air velocity. Particles larger than the equilibrium size move outward and are separated as coarse particles, while the smaller particles, classified as fine particles are caught by the collector.

Centrifugal air classifiers are used usually in combination with comminutors in a closed loop [1]. Centrifugal force is created either by airflow in cyclone-type classifiers, or by mechanical revolution in air separators. There are many centrifugal classifiers, for instance: Micron separator, Turbo classifier, Classiel (O-sepa), and Turboplex [2], the characteristics of which are given in Table 11.7.

Table 11.7 Characteristics of centrifugal air classifiers

Type of classifier	Cut size (μm)	Throughput (kg/h)	Rotor speed (rpm)	Power (kW)
Micron separator	5–150	150–12 000	200–2300	0.75–37
Turbo classifier	0.5–150	150–24 000	700–12 000	1.5–70
Turdoplex	2–180	40–36 000	120–22 000	1–45
Classiel	3–400	200–300 000	75–8400	4–400

(Source: Ref 2)

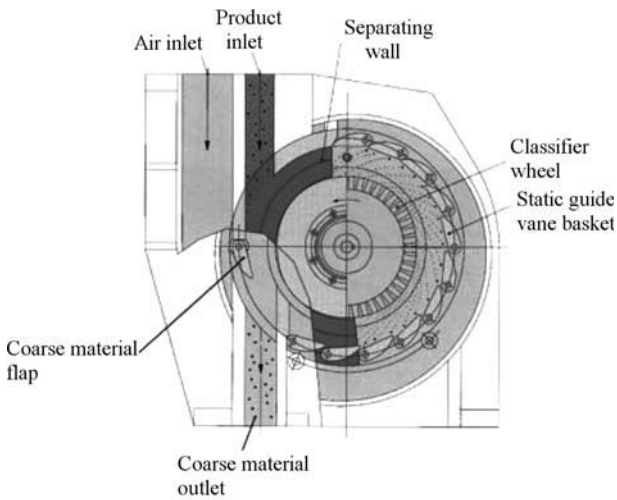

Figure 11.26 Schematic function of NETZSCH-CONDUX Fine Classifier CFS/HD-S. Courtesy of NETZSCH-CONDUX Mahltechnik GmbH.

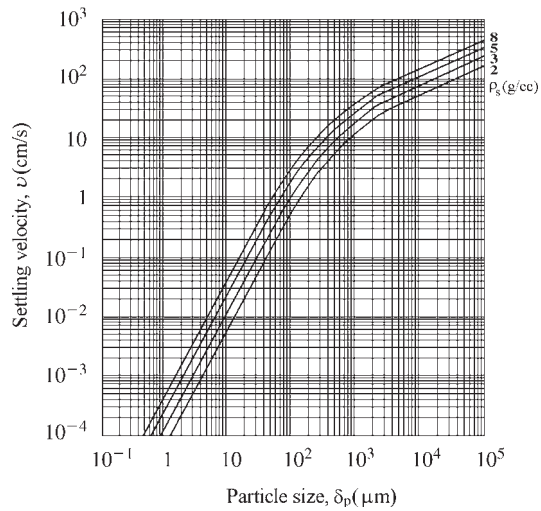

Figure 11.27 The relationship between the size of the spherical particles and their settling velocity in water (15°C).

The schematic function of NETZSCH-CONDUX Fine Classifier CFS/HD-S is shown in Figure 11.26. The necessary air which disperses the feed product through many adjustable guide vane slots and then leads it to the classifier wheel is fed via the air inlet. The classifier wheel separates coarse and fine particles. The fine particles are discharged via the hollow shaft. Coarse ones are rejected by the wheel and are discharged through the screw-shaped machine housing and via the coarse material outlet at the bottom. The discharge of coarse material can be adjusted by the position of the coarse material flap and so the cleanliness of the coarse material can be influenced.

Air classification cannot be used for potentially explosive powders such as aluminum and aluminum alloys, magnesium, titanium, etc. Explosion proof conditions can be ensured by means of inert atmospheres but that leads to a considerable price increase of the process.

In general, air classifiers are inferior to hydraulic classifiers in terms of efficiency and accuracy of separation [11].

Hydraulic Classification

Hydraulic classification of powders is based on the difference in the different size particle settling rates in a liquid medium in a gravitational field. Figure 11.27 illustrates the relationship between the size of the spherical particles and their settling velocity. In contrast to air classification where to prevent cohesion of particles a low concentration of particles 0.003–0.3 vol% in the gaseous medium is maintained, hydraulic classification can be performed under much higher solids concentrations. In fact, classification is fulfilled typically in the range 30–40 vol% in wet closed circuit grinding processes. The hydraulic classification process is normally performed with a cut size between 200 and 1 μm.

Two principles are used: (i) separation in the flow, direction of which coincides with that of main active forces (or in countercurrent action), and (ii) separation in the flow directed angularly to the latter.

The first principle is used by gravity classifiers, the second one by centrifugal classifiers (with separation

Table 11.8 Hydraulic classifiers

Classification technique	Type	Approximate range of cut size (μm)	Features
Gravity classifiers			
Settling reservoirs	Settling cone[a]	100–1 000	Simple structure; used mainly for coarse range
	Spitzkasten (multicones)	50–200	
	Settling reservoir with siphon discharge	20–200	Suitable for wide particle size
	Hydroseparator		
Mechanical classifiers	Spiral classifier		Usable for high density; medium to coarse range
	Drag classifier		
Centrifugal classifiers			
Hydrocyclone	Hydrocyclone (ordinary type)	3–200	High throughput; fine to medium size range; requires slurry pump
	Multiclone		
Centrifuge	Solid-bowl centrifuge (decanter type)	0.5–30	Very fine to medium size range
	Disk centrifuge (de Laval type))		

[a]Settling cone is described in subsection 'Dehydration' in this section, where its use as thickener is shown.

in the field of centrifugal forces). Table 11.8 lists major types of hydraulic classifiers that are useful for wet powder metallurgy processing.

Gravity settling reservoirs represent the simplest type of hydraulic classifier. Except for the hydro-separator, which is a modification of gravity thickeners, most gravity settling reservoirs are used for coarse size particle separation.

The gravity classifier is used for separation of off-size fractions from water-atomized powders. A classifier having a siphon unloading in comparison with bottom outlet ensures higher accuracy of classification (Figure 11.28). The classifier comprises a cylindrical tank; the pulp is fed through a branch pipe and the discharge drains into a concentric overflow chute. Water is also fed from the bottom via a tube to produce a suspended layer of particles. Coarse particles reaching the lower part of the tank are removed by siphons. The suspension flow rate is adjusted by valves connected to pressure pipes. The latter are sensors of the pulp density in the medium part of the tank. At the start of the classifier work, the siphons are actuated by water supply to their lower part via pipes.

Spiral classifiers are used for the discharge of the coarse particles in the feed pulp settled out from the pool in the reservoir, in which the spiral is partly submerged in the pool, while the fine particles overflow from the lip of the reservoir.

Hydrocyclones are extremely simple equipment with no moving parts except for rare modifications. The typical hydrocyclones are shown in the subsection

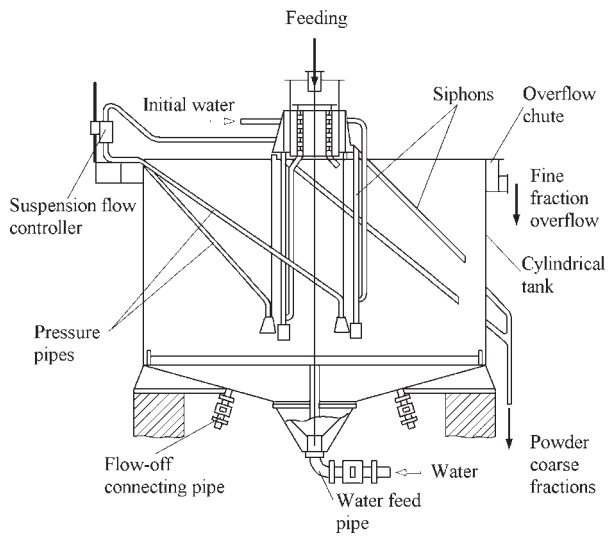

Figure 11.28 Gravity classifier with siphon unloading.

'Dehydration' in this chapter, where their use as thickeners is described. The applications of hydrocyclones for classification by size of water-atomized aluminum alloy powders are described in Chapter 13.

Hydrocyclones are manufactured in the size range 10–1200 mm in the diameter of the cylindrical part D_c (see Figure 11.2). Because the throughput of the hydrocyclone is reduced in proportion to the square

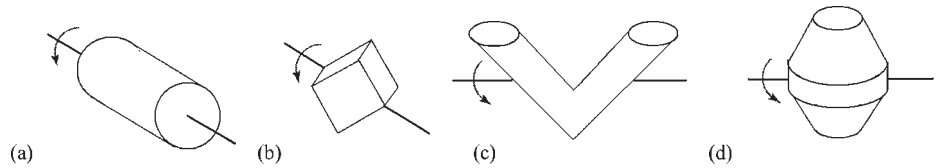

Figure 11.29 Schematic image of typical rotary vessel mixers.

of the unit size, very small cyclones are frequently fabricated in the form of batteries.

Based on consideration of fluid mechanical efficiency, the optimum parameters of the hydrocyclones have been derived [12] as follows:

$$\frac{L}{D_c} = 5,\ \frac{D_{ov}}{D_c} = 0.34,\ \frac{D_f}{D_c} = 0.38,\ \frac{L_0}{D_c} = 0.4 \quad (54)$$

where D_{ov} is diameter of the overflow nozzle, D_f is the inlet diameter (or the equivalent diameter of the inlet), L is the complete length, L_0 is the length of the cylindrical part.

In the centrifuge, in contrast to hydrocyclones, a forced vortex prevails, which is characterized by constant angular velocity over the whole radius of the slurry pool in which centrifugal settling of particles occurs. Centrifugal classifiers are commonly classified into two types of designs: solid bowl and disc (or de Laval type). According to the design features, solid bowl centrifuges can achieve coarse to ultrafine separation, while disc centrifuges are intended basically for very fine separation. The typical separation size ranges from 5 to 200 μm and from 0.2 to 10 μm, respectively.

Mixing

Powder mixing is an operation to prepare a homogeneous mixture from two or more powder ingredients with, if necessary, some liquid additions. Mixing is sometimes confused with blending, which is much the same technique but is used for mixing batches of powder of the same nominal composition, but differ in particle size or production lot. In mixing, the powders being combined are different in composition. Premixing is an operation to make a powder system composed of two or more ingredients with binders, which are mixed and bonded together to avoid segregation in handling. The bulk chemical composition might be the same as that found in wrought metallurgy but, at the particle level, there will be distinct differences. For example, bronze is made both as a prealloyed powder but also as a premixed powder. For a 90% copper and 10% tin bronze, the premixed material will consist of the proper ratio of pure copper and pure tin particles, but no bronze particle will be present [12].

Powder Mixers

Mixing is achieved in a mechanical device that rotates or in a stationary vessel with agitators, vibration unit, gravity motionless, etc. A few simple design rotary vessel mixers are schematically illustrated in Figure 11.29. Each revolves around some central axis which, in many cases, might also have a central intensifier bar with blades that spin at a high velocity to disrupt the particles during a tumbling motion. Most mixers split and recombine the powders to create new interfaces and to remove segregation and stratification. However, these same devices also can induce segregation of powders based on differences in particle size, particle shape, or density [13].

Table 11.9 comprises a classification of various powder mixers, based on the mode by which the powders are set in motion. The table also shows rough ranges of powder properties appropriate to each type of mixer.

Rotary Vessel Type

Although the rate of mixing is slow, a good final degree of mixing can be achieved. Powders to be mixed are charged up to 30–50% of the vessel volume. The rotational speed is set at 50–80% of the critical rotational speed, n_{cr}, given by

$$n_{cr} = \frac{0.498}{\sqrt{R_{max}}}(s^{-1}) \quad (55)$$

where R_{max} (m) is the maximum rotation radius of the mixer. For mixing powders with poor flowability and large differences in particle densities and diameters, various types of guide plates or other internals are installed in the rotating vessel. The addition of mixing aids or an operation at a rotational speed close to n_{cr}, may be useful in some cases.

Table 11.9 Classification of powder mixers and ranges of their use

Classification	Techniques and design characteristics	Mixer	Operation		Typical powder properties: Range of particle size (mm)				Flowability angle of repose (deg)				Differences in ingredients properties			Water content	
			Batchwise	Continuo	Over 1.0	1.0–0.1	0.1–0.01	Under	Under 35	35–45	Over 45	Cohesive	Small	Large	Abrasive	Dry	Wet
Rotary vessel	Horizontal axis of rotation	Horizontal cylinder (11.29a)*	○	○	○	○	●		○	●			○		○	○	
		Double cones (11.29d)	○		○	○	●		○	●			○		○	○	
		V–type (11.29c)	○		○	○	●		○	●			○		○	○	
		Cubic (11.29b)	○		○	○	●		○	●			○	●	○	○	
		Continuous V-type		○	○	○	●		○	●			○		○	○	
Stationary vessel	Horizontal axis of rotation	Ribbon agitator (11.31a)	○	○	○	○	○	○	○	○			○			○	●
		Screw agitator	○	○	○	○	○	○	○	○	○	○	○	●		○	○
		Rod or pin agitator	○	○	○	○	○	○	○	○	○	○	○	○		○	○
		Double-axle paddles agitator	○	○	○	○	○	○	○	○	○	○	○	○		○	○
	Vertical axis of rotation	Ribbon agitator (11.31b)	○	○	○	○	○	○	○	○	○		○	○		○	○
		Screw in cone agitator (11.31b)	○		○	○	○	○	○	○	○		○	●		○	○
		High speed agitator (11.31c)	○		○	○	○		○	○	●		○	○		○	○
		Rotating disk agitator		○	○	○	●		○	●			○			○	
		Muller agitator	○	○	○	○	○	○	○	○	○	○	○	○		○	○
	Vibration	Vibratory toroidal mixer (11.32)	○		○	○	○	○	○	○	○	○	○	●		○	
		Vibratory mill	○	○	○	○	○		○	○	○		○	●		○	
		Sieve		○	○	○	●		○	●			○		○	○	
	Gas flow	Moving other fluidized bed (11.31d)	○		○	○			○	●			○		○	○	
	Gravity	Falling under gravity action (11.31e)		○	○	○			○				○		○	○	
Complex	Internals in rotating vessel	Horizontal cylinder	○	○	○	○	○		○	○	●		○	●		○	○
		V–type	○		○	○	○		○	○	●		○	●		○	○
		Double cones	○		○	○	○		○	○	●		○	●		○	○
	Gas flow and mechanical agitation		○	○	○	○	●		○	○			○		○	○	
	Vibration and mechanical agitation (11.31f)		○	○	○	○	○	●	○	○	○	●	○	●	○	○	○

○, suitable; ●, usable; *the number and symbol of Figure, illustrating a mixer.

The double cone mixer of batch operation contains a body constructed from two cone bottoms with the apex angle 90°, having loading and unloading hatches equipped with sealed gates. Pivots of the body are mounted on the supports and connected with a reduction gear to the drive. Commercially available double cone mixers have geometric volumes 1.6 and 2.5 m^3, filled with components to be mixed up to 0.63 and 1.0 m^3, respectively. The throughput of the 1.6 m^3 mixer is 0.3 m^3/h. The work cycle includes the component loading (14 minutes), mixing (20 minutes) and mixture unloading (4 minutes). The mixer is powered by a 15 kW primary drive and a 0.75 kW secondary drive. Rotational speed of the primary drive is 20.5 rpm and of the secondary drive is 0.96 rpm. The throughput of the 2.5 m^3 mixer amounts to 0.5 m^3/h.

The mixing efficiency of double-cone mixers is somewhat lower than of vibrating toroidal ones, therefore, the mixing procedure requires longer time.

The joints of the loading and unloading hatches together with the corresponding loading device and receiving finite mixture device must be thoroughly made and reliably operating to be able to localize dust escape and leading dust to the exhaust system.

The Matson IBC batch blender allows mixing directly within the intermediate bulk container (IBC). An IBC with powder to be mixed is located in a revolving frame and clamped by means of a holding down device in an asymmetric axis of the rotation position (Figure 11.30).

Stationary Vessel Type

Stationary vessel mixers with mechanical agitation are shown in Figure 11.31.

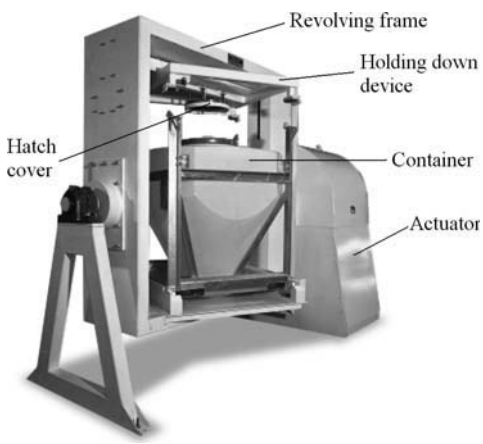

Figure 11.30 Matcon IBC batch blender. Courtesy of MATCON Company.

In stationary vessels using mechanical agitation, large amounts of powders can be handled in a small space. Specialized atmospheres as well as normal temperatures and pressures are accessible for multipurpose operations. The mixers of ribbon type (Figure 11.31(a)) are preferentially used for preparing mixtures of components noticeably differing in bulk density and their contents in the mixture. Some types of stationary vessel mixtures can be used in both batch and continuous mode.

The vibrating toroidal mixer, Consit CmV-1.0 of batchwise operation (Figure 11.32) consists of a toroidal chamber made of stainless steel, with loading and unloading hatches, a vibroexcitor and elastic supports. The tightness of joints between the loading hatch and the loading device branch tube and similarly between the mixture unloading device and the chute branch tube is achieved by means of corrugated elastic sleeve gaskets.

The volume of the mixing chamber is 0.7 m^3, maximum weight of loaded material occupying not more than 85% of the volume is 1400 kg; time of mixing is 10 to 20 minutes; vibration parameters on the outer diameter: vertical amplitude 1–3 mm, horizontal 1–2.5 mm; oscillation frequency 24.2 Hz. Efficient mixing is achieved by an intense corkscrew movement of powders in the toroidal chamber. The coefficient of heterogeneity varies from 1.5% to 3.0% and should be corrected for specific materials. There is commercially available a vibrating toroidal mixer series with mixing chamber volumes of 0.005, 0.04, 0.1, 0.4 and 1.0 m^3.

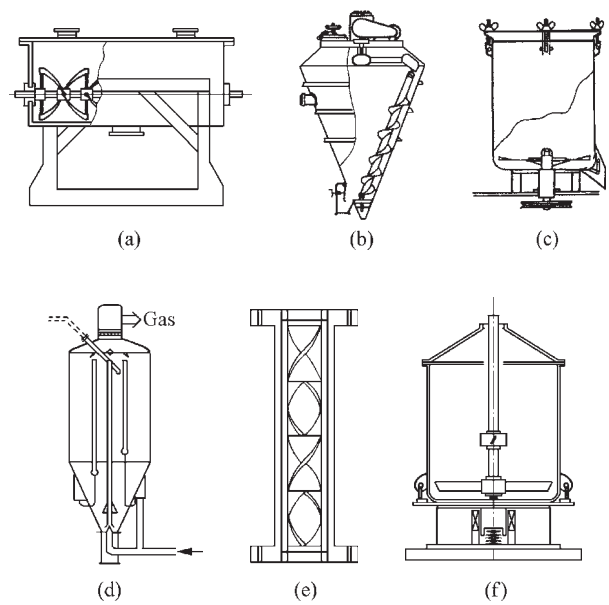

Figure 11.31 Typical examples of stationary vessel and complex type mixers.

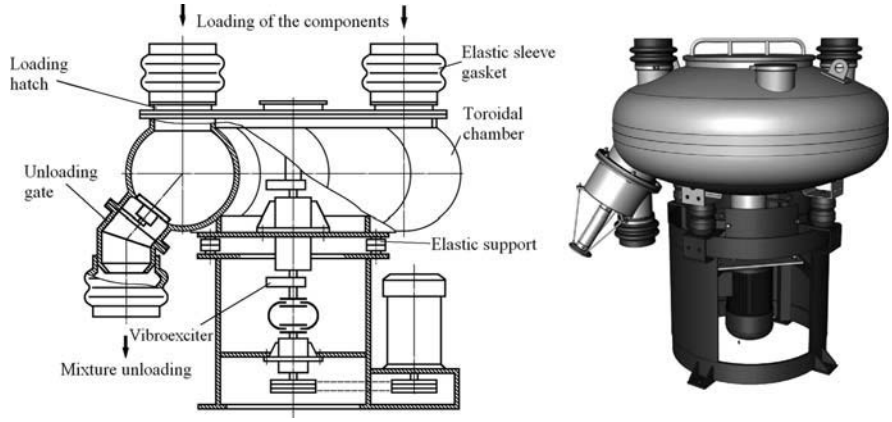

Figure 11.32 Vibrating toroidal mixer, Consit CmV-1.0 of batchwise operation. Courtesy of Consit Production Company, Moscow.

The stationary vessel mixers using gas-flow agitation are applied primarily for batch mode mixing. Powders to be mixed can be charged to more than 70% of the vessel volume. Additional equipment, including blowers, dust collectors and pressure regulators, is necessary so that the system as a whole usually becomes rather large.

In a stationary vessel with free gravity falling powders, the flow of powders is repeatedly divided and united to improve mixing and the degree of mixing can be adjusted by the number of repetitions.

Complex Type and Others

There are possible several combinations of mechanisms of powder mixing. Mechanical agitation can be fulfilled in addition to agitation by gas flow. Vibratory motion can also be added to stationary vessel mixers (see Figure 11.31(f)). All these types are to make the powder motion in mixers as free as possible from the force of gravity, improving the rate of mixing and extending the application of mixers to powders having rather large differences in physical properties.

Mechanism of Powder Mixing

Three types of particle motion are generally responsible for mixing of powders: convective mixing, shear mixing and diffusive mixing.

Convective Mixing

A circulating flow of powders is generally effected by the rotational motion of a mixer vessel, an agitating impeller such as a ribbon or a paddle or gas flow and vibratory motion. The circulating flow gives rise to convective mixing and contributes mainly to a microscopic mixing of bulk powder mixtures. Though the rate of mixing by this mechanism is rather high, its contribution to the microscopic mixing is unexpected. Convective mixing is beneficial for batch mode operation but gives unfavorable effects for continuous mode mixing.

Shear Mixing

The momentum exchange of powder particles having different velocities leads to shear mixing. The velocity distribution develops around the agitating device and the vessel walls due to compression and extension of bulk powders. It also developed in the powder layer in rotary vessel mixers, in gas-flow mixers at blowing openings and in suspended solid in vibratory mixers. Shear mixing can improve semimicroscopic mixing and be favorable in both batch and continuous operation.

Diffusive Mixing

Diffusive mixing is caused by random motion. The rate of mixing by this mechanism is low compared with convective mixing, but diffusive mixing is essential for microscopic homogenization.

During powder mixing, all of the above three mechanisms take place together.

Statistical Analysis of the Mixing

Analytical determination of the standard deviation of a mixture is described as a statistical measure of

how much the concentration of one constituent in a sample varies from the true concentration that characterizes the entire mixture. A statistical mixture of a typical two-component PM mix depends on the component mass ratio, the average component masses, the standard deviations of the component particle mass distributions and the sample size [15]. If the percentage of the component in a batch is X, and the percentage found in a spot sample is X_i, then the difference is $(X-X_i)$. The average of all the X_i readings could approach the value of X if enough samples are checked; the average of all the plus and minus variation of $(X-X_i)$ would approach 0. To obtain a measure of the overall sample – the significance of all the spot samples – the statistical variance and standard deviation are computed. The biased variance can be expressed:

$$\sigma_s^2 = \frac{\sum_{i=1}^{n}(X - X_i)^2}{n} \tag{56}$$

where σ_s^2 is biased sample variance, σ_s is biased standard deviation, i is spot sample number, X_i is spot sample measurement, X is actual content of the ingredient, and n is the spot numbers.

To compensate for the increased uncertainty entailed using very few spot samples, the unbiased variance is used. The difference is that $n-1$ is placed in the denominator instead of n. The expression then becomes:

$$\sigma_s^2 = \frac{\sum_{i=1}^{n}(X - X_i)^2}{n-1} \tag{57}$$

The degree of homogeneity (the degree of mixedness, M) for a powder mixture can be estimated by evaluating the magnitude of variance of the samples:

$$M = \frac{\sigma_0^2 - \sigma_s^2}{\sigma_0^2 - \sigma_r^2} \tag{58}$$

where σ_0^2 is variance for the initial segregated mixture, σ_r^2 is the variance anticipated for perfectly mixed random samples.

The final variance for a fully-mixed, randomly sampled systems should approach zero, that is $\sigma_r^2 = 0$ in the ideal. This gives a simplified form of M:

$$M = 1 - \frac{\sigma_s^2}{\sigma_0^2} \tag{59}$$

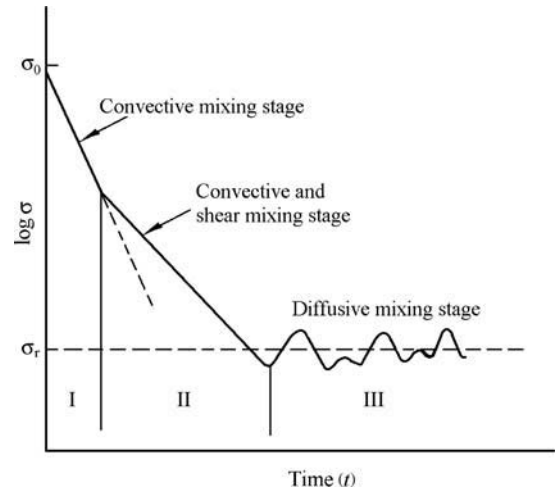

Figure 11.33 Schematic presentation of characteristic curve of mixing process.

Usually the homogeneity improves rapidly with initial mixing, but over time a steady-state homogeneity is attained that is less than unity; the maximum mixture homogeneity occurs when the rate of mixing equals the rate of segregation.

Powder mixing is accomplished in a mixer where the three mechanisms described above take place simultaneously. The characteristic curve of mixing is the chart of the degree of mixedness M against the mixing time t. Figure 11.33 illustrates a schematic example of a similar curve, where the standard deviation σ (on a logarithmic scale) shows the degree of mixedness M against the mixing time t (on the linear scale).

Generally, convective mixing is dominant in the initial stage (I) and the mixing proceeds steadily by the both convective and shear mechanisms in the intermediate stage (II). In the final stage (III), the effect of diffusive mixing appears and the dynamic equilibrium between mixing and segregation is reached. The degree of mixedness at this state is called the final degree of mixedness, M_∞. The characteristic curve of mixing is useful for the evaluation performance of mixers.

Various powder mixers show a variety of patterns in the characteristic curve of mixing. The value of M_∞ is also influenced perceptible by operating conditions and powder properties.

Passivating Techniques

Oleg D. Neikov, Irina B. Murashova
Frantsevich Institute for Problems of Materials Science (IPMS), Kiev, Ukraine
Ural State Technical University (UPI), Yekaterinburg, Russia

For most metals, the relationship between moisture and atmospheric oxygen is unstable. The property of metals to transform from the metallic state to another is characterized by the free energy decrease during the oxidation reaction.

In Table 11.10, the non-ferrous metals are listed in descending order of the negative normal electrode potential followed by increase of the positive one. This series is divided by hydrogen (−0.414 and 0.000 V) and oxygen (+0.815 and +1.23 V) equilibrium potential values on five metal groups different to their thermodynamically stability.

With regard to moisture and oxygen only very few metals from the fourth and fifth groups could be considered thermodynamically stable.

More information about the thermodynamic stability of metals can be obtained based on analysis of the metal potential–hydrogen ion exponent (pH) diagram.

Recent conceptions about corrosion processes are founded on electrochemical theory. Corrosion processes, which occur on a metal surface, have been more extensively studied and various processes for protection against corrosion of cast metal have been developed. At the same time, the powders, due to their large specific surface, are more vulnerable to corrosive action. The corrosion resistance of metals and alloys is characterized not only by thermodynamic stability but, to a greater extent, by process kinetics, i.e. its real rate of formation.

Table 11.10 Common thermodynamic characteristic of corrosion resistance of metals and their normal electrode potential

Group	Common characteristic of corrosion resistance	Electrode reaction[a]	Potential, E^0, V at 25°C
1	Metals with elevated thermodynamic instability (corrosion is virtual even in neutral aquatic environment free from oxidants).	Cs−e	−3.02
		Rb−e	−2.99
		Ba−e	−2.90
		La−3e	−2.52
		Mg−2e	−2.37
		Be−2e	−1.85
		Hf−3e	−1.70
		Al−3e	−1.66
		Ti−2e	−1.60
		Zr−4e	−1.63
		Ti−3e	−1.21
		V−2e	−1.18
		Nb−3e	−1.1
		Zn−2e	−0.782
		Cr−3e	−0.74
2	Metals are thermodynamically unstable, inconvertible in neutral environment durante absentia of oxygen; they can corrode in acid medium durante absentia of oxygen too	Cd−2e	−0.402
		Ti−3e	−0.336
		Co−2e	−0.227
		Ni−2e	−0.250
		Mo−3e	−0.200
		Sn−2e	−0.136
		Pb−2e	−0.126
		W−3e	−0.110
3	Metals of intermediate thermodynamic instability (in durante absentia of oxidants they are resistant in acid and neutral environments)	Bi−3e	+0.226
		Sb−3e	+0.240
		Cu−2e	+0.337
		Ag−e	+0.799
		Rh−3e	+0.800
4	High stability metals (they are corroded in neutral environmental in the oxygen presence and in acid environmental in the oxidants presence)	Pd−2e	+0.987
		Ir−3e	+1.000
		Pt−2e	+1.190
5	Full stability metals (they are resistant in acid environment in the presence of oxygen; they are not dissolved in complex-compounds in the presence of oxidants)	Au−3e	+1.500
		Au−e	+1.700

[a]Electrode reactions $M \leftrightarrow M^{ne} \pm ne$ are written summarily M−ne.

In accordance with an approximate scheme of the corrosion cell work in the case of linear dependence between the electrode reaction rate and potential, the expression for corrosion rate can be given as:

$$u = K\frac{E_c^b - E_a^b}{\frac{P_c}{S_c} + \frac{P_a}{S_a} + R} \tag{60}$$

where K is the conversion factor, $(E_c^b - E_a^b)$ is the difference between starting potentials of cathode and anode parts of a corrosion element; P_c and P_a are, respectively, the specific cathode and anode polarizability (dE/dI) by the corrosion current; S_c and S_a are the areas of cathode and anode parts respectively of the corrodent metal; and R is the ohmic resistance of the powder–liquid system.

Generally, the E_c^b and E_a^b values are determined experimentally or by evaluation of the corrosion motive force, the values of equilibrium potential of the depolarizator (E_e^{eq}) cathode reduction and anode reaction of metal solution (E_a^{eq}), calculable via Nernst's equation, are used (see Chapter 9). The value $(E_c^{eq} - E_a^{eq})$ is proportional to the change of free energy of the system and characterizes the extent of its thermodynamic instability. The denominator represents the summarized kinetic inhibition of cathode and anode processes taking into account the ohmic resistance and ratio of area of the electrode parts. The large surface of powders promotes their instability; therefore the anticorrosion effect during their production and processing is aimed at increasing polarizability of the cathode and anode processes and items on the rise of medium ohmic resistance.

Recent simulation of electrochemical process kinetics using computers allows corrosion rate to be evaluated more accurately by calculation of corrosion potential E_{cor} and corrosion current I equal for cathode and anode processes. The anode metal dissolution is described by the equation of retarded discharge, while the cathode process mechanism, depending on medium hydrogen ion exponent, is characterized by the kinetics of hydrogen emission ((a), acid medium) or limit diffusion current of oxygen solution reduction ((b), neutral and alkaline solutions):

$$\frac{I}{S_a} = i_{ex}^M \exp\frac{(1-\alpha_M)zF}{RT}(E_{cor} - E_{eq}^M) \tag{61}$$

$$\text{(a)}\ \frac{I}{S_c} = i_{ex}^H \exp\left(-\frac{\alpha_H F}{RT}\left(E_{cor} + \frac{2.303RT}{F}pH\right)\right) \tag{62}$$

$$\text{(b)}\ \frac{I}{S_c} = \frac{4FD_{O_2}C_{O_2}}{\delta} \tag{63}$$

where i_{ex}^M and i_{ex}^H, (A/m^2) are exchange current density of metal and hydrogen during reduction; α_M and α_H, are transport coefficients for metal and hydrogen; F is Faraday constant (k/mol); R (J/mol K) is absolute gas constant; T (K) is temperature; $D_{O_2}\,(m^2/s)$ is oxygen diffusion coefficient in corrosion medium; $C_{O_2}\,(mol/m^2)$ is oxygen solubility in the medium at respective temperature; δ is thickness of the diffused layer (about 100 μm). The values of i_{ex}, α, D and C are given in reference literature [16]. A joint resolution of Eqns (61) and depending on medium (62) or (63) is carried out in one of the mathematical application packages (for example, MathCAD) and the unknowns, current and corrosion potential, are found.

Passivation Methods

Passivating techniques are based on the following principles: reduction of the degree of thermodynamic instability; deceleration of cathodic processes; and rising of ohmic resistance of the system. These may be implemented in the following ways.

- A decreased thermodynamic instability of a metal can be achieved via alloying, protection of powder surface by an insulated coating, or by processing and storage of a product in an inert atmosphere.
  Alloying is restricted by requirements of purity of powders, to their processing characteristics and economic considerations. For instance, the thermodynamic stability can be increased by alloying copper with gold and nickel with copper.
  The powder surface insulation is possible by coating with polymer films, encapsulation of powders, forming oxide films, nitriding of surface and by applying greases.
  Thermodynamic stability of powders of aluminum, titanium, zirconium, niobium and other metals can be enhanced by nitriding their surfaces. Electromechanical passivity is attained through formation of insoluble corrosion productson on a reactive surface.
  Depending on the metal type, as inert atmospheres, nitrogen, argon, helium and other gases or gas mixtures not containing oxidants can be used, or with depleted content.
  To this group of powder passivating methods can be also added the air medium drying (using silica gels, aluminogels, and other moisture absorbing agents).
- Inhibition of cathode processes is achieved by the elimination of cathode contaminants from an alloy by introduction of additives that step up the cathode process overstress.

Stability of zinc, aluminum and magnesium is improved with an increase in their purity. The stability of commercial zinc can be improved by amalgamation of the surfac, or by cadmium introduction, while that of magnesium by the introduction of manganese. The use of these techniques in the production of commercial powders is restricted by technological requirements and economics.

- Inhibition of anode processes is achieved via alloying by introduction of cathode additives or cations into solution to reduce the overstress of cathode processes, as well as by introduction of oxidizers or anode inhibitors into the corrosive medium or by protective coating.
  Thus, the passivity is enhanced by alloying nickel with chromium, titanium with small additions of palladium. The cathode process overstress is decreased by the addition of chromates, nitrates, phosphates and perrhenates into the solution.
  Zinc chromate and other anode inhibitors are added to a paint film, or grease.
- No special actions are undertaken as a rule to reduce electrical conduction of the solution to increase ohmic resistance. This is contributed by creation of hydrophobic layers and poor conductive films on the powder particle surfaces.
  The techniques of the first group are of the greatest significance for passivation.

Hydrophobization

The work of a corrosion cell implies the transfer of charges between the cathode and anode in a liquid phase. A powder that possesses a developed surface adsorbs air moisture in which other gas ingredients of air have been dissolved and a current-conductive electrolyte is formed; otherwise electrochemical corrosion is not possible. The existing methods of drying air (use of silica gels, aluminogels, etc) are only valid for a limited period of time and require a reliable sealing for packages in which to store powders. On the other hand, imparting of hydrophobic properties to the surface of metal particles prevents formation of a moisture film and can essentially stop corrosion [17,18]. The hydrophobization of the metal powder surface is performed by treating powders with an aqueous solution of surfactant and organic compounds of fatty and aromatic series. Soda soap is an efficient stabilizer of copper powder against corrosion; the corrosion resistance of the powder as treated with stabilizing soap solution increases by 10 to 80 times (Table 11.11).

The powder as rinsed out after electrolysis, is treated with an inhibiter solution, washed with fresh water, de-watered by centrifuge, and dried in a current of hot air. To produce powders with retained hydrophilic properties, the powder is treated with gelatine or other surfactant (see Table 11.11) that prevent powder oxidation after the electrolysis treatment operations when the access of oxygen to the metal is enhanced through a thin moisture film (interoperation protection). Stabilizing surfactants can also be used directly at the electrolysis stage (see Table 11.11), which increases the interoperation protection. The effect of surfactant is manifested directly on the electrolysis kinetics and thus, on the properties of the powders produced. For instance, electrolysis conducted in the presence of polyvinylpyrrolidone leads to an increased content of fractions having a particle size between 45 and 71 μm.

When electrolytic copper powder is heated in hydrogen with further milling, its corrosion resistance is decreased by the removal of the stabilizing film during annealing. In which case, the powder can be treated immediately as milled in an organic solvent containing fatty acids.

Volatile inhibitors when added to hot gases allow simplification of the process of stabilization by combining it with drying (see Table 11.11). However, such a stabilization method has not found commercial application.

Copper powders produced by the method of melt spraying are prone to oxidation during the metal drop cooling. Surface hydrophobization of a molten metal is impossible, however; the use of water with added laundry soap in the receiving tank increases the stability of the powder against oxidation.

Nitriding and Oxide Formation

An ultrafine electrolytic powder containing 41.1% Cu, 1.8% Ni, 4.0% Al balance, iron, in its freshly produced state is pyrophoric; it can be passivated by producing an oxide or nitride film on its surface.

Nitriding is performed using ammonia which, mixed with a reducing gas, is introduced at the end of the recovery annealing of powders at 300–400°C. The flow rate of nitrogen-containing compound is at least 20 vol% of the reducing gas. Nitriding treatment for 15 minutes forms a nitride film on the powder surface.

When titanium is nitrided, a layer of nitrogen solution formed in α-titanium plays the role of protective film.

The oxide formation on the ultrafine powder surface can be achieved in the following way. After the recovery annealing is complete, the reducing gas is cut off, the powder is cooled down to room

Table 11.11 Methods of copper powder stabilization

Stabilizing component of solution	Unit	Concentration	Corrosion resistance increase degree[a]	Wettability	Hydrophobization operation
Stabilizing after electrolysis					
Without stabilizing	...	...	1.0	+[b]	
Laundry soap	wt%	0.01	81.0	−[b]	The powder is rinsed out after
Soapnaphtha	wt%	0.05	...	−	electrolysis. It is washing with
Benzothiazole	wt%	0.01	9.8	−	inhibitor solution – washing
Benzothiazole	wt%	0.06	57.8	−	out the excess of stabilizing
Glue	wt%	0.01	4.1	+	solution – moisture is removed
Glue	wt%	0.05	9.0	+	by a centrifuge–drying in hot air
Gelatine	wt%	0.01	3.5	+	current
Gelatine	wt%	0.02	8.0	+	
Gelatine	wt%	0.05	12.0	+	
Beta – naphtoquinoline	wt%	0.02	9.3	+	
Polyethylene polyamine	g/L	0.2–0.5	6.6	+	
Polyethyleneimine	g/L	1.0	6.4	+	
Benzothiazole	g/L	0.12–5.0	...	−	Dipping of powder in hot benzothiazole solution; airing
Stabilizing during electrolysis process					
Polyvinyl alcohol	g/L	0.2	4.44	...	Introduction of a surfactant
Gelatine	g/L	0.2	4.4	...	into electrolyte
Polyvinylpyrrolidinone	g/L	0.2	9.0		
Polyethylene polyamine	g/L	0.2–0.5	3.7	...	
Polyethyleneimine	g/L	1.0	5.8	...	
Stabilizing during drying in the fluidized bed					
Benzothiazole	...	...	2.2	...	Introduction of a saturated inhibitor vapor in hot air

[a]The action of each stabilizing matter is evaluated in comparison with conditions durante absentia of one, which is taken for unit;
[b]'Plus' and 'minus' indicate 'wettable' and 'non-wettable', respectively.

temperature in argon containing about 0.02% of oxygen [19].

Microencapsulation

Microencapsulation implies the application of polymer films either on the surface of each powder particle or granule.

The following microencapsulation methods are known [20]: physical–chemical methods (in water medium, in organic liquids media); chemical methods with use of polymers, polycondensation and polymerization; physical methods (via vapor condensation, extrusion, microcapsulaton in fluidized bed).

As film-forming material, the powder microencapsulation via vapor condensation uses a metal that is vaporized in a vacuum and condensed on the cold powder surface.

During extrusion, a thin tough film is formed on a small diameter screen perforated surface and the particles to be encapsulated are forced through this perforated surface. Centrifuges of specific design are used for this extrusion.

Microencapsulation in a fluidized bed is accomplished via formation of a fluidized bed of particles with spraying by a solution or suspension of a film forming material.

The aluminum powder of APV grade (in Russian classification) is microencapsulated with a film forming composition based on a silicon organic liquid [21] with the formation of aggregates consisting of fine, 5–20 μm particles, bonded to coarser ones. The presence of zones being blocked with a microfilm produces the effect on powder oxidation conditions in the low-temperature region. Thus, the temperature of onset oxidation for the microencapsulated powder of aluminum, APV (APV-M) is 90 degrees higher than for common APV (Figure 11.34(a)). Oxidation kinetics with heating of APV jointly with APV-M (Figure 11.34(b)) shows an endothermic effect (374.5 J/g).

Along with the decrease of dust formation when handling powders in processing steps, the microencapsulation also reduces the fire/explosion hazard [22].

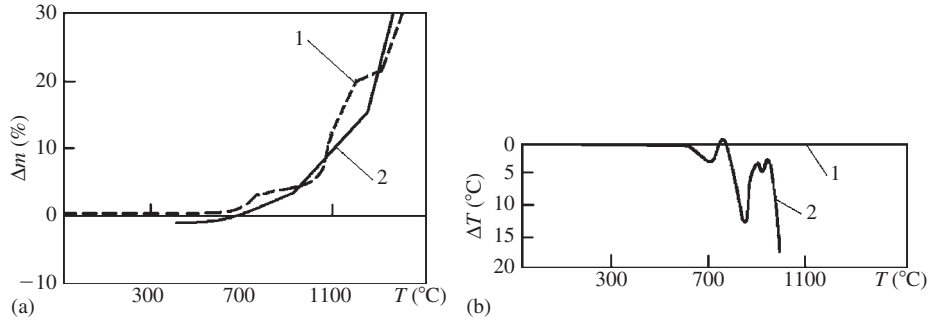

Figure 11.34 Mass increase of powder specimens during heating with rate 10 degree per minute (a) and thermogram (b) of synchronous oxidation of initial (1) and microcapsulated (2) powders: 1, APV; 2, APV-M.

Proportioning, Packaging and Inter-stage Transport

Proportioning

Proportioning of a material may be continuous, performed by means of feeders, or intermittent by feeding material in batches of preset weight or volume. Continuous uniform material feeding with a given flow rate is required, for instance, during drying and sizing of powders.

Powder feeders play an important role in powder processing such as feeding raw materials or discharging product materials from a storage vessel. The powder load to be treated in the process depends on the accuracy of feeders.

The static and dynamic characteristics of feeders depend on powder properties such as particle size, shape, internal friction coefficient and powder flowability. They also depend on the operating conditions, including moisture content of powder, temperature and pressure in the process.

Moreover, feeders are always associated with feed hoppers and their design might affect the function of feeders. If the feed hopper is not well designed, the flow mode in the hopper will be an unfavorable one called funnel flow and arch formation.

Unstable flow is caused by poor feeder selection or inappropriate hopper design. An unstable flow with bridging or flushing will also be caused by a variation in powder properties or operating conditions. The wall surface can be coated with ultrahigh-molecular-weight materials so as to reduce these problems. Suitable vibrators can also be utilized for this purpose. Granulation, drying or encapsulation can also decrease the friction so that the powder flow can be changed from the funnel flow mode to the mass flow mode, even for a hopper having a large wall angle.

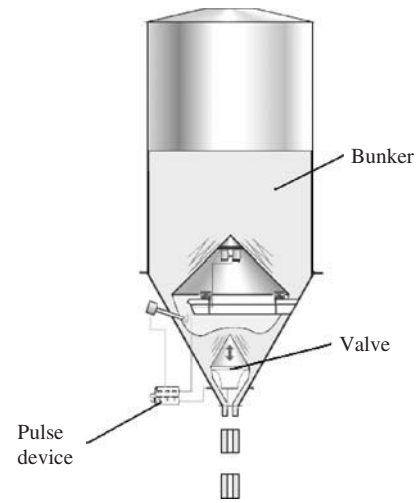

Figure 11.35 The lower discharger valve that lifts and vibrates to discharge product in either conditions or pulse mode. Courtesy of MATCON Company.

The pulp or slurry is supplied in batches for dehydration in apparatus of gravitational settling (batch operation) or of filtering (vacuum-filters of sampling action). Batch feeding is produced by filling containers (packages) with commodity powder, mixed with other components, and when components have to be delivered for passivation and microencapsulation of powders.

The feeder-activator design provides the powder outflow from bunker (or storage) through an annular slot between face plane of the discharge branch pipe and feeder cone. As a result of vibrating the powder, outflow occurs in a fluidized state. Such design helps to prevent arching. To prevent arch formation in large silo/hoppers, MATCON developed a design of a lower discharger valve that lifts and vibrates to discharge the product in either continuous or pulse mode (Figure 11.35).

The feeder intended for supplying a wet material is shown in Figure 11.36. It comprises a horizontal shaft with turning arms, which prevent adhering of wet material to the work element and allow the feeding rate to be adjusted. An agitator mounted in the discharge mouth of the feed bin eliminates arch formation and mouth occlusion with wet material. The maximum throughput is 0.8 m^3/h.

Various feeder types have been developed by Consit Company, including the screw feeder for slurry as well as for dry powder feeding, spiral feeders for dry particulate materials and vibrating feeders with throughput from 0.01 m^3/h and less up to 4.2 m^3/h.

For proportioning of the powder discharge, weight automatic dosing machines [23] are used, which are governed by means of the control station for the automatic batching line [24].

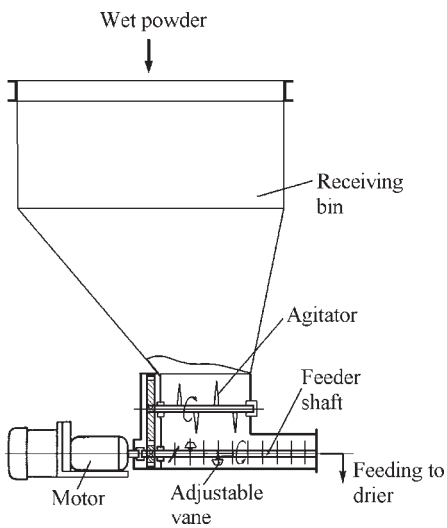

Figure 11.36 Screw feeder for feeding of wet powders.

Packaging

There is a variety of apparatus for proportioning and packaging powders. However, they are designed for handling foods, detergents, dyes, etc. These apparatus are, however, non-usable for metal powder handling because of higher density and higher volume containers of the latter.

On the other hand, there are completely automated units for proportioning and packaging of iron powders. However, these are very complicated and costly machines and their use is only justified at high production volume.

The Design Bureau of IPMS has developed simpler units for proportioning and packaging of powders. Their capacities correspond to production lines with a value up to 3 t/h. Two types of units have been developed to batch powders: for weight batching and volume batching.

For volume batching, the powder is charged into polyethylene packages of 15 and 20 liters inserted into steel barrels of the same volume. The package is weighed using an electronic scale and the weight recorded. It is then placed in a vessel. The orifice for charging is then welded, the chamber depressurized and the packed package is passed to the finished-products storage area. The throughput of the unit is 30 packages per hour.

The unit proportioning the powder by weight is complemented by commercial equipment, including weight batcher, rotary table and vacuum pump (Figure 11.37). The polyethylene bag is introduced into a cartridge of the packaging mechanism of the turntable (Figure 11.37a–c). Then the package, as was programmed, gradually takes positions to complete the following operations: filling with powder, vibrating densification with simultaneous partial welding of the loading package orifice, air extraction and final

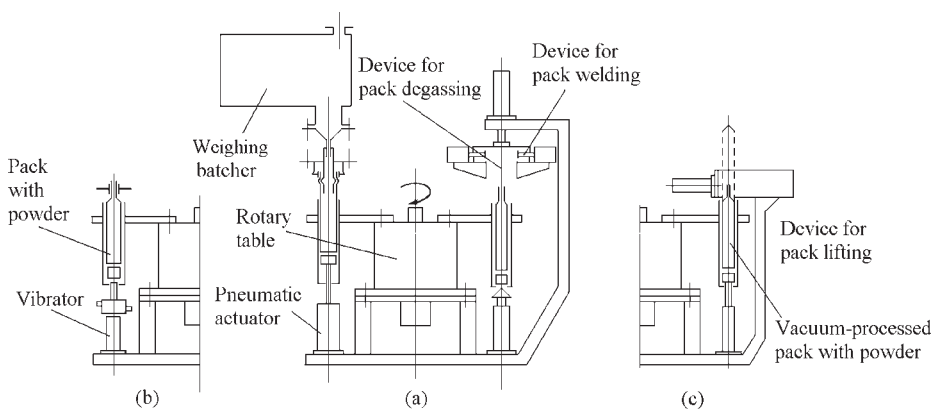

Figure 11.37 The unit for proportioning the powder by weight.

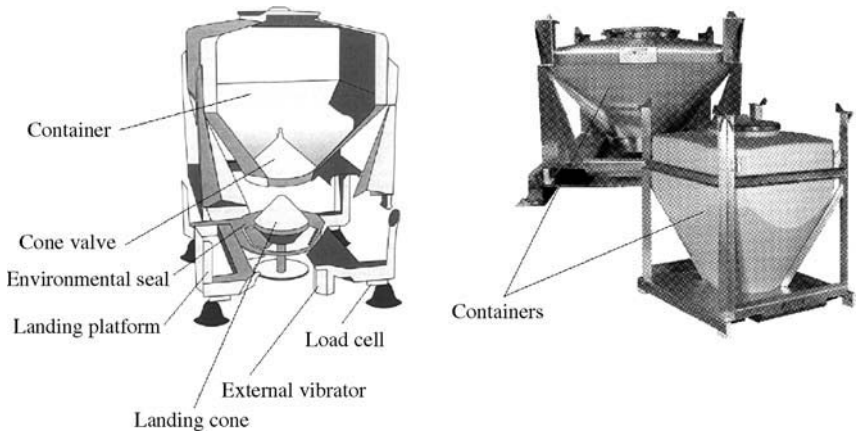

Figure 11.38 Container equipped by cone valve system. Courtesy of MATCON Company.

welding of the package loading orifice of the package, and unloading. Loading batch of powder is maximum 20 kg; maximum throughput of the unit is 30 packages per hour.

Inter-stage Transport

The type of the inter-stage transport chosen depends on the physical and mechanical properties of the material; assembling of processing equipment; production process management; and power of the production line.

Transportation of dry mixtures is done in special charge cans by material handling equipment (bridge cranes, electrical loaders fed via cables, crane jibs, telpher loaders, swing jib cranes), electric loaders, roller tables. The type of material handling equipment is chosen, taking into account the weight and height of the load to be lifted, material flow volume, load–displacement range, room geometry and category of fire/explosion safety.

The pulp is pumped by gravel pumps. Common types are pumps that provide a pulp flow rate of 63 m^3/h at a pressure of 22.5 m of water.

There are continuous and discontinuous inter-stage transports for powders. The discontinuous container transport is used for handling relatively small quantities. Advantages of such transport type are that compact placing of processing equipment is achievable, interoperational relations become simpler and mechanical material loss is reduced. Container volume is chosen taking into consideration the quantity of the powder to be processed during one shift. Containers can be simultaneously operated as storages (silos).

A container is designed so as to ensure the tightness of joints to the loading and unloading devices [25]. The container housing has a mounted bypass tube to exhaust the dust-laden air, which is forced from the filling tank to the upper portion of the container as its content decreases. Detailed information on this container design can be found in the subsection 'Definition of the local exhaust capacity' in Chapter 24.

The containers equipped with a cone valve system for joining to the receiving hopper during powder unloading are shown in Figure 11.38. Such containers produced by MATCON Company are commercially available.

Containers with a bottom fitting in spitzkasten form (Figure 11.39) provide a uniform settling of the powder throughout the horizontal cross-sections during its unloading from the container thus preventing powder segregation.

The conveyors (belt conveyors, vibrating conveyors, vertical spiral vibrating conveyors, spiral conveyors, and worm conveyors), bucket elevators and pneumatic transport are used as continuous types of transport.

Belt conveyors are used either for displacement of powders in a horizontal plane, or for low height lifting. The angle of inclination of a conveyor should be lower than the angle of friction of powder on the belt surface. Belt conveyors are favored when the loading sequence is in a straight line, for instance, when the melt is atomized in a horizontal chamber.

Belt conveyors can be set up at a steep angle of 60 degrees when wet powders are displaced, unloaded, for instance, from a dehydrating apparatus. The wet powder on a conveyor loaded side is pressed by the

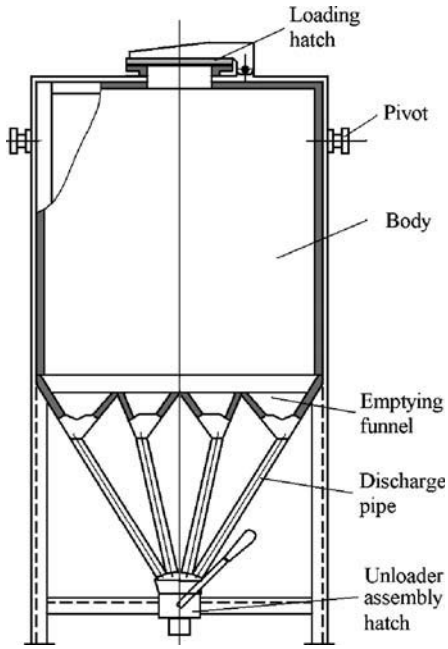

Figure 11.39 Container with bottom fulfilling in spitzkasten form for marketable powder.

belt of another conveyor moving synchronously with the former.

Vibrating conveyors are used for transport of powders in a horizontal plane, e.g. when the loading is performed at several points from hopper sections. Dustproof performance and simplicity of the design are advantages of vibrating conveyors.

Vibrating conveyors contain a load carrying element in the form of a tube mounted via elastic elements on a fixed frame. As vibroexciter, a debalance two-shaft vibrator or two electromechanical vibrators are used. The jump joint of overloads are tightened using elastic rubber gaskets. Throughput amounts to 6.0 t/h, length of transportation is 2.5–5.0 m.

A vertical vibrating conveyor is a conveying column with an inside spiral chute connected to supports by means of elastic ties and equipped with vibroexciters. The tightness of the loading and unloading subassemblies is reached via elastic corrugated rubber gaskets. The Consit conveyor KVV-0.5 has a column of 500 mm external diameter; lifting height of 5.0 m; throughput maximum 1.5 m^3/h apparent volume at a mark-to-space ratio of the chute breadth of 0.6–0.8. An upgraded design of the conveyor has vibroexciters mounted on the top of the column. A dustproof construction of the conveyor excludes dust emission. The vertical vibrating conveyor is a rather costly machine.

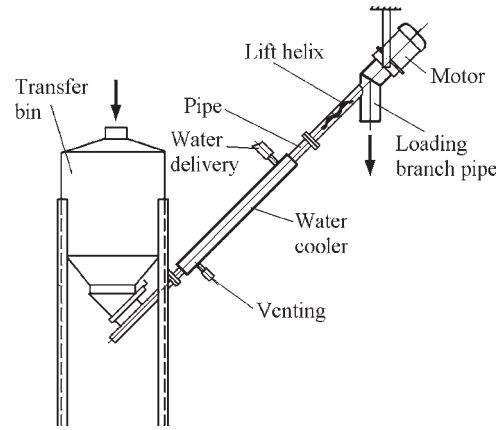

Figure 11.40 Spiral conveyor.

Vertical bucket elevators can also be used. However, their operation is accompanied by increased dust emission.

For transportation of a relatively small quantity of powders, inclined spiral conveyors are convenient to use (Figure 11.40). The powder is delivered to a transfer bin equipped with a gate. In a tube a lift helix is rotated, the upper end of which is connected to the electric motor shaft, while the lower end is free. The powder passes to the tube through a feed slot in the bin and is carried away by the lift helix and unloaded through a discharge branch pipe. The conveyor may, if required, be equipped with a water cooler, coaxially attached to the lift pipe; provision is made to feed and lead away water through nipples. The spiral rotates with 1000 R/hour speed. Volumetric throughput is 0.2 m^3/h apparent volume of powder; height of lifting is 4.0 m.

Pneumatic transport of powder is able to lift a powder, if required, to as much as 8–10 m in height, or to convey it to long ranges, especially by a cascade assembly of equipment. Recommendations relative to the design and calculation of transport systems are given in [26]. The use of pressurized pneumatic transport is preferred.

Pneumatic transport is used in pneumatic dryers (see Figure 11.11), in which the powder is conveyed suspended in a gas, while its movement is provided by a high pressure exhauster.

References

1. Bogdanova, O.S., Olevsky, V.A. (eds), *Handbook for Enriching of Ores. Preparatory Processes*. 2nd edn. Nedra, Moscow, 1982 (in Russian).
2. *Powder Technology Handbook*. Marcel Dekker, Inc. Publishers, New York, Basel, 1997.

3. Dytnerskiy, Yu.I., *Processes and Apparatuses of Chemical Technology*, 3rd edn. Chimija Publishers, Moscow, 2002 (in Russian).
4. Lykov, M.V., *Drying in Chemical Industry*. Chimija Publishers, Moscow, 1976 (in Russian).
5. Yurenjeva, V.N., Lebedeva, P.D., *Thermotechnical Handbook*, 2nd edn. Energija Publishers, Moscow, 1976 (in Russian).
6. Sazhin, V.S., *Technique of Drying*. Energija Publishers, Moscow, 1984 (in Russian).
7. Gorbis, Z.R., *Heat Exchange and Hydrodynamics of Disperse Through Streams*. Energija Publishers, Moscow, 1970 (in Russian).
8. Neikov, O.D., Logachev, I.N., *Aspiration and Air Dedusting During Manufacture of Powders*. Metallurgija Publishers, Moscow, 1986 (in Russian).
9. Brodskiy, Yr.A., Bazikov, V.I., Zubkov, I.V., Krylov, A. I., Stepanenko, V.D., Vibratory dryers for chemical industry. *Chemical and oil and gas engineering*, 2006, 10:7–10.
10. Soviet Union Patent 1,017, 891, November, 1981.
11. Barskiy, M.D., *Fractionating of Powders*. Nedra Publishers, Moscow, 1980 (in Russian).
12. Bradley, D., *The Hydrocyclone*. Pergamon Press Publishers, Elmsford, 1965.
13. German, R.M., A-Z of Powder Metallurgy. In *Metal Powder Technology*, ed. B. Williams. Elsevier Advanced Technology Publisher, Oxford, 2005.
14. Troitskiy, V.N., Brodsky, Yr.A., Application of vibratory mixers in powder metallurgy. *Powder Metallurgy and Metal Ceramics*, 1989, 1:91–94.
15. Schatt, W. (ed), *Pulvermetallurgie Sinter und Verbundwerkstoffe*, VEB Deutscher Verlag für Grundstoffindustrie, Leipzig, 1979.
16. Perry, J.H., *Chemical Engineers*. McGraw-Hill Book Company Publishers, 1969.
17. Usolceva, E.E., Pomosov, A.V., Electric precipitation of copper dispersed deposition over the organic additions. *Sov. Powder Metall. Met. Ceram.*, 1983, 8:1–8.
18. Nichiporenko, O.S., Pomosov, A.V., Naboychenko, S.S., *Powders of Copper and Copper Alloys*. Metallurgija Publishers, Moscow, 1986 (in Russian).
19. Zhelibo, E.P., Gamarnik, M.J., Polishin, E.V., Influence of annealing on composition, structure, and magnetic properties of superfine powders of iron and iron-cobalt alloy. *Sov. Powder Metall. Met. Ceram.*, 1989, 10:1–15.
20. Solodovnikov, V.D., The type of the in-process transport is chosen in dependence on physical and mechanical properties of a material. *Microcapsulation*. Chemija Publishers, Moscow, 1980.
21. Burykin, A.A., Neikov, O.D., Rabin, P.B., Sharova, L.C., Microencapsulation of metal powders for prevention of explosions and dust emissions during their production and processing. *Sov. Powder Metall. Met. Ceram.*, 1991, 6:98–103.
22. Neikov, O.D., Rabin, P.B., Vasiliyeva, G.I., Mcrocapsulated aluminium powders. *Material Science Forum*, 1997, 242:219–222.
23. Weight automatic dosing machines. Standards Publishers, Moscow, 1991 (in Russian).
24. *Control Station for the Automatic Dosing Line*. CNIITEItjachmash Publishers, Moscow, 1987 (in Russian).
25. Soviet Union Patent 1,126,508, July, 1983.
26. Spivakovskiy, A.O., Dijachkov, V.K., *Transporting Machines*. Mashinostroenie Publishers, Moscow, 1983 (in Russian).

SECTION 4 Production of Non-Ferrous Metal Powders

Contents

For a more detailed Section Contents list, please see the book Contents pages that start on page v

Chapter 12

Production of Aluminum and Aluminum Alloy Powders

Victor G. Gopienko, Russian National Aluminum-Magnesium Institute, Saint Petersburg, Russia

Aluminum and aluminum alloy powders are manufactured almost exclusively by gas atomization. Compressed air is used as the atomizing gas for most applications. Inert gases (nitrogen, argon and helium) have found application in special cases. Currently, the annual world production of aluminum powders amounts to 100 000 metric tonnes [1], while the productive capacity is estimated to be approximately twice this [2]. A large part of this capacity is in North America and in Russia. North American metal shipments in short tons in 1995–2006 (Figure 12.1) show the tendency of the dynamics of aluminum powder production in 1996–2000 and following stabilization at the level of 50 000 tons [3].

The ranges of aluminum powder applications are of a great variety. They include aluminothermic reduction in metallurgy, chemical processes, explosives, rocket fuel, pyrotechnics, thermite welding, additives for gas generation in aerocrete production, pharmaceuticals, pigments for paints and inks.

There are the following basic kinds of powder products from aluminum and its alloys:

- Powders: particles with a size from a few microns to 1.0 mm (usually not more than 0.5 mm) of spherical, oval, drop-like, irregular, fragmental or dendritic shape.
- Flakes: scaly (lamellar) particles with a thickness smaller than 1.0 μm and linear sizes 50–200 μm. Particles are usually coated with a thin layer of stearin, aluminum stearate, paraffin or other fats, the content of which is 0.2–4.0%.
- Pastes: compositions of flake particles (65–75%) and a liquid phase (water, hydrocarbons).
- Granules (grit): particles with a size larger then 0.5–1.0 mm of spherical, oval, drop-like, disk-shaped, needle or irregular shape.

Known methods of aluminum powder production can be divided into two basic groups.

- Physicochemical methods: electrolytic sedimentation from solutions or melts; reduction (or thermal decomposition) of aluminum compounds; evaporation and condensation of the metal from a vapor phase.
- Physicomechanical methods, i.e. without basic changes of chemical and phase

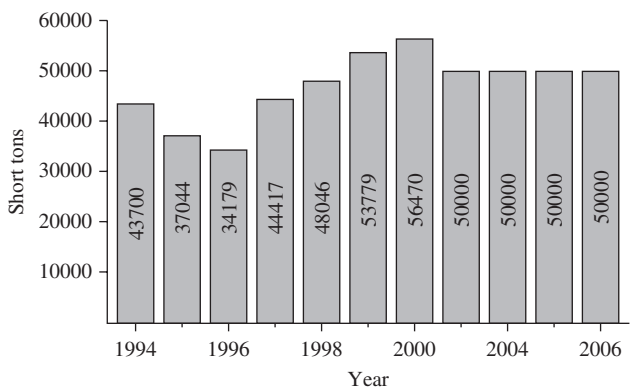

Figure 12.1 North American aluminum powder shipments in short tons in 1994–2006.

structure of the initial material: mechanical crushing of aluminum, fragile alloys of chips, foil; atomization of melts.

Besides of the main commercial gas atomization technique, the following methods for aluminum powders manufacture are known:

- *Crushing* of fragile aluminum alloys (Al–Ni, Al–Mg, Al–Si) in ball mills or other crushing devices (particle shape is fragmental).
- *Dry grinding* of aluminum powder or foil in the presence of surfactants in a protective gas atmosphere with monitored content of oxygen (production of pigment, pyrotechnic and clumpy powders).
- *Grinding of aluminum particles* in a liquid phase (hydrocarbons, water) containing surfactants (stearin) and other additives (production of pastes). Pastes can also be manufactured by mixing the powder with hydrocarbons or aqueous solutions with special additives.
- *Granulation*: free casting of the melt into a cooling medium through ground apertures of the melting pot (crucible); the size of granules is of 4–20 mm (the shape – disk-shaped).
- *Centrifugal atomization* of the melt through lateral apertures of the punched walls of a rotating glass, from a flat disk surface, edges of a cone glass, etc. The molten metal forms droplets that solidify in the cooling gas medium or in water. Plants for centrifugal dispersion of the melt are mainly used to manufacture granules with the grain size of more than 0.5 mm in size or coarse fractions of powders larger than 100 μm in size. Centrifugal dispersion is carried out through apertures of the rotating punched vessel (glass). Designs of plants with centrifugal dispersion are used in Russia and Ukraine [4].
- *Destruction of solid metal* at hot-brittleness temperature; the size of granules is 5–20 mm, their shape is irregular.
- *Lumping of fine foil scrap* into round granules of 3–6 mm in size.

The characteristics of aluminum powders produced by various methods are given in Table 12.1.

Gas Atomization

Atomization of melts by compressed gases or liquids provides for the manufacture of powders of aluminum and its alloys in a wide range of sizes from 1–2 μm to 1–2 mm with particle shape varying from spherical, drop-like to irregular. Uniformity of composition and fine microstructure of powder particles are achieved by atomization of aluminum alloys due to a high cooling rate of 10^4–10^6 K/s [5–7].

The greatest development and industrial application for producing metal powders by melt atomization by compressed gases use the following basic types of plant:

- Vertically upward aspirating plants, such as operated by Alcoa [2], allow the production of powders with the widest range of particle sizes.
- Horizontal aspirating installations, where the melt jet and the atomizing torch are directed horizontally or obliquely to the horizon. Ejection feed of the melt for atomizaton of aluminum, magnesium and their alloys is used at the aluminum mills in Russia, a feed under pressure is utilized at the Kluchevskoy ferroalloy mill in Russia, and a siphon feed is used at the Ekkart-Werke, Germany [4].
- Vertical installations, where a free flow stream of the liquid melt is atomized into droplets by impingement of high-pressure jets of gas or oil. They are used mainly to produce powders of heavy metals and alloys (iron, copper, complex alloys based on iron). In some cases, plants of such type are also used for producing light metals and alloys, including aluminum [4].

Numerous other variants of constructive design of the basic types of plant for atomization of molten metals and alloys listed above are known.

A scheme of the Alcoa process based on the vertically upward aspirating principle is shown in Figure 12.2 [8]. The molten metal is supplied from the holding or melting furnace to the atomizing tundish. The liquid is drawn from the tundish through a delivery tube into the atomizing nozzle. This is attained owing to the suction (aspiration) effect arising at the nozzle end by the flow of the high pressure atomizing gas in the nozzle. Meeting with the high-velocity gas jet, the liquid metal is broken up into droplets that are carried along by the gas flow and quenched by the gaseous cooling atmosphere in the chiller chamber. The particles formed together with the cooling air pass into the collection system that consists of two sets of cyclones. The powder collected in the cyclones is then transported in an inert gas atmosphere to the screens and packing station under inert gas.

However, this process requires careful adjustment and maintenance. An expected stopping or decreasing of the delivery of the cooling air in the chiller

Table 12.1 Characteristics of aluminum powders [4]

Type of powder, method of production	Shape of particles	Mass medium particle size (μm)	Density (g/cm^3)		Al_2O_3 (wt%)	Al content (wt%)
			Apparent	Tap density		
Powders produced by:						
Air	Oval with rough surface shape, irregular	50–200	0.73–1.24	1.15–1.25	0.1–1.0	99.5
Inert gas atomization	Spheroidal	45–100	0.5–1.4	0.90–1.70	0.1–1.7	99.5
Ultrafine powders produced by condensation from gas medium	Spheroidal	0.2–0.5	...	...	...	>99
Powders produced by grinding fragile alloys of Al–Mg, Al–Ni, Al–Si systems	Fission-fragment	40–2000	...	...	...	70–90
Flakes produced by dry grinding:						
Fine	Flaky	45	0.27–0.41	0.41–0.68	2–21	96–98
Coarse	Plate-shaped	150–1170	0.22	0.36	1	>99.5
Cloddy (for SAP)	Lump of flaky particles	210	1.08–1.21	1.35–1.49	6–14	The rest
Granules produced by melt atomization	Oval, tear-shaped, irregular, acicular	500–5000	1.8–1.5	1.6–1.8	...	87–99.5
Granules produced by free melt casting into the water or cooled surface	Disc-shaped	500–20 000	1.5–1.7	...	...	87–99.9
Paste produced by grinding in the fluid of liquid hydrocarbon	Flaky	45	...	...	2–20	...

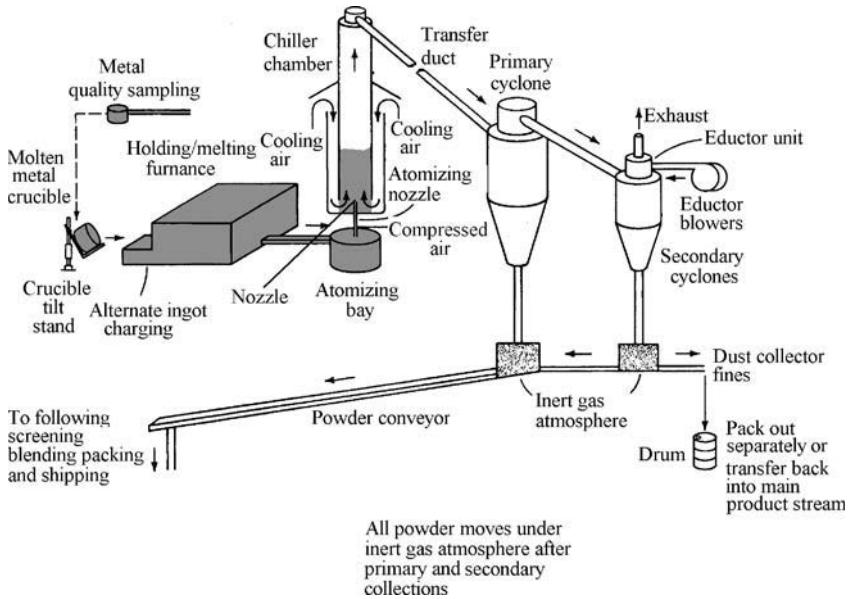

Figure 12.2 Schematic of the Alcoa process for atomizing aluminum powder.

chamber causes an increase of the airborne dust concentration of aluminum powder over the level which forms an explosive mixture. Generally, the technology of producing gas-atomized aluminum powders is a potentially explosive process and special safety measures are required that considerably increase the manufacturing cost. These safety measures, such as those accomplished by Alcoa, comprise cooling air delivered for the melt atomization in the chiller chamber, the carrying out under inert gas of all powder movement, including screening for separating into size fractions and packing into drums and, in addition, using sensitive systems controlling a low concentration of powder in the gas and the pressure rise.

Plants of horizontal type have the following advantages:

- impossibility of melt ingress into the dust-precipitating system in the case of a bath fracture
- relative ease of monitoring of the atomization process
- increase of the safety due to the division of stages and devices of atomizing (melting bath, atomizer) and primary classification (atomizing chamber, cyclones).

The disadvantage of such plants is the amount of area occupied, which is greater than for other types because a large part of the plant is in a horizontal plane.

Plants of vertical type with top-down atomization are more compact and occupy a smaller production space, however in this case the danger connected with an opportunity of melt inrush into the atomizing chamber is increased, the atomization process is more difficult to control and a large height of the chiller is necessary for supply of solidification of the molten particle stream.

The main characteristics of the explosion risks of the powders are shown in Table 12.2 [4].

The properties of typical commercial aluminum powders are given in Table 12.3 [9].

Plants of granulation type are more explosion-proof and have higher efficiency. However, they are not suitable for producing highly-dispersed powders.

The hardware-technological circuit (Figure 12.3) most widely used in Russia includes the high compressed gas (air or inert gas) atomization systems and powder separation. Devices with dry separation of atomization products (in cyclones, multi-cyclones, bag filters) and with melt atomization into liquid medium (hydrocarbons or aqueous solutions) are used. In the latter case, higher cooling rates are achieved. A disadvantage of atomization into a liquid is the necessity of powder drying and regeneration of the coolant, and received powders can be contaminated with carbon (in the case of the atomization into liquid hydrocarbons), oxygen and hydrogen (in the case of water atomization or gas atomization into water). The high activity of aluminum powders limits the opportunities of using devices for water atomization of aluminum and its alloys.

Water atomization is not used commercially for aluminum and its alloys for fear of the explosion risk

Table 12.2 Explosion risk characteristics

Type of powder	Composition, content (wt%)	Powder particles size (μm)	Explosion risk characteristics			
			LCIL (g/m^3)	p_{max}, MPa	v_{max} (MPa/s)	τ_{in} (s)
Al	99.95Al	160 max	60	0.43	6.6	0.10
		50 max	47	0.56	7.7	0.05
AD-33 (in Russian classification)	1.3(Zn + Mg)–0.3Cu–0.5Si–0.14 Mn Al–balance	160 max	80	0.39	4.3	0.15
		50 max	58	0.43	5.6	0.1
Al–Cr–Fe	90.5Al–8Cr–1.5Fe	63 max	101	0.43	2.0	0.3
		50 max	84	0.49	4.0	0.1

LCIL: the low concentration ignition limit; p_{max}: the maximal explosion pressure; v_{max}: the maximal velocity of its growth; τ_{in}: the induction period (the time from the start of igniter to the ignition moment of the powder suspension).

of the atomization process due to rapid hydrogen emission during powder–water interaction and the high reactivity of aluminum that can cause heavy oxidation of the surface of water-atomized powders.

In contrast to the traditional opinion, recent studies have shown that water atomization under optimized conditions could be used for production of high-quality Al alloy powders [10]. This technique is discussed in Chapter 13.

Typical chemicals analyses and physical properties of atomized aluminum powders are shown in Table 12.3.

Production of Granules

According to the properties and application fields, granules are a transition link between powders and ingots; the precise border between powders and granules in the range of particle size from 0.1 to 1.0 mm is practically absent. In some cases, powders can be successfully replaced by granulated aluminum and its alloys, in particular in the chemical industry, in the production of steel and ferroalloys, chromium, etc.

The advantages of granules in comparison with powders are their higher profitability and the lower explosion risk both of the production process and the product itself. It simplifies the organization of manufacture and use of such products.

The largest consumers of granules from primary and secondary aluminum are ferroalloy and steel works. The consumption of granules has increased with a corresponding decrease in the consumption of pig aluminum or powders.

In recent years, the technology for melted aluminum granulation has mainly developed in the direction of increase of granule uniformity in size, reduction of their oxide and gas content, and a possibility of regulation by coarseness, granule shape and microstructure of granulated alloys. Four basic hardware technological circuits of granulation allowing the manufacture of aluminum granules of various grain size, shape and hardening degree are used [4,9]. Hardware-technological schemes of granulation that are used in Russia are given in Table 12.4 and in Figure 12.4.

The scheme in Figure 12.4(a), circuit I (pouring into the water through a tundish with holes in the bottom) is used at the enterprises of the aluminum industry and ferrous metallurgy plants. Granules of aluminum of high and technical purity as well as granulated aluminum alloys are manufactured.

Mechanized lines with productivity up to 10 000 t per year working under the circuit I (pouring into the water via a tundish with holes in the bottom, Figure 12.4(a)) are used in the 'Volgograd Aluminum' plant of the SUAL company in Russia [4] to produce granules with granule size of 5–20 mm from high-purity aluminum (for gallium cementation from aluminate solutions) and granules from secondary aluminum with high iron content (for processing pig-iron and steel). In this circuit, the reduction of the size of granules is achieved by vibration of the pouring bowls. The plant is completely mechanized and provides a continuous technological process from melting of the metal to discharging the commodity product classified by granule size.

The technological circuit II (pouring to a cooled surface, Figure 12.4(d)) eliminates the contact of

Table 12.3 Properties of typical commercial atomized aluminum powders

Type of powder	Chemical and physical properties											Source
	Composition (wt%)					Apparent density (g/cm^3)	Sieve analysis (wt%) Sieve size (μm)					
	Al	Fe	Si	Each	Total		+250	+160	+100	+45	−45	
Atomized powders						0.8–1.3	Median diameter within 25–150 μm					[2]
Typical	99.7											
Max		0.25[a]	0.15[a]	0.05	0.15							
High-purity atomized powders						0.8–1.3	Median diameter within 25–150 μm					[2]
Min	99.97											
Typical	99.976	0.007	0.008	...	0.009							
Atomized aluminum powders	99.4	0.4	0.3	n-d	n-d	0.95–1.05	0	0	5–15	55–65	35–45	PM
Pigmentary aluminum powder[b]	Bal	0.5	0.4	4.06[c]	...	...	0	0	...	0.8		SUAL

[a] Fe + Si of 0.30 wt% max;
[b] Gas (nitrogen + 6 wt% oxygen) atomized powders are ground in ball mills with greasy additives;
[c] including 3.8% greasy additives; SUAL: JSC Siberian–Ural Aluminum Company; PM: Pometon.

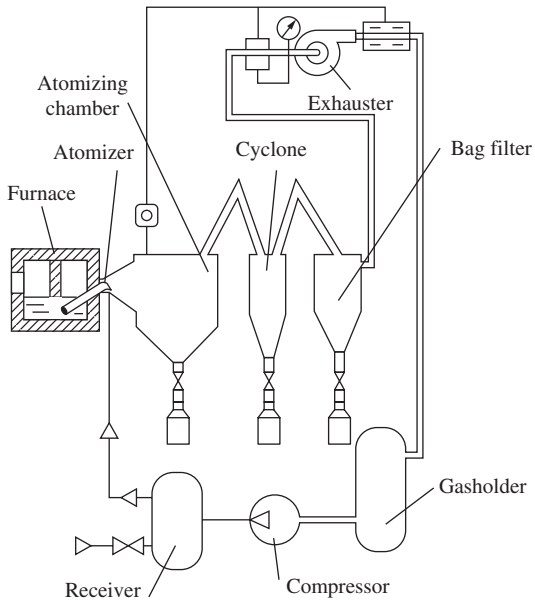

Figure 12.3 Schematic diagram of a gas atomization plant.

granules with water and the subsequent drying process. Despite the seeming simplicity in this circuit, there are serious difficulties connected with the necessity of fast heat removal from solidifying granules. As a rule, the productivity of such plants is of the order of 100–300 kg/h. Drop casting is carried out from the punched tube (funnel) radially placed over a water-cooled metal disk rotating in a horizontal plane. The granules, which have solidified on the disk, are cleaned off in the receiver, whence they are led to sieving and packing. Instead of a rotating disk, a moving belt can be used. Plants of this type are used by the firms Ekkart-Werke (Germany) and Pechiney (France).

Under industrial conditions, there are plants with units that generate electromagnetic oscillations acting on the melt stream, which has allowed a reduction of the size of granules up to 2–10 mm [4].

In centrifugal atomization, centrifugal force breaks up the molten metal as a spray of droplets which then solidify as powder particles. The circuits for centrifugal melt atomization (Table 12.4, circuits III and IV) produce granules of various shape and size (from 0.1 up to 2 mm) with a high crystallization rate. In all cases, the cup is 100–200 mm diameter, running at moderately high speeds, from 3000 to 10 000 rpm.

The scheme in Figure 12.4(c), circuit IV, assumes cooling of atomized particles in a gas atmosphere; in this process, needle-shaped (in air), drop-shaped or spherical (in inert atmosphere or under protection of particle surface by flux) granules are produced.

Granules manufactured by centrifugal atomization of the melt into water (Figure 12.4(b)) are used in powder metallurgy. The cooling rate of granules is close to that for gas atomized powders. Retardation of diffusion and fixing of high-temperature structure allows a two- to three-fold increase in the level of allowable impurities in alloys without a decrease in mechanical and corrosion properties of the material, i.e. to use effectively low-grade metal. In some cases, impurities traditionally considered as harmful, such as iron, form fine intermetallic phases that provide good elevated temperature strength and other mechanical properties.

The cooling rate estimated by calculation and experiment for the above circuits, I, II, III and IV, is within 100–200, 100–500, 10^3–10^4, and 10^2–10^3 K/s, respectively.

Granulated alloys of aluminum–silicon system have been developed based on cheaper electro-thermal silumin manufactured by direct reduction from ores, that essentially expand the raw-material base of the aluminum industry. Cooling of the melt at a high rate in the process of granulation has allowed an increase in the content of silicon in the alloy up to 35% and thereby provide its precision properties [4].

New designs of the spinning cup have allowed organization of the pouring of the metal from the cup channels as a torch that has ensured production of a finer product and has created an opportunity to carry out 'dry' atomization (circuit IV, Figure 12.4(c)). The size of the basic fraction of granules is decreased from 2.0–2.5 to 1.0–1.5 mm.

By increasing the rotation speed of the spinning cup, the centrifugal technology is capable of ensuring production of granules of 0.1–0.8 mm in size. The physical properties of the granules so produced do not differ significantly from those of gas atomized powders but they are distinguished by greater uniformity of granulometric composition and by the absence of dust fractions.

In aluminothermic processes, application of granules with a specific surface of 200–400 cm^2/g up to 1 mm in size produced by melt centrifuging are the most effective. Granules from 0.2 up to 2.0 mm in size are most effective for steel deoxidation. Coarse granules of spherical shape of 1–5 mm in size are most suitable for production of heat-conducting components for electric motors. Granules of spherical shape of 0.4–0.8 mm in size are used in the chemical industry in fluidized bed devices. Granules of 7–20 mm in size from high-purity aluminum are used in hydrometallurgical processes (for example, for cementation of gallium from aluminate solutions).

Nowadays, master alloys and modifiers are one of the most promising areas for using granules

Table 12.4 Characteristic of the main circuits of granulation melt

Technological circuit	Characteristic of granules		Particle weight (g)	Circuit characteristic		Application field of granules	Device productivity (t/h)
	Size (mm)	Shape		Advantage	Disadvantages		
I. Free or vibration pouring with cooling in a liquid; drying, classification	3–20	Disc-shaped, nodular	0.5–1.5	Stability of shape and size	Contact with liquid: necessity of drying; low cooling rate	Gallium cementation from aluminate solutions, ligatures, steel deoxidation, chemical industry	0.2–1.0
II. Free or vibration pouring with cooling on a cold surface	5–40	Hemisphere, petalous	0.5–1.5	No contact with liquid, no drying; high speed of cooling	The shape and size of granules are a disadvantage for pressure processing	Gallium cementation, chemical industry, semi-product for grinding, ligatures, steel deoxidation, sheet rolling, pigments	0.1–2.0
III. Melt centrifugal atomization with cooling in a liquid; drying, classification	0.1–2.0	Spindle-shaped, drop-like, nodular	0.002–0.05	Ease of coarseness and structure regulation, high rate of cooling	Contact with liquid, drying of granules is necessary	Powder metallurgy, pigments, deoxidation, aluminothermy	0.6–2.5
IV. Melt centrifugal atomization with cooling in gas medium; classification	0.2–2.0	Acicular, fibrous, spindle-shaped, spheroidal	0.002–0.006	No contact with liquid, no drying of granules	Large size of a collecting chamber (8 m in diameter), intensive heat mode, low rate of cooling	Aluminothermy, deoxidizers, powder metallurgy, ligatures, pigments	0.6–1.0

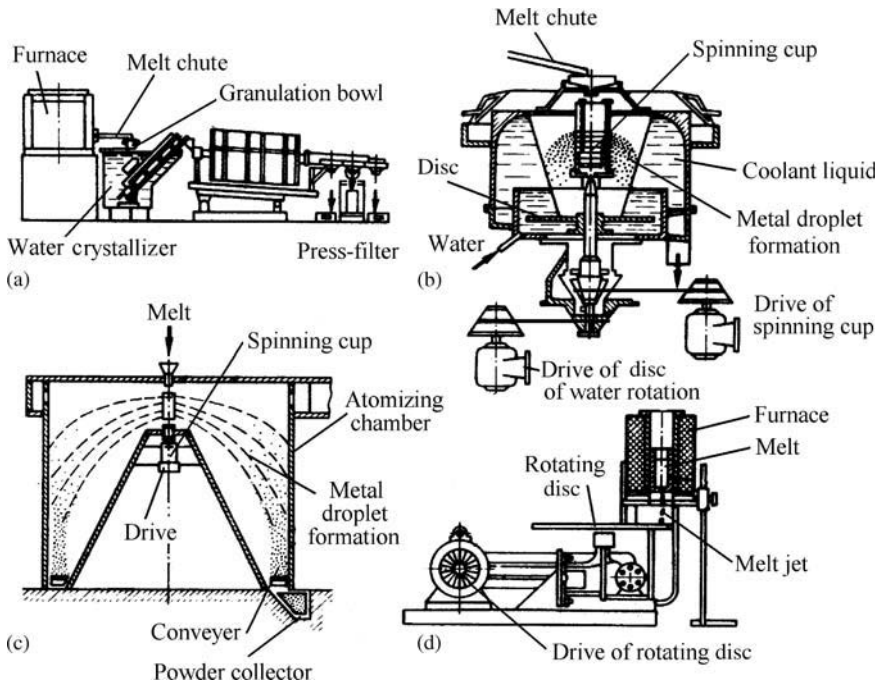

Figure 12.4 Hardware-technological circuits of the aluminum granulation: (a) scheme of the device for production of granules by the method of free casting into a liquid (water); (b) scheme of the device for granule centrifugal atomization with cooling in a liquid; (c) scheme of the device for centrifugal atomization with cooling in gas atmosphere; (d) scheme of the device for aluminum granulation with cooling on a cold surface.

5–20 mm in size. An advantage of granules in comparison with master alloys in the form of ingots or bars is the fine microstructure of the material. This provides a large number of crystallization centers while modifying the alloys and providing a heredity of structure, as well as the simplicity of batching and introduction of granules into the melt.

There are numerous application fields of aluminum granules, in the areas of powder metallurgy: the satisfactory properties of the products produced from low-grade aluminum and the unique properties of highly alloyed granulated alloys, explosion safety of the technology and the product distinguish granulation technology as an independent prospective direction of aluminum powder metallurgy.

The basic kinds of aluminum granules, which are produced commercially in Russia, are given in Table 12.5.

In hardware-technological schemes for producing aluminum granules developed in Russia, a magnetohydrodynamical granulator that provides manufacture of granules of the preset volume, granulation in an inert (protective) gas and dry method of crystallization on a moving belt are used.

Impulse atomization is capable of producing droplets of controlled size having a relatively narrow distribution and a predictable cooling rate [11]. The scheme of the process, shown in Figure 12.5, consists of an impulse generator, mechanical driver, a tundish and a nozzle plate with orifices. The impulses generate monodisperse droplets that free fall out of the orifices. The quiescent gas atmosphere, into which melts have been atomized, includes helium, nitrogen, argon and air. By varying the plunger acceleration, orifice size, orifice shape, melt temperature and gas atmosphere, the granule size and size distribution, shape and microstructure can be manipulated to the required specifications. Using this method, aluminum monodisperse granules from 2 to 10 mm in size are produced.

Production of Flake, Pigments and Pastes

Mechanical Milling of Aluminum and its Alloys

Aluminum flakes, pastes or powders from fragile alloys, such as Al–Mg, Al–Ni, Al–Si and others are produced by this method. For producing flakes,

Table 12.5 Aluminum granules

Granule mark	Sieve residue, wt% (max) on sieve with opening (mm)			Apparent density (g/cm^3)	Chemical composition (wt%)									Applications
					Al	Mg	Si	Fe	Mn	Cu	Zn	Ni	Sn	
	7	15	20		Minimum		Maximum							
AGUCH	95	0.3	–	1.0–1.5	99	...	0.03	0.01	...	0.005	...	0.006	...	For cementation of gallium from aluminum solutions, as a chemical reagent, etc.
AG	95	5.0	0.3	–	(Al + Mg) 97 min		0.6	3.0	0.5	0.3	0.5	·	0.3	In the metallurgical industry for deoxidation, modification of cast iron and steel

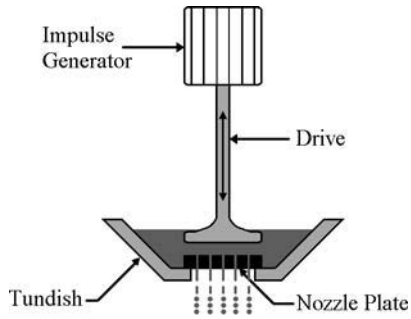

Figure 12.5 Schematic of the impulse atomization process.

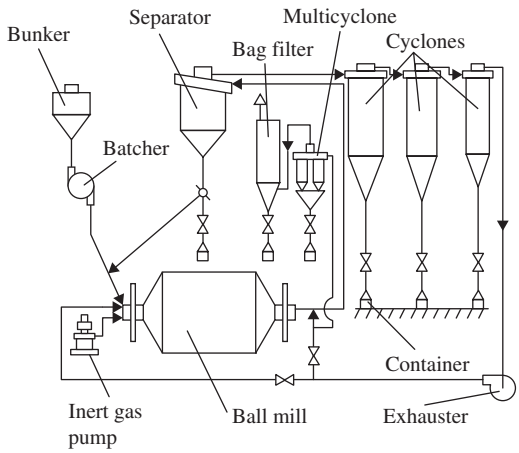

Figure 12.6 Schematic diagram of the pneumo-separation grinding installation.

aluminum stock material (powder, foil) is crushed in a protective gas atmosphere (dry scheme) or in a liquid (wet scheme).

The basis of the technology for producing aluminum fine is the process of plastic deformation that provides manufacture of particles in the form of thin flakes or leaflets. To prevent aluminum particles welding together and to reduce the friction between them and the milling balls, thus reducing the work required for deformation, stearin or another surfactant, in amounts from 0.3 to 4.0%, are added to the charge. Dry milling is carried out in a leak-tight mill working in a closed cycle in an atmosphere of nitrogen with the content of oxygen from 3 to 8%; the latter is necessary for the formation of a protective oxide film on the particle surface. At an oxygen content higher than 8%, an ignition inside the milling system is possible, and at an oxygen content lower than 2% self-ignition of the discharged powder is possible.

The scheme for the production of pigment (ПАП marks), pyrotechnic (ПП marks) flakes and lumpy flakes for sintering (АПС marks, in Russian classification) is shown in Figure 12.6. The main characteristics of aluminum flakes and lumpy aluminum flakes are presented in Table 12.6. Particles of aluminum lumpy flake are uniformly oxidized from the surface in the grinding process and agglomerated to the apparent density $0.9\,g/cm^3$ minimum. According to Russian GOST 10096-76, АПС marks contain of 6–17% $A1_2O_3$ [12].

The process of АПС lumpy flakes production consists of two stages. In the first stage, aluminum stock material is ground in the presence of 0.5–1.2 wt% of fats. The flakes produced have a lamellar particle shape no greater than 80 μm in size; its apparent density does not exceed $0.2\,g/cm^3$. On decreasing the content of the fatty additive to 0.5%, a further oxidation (second stage) and cold welding of the aluminum particles takes place. Conglomerates (lumps) of fine particles with apparent density $1.0–1.4\,g/cm^3$ are formed. The sizes of particles aggregated during balling are basically of 300–500 μm but can achieve 1 000 μm.

The charge of the fatty additive is increased with the increase of $A1_2O_3$ content in the final-product:

(Al_2O_3), wt%	6–11	11–17
Charge of the additive, wt%	0.60	0.6–0.9

Pastes are manufactured with petroleum-based or aqueous liquid phases. With the former, the aluminum flake content is of the order of 65% with 33% of volatile liquids such as white spirit, and 2% of fatty material (stearin acid). By the degree of fineness at grinding and the area of water coating ($1.5–3.0\,m^2/g$) on a mass unit, such paste considerably surpasses IIAII-2 – the finest aluminum flakes produced by dry grinding. Wet grinding is less explosive than the dry process of aluminum flake production.

The hardware-technological scheme that provides an opportunity of simultaneous or consecutive production of aluminum powders, flakes and pastes, includes the steps of initial material preparation, grinding, thickening, homogenizing and casing (Figure 12.7).

For the production of paste, aluminum powder manufactured by atomization, or scrap foil less than 50 μm in thickness, liquid hydrocarbons (white spirit, xylene, toluene, etc.) and fatty additives (stearin and oleic acids, etc.) are used.

Mixed material is ground in ball mills in one or several stages depending on the size of the initial aluminum particles and the required degree of particle fineness in the manufactured paste. The slurry from the mills is separated in a filter-press, a drum-type filter, or in a centrifuge.

Aluminum pastes are more convenient in use and in transportation because of the absence of dusting,

Table 12.6 Aluminum flakes and lumpy flakes

Trade name	Particle size (μm) (max)	Covering ability for water surface (cm^2/g) (min)	Apparent density (g/cm^3) (min)	Composition (wt%)							Applications
						Impurities						
						Mg	Si	Fe	Cu	Zn	Fat additives (max)	
				Al	Al_2O_3	Maximum						
Aluminum flakes												
ПАП-1*	80	700	0.3	90	...	0.01	0.4	0.5	0.05	...	3.8	Production of paints, enamels, resin glues. As a gas developing agent to produce aerocrete
ПАП-2*	45	1000	0.2	85	...	0.01	0.4	0.5	0.05	...	3.8	Is used in aircraft building, machine-building, instrument-making, polygraphic branch of industry
ПП-1	160	...	0.3	97	...	...	0.4	0.5	0.08(Cu + Zn)		0.8	Production of explosives and pyrotechnic components
ПП-2	100	...	0.4	95	...	...	0.4	0.5	0.08(Cu + Zn)		0.8	
ПП-3	63	...	0.5	93	...	...	0.4	0.5	0.08(Cu + Zn)		0.8	
Aluminum lumpy flakes												
АПС-1А	315	...	0.9	balance	6–8	...	0.25	0.20	...		...	Production of elevated temperature material SAP-1, capillary pipes and foil with the thickness from 0.3 to 0.1 mm resisting at 350–500°C
АПС-16	1000	...	1.0	balance	6–8	...	0.25	0.25	...		...	Production of profiled semi-product
АПС-2	1000	...	1.0	balance	9–12	...	0.25	0.30	...		...	Production of semi-product from SAP-2 with heat-resistance higher by 15–20% than SAP-1
АПС-3	1000	...	1.0	balance	13–17	...	0.25	0.30	...		...	Production of the semi-product from the most heat-resisting material SAP-3

*ПАП-1 and ПАП-2 produced for varnish-and-paint industry have the leafing of 80% min.

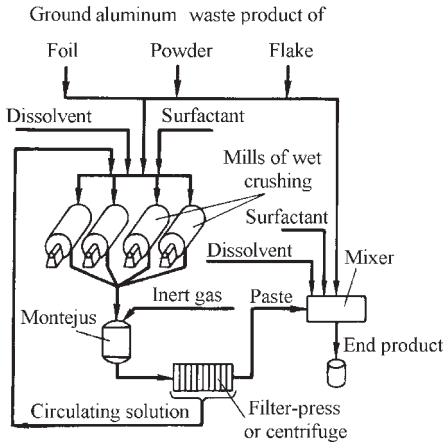

Figure 12.7 Schematic diagram of manufacture of the aluminum pastes.

greater bulk weight, etc. Mixing the paste with a lacquer gives a paint, which has high moisture-proofness and durability, high reflectivity and heat resistance. Leafing and non-leafing aluminum pastes are produced. Aluminum particles of the leafing paste rise to the surface of the varnish film and arrange themselves parallel to the surface which imparts a metallic shine and high reflectivity, complicates the penetration of moisture and increases the stability of the coating. Aluminum particles of non-leafing paste settle in the bottom part of the varnish film providing a polychromatic effect. Roof coatings comprise the largest market for non-leafing aluminum paste. The largest market for leafing aluminium paste is for automotive coatings.

Special application fields of aluminum paste are polygraphy, powder metallurgy, production of aerocrete.

Firms produce 30–40 types of aluminum pastes different in floating, granulometric composition, solvent and special additives. Characteristics of the aluminum pastes produced in Russia are presented in Table 12.7.

There are two processes for aluminum paste. In the first process, aluminum flakes are mixed with an aqueous solution containing phosphate ions, glycols aryl alkyl sulfonates, carbohydrates, polyatomic spirits, etc. as an inhibitor. Such technology is mastered both at factories producing aluminum flake and at some factories producing aerocrete.

In the second process, foil waste is ground in an aqueous solution containing fatty acids and inhibitors (salts of phosphoric and boric acids and colloid substances: albumin, casein, gelatin, glue or arabic gum). Grinding is carried out at the lowest possible temperature of 10–50°C.

Water aluminum pastes containing 50–65% of aluminum particles are fire- and explosion-proof, convenient to use and the content of the active metal keeps the properties stable for a long time. They are used as a gas forming agent to produce aerocrete, in the production of paints, in structure of water-filled explosives and in powder metallurgy.

The same technique is used for producing a water paste containing 20 wt% $A1_2O_3$. This paste is thickened, dried and ground to a powder state. Thus, a 'heavy' powder with the apparent density above 1.2 g/cm^3 suitable for use in PM is manufactured.

The Main Application Fields for Aluminum and Aluminum Alloy Powders

Powders and flakes of aluminum are ingredients of many industrial explosives used in the mining industry (ammonal, rock ammonites, alum trinitrotoluene). As a high-energy carrier, aluminum essentially raises the heat of the explosive transformation and the efficiency of the blasting operations. Powders such as ПА, pyrotechnic flakes of ПП marks, powders from secondary aluminum such as АПВ, ПА-ВВ, etc. (in Russian classification) are most widely used.

In ferrous metallurgy, aluminum powders (granules) are used as a reducing agent. Introduction of 0.1–1.5% of aluminum groats into the melt of iron completely releases it from the oxide (II) and thereby provides the production of a dense casting without sinks. Aluminum powders are also used for heating the riser part of the ingot in the casting of ferrous metals. A mixture of oxides and aluminum powders, tamped around the sprue opening and the riser, which 'ignites' from the melt, and during burning, provides cast metal in the liquid state for a long time so feeding the solidifying ingot and avoiding the formation of shrinkage cavities.

Aluminothermic reduction of refractory metal oxides is used in the production of ferromolybdenum, ferroniobium, ferrotungsten, etc.

The thermite mix containing 75% Fe_2O_3 and 25% Al provides a burning temperature of ≈2500°C.

In the chemical industry, aluminum powders and granules are active reducers as they quickly react in aqueous solutions of acids or alkaline media with emission of hydrogen: 1.0 kg of aluminum powders gives 1240 L of hydrogen. They are applied in the production of aluminum alkyls, polymerization of ethyls, for producing antidetonant, tetraethyl lead, etc.

Table 12.7 Aluminum pastes

Trade name	Particle size (μm) (max)	Covering capacity on water surface (m^2/g) (min)	Leafing (wt%) (min)	Substances soluble in organic solvents (wt%) (max)	Impurities (Fe, Si, Cu, Zn) total (wt%) (max)	Al	Application
Leafing aluminum pastes							
B-1	80	1.6	65	3.0	1.0	Balance	Finish paints with metallic shine
B-2	45	2.0	75	4.0	1.2	– ” –	
B-3	45	2.4	73	4.0	1.2	– ” –	
Non-leafing aluminum pastes							
H-1	80	–	–	3.0	1.2	Balance	Ground-coat protective paints
H-2	45	–	–	4.0	1.2	– ” –	
H-3	45	–	–	4.0	1.2	– ” –	
Special aluminum pastes							
C-1	80	0.7	65	3.0	1.2	Balance	Hammer enamels
C-2	45	1.7	75	3.5	1.2	– ” –	
C-3	45	1.7	–	4.0	1.3	– ” –	
МАП	160	1.3–1.7	50	3.5	1.0	– ” –	Thermoregulating coatings
ПД	80	2.0	30.0	3.5	1.0	– ” –	Slushing paints and enamels
ПДА	80	2.0	30.0	3.5	1.0	– ” –	Paints and enamels in aerosol packing

Aluminum powders are used for coating steel products by the methods of spray deposition, gas-flame or plasma spraying and thermal diffusion.

Aluminum powders and pastes are used as a colorful and protective pigment in compositions of various paints, varnishes and enamels. The paints obtained have a beautiful silvery color, protect products from moisture, heat and light.

The American Society for Testing and Materials (ASTM) has enacted the specifications for aluminum flake pigments (ASTM D 962, Part 28) [13]. The standard lining paste (ASTM D 962, type 2 class A) is used for structural steel coatings.

Aluminum-based sintered materials are distinguished by good pressing and sintering ability of powders, production profitability, high strength and good corrosion resistance.

In Russia, a range of Al-based powders is produced such as lumpy powder АПС, powders of high-purity aluminum (PA-VCh), of technical-purity aluminum such as ПА, aluminum groats АКП, powders of SAS alloys (Al–Si).

These materials are destined for PM production in machine building, electrical engineering, nuclear, electronic and other industries.

From the specified powders, strips, bars and profiles and cold-rolled sheets are manufactured. By hot extrusion of powders of aluminum alloys, materials with unique properties, high thermal resistance, such as SAS and SAP, low linear expansion such as SAS, high-strength alloys on the basis of the Al–Zn–Mg–Cu system, light fast alloys on the basis of the Al–Mg system, etc. are manufactured.

In addition, aluminum powders, flake pigments, pastes, paints and granules are applied in:

- production of high-density refractory materials (to increase the density, the thermal resistance and mechanical strength of refractory material)
- production of porous adsorption materials for cryogenic equipment
- production of a welding wire and lubricating cooling fluids (SOZh).

Aluminum powders are added to rubber to produce automobile tires with the purpose of increasing the heat conductivity of the protective rubber and to improve the operating conditions for the tire surface.

An addition of powders to plastics improves their mechanical properties, increases their wear resistance, imparts special properties (electric conductivity, heat conductivity, etc.).

Aluminum powder is applied as a filler material in plastics such as epoxy, polyester and phenolic resins. In particular, powder aluminum is used in the preparation of so-called 'cold solders' (fillers), which are used for filling of hollows, cracks and seams on the surface of a metal. More than 50% of the content of the cold solder is aluminum powder, which is mixed with the resin hardener.

Aluminum powder is used as a lubricant in producing ceramic details by the method of dry pressing for the reduction of the wear in molds, the obtaining of high-density pressings and the reduction of the pressing force.

Nickel-clad Aluminum Powders

A special class of aluminum powder materials is composite materials, which include powders of aluminum and its alloys or mixtures of such powders with powders of other compounds clad by nickel.

The production technology of the specified composite materials developed by the Norilsk Nickel Concern consists of coating powder particles of aluminum and its alloys with metallic nickel by the carbonyl process, i.e. by the decomposition of nickel tetra carbonyl vapor on the surface of the powder in the vibro-fluidized bed:

$$Ni(CO)_4 + Al \xrightarrow{180-250^{\circ}C} AlNi + 4CO$$

Depending on the chosen technological parameters of the process and the material-base, three main structural types of powder compositions are formed:

- clad powders, where particles of the base material are surrounded by a compact nickel coating
- conglomerated powders, where fine particles of the base material are conglomerated on the metallic nickel bundle
- capsulated powders, where particles of different composition, structure and properties are coated with a single nickel casing.

It is possible to form compositions that are combinations of the three above types. Thus, it is obviously possible to create a wide range of complex multicomponent compositions possessing a complex of predetermined physico-technological properties.

Composite powder materials metallized by nickel are subdivided into three main groups:

- metal–metal, metal–carbide compositions intended to increase the wear resistance and corrosion resistance of plasma coatings

- thermal reacting metal–metal and metal–metal–oxide compositions used for coating of wearproof, heat-resistant and heat-shielding coatings
- metal–solid lubricant and metal–carbide–solid lubricant compositions used for antifrictional coatings.

Nickel introduction into the makeup of clad, conglomerated and encapsulated compositions by the following thermal spraying provides:

- protection of the basic material of the coating against interaction with the plasma jet and oxidation
- more uniform distribution of components in the coating due to absence of the segragation
- interaction of separate components with the formation of solid solutions, intermetallics, etc.
- directed course of exothermic reactions that facilitate powder heating and improvement of coating quality
- creation of essentially new phases and structural components in the coating
- coarsening of fine powders that essentially expands the nomenclature of powders for spraying
- increase of fluidity, productivity of spraying and use factor of powder
- formation of essentially new multilayered powder compositions
- increase of durability, density and heat conductivity of coatings.

The low temperature of the process, the precise dosing of the nickel, the complete absence of a liquid phase and the fact that no additional process such as drying, filtration, regeneration of solutions is required and the complete absence of waste are the main advantages of the chosen method for producing composite powder materials in comparison with many liquid-phase and gas-phase processes.

Typical Physical Properties of Nickel-clad Aluminum Powders

- Powder composition, wt%: 4–23 A1; 96–77 Ni.
- Powder properties
  - thickness of the nickel coating on a particle of aluminum: from one to tens of microns
  - shape of particles: close to spherical
  - flow rate: 10–40 s
  - apparent density: 2.5–5.1 g/cm^3 (depending on the content of nickel)
  - the size of particles: 50–100 μm.
- Properties of plasma coatings:
  - microhardness: 4.0–8.0 GPa
  - porosity: 3–10%
  - strength of adhesion to the substrate: 30–38 MPa
  - exothermal effect while spraying of coatings comes at 625°C due to the reaction heat of the synthesis of the nickel–aluminum intermetallic in isothermal conditions
  - thickness of the coating layer that excludes peeling from the substrate: on Steel–3: 1.0 mm; on Steel–45: 0.8 mm; on D16T alloy: 3.0 mm. (The steel brands given in Russian classification.)
- Purpose: spraying of an intermediate layer on steels, cast irons, aluminum and titanium alloys, etc.

Processing of Aluminum Scrap into Powder Products

Production of Powder Products from Waste Aluminum Foil

It is known that remelting of the waste products of foil rolling is inefficient because of the great waste of aluminum at high temperatures that reaches several tens percent depending on foil thinness. Almost 100% of the use of foil waste products is achieved by their processing to aluminum powders (grit), flakes or paste.

The technology of foil processing is quite simple: crushing in cutting units such as the ones used for comminution of paper and plastic with subsequent use as the raw material for the production of aluminum flakes (dry crushing) or pastes (wet crushing). After rolling in mills (ball, jet-type, etc.), disintegrators and the like, the crushed flat particles of foil become rounded in shape, forming a special kind of powder product named ‘grit’. Grit has a wide application in the chemical industry as a reducing agent or gasifier, and in other industries as well.

Processing of Recycled Aluminum to Granules

In recent years, increasing attention is being paid to the processing of aluminum scrap (mainly chips and

used drink cans). Aluminum scrap has a complex chemical composition based on aluminum (>90%). Magnesium, zinc, silicon, iron, etc. are the main impurities. Sources of impurities are the composition of the alloy for producing drinks cans (mainly, Al–Mg alloy containing up to 3–4% Mg) and mechanical impurities that enter into the scrap due to inefficient sorting, classification and storage of the scrap.

Nowadays, all over the world, the main method of processing aluminum scrap is remelting in units of various types. The melt is usually cast into ingots. In some cases, the melt is granulated or gas-atomized to produce powder of recycled aluminum (for example, AIIB powders in Russia). These remelting–casting technologies are rather power-consuming.

Processing of aluminum scrap to powders and granules is an alternative to remelting of scrap to produce ingots. The advantage of this technology is that it is a simpler and cheaper process of producing granules from recycled aluminum. The size of granules is easily regulated by adjustment of grinders and varies from 1 to 10 mm. Such granules are used more effectively than ingots in ferrous metallurgy for steel deoxidation.

References

1. Dunkley, J.J., Atomisation of metals – craft or science?. In *Proceedings of 2nd International Conference on Spray Deposition and Melt Forming*, Vol. 1, Edited by: K. Bauckhage, U. Fritsching, V. Uhlenwinkel, A. Leatham, Universität Bremen, Bremen, 2003, pp. 3–11.
2. Unal, A., Leon, D.D., Gurganus, T.B., Hildeman, G.J., Production of aluminum and aluminum-alloy powder. In *ASM Handbook*, Vol. 7, *Powder Metal Technologies and Applications*. ASM International Publishers, 1998, pp. 148–149.
3. B. Williams, Powder metallurgy – a global market review. In *International Powder Metallurgy Directory & Yearbook*, 13th edn 1, 2008/2009, pp 5–14.
4. *Non-ferrous Metal Powders. Handbook*, Ed. S.S. Naboychenko, Metullurgiya, Moscow, 1997 (in Russian).
5. Dobatkin, V.I., Elagin, V.I., Fedorov, V.M., *Rapidly Solidified Aluminum Alloys*. All-Russian Institute of Light Alloys, Moscow, 1995 (in Russian).
6. Dunkley, J.J., Atomization. In *ASM Handbook* Vol. 7 *Powder Metal Technologies and Applications*. ASM International Publishers, 1998, pp. 35–52.
7. Lawley, A., *Atomization*. Metal Powder Industries Federation, Princeton, 1992.
8. Unal, A., Production of rapidly solidified aluminium alloy powders by gas atomisation and their applications. *Powder Metallurgy*, 1990, 33(1):53–64.
9. Neikov, O.D., Non-ferrous powder production technologies. In *International Powder Metallurgy Directory & Yearbook*, 13th edn 1, 2008/2009, pp 31–44.
10. Neikov, O.D., Krajnikov, A.V., Surface chemistry of water-atomised high-alloyed Al-Zn-Mg-Cu base powders. In *Proceedings of Vol. 1*, compiled by European Powder Metallurgy Association, Bellstone Shrewbury, UK, 1998, pp. 123–128.
11. H. Henein, Impulse atomization: an innovative approach for the generation of powders and spray deposits, In:, K. Bauckhage, U. Fritsching, V. Uhlenwinkel, A. Leatham, (Eds.), *Proceedings of 2nd International Conference on Spray Deposition and Melt Forming*, Vol. 1, 2003, Universität Bremen, Bremen, pp., 1-3–1-11
12. GOST 10096-76, Standard CIS (in Russian), Aluminium flake pigments.
13. ASTM Standard D 962, Aluminum Pigment, Powder and Paste, for Paint.

Chapter 13

Advanced Aluminum Alloy Powders

Oleg D. Neikov, Frantsevich Institute for Problems of Materials Science (IPMS), Kiev, Ukraine

Emerging processes, such as rapid solidification, mechanical alloying and spray forming, create powders that upon subsequent consolidation provide significant improvements in room and elevated temperature strength, fracture toughness, fatigue life and corrosion resistance. The real advantage of powder metallurgy processing is in the production of new alloys and composites with metallurgical structures and compositions that cannot be produced by ingot metallurgy. Rapid solidification extends the solubility of alloying elements, particularly transition and rare earth elements, and refines the structure of intermetallic phases responsible for improved mechanical properties. Mechanical alloying (MA) is a dry, high-energy milling process producing dispersions of insoluble oxides and carbides that stabilize the microstructure leading to high strength at elevated temperatures in the consolidated materials. By blending the alloy powder with a strengthening phase, discontinuously reinforced aluminum–matrix composites containing insoluble dispersoids (oxides and carbides), particulates, whiskers or fibers are produced for high-performance structural applications [1–5]. Table 13.1 contains the chemical composition commercially available of aluminum PM alloys and dispersion-strengthened composites.

The discontinuously reinforced aluminum–matrix composites are generally isotropic and less costly in comparison with continuous-fiber-reinforced aluminum–matrix composites. Silicon carbide or alumina-particle-reinforced aluminum composites have higher stiffness and, principally, high wear resistance in comparison with the unreinforced aluminum alloys. The PM route for producing the discontinuously reinforced composites involves blending elemental or pre-alloyed powder with the reinforcement, followed by canning, vacuum degassing and some form of consolidation, such as hot pressing or hot isostatic pressing (HIP), into a billet that is subsequently rolled, forged or extruded.

Mechanical Alloying

This technique is used for fabricating oxide-dispersion-strengthened alloys and discontinuously reinforced composites. High-energy ball milling results in mechanically alloying of pure metal powder and alloying components. During this process, intimate alloying by repeated welding, fracturing and rewelding take place. More detailed discussion of mechanical alloying can be found in Chapter 3.

In the case of aluminum alloys, carbon derived from process contribution agents and incorporated into the processed powder reacts with aluminum to form very fine carbides. These carbides and the fine oxide particles derived from the breakup of surface films on the initial powder particles create a dispersion that affects the fine-grained microstructure. This processing technique promotes the solution of the problem of low solubility according to the phase diagram or possibility of forming low-melting equilibrium or non-equilibrium phases. Thus, a metastable supersaturation can be achieved in systems such as aluminum–iron, aluminum–nickel, aluminum–copper, aluminum–titanium and aluminum–chromium. Another potential of MA is the generation of amorphous alloys that, following controlled crystallization, can create nanometer-scale microstructures [10].

IncoMAP alloy Al-9052 has a specific density 5% less than that of conventional age-hardenable aluminum alloy of comparable strength such as 2024 [11] and its combination of light weight, high strength and corrosion resistance makes it advantageous in aerospace applications.

In Ref. [12], MA is used to prepare composite powders of 7010 Al from elemental powder with or without SiC particulates. The addition of SiC improves the mechanical properties. The mechanical alloyed composites had higher modulus but lower strength values than the matrix at room temperature. However,

Table 13.1 Nominal chemical composition of aluminum PM alloys and dispersion strengthened composites

Alloy designation	Nominal mass elemental composition																		
	Be	C	Ce	Co	Cr	Cu	Fe	Li	Mg	Mn	Mo	O	Ni	Si	Ti	V	Zn	Zr	Al	(L)
Al–Cr–X	...	...	...	...	5.0	...	...	...	...	1.0	...	...	...	...		...	...	2.0	bal	...
Al–Ti–X	...	...	3.0	...	...	...	...	...	...	...	...	...	...	...	3.0	...	...	...	bal	...
Al–Be–X	22.6	...	...	...	...	...	...	10.8	...	...	...	...	...	...	...	...	...	...	bal	...
7090	...	...	...	1.5	...	1.0	...	...	2.5	...	...	0.35	...	...	...	...	8.0	...	bal	...
7091	...	...	...	0.4	...	1.5	...	...	2.5	...	...	...	...	...	...	...	6.5	...	bal	...
X7090	...	...	...	1.0–1.9	...	0.6–1.3	0.15	...	2–3	...	...	...	...	0.12	...	...	7	...	bal	...
X7091	...	...	...	0.2–0.6	...	1.1–1.8	0.15	...	1–3	...	...	...	...	0.12	...	...	5.8–7.1	...	bal	...
X7093	...	...		...	...	1.5	...	...	2.2	...	...	...	0.1	...	...	...	9.0	0.14	bal	...
8009	...	...	...	...	...	...	8.5	...	...	...	...	...	...	2.4	...	1.3	...	...	bal	...
X8019	...	...	4.0	...	...	...	8.3	...	...	...	...	...	...	...	..	...	...	...	bal	...
CZ42	...	...	6.0	...	...	...	7.0	...	...	...	...	...	...	...	...	...	...	...	bal	...
Al–Fe–Ni	...	...	...	...	...	...	8	...	...	...	...	...	1.7	...	...	...	...	...	bal	...
Al–Fe–Mo	...	...	...	...	...	...	8.0	...	...	...	2.0	...	...	...	...	...	...	...	bal	...
Al–Fe–V	...	...	...	...	///	...	10.5	...	...	...	...	...	...	...	...	2.5	...	...	bal	...
Al–Fe–Ni–Co	...	...	...	6.0	...	...	5.0	...	...	...	...	...	3.0	...	...	...	...	...	bal	...
Al–Fe–Mo–V	...	...	...	...	...	...	8	...	...	...	2	...	...	...	...	1	...	...	bal	...
Al–Fe–Mo–V–Zr	...	...	...	...		...	8.0	...		...	2.0	...	...	...	...	2.0	...	1.0	bal	...
Al–Fe–Cr–V–Si	...	...	...	...	3.86	...	8.29	...	...	...	...	...	...	2.31	...	1.19	...	...	bal	...
Al–Fe–Ti–V–Si	...	...	...	...	...	...	8.31	...	...	...	...	...	...	2.31	3.57	1.2	...	...	bal	...
FVS-0812	...	...	...	...	...	...	8.5	...	...	...	...	...	...	1.7	...	1.3	...	...	bal	...
RAE 72	...	...	...	...	7.5	...	1.2	...	...	...	...	...	...	...	...	...	...	...	bal	...
Al–Li–Cu	...	...	...	...	...	2–3.5	...	2.5–3.2	0.5	0.6	...	...	...	...	...	...	...	...	bal	...
Al–Mn–Ni	...	...	...	...	...	...	...	...	...	3–8	...	...	1.5–7.0	...	...	...	...	...	bal	...

(*Continued*)

Table 13.1 (Continued)

Alloy designation	Nominal mass elemental composition																		
	Be	C	Ce	Co	Cr	Cu	Fe	Li	Mg	Mn	Mo	O	Ni	Si	Ti	V	Zn	Zr	Al	(L)
Al–Mn–Co	...	...	...	1.6–6.5	...	...	...	...	...	3–8	...	...	...	...	...	...	...	...	bal	...
Al–Ni–Co				2–5	...	...	...	...	...	...	...	...	2–5	...	...	...	...	...	bal	...
601AB	...	...	...	...	...	0.25	...	...	1.0	...	...	...	...	0.6	...	...	...	...	bal	1.5
201AB	...	...	...	...	...	4.4	...	...	0.5	...	...	...	...	0.8	...	...	...	...	bal	1.5
602AB	...	...	...	...	...	...	...	...	0.6	...	...	...	...	0.4	...	...	...	...	bal	1.5
202AB	...	...	...	...	...	4.0	...	...	...	...	...	...	...	...	...	...	...	...	.bal	1.5
MD-22	...	...	...	...	...	2.0	...	...	1.0	...	...	...	...	0.3	...	...	...	...	bal	1.5
MD-24	...	...	...	...	...	4.4	...	...	0.5	...	...	...	...	0.9	...	...	...	...	bal	1.5
MD-69	...	...	...	...	...	0.25	...	...	1.0	...	...	...	...	0.6	...	...	...	...	bal	1.5
MD-76	...	...	...	...	...	1.6	...	...	2.5	...	...	...	...	...	...	...	...	...	bal	1.5
Dispersion-strengthened composites																				
Al–C	...	3	...	...	...	...	...	...	...	...	...	...	...	...	...	...	...	...	bal	...
Al–Cu–C	...	1.5	...	...	...	1	...	...	...	...	...	...	...	...	...	...	...	...	bal	...
Al–Mg–Co	...	1.5	...	...	...	...	...	...	2.0	...	...	...	...	...	...	...	...	...	bal	...
Dispal2	...	2	...	...	...	...	...	...	...	...	...	1.0	...	...	...	...	...	...	bal	...
7090	...	...	...	1.5	...	1	...	...	2.5	...	...	0.35	...	...	...	...	8.0	...	bal	...
Al–Fe–Ce	...	...	3.5	...	...	...	8.0	...	...	...	...	0.35	...	...	...	...	...	...	bal	...
Al–Fe–Co	...	...	...	2–7	...	...	3–8	...	...	...	...	0.35	...	...	...	...	...	...	bal	...
Al–Fe–Cr	...	...	...	...	1.5	...	8.5	...	...	...	...	0.35	...	...	...	...	...	...	bal	...
XAP001	...	0.4	...	...	...	...	0.2	...	...	...	...	6.0 (ox)	...	0.08	...	...	...	...	bal	...
XAPOO2	...	0.19	...	...	...	...	0.28	...	...	...	...	8.0 (ox)	...	...	...	...	...	...	bal	...
XAP004	...	0.39	...	...	...	...	0.29	...	...	...	...	14.0 (ox)	...	0.1	...	...	...	...	bal	...
IN9021	...	1.2	...	...	...	4	...	...	1.5	...	...	0.75	...	...	...	...	...	...	bal	...
IN9051	...	0.7	...		...	...	...	...	4.0	...	...	1.4	...	...	...	...	...	...	bal	...
IN9052	...	1	...	...	...	...	...	...	4.0	...	...	0.4	...	...	...	..	...	...	bal	...
905XL	...	1.1	...	...	...	...	...	1.3	4.0	...	...	0.4	...	...	...	...	...	...	bal	...

(L), lubricant; 601AB, 201AB, 602AB, 202AB, MD-22, MD-24, MD-69 and MD-76 grades are commercially available aluminum powder alloy compositions consisting of blends of atomized aluminum powders mixed with powders of alloying elements; (ox), oxide.
(Source: Refs: [1,6–9])

Table 13.2 Alloying addition nature dependence on phase composition and mechanical properties of Al–Mg–alloying compound–surfactant alloys

Alloying addition		Phase composition	Mechanical properties		
Matter	Content (%)		Hardness (MPa)	UTS (MPa)	El (%)
$Cu(OH)_2$	9.08	Al, Al_2Cu, Al_4Cu_9, Al_3Mg_2, Al_2O_3, MgO, Al_4C_3	1700	610	3
$Co(OH)_2$	6.82	Al, Al_5Co_2, Al_3Mg_2, Al_2O_3, MgO, Al_4C_3	1750	630	3
$Ni(OH)_3$	6.81	Al, Al_3Ni, Al_3Mg_2, Al_2O_3, MgO, Al_4C_3	1700	630	3
$Fe(OH)_3$	6.61	Al, Al_3Fe, Al_3Mg_2, Al_2O_3, MgO, $MgO{\cdot}Al_2O_3$, Al_4C_3	1700	620	3
LiOH	4.45	Al, Al_3Mg_2, Al_2O_3, MgO, $MgO{\cdot}Al_2O_3$, Al_4C_3	1650	640	4
$CuCO_3$	7.66	Al, Al_3Cu, Al_4Cu_9,Al_3Mg_2, Al_2O_3, MgO, Al_4C_3	1700	610	3
$Co(NO_3)_2{\cdot}3H_2O$	4.51	Al, Al_3Co_2, Al_3Mg_2, Al_2O_3, MgO, AlN, Al_4C_3	1800	660	2
$Ni(NO_3)_2{\cdot}6H_2O$	4.51	Al, Al_3Ni, Al_3Mg_2, Al_2O_3, MgO, AlN, Al_4C_3	1850	670	2
$Fe(NO_3)_2{\cdot}6H_2O$	4.43	Al, Al_3Fe, Al_3Mg_2, Al_2O_3, MgO, $MgO{\cdot}Al_2O_3$, AlN, Al_4C_3	1750	650	2
$H_2N{\cdot}CO{\cdot}NH_2$	2.50	Al, Al_2O_3, MgO, AlN, Al_4C_3	1900	720	2
$CH_3{\cdot}C_6H_3(NO_2)_2$	2.50	Al, Al_2O_3, MgO, AlN, Al_4C_3	2200	770	2
$C_{13}H_{14}N_4O$	2.50	Al, Al_2O_3, MgO, AlN, Al_4C_3	2200	760	2
$C_{10}H_{10}N_2O$	2.50	Al, Al_2O_3, MgO, AlN, Al_4C_3	2300	750	2

(Source: Refs 14–16)

at temperatures above 200°C they exhibited higher tensile strength than the matrix.

Using elemental powders as starting materials, nanocrystalline Al–4.9Fe–4.9Ni alloy powders were prepared by MA [13]. Ultimate tensile strength at room temperature of a consolidated semi-product achieves 650 MPa; while the yield strength remained above 280 MPa at 300°C.

It is typical that aluminum milling with aqua addition, as well its processing in carbon dioxide or sodium peroxide medium, gives significantly larger strengthening in comparison with mechanical alloying with oxides, Cr_2O_3, TiO_2 and ZrO_2, having high hardness and low value of Gibbs function of redox reaction. Mechanical alloying with oxides, such as CuO, Co_3O_4, MoO_3, and V_2O_5, which have higher values of Gibb's energy formation, is more advantageous.

The largest value of ultimate tensile strength was achieved in (Al–Mg)-alloying compound-surfactant materials, alloying by organic compounds [14]. These organic compounds belong to various classes, including oxalic acid ($COOH \cdot COOH$), carbamide ($H_2N \cdot CO \cdot NH_2$), dinitrotoluene $CH_3 \cdot C_6H_3(NO_2)_2$, 1.5-diphenylcarbazide ($C_{13}H_{14}N_4O$), and 3-methyl-1-phenyl-2-pyrazoline-5-one ($C_{10}H_{10}N_2O$) (Table 13.2).

The alloys produced have microcrystalline structure with grain sizes less 0.4 μm that consist of clusters less than 50 nm. The inclusion sizes of the main strengthening phases, MgO, $MgO{\cdot}Al_2O_3$, Al_4C_3 and AlN do not exceed 5 nm. The microcrystalline structure with ultrafine and nanosize main strengthening phases determines the high degree of strengthening. The MA alloys produced are heat-resistant (Table 13.3). They stand the test up to 500°C. Dependence of the ultimate tensile strength on the testing temperatures in the temperature ranges studied is near linear, while the elongation is a curve with maximum at 250–350°C.

Rapid Solidification Process

Rapid solidification is a metastable process that results in a significant undercooling of the molten metal leading to a refinement of microstructural features and constitutional effects such as extension of solubility limits, synthesis of novel crystalline phases and the formation of metallic glasses [11, 17–19].

Currently, gas atomization and centrifugal atomization methods for rapid solidified aluminum alloy powder production are the most highly developed and commercially available [20–25].

One of the centrifugal atomization processes used for this purpose is spinning cup atomization [23–25]. In all cases, the cup is 80–200 mm diameter, running at moderately high speeds from 3000 to 10 000 rpm. Solidification of the molten particles in a gaseous medium requires a very large chiller chamber, up to 12 m in diameter.

Spinning disk atomization is another form of centrifugal atomization [24], where a molten metal stream collides with a rapidly moving metal substrate surface such as a rotating disk rim. In this case,

Table 13.3 Temperature-dependent mechanical properties of aluminum alloys alloying with organic compounds

Alloying addition		Magnesium content (wt%)	Testing temperature, °C	Mechanical properties	
Matter	Content (wt%)			UTS (MPa)	Elongation (%)
$H_2N \cdot CO \cdot NH_2$	2.5	2.0	20	720	2
			200	420	8
			300	310	15
			400	240	12
			500	170	10
$CH_3 \cdot C_6H_3(NO_2)_2$	2.5	2.0	20	770	2
			200	480	8
			300	360	14
			400	260	10
			500	190	8
$C_{13}H_{14}N_4O$	2.5	2.0	20	760	2
			200	480	7
			300	370	15
			400	270	11
			500	190	9
$C_{10}H_{10}N_2O$	2.5	2.0	20	750	2
			200	470	8
			300	360	14
			400	250	11
			500	180	9

(Source: Ref 14)

material in the form of a ribbon is obtained. By melt extraction through melt atomization using a rotating disk that touches the melt surface, a product in the form of flake is obtained.

The material, in the form of thin ribbon, flake or wire, is rapidly cooled by heat conduction through the metal substrate followed by a grinding or chopping operation to the particulate state.

Additional information on spinning disk atomization and melt extraction can be found in Chapter 5.

The dendritic structure is a primary form in rapid solidification alloys, up to a cooling rate of 10^5–10^6 K/s. An important milestone in the study of dendritic structure was the discovery at the end of the 1940s of the hyperbolic dependence of the space between the second-order dendrite branches on solidification rate [26,27]. Such a characteristic has a physical meaning as determinative to a first approximation value of the separation diffusion volume by crystallization and is expressed by the hyperbolic equation

$$v = \left(\frac{A}{d}\right)^{1/n} \quad (1)$$

where d is the measured dendrite parameter in μm, v is the cooling rate in K/s, and A and n are constants [28]. Constant A, connected with alloy properties, increases as the coefficient of diffusion rises and alloying degree decreases. For high-strength aluminum alloys, $A = 100$; constant n value in the interval 0.25–0.5 depending on the grain shape. In particular, $n = 1/3$ for equiaxed grains.

The dendrite parameter is determined by means of calculation of average dendrite cell area in a metallographic section of powder particles at the most suitable magnification for current structure. The square root of this area gives the dendrite parameter, which is unambiguously dependent on solidification rate [19]. The dependence of dendritic branching on cooling rate is shown in Figure 13.1 [29]. A characteristic dendritic structure is observed in a 200 μm particle (Figure 13.1(a)); its dendritic parameter is equal to 2.8 μm which, according to Eqn (1) corresponds to a cooling rate of approximately 4.5×10^4 K/s. For a 90 μm particle (Figure 13.1(b)), the dendritic parameter is 1.57 μm and the corresponding cooling rate 2.5×10^5 K/s. The microcrystalline structure of a 50 μm particle (Figure 13.1(c)) is characterized by the dendritic parameter of 0.85 μm, which corresponds to the cooling rate of 1.6×10^6 K/s. The formation of non-dendritic grains with increasing cooling rate can be explained by increased supercooling

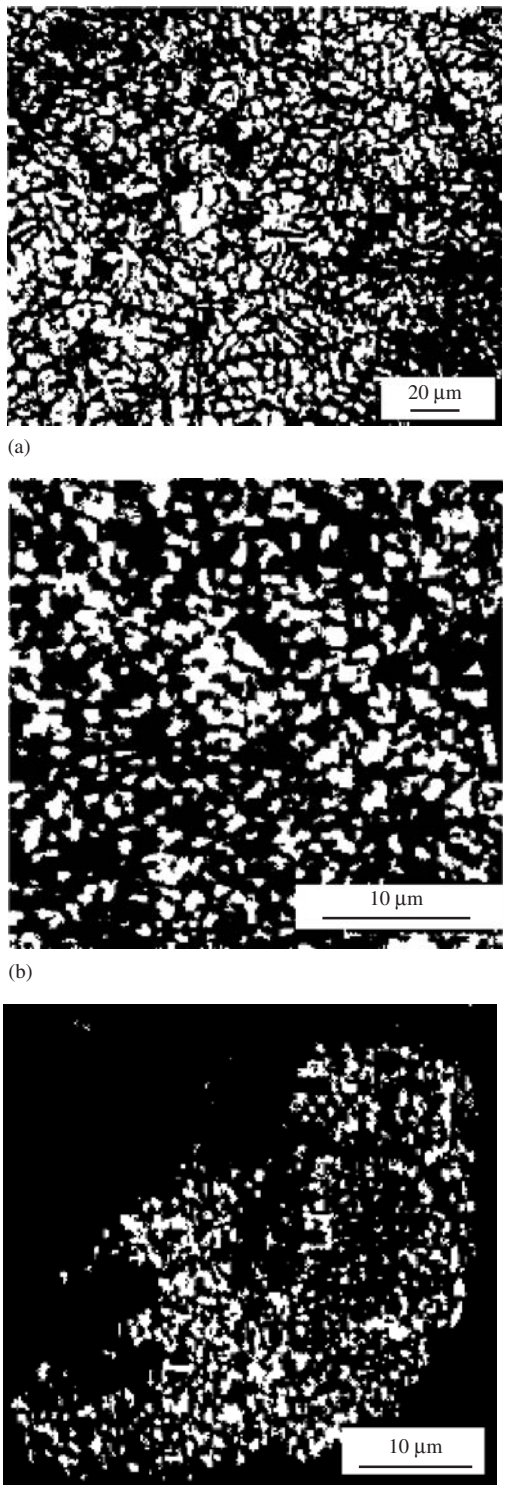

Figure 13.1 Structure of Al–9.5Zn–3.0Mg–1.2Cu alloy powder particles of various sizes with projected diameter equal to (a) 200 μm, (b) 90 μm and (c) 50 μm.

and by a significant intensification of the nucleation, respectively.

Approximate evaluation of dendritic parameter dependence on cooling rate during crystallization of aluminium alloys was made by Dobatkin [19] (Table 13.4). Non-dendritic grain sizes ranging from 0.02 to 0.05 μm (which correspond to a calculated cooling rate of 10^{10}–10^{11} K/s) were discovered and studied [19]. The 10–20 μm flakes of Al–6 wt%Zr alloy were obtained by means of drop firing on a copper substrate after melt heating up to a temperature exceeding the liquidus temperature by 50–100°C.

At a high cooling rate, along with the dendritic structure, the non-dendritic structure is formed without physical means of action by melt. And by still more higher cooling rates, only non-dendritic structure may be obtained [19]. The probability of increasing the non-dendritic grain by high cooling rates can be justified by a deep precrystallization undercooling and drastic intensification of the nucleation, accordingly. Here it is necessary to note that initial undercooling, which determines the intensification of the nucleation increasing, does not control the following crystallization process as a result of temperature increasing (recalescence) on the now first stage of alloy solidification. The deep undercooling can repress the crystallization process and will lead to formation of metallic glass.

Even at relatively low cooling rates, non-dendritic structures can be obtained by introducing a conditioning agent and by applying ultrasonics. Some conditioning agents, such as scandium, allow non-dendritic structures to occur without ultrasonic assistance. The non-dendritic structure of ingots, granules, powders and flake are shown in Figure 13.2.

The mechanism whereby the grain size is influenced by the cooling rate was discovered by Vladimir I. Dobatkin and his colleagues at the All-Russian Light Alloys Institute (VILS) [30]. It was shown that it is possible to obtain a non-dendritic structure whatever the cooling rate and that the grain size will not be dependent on factors other than cooling rate. Grain size refinement is achieved only by an increase in cooling rate and therefore the dendritic parameter curve is a lower boundary grain size depending on cooling rate (Figure 13.3). Above this boundary, dendrite grains are found. The upper boundary of dendrite grain sizes one can conventionally consider by monocrystal sizes when the grain occupies all the hardening molding volume.

In ingots of various size and shape of aluminum and magnesium alloys, non-dendritic structure was obtained at the expense of nucleation intensification by means of modifiers in combination with ultrasonic (cavitational) treatment. In granules, the

Table 13.4 Correspondence between dendritic parameter and cooling rate during crystallization of aluminum alloys

Cooling rate (K/s)	Dendritic parameter (μm)	Solidified material obtaining conditions
0.001	1000	Casting big ingot into the casting molds
1	100	Continuous casting of ingots
1000	10	Big granules
10^6	1	Fine granules and flakes
10^9	0.1	Ultrafine flakes
10^{12}	0.01	Crystallization of flakes with initial deep undercooling*
10^{15}	0.001	It is not obtained experimentally

*non-dendritic grain.

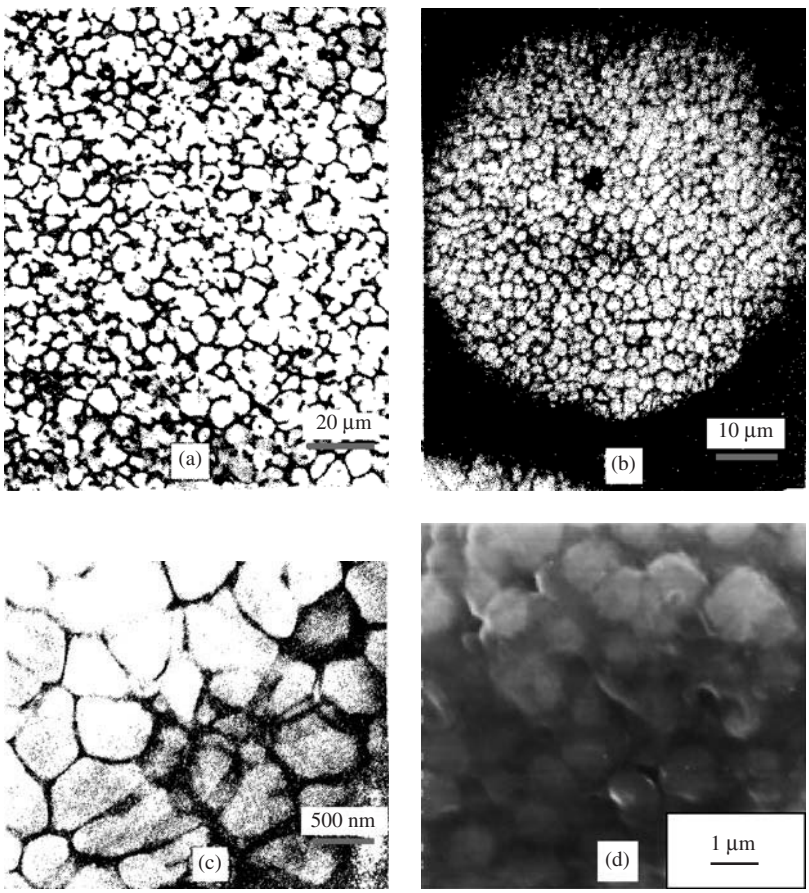

Figure 13.2 Non-dendritic structure of (a) ingots, (b) granules and (c) flakes of D16 alloy (in Russian grading analogous 2024 US grade), (d), powder particles of water atomised Al–5Fe–5Cr–2Ti alloy.

non-dendritic structure was obtained by ultrasonic atomization with cavitational effect on the melt before solidification and in flakes in response to deep precrystallization undercooling.

The phenomenon of heightened solubility by rapid crystallization is known as anomalous supersaturation [31]. Experimental data of attainable supersaturation in alloys of some duplex systems for ingots, granules of 1–3 mm diameter and flakes are compared with the maximum solubility in solid solution under equilibrium conditions in Table 13.5.

For the eutectic systems with limited confined solubility, peritectic systems and systems with one or several chemical compounds, the metastable diagrams

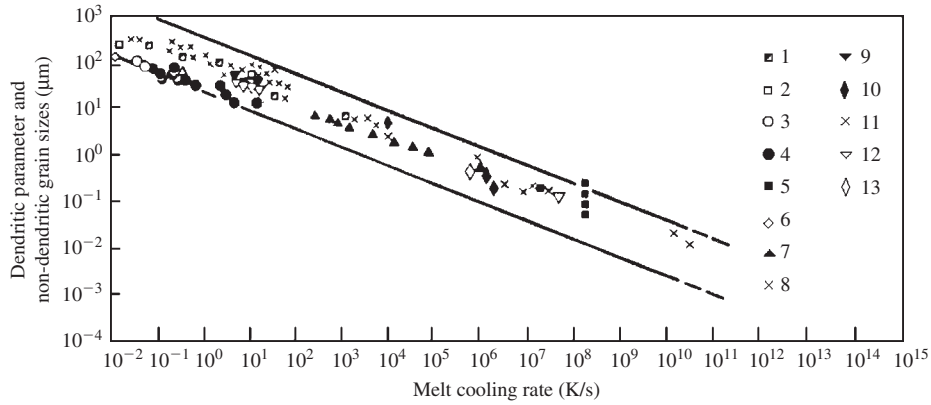

Figure 13.3 Dependence of non-dendritic grain size (11–13) and dendritic parameter (1–10) on melt cooling rate for aluminum alloys (1–8, 11), magnesium alloys (9, 12) and nickel elevated temperature alloys (1, 13). (Source: Ref 28)

Table 13.5 Content of alloying elements in solid solution of binary aluminum alloys

Second component	Maximum solubility under equilibrium diagram (wt%)	Content of alloying elements in solid solution (wt%)		
		in ingots by v_{cool} = 1 K/s	in granules by v_{cool} = 10^3–10^4 K/s	in flakes by v_{cool} = 10^5–10^6 K/s
Copper	5.7 [33]	2 [19]	...	33 [19]
Magnesium	17.4 [33]	3 [19]	...	34–38 [19]
Manganese	1.4 [33]	1.0 [19]	4.5 [19]	14.5 [19]
Zirconium	0.28 [33]	0.11 [19]	2.0 [19]	4.0 [19]
	...	...	1.2 [34]	...
Chromium	0.77 [33]	0.2 [19]	2.0 [19]	5.8 [19]
				5.7 [35]
Titanium	0.28 [33]	0.1 [19]	1.0 [19]	2.5 [19]
Vanadium	0.37 [31]	...	1.0 [19]	1.2 [35]
Molybdenum	0.2 [31]	...	0.6 [19]	1.0 [19]
Germanium	7.2 [33]	...	...	17.3 [19]
Iron	0.052 [31]	0.03 [19]	...	0.17 [19]
				0.2 [35]
Silicon	1.65 [33]	0.5 [19]	...	10.7 [19]
				11 [36]
Tungsten	0.22 [31]	...	1.2 [19]	...

differ from equilibrium ones. This is illustrated by reference to the aluminum–manganese system in a metastable equilibrium diagram (Figure 13.4) [32].

Depending on cooling rate, the location of the eutectic horizontal is changed but, in all cases, the liquidus and solidus lines of the equilibrium diagram are in continuation with the second component (manganese in this case) direction of equilibrium system liquidus and solidus lines. Thus it is possible to make at least two conclusions. First of all, at high cooling rates in hypereutectic alloys, one can prevent the formation of primary crystals of the second component or its compound and obtain a quasi-eutectic

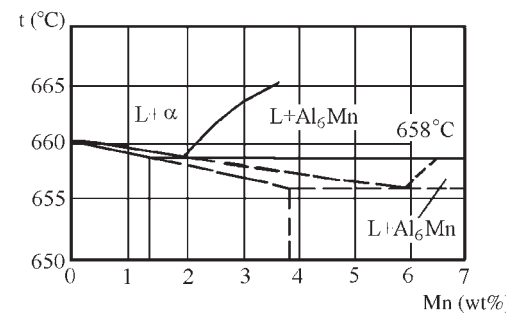

Figure 13.4 Scheme of metastable equilibrium diagram of Al–Mn system (dotted line).

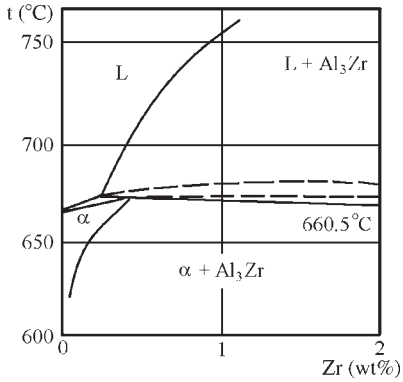

Figure 13.5 Scheme of metastable equilibrium diagram of Al–Zr system (dotted line).

or even quasi-hypoeutectic alloy structure. Secondly, the content of the second component in solid solution may be increased in comparison with maximum solubility as in the equilibrium diagram and solid solution compositions obtained by crystallization as in the equilibrium diagram have a eutectic structure.

In peritectic systems, by rapid cooling, the liquidus and solidus lines can be also continued in the second component direction. In this case, the liquidus and solidus lines are continued, not downwards as in eutectic systems (see Figure 13.4), but upwards, as shown in Figure 13.5 for the Al–Zr system [19].

The higher the melt cooling rate (and the attainable overercooling as a result), the greater becomes the concentration area in which solidification is of the solid solution type. The concentration area in which alloys without second component primary crystals and peritectic reaction products can be obtained is also widened.

For alloys of peritectic systems, with cooling rate rise, the change from primary intermetallic compound crystallization area directly to solid solution crystallization area is observed, which can be explained by suppression of the peritectic reaction (Figure 13.6).

The content curve of supersaturated solid solution usually has a remarkable bend in the cooling rate range from 10^3 to 10^6 K/s. This bend is also related to the beginning of precipitation of the second component crystals and the existence of non-equilibrium eutectics.

Two very important features of metastable diagrams – widening of solid solution area and displacement of the start of the second component primary crystal emission – are confirmed for complicated aluminum alloys. Property changes resulting from the aging of supersaturated solid solutions include increase of hardness and strength which can significantly exceed those of the primary solid solutions.

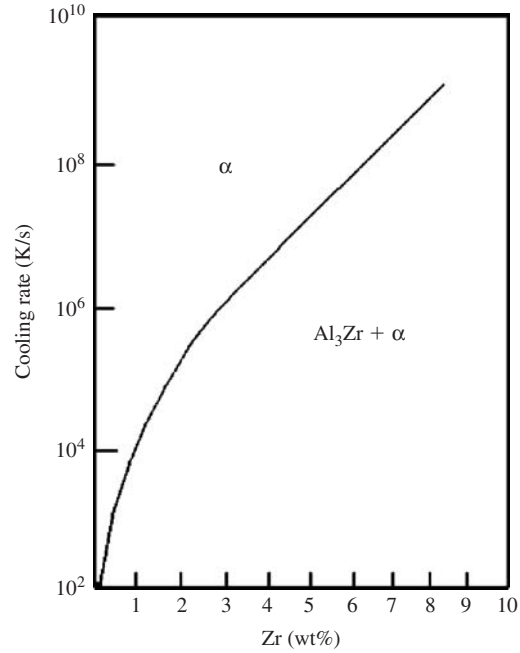

Figure 13.6 Phase diagram of Al–Zr system.

Consequently, the metastable crystallization effect allows the creation of alloys with strength, heat-resistance and other property levels unattainable in alloys produced by conventional technology.

Centrifugal Atomization

RSR Process

The mode of centrifugal atomization is the RSR (rapid solidification rate) process. The RSR process has been described by Cox et al. [37], Paterson [38] and Anderson [39]. The first RSR unit operated in late 1977, producing IN-100 powder in a pilot plant and patents were issued in 1978 [22] and 1982 [40]. The latter patented plant is shown in Figure 13.7.

The metal alloy is normally melted by vacuum induction. When the desired level of superheat is reached, the system is backfilled with helium. The pressure head of liquid metal in the tundish, the area of the nozzle, and the pressure difference between the upper chamber and lower chamber are controlled to obtain the desired flow rate of liquid metal through the nozzle. The liquid metal flows through the nozzle and onto the rotating disk, or atomizer rotor. The surface onto which the liquid metal flows imparts kinetic energy to it, the metal being flung from the edge of the rotor in the form of droplets, ligaments,

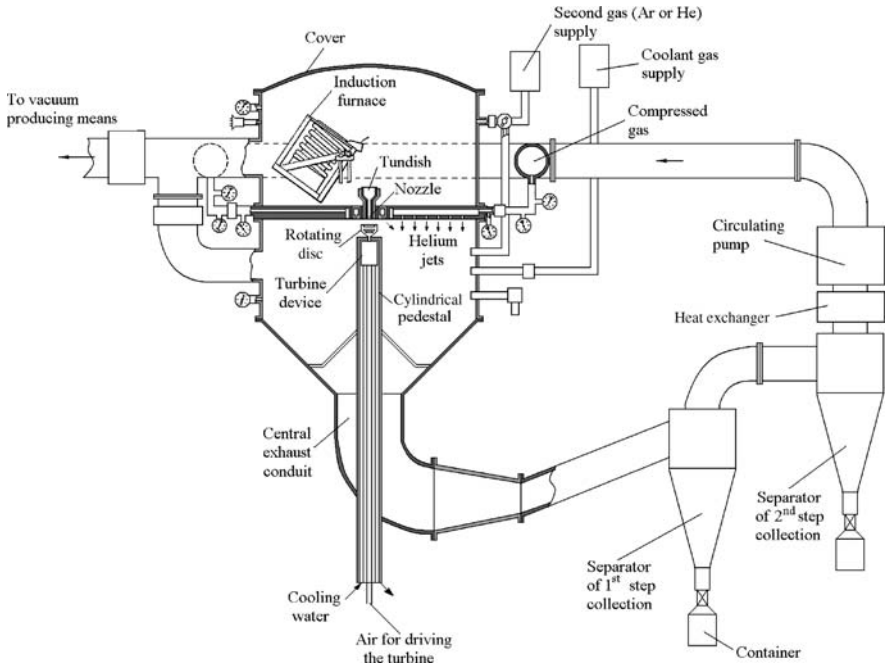

Figure 13.7 Schematic of spinning disk atomization.

or sheets, depending on the speed of the rotating disk, the flow rate of the liquid metal through the nozzle, atomizer rotor geometry and the fluid properties of the liquid metal. Such particles are rapidly cooled convectively by contact with the annular curtain of cooling helium jets directed downwards from the nozzle plate. The powder particles are carried from the lower chamber by the cooling stream and deposited in containers, according to particle size. The RSR plant incorporates closed-loop helium recirculation.

Total gas mass flow amounts to 0.9 kg/s, while a nozzle diameter of 4 mm was used to deliver a molten alloy at a mass flow rate of 0.15 kg/s. A speed of 18 000 rpm has been used with an atomizer rotor contoured as a cup having an inner diameter of 82.5 mm to produce metal particles in the range from 10 to 50 μm in diameter. In such conditions, the mean cooling rates are evaluated in a range of 10^5 K/s. To obtain these cooling rates with particle sizes up to 75 μm, it is necessary that a high thermal conductivity gas, such as helium, be used.

Parallel with nickel-base superalloys, the RSR process has been used to produce specialty aluminum alloy, beryllium alloy, molybdenum, titanium alloy, and silicide powders.

This technique allows the production of narrow size distribution powders and is used commercially to manufacture plasma spraying powders where size ranges such as $-150 + 53$ or $-100 + 38$ μm are needed. But, the uncontrolled geometry of the scull on the rotating disk and the problems of out-of-balance forces, degrades the size distribution greatly compared with that achieved with lower-melting metals where the cup or disk has precise geometry. It also results in heavy maintenance costs on the spinning cup assembly. The use of huge volumes of expensive helium is another drawback. As a result of these disadvantages, gas atomization has continued to dominate the production of higher-melting alloy powders. But the benefits of the rapidly solidified microstructures have yet to find major commercial paybacks outside the aerospace area. Thus, Pratt & Whitney, the main producer of RSR powder, remained the only operator in the 1990s and the few attempts that have been made to develop similar devices elsewhere have not been productive. Production is less than 1000 tonnes/year [25].

Spinning Cup Water Granulation Process

Conventionally, the spinning cup granulation process is carried out in open air because of the large size of plant needed to freeze coarse particles. In this case, a perforated steel or cast iron cup is used to make a series of streams of metal, which break up into needles due to the oxide film on them. Production is considerable, probably thousands of tonnes per year [25].

The spinning cup water granulation process [23] allows an increase of the cooling rate and a notable decrease of the size of plant owing to cooling the

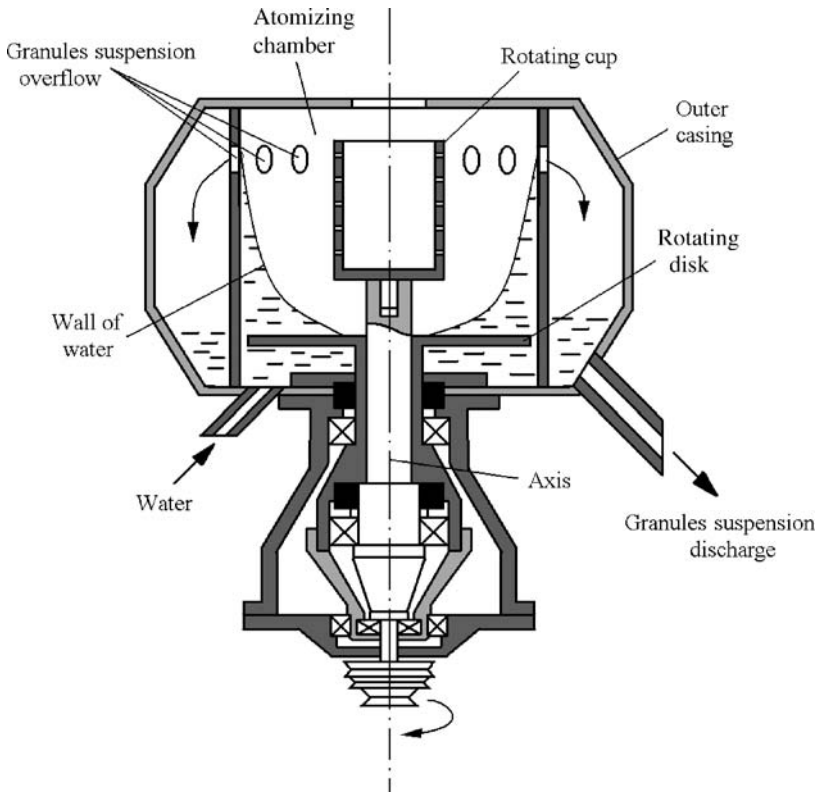

Figure 13.8 Schematic of spinning cup atomizer.

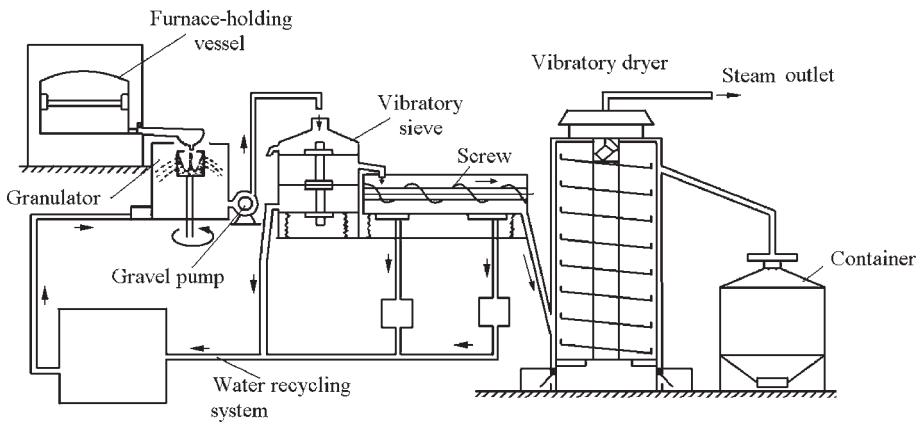

Figure 13.9 Flowchart of the spinning cup water granulation process.

molten granules in water. Thus, the chiller chamber is only 1.2–1.5 m in diameter in comparison with 12 m in diameter in open air granulation. A spinning cup water granulator, which was used in VILS, is shown in Figure 13.8. The cup with apertures in the walls is made from ceramics, which is non-wettable by aluminum and possesses high resistance and low heat conductivity. The rotating disk sets the water in the atomizing chamber in rotation and, under centrifugal force, the water is thrown away to the atomizing chamber walls and flows down to the overflow apertures. Thus, a mobile layer of water is formed on the inner surface housing walls. The liquid metal flows onto the rotating cup and is subjected to centrifugal force in the cup wall apertures in the form of droplets, such droplets being force cooled by contact with the annular wall of water. The solidified granules are carried from the atomizing chamber together with the cooling water through the overflow apertures. The flow diagram of the spinning cup granulation process with cooling of molten drops in water is shown in Figure 13.9.

Table 13.6 Dependence of calculated heat-transfer coefficient α_d on cooling medium

Cooling medium	Design equation	α_d (W/(m·°C))	Explanation
Air	$\alpha_m = \frac{Nu\lambda}{d_p}$	396	$Nu = 2 + 0.6Re^{0.5}Pr^{0.33}$; λ is coefficient of heat conductivity; d_p is diameter of drop; Re is Reynolds' number, $Re = wd_p/v_a$; w is drop velocity relatively to gas medium; v_a is kinematic viscosity; Pr is Prandtl number, $Pr = v_g/a$; a is thermal diffusivity; $w = 5$ m/s
Steam jacket	$\alpha_j = \frac{2\pi\lambda_s}{d_p(1-d_p/d_j)}$	803	λ_s is heat conductivity; d_s and d_j are diameters of drop and steam jacket, accordingly
Water	$\alpha = \frac{\rho r q_{cr}}{3(t_{cr} - t_w)\pi_{cr}}$	11200	q_{cr} is crystallization heat; t_w is water temperature; τ_{cr} is crystallization time; ρ is metal density; t_{cr} is metal crystallization temperature; r is drop radius

(Source: Ref 23)

Cooling rate of the particles in air is considerably lower than in water because of differences of the heat transfer process (Table 13.6). Therefore the flight time of particles before coming into contact with the water must be kept as short as possible. This is achieved by reducing the air space in the atomizing chamber and increasing the velocity of the molten droplets.

The dependence of granule fraction yield on cup rotary speed for Al-(1.4–2.0)Mn-(0.8–1.2)Cr-(0.5–0.9)Zr-(0.4–0.8)Ti-(0.4–0.8)V alloy is shown in Figure 13.10.

The main parameters of the spinning cup granulation process in ranges in which the investigations in VILS were carried out are given in Table 13.7. The conditions of the granulation process for −2.0 + 0.5 mm granule fraction yield were optimized:

- for high-strength Al–Zn–Mg–Cu-base alloys – slotted or with apertures, cup 125 mm in diameter; a cup speed of 1000 rpm; mass flow rate of molten alloy ranging from 170 to 250 kg/h; the temperature of the liquid metal on pouring ranges from 1000 to 1050°C;
- for elevated temperature – with apertures, cup 80 mm in diameter; a cup speed of 1500 rpm; mass flow rate of molten alloy in the range from 140 to 150 kg/h; the temperature of liquid metal on tapping ranging from 1200 to 1250°C.

The spinning cup granulation process with cooling of molten drops in water enables the cooling rates of granules in ranges from 10^3 to 10^4 °C/s to be achieved. This process is explosion-proof (owing to the absence of ultrafine and fine particles) and easy to operate.

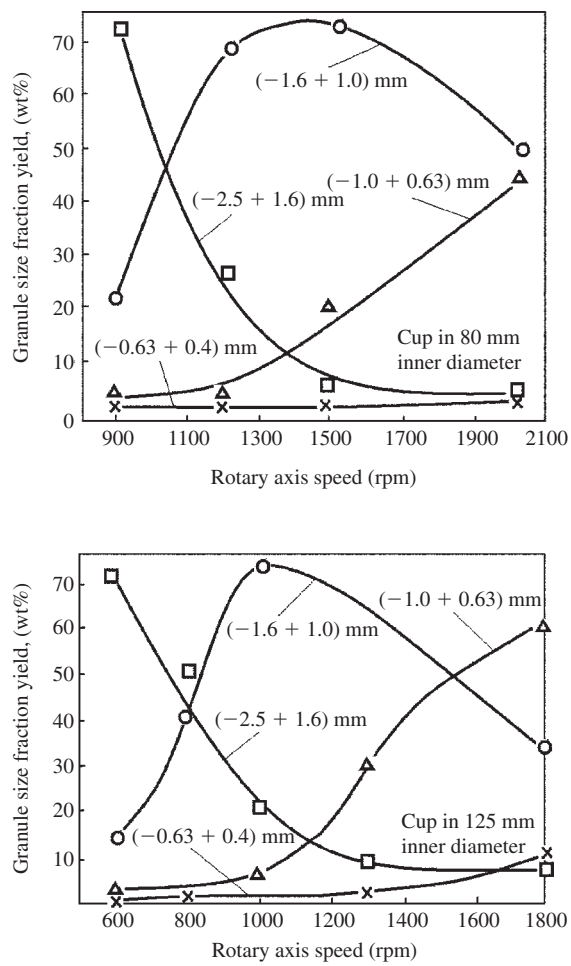

Figure 13.10 Dependence of granule fraction yield on cup rotary speed for 01419 alloy (in Russian grading). (Source: Ref 23)

Table 13.7 Main parameters of the spinning cup granulation process

Atomizer	Cup inner diameter (mm)	Aperture size (mm)	Cup rotary speed (rpm)	Molten mass flow rate (kg/h)
Breaking up from cup lip	150	...	600–2700	100–300
Cup with apertures	80–150	1.2–3.0	600–10000	100–600
Cup with slits	125–150	1.0–1.5	600–1000	100–600

(Source: Ref 23)

Table 13.8 Influence of cooling medium on surface properties of rapid solidified particles

Cooling medium	Impurities in cooling medium		Characteristics of powders and granules			
Composition	Aqua (wt%)	Oxygen (vol%)	Diameter (μm)	Oxygen content (wt%)	Adsorbed water content (wt%)	Oxide film thickness (nm)
Helium, high purity	max 0.002	max 0.002	50–350	0.01	max 0.001	3–4
Argon, highest grade	<0.0009	max 0.0007	50–350	0.005	max 0.001	3–4
Nitrogen, technical	0.09	max 0.5	50–350	0.1–0.4	max 0.01	3–5
Centrifugation in air, cooling in water	<100	<2	500–2000	0.05	max 0.01	3–5

(Source: Ref 23)

In comparison with gas-atomized powders cooled in technical nitrogen gas medium, the spinning cup granules cooled in water are less oxidated (Table 13.8) because of the high cooling rate.

The granulation technique followed by granule degassing and subsequent consolidation is applied for manufacturing alloys for various applications, including high strength, high strength weldability and elevated temperature aluminum alloys [19,23]. The total residual concentration of water and hydrogen should not exceed 0.3 ppm to provide sufficient quality of dense billets, including such important characteristics as plasticity, low-cycle fatigue and rate of crack propagation. Typical mechanical properties of high strength, high strength weldability and elevated temperature aluminum alloys on the basis of granules solidified in water are given in Table 13.9.

For comparison, the properties of ingot alloys of similar composition and function are included in Table 13.9. As may be seen, the high strength and weldable granular alloys show significantly better tensile properties than the ingot-based material. The semiproducts of elevated temperature alloy 01419 are inferior at room temperature in strength characteristics to semiproducts of AK4–1 conventional alloy, but at elevated temperatures and particularly creep-rupture strength are 1.5–2 times better.

The VILS granular technique enables the following to be produced [23]:

- billets with mass up to 350 kg up to 500 × 650 mm in size
- extruded semiproducts: rods from 10 to 200 mm in size, structural shapes from 0.8 to 130 cm^2 in cross-section area, tubes from 20 to 200 mm in diameter with wall thickness from 1.5 to 20 mm
- rolled semiproducts: sheets from 0.8 to 6 mm in thickness with width up to 1000 mm and length up to 3000 mm
- stamped semiproducts: pistons, coupler links, impellers and others in mass from 0.5 to 40 kg.

Water Atomization

For aluminum and its alloys gas atomization (GA) is widely used in industry [41–44]. The conventional process provides cooling rates up to 10^5 K/s. However, the GA technology is an explosive and dangerous process and special safety measures are required which raise the manufacturing costs considerably.

The well-known water atomization (WA) process allows one to increase the cooling rate. This technology is widely used for the production of ferrous

Table 13.9 Mechanical properties of aluminum alloy semiproducts made from water-atomized granules and ingot alloys

Alloy	Alloy composition (wt%)	Semiproduct	Condition strengthening	Temperature (°C)	Mechanical properties		
					UTL (MPa)	YS (MPa)	El (%)
High-strength alloys							
01969	Al-(8–9)Zn-(2–3)Mg-(1–1.5)Cu-(1.15–2.4)	Sheet in 2 mm thickness	T1	RT	670	640	10
		Rod in 5 mm diameter	T1	RT	690	660	6
01959	Al-(6–7)Zn-(1.8–2.5)Mg-(0.8–1.4) Cu-(0.8–2.15)	Sheet in 2 mm thickness	T1	RT	580	490	8
		Rod in 5 mm diameter	T1	RT	620	580	11
B95pch[a]	Al-6Zn-2.3Mg-1.7Cu-0.4Mn-0.17Cr	Sheet in 2 mm thickness	T1	RT	510	420	10
High-strength weldability alloys							
01949	Al-(4.5–5.5)Zn-(2.5–3.5)Mg-(0.1–0.4) Mn-(0.4–0.8)Cr-(0.4–0.8)Zr-(0.1–0.3)Ti	Sheet	T6	RT	590 500 (w)	500	10
1201[b]	Al-(4.0–5.0)Zn-(1.0–1.8)Mg-(0.2–0.7) Mn-(0.06–0.2)Cr-(0.08–0.2)Zr-(0.01–0.06)Ti-0,1Cu-0.4Fe-0,35Si	Sheet	T2	RT	410 280 (w)	330	10
Elevated temperature alloys							
01419	Al-(1.8–2.2)Mn-(0.8–1.2)Cr-(0.4–0.8) Zr-(0.4–0.8)Ti-(0.4–0.8)V-max 0.3Fe-max0,3Si	Extruded semiproducts	...	RT	340	310	15
			...	250	150	130	20
			After 1000 h	250	100	...	...
			...	350	110	90	21
			After 1000 h	350	50	...	...
AK4–1c	Al-(1.9–2.5)Cu-(1.4–1.8)Mg-(0.8–1.3) Ni-(0.8–1.3)Fe-(<0.3)Zn-(<35)Si-(<0.2)Mn	Extruded semiproducts	...	RT	420	360	7
			...	250	130	90	25
			After 1000 h	250	60	...	...
				350	50	40	90
			After 1000 h	350	30	...	...

[a]B95pch is ingot alloy (in Russian grading analogous 7050 US grade); [b]1201 is ingot alloy in Russian grading; [c]AK4–1 is ingot alloy in Russian grading; 01969, 01950, 01949, and 01419 are alloys made from water atomized granules in Russian grading, RT is room temperature.

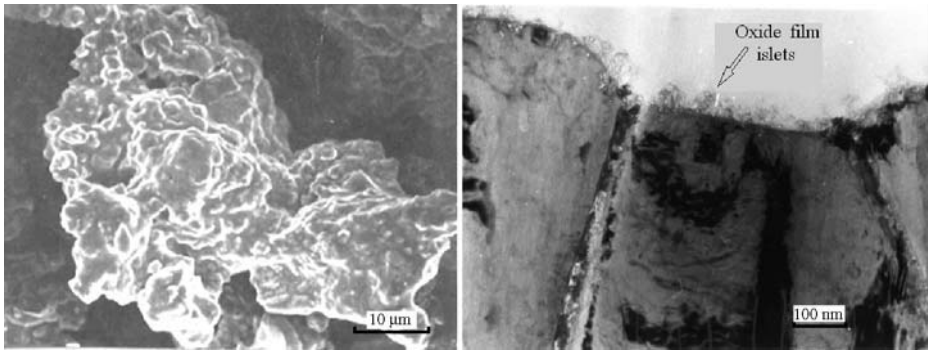

(a) (b)

Figure 13.11 SEM and TEM (microtome) micrographs illustrating irregular shape of particles and non-uniformity of the surface oxide film. Courtesy of Professor Krajnikov.

metals and some non-ferrous ones (e.g. copper). However, the process has not found application to aluminum alloys for two main reasons:

1. danger of explosion due to rapid hydrogen emission, and
2. high reactivity of aluminum that can cause heavy oxidation of the surface of atomized powders as a result of interaction between aluminum and water.

The problem of the powder quality and safety in the course of WA aluminum alloys powder production was solved at the Institute for Problems of Materials Science (Kiev, UA) [42–45]. This solution lies in the following:

- by using water solutions with inhibitors from the group of weak electrolytes and stabilizers of dispersions – protective colloids as well as their mixtures
- by hydrogen ion control
- by the control of suspension temperature
- by the hydraulic size classification of the atomized product
- by the optimization of the dehydration procedure.

Newly prepared aluminum powders strongly react with water at room and especially at elevated temperatures. During aluminum oxidation in water, multilayered films form on the metal surface and they are mainly composed of aluminum hydrate $Al(OH)_3$ and hydroxyhydroxide (AlOOH), the structure of those considerably depending on the oxidation temperature [46]. An aluminum oxide surface film is formed as follows.

A boehmite film forms as a result of dissolution of cell butts on the metal surface:

$$Al + 2H_2O = AlOOH + \frac{3}{2} H_2$$

then, boehmite is dehydrated:

$$2AlOOH = Al_2O_3 + H_2O$$

Thus the resulting reaction is

$$2Al + 3H_2O = Al_2O_3 + 3H_2$$

Evidently, the presence of structure defects such as grain and interparticle boundaries, pores, local chemical inhomogeneities, etc., accelerates the rate of the water–aluminum interaction.

Typical morphology of water-atomized high-strength aluminum alloy powder particles is shown in Figure 13.11(a). The powder particles have a very irregular shape and uneven surface. As the transmission electron microscopy shows, the surface oxide of water-atomized powders is non-uniform in its thickness (Figure 13.11(b)). Rather, three-dimensional film islets with a typical thickness of 30–40 monolayers usually cover 30–70% of the particle surface. The rest is covered with a thin oxide film of about 3 to a maximum of 8 monolayers.

Typical profiles of several elements as result of the study of depth distributions of electropositive elements with primary O_2^+ and secondary positive ions are shown in Figure 13.12. Only Mg exhibits a pronounced enrichment of subsurface layers. Both Zn and Cu are distributed more or less homogeneously with some deviations from an ideal plane profile. Main metallic impurities, Fe and Ca, are typically enriched in subsurface layers, as is seen from Figure 13.12(a). However, Mg, which is enriched and oxidized on the powder surface, also appears in the surface oxide. The average thickness of the surface oxide film, as well as the widths of the observed Mg, Fe and Ca segregation zones, are estimated on the basis of the available depth profiles and respective ion sputter rate data. These thicknesses are taken to be proportional to the sputtering times required for a 50% drop in the element profiles. The average thickness of the surface oxide usually varies from 4 to 10 nm.

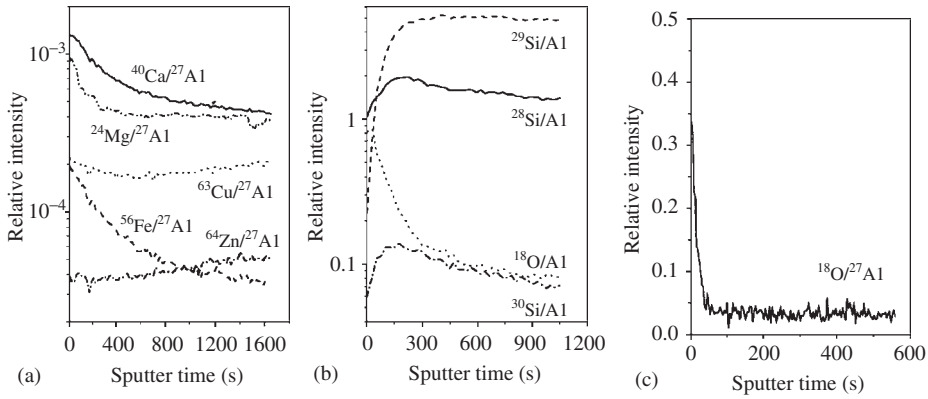

Figure 13.12 Typical depth profiles for: (a) Mg, Ca, Cu, Zn and Fe ions normalized to Al (primary O_2^+ and secondary positive ions), (b) Si and ^{18}O ions normalized to Al (primary Cs^+ and secondary negative ions), (c) $^{18}O/^{27}Al$ (primary O_2^+ and secondary negative ions). Courtesy of Professor Krajnikov.

The thicknesses of Mg, Ca and Fe enrichment layers range from 30 to 70 nm.

This conclusion is of importance from the viewpoint of further processing of water-atomized powders. Since the surface oxide is non-uniform in thickness, separate thick film islands do not impede transport processes in the course of powder compacting and thus sufficient cohesion of the interparticle boundaries can be achieved during compacting.

Microscopic kinetics emission as a result of metallic powder particle reaction with water enables the explosion risk of the process to be characterized. The experimental investigation of gas emission kinetics is carried out by means of a laboratory appliance which consists of a reaction vessel, a measuring dome to collect generated gases, a gas pressure sensor, a unit for pressure compensation and a recording device. The gas collected in the dome was analyzed by a chromatograph. This method is exact and permits gas emission to be measured with an accuracy within 1 ml per 1 kg of powder sample. The wet powder samples are taken for measurements preferably directly from the chamber of the vacuum filter, i.e. just after the operation of melt atomization and before drying. Characteristics of gas emission are usually measured for commercially available or experimental dry powder samples when the surface oxide film has already been formed and thus the reactivity of the powder has already been lowered. Evidently, the results obtained on primary wet powders are more exact.

The typical gas emission dependences on reaction time for high-strength aluminum alloys and elevated temperature ones at room temperature and at pH = 4.0 and 6.0 are shown in Figure 13.13. The rate of powder–water interaction strongly depends on the pH value. The nature of reaction kinetics abruptly changes with increasing pH to 6.0. The reaction activity of elevated temperature alloy powders with water is considerably lower in comparison with high-strength quaternary system Al–Zn–Mg–Cu alloys. But for both aluminum alloy types at pH = 4.0, which depends on composition and content of inhibitor, in given conditions, gas emission does not pose a danger.

Figure 13.14 represents the schematic diagram of the pilot plant for the production of aluminum alloy powders. The technological process consists of the following steps. The charge, which is prepared with the use of master alloys, containing all alloying elements, is melted in the induction furnace. The melt is fed into a tundish, whence it flows out through a nozzle in the bottom. The melt stream is atomized by jets of the cooled high-pressure water in the atomizing chamber. An inhibitor is introduced into the cooled water reservoir. A water suspension of the atomized metal powder forms at the bottom of the chamber and then flows into the suspension reservoir. The suspension is continuously pumped out from the reservoir and is supplied to the hydraulic classifier (Figures 13.15 and 13.16). The suspended powder is classified into various size fractions. The suspension with coarse fractions is returned into the suspension reservoir and is subjected to the mechanical dehydration by filtering under vacuum. The filtering by means of a high-performance porous filter dehydrates the suspension with fine fractions. All classified powders are dried in a vacuum. The automatic control system controls the hydrogen ion exponent (pH) value and the temperature of water and suspension.

The total concentration of gas impurities, such as adsorbed and chemisorbed oxygen and aqua, in gas-dried powders ranges from 800 to 2000 ppm depending on alloy composition and powder size distribution.

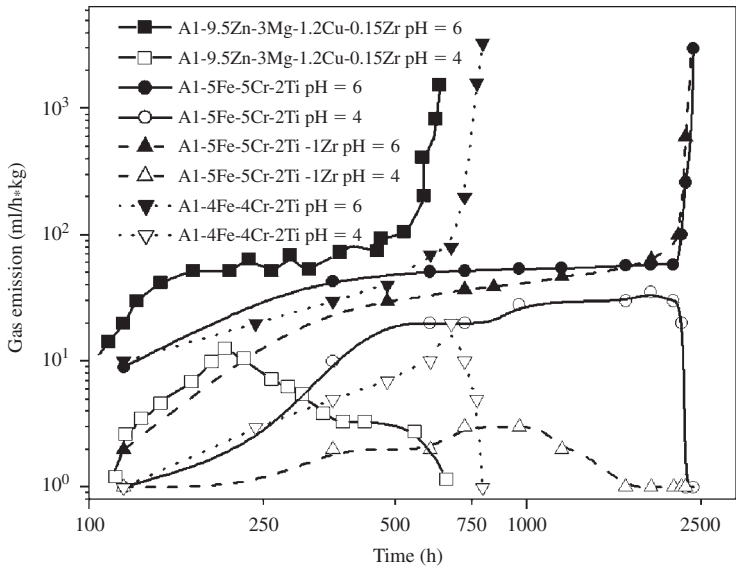

Figure 13.13 Gas emissions as a function of reaction time for several powders at pH 4.0 and 6.0.

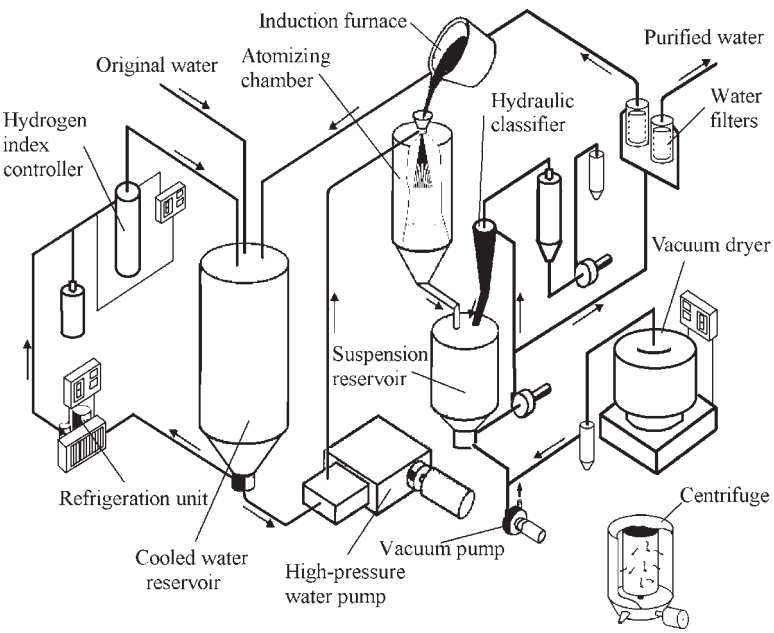

Figure 13.14 Scheme illustrating the developed water atomization technology.

In common use, the classifier permits sufficiently narrow particle fractions to be separated out provided that the separation regime is optimized. For example, for separation of fraction minus 20 μm of water-atomized $Al_{94}Fe_{3.0}Cr_{3.0}$ alloy powder, the most efficient hydroclassification regime is obtained using suspension hydraulic pressure $p_s = 0.02$ MPa, the corresponding suspension velocity at the entry to the hydrocyclone amounts to 1.35 m/s (v_c). Oversize particles are practically absent in the conditions of optimal hydroclassification (Figure 13.17(a)). It is significant that in relatively narrow particle size ranges the size distribution also obeys the normal logarithmic law (Figure 13.17(b)). This weight distribution is characterized by median diameter $d_{50} = 12$ μm and standard (mean square) deviation $\sigma = 1.65$, while the initial non-classified water-atomized $Al_{94}Fe_{3.0}Cr_{3.0}$ alloy powder contains up to 24 wt% of the fraction −20 μm.

Typical particle section micrographs of selected −20 μm fraction particles are shown in Figure 13.18. The specimens of powder particles for structural investigations were prepared from cold pressed

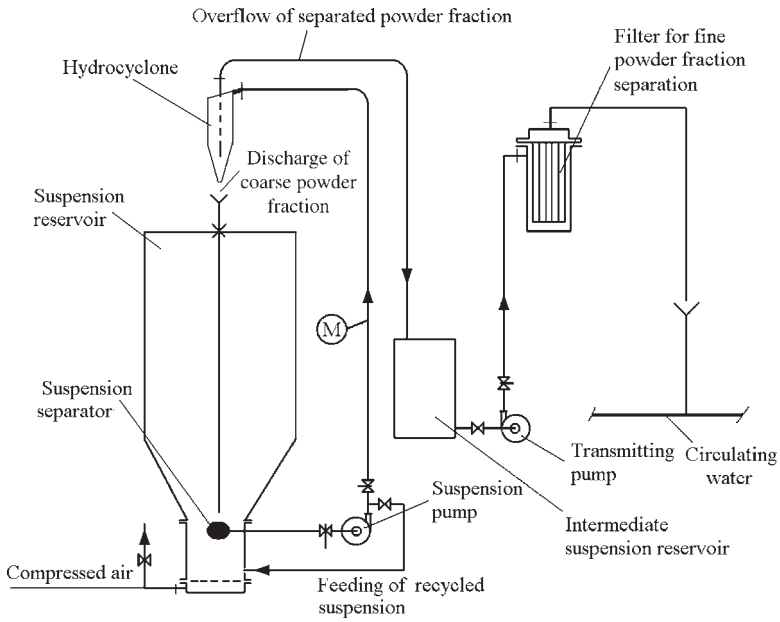

Figure 13.15 Scheme of hydroclassification system on particle size fractions.

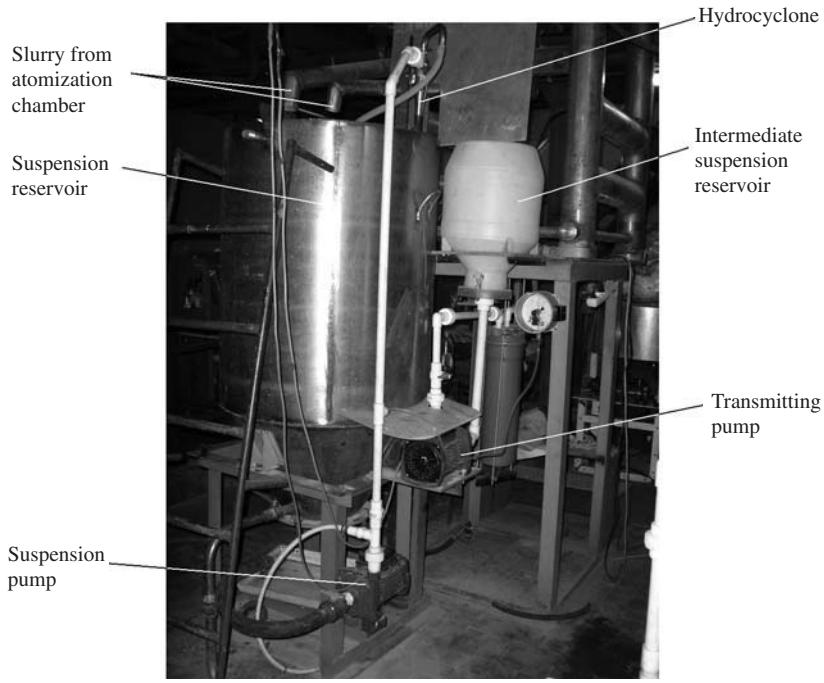

Figure 13.16 General view of the hydroclassification system of water-atomized powders.

briquettes with porosity about 30% followed by electrolytic polishing. The cooling rate of melts was estimated with the use of the dendrite parameter, which is equal to the average size of dendrite cells [19,28]. The sizes of the structural grains in the microphotographs of the particles with the projected diameters of 10.5 μm (Figure 13.18, left particle) and 17.0 μm (Figure 13.18, right particle) range from 0.3 to 1.0 μm respectively. Averaged melt cooling rates for the particles of such sizes of structural grains are 2.1×10^7 and 9.3×10^6 K/s respectively.

The technology used for powder compaction consists of two main stages, namely cold pressing followed

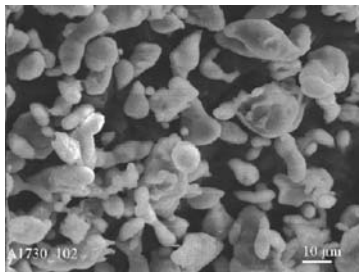

(a)

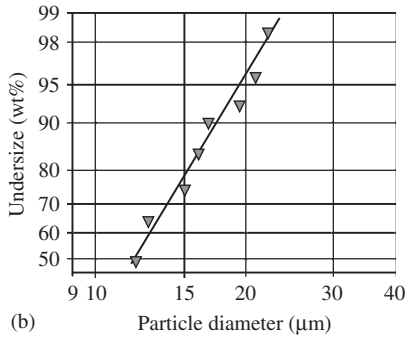

(b)

Figure 13.17 Up to 20 μm fraction of water atomized $Al_{94}Fe_{3.0}Cr_{3.0}$ alloy powder separated by means of hydroclassification: (a) SEM micrograph of separated powder fraction with undersize 20 μm; (b) size distribution of separated powder fraction with undersize 20 μm.

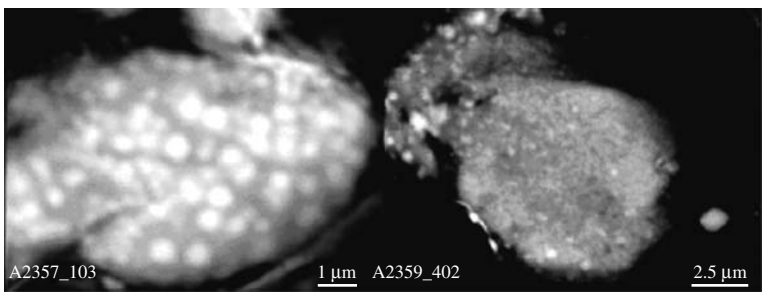

Figure 13.18 Particle section micrographs of selected −20 μm fraction particles.

by degassing and hot extrusion. Since the total concentration of water and hydrogen should not exceed 0.3 ppm to provide sufficiently dense billets [23], the main goal of degassing is reduction of residual gas concentrations to a necessary level followed by isolation of the degassed billets from the atmosphere. Compacting is aimed at the production of pore-free billets and conservation of the microstructure and phase composition of the RS powders.

At first, the powder is formed into green compacts in air at room temperature to a relative density of 30%, so that the particle surfaces remain accessible for vacuum outgassing and moisture removal. Further, the encapsulated green billet aluminum containers are degassed under 0.1 Pa vacuum at 400°C. After degassing, the properly sealed containers are extruded in air at 400°C, with a velocity of die travel of ≈0.3 mm/s and an extrusion ratio of about 12.8 to produce rods of 7 mm diameter.

The use of rapid solidification (RS) allows one to increase the solubility of insoluble impurities and alloying elements and thus to decrease the number and size of surplus phases [19]. As recently shown [45,47], the use of the newly developed technology based on high-pressure water atomization (WA) allowed the authors to produce a set of high-quality Al alloy powders which have been then consolidated for various applications. In particular, ultrahigh-strength, high-strength weldable and elevated temperature PM alloys showed very high mechanical properties that exceeded those of cast alloys of similar compositions [47–49].

One of the application areas of the new water atomization process may be in the recycling of secondary aluminum. Contamination of aluminum scrap by iron and silicon is the important problem of recycling of secondary aluminum [50]. Both iron and silicon have limited solubility in the aluminum matrix. As a result, cast ingots of secondary aluminum contain coarse Fe and Si base precipitates with diameters of a few microns. Such hardly-deformable inclusions are often located at grain boundaries or triple junctions and they usually have weak cohesion with the matrix [51]. Under load, cracks first of all nucleate at the interfaces of the matrix and the coarse precipitates. Therefore, such precipitates serve as principal fracture sources. As is known, if nucleation and propagation of the crack is connected with a single fracture source, then characteristics of the tensile strength and especially parameters of the fatigue strength decrease as compared with an opposite case when many cracks simultaneously arise from several sources. Coarse particles can, in a similar manner, influence corrosion resistance. Therefore, the use of cast secondary aluminum for production of high-quality alloys for crucial structural applications is hindered by the presence of coarse Fe and Si base precipitates in the microstructure [19].

Table 13.10 Alloy composition

Alloy No.	Alloying elements (mas.%)				Impurities (mas.%)		
	Zn	Mg	Cu	Total: Zn + Mg + Cu	Si	Fe	Fe + Si
1	9.3	0	1.9	14.1	0	0	0
2	9.4	2.8	1.6	13.8	0	0.4	0.4
3	9.4	4	1.3	14.7	0.3	0.15	0.45
4	9.4	2.9	1.44	13.74	0	0.6	0.6
5	10.0	3.2	1.35	14.55	0.55	0.13	0.68
6	10.0	2.9	1.38	14.28	0	0.93	0.93
7	8.6	3.5	1.3	13.4	0	1	1
8	9.4	3.3	1.3	14	0.9	0.9	1.8

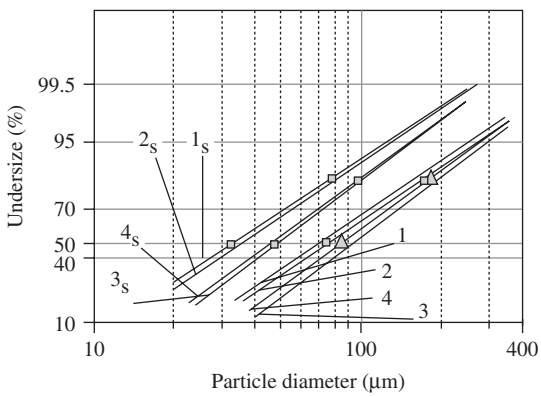

Figure 13.19 Weight (alloys 1–4) and surface (1_s–4_s) particle size distributions.

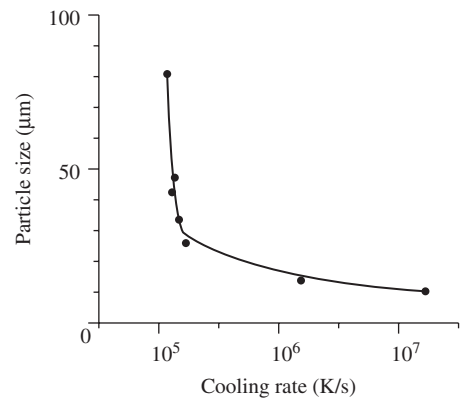

Figure 13.20 Correlation between powder and cooling rate.

In the work [52], possible effects of iron and silicon on the structure and properties of PM produced on the basis of water atomized powders were studied. The high strength Al–Zn–Mg–Cu system alloys were selected for investigation (Table 13.10). The total bulk concentration of all alloying elements lie between 13.4 and 14.55 mass%. Various combinations of Fe and Si with a maximum total concentration of 1.8 mass% were added to furnace charges during powder atomization in order to study their effect on the structure and mechanical properties.

The particle size distributions of the water atomized Al–Zn–Mg–Cu alloys obey a log normal law (Figure 13.19). The water atomization conditions were as follows: water pressure 10 MPa, superheat of the melt temperature equal 150–200°C, diameter of a gravity melt stream 7.0–7.5 mm. In these conditions, the median diameters of the mass distribution are in the range 72–83 μm and of the surface one equal to 33–47 μm. The geometric standard deviation represented the slope of the curve and the spread of particle size about the median value, respectively, is in the range 2.0–2.3.

The cooling rate of melts was estimated with the use of the dendrite parameter, which is equal to the average size of dendrite cells [19,28]. The correlation between particle size and cooling rate is shown in Figure 13.20.

PM alloys produced from WA powders generally show a high level of room temperature tensile strength (≈700 MPa) with sufficient plasticity (elongation ≈7–9%). A correlation between the characteristics of mechanical properties and the common bulk concentration of impurities is shown in Figure 13.21. The strength and hardness curves clearly demonstrate two regions. At lower impurity concentrations (up to 1%) both strength and hardness increase with impurity concentration without any evident loss of plasticity.

A further increase of the impurity concentration, however, reduces the level of strength. If the common concentration of Fe and Si rises from 1 to 1.8%,

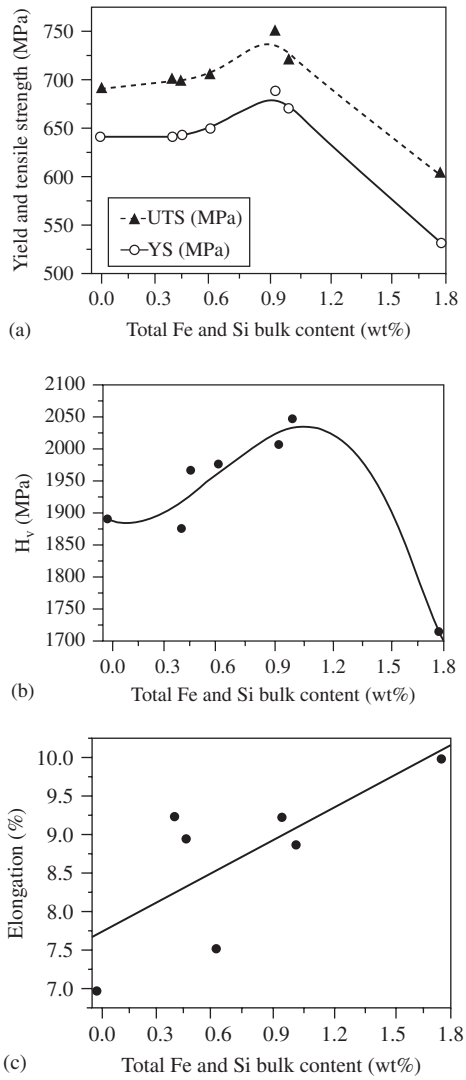

Figure 13.21 Correlation between the mechanical property characteristics and the common bulk concentration of impurities.

then the strength goes down from approximately 700 to 600 MPa while plasticity is less sensitive to the impurity concentration. The hardness behavior generally correlates with the strength.

The use of RS allows one to dissolve impurity atoms in the matrix. The atomization regimes used provide dissolution of at least 1.1 mass% Fe and Si. At higher impurity concentrations, coarse Fe and Si base particle precipitate and serve as fracture sources. As a result, the tensile strength of powder metallurgy alloys decreases. Higher cooling rates (or finer powder fractions) should be used to suppress precipitation of the above precipitates [52].

The water atomization process provides promising possibilities in advance of elevated temperature aluminum alloys. A comparative analysis of alloying principles for creating elevated temperate powder alloys shows the possibility of two approaches [19,48].

The first possibility is alloying with transition metals having some solubility in solid aluminum in accordance with the equilibrium diagram. At moderately high cooling rates (10^3–10^4°C/s), these metals form the supersaturated solid solutions in aluminum which, due to the influence of elevated temperatures and mechanical deformation during powder consolidation to semi-finished products, decompose into a dispersion of intermetallic or quasicrystalline phases. Prospective alloying elements in this class include Cr, Mn, Zr, Ti, W, Mo and Nb. High particulate density and uniform distribution of intermetallic and quasicrystalline phases are possible by increasing the supersaturation of the solid solution.

The second approach is the heterogenization of the cast structure by alloying with metals practically insoluble in aluminum even at cooling rates of 10^6°C/s, such as Fe, Co, Ni and rare earth elements. These elements precipitate upon crystallization in the form of dispersed intermetallics that are a part of the eutectic in the boundaries of dendrite cells, forming a framework.

Recently, the second approach has attracted greater attention. The data adduced in Table 13.11 have characterized the mechanical properties of elevated temperature aluminum alloys achieved by means of advanced water atomization technology [53, 54].

The developed RS technology allows the production of high quality alloys for elevated temperature applications. The technology is based on the modified WA process, which is more economically efficient than the known prototypes. The excellent compressibility of WA powders simplifies the procedure of powder consolidation which is based on hot extrusion of cold pressed degassed powders. The level of properties achieved here is comparable with that of other alloys of similar composition known from the literature and mainly exceeds them [54]. The ultimate tensile strength ranges of the aluminum alloys made from water-atomized powders are shown in Figure 13.22.

Spray Forming

Spray forming is a metal spraying process for the production of near-net shape parts. In this technique, the melt of metal is gas atomized to form a fine spray of molten particles that are deposited and sintered onto a stationary or moving substrate. Therefore, the

Table 13.11 Mechanical properties of elevated temperature aluminum alloys achieved by means of advanced water atomization technology

Alloy composition (at%)	Semi-product	Temperature (°C)	Mechanical properties			
			HV (MPa)	UTS (MPa)	YS (MPa)	El (%)
$Al_{94.9}Fe_{0.75}Cr_{4.35}$[a]	Rod, 6 mm in diameter	RT	...	483	402	4.5
		190	...	364	332	4.3
		300	...	261	236	4.7
$Al_{94\cdot7}Fe_{2.6}Cr_{2.7}$[a]	Rod, 6 mm in diameter	RT	...	459	398	10.6
		190	...	359	328	7,4
		300	...	247	221	3.1
$Al_{94.3}Fe_{4.7}Ce_{1.0}$[a]	Rod, 7 mm in diameter	RT	...	590	524	10
		300	...	320	270	6.5
$Al_{92.83}Fe_{6.03}Ce_{1.14}$[a]	Rod, 7 mm in diameter	RT	...	500	460	11
		300	...	290	260	7
$Al_{94}Fe_{2.5}Cr_{2.5}Ti_{1.0}$[b]	Rod, 10 mm in diameter	RT	2717	633	590	5.2
		190	...	...	...	...
		300	...	310	291	3.0
		400	...	199	177	6.7
$Al_{94}Fe_{4.1}Cr_{1.5}Ti_{0.47}Zr_{0.13}$[b]	Rod, 10 mm in diameter	RT	1980	701	653	6.0
		190	...	540	530	2.5
		400	...	165	145	8.0
$Al_{94}Fe_{2.5}Cr_{2.5}Ti_{0.7}Zr_{0.3}$[b]	Rod, 10 mm in diameter	RT	1920	642	611	7.4
		300	...	365	322	1.9
		400	...	190	188	5.4
$Al_{94}Fe_{2.5}Cr_{2.5}Ti_{0.5}Nb_{0.5}$[b]	Rod, 10 mm in diameter	RT	1880	647	597	2.7
		300	...	368	355	1.63
		400	...	202	171	4.7

[a]particle size fraction 0–63 μm; [b]particle size fraction 0–40 μm; RT is room temperature.

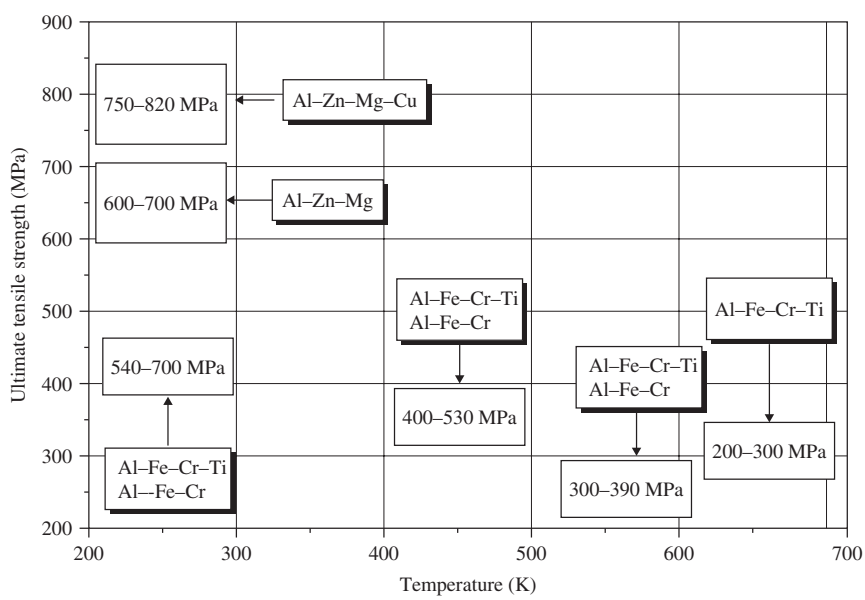

Figure 13.22 Ultimate tensile strength ranges of the aluminum alloys made from water atomized powders.

powder metallurgical process is accomplished omitting a cold solid powder state.

In a typical spray forming process, the metal melt is poured from the tundish into the atomization zone and is disintegrated by impinging high energy inert gas jets. In the resulting spray cone, the molten metal droplets partly solidify at high cooling rates and are accelerated towards the substrate where the mushy droplets are compacted to a solid preform. The principle of the spray-forming process is illustrated in Figure 13.23.

The idea of spray forming was developed in the late 1960s by Singer [55] at the University of Swansea in Wales, UK. The process of spray forming was further developed initially as an alternative to the production of thin metal sheets directly from the melt, which should replace the conventional metallurgical route of casting and subsequent forming of big slabs. For the first commercial application, scientists of Singer's group founded the Osprey Metals Ltd. [56]. Starting from here, several scientific groups all over the world took an active part in the research and development of the fundamentals and application potentials of spray forming [57–63].

The specific advantages of different spray formed materials as well as the properties of spray formed near net shaped products and the state of the art of research and industrial application of the process are documented in the periodical international user conferences on spray forming ICSF [64,65] and the International Conferences on Spray Deposition and Melt Atomization SDMA that took place in 2000, 2003 and 2006 at the University of Bremen [66–68] as well as in the publication series of the scientific contributions on spray forming in the special research programme at the University of Bremen since 1996.

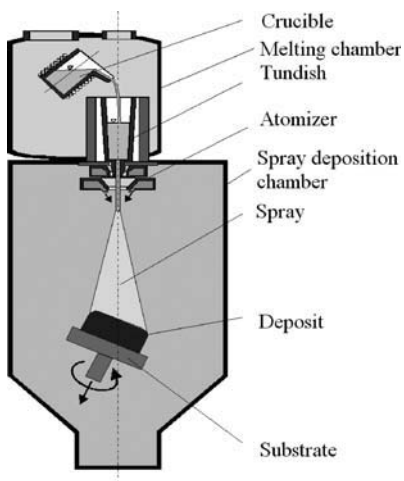

Figure 13.23 Spray forming process principle.

Different setups and ways of description and combination of fundamental process stages can be found in the literature [57,69,70]. The starting point of an analysis is the subdivision of the spray forming process into three main stages (Figure 13.24) [71]:

- preparation of the melt and atomization; this stage includes the preparation of the alloy composition, the delivery and the disintegration of the liquid from the continuous melt flow to the resulting droplet size distribution
- particle transport in the spray cone; here the spray cone behavior and development, described by the multiphase flow of metal droplets/particles and the gas, the momentum and heat transport within phases and exchange between phases are in focus
- impact and deposition of droplets; the impact of the droplets and compaction to the resulting deposit in combination with the behavior of the product occurs in this stage.

Modeling and simulation of the spray-forming process is an essential tool for process understanding and development [71–74]. Integral spray-forming models, especially for the thermal behavior in spray forming, have been derived by Bergmann et al. [75], Minisandram et al. [76] and Pedersen et al. [77,78]. Connection of various submodels is performed for transient temperature material behavior, from melt superheating in the tundish to room temperature in the preform via cooling and solidification.

In technical applications, the non-ferrous metals that are used for production of semi-finished products by spray forming are:

- conventional metals and alloys based on copper or aluminum

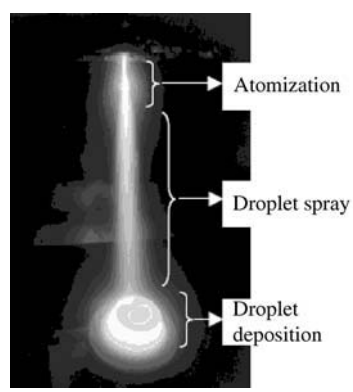

Figure 13.24 Subdivision of the spray forming process into three main stages. Courtesy of University of Bremen.

- metals and alloys which are difficult to cast (because they tend to segregate)
- superalloys (e.g. on nickel basis) and titanium
- particle reinforced metal–matrix composites (MMCs) [79–83].

The spray-formed products are typically free from macrosegregation and prior-particle boundaries that occur in conventional PM products. The spray forming is helpful in increasing the maximum solute content of alloying elements and achieving a finer distribution of second-phase particles in an equiaxed fine-grain structure. Such homogeneous, low-segregation, fine-scale alloy microstructures are useful for extrusion, rolling, forging and super plastic forming processes.

The main geometries which are produced by spray forming are as illustrated in Figure 13.25:

- flat products (sheets) are manufactured either by scanning (oscillating) the atomizer or by using (linear) slit nozzles in order to spread the spray cone over a certain area and spraying onto a linear moving substrate
- tubes and rings are produced by scanning the atomizer or stationary spraying onto a tube shaped or cylindrical substrate. The core will be drilled out or remains in the form for realization of a two-layered product (with different properties on the inside and the outside). Spray formed tubes are used in the chemical industry, spray formed rings will be used in big dimensions for applications in turbines and propulsion units (aeronautics and astronautics).

Billets are presently the most common manufactured geometries produced by spray forming. Cylindrical billets are commonly used as preform for a subsequent extrusion process. The manufacturing of a billet is realized by spraying at an inclined angle off-center on a rotating cylindrical substrate, which will be withdrawn during the process (commonly in vertical direction for a standing billet, but sometimes in a horizontal direction, producing a laying billet). To increase the production rate and throughput, sometimes two atomization units are used simultaneously [84]. Spray-formed billets are presently produced up to a diameter of approximately 0.5 m and up to a height of 2 m. Typically billets are deformed (e.g. extruded or forged) to be used, for example for applications in the automotive and aerospace industries.

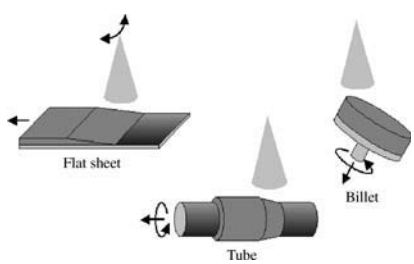

Figure 13.25 A schematic of the production of flat sheet, billet and tube by spray forming.

Figure 13.26 shows views of the equipment used in a pilot plant at the 'Spray Forming' Research Centre at the University of Bremen for obtaining spray forming products. This processing line includes separately three different modelling areas (with different time scales): (a) melt flow in the tundish, (b) particle cooling in the spray, (c) growth and cooling of the deposit. The melting capacities of the four spray forming facilities available within the center differ from 1 to 20 L and the maximum melting temperatures from 800 to 1600°C.

Contributions to fundamentals and applications of several non-ferrous metal material groups are: copper-based materials [85], aluminum-based materials [86,87], titanium and ceramic free superalloys [88], compound materials and MMCs [89], and lightweight materials (e.g. magnesium) [90].

Examples of spray formed Al–Li alloys are UL30 and UL40 having increased levels of lithium and zirconium in comparison with one of the most commonly used Al–Li alloys, 8090 (Al–2.5Li–1.0Cu–0.7Mg–0.12Zr). According to White et al. [91], UL30 (Al–3.0Li–1.0Cu–0.7Mg–0.3Zr) shows a 4.4% increase in specific modulus over 8090 and the strengthening is primarily by duplex particles Al_3 Zr (β') and Al_3 Li (δ') and copper and magnesium in solid solution. Palmer et al. [92] have spray formed UL40 (Al–4Li–0.2Zr) with the lithium content reaching the limit of solid solubility at the eutectic temperature. They found the as-sprayed grain structure equiaxed with grain sizes in the range 40–50 μm.

In another variation of the spray forming technology, Siemers et al. [93] used a low-pressure plasma spray deposition (PSD) technique for producing MMCs. In this process, plasma (near 9300–18 600°C) is formed in the interior plasma gun by the discharge of a DC arc through a flowing gas mixture (argon or nitrogen with additions of 2 to 15% hydrogen or helium). Powder is injected into the plasma jet through one or more injector ports. Then, the powder is entrained in the high-velocity plasma jet (Mach 2 to 3), melted, transported and impacted on a substrate where the molten droplets solidify at cooling rates of 10^5–10^6 K/s according to [93]. Siemers et al. [93] produced composites of metal–metal, metal–carbide and metal–oxide combinations. They also produced graded layered structures of near-theoretical density

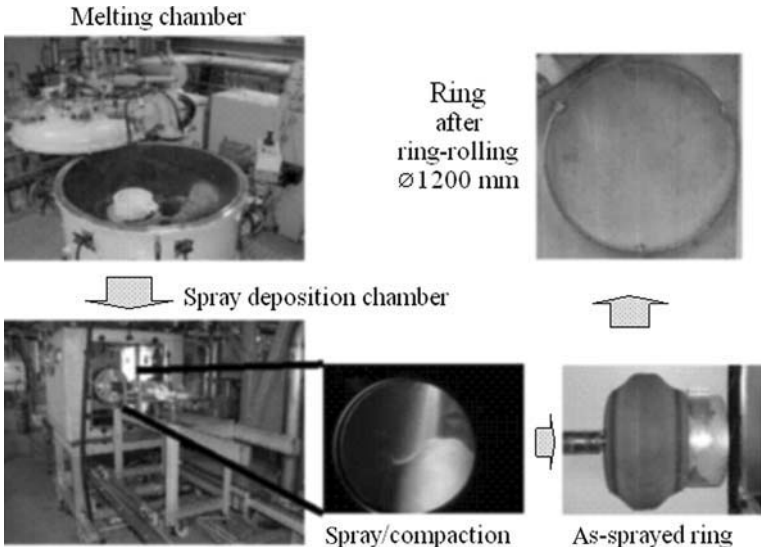

Figure 13.26 Equipment views used in a pilot plant by 'Spray Forming' Research Centre at the University of Bremen for obtaining spray forming products. Courtesy: University of Bremen, Germany.

to minimize the effects of interfacial stresses developed due to thermal mismatch between the constituents. Continuous as well as discontinuous composite can be fabricated by the PSD process. Continuous laminates, consisting of alternating layers of metal and reinforcement, are produced by first depositing metal, next depositing the reinforcement and repeating the sequence to build the desired final thickness. For fabricating discontinuous laminates of individual splattered particle lamellae (2–4 μm thick and 50–150 μm diameter), a powder blend of two or more different compositions can be injected into the plasma jet.

The PSD process is commonly used to apply a metal coating deposit onto engine components or protective ceramic for high temperature service in the aerospace, automotive and power generation industries.

Many works have been performed in the fundamental study of the PSD process, including its simulation by means of computational fluid dynamics to model the plasma flow, particle dynamic and heat transfer [94]. On the substrate part of the process, numerous studies have been carried out on the impact of the single liquid droplet on a solid surface. Both experimental and computational studies have been performed on materials such as zirconia [95], alumina [96], nickel [97] and tin [98] on mild or stainless steel, glass, or other substrates.

A new strip-casting process, termed 'spray rolling' (also 'spray strip casting'), combines elements of spray forming and twin-roll casting [99,100]. Thus the powder metallurgical process of a semi-product in the form of strips is accomplished omitting the cold solid powder state and billet compacts. In this process, molten metal is atomized with a high-velocity inert

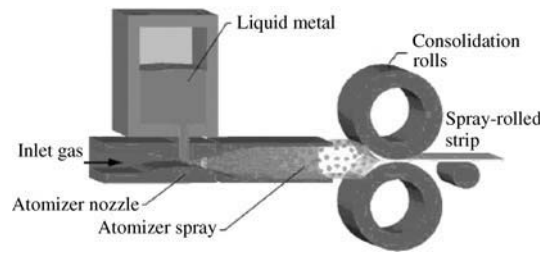

Figure 13.27 Schematic of spray rolling principle. (Source: Ref [99])

gas, the resultant droplets are quenched in flight and the spray is deposited onto mill rolls (Figure 13.27). In-flight convention heat transfer, extracting most of the metal's latent heat and conduction heat transfer at the rolls, rapidly removes the initial heat. Hot deformation of the semi-solid material by the rolls completely consolidates the rapidly solidified product. The high solidification rates in spray rolling allow a wider range of alloys to be processed and at higher production rates than is currently possible in commercial twin-roll casting practices [101–103].

Direct strip-casting techniques are attractive because they improve the economics of manufacturing of aluminum sheet products by eliminating the ingot casting, homogenization and hot-rolling unit operations in conventional ingot processing while significantly reducing energy consumption.

Tensile results for 2124 Al and 7050 Al alloys according to data of Idaho National Engineering and Environmental Laboratory (INEEL) [99,104] are summarized.

Table 13.12 Tensile properties of spray rolled and commercial 2124 and 7050 aluminum alloy strips

Alloy	Composition	*G*/*M*	Heat treatment	Tensile properties		
				UTS (MPa)	YS (MPa)	El (%)
Commercial 2124	Al-4.4Cu-1.5Mg-0.6Mn	...	T851	483	448	6
SR 2124	Al-4.4Cu-1.5Mg-0.6Mn	0.15	T851	441	407	6
SR 2124	Al-4.4Cu-1.5Mg-0.6Mn	0.3	T851	483	469	7
Commercial 7050	Al-6.2Zn-2.3Cu-2.3Mg-0.6 Mn-0.12Zr	...	T7651	510	448	12
SR 7050	Al-6.2Zn-2.3Cu-2.3Mg-0.6 Mn-0.12Zr	...	ST•2h•A	545	496	10
SR 7050	Al-6.2Zn-2.3Cu-2.3Mg-0.6 Mn-0.12Zr	...	ST•15h•A	545	503	7

SR is spray-rolled; ST is solution treatment at 471°C; A is aged (125°C, 12 h + 166°C, 15 h).

Commercial 2124-T851 and 7050-T7651 plates are remelted and spray-rolled. The alloys were induction melted under a nitrogen atmosphere, heated about 100°C above the liquidus temperature and pressure fed into an atomizer. Atomized droplets were directed horizontally and deposited into roll gap of a 200 × 300 mm 2-HI Fenn rolling mill operating at a roll surface speed of 4.1 m/min to produce strips measuring about 100 mm wide and 2.5 mm thick. The mill had standard tool-steel mill rolls. An inert gas atmosphere within the spray apparatus minimized in-flight oxidation of the atomized droplets. Strips were made under gas to metal mass flow rates (*G*/*M*) of 0.15 and 0.3 while maintaining other processing conditions constant. The production rate was 4100 kg/(h · m).

As shown in Table 13.12, for spray-rolled 2124 strip, increasing *G*/*M* from 0.15 to 0.30 resulted in an increase in tensile properties. The tensile properties of spray-rolled 2124-T851 produced at $G/M = 0.30$ compare favorably with those of commercial conventional material. Overall, tensile properties of the spray rolled and heat treated 7050 are similar to those of the commercial product.

Other Technologies

There are also other powder metallurgy processing techniques such as XD process, solid free-from fabrication (SFF) and self-propagating high-temperature synthesis (SHS), which one can regard as having potential for developing high-performance aluminum alloys and composites including functionally graded materials.

In the XD process, elemental components of the desired reinforcing phase are mixed with or incorporated into the metallic matrix material. The mixture is heated to a high temperature ($>T_m$) where a self-propagating reaction takes place. The elemental constituents react exothermally, forming a dispersion of ultrafine reinforcing particles in the matrix. As the particles of the reinforcing phase are formed by an exothermic reaction at an elevated temperature, they tend to be stable through subsequent processing at high temperatures. Larsen et al. [105] used the XD process to produce a master-alloy material containing (TBA-70 sponge: 70 wt% TiB_2 and 30 wt% Al), which was subsequently used for fabricating the discontinuously reinforced aluminum composites.

Solid free-form fabrication facilitates integrated manufacturing, from computer-aided design to finished parts, using only additive processing [106–108]. A solid or surface model is electronically sectioned into layers of predetermined thickness. Net-shape composite components can be directly produced from the elemental or prealloyed matrix powders mixed with suitable reinforcement by sintering, layer by layer, under a scanning laser beam.

Self-propagating high temperature synthesis is a process in which the synthesis reaction occurs through the reactant mixture in the form of a combustion wave [109]. Several advantages of the SHS process may include purity of the product, energy efficiency, formation of metastable phases and simultaneous synthesis and densification. And so the SHS process has the potential to be an available method for producing high-performance MMCs. Functionally graded materials including MMCs create a continuous

transition from a substantially ceramic material usable to high temperatures to a partly or fully metallic material [110–112].

References

1. Buhl, H., *Advanced Aerospace Materials*. Springer-Verlag Publishers, 1992.
2. Nembach, E., *Particle Strengthening of Metals and Alloys*. John Wiley & Sons Publishers, 1997.
3. Herrera, E.J., Gallardo, J.M., Rodriguez, J.A., New way to consolidate mechanically alloyed aluminium powder. In *Proceedings of 1998 Powder Metallurgy World Congress*, compiled by European Powder Metallurgy Association, UK, 1998, Vol. 1, pp. 317–322.
4. Li, P.Y. et al., Development of high damping aluminium alloys and composites using rapidly solidified powder metallurgy process. *Materials Science Forum*, 2003(426–432):411–416.
5. Sfat, C., Vasile, T., Vasilescu, M., Researches focused on structure of aluminium alloys processed by rapid solidification, used in automotive industry, In *Proceedings of 15th International Plansee Seminar*, Vol. 4, 2001, pp. 792–800.
6. *Powder Metallurgy*, Vol. 7, *Metals Handbook*, 9th edn. American Society for Metals, 1984.
7. *Aluminum and Aluminum Alloys, ASM Speciality Handbook*. ASM International Publishers, Metals Park, OH, USA, 1993.
8. Jung, T.K., Sung, T.J., Kim, M.S., Kim, W.Y., A comparative study of mechanical property in Al-8Fe-2Mo-2V-1Zr bulk alloys fabricated from an atomized powder and melt spun ribbon. In *Proceedings of 2006 Powder Metallurgy World Congress*, Korean Powder Metallurgy Institute, Busan, Korea, 2006, pp. 1105–1106.
9. Genkava, T., Yamasaki, M., Kavamura, Y., Microstructure and mechanical properties of rapidly solidified powder metallurgy Al-Fe-V-Si-X. In *Proceedings of 2006 Powder Metallurgy World Congress*, Korean Powder Metallurgy Institute, Busan, Korea, 2006, pp. 1123–1124.
10. Bhagat, R.B., Advanced aluminium powder metallurgy alloys and composites. In *ASM Handbook*, Vol. 7, *Powder Metal Technologies and Applications. ASM International Publishers*, 1998, pp. 841–858.
11. Murakami, Y., Aluminum-based alloys. *Materials Science and Technology*, 1996, 8:213–276.
12. Bhaduri, A., Gopinath, V., Ramakrishnan, P., SiC particulate reinforced aluminum matrix composites prepared by mechanical alloying. In *Proceedings* '*Advances in Powder Metallurgy & Particulate Materials*', Part 2. Metal Powder Industries Federation, 1996, pp. 3–12.
13. Wang, E., Hu, L, Nanocrystalline and ultrafine grained materials by mechanical alloying. In *Proceedings of 2006 Powder Metallurgy World Congress*, Korean Powder Metallurgy Institute, Busan, Korea, 2006, pp. 911–912.
14. Vitjaz, P.A., Lovshenko, F.G., Lovshenko, G.F., *Mechanical Alloyed Alloys Based on Aluminium and Copper*. Belaruskaja Nauka Publishers, Minsk, 1998.
15. Russian Federation Patent 2001715, January 1991.
16. Russian Federation Patent 2000882, July 1991.
17. Jones, H., *Rapid Solidification of Metals and Alloys*. Institute of Metallurgists Publishers, London, 1982.
18. Das, S.K., Rapidly solidified P/M aluminum and magnesium alloys – recent developments. *Rev. Part. Mayer*, 1993, 1:1–40.
19. Dobatkin, V.I., Elagin, V.I., Fedorov, V.M., *Rapidly Solidified Aluminum Alloys*. All-Russian Institute of Light Alloys Publishers, Moscow, 1995 (in Russian).
20. Savage, S.J., Froes, F.H., Production of rapidly solidified metals and alloys. *J. Metals*, 1984, 36(4):20–28.
21. Fleetwood, M.J., Rapid solidification processing. *Metals and Materials*, 1987, 3(1):14–20.
22. US Patent 4,078,873, March 14, 1978.
23. Bondarev, B.I., Shmakov Yu, V., *Technology of Rapidly Solidified Al Alloy Production*. All-Russian Institute of Light Alloys Publishers, Moscow, 1997 (in Russian).
24. Lawley, A., *Atomization*. MPIF Publishers, Princeton, New Jersey, 2003.
25. Dunkley, J.J., Atomization. In *ASM Handbook*, Vol. 7 *Powder Metal Technologies and Applications*. ASM International Publishers, 1998, pp. 35–52.
26. Dobatkin, V.I., *Continuous Casting and Casting Properties of Alloys*. Oboronizdat, Moscow, 1948.
27. Ghuljaev, B.B., *Solidification and Steel Heterogeneity*. Metallurgizdat Publishers, Moscow, 1950.
28. Eskin, G.I., Non-dendritic crystallization of light alloys. *Technology of Light Alloys*, 2000(2):17–25. (in Russian).
29. Neikov, O.D., Milman, Yu.V., Miracle, D.B., Lotsko, D.V., Sirko, A.I., Yefimov, N.A., Effect of Sc alloying additions on structure and mechanical properties of PM and cast high-strength Al alloys of same composition. In *Proceedings of PM 2001 Congress & Exhibition*, European Powder Metallurgy Association, Nice, 2001, pp. 219–224.
30. Dobatkin, V.I., Belov, A.F., Eskin, G.I., Borovkina, C.I., Golder, Yu.G., Crystallization regularities of

metallic materials. *Soviet Union Scientific discovery* #271, 1983.
31. Elagin, V.I., *Alloying of Wrought Alloys by Transition Metals*. Metallurgia Publishers, Moscow, 1975 (in Russian).
32. Novikov, I.I., Zolotorevskiy, V.S., *Dendritic Liquation in Alloys*. Nauka Publishers, Moscow, 1966 (in Russian).
33. Dric, M.E., Bochvar, N.P., Kadaner, E.S. et al., *Equilibrium Diagrams of Systems based on Aluminium and Magnesium*. Nauka Publishers, Moscow, 1977. (in Russian).
34. Dahl, W. et al., *Metallkunde*, 1977, 68(2):121–129.
35. Varich, N.I., Burov, L.M., Kolesnichenko, K. E., Izvestija, VUZov. *Non-Ferrous Metalurgija,* 1967(3):111–114.
36. Inol, A. et al., *Sci. Report Res. Inst. Tohoku Univ. A*, 1990, 35(1):101–114.
37. Cox, A.R., Moore, E.C., VanReuth, E.C., On the rapid solidification of superalloys. In *Proceedings 'Superalloys: Metallurgy and Manufacture'*. Claitor's Press, Baton Rouge, 1976, pp. 45–49.
38. Patterson, R.J., Rotating disc atomization. In *Metals Handbook*, 9th edn, Vol. 7, *Powder Metallurgy*. Am. Soc. For Metals, Metals Park, OH, 1984, pp. 45–54.
39. Anderson, R., Powder metallurgy at Pratt and Whitney. *Int. J. Powder Metall.*, 1990, 26(2):171–179.
40. US Patent 4,343,750, Aug. 10, 1982.
41. Unal, A., Leon, D.D., Gurganus, T.B., Hildeman, G. J., Production of aluminum and aluminum-alloy powder. In *ASM Handbook*, Vol. 7, *Powder metal technologies and applications*. ASM International Publishers, 1998, pp. 148–159.
42. Neikov, O.D., Rapidly solidified aluminium alloy powders. In *Proceedings of 1998 Powder Metallurgy World Congress*, European Powder Metallurgy Association, Shrewsbury, UK, 1998, Vol. 1, pp. 129–134.
43. Neikov, O.D., Water atomized powder technologies for advanced aluminium alloy production. In *Proceedings of 2000 Powder Metallurgy World Congress,* Japan Society of Powder Metallurgy, Kyoto, 2000, pp. 464–466.
44. Neikov, O.D., et al., Production of aluminium and its alloys, R.F. Patent No 2,078,427, Dec 1994.
45. Neikov, O.D., Krajnikov, A.V., Sameljuk, A.V., Vasilieva, G.I, Chaykina, N.G., An experimental study of water atomisation of aluminium alloys. In *Proceedings of 2002 Powder Metallurgy World Congress*, Metal Powder Industries Federation, Princeton, 2002, Vol. 3, 74–85.
46. Zhuravlev, V.A., Zakharov, A.P., Oxidation of Aluminum in Water at different temperatures. *Doklady AN USSR*, 1980, 252(5):1162–1166.
47. Neikov, O.D., Milman, Yu. V. et al., Properties of rapidly solidified powder aluminum alloys for elevated temperatures produced by water atomization, *Proc. 2002 World Congress of PM & Particulate Mater*. Metal Powder Ind. Fed., Princeton, NJ, 2002, 7, pp. 14–27.
48. Neikov, O.D., Milman, Yu. V. et al., Effect of powder size on mechanical properties of elevated temperature aluminium alloys. *Proceedings of PM 2001 Congress & Exhibition*, European Powder Metallurgy Association, Nice, 2001, pp. 219–224.
49. Neikov, O.D. et al., Production method of semiproducts from aluminium alloys, R.F. Patent No 2,238,172, Jul 2003.
50. Gjostein, N.A., Alternative materials for a new generation of vehicles. *Materials Science Forum*, Vol. 242. Trans Tech Publications, Switzerland, 1997. pp. 51–61.
51. Harushide Tsubakino, et al., Precipitation in deformed Al-Fe and Al-Fe-Si dilute alloys. *Materials Science Forum*, Vols. 331–337. Trans Tech Publications, Switzerland, 2000. pp. 951–956.
52. Neikov, O.D., Krajnikov, A.V., Milman, Yu.V. et al., Advanced PM aluminium alloys produced by new rapid solidification technology. *Proc. PM2004 World Congress*. European Powder Metallurgy Association, Shrewsbury, UK, 2004, Vol 1, pp. 237–242.
53. Neikov, O.D., Vasilieva, G.I., Sameljuk, A.V., Krajnikov, A.V., Water atomised aluminium alloy powders. *Materials Science and Engineering* A, 2004, 383:7–13.
54. Neikov, O.D., Milman, Yu.V., Sirko, A.I., Sameljuk, A.V., Krajnikov, A.V., Elevated temperature aluminium alloys produced by water atomisation. Water atomised aluminium alloy powders. *Materials Science and Engineering* A, 477, 2008, 80–85.
55. Singer, A.R.E., Recent developments and opportunities in spray forming. In *Koll. SFB 372.* University Bremen, 1996, 123–140.
56. Brooks, R.G., Moore, C., Leatham, A.G., Coombs, J.S., The Osprey process. *Powder Metall.*, 1977, 2:100–102.
57. Annavarapu, S., Apelian, D., Lawley, A., Processing effects in spray casting of steel strip. *Metall. Trans. A*, 1988, 190:3077–3086.
58. Lavernia, E.J., Wu, Y., *Spray Atomization and Deposition*. J. Wiley & Sons, Chichester, 1996.
59. Leatham, A.G., Lawley, A., The Osprey Process: principles and applications. *Int. J. Powder Metall.*, 1993, 29(4):321–329.
60. Mathur, P., Apelian, D., Lawley, A., Analysis of the spray deposition process. *Acta Metall.*, 1989, 37(2):429–443.

61. Bauckhage, K., Atomization of molten metals. In *Proceedings Int. Conf. Liquid Atomization and Spraying Systems ICLASS-91*, Gaithersburg, USA 1991.
62. Tsao, C.Y.A., Grant, N.J., Modeling of the liquid dynamic compaction spray process. *Int. J. Powder Metallurgy*, 1994, 30(3):323–333.
63. Reichelt, W., Stand der industriellen Anwendung des Sprühkompaktierens. In *Koll. SFB 372*, Vol. 1. University Bremen, 1996, pp. 189–198.
64. Wood, J.V. (ed.), *Proceedings 2nd Int. Conf. Spray Forming*, Swansea, UK 1993, Woodhead Publ. Ltd. Cambridge 1993.
65. Wood, J.V. (ed.), *Proc. 3rd Int. Conf. Spray Forming*, Cardiff, UK 1996, Osprey Metals Ltd. 1997.
66. Bauckhage, K., Uhlenwinkel, V., Fritsching, U. (eds), *Proceedings of the Spray Deposition and Melt Atomization Conference SDMA 2000*, 26–28. June 2000, Univ. Bremen, Bremen, 2000.
67. Bauckhage, K., Fritsching, U., Uhlenwinkel, V., Ziesenis, J., Leatham, A. (eds.), *Proceedings of the 2nd Spray Deposition and Melt Atomization Conference SDMA* 2003, 22–25. June 2003, Univ. Bremen, Bremen, 2003.
68. Fritsching, U., Uhlenwinkel, V., Bauckhage, K, Zoch, H.W., (eds.), *Proceedings of the 3rd Spray Deposition and Melt Atomization Conference SDMA 2006,* 4–6. Sept. 2006, Univ. Bremen, Bremen, 2006.
69. Lawley, A., Mathur, P., Apelian, D., Meystel, A., Spray forming: process fundamentals and control. *Powder Metall.*, 1990, 33:109–111.
70. Ottosen, P., Numerical Simulation of Spray Forming. PhD Thesis Tech. Univ. Denmark TM.93.27, 1993.
71. Mi, J, Grant, P. S., Fritsching, U., Belkessam, O., Garmendia, I., Landaherea, A., Multiphysics modelling of the spray forming process. *Materials Science and Engineering* A, 2008, 477:2–8.
72. Fritsching, U., *Spray Simulation – Modeling and Numerical Simulation of Sprayforming Metals*. Cambridge University Press, Cambridge, UK, 2004.
73. Hattel, J.H., Mathematical modelling and numerical simulation of casting processes. PhD Dissertation, Technical University Denmark, Lyngby, 1999.
74. Hattel, J.H., Pryds, N.H., Pedersen, T.B., Pedersen, A.S., Numerical Modelling of the Spray Forming process: The Effect of Process Parameters on the Deposited Material. In *Proc. SDMA 2000*, Bremen, 2000, 803–812.
75. Bergmann, D., Modellierung des Sprühkompaktierprozesses für Kupfer- und Stahlwerkstoffe. Dissertation Universität Bremen, 2000.
76. Minisandram, R.S., Forbes Jones, R.M., Kelkar, K.M., Patankar, S.V., Carter Jr., W.T., Prediction of thermal history of preforms produced by the clean metal spray. *Mater. Sci. Engng*. A, 2002, 326(1):184–193.
77. Petersen, K., Pedersen, A.S., Pryds, N., Thorsen, K. A., List, J.L., The effect of particles in different sizes on the mechanical properties of spray formed steel composites. *Mater. Sci. Engng*. A, 2002, 326(1):40–50.
78. Pryds, N., Hattel, J.H., Pedersen, T.B., Thorborg, J., An integrated numerical model of the spray forming process. *Acta Mater.*, 2002, 50:4075–4091.
79. Singer, A.R.E., Metal matrix composities made by spray forming. *Mater. Sci. Eng*. A, 1991, 135: 13–17.
80. Lawley, A., Apelian, D., Spray forming of metal matrix composites. In *Proceedings of Second Int. Conf. Spray Forming, ICSF2*. Woodhead Publishing, 1993, pp. 267–273.
81. Gupta, M., Juarez-Islas, J., Frazier, W.E., Mohamed, F., Lavernia, E.J., Microstructure, excess solid solubility and elevated-temperature mechanical behavior of spray-atomized and codeposited Al-Ti-SiCp. *Metall. Trans. B*, 1992, 23:719–736.
82. Srivatsan, T.S., Lavernia, E.J., Use of spray techniques to synthesize particulate-reinforced metal-matrix composites. *J. Mater. Sci.*, 1992, 27(22):5965–5981.
83. Wo, Y., Lavernia, E.J., Interaction mechanisms between ceramic particles and atomized metallic droplets. *Metall. Trans. A,* 1992, 23(10):2923–2935.
84. Markus, S., Fritsching, U., Spray forming with multiple atomization, In *Proceedings of 2nd Spray Deposition and Melt Atomization Conf*. Universität Bremen, Bremen, 2003, pp. 8-3–8-16.
85. Müller, H.R., Eigenschaften und Einsatzpotential Sprühkompaktierter Kupferlegierungen. In *Koll. SFB 372*, Vol. 1. University Bremen, 1996, pp. 33–56.
86. Hummert, K., Sprühkompaktieren von aluminiumwerkstoffen im industriellen maβstab – Stand der Entwicklung. In *Koll. SFB 372*, Vol. 1. University Bremen, 1996, pp. 199–215.
87. Kozarek, R.L., León, D.D., Mansour, A., An investigation of linear nozzles for spray forming aluminium sheets. In *Koll. SFB 372*, Vol. 1. University Bremen, 1996, pp. 141–160.
88. Müller, F.G., Benz, M.G., Carter Jr., W.T., Forbes, R. M., Leatham, A., Neues Verfahren zur Herstellung von Pulver, Formteilen oder halbzeugen aus titan oder keramikfreien superlegierungen. In *Koll. SFB 372*, Vol. 1. University Bremen, 1996, pp. 169–188.
89. Lavernia, E.J., Spray Atomization and Deposition of Metal Matrix Composites. In *Koll. SFB 372*, 1. University Bremen, 1996, pp. 63–122.

90. Ebert, T., Moll, F., Kainer, K.U., Sprühkompaktieren von Magnesiumlegierungen. In *Proc. 3rd Int. Conf. Spray Forming*, Cardiff, 1996, 177–185.
91. White, J., Mingard, K., Hughes, I.R., Palmer, I.G., Aluminum alloys with unique property combinations by spray casting. In *Proceedings of 2nd Int. Conf. Spray Forming*. Woodhead Publishing, 1993, pp. 355–364.
92. Palmer, I.G., Chellman, D.J., White, J., Evaluation of a spray deposited low density Al-Li alloy. In *Proceedings of 2nd Int. Conf. Spray Forming*. Woodhead Publishing, 1993, pp. 385–392.
93. Siemers, P.A., Jackson, M.R., Mehan, R.I., Rairden III, J.R., Production of composite structures by low-pressure plasma deposition. *Ceram. Eng. Sci.*, 1985, 6(7–8):896–907.
94. Ng, H.W., Remesh, K., Devasenapathi, A., Yu, S.C.M., Kang, C.W., Simulation on deposit topology in the plasma spray process. In *Proceedings of 2nd Spray Deposition and Melt Atomization Conf*. Universität Bremen, 2003, Bremen, pp. 8-53–8-65.
95. Planche, M.P., Normand, B., Suzon, E., Coddet, C., The relationships between in-flight particle characteristics and coating properties under plasma spraying. In *Proceedings of International Thermal Spray Conference*, 2001, pp. 771–777.
96. Pershin, L., Pasandideh-Fard, M., Mostaghimi, J., Chandra, S., Effect of substrate properties on the formation of plasma sprayed alumina splats. In *Proceedings of International Thermal Spray Conference,* 2001, pp. 813–820.
97. Pershin, L., McDonald, A., Chandra, S., Effect of substrate oxidation on the spreading of plasma-sprayed nickel. In *Proceedings of 3rd Spray Deposition and Melt Atomization Conf.* Universität Bremen, 2006, Bremen, pp. 56-1–56-11 (CD).
98. Pasandideh-Fard, M., Bhola, R., Chandra, S., Mostaghimi, J., Deposition of tin droplets on a steel plate: simulations and experiments. *Int. J. of Heat Mass Transfer*, 1998, 41:2929–2945.
99. McHugh, K.M., Delplanque, J.-P. et al., Spray rolling aluminum alloy strip. *Mater. Sci. Eng. A,* 2004, 383(1):96–106.
100. McHugh, K.M., Lin, Y., Zhou, Y., Lavernia, E.J., Delplanque, J.-P., Johnson, S.B. Spray rolling aluminum alloy strip for transportation applications, materials processing and manufacturing division. *Sixth Global Innovations Proceedings: Trends in Materials and Manufacturing Technologies for the Transportation Industry and Powder Metallurgy Research and Development in the Transportation Industry*, TMS, San Francisco, CA, 2005, pp. 219–224.
101. Gras, Ch., Meredith, M., Hunt, J.D., Microstructure and texture evolution after twin roll casting and subsequent cold rolling of Al-Mg-Mn aluminum alloys. *J. Mat. Process. Technol.*, 2005, 169:156–163.
102. Sun, N., Patterson, B.R. et al., Microstructural evolution in twin-roll cast AA3105 during homogenization. *Mat. Sci. Eng. A*, 2006, 416:232–239.
103. Yun, M., Lokyer, S., Hunt, J.D., Twin roll casting of aluminum alloys. *Mat. Sci. Eng. A*, 2000, 280:116–123.
104. McHugh, K.M., Lin, Y., Zhou, Y., Johnson, S.B., Delplanque, J.-P., Lavernia, E.J., Microstructure evolution during spray rolling and heat treatment of 2124 Al. In *Proceedings of 3rd Spray Deposition and Melt Atomization Conf. Universität Bremen*, 2006, Bremen, pp. 51-1–51-12 (CD).
105. Larsen, D.E., Adams, M.L., Kampe, S.L., Chritodoulou, L., Bryant, J.D., Influence of matrix phase morphology on fracture toughness in a discontinuously reinforced XD titanium aluminide composite. *Scr. Metall.*, 1990, 24:851–856.
106. Marcus, H.L., Bourell, D.L., Solid preform fabrication finds new application. *Adv. Mater. Process.*, 1993, 144(3):28–35.
107. Studt, T., Rapid prototyping key to fast development. R&D, May, 1994:55–56.
108. Belyavin, K., Minko, D., Bykov, R., Kuanichik, O., Investigation of pulse-periodical laser radiation power effect on stability of liquidmetallic contacts between powder particles by selective laser sintering. In *Proceedings of 2006 Powder Metallurgy World Congress*, Korean Powder Metallurgy Institute, Busan, Korea, 2006, pp. 911–912.
109. Munir, Z.A., The synthesis and consolidation of powders by self-propagating combustion methods. *Rev. Part. Mater.*, 1993, 1:41–74.
110. Mortensen, A., Koczak, M.J., The status of metal matrix composite research and development in Japan. *JOM,* 1993, 45(3):10–18.
111. Ford, R., Recent developments in functionally gradient materials. *Mater. Process. Rep.*, 1992:1–6.
112. Song, D.H., Park, Y.H., Park. Y.Ho., Park I.M., Cho, K.M., Thermomechanical properties of functionally gradient Al-SiC_p composites. In *Proceedings of 2006 Powder Metallurgy World Congress*, Korean Powder Metallurgy Institute, Busan, Korea, 2006, pp. 87–88.

Chapter 14

Production of Titanium and Titanium Alloy Powders

Victor G. Gopienko, Russian National Aluminum-Magnesium Institute, Saint Petersburg, Russia
Oleg D. Neikov, Frantsevich Institute for Problems of Materials Science (IPMS), Kiev, Ukraine

Titanium possesses an exclusive combination of low density, good mechanical properties at room and elevated temperatures and good corrosion resistance. Titanium and its alloys are used extensively in aerospace, biomedical industries and in other industrial applications. However, titanium ingots are expensive to produce and fabricate. Another problem is connected with segregation in highly alloyed titanium materials. The high cooling rate that PM technology makes possible ensures significantly greater amounts of alloying elements remain in the solid solution compared with ingot metallurgy and thus can substantially influence material phase composition and properties [1,2]. At the same time, PM processing permits articles close to their final shape and thus reduces material loss and accordingly lowers the production cost.

Many processes of titanium and titanium alloy powders manufacture are known. Currently, chemical reduction, hydrogenation/dehydrogenation, gas atomization, plasma-rotating electrode and plasma atomization processes are mainly used for commercial production.

Small amounts of titanium powder are produced by electrolysis of titanium compounds ($TiCl_4$, TiO_2) in melts, centrifugal atomization of the melt, amalgam metallurgy and the disproportionation method of low titanium halogenides.

Chemical Reduction

Generally, the initial source of titanium powder is 'sponge fines', so-called owing to their appearance. Sponge fines are nodular particles (see Introduction, Figure 14.2(h)) of pure titanium produced during the chemical reduction pro-cess from titanium tetrachloride. The commercial manufacture of titanium metal includes the chlorination of natural or synthetically produced rutile, TiO_2 [1,2]. The obtained titanium tetrachloride is reduced to metallic titanium by the sodium reduction method known as the Hunter process, the magnesium reduction method known as the Kroll process and the calcium hydride reduction process used in Russia.

In reduction processes of titanium tetrachloride, most of the residual chloride is removed by vacuum distillation or by water leaching. The final sponge fines typically contain from 0.12 to 0.15 wt% Cl.

Sodium Reduction Method

Characteristic sponge fines manufactured by the Hunter process are shown in Figure 14.1. A typical chemical analysis of commercial powders is given in Table 14.1. A screen analysis of sponge fines produced by sodium reduction is characterized by the content of the particle size fractions smaller than 105 μm in the amount of 78 wt% and fractions smaller than 64 μm amount of 40.8 wt% [3].

Table 14.2 gives typical technological characteristics of titanium powders and tensile properties of Ti–6Al–4V compacts produced from sponge fines and aluminum–vanadium master alloy.

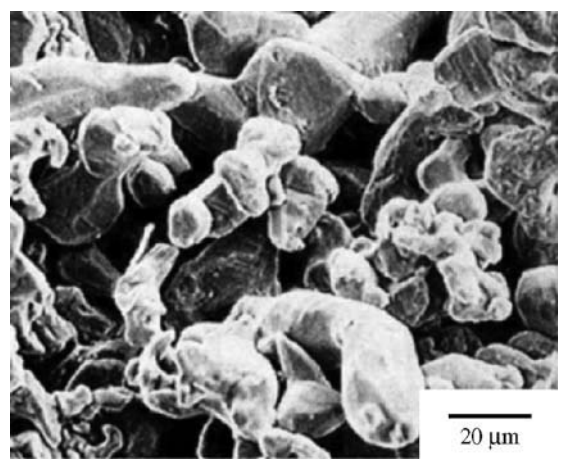

Figure 14.1 Sponge fines produced by the sodium process. (Source: Ref 3®)

Table 14.1 Typical chemical analysis of chemical reduction process titanium sponge fines and sinter compacted Ti–6Al–4V produced from these fines and Al–V master alloy powders

Elements (content, wt%)	Sodium process			Calcium hydride reduction process			Hydride/dehydride process		Electrolytic process
	CP[a]	[b]	CP[c]	CP[a]	[d]	CP[e]	P6/4-3[f]	CP[g]	CP[g]
Al	...	6.2	...	...	4.65	...	5.09	...	...
V	...	4.1	...	...	3.80	...	4.17	...	...
O	0.13	0.24	0.05–0.30	0.19	0.20	0.25–0.30	0.131	0.15–0.30	0.05–0.30
N	0.03	0.016	0.02–0.03	0.06	0.06	0.05–0.06	0.006	0.03–0.05	0.02–0.03
H	0.07	0.002	0.02–0.03	0.34	0.30	0.20–0.40	0.0015	0.06–0.15	0.02–0.04
C	0.02	0.02	0.01 max	0.03	...	0.04–0.05	0.02	0.015–0.020	<0.02
Fe	0.02	0.18	0.01–0.02	0.11	...	0.15–0.20	0.1	0.07–0.10	0.02–0.08
Na	0.10	0.10	...	...	...	...	...	...	...
Cl	0.13	0.12	0.10–0.13	0.004	0.003	0.003–0.005	...	0.06–0.08	0.03–0.08
Si	...	...	0.006 max	0.05	...	0.06–0.07	0.02	0.01–0.02	<0.02
Ca	...	...	...	0.04	0.06	0.08	...	...	...
Ni	...	...	...	0.07	...	...	...	...	...
Cu	...	...	...	...	...	...	<0.01	...	...
Sn	...	...	...	...	...	...	0.01	...	...
Nb	...	...	...	...	...	...	1.17	...	...
Mo	...	...	...	...	...	...	0.01	...	...
W	...	...	...	...	...	...	0.01	...	...
Cr	...	...	...	...	...	...	0.02	...	...
Ti	balance	balance	balance	balance	balance	balance	balance	balance	Balance

CP: commercially pure titanium; [a] source: Ref [3]; [b] sinter compacted Ti–6Al–4V produced from these sponge fines and Al-V master alloy powder, source: Ref [3]; [c] 630 + 180 μm powder sizes, source: Ref [1]; [d] sinter compacted Ti–6Al–4V produced from these fines, source: Ref [3]; [e] 100 + 40 μm (25%), 40 μm (75%) powder sizes, source: Ref [1]; [f] composition of alloys synthesized from blends of CP and master alloy powders; [g] 630 + 80 μm powder sizes, source: Ref 1

Table 14.2 Technological characteristics of titanium powders and sintered compacts produced from these powders

Technological characteristics	Sodium process			Calcium hydride reduction process			Hydride/dehydride process		Electrolytic process
	CP[a]	[b]	CP[c]	CP[a]	[d]	CP[e]	P6/4-3[f]	CP[g]	CP[g]
Tap density (g/cm^3)	...	...	0.9–1.2	...	...	0.95–1.40	...	1.35–1.70	1.4–1.8
Flow rate (s)	...	...	20 max	...	...	15 max	...	75 max	28 max
Yield strength (MPa)	...	868	...	...	865	...	868	...	...
Tensile ultimate strength (MPa)	...	945	...	...	966	...	965	...	...
Elongation (%)	...	15	...	...	13	...	14	...	...
Reduction of area (%)	...	25	...	...	32	...	31	...	...

CP: commercially pure titanium; [a] source: Ref [3]; [b] sinter compacted Ti–6Al–4V produced from these sponge fines and Al–V master alloy powder, source: Ref [3]; [c] 630 + 180 μm powder sizes, source: Ref [1]; [d] sinter compacted Ti–6Al–4V produced from these fines, source: Ref [3]; [e] 100 + 40 μm (25%), 40 μm (75%) powder sizes, source: Ref [1]; [f] composition of alloys synthesized from blends of CP and master alloy powders; [g] 630 + 80 μm powder sizes, source: Ref 1

Powder dispersivity grows with $TiCl_4$ bubbling through the melt, on the surface of which metallic sodium is supplied: the grain size of the basic mass of powder is lower than 20 μm.

More finely dispersed powders are produced by low-temperature reduction of titanium's compounds in organic media using alkaline metals or amalgams as reducing agents.

Magnesium Reduction Method

The titanium sponge produced is the sinter of crystals up to several centimeters in size. It is crushed to a required size. The riddlings (particles finer than 2 mm) are 3–5% of the mass of the sponge produced. They are used in powder metallurgy, in anticorrosive coatings, for production of titanium carbides, nitrides and other compounds. The yield of powder fractions of magnesium-thermal titanium essentially increases if vacuum separation of the reaction mass by hydrometallurgical processing is used. However, the quality of powders in this case is impaired.

Titanium powders can be produced by continuous reduction of $TiCl_4$ with gaseous magnesium in a stream of argon. In this process, the titanium powder and magnesium chloride are continuously carried out of the reaction zone.

To produce titanium powder, mechanical crushing of titanium sponge is used. However, in this case, there are some difficulties connected with the plasticity of high-purity titanium, therefore titanium is preliminarily oxidized or hydrogenated to embrittle it. Such a method is especially interesting for crushing titanium alloys, Ti–Al alloys in particular, produced by aluminothermic reduction of titanium dioxide.

Calcium Hydride Reduction Process

Reduction of titanium dioxide by calcium hydride is carried out at temperatures of 1150–1200°C:

$$TiO_2 + 2CaH_2 = Ti + 2CaO + 2H_2$$

The reaction product is processed by water solution of hydrochloric acid to remove CaO and $Ca(OH)_2$, then the powder is washed in distilled water, rinsed with alcohol and dried at 60–70°C in a vacuum.

Powder particles produced by the calcium hydride process have a spongy morphology similar to sponge fines produced by the sodium process and consist of conglomerations of small particles fused together during the reaction process. The powder produced (size fraction lower than 200 μm) contains up to 90% of particles less than 10 μm in size and has an apparent density of 0.6–0.8 g/cm^3. The powder contains up to 0.05% of calcium as its oxide. The average particle size of commercially pure titanium powder is 41 μm [4].

Table 14.1 shows a typical chemical analysis of commercial powders produced by calcium hydride reductions. Table 14.2 gives typical technological characteristics of titanium powders and tensile properties of Ti–6Al–4V articles produced from calcium hydride reduced titanium and aluminium–vanadium master alloy powders.

Plasma-Rotating Electrode Process (PREP)

PREP is a centrifugal atomization process where the end of a consumable metal bar is melted while being rotated about its longitudinal axis. The molten metal is centrifugally atomized in the form of droplets that solidify in an inert gas atmosphere to spherical powder particles. The consumable electrode can be melted by various energy sources. In the USA, helium plasma is used for producing titanium alloyed powders [3]. The electrodes are prealloyed bars of 60–65 mm in diameter and are rotated at speeds up to 15 000 rpm. Particle size depends on the alloy composition, the electrode diameter and the rotation speed. Typical sizes for Ti–6Al–4V powders are between 100 and 300 μm with a median diameter of about 175 μm. The PREP powder is spherical (Figure 14.2), has good flow characteristics and a tap density about 65% of solid substance. Various process modifications were investigated to produce finer powder [5]. In particular, the rotating electrode process (REP) was combined with gas atomization.

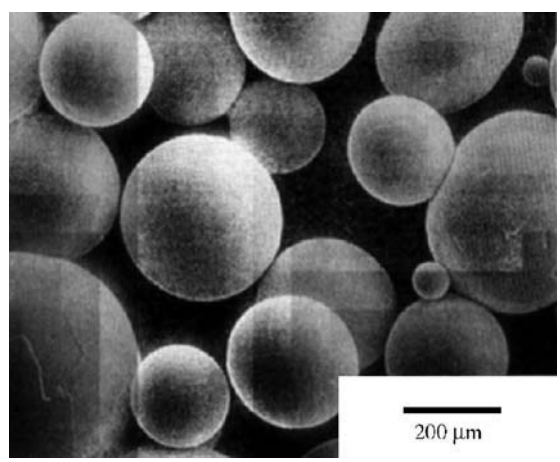

Figure 14.2 Ti–6Al–4V powder produced by the plasma rotating electrode process. (Source: Ref 3®)

The rotating electrode process is also used by similar technologies in Russia, China and Japan [1,3].

This process is discussed in more details in Chapter 5.

The PREP and REP powders are used to produce PM articles in aerospace, gas turbine engineering, environment control and biomedical applications.

Gas Atomization

The plasma atomization process was developed to produce fine spherical titanium powder using titanium wire as the starting material [6]. In this process, the wire is fed into the apex of three plasma torches, where it is melted and atomized in an argon atmosphere. Droplets are then cooled during their flight in argon with a cooling rate in the range of 10^2-10^3°C/s and solidi, forming spherical powder particles. Spherical titanium and Ti–6Al–4V alloy powders with particle size from 5 to 150–250 μm have been commercialized in four grades of differing particle size. The oxygen content depends on particle size and is in the range 0.1–0.3 wt%. The flow rate varies depending on particle size in the ranges from 23 to 200. PyroGenesis Inc. proposes the use of plasma atomized titanium powders for producing porous filters, applications in injection and thermal spray processes and biomedical applications [6].

Plasma melting induction guiding gas atomization (PIGA) is another variation for producing ceramic-free Ti alloy powders using a gas atomization process developed by GKSS Research Centre in Geesthacht, Germany [7]. In this process, a prealloyed rod is introduced into a conical induction coil where the tip of the rod is heated up and, once the melting temperature is reached, the melt drops down into the center of a nozzle. The obtained powder particles are predominantly spherical in shape. The resulting finer 45 μm powders are used in metal injection molding (MIM) and other areas.

Firm Leybold (Germany) has developed a technology to produce spherical powders of titanium and its alloys by melt atomization by inert gas [8]. The metal is melted in induction or electron-beam furnaces. Atomization is performed by argon or on a rotating disk.

For the purpose of decreasing the cost of argon atomized powder manufacture, a pre-mixed raw material consisting of titanium sponge and master alloy chips or granules is used [9]. Sintered MIM compacts using such Ti–6Al–4V alloy powder show that the tensile strength ranges from 810 to 880 MPa and the tensile elongation is around 10%.

For more information see Chapter 5.

Hydrogenation/Dehydrogenation (HDH) Process

The method is based on the reaction of titanium with hydrogen at 350–700°C, the formation of fragile hydrides, their mechanical crushing and subsequent dehydrogenation during 1–2 h at 700–800°C to a powder-form product. A saturation of titanium by hydrogen achieves 2–3.5 wt% depending on the purity of the initial material. The hydrogenated titanium is very brittle and can be simply ground to a fine powder. Mechanical crushing in ball mills allows the manufacture of powders of the required grain size. The disadvantages of the method are difficulties of hydrogen purification from oxygen and nitrogen as well as high sensitivity of titanium to the content of the residual hydrogen, causing fragility.

Typical chemical analysis and technological characteristics of titanium powders and sintered compacts are given in Tables 14.1 and 14.2.

Hydride of electrolytic titanium is distinguished by high purity and is used very effectively as a generator of hydrogen, in particular, in annealing of watch fibers and as an additive to the charge of various metal powders that activates the process of sintering. Crushed titanium hydride can serve as a raw material in production of materials such as titanium carbides, borides, nitrides and silicides.

For reducing the titanium powder cost, the hydrogenation process followed by hydrometallurgical processing was suggested [10]. The processes of dehydration with complete or partial removal of hydrogen was developed.

Amalgam Metallurgy Technique

Titanium tetrachloride is reduced by sodium amalgam obtained by electrolysis with a mercury cathode and graphite anode. The process is carried out in a reactor: titanium tetrachloride is bubbled through the amalgam at a temperature of 88–104°C in an inert atmosphere (helium, argon, neon). The discharged chlorine is used for the chlorination of titanium dioxide producing its tetrachloride:

$$TiCl_4 + 4Na(Hg) = Ti(Hg) + 4NaCl$$

The black powder formed is a mixture of titanium, mercury, sodium and sodium and titanium chlorides. Mercury is removed in a vacuum furnace (vacuum of $1–10^{-2}$ Pa) or in an inert atmosphere at 208–370°C. A mixture of titanium, its chlorides $TiCl_2$ and $TiCI_3$ and sodium chloride remains after

distillation. NaCl is separated from the mixture in the inert atmosphere at 815–1093°C. $TiC1_4$ reduction by mixed sodium-potassium amalgam is carried out at 650°C. Low titanium chlorides decompose and, at a lowered pressure, are removed. Sodium chloride is concentrated on the walls and titanium crystals form a sponge. An advantage of the method is production of particles of small size (1–10 μm) and high purity of the titanium sponge.

The amalgam metallurgy fundamentals are discussed in Chapter 9.

Electrolysis of Titanium Compounds

In the 1960s and 1970s, great attention was paid all over the world to titanium production by electrolysis of titanium halogenides (mainly, chlorides and fluortantalates) and titanium oxides (TiO_2, Ti_2O_3, etc.). However, the obtained electrolytic powder had a purity less than magnesium reduction powder so it did not gain commercial use.

The researches were carried out using chloride electrolytes based on chlorides of alkaline and alkaline-earth metals (KCl–NaCl, KCl–NaCl–$MgCl_2$). Difficulties of $TiCl_4$ and TiO_2 electrolysis (main kinds of Ti raw material) are connected with their low solubility in chloride solutions (<1%). At the same time, it was possible to manufacture fine titanium powders on the cathode at low current yields due to special construction designs for $TiCl_4$ (bubbling) and TiO_2 (hashing) disintegration.

The use of fluoride electrolytes increased the solubility of $TiCl_4$ and TiO_2 in the melt; however, in this case all the hardware-technological circuit of the electrolysis becomes very complicated and economically unprofitable.

One of the prospective electrolysis techniques, a two-level method of electrolysis, is considered. In this method, at the beginning, reduction of titanium tetrachloride in the melt to the tri- and bivalent condition at a low current density is carried out and then the current density is raised and titanium is precipitated on the cathode. Researches on primary titanium electrolysis (with insoluble anode) are being continued at present [11].

A new, electro-deoxidation (EDO) titanium powder process is currently being developed and is based on a technique invented at Cambridge University known as the FFC Cambridge Process [12]. The EDO process uses molten salt electrolysis to convert metal oxide into the pure metal. Unlike conventional electro-refining, in the EDO process, the metal oxide is not dissolved in the electrolyte, it is sintered into a ceramic material that then becomes the cathode of the electrolytic cell. During electrolysis, oxygen is extracted from the cathode and given off through the molten calcium chloride electrolyte on the anode. As the anode is made of graphite this is consumed in the process and mainly carbon monoxide is given off. At the end of the process cycle, the cathode is converted into oxygen-free metal.

The titanium alloys can be also made using the EDO process by means of adding oxides of the alloying additions to the initial oxide mixture used to make the cathode. These are mixed in the given quantities such that, after reduction, the metals are in the correct proportions for the alloy. A large range of standard titanium alloy has now been made in this way.

The process gives near-spherical titanium powder in the size ranges 20–250 μm in diameter. The powder particles are porous with a slightly irregular surface. The flowability of the dry powder is between that of atomized and HDH powders. Such a particle shape is favorable for good green strength in processes such as press and sinter or MIM.

Electrolytic Refining of Titanium

The technological circuit of the electrolytic process is shown in Figure 14.3 [13].

By anode dissolution of titanium metal, its waste products or alloys and cathode sedimentation of crystalline titanium, a titanium powder characterized by low content of impurities (Fe, Si, C, O, N, etc.) is produced. There are conditions where powders alloyed with aluminum, chromium, vanadium, manganese, zirconium and other metals can be produced.

Raw materials for anodes are: substandard titanium sponge; alloys based on titanium; conducting products of titanium raw material reduction (oxycarbides, oxycarbonitrides, etc.). The electrolyte is the molten NaCl, or NaCl + KCl, or NaCI + KCl + $MgCl_2$.

The preparation of the electrolyte consists of tetrachloride $TiCl_4$ reduction in molten NaCl and KCl using titanium scrap or sodium. Titanium ions are reduced to metal stepwise on the cathode; on the anode titanium is oxidized up to Ti^{2+} and Ti^{3+}. An average degree of oxidation (valency of titanium ions) in the electrolyte is 2.2–2.3.

The process of titanium refining was carried out in electrolyzers of VAMI design (Figure 14.4).

The electrolyzer is a two-cell device with a common heating furnace. Each cell consists of a retort with a bulk anode container and a cathode chamber hermetically connected with the retort. Both cells are electrically connected in parallel.

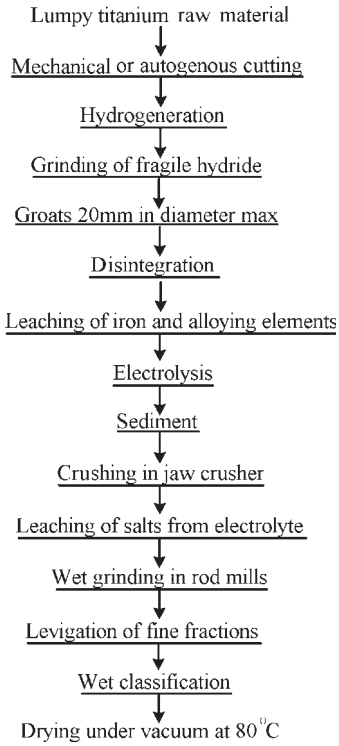

Figure 14.3 Technological scheme of titanium powder production by the method of electrolysis with soluble anode (electro-refining).

The cathode chamber is supplied with mechanisms for moving the cathode and for cutting off the deposit as well as the device for additional loading of the anode material, which consists of bunkers with feeders and discharge spouts with shutters. The device for unloading of the anode material in the form of a mobile tray with a folding bottom and the metal receiver are mounted on the retort. The cathode is freely suspended from a top bridge with shear device, which is connected with the elevating screw mechanism.

During electrolysis, the cathode is immersed in the electrolyte; a current supplying unit placed in the chamber performs the current feed to it. For deposit removal, the cathode is raised to the extreme top position and then is stopped; the top bridge falls downwards on the cathode and cuts off the deposit, which falls into the tray. Then the top bridge is raised, the cathode is released and dipped in the electrolyte and the cathode current circuit is closed.

The whole cycle of processing metal waste products, starting from the loading of the initial raw material and finishing by the unloading of the end product, is conducted inside the electrolyzer without breaking its leak-tightness under a small excess pressure of the inert gas.

Impurities not dissolved at the anode are collected in the anode slurry and are periodically removed from the electrolyzer by overspill through a tap-hole.

The current strength in the electrolyzers of VAMI is 10–15 kA. The capacity of the electrolyzer for titanium refining is 120–180 kg/day (of metal).

When using melt based on the KCl–NaCl mix with a content of 2–6% titanium and a temperature of 800–850°C, the cathode current density is maintained in the interval of 5–15 kA/m^2 and the anode current density is 4–8 times lower. Current yield counted as Ti^{2+} is 90% and the specific charge of electric power is 10–11 kW·h/kg. Titanium extraction under these conditions amounts to 95–96%, with the consumption of the electric power directly to electrolysis of 4.0–5.0 kW·h/kg.

A high purity of powder purification is achieved with respect to iron, nickel, tin, molybdenum, silicon, nitrogen, oxygen and carbon.

The powders produced by electrolytic refining are more plastic than the powders produced by hydrogenation/dehydrogenation of the same titanium waste products. The method of electrolytic refining is realized at experimental industrial plants in Russia.

Physical and chemical characteristics and technological properties of the various kinds of titanium powders are shown in Tables 14.l and 14.2.

In working with powders of chemical active metals, their transport, storage and processing carries a danger of ignition and explosion. To low the reactivity of powders various methods of passivation are used (Table 14.3).

Other Methods

Method of Disproportionation of Lower Titanium Halogenides

Low titanium halogenides ($TiCl_2$, $TiCl_3$) disproportionate with the formation of metal powder under certain conditions of atmosphere, temperature, and pressure. The process consists of transfer of low titanium halogenides of scrap metal or ores to titanium tetracloride ($TiCl_4$) at high temperatures.

During the process, the formed low chlorides are condensed in the colder zone of the furnace and, on heating, they disproportionate with the formation of highly dispersed titanium powder and titanium chloride which is returned to the beginning of the process. The produced powder is suitable for powder metallurgy.

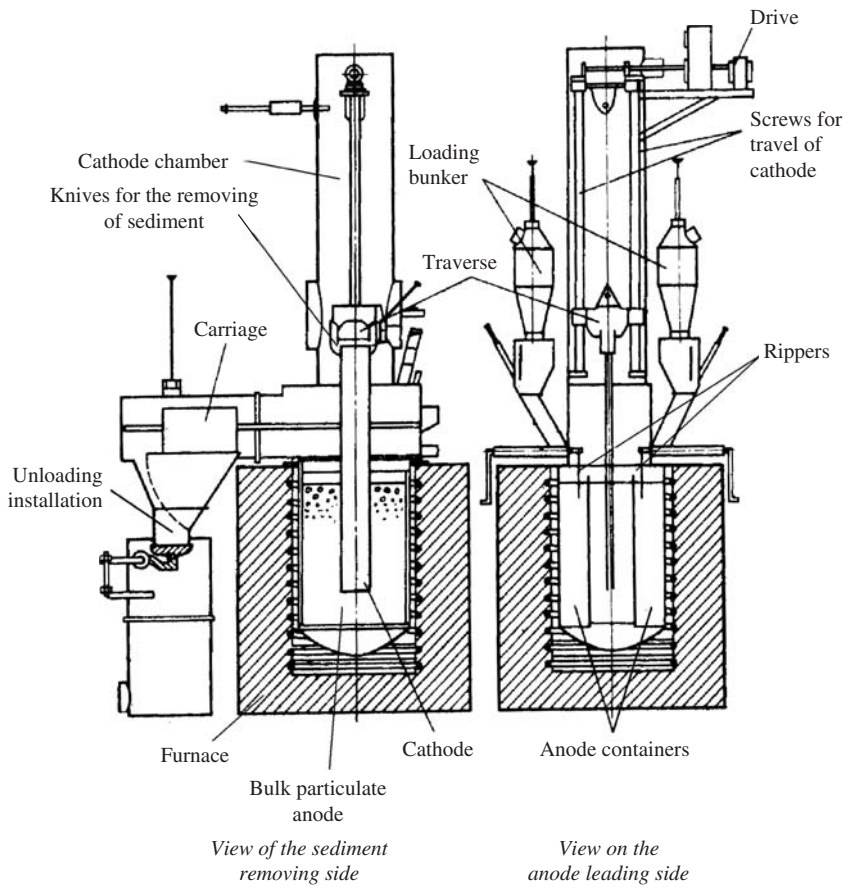

Figure 14.4 Electrolyzer with bulk anode for producing titanium powder.

Mechanical Alloying

The use of mechanical alloying to produce titanium-based alloys is relatively recent. The process is a simple technique to synthesize both equilibrium and non-equilibrium phases of materials starting with elemental powders where, generally, a mix of powders is processed in a high-energy ball mill [14]. Much of the work at present consists of the development of unique structural characteristics such as supersaturated solid solutions, metastable crystalline phases, amorphous phases, dispersion-hardened alloys and nanostructured materials [14–16]. Mechanical alloying is also being studied as a technique for the manufacture of nanostructured intermetallic composites such as Ti–6Al–4V/SiC [17]. A mechanical alloying process was used to synthesize $Ti_{45}Zr_{38}Ni_{17}$ powders for plasma thermal spraying [18]. The elemental powders mechanically alloyed by a planetary ball mill are led to an amorphous state. This amorphous phase primarily appeared in the thermally sprayed mechanically alloyed powders and is transformed into the icosahedral quasicrystal phase after annealing at 555°C. The Vickers hardness for the quasicrystal layers was about 7 GPa.

Applications

Titanium powders that have unique properties are used as alloying, refining and modifying components in the production of metals and alloys in ferrous and non-ferrous metallurgy. They have high chemical resistance to many organic and inorganic aggressive matters at normal and high temperatures. The high-temperature strength, good plasticity at low density and high corrosion resistance of titanium surpass many constructional and composite materials. The properties of titanium are realized most fully, and with high economic efficiency, by titanium powders. They are used as a basis of charges for production of refractory and composite materials and catalysts.

Table 14.3 Prevention of combustion of titanium powders

Manufacture	Branch of industry	Technique of powder passivation
Production of refractory compositions and materials on their base	Non-ferrous metallurgy, chemical and instrumental	Processing in acid solutions; high-temperature surface saturation; additives of aluminum oxide, nitrogen or carbon to argon plasma with dehydration
Production of friction materials by powder metallurgy	Engineering, petrochemical, etc.	Processing in aluminate solutions; processing by organosilicon composition liquids
Manufacturing of protective materials and coatings	Non-ferrous metallurgy, food and chemical	High-temperature oxidation (combustion synthesis, consists of solid-phase reaction of titanium with titanium dioxide mixture). Use of epoxy resins for powder passivation
Production of sorbents and gas absorbers, and pyrotechnic compositions	Nuclear plant, electronics, pyrotechnics	Processing in acid solutions with addition of the spirits; surface metallization by cementation or electrochemical copper plating; insertion of metals into argon plasma during dehydration
Manufacturing of sintered constructional and porous materials	Non-ferrous metallurgy, mechanical engineering	Processing in acids and solutions of halogenides; electrochemical and plasma-chemical surface metallization

Titanium powders are readily formed and sintered; products so made possess high corrosion resistance, strength and relative lightness. They are used for producing constructional details in mechanical engineering, ceramic-metal porous filters, welding and smelting electrodes and gas absorbers in various designs of electronic vacuum devices. Titanium powders are widely used as fillers of anticorrosive coatings based on epoxy resin, in the production of titanium carbide and nitride and in other fields of industry. One application field for powders of titanium and its alloys is the aviation industry.

Cases and bracelets for watches, surgical tools, prostheses, frames of lenses, weapon details, etc. are produced from titanium powders by the powder metallurgy processes.

Porous elements are applied as filters in various designs of cartridge filters, aerators in devices of regeneration and flotation saturation and in devices for biological purification of sewage [11]. They are used as filtering elements, in drainage devices, as gas absorbers and fire-resistors, dehumidifiers and oil separators. Elements can be welded by argon-arc, contact and diffusion welding and can be processed using metal-cutting machine tools.

Despite its high cost in comparison with traditional permeable materials, titanium elements are used with high economic efficiency due to high strength, exceptional corrosion resistance, biological inertness, low density and, additionally, filters can easily be regenarated, do not adversely affect the solutions being filtered, reduce losses and allow the pressure and rate of filtration or aeration to be increased.

Depending on the particle size of the initial powder, the parameters of pressing and sintering, permeable materials from titanium powders have the basic pore diameter between 25 and 200 μm, porosity of 30–50%, the minimal factor of permeability for various groups of products range from 1.0 to 2.5 mm/s.

The main mass of fine and medium titanium powders is used in the production of refractory compounds, particulate-reinforced titanium matrix composites and metal–polymer anticorrosive compositions. Using self-propagating high-temperature synthesis (SHS-process), it is possible to produce titanium carbide containing 79.3–79.6% of titanium, 18.12–19.42% of combined carbon and 0.18–0.28% of free carbon with high economic efficiency. The best results are achieved when using titanium powders finer than 0.1 mm.

Powders of coarse fractions are used mainly as briquettes between 20 and 100 mm in diameter and 20–30 mm in height in ferrous metallurgy. Thus, only a part of the low-grade spongy titanium, which has not been converted to powders of average and fine fractions, is used in ferrous metallurgy. Besides, due to the high density of briquetted titanium and the small size of briquettes, the waste in their use is approximately in 1.5 times lower than in direct use of spongy titanium. Batching and mechanization of briquette insertion into the molten steel is easily carried out.

References

1. S.S. Naboychenko, (ed.), *Handbook of Non-Ferrous Metal Powders*, Metullurgiya, Moscow, 1997 (in Russian).
2. Froes, F.H., Eylon, D., Powder metallurgy of titanium alloys. *Int. Mater. Review*, 1990, 32(3):162–182.
3. J.H. Moll, C.F. Yolton, Production of titanium powder. In *ASM Handbook*, Vol 7, *Powder Metal Technologies and Applications*, ASM International Publishers, 1998, pp. 161–166.
4. Moxson, V., Senkov, O.N., Froes, F.H., Production and characterization of titanium powder products for environmental, medical and other applications. In *Proc. Advanced Particulate Materials & Processes*, eds F.H. Froes, J.C. Hebeisen. American Powder Metallurgy Institute, 1997, pp. 387–394.
5. Nachtrab, W.T., Roberts, P.R., Newborn, H.A., Powder metallurgy of advanced titanium alloys. *Key Eng. Mate*, 1993, 77–78:115–140.
6. Smagorinski, M.E., Tsantrizos, P.G. Production of spherical titanium powder by plasma atomization. In *Proceedings of PM TEC 2002 World Congress*. Metal Powder Industrial Federation, Princeton, NJ, USA, 2002, pp. 3-248–3-260.
7. Limberg, W., Aust, E., Ebel, T., Gerling, R., Ogee, B. Metal injection moulding of an advanced bone screw 7Nb alloy powder. In *Proceedings of PM 2004 World Congress*, European Powder Metallurgy Association, 2004, 4, pp. 457–462.
8. Hohman, M., Bilkehor, L., *Ertl, M., TIZ – Fachber*, 1990, 114(2):111–119.
9. Fujita, M., Arimoto, N., Nishioka, K., Miura, H. New process for Ti alloy powder production by using gas atomisation. In *Proceedings of 2006 Powder Metallurgy World Congress*, Korean Powder Metallurgy Institute, Busan, Korea, 2006, pp. 12–13.
10. Griga, J., Petrunko, A., Drozdenko, V., Andreev, A., Yatsenko, A., New types of titanium powders: properties and applications. In *Proceedings of PM 2004 World Congress*. European Powder Metallurgy Association, 2004, 1, pp. 249–253.
11. Ginatta, M.V., Orsello, G., Perotti, P., Beruti, R., A newly designed plant for the electrowinning of titanium from molten salts. In *Proc. of Sixth. World Conf. on Titanium*. Societe Francaise de Metallurgie, 1995, pp. 753–757.
12. Ward-Close, C.M., Godfrey, A.B., Tompson, S.R., Advances in titanium alloy powder. In *Proceedings of PM 2004 World Congress*. European Powder Metallurgy Association, 2004, 1, pp. 261–266.
13. Gopienko, V.G., Ivanov, A.I., Ustinov, V.S. et al., Electrolytic refining of titanium. In *Proceedings of the Third International Titanium Conference*, Moscow, VILS, 1977, Vol. 1, pp. 77-83.
14. Froes, F.H., Suryanarayana, C., Powder processing of titanium alloys. *Rev. Part. Metals*, 1993, 1:223–275.
15. Ahn, J., Lee, K., Preparation of Ti-base intermetallic compounds by mechanical alloying. *Mater. Trans. JIM*, 1995, 36(2):297–304.
16. Overcoglu, M.L., Senkov, O., Srisukhumbowornchai, N., Froes, F.H. Microstructural evolution of a nanocrystalline Ti-47. 5Al-3Cr in the annealing range 725°C–1200°C produced by mechanical alloying and hot isostatic pressing. In *Proceedings of PM World Congress*, EPMA, 1998, pp. 305–310.
17. Chen, X., Baburaj, E.G., Froes, F.H., Vassel, A., Ti-6Al-4V/SiC composites by mechanical alloying and hot isostatic pressing. In *Proceedings of Advanced Particulate Materials & Processes*. American Powder Metallurgy Institute, 1997, pp. 165–192.
18. Takasaki, A., Uematsu, S., Kelton, K.F., Ti-based quasicrystal layers produced by plasma thermal spraying. In *Proceedings of 2006 Powder Metallurgy World Congress*, Korean Powder Metallurgy Institute, Busan, Korea, 2006, pp. 51–52.

Chapter 15

Production of Magnesium and Magnesium Alloy Powders

Victor G. Gopienko, Russian National Aluminum-Magnesium Institute, Saint Petersburg, Russia

Magnesium is a reactive material, as are aluminum and titanium (Table 15.1). Heat of formation, ΔH_0, of magnesium oxide equals 603.2 kJ/mol. Magnesium is potentially explosive in powder form. The lower explosive limit of the powder with particles smaller than 74 μm amounts to 10 g/m^3 and the rate of pressure rise equals 6.3 MPa/s (see Chapter 24). The development of the production methods should take these features of magnesium into account.

The basic methods of magnesium powder production are: mechanical crushing (scratching of an ingot from magnesium card tape fixed on a rotating drum, milling of an ingot), atomization of molten metal, evaporation–condensation and electrolysis.

Mechanical Crushing

The first industrial production of magnesium powder was organized for pyrotechnic purposes in the early twentieth century in Germany. The method consists of scratching a magnesium ingot by a cord tape fastened on a rotating drum.

The machine tool intended for this process, 'kratz-machine', has been improved for a long time. Powder dispersivity is adjusted by the speed of magnesium plate feeding, the speed of drum rotation and the diameter of cord tape needles. The drum also moved along its axis to enable all of the plane of the plate to be processed uniformly. Abrasion uniformity is provided by a continuous back and forth motion of the plate, which entered into the case of the machine tool through a special aperture. The cord tape was reeled on a steel drum. The diameter of the drum was 200 mm; the distance/speed on the surface was about 1000 m/min. The thickness of the magnesium plate was 40 mm, its width was 350 mm. The minimum diameter of the card tape needles was of 0.64 mm.

To prevent sparking while the needles were falling out from the tape, the case of the 'kratz-machine' was manufactured from aluminum–magnesium alloy. The received powder is stored in a box, which is installed in the casing of the 'kratz-machine'.

The finest magnesium powders – 'unfulbar' (intangible by touch) – were produced by additional crushing of the powder manufactured in the 'kratz-machine' in ball mills in an atmosphere of carbon dioxide.

Magnesium chips and grit are also produced by cutting cylindrical blanks 200–300 mm in diameter in a lathe using a special sawtooth cutter. The average particle size is 1 mm; the content of particles smaller than 0.75 mm in size is not higher than 35 wt%. The capacity of the machine tool is 8.8–15 kg/h.

Along with other methods, a method to produce magnesium powders by milling of an ingot with subsequent crushing of the chips in a grinding machine and a hammer mill is applied in the USA. This method is more efficient than the above method of producing powders with the help of the card tapes.

Special machine tools equipped with vertical and horizontal cutters are used (Figure 15.1). The produced chip-shaped powder is sucked into the catching system, precipitates in a cyclone and is divided by a screening machine to commodity fractions by particle size. The smallest fractions are caught by an oil filter placed in front of a ventilator. When necessary, powders are exposed to rolling in a ball mill for obtaining particles with a spherical shape.

Characteristics of the powders produced by the method of mechanical grinding are given in Table 15.2.

Powders of MPF grade (milled) contain not less than 99.5% Mg in magnesium powder and not more than 0.05% Fe, 0.005% Cl and 0.1% of moisture (in weight).

Table 15.1 Properties of reactivity of Mg in comparison with Al and Ti

Material	Density (g/cm^3)	Melting point (approximate) (°C)	Boiling point (°C)	Heat of fusion		Specific heat capacity		Combustion[a]	Heats of formation oxides		
				kJ/mol	kcal/mol	J/g ^{0}C	cal/g °C	°C	Oxide	Heat of formation (ΔH_0)[b]	
										kJ/mol	kcal/mol
Magnesium	1.74	649	1090	8.954	2.139	1.04	0.248	3100	MgO	−603.2	−144.090
Aluminum	2.70	660	2467	10.790	2.577	0.9	0.215	3500	Al_2O_3	−1691.5	−404.080
Titanium	4.51	1660	3287	20.9	4.99	0.52	0.124	3000	TiO_2	−955.9	−228.360

[a] Source: Ref 1. [b] The adiabatic combustion temperature in oxygen at 100 kPa pressure.

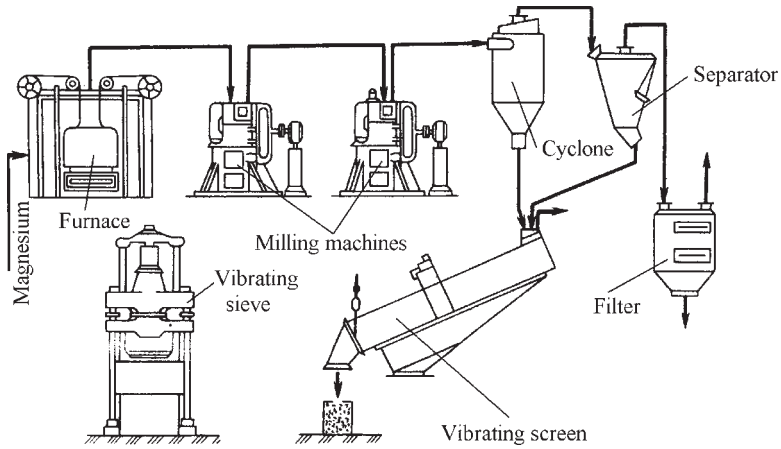

Figure 15.1 The hardware-technological circuit of magnesium powder production.

Melt Atomization

Magnesium powders produced by melt atomization with inert gas are polydisperse and have a particle size from several microns up to 0.5–1 mm. The hardware for the atomization is similar to that used for producing aluminum powders. Powders are classified into required fractions according to particle size.

The technology developed in VAMI consists of atomization of the melt by jets of nitrogen with an oxygen additive of 3 ± 0.1 wt%, the melt temperature being 50–70°C higher than the melting point of magnesium or its alloy. An optimum relation between the temperature of the melt and atomizing gas, the pressure of the gas, the ratio of gas to metal mass flow and other parameters, as well as the optimum hardware-technological circuit of production provide fire and explosion safety during the manufacture. Magnesium powders with particle size smaller than 200 μm ranging from spherical (particles smaller than 50–100 μm) to oval (larger particles) are produced by this technology.

Gas-phase Method

A high steam tension of magnesium vapor allows the use of the method of magnesium evaporation and vapor condensation for the production of fine magnesium powders.

The design of a continuous action device for producing magnesium powders by the condensation of its vapor in a vacuum or a rarefied atmosphere of inert gases is described in [2]. Vapor is condensed on a cooled brass drum 220 mm in diameter, its rotation speed being controlled; a special knife cuts off the condensate. A graphite crucible containing the melt is closed by a cover with an adjustable slot. Mixing of vapor with the inert gas takes place in a special branch pipe. An end face of a branch pipe is placed close to the rotating surface of a crystallizer. Heating of the crucible is inductive. To produce magnesium powder with particle size smaller than 1 μm, the temperature of the melt was 720°C, the gas pressure was 13.3 Pa and the rotation frequency of the condenser was $0.75\,\text{min}^{-1}$. Powder particle size at a constant pressure increases with the increasing temperature.

Key parameters determining hardware registration of the process are: the temperature of metal evaporation and condensation, nature and pressure of the inert gas and the method and the rate of condensate removal from the condensation zone. Characteristics of magnesium powders are given in Table 15.2.

Production of Magnesium Granules

Granulated magnesium is produced at the Kalush magnesium factory in Ukraine by atomization of the melt with the use of a salt flux for the protection of the metal against oxidation (Figure 15.2).

The atomizing chamber, in which the dispersion of magnesium and cooling and collection of the formed granules are carried out, has an internal diameter of 3.2 m. In the center of the chamber is a spinning-cup with punched walls, its rotation speed is in the range from 800 to 1600 rpm. The melted magnesium is introduced from the furnace into the granulator by a siphon. Simultaneously, the salt flux protecting magnesium from oxidation is admitted into the granulator. Melt droplets falling into the chamber are met by a counter air stream and solidify in flight. With the help of a screw and the pneumatic transport, the produced granules are removed from the

Table 15.2 Properties of typical commercial grades of magnesium powders

Type	Chemical requirements (wt%) max			Apparent density (g/cm^3)	Particle size distribution (μm)	Source
	Mg	Alloying elements	Admixture			
Turnings and chips						
MPF-1	99.5 min		0.05 Fe; 0.005 Cl; 0.1 moisture	0.36–0.47	500–μm, max[a]; 250–450 μm, basic fraction	SUAL
MPF-2	99.5 min		0.05 Fe; 0.005 Cl; 0.1 moisture	0.38–0.45	450 μm, max[a]; 140–250 μm, basic fraction	SUAL
MPF-3	99.5 min		0.05 Fe; 0.005 Cl; 0.1 moisture	0.40–0.45	250 μm, max[a]; 100–180 μm, basic fraction	SUAL
MPF-4	99.5 min		0.05 Fe; 0.005 Cl; 0.1 moisture	0.45–0.49	160 μm, max[a]; 100 μm, basic fraction	SUAL
LNR 11	99.5 min	...	...	0.4	1000–3000	ECKA
LNR 15	99.5 min	...	...	0.5	300–600	ECKA
LNR 16	99.5 min	...	...	0.6	3000–4000	ECKA
AZ91D	90	9Al-1.0Zn	...	0.6	1000–3000	ESKA
C	99.5 min	...	...	0.30–0.35	1500×1500×2000	PMTN
Powders						
PF 01/91	99 min	...	...	0.9	315–630	ECKA
PF 91/51 Type III	99.5 min	...	...	0.7	100–315	ECKA
PK 31 Type IV	97 min	...	...	0.5	<71	ECKA
MF 600/100	99.5 min	...	...	0.80 ± 0.05	>425 μm amounts 52 ± 5 wt%; >250 μm amount 97 ± 5 wt%; <45 μm totals 3 ± 3 wt%	PMTN
MF 250	99.5 min	...	...	0.60 ± 0.05	>250 μm amounts 2 ± 1 wt%; >150 μm amount 42±5 wt%; >106 μm amounts 75 ± 5 wt%; >63 μm amounts 92 ± 3 wt%; >45 μm amounts 98 ± 1 wt%; <45 μm totals 2 ± 1 wt%	PMTN
MF 90	99.0 min	...	...	0.55 ± 0.05	>63 μm amounts 40 ± 5 wt%; >45 μm amounts 85 ± 5 wt%; <45 μm totals 15 ± 5 wt%	PMTN
VDM-1[b]	94.6 min	...	...	...	1 μm, basic fraction	SUAL
VDM-20[b]	97.7 min	...	...	...	20 μm, basic fraction	SUAL

[a] Maximal size is considered when the sieve residue does not exceed 0.3% of the total mass of sieved particles; [b] produced by inert gas condensation technique; companies producing the commercial powders: SUAL: 'Siberian–Ural Aluminium Company' (Russia), ECKA: Eckart-Werke (trading companies – Eckart Austria and Eckart Switzerland); PMTN: Pometon S.p.A.

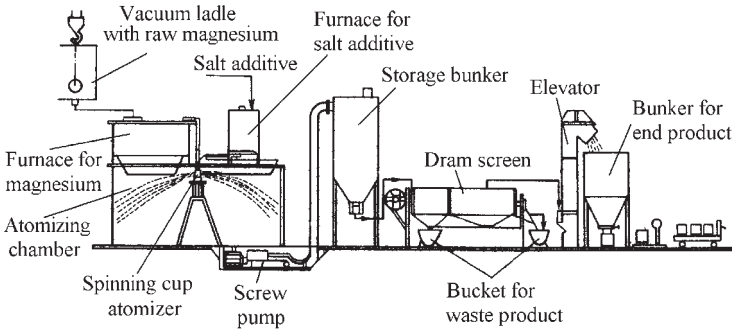

Figure 15.2 Device for producing granulated magnesium.

chamber and sieved into size fractions. The fraction 1.6–0.5 mm is the commercially useful fraction, yield of which is higher than 90–95%. The apparent density of granules is 0.85–0.95 g/cm^3. The capacity of the device is of 8000–10 000 tonnes per year.

Granules contain from 80 to 96 wt% of active magnesium, the rest is an oxide-salt film, which can be separated from metal particles by abrasion, screening or by dissolution of the crushed salt phase, after which the content of active magnesium in granules achieves 98.5–99.5 wt%.

In Russia, devices for producing large granules (5–20 mm in diameter) by the atomization of molten magnesium in a fusible mix of alkaline chlorides and alkaline earth metals are used.

The molten magnesium is atomized on the surface of a fusible salt melt at a temperature of 450–550°C, metal drops solidify into granules from 3 to 25 mm in size and emerge on the melt surface, whence with the help of a scoop with a perforated bottom, they are separated from the salt melt and are thrown into a rotating cooler drum. Granules at a temperature of 200–250°C are admitted into a drum-type screening device for the separation of the commodity fraction (5–20 mm in diameter). The commodity fraction contains 1.5–2.0% of salts.

The productivity of the device as a saleable fraction is from 1200 to 1500 kg/h with a yield of 90–92%. It was found that the temperature of the molten salt (the temperature of the melted magnesium was maintained automatically in the interval 710 ± 10°C) exerts a principal influence on the saleable fraction yield. A maximum is observed at temperatures of 500–550°C; when the salt melt temperature is raised to 600°C the fraction of +15 mm consists almost completely of non-spherical particles.

For manufacturing smaller granules, a spinning cup running at rotational speeds from 3000 to 10 000 rpm is used [3]. Yields of granules almost free of the dangerous −100 μm are obtained. Magnesium granules for flares were manufactured in several similar systems in the USA at rates of 1 t/h.

In the 'Avisma – titanium-magnesium integrated works' company (Russia), granulated magnesium is produced by a technique consisting of preparation of the melt of magnesium or its alloys together with the salt mix, and insertion into the melt of a dispersing agent (silicon oxide) with active stirring of the melt for metal dispersion in it. Then, the melt is cooled to a temperature below the melting point of the metal and granules are taken out from the melt. The extracted granules are separated from solid chloride salts by screening.

The granulated magnesium has roundish particles. The material is not caked and has a good flowability that provides good pneumatic transport in the technological process. In granulated magnesium, pellet particles and extraneous mechanical inclusions are absent.

Granules are also produced from alloys of magnesium with aluminum, zinc, titanium and other elements.

Granules of magnesium consist of 90–95% of spherical particles 0.5–2.0 mm in diameter; the content of particles of other shape (needles, etc.) should not exceed 10% as a greater amount reduces the flowability of the material.

Application of such granulated magnesium is effective for desulfurization and modifying of pig-iron, thermo-chemical, thermo-acid processing of oil wells in the oil-extracting industry and magnesium-organic synthesis of polyorganosiloxanes.

Coarse spherical granules of magnesium are produced in 'Avisma' by technology based on the disintegration of liquid-metal magnesium jets in a molten salt. Molten metal, in the form of the jets of the required diameter moving with a set speed, is inserted into the salt melt, the temperature of which is lower than the temperature of magnesium crystallization. Fluctuations of internal pressure are created in the metal jets and, with the help of the magneto-hydrodynamic method (MGD), they are transformed

into fluctuations of the jet surface resulting in their disintegration into drops of equal size. Drops are cooled to ambient temperature and separated from molten salt as granules.

The technology produces granules of magnesium and magnesium alloys of predetermined size in the range from 3 to 30 mm in diameter. The obtained granules are characterized by a dense structure, they contain up to 98% of metallic magnesium and not more than 2% of chloride. Apparent density of the product is 1.1 g/m^3.

Coarse spherical granules of magnesium of 5–15 mm in diameter are used for production of organosilicon compounds by the method of continuous magnesium-organic synthesis. It is necessary to use large and, therefore, heavy granules, because granules of smaller sizes and thus of a small weight are carried away with the products of synthesis and increase the explosion hazard of the process due to secondary reactions with the formation of hydrogen. Such granules have a dense structure and a high content of the basic component – magnesium.

A new method of producing fine spherical granules of magnesium was developed in 'Avisma' and OS 'RITM' (Russian Institute of Titanium and Magnesium). This method is based on capillary disintegration of magnesium jets under the action of regular fluctuations of the pressure created in the metal by the MGD method. In this technique, the inert atmosphere is created only during jet disintegration and drop spheroidization. Further, the drops get into the air atmosphere where they are finally crystallized and cooled down to the required temperature. The method is economical and it does not demand a hermetic chamber. The method produces granules of the set size ('monodisperse granules') between 0.3 and 30 mm in diameter. Granules have a shining metal surface and a spherical shape. The apparent density of the granules is 1.0–1.1 g/cm^3. The content of metallic magnesium is 99.7% min.

A magnetic field facilitates the refining of a granule structure and hence expands the area of their usage not only as a chemical reagent (ferrous and non-ferrous metallurgy, chemical industry, etc.), but also in powder metallurgy for producing high strength materials by virtue of their low density. Such products are potentially suitable for mechanical engineering applications – in the first instance in aviation and space technology.

Avisma and RITM have developed a new method of atomizing the molten magnesium by a magnetodynamic method in air. This is based on the discovery that magnesium droplets do not ignite in a strong magnetic field. The technology produces monodisperse granules of equal size, shape and weight with average characteristics varying within the ranges: weight of one granule: from 0.1 to 20 mg; size of granules (diameter of the head part): 0.3–3.0 mm; length of the granule: 1.5–15 mm; apparent density: 0.3–0.9 g/cm^3; content of metallic magnesium: over 99.5% or over 99.8%. The technology is used at the Solikamsk magnesium factory.

Applications

Powders and granules of magnesium and their alloys find various applications in modern technology, the main ones being:

- modifying metallurgical properties of metals, such as in the production of wrought steel and the removal of sulfur from hot iron products of blast furnaces
- manufacture of Grignard reagents, which are organometallic halides such as ethyl magnesium chloride (C_2H_5MgCl) that are used in organic synthesis to produce pharmaceuticals, perfumes and other fine chemicals
- chemical reduction, as in the manufacture of beryllium and uranium
- additives in electric welding electrode flux
- action as a light source in flares and photoflash bombs
- production of constructional purpose details in cases where only magnesium alloy powders and granules are applied
- as an initial material for producing construction products by the technique of the so-called thixotropic shaping: a new version of casting under pressure.

Nowadays, the basic consumer of granulated magnesium is ferrous metallurgy where granulated magnesium in the pure state or as mixes with lime and calcium carbide is applied for out-of-furnace pig-iron desulfurization. Granulated magnesium with a salt coating is applied in the pure state due to fire-explosion safety that provides the maximum effect.

Granulated magnesium is also applied in the structure of so-called 'powder' wire used for desulfurization of pig-iron by insertion of a wire into a ladle of melted pig-iron.

Granulated magnesium with a salt coating is used in the production of high strength spheroidal graphite cast iron.

Granulated magnesium is used for production of master alloys such as iron–silicon–magnesium and directly for intra-tuyere modifying of pig-iron amounting to a mechanical mix of granulated magnesium with ferrosilicon.

Granulated magnesium with salt additives can be effectively used as a source of hydrogen production.

Granulated magnesium of various coarseness (from 1 to 20 mm) is used in the development of effective technologies for the synthesis of silicon-organic monomers.

There is expected to be a consumption growth for fine granules of magnesium alloys in the production of computers, mobile phones, in the motor industry, where manufacture of thin-walled details by the methods of thixomoulding is required. The efficiency of this method significantly depends on the method of granule production, their structure and size.

References

1. Claeys, S., Lampman, S., Specialty applications of metal powders. In *ASM Handbook*, Vol. 7, *Powder Metal Technologies and Applications*. ASM International Publishers, 1998, pp. 1083–1092.
2. Frishberg, I.V., Kvater, L.I., Kuzymin, B.P., Gribovskii, S.V., *The Gas-phase Method of Preparing Powders*. Anoka Publishers, Moscow, 1978 (in Russian).
3. Dunkley, J.J., Atomization. In *ASM Handbook*, Vol. 7, *Powder Metal Technologies and Applications*. ASM International Publishers, 1998, pp. 35–52.

Chapter 16

Production of Copper and Copper Alloy Powders

Stanislav S. Naboychenko, Irina B. Murashova, Ural State Technical University (UPI), Yekaterinburg, Russia
Oleg D. Neikov, Frantsevich Institute for Problems of Materials Science (IPMS), Kiev, Ukraine

Copper-base powder metallurgy products rank third after iron and steel and aluminum-based PM products in terms of volume. Copper has high electrical and thermal conductivity and corrosion resistance. It can easily be wrought both hot and cold. Copper is exceeded only by silver among the materials used for electrical applications.

Copper-based powders are used to make self-lubricating bearings, the application of which in the PM industry dates back to the 1920s and still accounts for the major portion of PM copper and copper alloy applications. Other important uses for copper and copper-base PM materials include friction materials, electrical parts, filters, additives to iron as well as aluminum powder alloying, catalysts, paints and pigments.

The copper-based PM products achieved a record 54 100 mt globally in 2000 as is shown in Table 16.1 [1]. The development of copper powder production is different from the ferrous powder sector. Whereas the production of ferrous-based components has doubled over the past 10 years, copper-based products have achieved a global growth of less than 25% over the same period. One significant reason for this slowing down of growth has been the miniaturization of many products such as CD, DVD players, computers, etc. requiring ever smaller PM bearings.

Copper powders above 99% purity are commercially available. The four cardinal techniques of producing copper powders are: atomization, oxide reduction, electrolysis and hydrometallurgy. Of the above methods, atomization and oxide reduction are presently applied on a large global scale. Hydrometallurgical copper powders have not been manufactured in the USA since the early 1980s, but they are produced in Europe and Japan. A large portion of electrolytic powder manufacture is in Russia, where the Uralelectromed Company, located in immediate proximity to Yekaterinburg, annually produces about 6000 tonnes, while its production facility for copper powder is estimated at a total of about 12 000 tonnes per annum.

Atomization

In this process, molten metal flows from a tundish through a refractory nozzle and the liquid stream is disintegrated into droplets by the impact of water or gas jets. The droplets solidify into powder particles. Inert gas atomization produces spherical particles, while the shape of water-atomized powders can be regulated from irregular to nearly spherical by controlling the interaction conditions between the water jet and the metal stream, including liquid flow rate, water pressure and atomizer design. Particle shapes of gas- and water-atomized copper powder are shown in Figure 16.1.

Spherical copper powders have insufficient green strength for use in conventional PM. To give them compressibility, their particle shape and morphology may be transformed by means of mechanical processing and/or oxidation and reduction, as described below in 'Reduction of copper oxide'.

Table 16.1 Global shipments of copper and copper alloy powders (mt)

Cardinal point	1998	1999	2000	2001	2002	2003	2004	2005	2006
Europe (including E Europe)	16 500	16 000	18 500	15 500	14 000	14 000	14 700	12 500	15 500
N & S America	22 800	22 900	23 000	18 800	20 500	19 000	19 500	19 500	18 000
Asia & Oceania	9 150	8 900	12 600	12 150	11 500	13 500	15 900	16 500	19 000
Total	48 450	47 800	54 100	46 450	46 000	46 500	50 100	48 000	52 500

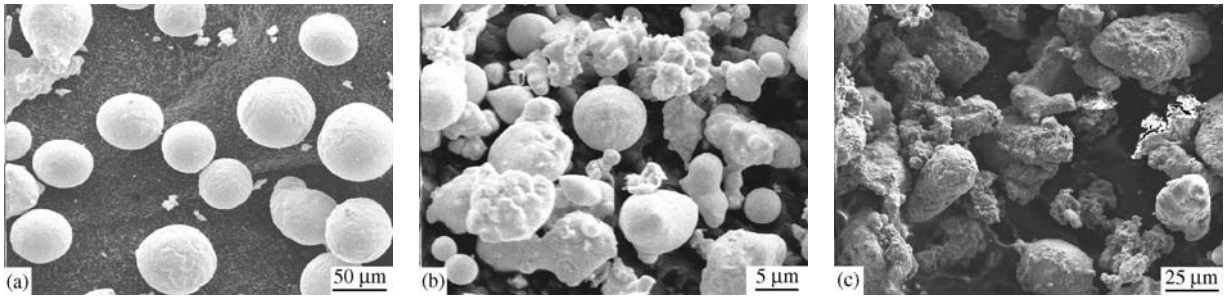

Figure 16.1 Scanning electron micrographs of gas- and water-atomized copper powders: (a) nitrogen atomized, (b) water-atomized, apparent density of 3.95 g/cm^3, (c) water-atomized, apparent density of 4.5 g/cm^3.

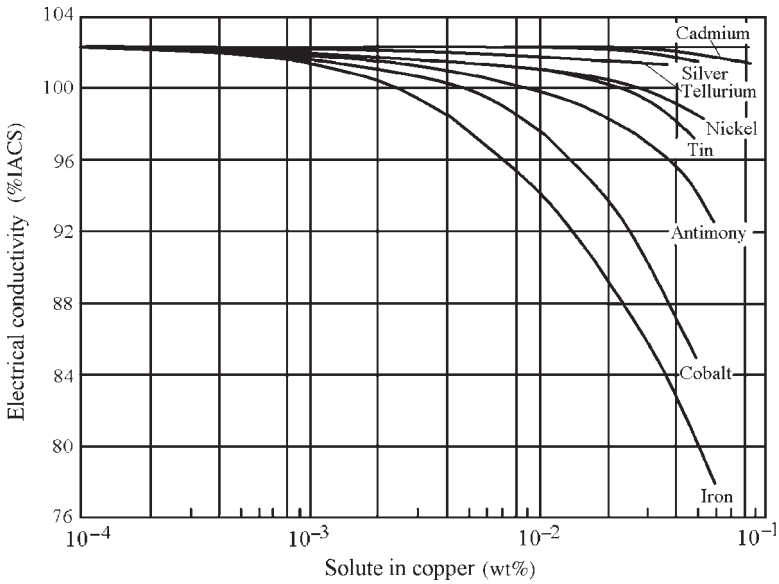

Figure 16.2 Influence of impurities in solid solution on electrical conductivity of oxygen-free copper (IACS is the abbreviation for International Annealed Copper Standard, is the % of conductivity a material has relative to copper, which is considered to be 100 % conductivity). (Source: Ref 2®)

Water is the preferred atomizing medium for producing copper and copper alloy powders. The copper powder of compacting-grade quality is produced from high quality copper by water atomization. The obtained dried powder may be then subjected to an elevated temperature in a reducing atmosphere.

Details of atomization, including fundamentals and atomizer design, are contained in Chapter 5.

Commercial Processes

Copper Powders

Generally, the copper is superheated to 100–150°C above the melting point, providing flow rates of nearly 28 kg/min through one nozzle. Ordinarily, to produce powder with particle size mainly less than 150 μm (100 mesh), water pressure must be in the range from 10 to 14 MPa.

The conductivity of copper depends very strongly on the impurities. The effect of impurities in solid solution on the electrical conductivity of oxygen-free copper is illustrated in Figure 16.2. Therefore, it is very important to control the impurity content during melt preparation to achieve high conductivity and good fluidity.

The need for oxygen control at this stage of the process depends on the subsequent processing and end use of the powder. In conventional refining of copper, poling and steam-generated hydrogen keep copper oxidation within the equilibrium curves shown in Figure 16.3 [2]. Increasing oxygen content results in the production of a more irregular powder and subsequent reduction of the atomized powder improves compactibility due to agglomeration and pore formation.

If the powder is used in the as-atomized state, lower oxygen contents are generally necessary, because of the deleterious effects of oxygen in many

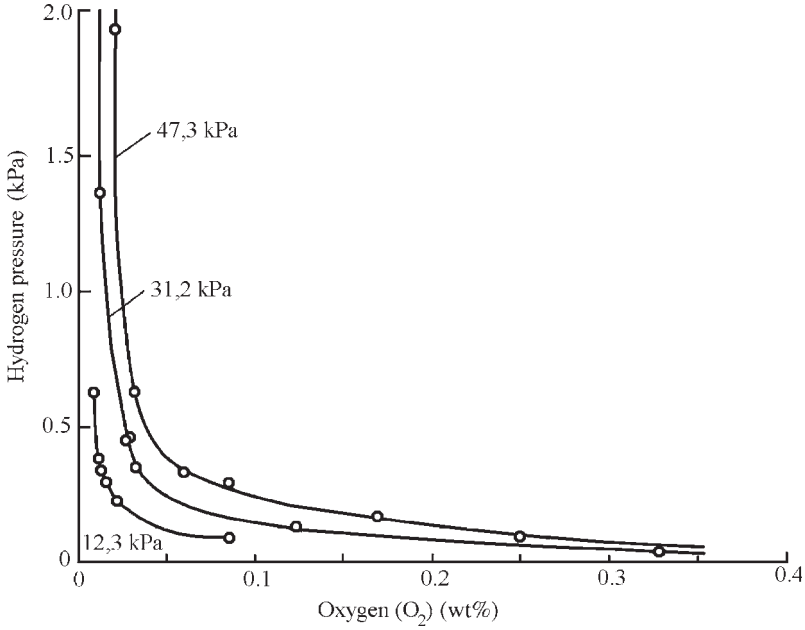

Figure 16.3 Effect of partial pressures of hydrogen and steam on oxygen content of liquid copper at 1150°C. $Cu + H_2 \leftrightarrow 2Cu + H_2O$ reaction at various water vapor pressures.

applications. Oxygen is present partly as surface oxide of copper particles and partly as copper oxide within the particles. Removal of oxygen requires reduction temperatures of approximately 700°C or higher. At this temperature some sintering takes place and it is necessary to mill the sinter cake to reduce it to powder.

In the reduction process, hydrogen readily diffuses through solid copper to react with oxygen and form steam. The large steam molecules, unable to diffuse through solid copper, break their way through grain boundaries, a phenomenon known as hydrogen embrittlement of copper, which reveals itself in the formation of blisters and cracks. These defects improve both compactibility and sintering rate during liquid phase sintering of copper mixed with tin.

There are applications of copper powders which require apparent densities lower than those reachable with water atomization. These powders can be produced by addition of negligible quantities, up to 0.2%, of certain elements, such as magnesium, titanium, calcium and lithium, to the copper melt prior to atomization. These metal additions decrease the surface tension of copper and/or form oxide films on the particle surface during atomization. Magnesium additions are usually used to produce compacting grade copper powder such as design parts, filters and additives for iron powders. Such powders may have apparent densities as low as 2 g/cm^3.

The addition of small amounts of phosphorus (0.1–0.3 wt%) to the molten copper before atomization, allows the manufacture of a spherical powder very low in oxygen. During atomization, even by means of air, the phosphorus oxidizes and forms protective gaseous phosphorus pentoxide (P_2O_5) compound. Such powders have apparent densities up to approximately 5.5 g/cm^3.

Spherical copper powders with controlled particle size are used in applications such as thermal spray coatings, metal impregnated plastics and heat exchangers. Irregular copper powders are used in compacting applications such as bronze mixes for self-lubricating bearings, friction materials, electrical brushes, electrical parts requiring high strength and electrical/thermal conductivity, additions to iron mixes, and diamond cutting wheels. Irregular copper powders are also used in brazing compounds and various chemical applications such as catalysts and in the production of copper compounds.

Typical properties of commercial grades of water- and gas-atomized copper powders are given in Table 16.2.

A flow diagram of the water atomization process for copper and copper alloy powders production is shown in Figure 16.4. Such a technological scheme with certain modifications is used at Polema metallurgical works, in Tula, Russia, and was also used at Alaverdsk mining-metallurgical integrated works, in Armenia, and at the powder metallurgy plant, in Baku, in Azerbaijan.

The first stage in the atomization process is the preparation of charge material for melting. Copper cathodes are cut by shears into pieces suitable for charging into the furnace. Charge components are weighed,

Table 16.2 Properties of typical commercial grades of copper powders produced by atomization

Chemical and physical properties											Source
Copper (wt%, min)	Acid insoluble (wt%, max)	Oxygen (wt%, max)	Apparent density (g/cm^3)	Flow rate (s/50 g)	Sieve analysis (wt%)						
					Sieve size (μm)						
					+250	+140	+100	+75	+45	−45	
99.0	...	...	4.5–5.5	...	...	20–50	30–60	10	trace	...	[2]
98.5(a)	...	...	4.5–5.5	...	...	Trace	5 max	2 max	bal	60–90	[2]
99.0(g.ph)	...	0.2 max	4.5–5.5	45 max	3 max	nil	3 max	15–35	...	40–70	MMP
99.95(g)	..	...	...	...	Mean size ranges from 22 to 5 μm depending on the grades						OSPR
99.0(w)	...	0.25	2.7–3.1	35	nil	1.0	...	20–40	20	35–50	MMP
99.3(w)	0.1	...	2.5–2.7	...	...	0.8 max	...	70 max	bal	30–45	[2]
99.5(w)	...	...	2.85v3.25	28	...	...	0.2	13	41	45.8	A-Ch
99.5(w)	...	...	2.77–2.73	45 max	...	nil	1 max	8 max	50 max	...	Pom
99.5(w)	0.01	...	2.85	27	...	trace	0.4	12	13	75	PYR
99.3(w.s)	...	0.3	3.3–3.5	35–30	...	less as 160 μm amounts 85 wt%					[3]
99.5(w.t)	...	0.21	3.0–3.1	38	...	...	18.4	17.6	28.1	29	[4]
99.8(w)	...	0.1	3.5	...	Mean diameter 5.1 μm						NIPP
99.0(m)	0.1	...	2.1–2.5	...	..	..	1 max	3 max	14 max	85 min	[2]

(a) Air atomized;
(g.ph) gas atomized with phosphorus addition;
(w) water atomized;
(m) water atomized aluminum with magnesium addition;
(w.s) without reduction treatment;
(w.t) after reduction treatment. Companies producing the powders: Pom: Pometon; MMP: Makin Metal Powders Ltd; OSPR: OSPREY Metals Ltd; PYR: PYRON Metal Powders; A-Ch: American CHEMET Co.; NIPP: Nippon Atomized Metal Powders Co.

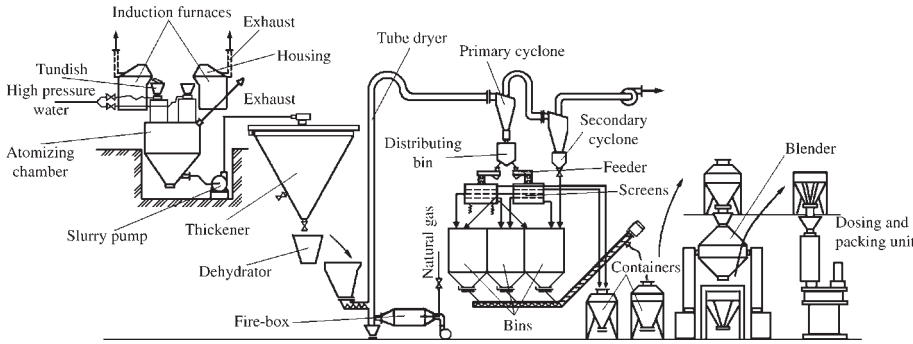

Figure 16.4 A flow diagram of the water-atomization process for production of copper and copper alloy powders.

heated up to a temperature of 150°C to exclude the moisture, and placed into boxes which are transferred to the melting zone. Then melting is carried out. Induction furnaces are usually used. They also may be used as holding for overheating and finishing of a melt prepared in other furnaces, for instance, in an air furnace or resistance furnace. Such duplex melting processes accomplish improvement of control of melt preparation and decrease energy consumption.

The procedure is as follows. The copper is charged into the furnace and heated to 1020–1040°C. After melting, the remaining ingredients are added, the melt being covered by a layer of dry charcoal. The melt is then transferred to the holding furnace and the temperature is raised to 1197 ± 10°C and held for 10 minutes. The slag is then removed and the melt 'poled' with green wood and sampled for chemical analysis.

The melt is superheated to approximately 1230–1280°C (147–197°C over melting point) and then poured into the tundish preheated up to 1100–1150°C, while the melt surface is covered by charcoal; liquid copper flows out through a calibrated pipe in the bottom, forming a melt stream which is atomized by water jets. Thus, a 'free fall' water-atomization design is used [5]. Water pressure is 13–15 MPa and the water consumption 14–17 liters per kilogram. The temperature of the copper melt at the beginning of atomization is 1200 ± 10°C, at the end of atomization it is not less than 1170°C.

The copper powder pulp in weight ratio of solid to water at approximately 1 to 10 is dewatered in vacuum filters. Powder with water up to 15 wt% is accumulated on the filter surface. Wet powder is dried in a convective dryer in an upward flow of gases such as combustion products of natural gas. Coarse powder particles above commercial powder size fall to the bottom of the container connected to the drier. Part of the commercial powder also falls into this container. This settling powder is then briquetted and in the form of briquettes is returned for remelting. Dried powder is separated in primary and secondary cyclones. The former separates powder fractions approximately coarser than 50 μm, while the latter separates the fine particle fraction. Subsequent separation of coarser fractions into given size ranges is done on a sealed round vibrating screen. Moisture content in dried powder is max 0.5 wt%.

To avoid moisture condensation in the duct of the drying unit, the system is preheated for about 15 minutes before setting in operation. Outside surfaces of the drying pipe, cyclones and connecting ducts are thermally insulated.

Powders from storage bins in the required ratio (depend on commercial powder size distribution) are blended in double-cone or in a toroidal vibrating mixer. To prevent oxidation, the powder is covered by a passivating addition based on polymeric compounds. The powder is charged into a container ensuring uniform descent of the powder layers in a container cross-section during powder unloading, which prevents its segregation.

A container with commercial powder is installed into a unit of proportioning and packing and powder is poured into polyethylene bags of capacity up to 20 kg, vacuum degassed and the bags are sealed.

Copper Alloy Powders

Commercial copper alloy powders, including brasses, bronzes and nickel silver, are manufactured in a similar way. Usually, the same integrated manufacturing facilities are used to complete the melting process, atomization, dewatering, drying, particle size separation and blending of a lot.

High purity raw materials are used. To ensure continuity and homogeneity, the molten batch is transferred to a second furnace with a greater holding capacity than the primary melting furnace. Induction heating is preferred for the final melting processing to ensure continuous induced liquid metal movement required for alloy homogeneity, including uniform

heavy alloying element dispersion, such as lead in lead-bearing alloys.

Atomization is achieved by maintaining a constant flow of molten stream from the secondary furnace and by controlling the pressure of the atomizing medium. Adjustment of powder properties, including particle size distribution, apparent density and green strength of compacts of each alloy is achieved by controlled variation of the atomizing process conditions comprising atomizing medium flow rate, molten metal superheating, atomizer design, etc. Subsequent reduction of oxides is not required for standard PM copper alloy grades.

Air-cooled, air-atomized powder is collected and passed over a primary screen to separate oversize particles. Usually, these are remelted during the processing of each alloy. In conclusion, the screened powder may be blended with dry organic lubricants, such as zinc stearate, for use in the manufacture of PM structural components.

Powder properties are maintained constant by periodically recording the atomizing parameters and evaluating the properties of representative samples from the in-process atomized product.

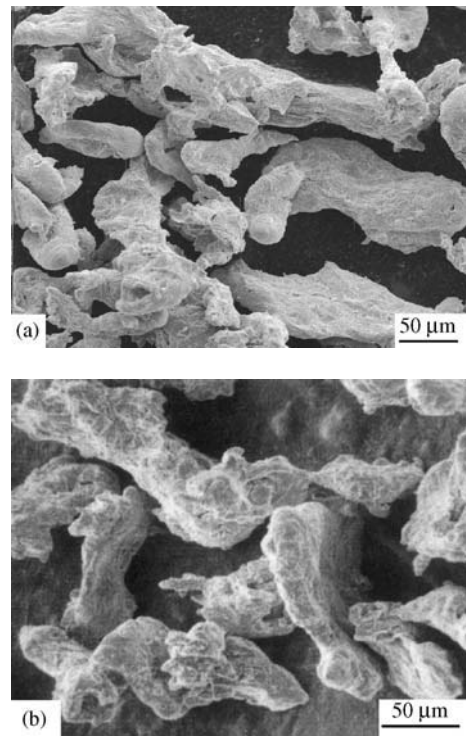

Figure 16.5 Scanning electron micrographs of water- and gas-atomized brasses: (a) water-atomized brass (80%Cu–19%Zn–1%Pb), (b) gas-atomized brass (80%Cu–18%Zn–2%Pb). Courtesy of A. Sameljuk.

Brasses

Brasses include the larger portion of copper-base alloy powders used for PM parts fabrication. Typical copper–zinc brass powders have zinc contents ranging from 10 to 30 wt%. Lead may be added in small amounts, from 1 to 2 %, to improve the machinability of the sintered compacts. The melting temperature is lowered as zinc content increases. Thus, the melting temperatures range from 1045°C for 90Cu–10Zn to 960°C for 70Cu–30Zn. A superheat in excess of the melting point depends on heat losses within the manufacturing system and the physical property requirements of the atomized powders. Typical micrographs of water- and gas-atomized brasses are shown in Figure 16.5. Particle morphology of both powders does not appreciably differ. Characteristic properties of commercial brass alloy powders are presented in Table 16.3.

For typical commercial brass the compressibility at 414 MPa is 7.6 g/cm^3 and green strength at 414 MPa is 10–12 MPa. Both compressibility and green strength data, which play a key role in PM processing, are determined on powders lubricated with 0.5% lithium stearate.

Bronzes

Ordinary compositions are 90%Cu–10%Sn and 85%Cu–15%Sn, produced by the same technique as brass powder, except that high purity copper and tin are used. As base powders for parts fabrication, the use of prealloyed atomized bronze compositions is hampered because of their nodular particle form and high apparent density, both of which contribute to poor compacted green strength. Typical properties of the bronze alloy compositions are given in Table 16.3. Prealloyed bronze powders are made commercially by air atomizing as well by water atomizing. The 90/10 bronze powders, which are introduced in bronze premixes for bearing manufacture, find wide application. Low green strength owing to high apparent density (3.2–3.6 g/cm^3) is overcome by the introduction of lower apparent density copper powders and choice of lubricants with a lower deleterious effect on green strength.

Fine bronze powder 80/20 (SF-BR8020) is produced by ultra-high-pressure water atomization. Such powders, manufactured by Nippon Atomised Metal Powders Co., have an irregular shape with mean diameter of 5, 10 and 15 µm for different powder grades. The tap density is 3.6 and 3.8 g/cm^3 for 5 and 10 µm mean size powders, respectively. Typical application of these powders is as metal bond for

Table 16.3 Properties of typical commercial grades of copper alloy powders produced by atomization

Chemical and physical properties											Source
Grade chemical composition (wt%)	Particle shape	Oxygen (wt%, max)	Apparent density (g/cm^3)	Flow rate (s/50 g)	Sieve analysis (wt%)						
					Sieve size (μm)						
					+250	+150	+100	+75	+45	−45	
Brasses											
10–30 Zn, 1–2 Pb(a)	Irregular	...	3.0–3.2	24v26	...	2.0 max	...	17–37	34–72	60 max	[6]
16–21 Zn, 1–2 Pb(w)	Irregular	...	3.1–3.3	40	−160 μm amounts 90 wt% min						[3]
212. (30 ± 1)Zn(a)	Irregular	...	2.9–3.5	45 max	0	...	...	...	10–25	60–90	Pom
212–63(w) (30 ± 1)Zn	Irregular	...	2.3–3.0	...	0	10 max	...	−53 μm amounts 95 wt% min			Pom
Grades II(w) 14–32 Zn, 1–2 P(b)	Irregular	...	2.8–3.4	...	0.2 max	2 max	...	13–33	26–46	26–56	NA
Bronzes											
85–90 Cu 10–15 Sn(a)	Irregular	...	3.3–3.5	...	...	2 max	...	17–37	32–72	60 max	[6]
86–88 Cu 9–11 Sn(w)	Irregular	0.2	3.7–3.9	35 max	−160 μm amounts 90 wt% min						[3]
CuSn10(a) 10 ± 1 Sn	Irregular	...	2.45–2.7	40 max	0	10 max	10	...	75–85	...	Pom
89/11 10.2–11.6 Sn 0.25–0.45 P	Spherical	...	4.75 min	6 grades in size range: −40 μm, 40/80, 80/160, 160/315, 315/630, and 630/1000 μm							NA
83.5–85.5 Cu, 14–16 Sn, 1 max Zn	Irregular		3.2–3.8	23–28	...	2 max	...	13–33	26–46	26–56	NA
SBP(w) 87.5–91 Cu, 9–12 Sn 0.2–0.45 P	Spherical ...	...	16 grades of spherical powders in narrow size range of 45/63 μm grade to 850/1180 μm grade								MMP

(*Continued*)

Table 16.3 (Continued)

Chemical and physical properties											Source
Grade chemical composition (wt%)	Particle shape	Oxygen (wt%, max)	Apparent density (g/cm^3)	Flow rate (s/50 g)	Sieve analysis (wt%)						
					Sieve size (μm)						
					+250	+150	+100	+75	+45	−45	
SFB95 (w) 4.5–5.5Sn	Irregular, highly porous structure		1.8–2.2	30–45	...	10 max	25 max	30–50	40–75	20–70	NIPP
Premix bronze powders											
MP-0 9.5–10.5 Sn 0.5–0.75 lubricant	...	...	2.7–2.9	30 max	...	1.1 max	10 max	5–25	20–40	40–60	MMP
PM-020 9–11 Sn, 0.2 C max 0.4 lubricant	...	...	2.75–2.95	35 max	0.2 max	1 max	2–6	20–35	31–46	25–35	NA
Grades MM 90 Cu, 10 Sn	...	...	3.1	30	...	trace	0.5	2.0	4.5	93	PYR
Nickel silvers											
Nickel Silver P. 60–64 Cu 17–23 Zn 17–19 Ni	(a)Irregular		2.9–3.3	27–35	...	2 max	...	13–33	26–46	26–56	NA
NS-2 64 Cu, 18 Zn, 18 Ni	(w)Irregular		...	...	Median diameter 10 μm						NIPP

(a) Air-atomized, (w) water-atomized. Companies producing the powders: Pom: Pometon; MMP: Makin Metal Powders Ltd; NA: Norddeutsche Affinerie [7]; PYR: PYRON Metal Powders; NIPP: Nippon Atomized Metal Powders Co.

diamond tools. The bronze powder 95/5 (SFB95) is also produced by the ultra-high-pressure water atomization. It has an irregular shape and high porosity. The apparent density is about 2.0 g/cm^3, and flow rate is close to 34.9. It may be used for bearings requiring high precision.

Compressibility for typical bronze powder, such as 90/10 composition, is 7.4 g/cm^3 at 414 MPa and green strength 414 MPa is 10–12 MPa. Both compressibility and green strength data are for the powders lubricated with 0.5% lithium stearate.

Spherical 89/11 and 90/10 bronze powders are used to manufacture filters. These powders are usually made by horizontal air atomizing and dry collection and separation. The spherical shape is attained due to addition of small amounts of phosphorus in the range from 0.2 to 0.45 wt%, which is introduced into the molten bronze in the form of a Cu–15%P alloy prior to atomizing. During air atomization, the oxygen predominantly reacts with phosphorus, forming phosphorus pentoxide, which is volatile at atomizing temperature. As a result, the surface oxidation of the droplets, which would lead to irregular shape on solidification, is avoided.

The spherical powders with particle size usually ranging from 45 to 850 μm are screened to produce a number of grades, each with a narrow particle size range. Thus, the commercial spherical bronze powders produced by Makin Metal Powder Ltd include 16 grades varying in size from 45/63 μm to 850/1180 μm. Each grade may contain up to 5% of particles above the upper size limit and up to 10% of particles below the lower size limit.

Properties of filter materials produced by loose powder sintering of spherical powders are strongly dependent on the particle size. Characteristically, a sintered filter made from spherical powder with particle size between 180 and 125 μm with filter thickness 1.6 mm has tensile strength of 33–35 MPa, viscous permeability coefficient of 9×10^{-6} m^2, and the lowest dimensions of particles retained by filter of 2.5–12 μm, while a filter with particle size between 850 and 600 μm with filter thickness 3.2 mm has tensile strength of 20–22 MPa, viscous permeability coefficient of 2.5×10^{-4} m^2, and the lowest dimensions of particles retained by filter of only 50–250 μm [6].

Irregular Cu–Pb–Sn Powders

Several compositions, such as 70Cu–30Pb, 84Cu–8Pb–8Sn, and 80Cu–10Pb–10Sn, are manufactured by water atomization. The apparent density is in range from 3.3 to 4.0 g/cm^3 for powders with fraction size below 100 and 160 μm. These powders play an important role in the manufacture of friction and sliding materials.

Varied commercial bronze powders for diamond tools are produced by ultra-high-pressure water atomization. These powder grades include: CuSnAl, contains 27–29 wt% Sn, 4.5–5.5 Al; SF–CuAl(80–20), contains 19–21 wt% Al, max 0.1 wt% Sn; SF–CuAg(80–20), contains 20 wt% Ag, max 0.1 wt% Sn; SF–CuNiSn, contains 9–11 wt% Sn, 19–21 wt% Ni; and others.

Nickel Silvers

Nickel–silver base alloy compositions, (60–65)Cu–(17–19)Ni–(17–23)Zn, are ordinarily used in the PM industry for sintered parts. These alloys can be modified by the addition of lead to improve machinability. Melting technique is similar to that used for brasses, except the melt temperature is 1093°C for superheat in excess of the melting point. Fine nickel silver powder consisting of 64Cu–18Ni–18Zn is produced by ultra-high-pressure water atomization. Median diameter of this powder is 10 μm. Water-atomized Cu–Ni alloy powders consisting of 74–76 wt% Cu and 24–26 wt% Ni are also required for the manufacture of sintered parts. Table 16.3 shows the characteristic properties of water-atomized nickel silver powders.

Compressibility for nickel silver powder at 414 MPa is 7.6 g/cm^3 and green strength at 414 MPa is 9.6–11 MPa. Both compressibility and green strength data are determined for powders lubricated with 0.5% lithium stearate.

Nickel silvers along with brasses, next to bronze bearings, are the most widely used materials for structural PM parts. Typical applications include hardware for latch bolts and cylinders for locks; shutter components for cameras; gears, cams and actuator bars in timing assemblies and in small generator drive assemblies; and decorative trims and medallions. In many of these applications, corrosion resistance, wear resistance and artistic appearance play important roles.

Currently, a number of companies manufacture premixed bronze powders in a ‘press ready’ condition and formulated to customer specific requirements (see Table 16.3). Thus, a wide variety of powder types can be used for the production of sintered bronze 90/10, e.g. mixed, partially prealloyed or prealloyed powders. Each type has certain advantages and drawbacks, and every decision as to powder type and mixing technique is a compromise that can turn out well or not so well. The use of premixes leads to improved quality of the parts produced because of the constancy of the properties of the mixes produced in standard grades in specialized factories with large mixers and reliable quality control systems. Additionally, the parts’ manufacturers’ costs are reduced as it is not required to buy, check, and store the separate ingredients and also avoids the cost of mixing and the associated risks.

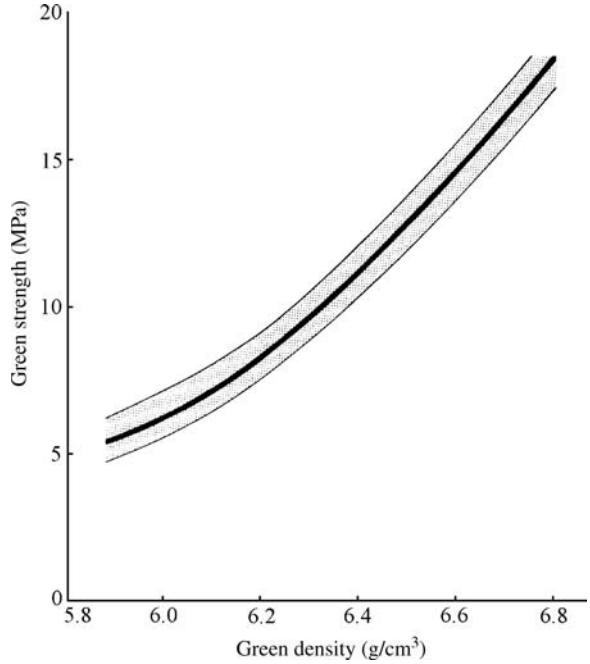

Figure 16.6 Dependence between the green density and the green strength of premixes for sintered bronze 90/10: PM-020 (88.5–90.5 wt% Cu, 9–11 wt% Sn, max 0.2 wt% C, 0.4 wt% lubricant); PMC-020 (87.5–89.5 wt% Cu, 9–11 wt% Sn, 1.0–1.5 wt% C, 0.25 wt% lubricant). Courtesy of Norddeutsche Affinerie AG.

Figure 16.6 shows the dependence between the green density and the green strength of premixes for sintered bronze 90/10 which are produced by Norddeutsche Affinerie (NA) in accordance with NA grade 41.1 for optimizing the selection of composition and processing conditions. The elevated green strength of NA premixes allows trouble-free manufacture even in the case of extremely thin-walled or highly porous bearings. Partially prealloyed powders (grades specified in 41.2) are added for better control of the sintering properties. The NA standard grades PM-020 and PMC-020 for sinter bronze 90/10 are the mixes of electrolytic copper powders, copper alloy powders, partially prealloyed powders and tin powders.

Production of Copper Powder by Solid Phase Reduction of Copper Oxide

The oxide reduction and electrolytic deposition were the first large-scale production of copper powders. In the USA, it still remains one of the main commercial processes for copper powder manufacturing. In

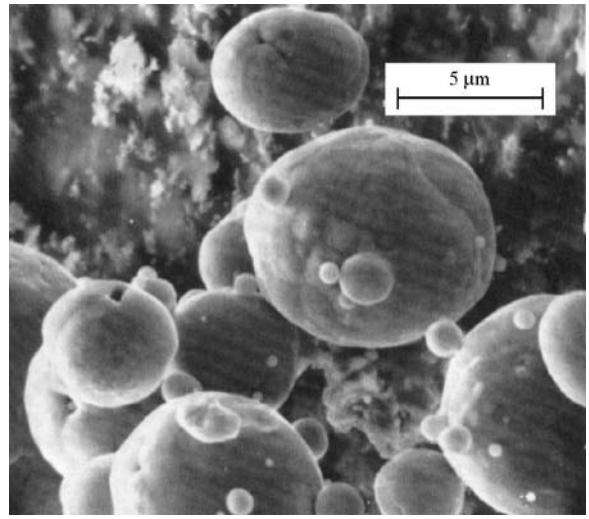

Figure 16.7 Scanning electron micrograph of air atomized copper powder. (Source: Ref 2®)

this process, particulate copper oxide is transformed to copper at elevated temperature in reducing gases. The sintered porous cake produced is then ground to powder. Originally, the initial charge for reduction was copper mill scale or cement copper. However, as copper powder of higher purity was required, particulate copper of high purity (chopped scrap or atomized powder) as starting material was oxidized to cuprous or cupric oxide or a mixture of both.

Melting is usually carried out in either fuel-fired or induction furnaces. It is important to ensure a very low content of elements that form very stable oxides, such as Al and Si which reduce the compressibility of the powder and also make it abrasive, while tin and lead additions cause difficulties in pouring the melt due to incrustation and clogging in the furnaces and nozzles. In the case of applications of copper powder for electrical and friction parts, it is important to remove the impurities with harmful effect on electrical and thermal conductivity (see Figure 16.2).

Large-scale atomization is usually run as a continuous process. Molten copper may be discharged through a tube in the side of the furnace wall and directly atomized, or through a tundish. Both air and water may be used as atomized medium, but horizontal air atomization into a rotating drum eliminates the need for dewatering and drying of the powder.

Micrographs of air-atomized and water-atomized powders are shown in Figure 16.7 and Figure 16.1(b), respectively. The water-atomized powder has a more irregular particle shape and its oxide content is somewhat lower due to higher cooling rate after atomization. At this stage in the process, particle

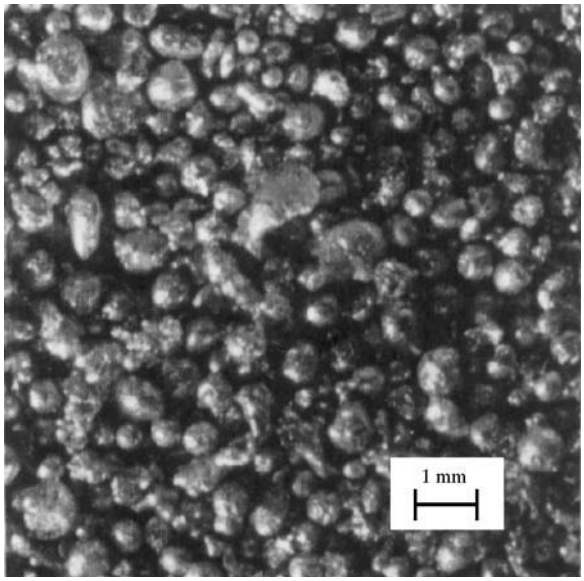

Figure 16.8 Scanning electron micrographs of air granulated copper. (Source: Ref 2®)

shape is not particularly important. The coarse shot-type particulate copper produced by low-pressure air or water atomization (Figure 16.8) is the typical starting material for the pure copper oxide process.

Oxidation of Copper Powder

There are two copper oxides, the red cuprous oxide, Cu_2O, and black cupric oxide, CuO. The oxidation of copper is a well known process. At high temperatures, oxidation follows the parabolic, in which film thickness increases with the square root of time. At low temperature, linear, logarithmic, and cubic oxidation rates have been observed, depending on the previous history of the oxide. The reaction of the copper oxide formation may be represented as follows:

$$2(Cu) + \tfrac{1}{2}(O_2) = [Cu_2O] \text{ exothermic}$$

$$\Delta G = -41{,}166 - 1.27 \times 10^{-3}\, T \ln T + 3.7 \times 10^{-3}\, T^2 - 1.80 \times 10^{-7}\, T^3 + 27.881T$$

where ΔG is free energy in calories per gram per mole, T is the absolute temperature, degrees Kelvin, R is the gas constant, ln is the natural logarithm

$$[Cu] + \tfrac{1}{2}(O_2) = [CuO] \text{ exothermic}$$

$$\Delta G = -37{,}353 - 0.16\, T \ln T - 1.69 \times 10^{-3}\, T^2 - 9 \times 10^{-8}\, T^3 + 25.082T$$

$$\Delta H = -38{,}170 + 1.30T + 0.99 \times 10^{-3}\, T^2 + 0.57 \times 10^{-5}\, T^{-1}$$

where ΔH is heat in calories per gram per mole;

$$(Cu_2O) + \tfrac{1}{2}(O_2) = 2[CuO] \text{ exothermic}$$

$$\Delta G = 33{,}550 - 0.95\, T \ln T - 3.75 \times 10^{-3}\, T^2 + 22.340T$$

$$\Delta H = -33{,}710 + 3.28\, T - 0.40 \times 10^{-3}\, T^2 - 0.20 \times 10^{5}\, T^{-1}$$

Oxidation or roasting of copper powder in commercial conditions is usually carried out in air at temperatures above 650°C. Oxidation in fluidized beds or in rotary kilns provides higher oxidation rates as a result of increasing the contact between powder and oxidizing gas. However, due to the strongly exothermic nature of the oxidation reaction, these operations are more difficult to control than roasting in a belt conveyer furnace.

Both cuprous oxide and cupric oxide powders are brittle and easy to grind to particle size below 150 μm. Furthermore, they are porous.

Reduction of Copper Oxide

Reducing atmospheres include hydrogen, dissociated ammonia, or other exothermic or endothermic gas mixtures. The typical reduction temperature ranges from 425 to 650°C. At temperatures of 700°C and above, sintering of the product may take place. Reduction of particulate copper oxide is generally accomplished in a continuous belt furnace with a stainless steel belt. The depth of copper oxide bed is approximately 25 mm in which reduction happens gradually from top to bottom during motion of the conveyor belt in the countercurrent of the reducing atmosphere. Exothermic reduction processes especially need a careful control of reducing atmosphere content, oxide particle size, reduction temperature and other processing parameters to optimize the reduction rate and to adjust the pore structure. Hydrogen is a more effective reducing agent than carbon monoxide, especially at low temperature. However, at higher temperatures all reduction reactions in the presence of either hydrogen or carbon monoxide go to completion. In the simultaneous presence of cations of alkali metals and 0.03–0.05 wt% Se or Te, the reduction is accelerated significantly, the process can be carried out at lower temperature, dispersivity and plasticity of powder particles increase [3].

The reaction of the copper oxide reduction can be written:

$$[Cu_2O] + (H_2) \leftrightarrow 2[Cu] + (H_2O) \text{ exothermic}$$

$$\Delta G = -16{,}260 + 2.21\, T \ln T + 1.28 \times 10^{-3}\, T^2 + 3.80 \times 10^{-7}\, T^3 - 24.768T$$

$$\Delta H_{298.1K} = -17{,}023$$

Temperature (°C)	900	950	1000	1050
p_{H_2} Pa (a)	1.39	2.0	2.76	3.77

$$[Cu_2O] + (CO) \leftrightarrow 2[Cu] + (CO_2) \text{ exothermic}$$

$$\Delta G = -27{,}380 + 1.47\,T \ln T - 1.4 \times 10^{-3}\,T^2 + 0.5 \times 10^{-6} T^3 - 7.01T$$

$$\Delta H = -27{,}380 - 1.47T + 1.4 \times 10^{-3}\,T^2 - 1.1 \times 10^{-6}\,T^3$$

Temperature (°C)	900	1050	1083
p_{CO} Pa (a)	2.8	9.06	11.3

$$2[CuO] + (H_2) \leftrightarrow [Cu_2O] + (H_2O) \text{ exothermic}$$

$$\Delta G = -24{,}000 - 0.01\,T \ln T + 5.4 \times 10^{-3}\,T^2 + 3.7 \times 10^{-7} T^3 + 22.896T$$

$$\Delta H_{298.1K} = -23{,}543$$

$$[CuO] + (H_2) = (H_2O) + [Cu] \text{ exothermic}$$

$$\Delta H_{290K} = -31{,}766$$

$$2[CuO] + (CO) \leftrightarrow (Cu_2O) + [CO_2] \text{ exothermic}$$

$$\Delta H = -33{,}300$$

where p_{H_2} is partial pressure of hydrogen, p_{CO} is partial pressure of carbon monoxide; values of p_{H_2} and p_{CO} are given in Pascals; other equation symbols are the same as in above equations and record the copper oxide formation; (a) total pressure is 1 atm.

Regulation of the reduction process controls the particle porosity, pore size and particle size distribution of the final powder over a wide range. As with other metal oxides, low reduction temperatures usually lead to the production of particles having fine porosity and correspondingly high specific surface. High reduction temperatures lead to the production of particles containing large pores and low specific surface. High reduction temperatures generally result in more complete reduction and interparticle sintering.

The reduced copper oxide appears from the reduction belt furnace as a porous cake. It is usually disintegrated in two stages. Primarily, the cake is broken into smaller pieces in a jaw crusher or similar equipment, accompanied by fine grinding in hammer mills. Then, the reduced and milled powder is screened and, if necessary, blended and generally treated by proprietary antioxidants to stabilize it against oxidation. Without this treatment, copper powders, especially when exposed to moist air, usually tarnish, with attendant detriment to green strength and other side effects. With increasing oxidation, the color of the powder changes from orange to purple to black. Oxygen content increases from a typical 0.1–0.2 wt% to several tenths of a percent, and may amount to 1 wt%. Powders with large specific surface area are more sensitive to discoloration.

Complete lots of powder are subjected to a series of tests designed to ensure performance in various applications.

When using copper mill scale as starting material for making oxide-reduced copper powder, additional treatment to remove impurities is required before reduction. Typical copper scale contains: 75–87 wt% Cu, 2–2.5 wt% SiO_2, 0.1–0.4 wt% Fe_2O_3, 1.0–1.2 wt% CaO; 1.0–1.3 wt% Al_2O_3 and contaminants of 1.0–1.5 wt% machine oils and 4–4.5% moisture. The amount of copper oxide in the scale ranges from 25 to 30 wt%. The size fractions of copper scale are generally below 150 μm.

The scale is normally annealed in air at temperatures above 627°C. Then, after accomplishment of the oxidation process, the copper oxide produced in the form of porous cake is finely ground. Before reduction, it is treated with a 10–15% solution of sulfuric acid at 177 ± 5°C; at which powder yield is 60–70%, however, etching solutions appear, sulfuric acid consumption is 0.9 tonne per tonne of finished powder. During reduction of copper oxide, a copper scale-to-slag weight ratio is up to 1:1. The apparent density of reduced copper powder with size fractions below 75 μm ground in ball mills is 3.05 g/cm^3. Finished powder yield is 60–65% of the initial copper scale weight.

A copper scale treatment technique is also known [3] where, after oxidation, 5–6 wt% soda is added to copper oxide and the mixture is ground for 3–4 hours and then the ground product is reduced at temperatures ranging from 827 to 877°C by converted gas. The sponge thus produced is wet ground using a liquid to solid ratio of 1 to 1 for a period of 3–3.5 hours. It is then treated with 3–5% solution of hydrochloric acid and subsequently washed, dried and finally further reduced. The reduced copper powder is of 98–98.5% purity, specific surface is 0.06 m^2/g, and particle shape is angular.

If the feed material includes impurities, they are preliminarily eliminated by hydrochemical processes. Thus, processing of a low-grade scrap by the ammonia method – ammonium-carbonate leaching and distillation of the solution (120–160 g/L Cu, treatment with steam or at 107–127°C during 2.5–3.0 hours) – results in precipitation of alkaline copper carbonate. Depending on scrap composition, the precipitate can include nickel, cobalt, zinc, arsenic and cadmium,

i.e. elements soluble in ammonia. The precipitate is washed, dried and converted to copper by hydrogen reduction. Finished copper powder is 98.5–99.4 wt% pure and the contaminants contain: max 0.03 wt% C and 0.05–0.15 wt% total volume of other elements, including S, Fe, Pb, Sn, Ca and Mg.

Typical properties of a commercial copper powder produced by the solid phase reduction of copper oxide are shown in Table 16.4. The single most important application for copper powder is for self-lubricating bronze bearings. In the USA, these bearings are manufactured predominantly from elemental mixtures of copper and tin. From about 1960, premixed and lubricated blends of 90% copper and 10% tin that have controlled dimensional change characteristics during sintering are increasingly in use. Apart from bronze bearings, applications of these powders include copper-base friction materials, electrical contacts and brushes, diamond wheels and copper additions to iron mixes for structural parts [7]. Non-compacting applications include copper fillers in plastics, catalysts and many chemical applications.

Production of Copper and Copper Alloy Powders by Electrolysis

In the electrolytic process, copper is electrodeposed to obtain a spongy powder deposit at the cathode rather than a smooth, adherent one. In this feature, it differs from the process of copper refining where a strongly adherent product is desired. Low copper ion concentration and high acid content in the electrolyte favor formation of powder deposits. High cathode current density and use of an electrolytically refined copper anode also facilitate the formation of powder. Along with these conditions, control of additional variables is necessary to produce powders that satisfy commercial requirements. These variable parameters include quantity and type of addition agent, temperature and circulation rate of the electrolyte, size and type of anode and cathode, electrode spacing and brush-down interval. A technological scheme of the electrolytic process is shown in Figure 16.9.

Electrodeposition of Copper Powders

Results of Electrolyte Composition

Copper content in the electrolyte must be fairly low to prevent adherent deposits. In the desired range, current efficiency rises with increasing ion concentration, with a maximum to 92% in the range from 23 to 33 g/L copper, as shown in [6]. Above approximately 33 g/L, current efficiency decreases and, simultaneously, the deposit becomes adherent instead of powdery. Apparent density and particle size also grow with a rise in copper ion concentration, while a high acid content promotes the formation of powder. As shown in [8], current efficiency increases to a maximum at a concentration of 120 g/L of sulfuric acid, then gradually falls as the acid content increases. Apparent density decreases with increasing acid content.

Certain additional agents to the sulfate/sulfuric acid electrolyte are used to alter powder characteristics. It was reported [6] that the addition of surfactants led to the production of powder with controlled particle size at a current density of 215 A/m^2, in contrast with the 700–1100 A/m^2 normally used, which results in considerable reduction in power cost. The addition of sodium sulfate, as was reported [9], reduces cathode current density and, as the sulfate content is increased, the powder becomes finer. By contrast, replacement of the normal sulfuric acid electrolyte by a sulfamate electrolyte favors the formation of a coarse copper powder [10]. Small quantities of copper chloride have been added to the electrolyte to increase the dendritic structure of powder particles and to increase the yield of fine powder due to the polarizing effect of the chloride ions [11].

Results of Processing Conditions

High current density accelerates the powder formation, but has a minor effect on current efficiency. An appreciable decrease in particle size takes place as current density is increased. Thus, in an electrolyte containing 25 g/L copper and 120 g/L free sulfuric acid, increasing the current density from 600 to 1000 A/m^2 raised the quantity of particles under 53 μm from 20 to 96%.

Raising the operating temperature of the cell increases the current efficiency and reduces the cell voltage. However, cell operation is hindered at temperatures higher than 60°C and powders produced at elevated temperatures are coarser than those obtained at lower temperatures. Therefore, electrolytic cells are operated at temperatures ranging from 25 to 60°C.

The method used to remove the powder deposit from the cathode and the brush-down intervals have a significant effect on powder properties. Commonly, the powder is removed mechanically by means of brushing. The brush-down interval assists in control of the particle size of the deposit. As shown in [6], the powder becomes coarser as the interval is increased from 15 to 60 min and the apparent density increases as the brush-down interval is extended.

Table 16.4 Properties of typical commercial grades of copper powders produced by oxide reduction

Property	Unit	Copper powder purity(wt% min) Source								
		99.8[a] [6]	99.8[a] [6]	99.8[a] [6]	99.6[b] [6]	99.5[b] [6]	99.53 [7]	99.64 [7]	99.62 [7]	99.36 [7]
Chemical composition										
Hydrogen loss	wt% max	0.13	0.13	0.16	0.28	0.26	0.23	0.24	0.26	0.39
Acid insoluble	wt% max	0.03	0.04	0.04	0.10	0.10	0.04	0.03	0.05	0.12
Copper	wt%	bal	bal	bal	bal	bal	bal	bal	bal	bal
Sieve analysis:										
+150	μm	0.1	...	...	...	...	0.3	...	...	0.1
+100	μm	0.6	0.1	0.1	0.1	0.1	11.1	0.6	0.3	1.0
+75	μm	15.5	9.5	7.3	2.8	0.2	26.7	8.7	5.7	4.9
+45	μm	42.8	33.4	29.0	10.3	1.4	24.1	34.1	32.2	12.8
−45	μm	41.1	57.0	63.6	86.7	98.6	37.8	56.6	61.8	81.2
Apparent density	g/cm^3	3.00	2.83	2.73	1.61	0.94	2.99	2.78	2.71	1.56
Hall flow rate	s/50g	22	23	24	...	...	23	24	27	...
Compacting properties at 165 MPa[c]:										
Green density	g/cm^3	6.15	6.12	6.03	6.0	5.9	6.04	5.95	5.95	5.76
Green strength[d]	MPa	8.6	9.7	10.4	20.0	29.0	6.15	7.85	9.3	21.4

[a]for bronze self-lubricating bearings;
[b]for friction materials and electrical brushes;
[c]measured with die wall lubrication only;
[d]transverse electrical brushes.

Processes to remove the deposit automatically from the cathode have been proposed. For this purpose, an organic extract was used in combination with sodium lauryl sulfate [12].

Details of operating conditions including fundamentals of the electroprocess are contained in Chapter 9.

Powder Production

As has been mentioned, the production of the electrolytic copper powder, as illustrated in Figure 16.9 generally follows the processes used in electrolytic refining of copper but with different operating conditions which are required to obtain a deposit of powder. Typical conditions for the production of electrolytic copper powder can be summarized as shown in Table 16.5.

Generally, the anodes are electrolytically refined copper and the cathodes are antimonial lead sheet. In a typical installation, the cathodes are $610 \times 860 \times 9.5$ mm in dimension [6]. The electrodes are arranged parallel to one another in rubber-lined or plastic electrolysis baths with the electrolyte, which flows from the top to the bottom of the bath. Both anodes and cathodes are short to allow enough space at the bottom of the bath for the collection of the deposited powder. Typically each cell is 3.4 m long by 1.1 m wide by 1.2 m high, and contains 18 cathodes spaced at 160 mm intervals and 19 anodes that are hung alternately. Copper is deposited on the cathodes in the form of dendritic particles removed periodically by brushing. Regularly, after operating the bath for several days, the power is turned off. Most of the electrolyte is drained from the bath and the powder slurry is removed. The powder is dewatered in a filter, washed several times and again dewatered. A treatment, for example, with an aqueous solution of gelatine protects the powder from oxidation during subsequent operations.

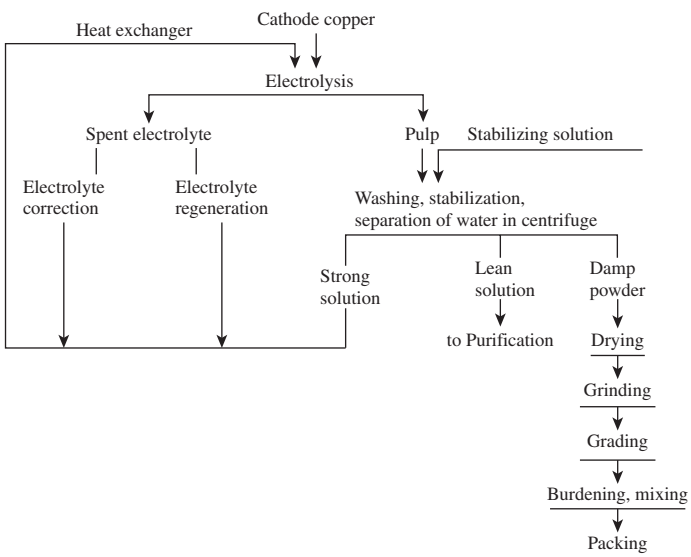

Figure 16.9 Technological scheme of electrolytic process of copper powder production.

Table 16.5 Summary of typical conditions for the production of electrolytic copper powder

Parameter	Quantity	
	Process by Ref [2]	Process by Ref [3]
Copper content in electrolyte	5–15 g/L	8–23 g/L
Sulfuric acid content in electrolyte	150–175 g/L	120–175 g/L
Chlorine ion	...	0.5–1.5 mg/L
Temperature	25–60°C	47–57°C
Anode current density	430–550 A/m^2	390–450 A/m^2
Cathode current density	700–1100 A/m^2	2500–3100 A/m^2
Bath potential	1.0–1.5 V	1.1–1.9 V

Then, the damp powder is subjected to a furnace treatment. The furnace processing also alters certain properties, including particle size and shape, apparent density and green strength of compacts made from the powder. Typically, an electric mesh belt furnace is used. To prevent the powder from spilling through the belt, a continuous sheet of high wet-strength paper is fed to the belt as undercoat for the powder. A roller compresses the powder to improve heat transfer. As it enters the furnace, water is vaporized and the paper burns, but not before the powder has been sintered enough to prevent it from spilling through the belt. The furnace atmosphere is produced in units in which natural gas and air are mixed to yield an atmosphere containing 17% H_2, 12% CO, 4% CO_2, the balance being nitrogen. By changing the furnace temperature between 480 and 760°C and altering the exposure time, the particle size distribution and apparent density may be varied to suit requirements. Upon completion of the furnace treatment, the cake is subjected to grinding and classifying.

In another method [3], the cathodes are of electrolytically refined copper as are the anodes. In a typical installation of this kind, anodes are manufactured in the form of a sheet 880 × 900 × 50 mm and cathodes in the form of rod (Figure 16.10).

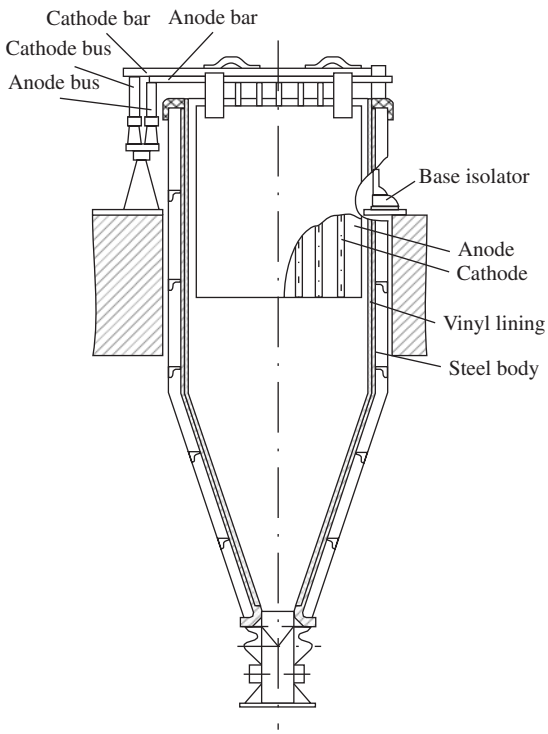

Figure 16.10 Electrolytic cell for copper powder production.

Such a technique is used at the copper-smelting plant of Uralelectromed Company. The electrolyte (copper sulfate and sulfuric acid) circulates in a closed loop system, passing through the electrolyzers, pressure tanks and heat exchanger. The dendritic copper powder deposited on the cathodes is removed once per 2–3 hours by shaking. On removal from the bath, the powder slurry is transferred to a centrifuge, where the electrolyte is removed and the powder washed. The addition of surface-active agents, such as certain fatty acid salts, during washing protects the powder from oxidation [13]. The damp powder is dried in a flow drying pipe by furnace gases. The dried powder is subjected to grinding in ball mills and to subsequent particle size classifying in an air classifier.

Grinding is another operation in which powder properties can be altered. When fine grinding is performed in high-speed hammer mills, feed rate, mill speed and discharge screen openings under the mill can be varied to obtain the powder characteristics desired. The powder leaving the hammer mills is delivered to screens where the oversize is separated and returned for additional grinding. The undersize of 150 μm powder is classified in an air classifier and the fines are transferred to the blending operation. Oversize product is returned for regrinding or is used as melting stock.

The finished powders are stored in the drams to which a drying agent such as silica gel or camphor is added to prevent further oxidation. In the case of high volume finished powder that meets customer specifications, powder is selected from various batches in appropriate proportions and mixed in a blender. The lot is sampled before being removed from the blender and, if required, corrections of the particle size distribution are made before the powder is packed in shipping drums.

Properties of Electrolytic Copper Powders

The properties of electrolytic copper powder depends on various parameters of the operation and, therefore, can be adjusted by modification of certain process variables. Properties of typical commercial grades of electrolytic powders are shown in Table 16.7.

A feature of powder produced by the electrolytic process is high purity, with a copper content usually exceeding 99.5 wt%. A measure of the oxygen content is obtained by exposing a sample of powder to hydrogen flow at an elevated temperature as specified in ISO 4491-2, ASTM E 159, MPIF 02, and CIS GOST 29006-91 (For detailed information on this method, see the description in the section 'Determination of oxygen content by reduction methods' in Chapter 1). Usually,

Table 16.6 Methods of producing electrolytic copper and copper alloy powders

Mode	Electrolyte composition	Current density (kA/m^2)	Temperature (°C)	Electrolysis parameters and conditions
Copper				
WS	7–35 g/L Cu 50–100 g/L H_2SO_4	0.5–0.9	25–57	Current efficiency 80–99%, particle size 20–100 μm, brush-down interval 15–60 minutes.
WS	4–24 g/L Cu 163 g/L H_2SO_4	1–2	40	Apparent density 0.8–2.2 g/cm^3, particle size 5–60 μm, current efficiency 75–96%
WS [15]	5–35 Cu 120–250 g/L H_2SO_4 0–6 g/m^3 Cl^-	0.5–6.0	42–60	Current efficiency 60–98%, apparent density 0.8–2.5 g/cm^3, specific surface 500–1800 cm^2/g
WS	25–30 g/L Cu 90 g/L NH_2HSO_3	1.5–4.0	. . .	Copper in the form of sulfamate; current efficiency 90–93%; circulation 1L(A·h), particles size 80 μm
WS [16]	6.4 g/L Cu 50 g/L H_2SO_4	–	14–50	Permanent overvoltage 0.3–0.7 V, particles size 2–200 μm
WS [17]	16–30 g/L Cu 160 g/L H_2SO_4	0.45–2.0	50	Permanent overvoltage 0.3–0.5 V; apparent density 2.7 g/cm^3; current efficiency 100 %
WS [18]	12–15 g/L Cu 160 g/L H_2SO_4	0.02–4.7	50	Linear current variation; current. efficiency 100%; particles size 20–100 μm in dependence of the current increasing rate
WS	6.4 g/L Cu 50 g/L H_2SO_4	–	25	Pulsing voltage with amplitude 600 mV; frequency 1–100 Hz; particles size 50–200 μm
WS	10–12 g/L Cu 150–200 g/L H_2SO_4	0.6	30–35	Pulse current; full period: pulse = 10:1; particle size 50 μm; current efficiency 98–99%; apparent density 1.5 g/cm^3.
EDC	3.2 g/L Cu H_2SO_4; 0.02–1% oleic acid	2.5	20	Drum rotation 10–40 rpm; dendrite size 0.3–3 μm
EDC [19]	3.2 g/L Cu Solutions of carbon acids in toluene	2.5	20	Rotation 10–40 rpm; oleic acid is changed to stearine to decrease Cu_2O yield; current efficiency is 93%
RSP	5.3–10.6 g/L Na_2CO_3	1.0	70	Raw material – CuO with particles 0.25 mm; cathode–copper; anode – coal; particle size to 0.5 mm; current efficiency 67–69%
M	0.2–10 wt% CuCl KCl–NaCl	0.01–20	447–897	At 447–567°C there are formed two-dimensional twin dendrites (112); at 897°C – three-dimensional (100)
C	H_2SO_4 to pH = 3.3–3.6; 12–15 g/L NaF	–	90–95	Drum rotation 3–5 rpm; cementing agent is aluminum
C	3–4 g/L Cu H_2SO_4	–	27–37	Cementing agent is Zn powder; mixing (Re = 10^3–10^4)
Copper–nickel				
WS	1 g/L Cu; 4 g/L Ni; 40 g/L NaCit, (a); 30 g/L NaCl; 20 g/L NH_4Cl			Cathode – stainless steel; anode – graphite; average particle size is 2 μm
Copper–lead				
WS	13–35.6 g/L Cu+Pb; (p = H 3)	2.5–3.0	40	(0.2–0.3) mole/L Cu+Pb; sulfamine solution; $(Cu/Pb)_{alloy} \cong (Cu/Pb)_{sol}$
Copper–tin				
WS	Cu/Sn 1.065 g/L; Na_3Cit 40 g/L; (pH = 2)	1.6	30	Alloy: 92Cu-8 Sn (solid solution) lattice constant – 0.3665 nm

(*Continued*)

Table 16.6 (Continued)

Mode	Electrolyte composition	Current density (kA/m^2)	Temperature (°C)	Electrolysis parameters and conditions
EDC	8 g/L Cu; 20 g/L Sn; 20 g/L HCl; 50 g/L NH_4Cl; (pH = 1.5); SAS 0.2%	1.5	20	Alloy: 90Cu-10 Sn; current efficiency 88%; voltage 12 V; cathode – graphite; specific surface is 3.76 m^2/g; apparent density is 0.97 g/cm^3; resistance is 7.5×10^{-4} Ohm·cm; copper is in the form of sulphate, tin is in the form of chloride
WS	7 g/L Cu; 41.5 g/L Sn; (pH = 6–8); natrium tripolyphosphate	1.5–2.5	30–41	Intensive mixing; white crystals
Copper–iron				
EDC	1.25–11.25 g/L Cu; 5.5–16.5 g/L Fe; 0.5 % oleic acid	0.4–2.8	11–50	Organic lay – toluene

Production mode: WS: electrolysis of aqueous solution; RSP: reduction of solid phase; EDC: electrolysis from double-layered cell; M: melt electrolysis; C: cementation; SAS: surfactant. Information on RSP, EDC, M, C and SAS is contained in Chapter 9. (a): NaCit: Sodium citrate.

the hydrogen loss ranges from 0.1 to 0.5 wt%, depending mainly on the specific surface. Nitric acid insolubles are determined according to ISO 4496, ASTM E 194, and MPIF 08 standards (see Appendix 1) and are usually less than 0.05 wt%.

Particle size distribution is selected to suit the application and can be varied over a wide range. Only several combinations are shown in Table 16.7.

Apparent densities of electrolytic powders are available usually from 0.65 to 3.2 g/cm^3. They differ in the quantity of apparent density of light and heavy. The powders with apparent densities below 1.2–1.3 g/cm^3 are generally referred to as light. The heavy powders are produced, as described above, by means of thermomechanical treatment of the former.

Generally, powders with density of less than about 1.3 g/cm^3 do not flow, powders with apparent densities ranges from1.3 to 2.3 g/cm^3 have poor flow rate and powders with higher apparent densities flow freely. The flow rates of the common blends of electrolytic copper powder range from 25 to 40 s/50 g.

The green density is a function of the compacting pressure. Depending on particle distribution of the dendritic powder blends used, the green densities amount to 6.0–6.3 g/cm^3 at compacting pressure 100 MPa, as is shown in Figure 16.11, and rise to 7.7–8.0 as the compacting pressure is increased to 550 MPa [7]. Green strength increases with the green density and therefore with compacting pressure, as shown in Figure 16.12 [7]. In this example, green strength for fine light copper powder such as the FS type (see Table 16.7) rises from 8 to 22 MPa as the green density is increased from 5.5 to 6.5 g/cm^3 and the green strength for heavy powder such as the SSM type (see Table 16.7) rises from 5 to 14 MPa as the green density is increased from 5.75 to 6.5 g/cm^3.

The particle shape of deposited electrolytic copper is generally dendritic, as is shown in Figure 16.13. However, during subsequent processing, including thermomechanical treatment, initial dendrites are enlarged due to welding together of small particles which rounds them somewhat (Figure 16.14).

The compacting pressure is an important variable to take into account, because the pressing and sintering conditions have an appreciable influence on the properties of sintered compacts. During sintering, the gases from the atmosphere, from the products of reduction, or from the lubricant must escape, if conducting compacts are to be obtained. So, when the compacting pressure is too high, the flow through interconnected pores may be hindered and gas cannot escape. Compacting pressures not higher than 275 MPa should be used in the production of large, thick parts from electrolytic copper powder, though, higher pressures can be used for thin-walled parts [20].

The tensile strength and elongation of parts made from a typical powder blend in relationship to compacting pressure and sintering time are shown in Figure 16.15 [21]. The powder was lubricated with lithium stearate, pressed at 1000°C in an atmosphere of dissociated ammonia. It shows that good tensile properties can be achieved with short sintering times.

Powder metallurgy techniques have long been successful in the production of parts containing highly

Table 16.7 Properties of typical commercial grades of copper powders produced by the electrolytic process

Properties	Unit	Source. Standard grades													
		NA				ECP		UEM		MMP		Pom		[6]	
		FFL	FS	SSM	GF	C100	C270	PML2	SA	SFG16–200	SFG22	LP0	SB		
Nominal composition															
Hydrogen loss	wt%	0.17 max	0.12 max	0.10 max	0.07 max	0.15	0.08	0.2 max	0.2 max	0.2 max	0.20 max	0.40 max	0.15 max	0.15 max	0.20 max
Acid insoluble	wt%	...	...	...	...	0.02	0.02	0.04 max	0.04 max	...	...	...	...	0.06 max	0.06 max
Copper	wt%	99.7 min	99.75 min	99.8 min	99.85 min	99.7	99.9	99.6	99.7 min	99.4 min	99.4 min	99.5 min	99.8 min	99.8 min	99.7 min
Sieve analysis:															
+250	μm	...	...	0.2 max	4 max	...	...	...	nil	...	...	...	nil	...	...
+150	μm	...	...	1 max	25–45	...	...	...	3–9	...	nil	...	5 max	1 max	...
+100	μm	...	...		...	...	...	...	25–35	nil	20 max	nil	15–25	6 max	...
+75	μm	0.2 max	0.2 max	23–29	50–70	...	...	...	...	3 max	10–25	0.2 max	38–48	...	trace
+45	μm	12 max	12 max	29–37	10 max	...	...	...	80–90	...	15–45	12 max	...	50–60	10 max
−45	μm	90 min	90 min	37–43		...	...	90 min	10–20	75–85	30–45	...	37–43	40–50	90 min
Apparent density	g/cm^3	0.95–1.10	1.75–1.95	2.30–2.50	2.10–2.70	1.0	2.7	0.90–1.10	2.25–2.55	1.50–1.70	2.10–2.40	0.65–0.75	2.35–2.55	2.3–2.5	0.9–1.1
Hall flow rate	s/50 g	none	none	40 max	36 max	none	26	none	40 max	45 max	45 max	none	40 max	37	none
Compacting properties at 165 MPa															
Green density	g/cm^3	6.3	6.3	6.5	6.5	5.9	6.1	...	...	6.40	6.40	...	...	6.4	6.0
Green strength (d)	MPa	25	21	14	12.5	27.5	10.3	...	...	15 min	5 min	...	...	14	18

NA: Norddeutsche Affinerie Aktiengeselschaft; ECP: ElectroCopper Products Ltd; UEM: Uralelectromed; PoM: Pometon; MMP: Makin Metal Powders Ltd.

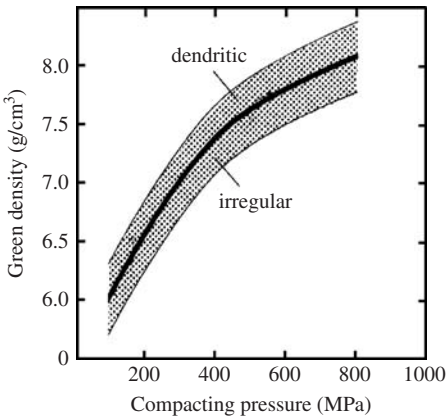

Figure 16.11 Effect of compacting pressure on green density.

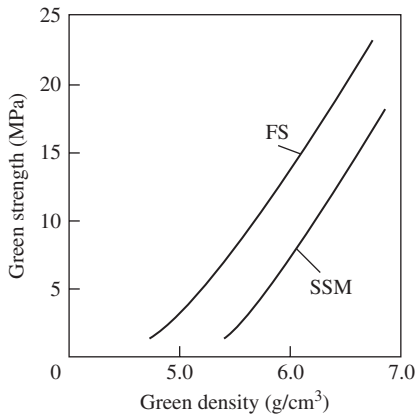

Figure 16.12 Relationship between green density and green strength.

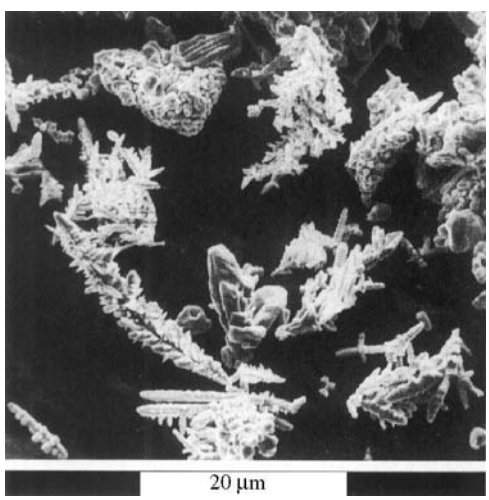

Figure 16.13 Dendritic structure of fine light electrolytic copper powder. Courtesy of Norddeutsche Affinerie AG

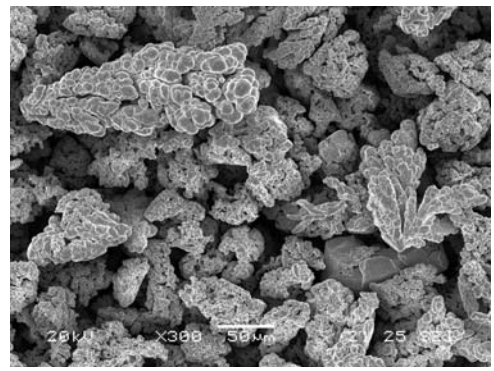

Figure 16.14 Structure of heavy electrolytic copper powder.

conductive copper. Even small amounts of impurities in the copper drastically reduce its conductivity. As conductivities above 90% IACS are required, only high-purity copper powder can be considered as starting material. In this connection, the electrolytic copper powder provides the best conditions for this. However, high conductivity can be achieved only in high-density compacts, as is shown in Figure 16.16, and the latter is generally possible only by means of re-compacting and re-sintering [21,22].

The test data represent an example of such processing (Figure 16.17). The starting material is electrolytic heavy copper powder of K grade produced by Norddeutsche Affinerie Company [22] which differs from powder of SSM grade (see Table 16.7) in a lower content of fine particle fractions, less than 40 µm. The sintering was done under cracked ammonia.

Compression should not be too high during the first compacting since this would hinder the escape of the lubricant from the specimen to be sintered. Even small lubricant residues spoil the electrical conductivity.

Applications

Currently, electrolytic copper powder is produced in England, Germany, Italy, Russia, Japan, India and Brazil, where it is used in most copper powder applications. The production of electrolytic copper powder has recommenced in the USA where, in the early 1980s, it was stopped and replaced by oxide reduction or water atomization.

Electrolytic copper powder is still the powder of choice in many electrical and electronic applications, where high electrical and thermal conductivity is required. Complex parts such as armature bearing blocks, contacts for circuit breakers, heavy-duty

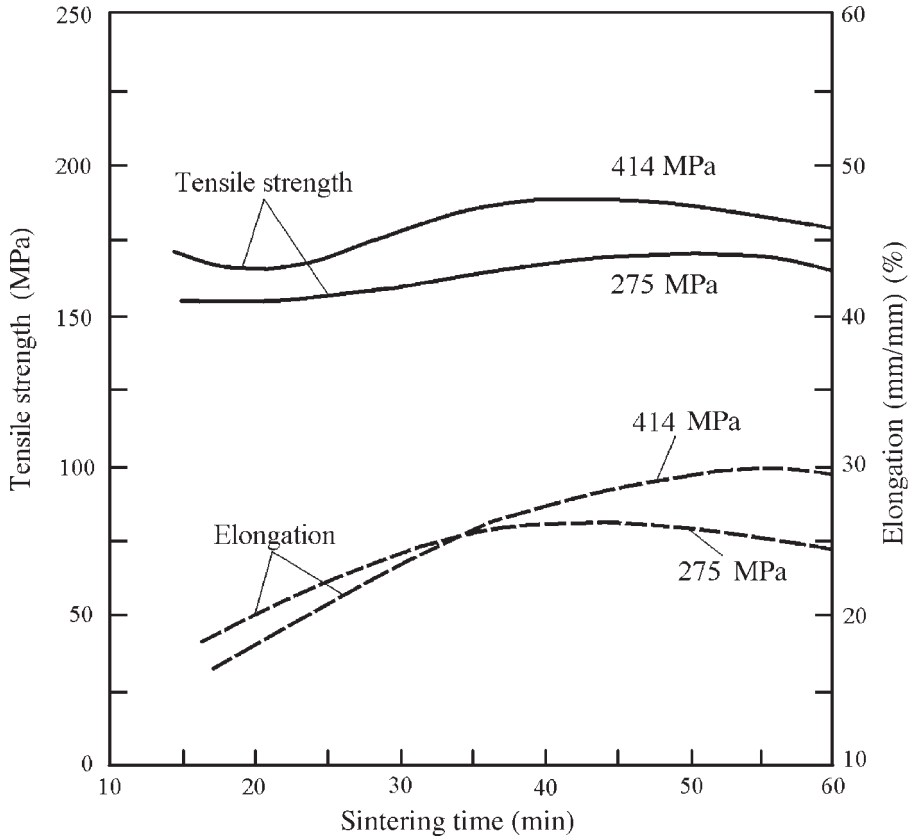

Figure 16.15 Effect of compacting and sintering conditions on tensile properties.

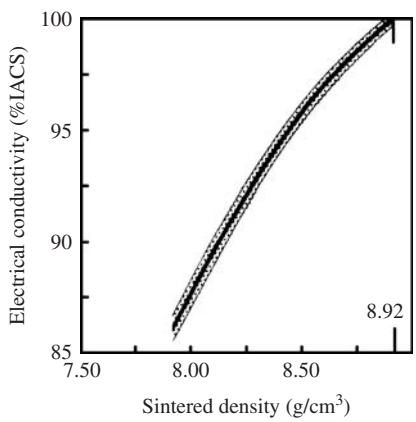

Figure 16.16 Dependence of electrical conductivity on sintered density.

contacts for circuit breakers, high-duty vacuum contact materials for contact tubes and electrode caps for welding, shading coils for contactors, switch gear components for use in switch boxes with capacities up to 600 A, and components for 150 and 250 A fuse blowouts are in regular production.

Electrolytic copper is still the preferred powder in the manufacture of electrical brushes due to possession of a combination of purity, high electrical conductivity, high surface area and particle dendritic shape which allow a large volume of graphite to be accommodated in a copper matrix with high conductivity and high green strength.

Electrolytic copper powder is used with various non-metallic materials to produce friction parts, such as linings for clutches and brakes. Premixes of iron–copper or iron–copper–carbon are utilized in various automotive applications (gears, camps, sprockets, piston rings) and similar components.

Production of Copper Powder by Hydrometallurgical Processing

The basic hydrometallurgical processing steps consist of leaching the raw material, accompanied by the precipitation of the metal from the solution. The most significant precipitation methods are cementation, reduction generally with hydrogen at normal or elevated atmosphere pressure, and electrolysis.

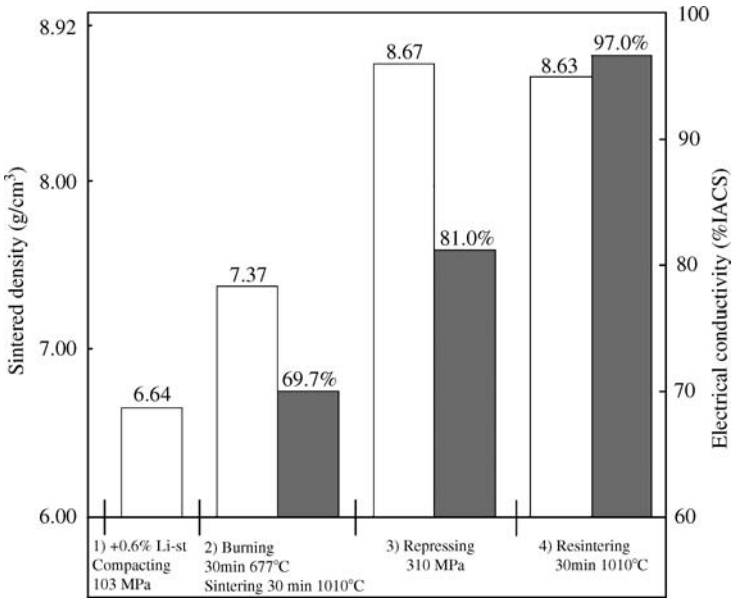

Figure 16.17 Effect of recompacting and resintering on sintered density and electrical conductivity. Courtesy of Norddeutsche Affinerie AG

Use of some leaching precipitation steps or the addition of solvent extraction, flotation or ion exchange improves the purity of the final product.

Leaching

The leaching of copper sulfide and copper oxide ores entails partial dissolution to cupric sulfate with sulfuric acid and iron sulfate. The presence of pyrites in many ore deposits, and its reaction with water and oxygen to form iron sulfate and sulfuric acid, creates an important source of acid. In dump leaching, the pH of the solution is maintained between 1.5 and 3.0, partly to preserve bacteria that promote and accelerate the oxidation of purity and copper sulfate minerals and also to prevent hydrolysis of iron salts. The copper content of the solution varies from less than 1 g/L to several grams per liter.

Other leaching methods include ammonia leaching, which is used for certain copper oxide ores. These methods are called leach-precipitation-flotation and are applied to mixed sulfide ores. There are also leaching technique involving the precipitation of the metal from organic phases [3]

Reduction Processes

Copper powders can be precipitated from ammoniacal, sulfurous and organic media by reduction with hydrogen, carbon monoxide and sulfur dioxide. The most effective reducer is hydrogen. Thermodynamic data for a number of reactions of copper precipitation under pressure are provided in Tables 16.8 and 16.9. Equilibrium residual concentration of Cu (II) ions depending on pH solution and hydrogen pressure p_{H_2} may be represented in accordance with Nernst as:

$$-\lg[Cu^{2+}] = \frac{E^{o}_{Cu^{2+}|Cu}}{0.0296} + 2pH + \lg p_{H_2}$$

where $E^{o}_{Cu^{2+}|Cu}$ is standard potential of the system $Cu^{2+} \leftrightarrow Cu$ (see abbreviations and symbols in Chapter 9).

Reduction of Cu (II) ions includes the stage of Cu (I) ions formation; their equilibrium concentration under the conditions, when temperature T ranges from 40 to 200°C, liquor contains 0.1–0.8 mole/L of Cu^{2+}; 0.3–2.0 mole/L of H_2SO_4 can be written:

$$[Cu^{+}] = [Cu^{2+}]_0^{0.5} - \exp\left\{\frac{5350}{(T+273)} - 10.52\right\}$$

The kinetics of copper precipitation from sulfate and ammoniacal media have special features as shown in the generalized equations given in Table 16.10.

Copper Precipitation from Sulfuric Acid Media

Kinetics of Cu (I) ion formation is described by the equation:

$$\frac{d[Cu^{+}]}{d\tau} = 4.3 \times 10^{9}[Cu^{2+}]_0 p_{H_2} \times \exp(-12900/(T+273))$$

Table 16.8 Equation and equilibrium constant values C of reaction Cu (II) ions reduction with gaseous reagents in acidic and ammonia solutions

Reaction	$-\Delta H°$ (kJ/(g·ion))	Equation of equilibrium constant (C)	C dependence on temperature T	C values at temperature	
				25°C	150°C
$Cu^{2+} + H_2 = Cu + 2H^+$	66.94	$C = \frac{a_{H^+}^2}{a_{Cu^{2+}} f_{H_2}}$	$\lg C = -0.24 + \frac{3497}{T}$	3.15×10^{11}	1.06×10^{8}
$Cu^{2+} + CO + H_2O = Cu + CO_2 + 2H^+$	64.09	$C = \frac{a_{H^+}^2 f_{CO_2}}{a_{Cu^{2+}} f_{CO} f_{H_2O}}$	$\lg C = 3.78 + \frac{3348}{T}$	1.025×10^{15}	4.95×10^{11}
$Cu^{2+} + SO_2 + 2H_2O = Cu + SO_4^{2-} + 4H^+$	109.28	$C = \frac{a_{H^+}^4 a_{SO_4^{2-}}}{a_{Cu^{2+}} f_{SO_2} f_{H_2O}^2}$	$\lg C = -12.74 + \frac{5716}{T}$	2.78×10^{6}	5.6
$Cu(NH_3)_2^{2+} + H_2 = Cu + 2NH_4^+$	114.46	$C = \frac{a_{NH_4^+}^2}{a_{Cu(NH_3)_2^{2+}} f_{H_2}}$	$\lg C = -3.62 + \frac{5984}{T}$	2.39×10^{16}	3.36×10^{10}
$Cu(NH_3)_2^{2+} + CO + H_2O = Cu + CO_2 + 2NH_4^+$	112.60	$C = \frac{a_{NH_4^+}^2 f_{CO_2}}{a_{Cu(NH_3)_2^{2+}} f_{CO} f_{H_2O}}$	$\lg C = 0.15 + \frac{5882}{T}$	7.53×10^{19}	1.12×10^{14}
$Cu(NH_3)_2^{2+} + SO_2 + 2H_2O = Cu + SO_4^{2-} + 2NH_4^+ + 2H^+$	158.56	$C = \frac{a_{NH_4^+}^2 a_{SO_4^{2-}} a_{H^+}^2}{a_{Cu(NH_3)_2^{2+}} f_{SO_2} f_{H_2O}^2}$	$\lg C = -17.15 + \frac{8282}{T}$	4.36×10^{10}	2.69×10^{2}

a_i is activity factor of an i-ion; f_j is fugitivity of a j-component.

Table 16.9 Values lgC of the reducing reaction of several copper compounds with gaseous reagents depending on temperature

Reaction	lgC at temperatures (°C)				
	327	427	527	627	827
$CuO + H_2 \leftrightarrow Cu + H_2O$	8.6	7.3	6.3	5.5	4.4
$Cu_2O + H_2 \leftrightarrow 2Cu + H_2O$	6.9	5.8	5.0	4.4	3.4
$CuO + CO \leftrightarrow Cu + CO_2$	11.1	9.5	8.3	7.3	5.8
$CuCl_2 + H_2 \leftrightarrow Cu + 2HCl$	2.9	3.1	3.4	3.7	4.4
$CuSO_4 + 2H_2 \leftrightarrow Cu + SO_2 + 2H_2O$	8.2	7.0	6.0	5.2	4.1
$CuCO_3 + Cu(OH)_2 + 2H_2 \leftrightarrow 2Cu + CO_2 + 3H_2O$	14.1	11.8	10.0	8.6	6.4

It is correct in ranges: $T = 117$–167°C, $p_{H_2} = 1.0$–3.5 MPa, $[Cu^{2+}] = (0.2-1.3)$mole/L, $[H_2SO_4]_0 < 0.2$mole/L.

Due to Cu (I) ion formation the accompanying ion-impurities have great importance which can lead to:

- the oxidation of Cu (I) ions (Fe^{+3}, Co^{3+}, CrO_4^{2-}, SeO_4^{2-}, etc.) that leads to slowing down of the process and increase of hydrogen consumption
- the formation of not readily soluble compounds with Cu (I) ions which thus pollute the powder (halides, thiocyanates, TeO_3^{2-}, etc).

Accumulated acid during equimolar copper precipitation impairs the kinetics of the process and increases solution activity. One expedient is to add ammonium sulfate or sulfates of the first-group metals (Na_2SO_4, K_2SO_4) which dilute the concentration of H^+ ions, but a more effective procedure is to introduce a slurry of oxides or copper hydroxides, or other soluble neutralizer.

Copper precipitation from sulfurous solutions is characterized by high selectivity towards the accompanying impurities. Co-precipitation of ions As (III), Bi (III) and Sb (III) occurs after precipitation of 90–95% Cu. Precious metals are removed quantitatively.

Mechanism of Cu (II) reduction with hydrogen is heterolytic and includes the following stages:

1. Solution of gas and saturation of the aqueous phase.
2. Activation of hydrogen with Cu (II) and Cu (I) ions

$$Cu^{2+} + H_2 \rightarrow (Cu_H^H)^{n+} \rightarrow Cu < H^{n-1} + H^+$$

3. Formation and accumulation of Cu (I) ions

$$Cu(II) + CuH^{n-1} \rightarrow 2Cu(I) + (H \text{ or } H^+)$$

4. Disproportionation of Cu (I) ions in excess of the equilibrium concentration.

Process parameters accelerating copper precipitation lead to the production of powder with more fine roundish particles. At $T > 147$°C agglomeration of dispersed particles is observed resulting in decreasing of the flow rate, apparent density and powder surface area. Variation of technological parameters within the limits that do not worsen copper precipitation rate affects powder properties weakly.

Increase in inert sulfate contents causes formation of dispersed roundish powder particles that increases its flow rate and apparent density. The particle shape depends on the sulfate type: roundish with (ammonia or Fe (II) sulfates), elongated with (zinc sulfate 0.08–0.16 mole/L NH_3; 0.015–0.03 mole/L PO_4^{3-}; 0.01–0.05 mole/L Cl^-).

Varying the type and surfactant consumption changes copper powder properties within the following limits: specific surface area ranges from 0.02 to 0.18 m^2/g, apparent density from 0.9 to 2.2 g/cm^3, particle size from 20 to 42 μm. Increase in surfactant consumption increases the carbon content in powder.

Increase in number of densifications from 1 to 6 results in an increase of powder apparent density and flow rate 1.6 times, powder size 1.67 times, powder surface decreases 2 times; conglomerates are formed, the sedimentation rate increases and dehydration becomes easier. Powder particle precipitation rate is 6–9.6 cm/min (particles size is 72–81 μm, apparent density is 0.6–0.84 g/cm^3 and specific surface is 1.9–2.3 m^2/g). On centrifuging (filtrational perchlorynevinyl fabric, separation factor 200–300, temperature 37–47°C), powder residual moisture content ranges from 10 to 15%, a maximum carry-over achieves 4.5%. If water consumption for powder washing exceeds water-to-powder weight ratios of up to 3 to 5 at temperature in the range from 27 to 37°C, residual content of sulfate sulfur is max 0.03–0.05%. Oxidation prevention is achieved by means of treatment of powder with 0.3–0.4% naphthenate soap solution.

Table 16.10 Kinetics parameters of copper reduction

Reducer	Medium	Kinetics equation	ΔE (kJ/mole)	Interval of examined parameters			
				p (MPa)	T (°C)	$[Cu^{2+}]$ ((g-ion)/L)	Solution composition
H_2	Ammoniac	$kSp_{H_2}^{0.5}$	67.4	1.0–3.0	167–217	1.0–2.5	6.5 MNH_3 1.5 $M(NH_4)_2SO_4$
	Acetate	$k\left[Cu^{2+}\right]p_{H_2}$	86 ± 0.5	0.5–2.0	373–423	0.1–0.2	25–50% HAc[a]
	Sulfuric acid	$k\left[Cu^{2+}\right]p_{H_2}$	107 ± 2.0	1.0–2.5	403–423	0.3–1.3	pH > 1.0
		$k\left[Cu^{2+}\right]p_{H_2}{}^{0.5}\left[H_2SO_4\right]^{-0.5}$	107 ± 2.5	1.5–4.5	403–423	0.3–1.3	pH < 1.0
SO_2	Sulfuric acid	$k\left[Cu^{2+}\right]^2 p_{SO_2}{}^{0.5}\left[H_2SO_4\right]^{-0.5}$	66.2	0.25–1.0	393–453	0.05–0.2	0.1–0.6 M H_2SO_4
CO	Sulfate	$k\left[Cu^{2+}\right]^2 p_{CO}$	140.0	1.0–4.0	423–463	0.1–0.8	Buffer
	Acetate	$\frac{k_1\left[Cu^{+}\right]\left[Cu^{2+}\right]}{\left[H^{+}\right]}+\frac{k_2\left[Cu^{2+}\right]^2 p_{CO}}{\left[H^{+}\right]}$	109 ± 1.3	1.5–3.4	378–396	0.048–0.12	0.25 MNaAc 0.5 MHAC[b]

[a]HAc is acetic acid;

[b]NaAc is sodium acetate; M denote mole/L.

k is the reaction rate constant the magnitudes of which are given in Ref [3].

On reduction of product in hydrogen, the temperature in the range from 247 to 397°C appreciably influences powder properties: the particles become more round and solid, powder apparent density and flow increase. At temperatures in the range from 597 to 827°C, the particle fractions less than 74 μm are sintered. During annealing substitute 40–60% of the sulfur, 60–70% of the carbon, and up to 98% of the oxygen are removed leaving residual impurities consisting of 0.005–0.016 wt% S, 0.05–0.1 wt% C and 0.03–0.05 wt% O_2. More complete elimination of impurities requires a primary oxygen content in the powder in the range from 2 to 3 wt% and annealing temperature in the range from 627 to 927°C. However, in this case, a cake arises that requires further grinding and particle size classifying. Such powder is characterized by higher apparent density and flow rate, though its yield is smaller due to screening out of coarse particles flattened during milling.

At compacting pressure p over 12 MPa, the useful green compacts are formed; the tensile strength of compacts made by isostatic pressing at $p > 500$ MPa from hydrogen-reduced powder and electrolytic powder are identical. Powder compactibility is described by the relationship $p/p_{max} = Q^{0,2}$ (Q – relative compact density). Compressibility of powders obtained from ground cake is 15–20% worse.

By varying the parameters of the powder precipitation and its subsequent processing, the powder properties can be altered within the following limits: apparent density of 0.5–2.5 g/cm^3, flow rate of 0.0–3.5 g/s and specific surface of 0.034–4.2 m^2/g. Powder surface composition is similar to electrolytic powder. Compared with the latter, copper powder precipitated from sulfuric acid media is characterized by higher apparent density and flow rate, smaller specific surface area, dispersivity and tendency to gas saturation and oxidation.

Copper as copper (I) chloride was precipitated from chloride solutions (25 g/L Cu; 20 g/L HCl) at 100°C and $p_{H_2} = 1.0$ MPa in an hour but even at 174°C and $p_{H_2} = 2.0$ MPa metallic copper is absent.

Organic reducing agents (sugar, glucose, starch, fructose and sawdust) precipitate copper powder at 160–170°C, density max 15–20 g/L, for 1.0–3.0 hours. However, incomplete copper precipitation, impurity of powder and recycled solution with reducer destruction substances indicate inadaptability (low technological effectiveness) of the tested agents.

For hydroxide pulp processing (127–177°C, $p_{H_2} = 2.0$–2.5 MPa), medium pH and temperature are governing process parameters: at pH > 4.5 and temperature lower than 140°C Cu(I) oxide forms; in a more acidic medium and at higher temperatures copper powder is obtained.

Copper Precipitation from Ammonia Media

Process rate with kienetics constant K does not depend on the original copper concentration; it decreases with increase in ammonia and ammonium sulfate concentration and increases with increase of temperature, the seed surface and hydrogen pressure raised 0.5 power:

$$d[Cu(NH_3)_n]^{2+}/d\tau = KS \cdot p_{H_2}^{0,5} \exp(-1860/(T + 273))$$

Optimal content of free ammonia should provide production of copper complexes $[Cu(NH_3)_n]^{2+}$ where $n = 2.2$–2.5.

Ammonia media stimulate co-reduction of nickel together with copper and powder contamination especially where the ratio of Cu^{2+} to Ni^{2+} is between 3.5 and 5.0 and there is a deficiency of ammonia. Copper residue should be over 10 g/L at $[Zn]_0 \leqslant 50$ g/L.

Zinc is present in the powder as a result of zinc ammoniate hydrolysis (insufficient amount of total ammonia, elevated temperature); its hydroxide or alkaline carbonates are eliminated from the powder by means of weak acid solution at the washing stage. Basic solution includes 150–160 g/L copper; if the copper content is higher, it becomes unstable during storage. Leaching of metallized feed yields a part of the copper in solution as Cu (I) ammoniate. It is significant for oxygen consumption reduction but does not influence the process rate. Usually, the ratio Cu (I) to Cu (II) is approximately 1.6–2.0.

If the temperature is raised from 163 to 204°C, treatment for 45 minutes is required to reduce the residual copper to 1 g/L starting with a solution containing 135 g/L. The recommended temperature is 237–247°C, hydrogen pressure must be not less than 2.1–2.5 MPa.

Surfactants as derivatives of polyacrylic acid or ammonium polyacrylate added in quantity of 0.005–0.5 g/L reduce the amount of powder deposited. Densification cycles increase the cooper precipitation rate, appreciably enlarge size and density of powder. Powder particle shape is non-equiaxed.

The process includes the following steps:

$$Cu(NH_3)_n^{2+} + 0.5H_2 \rightarrow (NH_3)_n^{+} + H^{+}$$
$$(NH_3)_n^{+} + 0.5H_2O \rightarrow 0.5Cu_2O + NH_4^{+} + (n-1)NH_3$$
$$2Cu_2O + H_2 + 2H^{+} \rightarrow 3Cu + Cu^{2+} + 2H_2O$$

The copper content usually exceeds 99.5%, powder particle size ranges from 5 to 40 μm. Up to 90% of copper in powder form is precipitated from ethylenediamine copper solutions by hydrogen under pressure (120–140°C, $p_{H_2} = 1.4$–4.2 MPa, for 1–3 hours).

The flowsheet of copper powder production by hydrometallurgical processing from scrap copper, cement copper and copper concentrate, matte and solutions supplied from adjacent fabrications is shown in Figure 16.18. This production flowsheet is similar to the hydrometallurgical methods of cobalt and nickel powder production. The main features are absence of seed preparation stage and limited number of densification cycles (does not exceed 4).

Copper Precipitation from Organic Phase

Processing of lean ores by heap or underground leaching yields weak solutions from which copper is extracted using organic agents to form a saturated metal-organic solution containing 2–10 g/L Cu. The solution undergoes a re-extract and then copper is precipitated from the obtained aqueous solution (30–40 g/L Cu) by electrolysis. Reduction of the saturated organic solution with hydrogen under pressure facilitates the production of copper powder without re-extract.

Promising results are obtained by treatment of an organic solution (33% tertiary carbonic acid + kerosene + 530 g/L Cu) with hydrogen at 230–310°C and $p_{H_2} = 2.0$ MPa. The mixture of heptane acid with kerosene saturated with copper was treated at 142°C and $p_{H_2} = 2.4$ MPa. This process passes through the Cu (I) ion formation stage and has an autocatalytic nature; addition of seed enlarges powder particle size. Preliminary treatment of organic solution also enlarges powder particle size, especially with an increasing ratio of NH_3. When the ratio amounts to 2.0, easy-filtered powder is formed.

Of the copper-impregnated extracting reagents (LIX-64, LIX-65N, SME-529, Acorgap-5100), the best results were observed on precipitation with reagent LIX-65N. Treatment of the organic solution including 30% LIX-65N, 20% decanol, 50% kerosene and 9.0 g/L Cu in the presence of copper powder (30–35% of total solution) at 197–227°C, $p_{H_2} = 1.7$–2.8 MPa for 1.0–1.5 hours yields more than 90% of precipitated copper.

Anhydride Process

During processing of ammoniacal solution by sulfur dioxide, the ammonium sulfite copper (I) salt is

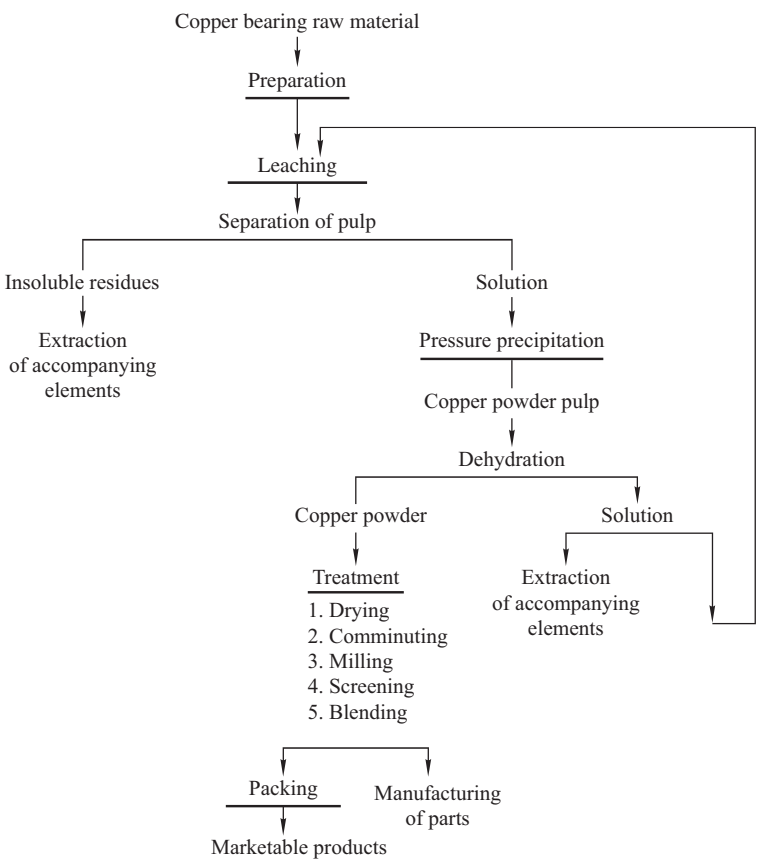

Figure 16.18 Flowsheet of copper powder production by hydrometallurgical processing.

precipitated and being decomposed hydrothermally (by treatment of aqueous solution at elevated temperature) or by acidification yields copper powder (Figure 16.19).

Copper scrap and metal-bearing precipitates are used rather than other copper-bearing materials. By leaching of copper scrap and metal precipitate (at 37–47°C and maintaining the weight ratio of NH_3 to Cu^+ at approximately 4.2 to 1, with aeration), solutions with enhanced content of Cu (I) ions are obtained thus requiring less sulfur dioxide to precipitate the copper.

At 27–77°C and $p_{H_2} = 1.6$–2.0 MPa about 70% of copper is precipitated selectively from the accompanying impurities (Zn, Ni, As, etc.):

$$2Cu(NH_3)_4SO_4 + 3SO_2 + 3H_2O \rightarrow 2Cu(NH_3)SO_4 + 3(NH_4)_2SO_3$$

Copper powder is produced by acidification of the slurry which contains $Cu(NH_3)SO_3$, or by elevated temperature hydrolysis (at 140–170°C and maintaining the weight ratio of liquid to solid at 1 to 1, during approximately 10–15 min):

$$2Cu(NH_3)SO_3 + H_2O \rightarrow 2Cu + (NH_4)_2SO_4 + SO_2 + 0.5O_2$$

Powder composition is as follows: 99.3–99.8 wt% Cu; 0.01–0.03 wt% S; 0.06–0.2 wt% O_2; 0.002–0.08 wt% Zn; and max 0.001% total Pb, Co, Ni, As, Sb, Bi, Fe, Mn and Sn. Particle size ranges from 12 to 60 μm and roundish is the general particle shape; apparent density is 1.3–3.0 g/cm^3, flow rate is 0.8–1.6 g/s. The powder properties depend on acid consumption, ammonium sulfate amount, presence of seed, treatment parameters and process hydrodynamics.

A process is known, where the copper salt is dissolved in acetonitrile (AN):

$$3Cu_2SO_3CuSO_4 \cdot 2H_2O + 5CuSO_4 \xrightarrow{AN} 7CuSO_4 + 2H_2SO_4 + 2SO_2$$

(57°C, 50% AN solution, 0.09 M SO_2 and 0.4 M H_2SO_4) the solution can be reduced in an autoclave (at 150°C) or by distillation (steam, 87°C, 0.5 hour) to precipitate about 50% of the Cu as powder and to regenerate AN. The particle size is below 53 μm; they are as crystals and not inclined to agglomerate. Content of Mg, Zn and Fe in the powder is max $(5–7) \times 10^{-4}$, which is 60–70 times lower than by direct hydrolysis of ammonium sulfite salt.

The anhydride method uses simpler equipment, consumes less power, production costs are lower in comparison with reduction under pressure. However, it is necessary to utilize bought-in ammonium sulfate and the yield of copper directly extracted is less, thus increasing the re-circulating costs.

Cementation

The precipitation of a metal from solution by the addition of another less noble metal is known as cementation. The fundamental equation for copper recovery from copper-bearing liquors using zinc is:

$$Cu^{2+} + Zn = Zn^{2+} + Cu$$

Sulfate solution contains 50 g/L of copper and 5–20 g/L of sulfuric acid. The latter hinders the hydrolysis of impurities present in the solution. An additional factor providing high purity of copper powder (97.0–98.5% Cu) is high residual content of copper in the solution (1–2 g/L). Consumption of zinc powder with particle size from 100 to 400 μm is

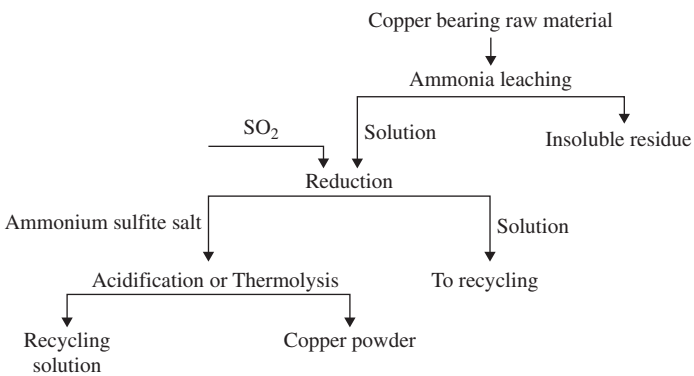

Figure 16.19 Flowsheet of copper powder production by the anhydride method.

determined by the stoichiometry of the above equation, taking into account residual content of copper in the solution.

The process is carried out at 50°C in the agitators with mechanic stirrers; the final slurry is filtered; the powder is washed with water, stabilized with 0.05% soap solution and dried.

The general precipitation reaction of copper recovery from cupric sulfate by the addition of iron is:

$$Fe + CuSO_4 = Cu + FeSO_4$$

Practically, scrap iron, such as detinned and shredded cans, is used. Subsequent separation, washing, reduction and pulverizing results in the production of a copper powder that contains considerable amounts of iron and acid insolubles, such as alumina and silica. For this process, chemical analyses of cement copper from different sources [6] show that total copper content ranges from 75 to 85 wt% and impurity contents, depending on scrap composition, vary in following ranges: 0.7–10.0 wt% iron, 0.5–1.1 wt% sulfur, 0.5–1.1 wt% nitric acid insolubles, 0.08 wt% calcium oxide, 0.5–1.2 wt% alumina, 0.4 wt% silicon dioxide, 0.2 wt% lead and 9.5 wt% oxygen.

Electrowinning

Electrowinning is used to recover copper from leach solutions containing more than approximately 25 g/L of copper (Harlan process). The electrolytic cells are equipped with insoluble lead–antimony anodes and 99% Ni cathodes. The copper powder deposits do not stick and gravitate to the bottom of the cells. The temperature of the electrolyte is maintained at 60°C; cathode current varies from 1350 to 2700 A/m^2. When the copper concentration falls below 15 g/L, the electrolyte is drained and used for feed ore leaching. Particle size of the powder prior to the heat treatment processing ranges from 1 to 25 μm. Copper content is excellent, >99.9%. However, the power requirements for electrowinning of copper are approximately ten times as large as those for electrowinning of copper using soluble anodes.

Copper may be precipitated from low content leach solutions by solvent extraction, followed by stripping with dilute sulfuric acid into an aqueous solution and electrowinning. Carboxylic acid and hydroxylamine-based compounds have been found to be selective solvents of low water solubility, to have good stability and to be compatible with inexpensive diluents.

Another technique is used for obtaining copper powder with electrochemical regeneration of the reducer. Copper is reduced in the solution by titanium ions (III) in the anode space of an electrolyzer (Figure 16.20) at room temperature [14]. The flow diagram of this process is shown in Figure 16.21. Metallic copper is precipitated from solution by the following reaction:

$$Cu^{2+} + 2Ti(III) = Cu(powder) + 2Ti(IV)$$

Copper ions go to the anode space from the soluble anodes. Powder permanently suspended in the electrolyte is recovered by filtration and the filtrate goes back into the cathode space, where the reducer, namely titanium ions (III), is regenerated on the perforated lead cathode.

Anode space is separated from the cathode by a diaphragm made of chlorine fiber previously tightened by boiling it in distilled water for 20 min. The level of the catholyte is higher than the anolyte level that ensures the electrolyte flows from the cathode space to the anode. The powder separated on the filter is washed with water to remove electrolyte, stabilized with 0.05% soap solution, then washed again, dried under vacuum at 100–120°C, cooled under vacuum to room temperature and classified. Electrolyte circulated with a speed of 22 L/h contains 184.2 g/L of $Ti_2(SO_4)_3$ and 98 g/L of H_2SO_4. The cathode current density at 25°C is 50 A/m^2 and anode current density is 400 A/m^2. The powder produced consists of particles of approximately 1.5 μm in size and having a distinctive angular shape.

Various characteristic methods for electrowinning copper and copper alloy powders from leach solutions can be found in Table 16.6.

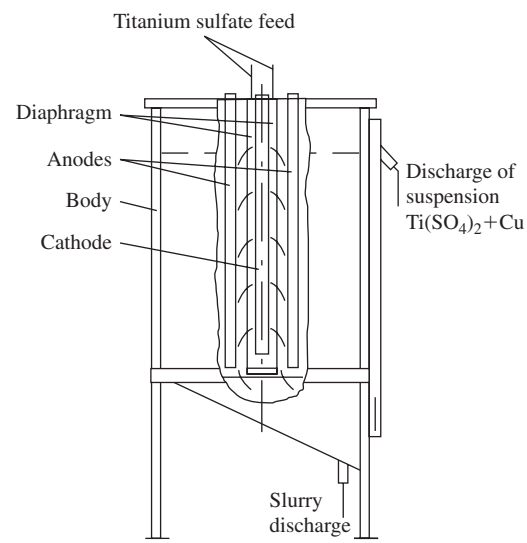

Figure 16.20 Electrolytic cell for production of copper powder by electrochemical regeneration of reducer.

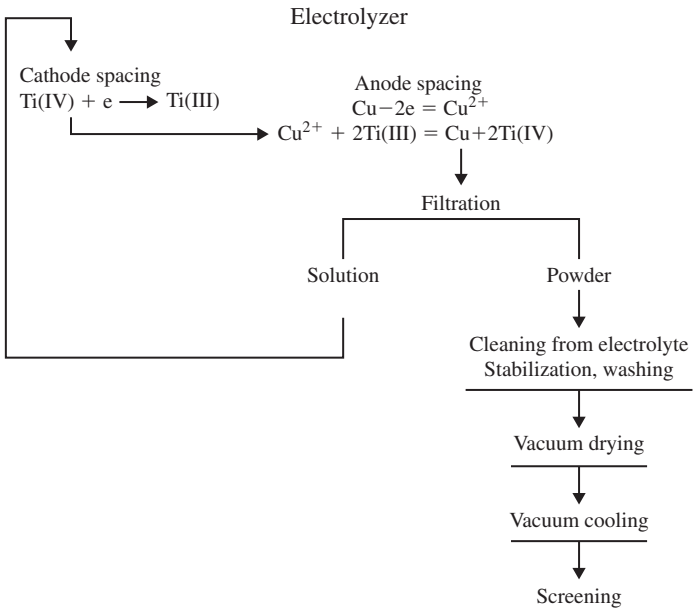

Figure 16.21 Flowsheet to produce copper powder by electrochemical regeneration of reducer.

Oxide Dispersion Strengthened (ODS) Copper Powder Production

Because of its high electrical and thermal conductivity, copper is widely used in industry; however, it has relatively low strength, especially at elevated temperatures. It can be strengthened by using stable oxides such as alumina, zirconia, titania, thoria or yttria. For this, the PM technique is used, because the above oxides are insoluble in molten copper. Dispersion strengthened copper cannot be made by conventional ingot metallurgy.

Manufacture

Oxide dispersion strengthened (ODS) copper can be produced by several methods [23]: simple mechanical mixing of the copper and oxide powders, coprecipitation from salt solutions, mechanical alloying [24] or by selective internal oxidation [25]. The latter produces the finest and most uniform dispersion. Size distribution and cost vary substantially among these methods. Alumina is a common strengthening phase used in the production of ODS copper.

The internal oxidation method is based on the principle that a copper–aluminum solid solution is internally oxidized at elevated temperature. For effective internal oxidation, oxygen must diffuse into the matrix (copper) several orders of value rather than the solute element (aluminum). Powder metallurgy offers the advantage that powder particles can be internally rapidly oxidized and then consolidated into the required shape.

The internal oxidation process involves the low aluminum addition in copper and atomizing the melt by mean of a high pressure inert gas such as nitrogen. The powder obtained is mixed with an oxidant that consists of fine copper oxide powder. Then, the mixture is heated to a high temperature at which the oxide dissociates and the oxygen produced diffuses into the particles of copper–aluminum solid solution. Because aluminum forms oxide more readily than copper, the aluminum in the alloy is preferably oxidized to aluminum oxide. After entire oxidation of the aluminum, surplus oxygen in the powder is reduced by heating the powder in hydrogen or a dissociated ammonia atmosphere.

Three grades of ODS copper are commercially available, where are designated as C15715, C15725, and C15760 by the Copper Development Association. The nominal compositions of these grades are: 99.7 wt% (99.3 vol%) Cu, 0.3 wt% (0.7 vol%) Al_2O_3 C15715 grade; 99.5 wt% (98.8 vol%) Cu, 0.5 wt% (1.2 vol%) Al_2O_3 C157215 grade; and 98.9 wt% (97.3 vol%) Cu, 1.1 wt% (2.7 vol%) Al_2O_3 C15760 grade.

The powder is consolidated into fully dense shapes by various techniques. Semi-products, such as rod and bar, are made by sealing the powder in a suitable metal container, usually copper, and hot extruding it to the given size. Strip is manufactured either by rolling rods of extruded rectangular bar or by directly

rolling powder with or without a container. Wire is produced by cold drawing of rod. HIP of powder sealed in container is used when large pieces cannot be made by hot extrusion. Such shapes can be also made by forging of sealed powder or green compacts.

Finished parts are made from semi-products by machining, brazing and soldering. Fusion welding is not applicable because it causes the aluminum oxide to precipitate from the liquid copper matrix, accompanied with the loss of dispersion strengthening. While flash welding, in which the liquid metal is squeezed out of the weld joint, and electron beam welding, in which a small heat-affected zone is created, have been used with success.

Properties

The properties of ODS copper strongly depend on the aluminum oxide content. They can be altered to meet a wide range of design requirements by varying the aluminum oxide content and/or cold work. Typical for rod stock in the hot extruded condition, increasing aluminum oxide content from 0.45 to 2.7 vol% increases the tensile strength from 340 to 670 MPa, while elongation is decreased from 27 to 19%.

The free or reducible oxygen content of the above three ODS coppers, usually about 0.02–0.05 wt%, is present in the form of dissolved oxygen and cuprous oxide. Alloys in this state are inclined to hydrogen embrittlement at high temperatures. In these low-oxygen compositions, the reducible oxygen can be converted to non-reducible oxide by adding up to 0.02 wt% boron as an oxygen getter. These grades are then resistant to hydrogen embrittlement.

Physical properties of ODS copper closely resemble those of pure copper, since the former contains small amounts of aluminum oxide as discrete particles in an essentially pure copper matrix. Table 16.11 shows the properties of the commercial ODS coppers comparing them with oxygen-free (OF) copper [23]. The melting point does not differ from that of copper because the matrix melts and the aluminum oxide separates from the melt. Density, coefficient of thermal expansion, and modulus of elasticity are similar to those of pure copper.

Electrical and thermal conductivities range from 78 to 92% of those for pure copper. In combination with the high strengths of these materials, they enhance the current-carrying or heat-dissipation capabilities for a given section size and structural strength. Therefore, they enable reduction of section size for component miniaturization without damage to structural strength or current and heat-carrying capabilities. At elevated temperature, the decrease in electrical and thermal conductivities of ODS coppers does not differ from those of pure copper.

ODS copper has high resistance to softening even after exposure to temperatures close to the melting point of copper because the aluminum oxide particles are stable at these temperatures and retain their original size and spacing. At typical brazing and glass-to-metal sealing temperatures (above 600°C), ODS coppers retain their strength while OF copper loses its strength. At above 600°C, the ODS coppers have tensile strength comparable to or better than some stainless steels. ODS copper has high thermal stability at elevated temperatures because the aluminum oxide particles retain their initial particle size and spacing even after prolonged heating and prevent recrystallization of the matrix.

Applications

Oxide dispersion strengthened copper has received wide market acceptance in series applications [23]. The main applications are enumerated below.

Lead wires. ODS copper wire is used in leads for incandescent lamps. Its high-temperature strength retention capability allows glass-to-metal seals to be made without abnormal softening of the leads. This in turn eliminates the need for expensive molybdenum support wires. Superior strength of the leads enables reduction in lead diameter to save material. ODS copper wire also can be used in leads for discrete electronic components such as diodes.

Relay blades and contact supports. These parts involve current-carrying arms that connect fixed contact points with electrical circuits. Generally, the relay blade and contact supports have silver contacts brazed or riveted to them. The strength retention capability of ODS copper after exposure to elevated temperature allows brazing of contacts to the blade without perceptible strength loss. Due to higher electrical conductivity of ODS copper; it has replaced conventional copper alloys, such as phosphor bronze and beryllium copper, in some relays.

Sliding electrical contacts. ODS copper bars are used in overhead sliding electrical contacts for high-speed electric trains. Their high resistances to abrasive wear provide up to 10 times contact life and reduce the maintenance costs significantly. The higher the train speed, the greater the advantage ODS copper base materials.

Resistance welding electrodes. ODS copper electrodes are widely used for resistance welding in automotive, appliance and other sheet metal processing industries. It is well known that sticking of the electrodes to the workpiece is a major problem when

Table 16.11 Properties of oxide dispersion strengthened (ODS) and oxygen-free (OF) copper powders

Properties				Unit	Material			
					C15715	C15725	C15760	OF Copper
Melting point				°C	1083	1083	1083	1083
Density				g/cm^3	8.90	8.86	8.81	8.94
Electrical resistivity at 20°C				Ω mm^2/m	0.0186	0.0198	0.0221	0.017
Electrical conductivity at 20°C				%IACS	92	87	78	101
Thermal conductivity at 20°C				W/m · K	365	344	322	391
Linear coefficient of thermal expansion for 20–1000°C				ppm/°C	16.6	16.6	16.6	17.7
Modulus of elasticity				GPa	130	130	130	115
		Thickness or diameter (mm)	Temper or condition[a]					
Tensile strength								
	Flat products	10	AC	MPa	413	434	517	...
		2.5	CW 75%	MPa	...	...	627	...
		2.3	CW 78%	MPa	...	586	...	...
		1.3	CW 88%	MPa	579	...	...	...
		0.15	CW 98%	MPa	661	675	737	...
	Plate	Up to 130	AC	MPa	365	413	...	...
		25	CW 60%	MPa	476	496	...	...
		16	CW 75%	MPa	483	524	...	...
	Rod	38–14	AC	MPa	393	441	551	...
		19	CW 55%	MPa	427	...		...
		13	CW 14%	MPa	...	...	572	...
		7	CW 94%	MPa	496	...	...	...
		7	CW 74%	MPa	...	...	620	390
	Wire	1.3	CW 99%	MPa	524	...	...	...
		0.4	CW 99.9%	MPa	606	...	...	...
	Rounds	up to 760	AC	MPa	365	413	469	...
Yield strength								
	Flat products	10	AC	MPa	331	345	413	...
		2.5	CW 75%	MPa	...	...	572	...
		2.3	CW 78%	MPa	...	544	...	...
		1.3	CW 88%	MPa	537	...	...	...
		0.15	CW 98%	MPa	613	613	655	...
	Plate	Up to 130	AC	MPa	255	296	...	...
		25	CW 60%	MPa	427	441	...	...
		16	CW 75%	MPa	455	467	...	...
	Rod	38–14	AC	MPa	324	358	517	...

(*Continued*)

Table 16.11 (Continued)

Properties				Unit	Material			
					C15715	C15725	C15760	OF Copper
		7	CW 94%	MPa	469	...	...	...
		7	CW 74%	MPa	...	...	599	...
	Wire	1.3	CW 99%	MPa	496	...	...	...
		0.4	CW 99.9%	MPa	579	...	...	...
	Rounds	Up to 760	AC	MPa	255	296	331	...
Elongation								
	Flat products	10	AC	%	20	21	13	...
		2.5	CW 75%	%	...	...	8	...
		2.3	CW 78%	%	...	8	...	...
		1.3	CW 88%	%	7	...	...	...
		0.15	CW 98%	%	6	6	6	...
	Plate	Up to 130	AC	%	26	19	...	...
		25	CW 60%	%	10	9	...	...
		16	CW 75%	%	10	9	...	...
	Rod	38–14	AC	%	27	24	22	...
		19	CW 55%	%	18	...	...	...
		13	CW 14%	%	...	...	16	...
		7	CW 94%	%	9	...	...	...
		7	CW 74%	%	...	...	14	...
	Wire	1.3	CW 99%	%	2		...	...
		1.3	HT 650%	%	10	...	...	...
		0.4	CW 99.9%	%	1	...	...	...
	Rounds	Up to 760	AC	%	26	19	4	...
Hardness								
	Flat products	10	AC	HRB	62	72	81	...
		2.5	CW 75%	HRB	...	...	85	...
		2.3	CW 78%	HRB	...	83	...	...
	Plate	Up to 130	AC	HRB	62	68		...
	Rod	38–14	AC	HRB	62	73	80	...
		19	CW 55%	HRB	68	...	...	...
		13	CW 14%	HRB	...	...	83	...
		7	CW 94%	HRB	72	...	...	...
		7	CW 74%	HRB	...	...	86	...
	Rounds	Up to 760	AC	HRB	...	68	76	...

[a]AC, as consolidated; CW: cold work % reduction in area; HT: heat treatment for 1 h.

welding galvanized and other coated steel. This usually results in electrodes pulling off their holders and necessitates stopping the assembly line to alter the electrodes. Such interruptions are very costly. ODS copper electrodes eliminate sticking to galvanized and other coated steel. Increasing use of coated steels in the automotive industry has predicted further wide usage of ODS copper electrodes.

Metal–inert-gas welding contact tips. Resistance of ODS copper to abrasive wear from the steel wire enables the tips to maintain the bore diameter and minimizes the wandering of the arc. This is important in automated welding lines. The non-sticking property of ODS copper also minimizes the material build-up.

X-ray and microwave tube components. Another example of ODS copper applications is the stems for the rotating anodes in X-ray tubes where high strength retention after brazing and glass-to-metal sealing are important. The high thermal conductivity of ODS copper also enables more efficient heat removal, thus lowering the operating temperature and providing longer tube life and quieter tube operation.

Particle accelerator components. Oxide dispersion strengthened copper plates and bars are used in mirrors and X-ray absorbers because of their high thermal conductivity, high strength, creep resistance and vacuum integrity.

Other applications. Other various applications of ODS copper include dissimilar circuit package components, high field magnet coils, anode stems chlorine cells, electrodischarge machining electrodes, high-speed motor and generator components, commutators and so forth.

Applications of Copper and Copper-base Powders

Basic applications for copper and copper-base PM materials are summarized in Table 16.12. These include bearings, electrical parts, friction materials,

Table 16.12 Applications of copper and copper-base powders

Applications	Powder type
Automotive and machinery	
Bearings	Bronze, copper–lead–tin, copper–lead, copper–lead–zinc, copper–nickel, ODS copper
Brake bands and linings	Copper, brass, copper–lead, copper–lead–tin, copper–tin–zinc–iron
Bushings	Bronze
Control panels, instruments	Nickel–silver
Counterweights	Copper–tungsten
Chemical	
Chemical catalysts	Copper
Filters	Bronze
Flame arresters	Bronze
Fungicide additive	Copper
Soil conditioning	Copper
Valves and pumps	Copper–nickel
Coatings and paints	
Conductive paints and plastics	Copper and brass
Antifouling paints	Copper
Decorative paints	Copper, brass, bronze
Lacquers	Brass, bronze
Mechanical plating	Copper, brass
Spray coating	Copper, brass
Vacuum metallizing	Copper
Construction hardware	
Conductive and non-sparking floors	Copper
Decorative plastics	Copper, bronze, and brass
Dissimilar circuit package components	ODS copper
Domestic water filters	Brass

(*Continued*)

Table 16.12 (Continued)

Applications	Powder type
Locks and keys	Brass, bronze, and ODS copper
Fastening bolt	Brass
Pipe joint compounds	Copper, brass
Electrical and electronic	
Brushes	Copper, copper–lead–tin–carbon
Brush holders	Nickel–silver
Contacts	ODS copper
Heatsinks	Copper
Printed circuits	Copper
Semiconductor stud bases	Copper, ODS copper
Telephone components	Brass, bronze
Particle accelerator components	ODS copper
Switch and contactor components	Copper, brass
Incandescent lamps	ODS copper
X-ray, microwave tube parts	ODS copper
Antigalling pipe joint compounds	Copper
Copper lubricants	Copper
Plastic-filled metal	Copper, bronze
Self-lubricating (oil-filled) parts	Bronze
Manufacturing and machining	
Abrasive wheel bonding	Copper
Brazing compounds	Copper, brass, bronze
Electrodischarge machining	Copper
Electrochemical machining	Copper
Resistance welding electrodes	Copper, copper–chromium, ODS copper
Metal-inert-gas welding contact tips	Copper, ODS copper
Ordnance	
Armor-piercing cores	Copper
Fuse parts	Brass
Projectile rotating bands	Copper, brass
Other equipment and uses	
Business machines	Brass
Coins, metals, medallions	Copper–nickel
Cordless devices	Copper
Fingemail polish	Copper
Lawn and garden equipment	Bronze
Metal bond for diamond tools	Bronze, copper–nickel
Photographic equipment	Bronze, brash, nickel–silver

structural materials, brushes, filters, additives to iron powders (alloying as well as infiltration), catalysts, pigments and paints.

An assortment of bearings and parts of sintered bronze are shown in Figure 16.22. Bearings made from sintered bronze have a uniform interconnected porosity ranging generally from 18 to 30%. The pore volume is impregnated once only with oil, after which the bearing functions maintenance-free and self-lubricating. Because of these advantages, self-lubricated bearings account for a significant part of PM applications. There are also many applications for sintered bronze parts.

Various configuration carbon brushes suitable for conducting electrical current in sliding contacts are pictured in Figure 16.23. Fine electrolytic copper powders form a durable matrix in which dispersed graphite serves as dry lubricant and prevents seizing of the brushes. The dendritic particle shape ensures good mixability with graphite and high green strength.

Friction materials are required as linings for clutches and brakes. Typical arrangements are shown in Figure 16.24. Friction linings have the property of converting mechanical energy of motion to heat by means of friction, the heat in turn having

Figure 16.22 Assorted bearings and parts made from PM bronze. Courtesy of Norddeutsche Affinerie Aktiengesellschaft.

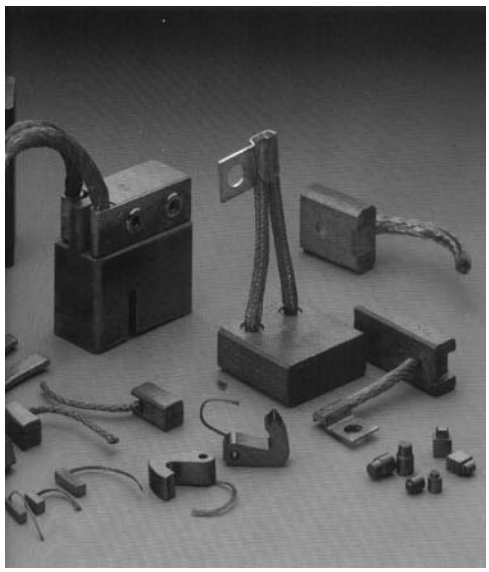

Figure 16.23 Typical carbon bronze brushes. Courtesy of Norddeutsche Affinerie Aktiengesellschaft.

to be continuously dissipated to prevent overheating. Various types of friction materials are employed depending on the amount of heat to be dissipated. In the capacity of friction components, silicon dioxide, aluminum oxide, silicon nitride, etc are employed. Graphite, lead, molybdenum sulfide, etc. play a part in lubricating components. In the case of smaller quantities of converted energy, it is sufficient to employ linings of the synthetic resin type, which

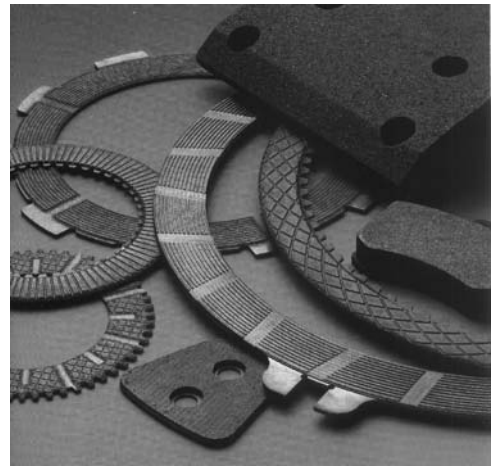

Figure 16.24 Friction PM parts assortment. Courtesy of Norddeutsche Affinerie Aktiengesellschaft.

may be reinforced with embedded metal particles, i.e. so-called semi-metallic linings. High-duty linings, on the other hand, contain continuous metallic solid which provides mechanical strength and good heat dissipation. In this matrix seizure preventing and friction producing components are embedded.

Formation and functional effectiveness of the supporting of the metallic matrix depend decisively on metal powder used. Dendritic copper powders ensure high green strength, intensive bonding between particles and high sintering activity, especially with the addition of elementary tin and liquid phase sintering.

Filters made of sintered bronze, exhibited in Figure 16.25, have a porosity of between 30 and 50%. A uniform distribution of interconnected pores having almost equal size and shape is characteristic. The size of the pores, and hence the permeability of the filter material, can be controlled by choosing suitable particle sizes in starting powder. Normally, the standard fractions used range from below 40 μm to 630–1000 μm.

Generally, manufacture is by the loose powder sintering process, and sintering is done in graphite or steel dies, mostly under hydrogen or cracked ammonia. Sintering temperatures are about 785°C, sintering times approximately 60 min. Spherical bronze powder contains about 0.35% phosphorus. The latter increases the surface tension of the melt to be atomized and so ensures a good spherical particle shape. The addition of phosphorus also reduces the solidus temperature of the tin bronze to about 700°C, which in turn allows the advantages of liquid phase sintering to be accomplished.

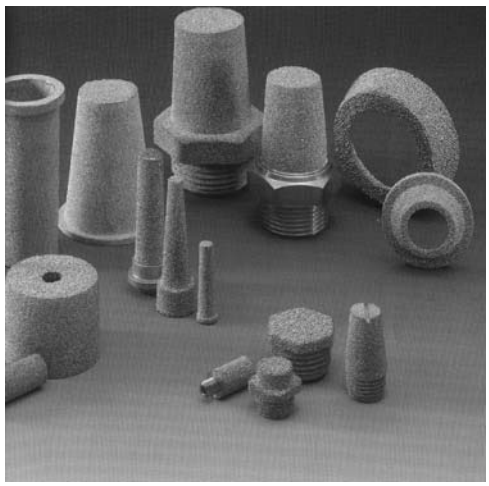

Figure 16.25 Filters made of sintered bronze spherical powders. Courtesy of Norddeutsche Affinerie Aktiengesellschaft.

Workplace Atmosphere Safety

Inspirable copper dust takes a predominantly fibrous effect. The ALV of copper aerosol in the workplace atmosphere as the shift time-weighted average concentration is 0.5 mg/m^3, while the threshold limit value (TLV) is 1.0 mg/m^3 and the copper powder production and processing is placed in the second class of danger of the four-class Standard system accordingly, State Standard 12.1.005-88 under the legislation in the Commonwealth of Independents States (CIS) [26]. The above State Standard standardizes ALV of copper phosphide, copper sulfhate, copper chloride, et al. The copper chromium phosphate is the most harmful inspirable substance among the standardized copper compounds and is placed in the first danger class. Its ALV limit is 0.02 mg/m^3.

Copper in drinking water imparts a foul taste and is related to the third, next to last class of danger and the TLV is 1.0 mg/l according to CIS State Standard 4630-88 [27].

Copper powder $<44\,\mu$m does not inflame in an aerogel state as well as in a suspended solid one in air. Data about combustibility of copper dust and some bronze and brass compositions also on prevention of inflammability can be found in Section 5, 'Safety Engineering in the Production of Powders'.

References

1. Williams, B., Powder metallurgy – a global market review. In *International Powder Metallurgy Directory & Yearbook*, 13th edn 1, 2008/2009, pp. 5–14.
2. Berry, D.F., Klar, E., Production of copper powders. In *ASM Handbook*, Vol. 7. ASM International Publishers, 1998, pp. 132–142.
3. S.S. Naboychenko, (ed.) *Handbook of Non-ferrous Metal Powders*. Metullurgiya, Moscow, 1997 (in Russian).
4. Sarkisjan, N.S. et al., Production of copper powders at the Alaverdsk mining-metallurgical integrated works. *Sov. Powder Metall. Met. Ceram.,* 1991, 5:91–96.
5. Neikov, O.D., Non-Ferrous powder production technologies. Article in *International Powder Metallurgy Directory & Yearbook,* 13th edn 1, 2008/2009, pp. 31–44.
6. Pelletiers, T.W., Berry, D.F., Production of copper alloy powders. In *ASM Handbook,* Vol. 7. ASM International Publishers, 1998, pp. 143–145.
7. Klar, E., Berry, D.F., Properties and selection: Nonferrous alloys and special-purpose materials. In *ASM Handbook,* Vol. 2. ASM International Publishers, 1990, pp. 392–402.
8. Kumar, D., Gaur, A.K., Electrochemical studies on production of electrolytic copper powders. *J. Electrochem. Soc. India,* July 1973:211–216.
9. Artamonov, V.P., Pomosov, A.V., Effect of foreign electrolytes on the production of copper by contact deposition. *Izv. V.U.Z. Cvetn. Metall,* 1976, 2:30–34 (in Russian).
10. Kotovskaya, S.L. et al., Manufacture of coarse copper powder from sulphamate electrolytes. *Sov. Powder Metall. Met. Ceram.,* February 1973:93–96.
11. Gurevich, L.I., Pomosov, A.V., The effect of chloride on electrodeposition of powdered copper precipitates. *Sov. Powder Metall. Met. Ceram.,* January 1969:10–15.
12. Singh, S.K., Akerkar, D.D., A continuous self-regulating method of making copper powder by electrolysis. *NML Tech. J.,* 1975, 17:23–26.
13. Pomosov, A.V., Numberg, M.I., Krymakova, E. G., Protection of copper powder against corrosion during manufacture and storage. *Sov. Powder Metall. Met. Ceram.,* March 1976:175–177.
14. Kotovskaya, N.L., Pomosov, A.V., Study various factors influence upon crystallization and dispersivity of copper powder produced by reduction. *J. Appl. Chem.,* 1970, 44(3):548–552 (in Russian).
15. Peissker, T., Production and properties of electrolytic copper powder. *Powder Met. Powder Technol.,* 1984, 18(2):87–90, 92–98, 100–101.
16. Popov, K., Maksimovich, M., Trnjancev, J., Dendritic electrocrystallization and the mechanism of powder formation in the potentiostatic electrocrystallization of metals. *J. Appl. Electrochem.,* 1981, 11:239–246.

17. Murashova, I.B., Potapov, O.A., Pomosov, A.V., Electroprecipitation of powder copper of homogeneous structure. *Sov. Powder Metall. Met. Ceram.,* 1988, 6:5–11.
18. Murashova, I.B., Korkin, S.L., Pomosov, A.V., Nikolskaya, N.R., Susloparov, D.G., Electroprecipitation of dispersed copper in terms of linear increase current. *Sov. Powder Metall. Met. Ceram.,* 1986, 10:8–11.
19. Balakina, M.L., Serpuchenko, E.A., Kourilenko, O.D., Copper powder production in two layer cells with fatty acids. *Sov. Powder Metall. Met. Ceram.,* 1984, 7:1–4.
20. Taubenblat, P.W., Smith, W.E., Evans, C.E., Production of P/M parts from copper powder. *Precis. Met.,* April 1972, 41.
21. Technical data from AMAX Metal Powders, AMAX Copper, Inc., 1968.
22. Peissker, E., *Metal Powders, Norddeutsche Affinerie.* Brillant-Offset Publ, Hamburg, 1986.
23. Nadkarni, A., Copper powder metallurgy alloys and composites. In *ASM Handbook,* Vol. 7. ASM International Publishers, 1998, pp. 859–873.
24. Benjamin, J.S., The International Nickel Company Inc., US Patent 3,785,801 (1974).
25. Nadkarni, A.V., Klar, E., SCM Corporation, US Patent 3,779,714 (1973).
26. Commonwealth of Independents States Standard GOST 12.1.005−88. Publishers of Standards, Moscow, 1988 (in Russian).
27. Sanitary Regulation and Standards of surface waters from pollution, SanPiP 4630–88. Publishers of MinZdrav, Moscow, 1988 (in Russian).

Chapter 17

Production of Nickel and Nickel-alloy Powders

Stanislav S. Naboychenko, Irina B. Murashova, Ural State Technical University (UPI), Yekaterinburg, Russia
Oleg D. Neikov, Frantsevich Institute for Problems of Materials Science (IPMS), Kiev, Ukraine

The two main processes for producing nickel powder are the carbonyl process, where nickel carbonyl is decomposed, and hydrometallurgical techniques, where the reduction of an aqueous solution of a nickel salt with hydrogen under pressure is realized (the Sherritt process). Nickel and nickel-alloy powders can also be produced by inert gas or water atomization, by electrolytic method, solid-phase reduction and by mechanical alloying.

Carbonyl Process of Nickel Powder Production

The manufacture of nickel powders by the decomposition of nickel carbonyl dates back to a process developed in 1889 by Ludwig Mond together with his collaborators Carl Langer and Friedrich Quincke. They found that carbon monoxide at atmospheric pressure and a temperature between 40 and 100°C reacts with active nickel to form a colorless gas and nickel tetracarbonyl:

$$Ni + 4CO \xleftrightarrow{50°C} Ni(CO)_4$$

They further showed that the reaction is easily reversible by heating the nickel tetracarbonyl to temperatures in the range 150–300°C:

$$Ni(CO)_4 \xleftrightarrow{230°C} Ni + 4CO$$

Formed nickel that has been in contact with air does not react with carbon monoxide, which is why carbonyls were not discovered earlier.

Mond built an experimental plant near Birmingham, England, and developed the carbonyl process for separating nickel from Canadian matte containing 40% Ni. Opening in 1895, the plant produced 1.5 tonnes of nickel weekly. Mond afterwards opened a refinery in Clydach, Wales and, during 27 years the refinery operated, the factory processed more than 90 000 tonnes of nickel in the form of pellets. In this process which, in modified form, is still used at the Clydach refinery, nickel oxide manufactured by roasting nickel sulfide is recovered to nickel sponge by hydrogen, activated by sulfiding and volatilized as carbonyl in an atmospheric reactor. Nickel carbonyl manufactured in this way is decomposed directly in the powder and pellet apparatus as a section of a continuous process of refining.

Nickel Tetracarbonyl Formation and Decomposition

Conversion of nickel to a carbonyl at a fixed temperature depends primarily on the partial pressure of the carbon monoxide present. For given conditions of surface activity, the rate of gaseous or liquid formation is determined by the reaction temperature and increases with increasing partial pressure of carbon monoxide. A feature of the dependence of system pressure and temperature on reaction rate in the formation of nickel tetracarbonyl is a peak corresponding to optimal temperature, as shown in Figure 17.1 [1]. The effect of increased system pressure on conversion of nickel to carbonyl has been shown experimentally and proved commercially.

The nickel tetracarbonyl formation reaction is highly exothermic:

$$Ni + 4CO \rightarrow Ni(CO)_4$$
$$\Delta_f H^{298} = +160.4\,kJ/(g \cdot mol)\ \{38.4\,kcal/(g \cdot mol)\}$$

Therefore, a high conversion-rate commercial nickel carbonyl process requires a large heat removal system.

At room temperature, nickel tetracarbonyl is a colorless volatile liquid with a high vapor pressure. It boils at about 43°C at atmospheric pressure and begins to decompose at 60°C or less, depending on the conditions, its melting point is −25°C, specific gravity amounts to 1.36135 at 0°C and 1.27132 at 36°C.

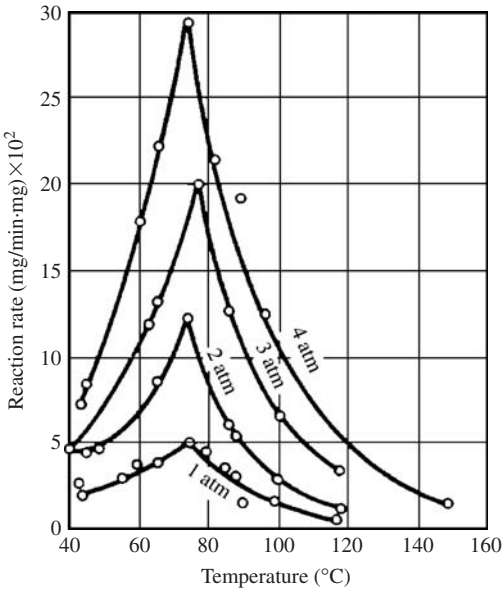

Figure 17.1 Dependence of system pressure and temperature on reaction rate in the formation of nickel tetracarbonyl.

Nickel tetracarbonyl is only weakly soluble in water, but is easily miscible with many organic solvents.

The stability of metal carbonyls varies a good deal. Nickel tetracarbonyl begins to liberate carbon monoxide and nickel at 0°C in a vacuum and the decomposition becomes appreciable above 60°C in an inert gas under atmospheric pressure.

In the formation of powder particles from the gaseous phase, several phenomena, jointly taking place, cause processes to come into play. They include the formation of complex nuclei, secondary crystallization of nickel on the surface of the finest particles and the interaction of particles in the crystallization process. At the specified temperature, the homogeneous part of the decomposition of nickel tetracarbonyl obeys the rate equation shown by H. Carlton and W. Goldberger [2]:

$$r = \frac{K_0\, p_{ca}}{1 + K_g\, p_{co}}$$

where r is the decomposition rate in grams per cubic centimeter per hour, K_0 is the rate constant in grams per square centimeter per hour, K_g is the adsorption constant of carbon monoxide on metal in $torr^{-1}$, p_{ca} is the partial pressure of carbonyl in torr, p_{co} is the partial pressure of carbon monoxide in torr. The decomposition rate for nickel tetracarbonyl is directly proportional to the partial pressure of the carbonyl and inversely to the partial pressure of the residual carbon monoxide.

Conditions that affect the formation of the nickel particles during carbonyl decomposition (such as processing temperature and the concentration and rate of the nickel tetracarbonyl feed to the decomposer) can vary significantly. These influence the physical and technical properties of the powders. Additions to the nickel tetracarbonyl into the decomposer can change the mechanism of powder forming, as well as particle morphology. Thus, hydroquinone sublimated with the carbonyl functions as a free radical trap, acting in the formation of macro particles of nickel metal.

The most important industrial application area of nickel tetracarbonyl is for refining nickel, where nickel pallets and powder products are manufactured. The plated products and a wide range of metallic and non-metallic (for example, nickel-coated graphite) powders can be produced by making coatings of nickel on various surfaces by means of decomposition of the carbonyl under special conditions. Nickel tetracarbonyl found application as a catalyst for organic synthesis, as well as providing a means for the manufacture of several organonickel compounds. It also serves to form nickel molds for the glass industry and for vapor plating on smooth surfaces such as plastic and metal.

Commercial Technique

Currently, the largest producers of high-purity nickel powders manufactured by the thermal decomposition of nickel tetracarbonyl are Inco Company with factories in Clydach, Wales, UK and in Copper Cliff, Sudbury, Ontario, Canada, and Norilsk Nickel Company, Russia.

The thermal decomposition of nickel tetracarbonyl processes are distinguished by pressure value as the low, atmospheric pressure carbonyl technique, as high pressure amounts to 20 MPa, and as average pressures ranging from 2 MPa to 7 MPa.

Spongy nickel (product of reduction of process wastes or natural nickel ores), copper–nickel converter mattes, natural ores, metallic nickel (metal-working cuttings), alloys of copper–nickel–iron system, anode scrap and etc. are used as raw materials.

Low Pressure Carbonyl Technique

The current Clydach refinery still uses the basic concept of the Mond–Langer process and produces nickel powders using the atmospheric pressure carbonyl technique. The use of feed matte as the granular nickel oxide containing small amounts of copper, cobalt, iron and siliceous matter make it possible to employ low pressure carbonyl processing. The latest

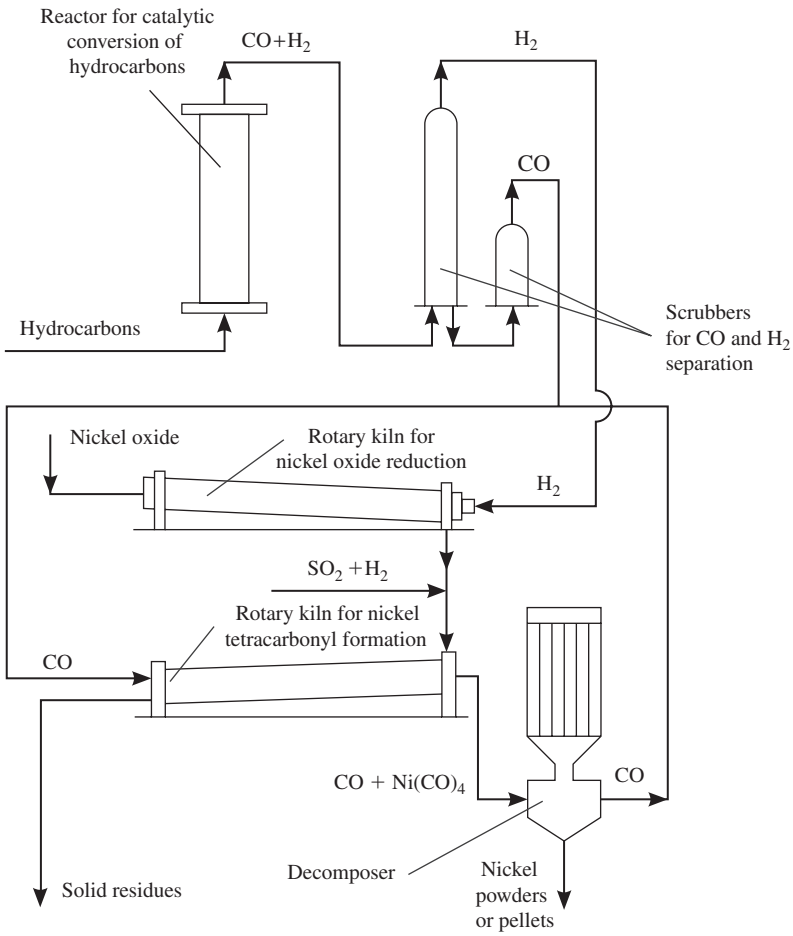

Figure 17.2 Schematic of the Mond-Langer process for manufacture of nickel products using atmospheric pressure carbonyl processing.

innovations comprised replacement of the many small hearth-type reducers and volatilizers of the original plant by large rotary kilns arranged in lines of two kilns with a smaller sulfiding unit. In the initial unit of each line, the nickel matte feed is reduced to metal by a countercurrent flow of preheated hydrogen at temperatures ranging from 400 to 500°C (Figure 17.2).

The reduced nickel matte is then activated by sulfiding with increasing sulfur concentration to 2 wt% and is sublimated in the final kiln at atmospheric pressure and temperature in range from 50 to 70°C by a countercurrent flow of carbon monoxide. This horizontal rotary kiln (5 m in diameter, 40 m length) has 200 tonne capacity (Figure 17.3). It is divided into two sections: the first section is equipped with scrapers for material intermixing and in it the extraction of the bulk of the nickel is accomplished; the second section completes the extraction of nickel. Collected dust is supplied into it by a screw conveyer. The carbon monoxide is injected along the whole reactor length. Duration of carbonyl processing is about 96 hours, nickel yield amounts to 95%. There is no necessity in the devices for carbonyl nickel cleaning owing to the soft mode of metal carbonyl formation practically excluding the formation of impurities (iron and cobalt carbonyls).

The obtained nickel tetracarbonyl vapor is transferred to the decomposition device where seed (carbonyl nickel powder) is added (Figure 17.4). A bucket elevator provides continuous circulation of formed pellets through the decomposer to achieve commercial size amounts of 5–10 mm.

Pellets (or powder) from the elevator are introduced into the top of a tubular heater (1.2 m in diameter, 6.7 m height) to separate the particles with commercial size. Commercial size particles are additionally processed in a classifier and removed from the cycle. Under seeding fractions are returned to the elevator. Non-commercial size particles are heated up to 200–230°C in a heater. Then they are transferred into a heat-insulated decomposer in which nickel tetracarbonyl vapor and carbon monoxide at 70°C are injected. Carbon monoxide containing 0.1% $Ni(CO)_4$ is removed from the top of the chamber and returned to the synthesis stage. Carbonyl content in the

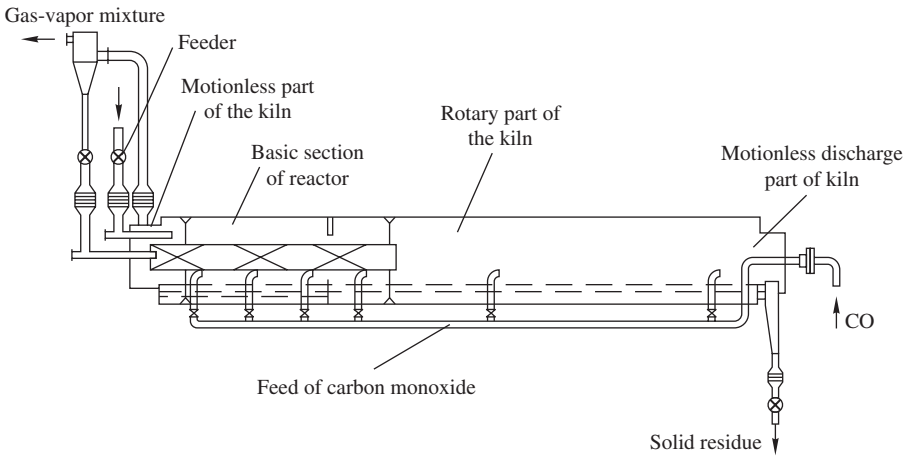

Figure 17.3 Rotary kiln for synthesis of nickel carbonyl at Clydach refinery.

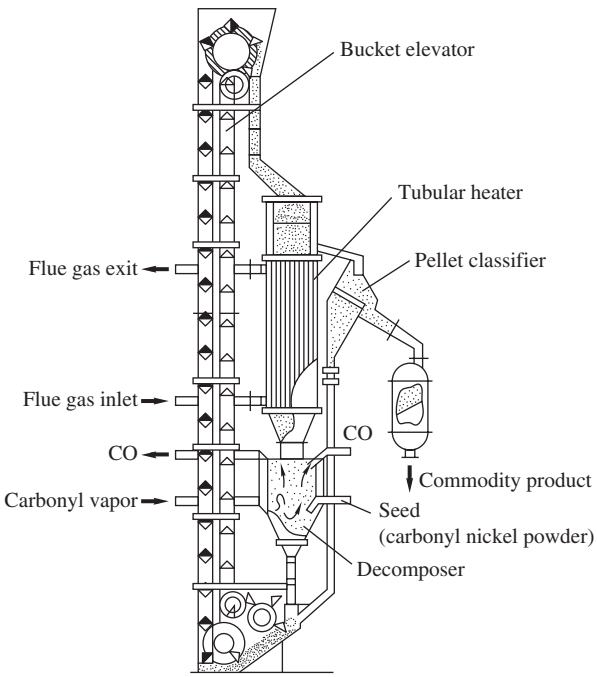

Figure 17.4 Schematic of the decomposer for carbonyl nickel pellet production.

gas–vapor mixture is max 15 wt% to prevent the pellet coalescence by high rate of nickel deposition.

The carbonyl low pressure process is continuous, automated and economical.

Average Pressure Carbonyl Technique

The Copper Cliff refinery uses the same basic process chemistries, but forms nickel tetracarbonyl at elevated pressure, which is necessary to extract nickel in the presence of high copper concentration. The plant feed is a mixture of oxides and sulfides of nickel, copper, iron and cobalt, other crude metallics and refinery residues that contain nickel.

This mixture is charged with coke into one of two 64 tonne capacity, top-blown rotary converters (Figure 17.5). In this process, silicates and some of the iron is slagged off and the liquid metal is then granulated by water atomization.

In this condition, the granules contain 65–75 wt% Ni, 15–20 wt% Cu, 2–3 wt% Fe and 3 wt% S represented as sulfides.

The dried metallic granules are batch fed into a 136 tonne capacity reactor (Figure 17.6), where they are reacted with carbon monoxide at temperatures up to 180°C and pressures up to 7 MPa. Nickel, and some iron, is extracted as a crude carbonyl sublimate, while copper, cobalt, precious metals and impurities are retained in the residue. Iron removal is controlled to between 20 and 50% of the input volume. Cobalt does not form carbonyl compounds, because they occur only when carbon monoxide pressures of 15 MPa are achieved. The reactors are water cooled because the nickel tetracarbonyl formation is exothermic.

Extracted carbonyl sublimates are condensed and stored at atmospheric pressure. The carbon monoxide carrier gas is recycled. The condensed product, containing both soluble nickel and iron carbonyls, is next pumped to rectifying columns, where it is separated into nickel tetracarbonyl vapor and iron rich liquid carbonyl. Rectifying the raw carbonyl liquid is achieved easily, owing to the fact that the boiling points of the nickel and iron carbonyls are 43°C and 102.8°C, respectively. The technique manufactures nickel tetracarbonyl vapor of 99.998% purity, with the bottom liquor having nickel-to-iron ratios of up

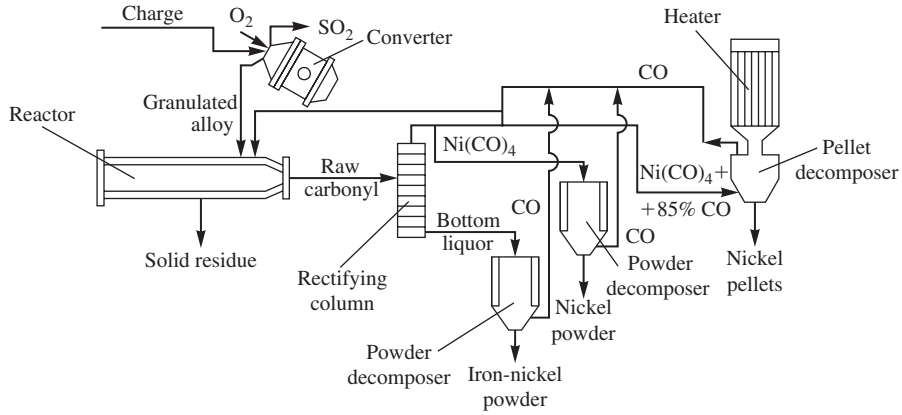

Figure 17.5 Flow sheet of the Copper Cliff nickel refinery process for manufacture of nickel products using elevated pressure carbonyl processing.

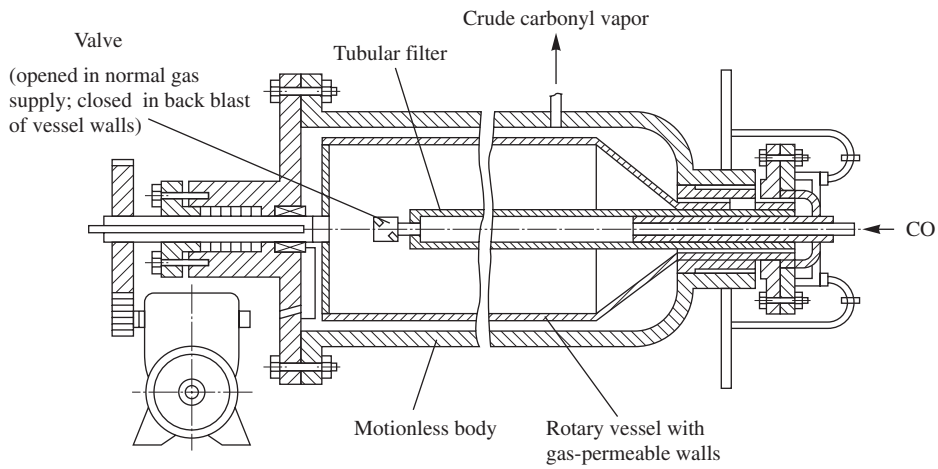

Figure 17.6 Reactor for synthesis of nickel carbonyl at elevated pressures.

to 3 to 7. From the top of the column, nickel tetracarbonyl vapor is exhausted off and fed into powder decomposers. A little below the top of the column, liquid nickel tetracarbonyl is taken off and either kept in storage or delivered to nickel pellet decomposers.

The powder decomposers are steel cylinders with heated jackets. Nickel carbonyl vapor is introduced into the decomposer chamber slightly above atmospheric pressure, where it contacts the heated decomposer walls that are preset at a temperature between 250 and 350°C. The nickel tetracarbonyl decomposes into nickel powder, with the release of carbon monoxide. The latter is recycled though filters and fed by a gas compressor to the pressure carbonyl reactors, while the powder is collected, gas purged, stabilized by a surface oxide film and transferred to storage completely free from carbon monoxide and carbonyl.

High Pressure Carbonyl Technique

High pressure carbonyl processes are required in the case of feed concentrates that contain high amounts of copper, cobalt and iron, as well as other impurities. This process is used at the Severonickel refinery, located approximately 200 miles from St Petersburg, Russia, where commercial production of carbonyl nickel powder was begun in the early 1960s. The feed matte is based on the ores of nickel–copper deposits in Norilsk, Siberia, and Pechenga, near the border of Russia with Norway. Currently, in these regions, the Norilsk Nickel company mines about 12 million tonnes per year.

The high-grade pyrite ores are ground in ball mills and the milled material is processed in a smelter, and is then converted to matte. The latter is reacted with carbon monoxide at pressures up to 25 MPa to

produce a high-purity nickel tetracarbonyl that is separated from the iron and other carbonyls as a result of condensation, distillation and vaporization. The thermal shock decomposes nickel tetracarbonyl into nickel powder, with the release of carbon monoxide. The powder is discharged from the decomposers and packed in steel drums.

Health and Environment Protection Measures in Carbonyl Nickel Production

Carbonyl nickel manufacture carries significant danger and harmful conditions. Nickel carbonyl is a highly toxic agent; the occupational exposure limits (OEL) of the nickel tetracarbonyl in the workplace atmosphere under the legislation in the Commonwealth of Independent States (CIS) [3], amounts to 0.0005 mg/m^3; lethal dose amounts to 0.1 mg/m^3. It causes acute and chronic intoxication and it is a weak carcinogen. Fatalities due to intoxication during production have been reported.

Toxic carbon monoxide can be responsible for acute and chronic poisoning in the manufacture process. Under 'Health and Safety' legislation in the European PM industry, the long- and short-term OELs for carbon monoxide in the workplace atmosphere are 50 vpm (60 mg/m^3) and 300 vpm (360 mg/m^3), respectively [4]. The long-term OEL for carbon monoxide in the workplace atmosphere is 20 mg/m^3 (≈17 vpm) according to 'Health and Safety' legislation in the Commonwealth of Independent States (CIS) [3].

Nickel carbonyl dissolves in process water up to dangerous concentrations due to significant water solubility amounting to 180 mg/L at a temperature of 10 °C. Its maximum allowable concentration in aqueous medium is not officially stated, but the admissible concentration limit of nickel amounts to 0.001 mg/L according to SanPiN 4630-88 [5]. Conditional admissible concentration limit of nickel carbonyl in water is 0.0003 mg/L providing the OEL in the air equilibrium layer with water surface.

Detailed information on health and environment protection measures in the carbonyl industry can be found in Chapter 7.

Powder Properties and Applications

Powder properties depend on the conditions of nickel carbonyl decomposition and their extra processing. Light (2–4 μm) and heavy (3–10 μm) nickel powders and also 5–10 mm pellets are mainly produced in industry.

Generally, four types of nickel powders produced by thermal decomposition of nickel tetracarbonyl are differentiated: acicular powder particles, chain-like, high surface area powders and high density semi-smooth particles. These powders exhibit uniform size and structure and high surface area and the technique ensures a high degree of purity.

Basic characteristics of Inco types and Norilsk Nickel types of carbonyl nickel powders are shown in Table 17.1. Inco heavy powders are marked by '100' series and light powders by '200'. Acicular particles are the characteristic type of nickel powder produced by carbonyl decomposition (Inco types 120–123 and Norilsk Nickel type IL5). They are fine and regular in shape, with rough surfaces (Figure 17.7) [6].

The Inco powder typically contains 700–900 ppm (0.07–0.09 wt%) oxygen, 3–5 ppm (0.0003–0.0005 wt%) iron, max 1 ppm (0.0001 wt%) sulfur and 600–700 ppm (0.06–0.07 wt%) graphitic carbon. The Fisher subsieve size is 3–7μm, apparent density is 1.8–2.7 g/cm^3 and surface area amounts to 0.4 m^2/g (BET) [7].

Chain-like nickel powders (Inco types 255, 287, etc., Norilsk Nickel type 1L7, 1L8, etc.) are characterized by their acicular, chain-like structure of relatively fine particles, which make them fluffy in character, with low apparent density 0.45–1.0 g/cm^3 and large specific surface area 0.6–0.7 m^2/g (BET). The typical structure and chain-like shape of this powder type are shown in Figure 17.8.

Ultra fine nickel powders (e.g. Inco type 210, Norilsk Nickel type S10 (Figure 17.9)) also have chain-like morphology, but the particles are finer, the Fisher subsieve size is 0.5–1.0 μm and specific surface areas range from 1.5 to 6 m^2/g depending on the grade.

Semi-smooth high density nickel powders exist in fine and coarse sizes. The fine Inco type 337 ranges from 10 to 40 μm in diameter and Norilsk Nickel type UT1 from 7 to 8.5 μm respectively (Figure 17.10); the coarse is 400–1000 μm in diameter. Powder apparent density ranges from 3.5 to 4.2 g/cm^3.

A large portion of the carbonyl nickel product is manufactured in the form of pellets (i.e. spherical granules) ranging from 5 to 13 mm in diameter. Pellets are characterized by a laminated (shaped like an onion) structure (Figure 17.11). This structure is formed as a result of multiple passing of particles through the decomposer to achieve the required pellet size.

The presence of iron carbonyl impurities, to 1–2 wt%, catalyzes the reaction of carbon monoxide thermal decomposition and influences the nickel powder particle shape formed at the stage of nickel carbonyl decomposition. Spherical nickel particles

Table 17.1 Basic characteristics of Inco and Norilsk Nickel carbonyl nickel powders

Type	Average particle size (μm)	Particle shape	Apparent density (g/cm^3)	Angle of repose (degree)	Content of impurities (wt%)			
					O	C	Fe	S
Inco powders[a]								
210	0.5–1.0	Chain-like	<0.5	...	0.10	0.05–0.15	<0.01	0.002
255	2.6–3.4	Chain-like	0.45–0.6	72	0.10	0.05–0.15	<0.01	0.0002
287	2.9–3.6	Chain-like	0.8–1.0	66	0.10	0.05–0.15	<0.01	0.0002
100	3–5	Acicular	1.6–2.1	65	0.10	0.05–0.20	<0.01	0.0002
122	4–7	Acicular	1.9–2.5	60	0.10	0.05–0.10	<0.01	0.0002
128	7–9	Acicular	2.5–3.0	48	0.10	0.05–0.10	<0.01	0.0002
337	40–300	Semi-smooth high density	3.5–4.0	...	0.25	0.08–0.10	0.01–0.05	<0.001
Norilsk Nickel powders and pellets[b]								
S 20	1.85–2.2	Chain-like	0.51–0.64	...	...	0.09	0.0015	0.0007
S 30	2.91–3.5	Chain-like	0.6–0.8	...	...	0.28	0.002	0.001
1L5	2.1–2.4	Acicular	1.01–1.4	...	...	0.28	0.002	0.001
1L8	1.4–1.6	Chain-like	0.45–0.6	...	...	0.001	0.002	0.001
UT1	7–8.5	High density	3.0–3.5	...	0.02	0.1	0.003	0.0001
UT3	3–6	Quasi-cubic shape	1.91–2.5	...	0.02	0.072	0.003	0.0001
DNK-0	7–13 mm	Spheroidal	...	...	...	0.015	0.015	0.001

[a]Content of other impurities, wt%: Zn, Zr < 0.01; Al, B, Mg < 0.005; Bi, Co, Cr, Cu, Mn, Mo, Pb, Si, Sn, Ti < 0.001.

[b]Content of other impurities <0.006 wt%; more information about Norilsk Nickel carbonyl products can be found on http://www.nornickel.ru.

with an 'onion-shaped' structure are formed due to carbon monoxide decomposition with a carbon content up to 1 wt%. Particle surfaces are transformed into acicular-shape (see Figure 17.7) during decomposition of nickel tetracarbonyl when carbon monoxide content is approximately 0.05 wt%. Detailed information on 'onion-shaped' structure forming can be found in Chapter 7.

Chemical composition of commercial pellets (e.g. Norilsk Nickel type DNK) includes 99.95–99.98 wt% Ni, 150 ppm C, 150 ppm Fe, 10 ppm Cu, 10 ppm S, 5 ppm Co, 1 ppm Pb, 1 ppm As. The low-melting-points elements and dissolved gas impurities in carbonyl pellets are higher than in all grades of electrolytic nickel products.

The Norilsk Nickel carbonyl powders are distinguished by high purity above 99.9 wt% metallic nickel, with a low level of oxidation, and of other impurities, especially iron and cobalt.

The properties of these high purity nickel powders have been tailored to meet the demanding requirements of the chemical, energy and metal industries. Currently, these products provide the basic nickel source for a wide range of specialized products.

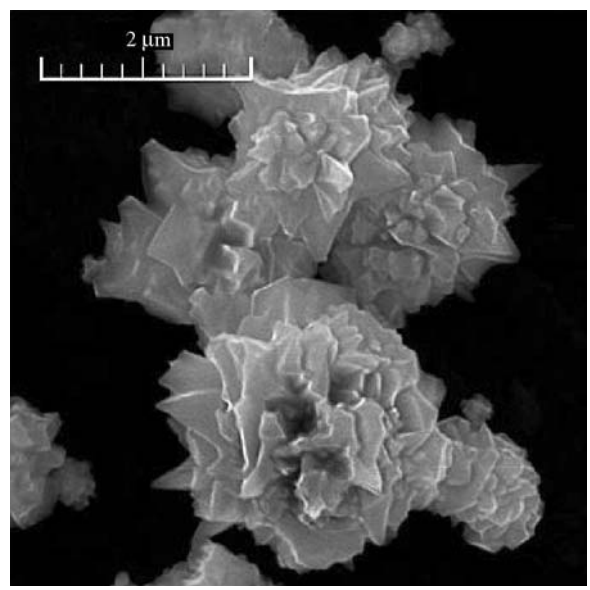

Figure 17.7 Scanning electron micrograph of ordinary type of nickel powder produced by carbonyl decomposition. Courtesy of Norilsk Nickel Company

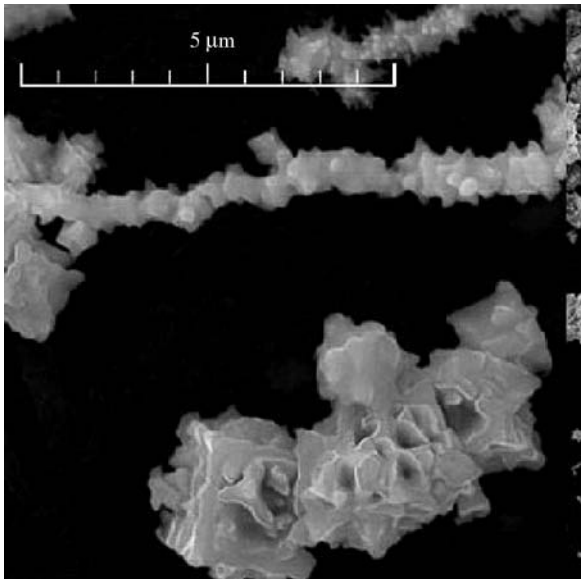

Figure 17.8 Scanning electron micrograph of chain-like type of nickel powder produced by carbonyl decomposition. Courtesy of Norilsk Nickel Company

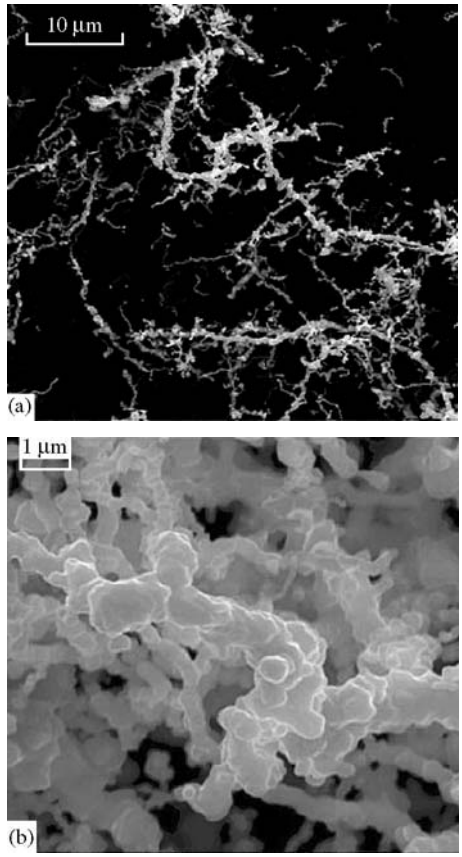

Figure 17.9 Scanning electron micrograph at lower (a) and higher (b) magnifications of ultrafine powder particles connected in the chains produced by carbonyl decomposition. Courtesy of Norilsk Nickel Company

Commonwealth of Independents States Standard GOST 9722 (see Appendix 2) differentiates the four brands of carbonyl nickel powder depending on their chemical composition: PNK-U, PNK-0, PNK-1, and PNK-2, respectively. Nickel content in PNK-U and PNK-0 is min 99.9 wt%, in PNK-1 and PNK-2 is min 99.7 wt%. Content of 18 impurities is regulated in these powders. According to the apparent density, the powders are divided as follows: T, heavy; L, light, K, coarse. Each of them is subdivided by particle morphology and size. Apparent density classification of carbonyl nickel powders accordingly with GOST 9722–97 is given in Table 17.2.

The carbonyl nickel powders and pellets have a wide application, including PM components, rechargeable batteries and fuel-cell electrodes, magnets, ferrites, hard alloys, chemical and catalysts, welding products, pigments and coatings, electronic alloys, getters, conductive resins and plastics. Application areas of Inco type and Norilsk Nickel type carbonyl nickel powders are given in Table 17.3.

The strongly linked chain morphology in combination with a low apparent density, high surface area of ultra fine carbonyl nickel powders is favorable for the production of sintered plates with a porosity approaching 90% which is strong enough to withstand the stresses during charging and discharging of rechargeable batteries. Nickel powders (Norilsk Nickel types S) are characterized by their unique, chain-like, highly convoluted structure, with low apparent density ranging from 0.52 to 0.56 g/cm^3 and specific surface area ranging from 1.5 to 2.0 m^2/g (Figure 17.12), which make them suitable for manufacturing rechargeable batteries. Ultra fine nickel powder Inco type 210 also answers the above demands.

Carbonyl nickel powders have an advantage over the conventional lead-acid batteries, the electrical power of which decays rapidly at low temperatures. This is of paramount importance for reliable starter batteries in countries with cold winters.

Generally, the requirements of nickel containing composition powders for PM applications consist of high purity, high rate diffusion transfer by interaction with the surrounding particles of other powders, high specific surface area and a reasonably narrow particle size distribution. These powders are fine and regular in quasi-cubic shape, with rough surface projections. Typical of such powders is Norilsk Nickel type UT3 (Figure 17.13).

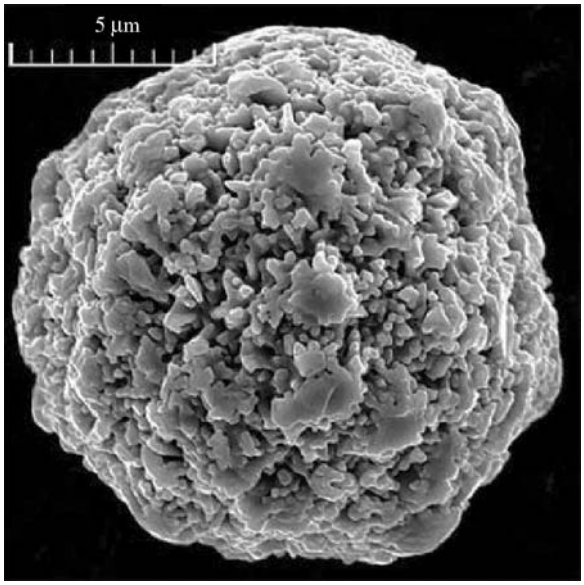

Figure 17.10 Scanning electron micrograph of semi-smooth high density nickel powder produced by carbonyl decomposition.

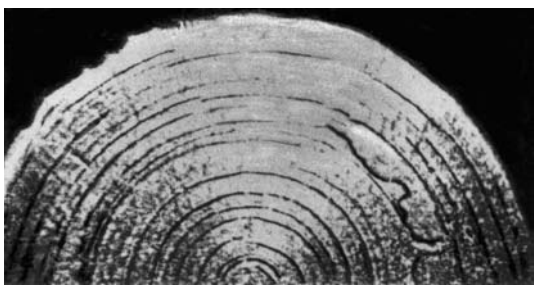

Figure 17.11 Micrograph of cross-section of a carbonyl nickel pellet.

Due to its purity, carbonyl nickel is used for the production of steel and special alloys, including cobalt-free steels and alloys for nuclear power and of refractory materials, because the absence of volatile impurities is very important for materials used under load at high temperatures.

In chemical and catalyst applications, the fine particle size and high specific surface area of carbonyl nickel powders promote their rapid dissolution in acid for the production of high purity nickel chemicals and catalysts. A particular interest is their use in the production of reformer catalysts in oil refining. During the reforming of crude oil, hydrogen is passed through a ceramic tube impregnated with nickel, and the process of converting crude oil to high octane fuel is appreciably accelerated.

In the area of paints and plastics, the inherent electromagnetic properties of nickel, coupled with its oxidation resistance, have enabled the carbonyl nickel powder to be used as a shield against electromagnetic interference (EMI). Currently, most electronic devices are enclosed in plastic casings to protect the components with an inexpensive, esthetically pleasing design. Plastics, however, lack one essential feature: they are not conductive and, consequently, do not shield electronic equipment from unwanted EMI. Although nickel is not quite as good a conductor as copper and silver, it absorbs more EMI than most metals because of its high magnetic permeability.

Carbonyl powders are characterized by free-flowing, good compressibility and easy-sintering.

Nickel-based alloys and compositions are characterized by high corrosion resistance and stability to high temperature oxidation and are used for gaseous thermal spraying to provide a protective coating on components operated in corrosion environments, conditions of abrasive wear and dry friction, at high temperatures.

Table 17.2 Apparent density of carbonyl nickel powders accordingly with GOST 9722-97 (CIS)

Powder type	Sub-group according to apparent density	Apparent density (g/cm^3)
PNK-UT1, PNK-OT1, PNK-2T1	1	3.00–3.50
PNK-UT2, PNK-OT2, PNK-2T2	2	2.50–2.99
PNK-UT3, PNK-OT3, PNK-2T3	3	1.91–2.50
PNK-UT4, PNK-OT4, PNK-2T4	4	1.41–1.90
PNK-1L5, PNK-2L5	5	1.01–1.40
PNK-1L6, PNK-2L6	6	0.81–1.00
PNK-1L7, PNK-2L7	7	0.61–0.80
PNK-1L8, PNK-2L8	8	0.45–0.60
PNK-2K9	9	1.30–1.70
PNK-2K10	10	min 1.20

The thermoreacting compositions, 'nickel-metal' (Ni-Al, Ni-Ti), 'nickel-carbide' (Ni-WC), 'nickel-oxide' (Ni-ZrO_2), and 'nickel-metal-oxide' (Ni-Al-WO_3), for spraying of resistant wear-refractory coatings and heat insulating plasma coatings and 'solid lubricant-nickel' composition for antifriction coatings and friction units working at dry friction or in water (nickel-graphite, nickel-boron nitride) are produced by vapor-phase precipitation of nickel on powder particles (cladding).

Characteristic nickel coated graphite (NCG) powders are of two types, containing nickel 60 wt% and 75 wt% respectively. The first clad type consists of 95 wt% sieve size fraction 100–250 μm in diameter, and apparent density of the powder ranges from 1.4 to 1.5 g/cm^3; the second clad type consists of 90 wt% sieve size fraction 200–325 μm in diameter and the apparent density ranges from 1.7 to 1.9 g/cm^3.

Combination of low density graphite with a layer of conductive nickel results in a lightweight filler suited for conductive gaskets (extruded, molded, sheet), sealants and plasma sprays.

In silicone gasket rings, conductive fillers are used manufactured from carbon black, NCG, silver plated materials (AgAl, AgCu, AgNi, Ag-glass) and pure silver. NCG is significantly better than carbon black, less effective than pure silver and comparable to silver coated materials. NCG is 3–4 times less expensive than silver plated materials and pure silver.

Carbonyl powders are characterized by free-flowing, good compressibility and easy-sintering.

High porous electrodes (porosity is in range from 70 to 90%) for nickel-cadmium accumulators and hydrogen-oxygen fuel element, elements of electronic equipment, sintered magnets, easy regenerated filters, catalysts are made of them.

Hydrometallurgical Processing

The production of nickel powders by hydrometallurgical processing involves leaching, solution purification and metal recovery operations. As the recovery stage is accomplished in the autoclaves at elevated pressures and temperatures, it is called also autoclave processing [8].

The Sherritt refinery in Fort Saskatchewan, Alberta, Canada, is an example of hydrometallurgical processing used in the manufacturing of nickel powders [9]. This process is adaptable to operate with a wide assortment of different feedstocks, predominantly the sulfide concentrates. A schematic diagram of the Sherritt process is shown in Figure 17.14. This process has been also adopted by Western Mining Corporation in a refinery at Kwinana, Western Australia.

Table 17.3 Application areas of Inco type and Norilsk Nickel type carbonyl nickel powders

Application area	Carbonyl nickel powder types	
	Inco type	Norilsk Nickel type [6]
Rechargeable batteries	210, 210, 255, 287	S10, S20
Fuel cells	210, 210H, 255, 287	S20, S27, S30, 1L5, 1L6, 1L7, 1L8
Domestic batteries	210	1L5, 1L6, 1L7, 1L8
Powder metallurgy components	4SP	UT1. UT2, UT3-PM, UT4, US3-1CG, US3-1CGL, 1L5, 1L6, 1L7, 1L8
Chemicals and catalysts	110, 210	UT1. UT2, UT3-PM, UT4, US3-1CG, US3-1CGL, 1L5, 1L6, 1L7, 1L8
Magnets	HDNP, 525	US3-1CG, US3-1CGL, 1L5, 1L6, 1L7, 1L8
Hard metals	210, 210H	US3-1CG, US3-1CGL, 1L5, 1L6, 1L7, 1L8, UT1. UT2, UT4
Electronics	110, 525	S20, S27, S30, 1L5, 1L6, 1L7, 1L8
Paints, inks	110, 525	S10
Welding	4SP	UT1. UT2, UT3-PM, UT4,US3-1CG, US3-1CGL

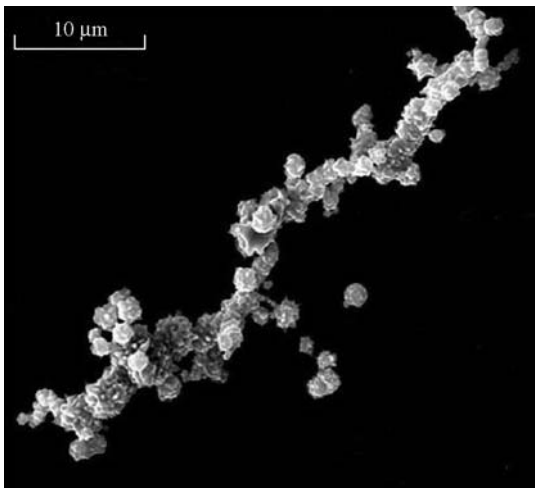

Figure 17.12 Scanning electron micrograph of linked particle nickel powder type produced by carbonyl decomposition. Courtesy of Norilsk Nickel Company

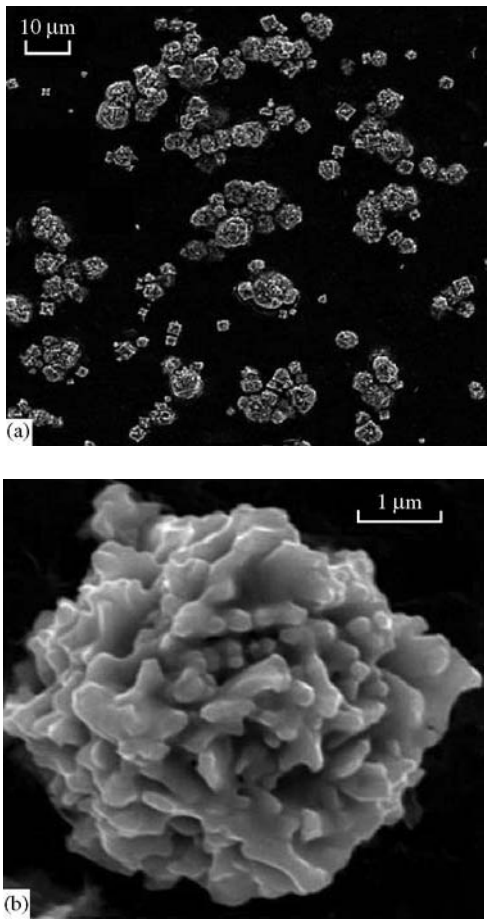

Figure 17.13 Scanning electron micrograph at lower (a) and higher (b) magnifications of quasi cubic shape powder produced by carbonyl decomposition. Courtesy of Norilsk Nickel Company

Feed Processing

Currently, the main feed to the Sherritt refinery is a nickel and cobalt sulfide produced in Moa Bay, Cuba. The sulfide ore from the Moa Bay deposits is high in iron along with cobalt. The processing of this ore is accomplished by means of high pressure leaching with sulfuric acid. The key operation in this process is the separation of nickel and cobalt from iron, which typically constitutes 50 wt% of the ore. It is possible to achieve the selective dissolution of nickel and cobalt with less than 1 g/L iron in the leach liquor. The typical chemical composition of nickel-cobalt sulfide produced in Moa includes 51–56 wt% Ni, 5.0–6.0 wt% Co, 0.5–0.8 wt% Fe, 0.1–0.2 wt% Cu, 1.0–1.3 wt% Zn, 32–37 wt% S. This concentrate is packaged in the form of a wet filter cake and transported to the refinery in Fort Saskatchewan.

Leaching

The first stage in the refining process is the leaching of the metal content from the sulfide feed. The leaching process is carried out at elevated temperature and pressure in continuous conditions during interaction between the fine sulfide concentrate and ammonium sulfate in the autoclaves. The typical conditions in the leach autoclaves are the following: temperature 90–95°C, pressure 0.77–0.84 MPa (110–120 psig), ammonia 80–110 g/L, ammonium sulfate 150–200 g/L. The resulting leach reaction is the oxidative dissolution of the metal sulfides to soluble amine complexes with the simultaneous oxidation of sulfide to salts including sulfate (SO_4^{2-}). The general equation for the ammoniacal leaching of the sulfides may be represented as:

$$MS + n NH_3 + 2O_2 \rightarrow M(NH_3)_n^{2+} + SO_4^{2-}$$

where M is nickel, cobalt, iron, copper, zinc; n ranges from 2 to 6.

The leaching process uses the differing stability of the amine complexes. The iron amine complex is hydrolyzed to a hydrated iron oxide, $Fe_2O_3 \cdot H_2O$, because it is the least stable. The leach slurry is delivered to a thickener where the leach liquor is separated from the solid residue of the precipitated hydrated iron oxide.

In reality, the reaction chemistry of the leaching process is significantly more complicated due to the peculiar behavior of sulfur in alkaline solutions. The reaction order of the oxidation of sulfur to form sulfate, sulfamate and a class of ammonium thiosalts may be described as follows:

$$S^{2-} \rightarrow S_2O_3^{2-} \rightarrow S_nO_6^{2-} \rightarrow SO_4^{2-} + SO_3NH_2^-$$

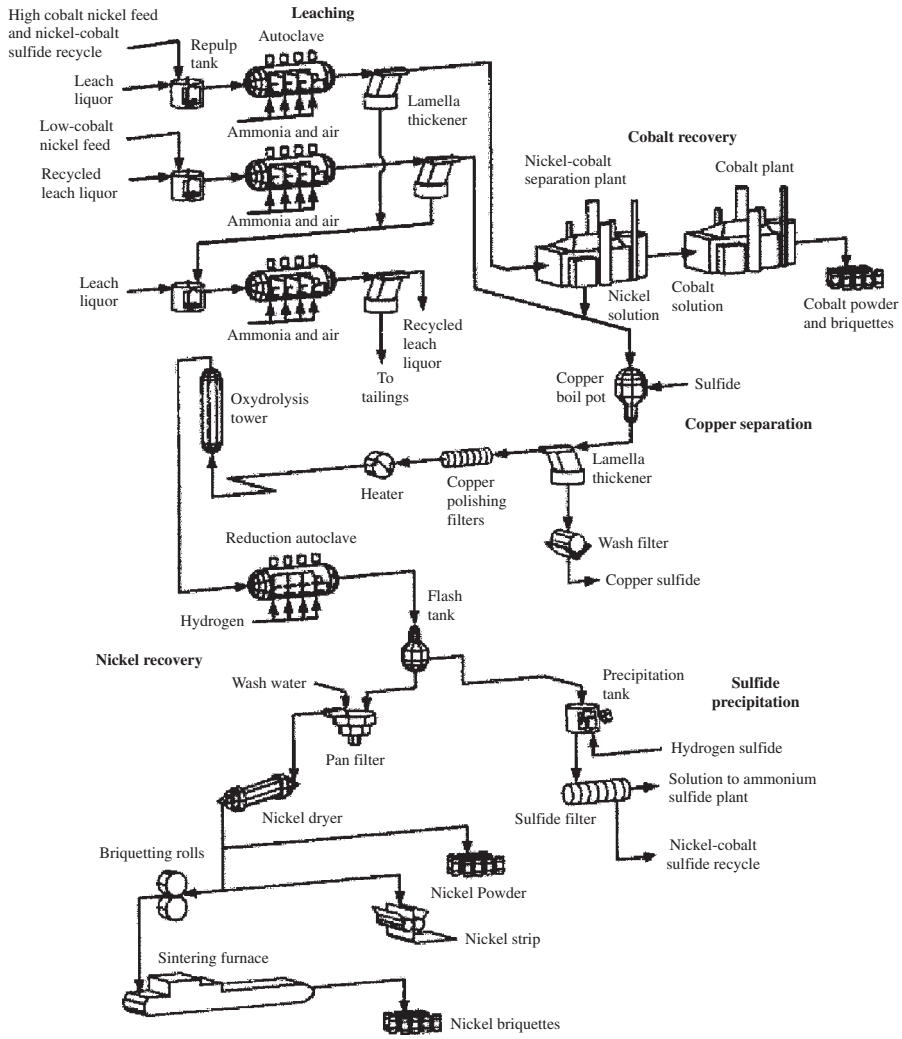

Figure 17.14 Flow diagram of the Sherritt's hydrometallurdical process. Source: Ref 9®

where n ranges from 2 to 6. The leach liquor contains sulfur in several forms depending on given time, up to 4 hours. The leach solution typically contains 60–70 g/L Ni, 6–9 g/L Co, 1–2 g/L Cu, 130 g/L NH_3, 200 g/L $(NH_4)_2SO_4$, and fluctuating quantity of other sulfur compounds.

Several solution purification steps must be accomplished before it is possible to reduce nickel as a pure metal from the leach solution.

Cobalt Separation

The next step of the refining process is the cobalt separation at the nickel–cobalt separation plant, where the leach liquor is transported. The Sherritt cobalt refining process is described in Chapter 18. After the removal of cobalt, the nickel-rich solution is subjected to a copper removal process.

Copper Removal

Copper is removed from the leach liquor and nickel-rich solution in a unit named a 'copper boil' (see Figure 17.14), where the combination of lowering the ammonia level by boiling to distill off the free ammonia and the addition of elemental sulfur and sulfur dioxide at elevated temperature arise out of the precipitation of copper sulfide. The copper sulfide is a mixture of cupric sulfide (CuS) and cuprous sulfide (Cu_2S).

The eliminating of copper is achieved because copper sulfide is less soluble than nickel sulfide. This copper sulfide as a by-product is filtered, washed, dried and then used in copper smelting.

Oxidation and Hydrolysis

The solution remaining after copper elimination contains an appreciable quantity of sulfamate and other forms of unsaturated sulfur compounds. If they are not fully converted to sulfate, the nickel powder product would contain an unacceptably high sulfur content. This is accomplished during hydrolyzing the sulfamate to sulfate at 245°C and oxidizing the thionates to sulfate with air at 4.8 MPa (700 psi) in one parallel stage called as 'oxydrolysis' (see Figure 17.14). Ammonium sulfamate ($SO_3NH_2^-$) is a herbicide and must be hydrolyzed to sulfate to avoid contamination of the ammonium sulfate fertilizer. Ammonium sulfate is crystallized from the reduction end solution.

Hydrogen Reduction by Autoclave Processing

In the final stage of the Sherritt process, nickel is precipitated from solution as a metal powder by hydrogen.

The essence of this process is to precipitate the nickel ions in the solution to nickel powder using hydrogen as a reductant. The reduction of metal from solution by hydrogen requires that the hydrogen potential of the system should exceed the electrode potential of the metal ions, in which case hydrogen will move into solution and the metal precipitates. The hydrogen potential is controlled by the pH of the solution and pressure of hydrogen.

The hydrogen reduction of nickel develops on the basis of the heterolytic mechanism, therefore the process rate is proportional to the seed powder surface. Changing type and quantity of seed powder makes it possible to produce nickel powders with different particle size and shape, different compositions and pseudoalloys (nickel coating of different materials stable under processing parameters).

The role of surfactant is important (typically, consisting of 0.001 mole/L thioacetamide, 0.01–0.005 g/L ethylene-malonic anhydride, 1 mg/gNi of anthraquinone, and derivatives on their base) due to which metal precipitates on seed powder surfaces with a constant rate. This provides for the production of powder with a more equiaxed (close to spherical) shape of particles; simultaneously, the duration of the induction period is reduced and the process accelerates.

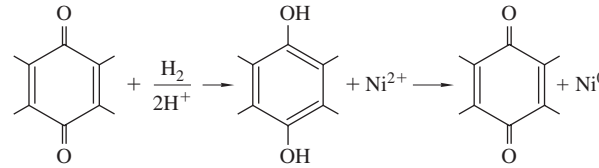

Figure 17.15 Hydrogen reduction pattern of nickel ions by participation of anthraquinon.

On the solid surface anthraquinone molecules absorb which, interacting with activated hydrogen in the alkaline medium, forms anthrahydroquinone, a strong reducing agent; as a result, chemical reduction of nickel ions (II) occurs and anthraquinone is regenerated according the scheme given in Figure 17.15.

For description dependence of the course of autoclave precipitation of a metal from ammonia solutions on the main parameters, the kinetic equations were proposed by V.N. Makhov (Canada, 1957):

$$-\frac{d[Ni^{2+}]}{dt} = k[Ni^{2+}]\cdot p_{H_2}\cdot S\exp\left(-\frac{5126}{T}\right)$$

by G.N. Dobrokhotov (USSR, 1962):

$$-d[Ni^{2+}]/d\tau = k[Ni^{2+}]\,p_{H_2}^{0.5}\cdot S\cdot\exp(-8930/T)$$
$$k = 4.2\times10^{-12}\,s^{-1}\cdot MPa^{-0.5}\cdot cm^{-2}$$

in both equations T is the temperature in K, S is the seed powder surface in cm^2; by M. Sato (Japan, 1972):

$$-d[Ni^{2+}]/d\tau = k_1[Ni^{2+}]^{0.5}\cdot p_{H_2}^{0.5}S\cdot k_2([H^+]-[H^+]^*)$$

where $[H^+]^*$ is concentration of hydrogen ions in solution with pH = 4.3, p_{H_2} is pressure in atm of hydrogen in the autoclave, S is the seed powder surface in cm^2, $k_1 = 5\times10^{-10}$ mole·$cm^{-2}\cdot s^{-1}$; $k_2 = 2.5\times10^{-5}$ mole $\cdot\, cm^{-2}\cdot s^{-1}$.

The reduction process is accomplished in mechanically agitated horizontal autoclaves at elevated pressures and temperatures. This batch process includes two separate stages: initial nucleation and subsequent densification. In the nucleation stage, fine nickel seed powder is formed in the autoclave. During the densification process, nickel from solution is reduced onto the seed powder particles, which then grow in size. The reduction process can be described as follows:

$$Ni^{2+} + 2NH_3 + H_2 \rightarrow Ni^0 + 2NH_4^+$$

The presence of free ammonia is necessary to neutralize the hydrogen ions arising during reduction. At low pH and lower hydrogen potentials, the reduction

Table 17.4 Typical densification operation parameters during nickel recovery using hydrogen

Serial number of operation	Hydrogen pressure (MPa)	Temperature (°C)	Duration (minutes)	Intermediate discharges (minutes)
0 (Initial nucleation)	2.1	117	28	...
1	2.1	182	16	...
2	2.5	182	15	...
13	2.8	204	19	...
18	2.8	199	27	1
19	2.8	199	27	...
23	2.8	199	28	1
24	3.2	199	26	...
27	3.2	199	29	1
28	3.2	199	30	...
31	3.2	199	35	1
35	3.2	199	36	1
36	3.2	199	39	...
39	3.2	204	35	1
40	3.2	204	47	...
43	3.2	204	41	1
44	3.2	204	45	...
47	3.2	204	53	1
48	3.2	204	55	...
50	3.2	204	63	1
51	3.2	204	65	Complete

of the metal ions ceases. During the reduction process, the slurry in the autoclave is agitated by means of impellers.

The initial nucleation stage is carried out in the autoclave at hydrogen partial pressure 2.5 MPa, and the solution is heated up to temperature 107–127°C. Under the stated conditions, the seed powder in the form of fine particles of metallic nickel is produced in 30–40 minutes. Then, the hydrogen supply is terminated, impellers are stopped; in 5 minutes a clarified solution is carefully decanted through the submerged tube into a separate reservoir and returned to the stage of raw material leaching.

The autoclave with seed powder is refilled with fresh nickel solution, the agitators are restarted, hydrogen pressure is applied, and the subsequent densification stage of the reduction process is started. This batch reduction process is repeated 50 to 60 times to create successive coatings of nickel on the powder particles. The process is complete when the powder has reached the required size.

Depending on the number of densification operations, hydrogen pressure ranges from 2.5 to 3.3 MPa (pressure is higher by the end of the whole precipitation operation); solution temperature is supported at the level from 182 to 204°C; the duration of a single densification operation ranges from 16 to 65 minutes. Typical densification operation parameters during nickel recovery using hydrogen are given in Table 17.4.

On the completion of the next recurrent operation (when the nickel content in the solution decreases down to 1 g/L), the impellers are switched off in sequence at regular intervals beginning with the most remote from the discharge assembly. The settling duration amounts 1 to 2 minutes and the solution is discharged into a flash tank. The fresh portion of solution is poured into the autoclave and, by analogy, the cycle is repeated in the presence of precipitated powder remaining from the preceding densification operation. The precipitated nickel powder is not discharged from the autoclave until the 15th densification cycle. Then, after every 3 or 4 cycles the part of powder is downloaded to decrease the load on the autoclave drive. The duration of the whole reduction process ranges from 70 to 80 hours. While the mixers are operated, the entire contents of the autoclave is downloaded into a flash tank; the autoclave is washed by circulating solutions for more complete powder removal.

While the number of the conducted cycles is increasing, their duration is also increasing from

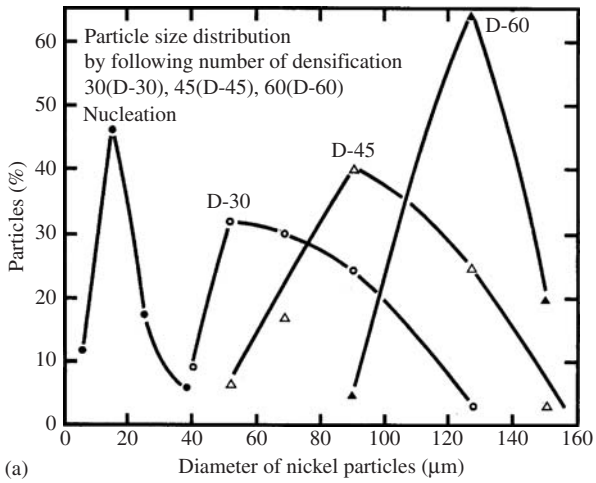

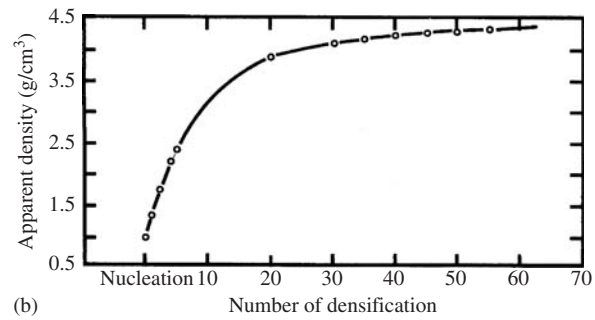

Figure 17.16 Dependence of the particle size distribution (a) and apparent density (b) on the number of densification cycles.

12 to 65 minutes. Figure 17.16 shows the increase of particle size (a) and apparent density (b) with the number of densification cycles in commercial operation [9].

Up to 2 wt% of powder remains on the walls of the autoclave during precipitation; so as to avoid clogging of the apparatus, this deposit is removed by a solution containing 3–4 g/L NH_3 and 200 g/L $(NH_4)_2SO_4$; the autoclave is blown by gas consisting of 93 vol% nitrogen and 7 vol% oxygen. The operation lasts about 6 to 7 hours at 107 ± 5°C, with gas pressure of 2.8 MPa. The obtained nickel-containing solution is returned to the stage of initial nucleation for seed powder formation in the autoclave for the next running cycle.

The addition of various organic additives to the densification reduction can also be used to ensure the means of controlling the size, shape and surface morphology of the powder manufactured.

The nickel feed solution also contains significant quantities of cobalt and zinc. Zinc is removed without problem, because it will not be reduced to the metallic state under the process conditions, while cobalt has a similar standard reduction potential to that of nickel (−0.267 V for cobalt compared to −0.241 V for nickel). In order to achieve complete reduction of nickel, the ammonia concentration is controlled in the reduction feed solution to give ammonia to total metals molar ratio of 1.9 to 1.0.

The slime consisting of nickel powder and reduction end solution is discharged from the autoclave and collected in flash tanks. Then the powder is let out from the flash tank cone as a 90 wt% solid slurry and is filtered and washed on a rotary pan filter. From the pan filter the wet powder with moisture residue amounting to 5 wt% is fed by a screw feeder into a rotary dryer, where it is dried at 127°C. Annealing in a current of moistened hydrogen at 427°C for 2 hours is carried out to remove carbon; dried gas is used for removal of oxygen under the same conditions. Powder sintering is observed at temperature >827°C. The dried powder is reloaded into the service reservoir by an elevator from where it is passed through vibrating screens and then fractions are mixed to obtain the required powder brands. Next, nickel powder is either packed as a powder product or transferred to the briquetting operation.

Typical properties of Sherritt's standard grade nickel powder are: chemical composition includes 99.9 wt% Ni, 0.08 wt% Co, 0.01 wt% Fe, 0.003 wt% Cu, 0.025 wt% S, 0.006 wt% C; granulometric composition is characterized with the following data: 0–10 wt% + 150 μm, 5–10 wt% (−150 + 100) μm, 20–45 wt% (−100 + 75) μm, 10–25 wt% (−75 + 63) μm, 10–35 wt% (−63 + 45) μm, 5–25 wt% (−45) μm; and apparent density ranges from 3.5 to 4.5. Figure 17.17 shows a scanning electron micrograph of a powder produced by Sherritt's hydrometallurgical processing.

For briquetting, the powder is first blended with an organic binder in a pug mill and is then compacted on a briquetting roll. Raw briquettes are sintered in an electric conveyor furnace for carbon and sulfur removal and sintering at a temperature of 957–967°C imparts structural integrity to the briquettes. The removal of carbon is achieved by oxidation in air and giving either carbon monoxide or carbon dioxide, while effect for sculpture removal depends on the maintenance of reductive conditions in the hydrogen atmosphere, with the eliminating of hydrogen sulfide. The sintering furnace therefore consists of three zones: the oxidizing zone for carbon removal, the reducing zone for sulfur removal and, finally, a cooling zone.

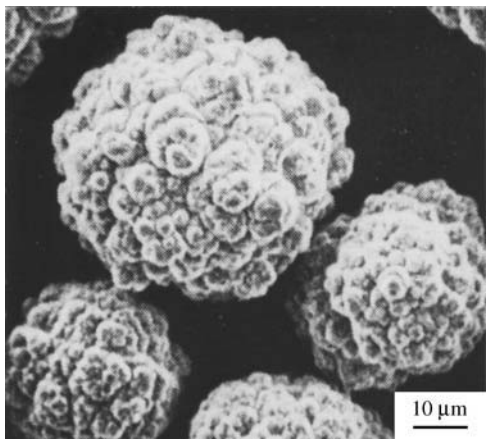

Figure 17.17 Scanning electron micrograph of a powder produced by hydrometallurdical processing.

Sulfide Precipitation

The liquor from hydrogen reduction contains residual nickel, cobalt and zinc. These metal ions are precipitated using hydrogen sulfide and recovered as sulfide precipitates. The common precipitation reaction can be written:

$$M^{2+}(aq) + H_2S \rightarrow MS(s) + 2H^+(aq)$$

where M is nickel, cobalt, zinc. Metals can be selectively removed from solution by controlling the pH of the sulfide precipitation reaction. The pH is controlled by the addition of ammonia to neutralize the acid generated in the precipitation reaction. The nickel and cobalt are then returned to leach the zinc, which is precipitated separately and is sold as by-product, and barren liquor (metal-free ammonium sulfate solution) proceeds to ammonium sulfate recovery. The latter, after removal of the metal values as metal sulfide, consists only of ammonium sulfate, which is referred to as 'barren solution'. This solution is then evaporated and ammonium sulfate, which is formed as a refinery by-product, is recovered in crystalline form. This crystalline ammonium sulfate recovery after centrifuging, drying and screening is sold as fertilizer.

For the production of especially pure powder, ordinary powder was dissolved into sulfuric acid. The solution was freed from: copper by means of cementation by nickel powder; iron (oxidization by H_2O_2, while the neutralization was carried out by using ammonia); cobalt by means of α-nitroso–β-naphthol. After the solution was thoroughly filtered, the residual content of each impurity was at the most 0.5 mg/L. Fine nickel carbonate powder is used for seed powder forming in the autoclave at a concentration of 5 g/L. The hydrogen reduction process is carried out at 277°C, and at hydrogen pressure 2.4 MPa. The ammonia concentration is adjusted in the nickel reduction feed to give an ammonia to metal molar ratio of 2.2. The produced powder is a purer nickel powder than that produced by carbonyl or electrolytic nickel processes.

Most hydrometallurgically produced nickel powder is compacted into briquettes for use as an alloying additive in the steel industry. Smaller amounts of powder are roll compacted into nickel strip or dissolved to produce various nickel salts.

Powders Covered by Nickel

Hydrometallurgical processing makes it possible to precipitate nickel on the surface of different solid materials (continuous powder, hollow granules, particles in the form of threads, etc.). Grain size of the powder produced is determined by the size of seed powder top-charged in the autoclave and ranges from 20 to 2000 µm. The particle size and shape is controlled during densification processing. Ammonium carbonate, ammonium sulfate solutions, aqueous pulps of nickel (II) hydroxide or alkaline nickel carbonate are used.

The parameters ensuring a uniform layer of seed powder cladding by processing of the ammonium sulfate solutions are the following: 147°C, hydrogen pressure ≥1.5 MPa, ammonium sulfate to metal molar ratio above 1.8, ammonia to metal molar ratio 2.5. Ammonium sulfate concentration should be not less than 115 g/L. If the ammonium sulfate content is more than 200 g/L, the solution viscosity increases which results in a decrease of the process rate, reduced apparent density, powder fluidity and degree of cladding, especially for seed powders with low specific density.

For maximum yield of clad powders, the difference in particle size of seed powder should be not over 60 µm. The coarser the seed powder, the thicker must be the nickel cover layer; several densification cycles are necessary to provide cladding continuity. Layer continuity of seed powder cladding is achieved if the rate of nucleation is higher than the speed of their growth. The lower the nickel precipitation rate, the higher the probability of non-uniformity of thickness and cladding continuity.

The kinetic equation is correct in the interval of 100–187°C and hydrogen pressure in the range from 0.5 to 2.0 MPa:

$$\tau = 48.6 \times 10^{-6}\ p_{H_2}^{0.94}\ \exp(1408/T)$$

Table 17.5 Properties and application areas of nickel composite powders covered by nickel

Type	Ni (%)	Properties	Application areas
Ni–C	50–85	Erosion resistance, increased strength, ease of handling by spraying	Coating of turbine buckets, evaporating surfaces by spraying method
Ni–Al	80–82	Spheroidal, heat resistance, wear resistant	Coating of parts working surfaces of rotary-piston engines
Ni–carbides (borides, nitrides)	...	Corrosion resistance, high strength, compressibility is better than mechanical mixtures have	Spraying of working surfaces of plasma generators, production of cutting tools by PM technique
(Ni, Cr, Al)–bentonite	...	Erosion resistance, heat resistance, ease of handling by spraying	Valves, heater nozzles, nozzles of turbines operating under conditions of high temperatures and flow velocities

where τ is transient time, h; p_{H_2} is the hydrogen pressure, MPa; T is temperature, K.

When in the range from 1.5 to 1.8 MPa and T is 150–200°C, a processing duration of 6–8 min is required to produce the cladding thickness of 1–5 μm containing 98–99 wt% Ni.

Depending on p_{H_2} and on particle size, composite Ni–Al powders have apparent densities between 1.42 and 1.83 g/cm^3 and specific surface area ranging from 0.3 to 4.1 m^2/g. Properties and application areas of typical composite nickel coated powders are given in Table 17.5.

The coating with nickel of chromium powders, technical diamonds, fiberglass and glass powder, and red phosphorus was accomplished by hydrometallurgical processing.

Autoclave Processing of Nickel Hydroxide and Carbonate Pulps

In 1962, G.N. Dobrokhotov (Hypronickel, Saint Petersburg, Russia) showed that during processing of a pulp containing 2–3 wt% nickel hydroxide at 190 to 247°C and hydrogen pressure in the range from 2 to 3.0 MPa, powder with a nickel content up to 99.7 wt% is obtained in 1 hour. It is characterized by increased dispersivity and low cementing activity in relation to copper.

An ordinary nickel powder is dissolved in ammonium-carbonate solution and then distilled in order to produce a high purity powder with low apparent density (0.5–1.0 g/L) and particle size of 2–3 μm. The feed to the autoclave process is a nickel carbonate with the following chemical composition: 46–47.5 wt% Ni, 12–14 wt% CO_2, 16.5 wt% OH^-, 0.7 wt% NH_3; apparent density of the precipitate is 0.22 g/cm^3, specific surface area is 24.4 m^2/g.

The precipitate is diluted by ammonia-carbonate solution to the following pulp composition: 75 g/L Ni, 29 g/L CO_2, 11 g/L NH_3. Fine nickel seed powder is introduced into an autoclave to give an Ni concentration in the pulp of 2 g/L. The reduction process is carried out at 147–187°C and hydrogen pressure in the range from 2.8 to 3.8 MPa. In order to effect the required properties of the powder, the ammonia concentration is adjusted in the nickel reduction feed solution to give an NH_3 to Ni molar ratio from 1.0 to 4 and a CO_2 to Ni molar ratio below 0.5.

The impurity content in the powder shall not be more than 0.04–0.07 wt% Co; 0.008–0.01 wt% Fe; 0.002–0.008 wt% Cu; 0.01–0.04 wt% C; 0.003–0.005 wt% S; 0.002 wt% Al; 0.001 wt% Ca; 0.001 wt% Si.

By varying the process conditions, powder with apparent density 0.3–3.6 g/cm^3 and specific surface area in the range from 0.5 to 10.0 m^2/g can be produced.

The following conditions are recommended for the reduction of aqueous carbonate pulp: hydrogen pressure 2.5–3.0 MPa, temperature 127–147°C, 0.01–0.05 g/L anthraquinone or palladium chloride as catalyst, initial pH value 5.9–6.4; less than 1.0 g/L Ni. The powder produced typically contains the following contaminates: 0.002–0.004 wt% Bi; 0.005–0.012 wt% Pb; 0.004–0.008 wt% Cu; 0.005–0.009 wt% Al; 0.002–0.008 wt% Mg; 0.0002–0.003 wt% Mn; 0.013–0076 wt% Si; 0.09–0.2 wt% Co; 0.003–0.043 wt% Fe; 0.076–0.174 wt% C; 2–6 wt% O_2 (because of surface oxidation). Particle shape is hexagonal, particle size is 1.0–2.0 μm, powder specific surface area ranges from 1.0 to

6.0 m^2/g, and apparent density is 1.0–2.0 g/cm^3. This powder is used in the production of nickel plates in alkaline accumulators.

The nickel hydroxide aqueous pulp typically contains 12–48 g/L nickel hydroxide, 1.5 mg/L $PdCl_2$, 4/g/L NaOH (pH value amounts to 13). The reduction process in the autoclave is carried out at a temperature above 157°C and hydrogen pressure 2.5–3.0 MPa. Powder produced particles have a spherical shape. Average particle size is in the range 50–70 nm, inclined to agglomeration and oxidation (up to 2–6 % oxygen). Powder apparent density is 0.3–0.6 g/cm^3, specific surface area 25 m^2/g.

The reduction by hydrogen of nickel hydroxide or alkaline carbonate is attractive because of the problem of nickel recovery from oxidized ores. In the acid leaching of ore, the metal is precipitated from the solution in the form of hydroxide using magnesium oxide. In the ammonia technology, the oxidized ore is reduced by roasting and subjected to ammonia-carbonate leaching and solution distillation resulting on alkaline nickel carbonate.

Atomization

Atomized nickel alloy powders are used mainly for hardfacing, aerospace components and electric power industry constituents. Nickel-based alloy powders are widely used in the manufacturing of PM superalloys.

Hardfacing Powders

Hardfacing is the application of hard, wear-resistant material to the surface of a component by welding, thermal spraying or a similar process, mainly to reduce wear. Hardfacing is used on original equipment, as well as for the repair of worn components. Hardfacing consumable materials are acceptable in different forms, such as powder, solid welding rods or wires and tubular rods or wires.

Gas and water atomization are the most widely used techniques for manufacturing hardfacing powders. Particle size intervals of different grades of powder used for various hardfacing processes fall within the range from 10 to 150 μm. For instance, the plasma spray operation requires fine powders in the 10–45 μm range, but special dispensing devices are required to prevent powder flow problems. In some conditions, in the case of plasma transferred arc, the particle size in the range from 45 to 150 μm is preferable. Use of excessive fines is damaging to the coating because fines tend to have higher surface oxides and burn-off tendencies. Certain hardfacing techniques, such as bulk welding process, require coarse powder in the 100–600 μm range.

Powder shape is also of great importance in any hardfacing operation. Spherical powders have the inside track to the service and solidity of the coating. Spherical powders flow better than irregular, which is important when using gravity powder-feed devices. Gas-atomized powders generally are spherical in shape but inclined to satellite formation. Water-atomized powders can be irregular or spherical, depending on alloy type and the cooling rate. Irregular particle shape, or narrow size distribution lowers apparent density and decreases the flow rate of the powder. The oxygen content of these powders is still below 0.1 wt%.

Commercially available nickel hardfacing alloys can be subdivided into three groups: boride containing alloys, carbide-containing alloys, and Laves phase-containing alloys. For the most part, nickel hardfacing powders are of the Ni–Cr–B–Si base and are self-fluxing during deposition because of the presence boron and silicon. Additions of these elements influence the melting temperature range of nickel-base alloys which is an important factor for hardfacing powders. Owing to the decrease of the melting point, an oxyacetylene torch can easily be used.

The elevated cooling rate makes it possible to form unstable intermetallic nickel–boron (Ni_3B, Ni_3B_4 and Ni_4B_3), nickel–chromium (CrB, Cr_2B, and Cr_5B) and other boride compound hard phases [10]. The unstable nickel–boron phases, the self-fluxing reactions and the wetting properties during fusing, lead to a much higher reaction rate with the oxides present on the substrate. The Laves phase is a kind of topologically close-packed intermetallic compound which has a hexagonal structure similar to M_7C_3 carbides, but the hardness value is less than that of carbides. Laves phase materials retain mechanical properties over a wide range of temperatures.

Generally, the finer structure produced by more rapidly cooling provides improved wear resistance in the final coating. These same features may also contribute to improved corrosion resistance.

Compositions and properties of several typical standard grades are given in Table 17.6. Deposit hardness of these alloys is as high as 60 HRC, depending on the chromium, boron and silicon contents. Alloys containing large amounts of boron and chromium, such as Ni–15.5Cr–4Si–3.5B–0.8C (alloy No. 60), are extremely abrasion resistant, but have poor impact toughness.

Table 17.6 Chemical composition and hardnesses of typical nickel hardfacing alloys

Property	Unit	Source. Trade name									
		Cabot Corp					ANVAL		Haynes International Inc.		
		Alloy No 22	Alloy No 35	Alloy No 40	Alloy No 50	Alloy No 60	B-60 C	625	C-22	Alloy C	Alloy 716
Nominal composition											
B	wt%	1.5	1.6	1.7	2.4	3.5	3.5	...	...	...	0.5
C	wt%	0.2 max	0.3	0.35	0.45	0.8	0.65	0.1 max	0.22 max	0.12	1.1
Co	wt%	...	...	...	...	...	...	...	...	...	11
Cr	wt%	...	3.7	7.5	11.0	15.5	15.5	21.5	21.5	17	26
Cu	wt%	...	...	...	...	...	2.5	...	...	...	...
Fe	wt%	1 max	1.2	1.5	3.0	4.0	4.0	5.0 max	5.0	...	29.0
Mo	wt%	...	...	...	...	...	2.5	9.0	13.5	17.0	3.0
Nb	wt%	...	...	...	...	...	...	3.6	...	...	...
Ni	wt%	Bal	Bal	Bal	Bal	Bal	Bal	Bal	Bal	Bal	Bal
Si	wt%	2.8	3.1	3.5	4.0	4.3	3.8	...	...	...	...
V	wt%	...	...	...	...	...	...	...	0.15	...	...
W	wt%	...	...	...	...	...	...	...	3.0	...	3.5
Nominal deposit microhardness											
HB	kgf/mm^2	220–250	320–365	350–415	525–575	710–790	...	...	...	...	...
HRC	HRC	19–24	32–37	35–42	49–52	59–62	...	...	...	...	32
Melting range	°C	940–1240	...	994–1152	976–1063	964–1003	...	...	...	...	...

The low-melting point eutectic of self-fluxing Ni–Cr–Si–B alloys combines with surface oxides on powders to form borosilicates, which promote wetting on the substrate. The most common use of these powders is in spray-and-fuse and manual torch applications in the glass industry. Additions of copper and molybdenum to self-fluxing alloys are introduced to improve corrosion and pitting resistance. These alloy powders have good abrasive and metal-to-metal wear resistance, although hot hardness and corrosion resistance are somewhat worse than those of cobalt-based alloys. The use of carbide-containing nickel alloys has been confined. The most widely used in this group is the Ni–Cr–Mo–C system. Hastelloy Alloy C is a typical alloy in this system which has good corrosion resistance and is normally deposited by the plasma spray technique. Carbide-containing alloys of the Ni–Cr–Mo–Co–Fe–W–C system are attractive as low-cost alternatives to cobalt-base alloys. A typical alloy in this system is Haynes Alloy 716 which, depending on precise composition, contains M_7C_3 or M_6C phase.

Superalloy Powders

The alloys with high strength at high temperature that are used primarily in turbine engines for aircraft and power generation are termed 'superalloys'. These materials are predominantly nickel-base alloys that are alloyed with refractory elements including molybdenum, tungsten, cobalt, niobium and tantalum. The PM superalloys are characterized by high homogeneous concentration of both solid solution strengthening elements and the γ'–forming aluminum and titanium intermetallic phases. The PM process makes it possible to form these structural features because of the high rate of crystallization.

The superalloys have been developed by the need for progressively higher strength at higher temperatures for advanced aircraft engines. With ingot-based material, segregation associated with more complex alloying is a problem and it is aggravated by the need for larger billets for larger turbine disks. A solution to this problem was to minimize segregation through rapid solidification of the alloy by atomization to powder and subsequent consolidation by a technique that does not melt the powder particles while attaining full density. To that end hot isostatic pressing (HIP) is widely used. Table 17.7 gives typical compositions of several common grades.

All powder used to produce PM superalloys is prealloyed which means that the powder is made from the molten state and each powder particle is a minibillet with the same composition as the molten alloy. Various methods are known to produce superalloy powders. Inert gas atomization and vacuum atomization are the most commercial superalloy powder making processes.

In gas atomization, high purity feed materials are vacuum induction melted and then atomized using inert gas. The liquid metal is atomized by high-pressure gas jets. The powder obtained, which is solidified at a rate in the range from 10^3 to 10^4 °C/s, is collected in a bottom chamber and/or cyclone collector. The particle size distribution resulting from this process depends mainly on the surface tension, γ, viscosity, η, and density, ρ, of the melt, as well as the velocity, *v,* of the atomizing gas, and the atomizer design. Oxygen contents are of the order of 100 ppm, depending on particle size. Argon is usually used to atomize superalloys. The use of nitrogen gas normally requires some modifications in composition to accommodate the nitrogen increase during the atomization process.

Vacuum atomization is based on the rapid evolution of gas when a molten metal is supersaturated with gas under pressure and is then suddenly exposed to a lower pressure. An arrangement consists of two vertical chambers connected by a transfer tube. The atomized powder particles, which are solidified at a rate of about 10^3 °C/s, fall to the bottom of the upper chamber. The cooled powder is collected under vacuum in another chamber, which is sealed and backfilled with an inert gas. This technique is capable of atomizing up to 1000 kg of superalloy spherical powder in one heat. This has been employed for LC Astroloy, MERL 76 and IN-100.

Superalloy powder is also produced using centrifugal atomization. One example of this technique is the rotating electrode process (REP) used in the early production of IN-100 and René 95 powders. In this process, a bar of the specified composition, 15–75 mm in diameter acts as a consumable electrode. The end of this rotating positive electrode is melted by a direct current electric arc between the consumable electrode and a stationary tungsten negative electrode. The process is carried out in helium gas. Centrifugal force causes spherical molten droplets to tear off the high-seed rotating electrode. These droplets rapidly solidify and are collected at the bottom of the chamber.

The plasma rotating electrode process (PREP) is the modification of the REP process and differs from the former in that plasma is used for melting the consumable electrode. Cooling rates amount to 10^5 °C/s for IN-100 [12].

The use of the rotating electrode technique is restricted because of the problem of rapidly solidified superalloy consumable electrode manufacturing.

Table 17.7 Chemical composition and tensile properties of typical PM superalloys

Property	Unit	Trade grade. Source								
		René 95 [11]	IN 100 [12]	LC Astroloy [13]	René 88DT [14]	Udimet 720, [15–17]	N 18 [18,19]	AF2-1DA-6 [15,20]	PA 101 [21,22]	MERL 76 [15,23,24]
Nominal composition										
Al	wt%	3.5	5.0	4.0	2.1	2.0	4.3	4.6	3.5	5.1
B	wt%	0.01	0.02	0.02	0.015	0.020	0.015	0.015	0.015	0.03
C	wt%	0.06	0.07	0.03	0.05	0.025	0.02	0.04	0.12	0.02
Co	wt%	8.0	18.5	17.0	13.0	14.7	15.5	10.0	9.0	18.6
Cr	wt%	13.0	12.4	15.0	16.0	16.0	11.5	12.0	12.6	12.4
Hf	wt%	0	0	0	0	0	0.5	0	0.95	0.35
Mo	wt%	3.5	3.2	5.0	4.0	3.0	6.5	2.8	1.9	3.3
Nb	wt%	3.5	0	0	0.7	0	0	0	0	1.4
Ta	wt%	0	0	0	0	0	0	1.5	4.0	0
Ti	wt%	2.5	4.3	3.5	3.7	5.0	4.3	2.8	4.1	4.3
Zr	wt%	0.05	0.06	0.04	0.04	0.03	0	0.1	0.04	0.06
V	wt%	...	0.8	0	0	0	0	0	0	0
W	wt%	3.5	0	0	4.0	1.25	0	6.5	4.1	0
Ni	wt%	bal	bal	bal	bal	bal	bal	bal	bal	bal
Tensile properties										
at RT										
UTS	MPa	1650	1591	1345	1232	1630	1580	1586	1472	1615
YS	MPa	1260	1102	930	1143	1194	1080	1138	945	1050
EL	%	18	26	22	20	22	20	12	15	...
at 427°C										
UTS	MPa	1557	...	...	...	1620	1570	...	...	...
YS	MPa	1109	...	...	...	1170	1070	...	...	...
EL	%	11	...	...	...	26	20	...	...	...
at 760°C										
UTS	MPa	1158	1267[1]	1068	1170	1170	1070	1550	1088	1060
YS	MPa	951	1068[1]	792	971	970	980	1100	875	990
EL	%	10	18[(1)]	22	13	20	6	21	11	...
at 900°C										
UTS	MPa	...	...	...	...	...	...	1200	...	...
YS	MPa	...	...	...	...	...	...	780	...	...
EL	%	...	...	...	...	...	...	10	...	...

UTS: ultimate tensile strength; YS: yield strength; EL: elongation; RT: room temperature; [1] at 700°C.

Obtained powders are screened to remove oversized particles and then blended to produce a uniform size distribution. All the powder handling processes are designed to eliminate the possibility of introducing foreign material into the powder. This involves the use of specially designed stainless steel containers, valves and inert gas handling or air handling of powder in clean rooms.

Depending on the application, powder size ranging from 250 to 45 μm is characteristic. Before being loaded into a die for consolidation, superalloy powders are evaluated for cleanliness by techniques such as water elutriation, which separates non-metallic inclusions from the powder. During preparatory processing, the powder is heated in a vacuum to remove air and adsorbed moisture. This procedure can be accomplished before loading or after loading into the die. In the former case, outgassed powder is loaded from an evacuated container into an evacuated consolidation container and then it is sealed. In the latter case, powder is loaded in air into a consolidation container which is next cold and hot outgassed and then sealed.

Superalloy powders are consolidated to full density using a combination of high pressure and high temperature. The primary consolidation methods for superalloys are HIP, extrusion and a combination of the two. For HIP, the powder consolidation container can be a simple geometric shape or a complicated near-net shape. The product can be in the form of billet ready for subsequent extrusion and/or forging. The HIP parameters usually used are 1040–1205°C at 105–205 MPa for 3–5 h [13]. Extrusion of superalloy powder can be done either as the extrusion of powder in the loose state or extrusion of preconsolidated billets. Extrusion ratios used for direct extrusion of powder are at least 7 to 1. With extrusion of preconsolidated billets, the powder may be preconsolidated by HIP, a separate forging press, or in the extrusion press. Extrusion ratios for solid billet are normally of the order of 3 to 1.

Table 17.7 gives the compositions of PM superalloys. Alloys that are commercially produced include René 95, IN-100, LC Astroloy, René 88DT and N18. Other alloys, such as Udimet 720, IN 706, AF2-1DA-6, PA101 and MERL 76 are in earlier stages of PM development.

It is of interest to note that when PM superalloys were introduced in the 1970s, the strength and fatigue properties were clearly superior to those of cast/wrought alloys [25,26] and, since then, process improvements have led to a decrease in the size and number of inclusions that initiate low level fatigue fractures.

The low cycle fatigue (LCF) life has improved impressively for an HIP PM superalloy in the last 20 years where the present average exceeds the maximum of 20 years ago [11]. It increased four times, from 50 000 to 160 000–210 000 average cycles to failure, depending on part type. In addition to the aforementioned, the number of these parts in service is approaching 150 000 worldwide and over 46 000 HIP PM parts have been produced and operated in Russian jet engines during the last 20 years [27,28].

Fundamentals about atomization are described in Chapter 5.

Mechanical Alloying

Mechanical alloying (MA) is usually a dry, high-energy ball milling technique and has been employed to synthesize composite metallic powders with both equilibrium and non-equilibrium phases starting from elemental powders.

It has been three decades since this technique was developed by John Benjamin and his colleagues at Inco [29], combining the advantages of precipitation hardening and oxide-dispersion strengthening (ODS) in several nickel- and iron-base superalloys for service at temperatures of 1000°C and above.

The mechanism of alloying changes at different milling stages [30]. During high-energy milling, the powder particles are repeatedly flattened, fractured and rejoined. Every time when two steel balls collide some powder is hit between them. The force of the impact plastically deforms the particles, creates new surfaces and causes the particles to weld together. The composite particles at this stage have a characteristic layered structure consisting of various combinations of the starting constituents. After milling for a certain length of time, the mechanical alloying process reaches the stage when each particle contains virtually all of the starting ingredients in the proportion they were mixed together. At this stage, steady state equilibrium is achieved when a balance is attained between the rate of welding and the rate of fracturing.

The ratio of balls to powder most commonly used is in the range from 10:1 to 20:1. The balls themselves range usually from 8 to 10 mm in diameter and are made from through-hardening steel.

The feed powders generally used for production of mechanically alloyed oxide dispersion-strengthened superalloys are widely accessible commercially pure powders with particle sizes in ranges from 1 to 200 μm. These powders fall into wide categories of pure metals, master alloys and refractory compounds. The pure metals include nickel, chromium, tungsten,

molybdenum and tantalum. The master alloys, containing nickel-base alloys with relatively large quantities of aluminum, titanium and zirconium, are quite brittle when cast and easily comminuted to powder. About 2 vol% of nano-size yttrium oxide, Y_2O_3 (25 nm) is added to form the dispersoid. This oxide, which is prepared by calcining of oxalate precipitates, consists of crystallites of about 50 nm agglomerated into pseudomorphous particles of about 1 μm. The yttrium oxide becomes entrapped along the interfaces between fragments in the composite metal powders. After completion of the powder milling, a uniform interparticle spacing of about 0.5 μm is achieved. For dispersion-strengthened superalloys, the amount of refractory oxide added ranges from about 0.4 to 1.5 wt%, in particular, yttrium oxide added is in range from 1 to 2.7 vol% [31].

For mechanical alloying, several types of high-energy ball mills are used. They differ in capacity, efficiency of milling, appliances for cooling, mill kinetics controlling, etc. Shaker mills and planetary ball mills are popular mills for carrying out MA experiments, which mill about 10 g (shaker mill) and few hundred grams (planetary ball mill) of the powder at a time. In attritors, a charge varying from a few kilograms to about 40 kg can be processed. Mechanical alloying accomplished in ball mills of up 1200 kg is widely used for commercial production of different superalloy powders. The milling time decreases with an increase in the energy of the mill. So, a process that takes only a few minutes in the shaker mill such as SPEX (SPEX CertPrep, Inc., Metuchen, NJ) lasts hours in an attritor and a few days in a commercial ball mill.

Currently, several types of high-energy mills are used for mechanical alloying including attritors, shaker mill, planetary ball mills, vibrating mills, rod mills and new designs that have been developed in recent years for specialized purposes. These include equipment suggested by Zoz Maschinenbau; HEMill from M.B.N. srl, Rome; Dymatron, Inc., Cincinnati, OH; Super Misuni NEV-MA-8 from Nisshin Giken, Co. The special data can be found in the available brochures or www-sites.

Characteristic mechanically alloyed nickel superalloy powder contains particles ranging from 10 to 500 μm with an average particle size between 50 and 200 μm. The internal structure of the powder is independent of particle size when the steady state during milling is achieved. A homogeneous distribution of ultrafine refractory oxide particles must be developed in a highly alloyed matrix for the production of ODS alloys.

Very high hardnesses, up to 520 HV, are reached in the powders as a result of the hard plastic deformation during mechanical alloying. In this connection, cold compaction as a consolidation method is not an option. The simple sintering process also is not available for consolidation of ODS alloys. The most generally used method of consolidation is hot compaction followed by hot extrusion, or by direct hot extrusion at temperatures greater than half the melting point. This process could be used if one is not concerned with the loss of the metastable condition, such as the crystallization of the amorphous phase in the powder. Several of the consolidation modes used for mechanical alloyed powders, both of laboratory and industrial scope, include hot isostatic pressing, powder rolling, plasma activated sintering and explosive compaction.

Powder contamination is an important problem in the mechanical alloying technique. Contamination of powders can be traced to chemical purity of the feed powders, milling equipment, milling atmosphere and the process control agents (PCA) added to the powders.

One way of minimizing contamination from the grinding medium and container is to use the same material for the container and grinding medium as the powder being milled. However, the problem is complex because the MA technique is applied to a variety of materials and it is impossible to get containers and grinding medium for all of these materials. If a container of the material to be milled is not available, then a thin coating on the internal surface of the container of the material to be milled can be used to minimize the contamination. Parallel with this, a simple rule that could be followed to minimize contamination is that the container and grinding medium should be harder then the powder being milled.

Contamination of powders is strongly dependent on the milling atmosphere. It has been ascertained that if the container is not properly sealed, the atmosphere surrounding the container contaminates the powder. It has also been observed that flushing with argon gas will not remove oxygen and nitrogen absorbed on the container internal surfaces. Schemes have been proposed to reduce the leakage of the ambient atmosphere into the container. For instance, experiments showed that pressurization and the use of high-purity argon (99.998 wt%) atmosphere resulted in the processing of high reactive metals such as high-quality titanium alloy powder with as little as 100 ppm oxygen and 15 ppm nitrogen [30]. This process, however, may not be economically viable and therefore may not be workable on a commercial scale.

Compositions and properties of several typical grades of the commercially mechanically alloyed nickel-base superalloys are given in Table 17.8.

Table 17.8 Compositions and properties of selected typical ODS mechanically alloyed nickel-based superalloys

Property	Unit	Trade grade. Source					
		MA 754 [31, 35]	MA 757 [32]	MA 758 [33]	MA 760 [31, 35]	MA 6000 [34]	TMO-2 [31, 35]
Nominal composition							
Al	wt%	0.3	4.0	0.3	6.0	4.5	4.2
B	wt%	...	...	...	0.01	0.01	...
C	wt%	0.05	...	0.05	0.05	0.05	...
Co	wt%	...	...	...	...	...	9.7
Cr	wt%	20	16	30	20	15	6
Mo	wt%	...	...	...	2.0	2.0	2.0
Ta	wt%	...	...	...	...	2.0	4.7
Ti	wt%	0.5	0.5	0.5	...	0.5	0.8
Zr	wt%	...	...	...	0.15	0.15	...
W	wt%	...	...	...	3.5	4.0	12.4
Y_2O_3	wt%	0.6	0.6	0.6	0.95	1.1	1.1
Ni	wt%	bal	bal	bal	bal	bal	bal
Mass density	g/cm^3	8.3	7.79	8.13	7.53	8.11	8.58
Melting point	°C	1400	...	...	...	1296–1375	...
Tensile properties							
at RT							
UTS	MPa	965	...	949	...	1294	...
YS	MPa	586	...	560	...	1284	...
EL	%	21	...	27	...	4	...
at 871°C							
UTS	MPa	248	...	339[a]	...	1156[b]	...
YS	MPa	214	...	214[a]	...	781[b]	...
EL	%	31	...	47[a]	...	6[b]	...
at 982°C							
UTS	MPa	190	...	173[c]	...	407	...
YS	MPa	169	...	151[c]	...	344	...
EL	%	18	...	29[c]	...	12	...

UTS: ultimate tensile strength; YS: 0.2 % yield strength; EL: elongation; RT: room temperature; [a] at 800°C; [b] at 760°C; [c] at 1000°C

The ODS nickel-base superalloys continue to find applications in a wide area of industries. Thus, the two production facilities of Inco have a combined annual powder capacity approaching 300 000 kg. The MA superalloys are intended mainly for three groups of applications including gas turbine vanes, turbine blades and sheet for use in corrosive atmospheres. Alloy MA 754 was the first mechanically alloyed nickel-base ODS superalloy to be produced on a large commercial scale. The largest application is as vanes and bands for aircraft gas turbine engines. This material is essentially a Ni–20Cr alloy strengthened by Y_2O_3 that results in higher strength and good resistance to thermal fatigue. Alloy MA 758 was developed for applications where its high chromium content is needed for greater oxidation resistance, in particular for internal combustion engine components, mainly in critical fuel injection parts. The alloy is also used in the glass industry for high-temperature parts requiring both elevated temperature strength and resistance to extremely corrosive molten glass. The mechanical properties of this alloy are similar to those of MA 754. Superalloy MA 760 is supplemented by γ' age hardening. Its composition was designed to provide a combination of high-temperature strength, long-term structural stability and oxidation resistance. The tensile strength properties of alloy MA 760 exceed those of MA 754 but are surpassed those of MA 6000. Its primary application is expected to be for gas turbines. The MA 6000 is a more complex alloy developed as a material for advanced gas turbines and is used for first and second turbine vanes and blades machined from solid rod. Superalloy MA 6000 combines γ' hardening and oxide-dispersion strengthening from the yttrium oxide addition. Aluminum and chromium

contents provide the oxidation resistance, while titanium, tantalum, chromium and tungsten jointly ensure sulfide resistance. The tungsten and molybdenum also function as solid solution strengtheners. MA 6000 is a perfect alloy for gas turbine vanes and blades when exceptionally high temperature strength is required.

Production of Nickel Powder by Reduction Processes

Solid Phase Reduction

The basic raw materials are nickel oxide produced by roasting of sulfide materials, or thermal decomposition of oxygen-containing compounds like hydroxides, carbonate, as well as salts and compounds of nickel thermally unstable at 727–927°C. The general equation for the solid phase reduction may be represented as:

$$NiO + R \rightarrow Ni + RO$$
$$NiA + R \rightarrow Ni + RA$$

where R is reducing agent, A is an acid radical.

Hydrogen, carbon monoxide, low-sulfur carbon containing materials (wood charcoal, oil coke, graphite) and natural gas are used as reducing agents.

While using hydrogen, the process is carried out at 500–550°C; the powder produced has high dispersivity and developed (sponge) particle surface. At higher temperatures (above 550°C) structure recrystallization, partial sintering and enlarging of particle size are observed. Reduction accelerates when the reducing operation is carried out in a fluidized bed or under pressure of hydrogen.

Heating nickel oxalate in hydrogen at 230–400°C produces ultrafine powder. To prevent sintering, organic reagents are added to the initial charge, for instance, a mixture of silicone oil and tetrahydrofuran. Powder is cooled in hydrogen current, washed with acetone for removal of organic traces and dried in air. Particle size is 0.3–1.0 μm. They are needle shaped. Sometimes nickel oxalate is converted to hydroxide by treatment of a precipitate by alkaline solution. Then this precipitate of $Ni(OH)_2$ is calcined in a hydrogen atmosphere at 550–930°C for two hours.

Powders of magnetic alloys based on Fe–Ni–Co are produced by an analogous method at 300–420°C.

The nickel formates are reduced at 200–300°C with the formation of ultrafine powder with specific surface 10–14 m^2/g, apparent density 0.4–0.45 g/cm^3 and particle size 0.1–0.3 μm.

Reduction by producer gas is carried out at 560–600°C in multi-hearth or in fluidized bed furnaces. The obtained powder is used in hydrometallurgy for purification of nickel–cobalt solutions from copper by cementation.

During reduction by solid carbon (700–830°C), the powder is inevitably contaminated by inclusions of the reducing agent and carbide formation. The charge is preliminarily granulated for increasing layer gas permeability. Powder sintering is avoided by the introduction of 0.5–1.0 wt% $CaCl_2/MgCl_2$ or by using fluidized bed furnaces.

Reduction by Organic Reagents

There are various methods of nickel powder production by reduction processes using organic reagents.

The nickel powders that are used as catalyst in the process of oil hydrogenization are produced by reduction by means of hydrazine from the following compositions:

- nickel borate solution in the presence of a catalyst (platinum or palladium salts)
- aqueous or ammoniacal solutions in the presence of platinum or palladium salts; final product contents 96–97 wt% Ni
- a mixture of nickel acetylacetonates in boiling ethanol
- an aqueous solution with addition of sodium borohydride at $p_{H_2} = 6–10$ MPa; $T = 27–87$°C; the powder is treated with glue, washed with alcohol and dried
- a nickel sulfate solution in the presence of Rochelle salt, platinum chloride; 96 wt% of the Ni was extracted in the colloidal product, which contained 99% of the Ni
- nickel hydroxide (II) (the ratio liquid to solid is 1 to 2.3, temperature 20°C); in 46 hours up to 99 wt% of the Ni in the form of powder with density of 6.78 g/cm^3 was precipitated; typical powder particle size distribution is characterized by following data: 5 wt% (+150) μm, 27.8 wt% (−150 + 100) μm, 14.1 wt% (−100 + 83) μm, 53.1 wt% (−83) μm
- for the production of nickel powder, oxide-dispersion strengthing by 2% zirconium dioxide, nickel salt is treated by alkali at 77–87°C and disulfo-zirconium acid is added, as well as 2.0–2.5 L hydrazine to 1 kg salt; the precipitate is filtered, washed, dried, calcined in hydrogen atmosphere at 450°C for 1 hour.

In the treatment of nickel salts by hydrazine, it is possible to influence the particle shape and size by varying the type of solution (aqueous, ethyleneglycol, diethylamine, di-, tri- ethyleneamine) and the process conditions (metal concentration, composition and specific consumption of reagents, temperature). When particle agglomeration is excluded, nano-size powders 0.1–1.25 μm are produced with narrow particle size distribution. Nickel content of the powder amounts to 99.8%.

During processing of basic nickel carbonate pulp using hydrazine-hydrate (hydrazine: nickel = 1.3 in moles) at 87°C, more than 96% of nickel is precipitated as ultrafine powder (particle size is 40–70 nm, surface is 21 m^2/g). Particle agglomeration was avoided by a polyvinyl alcohol addition.

Nickel powder properties are remarkably improved if nickel powder contains up to 1.0 wt% Mg or 0.1 wt% Ca. With this aim, the initial nickel solution containing alloying elements in the required amount is treated by sodium hydroxide and the precipitate obtained is processed with hydrazine. The articles manufactured from this powder show shrinkage characteristics close to ceramic backing shrinkage during sintering. It is important, in particular, for the production of inner electrodes in laminar ceramic capacitors.

Processing of alkaline nickel carbonate by sodium formate with phase transformations depending on temperature is given in the scheme below:

$$\left.\begin{matrix} NiCO_3 \cdot x Ni(OH)_2 \cdot y H_2O \\ NaCOOH \end{matrix}\right\} \xrightarrow{197\,^\circ C} \left.\begin{matrix} NiCO_3 \cdot x Ni(OH)_2 \\ NaCOOH \end{matrix}\right\}$$

$$\xrightarrow{277\,^\circ C} \left.\begin{matrix} Ni \\ Na_2C_2O_4 \\ NaCOOH \end{matrix}\right\} \xrightarrow{307\,^\circ C} \left.\begin{matrix} Ni \\ NiO \\ Na_2C_2O_4 \end{matrix}\right\}$$

$$\xrightarrow{347\,^\circ C} \left.\begin{matrix} Ni \\ NiO \\ Na_2C_2O_4 \\ Na_2CO_3 \end{matrix}\right\} \xrightarrow{597\,^\circ C} \begin{matrix} Ni \\ NiO \\ Na_2CO_3 \end{matrix}$$

The product is washed by water to remove sodium salts; then dried, annealed at 627–700°C in a hydrogen atmosphere, milled and screened. Chemical composition of the powder produced includes minimum 99.0 wt% Ni; 0.42 wt% Co; 0.003 wt% Cu; 0.09 wt% Fe; 0.02 wt% C; 0.02 wt% S; 0.06 wt% O_2. Powder particle size ranges from 2 to 9 μm, specific surface is 6–6.8 m^2/g, apparent density is 1.8–1.9 g/cm^3.

Nickel powder with a colloidal structure is produced when nickel salt is treated in an organic liquid (glycerol, silicone and vaseline oil) at a temperature not less than 247°C. For example, nickel formate is mixed with silicone oil in mass relation 1:1 and treated at 207°C for 1 hour. Powder is separated by centrifuge, washed with toluene and dried; it is monophase, particles have equiaxed shape, their size depending on the dispersivity of initial nickel salt. The powder purity is determined by raw material composition; there are problems connected with washing solution usage.

Processing of nickel formic precipitate by acetone (liquid-to-solid ratio of up to 6:1) is performed at the temperature 250°C in the presence of polyacrylamide oligomer that lyophilizes and protects powder particles from oxidization, thus excluding their pyrophoricity and allowing the production of powder with the following characteristics: mass density 8.4–8.6 g/cm^3, specific surface 8.0–9.6 m^2/g, particle size is 2–5 μm.

The aqueous-spirit solution of hydroxide pulp and nickel formate (ratio of spirit to water in the range from 0.1 to 10) is processed in an autoclave at 157–257°C and hydrogen pressure 2.5–5.0 MPa using surfactant (acrylonitrile, pyridine); powder particles are of spherical shape, their size ranges from 0.07 to 0.2 μm. The choice of conditions depends on the requirements of the powder properties. High hydrogen pressure, the proper surfactant and increased ratio of spirit to water promote production of fine powder.

For the production of powder with superhigh specific surface, a process is known where nickel chloride and metallic aluminum (nickel-to-aluminum ratio of up to 1 to 1) are mixed and treated in alkaline melt, inert gas atmosphere at 600°C for 4–5 hours. A reactor of special construction with electrical heating and mixing of reacting components is used. The powder produced has the specific surface up to 100 m^2/g and useful in chemical industry for production of catalysts or polymer compositions.

Production of Nickel Powder by Electrolysis

Nickel powder is produced by electrolysis from a sulfate electrolyte with soluble anodes which are produced by nickel refining (Figure 17.18). Chloride ions as hydrochloric acid are injected into the solution to prevent passivation of the nickel anodes.

Temperature in the range 47–57°C is maintained by the use of water cooled cathodes. The electrolyte consists of 2–5 g/L nickel; 45–60 g/L sulfate-ions and 0.05–0.15 g/L chloride-ions at pH ranging from

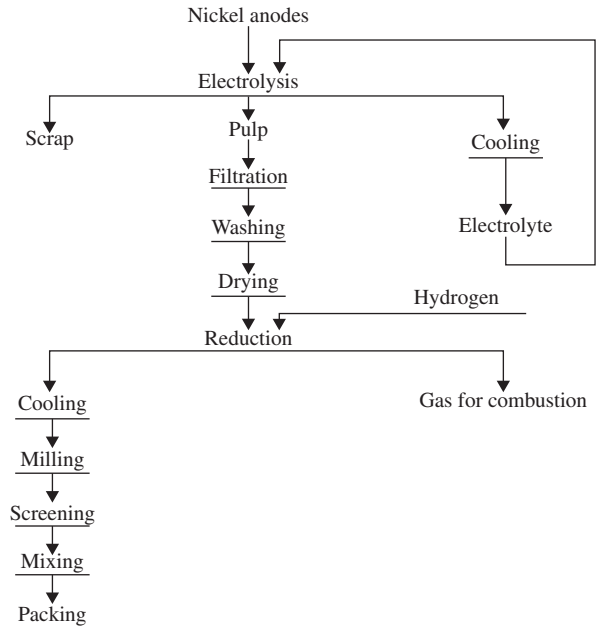

Figure 17.18 Flow sheet for nickel powder production by electrolysis.

5.5 to 7. Approximation of anode current efficiency to cathode one by chloride-ions concentration control provides the electrolyte composition stability. Cell voltage is 12–15 V at cathode density 1.8–2.2 kA/m^2. Electrolyzer is a bin-type one with hollow disk cathodes rotated in reciprocating directions. The powder precipitate is removed by knives.

Chemical composition of CIS's standard grade electrolytic nickel powders (GOST 9722-79) are given in Table 17.9, The powders typically contain 95.5 wt% nickel or more and 0.02 wt% oxygen or less. Powder type PNE-1 is purer than type PNE-3. The sieve content under 71 μm particle size of powder type PNE-1 is 96 wt% or more, while under 45 μm it is 30 wt% min. Its apparent density is 3.4 g/cm^3. The powder type PNE-3 is coarser: the sieve content less than 250 μm, is 97 wt% or more and oversize is not more than 3 wt%. Its apparent density is 5.0 g/cm^3.

Currently, the largest producer of electrolytic nickel powder in Russia is Norilsk Nickel Company [6].

There are various means of production of nickel and nickel-alloy powders by electrolytic processes. Several of them are summarized in Table 17.10.

Table 17.9 Chemical composition of CIS's standard grade electrolytic nickel powders (GOST 9722–79)

Brand	Nickel (minimum, wt%)	Impurities maximum (wt%)					
		O	Fe	Co	Si	C	S
PNE-1	99.5	0.02	0.10	0.20	0.03	0.06	0.008
PNE-3	99.5	0.02	0.20	0.50	0.03	0.08	0.010

Table 17.10 Production of nickel and nickel-alloys powders by electrolysis

Method	Chemical composition of electrolyte	Current density (kA/m^2)	Temperature (°C)	Electrolysis parameters
Nickel				
WS	20 g/L $NiSO_4 7H_2$; 20 g/L$(NH_4)_2SO_4$; 10 g/L NaCl (pH = 4–4.5)	0.5–3.0	30–35	Current efficiency is 40–60%; particles size ranges 40–60 μm
WS	50 g/L $NiCl_2$; 25 g/L NH_4Cl; HCl up to pH 1–1.5	. . .	20–40	Current efficiency is 66–75%
WS	20 g/L $NiCl_2$; 25 g/L NH_4Cl; 10 g/L NaCl (pH 5.2–7.3)	5	40	Powder consists of 55% of particles with size 60–25 μm; 30% of particles with size less than 25 μm; 20% of particles with size less than 10 μm

(*Continued*)

Table 17.10 (Continued)

Method	Chemical composition of electrolyte	Current density (kA/m^2)	Temperature (°C)	Electrolysis parameters
WS	15–25 g/L $NiSO_4 7H_2O$; 40 g/L NH_4Cl; 50–80 g/L NaCl; (pH 6.5–7.2)	5–10	20–30	Current efficiency is up to 65–70%; cell voltage is 7–12 V; easy removal of powder
WS [37]	47.8–57.4 g/L $NiSO_4 7H_2O$; 200 g/L NaCl	$i_{in} = 0.17$; $i_{end} = 0.56$;	50	Linear current time history; particles size 60–80 μm; specific current consumption 6.4–8 kW·h/kg
WS	4–8 g/L Ni; 20 g/L NH_4Cl; 10 g/L NaCl; (pH 5.5–6.5)	$i_k = 3–6$; $i_a = 0.4–0.5$	30–40	Current efficiency is 70–80%; cell voltage is 8 V
WS	17 g/L Ni; 200 g/L NaCl; 50 g/L NH_4Cl; (pH 6.3)	3.0	50	Current efficiency is 95%; particle size is 20–80 μm
WS	4–10 g/L Ni; 20 g/L H_3BO_3; 25 g/L Na_2SO_4; 20 g/L $(NH_4)_2SO_4$; 20–60 g/L urea	3.7–8.0	No data	Current efficiency is 55–80%; air agitation; period of precipitation is 20–30 min; particle size is 100 μm
Nickel–Cobalt				
WS	2–10 g/L $NiSO_4$; 2–8 g/L $CoSO_4$; 30–132 g/L $(NH_4)_2SO_4$; 12.4–24.8 g/L H_3BO_3; 10 g/L Na_2SO_4; (pH 2.1–9.6)	0.2–1.33	20	$[Ni/Co]_{alloy} = [Ni/Co]_{solution}$
Nickel–Tellurium [38]				
WS	7 g/L Ni; 33 g/L $(NH_4)_2SO_4$; 20 g/L K_2SO_4; 0.02–0.156 g/L Te	12	35	Current efficiency is 42%; average particle size is 50 μm; Te content in powder is 0.25 wt%
Nickel–Chromium				
WS	15 g/L $NiCl_2$; 94 g/L (Ni + Cr);	4–5	45	Current efficiency is 35%; $i = 10\ A/m^2$ on auxiliary cathode
Nickel–Zinc				
WS	5 g/L Ni; 16.2 g/L Zn; 20 g/L $(NH_4)_2SO_4$; 50 g/L NaCl;	8.9–20.8	25–70	Nickel as $Ni(NH_4)_2SO_4 \cdot 2H_2O$, zinc as sulfate; particles size is 5–10 μm; current efficiency is 34%
WS	10–20 g/L Ni; 18.2 g/L Zn; 20 g/L $(NH_4)_2SO_4$; 50 g/L NaCl	1.8–20.8	25–70	Nickel as salt $Ni(NH_4)_2SO_4 \cdot 2H_2O$, zinc as sulfate; particles size is 15–20 μm; current efficiency is 21–70%
WS	50–60 g/L Ni; 16.2 g/L Zn; 20 g/L $(NH_4)_2SO_4$; 50 g/L NaCl	1.8–13.3	25–50	Ni as salt $Ni(NH_4)_2SO_4 \cdot 2H_2O$, zinc as sulfate; dendrites 25–75 μm in size; current yield is 67–72%

(*Continued*)

Table 17.10 (Continued)

Method	Chemical composition of electrolyte	Current density (kA/m^2)	Temperature (°C)	Electrolysis parameters
Nickel–Iron–Molybdenum				
WS	9.5 g/L Ni; 1.7 g/L Fe; 0.48–0.45 g/L Mo; 19.8 g/L $(NH_4)_2SO_4$; (pH 2.5–2.7)	$i_k = 2.3$ $i_{aNi} = 0.1–0.2$ $i_{aFe} = 0.1–0.2$ $i_{aPb} = 1–2$	25	$i_{aFe}/i_{aNi} = 5/27$; on net near Fe anode $i = 50–70\,A/m^2$; Mo as $(NH_4)_2MoO_4$; Ni and Fe as sulfates; alloy is near permalloy
Nickel–Iron [39]				
WS	11.2–11.7 g/L (Ni + Fe); 50 g/L $(NH_4)_2SO_4$; 15 g/L KCl; 2.25 g/L NaF; (pH 5)	3.0	30	Optimum [Ni/Fe] = 1/1 (mole) $[Ni/Fe]_{alloy} = [Ni/Fe]_{solution}$ alloys are solid solutions; till 76% Fe fcc lattice; above - bcc; current efficiency is 73%; size 40 μm max; density 2.8–3 g/cm^3

WS: electrolysis in aqueous solution; Ce: current efficiency; i_a^{Pb}, i_a^{Ni}: current densities on insoluble (Pb) and soluble (Ni) anodes respectively

References

1. Goldberger, W.M., Othmer, D.F., The kinetics of nickel carbonyl formation. *Ind. Eng. Chem. Process Des. Dev*., 1963, July: 202–209.
2. Carlton, H.E., Goldberger, W.M., Fundamental consideration of carbonyl metallurgy. *J. Met., 1965*, 6:611–615.
3. Commonwealth of Independents States Standard GOST 12.1.005−88 (in Russian).
4. Guide to Legislation and 'Health and Safety' in the European PM Industry. EPMA, Bellstone, 1997.
5. Sanitary Regulations and Standards of Surface Waters from Pollution. SanPiN 4630-88 (in Russian).
6. Norilsk Nickel. Carbonyl powder and pellets. www.nornickel.ru
7. Tundermann, J.H., Carbonyl vapormetallurgy. In *ASM Handbook*, Vol. 7. ASM International Publishers, 1998, pp. 167–171.
8. Naboychenko, S.S., (ed.) *Handbook of Non-Ferrous Metal Powders*. Metullurgiya, Moscow, 1997 (in Russian).
9. Freeman, G., Production of nickel powders by hydrometallurgical processing. In *ASM Handbook*, Vol.7. ASM International Publishers, 1998, pp. 171–174.
10. Kammer, P.A., Simm, W., Steine, H.T., The influence of atomisation process and parameters on metallic powders and coating properties. Abstract in *Thermal Spray Research and Applications*. ASM International, 1990, pp. 773–776.
11. Conwey, J.J., Sperber, M.S., Rizzo, F.J., Enhanced properties of nickel-base superalloys using hot isostatic pressing (HIP) of powder metals. *Proceedings of 2002 World Congress on Powder Metallurgy & Particulate Materials*. MPIF, Princeton, 2002, pp. 8-123–8-137.
12. Coyne, J.E., Couts, W.H., Chen, C.C., Roehm, R.P., Superalloy turbine components – which is the superior manufacturing process: As-HIP, HIP + isoforge or gatorizing of extrusion. In *Proceedings of Powder metallurgy superalloys – aerospace materials for the 1980s*, Vol. 1, MPR, 1980.
13. Moll, J.H., McTiernan, B.J., Powder metallurgy superalloys. In *ASM Handbook*, Vol. 7. ASM. International Publishers, 1998, pp. 887–902.
14. Krueger, D.D., Kissinger, R.D., Menzies, R.G., Development and introduction of a damage tolerant high temperature nickel-base disk alloy, Rene 88 DT. In *Superalloys 1992*. The Minerals, Metals and Materials Society, 1992.
15. Furrer, D., Fecht, H., Ni-based superalloys for turbine discs. *Journal of Metals*, 1999, January: 14–16.
16. Hattory, H., Takekawa, M., Furrer, D., Noel, R.J., Evaluation of P/M U720 for gas turbine application.

Superalloys 1996. The Minerals, Metals and Materials Society, 1996, pp. 705–711.
17. Moll, J.H., Conway, J.J., Characteristics and properties of As-HIP PM Alloy 720. In *Proceedings of Superalloys 2000*, Conference Proceedings of Superalloys 2000, Seven Springs, PA, September 2000. TMS, Wareendale, PA, 2000, pp. 135–142.
18. Ducrocq, C., Lasalmonie, A., Honnorat, Y., N18, a new damage tolerant PM superalloy for high temperature turbine discs. In *Proceedings of the Sixth International Simposium on Superalloys,* 1988, Conference Proceedings of Superalloys 2000, Seven Springs, PA, September 1988. TMS, Wareendale, PA, 1988, pp. 63–72.
19. Soucail, M., Marty, M., Octor, H., Development of coarse grain structures in a powder metallurgy nickel base superalloy N18. *Scr. Mater.*, 1996, 34(4):519–525.
20. Gray, D.F., Mechanical properties of thick section AF2-IDA-6 powder metal turbine rotors. In *Proceedings Rapidly Solidified Materials*. American Society for Metals, 1985, pp. 387–395.
21. Ewing, B., Rizzo, F., ZurLippe, C., Powder metallurgy products for advanced gas turbine applications. In *Proceedings of the Second International Simposium of Superalloys*, Sept. 1972. TMS, Wareendale, PA, 1998, pp. BB1–BB20.
22. Ewing, B.A., A solid-to-solid HIP-Bond Processing concept for the manufacture of dual-property turbine wheels for small gas turbines. In *Proceedings Superalloys 1980*. American Society for Metals, 1980, pp. 169–178.
23. Dreshfield, R.L., Miner, R.V., Application of superalloy powder metallurgy for aircraft engines. In *Proceedings of 1980 International Powder Metallurgy Conference*, PM Superalloy Technology and Applications. Washington, DC, 1980, pp. 123–141.
24. Evans, D.J., Eng, R.D., Development of a high strength hot-isostatically-pressed disk alloy, MERL 76. In *Proceedings Modern Developments in Powder Metallurgy*, Vol. 14. Metal Powder Industries Federation, 1980, pp. 51–63.
25. Athey, R.L., Moore, J.B., Development of IN100 powder metallurgy discs for advanced jet engine application. In *Proceedings of the Eighteenth Sagamore Army Materials Research Conference*. Syracuse University Press, Syracuse, NY, 1972, pp. 281–301.
26. Chang, D.R., Krueger, D.D., Sprague, R.A., Superalloy powder processing, properties and turbine disk applications. In *Proceedings of the Fifth International Symposium on Superalloys.* TMS, Wareendale, PA, 1984, pp. 245–273.
27. Garibov, G.S., Current trends of PM superalloys discs production technology for gas turbine engines. In *Proceedings Advanced in Powder Metallurgy and Particulate Materials – 2001*. MPIF, Princeton, NY, 2001, 7, pp. 78–83.
28. Garibov, G. et al., Prospects of production of aerospace materials and techniques for their processing at the beginning of the 21 Century. *Technology of Light Alloys*, 2002, 4:80–89.
29. Benjamin, J.S., Dispersion strengthened superalloys by mechanical alloying. *Metall. Trans.*, 1970, 1:2943–2951.
30. Suryanarayana, C., Mechanical alloying. In *ASM Handbook*, Vol. 7. ASM. International Publishers, 1998, pp. 80–90.
31. de Barbadillo, J., Fischer, J., Dispersion-strengthened nickel-base and iron-base alloys. In *ASM Handbook*, Vol. 2. ASM International Publisher, 1990, pp. 722–729.
32. Inconel Alloy MA 754, *Alloy Dig.*, 1990, ASM International, Rev. March 1990.
33. Inconel Alloy MA 758, *Alloy Dig.*, 1990, ASM International, Rev. May 1996.
34. Inconel Alloy MA 6000, *Alloy Dig.*, 1980, ASM International, Rev. July 1983.
35. Gilman, P., Benjamin, J.S., Nickel- and iron-based dispersion strengthened alloys. In *ASM Handbook*, Vol. 7. ASM. International Publishers, 1985, pp. 722–726.
36. Krupin, S.V., Yuriev, B.P., Reasonable solution composition of nickel powder production by electrolysis. *Sov. Powder Metallurgy and Ceramics*, 1975, 1:20–23.
37. USSR Patent 1,257,120.
38. Krupin, S.V. Yuriev, B.P. Study of tellurium impurity co-precipitation at nickel powder production by electrolysis. *Sov. Powder Metall. Met. Ceram.*, (2):1–4.
39. Murashova, I.B., Pomosov, A.V., Artamonov, V.P., Electro precipitation of powder nickel-iron alloy. *Sov. Powder Metall. Met. Ceram.*, 1976, 6:1–4.

Chapter 18

Production of Cobalt and Cobalt-Alloy Powders

Stanislav S. Naboychenko, Irina B. Murashova, Ural State Technical University (UPI), Yekaterinburg, Russia
Oleg D. Neikov, Frantsevich Institute for Problems of Materials Science (IPMS), Kiev, Ukraine

Cobalt and cobalt-alloy powders are used in the PM industry predominantly in the production of permanent magnets, superalloys (high-temperature, creep-resistant) and wear-resistant hardfacing alloys. Cobalt powder is used also as an element in the tool and die steels and as a binder in cemented carbides.

About 60% of the feedstock of world production of cobalt originates in Zambia and Zaire.

Hydrometallurgical Process

The hydrometallurgical technique of cobalt powder incorporates three main processing stages: chemical dissolution (leaching), solution purification and metal recovery. Since the leaching stage is accomplished in the leach autoclaves it is also called autoclave processing [1].

Leach Autoclave Method

The leaching autoclave process is based on the ammoniacal pressure leaching of the sulfides to produce soluble nickel and cobalt hexammine sulfate complexes. This process is described in detail in Chapter 17.

The Sherritt (Corefco) refinery in Fort Saskatchewan, Alberta, Canada was the first to commercialize successfully the hydrometallurgical process for the treatment of a nickel sulfide concentrate. This refinery commenced operation in 1954. At present, the primary feed to the Sherritt refinery are nickel and cobalt sulfides which include 51–56 wt% Ni, 5.0–6.0 wt% Co, 32–37 wt% S and 1.0–1.3 wt% Zn. The first stage in the refining process is the leaching of the metal sulfides to soluble amine complexes with the simultaneous oxidation of sulfide sulfur (S^{2-}) to form a series of soluble thiosalts including sulfate. The general equation for the ammoniacal leaching of sulfides may be represented as:

$$MS + nNH_3 + 2O_2 \rightarrow M(NH_3)_n^{2+} + SO_4^{2-} \qquad (1)$$

where M includes nickel, cobalt, iron, copper, zinc and n is 2 to 6.

The typical conditions in the leach autoclaves are represented by following data: temperature 90–95°C, pressure of 110–120 psig (7.7–8.4 atm), ammonia 80–100 g/L and ammonium sulfate 150–200 g/L.

Before it is possible to reduce the nickel from the leach solution as the pure metal, several solution purification steps are completed. The leach liquor is transferred to the nickel–cobalt separation plant where cobalt is separated from the nickel as pure crystalline cobaltic hexammine salt [2].

A flow diagram of this process is shown in Figure 18.1. The nickel-rich solution remaining after the selective removal of cobalt is directed to the nickel plant for further solution purification processing and final nickel powder production.

Cobalt (III) hexammine sulfate, $[Co(NH_3)_6]_2(SO_4)_3$, is the basis for the separation and purification of cobalt from nickel. The initial step of this separation involves the precipitation of a cobalt–nickel hexammine salt. This precipitation is realized by the addition of ammonium sulfate and ammonia to the leach solution:

$$[Co(NH_3)_6]_2(SO_4)_3(aq) + 2[Ni(NH_3)_6](SO_4)(aq) + (NH_4)_2SO_4 \rightarrow 2(NH_4)[Co(NH_3)_6[Ni(NH_3)_6](SO_4)_3(s) \qquad (2)$$

The relatively insoluble cobaltic hexammine sulfate precipitates in the cobalt–nickel salt, while the more soluble nickel hexammine sulfate remains in solution. This selective nickel removal from the cobalt–nickel hexammine salt results in the isolation of a purified cobalt salt:

$$2(NH_4)[Co(NH_3)_6][Ni(NH_3)_6](SO_4)_3(s) \leftrightarrow 2(NH_4)^+(aq) + 2[Ni(NH_3)_6]^{2+}(aq) + 2[Co(NH_3)_6]^{3+}(aq) + 6(SO_4)^{2-}(aq)$$

and in continued reaction

$$2[Co(NH_3)_6]^{3+}(aq) + 3(SO_4)^{2-}(aq) \rightarrow [Co(NH_3)_6]_2(SO_4)_3(s) \qquad (3)$$

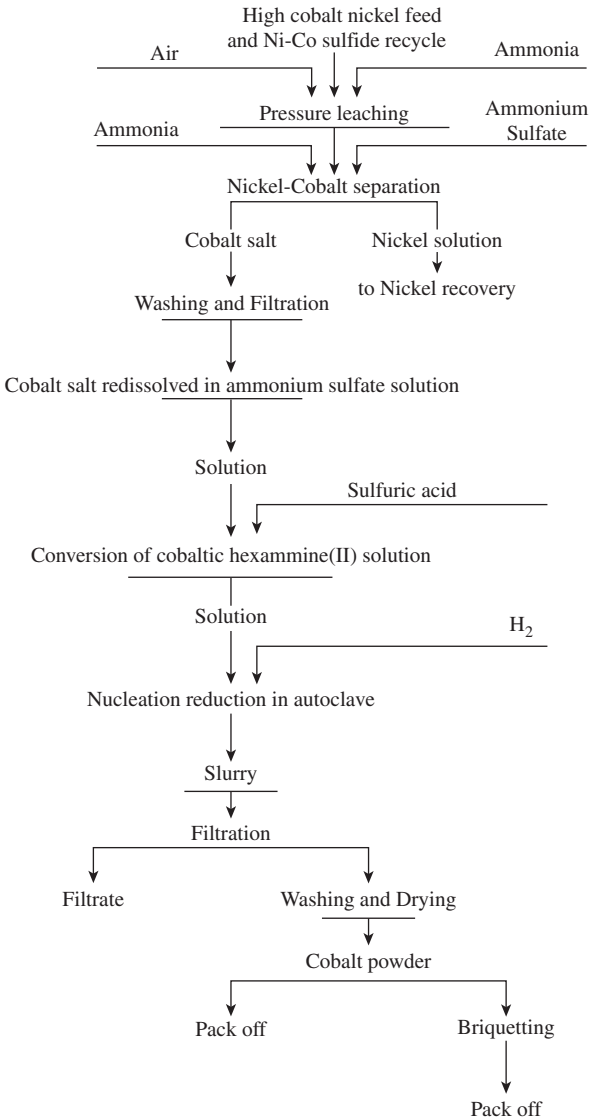

Figure 18.1 Flow diagram of the Sherritt cobalt refining process.

The cobalt hexammine salt is then recrystallized to remove the remaining nickel contamination. After washing and filtration, the pure cobalt salt is dissolved in an ammonium sulfate solution.

A step referred to as 'conversion' completes the reduction of the cobalt (III) present in the pure cobaltic hexammine solution to cobalt (II). The conversion of cobaltic hexammine to a cobaltous ammine is accomplished by the controlled addition of metallic cobalt powder as determined by the following stoichiometry:

$$[Co(NH_3)_6]_2(SO_4)_3 + Co(\text{powder}) \rightarrow 3[Co(NH_3)_4]SO_4 \quad (4)$$

The reduction of cobalt is a batch operation that occurs in a reduction autoclave under a hydrogen atmosphere at elevated pressure and temperature. Cobalt powder is produced in a cycle comprising one nucleation reduction, which refers to the hydrogen reduction process. By this process, fine cobalt seed powder is produced with the aid of a sodium sulfide/sodium cyanide catalyst. After the completion of the nucleation reduction, the solution is decanted from the seed powder, which remains in the autoclave for use as a catalyst. In the course of the cycle, the initially fine seed powder coarsens.

The objective of the densification reduction is to deposit reduced cobalt onto the seed particles until the desired powder density and particle size have been achieved. Every densification is an autoclave hydrogen reduction process where metallic cobalt precipitates from solution and is deposited on the seed powder by the following reaction:

$$[Co(NH_3)_2]SO_4 + H_2 \rightarrow Co(\text{metal}) + (NH_4)_2SO_4 \quad (5)$$

The rate of the process and its completeness depend on several factors, including the ammonium sulfate concentration, the ratio of ammonia to cobalt, the hydrogen pressure, temperature and the quantity of seed powder present.

At the end of every densification, the powder is deposited, the spent solution is decanted and the slurry is discharged from the autoclave to a flash tank, where the initial separation of cobalt powder from the end solution is accomplished. After washing the cobalt in a vacuum pan filter to remove ammonium sulfate, and drying, the product is packaged as powder or compacted into briquettes and sintered. Typical properties of the Sherritt cobalt powder are shown in Table 18.1.

The production of cobalt powder at the Sherritt refinery currently amounts to 2400 tonnes per year, representing about 10% of the world's shipments.

The kinetics of the reducing autoclave process was studied by Z.L. Ratner and G.N. Dobrokhotov (Gipronickel, USSR, 1966) in the temperature (T) interval 147–247°C hydrogen pressure, $p_{H_2} = 7 - 45$ atm, the ratio of ammonia to cobalt, $NH_3/Co = 3–7$, concentration of cobalt (II), $[Co^{2+}]_0 = 0.1–0.8$ mole/L, at seed consumption 0.11–0.7 mole/L. The kinetic indexes are shown in the first-order autocatalysis equation (Eqn 7):

$$[Co(NH_3)_n]^{2+} + H_2 \rightarrow Co + 2NH_4^+ + (n-2)NH_3 \quad (6)$$

$$-\frac{d[Co^{2+}]}{d\tau} = K_0 \frac{[Co^{2+}]_\tau}{\{[Co^{2+}]_0 - [Co^{2+}]_\tau\}} \cdot \frac{p_{H_2}}{1 + 0.9p_{H_2}} S \cdot n \cdot 10^{\frac{2695}{(T+273)}} \quad (7)$$

Table 18.1 Properties of the cobalt powder by hydrometallurgical processing

Property	Unit	Factory, Company		
		Sherritt International Corp.	UMEX of Union Miniere Belgium	OSRAM Bruntal Czech Republic
Chemical				
Co	wt%	99.9	99.8*	bal
Impurities max				
Ni	wt%	0.02	0.15	0.045
Fe	wt%	0.005	0.001	0.02
Cu	wt%	0.005	0.0005	0.001
Ag	wt%	...	0.12	0.001
Al	wt%	...	0.0005	0.01
Na	wt%	...	0.001	0.225
Mg	wt%	...	0.0005	0.005
Mn	wt%	...	0.0005	0.00025
Pb	wt%	...	0.002	...
S	wt%	0.03	0.006	0.0005
C	wt%	0.05	0.18**	0.04
O_2	wt%	...	0.7***	0.6
Screen size (μm)				
+150	wt%	0–15	...	...
−150 + 106	wt%	5–25	...	...
−105 + 75	wt%	5–15	...	...
−75 + 63	wt%	5–15	...	...
−63 + 45	wt%	20–45	...	...
−45	wt%	10–50	...	...
−38	wt%	...	99.98	...
Average powder size (FSSS)	μm		0.9	1.1–1.8
Apparent density	g/cm^3	2.5–3.5	1.2	0.9 min
Tap density	g/cm^3	...	2.5	...

*Determined by subtraction of non-organic content from 100% (e.g. cobalt = 100% −Ni −Cu −Ag −Fe −S).
**Carbon occurs in the form of residual organic material. 90% of the C is removed during treatment in hydrogen, vacuum or an inert atmosphere at temperatures up to 400°C.
***Oxygen occurs in the form of residual organic material. During treatment in vacuum or inert atmosphere up to 75% of the oxygen is removed at temperatures up to 400°C. During treatment in a hydrogen atmosphere, up to 90% of the oxygen is removed at similar temperatures.

where τ is time, s, $K_0 = 9.53\times10^{-2}$ $L^{-1}\cdot mole\cdot s^{-1}\cdot cm^{-2}$, S is surface of cobalt seed powder, cm^2; n is the molar ratio of NH_3 to Co(II), $\left|Co^{2+}\right|_0$ is the initial concentration of $\left|Co^{2+}\right|$, $\left|Co^{2+}\right|_\tau$ concentration of Co^{2+} at the moment τ.

Reduction type is heterolytic, therefore the seed is very important and there is the possibility of the cladding of the charging materials by cobalt as well as of recovery of cobalt powders of desired size, structure, apparent density, fluidity, and specific surface area.

Anthraquinone is not so significant; obviously, ions of Co(II) are not reduced to Co by generating anthrahydroquinone and the catalyst circle of anthraquinone functioning is broken down.

After treatment of the solution a period of hydrogen induction is observed, the duration of which decreases with a decrease of the sodium sulfide consumption. Its optimal consumption for fine powder production is of 0.01 M. Both the induction period and treatment duration are decreased in the presence of sodium cyanide. As a result, more dispersed and less agglomerated particles are produced, especially in the presence of surfactant and at high concentration of ammonium sulfate. The following parameters are operative for the nucleation stage: $T = 150$–$200°C$ $p_{H_2} = 1.5 - 3.0$ MPa; $(NH_4)_2SO_4 > 200$ g/L; $NH_3/Co = 2.3$–2.5.

From another surfactant, the compound containing 14 atoms of S at 0.001–0.004 mole of S^{2-} per 1.0 L is of interest.

The main method of powder property variation is to increase the number of densification cycles;

particles are of a porous structure capable of agglomeration; thus the powder surface is decreased.

The rate of the densification reduction increases with increasing of temperature, hydrogen pressure, and seed consumption. Addition of surfactant can influence the particle grain size and produce monodisperse powders, but they are a possible source of powder contamination by carbon and sulfur.

During the period 1968 to 1982, Outokumpu (Finland) produced by the leaching autoclave method up to 1500 t of cobalt powder per year from secondary raw materials, pyrite concentrate, and semi-finished products. The typical conditions in the leach autoclaves were the following: temperature of 177°C, total pressure of 4.0 MPa. The content of metallic cobalt in the powder produced was 99.8.

In 1983, Impala Platinum Company (Springs, South Africa) built a cobalt powder workshop on the basis of copper nickel converter matte processing.

Double sulfate ammonia salt $MSO_4(NH_4)_2SO_4\ 6H_2O$ was precipitated from the solution after autoclave extraction of nickel containing 1–3.0 g/L Ni; 0.5–1.0 g/L Co; 400–500 g/L $(NH_4)_2SO_4$. Composition of this salt includes 3.7 wt% Co, 11.2 wt% Ni, 0.025 wt% Fe, 0.004 wt% Cu, 0.015 wt% Mn; 60 wt% $(NH_4)_2SO_4$. It was dissolved in recycled ammonia solution, freed from impurities, the ratio of ammonia to cobalt adjusted to 2.3–2.5. The solution entering the cobalt precipitation contains 30 g/L Co, 500 g/L $(NH_4)_2SO_4$, 20 g/L NH_3; at most 5 mg/L Ni, 3 mg/L Fe, 1.0 mg/L Cu, 1.0 mg/L Mn. Residual cobalt content in the solution after precipitation is 1–2 g/L.

The use of carbon monoxide as reducer gas and the treatment of hydroxide suspensions and organic media by hydrogen have been investigated.

$$3[Co(NH_3)_6]^{2+} + 15CO + 6H_2O \rightarrow [Co(NH_3)_6][Co(CO)_6]_2 + 3(NH_4)_2CO_3 + 6NH_4^+ \quad (8)$$

Dobrokhotov (1962) showed the possibility of producing cobalt powder by processing cobalt (II) hydroxide pulp with content of solid matter 2–3 wt% at 117–147°C, $p_{H_2} = 2.5 - 3.0$ MPa; in 1 hour powder containing 99.7 wt% Co was produced.

There is also a possibility to precipitate cobalt from extractant 'Kelex-100' saturated with cobalt at 300°C.

Ultrafine powders (with particles less than 1 μm) are produced by the autoclave method due to prevention of particle growth. For this purpose, ammonium sulfate concentration is increased; the basic solution contains a residue of cobalt sulfate as a seed; then silver sulfate (catalyst) is added as well as an organic surface active substance to prevent particle agglomeration. Composition of the powder produced is: 0.15 wt% C, 0.75 wt% O_2, 0.006 wt% S, 0.17 wt% Ni and 0.15 wt% Ag. Apparent density is 1.1–1.6 g/cm^3. Specific surface area is 2.0–3.0 m^2/g. This powder is used in the production of magnetic compounds and as a bond in solid alloy production on the basis of carbides of high melting point metals and diamonds.

Sherritt also developed commercial production of composite powders, based on autoclave cobalt coating of different seed types (carbides, borides, metals). The properties of such composite powders are presented in Table 18.2.

Solid Phase Reduction

One of the main applications of cobalt powder is its use as a binder in the production of hardmetals (tungsten carbides). The greater part of this powder is produced by the reduction of cobalt oxide with hydrogen at relatively low temperatures, generally below 800°C to obtain the necessary degree of powder fineness. At low reduction temperatures (250–380°C) pyrophorus powder is produced; this property disappears at temperatures above 700°C. To protect the powder from oxidation it is cooled up to 60–70°C in an inert or reducing atmosphere.

Table 18.2 Properties of composite powders on the base of metal carbides (seed size is 44 μm)

Metal	Part of coating (%)	Content (%)		Average size (μm)	Apparent density (g/cm^3)
		Co	S		
W	81.3	18.6	0.01	14.8	...
Mo	77.9	20.0	0.035	6	1.56
Ti	78.0	19.5	0.09	3.8	1.23
Cr	80.7	18.4	0.046	7.0	2.0

The reduction of cobalt salts to metal may be represented as follows:

$$Co(Hal_2) + H_2 \xrightarrow{350-400\ ^\circ C} Co + 2H(Hal) \quad (9)$$

$$CoC_2O_4 + 2H_2 \xrightarrow{750\ ^\circ C} Co + 2CO + 2H_2O \quad (10)$$

$$Co(HCOO)_2 + H_2 \xrightarrow{700\ ^\circ C} Co + 2CO + 2H_2O \quad (11)$$

$$[Co(NH_3)_5]Cl_3 + 1.5H_2 \xrightarrow{700\ ^\circ C} Co + 3NH_4Cl + 2NH_3 \quad (12)$$

where Hal is a halide anion.

Typical properties of the reduced cobalt powders are given in Table 18.3 [3].

Cobalt powder can also be produced by the reduction of cobalt oxide with carbon, carbon monoxide and methane [1], but this technology has not been commercialized. Reduction by these reagents occurs in the following way:

$$Co_3O_4 + 2C \xrightarrow{930\ ^\circ C} 3Co + 2CO_2 \quad (13)$$

$$Co_3O_4 + 4CO \xrightarrow{350-830\ ^\circ C} 3Co + 4CO_2 \quad (14)$$

$$Co_2O_3 + CH_4 \xrightarrow{450\ ^\circ C} 2Co + CO + 2H_2O \quad (15)$$

Reduction temperature by carbon is 930°C, by charcoal and carbon black is 650°C, by methane is 450°C and by carbon monoxide is from 350 to 830°C. All processes are carried out in muffle electric furnaces over 1–2 hours; powders are contaminated by carbon and contain cobalt carbide.

In the case of metallothermic reduction of cobalt oxides, aluminum, boron, magnesium and silicon are used at temperatures ranging from 2427 to 2627°C:

$$Co_nO_m + M \rightarrow nCo + MO_m \quad (16)$$

$$3CoO + 2Al \xrightarrow{2500\ ^\circ C} 3Co + Al_2O_3 \quad (17)$$

$$CoO + Mg \rightarrow Co + MgO \quad (18)$$

Cobalt of high purity (99.9% Co) in the form of fine scales or needles is obtained as a result of treatment of cobalt chloride by aluminum at 830°C in molten NaCl−KCl.

Table 18.3 Typical properties of cobalt powders produced by solid phase reduction technique

Property	Unit	Value
Chemical		
Cobalt*	wt%	99.6
Impurities max		
Nickel	wt%	0.08
Iron	wt%	0.08
Silicon	wt%	0.035
Calcium	wt%	0.020
Manganese	wt%	0.020
Carbon	wt%	0.015
Zinc	wt%	0.010
Sulfur	wt%	0.008
Copper	wt%	0.001
Lead	wt%	0.003
Hydrogen loss	wt%	0.20
Screen analysis (μm)		
+150	wt%	0.01
−150 + 75	wt%	0.04
−75 + 45	wt%	0.15
−45 + 38	wt%	0.20
−38	wt%	99.60
Average particle size	μm	5
Apparent density	g/cm^3	1.8
Tap density	g/cm^3	3.0

*Hydrogen loss not included.
Source: Ref 4

Atomization

Atomized powders of cobalt-base alloys find a wide use for high-temperature applications. One of the major uses of these powders is hardfacing. This section discusses only hardfacing powders.

The carbide-containing alloys and alloys containing Laves phase are the two types of commercially effective cobalt-base hardfacing alloys. Typically, a carbide-containing alloy is a eutectic alloy inclusive of M_7C_3-type carbides in a cobalt-base matrix alloyed with chromium and tungsten. Laves phase is a kind of topologically close-packed intermetallic compound which has a hexagonal structure similar to M_7C_3 carbides, but the hardness value is less than that of carbides and amounts to 1000–1200 HB. Laves phase materials retain their mechanical properties over a wide range of temperatures. Their main uses are for plasma spray hardfacing operations such as plasma spray coating of gas turbine blades. There are two different Laves phase-containing cobalt-base alloys available for hardfacing applications: Co–28Mo–8Cr–2Si and Co–28Mo–17Cr–3Si alloys. These alloys contain at least 50 vol% of Laves phase.

In the microstructure of the carbide-containing alloys, the lightest colored phase is the matrix, which has a face-centered cubic (fcc) crystal structure. The dark phase is M_7C_3; the exact composition is $(Cr_{0.85}Co_{0.14}W_{0.01})_7C_3$, which has a hexagonal crystal structure. Generally, resistance to abrasive wear is imparted by the presence of carbides, whereas the resistance to corrosion and/or elevated temperature hardness retention is imparted by the matrix. Galling wear properties are similarly defined by the matrix alloy.

To minimize oxygen content, gas atomization is the most widely used technique for producing these powders. Some producers prefer vacuum melting and inert gas atomization (typically nitrogen or argon) to air melting and air atomization. The oxygen content in these atomized powders is significantly below 1000 ppm, while the nitrogen level may vary from 600 to 2000 ppm.

Composition and hardnesses of several typical alloys are presented in Table 18.4. The alloys in the Co–Cr–W–C system retain high hardness at elevated temperatures mostly from carbide and solid-solution strengthening rather than precipitation hardening. As shown, alloys RCoCrC and RCoCrB are higher hardness modifications of alloy RCoCrA because of higher carbon and tungsten contents. Alloy RCoCrC contains primary M_7C_3, eutectic M_7C_3 plus matrix and secondary M_6C. Alloy RCoCrB is similar to alloy RCoCrA, but it has more M_6C and, therefore, contains interdendritic eutectic carbide (chromium and tungsten rich).

Cobalt-base hardfacing powders are unsurpassable for use in combined wear-resistant, corrosion-resistant and high-temperature applications.

A gas atomization technology for the production of fine powders of cobalt alloys is used by Osprey Company (Osprey Metals Ltd). The commercial powders, depending on grades (MP/Co 452, MP/Co 502 and MP/Co 552), contain 28.5–30.0 wt% chromium, 3.0 wt% nickel, 4.0–13.0 wt% tungsten, 3.0 wt% iron and 1.2–2.5 wt% carbon. The particle shape is predominately spherical. The mean particle size ranges from 6.7 to 12.0 μm.

Carbonyl Processing

At present, the carbonyl method for cobalt powder production is very restricted by low capacity and unsatisfactory quality of powder [1].

Cobalt carbonyl $Co_2(CO)_8$ is produced by the action of carbon monoxide on fine powder of the freshly reduced cobalt-containing materials at 150–170°C

Table 18.4 Chemical composition and hardness of typical cobalt hardfacing alloys

Property	Unit	AWS designation or trade name					
		RCoCr A	RCoCr B	RCoCr C	Alloy 21	Alloy 20	Tribaloy T-800
Nominal composition							
C	wt%	1.1	1.4	2.5	0.25	2.5	...
Co	wt%	bal	bal	Bal	bal	bal	bal
Cr	wt%	28	29	30	27	32	17
Fe	wt%	3 max	3 max	3 max	2 max	...	...
Mo	wt%	1 max	1 max	1 max	5.5	...	...
Mn	wt%	1 max	1 max	1 max	1 max	...	...
Ni	wt%	3 max	3 max	3 max	2.8	...	...
Si	wt%	1	1.4	1	2 max	17	3
W	wt%	4	8	4	...		...
Nominal microhardness							
HB	kgf/mm^2	424	471	577	255	653	653
HRC	HRC	39–42	40–48	52–54	24–27	53–55	54–64
Approximate hardness of microconstituents							
Matrix	kgf/mm^2	370	420	510	250	540	800
Hard particles							
Alloy type		Eutectic	Eutectic	M_7C_3	Eutectic	M_7C_3 M_6C	Laves Phase
DPH		900	900	900	900	1700	1100

Source: Cabot Corp. AWS: American Welding Society

and pressure up to 20 MPa. Reductions of cobalt carbonate in benzene or hexane and synthesis from halide salts in the presence of metallic reducing agents are used. Joint synthesis of nickel and cobalt carbonyls from nickel–cobalt raw material followed by their separation is possible.

Fine black cobalt powder is produced by carbonyl decomposition in a current of carbon monoxide at 150–250°C with subsequent thermal treatment in a hydrogen atmosphere at a temperature ranging from 347 to 927°C. Passivated fine powder containing approximately 99.99 wt% cobalt and 0.01 wt% carbon is produced by decomposition of cobalt carbonyl in an inert organic solvent (decalin, silicone and vaseline oil, glycerol etc.). Organic fluid prevents the contact of the colloid particles formed with air and their agglomeration. A protective film, which prevents oxidation and powder inflammability, is formed due to liquid adsorption on the metallic particle surface.

Electrolytic Method

Powder is produced from sulfate electrolyte at pH = 5.5–6.0 using soluble cobalt anodes (Figure 18.2) [1]. Cobalt current efficiency is low (60%) due to low overvoltage of hydrogen on cobalt. A high value pH solution is necessary to keep cobalt current efficiency above the level. Equilibrium material balance in the electrolyzer is regulated by the pH value. The boric acid is introduced as a buffer addition agent. The cathode current efficiency is lower than the anode so that cobalt concentration in the solution is increased with time. Electrolyte is diluted by condensate to maintain a given concentration of the electrolyte. In the case of solution depletion, the metal dissolution procedure is intensified by the addition of concentrated sulfuric acid.

The anodes are cast from electrolytic cobalt. Sulfate electrolyte is circulated through the electrolyzers in a closed system including a heat exchanger supporting the required temperature in the cells. Electrolysis is kept at current density ranges from 1800 to 2500 A/m^2, temperature 60–70°C for about 2 to 3 hours. Powder is precipitated on titanium caissoned disk cathodes and, in due course, the anodes dilution gravitates to the bottom of the hopper type cell. Suspended solid is transferred to the settler after the accomplished electrolysis. Clarified electrolyte is returned for electrolysis after filtration and powder is treated by acid solution to wash out hydroxides and it is then washed with distilled water. Powder is dried (400–410°C, for about 3–4 hours) and reduced (900–960°C, for 10 hours) in a hydrogen

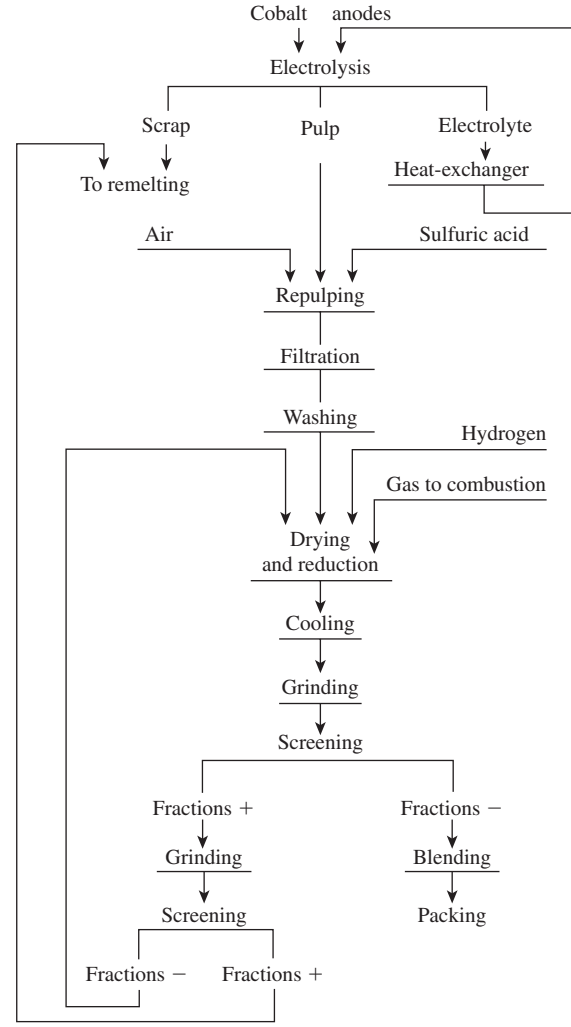

Figure 18.2 Flowsheet of cobalt powder production by electrolytic processes.

atmosphere. After cooling of the powder vessel with air for about 2–3 hours and then in a cell with running water (for 3 hours), the powder is milled in ball mills and screened. Produced fine fractions are passed through secondary reduction and large particles are transferred for remelting.

Electrolyte is prepared by anode dissolution of cobalt in sulfuric acid solution (at concentrations in the range from 30 to 35 kg/m^3) at current density 250–300 A/m^2. Electrolysis is stopped when the cobalt concentration has increased up to 18–20 kg/m^3, the solution is diluted down to 6–8 kg/m^3 of Co, then the pH of the solution is adjusted up to 5.5–6.0 by means of soda and boric acid is introduced as buffer addition agent (5–10 kg/m^3).

Table 18.5 Coercive force (Oe) at minus 70°C of cobalt powder produced by the amalgam technique

Temperature of heat treatment (°C)	Duration of heat treatment (min)				Note
	0	20	40	60	
120	0.530	1.080	1.110	1.110	Without tin addition
135	0.570	1.050	1.035	1.040	Without tin addition
150	0.530	1.135	1.100	1.055	Without tin addition
190	0.565	0.935	0.858	0.845	Without tin addition
30	...	1.060	1.100	1.080	With tin addition
150	...	1.116	1.065	1.065	With tin addition

Properties of the electrolytic cobalt powder are as follows:

- chemical composition includes 99.25 wt% Co, max 0.4 wt% Ni, max 0.04 wt% Cu, max 0.2 wt% Fe, max 0.025 wt% S, max 0.02 wt% C and max 0.1 wt% Cr
- granulometric composition consists of the particles max 4 wt% above 71 μm, min 30 wt% (−71 + 45) μm and min 66 wt% below 45 μm.

Amalgam Techniques

Electric precipitation of cobalt (or its alloys with iron and nickel) is kept at 40°C from a sulfate electrolyte with the cobalt weight-part concentration amounting to 94 g/L on an agitated mercury cathode in a cell with a soluble cobalt anode (or proper composition alloy) at interelectrode space of 1 cm. Anode and cathode current densities are equal at 500 A/m^2. The required value pH = 2 is achieved by adding hydrochloric acid. Amalgam is heat treated after electrolysis. Cobalt particles change their shape from dendritic to needle, or thread-like. Metals (for example, tin), for counteraction of particle agglomeration and a rise in the magnetic properties of suspensions, are introduced into the amalgam (Table 18.5) [1].

After heat treatment, the amalgam is concentrated by means of filtration and is exposed to orientation in a magnetic field with strength above 50 V/m. This treatment provides mechanically compact forms of hard material. The final mercury removal is accomplished by distillation and the sintered mass is reduced to fine thread-like particles. The particle size ranges from 0.5 to 1.5 μm with the fiber stem diameter about 0.02 μm.

Various electrolytic techniques of cobalt and cobalt-base alloy powders production are given in Table 18.6.

Other Hydrometallurgical Methods

The ultrafine powder is obtained as a result of reduction of cobalt formate in a vaseline medium (at temperature range 200–240°C for 1 hour). This powder is separated by centrifuge, washed by solvent (toluene) and dried. Particle size of the powder obtained ranges from 0.5 to 1.0 μm and the shape is close to spherical by using an ultrasonic field at frequency about 44 kHz and intensity of 750 kW/m^2. This method makes it possible to cover the cobalt particle surface with copper or silver films. For this purpose, the cobalt formate is mixed with glycerol, silver or copper salts (for example nitrates, ammoniates) soluble in the organic phase are added and the mixture is heated to 150–190°C. Cobalt powder with particle sizes about 0.2–0.5 μm clad with silver or copper is produced.

As powder properties are significantly dependent on the characteristics of the basic reduced solid phase, some decisions for preparation of the basic raw material before its reduction are proposed.

Thus, ammonia salts of cobalt:

- are evaporated at 80–100°C to obtain the dry salts
- are injected into the chamber at temperature 900–1200°C and produce cobalt (III) oxide
- are treated with sodium hydroxide solution which results in a precipitate of hydrated cobalt (II) oxide

Table 18.6 Production of cobalt and cobalt-alloy powders by electrolysis

Method	Electrolyte composition	Current density (kA/m^2)	Temperature (°C)	Electrolysis parameters
Cobalt				
WS	$CoSO_4$; $(NH_4)_2\,SO_4$, Na_2SO_4, H_3BO_3;	1.0	27	Particle shapes are needle-like and fan-like dendrites
EDC	5–74 g/L Co, chloride solution, pH = 1–6	0.5–8.0	10–60	Coercive force ranges from 0.1 to 0.87 Oe; particle size ranges from 0.5 to 4 μm
EDC	23–24 g/L Co; max 25 g/L NaCl chloride solution	3.0–4.0	15	Cobalt current efficiency amounts to 85–87%
EDC	5–74 g/L Co; chloride solution, pH = 1–6	4.5	25	Cl^-/SO_4^{2-} = 1/5; cobalt current efficiency amounts to 78–85%; with increasing content of SO_4^{2-} the cobalt current efficiency decreases
SPR*	400 g/L NaOH	1.0	80	Raw material is Co_3O_4 or $CoCO_3 \cdot 2CoO \cdot 2H_2O$; particle size about 0.5–1 μm; electrolysis duration is min 4–5 times as large as t_{theory}** for cobalt oxide, and 7–8 times as large as t_{theory} for $CoCO_3$
Cobalt–iron				
AM	62.4 g/L Co; 29.7 g/L Fe; HCl up to pH = 2	0.5	40	Anodes consist of 66.3 wt% Co, 33.3 wt% Fe; salts are the sulfates; after heat treatment at 189–200°C for 120–300 minutes; coercive force amounts to 1.7–1.85 Oe; particle size is about 0.5–1.5 μm
AM	31.2 g/L Co; 59.4 g/L Fe; HCl up to pH = 2	0.5	40	Anodes consist of 33.3 wt% Co, 68.6 wt% Fe; salts are sulfates; heat treatment at 180°C for 60–240 min; coercive force amounts to 1.66–1.93 Oe; particle size is 0.5–1.5 μm
Cobalt–tungsten				
WS	21.2 g/L Co; 21.3 g/L Na_2SO_4; 5.7 g/L W; 29.0 g/L citric acid; 20.0 g/L $(NH_4)_2SO_4$; pH = 2	3.0	20–30	Co in the form of sulfate; W in the form of Na_2WO_4; cobalt current efficiency amounts to 60–70%; cathode of Ni; $(Co/W)_{alloy}$~$(Co/W)_{solution}$ (in molar ratio); alloys up to 20% wt% W are solid solutions; particle shape is globular dendrites with size about 100 μm

Production method: WS: aqua solution electrolysis; EDC: electrolysis in two-layer cell; SPR: solid phase reduction; AM: amalgam metallurgy method (see 'Reduction from solution through film of surfactants' in Chapter 9).

*Electrochemical reduction occurs in thin surface film of the dispersoids.

**Cobalt current yield in that system is low so it is necessary to increase electrolysis duration in comparison with t_{theory} – calculated in accordance with Faraday law for known current.

- are treated with carbon dioxide at pressure $p_{CO_2} = 0.15 - 0.5\,\text{MPa}$, temperature up to 100°C and a sediment of alkaline cobalt carbonate is precipitated.

Further, the solid phase obtained is washed, dried and reground. The intermediate product is reduced in a hydrogen current at 400–630°C and an ultrafine cobalt powder is obtained.

In the case when cobalt is precipitated from solution in the form of oxalate, the sediment is treated by sodium hydroxide solution. Prepared cobalt (II) hydroxide is either washed, dried and reduced in hydrogen, or it is treated by hydrazine at 110 ± 5°C and pH = 9.0, or it is calcined and 0.2–2 wt% of tungsten carbide powder is added to the cobalt oxide to prevent powder sintering during reduction by hydrogen at 700–750°C.

References

1. S.S. Naboychenko, (ed.) *Handbook of Non-Ferrous Metal Powders*. Metullurgiya, Moscow, 1997 (in Russian).
2. Kerfoot, D.G.E., US Patent 5,468,281, 1995.
3. Freeman, G., Production of cobalt-base powders. In *ASM Handbook*, ASM International Publishers, Vol 7. 1998, pp. 179–181.
4. Powder, A.P., *Handbook of Metal Powders*. Reinhold Publ., 1966.

Chapter 19

Production of Zinc, Cadmium and Their Alloy Powders

Irina V. Frishberg, Fine Metal Powders R&D Company, Yekaterinburg, Russia

Production of Zinc Powders

There are different methods known for producing zinc powder, among them those employing cryogenic technique, electrolysis of aqueous solutions etc. Low melting and boiling points (419.5 and 907°C, respectively) and high chemical activity of zinc make the methods based on evaporation and condensation the most appropriate for the manufacture of zinc powder [1]. Due to a combination of high activity and high specific surface area, zinc powders find application in a variety of fields including metallurgy, chemistry, medicine, electrical engineering, etc.

Evaporation–Condensation Method

The evaporation–condensation or physical vapor deposition (PVD) method comprises melting the zinc, evaporation of the melt and condensation of the vapor in a neutral gas medium. In commercial production, the evaporation is carried out either in externally heated equipment or in electrothermal or induction furnaces.

The continuous process of zinc powder production (Figure 19.1) includes three sequentially arranged installations: a reverberating furnace for zinc melting and partial elimination of iron and lead, a rectification column and a condenser.

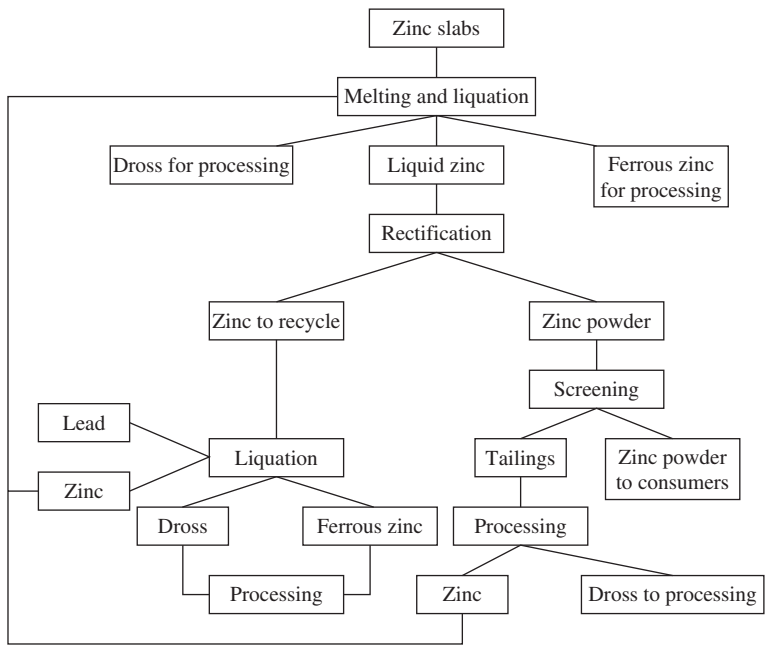

Figure 19.1 Flow-sheet of the process of producing zinc powder by rectification of the melt.

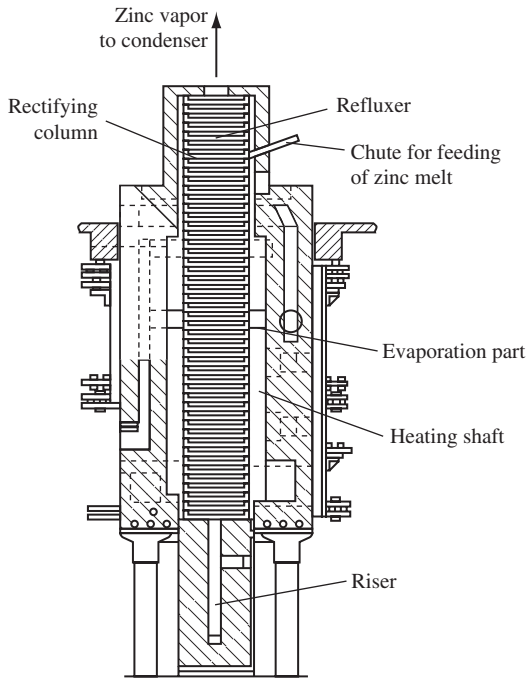

Figure 19.2 Rectification column.

The charge containing zinc of various grades is loaded into the gas-heated reverberating furnace that has three sections: a melting area, a liquation section and a superheater. In the melting area, the charge is melted at about 547°C; in the liquation section, some of the iron precipitates at 467–497°C as a sediment of ferrous zinc and lead, which is periodically removed. The dross accumulating on the surface of the melt is skimmed once a day and sent for recycling in kilns or muffle furnaces. Zinc with an iron content of less than 0.1 wt% is fed into the superheater at a temperature of about 597°C. From the superheater, the molten zinc is fed by a chute to a rectifying column (Figure 19.2) to one of the carborundum trays in the upper part of the column. The shaft of the column is lined with chamotte bricks and equipped with a gas supply duct and a waste gas flue. The shaft of the column consists of 20–24 W-shaped trays in the combustion section and 17–22 flat trays in the non-heated section.

Most of the zinc evaporates in the combustion chamber of the column at 1197–1297°C. The zinc vapor rises counter-currently to the metal melt flowing down from the top trays, gives up some heat to the melt and reaches the condenser, where condensation of the vapor and the formation of solid particles of zinc take place at temperatures of 247–397°C. The target is a highly active polydisperse powder.

Condensation occurs according to one of two patterns: vapor–liquid–crystal or vapor–crystal. The first pattern results in the formation of granules constituting the coarse fraction. The condensation in accordance with the second pattern proceeds in two condensers at a significant temperature difference between the incoming gas and the condensation surface. Tables 19.1 and 19.2 present the condensation conditions and the basic parameters of the process.

The temperature within the condenser volume varies depending on the distance from the wall: 67–87°C at a distance of 25 mm; 177–227°C at 1000 mm; 57–347°C at 1750 mm. The condensers are periodically cleaned by vibratory or mechanical methods.

After leaving the condenser, zinc powder undergoes separation by sieving. The +0.3 mm tailings are recycled.

The reflux part of the condensate amounting to up to 30% of the zinc charge, enriched in high-boiling components, passes from the lower trays of the column (see Figure 19.2) through a hydro-seal, to a recirculating tank.

An interaction of silicon carbide and iron in the reflux flow occurs at 1097–1297°C, according to the reaction (1):

$$\mathrm{Fe_{zn}} + n\mathrm{SiC} \leftrightarrow \mathrm{FeSi}_n + n\mathrm{C};\ \Delta G^0_{1500} = -16000\ \mathrm{J/mol} \quad (1)$$

The presence of iron in the zinc melt badly impairs the equipment; an increase of the iron content in the zinc from 0.04% to 0.06% reduces the service life of the column by 20%. Zinc is therefore subjected to liquation in order to reduce the iron content to 0.02% or lower. Besides iron, the zinc charge usually also contains lead, cadmium, copper and arsenic. The entire cadmium content passes to the zinc powder due to its lower boiling point. The lead content of the condensate, irrespective of its content in the zinc charge, can be reduced to a minimum under a certain temperature condition.

Copper does not interact with silicon carbide. Due to its accumulation in the recycled zinc, the formation of brass occurs that is prone to precipitate on the lower trays of the column thus hampering the process.

Aluminum present in the charge in the amount of 0.01–0.05 wt% and concentrating in the reflux is useful for refining the zinc.

Zinc from the precipitation tank is fed into the reverberatory furnace. In the case when zinc oxide is to be separated, the reflux is taken out of the main cycle and pro-cessed in liquation and retort furnaces.

A process comprising evaporation of the melt with simultaneous refining can also be used. It allows the

Table 19.1 Operating modes of rectification columns (I, II) and particle size distribution

Operating mode	Temperature (°C)			Composition of the gas phase in condensers (wt%)						Particle size distribution (%)					Change zinc capacity (t/day)
	In heating shaft	In column condensers		I			II			Fraction (mm)					
		I	II	CO	CH_4	H_2	CO	CH_4	H_2	+2.5	−2.5 +0.315	−0.315 +0.16	−0.16 +0.071	−0.071	
1	1257–1267	387	337	1.9	–	–	1.7	–	–	0.8	4.2	0.1	2.1	92.8	14.1
2	1267–1272	357	327	1.7	0.32	23.6	1.4	0.33	21.0	2.4	5.2	0.3	2.4	89.7	14.7
3	1257–1267	357	367	7.0	0.78	13.5	8.0	1.2	18.0	6.9	1.5	0.3	2.7	88.6	14.5
4	1217–1257	357	417	2.3	0.32	18.0	2.0	0.33	13.0	3.9	15.2	3.2	7.1	70.6	13.8

Note. Mode 1: characteristic of normal operation of the condensers; mode 2: forced cooling of condenser walls; mode 3: supply of ≈1 m^3/h carbon dioxide into condensers in counter flow to zinc vapor; mode 4: supply of water vapor into condenser (≈1 m^3/h).

Table 19.2 Typical characteristic of zinc powders produced by rectification of the melt

Mode	Fraction content,%				Particle size analysis of the fraction – 0.071 mm Content of particles of various size (μm), wt%						
	+0.16 mm		−0.16 mm								
	Zn total	Zn met	Zn total	Zn met	>15	10–15	8–10	6–8	4–6	2–4	<2
1	98.0	91.8	98.5	94.2	8.3	22.0	11.1	17.2	20.0	12.6	8.8
2	98.4	94.1	98.3	95.2	11.4	16.7	13.2	7.1	17.9	18.9	14.8
3	98.3	96.7	98.0	93.3	15.2	14.7	23.4	7.4	15.4	17.3	6.6
4	–	–	–	–	18.0	21.2	8.7	16.7	17.2	12.8	5.5

Note. See note to Table 19.1.

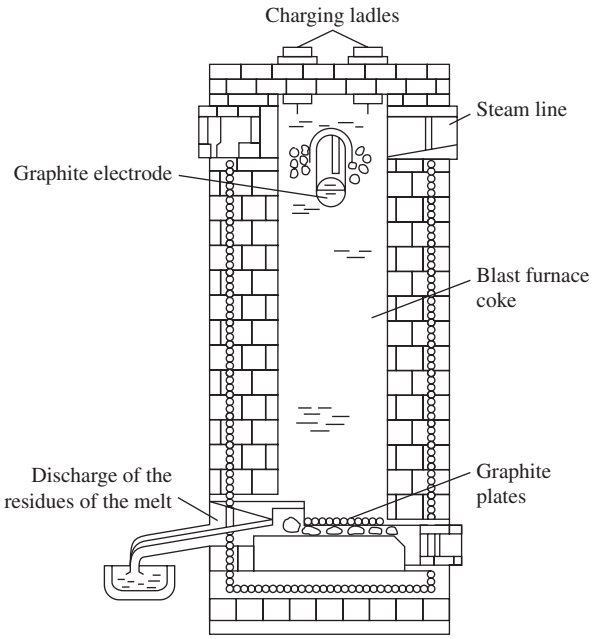

Figure 19.3 Electrothermal furnace for production of zinc powder.

content of high boiling point metallic impurities such as iron, copper, etc. to be reduced as much as 30 times. The installation yields up to 12 t a day. Lowering the process temperature, as well as using more pure source zinc also reduces the content of iron, copper, lead, tin, arsenic and other impurities.

A technique has been developed allowing the condensation of zinc vapor to be carried out in a single water-cooled condenser. The content of the fraction $<10\,\mu m$ in the powder increases up to 30–45 wt%. The tightness of the equipment accounts for a lower risk of autoignition of zinc vapor in the condenser; the conditions of column maintenance are improved.

The following advantages are features of the rectification method:

1. less pure, i.e. less expensive source zinc may be used, such as scrap
2. controllable powder properties
3. higher specific surface area of powder particles
4. powder particles of a regular spherical shape are produced.

Good technical performance and high economic indicators are features of the electrothermal process. The electrothermal furnace (Figure 19.3) of $520 \times 520\,mm^2$ in area is charged with blast-furnace coke sized between 380 and 20 mm. Graphite plates are connected to copper electrodes. The graphite electrode in the upper part of the furnace is sunk into the

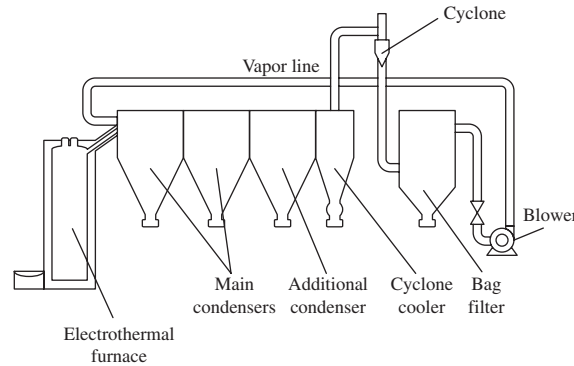

Figure 19.4 Electrothermal process flow-sheet.

coke to a depth of 900 mm at a distance of 2550 mm from the lower graphite plates. Liquid metal is fed by metering ladles into the upper part of the furnace. The remaining metal melt is tapped through the tap hole, while zinc vapor passes through a pipe connected with the condenser. The power rating of the transformer is of 360 kVA.

The condensation plant (Figure 19.4) consists of two main condensers with a surface area of $65\,m^2$ and one additional condenser of $37\,m^2$ surface area. The gas from the additional condenser is directed into a cyclone cooler and further on into the cyclone and a bag filter. The inert gas from the bag filter is recycled to the first condenser via the vapor line. The flow rate of the recirculating gas controls the particle size of the powder. The capacity of the blower is of $9.9\,m^3$/min, pressure 17.4 kPa. The capacity of the installation amounts to 2000 t/year, power consumption 1000 kWh per t zinc powder; the consumption of coke is 2 kg per t of powder.

Depending on the flow rate of the recirculating gas, the powder yield amounts to 29.6–32.4% from the first condenser, 30–36% from the second, 12.5–17.5% from the third one, 9–15% from the cyclone and 5–10% from the bag filter.

The electrothermal method does not ensure high purity of the zinc powder.

Inert Gas Condensation

A new method for producing fine zinc powder based on the inert gas condensation (IGC) process has been developed at the Institute of Metallurgy, Ural Branch of the Russian Academy of Science, and commercialized by the Fine Metal Powders Company in Yekaterinburg, Russia [2,3]. The 'Tuman'('Fog') installation of a modular type is the core of the process. The controlled process provides powders of a

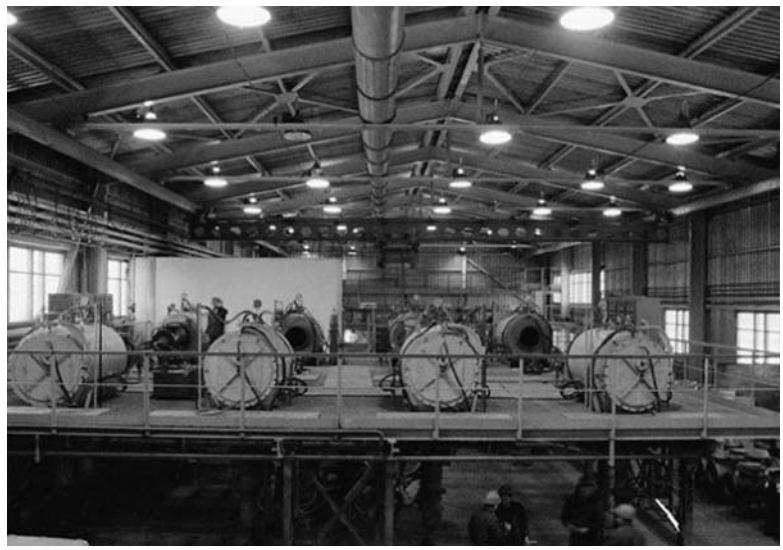

Figure 19.5 The 'Tuman' installations (The Fine Metal Powders Company's Advanced Technologies Plant).

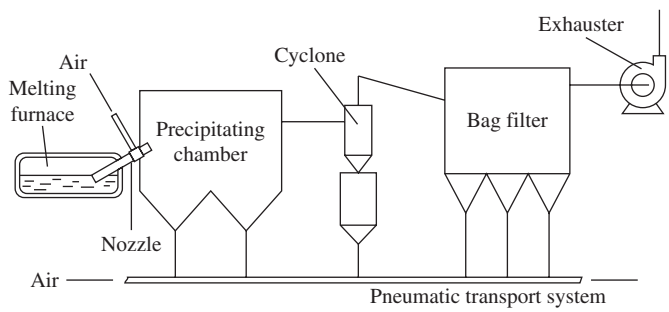

Figure 19.6 Flow-sheet for producing zinc powder by the atomization process.

targeted particle size at a high yield. The total plant capacity in terms of zinc powder is up to 1500 t/year (Figure 19.5).

The 'Tuman' unit operates on a 12-hour cycle. The power consumption of the evaporator totals 46.5 kW, the consumption of the inert gas (argon) amounts to 56 m^3 a month, the consumption of the cooling water is 3.5 m^3 per one modulus per hour. The zinc content is Zn = 99.98%; the trace impurities amount to: Pb = 76 ppm; Fe = 10 ppm; Cu = 6 ppm; Sn = 1 ppm and As = 2 ppm.

Melt Atomization

As shown in the Figure 19.6, zinc melt is fed to the spraying nozzle via a tube made of quartz glass, graphite or ceramic. The degree of rarefaction and the capacity of the unit depend on the diameter of the nozzle and its location in the ejector tube.

To obtain fine powder by gas atomization, different measures can be used, such as increasing the gas pressure and the gas flow rate; ultrasonic impact on the gas stream; heating the gas to 97–347°C prior to feeding it into the nozzle; instant cooling of the sprayed zinc by cold gas or liquid; nozzles of special design.

Figure 19.7 shows the dependence of particle size on the pressure of the atomizing agent (air). Higher pressure results in finer powders. Thus, at an air pressure of up to 20 MPa, the main part of the powder consists of particles <50 μm in size. The median mass diameter of this typical particle size distribution is 18 μm with geometric standard deviation of 2.1. The oxidation degree, being inversely proportional to the specific surface area of the powder, can also be used for the control of the particle size.

The dynamic vacuum method enables the content of <50 μm fraction in the powder to be increased by 20–80% as compared with the gas and ultrasonic

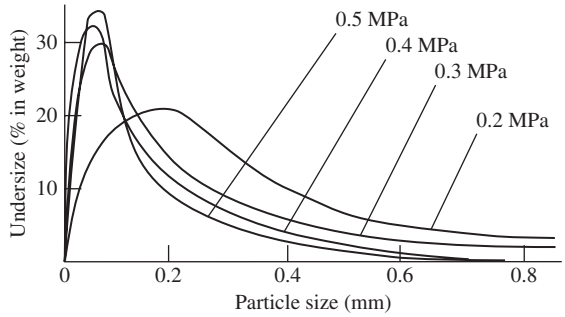

Figure 19.7 Relation between the air pressure (MPa) and particle size distribution of the powder.

atomization. The latter method comprises exposing the zinc melt to ultrasonic vibrations at a frequency of 22–44 kHz. The melt is atomized into small droplets, which solidify and drop into the receiving bin. Vacuum annealing is carried out for powder refining. To ensure the purity of the powder, all operations including separation, grinding, blending and packaging are carried out in a vacuum or in an inert gas medium.

As a rule, water atomization is not used for metals with a melting temperature below 500°C because of the forming extremely irregular particle shape due to extremely rapid solidification. Zinc is the lowest melting metal that is water atomized commercially. Thus, zinc powder for alkaline manganese batteries is produced by melt atomization under water pressure of about 5.5 MPa.The median mass particle size of this powder amounts 180 μm with geometric standard deviation about 2.34 [4].

Coarse powders with flake-shaped particles can be obtained by spraying the melt onto a rotating cooled surface. The superheated melt is fed through a nozzle onto a drum having a corrugated surface, the corrugation being made parallel to the axis of drum rotation.

Electrochemical Method

The electrochemical method allows the production of high-purity powders.

Cathodic precipitates of various types can be obtained:

- dense layers of flaky or crystalline particles; to obtain powder, these particles must be subjected to disintegration
- spongy soft precipitates easy for attrition
- loose precipitates of fine powder which do not require additional treatment.

Zinc sponge is produced from alkaline zincate electrolytes (18 g/L Zn, 250 g/L NaOH) obtained either by leaching oxidized zinc-containing source material with an alkaline solution or from recycling wastes of the manufacture of benzidine, hydrosulfate, etc.

The cathodes are conventionally made of nickel, stainless steel or magnesium. The electrolysis parameters are voltage of 3.5–4.0 V, current density of 2700 A/m^2, and temperature of 20–50°C. The spongy cathodic precipitate easily slides down the cathode. After washing, it is used as a reducing agent in chemical processes. Dry powder contains 99.3% Zn [1].

A process is known which uses an electrolyte consisting of sodium hydroxide and sodium zincate, Na_2ZnO_3 [5]. A zinc content of about 55 g/l yields a deposit of the suitable particle size. The current density is about 1076 A/m^2. Under these conditions, the deposit is a loosely adherent sponge that can be easily scraped or brushed off the cathode and processed to powder.

In the production of zinc powder from industrial wastes, the latter are leached in a 6-molar solution of sodium hydroxide at 57°C, bringing the zinc content of the solution to 30–40 g/l. Then the alkaline solution of the sodium zincate undergoes electrolysis at a temperature of 37–57°C and a current density of 2500–3000 A/m^2. The zinc sponge is removed by scraper blades. The precipitate is reduced to powder in an electrolyte medium, the disperser rotating at a speed of 1000–1500 rpm. The alkali residues are washed off the zinc powder.

The principal parameters of the electrochemical process are given in Table 19.3.

Other Methods

Extensive use is made of the method of obtaining fine zinc powder by mechanical grinding in various devices of ball, hammer, inertial, vibratory, jet type etc.

Air impact mills provide powders with the particle size in the range of 10–150 μm. The stability of the operation parameters and continuous recycled process are features of these plants.

Powders less than 1 μm in size can be produced by wet grinding in attritors in the presence of substances preventing autoignition of the powder such as nitrobenzene, salts of oleic or stearic acid. The addition of surfactants to the dispersing liquid will aid in reducing the particle size further.

Cryogenic methods enable fine and ultrafine powders to be produced. To obtain ultrafine powder, the powder is suspended in an aqueous medium and subsequently frozen under ultrasonic impact. The water is evaporated in a vacuum; the resulting product is a powder with particles size less than 1 μm.

Zinc powder can be produced as a by-product by treatment of zinc-containing wastes. The surface of

Table 19.3 Specification of electrolytic methods of manufacturing zinc powder

Process	Electrolyte composition (kg/m^3)	Current density (kA/m^2)	Temperature (°C)	Process characteristics
AS[a]	$ZnCl_2$ of 15–80; pH = 4.4–5.8	0.1–0.8	20–90	Graphite anode; electrolyte is periodically adjusted by concentrated solution of $ZnCl_2$
AS	$ZnCl_2$ of 20–40; NaCl of 300	0.54	–	Current efficiency of 95%; chlorides are easily washed out of the sponge
AS	Zn of 15–22; NH_4NO_3 of 10; HNO_3 to 63	0.2–0.3	20	...
AS	Zn of 10; NaOH of 200	1.1–1.5	30	Nickel anode, magnesium cathode; spongy deposit; powder yield of 90%
AS	Zn of 8–16; NaOH of 100–200	0.5–1.0	20–50	Current efficiency of 75–90%; deposit build-up time of 2–4 h; active zinc content of dry powder of 90–97%
AS	$ZnSO_4$ of 20–40; NaOH of 230	0.5–2.5	25–45	Powder apparent density of 0.32–0.45 g/cm^3; specific surface area of 0.35–0.58 m^2/g
AS	$ZnSO_4$ of 0.5–200; NaCl of 20	1.8–20.8	35–70	–
RSPh[b]	Na_2CO_3 of 159; ZnO	1.0	20	Raw material is ZnO; metallic zinc content of product of 90%; drying temperature of 333–338 K; particles are small, porous
AS	Zn of 40; NaOH of 220; oleate Na of 0.05; $CuSO_4$ of 0.5	3.0	60	Powder obtained in potentiostatic conditions (E = −2.04 V, normal hydrogen electrode) features elevated activity in the synthesis of rongalite
AS	$ZnSO_4$ of 60–65; NH_4Cl of 150; H_3BO_3 of 20; NH_3 of 20–25	0.3	17–20	Sedimentation of the powder at a potential of (−1.15– −1.2) V, normal hydrogen electrode; pH = 10
RSPh	Na_2CO_3 of 159; ZnO	1.0	20	Raw material is ZnO; metallic zinc content of product of 90%; drying after washing and stabilization at 60–65°C; particles are porous

[a]Water solution;
[b]reduction from solid phase

the zinc-containing melt is blown with an inert gas. Zinc vapor is condensed as a fine powder on the surface of a rotating water-cooled drum (a rotational speed of 0.5–10 rpm) located at a distance of 500–3000 mm from the surface of the melt. The average size of the resulting particles is <3 μm.

Zinc Powder Size Classification

There are a variety of classification techniques known that allow zinc powder of a targeted particle size distribution to be produced. Thus, for fine powders, a fluidized-bed air separation can be used. The starting powder is separated into three fractions: coarse (>20 μm) discharged through the baffle; fine (20–1 μm) carried out with the air to the cyclones; and the fraction <10 μm captured in a bag filter.

A combination of aero-gravitational and aero-centrifugal principles is employed in the installation for obtaining powder of targeted particle size (Figure 19.8).

A shelved aero-classifier measuring 300 × 300 mm in section contains 10 inclined shelves. Zinc powder is fed through a tangential inlet on the rotor (disk diameter is 400 mm) of a centrifugal aero-separator. The coarse fraction (>160 μm) is discharged at the bottom; the fine one (<10 μm) is captured in the bag filter. The system operates under a reduced pressure created by a ventilator at the outlet of the filter.

The process is controlled by the rate of the airflow and the rotational speed of the rotor.

The shelved aero-classifier ensures the extraction of the fractions under 160 μm up to 98.3% with a capacity of 1000 kg of source material per hour. The centrifugal separator segregates the powder incoming from the aero-classifier into two fractions with a 7–8 μm cut-off and extracts the fines containing 94.2–96.7% of the <10 μm fraction. A combination of various classification methods (screening + air separation) ensures the production of narrow powder fractions with targeted particle size limits.

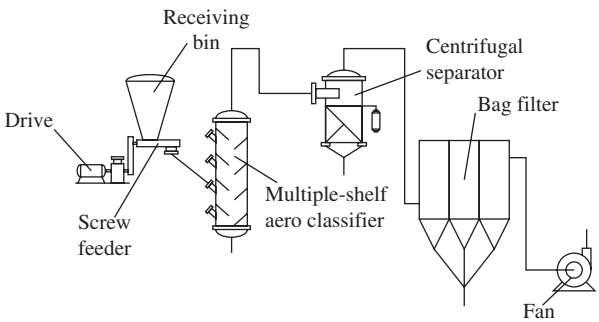

Figure 19.8 Flow-sheet of pilot-scale installation for aero-classification.

Properties of Zinc Powder

Zinc powders can differ essentially by particle size and shape as well as by basic physical and chemical properties depending on the manufacturing technique (Figure 19.9).

Water atomization of the melt provides low porosity particles of irregular shape. Gas atomization can result in elongated or spherical particles. Electrolysis provides high purity powders with particles of dendritic shape. Mechanical grinding can result in flaky particles. Chemical methods may provide particles of various shapes – spherical or irregular.

Safety Measures in Zinc Powder Production and Handling

High chemical activity of fine and, particularly ultrafine, zinc powders accounts for their flammability and explosiveness. Due to this fact, fire and explosion safety measures are necessary in zinc powder production and handling. For powder with particles <74 μm, the minimum spontaneous ignition temperature is 597°C and the minimum ignition

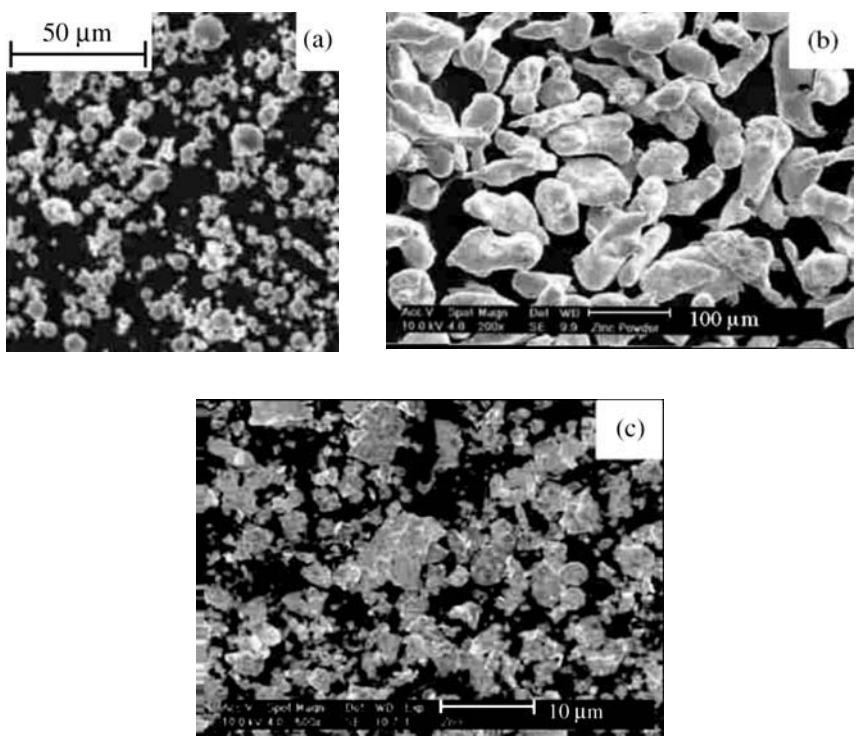

Figure 19.9 Zinc powder particle shape and size: (a) spherical particles of powder produced by IGC technique; (b) nodular particles of powders produced by gas atomization process; (c) flaky particles of centrifugal atomization.

energy is 640 mJ. The zinc sponge is removed by scraper blades. The lower explosive limit is 400 gm/m^3 (see Chapter 24). The spontaneous ignition temperature depends on the chloride content (>0.05%); moisture stimulates the spontaneous ignition process.

The presence of zinc oxide determines the degree of toxicity of zinc powder. Inhalation or swallowing zinc powder injures breathing organs and causes gastrointestinal disturbances.

The threshold limit value (TLS) in the air at the workplace (in terms of zinc oxide) adopted by Commonwealth of Independent States (CIS) is 0.5 mg/m^3 [6]. The TLS in drinking water (in terms of metal zinc) is 1.0 mg/L [7].

The operation area must be provided with fire fighting equipment and other protective means in accordance with the existing regulations.

Production of Cadmium Powders

All methods used for producing zinc powder are applicable to producing cadmium powder. Electrolytic deposition is the most common method (Table 19.4).

Table 19.4 Specification of electrolytic methods of manufacturing powders of cadmium and its alloys

Process	Electrolyte formulation (kg/$m^{3)}$	Current density (κA/m^2)	Temperature (°C)	Process characteristic
Cadmium				
EAS	$CdCl_2$; HCl	30–70	27	Sponge of fine two-dimensional dendrites; cadmium in the form of chloride
EAS	Cd of 0.11–11; H_2SO_4 of 50	0.05–0.2	27	Constant overvoltage of 80–150 mV; particle shapes – dendrites and needles with a length in the range of 70–300 μm
EAS	$CdCl_2$	3–0.75	25	Replacement of cementation by electrolysis reduced cost due to dust retention by a factor of 5
EAS	$CdSO_4$	5–15	25	Current efficiency of 86–93%; particle size of 50–80 μm; chemical cell capacity increases by of 20–30%, and their service life by a factor of 1.5–1.6
EAS	Cd_{start} of 100; CD_{end} of 20; H_2SO_4 of 10	0.6	25–28	Zinc present in the solution to 30–40 kg/m^3 is admissible; current efficiency of 93–96%; deposit building up time of 24 h.
ENAS	Dimethylformamide-solvent; NH_4BF_4 of 210; Cd $(BF_4)_2$ of 28.6–114.4	4	25	Constant overvoltage of 0.1–0.25 V; rotating electrode; deposit is washed off; at a rotational speed of 20–270 s^{-1} and operating time of 60 min; average particle size is of 6–29 μm
RSPh	CdO in form of tablets, NaOH of 40	3–4	25	Raw material is CdO, nickel anode; drying for 90 min at 323 K; current efficiency of 96%; particles: dendrite, polydisperse, porous
Cadmium–Zinc alloy				
AS	$CdSO_4$ of 8.4–37.5; $ZnSO_4$ of 2.4–48.3	1–15	20	Current efficiency of 90–96%; powder composition depends on deposit build-up time and concentration of cadmium in the solution
Cadmium–Iron alloy				
AS	Cd + Fe of 10; (NH_4) $2SO_4$ of 50; pH 2.7	35	20	Independent regulation of anodic currents of cadmium and iron; current efficiency of 65–67%; average particle size of 5 μm
Cadmium–Nickel alloy				
AS	$(CdSO_4 + NiSO_4)$ 0.2 mol/l; NH_4Cl of 5.4	3	20	Current efficiency of 65%; average particle size of 2 μm; phase composition – mechanical mixture of cadmium and nickel: (Cd/Ni) powder = (Cd/Ni) solution

EAS is electrolysis of aqueous solution; ENAS is electrolysis of non-aqueous solution; RSPh is reduction from solid phase; AS is aqueous solution.

Cadmium powder can be obtained by cementation from a solution of copper-cadmium cake in waste electrolyte and the removal of copper from it. The composition of the solution is (kg/m^3): Cd 6–12; Ni 0.01–0.04; Fe 0.02–0.06; Cu (0.2–0.3)$\times 10^{-3}$; Co 0.08–0.12.

Deposition is carried out in centrifugal reactor-separators using zinc dust. Thallium present in the solution is precipitated together with cadmium but, after the bulk of the zinc dust is utilized, thallium goes back into the solution. The cementation of cadmium is finished when the concentration of thallium in the solution gets close to the initial level. Ions of silver and indium promote the cementation of cadmium. The duration of the operation is 35–40 min. The precipitate contains up to 95–99% Cd. Power consumption is 1–2 kWh per solution volume of 1 m^3.

Cadmium powder with high electrochemical activity consisting of structurally uniform dendrite particles can be obtained from aqueous solutions on a horizontal cathode at varying current density. The composition of the electrolyte is (kg/m^3): Cd 5.6–20.2; acetic acid 90; potassium acetate 100–150; diethylene-triamine-penta-acetic acid 7.8–28 or diamine-cyclohexane-tetra-acetic acid 8.6–31. The current density rises with the duration of the process from a minimum value (i_0 = 1.0–1.5 kA/m^2) to a maximum of i_τ = 3.0 kA/m^2 following the parabolic law:

$$i = i_0 + (i_\tau - i_0) \cdot (t/\tau)^2 \qquad (2)$$

where τ stands for the current rise cycle.

The duration of growth of the disperse layer approaches 0.3–0.5 h. The powder is washed with a 5% solution of acetic or sulfuric acid, de-ionized water or acetone and dried in a vacuum. The cadmium anode without filler has a porosity of 60–70% and ensures a discharge current efficiency of 90%.

Production of Cadmium and Zinc Alloy Powders

Zinc- or cadmium-based alloys are conventionally produced by the electrochemical method (see Table 19.3) or by atomization (Table 19.5).

For producing an alloy with an atomic fraction of zinc of up to 40%, solutions of zinc and cadmium sulfate are used. Powders of targeted composition have been obtained by varying the composition of the solution and the current densities (Table 19.6). Alloys are precipitated at galvanostatic conditions.

The alloy powder presents a conglomerate of particles of dendrite shape with their longitudinal dimension approaching twice the cross-sectional dimension. An increase in the current density from 1000 to 15 000 A/m^2 leads to a reduction in particle size by a factor of 1.5–2 (from 250 $\times$ 140 μm to 150 $\times$ 75 μm). A change in the composition of the solution does not affect the particle size significantly.

Zinc–copper alloy powders can be produced by electrolytic deposition from cyanide as well as from pyrophosfate, ammoniate, tartrate, citrate and other solutions. For some alloys (Zn–Fe, Zn–Sn), there exists a nearly direct relation between the concentration of the metal in the solution and the ratio of the atomic fractions of the corresponding metals in the alloy. The composition of the alloy also depends on the current density, the temperature of the electrolyte and the intensity of agitation.

Spherically shaped powders of zinc, cadmium and their alloys can be produced by atomization of the melt that contains additives of alkali metals: Li, Na $\geq$ 0.001% or K, Ce, Rb $\geq$ 0.01%. Atomization of a zinc melt containing 0.4% Na (the temperature of the melt is 497°C, air temperature is 47°C, pressure is 0.3 MPa) provides a powder with up to 80% particles of spherical shape in the size range 150–480 μm. The apparent density of the powder is 4.2 g/cm^3. Without the addition of sodium, particles obtained under the same conditions have an irregular shape, the metallic luster is less marked and the apparent density is 3.2 g/cm^3.

A technique is known for producing zinc alloy powders by adding 5–80% iron and 0.2–5% aluminum or copper to the molten zinc. The melt is cooled and ground. The powder has elevated corrosion resistance and is hardly oxidized owing to the protective cathodic action of iron. It is used as filler in resins.

Applications

There are two basic sectors of application of zinc powders:

- protective coatings, including zinc-rich primers and paints; powder coating; sherardizing
- chemical processes: purification of zinc solutions before electrolysis at electrolytic zinc plants; manufacture of reducing agents (sodium and zinc hydrosulfites) for the paper and textile industries; in the mining industry (for the extraction of gold, silver and other precious metals); manufacture of alkaline batteries.

For manufacturing alkaline batteries and for other chemical applications, high-purity zinc powder is needed, which is produced using extra pure special high grade (SHG) zinc.

Table 19.5 Typical characteristics of zinc powder produced by ultrasonic atomization of the melt

Medium	Pressure (MPa)	Fraction yield (%)								Metal consumption (kg/min)	Proportion of oxygen in fraction <63 μm (wt%)	Apparent density, g/cm^3
		Particle size (μm)										
		+120	–120 + 80	+100	−100 + 50	−80 + 63	63 − 40	−50	−40			
Argon	–	10.6	20.3	–	–	10.4	51.1	–	7.6	–	0.02	–
Air	–	25.5	29.1	–	–	13.8	27.9	–	3.7	–	0.14	–
Vacuum	0.1	–	–	69.5	18.5	–	–	12	–	10.2	–	3.6
Vacuum	0.2		–	7.0	8.0	–	–	85	–	35.0	–	3.9

Table 19.6 Effect of electrolyte composition on powder composition and cathode potential (current density of 15 kA/m²)

Content in solution (g . ion/l)		Atomic fraction of Zn in powder (%)		Cathode potential (V)
Cd^{2+}	Zn^{2+}	Actual	Estimated	
0.18	0.15	6.9	6.5	−0.77
0.18	0.075	6.5	7.5	−0.78
0.18	0.03	5.6	6.2	−0.80
0.09	0.15	14.5	15.0	−0.78
0.07	0.15	20.6	22.3	−0.79
0.045	0.15	29.5	28.6	−0.81

Zinc Powders in Protective Zinc-Rich Coatings

Zinc-rich coatings combine the advantages of metallic (cathodic protection) and paint (barrier, hydroinsulating effect) coatings that make them perfectly suitable for 'cold' galvanizing of metals.

The most important applications of zinc-rich primers and paints are coatings exposed to severe corrosion-hazardous conditions: offshore oil fields, petroleum industry, power engineering, sea container production, ship building and repair. These materials are also widely used for protecting metal structures in the construction of buildings, bridges, etc.

Zinc-containing protective materials are divided into zinc primers containing 25–75% zinc and zinc-rich primers (85–92% Zn). They are also distinguished by the type of the binding agent: (a) organic compounds (e.g. systems based on epoxy ethers and epoxy polyamides or moisture curing systems based on polyurethane, vinyl and vinyl chloride rubbers); and (b) inorganic compounds on the base of ethyl silicates and alkaline silicates. Inorganic compounds display higher density and a greater abrasion resistance, but require a more careful pretreatment of the surface and perform lower flexural strength than organic zinc-rich compounds [8].

Zinc powders used as pigments in anticorrosive coatings should meet certain requirements. Thus, the metal zinc content in such powders should not be lower than 95% with a minimum of zinc oxide present. Limits are set on the content of lead (<0.15%) and iron (<0.004%); no moisture is admissible. Lead impairs the quality of the coating and threatens the labor safety conditions while welding. Elevated iron content of the powder reduces the protective potential of the primer, while moisture causes caking of the stored powder and creates a risk of emission of hydrogen prone to destroy the protective effect of the coating [9,10].

Zinc powders conventionally used in zinc-rich protective coatings have their particle size in the range of 3–12 μm (Table 19.7). The particle size of powders influences the density of particle packing. The maximum packing density of about 61% of the solids content (by volume) is peculiar to powders with an average particle size of 6 μm.

In recent years, powders with flaky particles (see Figure 19.9c), 0.2–0.4 μm thick and 20–30 μm long, have been used in primers and paints. When flaky powders are used, reliable corrosion protection is achieved at a powder content of 80% of the dry coating that reduces the consumption of zinc and increases the covering capacity and the elasticity of the coating.

Anticorrosive Zinc-Rich Coatings for Roll and Sheet Steel and Metal Ware

Protective coatings for roll and sheet steel based on pure fine zinc powder have been developed by Diamond Shamrock Corporation (now Metal Coatings International Inc, USA). These are DACROMET®, ZINCROMET®, ZINCROPLEX® and ZINCROMETAL®, widely used in the automotive industry.

DACROMET® is an inorganic coating composed of zinc and aluminum flake in a binding matrix of chromium oxides. Zinc and aluminum platelets align in multiple layers forming a metallic silver gray coating. Applied as a liquid material, the coating becomes totally inorganic after curing at 610°F/321°C. The corrosion resistance performances of DACROMET® are particularly high at a low thickness (from 5 to 10 μm). DACROMET® can serve as a base for most paints, including electrodeposited paint.

DACROMET® 320 is a non-electrolytic water-soluble thin-film coating for the corrosion protection of articles made from steel, cast iron or other metals. The coating contains zinc and aluminum flake in a chromium binder. The coating is metallic silver in appearance. The aqueous dispersion is applied by cold immersion or spray and is therefore free of any risk of causing hydrogen embrittlement. The coating

Table 19.7 Specification of zinc powders for protective coatings

Characteristics	ASTM Standard for Zinc Dust Type III (for use in zinc rich coatings)	Manufacturer, grade, manufacturing technique			
		Umicore, Belgium. Zinc Dust Grade 4P16, (Distillation)[1]	Trident Alloy, UK. Delaville Standard CP75 Zinc dust (Electrothermal Furnace technology)[2]	U.S.Zinc, USA Grade. USZ # 1 XL (Distillation)[3]	Fine Metal Powders Company, Russian Federation. Zinc powder Grade PZHD-1 (IGC technique)
Total zinc, calculated as Zn, min.%	99.0	99.0	98.0	98.5	99.0
Metallic zinc, min.%	96.0	96.5	95.0	95	96.0
Lead, calculated as Pb, max.%	0.002 (20 ppm)	0.003	0.1	0.01	0.013
Cadmium, calculated as Cd, max.%	0.001 (10 ppm)	0.0005	0.005	0.01	0.004
Iron, calculated as Fe, max.%	0.002	0.002	0.003	0.02	0.003
Medium particle size, μm	–	3.4–3.9	–	5–8	4–12
Coarse particles μm max.%					
+150	0.1	0.00	0.01	Trace	0.00
+75	0.8	0.00	0.3	0.1	0.8
+45	3.0	0.7	5.0	4.0	3.0
Specific weight, g/cm^3	–	–	7.1	7.1	7.1

Source: [1]http://www.jamesmbrown.co.uk/zincdust/zincdust.htm; [2]http://www.tridentalloys.com/Pigments/; [3]http://www.uszinc.com/ZincDust/ProductSpecs/XL_

thus produced is passivated throughout the film and provides high performance corrosion protection.

The corrosion resistance of DACROMET® 320 depends upon the thickness of the coating and is due to a combination of several mechanisms:

- a barrier effect due to the tile-like structure of the film
- controlled sacrificial protection of the zinc in relation to the metal substrate
- a film passivation, which reduces the consumption rate of zinc and aluminum.

Two DACROMET® coating types are commonly used to meet the automobile industry's requirements:

Grade A: coating weight >24 g/m², average thickness of 5–7 μm

Grade B: coating weight >36 g/m², average thickness 8–10 μm.

Coatings of greater thickness may be applied to increase the duration of the corrosion protection.

Several application techniques are used industrially, among them immersion, pneumatic or electrostatic spray.

Sherardizing (Thermo-Diffusion Galvanizing)

Sherardizing is a very reliable and versatile method of coating steel surfaces and therefore giving high protection against corrosion and abrasion. The metal articles are heated in the presence of zinc powder (dust). The process is normally carried out in a slowly rotating closed container at temperatures ranging from 320 to 500°C (Figure 19.10). Several after-treatments may be applied (chrome passivation, lubrication etc.).

A sherardized coating forms two layers of zinc–iron alloy: a diffused gamma layer containing 21–28% of iron and a compact delta layer containing 8–10% of iron. The thickness of the coating may be 10–110 μm.

The main benefits of the sherardized coating are: the thickness of the coating remains regular and uniform, even on irregular or complex shaped and recessed components; high adhesion due to the zinc–iron alloy diffusion; no hydrogen embrittlement; versatility; easy operation; environmental friendliness.

Figure 19.10 An installation for thermo-diffusion galvanizing (sherardizing): general view while container is being charged.

Usage: anti-corrosion treatment of metal articles (nails, bolts, screws, cast iron articles, metal pegs, medium-sized metal objects of irregular form, etc).

An important feature of thermo-diffusion galvanizing is that it does not impair mechanic properties of heavy-duty fixing parts (bolts and nuts), namely in bridge construction.

Mechanical Plating

Steel articles are placed in a drum with a mixture of a zinc powder, an activating solution and glass beads. The drum is then tumbled and the beads impact zinc onto the surface of the steel. The thickness of the resulting zinc coating is 10–12 μm. Also, cadmium powders and mixtures of Zn and Cd powders may be used.

References

1. *Handbook of Powders of Non-Ferrous Metals*. Metallurgia Publishers, Moscow, 1997, pp. 431-458 (in Russian).
2. Frishberg, I.V., Yurkina, L.P., Subbotina, O.Yu. et al., Experience in development and commercial implementation of new zinc-rich coatings for protection of steel against corrosion. In *Proceedings of the EuroPM 98 International Conference*, European Powder Metallurgy Association, 1998, Vol. 4, pp. 825–826.
3. Frishberg, I.V., Subbotina, O.Yu., Pavlyukova, O.N. et al., New Russian zinc-rich materials. *Promyshlennaya Okraska*, 2003, 1:8–15 (in Russian).
4. Dunkley, J.J., Atomisation of metal powders in powder metallurgy. *Institute of Metals*, 1991:2–21.
5. Taubenblat, P.W., Chemical and electrolytic methods of powder production, In *ASM Handbook*, Vol. 7, *Powder Metal Technologies and Applications*. ASM International Publishers, 1998. pp. 67–71.
6. Occupational Safety Standards System. General sanitary requirements for working zone air. *GOST* 12.1.005–88 (in Russian).
7. Sanitary regulations and Standards of surface waters from pollution. *SanPaN* 4630–88 (in Russian).
8. Zinc-rich paints for corrosion protection. *PCE*, 1997, 2(11):26–33.
9. Karakasch N., Zinc coating review – 2000 and beyond. *Corrosion Management*, 2001, No. 5.
10. High-quality coatings for steel bridges. *Tikkurilla Coatings*, 1999, 1:12–15.

Chapter 20

Production of Noble Metal Powders

Stanislav S. Naboychenko, Irina B. Murashova, Ural State Technical University (UPI), Yekaterinburg, Russia
Oleg D. Neikov, Frantsevich Institute for Problems of Materials Science (IPMS), Kiev, Ukraine

Properties of noble metals including silver, gold and platinum-group metals are listed in Table 20.1.

Chemical precipitation, thermolysis, electrolysis, hydrogen reduction and melt atomization are often used for the production of powders of these metals. Basic materials are solutions, salt pulps and hydroxides; in the latter case, solid phase properties significantly influence the properties of the powder produced complicating the reproducibility of a number of its characteristics (particle size, bulk mass, surface).

Among organic reagents let us note formaldehydes, alcohols, oxalic and formic acids and their salts and glycerin, and among non-organic ones hydrazine and its derivatives, borates of alkali and alkaline-earth metals, hypophosphites, Ti (III), Cr (III), V (III) salts are used most often. Organic reducers are safe, available and allow the process to be carried out at low temperatures. The produced powders have a developed surface, they are dispersed (1.0–10 μm), but gas-saturated and require a special finishing procedure. Formic acid and its salts, sodium formate in particular, are used most often. This is an available, non-toxic and easily soluble reagent. The precipitation factors depend on temperature, pH value, reagent consumption, but there is a problem of washing the powder free from sodium ions resulting in a high water consumption (up to 160–200 L per 1 kg of niello). Particle size of the produced residue is between 0.05 and 0.5 μm.

Reney's method is based on producing the alloy followed by selective leaching of the less noble component by acid or alkali solutions. The produced niello of metals or their alloys have large specific surface (80–100 m^2/g), but they are pyrophoric and the residues of the leached metal contaminate them, so they need to be passivated.

Thermolysis means the thermal decomposition of metal salts (nitrates, halides, ammoniates, carbonates, formates), which form volatile products on heating. The powders produced are distinguished by a non-uniform granulometric composition, small specific surface and contamination by thermolysis products.

Electrochemical methods (extraction from solutions, processing of salt pulp and hydroxides, electrolysis of wastes and recycled raw materials) are widely used in the production of noble metal powders.

Table 20.1 Basic properties of noble metals

Characteristic	Metals							
	Ag	Au	Ru	Rh	Pd	Os	Ir	Pt
Serial number	47	79	44	45	46	76	77	78
Atomic mass, g/mole	107.9	197	101.1	102.9	106.4	190.2	192.2	195.1
Relevant oxidation rates			3, 4, 6–8	3	2	4,6–8	3–4	2,4
Density, g/cm^3	10.49	19.32	12.45	12.41	12.02	22.61	22.65	21.45
Temperature °C:								
of melting	961	1064	2583	1966	1825	3033	2466	1768
of boiling	2212	2807	4150	3727	4253	5012	4428	3825
Specific heat capacity J/(°C mole)	25.4	25.4	24.0	26.0	26.0	24.8	25.1	25.9
Thermal conductivity (W/(°C m), at 25°C	433	318	117	152	75.2	87.6	147	71.6
Specific electrical resistivity, (nΩ · m), at 20°C	16.1	22.1	71	43.3	105.1	81.2	47.1	105

Powder properties depend on the electrolyte content, the current density, the hydrodynamic medium and the cathode shape.

A solid-phase reduction of salts and oxides of noble metals by hydrogen at 227–427°C is possible; however, the powders produced (especially palladium powders) have a tendency to hydrogen pickup and contain up to 0.1% of adsorbed hydrogen. Indices of hydrogen reduction (purity and physical properties of powder) are significantly improved when the hydrothermal method is used.

The hydrothermal method is the precipitation of metals from liquid (organic) media at an elevated temperature (107–177°C).

Basic methods of production are solid-phase reduction, chemical precipitation from solutions or pulp, electrolytic precipitation and electrolysis.

Production of Silver Powders

Chemical Processes

Most silver salts are easily reduced from solution, the only limitation being their solubility. The most common compounds are silver nitrate and silver oxide. Organic reducing agents such as alcohol, sugar or aldehydes are used to manufacture silver powder from silver oxide. For example, dextrose can be used to produce a very fine silver powder:

$$2AgNO_3 + 2NaOH \rightarrow Ag_2O_{(s)} + 2NaNO_3 + H_2O \quad (1)$$

$$12Ag_2O + C_6H_{12}O_6 \rightarrow 24Ag_{(s)} + 6CO_2 + 6H_2O \quad (2)$$

Organically precipitated silver powders have particle sizes ranging from 5 to less than 0.1 μm. However, these silver powders tend to agglomerate into aggregates 10 μm in size or larger. To avoid agglomeration, the powder can be precipitated in presence of a surfactant or de-agglomerated after the precipitation using a mechanical technique.

Silver powders are produced by mixing of an acidified solution with a solution of tin (II) salts in the presence of anion type surfactants, controlled pH values and temperature.

Silver powder with particles of a spherical shape is produced by atomization of silver nitrate solution and its pyrolysis.

To produce submicron particles of silver and palladium, their concentrated nitrate solutions are used, aerosol forming and drop separation by size are provided, and then drying and conversion of aerosol particles to the metallic condition are performed in a reducing atmosphere at elevated temperature.

Particles 7–10 μm in size are produced by evaporation of silver at 997°C with subsequent condensation in a nitrogen atmosphere.

Ceramic contacts of high wear resistance are produced from silver-based compositions (Ag-oxides of cadmium, copper, zinc, tin, lead, Ag–Ni), from nitric acid solutions of appropriate composition; the metals are jointly precipitated in the form of hydrates and carbonates. Powder mixtures with a particle size of 0.1–0.4 μm are produced after separation of precipitates, their washing, drying and calcination at 397–497°C. To provide a high yield, an agglomeration is carried out; the size of produced particles is 200–400 μm. Removal of cadmium oxide proceeds during sintering of products containing cadmium oxide at $T > 697$°C; a contact film of silver, which excludes oxidation, is formed in the surface layer.

A composition for the products that retain their electrical conductivity and wear resistance at low temperatures (for example, electrical contacts) and in a vacuum is produced by mechanical stirring of dispersed silver powders with additives of 2–49% of rhenium or molybdenum disulfide in water or alcohol.

Silver powder is produced by processing of a solution of silver nitrate (0.05 M) and 1-hydroxy-4-methylaminophenyl sulfate in the ratio of $[(C_7H_9ON)] \cdot H_2SO_4/AgNO_3 = 1.05$. The precipitate is washed by 3% solution of sodium nitrite, by hot water (57–67°C) and dried at 100 ± 5°C; the powder contains not less than 98.7% of Ag. Particle shape is regular polyhedrons 0.5–20 μm in size or ovals 0.3–4.5 μm in size. The powder surface is 0.19–0.21 m^2/g, the apparent density is 2.4 g/cm^3. The powder is used for film covering production (70% of Ag) with specific electric resistance not higher than $1.2 \times 10^{-7}\,\Omega \cdot m$.

Silver powder is produced also by processing hydroxide pulp with a solution of sodium formate; the precipitate is washed by water and dried. Powder properties (specific surface, S, apparent density, ρ, median mass diameter, d_m) significantly depend on the reduction conditions:

	S (m^2/g)	ρ (g/cm^3)	d_m (μm)
Production conditions:			
without surfactants	4.9	0.98	Aggregates
with surfactants	0.45–1.25	1.6–2.6	0.5–2.5
$L:S = 10$ (relation of liquid to solid)	1.3	...	10
$L:S = 1$	0.8	2.9	17

The consumption of reducing agent is 1.1–2.4% of the precipitated powder mass with a content of 99.9% of Ag.

It is possible to produce silver powder by a self-propagating low temperature reaction of precipitated silver chloride with zinc. In this process, powder of

silver or 'silver−zinc' alloy of Ag_nZn_m type is produced by means of chemical reactions considered as a kind of contact displacement:

$$2AgCl + H_20 \leftrightarrow Ag_2O + 2HCl \quad (3)$$

$$2AgCl + Zn \rightarrow 2Ag + ZnCl_2 \quad (4)$$

$$\Delta G = -150\,kJ/mole$$

Zinc consumption is stoichiometric; the duration of process is of 15–20 min, the transformation level is close to 100%. Powder surface area is $0.8\,m^2/g$, particle size is 1–2 μm, their shape is round.

Atomization

Silver powder is produced by atomization of a molten silver stream with gas or liquid. Average particle sizes generally are within the range 10–50 μm. The gas-atomized powder generally approaches a spherical shape, with a smooth surface, minimal porosity and a high powder density [1].

Spray pyrolysis technique for manufacture of silver powders is also used. This process involves the spraying of a silver nitrate solution into a flame formed by a coaxial burner. Control of the flame temperature and the spray conditions allow for the control of particle size and shape [2].

Spray pyrolysis produces solid, spherical, dense silver powders. An aerosol of silver nitrate solution is heated to temperatures as low as 600°C in nitrogen to decompose the silver salt and to produce a fully dense silver powder. Particle size of the powder is 5 μm and smaller.

Mechanical Comminution Processes

Mechanical milling is used to change the properties of silver powders including disintegration of particle aggregates, particle shape and particle surface characteristics. This process can be used for most types of silver powders with techniques such as ball milling, vibratory milling or attrition milling.

A feature of these processes is that they are time-consuming and require special precautions to prevent contamination from the mill and milling medium. Various types of milling media can be used including zirconia balls (ZrO_2), metallic balls and glass balls. Continued milling produces two-dimensional silver flake. The sizes of milling media vary between 10 and less than 1 mm depending on the sizes of initial powder and the size of the resulting silver flake required. Generally, an organic surfactant is introduced during the milling process to prevent the agglomeration of particles with each other while grinding and to control size and shape of the silver flake.

Production of Silver Powder from Solution by Electrolysis

The basic raw material is Dore's alloy that contains: 87–95% of Ag; 2–14% of platinoids and gold; 1–4% of Cu; 0.06–0.01% of Ni; 0.005–0.01% of As; 0.01–0.05% of Sb; 0.1–0.2% of Fe; 0.001–0.005% of Pb; 0.002–0.01% of Se; 0.005–0.1% of Te; silver-containing materials (80–84% of Ag; 16–20% of Cu). In accordance with State Standard 28595-90, silver of three brands (CpA-1 CpA-2 and CpA-3) is used in the cells with soluble anodes (respectively 99.99, 99.98 and 99.9% of Ag).

Silver is precipitated on the cathode as a loose needle-like deposit that is easily stripped from the cathode. The current efficiency in the nitrate solution is approximately 100%. The cause of electric loss is short circuits of silver dendrites and simultaneous reduction of NO_3^- anions to HNO_2, NO_2^-, NO_2 (gas) or NO (gas).

The respective O/R potentials are 0.94; 1.01; 0.77 and 0.95 V (nhe). Therefore the concentration of the free acid is decreased.

Fine silver powder is precipitated at the silver anode due to $Ag_2^+ = Ag + Ag^+$ reaction. Practically all impurities except gold and platinoids pass into solution. Part of the palladium can pass into solution from platinoids. Selenium and tellurium should be eliminated from the anode material during fire refining.

The powder is produced in cells with vertical or horizontal cathodes (Table 20.2) as well as on a rotating cylindrical cathode. Vertical cathodes in cells are sheets of silver, the purest aluminum, or stainless steel. The inter-cathode space is 16–20 cm. The anodes are put into a diaphragm-box with stretched bags of polyvinyl chloride (PVC) to collect the anode sludge. The ends of the cathode rods are pushed into slots welded to a bus. Vertical plates that perform reciprocal movements are installed for deposit removal. The silver deposit is stripped into a box with a filter bottom. A telfer for lifting the frame and the box with the silver powder is installed above the cells. The powder is removed from the cylindrical rotating cathode by knives and a bottom knife transfers the deposit to the sloping conveyor.

Cells with horizontal location of electrodes are manufactured from plastic or ceramics and lined with acid-proof tiles. A graphite dalle (cathode) is embedded into the cell bottom. Half of the cell bottom length is splayed to provide powder deposit discharge. An anode box with the bottom made of fire bars, on which a filtration nylon material, plastic grid and some layers of anode plates are placed, is installed above the horizontal part of the cell. The current is supplied by heavy contacting leads, to which the ends of a flexible cable are soldered. Anodic contacts are manufactured of 50% Ag + 50% Au alloy, cathodic contacts are fabricated from silver.

Table 20.2 Electrolysis conditions and process parameters

Parameters	Cell with vertical electrodes	Cell with horizontal electrodes
Electrolyte concentration (kg/m^3):		
Silver	10–20	40–50
nitric acid	10–15	15–25
Cathodic current density (A/m^2)	1500	400–500
Temperature (°C)	40–70	40–50
Deposit growth time (minutes)	2–10	1440
Cell voltage (V)	2–2.8	3.2–3.8
Current efficiency (%)	95–97	87–90

Once a day the deposit is discharged by knives on the filtration frame that is brought to the cell by a car. The deposit is washed by hot water acidified by nitric acid ($1\,kg/m^3$). Cleaning of the solution includes the elimination of lead and copper. Lead is precipitated by sulfuric acid. To eliminate copper, at first silver cementation from the solution is performed by copper plates, then the deposit is removed, copper cathodes and insoluble magnetite anodes are put into the cell; copper concentration is decreased to $10\,kg/m^3$ during electrolysis. The anodic sludge after refining Dore's alloy contains 30–70% of silver and much gold. Silver from the sludge is transferred to the solution and the solid residue is directed to electrolytic refining of gold.

It is possible to produce silver powder in the cells with insoluble anodes. Titanium sheets are covered by a thin platinum layer. Anode current density is twice as high in comparison with the cathode. The nitric acid concentration increases during electrolysis whereas silver ion concentration decreases. Periodically a part of the electrolyte is vented away for regeneration and removal of platinum metals and gold.

Silver powder produced by electrolysis meets the following requirements: >99.9% of Ag, maximum 0.02% of Cu; 0.04% of the sum (Fe, Pb, Al, Bi), 0.001% of NO_3^-, 0.005% of SO_4^{2-}, 0.08% of moisture (over 100%); particle size for PS1 brand: 97% of the size fraction of (−56) μm, for PS2 brand: 96% of the size fraction of (−160)μm.

Production of Silver Powder by Chemical Reduction with Electrochemical Regeneration of the Reducer

Fine silver powder is produced in the anodic space of the electrolyzer close to the surface of soluble silver anodes by chemical reduction with titanium (III) ions:

$$Ag^+ + Ti(III) = Ag + Ti(IV) \qquad (5)$$

The composition of the solution is 10% of $Ti_2(SO_4)_3$ and 10–15% of H_2SO_4. The electrolysis is carried out at 25°C providing cathode and anode current densities of 50–100 and $250\,A/m^2$, respectively. The finest powder formed with particle size of 1 μm is precipitated on the bottom of the electrodes. The solution of titanium sulfate goes to the cathodic space where titanium (IV) ions are reduced to Ti (III) ions. The powder is washed on a filter by 5% solution of sulfuric acid to eliminate titanium and then by water to eliminate sulfate ions. The water residue is eliminated by alcohol or acetone washing. Final drying of powder is performed under a vacuum at 42–52°C.

The several ways of production of electrolytic silver and silver-alloy powders are shown in Table 20.3.

Production of Fibrous Dendritic Silver Residue from Molten Electrolytes

Electrolysis is carried out using a silver nitrate melt based on the potassium–sodium eutectic (15–33 wt% of silver) at a temperature of 250–290°C in an open cell without additional stirring [6]. A flat anode in the form of a silver bar with insulated silver current supply is placed on the cell bottom. The cathode is a silver wire ($d = 1.5$ mm) clamped at the top between rolls of the lifting device. Prior to turning on the main current, a current of 0.1–0.2 A is applied for 1–2 minutes to provide stronger adherence of the fibrous deposit to the cathode. Without current interruption, the fibrous deposit is precipitated on the sublayer simultaneously providing cathode lifting (v) and current (i_a) regulation to the required level (in the range of 0.5–10 A). The speed of cathode lifting (from 0.25 to 12 cm/min) is controlled with the help of a gearbox and by changing the voltage applied to the motor from the electric power supply. Electrolysis conditions have to provide a part of the electrode of a constant length to be submersed into the electrolyte. After electrolysis, a tow of silver threads is washed to remove any adhering salt. Proper combinations of current and cathode lifting rate allow the production of fibers with a length up to 30 cm and various structures (Figure 20.1).

Table 20.3 Electrolysis conditions and process parameters of noble metal powder production

Method	Electrolyte composition (content of components (kg/m^3)	Current density (kA/m^2)	Temperature (°C)	Electrolysis parameters
Palladium				
WS	10 of Pd (pH 9)	0.5–7.0	20	Electrolyte: $Pd(NO_3)_2 + NH_4OH$; current efficiency is of 40%
Platinum				
WS	3–5 of $Pt(NH_3)_2(NO_2)_2$ 100 of $K_4P_2O_7 \cdot 3H_2O$; 50 of NH_4OH; (pH 10.5)	1.0	60	Current efficiency is 19–20%; deposit is black powder; apparent density is of $5\,g/cm^3$
Silver				
WS	32–48 of $AgNO_3$; 3–5 of HNO_3; 50–100 of $NaNO_3$	$i_k = 1.2$; $i_a = 0.3–0.4$	40–50	Current efficiency is 85–96%; voltage is 2 V
WS	15–20 of Ag; 10–15 of HNO_3	1.5	40–50	Time for deposit growth is 2 min, interelectrode space is 50 mm, voltage is 2–2.8 V; electric power consumption is 0.6 kWh/kg
WS [3]	20 of $AgNO_3$; 10 of $NaNO_3$; up to pH 1 of HNO_3	$i_k = 2.0$; $i_a = 0.5$	25	Current efficiency is 97–100%; particles size is 2–3 μm
WS	20–300 of H_2SiF_6	0.3–5.0	20–50	Silver anodes, stainless steel cathodes; 40–80% of particles with size 60 μm, apparent density is $1.1–2.5\,g/cm^3$
WS [4]	15–20 of Ag; 100–200 of NH_2SO_3H; (pH 0.5–1.5)	0.6–0.8	18–25	Current efficiency is 90–100%; particles size is 50–100 μm; mass use ratio is of 60–70%
EDC	50 of $AgNO_3$; 0.5% of oleic acid; (pH 1–2)	1.2	20	Graphite disk is used for cathode; rotation is of 60 rpm; precipitation time is 1 hour; voltage is 10 V; current efficiency is of 99.8%; powder surface is of $15–18\,m^2/g$
Palladium–silver				
WS [5]	10 of Pd + Ag (pH 9)	0.5–7.0	20	Current efficiency (42%) depends on total metals concentration. Particles size is 1–20 μm $(Pd/Ag)_{powder} = (Pd/Ag)_{solution}$
Palladium–platinum				
WS [10]	10–100 of Pd + Pt; (pH 2.5–2.7)	0.5–4.0	20	Particles size is 1–10 μm; alloys are solid solutions; salts are chlorides; $(Pt/Pd)_{powder} = (Pt/Pd)_{solution}$
Platinum–cobalt				
WS [11]	3–5 of $Pt(NH_3)_2(NO_2)_2$; 5–8 of $CoSO_4 \cdot 7H_2O$; 100 of $K_4P_2O_7 \cdot 3H_2O$; 50 of NH_4OH; (pH 10.5)	1.0–2.0	60	Black powder, current efficiency is of 20%; $(Pt + Co)_{sum} = 5–10\,kg/m^3$; at $(Pt/Co)_{solution} = 2/1$ $(Pt/Co)_{alloy}$ 1:1 (at); residue is absent under $i \leqslant 100–200\,A/m^2$
Silver–nickel				
WS	30 of Ag + Ni; 5–10 of Ag; 20–25 of Ni; (pH 4–6)	2.5–3.0	18–25	Sulfamic electrolyte; in solution Ni:Ag = 5:1; current efficiency is 40%; anodes: Ag:Ni = 1:4, the higher temperature the richer silver alloy
Palladium–nickel				
WS	4–14 of Pd + Ni; 20 of NH_4Cl; (pH 9.5)	10–15	20	[Pd/Ni] = 2/1; solid solutions; $(Pd/Ni)_{powder} = (Pd/Ni)_{solution}$; particles size is 85–107 μm; current efficiency is 65%
Palladium–copper				
WS	5–13.5 of Pd + Cu; 30 of NaCl; 60 of NH_4Cl; (pH 0.5)	3–4	20	$(Pd/Cu)_{powder} = (Pd/Cu)_{solution}$; particles size is 90–220 μm; current efficiency is of 65%; alloys are hard solutions

WS: water solution electrolysis; EDC: electrolysis from double-layer cell (see Subsection 'Reduction from solution through film of surfactants' in Chapter 2).

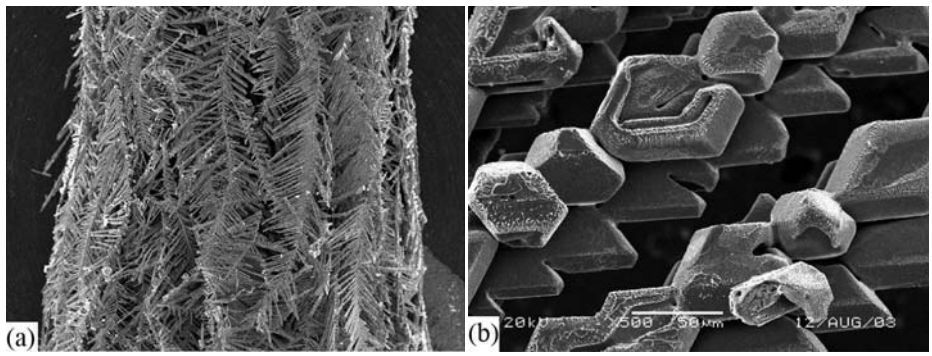

Figure 20.1 Silver fibrous deposits (current (i_a), A; velocity of electrode lifting (v), cm/min): (a) $i_a = 1$ A, $v = 5$ cm/min; (b) $i_a = 5$ A, $v = 3$ cm/min.

Production of Gold Powders

Gold bonding conductors, owing to their high reliability and conductivity, find a variety of applications in electronics and communication systems. The bonding behavior of gold, as well as its electrical conductivity, make it desirable in hybrid microcircuitry. A special reliability of gold is connected with its superior resistance to oxidation. The primary cost of using gold is rather high, but lost operating time and repair expenses as a result of the deterioration of electrical properties of non-gold elements due to the formation of oxide or sulfide films on contact surfaces are much higher [7].

Production of particles 3–180 µm in size is realized by gold vaporization in an inert gas atmosphere and condensation in ethanol.

Ultrafine gold powder particles are produced from the solution based on organic complexes by thermolysis of its aerosols (drops diameter is of 1–5 µm) in inert medium at temperatures higher than 497°C.

Many processes for manufacturing gold powder use an aqueous solution of $HAuCl_4$. This gold chloride solution is produced by dissolving gold grain or shot in aqua regia followed by heating to decompose and remove the nitric acid. A variety of reducing agents can be used to reduce gold to gold powder including other metal powders (zinc, magnesium, aluminum and iron), sulfur compounds (sulfur dioxide, sodium sulfite, potassium sulfite, and ferrous sulfate), hydrazines, aldehydes, oxalates, hydrogen peroxide and others.

Potassium sulfite or sodium sulfite can be directly added to aqueous gold chloride solution to produce spherical gold particles [8]:

$$2HAuCl_4 + 3Na_2SO_3 + 3H_2O = 2Au_{(S)} + 3H_2SO_4 + 6NaCl + 2HCl \quad (6)$$

Gold powder can also be produced by mechanical comminution. Sheets of gold are reduced by rolling to produce a foil between 10 and 20 µm thick followed by beating to produce a gold foil 0.2–0.5 µm thick. These foils are subjected to mechanical comminution ensuring an ultrafine gold powder production. Larger gold powders and gold flake can be manufactured by ball milling [9].

Production of Platinum-Group Powders

Powders of Platinum Metals

Chemical composition is shown in Table 20.4. Powders with a metal content not lower than 99.9% are produced according to special specifications. Each lot of powder corresponds to one brand of metal, foreign mechanical inclusions are not allowed.

Iridium powder. Particle size of the powder is not greater than 0.8 mm. The powder is used for the manufacture of alloys, special coverings and other products. The powder is supplied in lots of 250 kg.

Palladium powder. Particle size of the powder is not greater than 1.6 µm. The powder is supplied in lots of not more than 350 kg. It is used for the manufacture of contacts, alloys, chemicals, catalysts, special coatings and other products.

Platinum powder. Particle size of the powder is less than 1.6 µm; a content of the size fraction larger than 1.6 µm up to 2% is allowed. The mass of a powder lot is not larger than 350 kg. The powder is used for the manufacture of special units, alloys, coatings, semi-finished items and chemicals.

Rhodium powder. Particle size of powder is not greater than 0.8 µm; it is packed into plastic cans (net weight 25–5000 g) or in welded glass capsules (net weight 0.1–25 g). The mass of the powder lot is not greater than 350 kg. It is used for the manufacture of alloys, products and chemicals.

Osmium powder. Particle size of the powder is less than 1.0 µm; inclusions of the size fraction larger

Table 20.4 Chemical composition of refined powders of platinum metals

Chemical composition (wt%)												
			Impurities (max)									
Metal, Brand[a]	Basic metal content, min	Platinum metals, total	Pb	Fe	Si	Ba	Mg	Au	Al	Volatile matters	Sn	Total
Iridium												
IA-1	99.95	0.02	0.005	0.01	0.002	0.002	0.001	0.002	0.005	0.01	–	0.05[1]
IA-2	99.90	0.045	0.01	0.02	0.005	0.005	0.003	0.002	0.005	0.01	–	0.10
Palladium												
Pd AP-1	99.95	0.025	0.005	0.01	0.005	–	–	0.005	0.005	–	0.001	0.0[5]
Pd AP-2	99.90	0.050	0.005	0.02	0.005	–	–	0.010	0.005	–	0.005	0.10
Platinum												
PL AP-0	99.98	0.015	–	0.003	0.002	–	–	–	–	–	–	0.02[4]
PI AP-1[2]	99.95	0.025	0.005	0.010	0.005	–	–	0.005	0.005	–	0.001	0.05
PI. AP-2[3]	99.90	0.050	0.005	0.010	0.005	–	–	0.005	0.005	–	0.005	0.10
Rhodium												
Rh-Al	99.95	0.02	0.005	0.01	0.005	0.005	0.001	0.002	–	0.01	–	0.05[5]
Rh-A2	99.90	0.03	0.005	0.02	0.005	0.005	0.003	0.002	0.002	0.02	–	0.10
Osmium												
OsA-0	99.97	–	–	0.01	–	–	–	0.002	–	–	–	0.03[6]
Os A-l	99.95	–	–	0.01	–	–	–	0.002	–	–	–	0.05
OsA-2	99.90	–	–	0.03	–	–	–	0.002	–	–	–	0.10
Ruthenium												
Ru A-0	99.97	–	0.003	0.003	0.003	0.002	–	0.002	0.002	–	–	0.03[7]
Ru A-l	99.95	–	0.005	0.01	0.005	0.005	–	0.002	0.005	–	–	0.05
Ru A-2	99.90	–	0.01	0.02	0.01	0.005	–	0.002	0.005	–	–	0.10

[a]In Russian classification.
[1]Including Ag, Ni, and Cu.
[2]Including 0.00I of Sb.
[3]Including 0.005 of Sb.
[4]Including Ag,Mg,Cu,Ni, and volatile matters.
[5]Including Ag, Cu,Ni,Ti, and Al.
[6]Including Pt, Pd, Rh, Ir, Ag, Cu, and Ni.
[7]Including Pt, Pd, Rh, Ir, Ag, Cu, Ni, Mg, O.

than 1.0 μm (up to 2%) are allowed. The powder is packed into glass containers (25–5000 g) and capsules (0.1–25 g). It is used for the manufacture of alloys, semi-finished items, special products, coatings and chemicals.

Ruthenium powder. Particle size of powder is below 1.0 μm; inclusions of the size fraction larger than 1.0 μm (up to 2%) are allowed. The powder is packed into plastic containers (25–5000 g) and glass capsules (0.1–25 g). It is used for the manufacture of alloys, semi-finished items, special products, coatings and chemicals.

Chemical Reduction

The precipitation of platinum oxide at the interaction of H_2PtX_6 (where X is Cl^-, Br^-, I^-) with $NaNO_3$ and the processing of the oxide in hydrogen atmosphere is the oldest method of platinum niello production. Dispersivity is controlled at the stage of platinum oxide precipitation by variations of the salt nature, the inclusion of halides of alkali-earth metals (the latter are typical additions).

The process of reducing $[PtCl_6]^{2-}$ ion by sodium formate includes a number of consecutive stages: Pt (IV) → Pt (II) → Pt; the higher the (Cl^-) ion concentration, the slower the process rate; the activation energy for the interval of 95–60°C is of 105 kJ/mol.

The fractional conversion of the metal to powder achieves 99.9% in processing of chloro-amine compounds of platinum and palladium in sodium hydroxide solution by reducing agents (sodium formate, aluminum, hydrazine salts).

Platinum niello is produced by reaction of ammonium hexachlorplatinate with a 2.5 M solution of formic acid or sodium formate at 102 ± 5°C; pH of 6.0–6.5 is supported with the help of NaOH (or NH_3).

Metallic palladium powder is formed (without reducer) in the process of boiling dichloridiamminpalladium salt in a saturated alkali solution. If this salt is treated slowly (3 hours at 102 ± 5°C) in sodium hydroxide solution and sodium formate (0–20% of stoichiometric consumption) is used as the reducer, we can get palladium niello; an increase of sodium formate consumption from 10 to 80% of stoichiometrically necessary levels results in a decrease of palladium niello specific surface from 32 to 3 m^2/g. Palladium precipitation from chloride solutions by sodium formate is performed in accordance with the following scheme:

$$[PdCl_4]^{2-} \xrightarrow[Cl^-]{H_2O} [Pd(H_2O)Cl_3]^- \xrightarrow[\text{slowly}]{HCOO^-} [Pd(HCOO)Cl_3]^{2-} \rightarrow Pd + CO_2 + H^+ + 3Cl^- \quad (7)$$

The greatest influence on the increase of the process rate is exerted by an increase of temperature, sodium formate concentration and seed consumption. The process rate decreases at high pH and especially if chloride ions are introduced. It is explained by enhanced resistance of metal chloride components to the equation:

$$[M(NH_3)_2Cl_2] + H_2O \leftrightarrow [M(NH_3)_2H_2OCl]^+ + Cl^- \quad (8)$$

With the appearance of the metallic niello the process becomes autocatalytic.

Palladium powder is produced by processing its ammonium complexes with a mixture of formic acid and its ammonium salt prepared in the following manner: (CH_2O_2:$NH_4OH \geqslant 1.0$:0.3) at 77–87°C.

Cladding of powders of various metal oxides by platinum or palladium is achieved by the thermolysis method.

Powders of platinum, palladium, ruthenium and iridium are precipitated from acid–salt solution by cementation with zinc, copper, magnesium, aluminum or cadmium. The powder surface area is 0.1–1.0 m^2/g. A possible formation of intermetallics with the precipitator used reduces the powder quality.

Fine powders of platinum group metals are precipitated from aqueous or non-aqueous solutions of salts by radiation by election beam in doses of 10–30 mrad.

The Carbonyl Process

Powders of platinum group metals can be precipitated by the use of carbon monoxide:

$$MCl_x^{n-} + yCO \rightarrow M(CO)_yCl_{x-y}^{y-n} + yCl^- \quad (9)$$

$$M(CO)_yCl_{x-y}^{y-n} + yH_2O \rightarrow M + yCO_2 + 2yH^+ + (x-y)Cl^- \quad (10)$$

$$MCl_x^{n-} + yCO + yH_2O \rightarrow M + yCO_2 + 2yH^+ + xCl^- \quad (11)$$

There are several platinum carbonyl compounds:

$$Pt(CO)_2Cl_2,\ PtCOCl_2,\ Pt_2(CO)_3Cl_4,\ Pt(CO)_2Cl_6 \quad (12)$$

High carbonylchlorides are hydrolyzed to monocarbonylchloride; the latter is decomposed by interaction with water forming the platinum powder:

$$[PtCOCl_3]^- + H_2O \rightarrow Pt + CO_2 + 3Cl^- + 2H^+ \quad (13)$$

Platinum metals may exist in chloride solutions in different ion forms according to concentration of chloride ions.

$$PdCl_2 + CO \rightarrow PdCOCl_2 \quad (14)$$

$$PdCOCl_2 + H_2O \rightarrow Pd + CO_2 + 2HCl \quad (15)$$

Palladium complexes with maximal coordinate number 4 are formed in concentrated chloride solutions. In accordance with the above mentioned mechanism:

$$[PdCl_4]^{2-} + 2CO \rightarrow \left[Pd(CO)_2Cl_4\right]^{2-} \quad (16)$$

$$\left[Pd(CO)_2Cl_4\right]^{2-} + 2H_2O \rightarrow Pd + 2CO_2 + 4HCl \quad (17)$$

This process includes a number of subsequent transformations with complex ions of different structure as the participants.

The reduction is performed from the solutions (100–120 g/L of Pd; 1–2 M of HCl) or H_2PdCl_4 salt solution which is neutralized by alkali to pH of 6–8 and precipitated at 67–82°C.

The rate of palladium precipitation decreases in the presence of organic compounds (acetone, ethanol, butane); when the organic phase concentration is increased, the fine fractions output is increased also, and practically monodispersed powder can be produced; palladium powder with particle size of 1.2–1.7 μm was produced in the system palladium salt solution + about 10% of metal; particle shape is non-equiaxed, and their structure is porous.

The properties of palladium powders used for the manufacture of thin-walled ceramic capacitors are presented in Table 20.5.

Characteristic properties of palladium powders are homogeneity of phase and chemical composition, high particle size dispersity (0.3–3.5 μm), and insignificant pyrophorisity though of large specific surface (3.5–16.0 m^2/g).

Apparent density rises with the increase of the concentration of palladium salt and hydrochloric acid in the solution and the temperature and equals 0.8–2.8 g/cm^3. The specific surface is most significantly influenced by the content of palladium and acid in the solution and the temperature as well. To precipitate 1 kg of palladium, 262 g of carbon monoxide with the level of its usage of 80% is required.

Osmium powder is produced from platinum containing 0.6–1.0% of Os in two steps according to the scheme 'OsO_4 oxide sublimation– electrolysis'. Melting is done in an oxidizing atmosphere, and sublimates are collected in a 20% NaOH solution. Osmium bearing powder (50–70% of Os) is produced after the first stage by electrochemical precipitation. It is re-treated in the same way; the final cathode residue is washed free from impurities, dried and calcinated in a hydrogen atmosphere.

Autoclave Precipitation

Stable forms of noble metal ions that occur in aqueous solutions are complex compounds. Thermodynamic probability of their autoclave reduction by hydrogen is rather significant; the development of the process of metal powder precipitation is determined by the kinetic parameters and occurs at less rigid parameters than the precipitation of copper, nickel and cobalt powders.

The precipitation of gold from its thiosulfate, chloride and bromide complexes with 3+ charge proceeds at 57–67°C.

V.V. Ipatyev (1926) was the first who showed the possibility of platinum precipitation from the chloride complex. He carried out this process at 20–30°C, $p_{H_2} = 2.5 - 4.0$ MPa within 18–40 h; a positive influence of a seed was established and the precipitation rate increased in the series Pt, Ir, Rh, Pd. In general, this process can be described by the following reactions:

$$H_yMCl_x + \frac{y}{2}H_2 \rightarrow M + xCl^- + 2yH^+ \quad (18)$$

Similar reactions for actual platinum metals are presented below:

$$H_2PtCl_3 + 0.5H_2 \rightarrow Pt + 3Cl^- + 3H^+ \qquad E_0 = 1.47\,V \quad (19)$$

$$H_2IrCl_3 + 0.5H_2 \rightarrow Ir + 3Cl^- + 3H^+ \qquad E_0 = 1.02\,V \quad (20)$$

Table 20.5 The properties of palladium powders used for the manufacture of thin-walled ceramic capacitors

Property	Palladium	Alloy
Palladium content (min, %)	97	96
Chlorine-ion content (%)	0.01	0.04
Tap density (g/cm^3)	0.8–1.0	3.0–4.0
Specific surface (m^2/g)	10–16	3.5–6.0
Average particle size (μm)	0.3–0.6	2.0–3.5
Beginning of oxidation (°C)	197–217	547–597
Phase composition	Pd	Pd + (5–10)% of PdO
Level of transformation to oxide (%)	100	15–20

$$H_2PtCl_4 + H_2 \rightarrow Pt + 4Cl^- + 4H^+ \qquad E_0 = 0.73\,V \tag{21}$$

$$H_2PdCl_4 + H_2 \rightarrow Pd + 4Cl^- + 4H^+ \qquad E_0 = 0.62\,V \tag{22}$$

$$H_2RhCl_6 + 2H_2 \rightarrow Rh + 6Cl^- + 6H^+ \quad E_0 = 0.44\,V \tag{23}$$

Palladium and rhodium were reduced from the solutions containing 15–25 ppm (parts per million) of metal and 1 M of HCl at a hydrogen pressure of 0.1 MPa at 20–40°C and platinum and ruthenium were reduced at 70–80°C. The effect of increasing $p(H_2)$ to 0.35 MPa is established only for platinum and ruthenium.

In processing of acetate sulfate solutions of Rh (III), Pt (IV) and Ru (III), reduction to metal proceeded rather quickly and the process rate did not depend on the anion concentration and the ionic force of the solution. Cl^-, I^-, NH_3 ligands with their content higher than 3 N decelerate platinum metal precipitation and the process stops in the presence of CN^- ($p_{H_2} = 0.01$ MPa , 80°C). We can see an induction period in kinetic curves: the process rate is described by the equation of the first order of $-d[M]/d\tau = k[M^{n+}] \cdot [H_2]$ type. Experimental rate constants (c^{-1}) of reduction are as follows:

k: for $RuCl_6^{3-}$ is 1.0; for $RhCl_6^{3-}$ is 0.18;

for $PdCl_4^{2-}$ is 0.33; for $PtCl_4^{2-}$ is 5×10^{-4}

The precipitation of palladium from the solution bearing 2 g/DM^3 of Pd as H_2PdCl_4 requires the following: 30°C, $p_{H_2} = 0.3$ MPa; $\tau = 1$ h; the process is not developed in the presence of Cu (II) or Fe (III) ions.

Iridium can be reduced only to Ir (III) during the processing of chloride solutions bearing Ir (VI) ions at 30°C. Iridium metal is precipitated from the solution (64 mg/L, 20 g/L of HCl) only at 140°C, $p_{H_2} = 0.3$ MPa; within one hour. Platinum metals are precipitated at 80–147°C, within 0.5–1.0 h with sufficient stirring. Selective precipitation can be carried out depending on temperature and hydrochloric acid concentration.

Homogeneously sized silver powder with bulk weight of 0.3–3.0 g/cm^3 is produced by processing of silver oxide pulp bearing 10–200 g/L of solid, $t = 57$–117°C, $p_{H_2} = 0.5-2.5$ MPa within 10–40 min. Ammonia or silver salt is added to the pulp to increase the bulk weight and alkaline-earth metal sulfides or silver powders are added to decrease it. The powder produced is used for the manufacture of products, compositions and catalysts.

Noble metal powders can be precipitated by carbon monoxide in the interval of pH $\leqslant$ 7.0, the temperature of 20–200°C and $p_{CO} \geq 0.1$ MPa.

Production of Powders of Alloys Based on Noble Metals

The key condition of alloy production is phase composition uniformity achieved by alignment of the precipitation rate of components and their joint crystallization.

The most popular methods are chemical, contact displacement and electrochemical precipitation.

Silver–palladium powders used, in particular, as metallized paste fillers in capacitor production have to meet the following requirements: 70% of Ag and 30% of Pd, surface of not lower than 1.5–2.3 m^2/g, apparent density of 0.7–1.0 g/cm^3, content of the fraction (+90 μm) (with the particles of size $\geqslant$90 μm) not higher than 15%, homogeneous phase composition.

For their production, the basic raw material is dissolved in nitric acid, then the solution (80–100 g/L of Ag and Pd) is neutralized by alkali to pH 4.5–5.0 and the powder is precipitated by sodium formate to the residual content Σ(Pd, Ag) $<$ 1 mg/L at 67–77°C. The reducer consumption is 1.5–2.0-times the stoichiometric composition. The produced powder is annealed in a reducing atmosphere and screened. Due to a developed surface ($>$5–7 m^2/g) and the presence of residual nitrates, oxygen content in the powder can rise up to 1.5–2.0% which is intolerable.

Powders with the average particle size of 0.6 μm were produced using hydrazine as a reducer (47–57°C, 6-times consumption of stoichiometric quantity).

According to another method, the 'silver–palladium' composition is produced by stirring nitrate solutions (17 g/L of Ag, 3 g/L of Pd) with a reagent-precipitator (hydrazine + surfactants) at 53 ± 5°C. The surface of the produced powder is 2–7 m^2/g.

Pd–Cu alloy (55% of Pd) is produced from the solution of chlorides of these metals by reduction with hydrazine-sulfate. Two-three component alloys are produced by precipitation from hydroxy-ammonia and chloride ammonia complexes (the latter to provide the phase composition uniformity) of $(NH_4)_2MCl_4$ type where M is Pt (IV), Pd (IV), Os (IV), Ir (IV) with further treatment of the powder in hydrogen at 397°C.

A local reduction, first of all of palladium, is possible when using a pulp of salts of metals, which are constituents of the produced alloy, and its

precipitation by an organic reducer (most often sodium formate). Further, this results in a non-homogeneous distribution of solid solution components in the volume of a unit particle and a formation of up to 2–5% of individual metal inclusions.

Powders of Pt–Pd alloy are produced by joint precipitation by treatment of a solution of chloride complexes of these metals with sodium formate solution: at pH < 3.

$$H_2[PdCl_4] + HCOONa \rightarrow Pd + 3HCl + NaCl + CO_2;\ \Delta G = -158\ \text{kJ/mol} \quad (24)$$

at pH > 3

$$[PdCl_4]^{2-} + HCOO^- \rightarrow Pd + H^+ + 4Cl^- + CO_2 \quad (25)$$

$$[PtCl_6]^{2-} + 2HCOO^- \rightarrow Pt + 2H^+ + 6Cl^- + 2CO \quad (26)$$

The process includes: induction (1), precipitation and growth of nuclei (2); desorption and withdrawal into the solution of reaction products (3):

1. The induction stage is the diffusion of complex ions of the metal and the reducer to the seed surface.
2. The stage of precipitation and growth of nuclei is adsorption and an oxidation–reduction reaction:

$$[PdCl_4]^{2-}_{ads} + 2e \rightarrow Pd + 4Cl^-_{ads} \quad (27)$$

$$HCOO^-_{ads} - 2e \rightarrow CO_{2(ads)} + H^+_{ads} \quad (28)$$

accompanied by the growth of nuclei.
3. The stage of reaction products desorption and their diffusion into the solution.

In the case of multiple crystallization, the limiting stage is diffusion of Pt (Pd) (II) compounds to crystal surfaces. With an increase in pH, a part of aqua- and hydroxo forms in the composition of metal complex ions as well as the probability of an increase in niello precipitate formation.

The basic diagrams of alloy chemical precipitation are shown in Figures 20.2 and 20.3. They differ according to the type of the basic raw material: a slurry of metal salts or a solution. The proportion of components in the material that takes part in the precipitation provides further production of the alloy with a predetermined composition. It is adjusted in the starting material: for example, when producing the alloy PtPd-40p (in Russian classification), the proportion $[Pt]_0$:$[Pd]_0 = 1.4 \pm 0.1$ is kept in the solution. The precipitation is performed by sodium formate solution ($\gamma = 1.25$) at 162 ± 2°C, pH > 7. The precipitate is filtered out and thoroughly washed for complete elimination of Cl (I) and Na (I) ions. The

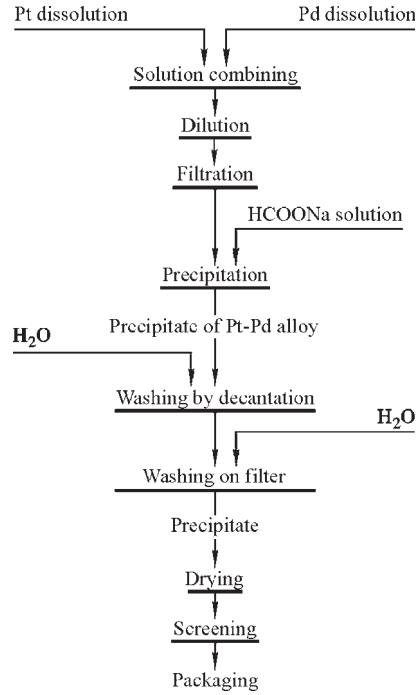

Figure 20.2 Flow-sheet of Pt–Pd chemical precipitation from solutions.

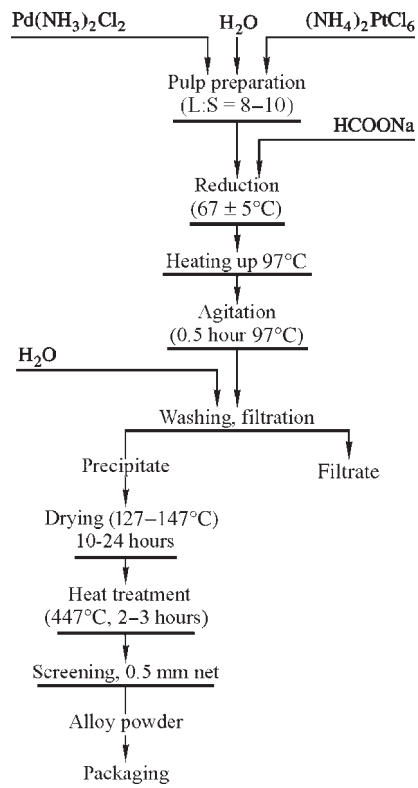

Figure 20.3 Method of Pt–Pd chemical precipitation from pulp.

precipitate is dried for 4–6 hours at 69°C and for 20–24 hours at 120°C. It is then screened and packed.

The composition of the alloy of PtPd-40p brand is: Σ(Pt, Pd) > 96.5 wt% including 58–61 wt% of Pt; not more than 0.04 wt% of Cl; 0.03 wt% of Na; 0.5 wt% of moisture; 0.05–1.0 wt% of volatile matter (O_2, H_2, CO_2, CO).

This alloy is a single-phase alloy; its apparent density is of 1.4–1.9 g/cm^3.

For example, per 1 kg of PtP-90 niello precipitate produced from metal, the consumption (in kg) is the following: 2.4 of HNO_3; 9.0 of HCl; 2.4 of Na_2CO_3; 3.0 of HCOONa; 200 of H_2O and 100 kW · h of electric energy.

In particular, this alloy is, like platinum, suitable for the metallization of pottery surfaces bearing bismuth or titanium.

In the processing of ammonium complexes of platinum and palladium (pH = 12–13; 147–157°C; L:S = 2; τ = 0.5–1.0 h), the latter are precipitated fully as powder.

The technique provides a quick and complete procedure with the minimum consumption of alkali and without an external reducer. The particles have a spherical form, their size is 0.3–0.4 μm and specific surface of the powder is 2–4.5 m^2/g [9]. The size of the particles decreases when the temperature of the process increases and the specific surface of the powder increases slightly.

Pt–Pd–Rh alloy is produced by thermolysis of a mixture of complex salts of $[Me(NH_3)_4]NH_4(RhCl_6)]$, $Me(NH_3)_4[RhH_2OCl_5]$ type, where Me is Pt (II), Pd (II). The products produced are solid solutions with compositions preset in the stage of mixture preparation; powder particles have a spherical shape, particle size is ⩾10 μm.

A powder with apparent density of 0.7–1.9 g/cm^3 and a porous structure of particle conglomerates 30–40 μm in size is produced by thermolysis of platinum and palladium glycine complexes.

Powders of palladium based compositions were produced by thermolysis of amino-oxalate complexes of $[Pd(NH_3)_4]$ $[Me(C_2O_4)_2]$ type, where Me is Zn, Cu, Ni, Co. An intermetallic was produced in the Pd–Zn system; in other cases, the solutions were mixed with the metal in the ratio of 1:1. Powder particle size for all compositions is not larger than 1 μm.

An isomorphic solution of platinum in palladium is precipitated by means of sodium bicarbonate from a solution bearing platinum and palladium. An alkaline medium of the obtained mixture brings about the reactions mentioned above. The larger the palladium content, the greater the process rate. Platinum is precipitated sufficiently completely at the atomic proportion Pt/Pd = (1–2)/1. The procedure is performed at 70°C, $[HCl]_0 = 0.75$ Me, $[NaCl]_0 = 1.25$ Me.

Increasing the Cl (I) ion concentration decelerates the process, but increasing acidity accelerates it; powder particle size is of 1.8–2.7 μm.

Temperature and duration are governing factors for Pt–Pd–Rh mixture precipitation: 26% of the metal was precipitated at 97°C within 3 h, 97% was precipitated in 8 h.

Production of Platinum Black Deposit (Niello)

Before platinization, the electrodes are thoroughly cleaned in a chrome mixture or by SiO_2 powder and calcinated. Platinization is carried out in the solution containing 30 kg/m^3 of H_2PtCl_6 and 0.2–2.3 kg/m^3 of $Pb(CH_3COO)_2$ at a current density that provides a moderate gassing on the electrodes (≈50 A/m^2) and at 22°C within 15 minutes. In the case of simultaneous platinization of two electrodes (for example, for application in cells of electrical conductivity measurement), the current is commutated from time to time.

After platinization, the electrodes are put into 10% solution of sulfuric acid and polarized cathodically within 5 minutes with an auxiliary platinum electrode as anode. The current strength in this case is also adjusted by gassing intensity. The adsorbed chlorine is reduced and eliminated more easily while washing as chloride ions. The electrodes are washed in running warm water and then in cold distilled water. The platinized electrodes have to be stored under a water layer as they lose wettability in air. Re-platinization is performed over 1–2 minutes.

Synthesis of Palladium Nanoparticles by Methods of Zone Electrochemistry

Palladium powder with a particle size of 5–15 nm is characterized by specific catalytic properties. Nanoparticles and their dendrite-shaped aggregates are produced from palladium chloride by means of cetyltrimethylammonia bromide (CTAB). The cylindrical part of the titanium rod is protected by plastic and rectangular pulses of direct current and ultrasound are supplied alternately to the electroactive disk part of the electrode. A predominant size of spherical particles (nuclei stripped from the electrode surface during ultrasound supply) is increased from 5 to 11–13 nm as the current density decreases from 130 to 80 A/m^2 in the solution with palladium salt concentration of 10 mol/m^3. A preferred range of concentration of palladium salt is 5–50 mol/m^3 and

the interval between adjacent ultrasound pulses is 5–10 s. The CTAB content can vary within a range from 20 to 30 kg/m^3. Dendrite aggregates from nanoparticle chains are formed by increasing the electrolysis duration to 2.5 h [12].

Manufacturing methods for electrolytic platinum-group powders and electrolytic platinum-group alloy powders are shown in Table 20.3.

References

1. Butts, A., Coxe, C.D., (eds), *Silver–Economics, Metallurgy, and Use*. Krieger Publishing, 1975.
2. Glicksman, H.D., Production of precious metal powders: silver, gold, palladium, and platinum. In *ASM Handbook*, Vol. 7. ASM International Publishers, 1998, pp. 182–187.
3. Baimakov, Yu.V., Zhurin, A.I., *Electrolysis in Hydrometallurgy.* Metallurgiya Publisher, Moscow, 1977 (in Russian).
4. Tomiltseva, A.K., Vyacheslavov, P.M., Burkat, G.K., Tsoi, Z.N., Silver powders electroprecipitation from sulphamine electrolyte. *Sov. J. Appl. Chem.,* 1978, 51(9):2094–2097 (in Russian).
5. Yurev, B.P., Shkuryakova, S.P., Electrolytic preparation of fine Pd-Ag powders of any given chemical composition. *Sov. Powder Metall. and Met. Ceram.*, 1973, 12(1):443–446.
6. Ivanovskiy, L.E., Rozanov, I.G., Zotin, I.V., Khramov, A.P., Production of dendrite metals deposits by ionic melt electrolysis and their application. *Liquid Melts*, 1997, (2):51–69.
7. Davies, R.R., New development in electronics and communications. In *Precious Metals*, eds R.O. McGachie, A.G. Bradley. Pergamon Publishing, 1981.
8. Short, O.A., US Patent 3,771,996 (1973).
9. Collier, N., Advances in gold powder technology. *Gold Bull.*, 1977, 10(3):62–66.
10. Shkuryakova, S.P., Yurev, Production of fine platinum-palladium alloy powders. *Sov. Powder Metall. Met. Ceram.*, 1974, 13(12):953–955.
11. Zayats, A.I., Perekhrest, N.A., Dispersed Pt-Co alloys precipitation. *Soviet J. Appl. Chem.*, 1972, 45(10):2248–2250 (in Russian).
12. Qiu, Xiao-Feng, Xu, Jin-Zhog, Zhu, Jian-Ming, Zhu, Jin-Jie, Xu, Shu, Chen, Heng-Yan, Controllable synthesis of palladium nanoparticles via a simple soundoelectrochemical method. *J. Mater. Res.*, 2003, 18(6):1399–1404.

Chapter 21

Production of Refractory Metal Powders

Stanislav S. Naboychenko, Ural State Technical University (UPI), Yekaterinburg, Russia
Irina B. Murashova, Ural State Technical University (UPI), Yekaterinburg, Russia
Oleg D. Neikov, Frantsevich Institute for Problems of Materials Science (IPMS), Kiev, Ukraine

Tungsten, molybdenum, niobium, tantalum and rhenium, classified as the refractory metals, are distinguished by several general characteristics, including high melting point, high density and superior resistance to wear and corrosion. With the exception of two of the platinum-group metals, osmium and iridium, they have the highest melting temperatures and lowest vapor pressures of all metals. Tungsten, for example, has a melting point of 3410°C, the highest of any of the elements and has a density over twice that of iron. Their feature, however, is heavy oxidation above 500°C and they must be protected for service at elevated temperatures by coatings or non-oxidizing atmospheres. These metals have body-centered cubic crystal structures (except for rhenium, whose crystal form is hexagonal).

The refractory metals are extracted from ore concentrates, transformed by processing into intermediate products and then reduced to the metal. Except for niobium, they are produced exclusively as metal powders, which are consolidated by sintering and/or melting. The process for niobium differs only in that the metal is generally reduced by aluminothermic reduction of oxide.

Production of Tungsten and Tungsten Carbide Powders

Tungsten was adopted in industry at the beginning of the 20th century due to its application as an alloying element in high-speed steels and as filament wire in incandescent lamps. In both applications, pure tungsten was manufactured in powder form.

At the end of the 19th century, very hard tungsten carbides, WC and W_2C, were studied by Henri Moissan [1,2]. However, for a long time all attempts to compact tungsten carbide powders resulted in porous and brittle products. In 1922, researchers of the OSRAM study group combined the brittle tungsten carbide with a ductile metal binder. After sintering such powder mixtures, a material of both high strength and toughness was obtained. Sintered hard metals, based on tungsten carbide bonded with cobalt, were first commercially produced by Widia in Germany in 1926. The global hard metal industry is estimated to have totalled 32 250 mt in 2002 with a sales value of over $8.5 billion followed by further rises to 51,900 mt in 2006 with sales an estimated $43 billion. Of this, around 60% is for sintered cutting tool materials used for machining all types of metallic components, for woodworking, mining tools, drilling tools used in oil exploration, etc., and the remainder for components such as rolls used in steel mills, metal forming dies and structural components for severe wear resistance applications [3].

Western Europe once led the market in this sector but its share diminished to 39% in 2006 while China's market share increased to 33%, USA is at around 13% and Japan accounts for 12% and others 3%.

Since 1993, the global production of tungsten, which is the main raw material used in sintered hard metal products, has fluctuated in a narrow range between 30 000 and 35 000 mt. China is the predominant tungsten producer accounting for almost 85% of global output in 1999. Further sources of raw materials include releases from strategic stockpiles in Russia and the USA. The usages of tungsten scrap as a raw material is estimated to be as high as 30% in some countries, with the incentive to use scrap increasing as tungsten prices increase. As a result, recent annual global consumption of tungsten has been in the range of 40 000–50 000 tonnes [4] and over half of the tungsten consumption is for tungsten carbide powder for hard metal production. Along with this, important products are based on tungsten alloy powders, such as:

- Heavy metal alloys (W–Fe–Cu–Ni–Co)
- Electrical contacts (W–Cu, W–Ag)
- Ductile tungsten, including lamp filaments.

Tungsten, as an alloying element for steels and superalloys, is predominantly used as ferro-tungsten, or as melting base alloys, which are prepared from

either ore concentrates or tungsten-bearing scrap. An insignificant part of the tungsten consumption is used in the form of various chemical products, such as catalysts, pigments, solid lubricants and heavy liquids.

Tungsten Metal Powder

Production of Tungsten Powder by Hydrogen Reduction

Feed to Process

Industrial raw materials to process tungsten-bearing minerals are wolframite ([Mn, Fe]WO_4), scheelite ($CaWO_4$), ferberite ($FeWO_4$) and hübnerite ($MnWO_4$). The lower limit of workable tungsten concentration ranges from 0.1 to 0.3 wt% WO_3. Concentrations of more then 2 wt% are infrequent. The average WO_3 content is usually about 0.5 wt% [5, 6]. Wolfram Bergbau and Hütten GmbH (WBH) in Austria, a world-leading producer of tungsten oxide, tungsten metal and tungsten carbide, mines recently about 400 000 tonnes of scheelite ore with a 536 306 peak in 1986, with average WO_3 content 0.55 wt% [7]. Depending on the mineral type, different techniques, such as gravity methods and flotation, are used to concentrate the ore up to reduced WO_3 contents of about 40–60 wt%. Tungsten-bearing scrap, which usually has a high tungsten content, is a considerable alternative tungsten source to the natural mineral resources.

Process

The main process steps from concentrates or scrap through the formation of high purity ammonium paratungstate (APT: $3(NH_4)_2O \cdot 7WO_3 \cdot 6H_2O$ and $5(NH_4)_2O \cdot 12WO_3 \cdot 11H_2O$) intermediate to tungsten metal powder [5] are shown schematically in Figure 21.1.

In the dissolution step, the tungsten-bearing feed materials (wolframite concentrate and oxidized tungsten scrap) are treated with NaOH or scheelite concentrate is treated with Na_2CO_3 to form water-soluble sodium tungstate Na_2WO_4

The purification steps include:

- Removal of the aluminum, arsenic, fluorine, phosphorus and silicon by precipitation.
- Substitution of sodium by NH_4 forms an ammonium solution $(NH_4)_2WO_4$. This is ordinarily done by solvent extraction, which is a liquid ion exchange process, where tungsten is extracted by means of an aliphatic amine dissolved in isodecanol and paraffin. This process is followed by re-extraction into aqueous ammonia solution.

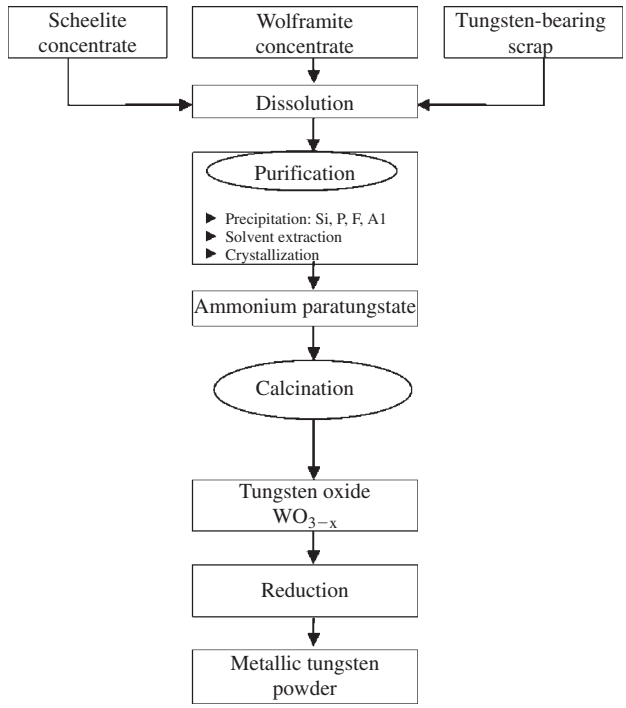

Figure 21.1 Tungsten metal powder production flowsheet.

- Crystallization of APT by evaporation of ammonia and water. APT is the intermediate product of highest purity for metallic tungsten and tungsten carbide powder production.

The calcination step includes heating the APT to 400–900°C, predominantly in rotary furnaces, for ammonia and water elimination. If accomplished in excess of air, the resulting oxide is WO_3 yellow tungsten oxide. In its absence, a slightly lower WO_{3-x} blue tungsten oxide is formed.

WO_3 is the most stable a-oxide with homogeneity range WO_3–$WO_{2.96}$; it has three crystalline modifications: monoclinic modification stable at temperatures lower than 727°C, tetragonal modification in the range from 727 to 1097°C and cubic modification at temperatures higher than 1097°C. It sublimes noticeably at 797–847°C and exists in the form of polymer molecules in the vapor phase.

Reduction step with hydrogen reducer. The reduction of the oxide to metal proceeds through several intermediate oxide phases. Generally, two furnace designs for the reduction process are used industrially: the multitube pusher type and the rotary furnaces. During the reduction process, the sequence in which oxides occur depends on the applied temperature and on the moisture within the powder bed, accordingly, static in pusher type popular furnaces and dynamic in rotary furnaces.

Tungsten reduction by hydrogen includes four steps:

$$WO_3 + 0.1H_2 \leftrightarrow WO_{2.9} + 0.1H_2O \qquad K_{eq} = -3792.0/(T + 273) + 4.8286$$
$$WO_{2.9} + 0.18H_2 \leftrightarrow WO_{2.72} + 0.18H_2O \qquad K_{eq} = -142.5/(T + 273) + 1.684$$
$$WO_{2.72} + 0.72H_2 \leftrightarrow WO_2 + 0.72H_2O \qquad K_{eq} = -801.7/(T + 273) + 0.8615$$
$$WO_2 + 2H_2 \leftrightarrow W + 2H_2O \qquad K_{eq} = -2219/(T + 273)$$
$$WO_3 + 3H_2 \leftrightarrow W + 3H_2O$$

The numerical value of summary equilibrium constant $K_{eq,sum}$ may be calculated as a composition of four previous equilibrium constants for preceding stages. It measures for temperature T°C

$$K_{eq.,sum} = \frac{9.61 \times 10^{11}}{(T + 273)^4} - \frac{1.26 \times 10^{10}}{(T + 273)^3} + \frac{2.67 \times 10^7}{(T + 273)^2} - \frac{1.55 \times 10^4}{(T + 273)}$$

In the pusher furnace, tungsten oxide is loaded into flat metal 'boats', which are pushed through the horizontal furnace tubes (Figure 21.2). Increased demand for tungsten products made it possible for WHB Company to modernize the reaction stage by replacing the manually operated pusher furnaces by automated furnaces (Figure 21.3). The powder layer preserves its static state throughout the whole reduction process. Typical reduction temperatures range from 600 to 1100°C. The boats are pushed at a rate usually in the range from 5 to 30 mm/min. The hydrogen flow is commonly in the countercurrent direction. Removal of the water vapor formed during reduction takes place from the powder layer surface and is carried away by the hydrogen flow. The cooler is located on the discharge end of the tube. Electrolytic hydrogen collected in gas-holders and freed from oxygen and steam is used. As the

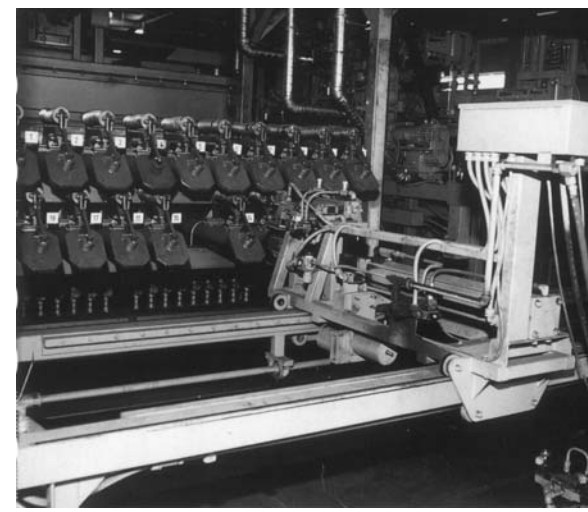

Figure 21.3 Automatic push type furnace. Courtesy: Wolfram Bergbau- und Hütten-GmbH.

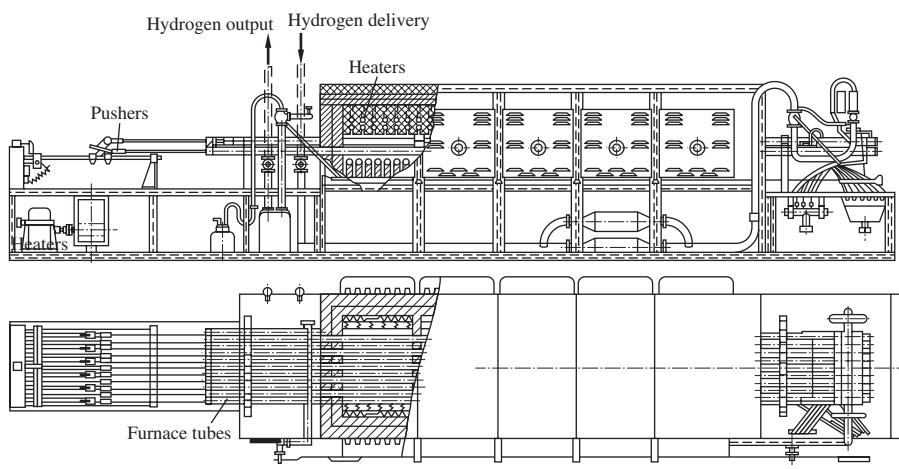

Figure 21.2 Multitube push type furnace.

hydrogen supply is greatly in excess of that required for the reduction (the efficiency is not more than 20%), the outgoing gas passes through a regeneration plant and returns to the process after drying. The boats are shifted in the direction of higher temperatures and less water damp concentrations. Reduction rate is controlled by water vapor diffusion through the layer of WO_3 powder and then transformation throughout the all layer section $WO_3 \rightarrow WO_{2.9} \rightarrow WO_{2.72} \rightarrow WO_2 \rightarrow W$ is accomplished.

The pusher type furnace is very adaptable to the manufacture of different particle size powders and can quickly be adapted to produce the desired powder properties.

By variation of reduction parameters such as temperature, powder layer depth in the boats and boat speed, the particle size of the metallic tungsten powder can be controlled. Grain size of the WO_2 particles influences significantly the tungsten particle size. Increase of the tungsten powder particle size is encouraged by high temperature and quick temperature increase along the furnace tube, high push rate, large depth of the powder layer, low hydrogen flow rate, and its high humidity.

By using the rotary furnaces, the tungsten oxide is directly introduced into the rotating furnace tube. An overall view of rotary furnace used at the refining plant of WBH Company is shown in Figure 21.4.

The rotating furnace tube has, as a consequence, not a static but a dynamic powder layer. Depth of the layer is influenced by the feed rate, rotational speed, incline and lifters inside the tube. The temperature range is comparable to that of pusher type furnaces and the hydrogen flow direction is also usually countercurrent. With respect to changes of particle size, the rotary furnace is not as flexible as the pusher furnace. A characteristic of application is the continuous production of powders with medium size ranging from 1 to 3 μm.

The intermediate oxides differ as regards both color and morphology. The latter is illustrated in Figure 21.5. The cause of these morphological changes is the transport of tungsten via the gas phase, i.e. chemical vapor transport (CVT) during the reduction sequence. Tungstic acid, $WO_2(OH)_2$, has been identified as the most volatile compound in the system W–O–H, and is responsible for the CVT. If the partial pressure ratio p_{H_2O}/p_{H_2}, is low enough, the reduction

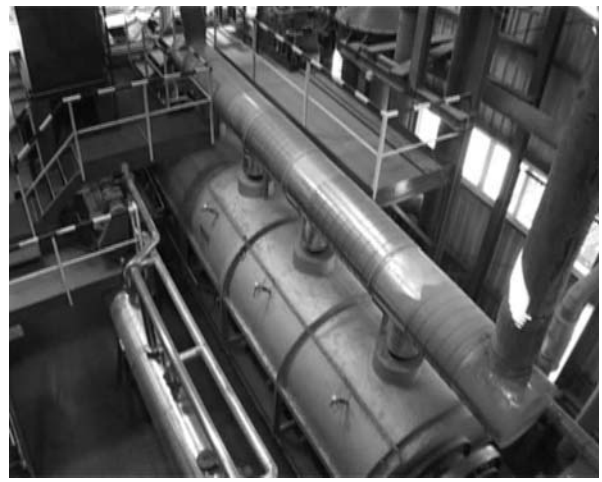

Figure 21.4 Rotary furnace. Courtesy: Wolfram Bergbau- und Hütten-GmbH.

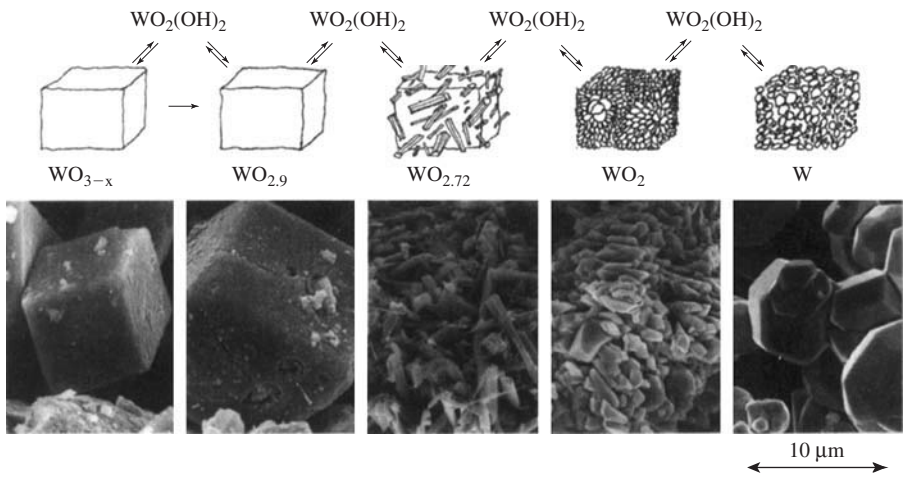

Figure 21.5 Morphological transformations of tungsten oxides during reduction at 1000°C. Source: Ref 6

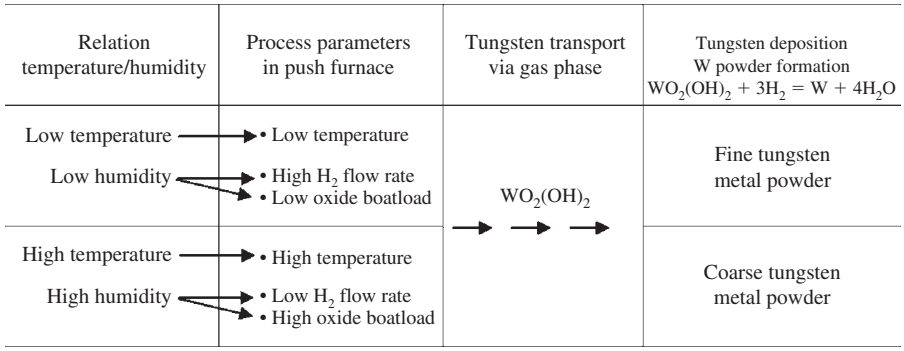

Figure 21.6 Control of the metallic tungsten particle size in the push furnace.

from WO_2 to tungsten starts. From a thermodynamic point of view, $WO_2(OH)_2$ may form from both WO_2 and tungsten, but the equilibrium pressure is lower above tungsten, which causes the CVT of $WO_2(OH)_2$ from WO_2 to tungsten, where the vapor deposits as metallic tungsten, thus leading to growth of the tungsten crystal. The CVT mechanism permits the control of the metallic tungsten particle size through the interaction of temperature and humidity (partial pressure ratio p_{H_2O}/p_{H_2}), which is shown schematically in Figure 21.6 for the pusher furnace.

Other Tungsten Powder Production Methods

Reduction by Solid Carbon

Reduction follows the relationship shown in Figure 21.7 and can be written:

$$WO_3 + 3CO = W + 3CO_2$$
$$3(CO_2 + C = 2CO)$$
$$WO_3 + 3C = W + 3CO \qquad K_{eq} = P_{CO}^{-3}$$

where K_{eq} is the equilibrium constant.

At temperatures lower than 727°C, the oxide is not reduced because of insufficient partial pressure of CO. The necessary temperature to accelerate the process is above 1197°C. Reduction is accomplished in pusher type furnaces with carbon tubes (Figure 21.8). Maximum temperature in the furnace is 1827°C; consumption power is 25 kW, daily yield is 350–380 kg [8].

To produce fine powders, the temperature is maintained in the range from 1397 to 1497°C, the boats are moved through the high temperature zone rather faster or some excess of black is injected. The powder produced contains inclusions of carbides and is friable. These powders are used for the production of tungsten carbide powders.

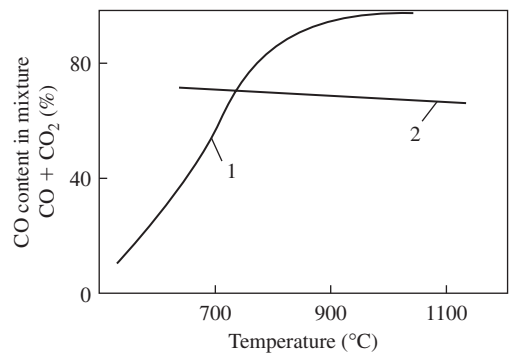

Figure 21.7 Equilibrium compositions of gaseous mix of CO and CO_2 depending on temperatures for $CO-CO_2$ and $CO-CO_2-WO_2-W$ systems. 1: $C + CO_2 \leftrightarrow 2CO$; 2: $WO_2 + 2CO \leftrightarrow W + 2CO_2$.

Precipitation from Gaseous Phase of Tungsten Hexafluoride and Tungsten Hexachloride

The powder is produced from gaseous substances:

- at low temperature by dissociation of tungsten hexafluoride or tungsten hexachloride in hydrogen
- by decomposition of tungsten hexachloride in neutral gas (argon or nitrogen)
- by high temperature decomposition of tungsten hexafluoride in hydrogen fluoride.

The melting point of tungsten hexafluoride is 3°C and its boiling point is 17.1°C. Melting point and boiling point of tungsten hexachloride are 281.5°C and 350°C, respectively. Reduction of tungsten halide ($WHal_x$) takes place according to the reaction with halide acid (HHal) formation:

$$WHal_x + 0.5xH_2 = W + xHHal,$$
$$k_{eq} = p_{HHal}^{x}/(p_{H_2}^{0.5x} p_{MHal_x})$$

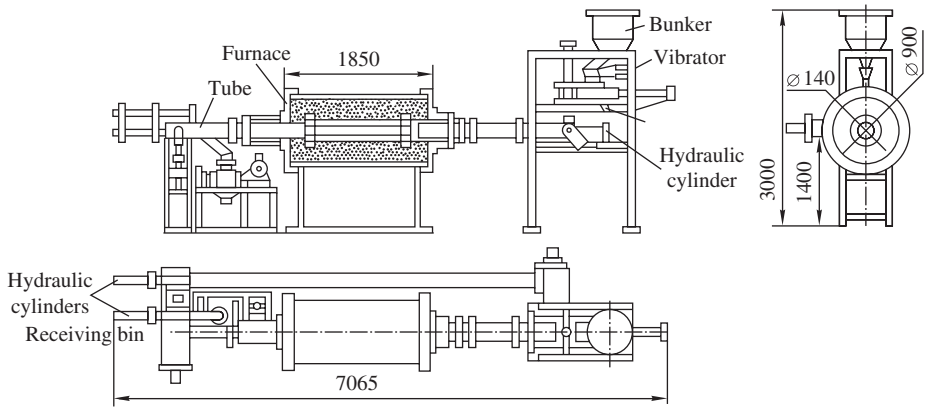

Figure 21.8 Push type furnace for tungsten anhydride reduction by carbon.

A flow diagram of the reduction process by precipitation from the gaseous phase of tungsten hexafluoride and tungsten hexachloride is shown in Figure 21.9. The plant consists of a halide evaporator, reactor of fluidized bed and devices for regeneration and gaseous product collection, a porous bottom made of sintered coarse tungsten powder replaced sometimes by a layer of tungsten small fragments (1–5 mm) or metal grate placed in the lower part of the reactor. Tungsten halide vapor from the evaporator, together with hydrogen and argon, are supplied by pump to the lower part of the preheated reactor where, at the bottom, tungsten fine powder (20–60 μm) as seed is found. During reduction, the seed is converted into granules which are discharged periodically or continuously. The hydrogen chloride or fluoride is collected in a scrubber. After discharge of the hydrogen and argon mixture from the desiccant, the hydrogen is absorbed by heated titanium sponge and argon is returned to the cycle. The sponge is dehydrogenated periodically and purified hydrogen is also returned to the cycle.

The temperature in the reactor influences the degree of metal precipitation. However, increasing the temperature above 897°C leads to eventual sintering of seed particles and, as a result, to the failure of the fluidized bed.

Tungsten reduction from WCl_6 is carried out at 747–797°C and from WF_6 at 547–597°C. In the first case, the molar ratio of hydrogen to tungsten hexachloride in the gas–vapor mixture is maintained at approximately 30–40 to 1; while the molar ratio of hydrogen to argon is approximately 1.75 to 1; tungsten recovery amounts to 90–99% and degree of precipitation on powder is 96–97%; in the second case, the molar ratio of hydrogen to tungsten hexafluoride, maintained at 15–18 to 1 provides full recovery of tungsten. The gaseous flow rate through the fluidized bed must be not less than 5–10 cm/s.

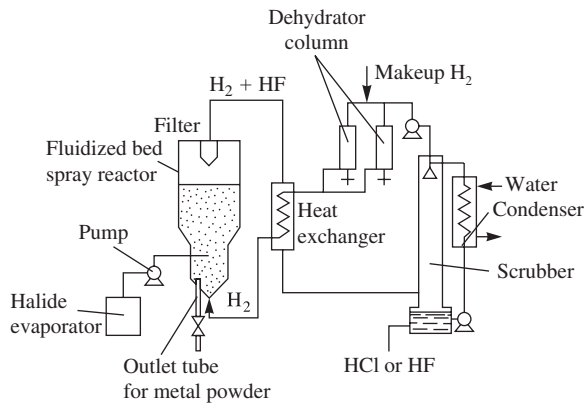

Figure 21.9 Flow diagram of the reduction process by precipitation from gaseous phase of tungsten hexafluoride and tungsten hexachloride in fluidized bed.

For the production of tungsten powders with spherical particle shape, the metal is reduced from concentrated solutions of salts, oxides, or hydroxides. Spheroidizing takes place in the high temperature zone where powder is transferred by carrier gas.

High purity tungsten nanopowders are produced from fluorine-containing compounds according to the following scheme: tungsten metal ion extraction from aqueous solutions (fluorine organic acids, ethers, amines, carbonyl acids, ketones and others), re-extract by solutions of fluorine compounds (hydrogen fluoride, ammonium fluoride, ammonium hydrogen fluoride), reduction of tungsten fluoride and tungsten oxyfluoride in hydrogen; metal powder particle size is approximately 30 nm. Similar powders are also produced by evaporation of volatile chlorides and hydrides in a reaction gas atmosphere (hydrogen, C_2H_5, ammonia), heating being done by high frequency induction or laser beam.

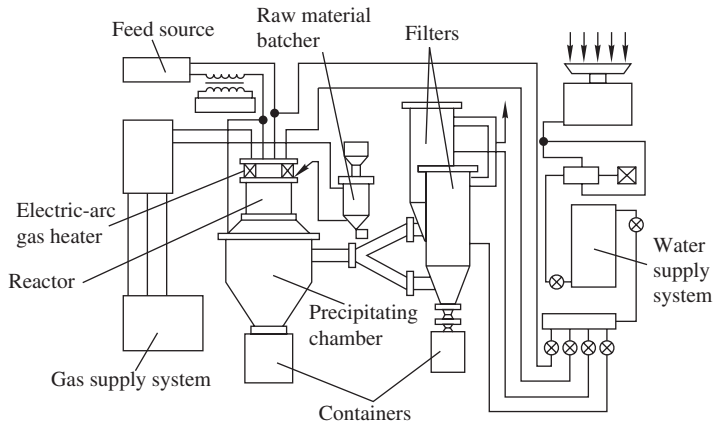

Figure 21.10 Electric arc device for tungsten and molybdenum oxides reduction by hydrogen.

Production of Powder by a Plasma Process

The plasma process is realized at temperatures much higher than the boiling point of the basic materials. Tungsten is produced in a vaporous state. Powder is formed by condensation, coagulation, crystallization accompanied by polymorphous transformations. Complete reduction to tungsten is achieved by processing tungsten trioxide in an argon–hydrogen plasma (by the molar ratio of argon to hydrogen at 1 to 1) at temperatures ranging from 3997 to 4997°C.

A two stage scheme is used for the production of powder with a narrow range of granulometric composition (0.6–2 μm) preserving its properties by storing in air. In the first step, the tungsten trioxide is preliminarily reduced at 1997°C to a residual oxygen content in the powder of 8%; in the second step, further reduction to metal is done at 747–797°C.

Plasma plant (Figure 21.10) contains a consumable tungsten electrode inside a chamber in which is a direct current arc (200 A, 30 V). The powder particles formed with average size about 0.05 μm are carried to a bag filter by a stream of hydrogen–argon mixture. The capacity up to 60 kg/h of tungsten powder with particle size 0.03–0.05 μm is provided for by control of jet temperature and reaction area geometry. Tungsten powder produced in compound current of arc and radio-frequency plasmas has average particle size about 10 nm and impurities content not more than 33 ppm Fe, 23 ppm Mo, 17 ppm Si and 280 ppm *C* (carbon).

Amalgam Method

Molybdenum and tungsten powders can be produced by reducing their pentachlorides by 2–5 wt% zinc amalgam Figure 21.11). The reduction reactions may be represented as follows:

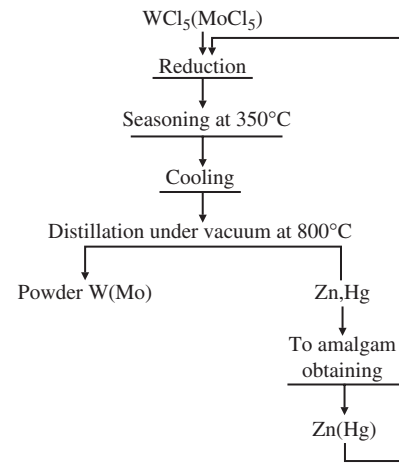

Figure 21.11 Flow sheet of molybdenum and tungsten powder production by amalgam method.

$$2MoCl_5 + 5Zn(Hg) = 2Mo(Hg) + 5ZnCl_2 + (Hg)$$
$$2WCl_5 + 5Zn(Hg) = 2W(Hg) + 5ZnCl_2 + (Hg)$$

Amalgam consumption is 110–200% of stoichiometry reactions. The temperature is a little bit lower than the boiling point of the zinc chloride formed (218°C). After metal reduction, the temperature is increased up to 350°C and kept for 30 minutes for growth of the crystals. Molten zinc chloride is floated on the amalgam surface, cooled and then a solidified cake of zinc chloride is separated from the amalgam surface and removed. Excess zinc and mercury are distilled in a vacuum by the increasing temperature to 800°C.

Carbonyl Technique

Tungsten and molybdenum carbonyl powders are produced by carbon monoxide action on their compounds (salts) at high pressures and temperatures with metal carbonyl formation and subsequent thermal decomposition. This process has been developed on enlarged laboratory and semi-industrial scales.

Synthesis of carbonyls is done in liquid media. Figure 21.12 shows a flow diagram of this process. Basic materials are: higher metal chlorides $MoCI_5$ and WCl_6 (their storage period is not more than one month), produced from ore concentrates, zinc powder as reducer and dichlorethane or ether as solvent. After solvent cleaning, basic materials are fed into an autoclave in the following sequence: dichlorethane, metal chloride, zinc and ether. For tungsten carbonyl production, the reaction components are charged in a weight ratio of tungsten hexachloride to zinc powder of 1 to 0.667 and volumetrical ratio of tungsten hexachloride to ether of 1 to 25. The process is carried out at 47–77°C and under 4–6 MPa of carbon monoxide pressure.

On completion of the synthesis, carbon monoxide is removed from the autoclave and the reaction mass is taken to the still where first solvents are eliminated and then carbonyl is evaporated off by live steam. Solvents then go to a regeneration unit and, after purifying, are returned to the process.

Carbonyl is supplied to a water spraying capacitor and the suspension is delivered to a nutsch-filter and the filtrate exhausted to the collector by vacuum pump. Squeezed carbonyl is fed to the topping still, cleaned from iron pentacarbonyl, $Fe(CO)_5$ by 1% NaOH aqueous solution and rectified. Cleaned carbonyl is filtered in the nutsh-filter, washed with distilled water and dried in a vacuum oven. The plant capacity is 200–500 kg per hour; autoclave volume is 1–15 liters, carbonyl efficiency amounts to 80–90%.

A process is known for dry synthesis from chlorides. The process uses iron swarf as the reducing agent and is conducted under carbon monoxide at a pressure up to 28 MPa and a temperature of 277°C. The advantage of the process is the absence of inflammable solvents.

Tungsten and molybdenum powders are produced by carbonyl decomposition under atmospheric pressure and at temperature ranges from 347 to 1197°C in a gas current (hydrogen, nitrogen and others). Sometimes it is decomposed at reduced pressure without using a carrier gas. Powder efficiency is about 90%. The flow sheet of powder production in hydrogen is shown in Figure 21.13. Crystalline carbonyl is charged into a horizontal sublimator of 'pipe-in-pipe' type with exterior heating. After sealing, the system is cleaned out by pure nitrogen. In the sublimator, carbonyl is heated up to temperatures ranging from 57 to 127°C and its vapor is carried by preheated and purified hydrogen to a decomposition unit provided with electroheating. Carbonyls are decomposed at temperatures ranging from 347 to 397°C. The powder is collected in a container.

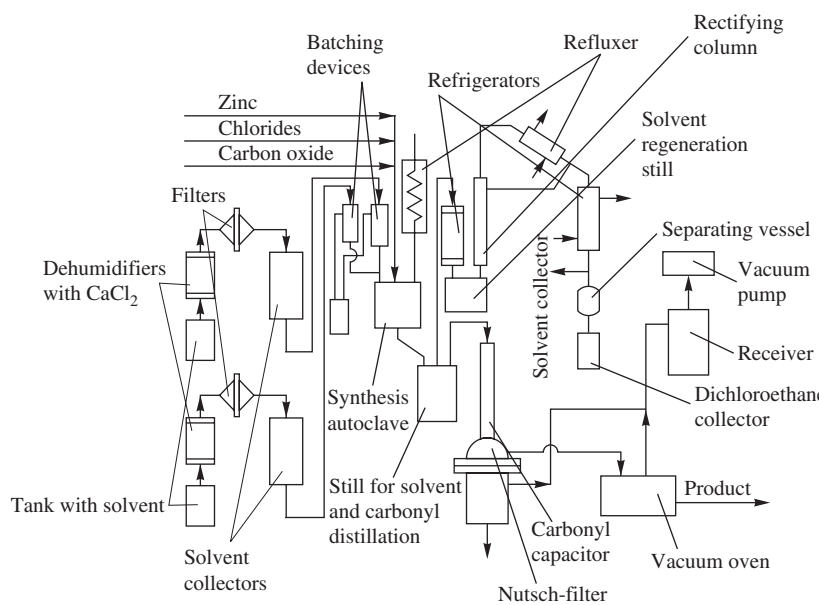

Figure 21.12 Diagram of plant for tungsten and molybdenum carbonyl synthesis in solvent media.

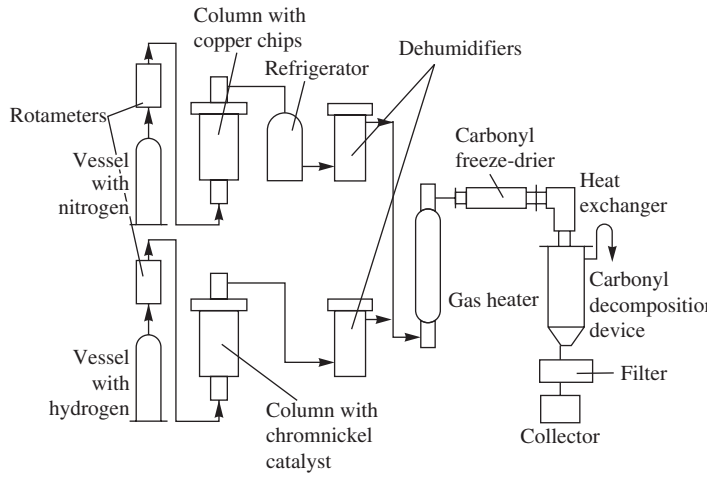

Figure 21.13 Flow sheet of powder production by carbonyl decomposition in hydrogen current.

Tungsten powder efficiency is 94%; molybdenum powder efficiency is 86%.

More detailed information on the carbonyl process is contained in Chapter 7.

Properties

Tungsten has two outstanding properties: the highest melting point of all metals at 3410°C and a very high density of 19.25 at 20°C [9]. It cannot be shaped by traditional casting techniques. Consolidation of tungsten powders is based almost exclusively on powder metallurgical methods. Therefore, definite and detailed powder specifications are very important in order to obtain the required final properties of a consolidated tungsten product. These specifications include physical and chemical properties.

The basic physical properties are particle size, flow rate and different powder density values. All the powder sizes, from ultrafine to hundreds of microns, are produced on an industrial scale, but the bulk of the powder used at present is in the size range 2–5 μm.

Particle sizes in the range from 1 to 10 μm are measured by Fisher subsieve sizer (FSSS) (ASTM B 330 and MPIF 32 standards) [10] and correspond to particle sizes observed directly by optical microscopy (OM) (MPIF E 20 and GOST 23402-78 standards) and by scanning electron microscopy (SEM). SEM and OM are also the best way to estimate the overall particle morphologies. Particle size distributions can be measured by light scattering techniques (ASTM B 822 standard [11]) or by sedimentation based on X-ray monitoring of gravity sedimentation scattering (sedigraph) (ASTM B 761 standard [11]). Controlling the reduction parameters makes possible the production of both narrow or wide size distribution and to provide any specific requirement on tungsten powders for various applications.

Apparent density (ISO 3923 standard and in accordance with it ASTM B 212, MPIF O4 and GOST 19440 standards), tap density (ISO 3953 standard and in accordance with it is accepted in ASTM B 527, MPIF 46, and GOST 25279 standards) as well as green density and green strength have great importance for determining the behavior of a powder during subsequent consolidation steps, including pressing and sintering.

A feature of tungsten powder is a relatively very high purity, in comparison with most other metal powders used for powder metallurgical products. Table 21.1 contains analytical data of typical tungsten powders produced by hydrogen reduction. Trace elements, including molybdenum, aluminum, arsenic, silicon, phosphorus, sodium, potassium, calcium, magnesium and sulfur are removed during ammonium paratungstate manufacture. The contaminants, such as nickel, chromium, iron and cobalt, characteristic alloying elements of reduction boats or furnace tubes, have to be avoided

Physical analyses of typical medium sized tungsten metal powders are given in Table 21.1. The characteristic morphology of the tungsten powders produced by hydrogen reduction is shown in Figure 21.14. The particles have angular prismatic shape in either coarse or submicrion sizes.

The powders reduced by solid carbon with characteristic particle size ranging from 1 to 10 μm include oxide 0.10–0.15 wt% and carbon under 0.5 wt% at stoichiometric carbon black consumption. Apparent density ranges between 3 and 7 g/cm^3. Such powders may be used in hard alloy manufacture to produce tungsten carbide.

Table 21.1 Properties of typical tungsten powders produced by conventional calcination/reduction process

Property	Unit	Source. Standard grades						
		WBH	OSRAM					
		2–5 µm	W 06	W 10	W 15	W 25	W 35	W 45	W 65
Particle sizes FSSS								
As supplied	µm	3.27	0.6 ± 0.1	1.0 ± 0.1	1.5 ± 0.2	2.5 ± 0.3	3.5 ± 0.3	4.5 ± 0.3	6.5 ± 1.0
Lab milled	µm	2.93	0.5 ± 0.1	0.8 ± 0.1	1.4 ± 0.2	2.4 ± 0.3	3.3 ± 0.3	4.2 ± 0.3	3.5 ± 1.0
Scott density	g/cm^3	3.17	2.0 ± 0.2	2.5 ± 0.3	2.8 ± 0.3	3.3 ± 0.3	4.0 ± 0.3	4.5 ± 0.4	4.7 ± 0.5
Tap density	g/cm^3	...	3.8 ± 0.3	4.4 ± 0.3	4.8 ± 0.3	5.2 ± 0.4	6.0 ± 0.4	6.3 ± 0.5	6.5 ± 0.8
Tungsten min. excluded oxygen	wt%	...	99.98		99.95				
			typ. virgin[a]	guar. virgin	typ. reclaimed[b]	guar. reclaimed			
Trace impurities:									
Aluminum	ppm	2	<20	<25	<20	<20			
Calcium	ppm	<2	<5	<10	<10	<15			
Carbon	ppm	11	...	...	...	...			
Chromium	ppm	<10	<5	<5	<5	<5			
Cobalt	ppm	...	<5	<20	<100	<100			
Copper	ppm	<2	<5	<5	<10	<15			
Iron	ppm	12	<20	<25	<20	<30			
Lead	ppm	...	<5	<5	<5	<5			
Magnesium	ppm	<1	<5	<5	<5	<5			
Manganese	ppm	...	<5	<5	<5	<5			
Molybdenum	ppm	<20	<50	<100	<150	<200			
Sodium	ppm	9	<5	<10	<10	<15			
Nickel	ppm	<5	<10	<15	<5	<15			
Oxygen	ppm	210	800	800	800	800			
Phosphorus	ppm	<20	...	...	...	...			
Potassium	ppm	<4	<5	<5	<5	<10			
Silicon	ppm	<10	<20	<20	<30	<30			
Sulfur	ppm	...	<10	<10	<20	<20			

[a]Tungsten powder made from tungsten ore;
[b]Tungsten powder made by recycling sintered carbide scrap; Companies: Wolfram Bergbau- und Hütten- GmbH; OSRAM: OSRAM Bruntál spol. s r. o.

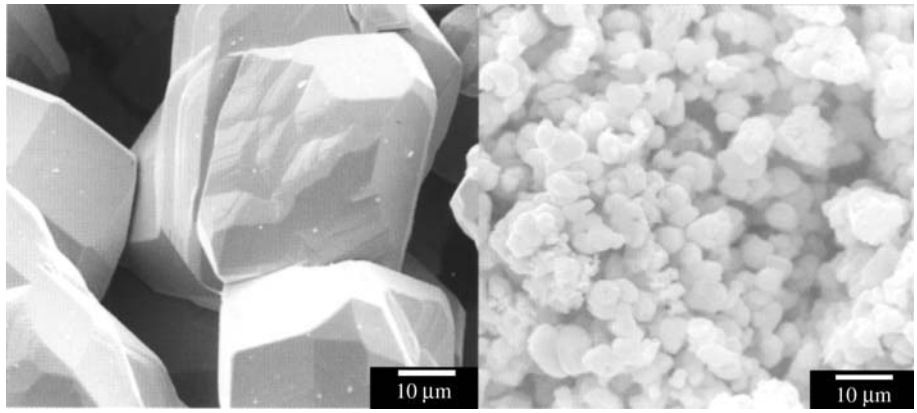

Figure 21.14 Scanning electron micrographs of coarse and submicron tungsten powders produced by hydrogen reduction.

Table 21.2 Composition of typical tungsten powders produced by reduction of highest halides

Property	Unit	Technique [6]		
		LTF	LTHL	HTF
Average particle size	µm	0.8	0.1	0.2
Trace impurities:				
Aluminum	ppm	...	...	14
Arsenic	ppm	...	...	80
Calcium	ppm	30	...	12
Chromium	ppm	...	7	...
Fluorine	ppm	130	...	900
Iron	ppm	1500	600	130
Magnesium	ppm	10	20	...
Manganese	ppm	30	5	...
Molybdenum	ppm	...	320	1300
Oxygen	ppm	200	6500	...
Silicon	ppm	10	60	300
Titanium	ppm	100	...	...

LTF: Low temperature dissociation by reduction of tungsten hexafluoride in hydrogen; LTHL: low temperature dissociation by reduction of tungsten hexachloride in hydrogen; HTF: high temperature decomposition of tungsten hexafluoride in hydrogen fluoride medium.

Tungsten powders obtained by precipitation from the gaseous phase of tungsten hexafluoride and tungsten hexachloride (reduction of highest halides) with particle sizes between 0.05 and 0.80 µm and roundish shape are of high purity (Table 21.2) and differ significantly from tungsten powder reduced from oxides.

Tungsten powders produced from WF_6 in hydrofluoric medium and by WO decomposition in hydrogen jet are finer than particles produced by high temperature WF_6 dissociation or by high temperature treatment of preliminary chlorinated wastes. High content of oxygen in some 'gas-phased' powders is caused by their high absorption properties in wet air.

Properties of carbonyl powders are shown in Table 21.3. Tungsten and molybdenum powders produced at decomposition temperature 347–397°C in hydrogen are represented by 60–70% of particles with round shape with rough and sharp spurs on the surface (Figure 21.15). Tungsten powders include up to 2.0% of oxygen.

Particles of tungsten and molybdenum powders reduced at temperatures in the range from 397 to 997°C in an argon current are spherical, non-uniform in size, especially at low decomposition temperatures. The surface of molybdenum particles is comparatively smooth; the surface of tungsten particles is

Table 21.3 Variation of properties with decomposition temperature for carbonyl tungsten powders

Decomposition temperature in current of argon (°C)	Color of powder	Average particle size (μm)	Specific surface area (m^2/g)	Carbon content (wt%)	Lattice spacing (nm)
400	gray	1.2	0.18	1.08	0.4178
500	gray	1.0	0.21	1.00	0.4172
600	dark-gray	0.74	0.30	1.50	0.4167
700	black	0.12	1.56	1.83	0.4163
800	black	0.07	3.00	1.82	0.4159
900	black	0.03	8.20	...	...
2000–3970	black	0.01–0.03	...	0.50–1.00	...

(a) SHF-discharge in nitrogen current.

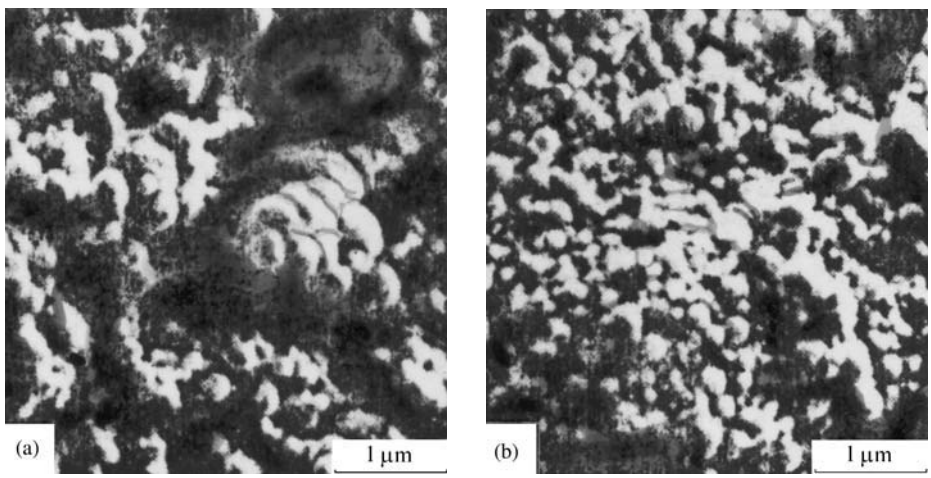

Figure 21.15 Scanning electron micrographs of (a) carbonyl tungsten and (b) molybdenum powders.

uneven and includes some separate spheroids. The particles become significantly less in size and specific surface increases on increase of the decomposition temperature from 397 to 997°C; for example, for tungsten powders, average size decreases from 1.2 to 0.03 μm, specific surface increases from 0.18 to 8.2 m^2/g, respectively. Carbon content in tungsten powders obtained in argon is 1.9 wt%, in molybdenum powders it amounts to 3.5 wt%. The addition of an oxidizing component to the carrier gas decreases the carbon content in the powder.

Sintering temperature of carbonyl tungsten and molybdenum powders are some hundreds of degrees lower than that of powder produced by other methods. They are used for the production of porous and compact parts by powder metallurgy.

Metal carbides, e.g. ZrC and other abrasive materials such as boron nitride, can be coated with tungsten or molybdenum by thermal decomposition of their carbonyls resulting in improved performance in service. For example, the hardness of cutting wheels of 'el'bor borazon' material (cubic boron nitride) metallized by tungsten is increased twofold. Diamond grains metallized by tungsten increase their cohesion in instrument assembly, preventing diamond chipping. Other methods of abrasives metallization are not very effective as they do not provide good coating cohesion.

The quantity of carbon and oxygen in the powder depends first of all on the process conditions in its production. Peak of carbon content is observed at about 697°C connected with free amorphous carbon formation because of catalytic decomposition of the carbon oxide. Carbon content can be decreased by a process of carbonyl $W(CO)_6$ decomposition in superhigh frequency discharge at temperatures ranging between 2730 and 3730°C in a nitrogen current. The particles have spherical shape and size ranges from 12 to 30 nm; nitrogen content is 0.3 wt% and oxygen content is not more than 1 wt%. Content of

other impurity elements does not exceed the value 1.0×10^{-4} wt%.

Carbonyl tungsten powders are metastable carbides with a face-centered cubic lattice. Their properties are changed with increasing temperature: lattice spacing decreased (see Table 21.3).

Powders obtained by plasma-chemical reduction are characterized by high dispersivity: particles of average size about 0.07 μm form weak conglomerates with developed specific surface and very low apparent density of 0.25 g/cm^3. When first produced, a large quantity of hydrogen chloride is absorbed on the surface which volatilizes during storage in air, while the oxygen concentration is increased to 4–8%.

Nanopowders of approximately 20 nm average particle size are produced by melt atomization in arc argon plasma. Tungsten particles of 510 nm sizes have face-centered or hexagonal close-packed lattice in comparison with typical body-centered for solid state.

Tungsten powders obtained by high temperature reduction in argon-hydrogen plasma represent double component systems consisted from α-W (body-centered lattice) and β-W (A-15) with main peaks (210) of β-phase and (110) of α-phase.

Tungsten Powder Applications

Ultrahigh purity powders are used for semiconductor manufacture. In particular, the incorporation of alpha emitters, such as uranium and thorium, are extremely crucial and must be held below 1 ppb. The mobile alkali ions, for instance sodium and potassium, have to be held below 0.1 ppm. Purification of APT by means of multiple extraction and crystallization steps ensures the required purity, where all production steps must be carried out in clean room conditions [5,12].

Pure tungsten powders. Pure tungsten powders are made into rods by pressing and sintering. In order to achieve high densification, a high temperature in the range 2500–3100°C is required [1,5]. The sintered tungsten bars thus obtained are forged or rolled at elevated temperatures in order to produce rods, which are subsequently drawn to manufacture wires, or sheet. Such pure tungsten materials are widely used for high temperature applications, for example in high-temperature furnace parts [1,5]. For these materials the powders produced by the highest halides reduction can be used.

Non-sag tungsten wires. To prevent sagging of tungsten filaments in incandescent lamps during high temperature operation, doping elements – aluminum, silicon and potassium – are included in the powder [1,13]. The present technique consists of addition of aqueous solution of compounds containing aluminum, silicon and potassium, into the tungsten oxide powder before reduction to tungsten metal. During this reduction, some part of the above trace elements is enclosed into the tungsten metal powder particles. In the sintering of the pressed tungsten powder, aluminum and silicon evaporate, while the potassium atom is too big to diffuse through the tungsten lattice.

This process results in the incorporation of potassium droplets as inclusions. During the wire drawing, the small potassium droplets are elongated and finally break into a multitude of little tiny potassium bubbles in lines along the wire axis, which results in an elongated interlocked grain structure. During recrystallization at elevated temperatures, the tiny potassium bubbles stabilize effectively by an effect similar to dispersion hardening, the movement of dislocations and thus the migration of the grain boundaries perpendicular to the wire axis. The large inclusions in the metal particles generate large potassium pores in the sintered ingot from which long bubble rows are formed in the wire. This characteristic structure explains the non-sag properties of the tungsten filaments in incandescent lamps [1,5, 3–16].

Tungsten composite materials. Tungsten metal powder blended with other powders, such as copper, iron, cobalt and nickel, form so-called 'tungsten heavy alloys' (WHAs), which typically contain 90–98 wt% W and can be liquid phase sintered at about 1500°C. Their properties include high density (17–19 g/cm^3) and ductility, energy penetration and radiation shields are the application fields of tungsten materials [5]. WHAs are typically formulated from elemental powders with mean particle sizes in the range from 1 to 7 μm.

Because of exclusive high melting temperature of tungsten, PM methods of manufacture of such materials are predominantly used.

Infiltration (INF) is used exclusively for making tungsten base composite contact materials. Refractory metal powder is first blended to the desired composition with or without a small amount of binder to impart green strength, then is pressed and sintered into a skeleton of the required shape. Silver or copper is next infiltrated into the pores of the skeleton. This technique produces the highest density composites, generally 97% or more of theoretical density. Because of the presence of some closed pores in the sintered skeleton complete densification is not possible.

The press-sinter method can be used for small refractory metal parts (not exceeding about 25 mm in diameter). A high density material is obtained by

pressing a blended powder of the exact final composition into shape and then sintering it at the melting point of the low-melting-point component (liquid-phase sintering). In some cases, an activating agent such as nickel, cobalt or iron is added to improve the sintering effect on the refractory metal particles. For this process, powders of much finer particle size are preferable so that more bonding surface exists. However, material formed by this process is weaker in comparison with the infiltration process.

The press-sinter-re-press (PSR) process is used for all categories of contact materials, especially the silver-based kind. Blended powders are compacted to the desired shape and then sintered. The materials are further densified by a second pressing (re-pressing). Sometimes the properties can be modified by a second sintering or annealing. The flexibility of this process makes it applicable to parts of any configuration and of any material. However, it is difficult to produce, by merely re-heating the sintered material, a product with as high density as is possible by the press-sinter-re-press process. Material thus produced may also have weaker bonding between particles.

The first heavy alloy developed was a W–Ni–Cu alloy. Alloys of this ternary system are still now used occasionally, mainly for applications in which ferromagnetic character and resistance must be minimized. However, the present industry standard W–Ni–Fe exceeds the above alloy in corrosion resistance and mechanical properties. Most of the current purposes for WHAs are best satisfied by the W–Ni–Fe system. Alloys such as 93W–4.9Ni–2.1Fe and 95W–4Ni–1Fe represent common compositions. Mechanical properties depend on the nickel to iron ratio. They are sensitive to hydrogen embrittlement due to the body-centered cubic (bcc) structure of the principal tungsten phase [17]. By means of the nickel to iron ratio selection and post-sinter heat treatment, optimal mechanical properties are obtained. There are two common post-sinter heat treatments for WHAs. Vacuum heat treatment is useful for the reduction of hydrogen embrittlement, so is resolution and quench for reduction of segregation-induced embrittlement. If alloys are subjected to vacuum heat treatment, nickel to iron ratios in the range 2.3–4 should be chosen, as better mechanical properties are generated [18,19]. For example 91W–6.3Ni–2.7 Fe alloy ensures ultimate tensile strength of 940 MPa, elongation of 35% and hardness of 29 HRC.

The addition of cobalt to a W–Ni–Fe alloy is a common approach for a slight increase of both strength and ductility. The presence of cobalt provides solid solution strengthening of the binder and slightly enhanced tungsten-matrix interfacial strength. Even higher mechanical properties are attainable from the W–Ni–Co system with nickel to cobalt ratios ranging from 2 to 9 [20]. These alloys provide high static tensile strength, ductility and hardness, e.g. for 91W–6Ni–3Co alloy, ultimate tensile strength is 960 MPa, elongation is 40% and hardness is 31 HRC. The use of such alloys is generally limited to defense applications requiring advanced mechanical properties.

A number of other special WHAs are known too. An example is an addition of molybdenum to the W–Co–Ni–Fe quaternary alloy to restrict tungsten dissolution and spheroid growth, resulting in higher strength, but reduced ductility, in the sintered state.

The addition of boron in the form of NiB and FeB to W–Ni–Fe system alloys leads to a small increase of hardness in some cases, in particular for W–7NiB–3Fe and W–7NiB–3FeB compositions [21]. The sintering temperature selected for these alloys was 1500°C.

A porous skeleton of pressed tungsten metal powder infiltrated with copper alloys or silver forming W–Cu as well as W–Ag composites are widely used as electrical contacts [22–24] due to their high electrical conductivity, low thermal coefficient of expansion and their resistance to damage caused by electrical arc formation.

Many researches have tried to obtain W–Cu alloys of full density without sintering additives by use of fine tungsten powder and increasing the homogeneity of the W–Cu powder in order to facilitate rearrangement of tungsten particles in liquid copper during liquid phase sintering [25,26]. By mechanical alloying of W/Cu or tungsten oxide and copper oxide, homogeneous W–Cu composite powders with nano-sized tungsten particles can be produced and fully densified specimens fabricated.

A mechano-thermo-chemical process using the liquid solution as starting material and a grinding process using salt-free oxide powder makes possible the production of ultrafine, homogeneous W–Cu composite powders [27]. The spheroidal composite W–Cu oxide powder is produced by spray drying an aqueous solution of tungsten and copper salts and subsequent oxidation. The spheroidal structure of the oxide powder is destroyed during ball milling and W–10 wt% Cu composite with nano-sized particles is produced by reduction of the ground oxide powder at 700°C in hydrogen. But, as the copper content in W–Cu composite powder decreases, densification of W–Cu powder compacts is difficult due to pore formation by local densification in agglomerated powders. W–10 wt% Cu-based oxide powders with tungsten trioxide addition before reduction sintered at 1400°C in hydrogen can achieve a sintered density of 17.05 g/cm^3, which amounts to 98.5% of theoretical density. The thermal and electrical conductivities of such a composite are 203 W/(m°C) and 36.5%IACS, respectively [27].

To fabricate the tungsten–copper nanocomposite powder, the tungsten–copper oxide mixture ball-milled in argon was reduced at low temperature of 300°C [28]. The reduced W–Cu nano-composite powder was consolidated at 1200°C for 1 h with a heating rate of 10°C/min.

It has been shown recently that porous tungsten can be obtained at approximately 1200°C, much lower temperatures than the 2000°C used in the conventional process. This has been achieved by employing the concept of reactive sintering. The method makes use of the addition of aluminum, the low melting phase of which decreases the process temperature while acting as a potential sintering aid. As a result higher homogeneity and uniform porosity distribution have been obtained [29].

The high-energy ball milling is a well known technique for producing of oxide-dispersion strengthened materials. Moreover, due to activation of a material during grinding without oxide and metal powder admixtures this method has essential advantages [30–32]. It makes the sintering stage easier and that results at both higher rate and lower temperature. The reduced size of mechanically ground particles and their high density in lattice defects promote the sintering transport phenomena. It also leads to finer and more homogeneous oxide dispersion. The latter feature together with the nanocrystalline structure of the ground powders results in a small grain size after sintering. As reported [33], long milling times of the order of 30 hours of W–1 vol% Y makes it possible to reach a relative density of 96.5% after sintering for 4 hours in vacuum at 1800°C, while within a milling time of 80 minutes, the relative density amounts only to 76.5%.

Recent developments [34,35] define the production of W/Cu composite powders which can be directly pressed to shape and sintered, thus without infiltration or machining, which is of particular importance with respect to the application as heat sink in the semiconductor industry.

Tungsten with oxide dispersions is manufactured with the addition of thorium-containing compounds, such as thorium oxide or thorium nitrate. The mixes consisting of tungsten metal powder and the above additives are pressed, sintered and further processed to wire or sheet. The main application of this material are welding electrodes which, due to the high electron emission ability of thorium, ensure easier arc formation and its stabilization and improved physical properties arise from dispersion hardening in sheets and wires, in particular for vibration resistant automotive lamps [1,5]. Because of the radioactive danger of thorium, alternatives have been developed. Cerium and lanthanum have been tried as potential candidates to replace thorium in welding electrodes.

Properties of typical tungsten based composites are shown in Table 21.4.

Recovery of Metallic Tungsten

Virtually almost all types of tungsten products, if available in large enough amounts and workable, are recycled at present [2,5]. Even unselected low quality scrap containing enough tungsten can be used as a feed material for the chemical ammonium paratungstate production process, electrochemical recovery, or for alloying in steel. But, any option or possibility to use selected tungsten scrap if practicable is, of course, desirable for economic reasons. Typical kinds of tungsten scrap include:

- Selected manufacturing scrap of pure tungsten can easily be crushed in high energy mills and directly re-used for applications with lower quality demands.
- Chips of heavy metal, obtained during the shaping operations, can be transformed into re-usable powder by means of oxidation and subsequent reduction. Large solid pieces can be machined into smaller pieces to enable subsequent recycling. The oxidation step leads to a total disintegration of the chips into oxide powder containing tungsten trioxide and tungstates of iron, nickel or cobalt. Hydrogen reduction resulted in a metal powder; in which all the components (W/Fe/Co/Ni) of the initial heavy metal are present.
- Composite scrap mixtures, such as W/Cu, are difficult to oxidize and are therefore not suitable for chemical recycling. Also, re-using in the steel industry cannot be realized due to the deleterious effect of copper in steel. A possible option is salt melt digestion with sodium nitrate, sodium nitrite and sodium carbonate mixtures. However, this process has environmental problems due to the nitrogen oxide formation. An alternative would be the electrochemical recovery of the tungsten.
- The slimes recovered from grinding of high-speed tool steel, such as containing up to 6 wt% tungsten, are de-watered by hot air and oxidized in a tube furnace in oxygen (0.05 m/s) with self-heating up to 947°C. The oxides are vaporized at a temperature higher than 1397°C and condensed on cold screens. Tungsten extraction yield reaches up to 86% after 6 hours at 1347°C. The condensate from tungsten and molybdenum oxides are reduced

Table 21.4 Properties of typical tungsten base composites

Nominal composition (%)	Manufacturing method[a]	Density (g/cm^3)		Electrical conductivity (% IACS)	Hardness	Tensile strength (MPa)	Modulus of rupture (MPa)	Data source[b]	Application examples
		Calculated	Typical						
Tungsten carbide-silver									
65Ag–35WC	INF	11.86	11.53–11.85	55–60	50–65 HRB	272	483	C, A	Aircraft contactors, lighting
60Ag–40WC	PSR	12.09	11.40–11.92	46–55	60–70 HRB	. . .	. . .	A	relays, low-voltage
50Ag–50WC	INF	12.56	12.12–12.50	43–52	75–83 HRB	276	793	C, A	switches, circuit breakers
40Ag–60WC	INF	13.07	12.0–12.92	40–47	90–100 HRB	379	827	C, A }	Heavy-duty
38Ag	INF	13.18	12.92–13.29	35–38	90–100 HRB	552	. . .	C . . }	circuit breakers
20Ag–80WC	PSR	14.23	13.2	19	400 HV[c]	. . .	. . .	M . . .}	Semiconducting material
Tungsten-copper									
50Cu	INF	11.39	11.0–11.27	42–47	90–100 HRB	. . .	1103	C, A	Arcing contacts in oil,
44Cu	INF	11.77	11.64	43	99 HRF	. . .	1241	C	wiping shoes in power
30Cu	INF	12.78	12.65	30	38 HRC	. . .	. . .	. . .	transformers
Ternary alloys									
91W–6.3 Ni–2.7Fe	PSR	. . .	. . .	. . .	29 HRC	940[c]	. . .	[20]	Defense applications
91W–6Ni–3Co	PSR	. . .	. . .	. . .	31 HRC	960[d]	. . .	[20]	

[a]INF, press-sinter-infiltrate; PSR, press-sinter-repress (blended powder of the desired composition are compacted to the required shape and then sintered. Afterwards, the material is further densified by a second pressing. Sometimes the properties can be modified by a second sintering or annealing);
[b]A: Advance Metallurgy, Inc., McKeesport, PA. C: Contacts, Materials, Welds, Inc., Indianapolis, IN. M: Metz Degussa, South Plainwille, NJ;
[c]elongation 35%;
[d]elongation 40%.

in hydrogen for 2 hours at 900°C. This yields powders with average particle size 15 μm and containing: 50 wt% tungsten, 50 wt% molybdenum, 0.02 wt% vanadium, 0.02 wt% chromium and 0.1 wt% iron.

- The process of recovery of tungsten bearing wastes includes following steps: oxidation in hot air; milling of formed mixture of tungsten oxide and cobalt–tungsten oxide; reduction at $T < 947$°C in endo-gas or dissociated ammonia with an addition of natural gas.
- The recycling of composites of tungsten with thorium-containing compounds has problems due to the radioactive radiation. Therefore, direct recycling in the steel industry is impossible. Chemical recovery in the conventional process leads to inadequate separation of thorium and is consequently also not applicable. At present, the only possible way to recycle this material is by electrolysis, such as one based on the electrolytic dissolution of tungsten in ammonia [36]. The difficulty is to carry out the process in such a way as to prevent dissolution of any of the radioactive products.

Accident Prevention when Working with the Powder

Metallic tungsten dust is not toxic and ranked in the fourth category according to State Standard 12.1.005-88 under the legislation in the Commonwealth of Independent States (CIS) [37]. Tungsten inspirable dust takes a predominantly fibrous effect. The limit for dust in the atmosphere of the work place unhealthy is 6 mg/m^3. Tungsten in drinking water is also unhealthy and falls into the second category. A limiting value of 0.05 mg/L is specified in CIS State Standard 4630–88 [38].

Fine oxidizable powder mixed with air can constitute an explosion hazard, but the risk with tungsten powder is minimal even with powder fraction $\leq$74 μm; a minimal ignition temperature of powder deposits (self-ignition temperature) is 310°C. The products with such characteristics of inflammability and explosion risk are relegated to the 'Low explosion hazard' class of danger according to the Guide to Legislation and 'Health and Safety' in the European PM Industry [39].

Common techniques are mainly used for pollution prevention and environmental control during powder manufacture and its processing. Detailed information on health and environment protection measures also on the prevention of inflammability risk in such conditions can be found in Section 5.

Tungsten Carbide Powder

Tungsten carbide powder is the base for the production of cemented carbides, the vast class of hard, wear resistant, refractory materials in which the hard carbide particles are bound together, or cemented, by a soft and ductile metal binder. Conventional manufacturing of tungsten carbide powders accounts world-wide for the bulk of the tungsten carbide powder produced. This technique permits the production of tungsten carbide powders with particle sizes ranging from 0.15 to 50 μm [40]. This field offers products for almost all industrial applications and is described below along with other methods.

Production

Conventional technique. There are two methods by which tungsten carbide powders are produced from the pure tungsten powder. In the first method, fine tungsten powders are blended with high purity carbon black, filled into graphite boats and pushed through a high temperature furnace under hydrogen at temperatures between 1400 and 1500°C. Compared to the reduction step for tungsten, temperatures are much higher and single tube pusher type furnaces (Figure 21.16) are used. Each particle is composed of numerous tungsten carbide crystals. The particle size of the tungsten carbide powder (Figure 21.17) for the most part preserves the particle size of the tungsten metal powder (see Figure 21.14). Further, cooled caked tungsten carbide powder is de-agglomerated. This step just separates particles from

Figure 21.16 Single tube push type furnace for tungsten carbide powder production. Courtesy: Wolfram Bergbau- und Hütten-GmbH.

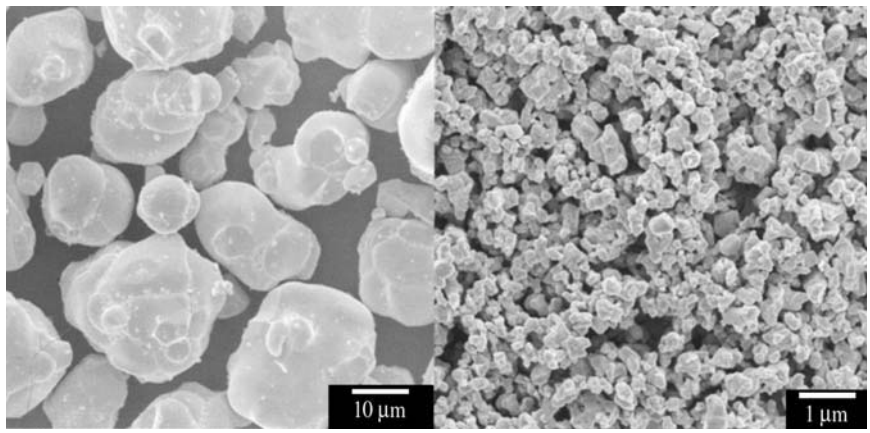

Figure 21.17 Scanning electron micrographs of coarse and ultrafine tungsten carbide powders. Courtesy: Wolfram Bergbau- und Hütten-GmbH.

sticking to each other and is not used to change the particle size. This process, including the ore processing steps, is also called the conventional calcination–reduction–carburization (CRC) process and offers the potential to manufacture commercial WC ultrafine powders with median grain sizes below 0.5 µm. Strict process control and a high degree of automation permits greater uniformity and batch to batch reliability to be achieved [41].

This process is unsuitable for the production of coarse-grained powder. Techniques of the former conventional tungsten carbide production are usually limited during carburization to temperatures around 2000°C. At these temperatures, carburization with tungsten powder with particles less than 100 µm can be achieved, but the resulting product is polycrystalline.

By the latter, the increase of tungsten carbide single crystals is realized by the use of a liquid phase, which is able to dissolve both tungsten and carbon. The formation of tungsten carbide within the melt of solvent metal, such as iron, is the basis of the Menstruum process, also called 'macro process' [42]. The powder mixtures of tungsten ore concentrates, iron oxide, aluminum, calcium carbide and/or carbon react exothermally (after ignition by a detonator) to generate tungsten carbide, iron, calcium oxide and aluminum oxide. A high temperature exothermic reaction ($2Al + 3FeO \leftrightarrow Al_2O_3 + 3Fe$) at about 2500°C produces a molten mass that, when solidified, consists of tungsten carbide crystals dispersed in iron and a slag containing impurities. This technique permits complete reduction and carburization of a batch of about 22 tonnes of tungsten carbide, which is achieved in 60 minutes. To get the tungsten carbide in powder form, the solidified solvent metal is dissolved, which is ordinarily done with hot hydrochloric acid. Separation of the obtained tungsten carbide powder according to desired particle size is done by sieving. Menstruum tungsten carbide powders have a high yield of well faceted single crystal particles with sizes of 400 µm and below.

Production of fine grained powder. Recently, the demands for tungsten carbide powders finer than 1 µm are increasing as material for precision tools such as drills and end mills for metal cutting, printed circuit boards, cutters and precision pins and so on. Together with the limitation of the conventional technique concerning the efficiency of fine grained metal powder production [43], there has been a strong motivation to develop alternative techniques.

Tokyo Tungsten Co. Ltd has developed [44] the direct carburizing process, where tungsten trioxide and carbon black react in the following steps:

$$WO_3 \rightarrow (WO_{2.9}) \rightarrow (WO_{2.72}) \rightarrow WO_2 \rightarrow W \rightarrow W_2C \rightarrow WC$$

at the $(WO_{2.72}) \rightarrow WO_2$ step, ultrafine particles are generated and then transformed into tungsten carbide without grain growth. The starting material is prepared in the form of pellets from a mixture of tungsten oxide with carbon black. Subsequent reaction is accomplished in rotary furnaces in two steps: first the direct reduction of the WO_3 to tungsten by carbon under nitrogen, followed by carburization under hydrogen at temperatures up to 1600°C to tungsten carbide powder.

This method permits the production of ultrafine powder with particle sizes ranging from 0.1 to 0.7 µm. Vickers hardness, HV (50 kg) decreases from

2150 to 1900 with increasing particle size from 0.1 to 0.3 μm.

Another direct carburization process has been developed by Dow Chemical Company [45,46]. A mixture of tungsten trioxide and carbon black falls through a vertical reactor at temperatures of approximately 2000°C. Accordingly, the reaction time is a few seconds and results in the formation of an intermediate mixture of W, W_2C, WC and C. This product has to be subjected to a second more conventional, carburization step. Particle sizes were reduced by controlling the milling time, carbon content, inhibitor addition and sintering temperature. The characteristic particle size range for this process is between 0.1 and 0.8 μm, which is identical to the lowest limits of the conventional process [43].

The spray conversion process has been developed for Nanodyne Inc. [47] to produce nanopowders. Aqueous solutions of tungsten and cobalt salts are spray dried, subsequently reduced and carburized with a gas mixture such as hydrogen and ammonia or carbon dioxide and carbon monoxide in a fluidized bed reactor. The product obtained is relatively large, about 75 μm, hollow WC–Co composite powder particles, which consist of tungsten carbide crystallites with a particle size of about 30 nm. This product is milled in order to obtain a powder suitable for consolidation.

Another technique to produce tungsten carbide nanopowders is a chemical vapor reaction process [48]. This process is based on the gas phase reaction of metal halides with different gas mixtures to produce nano-sized powder ranging from 5 to 50 nm. Production of tungsten carbides is possible in principle; however, the process seems to be better adapted to the production of nitrides or carbides of other group IV and V refractory metals.

Properties and Applications

High hardness is one of the most important properties of pure tungsten carbide and is the basis for the application in hard metals, also called 'cemented carbides'.

Hard Metals

Production of Grade Powders

Optimal interfacial bonding in hard metals is achieved by means of optimization of balance between the high hardness of the tungsten carbide and the high toughness of a ductile binder metal, such as cobalt, nickel, or iron [49,50]. The steps of hard metal manufacture include: blending of grade powders, milling, powder consolidation, liquid phase sintering, post-sintering operations and post-sinter forming. The excellent wetting of tungsten carbide by cobalt is one of the key properties. By variation of the tungsten carbide particle size and the percentage of cobalt, desired properties of the hard metals can be obtained [49–51]. A general rule, moreover, is the finer the carbide and the lower the cobalt content, the harder, but the less tough the composite is. But, higher binder content at a certain hardness (combined with a lower average WC grain size) does not necessarily mean a higher toughness. In particular, in the lower hardness range this relationship does not hold. At the higher hardness range, however, a higher binder can reduce the carbide contiguity and thus improve the hardness to toughness relationship. However, the improvements which can be obtained at a high hardness are obviously limited for hardness above 2000 HV30 [52].

Over the years, the basic WC–Co material has been modified to produce a variety of hard metals, which are used in a wide range of applications, including metal cutting, mining, construction, rock drilling, metal forming, structural components and wear parts. Approximately 50% of all carbide production is used for metal cutting applications.

Additions of other carbides such as titanium, tantalum and niobium, or titanium carbo-nitrides are used in steel cutting grades and are produced from metal oxides of titanium, tantalum and niobium. These oxides in particulate form are mixed with metallic tungsten powder and carbon black. The oxides are reduced under a hydrogen atmosphere or vacuum at elevated temperatures and form solid solution carbides WC–TiC, WC–TiC–TaC, or WC–TiC–(Ta, Nb)C. The menstruum process can be used to produce WC–TiC solid solution. In this method, both carbides are dissolved in liquid nickel, which functions as contributory metal. Solid solution carbides are then precipitated during cooling.

The hard metal powders may consist of tungsten carbide mixed with a finely dispersed metallic binder (cobalt, nickel or iron) or with additions of other above-named cubic carbides, depending on the desired properties and application of the tool. Intensive milling is necessary to disintegrate the initial carbide crystallites and to blend all components such that every carbide particle is coated with binder material. This process is accomplished in ball mills, vibratory mills or attritors, using carbide balls. The mills are usually lined with carbide sleeves; however, mills lined with low-carbon steel or stainless steel are also used.

Grinding is carried out under an organic liquid such as heptane or acetone to prevent oxidation of the powder. After milling, the liquid is distilled off and

the powder is dried. A solid lubricant, such as paraffin wax, is added to the powder mix in the final stage of the milling or subsequently in a blender. The lubricant protective coating prevents or greatly reduces the oxidation of the powder and imparts strength to the powder mix during its consolidation.

In the spray drying process commonly used in the hard metals industry, a hot inert gas such as nitrogen impinges on a stream of carbide particles. Thus, a product in the form of spheroidal powder aggregates is produced.

Powder Consolidation

A variety of techniques is used to compact the hard metal powders to the desired shape. Carbide tools for mining and construction applications are produced by uniaxial pressing as are metal cutting tool inserts, but the latter may require additional shaping after sintering. Rods and wires are formed by the extrusion. Cold isostatic pressing, in which the powder is subjected to equal pressure from all directions, followed by machining, is also in general use for wear and metal forming tools. Unlike most other metal powders, hard metal powders do not deform during the compacting process. Generally, they cannot be compressed to much above 65% of theoretical density. In spite of this, low green density carbide manufacturers have developed the technology for the achievement of good dimensional tolerance in the sintered product.

Sintering and Post-sintering Operations

The first step in the sintering process is the removal of the lubricant from the powder compact. Then the compacts are usually set on graphite trays coated with graphite paint. Using semicontinuous or batch type graphite furnace, the compacts are first heated to about 500°C in a hydrogen atmosphere or vacuum. Subsequent to lubricant removal, the compacts are sintered in a vacuum of 0.1 Pa (or 10^{-3} torr) at a final sintered temperature ranging from 1350 to 1600°C, depending on the content of the cobalt binder and the desired microstructure. This leads the cobalt melt and binds the carbide particles together. Shrinkage of the compact ranges from 17 to 25% on a linear scale and provides a practically pore-free, fully dense material.

In the 1970s, the hard metal industry took advantage of hot isostatic pressing (HIP), where vacuum-sintered material is re-heated under a gas (argon or helium) pressure of 100–150 MPa. The temperatures of this additional process are 25–50°C below the sintering temperature. The high temperatures and pressures employed in the HIP autoclave improve the nearly perfect properties of the hard metal parts by removing any residual internal porosity, pits and flows.

Subsequently, a further advance in sintering technology was the sinter-HIP process, developed in the early 1980s [53]. In this process, low-pressure hot isostatic pressing (up to about 7 MPa) is combined with vacuum sintering and pressure is maintained at the sintering temperature while the metallic binder is still molten. This technique facilitates the production of pore-free products at costs only slightly higher then those of vacuum sintering of the green compacts.

A large number of hard metal parts are machined after sintering because of surface finish, geometry and tolerance requirements. This operation is both time-consuming and expensive. The sintered parts are formed by means of metal-bonded diamond or silicon carbide wheels, turned with a single-point tool, or lapped with diamond-containing slurries.

Other Applications

Hardfacing

Hardfacing is the application of hard, wear-resistance material to the surface of a component by welding, thermal spraying or a similar process for the main purpose of reducing wear. Carbide/metal mixtures very like hard metal compounds are applied to machine parts to improve their resistance. This can be realized by flame or plasma spraying of powders or by welding techniques. Another category of hardfacing techniques is cladding. Hardfacing materials can be clad onto substrates by furnace fusing prearranged layers of loosely bonded hard metal onto the substrate. Cladding can also be done by HIP [54].

Sintered tungsten carbide powders are widely used for thermal spray coatings and torch welding hardfacing. Powder can be a product of crushing bulk WC–Co alloys or specifically made spherical shaped pellets. Tungsten carbide powders for thermal spray coatings usually contain from 6 to 18% cobalt. Particle sizes of WC–Co for thermal spray coatings range from 5 to 150 μm. Powder particle sizes for torch welding hardfacing ranges from 20 μm to 100 μm.

Macrocrystalline tungsten carbide powders are a special kind of tungsten carbide powder manufactured by a high temperature thermit process during which ore concentrate is converted directly to tungsten carbide. This product maintains the correct stoichometric carbon content of 6.13 wt%. Macrocrystalline tungsten carbide is grown in crystals ranging from 1 μm to 5 mm. Coarse mesh sizes of macrocrystalline

carbide are extensively used in abrasion erosion protection applications. The finer size powder is employed as wear rate modifier. Coarse tungsten carbide powder can also be obtained by conventional carburization method. Commercial grade powders such as MAS 2000, MAS 3000 and MAS 5000 are manufactured by H. C. Starck (Newton, MA). Particle sizes of these powders varies from 20 to 50 μm.

Cast tungsten carbide is another category of carbide that also finds wide applications in hardfacing. Cast carbide refers to eutectic of WC and W_2C that can range in carbon content from 3.5 to 4.5 wt%. It is manufactured by melting compounds of metallic tungsten, tungsten carbide and carbon at a temperature above 3000°C. The melt is cast into billets, which are then crushed to the size range of powder. The cast is crushed to powder less than 850 μm and as fine as below 45 μm. Cast carbide, mostly used in torch welding hardfacing, is often used in combination with sintered tungsten carbide and other carbides to enhance wear resistance. At the same time, addition of cast carbide tends to lower toughness coatings.

A relatively new spherical cast tungsten carbide product has all the basic characteristics of crushed cast carbide. However, this material has extremely high wear resistance and higher resistance to chipping and cracking in comparison with crushed cast carbide due to its spherical shape. Spherical cast carbide is manufactured by a technique ensuring rapid solidification of molten eutectic carbide droplets [55].

Electrical Contacts

Tungsten carbide analogous to other refractory metals and their carbides is distinguished by high melting and boiling points and also very high hardness at both room and elevated temperatures, but poor electrical and thermal conductivities and poor oxidation resistance. Forming a composite can compensate for these drawbacks. The development of composite contact materials involving silver with tungsten or molybdenum or their carbides has resulted in materials that can withstand higher currents and more arcing than other contact materials, without experiencing sticking or rapid erosion. Refractory metals, the content of which can vary from 10 to 90%, offer good mechanical wear resistance and resistance to arcing. The silver provides the good electrical and thermal conductivities.

Silver does not alloy with tungsten, molybdenum or their carbides. Therefore, PM processes are used in their manufacture. Depending on the composition, contact materials are accomplished either by pressing and sintering or by the press-inter-infiltrate method. At temperatures above the melting point of the infiltrant, the liquid metal penetrates and fills the interconnecting voids of the pressed and sintered compact. Densities of 96–99% of theoretical can be achieved by this technique. Infiltrated contact materials find use as current-carrying contacts in air- and oil-immersed circuit breakers, heavy-duty relays, automotive starters and switches. Copper infiltrant, which costs less but has very poor corrosion resistance, is used for parts that operate in non-corrosive environments such as oil, vacuum or inert atmospheres. Table 21.5 contains data of typical tungsten and carbide electrical contact grades published by manufacturers which usually include density, hardness and electrical conductivity.

Diamond Tools

Tungsten carbide powder, together with certain metal powders, find an application to adjust the characteristics of alloys in which the diamonds are embedded [49].

Physical and Chemical Properties

A number of physical and technological characteristic values are quite similar to those for tungsten metal powders. A feature of the tungsten carbide powders is the fact that the powder particle structure can be single or polycrystalline. Figure 21.18 illustrates, in diagram form, that tungsten carbide particles with equal particle size may quite well differ concerning the size of the individual crystals within the particles which, depending on the powder manufacturing process, can either be single or polycrystalline. This characteristic has a strong influence on the behavior of the powder during the manufacturing of the hard metal. Generally, the higher the number of subgrains per WC particle, the finer the microstructure of a hard metal can be [2].

SEM and bright field TEM images (Figure 21.19) show the typical morphology and physical constitution of ultrafine tungsten carbide [41]. The boundaries of grains within a single particle are revealed by dotted lines.

Recent developments in the field of standard ultrafine grades were driven above all by the need to control the sinter activity and grain growth tendency of ultrafine carbides. Table 21.6 shows the basic characteristics of standard ultrafine powder grades. Abbreviation CRC symbolizes the milestones of conventional process from tungsten concentrate to tungsten carbide through calcination, reduction and carburization. The values obtained by Fisher subsieve sizer (FSSS), based on the air permeability method of measuring the average particle size of powders, are not absolute and irreproducible in the range of ultrafine powders. It could be shown by scanning

Table 21.5 Properties of typical tungsten carbide electrical contact grades

Nominal composition (%)	Manufacturing method[a]	Density (g/cm^3)		Electrical conductivity (% IACS)	Hardness	Tensile strength (MPa)	Modulus of rupture (MPa)	Data source[b]	Application examples
		Calculated	Typical						
Tungsten carbide–silver									
65Ag–35WC	INF	11.86	11.53–11.85	55–60	50–65 HRB	272	483	C, A}	Aircraft contactors, lighting
60Ag–40WC	PSR	12.09	11.40–11.92	46–55	60–70 HRB	...	...	A	relays, low-voltage
50Ag–50WC	INF	12.56	12.12–12.50	43–52	75–83 HRB	276	793	C, A	switches, circuit breakers
40Ag–60WC	INF	13.07	12.0–12.92	40–47	90–100 HRB	379	827	C, A }	Heavy-duty
38Ag	INF	13.18	12.92–13.29	35–38	90–100 HRB	552	...	C }	circuit breakers
20Ag–80WC	PSR	14.23	13.2	19	400 HV (c)	...	...	M }	Semiconducting material
Tungsten carbide–copper									
50Cu	INF	11.39	11.0–11.27	42–47	90–100 HRB	...	1103	C, A	Arcing contacts in oil, wiping
44Cu	INF	11.77	11.64	43	99 HRF	...	1241	C	shoes in power transformers
30Cu	INF	12.78	12.65	30	38 HRC	...	...	...	

[a]INF, press-sinter-infiltrate; PSR, press-sinter-repress (blended powder of the desired composition are compacted to the required shape and then sintered. Afterwards, the material is further densified by a second pressing. Sometimes the properties can be modified by a second sintering or annealing);
[b]A: Advance Metallurgy, Inc., McKeesport, PA. C: Contacts, Materials, Welds, Inc., Indianapolis, IN. M: Metz Degussa, South Plainville, NJ.

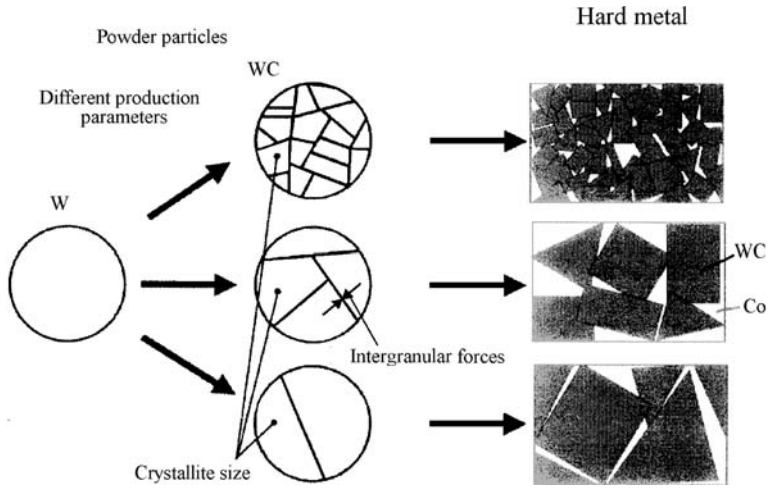

Figure 21.18 Influence of crystalline size of tungsten carbide particles on the microstructure forming of hard metal.

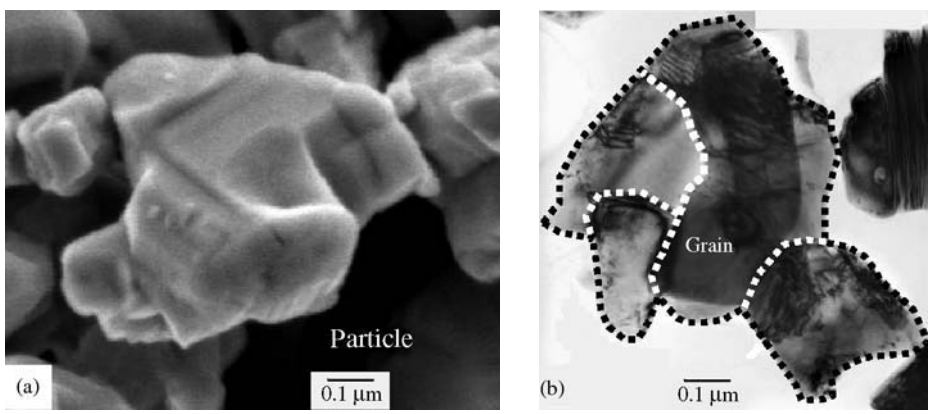

Figure 21.19 Morphology and physical constitution of ultrafine tungsten carbide. (a) Scanning electron micrograph of powder particles; (b) transmission electron microscopy image of single particle. Courtesy: Wolfram Bergbau - und Huttengesellschaft mbH NfG KG, Austria.

electron microscopy that obtained FSSS particle sizes are overstated by two to three times in comparison with reality [43,54]. While with field emission secondary electron microscopy (FESEM) particle sizes are slightly higher than calculated by BET (Table 21.6) because the surface roughness may give a high surface area measurement, leading to the wrong conclusion, that they are finer. In turn, an arithmetic mean FESEM particle size, calculated according to Eqn (c) in Table 21.6 used for particle size distribution:

$$\varphi(d) = \frac{\sum_{d_i}^{d_j} d}{\sum_{d_1}^{d_N} d}$$

where $\sum_{di}^{d_N} d$ the sum of particle diameter of all measured particles N (µm) does not represent reliable weight particle distribution. In consequence of cubic dependence of particle volume on its size, the weight distribution will be levelled by FESEM particle size distribution calculated by the sum of particle diameters. In reality, for example, if powder particle size boundaries ranged from 0.05 to 1.0, the linear particle sizes differ by 20 times, while their volumes differ by 8000 times. Thus the average FESEM particle size may be understated.

A higher fines yield can be advantageous in order to increase the sinter activity/densification rate (at low sintering temperatures during solid state sintering) or to enable a slight rise of hardness due to maximum grain growth inhibition. Special applications, in

Table 21.6 Properties of ultrafine tungsten carbide powder grades

Property	Unit	Standard grades				
		CRC025 WC O6		CRC020 WC 05		CRC015
FSSS[a] grain size	μm	0.63	0.64	0.55	0.56	0.49
BET specific surface area (S_{BET})	m^2/g	1.71	1.52	2.03	1.95	2.43–2.83
BET calculated particle size[b]	μm	0.22	0.25	0.19	0.20	0.16–0.14
FESEM particle size d_{SEM}[c]	μm	...	0.30	...	0.25	0.18
Total carbon	wt%	6.12	6.17	6.09	6.19	6.11–6.15
Free carbon	wt%	0.03	0.03	0.03	0.02	0.01–0.05
VC	wt%	undoped	0.1–0.5	undoped	0.3–1.0	0.3–1.0
Cr_3C_2	wt%	undoped	0.1–0.5	undoped	0.3–1.0	0.3–1.0
Oxygen	ppm	900	1030	1080	1450	1810–2800

[a]Fisher sub-sieve size;

[b]BET particle size calculated, based on measurement of minimum 300 particles, according equation: $d_{BET} \ll \frac{6}{15.6\ S_{BET}}\ \mu m$

[c]FESEM particle size according equation: $d_{SEM} \ll \sum_{d_i}^{d_j} d \Big/ \sum_{d_i}^{d_j} N\ \mu m$

where $\sum_{d_i}^{d_j} d$ is sum of diameter of all particles in range from d_i to d_j; $\sum_{d_i}^{d_j} N$ is total number of particles in range from d_i to d_j.

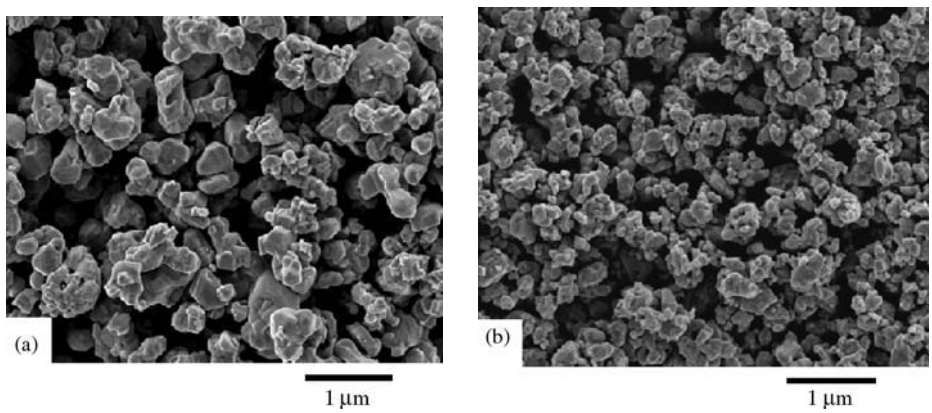

Figure 21.20 Scanning electron micrographs of standard tungsten carbide powder grades CRC025 (a) and CRC015 (b).

particular in the area of wear parts, set the demand for carbide grades with BET specific surface areas higher than $2.4\,m^2/g$. Developed grades CRC 015 satisfy these requirements (see Table 21.6). These carbides with calculated BET particle sizes of 0.15 μm are produced in full scale units by the conventional CRC process. Powder grades CRC 025 and CRC 015 differ appreciably in their particle sizes (Figure 21.20).

Added chromium plays an important role in the grain growth inhibition during sintering. The energy disperse analysis provides evidence [51] that chromium added already during powder processing is preferentially present at WC/WC grain boundaries even in the interior of polycrystalline particles or in necks between carbide particles; 10 wt% Co alloys produced by conventional liquid phase sintering at 1420°C and doped with chromium carbide (0.3–1.0 wt% Cr_3C_2) and vanadium carbide (0.3–0.6 wt% VC) resulted in coercitivity values ranging from 440 to 560 Oe with a corresponding increase in BET specific surface area from 1.5 to $2.8\,m^2/g$. Additionally, the increase in maximum coercitivity is directly proportional to the BET surface area.

The most important chemical side of tungsten carbide powder is its carbon content. Stoichiometric pure tungsten carbide has a total carbon content (C_t) of 6.135 wt%. From the point of view of thermodynamic equilibrium, WC has a very narrow stability range [1]. Thus, not even a small carbon shortage leads to W_2C subcarbide formation and excess of carbon

to the formation of free carbon (C_f). In commercial WC powders, there is always a small portion of free carbon present, about 0.03% at a stoichiometric C_t level. Even when the total carbon is below the stoichiometric level, the coexistence of traces of W_2C and C_f can occur. The carbon balance is important for hard metal manufacturing, because a shortage of carbon leads to the formation of the brittle phases, for instance, Co_2W_3C, and any excess in carbon leads to graphite precipitation. Thus, both cases result in a detrimental effect on the mechanical properties of the final product [1,51].

Elements such as vanadium, chromium, tantalum and niobium, due to their grain growth inhibiting effect during hard metal sintering, are added to tungsten carbide powder in amounts around 0.1–1.5 wt%. Such elements can be introduced as carbide to the tungsten carbide powder, or as oxide or carbide prior to the carburization step. Trace elements similar to nickel, iron and cobalt can be admitted in amounts around 100 ppm. At the same time, there are other impurities that should be limited in the very low ppm range because of their detrimental action on hard metal properties. Calcium, sulfur, silicon and phosphorus are typical of such elements [56,57]. Compositions and properties of several standard tungsten carbide powders are given in Table 21.7.

Recycling

Hard metal scrap containing tungsten carbide can be divided into two groups:

- Soft scrap, such as hard metal grinding sludge, filter dusts, broken green parts and floor sweepings
- Hard scrap, which represents sintered parts, consisting of either used parts or fragments.

The contamination of the scrap with the impurities is another criterion for classification. While particulate scrap contains impurity levels that cannot be admitted for direct reuse, hard scrap, even if heavily contaminated, can be classified, thus making direct reuse easier. Hard metal recycling processes can be subdivided into the following kinds:

- Direct conversion of sorted hard scrap into graded powder ready for pressing and resintering.
- 'Zinc process' is the most significant process [58]. It includes the following main processing steps: sorted, cleaned and crushed hard metal scrap; reaction in molten zinc at 900–1000°C in argon or hydrogen atmosphere; vacuum distillation at 1000–1050°C; obtained cake is consecutively crushed, ball milled and the resultant powder screened; then, oversize product (>75 μm) is returned to melting, undersize product (<75 μm) is ball milled, blend carbon adjusted resulting in graded hard metal powder.
- Also used on a commercial scale is the so-called 'Coldstream process', a high-velocity process. The cleaned, sorted and previously crushed hard metal scrap is entrained in a gas stream and projected against a stationary baffle plate. After the material has struck the target and shattered, it is removed from the impact chamber by suction. Material is then subjected to screening. The oversize product is returned into a feed vessel for subsequent impact against the baffle plate. Further classification of undersize material and mixing different size fractions result in graded hard metal powder ready for use.
- Removing the binder by means of leaching is another way of hard metal recycling. The composition of the hard metal scrap used for the leaching process determines the quality of the resulting carbide residue.
- Chemical conversion process can be used for all contaminated scraps, either soft or hard, to recover primary powders of the hard metal components. Figure 21.21 schematically shows the process from the contaminated and unsorted scrap via the conventional WC-powder manufacturing route which involves calcination, reduction and carburization intermediate to tungsten carbide powder.

Due to the intrinsic value of the hard metal components and the increasingly more severe legislation concerning waste disposal and the preservation of natural resources, recycling has today a considerable significance which will increase in the future.

Other Refractory Metals

Molybdenum Metal Powder

Molybdenum powders find application in different fields of technique. The major use for molybdenum is as an alloying element for alloy and tool steels, stainless and nickel- or cobalt-base superalloys to increase hot strength, toughness and corrosion resistance. Molybdenum ingots, produced by melting PM electrodes, are extruded, rolled into sheets or rods and subsequently worked to other mill product shapes, such as wire and tubing.

Molybdenum has outstanding electrical and heat conducting capabilities. The latter is approximately 50% higher than that of steel, iron and nickel alloys. It finds wide usage as heat sinks. The coefficient of thermal expansion of molybdenum plots almost

Table 21.7 Properties of typical tungsten carbide powders

Property	Unit	Source. Standard grades								
		WBH		OSRAM						
		WC 05D [2]	WC 06 [38]	BC04U	BC10U	BC45S	BC65S	BC75H	WC-TiC 70/30b	WC-Ti 50/50[b]
FSSS[a]	μm	0.53	0.64	0.5–0.7	0.91–1.20	4.31–5.00	11.01–15.00	>30	2.0 ± 0.3	2.0 ± 0.3
BET specific surface area	m^2/g	1.90	1.52	...	...	...	...	...	...	...
Nominal composition:										
Total carbon	wt%	6.23	6.17	6.13 ± 0.05	6.13 ± 0.05	6.13 ± 0.05	6.13 ± 0.05	6.13 ± 0.05	9.7–10.2	12.6 ± 0.2
Free carbon	wt%	0.04	0.03	max 0.08	max 0.08	max 0.06	max 0.06	max 0.06	max 0.25	max 0.4
VC	wt%	0.32	0.1–0.5	...	...	...	...	...	...	...
Cr_3C_2	wt%	0.64	0.1–0.5	...	...	...	...	...	...	...
Trace elements:										
Aluminum	ppm	10	<5	...	...	...	...	...	...	..
Calcium	ppm	3	<2	...	...	...	...	...	max 0.01	max 0.01
Chromium	ppm	...	...	100	100	50	50	75	...	...
Cobalt	ppm	<5	<5	...	...	...	...	...	...	...
Copper	ppm	<2	...	...	...	...	...	...	...	...
Iron	ppm	46	20	350	350	500	500	500	max 0.05	max 0.05
Magnesium	ppm	<1	...	...	...	...	...	...	...	...
Molybdenum	ppm	<20	<20	...	...	...	...	...	...	...
Nickel	ppm	<5	<5	150	150	100	100	100	...	...
Oxygen	ppm	1440	1030	3000	2500	500	500	500	...	...
Phosphorus	ppm	<20	...	...	...	...	...	...	...	...
Potassium	ppm	<4	...	...	...	...	...	...	max 0.01	max 0.01
Sulfur	ppm	6	<5	...	...	...	...	...	max 0.01	max 0.01
Silicon	ppm	<10	<10	...	...	...	...	...	max 0.005	Max 0.005
Density	g/cm^3			14.72	14.91	14.94	14.94	14.94	...	...
Hardness	HV30			2000	1650	1380	1220	<1050	...	...
Coercivity	O_e			500	260	122	80	<60	...	...

[a]Fisher sub-sieve size;
[b]Fine-grained grade; WBH: Wolfram Bergbau- und Hütten- GmbH; OSRAM: OSRAM Bruntál spol. s r. o.

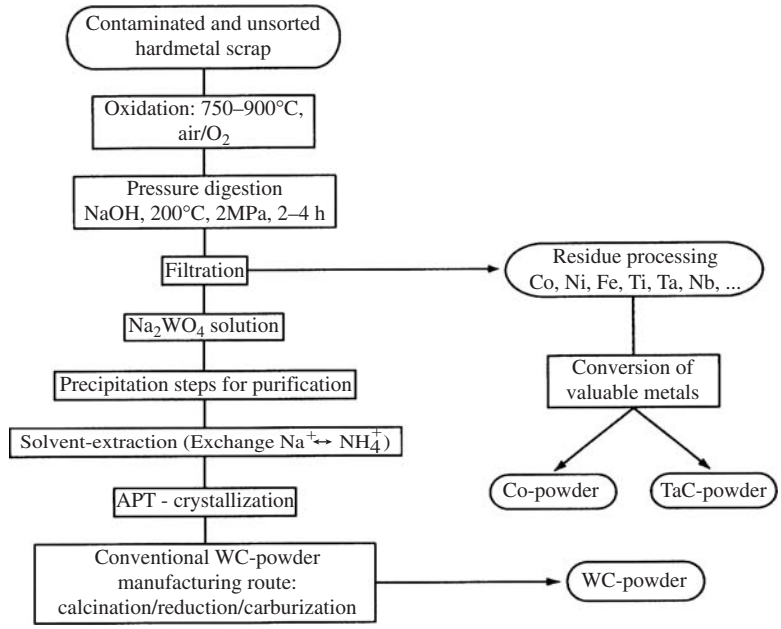

Figure 21.21 Flowsheet for the chemical conversion process. Source: Ref 2

linearly with temperature over a wide range. This characteristic, in combination with its heat conducting capabilities, accounts for its use in bimetal thermocouples. Methods of doping molybdenum powder with potassium aluminosilicate to obtain a non-sag microstructure comparable to that of tungsten have also been developed. In the electrical and electronic industries, molybdenum is used in cathodes, cathode supports, for radar devices, current leads for thoria cathodes and cores for winding tungsten filaments. Molybdenum is significant in the rocket industry, where it is used for high temperature structural parts. Molybdenum alloys satisfy the requirements for use in airframes because of their retention of mechanical properties after thermal cycling due to high recrystallization temperatures and good creep strength. Molybdenum has been also effective in the nuclear, chemical, glass and metallizing industries.

Production

Molybdenum powder is produced by a technique similar to that used for tungsten powder. Molybdenum disulfide (MoS_2) is the major source of raw material. Molybdenum disulfide is concentrated by flotation and transformed to an impure technical molybdenum trioxide (MoO_3) by means of roasting, which oxidizes the sulphur and removes it as gaseous sulfur dioxide [59].

Subsequent purification takes advantage of the sublimation characteristics of molybdenum trioxide. Above 550°C, it sublimes easily and can be distilled from its impurities and condensed again as pure molybdenum trioxide. Solvent extraction processes are also acceptable. Additional purification can also be achieved by dissolving molybdenum trioxide in ammonia to form ammonium molybdate, $(NH_4)_2MoO_4$. The pure molybdenum trioxide or ammonium molybdate is reduced in tube push type or rotary furnaces similar to those used for tungsten reduction. Typical purification reduction reactions can be written:

$$MoS_2 + 7/2O_2 = MoO_3 + 2SO_2 \text{ endothermic reaction}$$
$$MoO_3 + 3H_2 = Mo + 3H_2O$$
$$MoO_3 + 2NH_4OH = (NH_4)_2MoO_4 + H_2O$$
$$(NH_4)_2MoO_4 + 3H_2 = Mo + 2NH_4OH + 2H_2O$$

Reduction of molybdenum trioxide by dry hydrogen involves two steps: $MoO_3 \rightarrow MoO_2 \rightarrow Mo$. The bond strength metal–oxygen in MoO_3 is less than in WO_3, and in MoO_2 is vice versa larger than in WO_2. Below are values of the equilibrium constants for the two steps of Mo reduction ($K_{eq} = p_{H_2O}/p_{H_2}$).

Temperature (°C)	397	427	597	642	797	927
K_{eq}, 1st step	5.0×10^7	...	1.7×10^6	...	1.58×10^5	...
K_{eq}, 2nd step	...	0.076	...	0.234	0.389	0.55

Table 21.8 Properties of typical molybdenum metal powders produced by hydrogen reduction

Property	Unit	Source. Standard grades		
		[2]	SIC Standards	
		1–6 μm	TU 48-19-316	TU 48-19-313[c]
Particle sizes	μm	1–6[a]	<5	40–150
Nominal composition				
Molybdenum	wt%	99.9[b]	99.5	99.9
Trace elements:				
Aluminum	ppm	5–25	50	...
Calcium	ppm	3–15	70	70
Carbon	ppm	10–50	...	...
Chromium	ppm	5–25	...	...
Cobalt	ppm	...	...	...
Copper	ppm	5–10	...	...
Iron	ppm	10–100	140	...
Lead	ppm	5–10	...	...
Magnesium	ppm	1–10	30	30
Nickel	ppm	5–50	50	200
Oxygen + water	ppm	500–1000	3000	...
Potassium	ppm	...	500	...
Silicon	ppm	...	50	...
Sodium	ppm	...	150	150
Tin	ppm	15–50	...	...
Tungsten	ppm	100–300	400	...
NVM (summation of Ca, Na, K, S)	ppm	500–1000	...	...

[a]particle size FSSS;
[b]metallic molybdenum content, exclusive of gases;
[c]coarse powder for plasma spraying, CIS: Commonwealth of Independent States' standards.

The first step is conducted at temperatures ranging from 397 to 647°C providing slow increase of temperature in order to accomplish the formation of MoO_2 at 497–547°C and not to form molten material at 547–597°C (low-melting eutectic $Mo_4O_{11}-MoO_2$). The second reduction step is carried out at 647–947°C. The reduction parameters like temperature, reduction time and powder layer thickness (oxide load of the boats in push type furnace) are chosen so that the residual oxygen content falls below 1000 ppm during the second reduction step.

Properties of typical molybdenum metal powders produced by reduction of molybdenum trioxide by hydrogen are shown in Table 21.8.

There are also other known methods of producing pure molybdenum powder. However, they have not found commercial application.

To produce high purity molybdenum powder, an aqueous solution of ammonium molybdate is mixed with a solution of iron chloride (III); formed precipitate of iron molybdate is separated from the solution containing some of the impurities. A solution is acidified for the purpose of molybdic acid (H_2MoO_4) formation that is to transform separated and then dissolved in an aqueous solution of ammonia (NH_4OH). At the second stage of purification, the obtained solution of refined ammonium molybdate is mixed with a solution of iron chloride (III) and the cycle is repeated; formed precipitate of iron molybdate is separated, washed and, after acidifying the molybdic acid, is dissolved in an aqueous solution of ammonia. The solution is separated by filtration and finally pure ammonium molybdate is cooled. The crystals of pure ammonium molybdate are separated and reduced in a hydrogen atmosphere at 897–947°C.

Reduction of low boiling point molybdenum chlorides and fluorides also allows the production of high pure molybdenum powder. The melting point of molybdenum pentachloride ($MoCl_5$) is 194°C and boiling point is 268°C. A fluidized bed unit for reduction is described in Chapter 8, where molybdenum pentachloride is being supplied at the temperature in the range from 197 to 297°C ($MoCl_5$ is decomposed on $MoCl_4^+ + Cl^-$ above 268°C). Optimal conditions

Table 21.9 Variation of properties with decomposition temperature for carbonyl molybdenum powders

Decomposition temperature in current of argon (°C)	Color of powder	Apparent density (g/cm^3)	Carbon content (wt%)	Lattice spacing (nm)
400	gray	0.5	2.36	...
500	gray	...	3.28	0.42019
600	dark-gray	...	3.38	0.42030
700	black	...	3.53	0.42100
800	black	2.50	3.48	0.42220
2700–3700	black	...	0.10–0.20	...

providing metal precipitation of 88% and reduction degree of 98% are as follows: temperature range from 597 to 797°C, $MoCI_5$ concentration in gas vapor phase of 4–5 vol% and molar ratio of hydrogen to molybdenum pentachloride of approximately 30 to 1. Obtained fine powder contains: 40–60 wt% fraction minus 0.6 μm, 20–23 wt% fraction 0.6–1.2 μm, 10–20 wt% fraction 1.6–1.8 μm, and 1–3 wt% fraction 1.8–2.4 μm.

If a rotating reaction chamber is used, where ammonia paramolybdate is reduced by hydrogen, the porous conglomerates of dispersed powders are obtained, which are narrow in size and shape. Powders are distinguished by high bulk mass and good flow and their dispersivity depends on temperature condition. Highly dispersed (3–5 μm) powders of rhenium and molybdenum alloy (1:1) are produced by treatment of $ReOMoO(OCH_3)_7$ in two steps: calcinations in oxygen (250–300°C, 1–2 hours), reduction by hydrogen (800–900°C, 2–3 hours).

The carbonyl process for molybdenum powder production is based on the decomposition of carbonyl molybdenum ($Mo(CO)_6$). The powder particle sizes are around 1 μm and surface of the particles is rather smooth. Having increased the temperature of carbonyl decomposition, there have been changes in powder color, carbon content, apparent density and lattice spacing (Table 21.9). Carbonyl molybdenum powders enriched by carbon represent the metastable carbides with face-centered lattice. The increasing decomposition temperature leads to the extension of lattice spacing.

Impurities of carbon and oxygen are typical for molybdenum powders and the content of sulfur, phosphorus and arsenic does not exceed 1 ppm.

By execution of the carbonyl process in a hydrogen and nitrogen current, a peak of carbon (amorphous) content is observed at 697°C as a result of catalytic decomposition of its dioxide. Addition of oxidizing components into gas-bearer leads to decreasing of carbon content. For instance, the powder obtained in nitrogen with 2.2% of oxygen at 397°C contains 0.27 wt% carbon. To remove impurities, it is effective to heat treat powders at 897°C and above. The carbon amount goes down by a digit factor while carbonyl decomposition in ultrahigh frequency discharges.

Properties of Molybdenum and Molybdenum Alloy Powders

The high boiling and melting points of molybdenum 4610°C and 2612°C, respectively, are second only to those of tungsten, rhenium and osmium. Molybdenum is not used as widely as tungsten because it oxidizes more readily and erodes faster on arcing than tungsten. Nevertheless, due to the density of molybdenum (10.2 g/cm^3), which is about half that of tungsten (19.3 g/cm^3), use of the former is advantageous where mass limitation is important. The cost of molybdenum is also lower. In addition to its use in make-(before-) break contacts, molybdenum is widely used for mercury switches because it is not attacked, but only wetted, by mercury.

Like tungsten, molybdenum strip and sheet are made by swaging or rolling sintered powder compacts. Table 21.10 shows the properties of molybdenum in comparison with tungsten and Figure 21.22 illustrates the effect of temperature on various properties.

The mechanical properties of molybdenum and molybdenum alloys greatly depend on the amount of working treatment below their recrystallization temperature and on the ductile-to-brittle transition temperature. The minimum recrystallization temperature is 900°C. The metal keeps superior strength and hardness at elevated temperatures. However, when hot strength is required, a molybdenum alloy rather than elemental is the material of choice. Titanium and zirconium additions to molybdenum create alloys with hot strength and recrystallization temperatures above those of unalloyed molybdenum.

Table 21.10 Typical properties of molybdenum and tungsten

Property	Unit	Molybdenum	Tungsten
Density	g/cm^3	10.22	19.3
Hardness HB	GPa	1500	70
Modulus of elasticity			
at 20°C	GPa	325	405
at 1000°C	GPa	220	325
Melting point	°C	2612	3410
Boiling point	°C	4610	5660
Specific heat at 20°C	J/(kg · °C)	251	134
Thermal conductivity at 20°C	W/(m · °C)	155	130
Coefficient of linear thermal expansion at 20°C	μm/(m · °C)	5.53	4.43
Electrical resistivity at 20°C	nΩ · m	53.4	55
Electrical conductivity at 20°C	%IACS	33	31

Some of the physical properties of molybdenum and tungsten vary considerably with cross-sectional and grain structure.

Table 21.11 gives basic mechanical property data for 0.38 mm wire fabricated from pure molybdenum and several of the advanced molybdenum alloys.

At present, the molybdenum alloy of major technological importance is the high-strength, high-temperature alloy TZM. The material is manufactured either by PM or arc-melting processes. The composition of TZM consists of: (0.01–0.04) wt% carbon, (0.40–0.55) wt% titanium, (0.06–0.12) wt% zirconium, <0.0005 wt% hydrogen, <0.010 wt% iron, <0.002 wt% nickel, <0.002 wt% nitrogen, <0.0025 wt% oxygen, <0.008 wt% silicon and balance of molybdenum. At 1100°C, its strength is about 720 MPa which is approximately twice that of unalloyed molybdenum. The alloy is excellent for structural applications under conditions where unalloyed molybdenum is normally used [59].

In comparison with unalloyed molybdenum, TZM has a higher recrystallization temperature and higher strength and hardness at room and elevated temperatures. Its advanced mechanical properties are due to the dispersion of composite carbides in the molybdenum matrix. Basic application fields of TZM include:

- Die inserts for casting metals
- Die bodies and punches for hot stamping
- Tools for metalworking
- Heat shields and linings for furnaces, structural parts and heating elements
- Rocket nozzles.

To improve the elevated temperature strength of PM TZM alloys, the titanium and zirconium carbides have been substituted by hafniun carbide. An alloy containing 1% Hf and 0.06%C has a tensile strength of 580 MPa at 1315°C, in comparison with 480 MPa for TZM. Creep rate at 1205°C at a stress of 330 MPa is 0.038%/h, compared to 0.05%/h for TZM [60].

Table 21.12 presents the compositions and properties of various molybdenum–silver composites for electrical make-break contacts [61]. Because the properties of materials with the same composition depend on manufacturing methods, the manufacturing methods are also referenced in Table 21.13. These common methods of producing composite electrical contact materials are described in subparagraph 'Tungsten powder applications' (see above).

To improve the mechanical properties, including ductility and creep resistance of structural molybdenum-base materials, doped molybdenum alloys were developed by doping with a small amount of aluminum, potassium, silicon or rare-earth oxides [62]. Recently, high-toughness molybdenum alloys have been developed with fine grains and finely dispersed titanium carbide particles by mechanical alloying (MA) and hot isostatic pressing (HIP) processes, followed by hot forging and hot and warm rolling. The high toughness of the alloy may be due mainly to grain-boundary strengthening by fine carbide particles having semi-coherency with the adjacent matrix and the particles have the beneficial effects of increasing the recrystallization temperature and hindering grain growth. However, in both cases, a large amount of plastic working was required. Such working may limit the products available to thin sheets or thin wires shapes, which are inapplicable as structural materials.

More recently, molybdenum alloys with 0.8 mol% zirconium carbide (ZrC) or tantalum carbide (TaC) as dispersed particles were fabricated by mechanical alloying and HIP or spark plasma sintering (SPS) [63]. Powders of pure molybdenum (average particle size

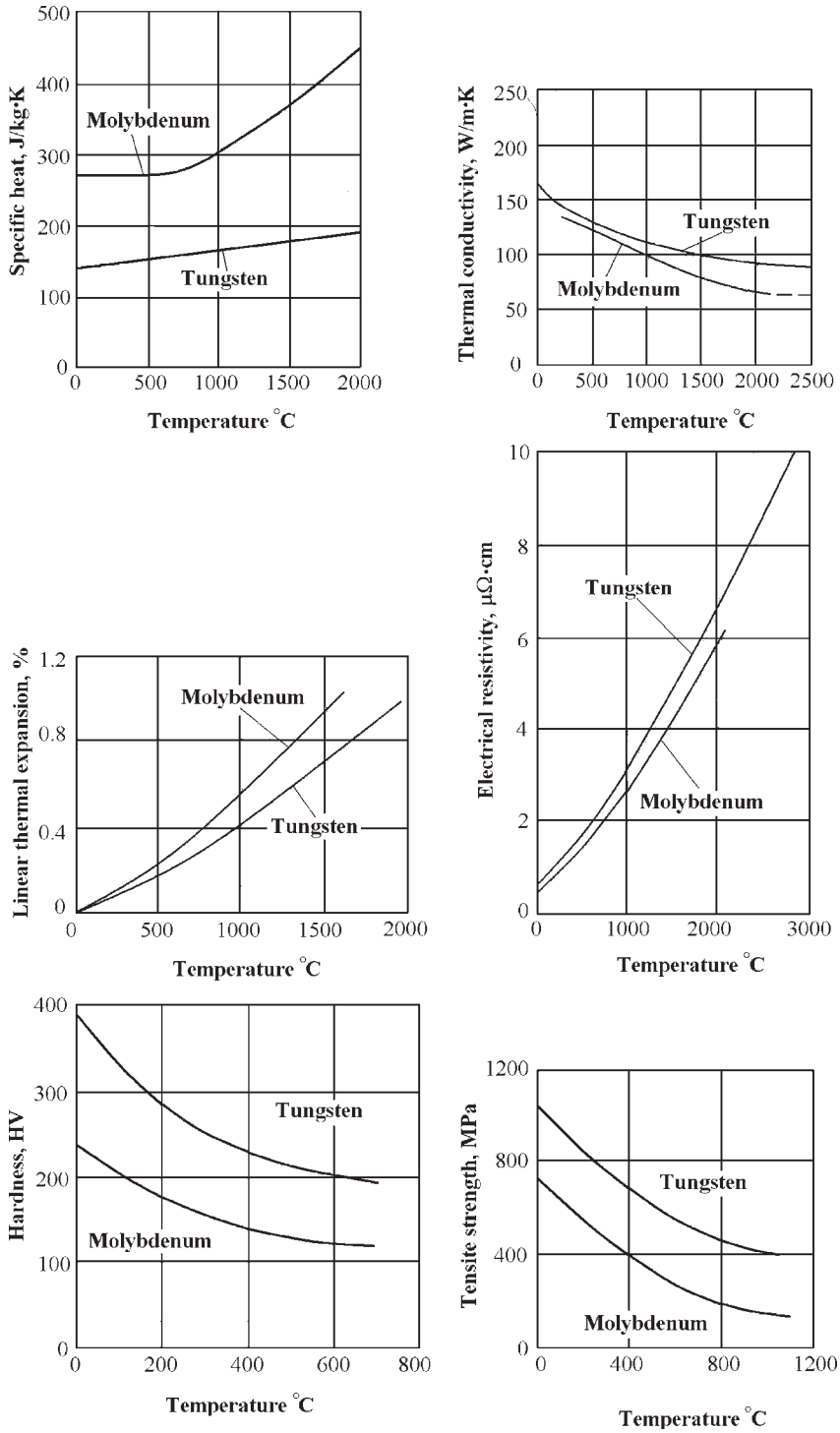

Figure 21.22 Properties depending on temperature for molybdenum and tungsten. Source: Ref 61

Table 21.11 Tensile properties of 0.38 mm molybdenum wire at room and elevated temperatures

Material sign	Composition	Temperature (°C)	Ultimate tensile strength (MPa)	Elongation (%)
Unalloyed molybdenum	Mo	20	1350	4.1
		1000	305	2.4
		1100	140	10.3
		1200	115	12.5
MT-104	Mo–0.5Ti–0.08Zr–0.01C	20	1565	3.1
		1000	1020	2.7
		1100	795	3.2
		1200	675	2.8
Mo + 45W	Mo–45W	20	1980	3.6
		1000	1095	2.3
		1100	950	2.3
		1200	745	2.2
HCM	Mo–1.1Hf–0.07C	20	1795	2.9
		1000	1270	3.4
		1100	1185	3.3
		1200	1035	3.0
HWM-25	Mo–25W–1.0Hf–0.035C	20	1935	3.2
		1000	1350	3.3
		1100	1250	3.1
		1200	1075	4.6
HWM-45	Mo–45W–0.9Hf–0.03C	20	2135	3.6
		1000	1460	3.3
		1100	1295	2.6
		1200	1170	2.4

Source: Ref 60

4.1 μm), ZrC (2 μm) and TaC (1.1 μm) were mixed to obtain the target composition in an argon atmosphere. These blended powders were subjected to mechanical alloying for 108 ks in a planetary type ball mill with lining and balls made of a cemented carbide (WC–Co). HIP and SPS were conducted at 1300°C and 147 MPa for 10.8 ks in argon, and at 1800°C and 74 MPa for 0.3 ks in a vacuum of 10 Pa, respectively. These alloys were annealed in a vacuum of 2.7×10^{-4} Pa at 1600–2200°C for 3.6 ks. Yield strength, ultimate tensile strength and elongation at 27°C and high temperature for Mo–0.8 mol%ZrC, Mo–0.8 mol%TaC and pure Mo conducted with tensile specimens in form of bar 4 mm wide, 25 mm long and 1 mm thick are shown in Table 21.13. The superplastic behavior was investigated on a gauge section 3 mm wide, 8 mm long and 2 mm thick. In both MA with HIP and MA with SPS specimens of Mo–08 mol%ZrC as sintered, the tensile strengths are 1.8 times higher than that of pure molybdenum, however, no plastic behavior is found. While both MA with HIP and MA with SPS specimens of annealed Mo–08 mol%ZrC are superior in terms of room temperature strength, their yield and tensile strengths are about 3 and 2.1 times higher respectively than that of pure molybdenum.

The carbide dispersed molybdenum alloys exhibit excellent strength up to 1100°C. Their tensile strengths are 3–5 times higher below 1200°C (about 0.5 melting point) and 1.5–2 times higher at 1500°C, than those of pure molybdenum and Mo–0.8 mol%TaC (Figure 21.23). The elongation of Mo–08 mol%ZrC with grain size of 3.0 μm obtained by means of SPS with MA increased rapidly in the temperature range over 1500°C, and a superior limit elongation of 180% is attained at 1700°C.

Variations in the nature of the oxide and consolidation method have been shown to have a significant effect on the mechanical properties of oxide dispersion strengthened (ODS) molybdenum material [64]. Comparison of the effect of doping technique and species on tensile properties of ODS molybdenum–lanthana and ODS molybdenum–yttria alloys

Table 21.12 Properties of typical molybdenum-silver composites for electrical make-break contacts

Nominal Composition (%)	Manufacturing method (a)	Density, g/cm^3		Electrical conductivity, % IACS	Hardness	Tensile strength, Mpa	Modulus of rupture, Mpa	Data source (b)	Application examples
		Calculated	Typical						
90Ag-10Mo	PSR	10.47	10.38	65–68	35–40 HRB	...	...	A	Air conditioner control
80Ag-20Mo	PSR	10.44	10.36	59–62	38–42HRB	...	...	A	Light- and medium- duty
75Ag-25Mo	PSR	10.42	10.33	58–61	44–47 HRB	. . .	...	A	applications, automotive circuit breakers switches, circuit breakers
50Ag-50Mo	INF	10.35	10.10–10.24	45–52	70–80 HRB	...	758	C, A	Air- and oil- circuit breakers,
	PSR	10.35	10.14	50	65	...	552	C,A	arcing tips, traffic signal relays, home circuit breakers
45Ag-55Mo	INF	13.33	10.10–10.32	44–58	75–82 HRB	...	...	A	
40Ag-60Mo	INF	10.32	10.10–10.32	42–49	80–90 HRB	...	. . .	C, A	Aircraft switches, breaker
	PSR	10.32	10.12	45	50–68	...	676	C, A	arcing tips, electric raisers, air and oil- circuit breakers
30Ag-70Mo	INF	10.29	10.00–10.31	35–45	85–95	414	931	C, A	Air-circuit breakers. low-
25 Ag-75Mo	INF	10.27	10.27	31–34	93–97	414	938	C, A	erosion arcing tips
20 Ag-80Mo	INF	10.26	10.23–10.26	28–32	96–98	407	965	C, A	Arcing contacts, heavy-duty
15 Ag-85Mo	INF	10.24	10.18	28–31	97–102	...	...	G	electrical applications
10 Ag-90Mo	INF	10.23	10.13	27–30	97–102	...	...	G	Semiconducting material

[a]INF, press-sinter-infiltrate; PSR, press-sinter-repress (blended powder of the desired composition are compacted to the required shape and then sintered. Afterwards, the material is further densified by a second pressing. Sometimes the properties can be modified by a second sintering or annealing)
[b]A: Advance Metallurgy, Inc., McKeesport, PA. C: Contacts, Materials, Welds, Inc., Indianapolis, IN. G: Gibson Electric Inc., Delmont, PA.

Table 21.13 Mechanical properties at 27°C for carbide dispersed molybdenum alloys

Alloy	Analyzed composition (wt%)				Manufacturing method	Relative density (%)	Condition	Grain size (μm)	Yield strength (MPa)	Ultimate tensile strength (MPa)	Elongation (%)
	Metal	C	N	O							
Mo–0.8ZrC	0.70Zr	0.100	0.022	0.140	MH	99.9	As sintered	0.3	...	827	0.0
							Annealed	1.8	1015	1053	0.6
Mo–0.8ZrC	0.69Zr	0.117	0.032	0.138	MS	99.9	As sintered	2.7	...	838	0.0
							Annealed	2.8	1038	1077	9.0
M0–0.8TaC	1.2Ta	0.110	0.019	0.137	MS	99.9	As sintered	10.9	559	707	12
							Annealed	11.2	547	639	38
Pure Mo	...	0.001	0.001	0.001	MH	100	Recrystallized	53.8	344	469	54

MH: Mechanical alloying and hot isostatic pressing; MS: mechanical alloying and spark plasma sintering.

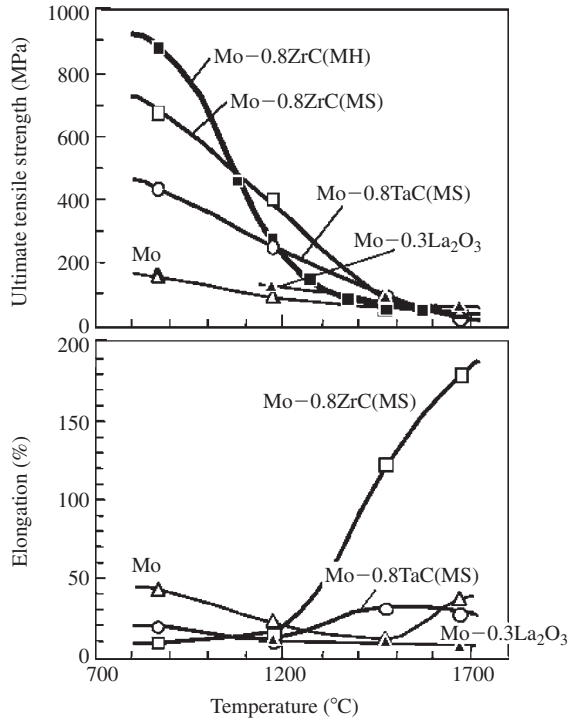

Figure 21.23 Dependence of ultimate tensile strength and elongation of the carbide dispersed molybdenum alloys on temperature. Source: Ref 63

illustrates that, for both oxide species, the wet doping technique results in a much finer dispersion of oxide, particles ranged from 0.08 to 0.12 μm. The wet doping process uses an aqueous tantalum nitrate solution to dope the molybdenum dioxide (MoO_2) precursor before its reduction to molybdenum metal powder [65]. At ambient temperature, the alloy's strength is not strongly sensitive to either doping technique but, at high temperatures, the wet doping technique produces superior material for a given oxide. Lanthana-doped material is also superior to yttria-doped material at elevated temperature. The ODS molybdenum material contains nominally 2 vol% La_2O_3 that corresponds to a lanthanum (La) content of 1.09 wt%.

The addition of a small amount of group VIII transition metals, such as nickel and palladium, can lower the activation energy of sintering and decrease the sintering temperature from greater than 1700 to less than 1300°C [66]. However, such activation-sintered compacts have no ductility and thus have restricted application in industry [67]. Through activated or liquid phase sintering, the addition of 1.5 wt% Ni to molybdenum was shown to improve the sintered density significantly to 97% at 1300°C, while the pure molybdenum only reached 82% theoretical density. But, it also impairs the ductility. This embrittlement appears to be caused by a grain boundary layer of a Ni–Mo compound about 2 nm thick formed during sintering [68]. Due to the brittle nature of this compound, the Ni-containing molybdenum fractures through this thin compound layer.

Workplace Atmosphere Safety

The aerosols of metallic molybdenum, either soluble or insoluble molybdenum compounds and molybdenum silicide, take a predominantly fibrous effect and are related to the third class of danger according to State Standard 12.1.005-88 under the legislation in the CIS [37]. The stated average limit value (ALV) of the metallic molybdenum aerosol in the workplace atmosphere as the shift time-weighted average concentration is 0.5 mg/m^3, while the threshold limit value (TLV) is 3 mg/m^3. The ALVs of the insoluble and soluble molybdenum compounds and molybdenum silicide in dust form are 1.0, 4.0 and 4.0 mg/m^3, respectively, while the ALV of soluble molybdenum compounds in the form of condensed aerosols is 2.0 mg/m^3. Molybdenum content in potable water has a toxicological effect and is related to the second class of danger and the TLV is 0.25 mg/L according to CIS State Standard 4630-88 [38].

Molybdenum powder even with particle sizes fraction $\leq 74\,\mu m$ in the air is not explosive; the minimum ignition temperature of powder deposits (self-ignition temperature) is 310°C. The products with such characteristics of inflammability and explosion risk are related to the 'Low explosion hazard' class of danger according to the Guide to Legislation and 'Health and Safety' in the European PM Industry [39].

Common techniques are mainly used to prevent pollution and environmental damage during powder manufacture and its processing. Detailed information on health and environment protection measures in such conditions can be found in Section 5.

Production of Niobium and Tantalum Powders

Niobium and tantalum are often found in close combination in their ores. The most important niobium–tantalum bearing minerals are columbite and tantalite, which form isomorphous series: $FeNb_2O_6-MnNb_2O_6$ and $FeTa_2O_6-MnTa_2O_6$ and the ores are variations of the compound $(Fe, Mn)(Nb, Ta)_2O_6$. Tantalum and niobium are separated from ore and from one another by digestion in aqueous hydrofluoric acid, followed by solvent extraction with methyl isobutyl ketone (MIBK), as illustrated in Figure 21.24 [69]. In the first contacting, only the niobium and tantalum fluorides are soluble in the MIBK. Thus they are separated from the contaminants iron, manganese, titanium and zirconium, which remain in aqueous solution. The fact that the solubility of tantalum in MIBK is high over an extensive range of acidity, while niobium is soluble only at high acidity is used for separation of tantalum fluoride and niobium fluoride. This is accomplished in a series of subsequent steps, where the MIBK is contacted with aqueous solutions of varying acidity.

Commercially, deposits of niobium are found also in the pyrochlore $[(Na, Ca)_2(Nb, Ta, Ti)_2O_4(OH, F) \cdot H_2O]$, which is mined in Canada and Brazil. These ores are mostly tantalum free and are enriched to concentrates containing 55–60% niobium pentoxide by means of a series of operations including grinding, flotation and leaching. The extraction of niobium by high temperature chlorination of the ore is also appropriate technique for niobium powder production [70].

Niobium

The use of niobium as an alloying element in steels is in commercial application. Nearly 75% of all niobium metal is used as minor alloying additions in low-alloy steel. About 20–25% is used as alloy additions in nickel-base superalloys and heat resisting steel. Only 1–2% of all niobium used is in the form of niobium base alloys and pure niobium metal including superconducting niobium–titanium alloy, which accounts for over one-half of all niobium alloys produced [71].

Aluminothermic Reduction

Initially, niobium metal was produced by PM methods which involved high temperature vacuum sintering and carbon reduction. However, in the early 1960s, aluminothermic reduction and electron beam purification came into general use. At present, the basic process for the recovery of niobium, along with recovery from columbite and tantalite ores shown in Figure 21.24, is the aluminothermic reduction of pyrochlore concentrates to ferroniobium. Niobium metal is purified by a chlorination process, where volatile niobium pentachlorate ($NbCl_5$) is distilled and then hydrolyzed to the oxide. The metal is next recovered by a second aluminothermic reduction

$$3Nb_2O_5 + 10Al \rightarrow 6Nb + 5\,Al_2O_3$$

During the exothermic reaction, oxide impurities are slagged and removed from the molten niobium.

Carbothermic Reduction

Carbothermic reduction is also practiced [72]. Reduction is conducted in two steps involving the formation of niobium carbide:

$$Nb_2O_5 + 7C = 2NbC + 5CO$$
$$Nb_2O_5 + 5NbC = 7Nb + 5CO$$

It is not desirable to conduct carbothermic reduction in one stage. Stock of Nb_2O_5 contains only 57.2% of niobium and even in briquette from it has low density ($\approx 1.8\,g/cm^3$). High volumes of CO ($\approx 0.34\,m^3$) are consumed per 1 kg of stock that leads to low capacity of the reduction process. Therefore, the first step is carried out in graphite-tube resistance push type furnaces in a hydrogen atmosphere at temperature of 1800°C. The graphite cartridge with the stock ($Nb_2O_5 + 7C$) is pushed through the furnace for 1–1.5 h. Lightly sintered niobium carbide is ground to powder and blended with Nb_2O_5 in a surplus of 3–5% against stochiometric ratio. Then this mixture is pressed into briquettes at a pressure of 100 MPa and calcined in a vacuum furnace at 1800°C and residual pressure 1.3–0.13 Pa for 6 hours. The niobium reduction goes by intermediary stages of lower oxide formation (NbO_2

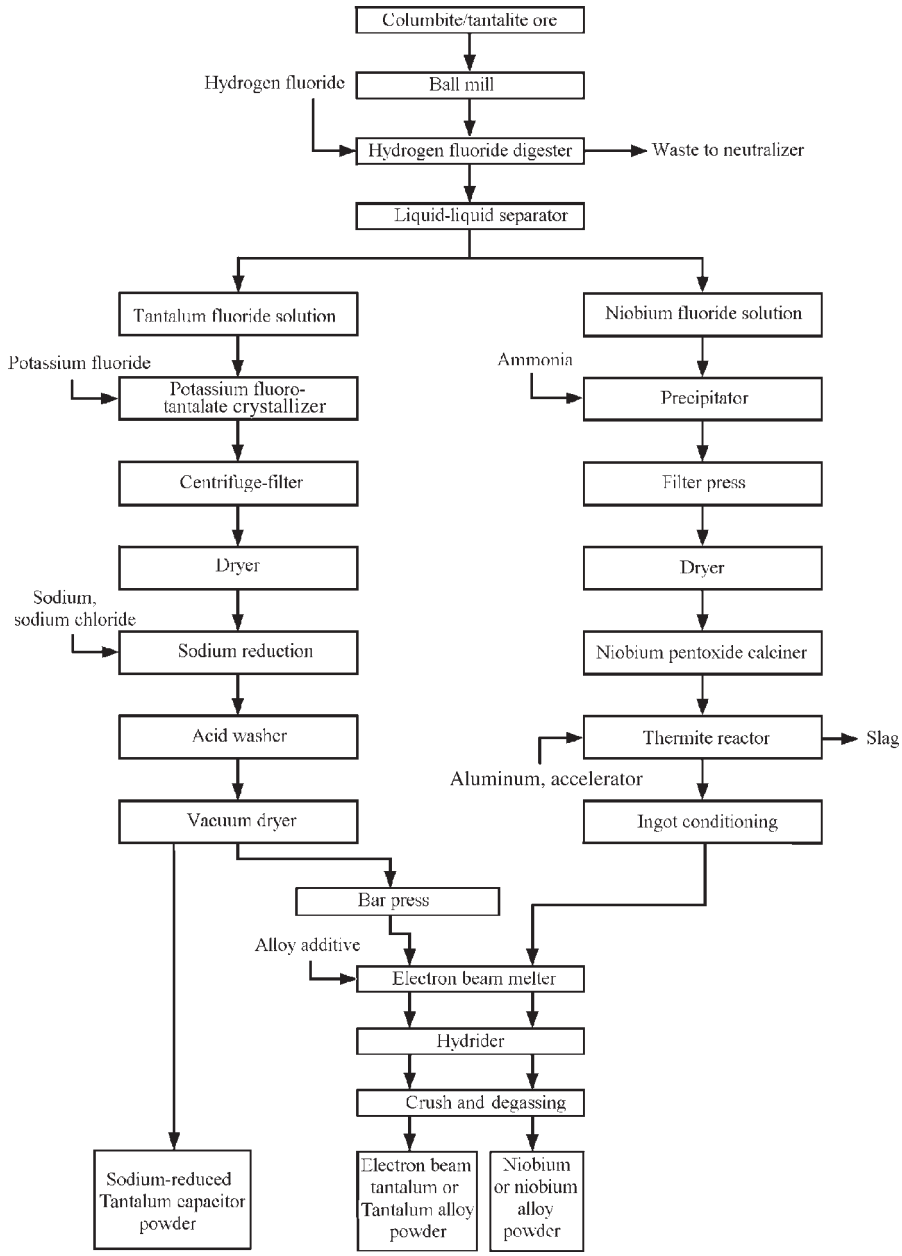

Figure 21.24 Niobium and tantalum production flowchart. Source: Ref 69

and NbO). It is important that, at temperatures above 627°C, a part of Nb_2O_5 is evaporated and NbO_2 and NbO are evaporated at higher temperatures. Niobium oxide vapor is adsorbed on the carbon and niobium carbide particles, where niobium is reduced. The second step goes with higher capacity as the mixture Nb_2O_5 + 5NbC has 82.4% niobium in briquettes with a density of about 3 g/cm^3.

Reduction by Sodium

The reduction of potassium fluorine niobate (K_2NbF_7) by sodium may be represented as follows:

$$K_2NbF_7 + 5Na = Nb + 2KF + 5NaF$$

This process is realized in a shaft furnace using a layerwise loaded charge in a steel crucible. Sodium

surplus (15–20%) in the form of sodium chloride layer is poured onto the top of the charge; the crucible is placed into the pre-heated furnace (up to 600°C) and kept for 1.0–1.5 h at 900–1000°C. Niobium powder is washed first in cold then in hot water, next washed by dilute nitric or hydrochloric acid (to eliminate iron, titanium and other impurities) and 2.5% cold hydrofluoric acid for 5–15 minutes to decrease the niobium oxide content.

Electrolysis of Melt

Electrolysis of melt is also used. Refined salts are melted in a nickel crucible (cathode) and Nb_2O_5 is introduced into the melt; the anode is a graphite rod; electrolyte temperature is 747°C. Voltage on the cell is 2.5 V; cathode current density ranges from 5 to 6 kA/m^2; current efficiency is not more than 30%. The niobium deposit is coarse-grained and contaminated with the lowest niobium oxides. Two types of electrolyte are used: K_2NbF_7–KCl–Nb_2O_5 and K_2NbF_7–KCl–NaCl (for refining). In liquid melt of the former, before Nb_2O_5 is introduced, the following reactions take place:

$$K_2NbF_7 + KF = K_3NbF_8 \text{ and/or}$$
$$K_2NbF_7 + KCl = K_3NbF_7Cl$$

Having added niobium pentoxide in surplus of KF the reaction can be written:

$$K_2NbF_7 + 13KF + 2Nb_2O_5 = 5K_3NbO_2F_4$$

Complex niobium containing ions admittedly NbF_8^{3-}, NbF_7^{2-}, and $NbO_2F_4^{3-}$ are present in the electrolyte. At temperatures in the range from 700 to 750°C and cathode current density ranging from 1 to 8 kA/m^2, it is possible to obtain niobium powder in which the impurities content in comparison with anode material is less by an order of magnitude: for iron 1–3, for silicon 1–1.5, for carbon 1–1.5, and for oxygen 1.0.

Niobium sponge can be produced also by electrodeposition from halide melts. Electrolysis of bromide and iodide melts (4–6% Nb) is carried out with addition of alkali metal chlorides at 700°C and cathode current density of 5 kA/m^2. Current efficiency is about 40%. The obtained sponge is lightly milled to powder. For niobium reduction from halide melts, the starting material is carbo-thermal niobium and the electrolyte is a mixture of NaCl and K_2NbF_7, with 10–40% of the latter. In an argon atmosphere, niobium is oxidized on the anode and reduced on the cathode using a cathode current density of 3.2–41 kA/m^2 and temperature between 827 and 927°C.

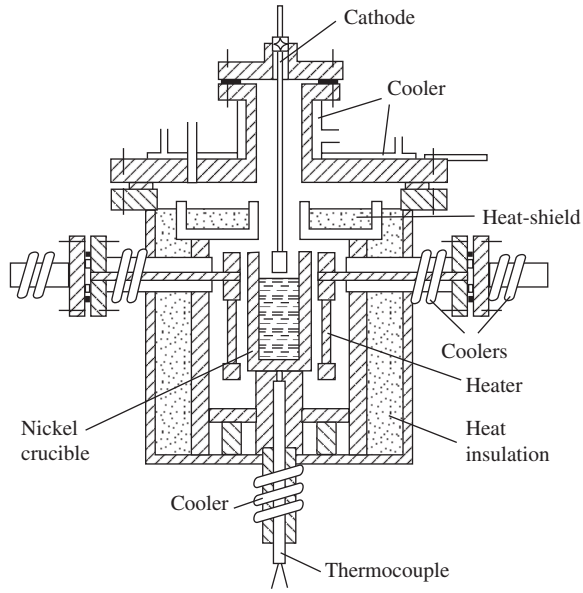

Figure 21.25 Electrolyzer for niobium refining.

The electrolysis cell (Figure 21.25) made of nickel is put into the furnace with graphite heaters and a heat shield. On the furnace cover a water-cooled chamber for charging is erected, in which the cathode is vertically moved. Current efficiency, calculated to Nb^{2+}, ranges from 23.1 to 34.6%. Compositions of contaminant elements in electrolytic refined niobium powders and in anodes are given in Table 21.14. The powders (cathode product) consist of modified coarse dendrites.

Hydride–dehydride Process

Powders are produced from ingots by means of hydriding, crushing and subsequent dehydriding of electron beam (EB) melted ingots. These melt-grade powders have higher purity than the sodium-reduced types and have better dielectric properties. However, unit capacitance is usually lower for EB-powder. Although the dielectric properties of niobium oxide are inferior to those of tantalum oxide, niobium has been evaluated as a means of manufacturing low-cost capacitors. Considerable niobium powder development work is required before niobium capacitors will be offered commercially. Usually, powders are crushed to pass a 180 μm (80-mesh) screen and a mean particle size of 10–15 μm is typical.

Typical compositions of niobium and niobium alloy powders are given in Table 21.15.

Niobium powder is frequently used as the starting material to blend with other alloying powders. The blend is pressed to bars and melted, thus promoting

Table 21.14 Compositions of contaminant elements in anodes and electrolytic niobium powder

Elements	Unit	Anode	Powder
Aluminum	ppm	10	10–20
Calcium	ppm	50	50
Chromium	ppm	20	10
Copper	ppm	10	1
Iron	ppm	30	70–150
Lead	ppm	...	10
Magnesium	ppm	10	10
Manganese	ppm	...	10
Nickel	ppm	10	100–500
Silicon	ppm	30	4–5
Tin	ppm	...	10
Titanium	ppm	1000	100
Vanadium	ppm	...	10
Zirconium	ppm	5000	100

alloy homogeneity. Niobium metal scrap, which is reduced to powder by the hydride–dehydride process, can also be incorporated into the alloy blends.

Some efforts [71] have been directed to producing complex metastable alloy powders, such as niobium–aluminum and niobium–silicon alloys, by liquid metal atomization and rapid solidification.

Most commercial niobium alloys are in wrought form. Primary (bulk) processing is generally done by high temperature extrusion or forging. Secondary working manufactures a variety of mill products such as rod, sheet, wire, foil and tubing. Powder metallurgy methods have been evaluated for common niobium alloys, such as C–103 (Nb–10Hf–1Ti) and Nb–30Hf–9W. It has been found that the high production cost of atomization prevents economic manufacturing of net shape parts. However, hydride–dehydride

Table 21.15 Typical compositions of niobium and Nb–10Hf–1Ti alloy powders made by the hydride–dehydride process

Property	Analysis (ppm)		
	Niobium		Nb-10Hf-1Ti (C-103 niobium alloy) Source: Fansteel Inc
	Source: Fansteel Inc	GOST 26252-84 I-grade	
Elements:			
Niobium	⩾99.7%	balance	⩾87.2%
Hafnium	<20	...	9.8%
Titanium	<20	<10	0.91%
Aluminium	<20	<10	<20
Boron	<1	...	<10
Carbon	500	<50	194
Cobalt	<10	<10	<10
Copper	<40	<30	<40
Hydrogen	150	<20	50
Iron	100	<30	200
Magnesium	...	<10	...
Manganese	...	<10	...
Molybdenum	<20	<30	100
Nickel	<20	<10	<20
Oxygen	1820	<2000	1980
Nitrogen	197	<200	62
Silicon	30	<30	<20
Tantalum	800	<600	2800
Tin	...	<10	...
Tungsten	<50	<30	1100
Zirconium	<20	<10	1800
Other elements[a]	<20	...	<20
Physical properties:			
Apparent density (g/cm^3)	...	0.7	...
Average particle sizes (μm)[b,c,d]	...	1.0; 1.1; 1.3	...
Surface area (m^2/g)	...	0.76	...

[a]Other elements include cadmium, chromium, magnesium, manganese, lead, tin, vanadium;
Method of particle sizes determination:
[b]BET particle size calculated;
[c]mercury porosimetry;
[d]FESEM particle size.

niobium powders are used to produce commercial quantities of hot working preforms of alloy Nb–30Hf–9W [71].

Tantalum

Several methods for reducing tantalum compounds to tantalum metal have been developed, but sodium reduction of the double salt, potassium tantalum fluoride (K_2TaF_7) to produce tantalum metal powder is the most commonly used. The general equation for the reduction with sodium may be represented as:

$$K_2TaF_7 + 5Na = Ta + 5NaF + 2KF$$

The reaction is carried out in a stirred reactor containing molten sodium chloride diluent under an inert atmosphere. The reaction is exothermic and accompanied by heat evolution amounting to 1500 kJ/mol (2 kJ per 1 g of molten sodium). After cooling, the resulting salt cake is removed from the reactor and crushed. The tantalum powder is recovered by thoroughly washing with hot distilled water with an addition of hydrochloric acid and subsequently dried at 107–127°C.

Particles are usually rounded in shape, with a tendency to form grape-like clusters during reduction. Individual particles in such clusters range in size from 1 to 10 μm, depending on reduction variables, including temperature, agitation and salt purity.

Electronic capacitor applications generally require fine particles with high surface area. In one modification of the process, potassium tantalum fluoride, sodium chloride and sodium metal are mixed into a paste and reacted without pre-melting [73]. Flake-shaped tantalum particles are produced by this technique. Since flakes have a higher surface-to-volume ratio than spheres, they are suitable for capacitor applications. In another modification of the process, tantalum powder with highly developed surface can be produced by conducting the process in the presence of small amounts of boron, phosphorus, sulfur and silicon. Even more appreciable effect is achieved by additions ranging from 0.002 to 0.5% of halides, oxides or sulfides of Ti, Zr and Hf.

Generally, a wide range of sodium reduced capacitor powders is currently available, with unit capacitances ranging from 5000 μF · V/g to greater than 25 000 μF · V/g. Capacitor powders are also manufactured from hydrided, crushed and degassed EB-melted ingot. The electron beam melting step allows improvement of the purification of tantalum metal powders. In this process, sodium-reduced powders are pressed into bars which are subsequently EB melted. The resulting ingot is placed in a furnace with a hydrogen atmosphere. The tantalum is fully hydrided on slow cooling from 800°C under hydrogen. The brittle hydride is crushed, ground and classified to yield powder with average particle sizes ranging from 3 to 6 μm. The particles have an angular shape.

Additions of small amounts (10–100 ppm) of sintering inhibitors, such as phosphorus, are frequently employed. These agents allow finer powders to be used than would be possible in the absence of an inhibitor. Alternatively, higher sintering temperatures can be used without loss of surface area, thereby aiding vaporization of undesirable impurities. Dielectric properties are thus improved.

Because capacitance is directly proportional to the tantalum surface area accessible to an electrolyte, a porous structure is desirable. Thus, it is desirable to press the powders to as low a density as possible, while retaining sufficient green strength for handling. In general, sodium-reduced powders can be pressed to lower densities than EB melted, degassed hydride powders. The former material is used in high-capacitance devices at lower voltage ratings (<50 V) as these powders can be produced in finer particle sizes and the material has improved pressing characteristics. However, because of the higher purity of the latter powders, they allow operation at higher voltage. Thus, comparing the two basic types of tantalum powders when used for capacitor manufacture shows that the sodium-reduced powder material has a higher capacitance per gram of powder and better green strength for pressed compacts, while electron beam melted, degassed-hydride powder material has higher purity, better flow characteristics and higher voltage capability in capacitor devices. Currently, sodium-reduced tantalum powders are generally used for 80–90% of capacitor applications.

There is also known an electrolytic process for producing tantalum using an electrolyte containing potassium fluoro-tantalate (K_2TaF_7), potassium (sodium) chloride and/or fluoride in which tantalum pentoxide is dissolved. Carbon dioxide and carbon monoxide are formed at the anode. An anode effect arises during electrolysis of the K_2TaF_7 melt. Potassium chloride and fluoride provide easy fusibility, fluidity and conductivity of the electrolyte, while the tantalum pentoxide improves wettability of the graphite anode. The cathode can be made of molybdenum, nickel, nichrome or steel.

Thus, the oxide-fluoride-chloride electrolytes contain ions of K^+, Cl^-, F^-, TaF_8^{3-}, $TaOF_6^{3-}$ (when the content of Ta_2O_5 in the electrolyte is less than 5%) or $TaO_2F_4^{3-}$ (when content of Ta_2O_5 in the electrolyte is 5% and more).

The discharge of Ta^{5+} ions occurs on the cathode:

$$Ta^{5+} + 5e \rightarrow Ta$$

The scheme of the anode process can be written:

$$TaOF_6^{3-} - 2e = TaF_5 + F^- + 0.5O_2$$
$$TaF_5 + 3K^+ + 3F^- = K_3TaF_8$$
$$0.5O_2 + C = CO\ (O_2 + C = CO_2)$$

Thus, Ta_2O_5 undergoes an electrolysis treatment after finally being introduced into the melt. Precipitation of tantalum on the cathode and oxygen on the anode can be described:

$$4Ta^{5+} + 20e \rightarrow 4Ta \text{ and } 10O^{2-} - 20e \rightarrow 5O_2$$

Reaction of graphite oxidation on the anode accompanied by evolution of energy leads to its depolarization, so that the amount of energy necessary to decompose of Ta_2O_5 is decreased.

The electrolyte contains: 2.5–8.5 wt% Ta_2O_5, 8.5–32.5 wt% K_2TaF_7; 27.5–57.5 wt% KF, 25.5–55 wt% KC1; melting temperature is about 647–697°C, depending on electrolyte composition. Electrolysis is accomplished at 697–747°C. An advanced electrolyte containing 3–3.5 wt% Ta_2O_5, K_2TaF_7; 66.5–72 wt% (NaCl + KCl) with reduced melting point 600°C allows the electrolysis to be conducted at 700°C.

There are two types of electrolyzers. In the first type, a graphite crucible serves as an anode and a metal bar located in the center of the crucible is the cathode. The second type includes a metal crucible as the cathode and a graphite rod or a hollow perforated graphite tube as anode disposed in the center of the crucible (Figure 21.26).

The latter is preferable. In this electrolyzer, Ta_2O_5 is loaded into the cell through the hollow anode and the gases are eliminated through the orifice in the side of the electrolyzer. Electrolysis is performed at a current density 5 kA/m^2 on the cathode and 1.2–1.6 kA/m^2 on the anode. Tantalum dendrites are deposited on the bottom and the sides of the crucible. The process is terminated as soon as the cathode deposit fills two-thirds of the crucible capacity. Tantalum powder particles are imbedded in the solidified electrolyte that protects the metal from oxidation on cooling. The powder particle sizes range from 30 to 120 μm.

The cathode product is milled in a ball-mill that operates in a closed cycle with an air separator. The electrolyte phase is separated and returned to the cell for electrolysis. The tantalum powder is washed on the shaking tables in water jets to eliminate electrolyte, then it is treated with a hot mixture of hydrochloric acid and nitric acid in porcelain reactors to eliminate molybdenum and iron, it is then washed with water again and dried.

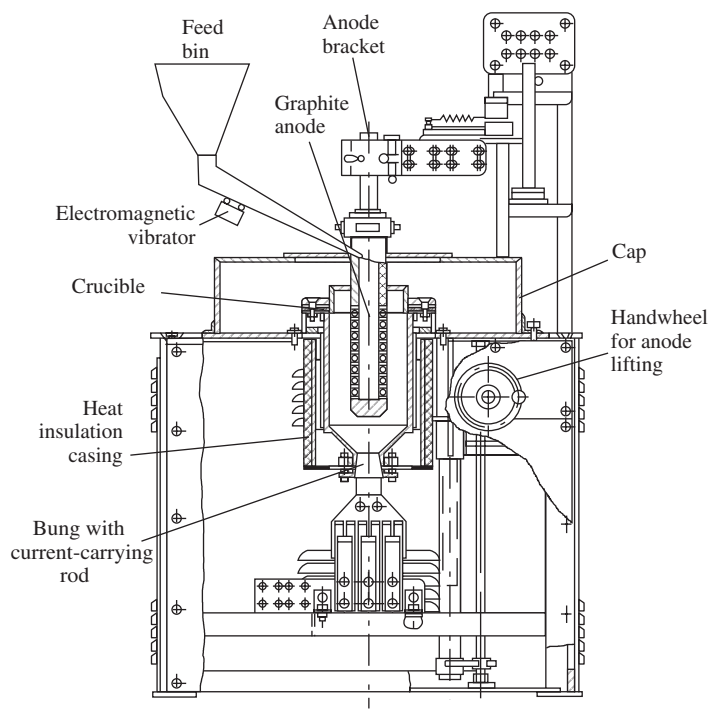

Figure 21.26 Electrolyzer for tantalum production.

A vacuum heating process is also available in which the cathode crucible is heated in argon to 900°C to melt the electrolyte. The vessel is then evacuated and the electrolyte sucked out. The metallic tantalum in form of weakly sintered dendrites in 100–120 μm sizes precipitated on the crucible walls is scraped off and ground. Current efficiency is 80–83%; power consumption is 2300 kWh per tonne.

Tantalum powder can be produced by electrolysis of melts containing tantalum pentachloride ($TaCl_5$). The liquid or vapor $TaCl_5$ (⩽10% of tantalum) is introduced into the melt (NaCl + NaF, NaCl + KCl, or NaCl + KCl + KF) at temperature ranges from 747 to 947°C, with voltage in the cell 6-8 V, cathode current density 5 kA/m^2 and anode current density from 10 to 20 kA/m^2; current efficiency amounts to 85–88%.

The method of tantalum refining in chloride–fluoride and fluoride melts is still attractive as the majority of impurities are eliminated completely; iron content is decreased 10–50 times, oxygen and hydrogen contents are decreased 10–100 times, molybdenum and tungsten content is decreased 10^4–10^5 times, but it is difficult to eliminate niobium.

Typical impurity compositions of sodium-reduced tantalum powder, electron beam melted degassed-hydride powder, electrolytic powder and purified electrolytic powder are given in Table 21.16.

Tantalum Carbide

The conventional technique for tantalum carbide powder production is similar to methods by which tungsten carbide powders are produced.

Stoichiometric tantalum carbide can be used as an additive to WC–Mo grade powder attritions to enhance the physical properties of sintered material. It can be also used as a grain growth inhibitor preventing the formation of large grains resulting in increased hardness of the sintered parts. Additions from a tenth of one percent to 30% are common and completely dependent on the particular application. Typical composition of commercial tantalum carbide powder, produced by OSRAM Sylvania Company, is given in Table 21.17. It also makes tantalum–niobium carbide (TaNbC) of several compositions, such as 90/10, 80/20, and 60/40.

Table 21.16 Typical impurity compositions of tantalum powders manufactured by different methods

Element	Powder analysis (ppm)			
	Sodium-reduced[(s)]	Electron beam melted degassed-hydride	Electrolytic from oxide chloride or oxide fluoride-chloride melts	Purified from fluoride-chloride or fluoride melts with K_2TaF_7
Aluminum	10	5	...	...
Calcium	10	5	...	...
Carbon	100	45	200–300	20–30
Chromium	25	5	...	...
Cobalt	10	5	...	...
Copper	10	5	...	...
Fluorine	...	...	10	...
Hydrogen	30	30	...	...
Iron	50	30	...	20–30
Iron + nickel	...	...	300–1000	...
Lead	10	5	...	...
Magnesium	10	5	...	...
Manganese	10	10	...	...
Nickel	50	5	...	...
Niobium	50	20	...	...
Nitrogen	90	40	...	...
Oxygen	2400	1650	1000–2000	100–200
Silicon	25	10	1000	...
Sodium	10	5	...	...
Tin	10	5	...	...
Titanium	10	5	1000	...
Tungsten	25	25	...	...
Vanadium	10	5	...	...
Zirconium	10	5	...	...

[(s)] Source: Fansteel, Inc.

Table 21.17 Typical properties of tantalum carbide powder

Property	Range	Typical
Particle size FSSS	0.5–2.0 μm	0.8–1.5 μm
Chemical analyses	Maximum percent	Typical percent
Total carbon	6.15–6.30	6.20–6.30
Free carbon	0.15	0.07
Calcium	0.02	0.005
Iron	0.05	0.04
Niobium	0.25	0.10
Oxygen	0.15	0.13
Silicon	0.02	0.01
Titanium	0.02	0.01

(Source: OSRAM Sylvania)

Consolidation and Manufacturing of Semi-products

Powder metallurgy semi-products of tantalum and its alloys are commonly made by cold isostatic pressing of the powders into bars. The bars are then resistance sintered in a vacuum furnace at 1.33×10^{-2} Pa. Heating occurs due to the passage of an electric current. For tantalum, temperatures above 2300°C are required to achieve full density and sufficient purification as a result of removal of interstitial impurity elements. Sintered bars are then rolled or drawn at room temperature, with suitable intermediate vacuum anneals.

Powder metallurgy products differ from those produced from cast materials primarily because surface oxides are present in the initial powders. These oxides are contained in the microstructure of the consolidated PM material. Recrystallization is inhibited and finer grained metal is obtained. The material is usually harder and has higher yield and tensile strength but is somewhat less ductile.

Microalloying additions, such as thoria and yttria, are sometimes added to control grain size and strength after recrystallization. Small quantities of silicon are also added, particularly to bars that are subsequently drawn to capacitor wire. Silicon promotes the retention of ductility of the wire by preventing embrittlement of the tantalum lead-wire embedded in the capacitor pellet. During vacuum sintering, oxygen diffuses from the surrounding powder into the embedded wire, which has lower oxygen, and collects at grain boundaries, thereby stimulating embrittlement. Silicon operates as getter for the excess oxygen. A part of the silicon vaporizes harmlessly in the form of volatile silicon monoxide.

Tungsten and hafnium are the alloying additions commonly added to improve the strength properties of tantalum. Typical properties for commercially produced tantalum and tantalum PM alloys and for comparison cast alloys are given in Table 21.18.

Ta–2.5%W is used for the fabrication of corrosion-resistant heat exchangers, valves and other chemical equipment. Less ductile Ta–10%W alloy is a harder, stronger and more wear-resistant alloy and is especially suited for the manufacture of furnace hardware, missile parts, nozzles and fasteners. A Ta–7.5%W alloy, made by powder metallurgy, is useful for springs, syphons and leaf springs in severe corrosion environments, such as hydrochloric acid, bromine or dry chlorine. Because the yield strength of the PM product is higher than that of ingot material of the same composition, its modulus of resilience is also considerably higher, as illustrated in Table 21.18.

Workplace Atmosphere Safety

The aerosols of metallic niobium and tantalum are not toxic and relegated to the fourth, lowest class of danger accordingly State Standard 12.1.005-88 under the legislation in the Commonwealth of Independents States (CIS) [37]. Inspirable dust of both metals takes predominantly a fibrous effect. The stated average limit value (ALV) of the aerosols of tantalum and its alloys in the workplace atmosphere, as the shift time-weighted average concentration, is 10 mg/m^3. As for niobium, the State Standard 12.1.005-88 standardizes only niobium nitride ALV, which amounts to 10 mg/m^3 (as the shift time-weighted average concentration).

Niobium in potable water has a toxic effect and is placed into the second class of danger and the TLV is 0.01 mg/L (for the inorganic compounds, including transition metals, subject to summation of all form contents) according to CIS State Standard 4630–88 [38].

The low concentration ignition limit (LCIL) of the metallic tantalum powder with particle sizes below 44 μm in the air is 200 g/m^3; minimum ignition temperatures of powder aerosols and aerogels (self-ignition temperature) are 630°C and 290°C, respectively. The products with such characteristics of inflammability and explosion risk are placed in the 'Moderate explosion hazard' class of danger according to the EPMA Guide to Legislation and 'Health and Safety' in the European PM Industry [39].

Common techniques are mainly used for pollution prevention and environmental control by powder manufacturing and its processing. Detailed information on health and environment protection measures and also on prevention of inflammability and explosion risk in such conditions can be found in Section 5.

Table 21.18 Typical properties for commercially produced tantalum and tantalum alloys

Property	Unit	Standard grades						
		Commercial pure tantalum		Ta-10W, EB melted[a]	Ta-7.5W, PM		Ta-7.5W, sheet[b]	
		EB melted[a]	PM		Wire	Sheet	Ingot	PM
Density, at 20°C	g/cm^3	16.9	16.6	16.8	16.8	16.8	...	...
Melting point	°C	3000	3000	3030	3025[c]	3025[c]	...	...
Hardness (HV)	HV	110	120	245	325	400	...	...
Hardness (DPH)	DPH	...	...	...	...	...	150	291
Tensile strength								
20°C	MPa	205	310	550	1035	1165	...	...
200°C	MPa	190	...	515	...	...	...	...
750°C	MPa	140	...	380	...	...	...	...
1000°C	MPa	90	...	305	...	...	...	...
Yield strength								
20°C	MPa	165	220	460	1005	875	483	676
200°C	MPa	69	...	400	...	...	...	...
750°C	MPa	41	...	275	...	...	...	...
1000°C	MPa	34	...	205	...	...	...	...
Elongation								
20°C	%	40	30	25	6	7	...	...
200°C		30	...	...	...	...	...	...
750°C		45	...	...	...	...	...	...
1000°C		33	...	...	...	...	...	...
Modulus of elasticity								
20°C	GPa	185	185	205	200	200	196	196
750°C	GPa	160	...	150	...	...	...	...
Modulus of resilience (U_R)[d]								
20°C	MPa	...	...	...	...	...	593	1172

[a]EB, electronic beam;
[b]Measured for 2.1 mm thick, annealed and recrystallized sheet;
[c]Estimated;
[d] $U_R = \sigma_0^2/2E$.
Source: Ref 78

Rhenium

Except for tungsten and carbon, rhenium, among the elements, has the highest melting point which is 3180°C. Its density is exceeded only by osmium, iridium and platinum. Rhenium has the highest modulus of elasticity among the refractory metals. A ductile-to-brittle transition temperature does not exist in pure rhenium. Rhenium is the only refractory metal that does not form carbides.

Production

The main method for rhenium powder production is reduction of ammonium perrhenate (NH_4ReO_4) by hydrogen. The reduction can be written:

$$NH_4ReO_4 + 2H_2 = Re + 1/2\ N_2 + 4H_2O$$

Typical impurity composition of hydrogen reduced powders is: ⩽5 ppm (Al + Fe + Cu + Mo), ⩽10 ppm (Ca + Si + P + Na), ⩽20 ppm (Mg + Ni + S), ⩽50 ppm K, ⩽1 ppm Mn, and Cu⩽0.5 ppm.

Raw material is milled in rubber-lined drums, then it is reduced in pusher type furnaces. The ammonium perrhenate is loaded into flat molybdenum boats, which are pushed through the furnace. Reduction takes place in two stages. At 343–363°C. ReO_2 is formed and a final reduction to metal is done at 947–967°C. The time of the boats in the hot zone of furnace is 1–2 hours. Average size of powder particles ranges from 1 to 3 μm. Apparent density ranges from 1.5 to 1.9 g/cm^3.

Among the refractory metals, rhenium has the highest tensile strength (Figure 21.27). Rhenium has high electrical resistivity. It typically exhibits higher resistivity than tungsten. This feature, associated with a low vapor pressure, makes it perfectly suited for filament applications; parallel with this, it preserves ductility and is not affected by the oxidation/reduction cycle experienced in these applications, as is tungsten. Rhenium does not react with molten copper, silver, tin or zinc. While readily soluble in molten iron and nickel, it is stable in the presence of aluminum.

Rhenium is resistant to hydrochloric acid and seawater corrosion and to mechanical effects of electrical erosion. At elevated temperatures, rhenium resists reaction in hydrogen and inert atmospheres.

Rhenium Alloys

Rhenium is used in combination with platinum in catalysts, especially for selective hydrogenation and crude oil reforming. Rhenium catalysts show high resistance to poisons, such as nitrogen oxides, sulfur and phosphorus.

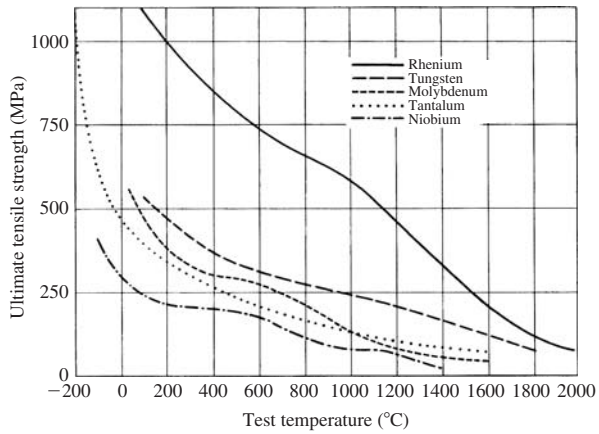

Figure 21.27 Dependence of ultimate tensile strength for pure refractory metals on temperature. Source: Ref 60®

Rhenium is an advantageous alloying addition with other refractory metals. It greatly enhances the ductility and tensile strength of refractory metals and their alloys. This tendency is retained on heating above the recrystallization temperature. For example, alloys of molybdenum and rhenium are more ductile than pure molybdenum. An alloy with 35% Re can be rolled at room temperature to more than 95% reduction in thickness before cracking. For economic reasons, molybdenum-rhenium alloys are not widely used commercially. Alloys of molybdenum with 5 and 41% Re are used for thermocouple wires.

Applications

Rhenium alloys are used in nuclear reactors, semiconductors, thermocouples, electronic tube components, gyroscopes, parts for rockets, electrical contacts, thermionic converters and various parts for high temperature aerospace applications.

Recent developments in the production of net shapes by powder metallurgy rhenium manufacturing techniques have generated significant saving in both time and budget. For instance, the thrusters of different and unique types of aerospace components (rhenium combustion chambers) were manufactured by means of near-shape technique [74]. As is known, near-net shapes are produced using elastometric molds with and without hard tooling inserts. The mold cavity is dimensioned so that after CIP and sintering, final dimensions require only a

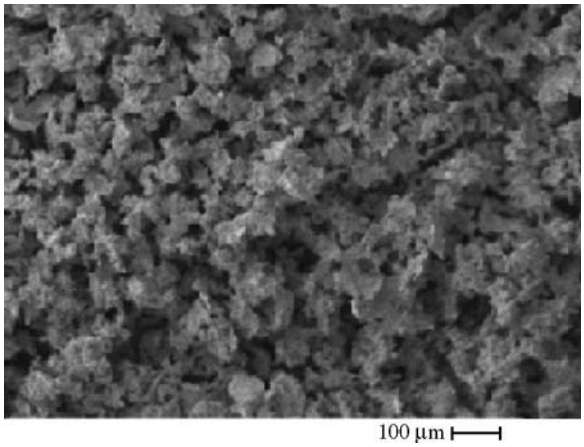

Figure 21.28 Scanning electron micrograph of the rhenium metal powder. Source: Ref 76

minimum amount of finish machining [75]. The use of this technique allows the making of parts with a density of 95–98% after sintering and 98.5–99.9% on subsequent hot isostatic pressing [76]. Typical microstructure of the initial rhenium metal powders is shown in Figure 21.28. The production of near-shape PM rhenium combustion chambers has reduced the manufacturing cost to 35%, and shortened the manufacturing time by 30–40%. The quantity of rhenium metal powder used to produce a chamber is reduced by approximately 70% and subsequent reduction in machining costs is nearly 50%. Thus, cold isostatic pressing to near-net shape has provided significant cost savings and also increased the quality and density of rhenium parts.

Tungsten–rhenium alloys, applied by vapor deposition, are used to coat the surface of molybdenum targets in X-ray tube manufacture. Other rhenium alloys, with tungsten and molybdenum, are used for filaments, grid heaters, cathode cups and ignitor wires in photoflash bulbs. One of the largest applications for rhenium is for mass spectrometer filaments. These are available in commercial (99.99%) and zone-refined (99.95%) purities.

References

1. Yih, S.W.H., Wang, C.T., Tungsten sources. In: *Metallurgy, Properties and Applications*. Plenum Press, 1979.
2. Lux, B., Zeiler, B., Production of tungsten and tungsten carbide powders. In: *ASM Handbook*, Vol. 7. ASM International Publishers, 1998, pp. 188–201.
3. Williams, B., Powder metallurgy – a global market review. In: *International Powder Metallurgy Directory & Yearbook*, 13th edn 3, 2008/2009, pp. 5–14.
4. Technical data, International Tungsten Industry Association.
5. Lassner, E., Schubert, W.D., Lüderitz, E., Wolf, H.U., Tungsten, tungsten alloys and tungsten compounds. In *Ullmann's Encyclopedia of Industrial Chemistry*, Vol. A27. VCH Verlagsgeselshaft GmbH, 1992.
6. Spross, M., Berg- und Huettenmaennische Montashefte. *J. Mining Metall., Mater. Geotech. Plant Eng*., 1996, 141(8):359–362.
7. Wolfram, 1975–2000. Wolfram Bergbau und Hütten GmbH.
8. Naboychenko, S.S. (ed.) *Handbook of Non-ferrous Metal Powders*. Metullurgiya, Moscow, 1997 (in Russian).
9. Lambert, J.B. (Chair) et al., *ASM Handbook*, Vol. 2, Nonferrous Alloys and Special-Purpose Materials, Art: Refractory Metals and Alloys. ASM International Publishers.
10. Method for Determination of Average Particle Size of Metal Powders Using the Fisher Subsieve Sizer, MPIF Standard 32. MPIF Publishers, Princeton, 2003, pp. 45–47.
11. ASTM Standards, American Society for Testing and Materials.
12. Wilhartitz, P., Ortner, H.M., Krismer, R., Analytical characterization of ultrapure refractory metals – a critical comparison of techniques. In *Proceedings of 12th Int. Plansee Seminar*, Vol. 3, 1989, pp. 575–586.
13. Pink, E., Bartha, L., (eds) *The Metallurgy of Doped Non-Sag Tungsten*. Elsevier, 1989.
14. Bartha, L., Lassner, E., Schubert, W.D., Lux, B., Special issue: The Chemistry of Non-Sag Tungsten. *Int. J. Refract. Met. Hard Mater*., 1995, 13.
15. Harmat, P., Grósz, T., Rosta, L., Bartha, L., A novel method for shape analysis: deformation of bubbles during wire drawing in doped tungsten. In *Proceedings of 15th International Plansee Seminar*, Vol. 4, 2001, pp. 108–117.
16. Horacsek, O., Bartha, L., Potassium incorporation into tungsten by entrapment of dopant particles formed on the surface of AKS-doped TBO. In *Proceedings of 15th International Plansee Seminar*, Vol. 1, 2001, pp. 658–668.
17. Dudder, G.B., Gurwell, W.E., Hydrogen embrittlement effects on tensile properties of tungsten heavy alloys. In: *Proceedings Tungsten and Tungsten Alloys – Recent Advances*. The Minerals, Metals and Minerals Society, 1991, pp. 161–167.
18. Caldwell, S.G., Variation of Ni/Fe ratio in W-Ni-Fe heavy alloys: a current perspective. *Proceedings Tungsten and Tungsten Alloys – 1992*. Metal Powder Industries Federation, 1993, pp. 89–96.

19. Rabin, B.H., Moyer, R.M., Microstructure and tensile properties of tungsten-nickel-iron compositions. *Metall. Trans. A*, 1998, 19:523–1532.
20. Spencer, J.R., Mullendspore, J.A., Relationship between composition, structure, properties, thermo-mechanical processing, and ballistic performance of tungsten heavy alloys. Report MTL TR 91-44, US Army Materials Technology Laboratory, Watertown, 1991.
21. Debata, M., Upadhyaya, A., Sintering of tungsten-based heavy alloys with NiB and FeB additives. In *Proceedings of 2004 Powder Metallurgy World Congress*, compiled by European Powder Metallurgy Association, Bellstone Shrewsbury, UK, 2004, Vol. 4, pp. 825–830.
22. Sebastian, K.V., Properties of sintered and infiltrated tungsten-copper electrical contact material. *Int. J. Powder Met. Powder Techn.*, 1981, 17(4):297–302.
23. German, R.M., Hens, K.S., Johnson, J.L., Powder metallurgy processing of thermal management materials for microelectronic application. *Int. J. Powder Metall.*, 1994, 30(2):205–215.
24. Wang, W.S., Hwang, K.S., The effect of tungsten particle size on the properties of infiltrated-Cu compacts. In *Proceedings Advances in Powder Metallurgy and Particulate Materials*, compiled by R.A. Mckotch, R. Webb. MPIF-APMI, Chicago, 1997, Vol.1, pp. 757–764.
25. Kim, J.C., Ryu, S.S., Kim, Y.D., Moon, I.H., Densification behavior of mechanically alloyed W-Cu composite powders by the double rearrangement process. *Scripta Materialia*, 1998, 39(6):669–676.
26. Yu, J.H., Kim, T.H., Lee, J.S., Particle growth during liquid phase sintering of nanocomposite W-Cu powder. *Nanostructured Materials*, 1997, 9:229–232.
27. Hong, S-H., Kim, T-H., Kim, B-K., Fabrication of W-10Cu alloy with high thermal conductivity. In *Proceedings of 2002 Powder Metallurgy World Congress*, compiled by V. Arnold, C.-L. Chu, W.F. Jandeska, H.I. Sanderow, Princeton, MPIF Publishers, New Jersey, 2002, pp. 7-180–7-190.
28. Kim, D.G., Lee, K.W., Kim, Y.D., Fabrication of nanostructural W-Cu powder using W-CuO mixture. In *Proceedings of 2002 Powder Metallurgy World Congress*, compiled by V. Arnold, C.-L. Chu, W.F. Jandeska, H.I. Sanderow, Princeton, MPIF Publishers, New Jersey, 2002, pp. 7-165–7-170.
29. Selcuk, C., Morley, N., Wood, J.V., Effect of post-sintering heat treatment on porous tungsten in relation to sintering swelling. In *Proceedings of 2004 Powder Metallurgy World Congress*, compiled by European Powder Metallurgy Association, Bellstone Shrewsbury, UK, 2004, Vol. 2, pp. 152–158.
30. Ivanov, E., Wickersham, C.E. Jr, Compaction of mechanically milled pure nanocrystalline tungsten. In *Proceedings of 14th International Plansee Seminar*, Vol. 1, 1997, pp. 207–216.
31. Öveçoglu, M.L., Ozkal, B., Suryanarayana, C., A composition of the sintering characteristics of ball milled and attritor milled W-Ni-Fe heavy alloys. *J. Mater. Research*, 1998, 11(7):1673–1682.
32. Povarova, K.B., Makarov, P.V., Luk'yanchikova, S.S., Zavarina, E.K., Effect of high-energy ball milling on structure and some properties of powder tungsten alloys. *Izvestiya Rossiiskoi Akademii Nauk, Metally*, 1994, (6):113–123.
33. Taillard, R.A., Avettand-Fènoel, M-N., Dhers, J., Foct, J., Ball-milling and sintering of blends of tungsten and yttrium-reach powders. In *Proceedings of 2002 Powder Metallurgy World Congress*, compiled by V. Arnold, C.-L. Chu, W.F. Jandeska, H.I. Sanderow, Princeton, MPIF Publishers, New Jersey, 2002, pp. 6-188–6-202.
34. Jech, D.E., Sepulveda, J.L., Traversone, A.B., Process for making improved copper/tungsten composites. US Patent 5,686,676 (1997).
35. Bose, A., Walker, D., Timmons, R., Graham, M., Complex shaped hardmetals by PM. In *Proceedings of 2004 Powder Metallurgy World Congress*, compiled by European Powder Metallurgy Association, Bellstone Shrewsbury, UK, 2004, Vol. 3, pp. 400–409.
36. Leichter, P., Trombitas, H., Vesely, A., AT-Patent AT 403,060 (Austria), 1997.
37. Commonwealth of Independents States Standard GOST 12.1.005−88 (in Russian).
38. Sanitary Regulation and Standards of surface waters from pollution. SanPiP 4630–88.
39. Guide to Legislation and 'Health and Safety' in the European PM Industry. EPMA, 1997.
40. Zeiler, B, The potential of conventional tungsten carbide powder manufacturing. In *Proceedings of 14th International Plansee Seminar*. RWF Werbegesellschaft, Vol. 4, 1997, pp. 265–276.
41. Bock, A., Zeiler, B., Production and characterization of ultrafine WC powders. In *Proceedings of 15th International Plansee Seminar*. 2001, Vol. 4, pp. 229–244.
42. McKenna, P.M., US Patent 3,379,503 (1968).
43. Schubert, W.D., Bock, A., Lux, B., General aspects and limits of conventional ultrafine WC powder manufacture and hard metal production.

In *Proceedings of 13th International Plansee Seminar*. RWF Werbegesellschaft, Vol. 4, 1993, pp. 283–305.
44. Yamamoto, Y., Matsumoto, A., Doi, Y., Properties of ultrafine tungsten carbide and cemented carbide by direct carburization. In *Proceedings of 14th International Plansee Seminar*. RWF Werbegesellschaft, Vol. 2, 1997, pp. 596–608.
45. Dunmead, S.D., Moore, W.D., Weiner, A.W., Eisman, G.A., Henley, J.P., Method for making submicrometer carbides, submicrometer solid solution carbides, and the material resulting there from, US Patent 5,380,688 (1995).
46. Carroll, D.F., Processing and properties of ultrafine WC/Co hard materials. In *Proceedings of 14th International Plansee Seminar*. RWF Werbegesellschaft, Vol. 2, 1997, pp. 168–182.
47. McCandish, L.E., Kear, B.H., Kim, B.K., Carbothermic reaction process for making nanophase WC-Co powders, US Patent 5,230,729 (1993).
48. König, T., Fister, D., Stark, H.C., GmbH & Co. KG, Goslar, EU Patent EP 0 568861 B1, (1993).
49. Schedler, W., Hardmetall für den Praktiker. VDI-Verlag GmbH, 1988.
50. Oyana, S.T. (ed.) *The Chemistry of Transition Metals Carbides and Nitrides*. Blackie Academic and Professional, 1996.
51. Brookes, K.J.A., *World Directory and Handbook of Hardmetals and Hard Materials*, 6th edn. International carbide data, Hertfordshire, UK, 1996.
52. Schubert, W.D., Neumaster, H., Kinger, G., Lux, B., Hardness to toughness relationship of fine-grained WC-Co hard metals. In *Proceedings of 14th International Plansee Seminar*. RWF Werbegesellschaft, Vol. 4, 1997, pp. 249–264.
53. Hellman, P.M., *Review of HIP Development, Hot Isostatic Pressing – Theories and Application*. Centek Publishers, 1988.
54. Fang, Z., Wear resistance of powder metallurgy alloys. In *ASM Handbook*, Vol. 7. ASM International Publishers, 1998, pp. 965–977.
55. Findeisen, E. et al., Process of manufacturing cast tungsten carbide spheres. US Patent 5,089,182 (1992).
56. Schubert, W.D., Kübel, E., Mechanical testing of specimens and impact of trace elements on properties of hard metals. In *Proceedings of 12th International Plansee Seminar*. Verlagenstalt Tyrolia, Vol. 2, 1989, pp. 869–909.
57. Uhrenius, B., Brandrup-Wognsen, H., Gustavson, U., Lethinen, B., Manninen, H., On the formation of impurity-containing phases in cemented carbides. In *Proceedings of 12th International Plansee Seminar*. Verlagenstalt Tyrolia, Vol. 2, 1989, pp. 71–96.
58. Kieffer, B.F., Baroch, E.F., Extractive metallurgy of refractory metals. AIME Publishers, 1981.
59. Molybdenum ore treatment – 1980 to December 1982, NTIS Published Search, PB83-857250, Dec 1982.
60. Lambert, J.B. et al., Refractory metals. In *ASM Handbook*, Vol. 7. ASM International Publishers, 1998, pp. 903–913.
61. Shen, Y.-S., Lattari, P., Gardner, J., Wiegard, H., Electrical contacts. In *ASM Handbook*, Vol. 2. ASM International Publishers, 1990, pp. 840–868.
62. Endo, M., Kimura, K., Udagava, T., Tanabe, S., Seto, H., The effects of doping molybdenum wire with rare earth elements. In *Proceedings of 12th International Plansee Seminar*. Metallwerk Plansee, Reutte, Vol. 1, 1989, pp. 37–52.
63. Takida, T., Kurishita, H., Mabuchi, M., Igarashi, T., Doi, Y., Nagae, T., Mechanical properties of fine-grained sintered molybdenum alloy processed by mechanical alloying. In *Proceedings of 15th International Plansee Seminar*. Plansee Holding AG, Vol. 1, 2001, pp. 293–304.
64. Mueller, A.J., Shields, J.A., Buckman R.W., The effect of thermo-mechanical processing on the mechanical properties of molybdenum–2 vol% lanthana. In *Proceedings of 15th International Plansee Seminar*. Plansee Holding AG, Vol. 1, 2001, pp. 485–497.
65. Bianco, R., Buckman, R.W., Geller, C.B., High strength, creep-resistant molybdenum alloy and process for producing the same. US Patent 5,868,876 (1999).
66. German, R.M., Labombard, C.A., Sintering molybdenum treated with Ni, Pd, and Pt. *Int. J. Powder Metall. Powder Tech.*, 1982, 18(2): 147–156.
67. Hwang, K.S., Huang, H.S., The liquid phase sintering of molybdenum with Ni und Cu addition. *Mater. Chemic. and Phys.*, 2001, 67:92–100.
68. Huang, H.S., Hwang, K.S., Embrittlement of activation sintered molybdenum. In *Proceedings of 2002 Powder Metallurgy World Congress*, compiled by V. Arnold, C.-L. Chu, W.F. Jandeska, H.I. Sanderow, Princeton, MPIF Publishers, New Jersey, 2002, pp. 6-77–6-88.
69. Kirk, R.E., Othmer, D.F., (eds), *Encyclopedia of Chemical Technology*, 3rd edn, Vol. 22. John Wiley & Sons, 1983.
70. Lerner, B.J., US Patent 3,294,482 (1966).
71. Wojcik, C.C., Processing, properties, and applications of high-temperature niobium alloys. In

Proceedings of 1994 Symposium, High Temperature Silicides and Refractory Alloys, Vol. 322, Materials Research Society, 1994, pp. 519–530.
72. Zelikman, A.N., Korshunov, B.G., *Metallurgy of Rare Metals*. Metallurgiya Publisher, Moscow, 1991 (in Russian).
73. Borchwes, P. et al., *Extractive Metallurgy of Refractive Metals*. Metallurgical Society of the American Institute of Mechanical Engineers, 1981.
74. Leonhardt, T., Hamister, M., Carlen, J.C., Near-net shape powder metallurgy rhenium thruster. AIAA paper 2000–3132, 2000.
75. Price, P.E., Cold isostatic pressing. In *ASM Handbook*, Vol. 7, ASM International Publishers, 1998, pp. 382–388.
76. Leonhardt, T., Downs, J., Near net shape of powder metallurgy rhenium parts. In *Proceedings of 15th International Plansee Seminar*. Plansee Holding AG, Vol. 1, 2001, pp. 647–657.

Chapter 22

Production of Rare Metal Powders

Stanislav S. Naboychenko, Irina B. Murashova, Ural State Technical University (UPI), Yekaterinburg, Russia
Oleg D. Neikov, Frantsevich Institute for Problems of Materials Science (IPMS), Kiev, Ukraine

Rare metals, listed in Table 22.1 [1], is a term dating from the beginning of the 20th century to denote elements the extraction of which had not been commercially realized or had found little application, less common was another term in use.

The majority of the rare metals (RM) are, in fact, widely distributed in the earth's crust but their extraction from rocks and refining present complicated technical problems. With improved extraction processes and increasing consumption, the term RM is losing its original significance.

In Table 22.1, the rare metals are divided into several classes, but this convention is of limited significance as many of the elements could be included in more than one group. For example, rubidium and cesium can be light or trace elements, while rhenium, a typical trace element, is, at the same time, a refractory metal, and titanium is a refractory metal but also a light metal. Thus, the group 'Rare metals' is not distinguished on some kind of scientific classification of the elements but was formed historically.

Table 22.1 Classification of rare metals

Group of periodic table	Elements	Group by techniques classification
I	Lithium, rubidium[a], cesium[a]	Lightweight
II	Beryllium	
IV	Titanium, zirconium, hafnium[b]	Refractory
V	Niobium, tantalum, vanadium	
VI	Molybdenum, tungsten	
VII	Rhenium[b]	
III	Gallium, indium, thallium	Trace elements
IV	Germanium	
VI	Selenium, tellurium	
VII	Rhenium	
VIII	Ruthenium	
III	Scandium, ittrium, lanthanum and lanthanides (14 elements from cerium to lutecium)	Rare-earth
II	Radium	Radioactive elements
III	Actinium and actinides (thorium, protactinium, uranium and transuranium elements)	
V	Polonium	

[a]Rubidium and cesium are the trace elements, but by their properties may be related also to light rare metals
[b]Hafnium and rhenium are typical trace elements, but by their properties may be related also to refractory metals.

Information on powder production of refractory metals, including tungsten, molybdenum, niobium, tantalum, and rhenium is given in Chapter 21, while information on titanium powders is contained in Chapter 14.

Vanadium

Among the rare elements, vanadium is one of the most common. The content of vanadium in the earth's crust exceeds that of copper, zinc or lead. A brittle metallic vanadium powder was first obtained by the English chemist G. Roscoe in 1869, but it was only in 1927 that D. Marden and M. Rich succeeded in producing ductile vanadium in the form of granules and beads. However, even today, vanadium is regarded as one of the most difficult metals to produce in pure form because of its non-homogeneous composition and high impurity content, especially interstitial impurity. In this connection, and because of the high cost, vanadium has mainly been used as an alloying addition [2].

As a base of heat-resisting alloys, vanadium is of interest because of such properties (Table 22.2) as high strength at elevated temperatures up to 600–800°C, relatively low density 6.1 g/cm^3, good corrosion resistance (approximately the same as that of titanium and chromium), resistance to attack by liquid alkali metals (nuclear reactor coolants), small thermal neutron capture cross-section ((4.5 ± 0.9) 10^{-28} m^2/at) and negligible capture cross-section of fast neutrons with energies of 100–1000 keV in the region of the maximum of the energy spectrum of sodium-cooled fast breeder reactors [3]. Vanadium has potential as a constructional material for reactors. The metal and particularly its alloys, being resistant to corrosion by carbon dioxide, show great promise as jet engine materials.

According to [5], at temperatures above 600°C vanadium and carbon dioxide vigorously react with each other, which manifests itself in an increase in the weight of specimens, a rise in their carbon content and a change in their surface phase composition (formation of oxides, following by carburization at temperature above 800°C). Thus, in carbon dioxide, vanadium base materials should not be used at temperatures exceeding 600°C.

Of the numerous methods of producing metallic vanadium, the following, usually yielding a sponge or powder product, can be cited:

- reduction of vanadium pentoxide by aluminum and subsequent vacuum treatment (aluminothermic process)
- reduction of pentoxide or trioxide by carbon or vanadium carbides in a vacuum (carbothermic process)

Table 22.2 Typical properties of vanadium

Property	Unit	Value
Density	g/cm^3	6.11
Crystal type[a]		bcc
Atomic diameter	nm	0.266
Brinell hardness	MPa	600
Melting point	°C	1900 ± 25
Boiling point	°C	3377
Specific heat at 0–100°C	J/(kg · °C)	498
Heat of fusion	kJ/mol	18.0
Heat of vaporization	kJ/mol	460
Thermal conductivity at 100°C	W/(m · °C)	30.9
Coefficient of linear thermal expansion at temperature ranges from 20 to 1100°C	°C^{-1}	$9.53 \cdot 10^{-6}$
Specific electrical resistance at 20°C	μΩ · m	0.26[b]
Volume diffusion	m^2/s	$4 \cdot 10^{-5}$
Volume diffusion activation energy	kJ/mol	317
Grain boundary diffusion	m^2/s	$5 \cdot 10^{-14}$
Grain boundary diffusion activation energy	kJ/mol	209
Section capture of thermal neutrons $n \times 10^{24}$	cm^2	5.1 ± 0.2

[a]Crystal type: bcc, body-centered cubic;
[b]after cold treatment. Source: Refs 1, 4

- reduction of various vanadium oxides by calcium in the presence of a halide flux (calciothermic process)
- reduction or decomposition of vanadium halides by hydrogen or metals (magnesium or sodium)
- electrolytic refining in a salt bath or precipitation out of a salt bath, using chloride and bromide melts.

Alumothermic reduction of the pentoxide (V_2O_5) is the simplest and cheapest method of manufacture of a crude product for subsequent refining and for the production of ferro-vanadium and titanium–vanadium–aluminium alloys [6].

Calciothermic reduction is widely used for obtaining vanadium powder from the vanadium trioxide [7]. A better than 99% pure metal can be produced (Table 22.3). A high concentration of impurities and variation of impurity content both within each batch and from batch to batch, which are linked with the specific nature of the calciothermic reduction process, constitute major obstacles to the use of calciothermic powder in powder metallurgy.

The magnesiothermic process, in which the complex physicochemical behavior of vanadium chlorides during reduction is of special interest, has potential for the manufacture of metal of low oxygen and nitrogen content at reduced cost. Vanadium containing 60–90 ppm oxygen was manufactured by magnesiothermic reduction [8].

Carbothermic reduction of oxides in a vacuum is the most economical method of producing vanadium intended for electrolytic refining. However, to obtain pure ductile vanadium containing, to say, 0.06% oxygen and 0.12% carbon, it is necessary to perform additional operations such as hydrogenation, crushing, milling and composition correction, which decrease productivity [9]. This method would appear to be the most suitable for the production of carbon-containing vanadium alloys by the simultaneous reduction of oxides with carbon or certain carbides.

Thermal decomposition of vanadium diiodide is an excellent laboratory method of refining vanadium but, because of low productivity, it is not suitable for commercial production.

So far, electrolytic refining is the only method of producing vanadium powder with an interstitial impurity content low enough to enable high density ductile metal to be obtained by powder metallurgy techniques. Vanadium of various origins (reduced by the carbothermic, calciothermic and others processes) is electrolytically refined in a chloride bath. A single refining increases the purity of metal from 99.4 to 99.98% and a second to 99.99%. Such characteristics of the electrolytic process as continuity, precise control and regulation of parameters and modest purity requirements for starting materials which do not an adverse effect on the quality of the end product, ensure a uniform impurity content and particle size distribution. These properties are particularly important in the production of materials by powder metallurgy.

Table 22.3 Nominal chemical composition of vanadium powders produced by different methods

Element	Unit	Method			
		Calciothermic reduction	Electrolysis grade[a]		Carbothermic reduction[c]
			VEL-1[b]	VEL-2	
Vanadium	wt%	99.00	99.99	99.40–99.92	98.00
Trace impurities:					
Aluminum	ppm	200	<100	<100	...
Calcium	ppm	1000	...	...	...
Carbon	ppm	400–2300	<100	<100	1200
Iron	ppm	200	<100	<1000	...
Hydrogen	ppm	20–50	...	...	...
Molybdenum	ppm	100	...	...	...
Nickel	ppm	...	<100	<400	...
Nitrogen	ppm	60–500	<500	<400	...
Silicon	ppm	...	<100	<100	...
Sulfur	ppm	...	<50	<50	...
Oxygen	ppm	200–1400	<500	<1000	600

[a]CIS (Commonwealth of Independents States) TU 48-4-335-86 standard

[b]After second refining

[c]Carbothermic reduction with subsequent refinement.

Vanadium powders VEL2 and VEL3 below 150 μm in size exhibit good compressibility. Double-ended pressing in steel dies under pressure of 1.0–1.2 GPa enables relative compact densities of 92–93% to be attained (Figure 22.1) [8].

Vacuum sintering at a residual pressure of 1.33 MPa is accompanied by a slight shrinkage of the compacts. The powder particle sizes below 200 μm do not affect the general character of the volume shrinkage on sintering (Figure 22.2), but a powder of particle size less than 100 μm exhibits greater activity during sintering, which leads to a higher degree of densification compared with coarser powder fractions.

A well known Ti–6Al–4V alloy is widely used for various industrial applications such as aerospace, chemical plants and so on, because of its high strength, good ductility, high corrosion resistance and low density. In order to improve its machinability and reduce the cost of producing parts with complicated shapes, the metal injection moulding (MIM) technique was used [10]. The starting material consisted of pure titanium powder with the particles below 45 μm and 10 wt% of coarse or fine 60Al–40V powder of particle sizes less than 40 and 20 μm, respectively. The powder mixtures were then kneaded with binder (30 wt% polypropylene, 40 wt% polymethyl methacrylate, 29 wt% paraffin wax and 1 wt% stearic acid) by means of a pressure-type kneading machine at 170°C for 8 ks. The powder loading was 65 vol%. The feedstock produced was then injection molded into compacts. After injection molding, extraction debinding, which vaporized the solvent, was conducted at 70°C for 21.6 ks in n-hexane, to remove partially the wax and polymethyl methacrylate. Final thermal debinding was performed from room temperature to 430°C in reduced pressure of argon gas and continuous sintering was accomplished in a vacuum (of the order of 10^{-2} Pa) with various sintering conditions.

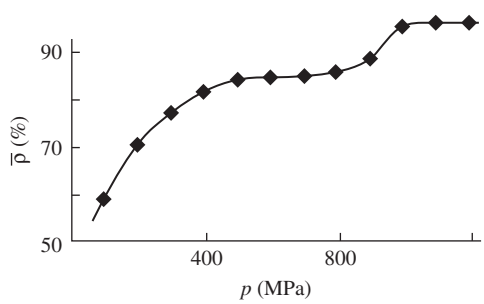

Figure 22.1 Variation of relative density ($\bar{\rho}$) of compacts of VEL1 and VEL2 powders depending on the pressing pressure (p).

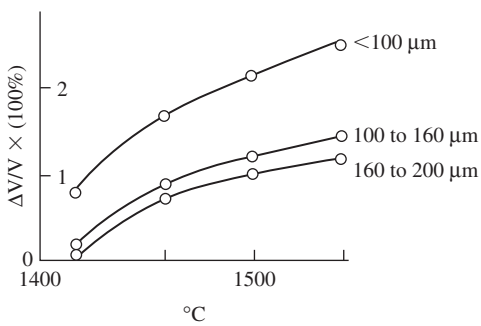

Figure 22.2 Variation of volume shrinkage of compacts from several fractions of VEL1 and VEL2 powders depending on the sintering temperature.

The relative density of the compacts for both, coarse and fine 60Al–40V powder types increases with increasing sintering temperature and reaches 97–98% at 1350°C. The relative density of the compacts using fine 60Al–40V powders is about 1% higher than that of the compacts using the coarse one (Figure 22.3). The tensile strength of the compacts increases with increasing sintering temperature, but it abruptly decreases at sintering temperatures above 1250°C (Figure 22.4). The behavior of the elongation as a function of sintering temperature is similar to that of the tensile strength.

Vanadium and vanadium alloys are widely used in particle metallurgy (PM) tool steels. In order to avoid the variant reading, we note that the term 'particle metallurgy' terminology applies exclusively to powder metallurgy (P/M) processes, where prealloyed and gas atomized powders are consolidated to full density by hot isostatic pressing (HIP). Particle metallurgy processing of tool steels was first introduced commercially by the Crucible Materials Corporation in 1970,

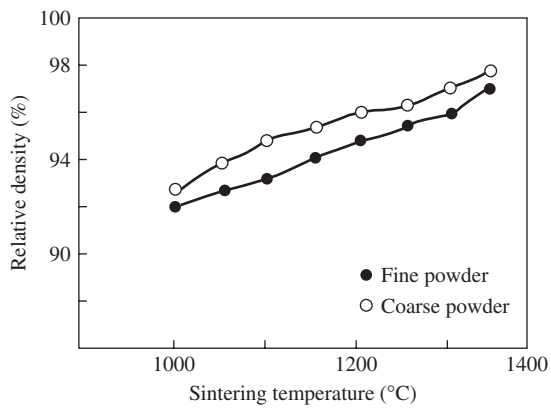

Figure 22.3 Influence of sintering temperature on the relative density of Ti–6Al–4V alloy compacts for two granulometric compositions of 60Al–40V powders (coarse and fine powders with particle sizes <45 and <20 μm, respectively). Source: Ref 10

and is currently the primary manufacturing method used for the development and production of high-performance high-alloy tool steel and tooling composites [11]. Particle metallurgy is used to distinguish such processing from traditional powder metallurgy techniques that typically employ mechanical pressing and high-temperature sintering to achieve varying degrees of densification in relatively small net shape parts.

Generally, the basic PM process consists of induction melting of prealloyed material (with or without secondary refining), gas atomization to produce a rapidly solidified spherical powder, screening and encapsulation of the powder and consolidation by HIP. There are a few select applications where it may be practical or technically necessary to use the HIP product directly, while the more common practice is to HIP a large cylindrical compact that is then hot worked to round or rectangular billets for subsequent hot rolling and finishing to round bar, flat bar, or plate and sheet products. These are the same product forms in which conventionally produced tool steels are stocked for sale to tooling or equipment component manufacturers. Consolidation by hot extrusion or other forging techniques is technically feasible, but usually not workable due to size limitations. It is also possible to produce near-net shapes using HIP technology, but it is commonly more economical to machine directly from semi-finished products.

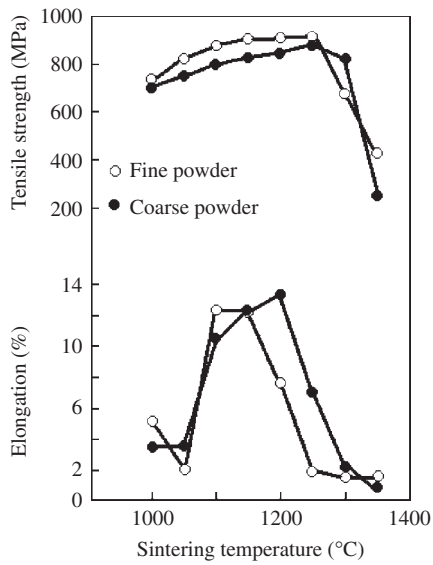

Figure 22.4 Influence of sintering temperature on the tensile properties of 60Al–40 V alloy compacts in the form of strip with length 75 mm, width 5 mm and thickness 2 mm for two granulometric compositions of 60Al–40V powders (coarse and fine powders with particle sizes <45 and $<20\,\mu$m, respectively). Source: Ref 10

The distinguishing characteristic of wrought PM high-alloy tool steels, compared to conventionally ingot cast and wrought materials of similar composition, is the uniform distribution and small size of the primary carbides that form in the PM tool steels due to rapid solidification of the particles obtained by atomization. Figure 22.5 shows the primary carbide distribution observed in the heat treated microstructures of 51 mm diameter wrought PM and conventional T15 alloy (1.5C–12W–5V–5Co), where the primary carbides are a combination of vanadium-rich MC and tungsten-rich M_6C types.

Many of the PM high-speed steels are also used in cold work operations, where a combination of good wear resistance and high hardness is required. PM M3 and PM M4 (Table 22.4) are particularly well suited for cold working application because of their excellent

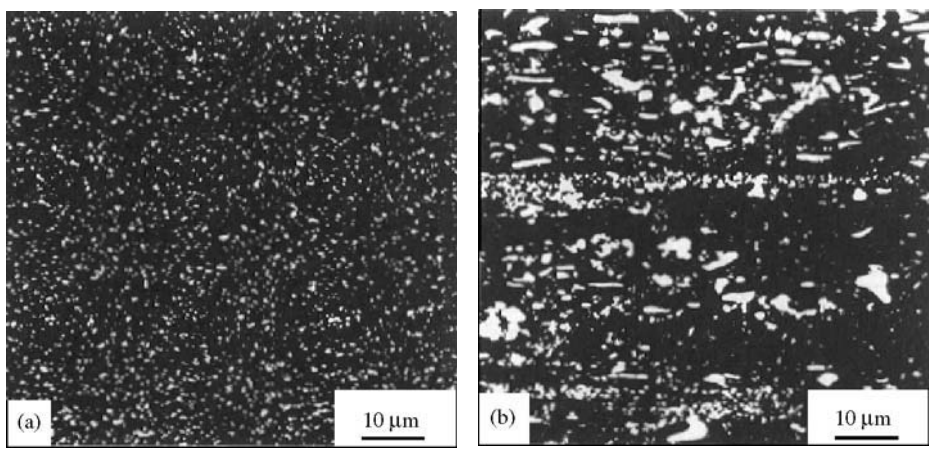

Figure 22.5 Primary carbides in heat treated PM (left) and conventional cast (right) 1.5C–12W–5V–5Co high speed steel alloys. Source: Ref 12

Table 22.4 Nominal compositions for several of the commercially available PM high speed steels and PM cold-work tool steels

Property	Unit	Particle metallurgy steels						
		High speed steels[a]			Cold-work tool steels, grades[b]			
		FAX 23	DEX 80	CPM Rex 25	PM 3V CPM 3V	PM 8Cr4V Vanadis 4	PM 8Cr10V Vanadis 10	PM 18V CPM 18V
Nominal chemical composition:								
Carbon	wt%	1.3	2.1	1.8	0.80	1.50	2.90	3.90
Chromium	wt%	...	...	...	7.50	8.00	8.00	5.25
Manganese	wt%	<0.30	<0.30	<0.30	...	...	...	...
Molybdenum	wt%	5.0	6.0	6.5	1.00	1.00	1.50	1.30
Silicon	wt%	<0.50	<0.50	<0.50	...	...	...	...
Sulfur	wt%	<0.03	<0.03	<0.03	...	...	...	...
Tungsten	wt%	6.25	14.0	12.5	...	...	...	...
Vanadium	wt%	3.0	5.5	5.0	2.75	4.00	9.80	17.50
Carbide content:								
MC	vol%	...	...	...	4.7	6.6	13	30.5
M_7C_3	vol%	...	...	...	0.4	5.7	14	...
Total	vol%	...	...	...	5.1	12.3	27	30.5
Hardness	HRC	65–67	68–70	67–69	60[c]	60[d]	60[e]	62[f]

[a]Commercial equivalent grade
[b]in denominator it is given commercial equivalent grade;
[c]Heat treatment 1121°C/30 min + air cool + 524°C temper (3 × 2 h);
[d]Heat treatment 1021°C/30 min + air cool + 524°C temper (2 × 2 h);
[e]Heat treatment 1060°C/30 min + air cool + 552°C temper (2 × 2 h);
[f]Heat treatment 1121°C/30 min + oil quench + 552°C temper (2 × 2 h).
Company suppliers of PM high-alloy tool steels (their names, location and trade name prefixes): Bohler/Uddeholm Corporation (Austria, Vanadis/Isomatrix PM); Hitashi Metals (Japan, HAP); Daido Steel (Japan, DEX); Nachi Fujikoshi (Japan, FAX); Erasteel Kloster AB (Sweden, ASP); Bodycote Powdermet AB, (Sweden, APM); Crucible Materials Corporation (USA, CPM); Carpenter Technology Corporation, (USA, Micromelt PM). Source: Refs [12, 13, 14, 15]

combination of wear resistance, toughness and grinding characteristics over a wide range of hardness.

Recent PM tool steel development has tended to focus on the following: (a) even more wear resistant vanadium compositions containing 15–18% vanadium with up to 30% by volume of primary MC-type carbides; (b) low-to-intermediate carbide volume fraction materials moderately alloyed with vanadium and chromium to optimize the toughness properties by maintaining good wear resistance; and (c) high vanadium and high chromium compositions for wear applications that also require good corrosion resistance.

Table 22.4 lists the nominal compositions for several of the commercially available PM high speed steels and PM cold-work tool steels. All of the tool steels listed in the table are capable of attaining 60–62 HRC during heat treatment, which is the typical application hardness range for cold work tooling.

In recent years, much work has been done to develop the potential of cemented carbides where a substantial amount of the tungsten carbide of conventional WC–Co alloys has been replaced by vanadium carbide (i.e. WC–$(V,W)C_x$ alloys, with x always <1) [16].

For the purpose to optimize the composition, 15 V–W–C–Co alloys varying in composition were examined. They were prepared by mechanical alloying [16]. The cobalt content of the alloys was kept constant at 50 at%. The high cobalt content was selected to permit the favorable formation of each phase. The carbon content was 27.8 at% in seven of the alloys (high-carbon or HC alloys) and 22.8 at% in eight of the alloys (low-carbon or LC alloys), so that the (V + W)/C ratio would be 0.8 and 1.2 respectively and the substitution of vanadium for tungsten in VC_x was systematically increased. The lattice parameter of $(V,W)C_x$ decreases with increasing V/(V + W) ratio (i.e. with decreasing W content) (Figure 22.6). It is also shown that for V/(V + W) ratio the lattice parameters of $(V,W)C_x$ in carbon rich (HC) alloys are consistently larger than in carbon depleted (LC) alloys.

Figure 22.7 shows that the microhardness of $(V,W)C_x$, measured at 50 g, varies with the V/(V + W)

ratio value. The scatter in the microhardness results is large (mean standard deviations ±150 HV0.05) because the measurements were carried out on random cross-sections of $(V,W)C_x$ particles. In spite of the scatter, the results show that the microhardness appears to reach a maximum value at V/(V + W) between 0.8 and 0.88. It is also shown that the microhardness of LC is consistently higher than the microhardness of HC alloys, while the lattice parameter in low carbon alloys has been found to be consistently smaller than in high carbon alloys.

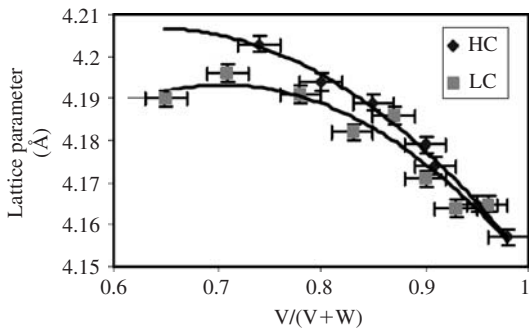

Figure 22.6 Dependence of the lattice parameter of $(V,W)C_x$ on the V/(V + W) ratio in $(V,W)C_x$. HC stands for 'high carbon V–W–C–Co alloys' with nominal carbon content 27.8 at% and LC stands for 'low carbon V–W–C–Co alloys' with nominal carbon content 22.8 at%. Source: Ref 16

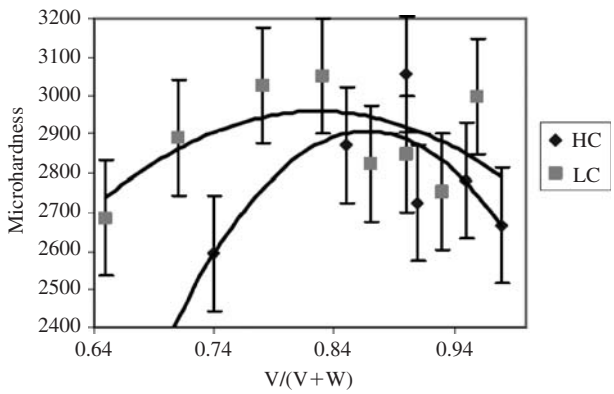

Figure 22.7 Dependence of the microhardness (HV0.05) of $(V,W)C_x$ on the V/(V + W) ratio in $(V,W)C_x$. HC and LC have the meaning as in Figure 22.6. Source: Ref 16

Workplace Atmosphere Safety

Inspirable dust of vanadium compounds has a predominantly carcinogenic effect. Data of the stated average limit value (ALV) of the aerosols of vanadium compounds in the workplace atmosphere, as the shift time-weighted average concentration, and the classes of danger according to State Standard 12.1.005-88 under the legislation in the Commonwealth of Independents States (CIS) [17], are given in Table 22.5. As for vanadium, the State Standard 12.1.005-88 standardizes ALV of vanadium pentoxide, vanadium trioxide, ferrovanadium and vanadium containing slags. The vanadium pentoxide fume is the most harmful inspirable substance and is related to the first most dangerous class according to above State Standard.

Vanadium in potable water takes toxicological action and is related to the third, next to last class of danger and the TLV is 0.1 mg/L according to CIS State Standard 4630-88 [18].

The flammability and explosivity of metallic vanadium are characterized by the following data. Solid vanadium becomes brittle on heating above 300°C and intensive oxidation occurs at 600–700°C with vanadium pentoxide formation; at 700°C it reacts with nitrogen, forming a yellow-bronze vanadium nitride. A powder, containing 86.4 wt% vanadium, with particle size below 74 μm forms a settled dust (aerogel) with a self-ignition temperature of 490°C; minimum aerogel ignition energy is 8 mJ; self-ignition temperature of suspended solid in air is 500°C; the low concentration ignition limit of airborne powder is 220 g/m^3; explosion pressure of suspended solid concentration in air is 350 kPa; maximum rate of pressure rise is 6.9 MPa/s; maximum explosion-proof oxygen content in suspension of matter in gas with diluted carbon dioxide is 10 vol%; minimum suspended solid ignition energy in air is 60 mJ.

The products with such characteristics of inflammability and explosion risk are placed in the 'Moderate

Table 22.5 Average limit value (ALV) of the aerosols of vanadium compounds in the workplace atmosphere

Vanadium compound	Condition of harmful agent	ALV (mg/m^3)	Class of danger
Vanadium pentoxide	Fume	0.1	I
Vanadium trioxide	Dust	0.5	II
Vanadium pentoxide	Dust	0.5	II
Ferrovanadium	Dust	1.0	II
Vanadium containing slags	Dust	4.0	III

explosion hazard' class of danger according to Guide to Legislation and 'Health and Safety' in the European PM Industry [19].

Voluminal quenching of burning vanadium can be done by special powder compounds, but argon is the best medium [20].

Common techniques are mainly used to prevent pollution and for environmental control during powder manufacture and processing. Detailed information on health and environment protection measures and also on prevention of inflammability and explosion risk in such conditions can be found in Section 5.

Zirconium

Zirconium powders find wide application in electronics, pyrotechnics, engineering, steel production, nuclear power industry, refractory, ceramics, enamels and in casting. The ability of zirconium powder to absorb gases ensures the keeping of a high vacuum; to this end it is plated on the surface of anodes, grids and other parts in electronics.

Zirconium powders are characterized by low temperature of inflammability and high rate of pressure rise. Due to these properties, they are used as the igniter in detonators, photoflashes and in manufacturing of smokeless powder.

Zirconium is used to deoxidize and denitride steels and for alloying in armor and gun steels, as well corrosion-resistant and heat-resistant steels. Zirconium improves the strength characteristics of copper (0.1–6 wt% addition); it imparts fine grain structure to magnesium alloys and prevents lead segregation in leaded bronze.

The zirconium content in the earth's crust is relatively high, about 0.025 wt%, and exceeds that of copper, zinc and lead. There are nearly 20 zirconium-containing known minerals but, at present, only two minerals, zircon (zirconium ortho-silicate) and baddeleyite (with up to 98 wt% ZrO_2) are the main commercial sources.

The zircon ores are enriched by gravitational technique in combination with magnetic and electrostatic separation. High purity zirconium dioxide is used as the initial product for zirconium powder production. Physical properties and diffusion factors for zirconium are given in Table 22.6.

The production of zirconium powders is accompanied by considerable technological difficulties because of their high chemical activity. Reaction of zirconium with oxygen, nitrogen, carbon, carbon oxides and water vapor is followed by a large decrease of Gibbs' energy. Zirconium is more easily ignited than aluminum because its oxide is a less protective coating than Al_2O_3, therefore aluminum melts before it ignites, while zirconium particles ignite before they melt.

Table 22.6 Typical properties of zirconium

Property	Unit	Value
Density	g/cm^3	6.52
Crystal type[a]		bcc
Atomic diameter	nm	0.316
Brinell hardness	MPa	640–670
Melting point	°C	1852 ± 10
Boiling point	°C	4377
Specific heat		
at 0–100°C	J/(kg · °C)	264
Heat of fusion	kJ/mol	23.0
Heat of vaporization	kJ/mol	567
Thermal conductivity at 100°C	W/(m · °C)	30.9
Coefficient of linear thermal expansion in the temperature ranges from 20 to 1100°C	$°C^{-1}$	$8.9 \cdot 10^{-6}$
Specific electrical resistivity at 20°C	μΩ · m	0.41
at 800°C	μΩ · m	1.43
Volume diffusion	m^2/s	1.3×10^{-4}
Volume diffusion activation energy	kJ/mol	272
Grain boundary diffusion	m^2/s	6×10^{-16}
Grain boundary diffusion activation energy	kJ/mol	184
Section capture of heat neutrons, $n \times 10^{24}$	cm^2	0.18

[a]Crystal type: bcc, body-centered cubic
Source: Refs 1, 4

Methods of producing zirconium powder or sponge can be classified into five groups:

- reduction of zirconium tetrachloride by magnesium or sodium
- reduction of zirconium fluoride (ZrF_4) by calcium or of potassium hexa-chlorozirconate (K_2ZrF_6) by sodium
- reduction of zirconium dioxide by calcium or calcium hydrate
- electrolytic methods for production or refining of zirconium powders
- iodide method of zirconium refining.

Some of the methods for zirconium powder and sponge production are discussed below.

Reduction of Potassium Hexachlorozirconate by Sodium

This reaction requires external heating:

$$K_2ZrF_6 + 4Na = Zr + 4NaF + 2KF$$

The specific reaction heat effect amounts to 1110 kJ per 1 kg of (K_2ZrF_6 + 4Na) mixture.

The process is performed in a sealed steel reactor in a vacuum or in an argon atmosphere at 800–900°C with sodium excess of 15–20%. After cooling, the cake is knocked out from the reactor and treated with water or NH_4Cl-solution to remove sodium skulls, then it is ball milled and the fluorides leached with water in the reactors with an agitator. To eliminate iron, the powder is treated with hydrochloric acid, washed with water, filtered and dried in a vacuum at 57°C.

Reduction by Calcium or Calcium Hydrate

Reduction of zirconium dioxide by calcium or calcium hydrate is accomplished in an argon atmosphere at temperatures from 1000 to 1100°C. Reduction by calcium hydride is a modified calciothermic process because the calcium is the main reducing agent. The calcium hydride is obtained as a result of action by dry hydrogen on calcium at 400–600°C. The reduction of zirconium dioxide by calcium and calcium hydride may be represented by the following reactions:

$$ZrO_2 + 2Ca = Zr + 2CaO$$

$$ZrO_2 + 2CaH_2 = ZrH_2 + 2CaO + H_2$$

Reaction heat is insufficient for a self-sustained process. It requires continuous heat admission.

The process is carried out in sealed heat-resistant steel reactors, where a briquetted mixture of zirconium dioxide and dry pure calcium is charged. Calcium chloride is added to the feed to regulate the grain size of the zirconium powder. The reactor atmosphere is evacuated and replaced by argon. The reduction process is continued for 1 h at 1000–1100°C. The reduced product after cooling is ground, washed with a large volume of water for calcium oxide removal, treated by dilute hydrochloric acid, washed by water and dried in a vacuum at 40–50°C.

In the case of reduction by calcium hydrate, a briquetted mixture of zirconium dioxide and calcium hydride is charged into a reactor. As calcium hydrate decomposes in moist air, it is preserved in sealed containers, while grinding and blending are kept in leakproof grinders and blenders under argon. After exhausting, the reactor is filled with dry hydrogen and reduction is accomplished at 900–1000°C. In contrast to the calciothermic process, as a result of reduction by calcium hydrate, zirconium hydride (ZrH_2) is obtained. This gives a certain advantage, since zirconium hydride is less oxidized by washing from calcium oxide, in comparison with zirconium powder.

Typical properties of zirconium powders produced by calciothermic and natriothermic processes are given in Table 22.7.

Production of Zirconium Powders by Electrolysis

Zirconium can be obtained by electrolysis of zirconium halides in a salt melt. The best results are obtained with electrolytes containing K_2ZrF_6 in a melt of KC1 or NaCl. Potassium chloride is preferable because its decomposition voltage is higher than that of sodium chloride and an anode effect on the graphite anodes occurs only at high current density. A mixture of 70% KC1 + 30% K_2ZrF_6 melts at 727°C so that the electrolysis can be conducted at 747–797°C. Solubility of the KF obtained during electrolysis is better than that of NaF which simplifies separation of electrolyte from the cathode precipitate (zirconium powder). The major reactions taking place on the cathode in the electrolyzer are:

$$ZrF_6^{2-} \leftrightarrow Zr^{4+} + 6F^-$$

$$Zr^{4+} + e \rightarrow Zr^{3+} + e \rightarrow Zr^{2+} + 2e \rightarrow Zr^0$$

Table 22.7 Properties of zirconium powders produced by different methods

Property	Unit	Method				
		Calciothermic reduction, grade[a]		Natriothermic reduction, grade[b]		
		PZrC1	PZrC2	PZrN–A	PZrN–B	PZrN–V
Chemical composition:						
Zirconium:						
Active	wt%	⩾96	⩾96	73.0–76.9	71.1–73.5	67.2–71.1
Whole	wt%	...	...	93–94	92.5–93.1	91.5–92.5
Calcium	ppm	500	500	⩽1500	⩽1500	⩽1500
Carbon	ppm	⩽500	⩽500	⩽2500	...	1000–3000
Chlorine	ppm	⩽30	⩽30	⩽30	⩽30	⩽30
Fluorine	ppm	...	...	⩽100	⩽100	⩽100
Hydrogen	ppm	⩽1500	⩽2000	⩽2000	...	1000–3000
Iron	ppm	⩽500	⩽500	⩽3000	⩽3000	⩽3000
Magnesium	ppm	...	...	⩽1500	⩽1500	⩽1500
Sulfur	ppm	...	...	⩽7000	⩽7000	⩽7000
Moisture	wt%	...	...	⩾14	⩾14	⩾14
Granulometric composition:						
10 μm under seeding	wt%	⩾50	⩾50	44–58	44–50	43–47
from 10 to 20 μm	wt%	...	...	20–47	29–39	31–38
from 20 to 50 μm	wt%	...	...	10–22	17–21	19–22
50 μm oversize	wt%	⩽1.0	⩽1.0	⩽0.5	⩽1.0	⩽2.0
Specific surface	m^2/g	0.19–0.25	0.15–0.19	...	...	...

[a]CIS TU 48-4-234-84 standard
[b]CIS TU 48-4-376-76 standard.

Chlorine is formed on the anode (current density is $4\,kA/m^2$):

$$4F^- + 4KCl(4NaCl) - 4e \rightarrow 4KF(4NaF) + 2Cl_2^{\uparrow}$$

During the electrolysis, the electrolyte is enriched with fluorine ions that interact with the carbon of graphite anodes forming CF_4. Optimum cathode current density for an electrolyte of 25–30%K_2ZrF_6 + 75–70%KC1 composition ranges from 3.5 to $4.5\,kA/m^2$. The cathode deposit includes 30% of zirconium powder with particle size ranging from 50 to 200 μm; the remainder is electrolyte salts. Current efficiency amounts to 60–65%.

A scheme of a typical electrolyzer for zirconium powder production is shown in Figure 22.8. Four graphite electrodes (two anodes and two alternating current electrodes for electrolyte melting) are sited in a stainless steel vessel with water-cooled walls. The cathodes are made of steel.

After the electrolyte has been melted by alternating current, the cathode is submerged into the melt and direct current is applied. Electrolysis is performed in an argon atmosphere. A wall accretion of solidified electrolyte is formed on the bath walls and protects the electrolyte from iron contamination and the walls

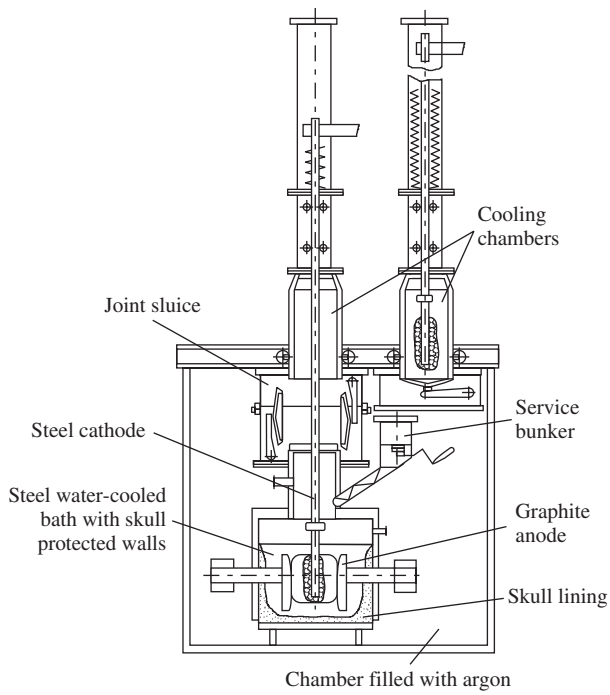

Figure 22.8 Scheme of typical electrolyzer for zirconium powder production.

from a corrosive electrolyte. On completion of the electrolysis, the cathode with precipitate passes to the cooling chamber; the sluice and chamber are evacuated and filled with argon. The precipitate is cooled in the argon atmosphere and then it is brushed off the cathode, jaw-crushed into pieces of 8–10 mm and followed by wet grinding (in order to avoid of zirconium oxidation and combustion in the air). The salts are removed by washing at 57°C, then the powder is washed with 10% solution of hydrochloric acid, subsequently with distilled water, next by alcohol or acetone and finally dried in a vacuum at 50–60°C. Fine fractions are used in powder metallurgy; coarse particles are either remelted or reground.

Typical contaminants of the obtained powder are: 60 ppm oxygen, 30 ppm nitrogen, 500 ppm carbon, 1 ppm copper, 130 ppm iron, 700 ppm nickel, 200 ppm titanium; ⩽20 ppm manganese, 30 ppm chromium, 50 ppm cobalt; 20 ppm chlorine; 100 ppm magnesium and 500 ppm silicon.

Amalgam Method

Zirconium powder can be produced by an amalgam method. Zirconium tetrachloride is reduced by potassium–lithium amalgam:

$$2KLi(Hg) + ZrCl_4 \rightarrow Zr(Hg) + 2KCl + 2\underset{melt}{LiCl}$$

The amalgam concentration amounts to 0.8%, with the potassium-to-lithium ratios of up to 4 to 1 and excess metal-reducer 1–4%. Reduction is performed in a column at 400°C in the lower part while the upper part of the column is water cooled. The mixture of zirconium tetrachloride, lithium amalgam and potassium amalgam is pumped continuously to the heated area where it is kept for several minutes to ensure 100% reduction of the tetrachloride. The reduction is performed in the column under pressure to prevent evaporation of mercury at 400°C. In the cold part of the column, the salt melt solidifies and floats up while amalgam enriched with zirconium accumulates under the mercury layer. The amalgam is filtered through porous partitions. Residues of mercury, potassium and lithium are sublimated under vacuum at 1400°C. Zirconium is obtained in the form of sponge. The sublimation products are returned to the reaction zone.

Combustion Synthesis of Zirconium Nitrides

This method was discovered in the late 1960s in the former Soviet Union [21]. Zirconium nitride (ZrN) has been produced by combustion synthesis with phosphorus [22,23]. This powder can be used to form refractory corrosion-resistant coatings and conducting materials in electronic applications. Depending on the nitrogen pressure, zirconium nitrides with a wide range of nitrogen compositions have been synthesized, ranging from solid solution with a minimum amount of nitrogen ($ZrN_{0.1}$) to single-phase supersaturated solutions ($ZrN_{0.34}$ $ZrN_{0.45}$), as well as stoichiometric ZrN. Full conversion to the stoichiometric compound can be achieved by dilution of the initial metal powder with the corresponding nitride product [24,25].

Workplace Atmosphere Safety

Inspirable dust of zirconium metals and zirconium compounds takes a predominantly fibrous effect. Data of the stated average limit value (ALV) of the aerosols of zirconium and its compounds in the workplace atmosphere, as the shift time-weighted average concentration, and the classes of danger accordingly State Standard 12.1.005-88 under the legislation in the Commonwealth of Independents States (CIS) [17] are given in Table 22.8. The above State Standard standardizes ALV of metallic zirconium, zirconia, zirconium dioxide, zirconium carbide, zirconium nitride and zirconium fluoride. Zirconium fluoride is the most harmful inspirable substance among the standardized

Table 22.8 Average limit value (ALV) of the aerosols of zirconium and its compounds in the workplace atmosphere

Denomination	Condition of harmful agent	ALV (mg/m^3)	Class of danger
Zirconium metallic	Aerosol	6	III
Zirconia	Aerosol	6	IV
Zirconium dioxide	Aerosol	6	IV
Zirconium carbide	Aerosol	6	IV
Zirconium nitride	Aerosol	4	III
Zirconium fluoride	Aerosol	1	II

zirconium compounds and is placed in the second danger class of the four-class Standard system.

Metallic zirconium is characterized by the following data of flammability and explosivity. Zirconium is a combustible metal. Solid zirconium in the air at room temperature is stable. On heating to less than 400–500°C, it develops a protective film. At higher temperatures, simultaneously with increasing oxidation rate, solution of oxygen occurs that markedly decreases the ductility. An aerogel of powder below 74 μm in size has a self ignition temperature of 190°C; the low concentration ignition limit of suspended solid (airborne powder) is 40–64 g/m^3; maximum explosion pressure by suspended solid concentration in air is 630 kPa; maximum rate of pressure rise is 28.4 MPa/s; maximum explosion-proof oxygen content in suspended matter in argon gas is 4 vol%; minimum suspended solid ignition energy in air is 5 mJ.

The products with such characteristics of inflammability and explosion risk are placed in the 'High explosion hazard' class of danger according to the Guide to Legislation and 'Health and Safety' in the European PM Industry [19].

The voluminal quenching methods and special powder compounds are used for quenching of burning zirconoum powders. Talc is a better medium for voluminal quenching [20].

Zirconium hydride (ZrH_2). Powder with particle size below 74 μm displays self-ignition temperature an aerogel at 270°C; the low concentration ignition limit of suspended solid in air about 85 g/m^3; maximum explosion pressure by suspended solid concentration in air is 630 kPa; maximum explosion-proof oxygen content of a suspended solid in argon is 6 vol%; minimum suspended matter ignition energy in air is 60 mJ.

Zirconium carbide. Powder with particle size below 53 μm exhibits self-ignition temperature of an aerogel at 342°C; the low concentration ignition limit of airborne powder is about 142 g/m^3. Common techniques are mainly used to prevent pollution and environmental control during powder manufacture and its processing. Detailed information on health and environment protection measures and also on prevention of inflammability and explosion risk in such conditions can be found in Section 5.

Indium

The content of indium in the earth's crust amounts to 1.5×10^{-5}%. Indium-only minerals are very rare and do not have commercial significance. The greatest indium concentrations are found in the minerals kilindrite $Pb_6Sb_2Sn_6S_2$ (from 0.1 to 1.0 wt% In), franckeite $Pb_5Sb_2Sn_2S_{12}$ (under 0.1 wt% In) and stannite $CuFeSn\ S_4$ (under 0.1 wt% In). In the sphalerites, indium content ranges from 0.1 to 0.0001 wt%. Indium content is higher in zinc ores with high concentration of iron and stibium.

Indium is distinguished for its high capture cross-section for thermal neutrons (Table 22.9) and so can be used in control rods in nuclear reactors.

Various waste and semi-finished products of zinc and lead manufacture are the main sources of

Table 22.9 Typical properties of indium and thallium

Property	Unit	Value	
		Indium	Thallium
Density	g/cm^3	7.362	11.83
Crystal type[a]		fct[a]	H[b]
Atomic diameter	nm	0.322	0.342
Hardness HB	MPa	10	30
Melting point	°C	156	303
Boiling point	°C	2080	1406
Specific heat at 0–150°C	J/(kg · °C)	243	137
Heat of fusion	kJ/mol	3.3	4.3
Heat of vaporization	kJ/mol	226	163
Thermal conductivity from 0 to 100°C	W/(m · °C)	25.1	38.9
Coefficient of linear thermal expansion at 20°C	°C^{-1}	$24.8 \cdot 10^{-6}$	$28 \cdot 10^{-6}$
Specific electrical resistance	μΩ · m	0.082 (0°C)	0.18 (20°C)
Section capture of thermal neutrons, n · 10^{24}	cm^2	190	3.3

Crystal type:
[a]fct, face-centered tetragonal.
[b]H, hexagonal for α modification, stable under 230°C; fcc, face-centered cubic by above 230°C temperatures β modification is stable. Source: Refs 1, 4

indium. As well as indium, these products often contain other trace elements: cadmium, gallium, thallium and germanium. In zinc pyrometallurgy, the dust of coking furnaces and lead obtained as a result of rectifying purification of preliminary indium can serve as a source of indium. In zinc hydrometallurgy, the sublimation of rotary-kiln or fuming processes and copper–cadmium cakes may be used for indium sources. In lead production, the refinement of lead products and various waste products (for example, dust and copper removing slags of reverberatory process) can also serve as sources of indium.

Indium recovery technique usually includes two steps:

- obtaining of indium concentrate with indium content over 1 to 2 wt%
- production of black indium.

Black indium is recovered from a solution by cementation on zinc or aluminum sheets. Low standard indium potential (−0.34 V) allows purification of the solution from impurities of the elements with less negative standard potentials such as copper, arsenic and antimony (Table 22.10) while it is shown that indium and a number of other metals can be precipitated by cementation on zinc and aluminum.

A feature of indium powder production by electrolysis is low yield (10 %) of powder fraction under 50 μm. A cementation technique has the advantage for indium sponge production, where the indium is precipitated from sulfate solutions as sponge by zinc dust cementation on aluminum sheets at 57°C. In solution with excess of sulfate ions, complete deposition of indium is made difficult because of its tendency to form complex ions $[In(SO_4)_2]^-$; therefore hydrochloric acid is introduced on the basis of 10–20 ml per 1 L of solution. From chloride solutions, indium is precipitated by cementation on zinc sheets. The sponge is separated easily from the metal precipitator; it is washed with water, dried and ground.

Production of powder by air atomization of a melt allows an increase in productivity and yield of powder fraction below 50 μm, but this process has the problem of nozzle freezing owing to the low melting temperature. Reduction or avoidance of nozzle freezing is possible by means of hot gas atomization. Simultaneously, such a technique also contributes to reducing the energy consumption [26].

At air pressure 1.2–1.3 MPa, the yield of below 45 μm powder exceeds 80 wt%. In powder PIR grade (TU 48-0213-5/0-86 Standard), the 160 μm oversize does not exceed 1 wt%, while in the 45 μm product there is not less than 70%.

The main application for high-purity indium is in semi-conductor techniques. As was referred to above, indium has a remarkably high cross-section capture for thermal neutrons. Due to this, indium is used in alloys containing 19% In, 71% Ag and 10% Cd and 54–62% In, 8–18% Cd and balance B for the control rods in nuclear techniques. Wear-resistant coatings of indium are used for protection of bearings from corrosive action of hot lubricants in powerful engines (for example, in aviation and automotive industry). Indium coatings possess high reflecting ability and do not grow dim. Therefore, they are used as reflectors.

Alloys In–Sn–Cd–Bi and In–Pb–Sn are used as solders for joining of metals, glass, quartz and ceramics. In vacuum techniques, solders of indium alloy with tin (50% In and 50% Sn) serve for joining glass with glass or metal. They ensure vacuum tight joins.

Workplace Atmosphere Safety

State Standard 12.1.005-88 [17] lays down the admissible content of indium oxide (In_2O_3) in workplace atmospheres. Its occupational exposure limit (OEL) of the inspirable fraction of dust in the workplace atmosphere is 4 mg/m^3. Indium oxide is not toxic and is relegated to the third class of danger according to the above standard.

Thallium

The thallium weight content in the earth's crust amounts to 3×10^{-4}%. Thallium-only minerals are very rare and, in general, thallium is widely

Table 22.10 Standard potential valuations of series metals

Element	Standard potential	Element	Standard potential	Element	Standard potential
Al^{3+}/Al	−1.53	Cd^{2+}/Cd	−0.40	Ge^{4+}/Ge	−0.15
Zn^{2+}/Zn	−0.76	In^{3+}/In	−0.34	Sn^{2+}/Sn	−0.136
Ga^{3+}/Ga	−0.52	Ti^{+}/Ti	−0.336	As^{3+}/As	+0.247
Fe^{2+}/Fe	−1.53	Pb^{2+}/Pb	−0.126	Cu^{2+}/Cu	+0.34

dispersed. The greatest thallium concentrations are found in iron sulfides (pyrites and marcasites), where its content reaches 0.1–0.5%. At present, waste and semi-finished products serve as major raw material sources.

Crude thallium is usually recovered from sulfate solution by cementation on zinc sheets (standard potential Tl^+/Tl is -0.336 V). This process allows the removal from solution of impurities of the series elements such as zinc, lead, chromium and others. Cementation with subsequent alkali refinement makes it possible to produce metal not less than 99.96% pure which is suitable for use in alloys or for the manufacture of salts for infra-red optics. Typical physical properties of thallium are given in Table 22.9.

Ultrafine thallium powder is produced by electrolysis. Electrolyte composition is: 0.005–0.020 mol/L $TlSO_4$; 0.1–0.23 mol/L $(NH_4)_2SO_4$; 0.1 mol/L H_3PO_3; 0.07 mol/L $Na_2SO_4 \cdot 10H_2O$. Current efficiency amounts to 17% at current density 0.667 kA/m^2. Decreasing the thallium sulfate content leads to a fall in the current efficiency. Powder is precipitated in the form of dendrites. The lower the concentration of thallium ions and ammonia sulfate and the lower the pH, the smaller the grain size of the deposit. Powder contains small amounts of thallium oxides Tl_2O and Tl_2O_3. Quantity of oxides in the deposit is minimal at ammonia sulfate concentration 0.1 mol/L and pH = 2.4 [27].

Thallium powder is used as an alloy addition to powder alloys with the object of decreasing the alloy grain size.

Workplace Atmosphere Safety

State Standard 12.1.005-88 [17] refers only to the admissible content of thallium bromide and thallium iodide in workplace atmospheres. Their occupational exposure limits (OEL) of the inspirable fraction dust in workplace atmosphere are 0.01 mg/m^3. Thallium is placed in the highest, first class of danger according to the above standard.

Thallium content in potable water takes sanitary-toxicological effect and is in the exceedingly dangerous (First) class. The TLV is 0.0001 mg/L (for the inorganic compounds, including transition elements subject to summation of all form gross contents) according to CIS State Standard 4630-88 [18].

Ruthenium

Ruthenium is one of the platinum group metals. Solid metallic ruthenium is silvery-white, while the powder has a gray color. Ruthenium is an extremely rare and very scattered element. Its weight content in the earth's crust amounts to 5×10^{-7}%. It appears in the form of isomorphous admixture in the minerals of the osmium–iridium group, together with other platinum minerals. Ruthenium is also contained in copper–nickel sulfide ores and concentrated in the process of nuclear reactor work. Physical properties and diffusion factors for ruthenium are given in Table 22.11.

Table 22.11 Typical properties of ruthenium

Property	Unit	Value
Density at 20°C	g/cm^3	12.45
Crystal type[a]	...	H
Atomic diameter	nm	0.268
Brinell hardness	MPa	2160[b]
Melting point	°C	2334 ± 10[c]
Boiling point	°C	4100
Specific heat at 25°C	J/(kg · °C)	238
Steam saturated pressure at 2300°C	Pa	1
Thermal conductivity at 20°C	W/(m · °C)	105
Coefficient of linear thermal expansion at temperature ranges from 0 to 100°C	μm/(m · °C)	9.1
Specific electrical resistance at 25°C	μΩ · m	0.074

[a]Crystal type: H hexagonal.
[b]Value ranges are determined by anisotropy.
[c]Monocrystalline purity 99.98%. Source: Ref 28

In the form of solid metal it is not soluble in acids, including aqua-regia, though it is attacked by solutions of alkali metal hypochlorites, alkali melts and peroxides. Ruthenium is not oxidized at room temperature, while at elevated temperatures it is oxidized to ruthenium dioxide, RuO_2. Fine powdered ruthenium readily absorbs hydrogen (ruthenium niello can absorb 1500 times its own volume of hydrogen).

Ruthenium is present in the semi-finished product of the platinum metals refining process which is the principal source of the metal. Ruthenium concentrate is melted with a mixture of alkali and nitre or heated with either sodium or barium peroxides, sublimated in the form of ruthenium tetroxide. This is dissolved in hydrochloric acid and the ruthenium precipitated in the form of ruthenium ammonium hexachloride. This is reduced in a hydrogen current. The resulting ruthenium powder is 99.9% pure [28].

Ruthenium additions appreciably increase hardness, strength and corrosion resistance of various alloys.

One likely field of application is in hard metals based on tungsten carbide with a cobalt binder. The effect of the ruthenium is a modification of the liquid phase during sintering which restricts grain growth. This leads to increased strength and hardness and, thus, improved cutting performance. Recently, several compositions of hard metal have been studied [29,30]. The starting materials for the powder mixtures containing tungsten carbide, cobalt, vanadium carbide, chromium carbide, Co–Fe–Ni alloy and ruthenium powders were tried in different combinations (Table 22.12). The powders were mixed and milled with the ball mill with surfactant addition. After milling, the mixtures were granulated. Pressing under 300 MPa pressure produces samples of $55 \times 10 \times 5$ mm. The ratio of green density to thereotical density was 0.52 and the flexural strength of obtained specimens amounts to 4 MPa. Sintering was done using three different cycles depending on cobalt and ruthenium content and at temperatures ranging from 1415 to 1490°C.

For all the alloy types, it appears that ruthenium acts as a grain growth inhibitor. The reduction in the particle size of tungsten carbide is noticeable for the compounds only doped with ruthenium (see Table 22.12). Addition with other inhibitors of grain growth, such as the vanadium and chromium carbides, has only a weak effect on the grain size. The increase is approximately 20%. At the same time, it has an influence comparable with the other inhibitors on the mechanical properties. Typical microstructures of WC/Co and (WC–Cr_3C_2–VC)/Co systems without and with ruthenium addition are shown in Figure 22.9.

Doping with ruthenium improves the flexural strength in particular for grades with vanadium and chromium carbides. The increase is particularly high, above 20%, for the (WC–Cr_3C_2–VC)–11Co–0.16Ru system. Ruthenium additions improve the performances in machining over the conventional hard metals.

Ruthenium is introduced into platinum and palladium base alloys used for manufacturing wear-resistant parts of various measuring instruments, electrical make-break contacts and jewelry. Thermocouples for use at temperatures up to 2000°C are made of iridium–ruthenium alloys. Metallic ruthenium, its alloys and metallo-organic compounds are used as catalysts in the synthesis of organic and inorganic products.

Workplace Atmosphere Safety

State Standard 12.1.005-88 [17] contains only a requirement as to admissible content of ruthenium dioxide in workplace atmospheres. The occupational exposure limit (OEL) of the respirable fraction dust in workplace atmosphere is 1 mg/m^3. It is placed in

Table 22.12 Nominal composition (wt%) of WC/Co, (WC–Cr_3C_2–VC)/Co and WC/(Co–Fe–Ni) systems and grain size after sintering (d_g)

WC/Co				(WC–Cr_3C_2–VC)/Co				WC/(Co–Fe–Ni)			
WC	Co	Ru	d_g (μm)	WC–Cr_3C_2–VC	Co	Ru	d_g (μm)	WC	Co–Fe–Ni	Ru	d_g (μm)
94.0	6.0	...	2.5	94.0	6.0	...	0.70	88	12	...	1.48
94.0	5.2	0.8	1.55	94.0	5.2	0.8	0.70	88	10	2	0.87
90.8	9.2	...	2.09	90.8	9.2	...	0.79				
90.8	8.0	1.2	1.26	90.8	8.0	1.2	0.65				
87.4	12.6	...	2.31	87.4	12.6	...	0.79				
87.4	11.0	1.6	0.73	87.4	11.0	1.6	0.65				

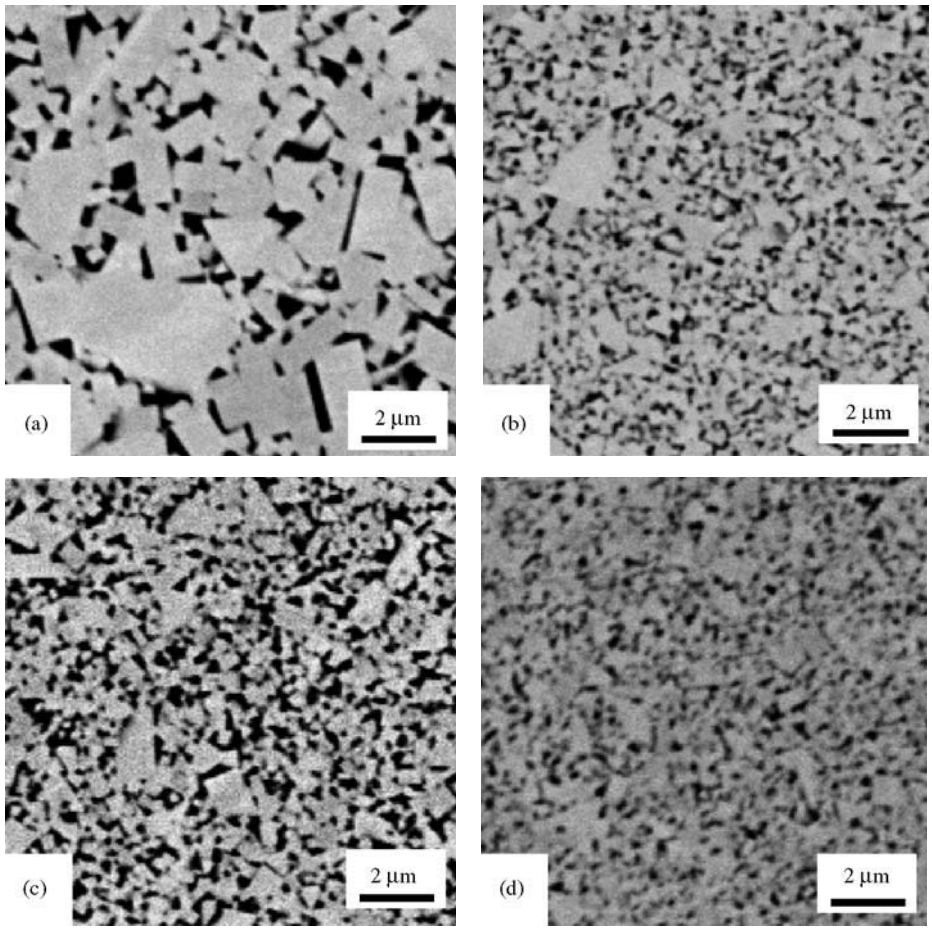

Figure 22.9 Typical microstructures of WC/Co (a, c) and (WC–Cr_3C_2–VC)/Co (b, d) with binder content 9.2%Co (a, b) and 8%Co + 1.2%Ru (c, d). Source: Ref [29]

the second class of danger according to the above standard.

Production of Rare Earth Metal-Alloy Powders

The collection of 14 elements with ordinal numbers from 58 (cerium) to 71 (lutecium) disposed in group VI of the periodic table behind lanthanum and with similar properties are called rare earth (RE) elements. Therefore, lanthanum is usually included in this group and the elements are named lanthanides (Ln) (i.e. similar to lanthanum). In addition, elements of the third group, yttrium and scandium, are chemical analogs of lanthanides. In its properties, yttrium is closer to the lanthanides than is scandium. In view of the fact that scandium essentially differs from lanthanides and has little geochemical connection with them, scandium is considered below in a separate sub-section.

Due to their physicochemical properties, lanthanides are similar. This is explained by features of their electron shells: with growth of the atomic nucleus (growth of the ordinal numbers), the structure of the two outer electron levels of lanthanide atoms remains the same, as since by transition from element to element the electrons appear in the deep underlying electron level 4*f*. The maximum possible electron number in the 4*f*-level is 14 and determines the number of lanthanide elements.

Bond strength of the electrons is increased as the 4*f*-level is filled by half (to seven electrons) or full to the complete 14 electrons. Therefore, the gadolinium and lutecium atoms are distinguished by the most

stable configuration of the 4*f*-level. Oxidation level +4 is shown by cerium and praseodymium (due to the easy passage of first *f*-electrons on the 5*d*-level) and by terbium and dysprosium, following after gadolinium. Oxidation level +2 is observed in samarium, europium and ytterbium, i.e. by elements with electron number on the *f*-level near to 7 and 14.

Rare earth elements are divided into two subgroups: cerium [(La), Ce, Nd, Pm, Sm and Eu] and yttrium [Gd, Tb, Dy, Ho, Er, Tm, Yb, Lu and (Y)]. This division was originally based on the difference in the solubility of the double sulfates formed by lanthanides with sodium or potassium sulfates. In succeeding years, periodicity of variation of several properties was ascertained within the collection of lanthanides, corresponding to their division into two subgroups.

Contrary to the above enumerated properties, some properties of elements are changed continuously. Thus, as the ordinal number is increased, the radii of atoms and ions are continuously decreased. This fact, called 'lanthanide compression', explains the gradual basicity reduction of elements from cerium to lutecium and stipulates the distinctions in dissolubility of lanthanide salts and the stability of their composite compounds.

Physicochemical Properties

Physical Properties

Lanthanides are silvery-white metals. Some of them (for example, praseodymium and neodymium) have a slightly yellow color. Physical properties of the lanthanides are given in Table 22.13.

The melting points of elements of the cerium subgroup are lower than those of elements of the yttrium subgroup. It is notable that the boiling points of samarium, europium and ytterbium, indicated valency 2+, are considerably lower than for the other lanthanides. Also notable is the high capture cross-section for thermal neutrons of gadolinium, samarium and europium.

The high pure lanthanides are plastic and easily yield to deformation (forging and rolling). The mechanical properties are strongly dependent on impurity content, particularly hydrogen, sulfur, nitrogen and carbon. Values of ultimate strength and modulus of elasticity of the yttrium subgroup metals (except for ytterbium) are higher than those of metals of the cerium subgroup.

All lanthanides, including lanthanum, are paramagnetic; some of them (gadolinium, dysprosium and holmium) reveal ferromagnetic properties. α-lanthanum is transformed into a superconductivity state at 4.9 K and into β-lanthanum at 5.85 K. Other lanthanides do not show superconductivity even at temperatures below tenth degree K.

Chemical Properties

The lanthanides are distinguished by high chemical activity. They form stable oxides, halogenides and sulfides and react with hydrogen, carbon, hydrocarbons, carbon monoxide and dioxide, nitrogen and phosphorus. Metals decompose water (slowly in the cold, more rapidly at elevated temperature) and readily dissolve in hydrochloric, sulfuric and nitric acids. At temperatures above 180–200°C, the metals are rapidly oxidized in air.

The lanthanide oxides are characterized by chemical stability and high melting points. Thus, cerium dioxide melts at about 2500°C and lanthanum oxide at above 2000°C.

The lanthanide hydroxides, $Ln(OH)_3$, have an alkaline nature and are weakly soluble in water and alkalis. The pH at which they are precipitated decreases from 7.62 for cerium to 6.82 for lutecium, corresponding to decreasing basicity in the lanthanides' row from cerium to lutecium.

Chlorides, sulfates and nitrates of the trivalent lanthanides are soluble in water and crystallized for the most part in the different form of crystallohydrates.

Fluorides and oxalates are weakly soluble in water and in dilute mineral acids. Fluorides are precipitated in the form of crystallohydrates of $LnF_3 \cdot 0.5H_2O$ composition or non-aqueous salts (for example, Pr and Nd salts). For oxalates, the most typical composition is $Ln_2(C_2O_4)_3 10H_2O$. Solubility in water of oxalates of the yttrium subgroup elements is higher than that of the cerium subgroup elements. On heating to 500–600°C, the oxalates are decomposed with the formation of Ln_2O_3 type oxides.

Phosphates, carbonates and ferrocyanides are also weakly soluble in water. Most single lanthanide salts are inclined to form double or composite salts with alkali metals and ammonia as well with bivalent elements.

Lanthanides form composite compounds with many organic substances. Among them the compounds with citric acid and series of aminopolyacetic acids are of great importance. Stability of composite compounds with organic acids is generally increased in series from lanthanum to lutecium and that is widely used in some methods for separation of lanthanides.

Sources of Raw Material

The lanthanides content in the earth's crust is about 0.01 wt%, which equals the copper content. There

Table 22.13 Physical properties of lanthanides and yttrium

Element	Atomic number	Atomic diameter (nm)	Crystal type[a]	Density (g/cm^3)	Melting point (°C)	Boiling point (°C)[b]	Specific electrical resistance ($\mu\Omega \cdot m$)	Capture cross-section of thermal neutron, $n \times 10^{24}$ (cm^2)	E (GPa)
Lanthanum	57	0.374	H	6.162	920	3470	0.615	8.9	39.15
Cerium	58	0.365	fcc	6.768	795	3470	0.75	0.70	30.58
Praseodimum	59	0.3656	H	6.772	935	3212	0.68	11.2	35.92
Neodymium	60	0.3642	H	7.007	1024	3030	0.64	44	38.6
Promethium	61	0.370	H	7.26	1035	3200	0.75	...	46
Samarium	62	0.3604	R	7.563	1072	1900	0.92	6500	34.80
Europium	63	0.398	bcc	5.245	826	1597	0.81	4500	18.2
Gadolinium	64	0.358	H	7.886	1313	3266	1.34	44000	57.3
Terbium	65	0.356	H	8.258	1356	3230	1.16	44	58.64
Dysprosium	66	0.3546	H	8.559	1407	2600	0.91	1100	64.33
Holmium	67	0.3552	H	8.779	1461	2600	0.94	64	68.50
Erbium	68	0.3514	H	9.062	1497	2900	0.86	166	74.74
Thullium	69	0.3492	H	9.318	1545	1730	0.90	118	...
Ytterbium	70	0.388	fcc	6.943	824	1196	0.28	36	18.15
Lutecium	71	0.3468	H	9.849	1652	3330	0.582	108	68.6
Yttrium	39	0.3602	H	4.472	1510	3336	0.589	1.38	67

[a]Crystal types: H, hexagonal; fcc, face centered cubic; R, rhombohedral; bcc, body-centered cubic.
[b]Approximately.

are more than 250 known minerals containing RE, 60–65 of them can be classed as RE minerals, which contain RE oxides in amounts more than 5–8%. As regards their chemistry, phosphates, fluorides, silicates, silico-titanates, titanium silicates, niobium tantalates and titanium niobates are the main minerals.

The following minerals have the largest commercial importance:

- monazite, (Ce, La, ...)PO_4 contains 50–60% Ln_2O_3 and 4–7% ThO_2
- bastnaesite, (Ce, La, ...)FCO_3 contains 73–77% Ln_2O_3
- loparite, (Na, Ca, Ce,...)$_2$ (Ti, Nb, Ta)$_2O_6$ contains 39.2–40% TiO_2; 32–34% (Ce, La, ...)$_2O_3$ and 8–10% (Nb, Ta)$_2O_5$
- parisite, Ca(Ce, La, ...)$_2[CO_3]_3F_2$ contains 53–64.5% RE_2O_3 and from traces to 8% yttroparisit
- euxenite, (Y, Ce, Ca, ...) (Ti, Nb, Ta)$_2O_6$ contains 18.2–27.7% (Y, Er, ...)$_2O_3$, 0.2–4.3% (Ce, La, ...)$_2O_3$, 16–30% TiO_2, 4.3–1.4% Nb_2O_5 and 1.3–23% Ta_2O_5
- xenotime, YPO_4 contains 52–62.6% Y_2O_3.

One of the basic sources of cerium subgroup elements is monazite, which is commonly found in gravel deposits together with ilmenite, zirconia, loadstone and other minerals. Using gravitational and magnetic enriching methods, monazite concentrates with 58–65% Ln_2O_3 are obtained. From them, simultaneously with thorium, the lanthanides are eluated.

The largest ore deposits are in India, Brazil, the USA, Australia, Madagascar and Sri Lanka. Commercial deposits of bastnaesite are located in the USA and Burundi. Concentrates, containing nearly 60% Ln_2O_3, are produced from such ores by means of flotation. Combination of concentrate roasting with subsequent acid processing enables the production of a concentrate with 90% of Ln_2O_3.

In Russia, laporite is an important commercial source of RE, deposits of which are situated on the Kolsky peninsula. Laporite ores are easily reduced yielding concentrates containing 80–90% mineral. During the process, the lanthanides are simultaneously reduced along with niobium, tantalum and titanium.

Euxenite, xenotime, as well the tailing of certain uranium-containing ore processing, are important raw materials for the recovery of yttrium subgroup elements.

Whatever the RE raw material, the metals are recovered in the form of oxide and hydroxide which must then be separated to obtain the individual elements. Scrap in the form of (RE)Co_5 or (RE_2)Co is also used. Scrap is heated up to 797°C in air to remove organic impurities. The oxygen content is reduced to 0.07% during the following treatment with metallic calcium at 1097°C. The scrap then is ground and washed with acid solution to free it from calcium oxide. Produced powder is added to material for the production of magnets. Rare-earth metal scrap cobalt magnets are treated with hydrochloric or oxalic acid. As a result, the RE elements are precipitated, while cobalt is taken into solution.

Methods of RE Elements Separation

As a consequence of the similarity of lanthanides properties, their separation is a complicated problem. Earlier separation methods were mainly based on difference in solubility of lanthanide compounds. As a result of numerous separate crystallizations or precipitations, the individual elements of different purity were obtained. For separation of certain elements, their ability to be oxidized to the tetravalent state (Ce, Pr and Tb) or to 2+ valency state (Sm, Eu and Yb) was used. In this case, the separation is facilitated by the appreciable differences in properties of lanthanide compounds with oxidation level +4 and +2 in comparison with lanthanide compounds with oxidation level +3.

Recent lanthanide separation schemes are based on using more effective methods: liquid extraction and ion exchange. In some separation schemes, selective oxidation and reduction are applied.

Separation of RE by Extraction

At present, the extraction methods have become the main ones in RE separation schemes. In commercial production, organophosphorus extracting agents are mainly used: tributylphosphate (TBP), diethyl hexyl phosphoric acid and carbonic acids [1]. Separation is based on regular variation of distribution coefficient values along the lanthanides row.

In commercial production, the RE separation by TBP extraction is, for the most part, done from nitric acid solutions containing RE nitrates. The extraction proceeds with trisolvate formation:

$$Ln^{3+}_{(aqu)} + 3NO^{-}_{3(aqu)} + 3TBP_{org} \leftrightarrow Ln(NO_3)_3 \cdot 3TBP_{org}$$

$$D = K_c[NO^{-}_3]^3_{(aqu)} \cdot [TBF]^3_{(org)}$$

where K_c is the equilibrium constant of the extraction reaction and D is the distribution coefficient.

The D values in the TBP–HNO_3 system at high concentrations of HNO_3 in the 11–15 mol/L range

increase continuously with increase of lanthanide atomic number. However, in solutions with HNO_3 concentrations lower 5 mol/L, the inversion of regularity variation of distribution coefficients for the europium–lutecium row occurs (Figure 22.10). This is explained by hydration energy growth along the heavy RE elements row, becoming apparent at low acidity that makes difficult the displacement of aqueous molecules from hydrates.

At high acidity (more than 12 mol/L), the average value of the division coefficient β of the adjoined elements from lanthanum to terbium $\beta = D_{z+1}/D_z$ amounts to 1.9. For elements from terbium to lutecium, this value is lower. Therefore, for all the RE group, one can accept on average $\beta = 1.5$. By using TBP extraction for division of RE on subgroups, the process is carried out in nitrate solutions with HNO_3 concentration ranging from 7 to 10 mol/L. In this process, yttrium falls into the heavy RE subgroup (Dy–Lu).

In the RE separation by extraction, the process is usually conducted in a cascade of the mixer–clarifier type. A countercurrent system is used, consisting of extraction, flushing and re-extraction sections. The total number of cascade steps ranges from 50 to 90.

RE Separation by Ion-Exchange Chromatography

At present, ion-exchange chromatography is a complementary method usable for obtaining individual high purity RE, mainly heavy ones.

For separation of lanthanides by ion-exchange chromatography, various cationite resins are used.

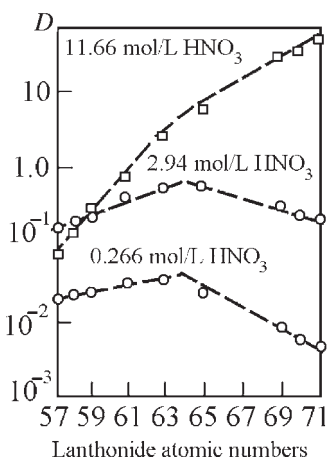

Figure 22.10 Dependence of distribution coefficient *D* on lanthanide atomic number by TBP extraction for europium–lutecium row. Source: Ref 1

Separation is usually accomplished by elution chromatography. Lanthanide ions' affinity to a resin is diminished from La^{3+} to Lu^{3+}, i.e. in order of decreasing hydrated ion size. However, RE ions' affinity to resin is very close and does not ensure sufficiently effective division. Better separation is achieved by using eluting solutions containing organic compounds which form various stability complexes with RE ions.

Washing out efficiency corresponds to the durability of anion lanthanide complexes. With the motion of washing-out solution along a column (or connected in-series columns), the composite of cations is divided on the separate sorption zones (stripes) moving with certain rates to the column exit. For the washing out, various organic compounds, forming complexes with lanthanides, are used. Ethylene diamine tetraacetic acid (EDTA) is widely employed for chromatography RE division. EDTA is one of the α-amino acids. It is a tetrabasic acid with two nitrogen atoms and is denoted H_4V. With triple-charged ions of lanthanides, EDTA forms the chelate compounds, in which nitrogen atoms are connected with the lanthanide ion by coordinating bonds.

The stability constant of these complex compounds is defined by the equation:

$$Ln^{3+} + HV^{3-} \leftrightarrow H(LnV)$$

$$K = \frac{[H(LnV)]}{[Ln^{3+}] \cdot [HV^{3-}]}$$

As is obvious from Figure 22.11, the stability constants of lanthanide complexes with EDTA increases from lanthanum to lutecium, i.e. with rise of lanthanide atomic number. The stability complex constants of two adjoined elements differ from each other on average by 2.4 times. This determines the conditions for highly selective action of EDTA for using elution RE cations from a resin.

Schemes of Complete Separation

Various schemes are used for complete separation of RE, in which the methods described above are combined. By way of illustration, Figure 22.12 shows a scheme for the separation of the cerium subgroup elements. A mixture of hydroxides is usually fed for separation. Initially, from the mixture, cerium can be extracted by oxidation. Then separation by means of countercurrent extraction is performed on three fractions: light RE (lanthanum, cerium, praseodymium and neodymium), middle RE (praseodymium,

neodymium, samaruim and europium) and enriched fraction by gadolinium and elements of the yttrium subgroup (neodymium, samaruim, europium, gadolinium + ytterbium). From the second and third fractions, samarium and europium, one can proceed by sodium amalgam reduction and separate as described above. The separation of elements in each of the separate fractions is accomplished by extraction and ion-exchange chromatography methods.

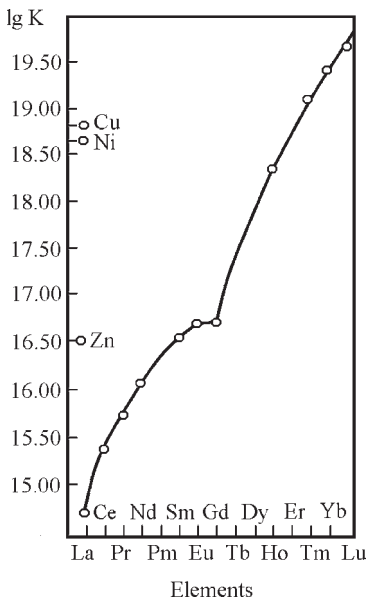

Figure 22.11 Dependence of stability constant of lanthanide complexes with EDTA on lanthanide atomic number from lanthanum to lutecium. Source: Ref 1

During separation of yttrium subgroup elements (for example, using extraction in chloride-thiocyanate system), a fraction containing Gd, Tb and D, and a fraction, containing Ho, Er, Tb, Tm and Lu, are obtained. Subsequent separation is done using extraction and ion-exchange chromatography. Ytterbium is produced by reduction from nitrate solutions using sodium amalgam.

Production of RE Powders

In view of the high chemical durability of lanthanide compounds (oxides and halogenides), pure metals and their alloys are obtained by thermal reduction or electrolysis of melts.

Initial Compounds for Metals Production

Rare earth metals are mainly produced from non-aqueous chlorides or fluorides.

Production of Chlorides

Dehydration of $RECl_3 \cdot nH_2O$ crystallohydrate or the oxide chlorination 'dry' method is applied for the chlorides.

In order to prevent the formation of oxychlorides, LnOCl, as a result of hydrolysis, the dehydration of crystallohydrates is done in dry hydrogen chloride at temperatures ranging from 400 to 450°C. In this way, oxychlorides are converted into chlorides:

$$LnOCl + 2HCl = LnCl_3 + H_2O$$

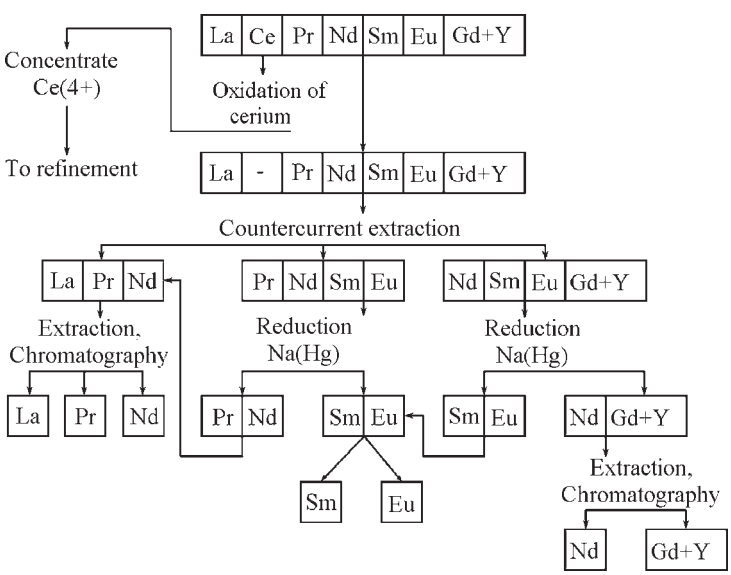

Figure 22.12 Principal circuit of cerium subgroup elements separation.

Dry methods are based on the interaction of RE oxides with various chloridizing agents: chlorine in the presence of carbon, ammonium chloride and hydrogen chloride. Chlorine in the presence of carbon and carbon tetrachloride reacts with RE oxides at temperatures ranging from 700 to 800°C and molten chlorides are obtained. The interaction with ammonium chloride at 200–300°C is represented by the equation:

$$Ln_2O_3 + 6NH_4Cl = 2LnCl_3 + 6NH_3 + 3H_2O$$

After the reaction has ended, the NH_4Cl excess is sublimated by heating at temperatures from 300 to 320°C and atmospheric pressure ranging from 66.5 to 267 Pa. Anhydrous RE chlorides are hygroscopic. Therefore, it is necessary to avoid their contact with moist air during processing and to keep them in a dry inert gas atmosphere.

Production of Fluorides

RE fluorides are obtained by dehydration of hydrated salts, precipitated from solutions, or by the action of hydrogen fluoride on RE oxides. RE fluorides are precipitated from nitrate or muriatic solutions by hydrofluoric acid. Some of the RE (lanthanum, cerium and others) are precipitated in the form of semi-hydride $LnF_3 \cdot 0.5H_2O$, the others (praseodymium, neodymium) without crystal water. By heating a solution with fluoride residues by an infra-red source, the hydrated fluorides are transformed into anhydrous ones. The precipitates are then washed with alcohol and dried at 400°C in a dry argon atmosphere. Fluorides produced in this way contain impurities of oxyfluorides, LnOF. It is possible to remove them by drying in a current of hydrogen fluoride.

Purer fluorides are obtained by the action of hydrogen fluoride on oxides at 550–575°C:

$$Ln_2O_3 + 6HF = 2LnF_3 + 3H_2O$$

Fluoridation of oxide pellets is conducted in push type tube furnaces through which boats with oxides are pushed in a gas countercurrent. It is possible to perform the fluoridation of oxides in a fluidized bed. Fluorides, in contrast to chlorides, are less hygroscopic, which makes processing easier.

Electrochemical Methods

A number of methods of producing lanthanides by the electrolysis of molten salts have been developed. Among them, electrolysis of non-aqueous RE chlorides in molten alkali and alkaline-earth metal chlorides is more extended. This technique is used on a commercial scale mainly for the production of cerium subgroup mischmetal and individual metals. During electrolysis, these metals are precipitated on the cathode in the molten state due to their comparatively low melting points.

The production of the yttrium subgroup metals by electrolysis is more difficult because, with the exception of ytterbium, they have comparatively high melting points (from 1350 to 1700°C). Because of the evaporation of the halogen salts, as well as difficulty in selecting suitable materials for the salt bath, and for the electrodes, the production of the yttrium subgroup metals by electrolysis is practically impossible and is, therefore, not used.

The electrolytes used for mischmetal or cerium subgroup metals usually contain 50% KCl + 50% $CaCl_2$, corresponding to the eutectic with melting point 660°C or 50% KCl + 50% NaCl, melting at 658°C. In melts of these salts, the lanthanide chlorides are readily soluble. The electrolyzer bath contains approximately 58–60% $LnCl_3$ and the rest alkali and alkaline-earth metal chlorides with a small addition of calcium fluoride. The scheme of a typical electrolyzer usable for mischmetal is shown in Figure 22.13. Electrolyte temperatures range from 800 to 900°C. The process is carried out at a tension of 10–15 V and a current of 1000–2000 A depending on electrolyzer size. Current efficiency ranges from 50 to 70%.

The mischmetal or cerium produced contains 94–99% RE and impurities: <1% silicon, 1–2.5% iron, also carbon, calcium, aluminum and others. It is possible to increase the RE purity by applying metals, such as tantalum, non-interacting with lanthanides, for electrodes, high purity magnesia and beryllia for crucible linings, as well as by accomplishing the electrolysis in inert gas.

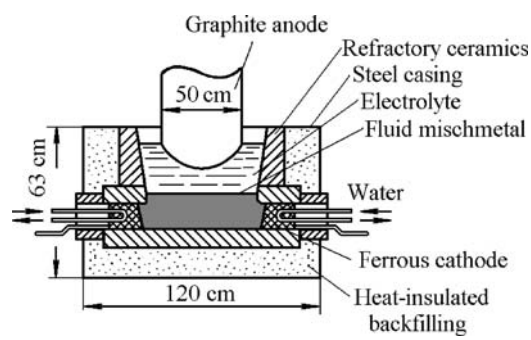

Figure 22.13 Scheme of typical electrolyzer usable for producing mischmetal.

Metallothermic Methods

The metallothermic methods can be used to obtain all lanthanides, except samarium, europium and ytterbium. The process is applicable only to the lower halogenides and for the other metals reduction of oxide with lanthanum or carbon and sublimation in a vacuum are developed. Reduction of fluorides or chlorides by calcium is also used. Otherwise, the production of the heavier RE and yttrium is done using calcium.

Lanthano-Thermic Method

Reduction of samarium, europium and ytterbium from their oxides by lanthanum is implemented in a vacuum simultaneously with distillation of the metals formed, which have higher vapor pressure than lanthanum:

$$Sm_2O_3 + 2La = 2Sm\uparrow + La_2O_3$$

Typically, the process is carried out in a tantalum crucible. The unit includes an assembled condenser in its upper part. A mixture of oxide and 20% surplus lanthanum chips is placed in the crucible, which is heated in a vacuum induction furnace to about 1400°C. During heating, the vacuum is maintained at not lower than 1.33×10^{-2} Pa. The sublimation is accompanied by abrupt pressure fall to 1.33×10^{-5} Pa, because the evaporated metals actively absorb the residual gases. Condensation takes place at temperatures from 300 to 400°C. In this case, metal is obtained in the form of a coarse-crystalline crust. At lower temperatures metal powder is produced. The samarium, europium and ytterbium so produced are practically free from Ta and Ln. Impurities content of carbon, nitrogen, hydrogen and oxygen do not exceed 0.01%. Cerium or mischmetal, instead of lanthanum, can serve in the capacity of reducing agent.

Carbo-Thermic Method

This technique includes two steps:

- reduction of Ln_2O_3 by carbon at temperatures between 1600 and 1700°C, lanthanide carbide being produced:

$$Ln_2O_3 + 7C = 2LnC_2 + 3CO$$

- dissociation of the carbide in a vacuum with sublimation of the lanthanide:

$$Ln_2C_2 = 2Ln\uparrow + 2C$$

This method is used for the production of samarium, europium and ytterbium, which have relatively low boiling temperatures, 1900, 1400 and 1430°C, respectively.

The process is led in a graphite crucible where a briquette mixture of oxide with 10% surplus carbon (black) is placed into the crucible which is heated in a vacuum induction furnace.

The first step is led by pressure in the furnace of 13.3 Pa at temperatures 1600–1700°C for about 3 h. As a result lanthanide carbide is obtained. The second step is accomplished by pressure of 0.13 Pa and temperatures ranges from 1600 to 1900°C. Lanthanide sublimates arise from carbide dissociation and are precipitated on a cooled condenser made from tantalum or molybdenum. Samarium obtained by this method contains the following impurities: 0.05% carbon, 0.1% oxygen, 0.035% hydrogen and $<0.1\%$ nitrogen.

Refinement of RE by Distillation

Refinement of rare earth metals, obtained by one of the methods described, is accomplished by distillation in a vacuum. This method is particularly effective for refining of refractory metals of the yttrium subgroup, including yttrium.

Metal is placed in a tantalum crucible conjoined with a tantalum condenser and both are connected to a vacuum system. The crucible is heated by induction. The fusion is led by vacuum $\leqslant 0.0013$ Pa. During fusion of dysprosium, holmium and erbium, the temperatures in the crucible are maintained in the range 1600–1700°C, while in the condenser from 900 to 1000°C. For more refractory yttrium, terbium and lutecium, the temperatures in the crucible is kept at 2000–2200°C and 1300–1400°C, respectively.

Workplace Atmosphere Safety

State Standard 12.1.005-88 [17] contains requirements as to the admissible content of cerium dioxide, cerium fluoride and yttrium oxide in workplace atmospheres.

The stated average limit value (ALV) of the cerium dioxide aerosol in the workplace atmosphere as the shift time-weighted average concentration is 5 mg/m^3. It is placed in the third class of danger according to the above standard. The ALV of cerium fluoride aerosol in the workplace atmosphere as the shift time-weighted average concentration is 0.5 mg/m^3, while the threshold limit value (TLV) is 2.5 mg/m^3. It is placed in the third class of danger, next to the

last, according to the above standard. Yttrium oxide aerosol is also placed in the third class of danger. Its ALV is 2 mg/m^3 in the workplace atmosphere.

Cerium is a combustible metal. Cerium powder in suspended solid state in air is explosive. A powder with particle sizes finer than 80 μm exhibits: self-ignition temperatures in aerogel and in suspended solid state in air states of 100 and 148°C; the minimum explosion concentration of suspended solid in air is 36 g/m^3 [20]. The products with such characteristics of inflammability and explosion risk are placed in the 'High explosion hazard' class of danger according to the Guide to Legislation and 'Health and Safety' in the European PM Industry [19].

Argon and special powder compounds are used for quenching of burning cerium powder [20].

Yttrium powder is a combustible substance. Milled yttrium with particles ranging from 50 to 400 μm is characterized by following combustibility parameters: self-ignition temperatures in aerogel state is 313°C, while by radiation heating it is 155°C; self-ignition temperature suspended solid in air is 432°C. The low concentration of ignition limit of suspended solid in air was not found up to 1000 g/m^3. Yttrium powder with particle sizes finer than 80 μm, obtained by means of milling in argon, has an ignition temperature of 170°C and minimum explosion concentration of suspended solid in air is 36 g/m^3. Consequently, the latter product can also be placed in the 'High explosion hazard' class of danger.

As for cerium powder, the voluminal quenching method by argon and special powder compounds are used for quenching of burning yttrium powder [20].

Samarium hexaboride (SmB_6). Samarium hexaboride is a combustible material. Powder with particles less than 56 μm has a self-ignition temperature of 665°C.

Range of Applications

Rare earth elements in the form of metals, alloys and chemical compounds have found wide application in metallurgy, glass and ceramic production, nuclear power, lighting, television and laser techniques, chemical industry, medicine and agriculture. Possibilities of their use far from being exhausted and are being expanded as properties of lanthanides, their alloys and compounds are being studied.

The powder metallurgy technique discovers new possibilities in the creation of materials containing rare earth elements with properties unachievable by traditional metallurgy. Rapid solidification processes and mechanical alloying permit the synthesis of a variety of stable and metastable phases including supersaturated solid solutions, fine crystalline and quasicrystalline intermediate phases and amorphous alloys.

Refractory and Elevated Temperature Alloys

The 2 vol% lanthana- and 2 vol% yttria-doped molybdenum materials exceed appreciably in mechanical properties of arc-melted and cast molybdenum and Z6 grade, a commercial zirconia-doped material [31,32]. The creep rupture strength values of oxide dispersion strengthened (ODS) 2 vol% lanthana-doped molybdenum material [32] is twice that of arc-melted and cast and of Z6 zirconia-doped materials.

Variations in oxide kind and consolidation method have been shown to have a significant effect on the mechanical properties of ODS molybdenum material [32]. Comparison of the effect of doping technique and species on tensile properties of ODS molybdenum–lanthana and ODS molybdenum–yttria alloys illustrates that, for both oxide species, the wet doping technique results in a much finer dispersion of oxide particles ranging from 0.08 to 0.12 μm. The wet doping process is based on using an aqueous lanthanum nitrate solution to dope the molybdenum dioxide (MoO_2) precursor before its reduction to molybdenum metal powder [33]. At ambient temperature, the alloy's strength is not strongly sensitive to either doping technique but, at high temperatures, the wet doping technique produces superior material for a given oxide kind. Lanthana-doped material is also superior to yttria-doped material at elevated temperatures. The ODS molybdenum material contains nominally 2 vol% La_2O_3 that corresponds to a lanthanum (La) analyzed content of 1.09 wt%. The tensile properties of this material as a function of temperature are shown in Figure 22.14. The total amount of product in the final material forms varied from 92% to 99.6% (relative density, RD). Flat sheet was produced by cold isostatic pressing (CIP). The 4.8 mm diameter rod was processed from a 70 mm diameter CIPed billet which was sintered, and then processed to a final condition by a combination of rolling and swaging at elevated temperature. The 38 mm rod was consolidated by CIPing nominal 280 mm diameter billet which was sintered and then hot extruded to bar at 4 to 1 ratio. A section of the bar was then turned to a 70 mm diameter round and then rod rolled to final diameter. After a high temperature (>1600°C) annealing treatment, a highly elongated interlocking grain microstructure, typical of an oxide dispersion strengthened material, is obtained [34].

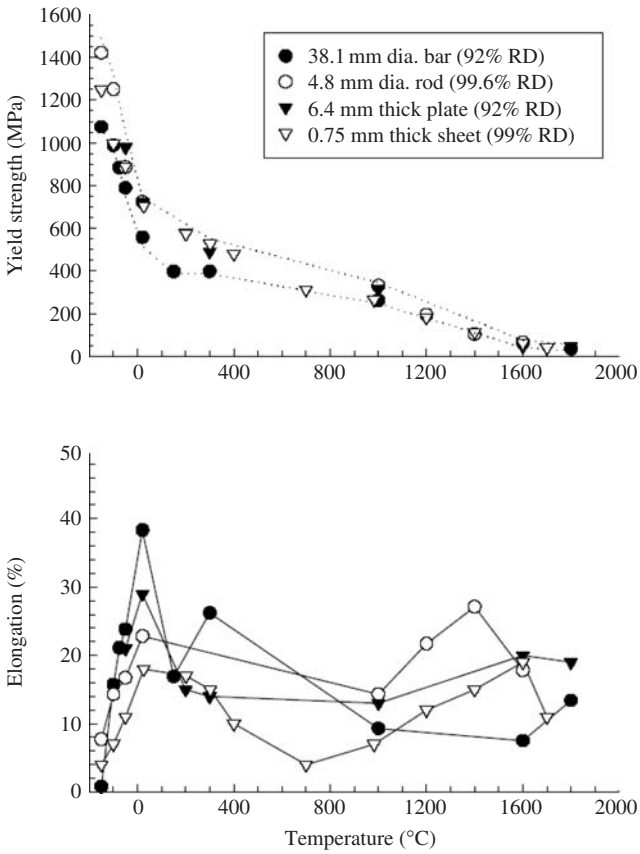

Figure 22.14 The tensile properties of ODS molybdenum-2 vol% lanthana specimens as a function of temperature. Source: Ref 32

So as to synthesize several yttria dispersed tungsten alloys resistant to high temperature liquid metal corrosion and with improved mechanical behavior at rather high temperatures, the ODS process by ball milling and sintering of tungsten and yttria powders was developed [35,36].

The W–Y system by the ODS process behaves in a more ductile way during milling, the higher yttrium content was studied in the range from 1 to 17 vol% [37]. Long milling times of the order of 30 hours are necessary to reach both a significant reduction of particle size, a grain size of a few tens of nanometers, and to the finest microscopic distribution of yttrium. The milled powders were axially compacted into green pellets at pressure of 1.2 GPa. The resulting pellets were subsequently sintered using a 300°C/h heating rate. Four hours at 1800°C vacuum sintering treatment may give rise to a significant 96.5% relative density. Vacuum sintering is much to be preferred to a treatment under hydrogen. The vacuum sintered samples may exhibit levels of microhardness up to 840 HV_{100}. Comparison of the evolution of relative density with variation of microharness of the W–1 vol% Y vacuum sintered samples is shown in Figure 22.15.

Molybdenum disilicide is a promising material for high temperature structural applications because of its high thermal conductivity, high melting point, lower density and elevated oxidation resistance. However, its use is limited by poor toughness and poor creep strength at elevated temperatures. Attempts have been made to improve it by synthesizing RE–$MoSi_2$ composites [38].

The mixtures of 99.9% pure molybdenum with particle size ranging from 2 to 4 μm, 99.5% pure silicon

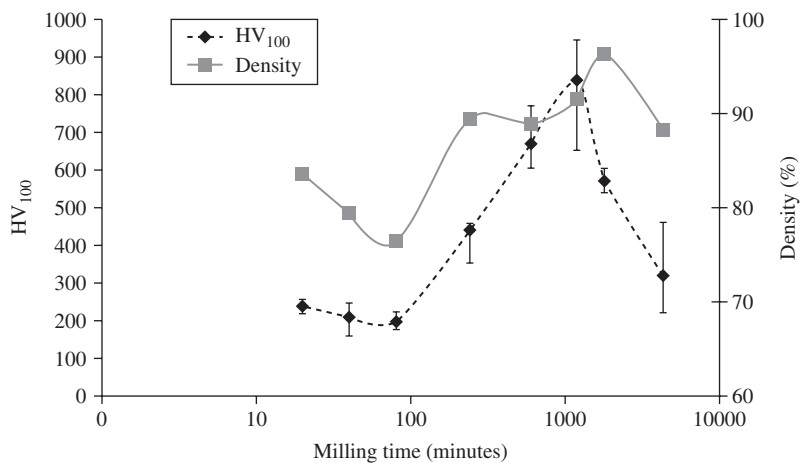

Figure 22.15 Comparison of the evolution of relative density with variation of microhardness of the W–1 vol% Y vacuum sintered samples.

less than 45 μm in size and 99.9% pure RE with nearly 1 μm particle sizes were used for preparation of composites. The RE content in the composites was 0.2, 0.4, 0.6, 0.9 or 1.2 wt%, respectively. The composites were synthesized by mechanical alloying (MA) and self-propagating high-temperature synthesis (SHS). The resulting powders were then hot pressed in a graphite die at 1300–1400°C for 20 min. The hardness and fracture toughness of molybdenum disilicide material at elevated temperatures in the range from 800 to 1400°C were improved by the addition of rare earth elements. They are increased nearly by 50%, when adding the optimum amounts, 0.9 wt%.

Rare earth elements are used as alloying additions in aluminum and magnesium alloys to improve mechanical properties of the latter, particularly, at elevated temperatures [39–41].

One such alloy, aluminum with 8% of iron and 4% of cerium is of interest. It is obtained on the basis of powders made by high pressure gas atomization of a melt composed of high purity 99.999 aluminum, 99.99 iron and 99.9 cerium. This atomization process [42] produces a powder with a relatively thin oxide film compared to current commercial atomization. A scanning electron micrograph of as atomized powder is shown in Figure 22.16. The atomized powder composition determined by chemical analysis contained: 8.06 wt% iron, 3.84 wt% cerium, 45 ppm nitrogen, 676 ppm oxygen, 176 ppm carbon, balance aluminum. The minus 75 μm powder was poured into a copper can which was then evacuated and sealed before extrusion. The latter is done at 370°C with a 9 to 1 extrusion ratio. The extruded material in the form of a 10 mm rod was then machined into miniature tensile specimens. Three replicate tensile specimens were tested at room temperature, 250°C and 325°C. In addition, separate tensile specimens were annealed at 250°C and 325°C for 100 hours and subsequently tested at room temperature. The use of cleaner powders simplifies the process by eliminating the degassing and hot pressing of the compacts that are required with the commercial RS process [39]. According to the authors [41], although the cost of producing the cleaner powder will be higher than current atomization costs, the overall costs should be much less in comparison with the commercial process because of the elimination above mentioned processing steps. However, high pure aluminum and cerium powder processing relates to technical difficulties owing to explosion risk of such powders.

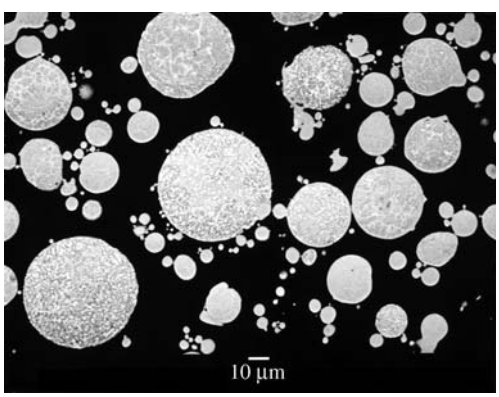

Figure 22.16 Scanning electron micrographs of atomized Al–8wt%Fe–4wt%Ce alloy powder. Source: Ref 41

The tensile properties of PM Al–8wt%Fe–4wt%Ce are given in Table 22.14. For comparison, data for commercial alloys of similar composition are also included in this table. As is obvious, the PM specimens retain quite high mechanical properties at temperatures up to 315–325°C.

Manufacture of Electrodes

Thorium oxide is added to tungsten electrodes, because of its high electron emission and easy arc formation. Environmental control and safety regulation associated with the use of radioactive thorium, have led to the development of alternatives.

Since the 1970s, tungsten electrodes activated by rare earth metal oxides to avoid thorium radioactivity have been researched and developed in China, the Soviet Union, Japan and elsewhere. It was reported that in the case of low current welding W–CeO_2 electrodes can replace W–ThO_2 electrodes. Recently, it was reported [44] that tungsten electrode properties can be improved by adding combined rare earth oxides to tungsten and W–ThO_2 electrodes can be replaced by tungsten electrodes activated by combined rare earth oxides, namely La_2O_3, CeO_2 and Y_2O_3.

As an alternative to ThO_2 cathodes, La_2O_3–Mo cathodes appeared in the middle 1970s. However, because of their poor emission stability, La_2O_3–Mo cathodes have not been used commercially [45]. Attempts have been made to improve them by means of cathode carburization, i.e. forming of a porous carbide layer on the cathode surface. As it is shown, the porous carbide layer can store active substances and carry them to the surface. The bulk diffusion of lanthanum atoms increases after carburization as carbon reduces the bonding between lanthanum atoms and the molybdenum surface [46,47]. Mo_2C formed in the carburization process can reduce La_2O_3 to metallic La which is favorable for emission. According to [45], the carburization process of La_2O_3–Mo cathodes can be divided into three steps:

- carbon, formed by the decomposition of benzene is absorbed on the surface of carbide layer

Table 22.14 Tensile properties of elevated temperature alloys doped by cerium

Property	Unit	Alloy (Source)			
		CU78 [43][a,b]	CZ42 [39][a,b]	Al-Fe-Ce [39][a,b,c]	Modified CU78 [41][a]
Nominal composition					
Iron	wt%	8.3	7.0	8.0	8.0
Cerium	wt%	4.0	6.0	7.0	4.0
Aluminum	wt%	balance	balance	balance	balance
Tensile strength at room temperature	MPa	428	448	484.9	447 ± 13
At 166°C	MPa	...	365	...	...
At 250°C	MPa	...	...	...	391 ± 14
At 260°C	MPa	...	283	...	...
At 316°C	MPa	...	221	193.8	...
At 325°C	MPa	...	...	...	362 ± 23
Yield strength at room temperature	MPa	352	379	418.9	325 ± 15
At 166°C	MPa	...	345	...	...
At 250°C	MPa	...	...	...	300 ± 15
At 260°C	MPa	...	262	...	...
At 316°C	MPa	...	200	178.1	275 ± 25
At 325°C	MPa	...	...	...	
Modulus of elasticity at room temperature	MPa	...	78.6	...	...
At 166°C	MPa	...	68.9	...	...
At 232°C	MPa	...	64.1	...	...
At 260°C	MPa	...	62.1	...	...
At 316°C	MPa	...	56.5	...	...
Elongation, at room temperature to 316	%	...	5.0	7.0–7.6	3.0–5.7

[a]Oxygen also present.
[b]supplier: Alcoa.
[c]thin-sheet specimens.

- carbon diffuses to the Mo–Mo_2C interface through the carbide layer
- carbon has a chemical reaction with Mo at the interface to form Mo_2C.

Permanent Magnets

Rare earth alloys magnets are characterized by a high coercive force (H_c) and residual induction (B_r). These alloys are processed to provide the maximum energy product, which is the numerical value of energy product $H_c \cdot B_r$ in the second quadrant (top left) of the hysteresis curve (Figure 22.17). The energy product is measured by approximation of the largest rectangle to the demagnetization curve, found in the second quadrant of the hysteresis loop.

The high coercivity of the rare earth elements is based on nucleation and pinning of domain walls at surfaces and at grain boundaries. Generally, the blended fine particles are compacted in a magnetic field, sintered, heat treated, machined to size, coated and magnetized. Typical energy products range from 130 to 160 kJ/m^3 (16–20 MG · Oe) by conventional processing. $SmCo_5$ single phase magnets are widely used. In precipitation hardened $Sm(Co, Cu)_{7.5}$, copper is substituted for some of the cobalt. This produces a fine, coherent precipitate, about 10 nm, when aged at 400–500°C.

Recently, neodymium has attracted increasing attention [48–52]. It is more abundant and less costly than other rare earth metals. Commonly, an alloy close to the composition of $Nd_{15}Fe_{77}B_8$ is melted and then rapidly solidified by pouring a stream of molten metal on to a rotating cold disk. This rapid solidification process produces a thin, amorphous ribbon. The ribbon, in turn, is chopped and crushed into 200 μm particles. The particles can be bonded with polyamides and injection molded to form magnets.

The technique is known for preparing compacts by hot pressing. The $Nd_{13.6}Fe_{73.7}Co_{6.6}Ga_{0.6}B_{5.5}$ ribbon

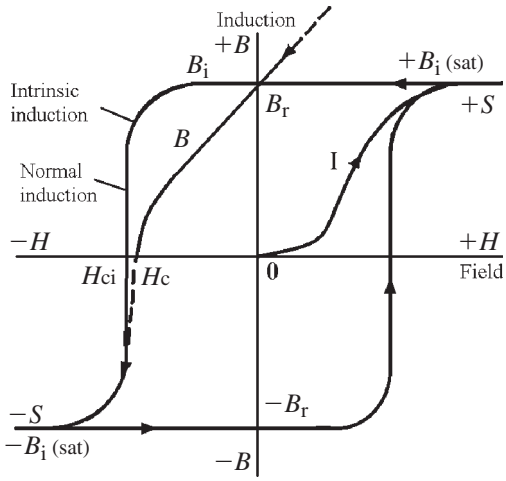

Figure 22.17 Typical hysteresis loop for a permanent magnet material.

powder was hot pressed and the fully dense compacts were subsequently hot deformed [48]. Minimum deformation required to achieve good texture was around 50%. Deformation temperatures, in the range from 600 to 1000°C, enabled useful anisotropy to be achieved. With the optimum processing parameters, a maximum energy product ($H_c \cdot B_r$) as high as 409 kJ/m^3 was achieved.

The influence of heat treatment on properties of Nd–Dy–Fe–Co–Nb–Al–Cu–B sintered magnets is shown in publication [49]. The alloys were prepared by vacuum induction melting of 99.9 to 99.99% purity elements. In three initial alloy types, the rare earth element nominal contents were in the following ranges: from 13.8 to 12.0 at% Nd, 0.75 at% Dy and 3.4 at% Tb. For comparison, different compacting techniques were used: sintering at temperatures 1062 and 1100°C and hot isostatic pressing at temperatures in the range from 800 to 1077°C and pressure from 60 to 180 MPa at exposures from 3 to 10 ks. Optimized heat treatment parameters depend on various alloying elements: for example, on alloying with the optimized treatment temperatures range from 527 to 577°C (3.6 ks), while with copper the optimized temperature interval ranges from 452 to 502°C (3.6 ks). The maximum energy product ($H_c \cdot B_r$) values for given magnet compositions lie between 320 and 360 kJ/m^3.

The Nd–Fe–B magnets were produced from gas atomized powders (GA) [50]. The neodymium content in five initial alloys ranged from 14.5 to 16 at%. There were included additions of terbium, dysprosium, titanium, molybdenum, boron, vanadium and aluminum. Alloys were prepared by induction melting of raw materials with purity above 99.9% under high purity argon. The magnets were sintered at 1050°C for 1 h. The main phases of rapidly solidified alloys are tetragonal $Nd_2Fe_{14}B$ and the rest is $Nd_{1.11}Fe_4B_4$ and a solid solution on an Nd base. The dendrite structure is typical for all five investigated alloy compositions. Isothermal annealing of GA magnets at 800°C leads to formation of an optimum structure. Heavy rare earth elements, dysprosium and terbium, enhance the main magnetic $Nd_2Fe_{14}B$ type phase lattice that leads to an increase of magnetic properties. The best coercivity achieved for GA magnets was $H_c = 800$ kA/m.

In order to examine the compacting of the Nd–Fe–B magnetic powder as well as the applied technology on the physical properties of the Nd–Fe–B dielectromagnets, two powder types were used [51]. Both types were manufactured by the company Magnequench and are marketed under the names MQP–B and MQP-S-11-9. The MQP-B powder is produced from Nd–Fe–B alloy by the melt spinning technique. The average size of particles in ribbon form of this powder is about 200 μm. The MQP-S-11-9 powder is manufactured by atomization. The average size of particles for this type of powder ranges from 35 to 50 μm. Both powder types are used for manufacturing of compression molded as well as injected molded magnets.

The injection molded dielectromagnet manufacturing process consisted of injection of a mix composed of magnetic powder and polystyrene as a binder agent. The injection molding process was accomplished at temperatures in the range from 160 to 240°C and under injection pressures of either 100 or 130 MPa. The compression molded dielectromagnets consisted of compression molding of the magnetic powder bound by Epidian100 heat-hardening resin which contributed 2.5% of the total weight of powder and resin mixture. Figure 22.18 shows microscope photographs of cross-sections of the injection molded dielectromagnets made from powders. Magnetic properties of the atomized powder magnets are lower than the ones of the ribbon powder magnets (Table 22.15). The advantage of the former lies in better technological features: preparation of the atomized powder is easier, the mold is more densely filled with the material and manufacturing of injection molded magnets with a higher content of hard magnetic powder (about 62% volume ratio) is possible.

New metastable nanocrystalline multicomponent systems prepared by mechanical alloying or by mechanochemical methods show an enhanced remanence or improved high temperature properties [52]. For isotropic magnets, high energy ball milling is used as a versatile technique for the preparation of nanocomposites in the (PrNd)FeB system. Alloy composition optimization and mixing with iron lead to

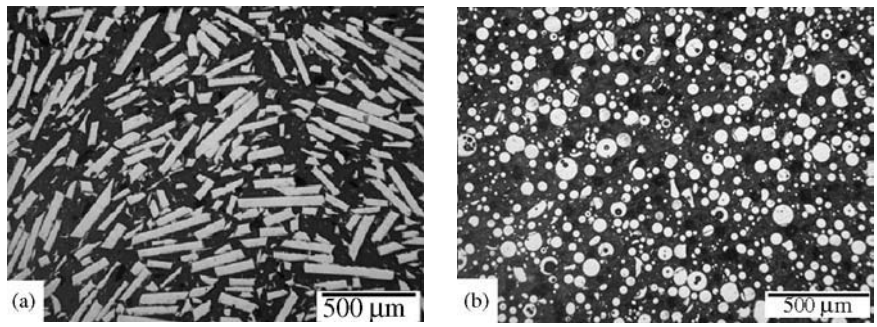

Figure 22.18 Photographs of cross section of the injection moulded dielectromagnets from ribbon (a) and from atomized (b) powders. Source: Ref 51

Table 22.15 Magnetic properties of the Nd–Fe–B dielectromagnets

Powder grade	Powder obtaining process	Particle shape	Magnet production process	Magnetic properties		
				B_r, T	H_c (kA/m)	$(BH)_{max}$ (kJ/m^3)
MQP-B	Melt spinning	Ribbon	Compression molded	0.71	735	82.72
MQP-S-11-9	Melt atomization	Spheroidal	Compression molded	0.572	796	51.17
MQP-B	Melt spinning	Ribbon	Injection molded	0.467	829	40.71
MQP-S-11-9	Melt atomization	Spheroidal	Injection molded	0.363	812	24.03

B_r is residual magnetic induction; H_c is high coercive force; $(BH)_{max}$, is energy product measured by fitting the largest rectangle to the demagnetization curve, found in the second quadrant of the hysteresis loop (see Figure 22.17)

hard magnetic multiphase powders with improved corrosion resistance suitable for high performance bonded magnets. The high values of maximum energy product $(H_c \cdot B_r)_{max}$ and magnetic induction are due to the presence of α-Fe and an exchange-coupling effect resulting in effectively single-phase demagnetization curves (see Figure 22.17).

Generalized typical magnetic properties of the bonded and of the sintered magnets, made from rare-earth alloys as well as from ferrites for comparison, are given in Figure 22.19.

Rare earth magnets are used in electronic watches and traveling-wave tubes. Direct-current and synchronous motors and generators include rare earth magnets for size reduction. The reasons for usage comprise high flux density, high coercive field, high energy size value and temperature stability. Rare earth magnets are also used in medical devices, such as thin motors in implant pumps, valves and in aiding eyelid motion.

It is significant that more than thirty parts of a present-day car (for example, door locks, oil pump, windows, seat supports, wipers, headlight direction, brakes, steering, etc) include rare earth alloy magnets.

Cemented Tungsten Carbides

The study of RE metal-doped cemented carbide was started in the early 1960s in China and intensive investigations in this field have been reported lately [54–56]. Recently, an enrichment effect of RE metal on the sinter skin was observed during the sintering process of high activity mischmetal (mainly containing lanthanum and cerium) doped cemented carbides with low and medium carbon levels [57].

Beryllium

Beryllium is a light gray metal and has the lowest density among the construction metals. This metal, due to its unique mechanical and physical properties, is used in various nuclear, aerospace, X-ray, and consumer fields.

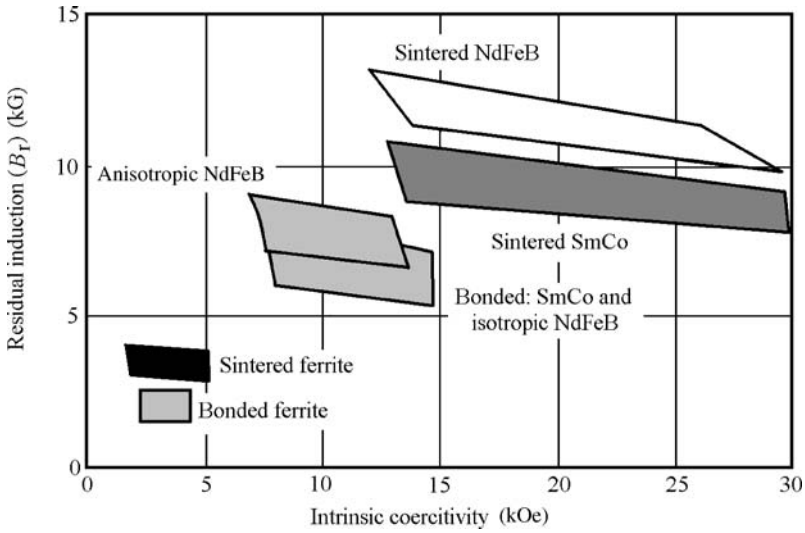

Figure 22.19 Generalized typical magnetic properties of bonded and of sintered magnets. Source: Ref [53]

Table 22.16 Typical properties of beryllium

Property	Unit	Value
Density	g/cm^3	1.847
Crystal type[a]		HCP
Atomic diameter	nm	0.228
Brinell hardness	MPa	1000–1500
Modulus of elasticity	GPa	275–300
Melting point	°C	1289
Boiling point	°C	2970
Specific heat at room temperature	kJ/(kg · °C)	1.88
Heat of fusion[b]	kJ/mol	9.8
Heat of vaporization[b]	kJ/mol	308
Thermal conductivity	W/(m · °C)	190
Coefficient of linear thermal expansion at temperature ranges[c]:	μm/(m · °C)	
at 25 to 100°C	μm/(m · °C)	11.6
at 25 to 300°C	μm/(m · °C)	14.5
at 25 to 600°C	μm/(m · °C)	16.5
at 25 to 1000°C	μm/(m · °C)	
Electrical conductivity[b]	% IACS	40
Volume diffusion[b]	m^2/s	6×10^{-5}
Volume diffusion activation energy[b]	kJ/mol	161
Capture cross section of heat neutrons n · 10^{24}	cm^2	0.009
Transmits sound[c]	m/s	12 600
Reflects light[c]:		
optical reflectivity	%	50
ultraviolet reflectivity	%	55
infrared (10.6 μm)	%	98

[a]Crystal type: H, hexagonal. Source: Refs [a][1], [b][4], [c][58]

Cast beryllium usually has a coarse crystalline structure and, because of its high crystal anisotropy, wrought processing is not feasible. Therefore, powder metallurgy is the only acceptable technique for manufacturing strong homogeneous beryllium billets.

Physical Properties

Beryllium is a light metal with a combination of physical properties that is not found in any other metal (Table 22.16). A close packed hexagonal crystal

structure, α-modification (with $a = 0.2286$ nm and $c = 0.3584$ nm and c/a ratio of 1 to 1.56) at above 1250–1260°C, near to melting point is transformed into cubic β-form. The value c/a of beryllium crystal structure is low compared with other metals such as titanium (1 to 1.58).

Beryllium has a relatively high melting point, high modulus of elasticity, relatively high electrical conductivity (35–45% IACS), high specific heat, low coefficient of thermal expansion and highest among metals of heat capacity; beryllium is distinguished by very small capture cross-section for thermal neutrons and high ability to scatter them. Beryllium penetrability by X-rays is 16–17 times as large as aluminum penetrability. Beryllium is non-magnetic.

Wrought beryllium has the highest strength-to-weight ratio of all construction metals and retains durability at elevated temperatures up to 600°C. However, mechanical properties strongly depend on the processing technique and subsequent thermal and mechanical processing. Extrusion and rolling lead to anisotropic properties caused by orientation of hexagonal beryllium crystals in a certain direction. Consequently, for example, the tensile strength of extruded rod or rolled bar in the longitudinal direction is one and a half to twice that in the transverse direction. Anisotropic mechanical properties are not observed in articles obtained by PM (usually by hot pressing), because of the random orientation of the crystals.

In dry air, beryllium does not oxidize significantly at temperatures up to about 600°C because it forms a protective oxide film, similar to that of aluminum, formed in air. Rapid oxidation is observed at 900–1000°C. Above 650°C, beryllium slowly reacts with nitrogen, forming beryllium nitride (Be_3N_2). Hydrogen does not react with beryllium right up to melting point. Halogens react with beryllium at elevated temperatures, beginning at 300°C forming BeX_2 (X is halogen). High purity beryllium is stable in pure water up to 100°C, but the presence of inclusions of chlorides and/or carbides in the metal and of chloride, sulfate, etc. ions in the water accelerates corrosion.

Beryllium is dissolved in hydrochloric and sulfuric acids, slowly reacts with dilute nitric acid in the cold, but is dissolved on heating. It is dissolved by caustic alkali solutions forming the beryllate ($MeBe\ O_2$).

At temperatures down to 500–700°C, beryllium is stable in contact with melted metals and alloys that can be used as a heat-transfer medium in nuclear reactors. Bismuth, Bi–Pb alloys, Bi–Pb–Sn alloys, sodium, potassium, Na–K alloys and lead are relevant in this context.

Molten beryllium reacts with carbon with the formation of beryllium carbide (Be_2C) and reacts with such durable and refractory oxides as magnesium oxide, aluminum oxide, calcium oxide and zinc peroxide, due to high beryllium affinity for oxygen.

Beryllium Compounds

Only one oxide, BeO, is known in the beryllium–oxygen system. It is a refractory compound with melting point 2550°C and high chemical stability (enthalpy formation is 599 kJ). Beryllium oxide is remarkable for high heat conductivity that ensures heat resistance. Burnt at 1800°C, beryllium oxide is virtually insoluble in acids and does not react with fused metals (uranium, iron, nickel, calcium and others).

Beryllium fluoride, BeF_2, is a colorless crystalline material and very hygroscopic. It is highly soluble in aqua (about 18 mol/L). Beryllium fluoride with alkali metal fluorides and ammonium forms composite salts. The salts, Na_2BeF_4 and $(NH_4)_2BeF_4$, play an important part in technology. Beryllium fluoride is obtained by thermic decomposition of ammonium fluoro-beryllate at 900°C.

Beryllium hydroxide, $Be(OH)_2$, precipitated from beryllium salt solutions in the pH interval from 6 to 8, possesses amphoteric properties: beryllium salt solutions are formed by dissolving in acids, while beryllates (Me_2BeO_2) are formed by dissolving in alkalis. Beryllium hydroxide is dissolved in ammonium carbonate, forming a carbonate complex, $(NH_4)_2[Be(CO_3)_2]$. Solutions of the latter are decomposed on boiling, a slightly soluble basic carbonate $BeCO_3 \cdot n Be(OH)_2 \cdot mH_2O$ being precipitated.

Beryllium forms alkaline salts with a series of organic acids with general formula $Be_4O(RCOO)_6$, which are produced by the action of organic acids on beryllium hydroxide. In technology, compound $Be_4O(CH_3COO)_6$ is used. Salt is sublimed without decomposition at temperatures 360–400°C.

Beryllium forms intermetallic compounds with a series metals, differing by infusibility, low density and oxidation resistance up to 1500–1600°C. Of greatest interest are the following beryllides: Zn Be_{13}, $TaBe_{17}$ and Mo Be_{12} with melting temperatures about 1930, 1980 and 1700°C, respectively.

Sources of Raw Material

The beryllium content in the earth's crust is about 6×10^{-4} wt%. Nearly 40 beryllium minerals are known, mainly various complicated silicates. The following minerals have the largest commercial importance: beryl, chrysoberyl, phenacite, helvite, bertrandite and donalite.

Beryl ($Be_3Al_2(Si_6O_{18})$) is the most prevalent beryllium mineral. It contains up to 14.1 wt% BeO and

often admixtures of alkaline metals. The hardness of beryl is 7.5–8 on the Mohs scale.

Phenacite (Be_2SiO_4) is the richest mineral as regards beryllium content – 46 wt%. The hardness of phenacite is 7.5. At present, phenacite, along with beryl, has a large commercial significance.

The commercial beryllium ore deposits are confined to pegmatitic and hydrothermal-pneumatolytic types. At present, the hydrothermal-pneumatolytic type ore deposits contain mainly phenacite, chrysoberyl, helvite, and bertrandite, opened at the beginning of the 1950s in the USA, are becoming commercially important.

Beryllium ores are usually lean: BeO content ranges from 0.03 to 2%. They are difficult to concentrate because of their similarity to the rocks with which they occur in association. The major ore concentration methods are the following:

- selective grinding is used for ores which contain soft rocks (soft slates, talc and others). The hard beryllium minerals are separated from barren rock minerals on screens or in separators
- flotation is used for disseminated beryl ores. Beryl is floated with fatty acids (rapic acid). For concentrating phenacite and bertrandite ores, the concentration schemes include gravitation in heavy liquids (for medium-and coarsely disseminated ores) and flotation for finely disseminated ores.

Standard beryllium flotation concentrates in Russia contain from 9.7 to 6.12%BeO.

Beryllium concentrates are usually processed to beryllium oxide or beryllium hydroxide, from which beryllium fluoride or chloride is produced – the initial materials for beryllium production. The fluoride and sulfate methods are used in commercial practice for processing beryllium concentrates.

The fluoride technique is based on beryllium conversion by means of complex fluorides, Na_2SiF_6 and Na_3FeF_6. As a result of the interaction of beryl with complex fluorides at temperatures ranging from 750 to 800°C, fluorberyllate (Na_2BeF_4), which is soluble in aqua, is formed. Compounds of other elements have low solubility.

The sulfate technique is based on conversion of beryllium together with aluminum and iron into a sulfate solution, while the main bulk of silicon dioxide remains as an insoluble residue. As long as beryllium slowly reacts with concentrated sulfuric acid, even at 200–250°C, preparatory operations of concentrate alloying with lime or thermal activation of beryllium are conducted.

At present beryllium is obtained by two methods:

- reduction of beryllium fluoride by magnesium
- electrolysis from chloride electrolyte.

Magnesium-Thermal Reduction of Beryllium Fluoride

Magnesium is used as a reducing agent, because it does not form compounds in solid solution with beryllium:

$$BeF_2 + Mg = Be + MgF_2; \quad \Delta G^0_{1000K} = -118\,kJ$$

The redundant BeF_2 is introduced in a flux composition. Reduction is done in graphite crucibles in induction furnaces. A mixture of magnesium fluoride and beryllium fluoride, not avoiding additional impurities, is used as flux for protection from oxidation. Magnesium is introduced in 75% stochiometric quantity. Reduction is conducted in an inert atmosphere at temperatures ranging from 900 to 1000°C. Next, the temperature is raised to 1300°C (higher than beryllium melting point). The prill float to the surface and are assembled in an ingot ('lens'). During cooling, beryllium solidifies before the flux which allows the ingot to be withdrawn from fused flux. The ingots obtained contain to 1.5% Mg, about 0.1% BeO, 0.1% Fe and Al and other impurities. They are refined by remelting at 1500°C.

Electrolysis from Chloride Electrolyte

The electrolyte contains $BeCl_2$ and NaCl in weight ratio 1 to 1. It is close to eutectic composition (58.7% $BeCl_2$ + 41.3% NaCl) with melting point 215°C that

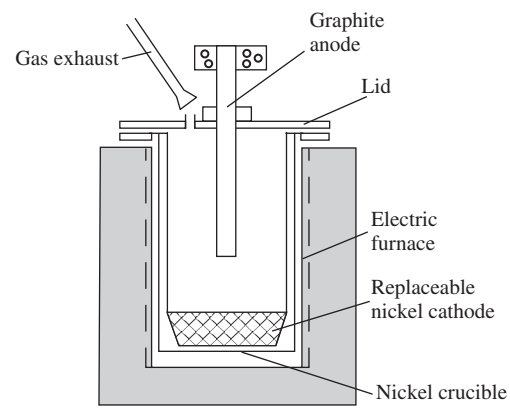

Figure 22.20 Scheme of electrolyzer for flake beryllium production.

permits electrolysis to be conducted at low temperatures around 350°C. Beryllium is deposited on the nickel electrodes; chlorine is evolved on the graphite anode:

$$Be^{2+} + 2e = Be$$

$$2Cl^{-} - 2e = Cl_2$$

An electrolytic cell made of nickel is put into a furnace (Figure 22.20). Replaceable cathodes are perforated nickel crucibles. Chlorine evolved on the graphite anode is removed by the exhaust system.

Originally, the electrolyte is refined from impurities of more electropositive metals as compared with Be (such as Cu, Fe, Ni, and others) at voltage of about 1.5 V. Then the cathode is replaced and the voltage increased to 2.08 V. Cathode current density is 1 kA/m^2, anode current density is 4 kA/m^2. Electrolysis is conducted at 420°C. Current efficiency is 60–65%. The cathode, with precipitated beryllium, is removed from the electrolyzer while still hot. On cooling, the beryllium flake is removed from the cathode and sequentially washed by water, alkali solution, diluted nitric acid and again with water and then it is centrifuged and dried.

Dried beryllium flakes are pressed into briquettes, which are vacuum remelted and cast into ingots. Typical impurity contents of electrolytic beryllium after vacuum remelting are 30 ppm Al, 30 ppm Ca, 20 ppm Cl, 20 ppm Cu, 70 ppm Fe, 30 ppm Ni and 20–30 ppm Si.

Production of Leafed Beryllium by Electrorefining from Melts

The feed is preliminary beryllium in disks. The electrolyte consists of 40–50 wt% $BeCl_2$ and 50–60 wt% NaCl. Temperature ranges from 320 to 330°C. Cathode current density is 830 A/m^2, anode current density is 3000 A/m^2. The electrolyzer has a construction similar to the one for beryllium recovery with insoluble anodes (see Figure 22.20). Preliminary beryllium disks are set on the graphite rod. Another type of electrolyzer is equipped with a gradually extending anode made of refined beryllium. After extraction, cathode deposits are washed with 10% solution of ammonium carbonate, oxalic acid and ethyl alcohol. The impurity content in the final product is as follows: 60–100 ppm Fe, 80–300 ppm Ni; and 6–20 ppm Mn. Current efficiency is up to 80%, beryllium recovery amounts to 80%.

Powder Production

The vacuum remelted beryllium ingots are cut into chips by lathe turning. But chips produced in this way are relatively coarse and must be reduced to fine particle sizes before consolidation into homogeneous, fine grained billets.

Grinding

Until recently, ball milling and attrition grinding were the only processes used to reduce machining chips to powder. Attrition milling is accomplished by impact and shear forces which may be classified as a high-energy ball milling process [59], where the rotating charge of balls and milling product form a vortex by means of a rotating impeller.

This milling process results in basal plane cleavage. Thus, the powder particles produced by attrition technique tend to form flakes (Figure 22.21(a)) with flat corresponding to {0002} basal planes. Ball milled powders have a similar shape. As a result of their particle shape and crystallographic texture, consolidated billets reveal anisotropy of both physical and mechanical properties.

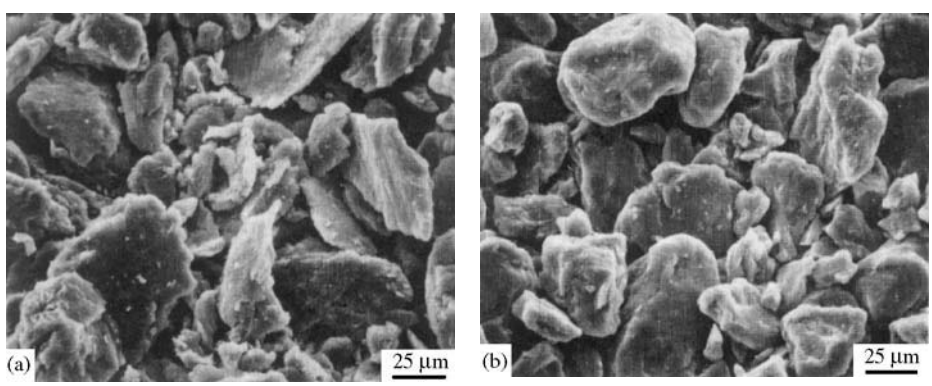

Figure 22.21 Scanning electron micrographs of flake like attritional (a) and blocky impact ground (b) powders. Source: Ref 60®

By vibratory die loading for pressing and following consolidation, usually by uniaxial vacuum hot pressing, the imposed stress causes many flake particles to turn so that the *c*-axis poles align to the stress axis. In compacts made with attrition powder, *c*-axis poles exist with two to three times the frequency in the longitudinal as compared to the transverse direction. This leads to substantial anisotropy of mechanical and physical properties [58].

Milling chips in a water-cooled disk grinder with a beryllium lining in a dry inert gas atmosphere is also used. Another known process is ball milling in an aqueous medium, the powder being subsequently washed with dilute nitric acid and, to prevent oxidation, organic liquid(s) [7]. These powders have also particles tending to flake shape.

The coldstream impact process is used to reduce anisotropy. Chips and powder are entrained in a high speed gas stream and are impacted against a stationary beryllium target. Rapidly expanding gases leaving the nozzle create a strong cooling effect by adiabatic gas cooling, which is greater than the heat generated by pulverization. Therefore, the process occurs at well below room temperature. The high speed pulverization process, coupled with the latter, activates the secondary and tertiary non-basal cleavage systems. The resultant particles have roundish facets (Figure 22.21(b)), rather than flake like.

After the material has struck the target and shattered, it is removed from the impact chamber by suction. It is then transported to a primary classifier, which allows the oversize to return to the feed hopper for subsequent impact against the target. The finished product is separated by the secondary classifier and transported to collection containers. More detailed information on coldstream impact grinding as well as on other grinding technique can be found in Chapter 2.

The particle shape and crystallographic texture, obtained by impact grinding leads to substantially reduced correlation between crystallographic basal planes and flat powder particle faces, leading to decreased anisotropy and an improvement in longitudinal tensile elongation. The transverse-to-longitudinal ductility ratio for attrition milled powder is about 3 to 1. For impact ground powder, this value is approximately 1.6 to 1.

The strength of beryllium is related directly to grain size which is primarily a function of the particle size, oxide content and consolidation temperature of the powder used. Because oxides are a primary grain-boundary pinning agent, fine particle size enhances oxide content and, therefore, strength. The strength imparted by fine grain size and the potential embrittlement effect of excessively high oxide content must be balanced against each other. Characteristics of beryllium powders used to manufacture billets are given in Table 22.17.

Gas Atomization

Inert gas atomization enables beryllium powder to be produced in semi-manufactured condition without a chip-forming step [60]. Parallel with this, the major advantage of this process over conventional impact ground powder technique is the increased isotropy of the consolidated material. This is especially important in optical systems, where isotropy is a primary factor in component performance, particularly in cryogenic systems in which thermal constructions can cause distortion in anisotropic components. Economic benefits may also be obtained if this process is used on a commercial production scale. The typical chemical composition of inert gas atomized beryllium powder is given in Table 22.17.

Microalloying Influences

The impurity elements that have an influence on the beryllium properties include aluminum, cobalt, copper, iron, magnesium, nickel, silicon, oxygen and carbon.

Aluminum and iron can cause deleterious effects in beryllium. The presence of aluminum at the grain boundaries leads to reduced ductility in components for elevated temperature applications. Iron forms the compound $FeBe_{11}$, which results in precipitation hardening. Yield point feature observed in beryllium has been attributed to the pinning of dislocations by $FeBe_{11}$ precipitates [58]. If it persists until the ultimate strength is reached, the beryllium fractures with little plastic deformation. Aluminum and iron, when present together in beryllium, can form the compound $FeAlBe_4$. The appropriate balancing of aluminum and iron content eliminates the embrittlement action of aluminum or $FeBe_{11}$ precipitation without the use of ultra-high purity.

Silicon acts as a sintering assistant in the consolidation of beryllium powder. In practice, the hot pressing of beryllium powder with silicon content is difficult because of the pressure limitation when using graphite dies. The high pressure capability of hot isostatic pressing is often used for the consolidation of low-silicon, high-purity electrolytic powder. A variant is to dope the material with trichlorosilane at the vacuum hot pressing stage. In general, aluminum, iron and silicon cause agglomeration and growth of beryllium oxide and also act on recrystallization, grain growth and creep strength of beryllium.

Table 22.17 Characteristics of beryllium powders used to manufacture billets

Property	Unit	Grade				
		SP-65B[a]	SP-200F	IP-70	IP-220	GA[b]
Elements:						
Beryllium assay	% min	99.0	98.5	99.0	98.0	balance
Beryllium oxide	% max	1.0	1.5	0.7	2.2	0.32
Aluminum	ppm max	600	1000	700	1000	300
Boron	ppm max	2	...	...	...	...
Cadmium	ppm max	2	...	...	...	...
Calcium	ppm max	100	...	...	...	...
Carbon	ppm max	1000	1500	1000	1500	700
Chromium	ppm max	100	...	...	...	...
Cobalt	ppm max	10	...	...	...	...
Copper	ppm max	150	...	...	...	...
Iron	ppm max	800	1300	1000	1500	900
Lead	ppm max	20	...	...	...	...
Lithium	ppm max	3	...	...	...	...
Magnesium	ppm max	600	800	700	800	100
Manganese	ppm max	120	...	...	...	...
Molybdenum	ppm max	20	...	...	...	...
Nickel	ppm max	300	...	...	...	...
Nitrogen	ppm max	300	...	...	...	...
Silicon	ppm max	600	600	700	800	...
Silver	ppm max	10	...	...		...
Other metallic impurities[c]	ppm max	200	400	400	400	...
Particle sizes 45 μm under seeding	min %	98	98	98	98	...

[a]Nominal composition of nuclear grade of beryllium powder.
[b]Typical chemistry of inert gas atomized beryllium powder.
[c]Each; determined by normal spectrographic methods.
Source: Refs 60, 61

Copper, cobalt and nickel show extensive solubility in beryllium.

Among the non-metallic impurities, only carbon and oxygen are observed to any appreciable extent. Both have minimal solubility in beryllium. Carbon occurs as the cubic refractory beryllium carbide compound, which is usually found within the grains. This carbide accelerates the corrosion of beryllium, as it slowly hydrolyzes in the presence of moisture.

Oxygen forms stable beryllium oxide, which is principally a grain-boundary constituent. However, it may also be found in the matrix. Typical concentrations of beryllium oxide in beryllium powders in commercial billets range from 0.7 to about 2.0%.

Powder Consolidation and the Production of Wrought Products

The most common powder consolidation methods are vacuum hot pressing and hot isostatic pressing. Other methods, such as cold pressing and sintering and vacuum sintering, have also been used to consolidate beryllium and beryllium alloy powders.

Vacuum Hot Pressing (VHP)

This technique was most frequently used for manufacturing commercial beryllium billets. Graphite dies are commonly used due to a low coefficient of thermal expansion, which simplifies removal of the beryllium billet after cooling. Graphite is available in sufficiently large sizes to produce vacuum hot pressings above 560 mm in diameter. Pressings that are too large in diameter for graphite dies are accomplished in nickel alloy (IN-100) up to 1830 mm in diameter.

Beryllium powder is vibratory loaded into the dies to achieve a density of about 55%. The assembly is then placed in a vacuum hot pressing chamber. Typical pressing temperatures range from 1000 to

Table 22.18 Properties of beryllium hot pressed billets

Property	Unit	Grade				
		S-200F	S-65B	I-70A	I-220B	EP[a]
Chemical composition:						
Beryllium assay	% min	98.5	98.5	99.0	98.0	balance
Beryllium oxide	% max	1.5	1.0	0.7	2.2	...
Aluminum	% max	0.10	0.06	0.07	0.10	0.03
Carbon	% max	0.15	0.12	0.07	0.15	...
Iron	% max	0.13	0.12	0.10	0.15	0.10
Magnesium	% max	0.06	0.08	0.07	0.08	0.05
Silicon	% max	0.06	0.06	0.07	0.08	0.03
Other metal impurities	% max	0.04	0.04	0.04	0.04	0.03
Powder type		Impact ground	Impact ground	Impact ground	Impact ground	Flakes
Minimum density	g/cm^3	1.84	1.84	1.84	1.84	...
Theoretical density	%	99	99	99.3	99	...
Average grain size	μm max	25	15	20	25	...
Ultimate strength (min)	MPa min	324	289.6	241.3	379	...
Yield strength (min)	MPa min	241	206.8	172.3	275	...
Elongation (min)	% min	2	2	2	2	...

Note: Pressing sizes can range from 188 to 1830 mm in diameter and 150–1680 mm in length, depending on grade and compositions.
[a]Electrolytic beryllium flakes are pressed in briquettes, which are vacuum remelted and cast into ingots.
Source: Refs 1, 60

1100°C and compacting pressure ranges from 3.5 to 14 MPa. Properties of vacuum hot pressed billets are given in Table 22.18.

Hot Isostatic Pressure (HIP)

Improved isotropy of both microstructure and mechanical properties is a major advantage of isostatic pressing. This is achieved because the pressure is applied from all sides, shrinkage is uniform in all directions and directionality originating from the pressing operation is prevented.

In the HIP process, the powder is loaded into a mild steel container, degassed to remove air and vapor, and the container is sealed. Hot isostatic consolidation at pressures of about 103 MPa and at temperatures from 760 to 1100°C is the only effective means of reliably consolidating high purity beryllium powders to full theoretical density. While ordinary purity beryllium powder, which contains sufficient concentration of impurity elements such as aluminum and silicon that act as sintering aids in the hot pressing, can be vacuum hot pressed to nearly theoretical density by pressing at about 7 MPa at 1050°C, high purity powder can be consolidated by the latter technique to only 98% theoretical density at the same temperature even when employing pressures as high as 24 MPa or more. These pressures are close to the upper limit at which consolidation can be performed using graphite die tooling.

The mechanical properties of three grades of hot isostatic consolidated beryllium are compared to their vacuum hot pressed parallel parts in Table 22.19. Isostatic consolidation of high purity powder material improved physical and mechanical properties, including fine grain size, well distributed oxide content, a high degree of isotropy, good compression creep properties, good elevated temperature properties, and no grain growth up to 1260°C.

Beryllium powders are consolidated to near theoretical density also by:

- Cold isostatic pressing followed by vacuum hot pressing
- Cold isostatic pressing followed by pressureless sintering
- Cold isostatic pressing followed by hot isostatic pressing
- Direct hot isostatic pressing

The technique of uniaxial cold pressing followed by sintering in a vacuum and final sintering in an argon atmosphere has been used for specific applications, such as the production of aircraft brakes, heat sinks, rotors and stators [58].

Wrought Product Forms

After beryllium powder consolidation, it is easily processed by conventional metalworking techniques.

Table 22.19 Mechanical properties of VHP and HIP beryllium

Property	Unit	Grade					
		S-200F		I-70		I-220	
		HIP	VHP	HIP	VHP	HIP	VHP
Ultimate tensile strength	MPa	414	324	345	241	448	379
Yield strength	MPa	296	241	207	172	345	275
Elongation	%	3	2	2	2	2	2

Source: Ref 58

Table 22.20 Typical tensile properties of beryllium wrought specimens

Product	Manufacturing method	Test orientation	Ultimate tensile strength (MPa)	Yield strength (MPa)	Elongation[a] (%)
Block					
Ordinary purity[b]	VHP	L	370	266	2.3
		T	390	273	3.6
Hugh purity	HIP	L	455	287	3.9
		T	455	287	4.4
High-oxide instrument grade	VHP	L	476	406	1.5
		T	511	413	2.7
Fine grain size	HIP	L	580	407	3.7
		T	587	407	4.2
Sheet (1–6.4 mm, thick) Ordinary purity powder	Hot rolled	...	531	372	16
Ordinary purity ingot	Hot rolled	...	352	172	7
Extrusion					
Ordinary purity powder	Hot extrusion	...	655–690	345–518	8–13
Ordinary purity ingot	Hot extrusion	...	628–655	345–518	8–13
Forgings Ordinary purity	...	...	483–600	435–600	0–4.5

L, longitudinal; T, transverse.
[a]Elongation in 50 mm.
[b]Structural grade contains about 1.8%BeO.
Source: Ref 62

Wrought forms of beryllium with optimum properties are produced from vacuum hot pressed billets by conventional hot-working techniques. Wrought products show improved mechanical properties in the predominant direction of metal flow. Mechanical properties of wrought products depend greatly on crystallographic orientation. Biaxial or triaxial deformation procedures are often used to produce semiproducts with balanced directional properties.

Sheet, plate and foil are the most commonly manufactured wrought forms of beryllium. These flat products are produced by encasing beryllium billets in steel jackets, followed by cross rolling at moderate temperature. Beryllium foil is available in thicknesses from 0.025 to 0.5 mm and panel sizes up to 125 × 300 mm.

Rod, tubing and structural shapes are available by beryllium extrusion. Their mechanical properties in the direction of metal flow are superior to the mechanical properties of hot pressed billets in the direction of metal flow. Input billets for extrusion are usually machined from hot pressed blocks. Extrusion billets are jacketed in low-carbon steel containers that have been shaped during extrusion through a steel draw plate at 900–1065°C. Then, the steel jackets are chemically removed from the extrusions.

Conventional rod is produced in sizes from 9.5 to 135 mm in diameter. Tubing is available from 6.4 mm outside diameter by 1 mm wall thickness up to 150 mm outside diameter by 3.2 mm wall thickness.

Typical tensile properties of beryllium sheet and extrusions are listed in Table 22.20.

Applications of Beryllium

Nuclear and X-Ray Applications

Beryllium is used as a reflector material, in research and fast reactors, as well as in power reactors, for moderators, reflectors and fuel cladding material.

Exclusive combination of properties of beryllium greatly improves the control of nuclear fusion energy reactors such as the Joint European Torus (JET). The excellent oxygen gathering performance of beryllium with its low atomic number eliminates plasma density disruptions, increases the time scale of magnetohydrodynamic effects and reduces runaway photoneutron production.

Because of excellent transparency to soft X-rays and other radiation such as gamma rays, beryllium is used in X-ray tube windows. Owing to its low density, beryllium passes X-rays 17 times better than an equivalent thickness of aluminum.

In medical radiation detection devices such as axial tomographic scanners and other related equipment with pressurized detection chambers, the transparency of beryllium to X-rays and its stiffness are united. A stiff beryllium window resists the internal gas pressure with minimum deflection. Most of this equipment requires disks thinner than 0.25 mm and are cut from sheet or machined from vacuum hot pressed blocks.

Aerospace Applications

The unique combination of low density, high modulus of elasticity and dimensional stability of beryllium makes it an ideal choice for structural parts in aerospace components. In particular, a beryllium structure as well as beryllium optical system was applied in the Hughes MODIS satellite; a beryllium thrust tube assembly was used in the Japanese CS-2 satellite. Beryllium is also exploited in the optical bench for the McDonnell Douglas mast-mounted helicopter sight system. Laser, television and infrared sensors are mounted to the bench, which must maintain precise alignment for proper operation of the target detector and designator system [58].

The development of higher ductility grades of beryllium in various wrought forms, including sheet metal, has increased the potential application of beryllium in the aerospace sphere.

High Temperature Conditions

Beryllium has the highest specific heat among all the structural materials, good thermal conductivity, relatively high melting point and resistance to oxidation up to about 700°C. It is a highly efficient heat sink, heat shield and airplane and automobile brake material. Beryllium is also used for making thrust chambers and nozzles of rocket engines.

Apparatus Applications

Beryllium is used in components in inertial guidance systems. It is used in precision navigational aids for aircraft, spaceship, missiles, ships and submarines. The high modulus, high precision elastic limit and dimensional stability under high g-forces make beryllium the elect material for these conditions.

Alloys of Beryllium

An alloy of 68 wt% beryllium with aluminum is known under the commercial alloy name AIBeMet 162. The physical properties and mechanical properties of the three commercial available forms (extrusions, sheet and hot isostatic pressed block) are presented in Table 22.21.

In comparison with unalloyed beryllium, fabrication such as welding and joining of AIBeMet can be easier. This makes AIBeMet an alternative when the properties of beryllium are well in excess of required values. The properties of AIBeMet make it a candidate for many applications in which aluminum or titanium could also be used.

Current aerospace uses AIBeMet, including electronic modules for the F-22 tactical fighter and antenna and structures of several commercial communication satellites. In commercial products, AIBeMet served as the voice coil actuator in high-performance hard disk drives in the early 1990s due to its light weight and high stiffness. Along with this, the brake calipers of Formula I automobiles have been made from AIBeMet and used by many racing teams.

The solid solubility limit of beryllium in aluminum is low (0.3 at.%). This alloying limit can be extended by rapid solidification (RS) PM technology. Lewis et al. at Lockheed Corporation have examined Al–Be–Li alloys by RS-PM and have attained values of specific modulus that are significantly higher than those attained in conventional aluminum alloys [63]. They used melt spinning to examine Al–Be–Li and Al–Be alloys designed to be age hardenable and to have ultralow density. Al–20.5Be–2.4Li and Al–29.6Be–1.3Li alloys illustrated the best properties.

Workplace Atmosphere Safety

Inspirable dust of beryllium and its compounds are both carcinogens and able to cause allergic illnesses.

Table 22.21 Properties of AlBeMet 162 and aluminum–beryllium–lithium alloys

Property	Unit	Alloy		
		AlBeMet 162	Al-20.5Be-2.4Li	Al-29.6Be-1.3Li
Nominal chemical composition:				
Beryllium	wt%	68.0	20.5	29.6
Lithium	wt%	...	2.4	1.3
Aluminum	wt%	balance	balance	balance
Physical properties:				
Density	g/cm^3	2.01	2.298	...
Elastic modulus at 25°C	GPa	200	123	142
Elastic modulus at 200°C	GPa	195	...	...
Linear coefficient of thermal expansion at 25–100°C	μm/(m · °C)	16.35	...	...
Thermal conductivity at 25°C	W/(m · °C)	212	...	...
Specific heat	kJ/(kg · °C)	1.5	...	...
Electrical resistivity	μΩ · cm	3.43	...	...
Solidus temperature	°C	644	...	...
Mechanical properties:				
Ultimate tensile strength:				
As-quenched	MPa	...	451	...
Underaged	MPa	...	...	494
Peak aged	MPa	...	531	536
AMS 7911, HIPed block	MPa	262	...	...
AMS 7913, sheet	MPa	386	...	...
AMS 7912, extrusion (longitudinal)	MPa	358	...	...
Yield strength				
As-quenched	MPa	...	321	...
Underaged	MPa	...	...	434
Peak aged	MPa	...	483	497
AMS 7911, HIPed block	MPa	193	...	...
AMS 7913, sheet	MPa	276	...	...
AMS 7912, extrusion (longitudinal)	MPa	276	...	...
Elongation				
As-quenched	%	...	6.4	...
Underaged	%	...	...	5.0
Peak aged	%	...	3.3	2.6
AMS 7911, HIPed block	%	2	...	...
AMS 7913, sheet	%	5	...	...
AMS 7912, extrusion (longitudinal)	%	7	...	...

Source: Refs 39, 58

Their occupational stated average limit value (ALV) in the workplace atmosphere, as the shift time-weighted average concentration, and the classes of danger according to State Standard 12.1.005-88 under the legislation in the Commonwealth of Independents States (CIS) [17] is 0.001 mg/m^3. It is classed with the extremely dangerous powders, the first class of danger class according to the above State Standard.

Because of the high toxicity of beryllium and its compounds, a complex of industrial safety measures at the beryllium manufacturers is provided. The processes are especially dangerous where beryllium and its compound powders are used and processed, solutions are filtered, evaporated and decanted, molten and volatile compounds are sublimated. These industrial safety measures include maximum encapsulation of all units and interoperational transport, maximum mechanization and automation of the processes, remote control units, conducting of manual operations by means of manipulators in airproof boxes. In vented chambers, where equipment is located, an underpressure is maintained, in order to prevent an escape of airborne beryllium.

The beryllium containing suction gases are subjected to high-performance cleaning. Beryllium trace concentrations are continuously controlled in workplace atmospheres and in factory ambient air.

The combustibility of metallic beryllium is characterized by the following data. Solid beryllium is noncombustible. Self-ignition temperatures of beryllium powders in air range from 540 to 700°C, in water vapor from 350 to 450°C, in carbon dioxide at 570°C and in nitrogen above 1300°C. In humid gases, self-ignition temperatures for all cases are lower, than in dry ones. A suspended solid with particles coarser than 100 μm in air is explosion-proof. The burning temperature of beryllium amounts to 2000°C. The diffusion burning rate front on the powder surface amounts to 0.64 mm/s.

The products with such characteristics of inflammability and explosion risk are placed in the 'Moderate explosion hazard' class of danger according to the Guide to Legislation and 'Health and Safety' in the European PM Industry [19].

To extinguish burning beryllium it is necessary to use calcium fluoride powder (with consumption about 150 kg per 1 square meter) or dry sand. For voluminal quenching method, argon is used in concentration 35 vol% min in burning zone. Fire-fighting water foam, carbon dioxide and fire-extinguishing refrigerants must not be used [20].

As regards permissible beryllium concentration in potable water, the harmfulness limiting sign of beryllium threshold limit values (TLV) in potable water is sanitary-toxicological effect. Beryllium is, therefore, classed as an extremely dangerous substance, in the first class of danger according to the State Standard 4630-88 [18]. Its TLV is 0.0002 mg/L (subject to summation of all form contents).

Scandium

Physical Properties

The ordiecutive number of scandium is 21. Among the light metals, scandium is unique in its combination of low density with high melting point. Typical physical properties of scandium are given in Table 22.22.

Compact scandium is a silvery-white metal. It reacts with oxygen, halogens, sulfur and carbon. The surface film formed in air prevents further oxidation. With nitrogen, scandium reacts at temperatures above 500°C with nitride, ScN, formation. Scandium is easily dissolved in mineral acids, except for chromic and hydrofluoric acids and it reacts slowly with concentrated sodium hydroxide. The ion radius $Sc3^+$ (0.083 nm [1]) is less than Y^{3+} (0.097 nm) and

Table 22.22 Typical properties of scandium

Property	Unit	Value
Relative atomic mass	...	44.9559
Density	g/cm^3	2.989
Crystal type[a]:		c-p H
α-Sc (till 1337°C)		
lattice parameters	nm	$a = 0.33083$;
β-Sc (above 1337°C)		$c = 0.52680$
		bcc
Atomic diameter	nm	0.328
Brinell hardness	MPa	390
Melting point	°C	1541
Boiling point	°C	2836
Specific heat		
at 25°C	J/(mol · °C)	25.52
at 1500°C	J/(mol · °C)	39.80
Heat of fusion	kJ/mol	14.1
Heat of vaporization	kJ/mol	377.8
Thermal conductivity at 100°C	W/(m · °C)	15.7
Coefficient of linear thermal expansion in the temperature range from 20 to 1100°C	μm/(m · °C)	10.2
Specific electrical resistance at 25°C (polycrystalline specimen)	nΩ · m	410

[a]Crystal type: c-p H, close-packed hexagonal; bcc, body-centered cubic.
Source: Refs 1, 64

triple-charged RE ions (0.088–0.103 nm). Therefore, in scandium compacts the tendency to hydrolysis is greater than in similar rare earth compounds.

With metals of I, II, VII, VIII and VI by-subgroups and II, III, IV and V main subgroups of the Periodic Table, scandium forms intermetallic compounds ScMe, Sc_2Me, $ScMe_2$ and $ScMe_3$, and other types. The elements of III, IV, V and VI by-subgroups form eutectics with scandium.

Scandium forms compounds with oxidation level of element +3. Others element oxidation levels are not characteristic for scandium.

Sources of Raw Material

Scandium is a typical trace element of rocks. Its content in the earth's crust is about $6 \cdot 10^{-3}$ wt%. Scandium does not form its own deposits. Scandium minerals, thortveitite ($Sc_2[Si_2O_7]$) and sterrettite ($ScPO_4$ $2H_2O$), are very uncommon and have no commercial significance. Minerals, in which scandium is present in the form of isomorphous admixtures with concentration of Sc_2O_3 ranging from 0.005 to 0.3%, are more extensive.

Scandium mineral raw materials are concentrated in Australia, China, Kazakhstan, Norway, Russia, Ukraine, the USA and Madagascar. In Australia, scandium mineral reserves are contained in nickel and cobalt ore deposits, in Kazakhstan in uranous deposits, in Madagascar and Norway in pegmatite rocks. In Ukraine, scandium is contained in iron ores. In China, scandium mineral reserves are contained in tin, tungsten and iron ore deposits.

Because scandium is a trace element, currently it is usually obtained by means of extraction from waste and middling of metallurgical production, uranium-containing phosphorites, hydrolytic sulfuric acid, scandium–vanadium ores, mine waters and aluminum–scandium alloys.

Scandium content in processing products of raw material amounts to 1–10 ppm. Therefore, starting with the material, initial concentrates are obtained, which are further processed into scandium compounds.

Scandium-containing materials are taken into solution by treatment with acids, sodium hydroxide or by chlorination followed by washing with water or acid.

To recover scandium from solution, the following basic methods are used: precipitation of low-solubility compounds, extraction by organic solvents and ion exchange.

At present, the largest quantity of scandium is mined together with bauxites. Methods of its extraction from the red slime of alumina production are based on direct opening by mineral acids. The distribution of scandium in various minerals is shown in Table 22.23 [65].

Scandium Production

Currently, metallic scandium is produced mainly by metallothermic reduction of non-aqueous scandium fluoride or scandium chloride by magnesium or calcium in an inert gas atmosphere:

$$2ScF_3 + 3Ca = 3CaF_2 + 2Sc$$

The starting material is pure scandium oxide. Scandium oxide grade compositions according to CIS (Commonwealth of Independents States) TU 48-4-335-86 standard are illustrated in Table 22.24.

A technological line diagram of high-purity metallic scandium production is shown in Figure 22.22. Pure scandium oxide is heated in a current of hydrogen fluoride at 600°C. Reduction is conducted in tantalum or molybdenum crucibles.

The scandium fluoride thus produced is reduced at 850°C, rising to 1600°C, after which scandium and the slag separate and the reduction is complete. Then the metal is remelted under vacuum 10^{-3} Pa to eliminate the volatile residual impurities. At a temperature of 1700°C, scandium is sublimed. In order to reduce contamination by tantalum, it is recommended

Table 22.23 Distribution of scandium in various minerals

Raw source	Raw processing scope (10^3 tonnes per year)	Sc content (ppm)	Sc_2O_3 yield (tonnes per year)
Bauxites	71 000	1–20	710–1420
Uranic ores	50 000	1–10	50–500
Ilmenites	2000	10–20	20–40
Wolframites and cassiterites	200	100	20
Zircons	100	50–100	5–10

Source: Refs 64, 65

Table 22.24 Chemical composition of scandium oxide and metallothermic metallic scandium grades

Elements	Unit	Grades					High refined scandium	
		Scandium oxide[a]		Metallic scandium[b]				
		OS-99.9	OS-99.0	ScM-1	ScM-2	ScM-3	D[c]	E[d]
Scandium oxide	wt% min	99.9	99.0	...	...	...	...	...
Scandium	wt% min	...	...	99.85	99.74	99.65	99.998	99.996
Impurities:								
Aluminum	ppm max	30	100	100	100	100	9.00	0.7
Calcium	ppm max	100	500	300	200	200	0.08	3.0
Chromium	ppm	...	...	...	...	...	0.3	1.0
Cobalt	ppm max	...	...	...	...	...	0.10	1.0
Copper	ppm max	50	100	100	100	100	0.10	1.0
Iron	ppm max	50	500	300	600	1000	4.00	2.0
Magnesium	ppm max	30	100	100	200	200	0.01	2.0
Manganese	ppm max	30	100	...	...	...	0.20	1.0
Nickel	ppm max			...	...	...	0.01	1.00
Phosphorous	ppm max	100	200	...	...	...	...	...
Potassium	ppm max	...	...	...	...	...	0.05	0.5
Silicon	ppm max	100	500	200	500	600	0.1	3.0
Titanium	ppm max	50	500	100	200	200	0.4	1.00
Vanadium	ppm max	...	...	...	...	...	0.05	2.00
Ytterbium	ppm max	50	500	100	100	100	...	...
Yttrium	ppm max	50	500	100	100	100	...	...
Zirconium	ppm max	50	1000	100	100	100	...	...
Impurities total	wt% max	0.1	1.0	...	...	...	...	...

[a]CIS TU 48-4-335-86 Standard
[b]CIS TU 48-4-483-87 Standard
[c]D, calcium-thermic scandium produced by distillation refining technique at Giredmet' pilot plant, in Russia
[d]E, calcium-thermic scandium obtained by electrorefining in halogenide melts.

to add metals which alloy with the scandium and allow reduction to be carried out at a lower temperature. As calcium does not alloy with scandium, zinc is added and, in order to lower the melting point of the slag, lithium fluoride is introduced. In this case, the scheme of reduction process may be represented as follows:

$$2ScF_3 + 3Ca + 8Zn + 12LiF = 2(Sc \cdot 4Zn) + 3(CaF_2 \cdot 4LiF)$$

The process is carried out in argon at 1100°C. After reduction, zinc and calcium admixtures are sublimed from sponge scandium in a vacuum. The initial calcium-thermic scandium is refined to high purity by one of following methods:

- vacuum fusion; duration of processing is over 10 h; metal is manufactured in the form of ingot
- vacuum distillation at temperatures above 1539°C; high purity scandium in fine crystalline form results. Aluminum sublimes first of all, iron the last, which complicates the process during refining of a high purity residuum. Contamination of scandium occurs due to interaction with the material of the container
- zone melting; produces a monocrystalline ingot with perfect structure, but productivity is low as it is necessary to repeat the process 15–20 times
- electrorefining; the refinement coefficient amounts to 100–1000 times. This process is effective for purification from RE, aluminum, calcium, copper, iron, magnesium, silicon and radioactive elements.

The metallothermic scandium is a silvery-white powder with a golden tint. The minimum scandium contents for ScM-1, ScM-2 and ScM-3 grades are 99.85, 99.74 and 99.65%, respectively, according to CIS TU 48-4-483-87 standard (Table 22.24). The high purity calcium-thermic scandium is produced in Russia at Giredmet pilot plant using a highly productive distillation technique. The scandium purity reaches 99.998% and higher.

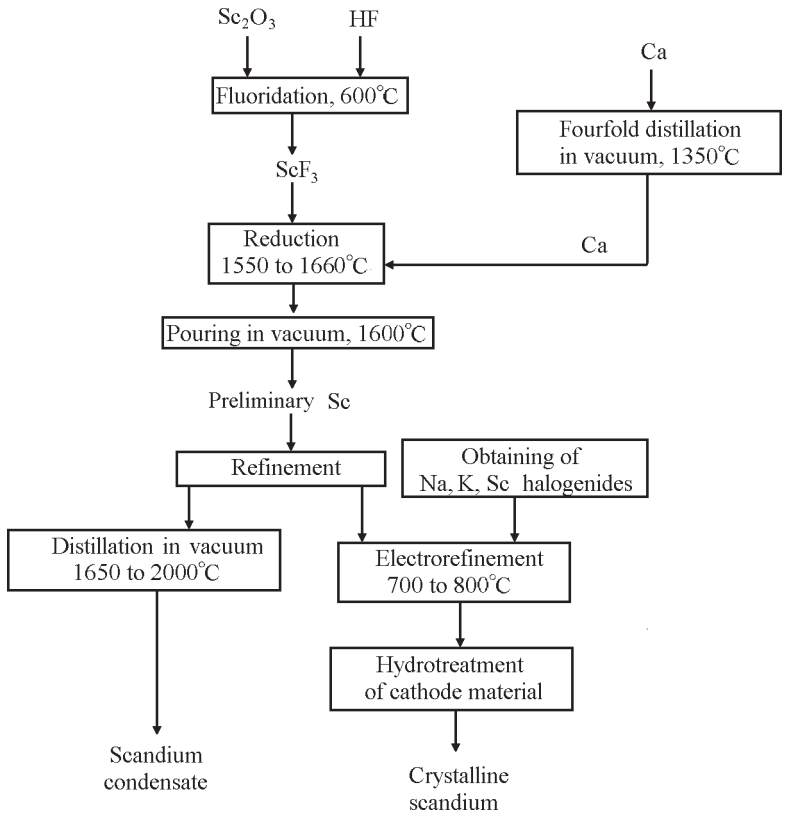

Figure 22.22 Technological line diagram of the production process for high-purity metallic scandium.

Applications

One of the major scandium application areas is the development of high strength light aluminum alloys. Scandium influences the alloy structure, promotes formation of a subgrain structure and prevents the recrystallization due to the following features:

- scandium interacts with aluminum under the eutectic type phase diagram with variable solubility. It is inclined to form supersaturated solid solutions in non-equilibrium conditions even at low solidification rate
- crystalline lattice of intermetallic Al_3Sc, formed by interaction of scandium with aluminum, almost coincides with structural lattice of aluminum under dimensionally structural parameters. This property is the basis of its strongest influence on the properties of alloys.

Due to these features, a small scandium addition (0.15–0.25 wt%) produces aluminum alloys and welds with non-dendritic structure and, as a result, improved performance.

Maximum scandium solubility in solid aluminum amounts to approximately 0.24 wt% [64], while even at solidification rates above 100°C per second, scandium levels up to 0.6 wt% are retained in Al solid solution [66]. According to [67], at 300°C per second, scandium levels up to 1 wt% are preserved in Al, Al–Mg, Al–Mg–Ag and Al–Zn–Mg alloys. In accordance with reference [66] at a cooling rate of 10^7 K/s, scandium concentration in solid solution can be retained at 5.0 wt%.

According to aluminum–scandium phase diagram (Figure 22.23), the eutectic reaction L ↔ α-Al + Al_3Sc is observed at Al–0.55 wt% Sc alloy [68]. In this case, after solidification and aging, the alloy contains α-Al and dispersed precipitate of Al_3Sc. With scandium concentrations above 0.55 wt%, primary precipitation of Al_3Sc occurs and this leads to a decrease of grain size in the solid. However, this concentration is decreased by the presence of other alloying elements (in particular titanium, zirconium and hafnium) [69].

Aluminium alloys alloyed with scandium are usually classified [64] into four groups:

- thermally non-strengthened weldable Al–Mg base alloys
- thermally strengthened high-strength weldable Al–Zn–Mg base alloys
- thermally strengthened ordinary and high-strength weldable Al–Li base alloys
- thermally strengthened high-strength Al–Zn–Mg–Cu base alloys.

Alloys based on the Al–Zn–Mg system have a favorable combination of mechanical properties and corrosion resistance and technological effectiveness (good weldability, plastic deformability and ability to self-quench). However, they yield to Al–Zn–Mg–Cu base alloys as regards tensile strength. Thus, the cast alloys 7178 (US specification) and its analogue B96 (Russian specification) have ultimate tensile strength (in T6 condition) at room temperature of 605 and 660 MPa, respectively, while the ultimate tensile strength of advanced ternary alloys, as the e.g. 7039 amounts only to 450 MPa [39].

Further increase of properties of Al–Zn–Mg alloys is impossible by traditional ingot technology, because increasing the main alloying element (Zn + Mg) content reduces corrosion resistance and the addition of refractory transition metals is usually limited by their low solubility in solid alloys at low cooling rates.

Powder metallurgy opens the possibilities for additional alloying of aluminum alloys by crystallization with high cooling rates.

Rapidly solidified Al–Zn–Mg alloys (with total Zn + Mg content of 8–10 wt%) have been produced by high pressure water atomization of the melt, providing cooling rates up to 10^6 K/s. Advanced technology of aluminum and aluminum alloy powders is described in Chapter 13. The alloys were doped with scandium, zirconium and other transition metals. After hot degassing in a vacuum of porous green powder briquettes, they are direct hot extruded to the rods and sheets. Under another consolidation scheme, the degasified porous green powder briquettes were hot pulse pressed in vacuum at a pressure 1 GPa. Then, these compacts are extruded as in the former scheme. Both scheme products are subsequently subjected to thermal treatment [70].

Typical water-atomized powder particles of ternary Al–Zn–Mg base alloy are shown in Figure 22.24, including their morphology (a) and surface microstructure of the individual particle (b). The size of individual particle grains ranges from 0.5 to 2.0 μm, with an average 1.0 μm (Figure. 22.24(b)), which corresponds to a cooling rate of the melt of 10^6 K/s [71]. The compositions of PM Al–Zn–Mg base alloys are given in Table 22.25. For comparison, similar cast alloys were also made in parallel. For the PM alloys, minus 100 μm powder was selected. Samples of PM and cast alloys were subjected to similar thermomechanical treatment.

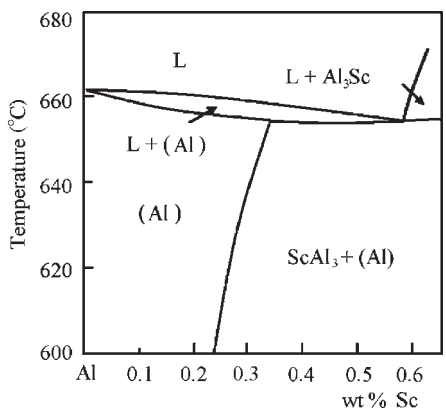

Figure 22.23 Al–Sc system phase diagram at the aluminum rich end.

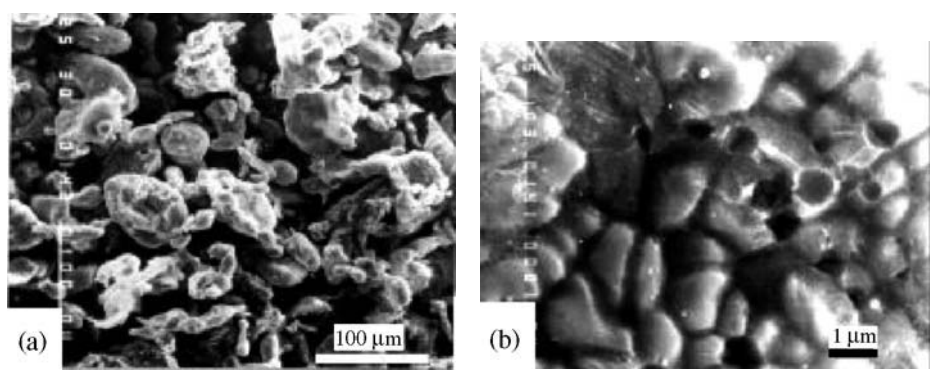

Figure 22.24 Typical scanning electron micrographs of the particles (a) and surface microstructure of a separate particle (b).

Very rapid solidification of the melt ensures that a fine, non-dendritic structure forms without participation of scandium in contrast to slow solidification processes, where scandium plays the main role in grain and non-dendritic structure formation. A dislocation cellular structure, with a cell size of about 1 μm, was evident in all PM alloy rods after T6 treatment (Figure 22.25). A polygonal cell structure was observed in all PM alloys. The dislocation density is increased in the cell walls. A disorientation of the cells is observed, which facilitates improvement of mechanical properties.

Two types of the secondary dispersoids in Al–Zn–Mg base extruded rods, $Al_3(Sc_{1-x}\ Zr_x)$ and $MgZn_2$, are seen in transmission electron microscopy images (Figure 22.26). Comparison of the contributions of both phases to alloy strengthening is possible, based on the present concept of precipitation strengthening in Al–Zn–Mg alloys [72,73]. Essentially, there are two different types of dislocation movement in particle strengthened crystals (Figure 22.27), the cutting in Guinier–Preston zones by small sized second phase particles and the Orowan mechanism by precipitated particle sizes increasing amounts to d_{cr}, where

Table 22.25 Typical tensile properties of Al–Zn–Mg extruded rods

Property	Unit	Alloy						
		3P[a]	3C	5P	5C	7P	23P	24P
Nominal chemical composition:								
Aluminum	wt%	balance	balance	balance	balance	balance	balance	balance
Zinc	wt%	5.0	5.0	5.0	5.0	5.8	5.5	5.5
Magnesium	wt%	3.0	3.0	3.0	3.0	4.0	3.0	3.0
Scandium	wt%	0.3	0.3	0.3	0.3	0.3	...	0.3
Zirconium	wt%	0.5	0.5	0.85	0.85	0.3	0.8	0.3
Cobalt	wt%	...	...	...	...	...	...	...
Copper	wt%	...	...	...	...	0.6	0.6	0.6
Chromium	wt%	...	...	0.22	0.22	...	0.3	...
Manganese	wt%	0.5	0.5	...	...	0.5	0.5	0.5
Nickel	wt%	...	...	0.17	0.17	...	0.15	...
Titanium	wt%	...	...	0.22	0.22	...	0.15	...
Tensile properties[b]:								
Hardness	MPa	1860	1710	1770	1400	1980	...	...
Ultimate tensile strength	MPa	651	590	618	427	719	655	700
Yield strength	MPa	596	531	553	356	652	614	656
Elongation	%	7.7	10.3	8.1	15.5	9.4	8.8	7.1

[a]The PM and cast alloys are denoted by the letters 'P' and 'C', respectively.
[b]Samples of PM and cast alloys were subjected to similar thermomechanical treatments. They were hot extruded in air at 400°C, with the rate of die travel in ranges 0.3 to 1.2 mm/s and extrusion ratio about 17 to 1 (ratio of sample initial cross section to final one); rods of 6 mm diameter are tensile tested in condition T6.

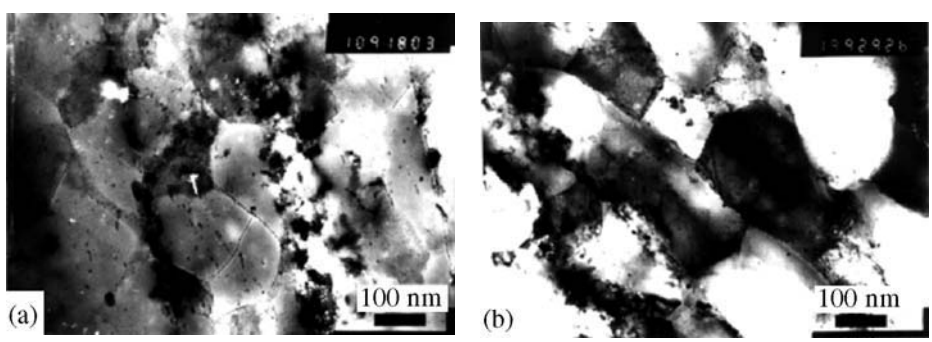

Figure 22.25 Transmission electron micrographs of PM rods in T6 condition in the longitudinal section: (a) Al–5Zn–3 Mg–0.7Zr–0.3Sc–0.5Mn alloy and (b) Al–5.5Zn–3 Mg–0.3Zr–0.3Sc–0.5 Mn–0.6Cu alloy.

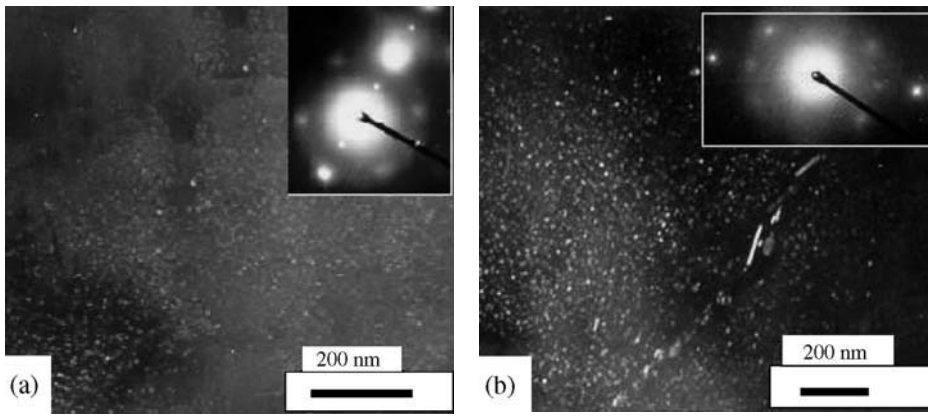

Figure 22.26 Secondary dispersoids in the PM rod longitudinal section of ternary Al–Zn–Mg base alloy doped with scandium and zirconium: (a) dark-field images in reflection (001) of the phase $Al_3(Sc_{1-x}\ Zr_x)$; (b) dark-field images in reflection (201) of the phase $MgZn_2$.

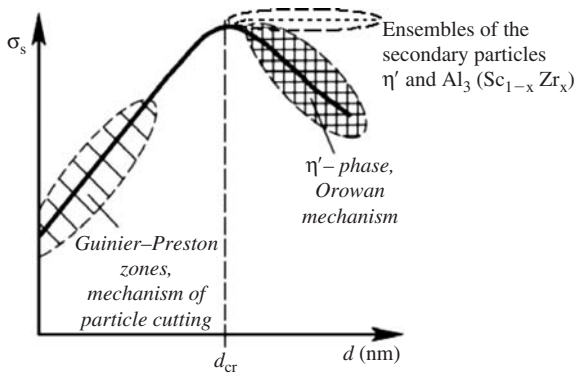

Figure 22.27 Scheme illustrating dependence of yield strength σ_s on the average size of second phase particles in Al–Zn–Mg alloys doped with scandium and zinc.

dislocations bypass the generally incoherent and unshearable particles to form a ring-shaped dislocation loop (Orowan loop). However, according to both theories, the strengthening by particles depends on their volume fractions.

Thus, the strengthening contribution of $Al_3(Sc_{1-x}\ Zr_x)$ is significantly smaller than that of $MgZn_2$, because of its appreciably reduced volume fraction and increased size, while an additional strengthening effect is connected with $Al_3(Sc_{1-x}\ Zr_x)$ or Al_3Zr. These particles precipitate within the grains from the supersaturated solid solution during heating prior to quenching. The particle dimensions do not exceed 4–5 nm and increase only on lattice defects. The main role of $Al_3(Sc_{1-x}\ Zr_x)$ and other intermetallics is in preventing recrystallization and the preservation of the cellular structure.

The maximum strength and the strong age-hardening of Al–Zn–Mg alloys are considered to be associated with precipitation of the metastable η′-phase. Its hexagonal structure, similar to the equilibrium η-phase, is plausible with the following precipitation sequence for alloys of relatively high Zn to Mg ratio: solid solution → GP zones → η′-phase → η-phase. The equilibrium phase η is the binary intermetallic of composition $MgZn_2$, η′ is the corresponding metastable phase.

As was found experimentally, a simultaneous increase of the strength and plasticity can be achieved for wrought semi-finished products alloyed with Sc in combination with other TM and RE metals after T6 treatment. A principal explanation of this effect was found [73,74] by analyzing the dependence of yield strength as a function of particle size (see Figure 22.27). Sc increases the size of η′-particles. In this case, the size of η′-particles, $2r$, can exceed the critical size d_{cr}, which leads to a transition from the mechanism of cutting the particles by dislocations to the mechanism of detour according to the Orowan model. Under such a transition, the plasticity of an alloy increases. At the same time, the strength can decrease. However, on alloying with Sc, a second ensemble of dispersed particles of $Al_3(Sc_{1-x}\ Zr_x)$, is formed that eliminates the loss of strength. Thus, the alloying with Sc can, in principle, lead to the simultaneous increase in strength and plasticity.

Ultimate tensile strength (UTS), yield stress (YS), elongation (EL) and Vickers hardness (HV) of PM and cast alloy rod specimens of Al–Zn–Mg alloys in T6 condition at room temperature are summarized in Table 22.25. Tensile strength comparison with cast alloys shows that PM alloys based on WA-N powder technology have considerably higher strength characteristics.

These products are characterized by excellent weldability. The welding seam has fine crystallized

Table 22.26 Typical properties of thorium and uranium

Property	Unit	Value	
		Thorium	Uranium
Density at 20°C	g/cm^3	11.72	19.10
Crystal type		fcc[a]	O[b]
Atomic diameter	nm	0.360	0.276
Hardness HB	MPa	530–700[c]	1500[d]
Modulus of elasticity at 25°C	GPa	70	190
Melting point	°C	1750	1132
Boiling point	°C	3850	3745
Specific heat	J/(kg · °C)	100	117
Heat of fusion	kJ/mol	19.2	15.5
Heat of vaporization	kJ/mol	544	423
Thermal conductivity	W/(m · °C)	37.7[e]	25.1[f]
Specific electrical resistance	μΩ · m	0.13 (20°C)	0.30 (20°C)
Section capture of heat neutrons, $n \times 10^{24}$	cm^2	7.31	7.68

Crystal type:
[a]fcc, face-centered cubic for α-thorium crystal modification at temperatures up to 1400°C;
[b]O, orthorhombic for α-uranium crystal modification at temperatures up to 662°C.
[c]depending on annealing conditions of wrought metal.
[d]after annealing of wrought metal at 770°C.
[e]at 110°C.
[f]at 20°C
Source: Refs 1, 4

equiaxial microstructure without columnar crystallites, while no recrystallization took place in a heat-affected zone. Tensile strength ratio of sheet to weld ranges from 0.85 to 0.89.

The features of scandium effect on ternary Al–Zn–Mg base alloys as discussed above are similar for thermally strengthened high-strength Al–Zn–Mg–Cu base alloys and also depend on the melt solidification rate.

Radioactive Metals: Thorium and Uranium

Physical and Chemical Properties

Thorium is soft silvery-white metal when freshly cut. Two crystalline forms exist: α-thorium with face-centered cubic lattice is stable up to 1400°C and above 1400°C β-thorium has body centered cubic lattice.

Uranium is a plastic gray steel-blue metal. Three uranium crystal modifications are known: α-uranium is in the orthorhombic system, which is stable up to 662°C, β-uranium with tetragonal lattice is stable in the range from 662 to 769°C, γ-uranium with face-centered cubic lattice is stable at temperatures above 769°C. Typical physical properties of thorium and uranium are given in Table 22.26.

In air at room temperature thorium as well as uranium are slowly oxidized, giving a black oxide film, which retards the corrosion but does not prevent it. Uranium at temperatures above 150°C and thorium above 400°C are rapidly oxidized.

In the thorium–oxygen system only one oxide, thorium dioxide (ThO_2) exists. Its melting point is 3200°C and it possesses a high chemical stability. In the uranium–oxygen system there are six known oxides, UO_2, U_2O_8 and UO_3 being the most important. Oxygen solubility in thorium and uranium is insignificant. Thorium and uranium actively react with hydrogen to form hydrides (ThH_2, $ThH_{3.75}$ and UH_3).

Both metals react with nitrogen at 600–800°C, forming nitrides. Uranium nitrides are not readily soluble in acids and are inactive to alkali solutions. Thorium nitrides are decomposed by water with the emission of ammonia. Uranium and thorium form carbides with carbon, which are decomposed by water producing hydrocarbons.

With fluorine, uranium and thorium react in the cold, while with other halogens on heating. The most important uranium fluoride is the hexafluoride, UF_6, which is used in the separation of the isotopes, while the tetrafluoride, UF_4, is the starting material for the production of uranium metal.

Both metals slowly corrode in water up to 100°C, while steam above 200°C strongly oxidizes uranium

and thorium forming UO_2 and ThO_2. At room temperature, thorium slowly dissolves in nitric, sulfuric and hydrofluoric acids, but is readily soluble in hydrochloric acid. Alkali solutions react slowly with thorium.

Hydrofluoric acid reacts slowly with uranium. At room temperature, the metal does not react with dilute sulfuric acid and, on heating, the corrosion rate is the same as in water. Hydrochloric acid rapidly dissolves uranium; in nitric acid the dissolution rate is moderate.

Thorium Powder Production

Commercially, thorium is produced by metallothermic reduction of its compounds (thorium dioxide and halogenide) or by electrolysis of melts. To produce particularly high purity thorium (predominantly for research purposes) thermo-dissociation of thorium iodide is used.

In view of the high melting point, thorium is produced in powder or sponge form, which is then transformed into compact metal by PM method or by melting.

Reduction of Thorium Dioxide by Calcium

High purity thorium dioxide is for the most part obtained by thermal decomposition of thorium oxalate at 600–650°C.

Calcium is used to reduce the oxide to metal:

$$ThO_2 + 2Ca = Th + 2CaO$$

$$\Delta H^0_{1,300K} = -60\,\text{kJ}; \quad \Delta G^0_{1,300K} = -24.7\,\text{kJ}$$

Reaction heat is insufficient for out-of-furnace processing. Reduction is conducted in a pure argon atmosphere in an apparatus of the form shown in Figure 22.28. The charge (a mixture of thorium dioxide with calcium chips) is fed into a steel crucible, lined with molybdenum sheet or calcium oxide.

The reduction is accomplished in an argon atmosphere at temperatures ranging from 1000 to 1100°C. After cooling, the reaction product is leached by water and dilute hydrochloric acid for the elimination of calcium and calcium oxide. For the separation of fine fractions, thorium powder is washed on a concentration table. For eliminating thorium dioxide films from the surface of particles, the powder is washed in turn by 15% nitric acid and water, and then dried under vacuum.

To produce coarse particles, calcium chloride is included in the charge. This chloride is molten at the reduction temperature and takes part of the calcium oxide into solution and this reduces the influence

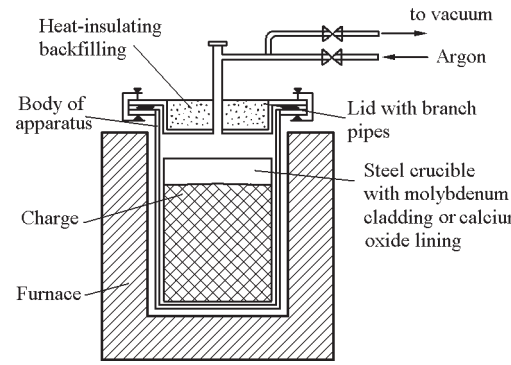

Figure 22.28 Scheme of apparatus for thorium dioxide reduction by calcium.

that the CaO has in retarding the growth of the thorium powder particles. For better use of crucible volume, the charge (ThO_2 + Ca + $CaCl_2$) is preliminarily briquetted. In this case, for complete reduction, a 25% calcium excess against its stochiometric content is enough. The yield of thorium recovery yield in powder amounts to 90%. Its purity ranges from 99.6 to 99.8%.

Electrolysis of Melts

Thorium is electro-refined from chloride–fluoride melts containing 30–45% $ThCl_4$ and eutectic KC1 + LiCl. The process is performed at 597–647°C, at current density 1.5 kA/m^2 and cell voltage 2.0 V. Thorium is oxidized stepwise to Th^{4+} on the anode and is reduced to metal on the cathode.

The electrolyzer is placed into a resistance furnace quartz vessel with an inside diameter of 67 mm and height of 432 mm, sealed with a rubber plug through which a molybdenum cathode, thorium anode and a tube for argon entrance are interposed. Electrolysis is complete in 6–8 hours; the cathode with powder precipitate is taken out, submerged in cold water and subsequently washed in water, 10% nitric acid, distilled water, acetone, ethyl alcohol and dried. The product is in the form of coarse dendrites. Their size decreases with increase of cathode current density.

Production of Thorium Compacts

Thorium powders possess high plasticity and allow high compacting pressure. The pressure levels for calcium thermic and electrolytic thorium powders range from 0.8 to 1.2 and 0.6 to 0.8 GPa, respectively.

Pressed billets are sintered in a vacuum 0.1–0.6 Pa at temperatures from 1100 to 1400°C for 30–60 minutes. Sintered billets have density

11.5–11.6 g/cm^3 (about 98.3% theoretical). Their Brinell hardness ranges from 520 to 700, while ultimate tensile strength ranges from 170 to 220 MPa.

It is also possible to produce dense material by melting. Thorium powders or sponge are melted in electric-arc furnaces or in vacuum induction furnaces. In the latter case, thorium is melted in beryllium oxide crucibles, which are heat-resistant to thorium up to 1800°C. The beryllium crucible is inserted into a graphite one, which is heated by induction. Melting is conducted under vacuum 0.133 Pa and lower.

Uranium Powder Production

Metallic uranium can be produced by the following methods:

- reduction of uranium oxides by calcium or calcium hydride
- reduction of uranium tetrafluoride or uranium tetrachloride by calcium or magnesium
- electrolysis of halogen salts in molten media.

As a result of uranium oxide reduction as well as electrolysis of melts, metallic uranium powders are obtained which are separated from the oxides and salts by treatment with water and acids. On the other hand, metallothermic reduction of halogen salts produces uranium in the form of ingots which readily separate from the slag. The advantage of this explains why this process is widely used.

Uranium tetrachloride in contrast to fluoride is very hygroscopic, which makes it difficult to work with. Additionally, the chloride boils at 800°C, which causes further difficulties. Therefore, production of uranium is based predominantly on reduction of uranium tetrafluoride.

Applications

A potential use of thorium is in nuclear power engineering. Under the action of thermal neutrons, natural thorium (isotope ^{232}Th) is converted to fissionable isotope ^{233}U. However, at present, consumption of thorium in this direction is restricted owing to sufficient resources of uranium.

Thorium and its compounds are used for alloying in alloys based on nickel, cobalt, magnesium and aluminum. Due to high electron emission capability of thorium, it is used to create tungsten based material with an oxide dispersed phase. This material is produced by means of PM. Tungsten metal powder and thorium-containing compounds (such as thorium dioxide or thorium nitrate) are mixed, pressed, sintered and further processed to wire or sheet. They have two major applications [75,76]:

- welding electrodes, whereby the high electron emission capability of thorium is used for easier electric arc formation and its stabilization
- improved physical properties (dispersion hardening) in tungsten wire and sheet, e.g. for vibration-resistant automotive lamps.

Commercially produced mechanically alloyed TD-Ni alloy is an elevated temperature nickel-base alloy, containing 2.0 wt% thorium oxide. Its ultimate tensile strength at 700°C amounts to 150 MPa (Source: Inco Alloys International [77]); thorium dioxide is used as the refractory material.

Metallic thorium, thorium dioxide, as well as other thorium compounds are used in catalyst compositions in organic synthesis in the chemical industry.

Uranium serves as basic nuclear fuel. Two isotopes ^{235}U and ^{233}U are able to maintain a chain reaction with slow neutrons. The former is contained in natural uranium, therefore, it is the primary nuclear fuel. The latter fissile isotope is obtained by radiation of thorium with thermal neutrons.

Safety Engineering

The IAAE international basic safety standards for protection from ionizing radiation and safety processing with radiation sources [78] serve as the basis for the corresponding Commonwealth of Independents States (CIS) standards [79–81] as well as for other countries.

The International Commission on Radiological Protection (ICRP) has published the limit values of ionizing radiations and recommendations on radiological protection [82–85]. Table 22.27 contains the volume radionuclide limits in workplace atmospheres and age-dependent doses for working with radioactive thorium and uranium in open conditions. In this Table, there are also cited data age-dependent doses to members of the public from intake through ingestion as well as inhalation.

Thorium is characterized by the following data of flammability and explosibility. It is a combustible metal. Thorium powder is pyrophorus. The self-ignition temperatures of aerogel and suspended solid in air are 280 and 270°C, respectively; the low concentration ignition limit of suspended solid in air is 75 g/m^3; explosion pressure is 630 kPa max; maximum rate of pressure rise is 84 MPa/s; explosion-proof oxygen content in inert gas is 4 vol% max; minimum

Table 22.27 Numerical magnitude limits of ionizing radiation for radioactive thorium and uranium

Radionuclide	Half-life (years)	ADD_A^{inhal} [a](Bq per year)	ADD_A^{ingest} [a](Bq)	ADD_B^{inhal} [b](Bq per year)	CL_C^{inhal} [b](Bq/m^3)	ADD_B^{inhal} [b](Bq per year)	CL_B^{ingest} [b](Bq/m^3)
^{232}Th	1.405×10^{10}	90	5×10^4 (Class W)	2	0.0004	200	700
^{234}U	2.445×10^5	600	3×10^6 (Class W)	5	0.003	3000	10000
^{235}U	703.8×10^6	600	3×10^6 (Class W)	6	0.003	3000	10000
^{238}U	4.468×10^9	600	3×10^6 (Class W)	6	0.003	3000	10000

ADD_A^{inhal} and ADD_A^{ingest} are the age-dependent inhalation and ingestion doses in workplace atmospheres, correspondingly, by working with radioactive thorium and uranium in open conditions. ADD_A^{inhal} and CL_C^{inhal} age-dependent doses and volume radionuclide limits to members of the public from intake through inhalation, correspondingly. ADD_B^{inhal} and CL_B^{ingest} age-dependent doses and volume radionuclide limits to members of the public from intake through ingestion, correspondingly. Bq = 1/s Curie, Ci = 3.7×10^{10} Bq. Source: Refs [a][85], [b][81]

suspended solid in air ignition energy is 5 mJ. The products with such characteristics of inflammability and explosion risk are placed in the 'High explosion hazard' class of danger according to the Guide to Legislation and 'Health and Safety' in the European PM Industry [19].

Methods used to extinguish thorium-fires include: high volume carbon dioxide (12 kg/m^3 for 2–5 minutes); special powder mixes based on potassium and sodium chlorides, and voluminal quenching by argon [20].

Uranium flammability and explosibility are characterized by the following data. Fine uranium powder is energetically oxidized and can easily ignite spontaneously. A powder with particle size below 74 μm exhibits: self-ignition temperatures of aerogel and suspended solid in air of 100 and 20°C, respectively; the low concentration ignition limit of suspended solid in air is 60 g/m^3; explosion pressure is 480 kPa max; maximum rate of pressure rise is 35 MPa/s; explosion-proof oxygen content in nitrogen is 1.5 vol% max, in helium 2.5 vol%, in argon 2.0% and in carbon dioxide 0 vol%; minimum suspended solid in air ignition energy is 45 mJ. The products with such characteristics of inflammability and explosion risk are placed in the 'High explosion hazard' class of danger [19]. Uranium spontaneous ignition is possible under water and even in a moist argon atmosphere. A mechanical loading increases the tendency of uranium to spontaneous ignition. Steam reacts with uranium at 150–250°C and interaction occurs more readily than with oxygen. At 750°C, uranium readily reacts with carbon dioxide. There are known cases of spontaneous ignition in carbon dioxide [1]. Uranium chips burn in nitrogen oxide at 400–500°C.

Extinguishing facilities of uranium are the same as for thorium and consist of the voluminal quenching method by argon (more efficient than carbon dioxide) and fire extinguishing powders which are represented by mixtures of potassium and sodium chlorides.

References

1. Zelikman, A.N., Korshunov, B.G., *Metallurgy of Rare Metals*. Metallurgiya Publisher, Moscow, 1991 (in Russian).
2. Eisen, W.B. PM tool and high speed steel – a comprehensive review. In *Proceedings of 5th International Conference on Advanced Particulate Materials and Processes*. Metal Powder Industries Federation, 1997, pp. 55–63.
3. Trefilov, V.I., Moiseev, V.F., *Fine Particles in Refractory Metals*. Naukova Dumka Publishers, Kiev, 1978 (in Russian).
4. German, R.M., *Sintering Theory and Practice*. John Wiley & Sons Publishers, 1996.
5. Vlasyuk, R.Z., Kurovskii, V.Ya., Lyapunov, A.P., Radomysel'skii, Interaction of titanium and vanadium with carbon dioxide on heating. *Sov. Powder Metall. Met. Ceram.*, 1986(1):64–68.
6. Wang, C.T., Baroch, E.F., Worcester, S.A., Shen, Y.S., Preparation and properties of high-purity vanadium and V–15 Cr–5 Ti. *Metall. Trans.*, 1970, 1(6):1683–1689.
7. Naboychenko, S.S. (ed.) *Handbook of Non-ferrous Metal Powders*. Metullurgiya, Moscow, 1997, pp. 281–304 (in Russian).
8. Radomyselsky, I.D., Solntsev, V.P., Evtushenko, S.V., The features of powder metallurgy of vanadium

and its alloys. *Sov. Powder Metall. and Met. Ceram.*, 1987, 5:367–372.
9. US Atomic Energy Commission, Carbon reduction process, Patent USA 3,463,634.
10. Itoh, Y., Harikou, T., Sato, K., Miura, H., Improvement of ductility for injection moulding Ti-6Al-4V alloy. In *Proceedings of 2004 Powder Metallurgy World Congress*, compiled by European Powder Metallurgy Association, Bellstone Shrewsbury, UK, 2004, Vol. 4, pp. 445–450.
11. Consemüller, K., Hribernik, B., Schneider, G., Tool steels present and future. In *Proceedings of 4th International Conference on Tooling*. Ruhr University–Bochum, 1996, pp. 3–16.
12. Dixon, R.B., Stasko, W., Pinnow, K.E., Particle metallurgy tool steels. In *ASM Handbook*, Vol. 7. ASM International Publishers, New York, 1998, pp. 786–802.
13. Haswell, W.T., Stasko, W., Dax, F.R., Cobalt-free CPM high speed steels. In *Proceedings: Processing and Properties of High Speed Tool Steels*. TMS/AIME, 1980, pp. 147–158.
14. Riedl, R. et al., Developments in high speed tool steels. *Steel Res.*, 1987, 58(8):339–352.
15. Westin, L., Wisell, H., Powder metallurgy high speed steels. *Scand. J. Metall.*, 1996, 25(1):41–46.
16. Zinyana, J. et al., Effect of composition on the (V,W)C in V-W-C-Co alloys. In *Proceedings of 15th Int. Plansee Seminar.* Plansee Holding AG, Vol. 4, 2001, pp. 291–299.
17. Commonwealth of Independents States Standard GOST 12.1.005−88, Publishers of Standards, Moscow 1988 (in Russian).
18. Sanitary Regulation and Standards of surface waters from pollution. SanPiP 4630–88. MinZdrav, Moscow, 1988 (in Russian).
19. Guide to Legislation and 'Health and Safety' in the European PM Industry. EPMA, 1997.
20. Fire- and explosion-proof of matters and materials and means for their quenching. *Handbook*, ed. A.N. Baratov, A.J. Korolychenko. Chimia, Moscow, 1990 (in Russian).
21. A.G. Merzhanov, V.M. Shkiro, I.P. Borovinskaya, Soviet Union Certif [Patent], 255221, 1971.
22. Merzhanov, A.G., Borovinskaya, I.P., Self-propagating high-temperature synthesis of refractory inorganic compounds. *Dokl. Akadem Nauk USSR*, 1972, 204(2):366–369 (in Russian).
23. Muchnik, S.V., Lomnitskaya, Y.F., Chernogorenko, V.B., Lynchak, K.A., Interaction under combustion in powder mixtures of copper-zirconium-phosphorus. Sov. *Powder Metall. Met. Ceram.*, 1993, (11–12):670–865.
24. Borovinskaya, I.P., Loryan, V.E., Self-propagating synthesis of solid solution in zirconium-nitrogen system. *Dokl. Akadem. Nauk USSR*, 1976, 231(4):911–914 (in Russian).
25. Borovinskaya, I.P., Loryan, V.E., Self-propagating high-temperature synthesis of titanium nitrides under high pressure of nitrogen. *Sov. Powder Metall. Met. Ceram.*, 1978 (11–12):655–851.
26. Dankley, J.J., Hot gas atomisation – economic and engineering aspects. In *Proceedings of 2004 Powder Metallurgy World Congress,* compiled by European Powder Metallurgy Association, Bellstone Shrewsbury, UK, 2004, Vol. 1, pp. 13–18.
27. Abd El-Halim, A.M., Khalil, K.M., Electrolytic production of thallium powder in sulphate bath. *Surface Texhnol*, 1984, 23(4):215–223.
28. *Encyclopedia of Inorganic Materials*, ed. Fedorchenko, I.M. Glavnaja Redakcija Ukrainskoy Sovetskoy Encycpopedii, Kiev, 1977 (in Russian).
29. Bonjour, Chr., Actis-Data, A., Effects of ruthenium additions on the properties of WC-Co ultra micrograins. In *Proceedings of 2004 Powder Metallurgy World Congress*, compiled by European Powder Metallurgy Association, Bellstone Shrewsbury, UK, 2004, Vol. 3, pp. 515–521.
30. Bonjour, Chr., Effects of ruthenium additions on the properties and machining behaviour of WC-Co hard metals. In *Proceedings of 2004 Powder Metallurgy World Congress*, compiled by European Powder Metallurgy Association, Bellstone Shrewsbury, UK, 2004, Vol. 3, pp. 528–534.
31. Conway, J.B., Flagella, P.N., *Creep-rupture Data for the Refractory Metals to High Temperatures*. Gordon & Breach Science Publishers, New York, 1971.
32. Mueller, A.J., Shields, J.A., Buckman, R.W., The effect of thermo-mechanical processing on the mechanical properties of molybdenum–2 vol% lanthana. In *Proceedings of 15th International Plansee Seminar*. Plansee Holding AG, Vol. 1, 2001, pp. 485–497.
33. Bianco, R., Buckman, R.W., Geller, C.B., High strength, creep-resistant molybdenum alloy and process for producing the same. US Patent 5,868,876 (1999).
34. Bianco, R., Buckman, R.W., Mechanical properties of oxide dispersion strengthened (ODS) molybdenum. In *Proceedings 'Molybdenum and Molybdenum Alloys*'. The Minerals, Metals & Materials Society, 1998, pp. 125–142.
35. Povarova, K.B., Makarov, P.V., Luk'yanchikova, S. S., Zavarina, E.K., Effect of high-energy ball milling on structure and some properties of powder tungsten alloys. *Izvestiya Rossiiskoi Akademii Nauk, Metally*, 1994, (6):113–123.
36. Itoh, Y., Ishivata, Y., Strength properties of yttrium-oxide-dispersed tungsten alloys. *JSME Int. J., Series A*, 39(3):429–434.

37. Taillard, R.A., Avettand-Fènoel, M.N., Dhers, J., Foct, J., Ball-milling and sintering of blends of tungsten and yttrium-rich powders. In *Proceedings of 2002 Powder Metallurgy World Congress*, Princeton, MPIF Publishers, New Jersey, 2002, pp. 6-188–6-202.
38. Zhang, H., Liu, X., Ning, A., Microstructures and properties of rare earth-particles reinforced $MoSi_2$ composites. In *Proceedings of 15th International Plansee Seminar*. Plansee Holding AG, Vol. 1, 2001, pp. 339–352.
39. Aluminum and aluminum alloys, *ASM Speciality Handbook*. ASM International Publishers, 1990.
40. Anderson, I.E., Foley, J.C., Flumerfelt, J.F., Simplified aluminum powder metal processing routes for automotive applications. In *Proceedings of First International Conference on Powder Metallurgy Aluminum & Light Alloys for Automotive Applications*. MPIF, Princeton, NJ, 1998, pp. 75–82.
41. Foley, J.C., Hunt, W.H., Barnard, D.J., Laabs, F.C., Simple powder metallurgy processing of Al-8Fe-4Ce alloys. In *Proceedings of 2002 Powder Metallurgy World Congress*, Princeton, MPIF Publishers, New Jersey, 2002, pp. 1-103–6-114.
42. Kim, Y-W., Processing, microstructure, properties of Al-Fe-Ce alloys. In *Proceedings 'Dispersion strengthened aluminum alloys'*. TMS, Warrendale, PA, 1988, pp. 157–180.
43. Lee, D.Y., Zupon, D.Y., High temperature performance of dispersion strengthened PM aluminum alloys. In *Proceedings 'Dispersion strengthened aluminum alloys'*. TMS, Warrendale, PA, 1988, pp. 265–281.
44. Nie, Z., Chen, Y., Zhou, M., Zuo T., Research and development of tungsten electrodes added with rare earth oxides. In *Proceedings of 15th International Plansee Seminar*. Plansee Holding AG, Vol. 1, 2001, pp. 568–574.
45. Wang, J., Zhou, M., Zuo T., Zhang, J., Nie, Z., Carbonization kinetics of La_2O_3–Mo cathode materials. In *Proceedings of 15th International Plansee Seminar*. Plansee Holding AG, Vol. 1, 2001, pp. 684–694.
46. Sreenivasa Rao, G., Dhamadhikari, C.V., Nigavekar, A.S., Effect of carburization on diffusion and desorption properties of La–Mo system. *J. Vac. Sci. Technol.*, A, 1989, 7(6):3269–3272.
47. Sreenivasa Rao, G., Dhamadhikari, C.V., Nigavekar, A.S., Some aspect of adsorption, diffusion, and thermal desorption properties of a La–Mo system. *J. Vac. Sci. Technol.*, A, 1989, 6(5):3005–3012.
48. Leonowicz, M., Derewnicka, D., Krzton, H., Panchanathan, V., Structural anisotropy in Nd-Fe-B magnets processed by hot working of melt-spun ribbon powder. In *Proceedings of 2002 Powder Metallurgy World Congress*, Princeton, MPIF Publishers, New Jersey, 2002, pp. 14-1–14-10.
49. Lukin, A., Matveyenkov, A., Influence of heat treatment parameters on properties of Nd-Dy-Fe-Co-Nb-Al-Cu-B sintered magnets. In *Proceedings of 2004 Powder Metallurgy World Congress*, compiled by European Powder Metallurgy Association, Bellstone Shrewsbury, UK, 2004, Vol. 4, pp. 511–534.
50. Vystavkina, V., Brecharya, G., Vasilyeva, E., Microstructure and properties of Nd-Fe-B magnets, produced from gas-atomized powders. In *Proceedings of 2004 Powder Metallurgy World Congress*, compiled by European Powder Metallurgy Association, Bellstone Shrewsbury, UK, 2004, Vol. 4, pp. 539–544.
51. Ślusarek, B., Paszkowski, L., Biało, D., The influence of kind of powder on physical properties of Nd-Fe-B dielectromagnets. Microstructure and properties of Nd-Fe-B dielectromagnets. In *Proceedings of 2004 Powder Metallurgy World Congress*, compiled by European Powder Metallurgy Association, Bellstone Shrewsbury, UK, 2004, Vol. 4, pp. 555–560.
52. Schultz, L., Gutfleisch, A., Kirchner, A. et al., Keynote: high performance nanocrystalline functional materials. In *Proceedings of 2004 Powder Metallurgy World Congress*, compiled by European Powder Metallurgy Association, Bellstone Shrewsbury, UK, 2004, Vol. 4, pp. 569–575.
53. Ormerod, J., Constantinides, S., *PM Magnetic materials and applications, short course*, 22–23 June 1993. Metal Powder Industries Federation Publishers, 1993.
54. Ji, Ch., Jiangao, Y., Xinghua, G., Application of rare earth elements in cemented carbide inserts, drawing dies and mining tools. *Mater. Sci. Eng.*, A, 1996, 209:287–293.
55. Chonghai, Xu., Xing, Y., Chuanzhen, H., Research and development of rare-earth cemented carbides. *Int. J. Refract. Met. Hard Mater.*, 2001, 19(3):159–168.
56. Zhang, L., Schubert, W-D., Huang, B., Chen, S., Zhang, Ch., Cerium enrichment phenomena on the sinter skin of cemented carbide. In *Proceedings of 2004 Powder Metallurgy World Congress*, compiled by European Powder Metallurgy Association, Bellstone Shrewsbury, UK, 2004, Vol. 3, pp. 443–449.
57. Zhang, L., Schubert, W-D., Huang, B. et al., Surface observation of rare earth doped cemented carbide. *PM Science & Technology Briefs*, 2003, 5(3):17–23.
58. Marder, J.M., Wellman, B., Powder metallurgy beryllium. In *ASM Handbook*, Vol 7. ASM International Publishers, 1998, pp. 941–946.

59. Courtney, T.H., Modeling of mechanical milling and mechanical alloying. *Reviews in Particulate Materials 2*. Metal Powder Industries Federation Publishers, 1994.
60. Marder, J.M., Wellman, B., Production of beryllium powders. In *ASM Handbook*, Vol. 7. ASM International Publishers, 1998, pp. 202–205.
61. Hashiguchi, D., Marder, J.M. Structure and properties of beryllium powder. In *Proceedings 'Modern Development in Powder Metallurgy'*, Vol. 20, Metal Powder Industrial Federation, 1998, pp. 109–119.
62. Floyd, D.R., Lowe, J.N., *Beryllium Science and Technology*. Plenum Press Publishers, 1979.
63. Lewis, R.E., Yaney, D.L., Tanner, L.E., The effect of lithium in Al-Be alloys. *Proceedings 'Aluminum-Lithium Alloys V'*. ASM International Publishers, 1990, pp. 731–740.
64. Alexandsandrovsky, S.V., Siziakov, V.M., Kucenko, D.V., Ratner, A.H., *Metallothermic Obtaining Methods of Heightened Purity Scandium and its Alloys*. Ore and Metals Publishers, Moscow, 2004 (in Russian).
65. Korshunov, B.G., Reznik, A.M., Semenov, S.A., *Scandium*. Metallurgija Publishers, Moscow, 1987 (in Russian).
66. Driz, M.E., Kadaner, E.S., Dobatkina, T.V., Turkina, N.I., Interaction of scandium with aluminium on the aluminium rich part of Al–Sc system. *Izv. AN USSR, Metals*, 1973 (4):213–217.
67. Parker, B.A., Zhou, Z.F., Nolle, P., The effect of small additions of scandium on the properties of aluminium alloys. *J. Mater. Sci.*, 1995, 30:452–458.
68. Driz, M.E., Toropova, L.S., Bykov, Yu.G. et al., Al–Sc metastable phase diagram of the aluminium-rich part. *Izv. AN USSR, Metals*, 1983 (1):179–182 (in Russian).
69. Hyde, A.F., Norman, A.F., Prangnell, P.B., The effect of cooling rate on the morphology of primary AI_3Sc intermetallic particles in Al–Sc alloy. *Acta Mater.*, 2001, 49:1327–1337.
70. Neikov, O.D. et al., Properties of rapidly solidified powder alloys of the Al–Zn–Mg system. Vols. 396–402. In *Materials Science Forum*. Trans. Tech. Publications, Switzerland, 2002, pp. 1223–1228.
71. Eskin, G.I., Non-Dendritic crystallization of light alloys. *Technology of Light Alloys*, 2000, (2):17–25 (in Russian).
72. Lendvai, J., Precipitation and strengthening in aluminium alloys. In *Materials Science Forum* Vols. 217–222. Trans. Tech. Publications, Switzerland, 1996, pp. 43–56.
73. Milman, Yu.V. Influence of scandium on structure, mechanical properties, and corrosion resistance of aluminium alloys, In *Proceedings 'Advance Materials and Technologies'*, National Academy of Sciences of Ukraine, 2003, pp. 335–360.
74. Milman, Yu.V., Sirko, A.I., Lotsko, D.V., Senkov, O. N., Miracle, D.B., Microstructure and mechanical properties of cast and wrought Al-Zn–Mg–Cu alloys modified with Zr and Sc. In *Materials Science Forum* Vols. 396–402. Trans. Tech. Publications, Switzerland, 2002, pp. 1217–1222.
75. Yih, S.W.H., Wang, C.T., *Tungsten Sources, Metallurgy, Properties, and Applications*. Plenum Press Publishers, 1979.
76. Lassner, E., Schubert, W.D., Lüderitz, E., Wolf, H. U., Tungsten, tungsten alloys, and tungsten compounds. In Ulmann's Encyclopedia of Industrial Chemistry, Vol. A27. VCH Verlagsgesellshaft GmbH, 1992.
77. Suryanarayana, C., Mechanical alloying. In ASM Handbook, Vol. 7. ASM International Publishers, 1998, pp. 80–90.
78. International basic safety standards for protection from ionizing radiations and safety handling with radiation sources, Series 115. ICAAE, Vienna, 1997.
79. Radiation safety standards (NRB–99), SP 2.6.1.758–99. Energoatomizdat, Moscow, 1999 (in Russian).
80. Basic sanitary standards of working of radiation safety. (OSPORB–99) SP 2.6.1799–99. Energoatomizdat, Moscow, 1988 (in Russian).
81. Radiation safety standards of Ukraine (NRBU–97), Kiev, 2001 (in Ukrainian).
82. ICRP, Publication 69. *Age-Dependent Doses to Members of the Public from Intake of Radionuclides*: Part 3, *Ingestion Dose Coefficients*. Oxford Pergamon Press, 1995.
83. ICRP, Publication 71. *Age-Dependent Doses to Members of the Public from Intake of Radionuclides*: Part 4, *Inhalation Dose Coefficients*. Oxford Pergamon Press, 1995.
84. ICRP, Publication 60. Radiation protection 1990: *Recommendations of the International Commission on Radiological Protection* (ICRP). Pergamon Press, 1991.
85. ICRP, Publication 61. *Annual Limits on Intake of Radionuclides by Workers Based on the 1990 Recommendations*, Pergamon Press, 1991.

Chapter 23

Production of Powders of Lead, Tin, Bismuth and their Alloys

Stanislav S. Naboychenko, Ural State Technical University (UPI), Yekaterinburg, Russia
Irina B. Murashova, Ural State Technical University (UPI), Yekaterinburg, Russia
Oleg D. Neikov, Frantsevich Institute for Problems of Materials Science (IPMS), Kiev, Ukraine

Lead, tin and bismuth are distinguished by low melting points. Their typical physical properties are given in Table 23.1.

Because of the low melting point, the atomization process is simplified: as there are fewer problems with the selection of refractory material for the manufacture of melting furnaces, fused metal tubes and atomizers, hot gas atomization can be employed. The latter increases the stability of the atomizer operation (melt drops welding on the atomizer is prevented) and results in yields of finer powder [3–5].

Atomization

Currently, most lead, tin and bismuth powders are produced by atomization because it presents a

Table 23.1 Typical properties of lead, tin and bismuth

Property	Unit	Value		
		Lead	Tin	Bismuth
Physical properties				
Density[a]	g/cm^3	11.10	7.30	9.8
Crystal type[b]		fcc	Tetra.	R
Atomic diameter	nm	0.350	0.316	0.326
Melting point	°C	328	232	271.2
Boiling point	°C	1740	2270	1560
Specific heat	kJ/(kg · °C)	130	226	120
Heat of fusion	kJ/mol	5.0	7.2	11.3
Heat of vaporization	kJ/mol	178	290	151
Solid–vapor surface energy	J/m^2	0.61	0.68	...
Elastic modulus at 25°C	GPa	16	55	32
Linear coefficient of thermal expansion from 25 to 100°C	μm/(m·°C)	27.56	22.4	13.3
Thermal conductivity at 25°C	W/(m·°C)	35.3	66.6	7.8
Electrical resistivity	μΩ · m	0.207	0.115	1.07
Mechanical properties:				
Ultimate tensile strength:	MPa	12–13	10–50	5–20
Hardness HB	MPa	30–40	50	93
Elongation	%	55	40	...

[a] At room temperature
[b] Crystal type: fcc, face-centered cubic (polymorphic at temperatures below 13.2°C); Tetra, tetragonal; R, rhombohedral.
Source: Refs 1, 2

convenient and cost-effective means of production of large batches of powder.

The molten metal can be atomized vertically (up or down stream) or horizontally, depending on the nozzle direction. Generally, there are two atomization techniques: annular nozzle and cross-jet atomization. In an annular nozzle, the gas stream aspirates liquid metal into the nozzle where it is disintegrated into tiny droplets by the high velocity gas stream. In cross-jet atomization, the gas is at right angles to the melt stream. This method usually produces coarser particles than annular nozzles.

Lead Powder Production

A typical lead powder production process based on hot gas atomization is described in [3]. The bars of lead brands (C0 and C1 brands in Russian Standard GOST 16138) serve as raw material. Superheating of the molten lead above 547°C noticeably decreases the surface energy and viscosity and that results in finer powder; however, the sublimation with the production of toxic lead vapor limits the superheat up to 447°C.

Lead bars are melted in a crucible; the melt is superheated and poured into a tundish, where a constant melt level is maintained. From the tundish, through a calibrated bottom orifice of 4–5 mm diameter, metal flows into the atomizer action zone where it is atomized by an annular jet of air heated to between 197 and 247°C at a pressure between 0.6 and 0.8 MPa. To prevent the drops sticking to the chamber walls, the vertical metal gas stream is deflected in a horizontal direction by auxiliary airflow. Air consumption for atomization ranges from 1.8 to 2.2 m^3 air per 1 kg melt. Powder from the chamber is transferred to sieving and the used air is subjected to dedusting in a cyclone and a bag filter.

Table 23.2 gives the chemical and sieve analysis data for several commercially available lead powders produced by atomization. Air-atomized lead particles are roundish in shape. Figure 23.1(a) illustrates typical particle shapes and surface topography.

Methods of lead powder production by electrolysis are of secondary importance. Electrolysis process parameters are given in Table 23.3.

Ultrafine lead powders, usable in lubricant compositions for formation of a protective layer against radiation, are produced by thermolysis: alkylamide of oleic acid is mixed with lead formate in proportions ensuring 20% lead content in the mixture, which is then processed at 237°C for 1 h. As a result, powder with roundish particles and sizes ranging from 0.2 to 0.8 μm is produced.

Table 23.2 Properties of commercially available lead powders produced by atomization

Property	Unit	Standard grades		
		ПСА[a]	63[b]	CSC[c]
Nominal composition				
Lead	wt%	99.7 min	99.7 min	99.6 min
Trace elements:				
Antimony	ppm	5 max	...	...
Arsenic	ppm	5 max	...	...
Bismuth	ppm	50 max	...	...
Copper	ppm	10 max	...	...
Iron	ppm	20 max	...	...
Oxygen	wt%	0.3 max	...	...
Total impurities	wt%	0.3 max	...	...
Calcined residue after treatment by nitric acid	wt%	0.01 max	...	...
Sieve analysis:				
−106 + 80 μm	wt%	...	...	5 max
−80 + 75 μm	wt%	1.0 max	nil	
−75 + 63 μm	wt%	1.5 max	0.2 max	15 max
−63 + 45 μm	wt%	...	10 max	
−45 μm	wt%	75–90	...	85 min
Apparent density	g/cm^3	5–6	4.5±0.5	4.5–6.0

[a] The requirements of Russian Federation Standard GOST 16138.
[b] Pometon S.p.A. standard grade.
[c] Chang Sung Corporation.

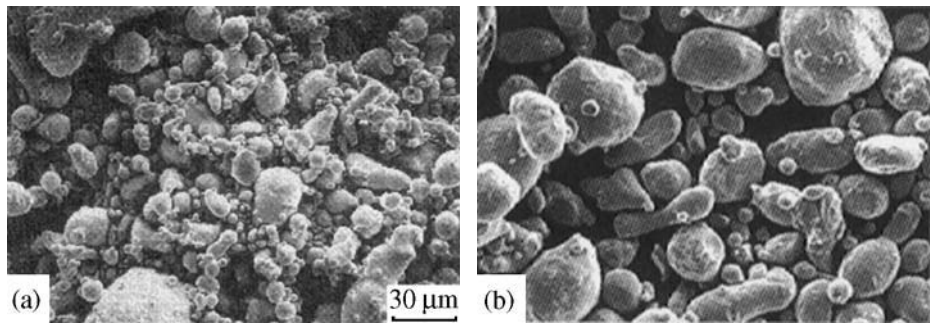

Figure 23.1 Scanning electron micrographs of atomized (a) tin and (b) lead powders.

Table 23.3 Production of electrolytic powders of bismuth, tin, lead, antimony and their alloys

Method	Electrolyte composition	Current density (kA/m^2)	Temperature (°C)	Electrolysis conditions and ready powder properties
Bismuth [6]				
EDC	59.5 g/L Bi, 100 g/L NH_4Cl; 65.0 g/L glycerin; (pH from 0.2 to 2); 0.2% oleic acid	3.0	5	Cathode rotation 70 rpm; upper layer is mixture of cyclohexane and toluene; particle sizes: 0.05–0.1 μm
EDC	59.5 g/L Bi; 20.0 g/L HCl; 150 g/L NH_4Cl; oleic acid 0.5% in toluene	3.0–4.0	15–25	Cathode rotation 60 rpm; ready particulate product is aggregates of small particles
Tin				
EDC [7]	31.3–62.6 g/L *Sn* 0.5% Oleic acid	0.5–8.0	5–60	Top layer solvent is toluene; powder particle sizes: 0.2–0.5 μm
CED	12–119 g/L Sn	...	20–60	Substituting metal: Zn; solution: $SnCl_4$; drum rotation 12 rpm; particle sizes <300 μm; apparent density 1.51 g/cm^3
CED	12–119 g/L Sn	...	27	Substituting metal: Zn; solution: $SnCl_2$; rate of solution depletion 39.7 g/(L·h); average size of particles 222 μm; apparent density 0.67 g/cm^3
CED	12–119 g/L Sn	...	27	Substituting metal: Al; solution $SnCl_2$; rate of solution depletion 53 g/(L·h); average size of particles 249 μm; apparent density 0.56 g/cm^3
CED	Sn saturation	-	27	Substituting metal: Zn; solution $SnSO_4$; rate of solution depletion 10.7 g/(L·h); average size of particles 154 μm; apparent density 1.08 g/cm^3
Lead				
WS	20–30 g/L Pb; NaOH 100–160 Pb; NaCl; 26.7–40 Pb; KCl up to 50.0 Pb	0.2–1.5	20	Solution on the basis of PbCl2; lead anodes; current efficiency: approx. 100%
WS	7.5 g/L Pb; 200 g/L NaCl; 130 g/L NaOH	0.4–1.5	20	Current efficiency: 70–82%; precipitate deposition time is 5 min
WS	40 g/L Pb; 300 g/L NaCl	0.5–2.0	45	Current efficiency: 80.6–89.1%; voltage on the cell: 3–4.7 V

(*Continued*)

Table 23.3 (Continued)

Method	Electrolyte composition	Current density (kA/m^2)	Temperature (°C)	Electrolysis conditions and ready powder properties
WS	40 g/L Pb; 300 g/L NaCl	0.5–2.0	45	Current efficiency: 80.6–89.1%; voltage on the cell: 3–4.7 V
WS	28 g/L Pb; 100 g/L NaOH; 29 g/L Na_2CO_3	3.0–4.0	18–23	Precipitate deposition time: 40–60 min
M	0.2–0.9 g/L Pb; NaOH	5.0–12.0	350–370	Lead in the melt is in form of Na_2PbO_2; nickel anodes
Lead–tin				
M	10 g/L Pb; 59.6 g/L $SnCl_2$; 26.4 g/L KCl	5.0–6.0	237–277	Lead is contained in the melt as $PbCl_2$; current efficiency: 75%; 93–95% Pb content in ready product; average size of particles 100 μm
Lead–bismuth [8]				
EDC	35 g/L (Pb + Bi); 50 g/L NH_4NO_3; 30 ml/L HNO_3	2.0	20	Top layer: 0.03% oleic acid solution in toluene; ratio Pb to Bi is 10 to 1 in ready powder; current efficiency: 45–50%; particle sizes: 0.1–5 μm
Bismuth–tin [9]				
EDC	(30–60) g/L (Bi + Sn); 50 g/L $(NH_4)NO_3$; 30 ml/L HNO_3 conc.	2.0	20	Alloys contains 70–90% Bi; particle sizes: 0.1–5 μm
EDC	33.2 g/L Bi; 31.4 g/L Sn; 100 g/L NH_4Cl; 30 g/L HCl	1.5	25	Cathode rotation −60 rpm; upper layer: toluene with 0.5% oleic acid; current efficiency: 50%; alloy consists about 80% Bi; salts: chlorides
Tin–antimony				
EDC	(63–200 g/L (Sn + Sb) (80–100) g/L NH_4F pH = 3.54	0.2–0.6	25	Ratio $SnCl_2$ to $SbCl_3$ is 1.0 to 1.0; alloys: mixture of tin and intermetallides; current efficiency: 60–85%; particle sizes: 0.1–2 μm

Technique: WS, water solution electrolysis; EDC, electrolysis from double-layer cell (see section 'Reduction from solution through film of surfactants' in Chapter 9); CED, contact electrolytic displacement (see section 'Contact displacement method (Cementation)' in Chapter 9); M, electrolysis from the melt [composition -% (by mass)]

Tin Powder Production

For tin powder production, the horizontally cross-jet air atomization technique is often used [10]. Pressures commonly employed range from 345 to 1725 kPa. Compressed air is preheated in a gas-fired heat exchanger to prevent freezing of tin within or around the nozzle orifice arising from the chilling effect of the expanding air as it is streaming through the nozzle. The air stream with atomized particles enters the horizontal atomization chamber from where it is sucked by fan into a cyclone where the powder is collected. The finest particles, which have not separated in the cyclone, are then retained on a filter.

The vertical melt atomization technique also finds application for tin powder production. One such unit is shown in Figure 23.2 [11]. It consists of a reservoir to which molten metal is fed by gravity. From the reservoir, the metal flows into the tundish; the flow being controlled by an electromagnetic arrangement device so as to maintain a constant level in the tundish and, therefore, a constant flow rate to the atomizer. The reservoir, tundish, batcher, atomizer and the fused metal tubes connecting them are provided with electric heaters. The atomizer is mounted on the lid of the cylindrical atomization chamber into which a jet of melt is atomized by an annular air jet, forming a metal–air stream. Cold air is fed into that

stream by directed jets formed by a manifold with apertures placed under the chamber lid.

The additional cooling by means of air jets increases the turbulence of the metal–air stream, raises the cooling rate of the particles and decreases the adhesion of powder on the chamber walls. Atomized powder accumulates in the container at the bottom of the atomization chamber. The finest particles, which have not separated in the chamber, are then retained on a filter.

The closed nozzle design [12] has been used (Figure 23.3). The atomizer was equipped with changeable parts, nozzles and sleeve, to ensure various operating modes. The nozzles differ by arrangement of the discharges and their diameters: one central discharge for melt outflow (a) and three radial discharges with axes perpendicular to the outside wall (b) of the nozzle. Table 23.4 contains the technological parameters of tin powder production by means of a vertical melt atomization.

Physical properties of tin powder depend on atomization conditions and sieving procedures. Coarse grades are atomized by larger metal streams using lower air pressures. The finer grades of powder require higher pressures and a small molten metal stream. Sieving is an independent means of controlling the size of the largest particles in the powder.

Table 23.5 gives properties of commercially produced tin powders. Impurities in the tin melt stock carry over to the powder. The tin powder purity is directly related to the purity of the ingot melted.

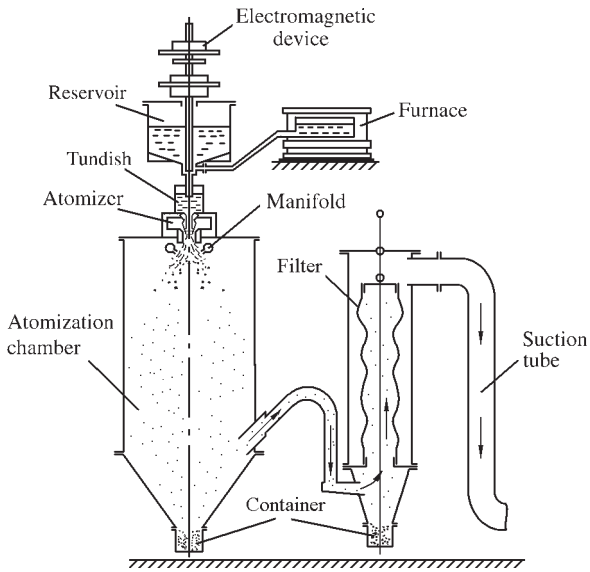

Figure 23.2 Vertical melt atomization technique of tin powder production.

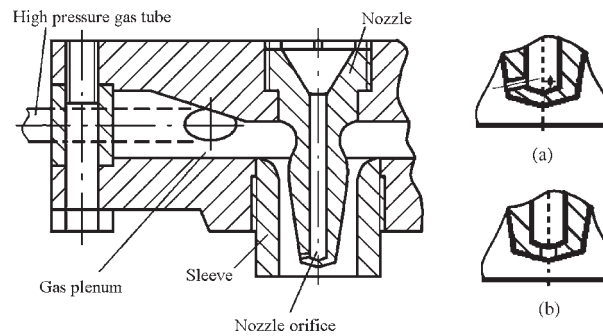

Figure 23.3 Close-coupled atomizer with changeable nozzles and sleeves: (a) nozzle with three radial discharges with axes perpendicular to the outside nozzle wall; (b) nozzle with one central orifice for melt outflow.

Table 23.4 Technological parameters of tin powder production by means of vertical melt atomization technique

Atomizer type	Melt mass flow (kg/h)	Discharge time of 1.0 kg melt(S)	Melt temperature (°C)	Operating gas pressure in atomizer (MPa)	Temperature of operating gas in atomizer (°C)	Pressure of cooling gas (MPa)	Powder yield (%)[c]
3w/3.0[a]	498.3	7.2	350	0.55	350	1.8	87.1
3w/2.8	478.8	7.5	350	0.53	320	1.4	93.2
3w/2.0	264.6	13.0	350	0.50	330	3.0	93.9
1/3.0[b]	361.2	10.0	350	0.51	320	1.5	83.7
1/2.5	297.4	12.1	350	0.50	360	2.5	66.7
1/2.0	198.7	15.1	350	0.52	385	2.5	94.6
1/1.5	185.0	19.5	350	0.50	385	2.2	98.8

[a] Fraction numerator signifies 'three radial discharges with axes perpendicular to the outside nozzle wall', in denominator is value of the orifice diameters (mm).
[b] fraction numerator signifies 'the nozzle with one central orifice for melt outflow', in denominator is value of the orifice diameters (mm).
[c] percentage of initial material efficiency for the various nozzle types.

Table 23.5 Properties of commercially tin powders

Properties	Unit	Standard grades									
		ASTM grade, sample			GOST 9723[a]			MMP[b]		Pometon[c]	
		A	B	C	PO1	PO2	PO3	−100	−600	106	IMP
Nominal composition											
Tin	wt%	99.8 min	99.8 min	99.8 min	99.1 min	99.0 min	99.0 min	99.85 min	99.85 min	99.7 min	98.0 min
Trace elements, max:											
Antimony	wt%	0.04	0.04	0.04	0.05	0.05	0.05	...	...	..	..
Arsenic	wt%	0.05	0.05	0.05	0.015	0.015	0.015	...	...	..	..
Bismuth	wt%	0.015	0.015	0.015	0.05	0.05	0.05	...	...	...	..
Copper	wt%	0.04	0.04	0.04	0.03	0.03	0.03	...	...	...	..
Iron	wt%	0.015	0.015	0.015	0.02	0.02	0.02	...	...	...	..
Lead	wt%	0.05	0.05	0.05	0.15	0.25	0.215	...	...	...	..
Oxygen	wt%	...	...	...	0.5	0.5	...	0.15	0.15	...	...
Sulfur	wt%	0.1	0.1	0.1	0.016	0.016	0.016	...	...	...	...
Sieve analysis											
+150 μm	wt%	48.0	0.3 max	...	...	...	...	0.5 max	...	...	..
+125 μm	wt%	...	...	...	...	...	...	...	...	nil	...
+100 μm	wt%	46.5	3 max	...	...	...	...	15 max	...	0.1 max	nil
+80 μm	wt%	...	...	...	0.5 max	0.5 max	...	...	...	...	...
+75 μm	wt%	4.0	3–8	...	...	...	...	15–35	nil	...	...
+71 μm	wt%	...	...	...	2.0 max	2.0 max	...	...	...	...	...
−63 μm	wt%	...	...	...	...	...	100	...	...	...	...
+53 μm	wt%	...	...	...	...	...	...	10–30	0.5 max	...	0.5 max
+45 μm	wt%	1.0	12–25	...	...	...	...	10 max	2.0 max	15–45	2 max
−45 μm	wt%	0.5	70–85	98 min	85–95	80 min	95 min	35–55	98 min	...	...
Fisher subsieve size, average size of particles	μm	...	10–15	1–3	...	...	...	...	...	...	...
Apparent density	g/cm^3	3.35	3.7–4.2	1.3–2.0	3.0–4.0	3.2–4.2	3.2–4.2	...	...	3.8±0.4	2.5±0.5

[a] Commonwealth of Independent States (CIS).
[b] MMP: Makin Metal Powders Ltd.
[c] Pometon. S.p. A., Metal powders and granules.

Production of active powder used as a catalyst is based on transformation of white tin (β) into gray tin (α) at a temperature below 13.2°C. The gray tin modification has a cubic diamond type structure with lattice spacing $a = 6.4891$ Å. This conversion process takes place at temperatures below −16.6°C with significant volumetric expansion ($\Delta V = 26.6\%$) and depends on temperature and metal purity. Powder particles have an irregular fission-fragment shape with a rather developed surface, which is 30 to 40 times that of the atomized powder.

By means of electric explosion of tin wire in an ethyl alcohol medium, a powder with particle sizes from 13 to 20 μm is produced. The powder particle sizes were decreased still further, 2 to 3 times by including 1.0 wt% cadmium or 0.56 wt% bismuth in the melt.

By cementation of tin from its chloride solutions, by means of zinc or aluminum, powder with apparent density 0.6–1.1 g/cm^3 and particle sizes from 150 to 250 μm was produced. The residue percent of substituting metal in the powder amounts to 0.3–1.2%.

Ultrafine tin powders with particle size ranging from 0.3 to 0.8 μm are produced by electrochemical precipitation from a double layer bath consisting of an aqueous phase represented by chloride/fluoride electrolyte (150 g/L $SnCl_2 \cdot 2H_2O$ and 60 g/L NH_4F) and organic medium – a solution of oleic acid in toluene [7]. At current density in the range from 50 to 500 A/m^2 and temperature ranging from 20 to 60°C, tin is reduced from complex anions $[SnClF_2]^-$ and appears in the form of black powder with particles being distributed uniformly in the organic layer of the bath. Sodium salts are not desirable due to possible formation of sodium oleate. After electrolysis, the powder is extracted from the organic phase, separated from organic liquid by centrifugation, washed free from electrolyte by hot distilled water (87°C) and an aqueous solution of acetone or ethyl alcohol in relation 1.0 to 1.0. Washed powders are dried under vacuum at room temperature to constant mass. Oxide phases are absent due to adsorption by oleic acid. Current efficiency reaches 100%. The shape of particles is dendritic with short branches of the second order axes (Figure 23.4). The structure of powders also depends on the cathode material. Comparison of silver, nickel, stainless steel and aluminum cathodes shows that coarser particles are formed on silver cathodes, which has the most positive potential, while the finest particles are observed on deposition on the aluminum cathode, which has the most negative potential.

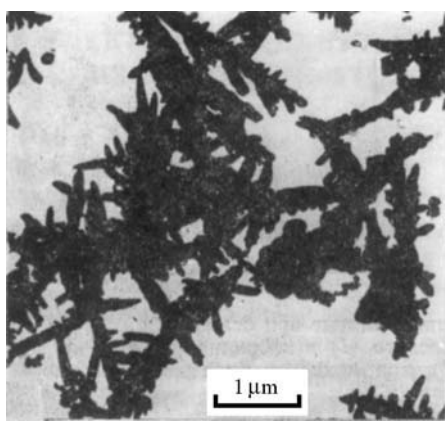

Figure 23.4 Typical scanning electron micrograph of powder produced by electrochemical precipitation from double layer bath.

Electrolytic Bismuth Powder Production

Bismuth powder is produced by the same method as tin powder in a two layer bath with rotating cathode and soluble anode [6]; electrolyte composition: aqueous phase of 59.5 g/L Bi, 20 g/L HCl and 150 g/L NH_4Cl; organic phase: toluene and 5% oleic acid. The process is carried out at current density 3–4 kA/m^2 and at temperature ranging from 15 to 25°C; current efficiency is between 65 and 70%.

Ultrafine powder modified by oleic acid is separated from the organic phase by centrifugation, freed from electrolyte by hot distilled water (87°C) and aqueous solution of acetone or ethyl alcohol 1.0 to 1.0. Powders are dried under vacuum at room temperature to constant mass. Powders produced have particle sizes in the range from 0.1 to 0.5 μm.

Other electrolytic production methods for bismuth, tin and lead powders, as well as their alloys [6–9], are given in Table 23.3.

Health and Environment Protection

Lead and manufacture of its inorganic compounds carry grave danger and harmful conditions. Lead is a highly toxic agent; its occupational exposure limits (OEL) in the workplace atmosphere under the legislation in the Commonwealth of Independents States (CIS) [13], amounts to 0.005 mg/m^3 as the shift time-weighted average concentration and 0.01 mg/m^3 as peak concentration. It is classed with the extremely dangerous powders, the first class according to the above State Standard.

Because of the high toxicity of lead and its inorganic compounds, a complex of the industrial measures of lead powder manufacture is provided. These

industrial safety measures include maximum encapsulation of all units and interoperational transport, maximum mechanization and automation of the processes, remote control of units, conducting of manual operations by means of manipulators in airtight boxes. In vented chambers, where equipment is located, an underpressure is maintained, in order to prevent an escape of airborne lead. The lead-containing suction gases are subjected to high-performance cleaning. Lead trace concentrations are continuously controlled in the workplace atmospheres and in the ambient factory air.

The admissible concentration limit of lead in aqueous medium per toxicological indication is 0.03 mg/L. It is classified as a highly dangerous agent in the second dangerous class according to SanПiN 4630–88 Standard [14].

The occupational exposure limit in the workplace atmosphere of bismuth and its inorganic compounds is 0.5 mg/m^3. It is placed in the second class of danger according to CIS Standard [13].

The admissible concentration limit of bismuth in aqueous medium per toxicological indication is 0.1 mg/L (for the inorganic compounds, including transition elements, subject to total contents of all forms). It is classified as highly dangerous agent in the second dangerous class according to SanПiN 4630–88 Standard [14].

The vapors of toluene used for the electrochemical precipitation of tin powder in a double layer bath process are classed as third class danger. Its occupational exposure limit in the workplace atmosphere amounts to 50 mg/m^3. Toluene is a substance with pencil-beam action demanding the automatic monitoring of its content in air. It is capable of causing allergic illnesses in working conditions.

The admissible concentration limit of toluene in aqueous medium per organ-oleptic indication, changing the smell, is 0.5 mg/L. It is classed as a moderately dangerous agent in the fourth dangerous class.

Metallic tin in particulate form is a combustible material, while solid metal is non-combustible. Self-ignition temperatures of tin powder, containing 98 wt% with particles below 74 μm in size in aerogel and suspended solid conditions are 520 and 660°C, respectively. The low concentration ignition limit (LCIL) is 220 g/m^3; maximum explosion-proof oxygen content in airborne powder (LOC) diluted by carbon dioxide is 15 vol%. The combustibility and explosibility of tin alloy with 2 wt% lead is characterized by the following data. Self-ignition temperatures of the powder with particles below 74 μm in size in aerogel and suspended solid conditions are 430 and 630°C, respectively [15]; the LCIL is 190 g/m^3; maximum explosion pressure by airborne powder content 1000 g/m^3 is 340 kPa; maximum rate of pressure rise is 12 MPa/s; minimum airborne powder ignition energy is 80 mJ; LOC diluted by carbon dioxide is 16 vol%.

The products with such characteristics of inflammability and explosion risk are placed in the 'Moderate explosion hazard' class of danger according to the Guide to Legislation and 'Health and Safety' in the European PM Industry [16].

To extinguish burning tin powder it is necessary to use a mix of potassium and sodium chloride powder (with consumption about 15–50 kg per 1 square meter), or dry sand. For the voluminal quenching method, argon is used consuming about 12.0 kg/m^3 in the burning zone.

Lead in particulate form is difficult to ignite. Self-ignition temperatures of lead powder with particles below 53 μm in size in aerosol and suspended solid conditions are 210 and 710°C, respectively.

The oleic acid, used for electrochemical precipitation of tin, bismuth and their alloy powders in the double layer bath process, is a combustible liquid. Its properties are characterized by the following data. Melting point is 14°C; boiling point is 380°C; heat of combustion 10370 kJ/mol. Oleic acid is insoluble in water. Its self-ignition and ignition temperatures are 280 and 180°C, respectively. To extinguish burning oleic acid, it is necessary to use bicarbonate of soda powder or the voluminal quenching method by means of carbon dioxide, consumption of about 0.7 kg/m^3 in the burning zone.

The cyclohexane, which is also used in the electrochemical precipitation of tin, bismuth and their alloy powders in the double layer bath process, is a highly inflammable liquid. Its properties are characterized by the following data. Melting point is 6.5°C; boiling point is 80.7°C; heat of combustion is 3689 kJ/mol. Cyclohexane is insoluble in water. Its self-ignition temperature is 259°C. The lower and upper flame propagation limits in air are 1.3 and 7.8 vol%, respectively. Maximum explosion pressure is 858 kPa; maximum rate of the flame propagation is 0.436 m/s; minimum ignition energy is 0.22 mJ; the burning temperature amounts to 1997°C. The means of extinguish burning cyclohexane are the same as for oleic acid [15].

Applications

Tin powders are used extensively in the production of porous, self-lubricating bronze bearings and as constituents in soldering and brazing powders and pastes. Tin powders are also used in powder metallurgy structural parts, friction disks, clutches, brake linings, bonded resin friction materials, metal graphite brushes, diamond abrasive grinding wheels,

Table 23.6 Typical solder alloy powder grades

Property	Unit	Standard grades													
		ASTM grade, samples						GOST 1499, samples[a]						Nippon AMP	
		10 B	30 B	50 B	63 B	62 P	96.5TS	ПОС 10[b]	ПОС 40[b]	ПОС 61[b]	ПОС 90[b]	ПОССу 61-0.5[c]	ПОССу 95-5[d]	80-20	60-40
Composition															
Main components:															
Tin	wt%	8–12	28–32	48–52	61–65	61.5–67.5	95–96	9–10	39–41	60–62	89–91	60–62	94–96	80	60
Antimony	wt%	0.2–0.5	0.2–0.5	0.2–0.5	0.2–0.5	0.3–0.5	0.2–0.5	...	...	...	...	0.2–0.5	4.0–5.0	...	...
Lead	wt%	bal	bal	bal	bal	bal	bal	bal	bal	bal	bal	bal	bal	20	40
Trace elements, max															
Aluminum	wt%	0.005	0.005	0.005	0.005	0.005	0.005	0.002	0.002	0.002	0.002	0.002	0.002	...	...
Antimony	wt%	...	...	...	...	...	...	.0.05	.0.05	.0.05	.0.05	...	...	...	...
Arsenic	wt%	0.02	0.02	0.02	0.02	0.02	0.02	0.03	0.03	0.03	0.02	0.03	0.05	...	...
Bismuth	wt%	0.25	0.25	0.25	0.25	0.25	0.25	0.1	0.1	0.1	0.1	0.1	0.2	...	...
Copper	wt%	0.08	0.08	0.08	0.08	0.08	0.08	0.05	0.05	0.05	0.05	0.08	0.1	...	...
Iron	wt%	0.02	0.02	0.02	0.02	0.02	0.02	0.02	0.02	0.02	0.02	0.02	0.02	...	...
Lead	wt%	...	...	...	...	...	...	...	...	...	...	...	...	...	...
Nickel	wt%	...	...	...	...	...	...	0.02	0.02	0.02	0.02	0.02	0.08	...	...
Silver	wt%	...	...	...	...	1.75–2.25	3.3–3.7	...	...	...	...	...	...	...	...
Sulfur	wt%	...	...	...	...	...	...	0.02	0.02	0.02	0.02	0.02	0.02	...	...
Zinc	wt%	...	...	...	...	...	...	0.002	0.002	0.002	0.002	0.002	0.002	...	...
Particle sizes	μm	...	...	...	...	...	...	⩽50	⩽50	⩽50	⩽50	⩽50	⩽50	5[e]	10[e]
Solidus temperature	°C	268	183	183	183	179	221	...		...	...	...	...	...	...
Liquidus temperature	°C	299	255	216	183	179	221	...		...	...	...	...	...	...
Soldering range	°C	329–369	285–325	213–282	212–253	209–249	251–291	...		...	...	...	...	...	...

[a] Commonwealth of Independents States (CIS).
[b] Antimonousless.
[c] Low-antimonous.
[d] Antimonous.
[e] Median diameter. Nippon AMP: Nippon Atomized Metal Powders CO.

bronze filters, peen plating, plasma arc spraying, chemical formulations, additives for rubber and plastics, chemical manufacturing, smokeless powder for pyrotechnics, foams and tin flake.

The requirements for powders utilized for soldering paste production are a high content of fine particles and a low oxygen content. Some typical solder alloy powder grades used in soldering pastes and creams are listed in Table 23.6.

Because copper and lead have limited solubilities in each other, they are difficult to alloy by conventional ingot metallurgy. Copper–lead powder mixtures have excellent cold pressing properties. They can be compacted at pressures as low as 76 MPa to densities as high as 80% of theoretical density. After sintering, they can be re-pressed at pressures as low as 152 MPa to become practically non-porous bearings.

Cu–Pb–Sn PM materials are also used to replace solid bronze bearings. They are produced by spreading the powder in a predetermined thickness on a steel strip, sintering, rolling to theoretical density, resintering and annealing. The end product has a residual porosity of about 0.25%. These materials include Cu–25Pb–0.5Sn, Cu–25Pb–3.5Sn, Cu–10Pb–0.5Sn and Cu–50Pb–0.5Sn.

Tin, lead and bismuth powders are used as compacted metal powders in the production of metallic foams. The metal powders are mixed with foaming agents to give a completely homogeneous mixture. The result of the subsequent densification step is a foamable material that, upon heating to temperatures within the range of the melting point, expands into a highly porous cellular solid with a closed pore structure. The typical structure of lead foam is shown in Figure 23.5. More information about metallic foam technology can be found in Chapter 10.

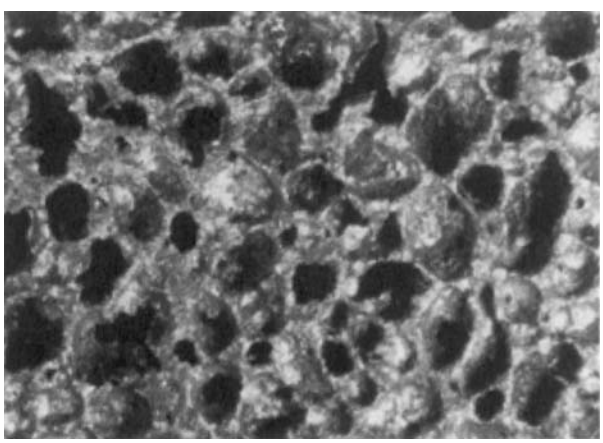

Figure 23.5 Optical micrograph of cross-section of lead foam. Source: Ref 17®

References

1. Fedorchenko, I.M., ed. *Encyclopedia of Inorganic Materials*, Glavnaja Redakcija USE, Kiev, 1977 (in Russian).
2. German, R.M., *Sintering Theory and Practice*. John Wiley & Sons Publishers, 1996.
3. Nichiporenko, O.S., Naida, Yu.I., Medvedkovsky, A.B., *Powder Atomisation from Melts*. Naukova Dumka Publisher, Kiev, 1980 (in Russian).
4. Wolf, G., Till, K., Scholz, R., Hot gas atomisation. In *Proceedings of 2002 Powder Metallurgy World Congress*, Princeton, MPIF Publishers, New Jersey, 2002, pp. 3-163–3-177.
5. Dunkley, J.J., Hot gas atomisation – economic and engineering aspects. In *Proceedings of 2004 Powder Metallurgy World Congress*, compiled by European Powder Metallurgy Association, UK, 2004, Vol. 1, pp. 13–18.
6. Zhelibo, E.P., Grechanjuk, V.G., On bismuth fine powders deposition on passivated electrodes. *Sov. Powder Metall. Met. Ceram.*, 1978(6):1–6.
7. Zhelibo, E.P., Grechanjuk, V.G., Electrodeposition of tin fine powders from cloride-fluoride electrolytes. *Sov. Powder Metall. Met. Ceram.*, 1978(7):4–7.
8. Fil', T.N., Khimchenko, E.I., Isaj, V.N., Romanova, A.V., Electrodeposition and X-ray diffraction examination of high-disperse lead–bismuth alloy. *Sov. Powder Metall. Met. Ceram.*, 1977(3):12–19.
9. Zhelibo, E.P., Grechanjuk, V.G., Effect of electrolyte composition on conditions of tin–bismuth high-dispersed alloy formation. *Sov. Powder Metall. Met. Ceram.*, 1978(8):5–9.
10. Ullrich, W.J., Production of tin powders. In *ASM Handbook*, Vol. 7. ASM International Publishers, 1998, pp. 146–147.
11. Adamchik, L.V., Bondarenko, S.G., Koval'chuk, V. G., Pavlenko, D.V., Statsenko, I.D., Gas-sprayed tin powders. *Sov. Powder Metall. Met. Ceram.*, 2003, 42(1–2): 100–104.
12. Lawley, A., *Atomization*. Metal Powder Industries Federation Publishers, Princeton, New Jersey, 2003.
13. Commonwealth of Independent States Standard GOST 12.1.005−88. Publishers of Standards, Moscow, 1988 (in Russian).
14. Sanitary Regulation and Standards of surface waters from pollution. SanПiN 4630–88. MinZdrav, Moscow, 1988 (in Russian).
15. Baratov, A.N., Korolychenko, A.J. (ed.), Hand book Fire- and explosion-proof of matters and materials and means for their quenching. Handbook, Chimia, Moscow, 1990 (in Russian).
16. Guide to Legislation and 'Health and Safety' in the European PM Industry. EPMA, 1997.
17. Banhart, J., Baumeister, J., Weber, M., Metallic foam. In ASM Handbook, Vol. 7. ASM International Publishers, 1998, pp. 1043–7.

SECTION 5 Safety Engineering in the Production of Powders

Contents

Chapter 24

Safety Engineering in the Production of Powders

Oleg D. Neikov, Frantsevich Institute for Problems of Materials Science (IPMS), Kiev, Ukraine

Dangerous and Harmful Manufacturing Factors

Open flames, heat radiation, molten metal, fire and explosive dusts and gases, and elevated temperatures in the workplace atmosphere, elevated temperatures of equipment surfaces, noise and vibration, voltage in electric circuits, electrostatic electricity, movable mechanisms and mobile parts of equipment are dangerous and harmful agents in the production of powders.

Generally, the dangerous and harmful factors in powder productions as well as in subsequent powder processing are classified as chemical and physical agents. The latter include:

- the risks to health from exposure to noise
- hand transmitted mechanical vibrations and whole body vibrations
- effects of electric and magnetic fields.

Chemical agents are determinated by the properties of the substances concerned.

The physical-chemical properties of the dusts are characterized by chemical composition, particle size distributions, specific surface, flammability, explosive properties, oxidizability, relative density, specific electrical resistance, adhesion property, wettability, abrasivity, solubility, etc.

Dust Gaseous and Vapor Emissions

The main source of dust and emission of gas and vapor are melting furnaces, stands for heating of the crucibles and tundishes, atomization units, powder drying, classification, loading and unloading units, dosing and packing. The heating of crucibles and tundishes by means of natural gas forms combustion gas containing approximately 12 vol% carbon dioxide, about 2 vol% carbon monoxide and 2 vol% hydrogen and maximum 0.2 vol% nitrogen oxides. The fusion of metals and atomization of melts are accompanied mainly by emission of metal oxides (Table 24.1). Thus, during copper melting in a 0.4-tn induction crucible furnace, the concentration of copper oxides in the convection current of sublimates over the melt amounts to 250 mg/m^3, in brass melting, between 830 and 2700 mg/m^3, while during the pouring of the melt into the tundish, the concentration amounts to 5700 mg/m^3 and, in the pouring of bronze, to 7500 mg/m^3. The sublimates contains up to 90 wt% of particles with sizes below 2.5 μm.

Typical data of dust concentration and particle size distribution in aspiration exhausts by copper and copper alloys atomized powder production are given in Table 24.2.

The content of vapor in aspiration gas is determined starting with the intensity of the vapor emission with assignment of its per mass flow of aspiration gas. Thus, during drying in the vibrodryer

Table 24.1 Typical composition of the sublimates formed during melting and atomization

Metal	Content of elements (wt%)					
	Copper	Zinc	Lead	Tin	Carbon	Oxygen and other
Copper	92–96	...	...	...	...	5–8
Brass 63	9	24	...	...	38.4	28.6
Bronze	34	45.4	0.41	15.7	4.3	0.2
Zinc	...	77.0	...	...	...	23.0

Table 24.2 Typical data of dust concentration and particle size distribution in aspiration exhausts by copper and copper alloy atomized powder production

Technological operation	Dust concentration in aspiration exhausts (g/m^3)	Weight powder distribution by particle size (μm) fractions (%)						
		<4	4–6.3	6.3–10	10–16	16–25	25–40	>40
Melt preparation:								
in induction furnace:		All particles are finer than 2.5 μm						
Copper	0.007							
Bronze (Cu–5Sn–5Zn–5Pb)	0.009							
Brass (Cu–20Zn)	0.031							
in reverberatory furnace:								
Zinc	2.56	90 wt% particles are finer than 2.5 μm						
Water atomization of melt:		All particles are finer than 10 μm						
Copper	0.02							
Bronze (Cu–5Sn–5Zn–5Pb)	0.03							
Brass (Cu–20Zn)	0.15							
Drying in vibrodryer[a]:		38.0	22.0	26.0	10.0	4.0	...	...
Copper	0.1							
Bronze (Cu–5Sn–5Zn–5Pb)	0.12							
Brass (Cu–20Zn)	0.15							
Sieving of powders	0.05–1.2	36.5	8.0	12.5	15.0	18.3	4.8	4.9
Blending in mixers:								
Double-cone mixers	0.36	24.1	22.6	20.9	1.6	0.8	24.0	16/0
Impeller mixers	3.2	16.0	24.0	0.8	1.6	2.9	22.6	14.1
Dry continued mills (discharge places)	4.5	4.1	1.8	3.2	2.2	6.4	15.8	66.7
Weight batchers	0.05	38.0	22.0	26.0	10.0	0.4	...	...
Unloading from conveyor into bin or technological apparatus	1.0	14.8	6.8	...	9.0	31.8	16.8	20.0
Loading–unloading of powder from conveyor to conveyor	2.7	13.9	5.3	3.2	8.9	31.9	16.1	20.7
Elevators (charge places)	2.96	6.5	39.3	32.1	11.6	6.6	4.0	...

[a]'Thermal Drying' in Chapter 11 contains data about this vibrodryer

of water atomized copper alloy powder with initial 8 wt% and residual 0.5 wt% water content with gas mass flow 1500 m^3/h, after 5 minutes in the drier the vapor concentration in the aspiration gas is 21.4 g/m^3.

Properties of Powders

Adhesion

The ability of particles to form aggregates and to adhere to apparatus walls is a function of autohesion and adhesion interaction. Autohesion is the interaction of particles with each other, and adhesion is the interaction of particles with the monolayer of the surfaces. The breaking strength of a dust layer characterizes the dust autohesion. Under autohesion, the dust is classified into three groups: non-agglutinated dust with breaking strength below 60 Pa, weakly agglutinated with breaking strength ranging from 60 to 300 Pa, and strongly agglutinated – higher than 600 Pa.

For example, bronze powders are referred to as weakly agglutinating with breaking strength from 60 to 244 Pa depending on particle size distribution. A brass powder coarser than 160 μm is placed into the non-agglutinating group, having the breaking strength 44 Pa. The powder-like fractions of the brass powders are referred to as weakly agglutinating, with breaking strength of the order of 200 Pa.

Powder flowability is characterized by the angle of repose. The static and dynamic angles of repose are discriminated. The former refers to the angle at which the side surface of particulate material is located after removal of a supporting wall. The dynamic angle is the angle between the basis and element cone obtained by free fall of powder on a flat horizontal surface.

More detailed interpretation of flowability and angle of repose is contained in Chapter 1.

Hygroscopicity and Wettability

Hygroscopicity, that is the ability to absorb moisture from the environment, influences on dust properties, such as autohesion and adhesion interaction, flowability and electrical conductivity of the dust layer, which are necessary to take into account in the designing of aspiration installations.

The so-called equilibrium moisture content is the content in the powder appropriate to every ambient gas humidity. The hygroscopic moisture content is determined by drying a sample to constant weight. This method is most widely used, but is not applicable to substances with decomposition or fusion temperatures below 110°C.

The wettability of dust is determined by interaction of molecules on the boundary of solid, liquid, and gaseous phases and leads to a liquid film forming on the surface of the particles. The wetting of dust particles by water droplets is the base of the wet dedusting process.

The tendency of the dust to wetting is evaluated by the film floatation method, which consists of determination of the weight of a powder placed on the surface of water that sinks in a specified time. At wettability, the dust is divided on three groups: bad, medium and good wettability, for which the percentage of particles that sink is 30, 30–80 and greater than 90 wt%, respectively.

Abrasiveness

The abrasive properties of dust depend on the hardness, particle shape, density, and particle sizes and can be expressed as the abrasive coefficient K_a. A laboratory method of K_a determination for their values, exceeding 0.5×10^{-12} m^2/kg, is based on determination of the degree of wear of a plate, located at an angle of 45° by a stream of the powder investigated.

Ambient Noise and Vibration

The furnaces, atomizing installations, high pressure pumps, equipment for crushing, comminution, and sieving, and lifting-transport equipment are noise sources. Data about characteristic levels of noise created by certain operations are given in Table 24.3. The measures for reducing the general noise level and pressure levels in octave bands up to admissible sizes are regulated by standard acts [1,2].

Vibrosieves are the major vibration source in powder production. Their levels of common vibration by geometric mean frequencies are characterized by the following data: 89.5, 82.5 and 75 dB along with 16, 31.5 and 63 Hz, respectively, while the admissible limit is 92 dB.

Heat Radiation

Molten metal, furnace equipment and burning torches, used for heating crucibles and tundishes, are the main sources of heat radiation. Thus, in a tundish heating zone, at 1 m from the torch, the heat radiation amounts to 2250 J/(m$^2 \cdot$ h), while the melting area near an induction furnace achieves about 12880 J/(m$^2 \cdot$ h). In such zones, protection from heat radiation is necessary.

Electrostatic Electricity

The electrical conductivity of dust is characterized by the value of resistivity of the dust layer. Resistivity values are subdivided into good (below $10^2 \Omega \cdot$ m), medium (from 10^2 to $10^9 \Omega \cdot$ m) and high ohmic resistance (above $10^9 \Omega \cdot$ m). For resistivity determination, a dust layer is formed and its electrical resistance measured.

The movement of powder and dust streams is accompanied by their electrization, here the value of charge depends on both the nature of the dust and the material of the contacting surface. The lowest

Table 24.3 Characteristic noise levels by fulfillment of certain operations

Manufacturing process	Common noise level (dB)	Pressure level (dB) in octave bands (geometric mean frequencies, Hz)							
		63	125	250	500	1000	2000	4000	8000
Shears cutting of copper bars	84	93	88	84	81	80	78	76	72
Fusion in induction furnace	101	77	74	80	76	91	70	70	61
Water atomization	86	80	80	83	80	82	71	70	68
Sieving of the powders	92	87	87	87	90	87	81	76	70

specific charge value for bronze and brass powder and dust is observed by using copper as the contacting material. The movement of bronze and brass powder streams leads to the appearance of specific charge 3.35 C per 1 g bronze powder and 2.99 C per 1 g brass powder. On a surface of aluminum alloy or chromium, the electrostatic electricity charges for bronze and brass particles are 5.5 and 3.5 C/g, respectively, and on a steel contacting surface 6.35 and 3.88 C/g, respectively.

Inflammability and Explosivity of Powders

Metals which have the potential to combine with oxygen have the further potential to ignite or explode when in their dispersible condition. Powders in layer or dust deposits do not explode, but by action of an applicable ignition source, they can ignite and burn. A local initial explosion usually breaks up the deposit leading to dust cloud formation. Here, the flame is able to expand throughout the cloud and can generate an explosion of large-scale destructive strength.

Inflammation and explosion can occur not only due to oxygen, but also via other exothermic reactions, for example, as a result of interaction of magnesium with nitrogen and aluminum and magnesium with freon.

The evaluation of combustibility of the powder in layer or dust deposit consists of minimal ignition temperatures, smoldering temperature and combustibility group.

The tests for an explosion assessment of powder or dust in suspended solid state are follows:

- low concentration ignition limit
- minimum ignition and self-ignition temperatures
- maximum explosion pressure
- maximum rate of pressure rise
- minimum ignition energy
- limiting oxygen concentration to prevent ignition.

Conditions for explosion to occur include the following criteria:

- the powder must be combustible
- the powder must be capable of becoming a suspended solid
- the concentration of airborne powder particles in the dust cloud must be within the critical ignition limit range
- the suspended solid in contact with an ignition source in air must be capable of initiating and sustaining flame propagation
- the atmosphere into which the dust is suspended must contain sufficient oxygen to support combustion.

Combustibility is the ability of a material to burn; the materials can be divided into combustible, difficult and incombustible. Depending on the material combustibility group, an appropriate category of manufacture is accepted, as well as the technical decisions, providing the fire-explosion safety of powder production, storage and transportation.

The low concentration ignition limit (LCIL), in g/m^3, is the minimum concentration of suspended solid in the oxidizing atmosphere which can sustain flame propagation. The determination of classes and zones of the manufacturing rooms is based on LCIL values [1,2].

Minimum ignition temperature (T_i, °C) is the minimum temperature of powders at which, in the presence of an external ignition source, the temperature increases through the exothermic reaction, ending in spontaneous flame appearance. According to the size of T_i, the material is classified on combustibility grade and fire hazard of equipment and technological processes.

Self-ignition temperature (T_{si}, °C) is the minimum temperature of powders (in aerogel state), at which exothermic reaction rate abruptly increases, ending in spontaneous flame production. A reacting chamber containing a powder sample is heated. The powder heating occurs from wall heat transfer or during rapid mixing of previously heated components of a mixture. The knowledge of T_{si}, is necessary for temperature heating limitations of equipment surfaces and combustible mixtures.

The self-ignition temperature of suspended solid ($T_{s\cdot ab}$, °C) is the minimum temperature of suspended solid in air at which the exothermic reaction rate abruptly increases, ending by spontaneous flame production.

Self-heating temperature is the lowest temperature at which the exothermic reaction appears from environmental heat.

Smoldering temperature (T_{sm}, °C) is the temperature during self-heating, at which the exothermic reaction rate increase leads to appearance of smoldering.

Minimum ignition energy (w_{min}, mJ) is the lowest energy of spark discharge able to ignite the most easily ignitable dust air stream.

Maximum explosion pressure (p_{max}, MPa) is the maximum pressure, incipient by explosion of airborne powder in a closed vessel with initial pressure 101.325 kPa. These data are necessary for strength design of the equipment.

Maximum rate of pressure rise (v_{max}, MPa/s) is the relation of an increment pressure, developed during explosion in a closed vessel, to the time interval in the course of which this increment occurs. Magnitude of v_{max} is necessary for design of the equipment and design of devices, discharging the explosion pressure.

Limiting oxygen concentration to prevent ignition (LOC) is the minimum oxygen concentration in combustible gas-borne powder mixture, below which the ignition and combustion become impossible whatever the fuel content in the mixture. LOC size is used for determination of the explosion-proof regimes of the technological processes, pneumatic transport and designing of explosion suppression and fire quenching systems and installations.

Thermophysical Properties

Thermophysical properties comprise specific heat capacity, thermal conductivity, coefficient of linear thermal expansion, heat of vaporization and heat of combustion. Thermophysical magnitudes of the materials are given above, in sections, where powder production is described.

Heat (enthalpy) of combustion of a material (ΔH) is a variation of enthalpy through course of combustion reaction of the material weight unit with equivalent oxygen amount. ΔH quantity (Table 24.4) is used for determination of manufacturing areas and building categories for explosion and fire hazard. ΔH quantity of composite materials is calculated on ΔH quantities of elements contained in them.

Explosion-proof characteristics of the gaseous reducing agents and easily combustible liquids used in the production of non-ferrous powders are given in Table 24.5.

Combustibility and explosibility values of non-ferrous powders are given in Table 24.6 (the powders are placed in decreasing order of activity).

Figure 24.1 illustrates the dependence of LCIL, p_{max}, and average rate of pressure rise v_{mid}, on the particle sizes for water atomized aluminum alloy powder [4]. The values of LCIL increase and v_{mid}, decrease continuously with increasing particle size in ranges from 50 to 130 μm. The p_{max}, quantities show a weak dependence on particle size in the range from 50 to 80 μm followed by a stronger decrease of p_{max}, for coarser powders.

A feature of aluminum and aluminum-based alloy powders is the risk of powder ignition resulting from either exothermal reactions with air or formation of hydrogen on contact with water. They lightly react

Table 24.4 Heat of oxide formations and combustion of materials

Element	Oxide	Heat of oxide formation (kJ/kg)	Heat combustion of element (kJ/kg)
Aluminum	Al_2O_3	16470	34170
Barium	BaO	3620	4040
Calcium	CaO	11340	15900
Carbon	CO_2	8970	32860
Magnesium	MgO	15050	25080
Silicon	SiO_2	15200	32550

Table 24.5 Explosion-proof characteristics of gaseous reducing agents and easily combustible liquids

Substance	Concentration limits of flame propagation (vol%)	Maximum explosion pressure (MPa)	Rate of pressure rise (MPa/s)[a]
Hydrogen	4–75	0.65	64/70
Ammonia	18–28	0.60	...
Dissociated ammonia with hydrogen content (vol%):			
75	5.4–73.1	...	...
40	10.6–75.1	...	...
20	21.5–76.1	...	...
Endogas with hydrogen content (vol%):			
40	8.8–71.8	...	...
20	16.2–69.2	...	...
Ethyl alcohol	3.6–19.0	0.62	10/16
Methyl alcohol	6.34–7.0	0.63	10.55/21.3
Isopropyl alcohol	2–12	0.69	8.3/12.3
Benzine	1.2–6.9	...	...

[a]Average rate of pressure rise/maximum rate of pressure rise

Table 24.6 Combustibility and explosibility values of non-ferrous powders

Material	Particle sizes (μm)	Powder			Suspension of airborne powder					Combustibility group
		T_i (°C)	T_{si} (°C)	$T_{s\cdot ab}$ (°C)	w_{min} (mJ)	LCIL (g/m^3)	p_{max} (MPa)	v_{max} (MPa/s)	LOC (vol%)	
Magnesium[BM]	<74	490	420	450	0.025	10	0.66	6.3	0Ar; +C; +N[b]	CB[c]
Magnesium, spheroidal[5]	<280	...	...	600	...	20	0.67	12.3	2N	CB
Magnesium, milled[5]	<100	...	...	520	...	40				
Zirconium[d]	<75	...	190	20	5	40–64	0.63	9.1	3N; 5Ge; +Ar; +C	CB
Zirconium[BM]	3–6	180	190	...	0.0004	40	0.45	4.45	3N; 5Ge; +Ar; +C	CB
Uranium[BM]	<10	...	100	20	25	60	0.37	23.8	+C; 1N; 2Ar; 2Ge	CB
Titanium, calcium hydride[5]	<50	...	...	520	10[d]	13	0.64[6]	11.8.	2.5N	CB
Titanium, electrolytic[5]	<50	...	...	340	...	40	0.39	9.8	3N	CB
80Ti–20Ni alloy[d]	<50	...	150	...	...	10	...	...	...	CB
Aluminum dust[d]	<27	320	520	410[e]	...	40	1.3	6.86	3N	CB
Aluminum flakes[5]	<20	...	...	520	...	45	0.78	6.87	8N	CB
Aluminum, spheroidal[5]	<50	...	...	750	...	45	0.72	3.5	8N	CB
85Al–15Li alloy[d]	149	...	400	...	140	100	0.66	25.5	...	CB
50Al–50Mg alloy	<71	...	660	...	...	90	0.49	6.37	2.5N	CB
50Al–50Cu alloy[d]	44	...	830	...	100	100	0.468	17.9	...	CB
58Al–42Ni alloy[d]	44	...	540	...	80	190	0.544	...	14N	CB
Thorium[d]	7	...	280	270	5	75	0.57	...	2Ar; 2N; 5He; 7C	CB
Yttrium, milled[d]	<80	...	170	...	...	36	...	...	...	...
Silicocalcium[5]	<50	...	...	490	...	42	0.66	20	8N	CB
Silicon[d]	<74	...	760	780	80	100	0.75	8.4	11Ar; 12C	CB
80Si–20Zr alloy[d]	<53	...	546	...	...	104	...	...	...	CB
Boron[BM]	<44	...	400	470	60	100	0.63	1.7	11N	CB
Chromium[BM]	<74	...	400	...	140	190	0.4		14C	CB
Hafnium[d]	<180	...	250	390	...	210	...	...	...	...
Tantalum[d]	<44	...	300	630	120	200	0.35	3.03	...	CB

Zinc[d]	<74	...	310	600	640	480	0.490	1.8	10C	CB
Vanadium[d]	<74	...	490	500	60	220	0.35	0.69	10C	CB
Bronze[BM]	<53	...	190	370	...	10	0.3	0.9	...	
Tin[BM]	<53	...	430	...	80	190	0.26	0.9	16C	dCB
96Sn–2Pb alloy[d]	<74	...	430	630	80	190	0.340	1.2	16C	dCB
Antimony[BM]	<74	...	330	420	1920	420	0.056	0.7	16C	dCV
Cadmium[BM]	<74	...	250	570	4000	...	0.05	0.7	...	dCB
Lead[BM]	<53	...	270	710	...	...	...	...	...	dCB
Tellurium[BM]	<44	...	340	550	...	...	...	...	...	dCB
Molybdenum[BM]	<74	530	310	720	...	...	...	...	...	dCB
Cobalt[BM]	<44	...	370	760	...	...	...	...	...	dCB
Tungsten[BM]	<74	...	430	717	...	...	...	...	...	dCB
Nickel	<50	...	470	...	...	220	...	...	...	dCB
Beryllium[BM]	1	...	540	910	...	...	...	...	...	dCB
Copper	<44	Does not inflame								iCB
Copper dust	80 wt% <40 μm 14 wt% <10 μm	470	193	Does not inflame in airborne state						dCB
Brass (87Cu–10.9Zn)	27 wt% <10 μm	Does not inflame in layer as well in airborne state								iCB
Brass dust (88.1Cu)	88 wt% <10 μm	450	205	Does not inflame in the airborne state						dCB
Bronze (Cu–5Sn–5Zn–5Pb)	80 wt% <100 μm	620	615	Does not inflame in the airborne state						dCB

(+) is designated that suspension of airborne powder is fired in specified inert gas;
[a]Ciphers in LOC column figure an oxygen explosion-proof content in vol%;
[b]Abbreviation of the gas-diluted: Ar: argon, C: carbon dioxide, N: nitrogen, He: helium;
[c]Abbreviation of the material combustibility group: CB: combustible, dCB: difficult by combustible, iCB: incombustible;
[BM]Source: Report of Investigation Bureau of Mines, V.S. GPO, 1964, 6516;
[d]Source: Fire and explosion risk of the substances and matrials and quenching means, Handbook, Ed. Baratov, A.N., Korolychenko, A.J. Chemija Publishers, Moscow, 1990;
[e]Smoldering temperature;
[5]The cipher located overhead, at the right top of material name is the reference source.

at room temperature with aqueous alkali solution accompanied by hydrogen emission. The mixing of aluminum powder with alkali solution might lead to an explosion. Such powders react strongly with many metalloids. Thus, aluminum chip burns in bromine, forming aluminum bromide. On heating, aluminum combines with sulfur. Finely ground aluminum reacts with halogenated hydrocarbons; if present in small amounts, aluminum chloride (which forms during this reaction) acts as a catalyst, which accelerates the reaction, leading to explosion in some cases. Such an occurrence is observed on heating of aluminum powder with methyl chloride, carbon tetrachloride and a mixture of chloroform with carbon tetrachloride up to a temperature of about 150°C. A mixture of aluminum powder with copper oxide, silver oxide and especially lead dioxide burns with a blast. A mixture with carbon or nitro-compounds is explosive.

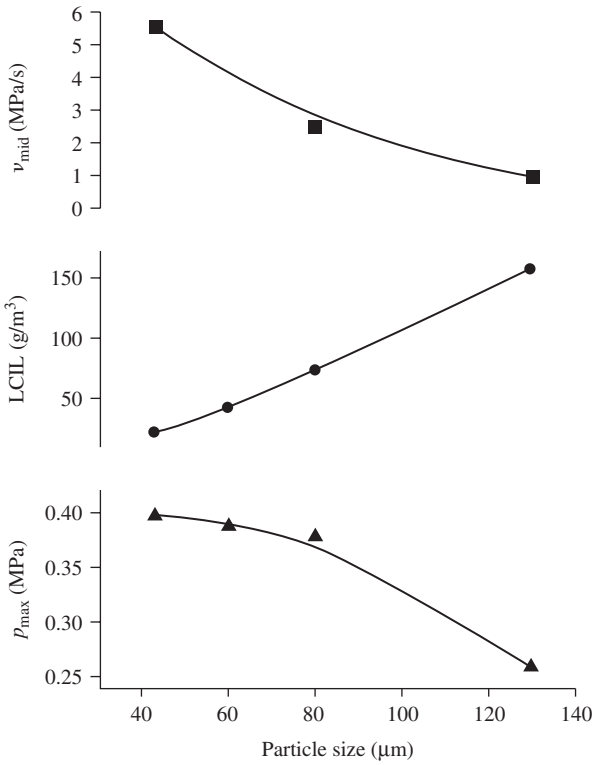

Figure 24.1 Dependence of low concentration ignition limit (LCIL), maximum explosion pressure (p_{max}) and average rate of pressure rise v_{mid}, on particle size for water atomized aluminum alloy powder. Source: Ref 4

Guide to EU Legislation [3] includes recommendation to categories high, moderate or low hazard depending on minimum ignition temperature, explosion limits and oxygen content (Table 24.7).

Workplace Atmosphere Limited Powder Threshold Values

The proportion of total particulate matter which is inhaled into a human body depends on the properties of the particles, on the speed and direction of air movement near the body, on breathing rate, and whether breathing is through the nose or mouth. Inhaled particles can then deposit somewhere in the respiratory tract or can be exhaled. The site of deposition, or probably of exhalation, depends on the properties of the particle, respiratory tract, breathing pattern and other factors.

The European Standard EN/481/1993 on 'Workplace Atmospheres. Size fraction definitions for measurement of airborne particles' includes the planning and performing of measurements. The introduction to this standard states that there is a

Table 24.7 Explosion assessment of metals according to Guide to EU Legislation [3]

Explosion-proof characteristics	Explosion hazard category		
	High explosion hazard	Moderate explosion hazard	Low explosion hazard
Minimum oxygen requirement	<3 vol%	>3 wt%	. . .
Minimum ignition temperature	<600°C	from 300 to 800°C	>700°C
Explosion concentration limit	from 20 to 50 g/m^3	from 100 to 500 g/m^3	. . .
Examples	Zirconium, magnesium and aluminum	Copper, silicon, tin and zinc	Cobalt, lead and molybdenum

wide variation from one person to another in the probability of particle inhalation, deposition, reaction to deposition and clearance. Nevertheless, it is possible to define conventions for size selective sampling of airborne particles when the purpose of the sample is health related. These conventions are relationships between aerodynamic diameter and the fractions to be collected or measured, which approximate to the fractions penetrating to the regions of the respiratory tract under average conditions. A view of the penetration of respirable particle fractions in a human body is typically determined in the following way: particles finer than 100 μm penetrate to the larynx, particles with average size 11.64 ± 1.5 μm penetrate to the bronchi and particles with average size 4.25 ± 1.5 μm penetrate to the alveolus.

Recommended values of size ranges for occupational and environmental health related air sampling are represented in Figure 24.2. There are three optional boundaries between the tracheobronchial and alveolar components of the thorax fraction. Two of these are the traditional recommendations for working adults of the British Medical Research Council (BMRC) and the American Conference of Governmental Industrial Hygienists (ACGIH). The third, labeled other populations, corresponds to sensitive members of the general public who have constricted bronchial airways (from American Industrial Hygiene Association Journal, May 1981).

The TLV values of harmful materials in workplace atmospheres, classification and prior phase conditions are contained in Table 24.8. Depending on the degree of danger of the substances and materials, the four danger classes are listed as: highest dangerous class I reducing down to class IV. These values are accepted by the Commonwealth of Independent States (CIS) Standard, GOST 12.1.005–88 [6] and are close to the European Standard on workplace atmospheres – EN/481/1993, including Directive (88/642/EEC) on limit values.

The classification of dangerous substances according to EU Directives, means chemical elements and their compounds as they occur in the natural state or as produced by industry, including any additives required for the purpose of placing them on the market, or any impurity deriving from the production process/materials used. There are two different types of 'substances' which may be classified as dangerous: those already listed in Annex I of Directive 67/548/EEC (European Inventory of Existing (Commercial) Chemical Substances or EINECS for short), or new substances not listed in EINECS and which will need classification by the producer or importer. The procedure for classifying new substances is given in Annex V of Directive 67/548/EEC. The Annex I contains literature references and data banks with limit values, including references [7–9].

Most of these substances are able to cause fibrogenesis and allergic diseases; beryllium, its compounds and vanadium chloride are carcinogenic. The systematic contact with metallic powder aerosols leads to occupational diseases.

A danger level of metallic dusts for human health depends on chemical composition and their oxidation level, particle size, concentration, action duration, penetration routes into organs, presence of impurities, etc. By means of suitable control, the dust concentration in workplace atmospheres must be maintained below TLV level.

Table 24.9 gives the main data about biological influence of metallic powders on humans [6].

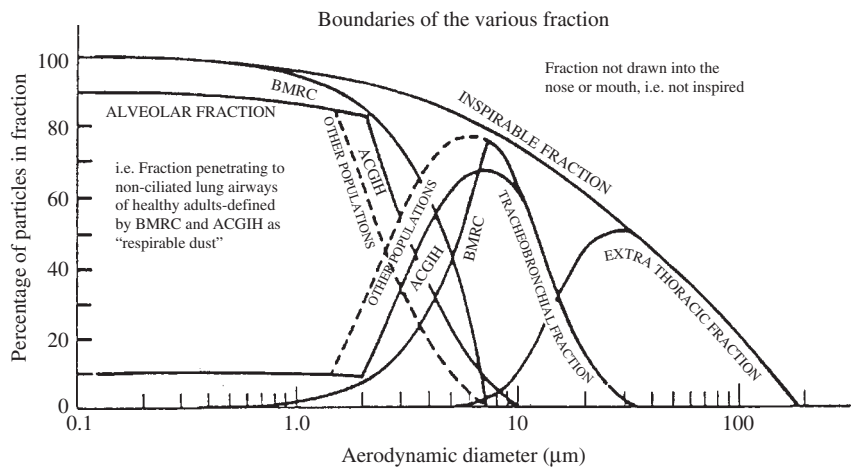

Figure 24.2 Recommended values of size ranges for occupational and environmental health related air sampling.

Table 24.8 TLVs values of harmful materials in workplace atmospheres

Substance	Phase state	TLV (mg/m^3)	Danger class
Aluminum oxide (alumina, electrolytically produced corundum)	Aerosol	6.0	IV
Aluminum alloys, on aluminum basis	Aerosol	2.0	IV
Antimony	Aerosol	0.5/0.2[a]	II
Arsenic non-organic compounds (on As basis):			
Arsenic content below 40 wt%	Aerosol	0.04/0.01	II
Arsenic content more than 40 wt%	Aerosol	0.04/0.01	I
Barium	Aerosol	6.0	IV
Beryllium and its compounds on beryllium basis	Aerosol	0.001	I
Bismuth	Aerosol	0.5	II
Cadmium	Aerosol	0.05/0.01	I
Cobalt	Aerosol	0.5	II
Copper	Aerosol	1.0/0.5[a]	II
Chromium oxide (on Cr^{+3} basis)	Aerosol	4.0	III
Chromate, bichromate (on Cr_2O_3 basis)	Aerosol	0.1	I
Lead and its inorganic compounds	Aerosol	0.01/0.06	I
Magnesium chlorate	Aerosol	5.0	III
Manganese oxides (on MnO_2 basis)			
mechanical grinded	Aerosol	0.3	II
condensation aerosol	Aerosol	0.05	I
Mercury metallic	Mist	0.01/0.006	I
Molybdenum metallic	Aerosol	3.0/0.5	III
Molybdenum silicide	Aerosol	4.0	IV
Molybdenum sulfide	Aerosol	6.0	IV
Nickel	Aerosol	0.05	I
Silicon dioxide by its contain in dust, wt%:			
>60	Aerosol	1.0	II
10–60	Aerosol	2.0	II
2–10	Aerosol	4.0	III
Titanium and its oxides	Aerosol	10	IV
Titanium sulfide	Aerosol	6.0	IV
Titanium tetrachloride (on HCl basis)	Mist	1.0	II
Thorium	Aerosol	0.05	I
Tungsten, tungsten carbide, tungsten silicide	Aerosol	6.0	IV
Vanadium and its compounds:			
vanadium oxide fume	Aerosol	0.1	I
vanadium oxide dust	Aerosol	0.5	II
vanadium containing slag dust	Aerosol	0.5	II
Zinc oxide	Aerosol	0.5	II
Zinc sulfide	Aerosol	5.0	III
Zirconium and its compounds:			
zirconium metallic	Aerosol	6.0	III
zirconium dioxide	Aerosol	6.0	III
zirconium nitride	Aerosol	4.0	III

[a]Numerator is the short-term maximum value; denominator is the average during shift value

Techniques for the Prevention of Exposure to Hazards

Common Demands to Production Area, Equipment and Processes

The workplace atmosphere parameters must be in conformity with the standards. The European Standard is related to the requirements of Directives 80/1107/EEC and 88/642/EEC. Commonwealth of Independent States (CIS) follows the GOST 12.1.005–88, GOST 12.1.003–83, and GOST 12.1.012–78.

For powder production there are no special requirements as regards buildings, constructions and production area with respect to air environment, harmful impurity contents, sonic level and vibration.

Table 24.9 Biological influence of metallic powders on humans

Material	Danger class	TLV (mg/m^3)	Influence on humans
Copper	II	1.0/0.5[a]	Disease of the breathing organs, cardiovascular system and gastrointestinal tract
Chromium anhydride, chromate, bichromate (on Cr_2O_3 basis)	I	0.1	It causes allergic rash and appearance of pits the on skin and nose cavity
Lead	I	0.01/0.005	It is toxic and tends to acute and chronic poisoning with lesions of many systems and organs of humans
Manganese oxides (on MnO_2 basis) mechanical ground	II	0.3	Toxic and causes acute and chronic poisoning with lesion of many systems and organs of humans
Nickel	I	0.05	Evidence of common toxic effect. It causes acute and chronic poisoning with pre-emptive lung lesions
Zinc oxide	II	0.5	Fever condition
Aluminium	IV	2.0	Moderate fibrogenesis and weak common toxic influence
Magnesium	IV	2.0	Moderate fibrogenesis and weak common toxic influence
Titanium	IV	10.0	Weakly toxic

[a]Numerator is short-term maximal value; denominator is average during shift value

The common recommendations for preventing and controlling exposure hazards [3] include:

For preventing exposure

- Change the process so that the operation is unnecessary
- Modify the process to eliminate the hazardous substances
- Substitute a less hazardous substance or the same substance in a less hazardous form.

For controlling exposure hazards

- Totally enclose the process
- Design the plant or system to operate so as to minimize generation of gravitational spills and, in the event of spills, minimize the area of contamination
- Design the plant to minimize powder transfers
- Provide for partial enclosure with local exhaust ventilation (aspiration)
- Provide for local exhaust ventilation
- Design the transfer units and local exhaust to minimize powder entrainment and suction rate
- Provide for sufficient general ventilation by dilution
- Reduce the number of employees exposed
- Exclude non-essential access
- Reduce the period of exposure
- Exclude contacts of powders with substances leading to oxidation, combustion or explosion
- Regularly clean contamination from walls, surfaces, etc.
- Provide for safe means of storage and disposal of hazardous substances
- Provide for adequate facilities for washing, changing, storage of clothing, including laundering of contaminated items

- Prohibit eating, drinking, smoking, etc. in contaminated items
- Where the above measures do not prevent exposure hazards or provide adequate control then, in addition, use suitable personal protective equipment.

Equipment, in which there are places in which explosive mixtures could form, must be equipped with a safety valve or diaphragm. Explosion parameters are basic data for the calculation of safety valves and diaphragms [10]. For apparatus and pipelines destined for liquid and gaseous toxic and explosive products, arrangements for blow-through must be provided.

In order to avoid entry of explosive or toxic gases from technological pipelines in water, air and steam communications, it is necessary to provide check valves or hydroseals. The apparatus and communications for toxic, combustible and aggressive liquids must have emergency capabilities permitting fully to remove liquids contained in them by self-flowing. It is necessary provide for techniques to eliminate the generation of a pressure in an enclosure or to minimize it, if the maintenance of overpressure is not conditioned by a technological requirement.

It is necessary to provide in the design of reloading units and local exhaust systems (aspiration) minimal powder entrainment and suction rate by decreasing the number and height of the reloadings and final velocity of the gravitational powder stream, elimination of the possibility of 'free pass' through the bins, and the provision for powder delivery through sealed feeders.

For powder loading by volume, facilities must be provided for preventing dust emission and, as a rule, without local exhaust ventilation by means of the tight sealing of loading units, and arrangements to ensure that the contaminated air from the loaded vessel is overflown in to discharged capacity are recommended.

In crushing and grinding equipment, in which overpressure and directed flows are formed, it is necessary to provide for tight sealing of charge and unloading units, eliminating aerodynamic connections with ambient air and conjugated equipment; along with this, for decreasing overpressure, the zones under such pressure are connected with underpressure zones by means of by-passes [10].

Surfaces of walls, ceilings and floors of production area and storage facilities must be smooth, with minimum quantity of ledges, and moisture-resistant, allowing wet mechanized cleaning.

Explosion and Fire Safety

The classification of production areas and buildings as regards explosion-fire and fire risk in the Commonwealth of Independent States (CIS) is defined according to Technological Designing Standard ONTP-24–86 [11]. The categories are determined for the most disadvantageous conditions subject to type of combustible substance and materials, their quantity, fire-danger and features of technological processes (Table 24.10). The category of risk is indicated by a letter – A(higher) down to D (lower).

The quantity of substances which come into production areas and can form explosive gas–air or

Table 24.10 Categories of production areas and buildings on explosion-fire and fire risk

Building category	Substance and material characteristics situated (circulating) in production areas
A (explosion-fire risk)	Combustible gas, highly inflammable liquids with flash temperature up to 28°C in such quantity that can form steam–air explosive mixtures by which ignition the calculated explosion overpressure in the building exceeds 5 kPa. The substance and materials able to burst and burn by interaction with water, air oxygen, or with each other in such quantity, that the calculated explosion overpressure in the building exceeds 5 kPa
B (explosion-fire risk)	The combustible dust and fibers, highly inflammable liquids with flash temperature above 28°C and combustible liquids in such quantity that can form air-dust or steam-air explosive mixtures by which ignition the calculated explosion overpressure in the building exceeds 5 kPa
V (fire-risk)	The combustible and difficult to combust liquids, solid combustibles, difficult to combust substances and materials (including dusts and fibers) and substances and materials able, by interaction with water, air oxygen, or with each other, only to burn in conditions that the buildings in which they are positioned or circulate, do not relate to categories A and B
G	Incombustible substances and materials in hot, glowing or fused condition in which processing is accompanied by emission of radiant heat, sparks and flame; burning gases, liquids and solid substances, which are burned or utilized as fuel
D	Incombustible substances and materials in the cold condition

steam–air mixtures, needs to be assessed, starting from a possible emergency on the basis of the largest amount of substances or materials which are the most hazardous with respect to explosion occurrence. In production areas where the emission of explosive gases or vapor in workplace atmospheres is most likely, it is necessary provide for automatic control of their content.

Thermoprocessing equipment is widely used for manufacturing non-ferrous metal powders. The safety of such equipment and also the controlled atmospheres often used as part of the manufacturing process are therefore of paramount importance to the PM technique.

The European Standard (EN 746) provides for the safety of persons and property during commissioning, start-up, maintenance periods and dismantling, as well as in the event of foreseeable faults or malfunctions which may occur.

Furnaces with annealing atmospheres must be equipped with a control system of a gas reburning torch which must prevent the spontaneous break and extinction of the torch; this system must be assembled with a gas supply system and emergency ventilation. Furnaces operating with hazardous atmospheres must also be equipped with a purging system, which is actuated (automatically as far as possible) in cases of danger, for example by decreasing hazardous atmosphere pressure, in order to bring the equipment to a safe condition by replacing the atmosphere with an inert gas.

As [3] shows, the European Development Centre, in Sheffield, UK, has available Material Safety Data Sheets (MSDS) for industrial gases and gas mixtures in printed form or on CD-ROM.

Quenching Means

As quenching means for combustible metallic powders, gases and liquids, fire-extinguishing refrigerants, powders and combined compositions are used. Typical physico-chemical properties of fire-extinguishing refrigerants which are used in the Commonwealth of Independent States countries are given in Table 24.11. The aliphatic hydrocarbons (alkanes) are the basis of the refrigerants.

Fire-extinguishing powders are finely ground mineral salts with various additions, obstructing caking. For the basis, the phosphorus-ammonium salts (mono-, diammoniumphosphates and ammophos), sodium carbonate and bicarbonate, sodium and potassium chlorides, and others are used. As additions the organosilicon compounds, metal stearates, nepheline, talc and others are used. A mechanism of the extinguishing effect is the inhibition of burning as a result of binding of chain reaction active centers. A heterogeneous recombination of these centers occurs on the powder surface as well as a homogeneous interaction of sublimation products with active centers.

The extinguishing ability of powders depends not only on the chemical nature of powders but on their fineness. The finer the powder particles are, the larger their surface, and the higher their effectiveness. However, the possibility of ultrafine powder production and use is restricted. Optimal particle sizes of commonly used powders range from 40 to 80 μm. Typical data about fire- extinguishing powders used in the Independent States countries are given in Table 24.12.

In combined compositions, the properties of several fire-extinguishing means are associated. The compositions which represent the combinations of a carrier with intense burning inhibition are the most effective. For example, aqueous-refrigerant emulsions and combinations of air-based foam with refrigerants related to them.

For voluminal quenching, nitrogen-refrigerant and carbon dioxide-refrigerant compositions have been developed. These compositions ensure a 4 to 5 times decrease in the specific rate of expensive bromine refrigerants. The composition containing 85 wt%

Table 24.11 Typical physicochemical properties of fire-extinguishing refrigerants

Physicochemical properties	CF_3Br	$C_2F_4Br_2$	CF_3Br
Refrigerant sign	13B1	114B2	12B1
Molecular mass	148.93	259.89	165.4
Temperature (°C):			
boiling point	−57.8	+47.5	−4.0
freezing point	−168.0	−11.5	−160.5
Steam pressure at 20°C (kPa)	1480	38	266
Density of liquid (g/cm^3)	1.575	2.18	1.83
Viscosity at 20°C (Pa·s)	160	762	520
Self ignition temperature (°C)	695	542	...
Fire-extinguishing concentration (kg/m^3)	220–250	195–220	255
for petroleum product (vol%)	(14–16)	(9–10)	(14)

Table 24.12 Fire-extinguishing powders

Powder trademark[a]	Main component	Area application (Fire class)	Fire-extinguishing ability (kg/m^2)
ПСВ-3	Sodium bicarbonate	BCE	1.6
ПФ	Diammonium phosphate	ABCE	1.4
ПС	Sodium carbonate	D	40
П-2АП	Ammophos	ABCE	1.8
Пirant A	Ammophos	ABCE	1.8
ПГС-М	Mixture potassium and sodium chlorides	BCD	26D 1.4BC
CI-2	Silicagel saturated by 114B2 refrigerant	D (metal-organic compounds and metal hydrides)	20–32D 0.2B
PC	Swelling graphite	D (potassium alloys sodium alloys)	6.0 9.0
МГС	Graphite with lowered density	D, for sodium for lithium	3.0 10.0

[a]Data about fire-extinguishing powders used in Independent States countries; ; Fire classes: A – combustion of solid matters; B – combustion of liquid matters; C – combustion of gaseous matters; D – combustion of metals and metal-containing matters.

carbon dioxide and 15 wt% 114B2 refrigerant is especially advantageous. The reciprocal solubility of components in the ratio cited in the condensed state contributes to its merits. For this reason, the possibility of joint composition storage is simplified and the cost of using it is reduced.

By voluminal quenching, the calculated composition weight m (in kg) amounts to:

$$m = KVq_n \quad (1)$$

where K is the coefficient taking into account the unsealed production area; V is the volume of production area, m^3; q_n is the supply rate of quenching composition amounting to 0.27 kg/m^3 for supply duration $\tau = 30$ s and 0.4 kg/m^3 by $\tau = 60$ s.

Recomended quenching means are given in Table 24.13 with the parameters being taken as reference values.

The most effective quenching means for alkaline metals are МГС and ПС powders and voluminal quenching by means of gaseous mixture nitrogen and carbon dioxide. The best quenching compositions for alkaline-earth metals are ПГС-М powders and argon for voluminal quenching. For polar hydrocarbon liquids (alcohols, acetone, either, etc), the best quenching means for large spillages are water spray, foam and ПСВ powder and, for small fires, water and carbon dioxide. The most effective quenching means for hydrogen and hydrocarbon gases, including liquefied gases, are cooling by water and voluminal quenching.

For fire quenching on combustible gas supply systems, high pressure water, inert gas, steam or air delivery provides for flame break followed by filling the system with inert gas.

Isolation of Powder-gas Emissions

Aspiration involves isolation of the powder–gas emission origin, removal of these emissions via an exhaust and separation of particles from aspirated gas before its ejection into the environment. It is also possible, in certain conditions, that aspiration can provide heat removal and prevent overheating of the material being processed.

There are open-loop and closed-loop aspiration systems. The latter is much more complicated and requires the provision of protective gas and a leak-tight construction. Resort to closed-loop systems in the case of suspended solid with low values of LCIL and LOC is favorable.

Dust or harmful gases formed as a result of mechanical and thermal processes or chemical reactions in the equipment and aspiration covers flow out when overpressure arises in non-hermetic systems. The main processes responsible for such pressure formation are the following:

- Dynamic interaction of particle gravitation flow with the gaseous medium causes ejection pressure, p_e
- When closed chambers and volumes are filled with particulate materials, excess pressure, p_v appears as a result of a decrease of the empty volume and redistribution of pressure in the loading apparatus as ejection pressure acts
- In equipment with moving parts, a high peripheral velocity excess pressure, p_{eq}, arises and directed air flows result
- As a result of heat exchange during the processing of heated materials, the density of gaseous

Table 24.13 Recommended quenching means

Quenching means		Substances and materials							
Composition	Parameters	NP-HCL	P-HCL	H-CM	HC-G	Hydrogen	AM	AEM	AOrg
Water	I (L/(m^2· s)) τ = 30–60 minutes	0.2	0.25	0.2	0.1d	0.08d	...	...	0.3
Air-mechanical mean multiplicity foam	I(L/(m^2· s)) τ = 30–60 minutes	0.08	...	0.05	...	...	...	...	...
Voluminal quenching									
Carbon dioxide	G (kg/m^3), τ = 2 min	0.7	0.7	0.7	...	...	...	12[i] τ = 2–5	...
Refrigerants[a]	G (kg/m^3), τ = 0.2 min	0.22[b]	0.22	0.22[c]	0.32 τ = 0.5	1.16 τ = 0.5	...	...	...
85 wt%CO_2+15 wt% $C_2F_4Br_2$ (CF_3Br)	G (kg/m^3) τ = 0.5 min	0.27	0.27	0.27[c]	0.4	0.57	... 2.0–2.5[f] τ = 0.5–5.0	...	...
Powder									
ПСВ-3	G (kg/m^2)	0.66	0.66	...	4.0[e]	...	...	...	...
П-2АП,	G (kg/m^2)	0.89	0.89	0.4	5.0[e]	...	...	...	...
Пirant A,		0.65	0.65	0.31					
ПФ		0.47	0.47	0.23					
ПГС-М,	G (kg/m^2)	...	...	...	...	...	...	15–50[j]	...
ПС,		...	...	...	...	...	40–60	...	...
МГС,		...	...	...	...	...	10[g]	...	...
РС,		...	...	...	...	...	9[h]	...	...
ПФК		...	...	...	...	...	...	100[k]	...
СІ-2		...	...	...	...	...	...		20–32

Symbols: I is supply rate of quenching means; τ is quenching time; Substances and materials: NP-HCL is non-polar hydrocarbon liquids (including petroleum products); P-HCL is polar hydrocarbon liquids (alcohols, acetone, ether, etc); H-CM is hard carbonic products; HC-G is hydrocarbon gases, including liquefied gases; AM is alkaline metals (sodium, potassium, etc); AEM is alkaline-earth metals (magnesium, aluminum, etc); AOrg is organoaluminum compounds. Quenching compositions: [a]114B2 and 12B1 refrigerants; [b]G = 0.37 kg/m^{3}for work categories A and B; [c]for glowing materials the G is increased to twice; [d]for cooling the equipment adjacent to burning centre; [e]powder rate on 1 kg of effluent gas; [f]mixture 94 vol% nitrogen and 6 vol% carbon dioxide; [g]for quenching of sodium and lithium; [h]for quenching of sodium and sodium-potassium alloy; [i],argon; [j]for quenching of magnesium and aluminum; [k]for quenching of calcium and beryllium by means of calcium fluoride powder (ПФК)

Source: *Fire and explosion risk of substances and materials and quenching means, Handbook,* Ed. Baraov, A.N., Korolychenko, A.J. Chemija Publishers, Moscow, 1990

media in the equipment and covers differs from the density of the surrounding air and, hence, the pressure of the gaseous medium is redistributed: heat pressure p_t appears

- Mass transfer as a result of chemical transformations or vaporization causes pressure p_{mt}.

Ejection Pressure p_e

During the movement of particulate materials in closed chutes of non-hermetic units, a directed flow of ejected air is created. This is typical for numerous operations: reloading from one conveyor to another, feeding of materials by conveyors into units, and discharge of material from units onto conveyors or into adjacent equipment.

During transportation of powder, it is necessary to provide sloping chutes with minimum inclination (under conditions of powder motion), in order to decrease harmful emissions.

The interaction with air of the surface of moving powder on the bottom chute is described by the equation [12]:

$$F\sum \zeta v_2^2 \rho_2 = \int_0^l c_\tau b|v_1 - v_2|(v_1 - v_2)\rho_2\, dx \qquad (2)$$

where F is the square of the chute cross-section, $\sum\zeta$ is the sum of local resistance to motion of the ejected air, v_1, v_2 are velocity of movement, c_τ is the coefficient of dynamic interaction of the surface of the moving powder with gaseous medium/air, b is the width of the chute, l is the length of the chute, ρ_2 is air density; here and below by subscript '1' the magnitudes characterizing the material movement are denoted, and by subscript '2', the air.

The left part of the above equation shows the resistance force to the ejected air motion, while the right part describes the force causing this motion as a result of interaction between the moving material free surface and the gas medium. With the decrease of v_1, l and b and the increase of $\sum\zeta$, the force causing ejection decreases, as well as the ejected air rate and, therefore, the value of the required suction capacity L_a. The decrease of v_1 and l is achieved by a decrease of the overfall. Decrease of v_1, as was noted, is also possible at the expense of the sloping chutes with minimum inclination (under conditions of powder movement), however, as a result, Fv_2 is decreased, since Fv_2 depends more strongly on v_1, than on l.

The aspiration cover with double walls (Figure 24.3) has an aerodynamic advantage. Such a design ensures the removal of the overpressure focuses from leak-stop-sealing systems and equalizes pressures on the inner surface of the outer walls of the aspiration

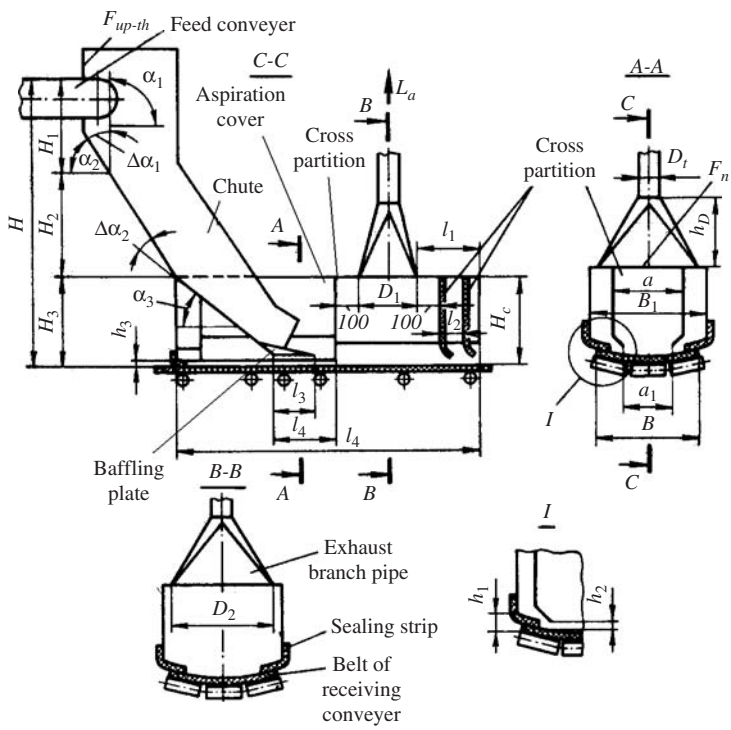

Figure 24.3 Diagram of the belt conveyor reloading unit.

covers. Typical parameters of the belt conveyor reloading unit are given in Table 24.14.

Reloading units that maintain powder in quasi-interconnected motion condition unchanged during changes in powder-consumption rate have been designed. These units achieve a considerable decrease of the free powder surface during powder gravitation flow for interaction with the gaseous medium. Such conditions are achived in chutes in the form of a three-edged prism with one of the ribs directed down [12,13].

The use of such a device during processing of metallic powder decreased aspirated air consumption by 1.7 to 2.3 times and reduced powder loss by 2.5 to 3 times [5].

Overpressure in Closed Chambers

When closed chambers and volumes are filled with particulate material, excess pressure p_Σ appears as a result of a decrease in the unoccupied volume p_v and redistribution of pressure in the loading apparatus as ejection pressure acts:

$$p_\Sigma = p_v + p_e \tag{3}$$

Diagrams of various filling units are shown in Figure 24.4. In the case where a closed sagger is filled from a pressurized batcher (Figure 24.4(a)), during the process the forced out air is displaced, moves in the chute and further through the powder layer in the consumed volume. Then, in the chute, at the site of its junction with the consumed volume, the maximum pressure corresponds to pressure p_v necessary for overcoming the powder layer resistance to forced out air flow:

$$p_v = G_1 g \rho_2 H_m / K_f \rho_1 F_m \tag{4}$$

where G_1 is a material mass flow during sagger filling (kg/s), ρ_1 is the material density (kg/m^3), H_m is the highest material level in the consumed volume

Table 24.14 Typical parameters of the belt conveyor reloading unit

B	B_1	a	a_1	H_C	l	l_1	l_2	L_3	l_4	h_1	h_2	h_3
400[a]	520	300	280	300	1400	250	100	200	400	2.5δ	1.5δ	3.5δ
500	650	375	350	380	1500	250	100	250	500	2.5δ	1.5δ	3.5δ
630	820	485	455	500	1820	325	100	330	630	2.5δ	1.5δ	3.5δ
800	1040	600	560	600	2200	400	100	400	800	2.5δ	1.5δ	3.5δ

[a]All dimensions are given in millimeters, δ is the belt thickness

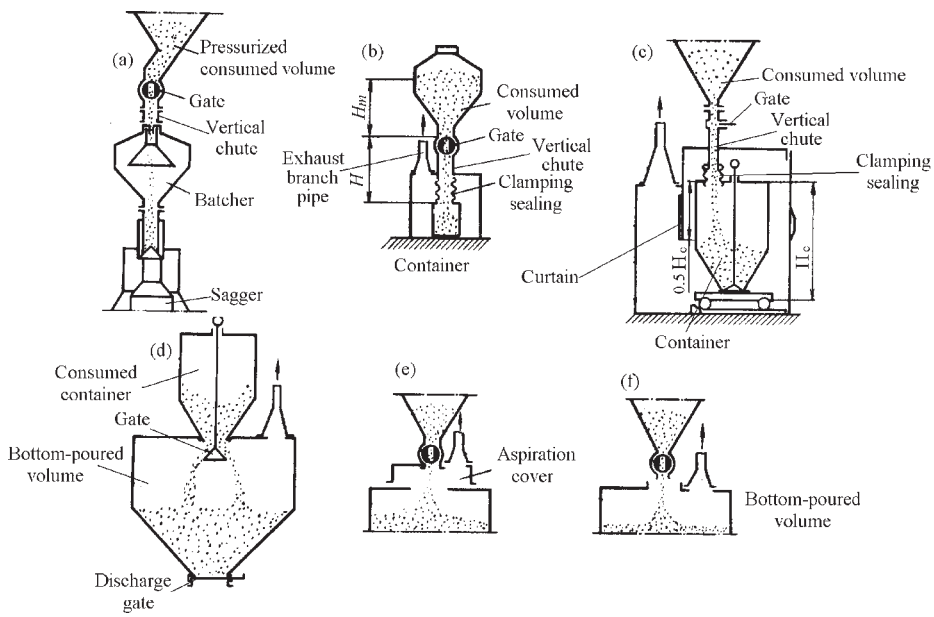

Figure 24.4 Diagrams of various filling units: (a) closed sagger filled from pressurized batcher; (b) and (c) loading of container in cabin type aspiration covers; (d) bottom-poured volume from container; (e) (f) loading of movable containers.

(m), F_m is the horizontal square occupied by material in the consumed volume (m^2), K_f is the filtration coefficient whose values are given in the Directive for designing and computation of aspiration in metallic powder production including combustible and explosive material [14].

At the inlet to the chute, the site of its joining the consumed volume, the overpressure is minimal:

$$p_{\Sigma_{min}} = p_v \tag{5}$$

while, at the outlet end, the sagger entrance, the summarized pressure amounts to

$$p_{\Sigma_{max}} = p_v + p_e \tag{6}$$

$$p_e = 145\psi G_1 \rho_2 v_{1_k}^3 (gF\rho_1 d_a)^{-1} \tag{7}$$

where ψ is an aerodynamic resistance coefficient of the particles, v_{1k} is the material velocity in the chute outlet and d_a is the average particle size.

A design for joining and the sort of sealant material are selected depending on the value of $p_{\Sigma max}$.

In the case of non-hermetic receiving volume, the required suction capacity is determined by the equation

$$L_a = L_v + L_n \tag{8}$$

where L_v is the air flow displaced from the receiving volume during filling, L_n is the air flow which is sucked through the non-compactnesses in the receiving volume or aspiration cover. The value of the discharge coefficient through the openings amounts to 0.65:

$$L_n = 3300F_n(p_c/\rho_2)^{0.5}, m^3/h \tag{9}$$

where p_c is the normalized underpressure in the cover (Pa).

In case of the suction connected directly to the loading volume (see Figure 24.4(e)), the required suction capacity L_a, must be calculated subject to the flow rate value ejected by powder gravitation flow.

To decrease p_v in powder-filled chambers, pressurized chambers and loading devices should be used. At the same time, if suction is connected to the casing of the charging unit (but not to the volume being loaded), the influence of p_e on the required suction capacity L_a, is absolutely excluded, because $\Sigma\zeta \to \infty$. Using pressurized chambers and loading devices, the air being displaced as a result of the powder coming is realized best by means of the by-passes connecting the bottom-poured vessel with the receiving one, or a combination of a discharge nipple with the ejection exhaust (Figure 24.5).

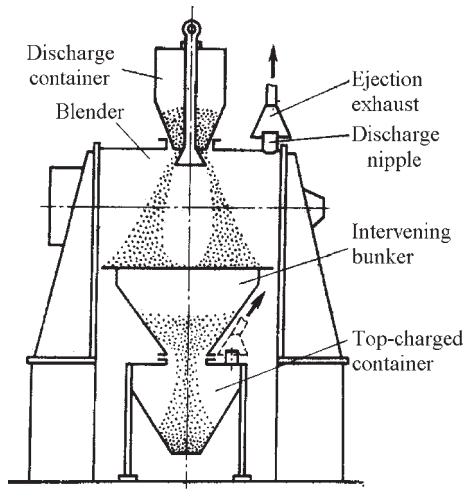

Figure 24.5 Diagram of the feeding and unloading of a blender.

Pressure Created by Equipment Moving Parts

The most effective means of eliminating the action of excess pressure p_{eq}, created by moving parts, is pressurized filling of loading and unloading units, isolated from the environment and from other equipment. Pressurized packing should withstand maximum pressure. By-pass pipes should be used to discharge excess pressure. They should connect zones of overpressure with underpressure zones.

The maximum pressure p_{eq}, created by moving parts of a hammer crusher (Figure 24.6), is determined from the equation:

$$p_{eq}^* = c_h \left(1.5\frac{c_m G_1}{c_h \rho_1 d_a} + nF_{h1}\, i\right)\frac{\rho_2 l_R}{4F}\,\overline{v} \tag{10}$$

where c_h is the coefficient of dynamic interaction of the rotating parts with air, G_1 is a material mass flow, c_m is the coefficient of dynamic interaction of the particulate material with air in the crusher chamber, ρ_1 is the material density, d_a is the root-mean-square diameter of material after collision with hammers and bumper slabs, $F_{h\cdot l}$ is the sum area of one row of rotating parts, F is the cross-section of the hammer body, in which the parts revolve (the section is orientated normally to root-mean-square air velocity vector in the inner crusher), n is the rotation velocity of hammers, l_R is the trajectory length of the active part rotor center diameter D_{ac} from the material entrance site in hammers action zone and the end of the separation grate, i is the

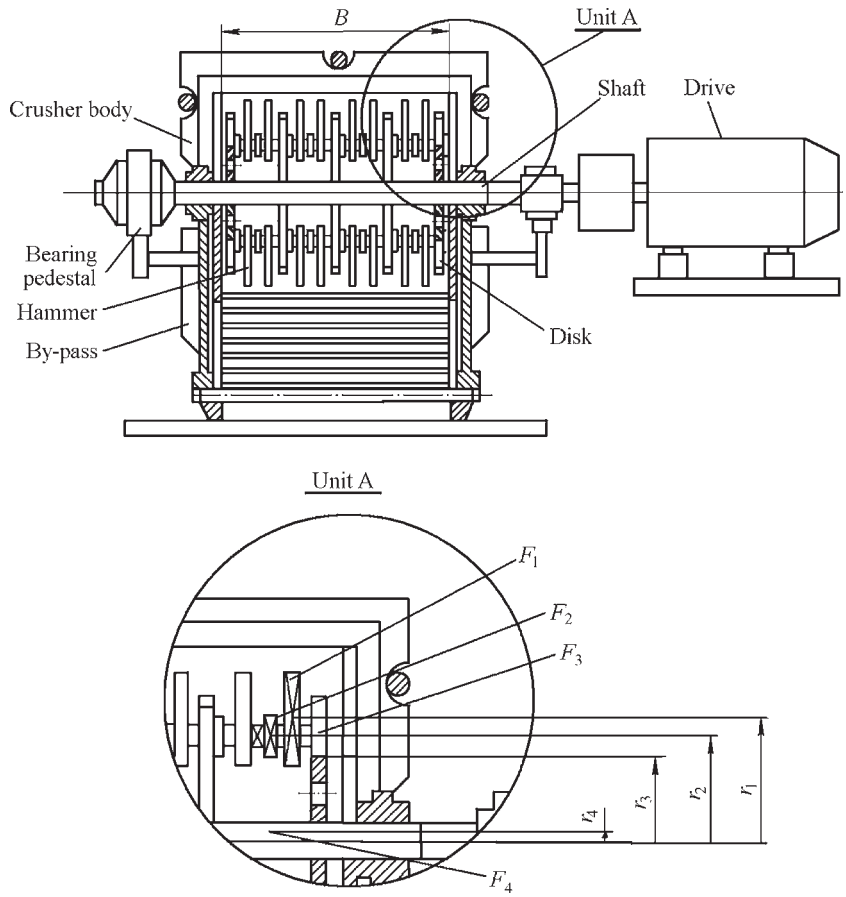

Figure 24.6 Hammer mill with built-in by-pass pipes.

number of hammer rows, $\bar{v}$ is the root-mean-square peripheral velocity of the active rotating parts D_{ac}

$$D_{ac} = \frac{2\sum_{i=1}^{n} F_{ha} \times r}{\sum_{i=1}^{n} F_{ha}} \qquad (11)$$

where r is the distance from the hammer mill axis to the mass center of the corresponding constituent of the active rotor parts; F_{ha} is the constituent cross-section area of the active rotor parts.

In crushing conditions, in comparison with idle running, the created pressure is appreciably higher.

Heat Pressure p_t

In equipment bodies and aspiration covers, the gaseous medium pressure is redistributed if its density differs from the environment as a result of heat exchange during processing of the elevated temperature materials. The value of p_t is determined by the equation

$$p_t = 0.5g(\rho_{2_{env}} - \rho_{2_{r.v}})H \qquad (12)$$

where $\rho_{2_{env}}$ is the density of the environment medium, $\rho_{2_{r.v}}$ is the density of the gaseous medium in the lower aspiration cover, H is the maximum value of the difference between the apparatus (cascade) cross-sections levels which are aerodynamically connected.

Pressure p_{mt} – mass transfer result

Pressure p_{mt} arising from the mass transfer is the result of chemical transformations or vaporization. Overpressure originating in pressurized capacity

during phase transfer with gas (vapor) volume yield, J (kg/(m^3 · s)) with density ρ_2 (kg/m^3) during τ (s) may be represented as follows:

$$p_{mt} = (p_{mt_\tau} - p_{mt_0}) = p_{mt_0}(e^{J\tau/\rho_2} - 1) \quad (13)$$

where p_{mt_τ} and p_{mt_0} are the pressure in pressurized capacity at τ and the starting moment, respectively.

Capacity of Local Suctions

In practice, one of the above mechanisms may function independently but, more often than not, they occur in combination.

The mass balance equation is the initial one for determination of the required suction capacity:

$$\sum_{i=1}^{N} L_{a_i} = \sum_{j=1}^{n} L_{d_j} \quad (14)$$

where L_{a_i} and L_{d_j} are air flow arriving in the cover through j-th channel (chute, opening) and receding from cover by i-th suction (or going off through i-th channel), respectively.

The value of the gaseous component deleted is determined by the difference of pressure and hydraulic resistance of the channel or openings. Generally, by the simultaneous action of several of the above mechanisms

$$L_c = F_c\sqrt{\frac{2p_e - p_t \pm p_{eq} + p_v + \Delta p}{\rho_2 \sum \zeta}} \quad (15)$$

$$L_n = \sum_{i=1}^{n} F_{o_i}\sqrt{\frac{2p_c}{\zeta_i \rho_2}} \quad (16)$$

where $\sum\zeta$ is a sum of resistance coefficients to gaseous component motion, ζ_i is the resistance coefficient of i-th opening to suction air, p_c is a normalized underpressure in aspiration cover, Δp is a pressure difference determined by action of local exhausts, F_{o_i} is the area of i-th opening.

If gas emission occurs and its density differs from that of the gas filling the unit, it is more convenient to operate by flow mass values G_a but not by the volumes of aspiration gas. In the case when pressure arises only as a result of gas emission

$$G_a = \sum_{i=1}^{n} F_{o_j}\sqrt{\frac{2p_c\rho_{2_{en}}}{\zeta}}\,\frac{(1+m_c)}{(1+m_{en})} \quad (17)$$

where m_c and m_{en} are the emission gas content in cover and environment, respectively.

Aspiration in Combustible Powder Conditions

Aspiration for controlled heat removal, to prevent excessive heating of the processed material, can be used in conditions of material grinding with relatively high energy activation of the oxidation reaction (50–60 kJ/mol and higher). The critical temperature $t_{1_{cr}}$ of the ground material coming from the mill is considered to be that at which glowing particles appear in them. In [15], the heating process of the material during milling is described and an account of $t_{1_{cr}}$ is given.

During mechanical processing of materials with low energy activation values, fire and explosion safety can be ensured by the use of controlled protective atmospheres.

The method for production of powders, granules and briquettes of chemically active metals and their alloys is described in [16]. This technique comprises the comminution of initial bulky material in a shielding gas over a film-forming composition, followed by sieving size classification, blending and subsequent compacting (Figure 24.7).

This processing line includes a vibro jaw crusher unit (A) (in this flowchart the unit boundaries are marked by dotted lines), cone inertia crusher unit (B), vibro size separator unit (C), vibro blender unit (D), briquetting press unit (E), film-forming composition generation unit (F) and closed-loop shielding gaseous change system (Q). Each unit is developed as autonomous with cascade equipment location and is connected with the delivery and returning pipes by means of pipe-bends. The transportable containers (Figure 24.8) serve the consumed volumes. The containers are equipped with a gas distributing design and a by-pass which lets in the controlled protective atmospheres.

The introduction of a film forming composition comprises an organosilicon compound and surfactant and increases the explosion safety, capacity and finished powder yield [17]. Reducing the dust-like powder fraction emission by means of film formation contributes to increased explosion safety. During the comminution, the film forming composition covers the freshly formed surface of the particles and dust-like fractions form particle aggregates. By means of the available controlled comminution process parameters, it is possible to obtain powders with specified improved properties. Table 24.15 shows typical conditions of process parameters choice in

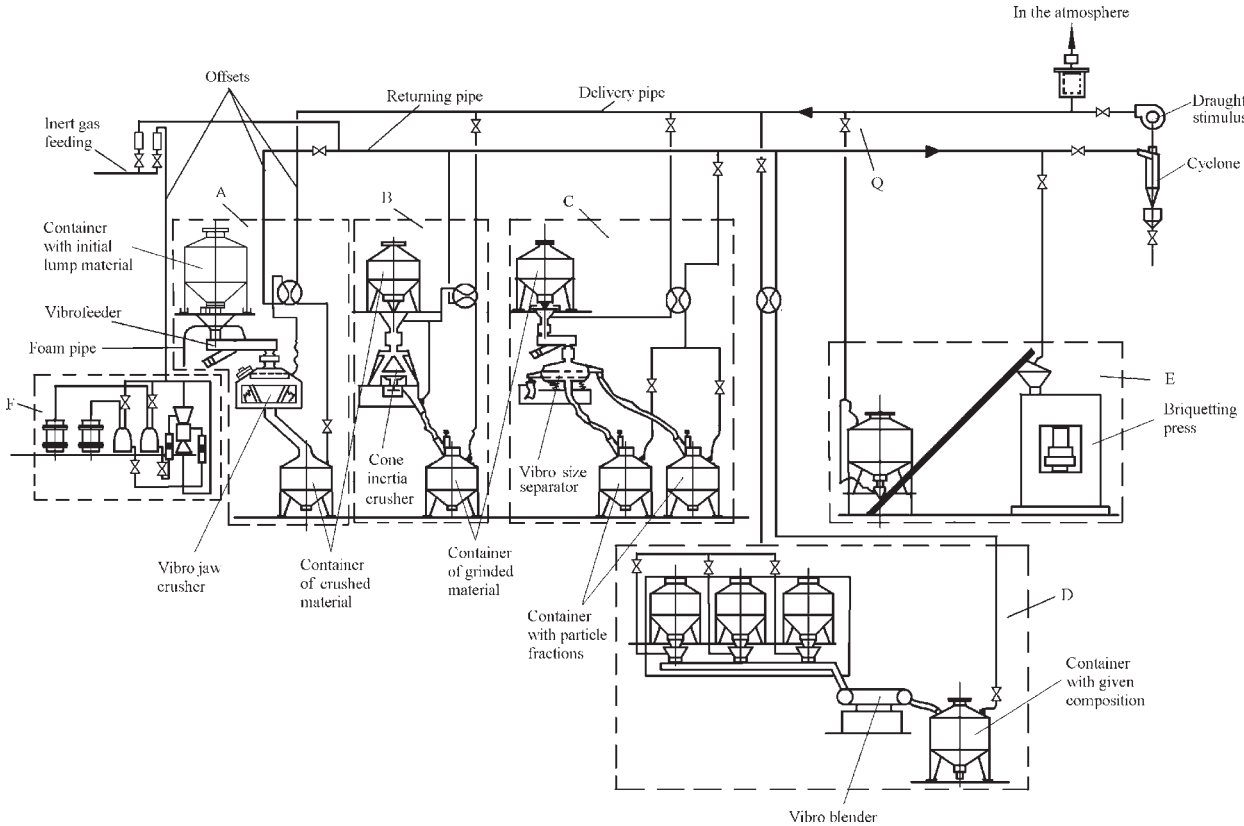

Figure 24.7 Flowchart of the process of production of powders, granules and briquettes of chemical active metals and their alloys.

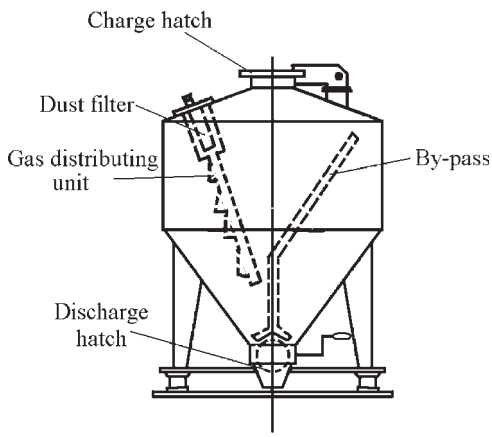

Figure 24.8 Transportable container.

silicocalcium powder production. As is shown, the treatment of the initial particulate material by the organo-silicon compound and surfactant ensures increasing the finished powder yield, decreasing the temperature of the ground material and explosion safety improvement.

In the given case, the acceptable size fraction yield ranges from 1.0 to 0.05 mm with improved explosion safety and capacity. The developed technique (see Table 24.15) allows such requirements to be met.

Melt Atomization Units

An aspiration cover over an induction melting furnace in the form of a housing located above the crucible and hinged to the furnace frame and exhaust duct (Figure 24.9) is recommended. Such a design ensures cover location above a dust-gas emission source in whatever furnace position, and highly effective aspiration during the whole technological cycle, including melt preparing and pouring [18]. Melt pouring into the tundish is shown in Figure 24.10.

Typical data of dust concentration and volume of aspiration gas from induction furnaces are given in Table 24.16.

Table 24.15 Process parameters of choice for silicocalcium powder production

FFC (wt%)	G_m (kg/h)	T_m (°C)	Dust content g/m^3		Particle size (mm)			Fraction content (wt%)		Explosibility	
			C_1	C_2	+1.0	−1.0 +0.4	−0.4 +0.1	−0.1 +0.05	−0.05	LCIL (g/m^3)	LOC (vol%)
0.0	230	80	6.29	16.6	9.9	24.1	30.2	15.3	20.5	150	14
0.2	418	45	6.09	13.3	11.2	34.1	24.3	18.2	12.2	370	14
0.3	969	35	5.29	4.55	9.3	37.3	29.5	16.3	7.6	400	16
0.5	983	35	4.70	1.15	0.5	57.0	21.2	15.5	5.8	400	16
0.6	971	45	4.40	1.87	1.1	44.7	29.7	19.3	5.2	400	16

FFC is the film forming composition content, G_m, is the finished powder yield, T_m is the temperature of powder on discharge from cone inertia crusher, C_1 is the dust content in air of aspiration cover of the vibro jaw crusher, C_2 is the dust content in air of aspiration cover of the cone inertia crusher, LCIL is the low concentration ignition limit. LOC is an oxygen explosion-proof content of nitrogen in gas-diluted protective atmospheres.

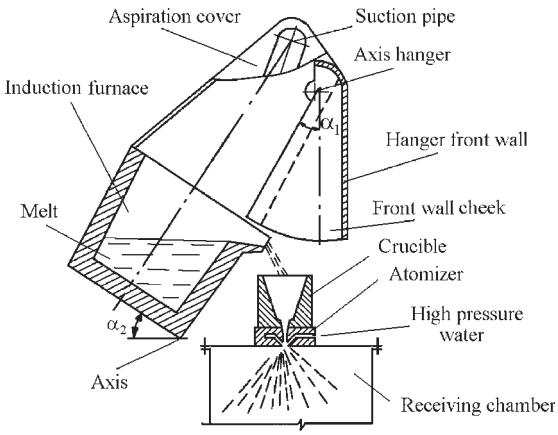

Figure 24.9 Aspiration cover of an induction melting furnace.

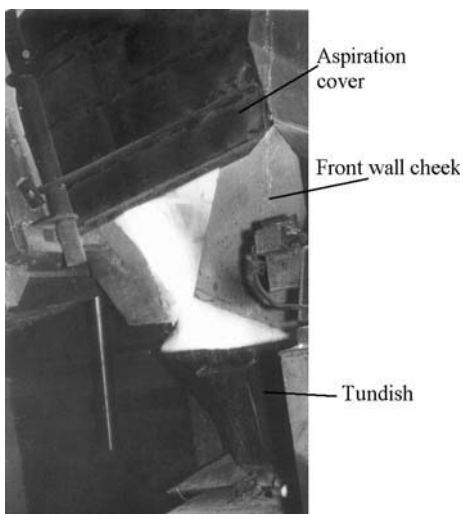

Figure 24.10 Position of the aspiration cover during melt pouring into tundish.

Grinding Units

During the operation of some kinds of equipment pulsating motion occurs. For example, in drum mills, pulsations can appear as a result of displacement of milled bodies. In such cases, dust emissions are effectively localized through the employment of covers with inside and outside chambers [19] (Figure 24.11).

The use of such devices [20] during grinding copper shot in tumbling mills (Figure 24.12) decreased the required suction capacity L_a by 1.3 times in comparison to ordinary aspiration covers and powder loss to the aspirated air was decreased by 7 times.

Definition of the Local Exhaust Capacity

Aspiration During Particulate Material Reloading in Closed Gravity Chutes

Unsealed and pressurized reloading units are distinguished. To decrease the dust emission, air exhaust capacity and loss of the particulate material, the following are recommended:

- to provide sloping chutes with minimum inclination (that allows material movement); it is necessary to avoid the vertical end of the chute leading to the entrance to the cover of the receiving unit
- to maximize the decrease in the fall height of the gravitational material flow; in case of necessity, the turns in vertical flat (Figure 24.13) perform according to scheme (a), but not scheme (b)

Table 24.16 Dust concentration and volume of aspiration gas from induction furnaces

Induction furnace type (ISC)	Powder commercial grade (ISC)	Aspiration gas volume at 40°C (m^3/h)	Average dust concentration (mg/m^3)
Copper powder[w]			
IST – 0.16[a]	PMR[b]	1000	2.7
ILK – 0.4[c]	PMR	3000	7.0
IST – 0.4	PMR	3000	7.0
IST – 1.0	PMR	4500	18.0
Brass powders[w]			
IST – 0.16	PLS – 60[d]	1100	9.0
ILK – 0.4	PLS – 60	3000	31.0
IST – 0.4	PLS – 60	3000	31.0
IST – 1.0	PLS – 60	5000	72.0
Bronze powders			
IST – 0.16[w]	Cu–5Sn–5Zn–5Pb	1100	3.4
ILK – 0.4[w]	Cu–10Sn	3000	10.0
IST – 0.4[w]	Cu–5Sn–5Zn–5Pb	3000	10.0
IST – 1.0[g]	Cu–10Sn–0.3P	5000	9.0
Aluminum powder[g]			
IAT – 0.4	PA-5[f]	4000	12.0

(ISC) Independent States Countries grades; [a]IST imply a crucible induction furnace, while the quantity – metric ton capacity of charge with iron; [b]water atomized powder; [c]ILK imply a channel induction furnace; [d](30 ± 1)Zn; [e]the quantity – metric ton capacity of charge with aluminum; [f]99 wt% Al; [w]water atomized powder; [g]gas atomized powder.

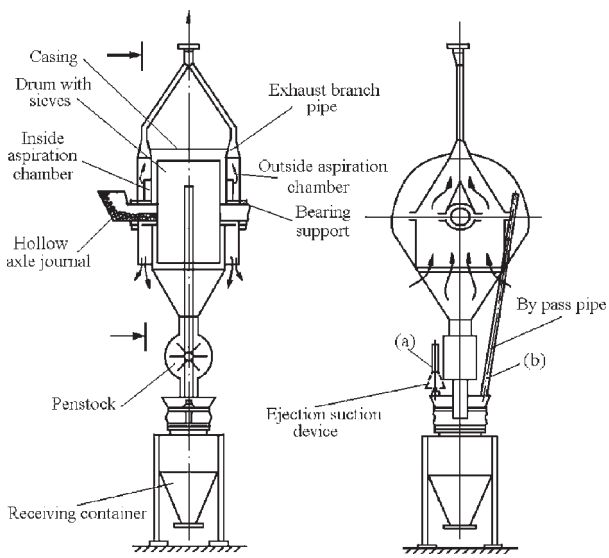

Figure 24.11 Aspiration of the ball mill with peripheral milled powder discharge. Modifications: (a) with ejection suction device; (b) with by-pass pipe. Source: Ref 17

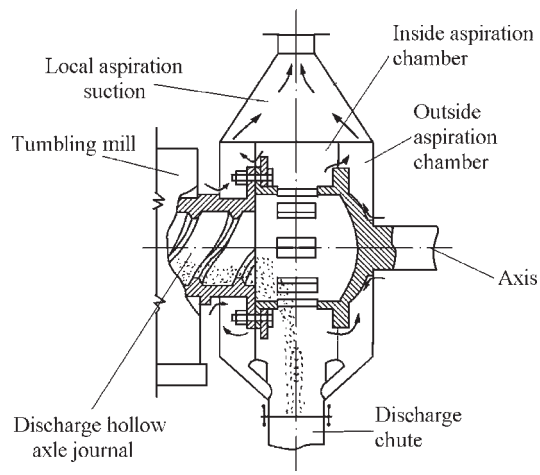

Figure 24.12 Discharge unit of a tumbling mill.

- the aspiration covers of the belt conveyer loading locations perform with double walls (see Figure 24.3) for various particulate materials, or with single concave walls (Figure 24.14) mainly for powder reloading
- in the case of powder reloading, the chutes are rather in the form of a three-edged prism with one of the ribs directed down (Figure 24.14)
- in the case of the pressurized receiving volume capacity, the local exhaust must be attached to the feed conveyer unloading heading cover
- the air velocity in the exhaust branch pipe opening attached to the conveyer cover which

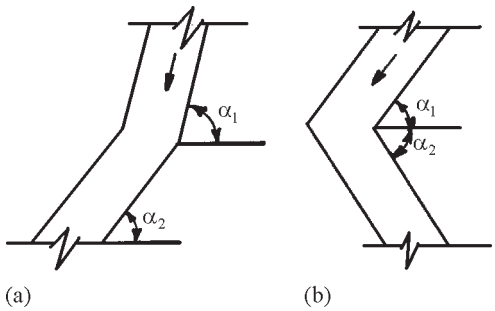

Figure 24.13 Scheme of the chute turns in vertical flat.

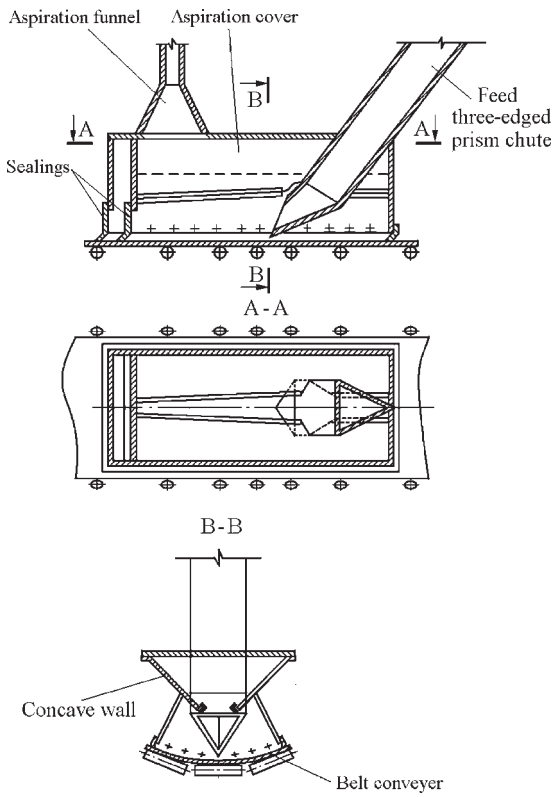

Figure 24.14 Receiving belt conveyer cover with single concave walls.

is acceptable for materials with average particle sizes in the range from 0.2 to 3 mm by $\rho_1 \geqslant 2000\,kg/m^3$ and average particle sizes in the range from 0.2 to 7 mm by $\rho_1 \geqslant 1200\,kg/m^3$ at most 1 m/s; for materials containing particles with diameters of to 0.3 mm and above with 50% of maximum size particles 3.0 mm with ρ_1 ranges from 1200 to 4500 kg/m^3 and with $\rho_1 > 4500\,kg/m^3$ up to 0.4 and 0.7 m/s, respectively.

The determination of the local exhaust device comprises following steps:

1. For the local exhaust definition the initial data given in Table 24.17 and basic calculated magnitudes (Table 24.18) are used.
2. The entrance rate into the receiving apparatus cover v_{1f} is calculated by means of step-by-step definition of rates for rectilinear chute lengths over formulas or nomogram (Figure 24.15).

   For the vertical initial length

$$v_{1v,i=1} = \sqrt{19.6H_i} \tag{18}$$

   for the incline lengths

$$v_{1ch,i} = \sqrt{(v_{1f,i-1}k_{tn})^2 + 19.6H_i(1 - 0.9f_{fr}\,\mathrm{ctg}\alpha_i)} \tag{19}$$

   where $v_{1f,i}$ is the material moving rate at the end of the chute's previous length, m/s; f_{fr} is the friction coefficient of particulate material moving along the steel bottom chute (it is accepted to be 0.625 for coarse and 0.9 for fine powders); k_{tn} is the rate reduction coefficient of material flow turn (due to change of the inclination of the chute), the magnitudes of which are given in Table 24.19.
   The initial material rate on the first chute length, on feed conveyer level is taken to be equal to zero.
3. The average diameter of the material particles is given by the formula

$$d_m = 0.01\sum_{i=1}^{n} d_i m_i \tag{20}$$

   where d_i is the average diameter of particles in the *i*-interval, mm; m_i is the mass part of particles in *i*-interval, wt%; *n* is number of intervals.
4. The sum of the local resistances to the covers and chute $\sum\zeta$ is determined from the equation

$$\sum\zeta = \zeta_{en} + \zeta_{ch} + \zeta_{par} \tag{21}$$

   The size of ζ_{en} is calculated from the formula

$$\zeta_{en} = 2.4\,(F_{ch}/F_{n.f})^2 \tag{22}$$

   For vertical chutes $\zeta_{ch} = 1.5$; for the inclined chutes and chutes with turns $\zeta_{ch} = 2.5$.

Table 24.17 Initial data for the definition of the local exhaust capacity of particulate material reloadings on closed gravity chutes

Parameter	Symbol	Unit	Note
Material mass flow	G_1	kg/s	
Density of the material	ρ_1	kg/m^3	
Temperature of the material	t_1	°C	
Granule composition	$g/(d)$	%	
Belt width of receiving conveyer	B	m	see Figure 24.3
Material fall height from feed conveyer to entrance to the receiving conveyer cover	H	m	In case of sectional chutes with bends, the fall height of every chute part is taken into account (see Figure 24.3)
Length of the inclined chute	l_{ch}	m	In case of sectional chutes, the length of every section
Inclination of the chute to the horizontal plane	α	grade	In chutes with bends, the inclinations of every chute part
Angle changing of chute inclination at a bend location	$\Delta\alpha$	grade	See Figure 24.3
Cross-section area of the chute at site entrance of the material in receiving conveyer cover	F_{ch}	m^2	
Width of the chute cross-section area	b	m	
Height of the chute cross-section area	h	m	
Air density	ρ_2	kg/m^3	

Table 24.18 The basic calculated magnitudes for the definition of the local exhaust capacity for particulate material reloadings on closed gravity chutes

Parameter	Symbol	Unit	Note
Specific material mass flow	G_1/b	kg/(s · m)	
Material rate at the first inclined chute	v_{1c}	m/s	Eqn (18)
Material rate under entrance receiving conveyer cover	v_{1r}	m/s	
Material rate under meeting with bottom of receiving unit (conveyer belt)	v'_{1r}	m/s	
Relation of initial material rate to the final one in the chute	n		
Average material particle size	d_m	mm	Eqn (19)
Local resistance coefficient:			
of entrance in the feed conveyer cover	ζ_{en}		Eqn (22)
of the chute	ζ_{ch}		Eqn (21)
of the cross partition in receiving conveyer cover	ζ_{par}		Table 24.20
Underpressure on the inside surface of the outer receiving conveyer cover walls	$p_{c.r}$	Pa	Table 24.21
Underpressure on the inside surface of the outer feed conveyer cover walls	$p_{c.f}$	Pa	Table 24.21
Area of the non-compactnesses in cover:			
of the feed conveyer	$F_{n.f}$	m^2	
of the receiving conveyer	$F_{n.r}$	m^2	Eqn (24)
Heat pressure originating from overload of the heated materials	p_t	Pa	Is taken into account, when $t_1 \geqslant 50$°C Eqns (25–27)
Coefficient of dynamic interaction of the moving material surface in the sloping chute with air	c_τ		Eqns (28, 29)
Ejection coefficient	φ		Eqn (31)
Local exhaust capacity of pressurized covers of the receiving apparatuses, volumes, and conveyers	$L_{a.f}$	m^3/h	Eqn (32)
Air flow volumes, which are sucked through the non-compactnesses of a feed conveyer head unloading cover	$L_{n.f}$	m^3/h	Eqn (34)
Air flow volumes, which are sucked through the non-compactnesses of a receiving conveyer cover	$L_{n.r}$	m^3/h	Eqn (36)
Air flow volumes ejected by particle gravitation flow	L_{ej}	m^3/h	Eqn (37)
Local exhaust capacity of unpressurized covers of the receiving apparatuses, volumes, and conveyers	$L_{a.r}$	m^3/h	Eqn (33)

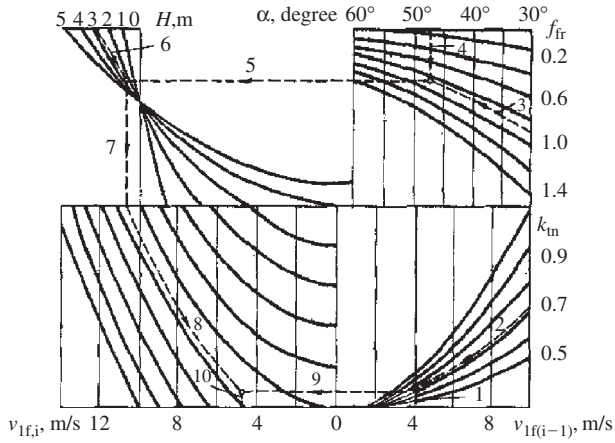

Figure 24.15 Nomogram for definition of the material rate under entrance of receiving conveyer cover, v_{1r}. Example: it is given $v_{1f,\,(i-1)}$; $k_{tn} = 0.72$; $f_{fr} = 0.9$; $\alpha_i = 47°$; $H_i = 2.9$ m. Answer: $v_{1f,i} = 4.76$ m/s.

Table 24.19 Values of the rate reduction coefficient k_{tn} depending on change of inclination of the chute

$\Delta\alpha = \lvert\alpha_{i-1} - \alpha_i\rvert$ (degree of arc)	k_{tn}	$\Delta\alpha = \lvert\alpha_{i-1} - \alpha_i\rvert$ (degree of arc)	k_{tn}
60	0.47	30	0.85
50	0.64	20	0.93
45	0.70	10	0.97
40	0.75	0.00	1.00

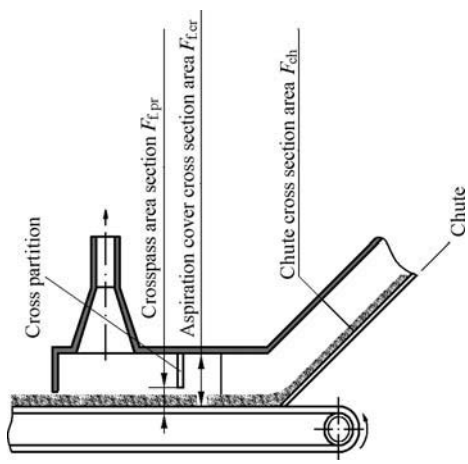

Figure 24.16 Scheme to the calculation of ζ_{par} for cover with double walls and solid cross partition.

The value of ζ_{par} (see Figures 24.3 and 24.16) is determined from Table 24.20 depending on the relations $F_{ch}/F_{f\cdot cr}$ and $F_{f\cdot pr}/F_{f\cdot cr}$, where $F_{r\cdot pr}$ is the cross area passing under the partition wall, m^2; $F_{r\cdot cr}$ is the cross area of the receiving conveyer cover, m^2. The ble value of $F_{f\cdot pr}/F_{f\cdot cr} = 0.25$–$0.3$.

Table 24.20 Dependence ζ_{par} on the relations $F_{ch}/F_{f.cr}$ and $F_{f.pr}/F_{f.cr}$

$F_{ch}/F_{f.cr}$	ζ_{par} values by $F_{f.pr}/F_{f.cr}$ relation				
	0.1	0.2	0.3	0.4	0.5
1.0	193	44.5	17.8	8.12	4.02
0.8	124	28.5	11.4	5.19	2.57
0.6	69.5	16.0	6.41	2.92	1.45
0.4	30.9	7.12	2.84	1.30	0.64
0.2	7.72	1.78	0.71	0.32	0.16

5. The underpressure on the inside surface of the outer receiving unit cover walls is defined by the formula (Eqn 23)

$$p_{cr} = 0.163 k_{c.r} (v'_{1r})^2 \qquad (23)$$

where v'_{1r} is the material rate on meeting with the bottom of the receiving unit (conveyer belt), which is determined by the formula in Eqn (19), here H must be increased by the fall height of material in the receiving unit cover; $k_{c\cdot r}$ is correction coefficient, which is taken from Table 24.21.

6. The area values of the non-compactnesses in the cover of the feed conveyer $F_{n\cdot f}$ and of the receiving conveyer $F_{n\cdot r}$ are accepted on the constructive data:

   $F_{n\cdot f}$ amounts to 0.3 and 0.5 m^2 for belt width in the range from 0.5 to 0.8 m and 1.0 m, respectively;
   $F_{n\cdot r}$ must be not exceed the values, calculated from the formula

$$F_{n.r} = 2(l + B_1)\delta \qquad (24)$$

   where l and B_1 are the length and width of cover in its part lower (see Figure 24.3); δ is the width of a conditional opening, 0.015 m.
7. The heat pressure p_t is determined from Eqn (12) reduced to the form

$$p_t = p_{t.m} H \qquad (25)$$

   where $p_{t\cdot m}$ is the specific heat pressure (by $H = 1.0$ m), as shown in Table 24.22, which is constituted by the formulae in Eqn (26) and Eqn (27) for various technological parameters

$$p_{t.m} = 4.905\,(\rho_{2.a} - \rho_{2.d}) \qquad (26)$$

Table 24.21 Correction coefficient, $k_{c.r}$ values

Reloading unit type	Cover design	Cover parameters		Correction coefficient	
		$H_{c.r}/B_{c.r}$	$l_1/B_{c.}$	Initial particulate stock	Metallic powders
Reloading from feed conveyer to receiving conveyer	Receiving conveyer cover:				
	• no-go with single flat walls	From 0.4 to 0.75	From 0.4 to 0.75	0.65	0.75
		Till 0.75	From 0.75 to 1.0	0.55	0.65
		0.4	Till 0.45	1.3	1.35
	• no-go with double flat walls (Fig. 3)	From 0.75 to 1.0	From 0.4 to 0.75	0.45	0.50
	• no-go with single concave walls (Fig. 14)	From 0.8 to 1.0	...	0.45	0.50
	• through-pass with single flat walls	From 0.4 to 0.75	...	4.0	4.5
Elevator or other equipment, which is loaded by gravitation chute	Single cover	...	...	3.5	4.5
Elevator	'Sheath' type cover of the elevator stretching station	...	...	3.0	4.0
Load by gravitation chute of a non-pressurized bin	The local exhaust is attached to bin covering	...	...	2.0	2.5
Load by gravitation chute of a pressurized bin	The local exhaust is attached to the feed conveyer head cover	...	...	0.8	1.2

Table 24.22 Specific heat pressure (values $H = 1$ m) p_t for various temperatures of incoming particulate material t_1 and aspirated air $t_{2.d}$

t_1 (°C)	$t_{2.d}$ (°C)	k_t	$\rho_{2.d}$ (kg/m^3)	p_t (Pa)
50	32	1.0	1.16	0.29
75	43	0.95	1.11	0.49
100	52	0.90	1.08	0.69
150	62	0.75	1.05	0.88
200	75	0.70	0.99	1.08
250	87	0.65	0.98	1.18
300	95	0.60	0.96	1.28
350	104	0.57	0.94	1.37
400	114	0.55	0.92	1.47
450	122	0.52	0.90	1.57
500	128	0.50	0.88	1.67
600	138	0.45	0.86	1.77

where $\rho_{2\cdot a}$ and $\rho_{2\cdot d}$ are air density at ambient air temperature $t_{2.a} = 16$°C and air temperature in receiving conveyer cover $t_{2\cdot d}$.

$$t_{2.d} = 0.5\,k_t(t_1 - t_{2.a}) \tag{27}$$

where k_t is the correction factor.

8. The dynamic interaction coefficient with air of the material surface, as it moves along an inclined chute, is determined by formulae (Eqn 28 and Eqn 29) or nomogram (Figure 24.17)

$$c_\tau = 0.09\alpha^{-1}(d_m c_\tau^*)^{0.4} \tag{28}$$

where α is chute angle of slope in radians

$$c_\tau^* = 3.26\,m_v - 3.6\,m_v^2 + m_v^3 \tag{29}$$

$$m_v = 10^3 G_1/\rho_1 b$$

b is a size which characterizes the material moving stream contact surface with air in the chute, m; b is the chute width for rectangular cross-section chutes;

$b = 0.5d_c\sqrt{\pi}$ *for* round cross-section chutes;

$$b = \sqrt{\frac{4G_1\ \mathrm{tg}(0.5\gamma_{rib})}{\rho_1\beta_1 v_1}} \tag{30}$$

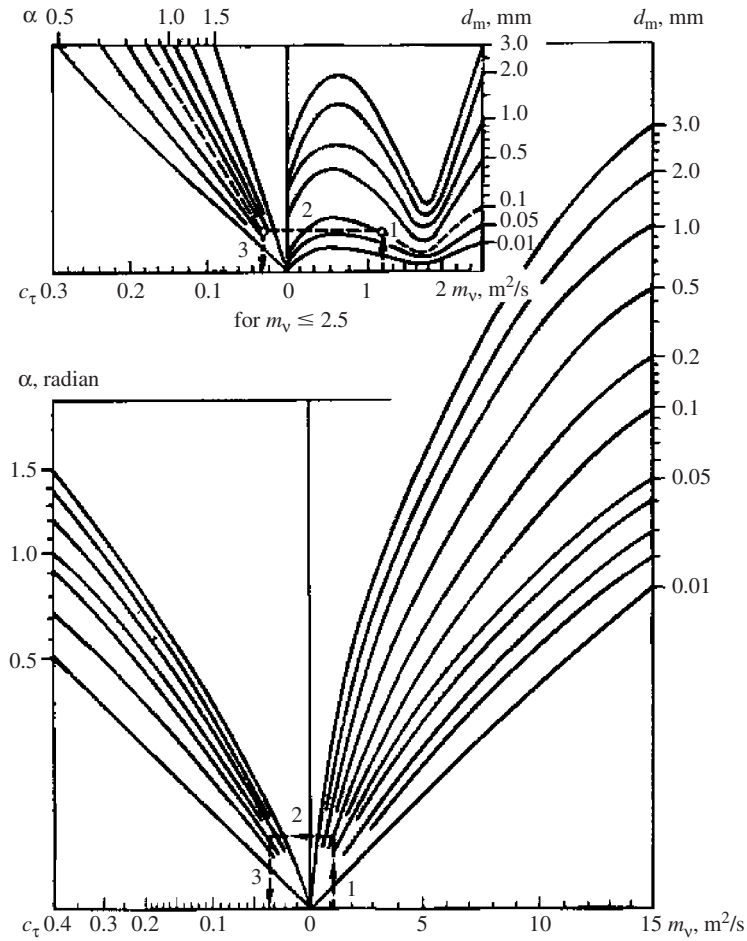

Figure 24.17 Nomogram for the c_τ definition. Example: it is given $G_1 = 1.945$ kg/s; $\rho_1 = 7800$ kg/m^3; $b = 0.2$ m; $d_m = 0.11$ mm; $\alpha = 0.82$ radian. Answer: $m_v = 10^3 \frac{1.945}{7800 \times 0.2} = 1.248$ m^2/s; $c_\tau = 0.031$.

for the chutes in the form of a three-edged prism with one of ribs directed down (see Figure 24.14) γ_{rib} is the angle between facets convergent to the rib directed down, degree; β_1 is the solid volumetrical concentration in quasi-interconnected motion, in the chute, (it is accepted in range from 0.035 to 0.05).

9. The ejection coefficient φ is defined by Eqn (31) or nomograms (Figures 24.18, 24.19 and 24.20)

$$\varphi = \frac{\sqrt{0.44(1-n^3)^2 + 2(1-n^2)^2(A-1)[B+0.25(1+n^2)]}}{(1-n^2)(A-1)} - 0.67(1-n^3) \quad (31)$$

where

$$A = \frac{h\Sigma\zeta}{c_\tau l_{ch}}; \quad B = \frac{AC}{\Sigma\zeta v_{1f}^2}; \quad C = \frac{p_{c.r} - p_t}{\rho_2}$$

10. The formulas for calculation of the reloading unit local exhausts with various degrees of pressurization of the covers and temperature of materials are given in Table 24.23.

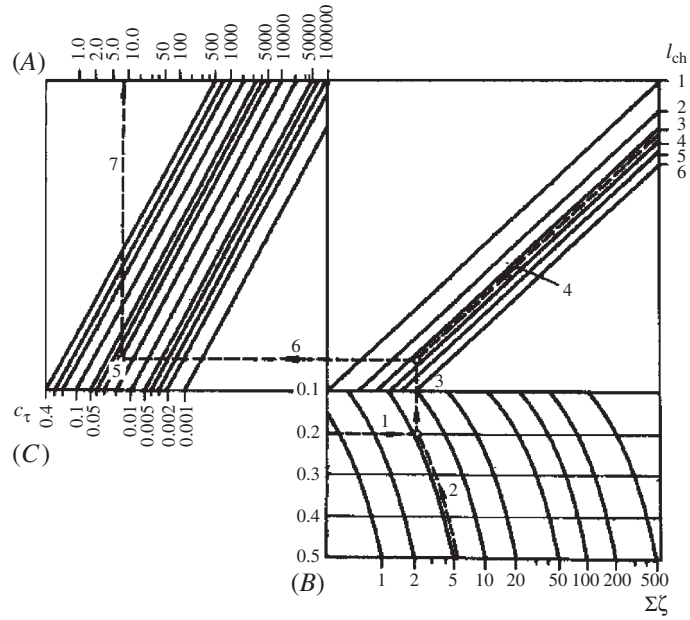

Figure 24.18 Nomogram for the A definition. Example: it is given h = 0.2 m; Σζ = 5.2; c_τ = 0.031; l_{ch} = 3.28. Answer: A = 8.65.

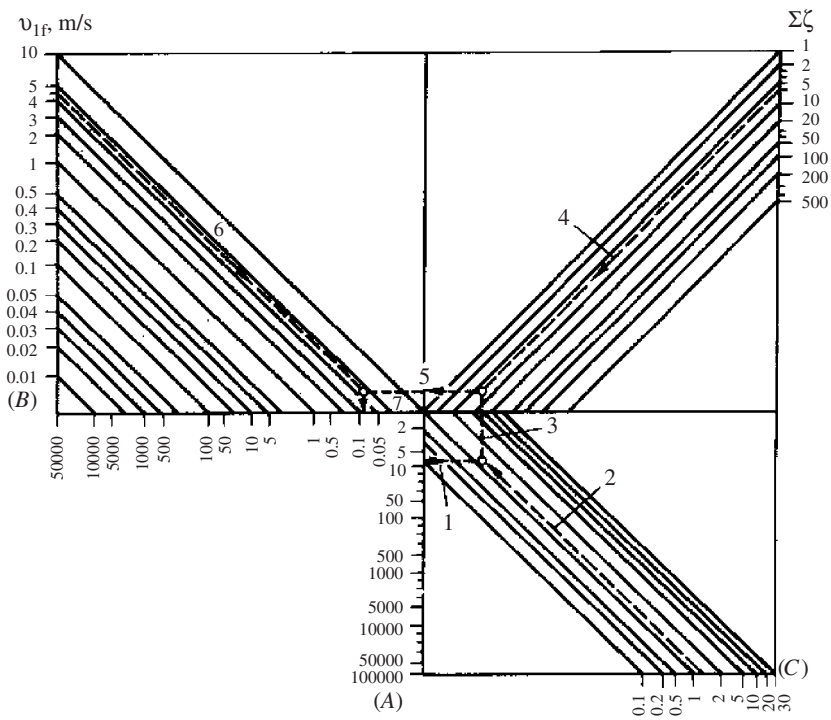

Figure 24.19 Nomogram for the B definition. Example: it is given A = 8.65; $p_{c\cdot r}$ = 1.64 Pa; p_t = 0; $t_{2.d}$ = 20°C (ρ_2 = 1.2 kg/m^3); Σζ = 5.2; $v_{1.r}$ = 4.71 m/s; $C = \frac{p_{c.r} - p_t}{\rho_2} = \frac{1.64 - 0}{1.2} = 1.37$ Answer: B = 0.09.

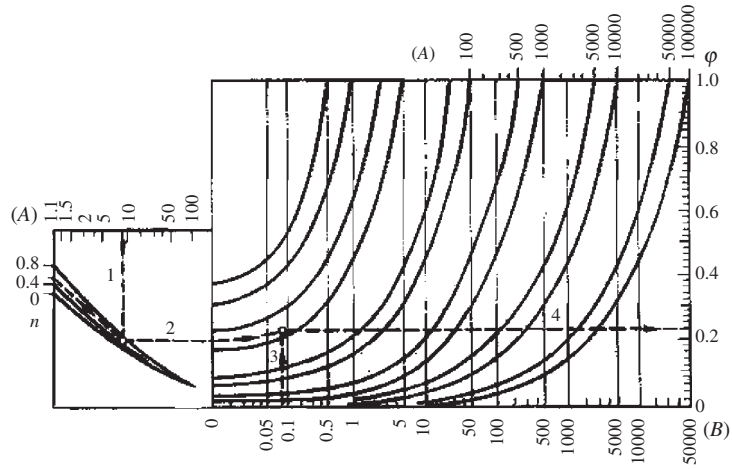

Figure 24.20 Nomogram for the φ definition. Example: it is given A = 8.65; n = 0.6; B = 0.09. Answer: 0.247. Note: For A > 100 the n quantity does not take part in the φ definition.

Table 24.23 Formulas for the determination of the local suctions (m^3/h)

Cover characteristic	Attaching location of the local suction	Symbol	Formula	
Pressurized	to the unloading head of feed conveyer	$L_{a.f}$	$L_{af} = L_{nf} = 3300\,F_{nf}\sqrt{\frac{p_{cf}}{\rho_2}}$	(Eqn 32)
Unpressurized for:				
unreheated materials (temperature below 50°C)	to the receiving unit cover	$L_{a.r}$	$L_{a.r} = L_{n.r} + L_{ej}$	(Eqn 33)
heated materials (temperature above 50°C)	both to the receiving unit cover and to the unloading head of feed conveyer	$L_{a.r}$, $L_{a.f}$	$L_{af} = 400\,B_{c.f}$ where $B_{c.f}$ is the width of head feed unit cover (m)	(Eqn 34)
			$L_{a.r} = (L_{n.r} + L_{ej})$	(Eqn 35)
			where	
			$L_{n.r} = 3300\,F_{n.r}\sqrt{\frac{p_{c.r}}{\rho_2}}$	(Eqn 36)
			$L_{ej} = 3600\,F_{ch}\varphi\,v_{1f}$	(Eqn 37)

Example of the Computation

The determination of the local exhaust capacity of the belt conveyer reloading unit. The receiving cover is no-go and is with double flat walls (see Figure 24.3).

The initial data by selected $F_{n\cdot f}$, $F_{n\cdot r}$, and F_{ch} values: $G_1 = 1.945\,kg/s$; $\rho_1 = 7800\,kg/m^3$; $t_1 = 20°C$; $F_{ch} = 0.0258\,m^2$; $d_m = 0.11\,mm$; $F_{n\cdot f} = 0.04\,m^2$; $F_{n\cdot r} = 0.02\,m^2$; $H_1 = 0.8\,m$; $H_2 = 0.8\,m$; $H_3 = H_{c\cdot r} = 0.38\,m$; $\alpha_1 = 90°$; $\alpha_2 = 47°$; $\alpha_3 = 40°$; $b = 0.2\,m$; $l_{ch} = 3.88\,m$; $p_t = 0$; $F_{c\cdot r} = 0.09\,m^2$.

Solution:

The powder gravitational movement rate at the end of the initial vertical tract of the chute is determined by Eqn (18):

$$v_{1v,i=1} = \sqrt{19.6 \times 0.8} = 3.96\,m/s$$

The powder movement rate at the end of the inclined part of the chute at the site entrance in the receiving

conveyer cover is defined by Eqn (19) or nomogram (see Figure 24.15)

$$v_{1sh,i} = \sqrt{(3.96 \times 0.72)^2 + 19.6 \times 2.9(1 - 0.9 \times 0.9 \times 0.93)} = 4.71\,\text{m/s}$$

where $f_{fr} = 0.9$, $k_t = 0.72$ by $\Delta\alpha = 43°$ (it is found from Table 24.19).

The sum of the local resistances per Eqn (21) and Eqn (22) amounts to

$$\sum \zeta = 2.4 \left(\frac{0.0258}{0.09}\right)^2 + 2.5 + 1.7 = 5.2$$

where ζ_{par} is found from Table 24.20 by $F_{f\cdot pr}/F_{f\cdot cr} = 0.3$ and $F_{ch}/F_{f\cdot cr} = 0.286$.

The coefficient c_τ is determined by Eqn (28) and Eqn (29) or nomogram (see Figure 24.17):

$$m_v = 10^3 \frac{1.945}{7800 \times 0.2} = 1.247\,\text{m}^2/\text{s}$$

$$c_\tau^* = 3.26 \times 1.247 - 3.6 \times 1.247^2 + 1.247^3 = 0.4$$

$$c_\tau = 0.09\,(0.82)^{-1} \times (0.11 \times 0.4)^{0.4} = 0.031$$

$$\alpha_2 = 47° = 0.82 \text{ radian.}$$

The powder movement rate at the end of the inclined chute on meeting the bottom of the receiving unit (conveyer belt) is defined according to Eqn (19) or nomogram (see Figure 24.15):

$$v'_{1r} = \sqrt{(4.71 \times 0.98)^2 + 19.6 \times 0.38(1 - 0.9 \times 0.9 \times 1.19)} = 4.64\,\text{m/s}$$

The underpressure on the inside surface of the outer receiving unit cover walls is defined by Eqn (23), and amounts to

$$p_{cr} = 0.163\,k_{c.r}\,(v'_{1r})^2 = 0.163 \times 0.5 \times 4.64^2 = 1.64\,\text{Pa}$$

The ejection coefficient φ is defined by Eqn (31) or nomograms (see Figures 24.18, 24.19 and 24.20)

$$\varphi = \frac{\sqrt{0.44(1 - 0.6^3)^2 + 2(1 - 0.6^2)^2(8.65 - 1)}}{[0.1 + 0.25(1 + 0.6^2)] - 0.67(1 - 0.6^3)} = 0.2$$
$$(1 - 0.6^2)(8.65 - 1)$$

where

$$n = \frac{3.96 \times 0.72}{4.71} = 0.6; \quad A = \frac{0.2 \times 5.2}{0.031 \times 3.88} = 8.65;$$

$$B = \frac{8.65 \times 1.37}{5.2 \times 4.71^2} = 0.1; \quad C = \frac{1.64}{1.2} = 1.37.$$

Air flow volumes ejected by particle gravitation flow in the receiving conveyer cover per Eqn (37) (see below) at Table 24.23 amount to:

$$L_{ej} = 3600 \times 0.25 \times 4.71 \times 0.0258 = 110\,\text{m}^3/\text{h}.$$

The air flow volumes which are sucked through the non-compactness of the receiving conveyer cover are defined by Eqn (36)

$$L_{n.r} = 3300 \times 0.02 \sqrt{\frac{1.64}{1.2}} = 78\,\text{m}^3/\text{h}$$

The local exhaust capacity according to Eqn (35) amounts to

$$L_{a.r} = 110 + 78 = 188\ \text{m}^3/\text{h}.$$

Discharge of Containers

The pressurized performance of the container discharge unit and receiving vessel allows the effective use of by-pass pipes to reduce excess pressure by means of a connection zone of excess pressure with a thinning zone that leads the flow of dust-laden gas from the receiving vessel into the container, in the space above the falling powder level (Figure 24.21).

The taper conjunction in the abutment of the container delivery cell to the receiving bin checkerwork provides airtightness. The entrance to the by-pass tube is cleared by a container placed on the receiving bin. Table 24.24 contains the necessary data for designing by-pass pipes. Such a design is useful for powder processing in air as well in protective atmospheres for combustible and explosion-risk powders.

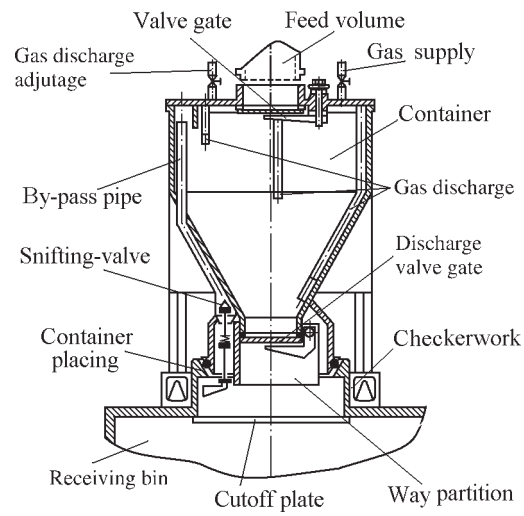

Figure 24.21 Container at discharge position by pressurized matting with a pressure sealed receiving vessel.

Table 24.24 Necessary data for designing of by-pass pipes

Parameter	Symbol	Unit
Density of materials	ρ_1	kg/m^3
Apparent density	ρ_{ap}	kg/m^3
Material mass flow	G_1	kg/s
Atmosphere underpressure in the space above the falling powder level in volume which is unloaded	p_f	Pa
Atmosphere overpressure in receiving volume (bin)	p_r	Pa
Cross-section of the by-pass pipe	F_{b-p}	m^2
Diameter of the by-pass pipe	D_{b-p}	m
Sum of the local hydraulic resistances of the by-pass pipe	$\Sigma\zeta_{b-p}$	
Gas volume being displaced from receiving bin	L_{b-p}	m^3/s

The gas volume being displaced from the receiving vessel during powder discharge amounts to

$$L_{bp} = \frac{G_1}{\rho_{ap}}, \text{ m}^3/\text{s}$$

The cross-section of the by-pass pipe

$$F_{b\text{-}p} = \frac{L_{b\text{-}p}}{v_{2(b\text{-}p)}}, \text{ m}^2$$

where

$$v_{2(b-p)} = \sqrt{\frac{2(p_r - p_f)}{\rho_2 \Sigma\zeta_{b-p}}} \text{ m/s.}$$

Single Rotary Hammer Mills

The most effective means of eliminating the effect of excess pressure created by moving rotary parts, as noted before, is pressurized performance of loading and unloading units, isolation from the equipment installation in the order in which it must function. It is effective to provide the hammer mill with by-pass pipes to reduce excess pressure. They connect the mill cavity, situated at underpressure, with the discharge unit, situated at overpressure (Figure 24.22).

The initial data that are necessary for the determination of the capacity of the suction devices are enumerated in Table 24.25.

Determination of the Basic Calculated Magnitudes

1. The root-mean-square diameter of crushed material particles is defined on sieve analysis data base by Eqn (20):

$$d_m = 0.01 \sum_{i=1}^{n} d_i m_i$$

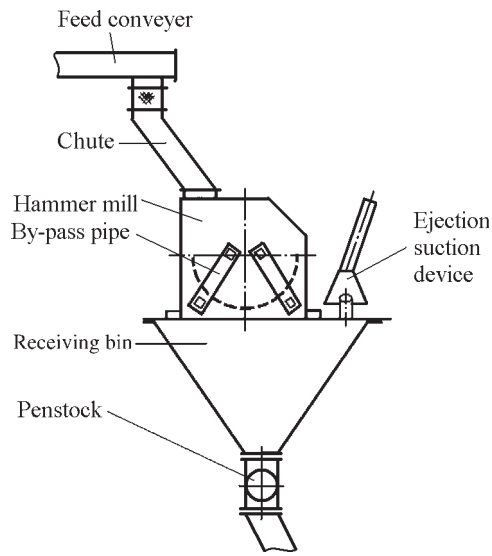

Figure 24.22 Scheme of a hammer mill installation.

2. The conditional diameter of circle described by mass center of the active rotor part rotation is calculated from Eqn (11):

$$D_{ac} = \frac{2\sum_{i=1}^{n} F_{ha} \times r}{\sum_{i=1}^{n} F_{ha}}$$

where

$$\sum_{i=1}^{n} F_{h.a} \times r = F_{h.a(1)} \times r_1 + F_{h.a(2)} \times r_2 + \cdots + F_{h.a(n)} \times r_n$$

$$\sum_{i=1}^{n} F_{h.a} = F_{h.a(1)} + F_{h.a(2)} + \cdots + F_{h.a(n)} \quad (32)$$

Table 24.25 Data for the determination of the capacity of hammer mill suction devices

Parameter	Symbol	Unit	Note
The installation scheme and initial data			
Maximum pressure, when tightness is retained	P	kPa	
Material mass flow	G_1	kg/s	
Material density	ρ_1	kg/m^3	
Type of the hammer mill			
Number of the hammer rows	i		
Rotation velocity of hammers	n	s^{-1}	
Root-mean-square diameter of crushed material particles	d_m	m	Eqn (20)
Coefficient of dynamic interaction			
of the material pieces with mill chamber atmosphere	c_m		Eqn (50)
of the rotating parts with mill chamber atmosphere	c_h		Eqn (49)
The basic calculated magnitudes			
Sum area of the one row of rotating parts	$F_{h.1}$	m^2	Calculated by summation of the constituents
Constituent cross-section area of the active rotor parts	$F_{h.a}$	m^2	See Figure 24.6
Distance from the hammer mill axis to mass centre of the corresponding constituent of the active rotor parts	$r_1, \ldots r_n$,	m	See Figure 24.6
Conditional diameter circle describable by mass centre of the active rotor part	D_{ac}	m	Eqn (32)
Root-mean-square rotary velocity of hammers	$\overline{v}_h$	m/s	Eqn (33)
Trajectory length of active part rotor centre diameter D_{ac} from the material entrance site in hammers action zone and the end of separation grate	l_D	m	Eqn (34)
Cross-section of hammer mill chamber, orientated normally to the D_{ac} trajectory, in the zone of flow components movement	F	m^2	See Figure 24.6
Sum of the local aerodynamic resistances to the gas movement in hammer mill	ζ_h		receptee amounts to 10
Underpressure in zone around of the hammer shaft close to the inside surface of body side walls (position of by-pass attachment)	p_h	Pa	Eqn (52)
Area cross-section of the feed chute	F_f	m^2	
Area cross-section of the discharge chute	F_{des}	m^2	
Sum of the local hydraulic resistance coefficients to the gas movement in by-pass pipes	$\Sigma\zeta_{b.p}$		Eqn (42)
Local resistances to the gas entrance from the by-pass pipe to mill chamber	$\zeta_{en.h}$		Eqn (41), See Table 24.24
Hydraulic characteristic of the by-pass pipes	$R_{b.p}$	kg/m^7	Eqn (35)
Maximum gas medium pressure originating by hammer mill	p_{h-m}	Pa	Eqn (10), Eqn (44)
Sum of the local hydraulic resistance coefficients to the gas movement in the net	$\Sigma\zeta_{-net}$		Eqn (48)
Hydraulic characteristic of the net	R_{net}	kg/m^7	Eqn (51)

where $F_{h\cdot a(1)}$, $F_{h\cdot a(2)}$, ... $F_{h\cdot a(n)}$, are constituent cross-section areas of the active rotor parts; r_2, r_1, ... r_n, are the distance from the hammer mill axis to the mass center of the corresponding constituents of the active rotor parts.

3. The root-mean-square circumferential speed of the hammers equals

$$v_h = 3.14\, D_{ac} n \tag{33}$$

4. Trajectory length of active part rotor centre of diameter D_{ac} from the material entrance site in hammers action zone and the end of separation grate is

$$l_{D_{ac}} = 8.72 \times 10^{-3}\, D_{ac} \alpha_i \tag{34}$$

where α_i is the angle between the particulate material entrance in the action zone of the hammers and conventional plane passing through the shaft center and the grate end measured in the course of shaft rotation.

5. The cross-section of the hammer mill cavity, orientated normal to the D_{ac} trajectory, in

the zone of the flow components movement is determined as the product of the mill cavity width and the distance between the axis surface up to the fire-grate radius course (see Figure 24.6).

6. Hydraulic characteristic of the by-pass pipes $R_{b\cdot p}$:

$$R_{b.p} = 0.5\sum \zeta \rho_2 (F)^{-2} \tag{35}$$

where $\sum\zeta$ is sum of the local hydraulic resistance coefficients to the gas flow in the by-pass pipes; F is the cross-section of hammer body, in which the parts rotate (the section is orientated normally to root-mean-square air velocity vector in inner crusher).

7. The sum of the local hydraulic resistance coefficients is defined in the following way:
   (a) for the feed section of the hammer mill installation including feed conveyer unpressurized cover with non-compactnesses in the form of slots and gravitational chute:

$$\sum \zeta_f = \zeta_{en} + \zeta_{f\text{-}ch} \tag{36}$$

where ζ_{en} is the local hydraulic resistance coefficient of the slot determined by the formula

$$\zeta_{en} = 2.4\left(\frac{F}{F_{en}}\right)^2 \tag{37}$$

F_{en} is the cross-section of the slots; $\zeta_{f\text{-}ch}$ is the local hydraulic resistance coefficient of the feed chute: for inclined chutes and chutes with corners $\zeta_{en} = 2.5(F/F_f)^2$, F_f is the cross-section of the feed chute, while for vertical chutes $\zeta_{en} = 1.5(F/F_{ch})^2$, respectively;

   (b) for the discharge section:

$$\sum \zeta_d = \zeta_{fun} + \zeta_{d\text{-}ch} + \zeta_{d\text{-}f} \tag{38}$$

where $\sum\zeta_{fun}$ is the local hydraulic resistance coefficient of the receiving funnel; $\sum\zeta_{d\text{-}ch}$ is the local hydraulic resistance coefficient of the discharge chute; $\sum\zeta_{d\text{-}f}$ is the local hydraulic resistance coefficient of the unit feed of the adjoining inter-operational transport or processing apparatus.

Using an unpresserized receiving bin, in which it is necessary to support the underpressure

$$\sum \zeta_d = (\zeta_{fun} + \zeta_{en.b})\left(\frac{F}{F_{en.b}}\right)^2 \tag{39}$$

durante absentia of funnel $\zeta_{fun} = 0$.
By mounting the hammer mill direct on the bin equipped with an ejection suction device (see Figure 24.22):

$$\sum \zeta_d = \zeta_{en.b}\left(\frac{F}{F_{en.b}}\right)^2 + \zeta_{d.s}\left(\frac{F}{F_{d.s}}\right)^2 \tag{40}$$

where $\zeta_{en\cdot b}$ and $\zeta_{d\cdot s}$ are the hydraulic resistance coefficients of the entrance in the receiving bin and its exit to the socket, respectively; $F_{en\cdot b}$ and $F_{d\cdot s}$ are the cross-section areas of the entrance to the bin and the discharge socket, respectively. The $\zeta_{en\cdot b}$ and $\zeta_{d\cdot s}$ values for conditions (see Figure 24.22) can be received equal to 0.5 and 1.0, respectively;

   (c) for the by-pass pipes:

$$\sum \zeta_{b.p} = (\zeta_{en.h} + \zeta_{en\text{-}b.p} + \zeta_{fr\text{-}b.p})\left(\frac{F}{F_{b.p}}\right)^2 \tag{41}$$

where $\zeta_{en\cdot h}$ is the hydraulic resistance coefficient at the entrance from by-pass pipe to the hammer mill cavity (Table 24.26); $\zeta_{en\text{-}b\cdot p}$ is the hydraulic resistance coefficient at the entrance of the flow to the by-pass pipe, equals 0.5; $\zeta_{fr\text{-}b\cdot p}$ is the flow friction coefficient of the by-pass pipe (Table 24.27); $F_{b\cdot p}$ is the cross-sectional area of the by-pass pipe.

In the case of several by-pass pipes $\sum_{i=2}^{i=N} \zeta_{b.p_i}$ is determined from a relation:

$$\sum_{i=2}^{i=N} \zeta_{b.p_i} = \left[\sum_{i=2}^{i=N}\left(\frac{N_{b.p_i}}{\Sigma\zeta_{b.p_i}}\right)\right]^{-1} \tag{42}$$

where $N_{b.p_i}$ and $\Sigma\zeta_{b.p_i}$ are numbers of the parallel *i*-type by-pass pipes and sum of the hydraulic resistance coefficients of each of them, respectively.

Table 24.26 Values of the hydraulic resistance coefficient of the entrance flow from by-pass pipe into the hammer mill chamber dependence on design geometry

Relation $r/D_{b.p}$[a]	$\zeta_{en.h}$ values by relation $\Delta/D_{b.p}$[b]						
	0.05	0.07	0.10	0.15	0.20	0.25	0.30
0,1	5.6	3.7	2.3	0.62	0.57	0.76	0.93
0.2	4.5	2.3	0.9	0.52	0.51	0.62	0.75

[a] r is the rounding radius in the location of the connection of by-pass pipe with mill chamber by gas flow entrance into it;
[b] Δ is the gap between the by-pass pipe plane opening by gas flow entrance into mill chamber and mill rotating body flank

Table 24.27 Values of the by-pass pipe flow friction coefficient ($\zeta_{fr\text{-}b.p}$) in dependence on pipe cross-section area ($F_{b.p}$)

$F_{b.p}$	$\zeta_{fr\text{-}b.p}$	$F_{b.p}$	$\zeta_{fr\text{-}b.p}$	$F_{b.p}$	$\zeta_{fr\text{-}b.p}$
0.005	0.474	0.02	0.350	0.04	0.260
0.0078	0.463	0.03	0.310	0.05	0.200
0.01	0.420	...	...	...	...

For the cover permeability

$$\sum \zeta_n = 2.4\left(\frac{F}{F_n}\right)^2 \tag{43}$$

8. The gas pressure created by the hammer mill ($p_{h\cdot m}$, Pa) in the absence of by-pass pipes (see also Eqn 10):

$$p_{h.m} = \left(\frac{B_{h.m} - \sqrt{B_{h.m}^2 - 4A_{h.m}}}{2A}\right)^2 \tag{44}$$

where

$$B_{h.m} = \sqrt{\frac{k_r}{v_h}} \tag{45}$$

$$A_{h.m} = \frac{k_r}{v_h^2} - \frac{\rho_2 \zeta_{h.m} k_r}{2k_{h.m}} - \frac{1}{k_{h.m}} \tag{46}$$

$$k_{h.m} = c_h\left(1.5\frac{c_m G_m}{c_h \rho_1 d_m} + nF_h i\right)\frac{\rho_2 l\, D v_h}{4F} \tag{47}$$

$$k_r = \frac{2}{\rho_2 \sum \zeta_{net}} \tag{48}$$

where $\sum \zeta_{net}$ is the sum of the net hydraulic resistance coefficient related to area F (the net contains feed and discharge units up to entrance into the aspiration funnel); $\zeta_{h\cdot m}$ is the hammer mill hydraulic resistance coefficient, which is accepted as equal to 10.

The c_h and c_m values in the absence of the by-pass pipes are accepted as $c_h = c_h^*$ and $c_m = c_m^*$ (see Table 24.28).

9. The dynamic interaction coefficients in the presence of the by-pass pipes are defined by the formulae:

$$c_h = 1.07(c_h^*)^{0.94}\left(\frac{R_{net}}{R_{b.p}}\right)^{0.01} \tag{49}$$

$$c_m = 1.07(c_m^*)^{0.94}\left(\frac{R_{net}}{R_{bp}}\right)^{0.01} \tag{50}$$

where R_{net} is the hydraulic characteristic of the net:

$$R_{net} = 0.5\rho_2 \sum \zeta_{net}(F)^{-2} \tag{51}$$

10. Underpressure in the zone around the hammer shaft close to the inside surface of

Table 24.28 Values of the c_h^* and c_m^* coefficients

Dynamic interaction coefficients	Coefficient values by F_h/F		
	0.4–0.6	0.6–0.65	0.65–0.7
c_h^*	0.04	0.1	0.18
c_m^* for different σ, MPa:			
19.6	5.5	13.7	24.7
36.0	6.46	16.1	29.0
96.0	11.2	28.7	...

σ is the compressive strength of grinding material.

body side walls (position of by-pass attaching) (Pa):

$$p_h = 1.93\, p_{h.m}^{0.88} \left(\frac{\sum \zeta_{b.p}}{\sum \zeta_{net}} \right)^{0.11} \left(\frac{F}{F_h} \right)^{3.27} \quad (52)$$

11. The diameter of the ejection suction device discharge socket:

$$D_{d.s} = 0.905 \left(\frac{G_1}{\rho_1} \right)^{0.5} \left(\frac{\zeta_{d.s} \rho_2}{p_{d.r}} \right)^{0.25} \quad (53)$$

where $p_{d\cdot r} = p_{h\cdot m}$ for direct discharge of the milled material into technological apparatus (or inter-operation transport); $p_{d\cdot r} = p_{h\cdot m} + p_{ej}$ for discharge of the milled material via a chute; p_{ej} is calculated from (Eqn 7).

12. The diameter of the ejection suction funnel entrance:

$$D_{f.en} = (10 - 15) D_{d.s} \quad (54)$$

13. The gas volume flow through the ejection suction device discharge socket under the action of the overpressure in the receiving cover:

$$L_{d.s} = 1.11 D_{d.s}^2 \sqrt{\frac{p_{d.r}}{\rho_2 \zeta_{d.s}}} \quad (55)$$

Water Treatment

The treatment of recirculated water and waste waters depends on the extent of their pollution and are therefore subjected to different treatments.

- Mechanical treatment methods consist of removal of solid material by separation under the action of gravity, centrifugal forces or on filtration membranes.
- Chemical treatment methods are based on the use of the processes and reagents, producing the insoluble precipitates. For chemical purification processes, oxidation, neutralization and other chemical reactions are used. In treatment, slaked lime, limestone, calcium chloride, calcium hypochloride, ferric sulfate and other substances are used.
- Of the physical-chemical methods, sorption, coagulation, electrolysis, ion-exchange, extraction, crystallization and decontamination are used.
- Biochemical methods are based on processes providing mineralization.

Mechanical Treatment Methods

The gravity precipitation is accomplished in the precipitators, while the separation under action of the centrifugal forces is in the hydrocyclones and precipitation centrifuges (information about details can be found in Chapter 11).

During powder production by water atomization it is usually enough to clean the recirculated water by mechanical means.

The flow chart of the recycling of the water during the water atomization of copper alloy powder is shown in Figure 24.23. The water from the initial water reservoir is fed by high pressure pump to the atomizer. The sludge (typically having water-to-solid ratio up to 8 to 10) from the atomization chamber is delivered by a slurry pump into the thickener. The thickened underflow is loaded into a vacuum cartridge filter chamber (see Chapter 11). The vacuum pump sucks off the water. The clarified water from the thickener and loosened in the water-drop eliminator condensed moisture are collected and pumped to a cartridge filter from which refined water goes, via a cooler if necessary, to the initial water reservoir.

Chemical Treatment Methods

Water with high acidity is neutralized with lime. This can be crushed lime, chalk, dolomite or marble filters. The filter layer with 3–8 cm size fragments is from 0.8 to 1.2 m thick. The filtering rate does not exceed $5\,m^3/(m^2 \cdot h)$.

Acidic waste water contains metal cations, the lime is neutralized and it is possible to recover copper, nickel, zinc, lead, cobalt, cadmium and other metals. During deposition from acid and neutral solution the hydrogen ion exponent (pH) changes as is shown in

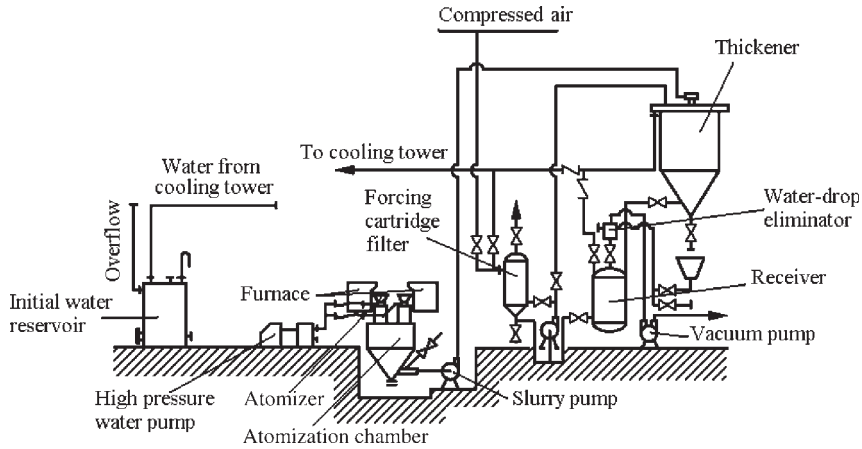

Figure 24.23 Flow chart of the water recycling in water atomized copper alloy powder production.

Table 24.29 Changing of the hydrogen ion exponent (pH) during deposition from acid and neutral solutions

Deposition process advance	Hydrogen ion exponent in waste waters inclusive of metal cations					
	Cu^{2+}	Ni	Zn^{2+}	Pb	Co	Cd
At the start of deposition	5.3	6.7	5.4	6.0	6.7	7.2
When deposition is complete	8.0–9.0	9.0–9.5	8.0–9.0	8.5	8.0	8.5–9.0

Table 24.29. For 1 m^3 of water with elevated acid content 0.5–1 kg of quicklime is consumed.

The cementation of copper on broken iron is the basic and simplest technique for copper extraction; here the iron cations go into solution, while copper is precipitated on the scrap as metal. The acid waste waters, saturated with iron, are treated with lime and passed to a thickener. The clarified water is returned to the process. The best reagent is low-grade lime including calcium carbonate.

Nickel is recovered by precipitation as hydroxide or carbonate salt compositions.

The waste water treatment from zinc and its extraction is produced by lime milk, prepared from third grade lime. During processing, the deposition is precipitated in the form of hydroxide and basic salt. Lead can be recovered by analogous processes.

Mercury is usually extracted either by precipitation in the form of sulfide or by means of filtering through a highly alkaline medium, such as sodium. In the former, the mercuric sulfide is in the colloidal state, therefore it is coagulated with aluminum sulfate $Al_2(SO_4)_3 \cdot 18H_2O$, iron sulfate $FeSO_4 \cdot 7H_2O$, lime or a mixture of these reagents.

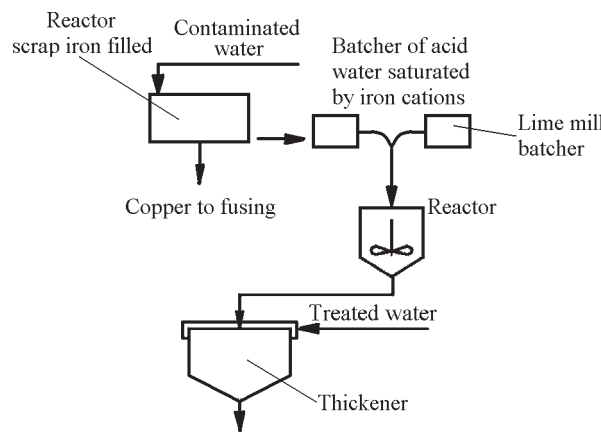

Figure 24.24 Scheme of the contaminated water purification from copper cations by the cementation technique.

Cyanide in cyanide-containing waste is converted into non-toxic insoluble ferrocyanides or oxidized by hypochlorite followed by sedimentation and filtration.

A typical flow chart of the recovery of the heavy metal cations is shown in Figure 24.24. The waste

water in the reactor is mixed with the slaked lime, a precipitate is formed in the thickener and the treated water is re-used. The lime suspension is made by wet grinding in the mill, in closed circuit with the hydrocyclone. The lime quantity is determined based on the nature and concentration of the impurities.

The sizeable lime expenditures and large volumes of the obtained metal oxide hydrates are features of the imperfections of the chemical treatment methods. Furthermore, the precipitation of the oxide hydrates demands maintaining the pH outlets exactly in the given ranges.

Ion-exchange Method

Ion exchange is a more recent technique. By means of the ion-exchange resins, the following metals are extracted: zinc, copper, nickel, silver, chromium and others. The synthetic ion exchange in aqua resin-ionites are extended.

Also used are the strong acid sulfonic cationics KY–1 and KY–2, sub-acid carboxyl cationic KB–4 and anionites, AB–17, EDE–10II and AN–31 (Russian commercial grades).

The absorption capacity of 1 g ionite amounts to 6–10 mg-eq/h. The ion-exchange rate depends on the rate of ion diffusion from solution into ionite, chemical reaction of double ion exchange in ionite and displaced ion diffusion from ionite into the solution.

By ion exchange on the sulfonic cationic KY–2, the ions are disposed in the following order of displacement energy: $H^+ < Na^+ < Mg^{2+} < Zn^{2+} < Co^{2+} < Cu^{2+} < Cd^{2+} < Ni^{2+} < Ca^{2+} < Sr^{2+} < Pb^{2+} < Ba^{2+}$. The cations, to the right, are absorbed less readily than those on the left.

The weak acid anions CO_3^{2-} and SiO_3^{2-} are removed only by strong alkaline anionite such as AV–17 (in the absence of the strong acid anions), while the strong acid anions are removed by weak alkaline anionite such as AN–31.

During the anion exchange process, the anions are removed in following order: $SO_4^{2-} > Cl^- > NO_3^- > NO_2^- > CO_3^{2-} > SiO_3^{2-}$.

The filtering rate through the fixed-bed or fluidized layer of the ionite is about 16 m per minute. The latter is more effective.

The purification process is accomplished in absorbtion columns. Of the known designs, columns with grates and downcomers are the most efficient. On the column top, the annular overflow chute and ionite feed funnel are placed.

The waste water is fed into the column bottom and during upward flow it creates a fluidized layer on the fall-through grates. The treated water is discharged through the annular overflow, while the saturated ionite is discharged from the column bottom and by air-lift is fed from above into a regeneration column, into which the regeneration solution is fed from below. Washed regenerated ionite is returned in the ion-exchange column.

The ion-exchange technique is used also for desalting the recirculating water used for melt atomization, washing of the powders, equipment and for powder cooling.

The process of partial desalting includes two basic stages: cation exchange (i.e. removal of cations) and anion exchange (i.e. removal of anions).

The cation exchange is done by passing the processed liquid through the hydrogen–cation–exchange filters. On the hydrogen–cation–exchange filters the cations are exchanged for hydrogen, and the equivalent amount of acid is generated in the filtrate. The subsequent acid filtrate passes through the anion-exchange filters leading to the retention of the acid anions by the anionite. As a result desalted water, from which cations and anions are eliminated, is obtained.

The operating exchange capacity of cationite is defined by the equation

$$E_c = \alpha_{ef\text{-}c}\ E_{f\text{-}c} - 0.5 q_c (h_w + C_{Na})$$

where $\alpha_{ef\text{-}c}$ is coefficient of regeneration efficiency, in the range 0.9–0.93; $E_{f\text{-}c}$ is total dynamic exchange capacity of cationite, (g-eq)/m^3; q_c is specific consumption of water, m^3 per one wastewater m^3; h_W is total water hardness, (g-eq)/m^3; C_{Na} is sodium content in the treated water, (g-eq)/m^3.

Table 24.30 includes data for the hydrogen–cation–exchange filter calculation.

By countercurrent cation exchange with total salt content in the treated wastewater of 20 mg-eq/L and specific acid consumption 110 g/(g-eq), the full softening is obtained with simultaneous removal of the Na^+ cation up to a residual of about 0.08 mg-eq/L.

The anionite-exchange filters, designed for the elimination of strong acid anions, contain a weak basic anionite, for example, AN–31 (trademark), while for the elimination of weak acids (CO_3^{2-} and SiO_3^{2-}), strong basic anionite AB–17 type are used.

The operating exchange capacity of anionite AN–31 (trademark) is defined by the equation

$$E_a = \alpha_{ef\text{-}a}\ E_{f\text{-}a} - 0.8 q_a C_a$$

where $\alpha_{ef\text{-}a}$ is the coefficient of the anionite regeneration efficiency dependent on the alkali discharge intensity (by its discharge intensity 60 g on 1 g-eq of the absorbed sulfates and chlorides, the $\alpha_{ef\text{-}a}$ is taken to amount to 0.8–09); $E_{f\text{-}a}$ is the total anionite

Table 24.30 Data for the calculation of hydrogen–cation–exchange filters

Parameters	Unit	Normative values
Cationite type		Sulfonated coal CK–1, cationite KY–2
Grain size:		
CK–1	mm	1.0–1.1
KY–2	mm	1.0–1.25
Allowable bed height	m	up to 3.3
Apparent density of commercial cationic aterial:		
CK–1	kg/m^3	550
KY–2	kg/m^3	690
Temperature of treatment water	°C	15–40
Number of maintained filters	pcs	Not less as 3 operational and 1 reserve
Advisable filtering rate, at water hardness (mg-eq/l):		
under 5	m/h	20 (30)[a]
under 10	m/h	15 (25)
under 15	m/h	10 (20)
Hydraulic resistance of filters according to cationite type:		
CK–1 by filtering rate (m/h)		
10	m-water column	20
20	m-water column	24
30	m-water column	28

[a]Maximum at the time when one of the filters is in regeneration regime

Table 24.31 Technological data for calculation of the AN-31 brand anionic material filters

Parameters	Unit	Normative values
Moisture load	%	15
Apparent density	g/cm^3	0.72–0.75
Grain sizes in turgid condition	mm	0.4–2.0
Anionic yield	%	5–10
Total anionic dynamic exchange capacity	(g-eq)/m^3	>800
Number of as maintained filters	pcs	Not less as 3 operational and 1 reserve
Advisable filtering rate, taking into account of full E_{f-a} using	m/h	15–20
Regeneration of anionic material with alkali:		
Specific consumption	g/(g-eq)	60
Solution strength	%	4
Passage rate	m/h	20
Cleaning of anionite material:		
Specific water consumption	m^3/m^3	20
Passage rate of washing water	m/h	8–10

dynamic exchange capacity, (g-eq)/m^3 (in accordance with Table 24.31); q_a is the specific consumption of anionite cleaning (it takes 20 m^3 water per 1 m^3 of the anionic); C_a is anion concentrations of strong acids in the water fed to the anionic filters. The technological data for calculation of the anionite filters in desalting circuits are given in Table 24.31.

Sorption, Evaporation and Flotation Methods

Sorption Method

Sorption method is used for the removal of phenols, acetone, trichloroethylene and other solvents which

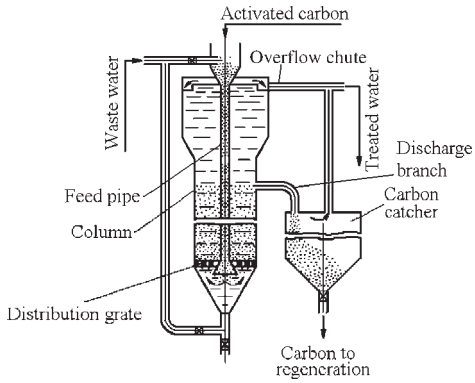

Figure 24.25 Sorption technique for the waste water purification.

are used in the electrochemical methods of powder production. As adsorbents, activated carbon, breeze coke, peat, chalk and limestone in the form of irregular shaped grains from 1.5 to 5 mm in diameter are used. Reduction of adsorbent is done by chemical dissolvents, steam or heat treatment.

Motionless as well as fluidized beds of adsorbent are used in adsorbers. The design of the former is simpler but the adsorbers with fluidized beds are more effective.

Commercial plants usually contain a column (Figure 24.25), with a larger diameter in the upper section head part, equipped with an overflow chute for venting of the treated water. The waste water is fed into the conic end, over which a distributive grating with 5–10 mm diameter apertures is located. A 2.5–2.7 m activated carbon layer is formed on the grating. The activated carbon is fed into the column by a batcher through the vertical pipe. The flow rate is such as to maintain the carbon in the fluidized state. Part of the treated water containing spent carbon is removed through a discharging branch to the carbon catcher. The treated water from the column is discharged in the overflow chute and is vented with water from the carbon catcher.

The activated carbon is subjected to regeneration, after which is returned to the adsorber. The adsorbed substances are taken out during regeneration by means of organic solvents, steam distillation and evaporation with a heated gas current.

Evaporation Method

Evaporation represents the distillation of the volatile matter contaminating the water with water steam. This technique can be used for the removal of phenols. Here the waste water is not polluted by chemical reagents.

Flotation Method

Flotation is used for the removal of surfactants, fats and oil products. The process is based on the floating-up of air blebs with particles spoiling the waste water.

Numerous companies specialize in the area of waste water treatment and recirculation: Rochen UF System, Germany, designs and assembles the water-purifying equipment; National Water storage group Companies, Russia, deal with the treatment of waste water and water conditioning; Jurby Water Tech International, UK, produces decarburization, reverse osmosis and demineralization installations and chemical reagents for technological water treatment; KWI Co, Russian branch, produces flotation equipment for waste water treatment; Kreal-water purification and conditioning Co, Russia, builds waste water treatment installations, purification filters and water conditioning equipment; and OY LABKO AB, Finland, produces equipment for waste water treatment.

Dust and Gas Cleaning

The selection of equipment for dust removal is based on the following criteria:

- the degree of dust removal required
- the physical and chemical properties of the dust
- temperature, moisture content, chemical reactivity, dust concentration and the volume of the gas to be treated
- the operating regime of the equipment.

Dust arresters are subdivided into coarse, medium and fine depending on their guaranteed gas cleaning efficiency. The coarse dust arresters efficiently collect particles bigger than 10 μm, while particles smaller than 2 μm are not collected. The medium cleaning plants efficiently collect up to 2 μm and fine cleaning plants collect particles in the range below 2 μm.

Depending on the dust collecting mechanism, dust arresters are subdivided into mechanical (dry and wet), porous and fibrous filters, electrical precipitation and plants based on some other effects (such as acoustical and condensation coalescence of the particles). Such coagulated particles are caught further in some coarse or medium cleaning plants.

A magnetic effect, thermophoresis, and others mechanisms have been explored. However, such processes are still in the experimental stage.

Table 24.32 Gas cleaning plants

Parameter	Unit	Plant type[a]				
		KP-1.6-2Y-01	KP-3.15-2Y-01	KP-6.3-2Y-01	KP-12.5-2Y-01	KP-25-2Y-01
Capacity (max)	m^3/h	1600	3150	6300	12 500	25 000
Heat transfer area (min)	m^2	35	39.4	110	400	715
Hydraulic resistance (max)	kPa	10	10	10	10	10
Catalyst total volume (min)	m^3	0.2	0.36	0.65	0.86	1.6
Temperature of exhaust gas emissions:						
before catalyst layer, not more than	°C	450	450	450	450	450
maximum in apparatus	°C	500	500	500	500	500
Maximum concentration of impurities in gases						
carbon monoxide and organic compositions (converting to carbon)	g/m^3	10	10	10	10	10
dusts	g/m^3	0.01	0.01	0.01	0.01	0.01
Purification efficiency, minimum	%	95	95	95	95	95
Consumption of fuel gas, maximum	m^3/h	10.1	22.1	38.9	64.8	118.0
Specific power consumption, maximum	kWt·h/(1000 m^3)	58.6	65.2	57.5	48.4	44.7
Weight (max)	ton	2.62	3.13	5.85	13.63	24.82

[a]Russian Standards.

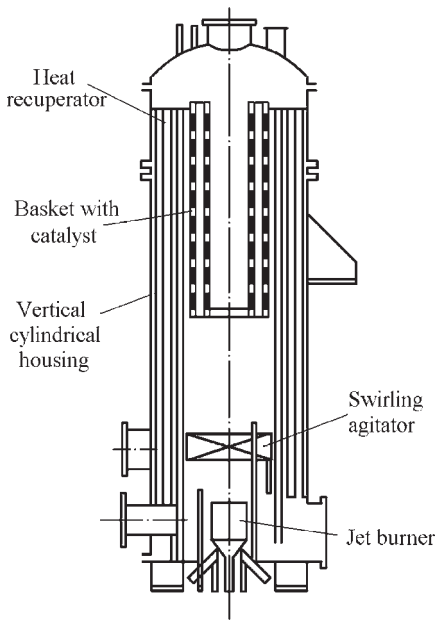

Figure 24.26 Type KP apparatus for the purification from carbon monoxide and organic compounds of effluent gas.

The gas cleaning plants, KP type (Table 24.32) are intended for cleaning exhaust gas emissions from carbon monoxide and organic compositions with weight concentration up to 10 mg/m^3. The apparatus (Figure 24.26) consists of a vertical cylindrical body, within which is the basket with catalyst, dividing sidewalls and shell-and-tube circular heat exchanger are coaxially assembled. Under the basket, the jet burner and turbulence promoter are located. The basket consists of two concentrically situated cylinders. The space between cylinders is filled with catalyst.

Preliminary heating of the exhaust gas emissions is realized by the heat of the refined gases in the shell-and-tube circular heat exchanger. The turbulence promoter ensures temperature uniformity in front of the catalyst layer.

The exhaust gas emissions come via the intertubular space of the heat exchanger to the jet burner, which warms them up with admixtures of oxidizers to the temperature range from 250 to 450°C, whereupon the gases through the turbulence promoter reach the catalyst layer. The catalyst type and operating temperature are chosen depending on the exhaust gas emissions composition and the concentration of impurities.

As a result of the catalytic oxidation of the impurities, carbon dioxide and water are formed. The characteristics of the exhaust gas emissions cleaning apparatus are given in Table 24.32.

The operating details and special features of dust and gas cleaning equipment can be found in respective brochures available from the manufacturers. The Suomen Imurikeskus Oy specializes in area of gas cleaning from ultrafine dust.

Waste Products Utilization, Storing and Transportation

Waste Utilization

The hazardous waste products legislation in the EU as well as internationally becomes increasingly important for the metals and alloys industry. It is also an area where end-users must try to eliminate or restrict the use of such metals or alloys because they are classified, prompted by fear of downstream disposal problems, or fear of damaging the company's 'green' image.

It is accepted that waste products can be subdivided into three main areas: scrap for recycling, scrap for disposal (waste) and scrap components within assemblies.

Scrap for recycling is not 'waste' and therefore is not subject to waste regulations. This type of scrap should be returned to the producer or it can be sold to authorized scrap dealers.

The off-size waste products are pressed into briquettes and returned to the technological process, if they correspond with the composition conditions, or transferred to processing as secondary raw materials. In that case, the safety requirements are regulated by corresponding statutory acts, as GOST 12.2.055-81 and OST 4 GO.091.266-87 in the Russian Federation.

Scrap for disposal (waste) is defined within the framework Directive 91/156/EES if it cannot be recycled and must be disposed of. It is important to establish whether the scrap or waste meets the Special Waste definition. This can be established by the following conditions:

- if it is a listed waste (this includes waste arising from surface treatment of metals; liquid waste or sludge containing metal or compounds; dust or waste powder containing metal compounds)
- if it contains a listed substance (this includes many metals and/or their compounds)
- if it falls into either of the above categories, does it also have dangerous properties.

Such scrap is classified as a special waste and the waste generator has the duty of care in the disposal of the waste. It must also be handled by an authorized waste disposal agent and disposed of in an authorized land fill site.

Scrap components within assemblies. Here the scrap producer first has to establish whether it is economically feasible to extract the components made from the classified material for recycling. There is, however, no legal requirement to remove the components prior to disposal. In disposing of the equipment with the components still in it, the scrap producer must carry out a risk assessment whether the waste falls under Special Waste Regulation to determine the technique of disposal.

A typical metal machining scrap recycling process is schematically shown in Figure 24.27. The initial chips (includes copper, brass, tin or titanium) with size up to 500 mm are fed to a hammer crusher. Crushed chips less than 5 mm are cleaned in a vibratory washing machine followed by drying and subsequent milling in a vibratory cone mill. The milled product is divided by means of vibratory sieve into fractions $+100\,\mu m$ and $-100\,\mu m$. The former is returned for further milling, while the latter is subjected to gravity concentration.

Waste disposal as related to the metals and alloys industries will be affected by a new EU legislation which will require ecotoxicology classification.

Directive 91/686/EEC contains a new and wider definition of hazardous waste which extends to

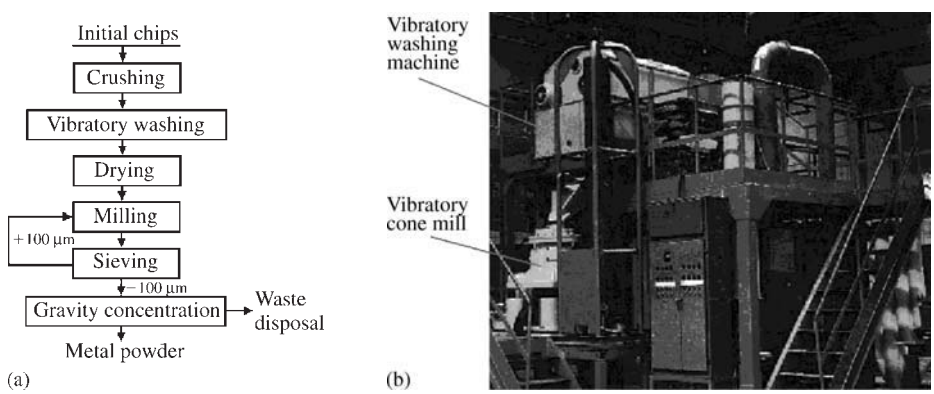

Figure 24.27 Metal chip waste recycling: (a) scheme of process; (b) overview of the installation. Courtesy of the Mekhanobr Institute, Saint Petersburg

metallic dusts and powder as well as liquid or sludges containing metals or metal compounds. Components of wastes which render them hazardous include nickel compounds.

Demands of this Directive include:

- competent authorities to draw up hazardous waste management plans and to make these public
- Member States to identify and record all hazardous waste being disposed of within their borders
- inspection of hazardous waste collection and transport activities must, in particular, cover the origin and destination of the waste
- operators who dispose, recover and collect or transport hazardous waste must not mix different categories of waste or mix hazardous waste with non-hazardous waste
- wastes must be suitably packaged and labelled in accordance with international and community standards in force.

The European Waste Catalogue is a non-exhaustive list of wastes, which unconditionally includes waste containing nickel and its compounds, intended to provide a common terminology for waste management activities throughout the EU. The Catologue represents a list of waste which the EC was required to produce under Article 1 of the Waste Framework Directive 75/442/EEC, as amended by 91/156/EEC. The catalogue is no longer directly relevant to the definition of hazardous waste for which a separate list is be drawn up by the European Commission [3].

Storing and Transportation of Hazardous Powders

The storing and transport of dangerous goods are governed by a large number of international treaties and national legislation. The principal regulations, based on the 'Recommendations on the transport of dangerous goods' (as published in the eighth revised edition by the United Nations (UN), New York, 1993, ISBN 92 1 139042 7), are:

- the European Agreement concerning the international carriage of dangerous goods by road (ARD) which applies to the international (as well as in some cases also to the national) transport of harmful substances in Europe. The agreement has been signed by most European countries
- the International Regulations concerning the carriage of dangerous goods by rail (RID) which are part of the Treaty on the International carriage by rail (COTIF), which has been signed by most European states
- the International Maritime Dangerous Goods Code (IMDG Code) is applicable worldwide and applies to ships carrying dangerous goods in packaged form or in solid form in bulk
- the IATA dangerous goods regulations which are applicable worldwide to all airlines which are members or associate members of IATA.

The Standards GOST 12.2.055-81 and OST 4 GO.091.266-87 stipulate in CIS the safety regulations for storing, transportation and using active and harmful materials. The categories of production areas and buildings on explosion-fire and fire risk are determined in Commonwealth of Independent States (CIS) in accordance with Technological Designing Standard ONTP-24–86 [11].

Dangerous goods are products which can represent a significant risk to health, safety or property during transportation. They are assigned to one or more of the nine UN hazard classes by descending order of danger and, where applicable, to one of three UN packing groups. The flammable solids are placed in Class 4, while flammable liquids are in Class 3 and corrosives in Class 8. The criteria for classification and packaging of dangerous goods are based on the Recommendations of the United Nations Committee of Experts on the Transport of Dangerous Goods (as published in the eighth revised edition by the United Nations, New York, 1993; ISBN 92 1 139042 7).

The Packing groups include:

- Packing group I: Great danger
- Packing group II: Medium danger
- Packing group III: Minor danger

For metal powders, the main classification area is for flammability (Class 4). This class is subdivided as follows:

- Division 4.1: flammable solids are solids, other than those classed as explosives which, under conditions encountered in transport, are readily combustible or may cause or contribute to fire through friction
- Division 4.2: pyrophoric are substances liable to spontaneous combustion or self-heating under normal conditions encountered in transport, or to heating up in air and being then liable to catch fire
- Division 4.3: emission of flammable gases covers the substances which, on contact with water, are liable to become spontaneously flammable or to give off flammable gases in dangerous quantities.

Table 24.33 Classification for transportation of a range of metal and alloy powders

Metal powders	Class 4.1	Class 4.2	Class 4.3	Thermal stability	Conclusions
Lead <40 μm	Packaging group III	Packaging group II	...	High reactive	Class 4.2 Packaging group II
Lead <63 μm	...	...	...	High reactive	...
Coarse copper	...	...	...	Low reactive	...
Copper <63 μm	...	...	...	Reactive	...
Bronze <40	...	...	...	Low reactive	...
Brass <63 μm	...	...	...	Low reactive	...
Phosphor-copper <80 μm	...	...	...	Reactive	...
Copper flake <40 μm	...	Packaging group II	...	High reactive	Class 4.4 Packaging group II
Tungsten <2 μm	Packaging group II	...	...	Reactive	Class 4.1 Packaging group II
Zinc <63 μm	...	...	Class 4.3	Low reactive	...
Tin <40 μm	...	...	...	Low reactive	...
Bronze premix with lubricant	...	...	...	High reactive	..

Source: Ref 3®

Table 24.34 UN method final test and EC method A10 final test for 10 cm length samples

PG	UN class 4.1		EC class F, R11	
	Burning rate (10 cm length)		Burning rate (10 cm length)	
	Metal powders (minutes)	Other solids (seconds)	Metal powders (minutes)	Other solids (seconds)
II	5	<45*	10	45
III	10	<45**		

*Wetted barrier zone passed;
**wetted barrier stops flame in ≤4 minutes.
Source: Ref 3

Some examples of tests undertaken by EPMA members on the classification for transportation of a range of metal and alloy powders are given in Table 24.33.

The EC criteria for classification, choice of symbols, and indication of danger with risk (R) phrases are given in Directive 67/548/EES. Thus, R10 is Flammable, R12 is Extremely Flammable, R11 is Highly Flammable (idem Class F), R15 is Contact with water liberates extremely flammable gases and R17 is spontaneously flammable in air.

Table 24.34 compares the UN and EC two packing groups (PG) — I and II, whereas the EC class is not subdivided. The UN preliminary burning rate test criteria for Class 4.1 are less severe than the preliminary EC test criteria.

The limits for 10 cm length and time in minutes for pyrophoric substance and self heating powders (UN class 4.2) defined by the UN method and EC method A10 equal 20 and 40, respectively.

References

1. Commonwealth of Independent States Standard GOST 12.1.003-83, Occupational Safety Standards System. Noise. General Requirements of Safety (in Russian).
2. Commonwealth of Independents States Standard SNiP II-12-77, Occupational Safety Standards System. Protection away from the Noise. Designing Standards (in Russian).
3. *Guide to Legislation and 'Health and Safety' in the European PM Industry*. EPMA, 1997.
4. Neikov, O.D. et al., Explosion-security of manufacture processes of advanced water atomized

aluminium alloy P/M technology. In *Proceedings of 2002 Powder Metallurgy World Congress*, compiled by V. Arnold, C.-L. Chu, W.F. Jandeska, H. I. Sanderow, Princeton, MPIF Publishers, New Jersey, 2002, pp. 7-60–7-69.
5. Alekseev, A.G., Neikov, O.D., The explosion risk of metal powders. Staub, 1990, 50:245–250.
6. Occupational Safety Standards System. General sanitary requirements for working zone air. GOST 12.1.005−88 (in Russian).
7. Hazard classification of metallic alloys – a proposal for special concentration limits. EIMAC, for EU Expert Meeting, 1996.
8. ECDIN, Datebase. Commission of the European Communities (CEC). Environmental Chemical Data and Information Network. Joint Research Centre, Environment Institute, Italy, 1992.
9. EINECS-Plus, CD-ROM on three EU chemical inventories. EUR-OP, Luxembourg (JX-87-95-001-8C-Z), 1996.
10. Soviet Union Patent 1,044,328, June, 1981.
11. Technological Designing Standard ONTP-24–86 (in Russian).
12. Neikov, O.D., Logachev, I.N., *Aspiration and Air Dedusting During Manufacture of Powders*. Metallurgija Publishers, Moscow, 1981 (in Russian).
13. Soviet Union Patent 842015, December, 1981.
14. *Directive for designing and computation of aspiration in metallic powder production including combustible and explosive*. IPMS Publishers, Kiev, 1995.
15. Neikov, O.D., Prevention of ignitions by comminution of sponge iron. *Powder Metall. Met. Ceram.*, 1977, 11:102–106.
16. RU Patent 2,122,926, May, 1997.
17. Soviet Union Patent 1,436,341, February, 1987.
18. Soviet Union Patent 1,460, 831, January, 1987.
19. Soviet Union Patent 1,131,536, March, 1983.
20. Soviet Union Patent 413,990, March, 1972.

Appendix 1

Methods of Powder Characterization and Testing

Standard title	Origin				
	ISO	ASTM	MPIF	CIS	Other
Metallic Powders – Determination of Apparent Density – Part 1: Funnel Method	3923/1	B 212	04	GOST 19440-94	...
Density, Apparent of Metal Powders using the Arnold Meter	...	B 703	48	...	...
Density, Apparent of Non-Free-Flowing Metal Powders	...	B 417	28	...	...
Metallic powder – Determination of apparent density – Part 2: Scott Volumeter Method	3923/2	B 329	...	GOST 19440-94	
Flow Rate of Metal Powders	4490	B 213	03	GOST 20899-75	...
Measuring Dimensional Change of Metal Powder Specimmens due to Sintering	4492	B 610	44	GOST 29012-91	...
Metallic Powders – Determination of Oxygen Content by Reduction Methods – Part 1, Part 2, Part 3, Part 4	4491-1, 2, 3, 4	E 159	02	GOST 29006-91 GOST 27417-87 GOST 18897-73	...
Metallic Powders – Determination of envelope – specific surface area from measurements of the permeability to air of a powder bed under study-state flow conditions	10070	...	...	GOST 23401-90	...
Metallic Powders – Determination of particle size distribution by gravitational sedimentation in a liquid and attenuation measurement	10076	...	...	...	...
Metallic Powders – Determination of acid insoluble content in iron, copper, tin and bronze powders	4496	E 194	6	GOST 30550-98	...
Metallic Powders – Determination of Particle size by Dry Sieving	4497	B 214	05	GOST 18318-94	MIL-STD-1233
Metallic Powders. Determination of particle shape	...	...	...	GOST-25849-83	...
Metallic Powders, excluding Powders for Hard metals – Determination of Compactibility (Compressibility) in Uniaxial Compression	3927	B 331	45	GOST 25290-90	...
Metallic Powders – Determination of Green Strength by transverse rupture of rectangular compacts	3995	B 312	15	GOST 25282-93	...
Particle Size Distribution of Metal Powders and Related Compounds by Light Scattering	...	B 822	...	...	...

(*Continued*)

Standard title	Origin				
	ISO	ASTM	MPIF	CIS	Other
Particle Size Distribution of Refractory Metals and their Compounds by X-Ray Monitoring of Gravity Sedimentation	...	B 761	...	...	...
De-Agglomeration of Refractory Metal Powders and their Compounds Prior to Particle Size Analysis	...	B 859	...	...	...
Particle Size Distribution of Refractory Metals-Type Powders by Turbidimetry	...	B 430	...	...	...
Particle Size, Average, of Metal Powders by Fisher Subsieve Sizer	...	B 330 C 721	32	...	MIL-STD-1233
Particle Size Analysis of Particulate Substances by Optical Microscopy		E 20	...	GOST 23402-78	...
Permeable sintered metal materials – Determination of bubble test pore size	4003	...	...	GOST 26849-86	...
Pore Volume Distribution of Catalysts by Mercury Intrusion Porosimetry	...	D 4284	...	...	...
Bulk Density and Porosity of Granular Refractory Materials by Mercury Intrusion Porosimetry	...	C 493	...	...	...
Sampling and Testing Aluminum Powder and Paste	...	D 480	...	...	...
Sampling Finished Lots of Metal Powders	3954	B 215	01	GOST 23148-78	
Standard Shear Testing Method for Bulk Solids Using the Jenike Shear Cel	...	D 6128	...	...	...
Subsieve Analysis of Granular Metal Powders by Air Classification	...	B 293	12	...	...
Tap Density of Metal Powders	3953	B 527	46	GOST 25279-93	MIL-STD-1233
Tension Test Specimens for Pressed and Sintered Metal Powders	2740	E 8	10	...	...
Testing Copper-Base Infiltrating Powders	...	...	49	...	...
Terms Used in Powder Metallurgy	3252	B 243	9	GOST 17359-82	
British Standards 2955 Glossary of Terms Relating to Powders	...	...	...	...	British Standards 2955
Wire-Cloth Sieves for Testing Purposes, Specification	565 3310/1	E 11		GOST 3584	RR-S-366

Standards referenced include those of the American Society for Testing and Materials (ASTM), International Organization for Standardization (ISO), Metal Powder Industries Federation (MPIF), Commonwealth of Independent States (CIS), MIL-STD: Superintendent of Documents, US Government Printing Office, Washington, D.C.20402.

Appendix 2

Metal Powder Specifications

Standard title	Designation		
	ASTM	CIS	Other
Aluminum Pigment, Powder and Paste, for Paint	D 962	GOST 5494-95	TT-P-320B
Aluminum Powder, Flaked, Grained and Atomized	. . .	. . .	MIL-A-512A
Aluminum Lumpy Pigment	. . .	GOST 10096-76	. . .
Antimony, Powdered, Technical	. . .	. . .	MIL-A-10841B
Brass Powder (for sintering)	. . .	. . .	MIL-B-11552B
Bronze Powder, Gold	D 267	. . .	TT-P-340
Copper Powder	. . .	GOST 4960	. . .
Copper Powder (for use in ammunition)	. . .	. . .	JAN-C-768
Copper Electrolytic Powder, Ultrafine, Stabilized	. . .	TU 17911-368-094-96	. . .
Copper Reduced Powder, Stabilized	. . .	TU 48-0318-083-94	. . .
Copper Powder for Use in Antifouling Paints	D 964	. . .	. . .
Cobalt Powder	. . .	GOST 9721-79	. . .
Iridium, Powdered	. . .	GOST 12338-81	. . .
Magnesium-Aluminum Alloy, Powdered	. . .	. . .	JAN-M-454
Magnesium Powder (for use in ammunition)	. . .	. . .	JAN-M-382A
Manganese, Powdered (for use in ammunition)	. . .	. . .	JAN-M-476A
Nickel Powder	. . .	GOST 9722-79	. . .
Nickel Powder (for use in ammunition)	. . .	. . .	JAN-N-412A
Niobium Powder	. . .	GOST 26252-84	. . .
Palladium, Powdered	. . .	GOST 14836-82	. . .
Powders, Metal, Atomized (Aluminum, Magnesium, Magnesium-Aluminum)	. . .	. . .	MIL-P-14067B
Rhodium, Powdered	..	GOST 12342-81	. . .
Tin Powder	. . .	GOST 9723-79	. . .
Tin, Pulverized	. . .	. . .	JAN-T-458
Titanium, Powdered	. . .	. . .	MIL-T-13405
Tungsten, Powdered	. . .	. . .	MIL-T-13827
Zinc Powder	. . .	GOST 12601-76	. . .
Zinc Dust (for use in pyrotechnics)	. . .	. . .	JAN-Z-365
Zinc Dust (metallic zinc powder); Dry (paint pigment)	D 520	. . .	TT-P-460 No. 1
Zirconium-Nickel Alloy Powder (for use in delay compositions)	. . .	. . .	MIL-Z—11410A
Zirconium powder (calciothermic)	. . .	TU 48-4-234-84	. . .
Zirconium powder (natriothermic)	. . .	TU 48-4-376-76	. . .
Zirconium, Powdered (for use in ammunition)	. . .	. . .	JAN-Z-399A

(*Continued*)

Standard title	Designation		
	ASTM	CIS	Other
Miscellaneous:			
Brushes, Electrical Contacts and Carbon Stock, Electrical Contact Brush			MIL-B-003743D
Precision Electroformed Sieves, Specification for	E 161	. . .	. . .
Terms used in Powder Metallurgy	B 245	. . .	MPIF: 9

Standards referenced include those of the American Society for Testing and Materials (ASTM), Metal Powder Industries Federation (MPIF), Commonwealth of Independent States (CIS), JAN, MIL, TT: Superintendent of Documents, US Government Printing Office, Washington, DC 20402.

Appendix 3

Abbreviations and Symbols

A	ampere
Å	angstrom
ac	alternating current
AES	Auger electron spectroscopy
AMS	Aerospace Material Specification
ANSI	American National Standards Institute
ASM	International The Materials Information Society
ASTM	American Society for Testing and Materials
at.%	atomic percent
atm	atmosphere (pressure)
bal	balance
bcc	body-centered cubic
BEI	back scattering electron image
bet	body-centered tetragonal
Btu	British thermal unit
CIP	cold isostatic pressing
cm	centimeter
CMC	ceramic-matrix composite
CP	Commercial pure
cpm	cycles per minute
cps	cycles per second
CSA	Canadian Standards Association
cSt	centiStokes
CTE	coefficient of thermal expansion
CVD	chemical vapor deposition
CVI	chemical vapor infiltration (impregnation)
d_a	project area diameter of the particle
dB	decibel
dc	direct current
DCA	differential calorimetric analysis
diam	diameter
DIN	Deutsche Institut für Normung
d_p	perimeter diameter of the particle
DTA	differential thermal analysis
e	charge of an electron; natural log base, 2.71828
E	modulus of elasticity; Young's modulus; potential
E_s	secant modulus
EIMAC	European Industry Metals and Alloys Classification Group
EL	elongation
emf	electromotive force
EMI	electromagnetic interference
Eq	equation
EPMA	European Powder Metallurgy Association
ESC	environmental stress cracking
esu	electrostatic units

et al.	and others
eV	electron volt
F	Faraday constant; force
fcc	face-centered cubic
FCGR	fatigue crack growth rate
fct	face-centered tetragonal
Fig.	figure
FM	figure of merit
ft	foot
g	gram
G	gauss
GA	gas atomized
gal	gallon
GPa	gigapascal
gpd	grams per denier
gr	grain
h	hour
h	thickness
H	henry
H	change in height; degree of homogenization; enthalpy; hardness; height; magnetic field
HB	Brinell hardness
hcp	hexagonal close-packed
HDT	heat-deflection temperature
HDVC	hot dynamic non-capsule vacuum compacting
HE	hot extrusion
HERF	high-energy-rate forging
HIP	hot isostatic pressing
hp	horsepower
HPWA	high pressure water atomization
HR	Rockwell hardness (requires a scale designation, such as HRC for Rockwell C hardness)
HV	Vickers hardness
Hz	hertz
i	current (measure of number of electrons)
I	current; emergent intensity
IACS	International annealed copper standard
IC	integrated circuit
ID	inside diameter
in.	inch
IPD	integrated product development
IPMD	International Powder Metallurgy Directory Yearbook
IPMS	Institute for Problems of Materials Science
IPPC	integrated pollution prevention and control
IPTS	International Practical Temperature Scale
IR	infrared (radiation)
ISO	International Organization for Standardization
ITS	International Temperature Scale
IV	intrinsic viscosity
J	joule
JIS	Japanese Industrial Standard
k	karat
k	Boltzmann constant; notch sensitivity factor; thermal conductivity; wave number
K	Kelvin
K	bulk modulus of elasticity; coefficient of thermal conductivity; empirical constant; interface reaction; mean integrated thermal conductivity
K_{Iscc}	threshold stress intensity for stress-corrosion cracking

kg kilogram
km kilometer
kN kilonewton
kPa kilopascal
ksi kips (1000 lb) per square inch
kV kilovolt
kW kilowatt
l mean free path; length
L liter; longitudinal direction; liquid
L length
lb pound
lbf pound-force
LCA life cycle analysis (or assessment)
LCFS low-cycle (3 Hz) fatigue strength on the base of 10^5 cycles
LCIL low concentration ignition limit
LOC explosion proof limit oxygen content
L/D length-to-diameter ratio
LED light-emitting diode
LEFM linear-elastic fracture mechanics
ln natural logarithm (base *e)*
log common logarithm (base 10)
m matrix; meter
m ion mass; Weibull modulus
M metal atom
M molecular weight
MA mechanical alloying
mA milliampere
MeV megaelectronvolt
mg milligram
Mg megagram
MIM metal injection molding
min minimum; minute
MJ megajoule
mL milliliter
MLCCs multilayer ceramic capacitors
MLT marketing lead time
mm millimeter
MMC metal-matrix composite
mod modified
mol% mole percent
MOR modulus of resilience; modulus of rupture
mPa millipascal
MPa megapascal
mpg miles per gallon
mph miles per hour
MPIF Metal Powder Industrial Federation
ms millisecond
MS megasiemens
MSDS material safety data sheets
mT millitesla
MTBF mean time between failures
MTTF mean time to failure
mV millivolt
MV megavolt
MW molecular weight

n	growth exponent
n	integral number; section capture of thermal neutrons
N	Newton
N	fatigue life (number of cycles)
NASA	National Aeronautics and Space Administration
NBS	National Bureau of Standards
NC	numerical control
NDE	non-destructive evaluation
NDI	non-destructive inspection
NDT	non-destructive testing
NISI	National Institute of Standards and Technology
nm	nanometer
No.	number
OD	outside diameter
ODS	oxide-dispersion strengthened
Oe	oersted
OELs	occupational exposure limits
OHA	operating hazards analysis
ORNL	Oak Ridge National Laboratory
OSHA	Occupational Safety and Health Administration
oz	ounce
p	page
p	pressure
P	applied load; power; pressure
Pa	pascal
PCA	process control agent
PCE	pyrometric cone equivalent
PDS	product design specification
PDT	product design team
P/F	powder forging
pH	negative logarithm of hydrogen-ion activity
PM	powder metallurgy
ppb	parts per billion
ppba	parts per billion atomic
ppm	parts per million
ppt	parts per trillion
Pr	Prandtl number
psi	pounds per square inch
PTC	positive temperature coefficient
PVD	physical vapor deposition
QC	quality control
QFD	quality function deployment
QLF	quality loss function
r	radius vector in a plane normal to the axis
r	particle radius; radius of curvature; rate of reaction; reflectivity; spherical particle radius
R	roentgen
R	average particle radius; gas constant; radius; ratio of the minimum stress to the maximum stress; resistance; reliability
R_a	surface roughness in terms of arithmetic average
RA	reduction of area
rad	absorbed radiation dose; radian
Re	reynolds number
REM	rare earth metal
Ref	reference
rem	remainder

rf, RF	radio frequency
RH	relative humidity
rms, RMS	root mean square
rpm	revolutions per minute
RS	rapid solidification
RT	room temperature
RTI	relative thermal index
s	second
S	Siemens
S	distance traveled
SAE	Society of Automotive Engineers
scfm	standard cubic foot per minute
SEM	scanning electron microscopy
sfm	surface feet per minute
SG	standard grade
SI	Systèm International d'Unités
sineh	sine hyperbolic
S/N	signal-to-noise (ratio)
S-N	stress-number of cycles
SPC	statistical process control
SPF	superplastic forming
sp gr	specific gravity
SRIM	structural reaction injection molding
std	standard
STEM	scanning transmission electron microscopy
STM	scanning tunneling microscopy
t	thickness; time
T	Tesla; transverse direction
T	absolute temperature; temperature; tenacity; total dispersion; transmittance
T_m	melt temperature
TEM	transmission electron microscopy
TGA	thermogravimetric analysis
TLVs	threshold limit values
TM	transition metal
TMA	thermomechanical analysis
TMS	The Minerals, Metals and Materials Society
TP	thermoplastic
UMIST	University of Manchester
UNI-Bremen	University of Bremen
UTS	ultimate tensile strength
UV	ultraviolet
v	workpiece velocity
V	volt
VD	vacuum degassing
V_f	volume fraction of fiber
V_m	volume fraction of matrix
V_v	volume fraction of void content
VILS	Al-Russian Institute of Light Alloys
VI	viscosity index
vol	volume
vol%	volume percent
w	whisker
W	watt
W	total radiation; width
WA	water atomization

wt%	wight percent
x	axial distance
X	neck diameter
XRD	X-ray diffraction
Y	scale of microstructural segregation
YAG	yttrium aluminum garnet
yr	year
YS	yield strength
z	ion charge
Z	atomic number; impedance
°	angular measure; degree
°C	degree Celsius (centigrade)
°F	degree Fahrenheit
0°	fiber direction
90°	perpendicular to fiber direction
α	coefficient of thermal expansion
γ	shear strain; surface energy; surface tension
γ_i	interfacial energy
γ_s	surface energy
δ	an increment; a range; change in quantity; grain boundary width; thickness of liquid boundary
Δ	an increment; a range; change in quantity
Δ*T*	temperature difference or change
ε	strain
έ	strain rate
η	loss coefficient; viscosity
θ	angle; geometrical constant
θ_i	angle of incidence
θ_r	angle of refraction
κ	dielectric constant
λ	thermal conductivity
μ	friction coefficient; linear attenuation coefficient; magnetic permeability; the mean (or average) of a distribution
μin	microinch
μm	micrometer (micron)
μs	microsecond
ν	Poisson's ratio; velocity
π	pi (3.141592)
ρ	density; resistivity
σ	Stefan-Boltzmann constant; strength; stress; tensile stress; tensile strength
σ_a	applied stress
σ_f	applied axial load
Σ	summation of
τ	shear stress
ϕ	angle of internal friction; dihedral angle; porosity; power
Φ	reaction rate (kinetic function); volume concentration of impurity ions
ψ	damping; geometrical constant
ω	frequency
Ω	atomic volume; electrical conductivity; molecular volume of solute; ohm
∂	partial derivative
∂η/∂t	kinetic function
⇄	direction of reaction
÷	divided by
=	equals

≈	approximately equals
≠	not equal to
≡	identical with
>	greater than
≫	much greater than
⩾	greater than or equal to
∞	infinity
∝	is proportional to; varies as
∫	integral of
<	less than
≪	much less than
⩽	less than or equal to
±	maximum deviation
−	minus; negative ion charge
×	diameters (magnification); multiplied by
·	multiplied by
/	per
%	percent
+	plus; positive ion charge
√	square root of
~	approximately; similar to

Greek Alphabet

A, α	alpha
B, β	beta
Γ, γ	gamma
Δ, δ	delta
E, ε	epsilon
Z, ζ	zeta
H,η	eta
Θ, θ	theta
I, ι	iota
K, κ	kappa
Λ, λ	lambda
M, μ	mu
N, ν	nu
Ξ, ξ	xi
O, ο	omicron
Π, π	pi
P, ρ	rho
Σ, σ	sigma
T, τ	tau
Y, υ	upsilon
Φ, ϕ	phi
X, χ	chi
Ψ, ψ	psi
Ω, ω	omega

Index